

FINAL REPORT
ON
THE UPPER MIDDLE FORK PROJECT

by

A. Dib, S. Ceyhan, K. Ishida, M. L. Kavvas, S. Jang, N. Ohara

Hydrologic Research Laboratory
Department of Civil and Environmental Engineering
University of California, Davis

Principal Investigator: M. L. Kavvas

Report to Plumas County

December 2016

Table of Contents

I. SUMMARY AND OBJECTIVES OF STUDY	1
II. UPPER MIDDLE FORK WATERSHED	3
1. OVERVIEW OF THE PROJECT SITE	3
2. METHODOLOGY	4
3. GROUND OBSERVATION DATA COLLECTION	6
4. DEVELOPMENT OF A GEOGRAPHIC INFORMATION SYSTEM (GIS) DATABASE FOR THE UPPER MIDDLE FORK WATERSHED	8
A. <i>Digital Elevation Model (DEM) Data</i>	9
B. <i>Land Use/Land Cover and Vegetation Data</i>	9
C. <i>Soil Survey Data</i>	9
5. RECONSTRUCTION OF HISTORICAL HYDRO-CLIMATE DATA OVER THE UPPER MIDDLE FORK WATERSHED	10
A. <i>Using a Regional Climate Model to Reconstruct the Atmospheric Data over UMF</i>	11
B. <i>Validation of the Reconstructed Historical Climate</i>	13
6. GLOBAL CLIMATE MODELS AND THE RECONSTRUCTION OF THEIR HISTORICAL AND PROJECTION OF THEIR FUTURE CLIMATE SIMULATIONS	18
A. <i>Discussion on Global Climate Models</i>	19
B. <i>Validation of GCM-based Precipitation Estimates Simulated by MM5</i>	20
7. HYDROLOGIC MODELING OF THE UPPER MIDDLE FORK WATERSHED	23
A. <i>Implementation and Use of the WEHY Snow Module over Upper Middle Fork</i>	24
B. <i>Implementation and Use of the Hydrologic Module of the WEHY Model over Upper Middle Fork</i>	31
8. SIMULATING HISTORICAL CONDITIONS AND FUTURE PROJECTIONS OF WEHY USING ATMOSPHERIC INPUTS FROM GLOBAL CLIMATE MODELS	41
A. <i>Comparison of Future Projected Flows at the Upper Middle Fork Watershed</i>	49
B. <i>Trend Analysis of the Future Projected Flows at the Upper Middle Fork Watershed</i>	55
C. <i>Flood Frequency Analysis for Future Projected Flows over the Upper Middle Fork Watershed</i>	57
III. LAKE DAVIS BASIN	62
1. OVERVIEW OF THE PROJECT SITE	62
2. HYDROLOGIC MODELING OF THE LAKE DAVIS BASIN	63
A. <i>Implementation and Use of the WEHY Snow Module over the Lake Davis Basin</i>	63
B. <i>Implementation and Use of the Hydrologic Part of the WEHY Model over the Lake Davis Basin</i>	66
3. HISTORICAL ANALYSIS OF THE GRIZZLY VALLEY DAM	75
4. FUTURE ANALYSIS OF THE GRIZZLY VALLEY DAM	83
A. <i>Comparison of Future Projected Inflows into the Grizzly Valley Dam</i>	85
B. <i>Trend Analysis of the Future Projected Inflows into the Grizzly Valley Dam</i>	86
C. <i>Analysis of Reservoir Operations under Future Projected Inflows into the Grizzly Valley Dam</i>	88
IV. SIERRA VALLEY GROUNDWATER SYSTEM	113
1. OVERVIEW OF THE PROJECT SITE	113
2. METHODOLOGY	114
3. GROUND OBSERVATION DATA COLLECTION	115
4. GEOHYDROLOGIC MODELING OF THE SIERRA VALLEY GROUNDWATER SYSTEM	116
A. <i>Implementation and Use of the WEHY Snow Module over the Sierra Valley Basin</i>	116
B. <i>Implementation and Use of the Hydrologic Module of the WEHY Model over the Foothills Watersheds</i>	120
C. <i>Implementation and Use of the IWFM over the Sierra Valley Aquifer</i>	126
5. HISTORICAL ANALYSIS OF THE SIERRA VALLEY GROUNDWATER SYSTEM	150
6. FUTURE ANALYSIS OF THE SIERRA VALLEY GROUNDWATER SYSTEM	157
V. SUMMARY AND CONCLUSIONS	185

List of Figures

FIGURE 1. LOCATION OF UPPER FEATHER RIVER (UFR) AND UPPER MIDDLE FORK (UMF) WATERSHEDS WITHIN CALIFORNIA. THE ZOOMED-IN FIGURE REVEALS ELEVATIONS INSIDE THE UMF WATERSHED. [ELEVATION DATA SOURCE: DIGITAL ELEVATION MODEL (DEM) FROM THE NATIONAL ELEVATION DATASET (NED): [HTTP://NED.USGS.GOV/](http://ned.usgs.gov/)].3

FIGURE 2. VEGETATION AND LAND-COVER TYPES AT 100-M (328-FT) RESOLUTION OVER THE UPPER MIDDLE FORK WATERSHED.4

FIGURE 3. A SIMPLIFIED, GENERALIZED FLOW CHART OF THE STEPS USED FOR RUNNING THE WEHY-HCM OVER A WATERSHED. MCU: MODEL COMPUTATIONAL UNIT – THE COMPUTATIONAL UNIT USED BY THE WEHY MODEL TO UNDERGO THE SIMULATION; IT IS EQUIVALENT TO THE HILLSLOPE.5

FIGURE 4. LOCATIONS OF USEFUL FINE-INTERVAL, LONG-TERM PRECIPITATION, SNOW, AND FLOW STATIONS USED FOR THIS UMF PROJECT.7

FIGURE 5. SPATIAL SOIL MAP BASED ON SSURGO DATA FROM CALIFORNIA USDA-NRCS OVER THE UMF WATERSHED.9

FIGURE 6. SPATIAL EXTENT OF THE FOUR NESTED GRIDS FOR ATMOSPHERIC DATA RECONSTRUCTION BY MM5. D1: 81 x 81 KM (50.3 x 50.3 MI.), D2: 27 x 27 KM (16.8 x 16.8 MI.), D3: 9 x 9 KM (5.6 x 5.6 MI.), D4: 3 x 3 KM (1.86 x 1.86 MI.).13

FIGURE 7. LOCATIONS OF SELECTED MONTHLY, LONG-TERM GROUND PRECIPITATION STATIONS FOR USE IN COMPARISON AGAINST MM5-NCEP SIMULATED RESULTS.14

FIGURE 8. TIME-SERIES COMPARISONS OF MONTHLY PRECIPITATION BETWEEN GROUND OBSERVATIONS AND MM5-NCEP SIMULATED VALUES. NO BIAS CORRECTION WAS APPLIED.14

FIGURE 9 (CONTINUED). MEAN MONTHLY COMPARISONS OF SIMULATED PRECIPITATION FIELDS (BASED ON MM5 DOWNSCALING OF NCEP/NCAR REANALYSIS HISTORICAL DATA) AND PRISM DATA DURING THE PERIOD SPANNING FROM WATER YEAR 1951 TO WATER YEAR 1999 OVER THE UMF WATERSHED.....17

FIGURE 10. TIME-SERIES COMPARISONS OF THE UMF WATERSHED-AVERAGE MONTHLY PRECIPITATION BETWEEN MM5-SIMULATED AND PRISM VALUES. NO BIAS CORRECTION WAS APPLIED.17

FIGURE 11. TIME-SERIES COMPARISONS OF UMF AVERAGE MONTHLY PRECIPITATION BETWEEN GCM (CCSM3 AND ECHAM5)-BASED ESTIMATES AND PRISM VALUES. NOTE: ECHAM5 IS ABBREVIATED AS EH5 IN THE ABOVE FIGURE.....21

FIGURE 12. PRECIPITATION TRENDS BASED ON THE 10-YEAR BASIN AVERAGE ANNUAL PRECIPITATION FROM GCM (CCSM3 AND ECHAM5)-BASED ESTIMATES AND PRISM VALUES. NOTE: ECHAM5 IS ABBREVIATED AS EH5 IN THE ABOVE FIGURE.22

FIGURE 13. COMPARISON OF THE QUARTILE-QUARTILE PLOT BETWEEN CCSM3-BASED SIMULATED VALUES AND PRISM MONTHLY PRECIPITATION VALUES.23

FIGURE 14. COMPARISON OF THE QUARTILE-QUARTILE PLOT BETWEEN ECHAM5-BASED SIMULATED VALUES AND PRISM MONTHLY PRECIPITATION VALUES. NOTE: ECHAM5 IS ABBREVIATED AS EH5 IN THE ABOVE FIGURE.23

FIGURE 15. SKETCH OF THE SPATIALLY DISTRIBUTED SNOW MODEL. SOURCE: OHARA & KAVVAS (2006).25

FIGURE 16. ILLUSTRATION OF THE APPROXIMATION OF SNOW TEMPERATURE VERTICAL PROFILE. SOURCE: OHARA & KAVVAS (2006).25

FIGURE 17. TIME SERIES OF THE OBSERVED AND SIMULATED SNOW WATER EQUIVALENT (SWE) AT THE SELECTED FIELD OBSERVATION SITES FROM OCTOBER 2005 THROUGH SEPTEMBER 2006 (CALIBRATION PERIOD).....27

FIGURE 18. TIME SERIES OF THE OBSERVED AND SIMULATED SNOW WATER EQUIVALENT (SWE) AT THE SELECTED FIELD OBSERVATION SITES FROM OCTOBER 2000 THROUGH SEPTEMBER 2010 (VALIDATION PERIOD). WATER YEARS 2003 AND 2005 WERE NEGLECTED FROM THE ANALYSIS OF PLP DUE TO OBVIOUS ERRONEOUS DATA FOR THESE YEARS.29

FIGURE 19. MODEL-SIMULATED SNOW WATER EXTENT AND THEIR CORRESPONDING OBSERVED SNOW COVER PERCENT (MODIS) FOR THE MONTH OF APRIL FOR EACH OF 2008, 2009, AND 2010 (WITHIN THE VALIDATION PERIOD).30

FIGURE 20. SCHEMATIC DESCRIPTION OF THE WEHY MODEL. SOURCE: KAVVAS ET AL. (2004).....32

FIGURE 21. STRUCTURAL DESCRIPTION OF THE WEHY MODEL. SOURCE: KAVVAS ET AL. (2004).33

FIGURE 22. DIGITAL ELEVATION MODEL (DEM) FROM THE NATIONAL ELEVATION DATASET (NED) OVER THE UMF WATERSHED.....34

FIGURE 23. SURFACE SLOPE OVER THE UMF WATERSHED.34

FIGURE 24. MODIS MONTHLY LEAF AREA INDEX (LAI) OVER THE UPPER MIDDLE FORK WATERSHED.36

FIGURE 25. SAMPLE OF DISTRIBUTED LAND SURFACE PARAMETERS FROM DATABASE OVER THE UPPER MIDDLE FORK WATERSHED.36

FIGURE 26 (CONTINUED). SAMPLES OF DISTRIBUTED SOIL HYDRAULIC PARAMETERS FROM DATABASE OVER THE UPPER MIDDLE FORK WATERSHED.38

FIGURE 27. TIME SERIES OF THE OBSERVED AND MODEL-SIMULATED DAILY FLOW DISCHARGES AT THE MER STATION FROM OCTOBER 1996 THROUGH SEPTEMBER 1997.39

FIGURE 28. TIME SERIES OF THE OBSERVED AND MODEL-SIMULATED DAILY FLOW DISCHARGES AT THE MER STATION FROM OCTOBER 1979 THROUGH SEPTEMBER 2010 (VALIDATION PERIOD).40

FIGURE 29. ANNUAL BASIN AVERAGE PRECIPITATION PROJECTED OVER THE UMF WATERSHED AS PROJECTED BY THE 13 DIFFERENT GCM SCENARIOS. THE ENSEMBLE MEAN AND TRENDLINE ARE SHOWN BY THE BLACK BOLD AND RED DASHED LINES, RESPECTIVELY.	42
FIGURE 30. ANNUAL MEAN BASIN AVERAGE TEMPERATURE OVER THE UMF WATERSHED AS PROJECTED BY THE 13 DIFFERENT GCM SCENARIOS. THE ENSEMBLE MEAN AND TRENDLINE ARE SHOWN BY THE BLACK BOLD AND RED DASHED LINES, RESPECTIVELY.	42
FIGURE 31. SPATIAL MAPS SHOWING THE ENSEMBLE AVERAGE SNOW DEPTH OF ALL PROJECTIONS FOR THE MONTH OF JANUARY, AVERAGED OVER 10-YR PERIODS THROUGHOUT THE FUTURE 21 ST CENTURY (CONTINUED BELOW).....	44
FIGURE 32. SPATIAL MAPS SHOWING THE ENSEMBLE AVERAGE SNOW DEPTH OF ALL PROJECTIONS FOR THE MONTH OF MARCH, AVERAGED OVER 10-YR PERIODS THROUGHOUT THE FUTURE 21 ST CENTURY (CONTINUED BELOW).....	46
FIGURE 33. SPATIAL MAPS SHOWING THE ENSEMBLE AVERAGE SNOW DEPTH OF ALL PROJECTIONS FOR THE MONTH OF MAY, AVERAGED OVER 10-YR PERIODS THROUGHOUT THE FUTURE 21 ST CENTURY (CONTINUED BELOW).....	48
FIGURE 34. HOURLY FLOW PROJECTIONS AT THE UMF OUTLET FOR YEARS 2010 TO 2100, USING THE 13 DIFFERENT CLIMATE PROJECTIONS FROM THE TWO GCMs (CCSM3 AND ECHAM5). NOTE: ECHAM5 IS ABBREVIATED AS EH5 IN THE ABOVE FIGURE.	50
FIGURE 35. ENSEMBLE AVERAGE HOURLY FLOW PROJECTIONS AT THE UMF OUTLET FOR THE PERIOD 2010 TO 2100 FOR EACH OF THE CLIMATE PROJECTIONS OF (A) CCSM3 AND (B) ECHAM5. NOTE: ECHAM5 IS ABBREVIATED AS EH5 IN THE ABOVE FIGURE.	52
FIGURE 36. ENSEMBLE AVERAGE HOURLY FLOW PROJECTIONS AT THE UMF OUTLET FOR THE YEARS 2010 TO 2100 FOR ALL 13 PROJECTIONS (I.E., RESULTS FROM BOTH CCSM3 AND ECHAM5).	52
FIGURE 37. DAILY MEAN FLOW PROJECTIONS AT THE UMF OUTLET FOR THE YEARS 2010 TO 2100, USING THE 13 DIFFERENT CLIMATE PROJECTIONS FROM THE TWO GCMs (CCSM3 AND ECHAM5). NOTE: ECHAM5 IS ABBREVIATED AS EH5 IN THE ABOVE FIGURE.	53
FIGURE 38. ENSEMBLE AVERAGE DAILY MEAN FLOW PROJECTIONS AT THE UMF OUTLET FOR THE YEARS 2010 TO 2100 FOR EACH OF THE CLIMATE PROJECTIONS OF (A) CCSM3 AND (B) ECHAM5. NOTE: ECHAM5 IS ABBREVIATED AS EH5 IN THE ABOVE FIGURE.	53
FIGURE 39. ENSEMBLE AVERAGE DAILY MEAN FLOW PROJECTIONS AT THE UMF OUTLET FOR THE YEARS 2010 TO 2100 FOR ALL 13 PROJECTIONS (I.E., FROM BOTH CCSM3 AND ECHAM5).	54
FIGURE 40. HOURLY FLOW PROJECTIONS AT THE UMF OUTLET FOR THE YEARS 2000 TO 2010 FOR ALL 13 PROJECTIONS (I.E., FROM BOTH CCSM3 AND ECHAM5), COMPARED TO CORRESPONDING OBSERVED FLOWS.	55
FIGURE 41. ENSEMBLE AVERAGE HOURLY FLOW PROJECTIONS AT THE UMF OUTLET FOR THE YEARS 2000 TO 2010 FROM ALL 13 PROJECTIONS (I.E., FROM BOTH CCSM3 AND ECHAM5), COMPARED TO CORRESPONDING OBSERVED FLOWS.	55
FIGURE 42. ANNUAL AVERAGE FLOWRATES FROM THE OUTLET OF THE UMF WATERSHED. FLOWRATES ARE PROVIDED FOR EACH OF THE 13 FUTURE PROJECTIONS, AS WELL AS FOR THE ENSEMBLE AVERAGE OF ALL PROJECTIONS. A LINEAR TRENDLINE IS ALSO PLOTTED TO SHOW THE GENERAL TREND OF THE ENSEMBLE AVERAGE.	57
FIGURE 43. (A) FREQUENCY HISTOGRAM OF ANNUAL FLOOD PEAKS, AND (B) INTEGRATED HISTOGRAM OF ANNUAL FLOOD PEAKS OVER THE UMF WATERSHED USING DATA FROM ALL 13 PROJECTIONS (2010-2100).	58
FIGURE 44. FREQUENCY CURVE OF ANNUAL FLOODS FOR THE UMF WATERSHED (2010-2100).	59
FIGURE 45. LOCATION OF LAKE DAVIS BASIN AS A PORTION OF THE UPPER MIDDLE FORK WATERSHED (UPPER FIGURE); LOCATION OF LAKE DAVIS AND GRIZZLY VALLEY DAM WITHIN THE LAKE DAVIS BASIN (LOWER FIGURE).....	62
FIGURE 46. LOCATION OF THE SELECTED SNOW FIELD OBSERVATION STATION (GRZ) WITHIN THE LAKE DAVIS BASIN.	64
FIGURE 47. TIME SERIES OF THE OBSERVED AND MODEL-SIMULATED SNOW WATER EQUIVALENT (SWE) AT THE SELECTED FIELD OBSERVATION SITE FROM OCTOBER 2005 THROUGH SEPTEMBER 2006 (CALIBRATION PERIOD).	64
FIGURE 48. TIME SERIES OF THE OBSERVED AND MODEL-SIMULATED SNOW WATER EQUIVALENT (SWE) AT THE SELECTED FIELD OBSERVATION SITE FROM OCTOBER 2000 THROUGH SEPTEMBER 2010 (VALIDATION PERIOD).	65
FIGURE 49. VEGETATION AND LAND-COVER TYPES OVER THE LAKE DAVIS WATERSHED.	67
FIGURE 50. SPATIAL SOIL MAP BASED ON SSURGO DATA FROM CALIFORNIA USDA-NRCS OVER THE LAKE DAVIS WATERSHED.	67
FIGURE 51. DIGITAL ELEVATION MODEL (DEM) FROM THE NATIONAL ELEVATION DATASET (NED) OVER THE LAKE DAVIS WATERSHED.	68
FIGURE 52. SURFACE SLOPE OVER THE LAKE DAVIS WATERSHED.	68
FIGURE 53. MODIS AVERAGE MONTHLY LEAF AREA INDEX (LAI) OVER THE LAKE DAVIS WATERSHED.	69
FIGURE 54. SAMPLES OF DISTRIBUTED LAND SURFACE PARAMETERS FROM DATABASE OVER THE LAKE DAVIS WATERSHED.	70
FIGURE 55 (CONTINUED). SAMPLES OF DISTRIBUTED SOIL HYDRAULIC PARAMETERS FROM THE DATABASE OVER THE LAKE DAVIS WATERSHED.	71
FIGURE 56. LOCATION OF THE SELECTED FLOW FIELD OBSERVATION STATION (DAV) IN THE LAKE DAVIS WATERSHED (DELINEATED BY THE BLACK BOUNDARY).	72
FIGURE 57. TIME SERIES OF THE OBSERVED AND MODEL-SIMULATED MONTHLY FLOW DISCHARGES AT THE DAV STATION FROM OCTOBER 1985 THROUGH SEPTEMBER 1986.	73

FIGURE 58. TIME SERIES OF THE OBSERVED AND MODEL-SIMULATED MONTHLY FLOW DISCHARGES AT THE DAV STATION FROM OCTOBER 1985 THROUGH SEPTEMBER 1995 (VALIDATION PERIOD).	74
FIGURE 59. SAMPLE PLOT OF INFLOW AND DEMAND TIME SERIES FOR A DAM. [SOURCE: KLEMES (1979)].	76
FIGURE 60. SAMPLE PLOT OF INFLOW AND DEMAND MASS CURVES. [SOURCE: KLEMES (1979)].	76
FIGURE 61. MINIMUM FLOW RELEASE SCHEDULE FOR LAKE DAVIS. [SOURCE: DWR BULLETIN No. 117-3 OF JULY 1965].	77
FIGURE 62. HISTORICAL ANNUAL INFLOWS TO GRIZZLY VALLEY DAM. BLACK OVALS: WET YEARS; RED OVALS: DRY YEARS.	78
FIGURE 63. RULE CURVES DERIVED FROM HISTORICAL RECORDS FOR GRIZZLY VALLEY DAM: WET YEARS, DRY YEARS, AND ALL THE YEARS OF THE HISTORICAL PERIOD. A USER-DEFINED CUSTOM RULE CURVE IS ALSO PLOTTED.	78
FIGURE 64. TIME SERIES OF SIMULATED AND OBSERVED RESERVOIR STORAGES FOR GRIZZLY VALLEY DAM OVER THE HISTORICAL PERIOD. THE SIMULATIONS WERE RUN USING: (A) THE DERIVED "WET" RULE CURVE, (B) THE DERIVED "DRY" RULE CURVE, (C) THE DERIVED "AVERAGE" RULE CURVE; AND (D) THE CUSTOM RULE CURVE. EOM: END OF MONTH.....	79
FIGURE 65. TIME SERIES SIMULATED AND OBSERVED RESERVOIR STORAGES FOR GRIZZLY VALLEY DAM OVER THE HISTORICAL PERIOD. THE SIMULATIONS WERE RUN WITH NO RULE CURVE. VERTICAL ARROWS EMPHASIZE THE DIFFERENCES BETWEEN HISTORICAL AND SIMULATED VALUES.	80
FIGURE 66. TIME SERIES OF SIMULATED AND OBSERVED RESERVOIR STORAGES FOR GRIZZLY VALLEY DAM OVER THE HISTORICAL PERIOD. THE SIMULATIONS WERE RUN USING THE THRESHOLD METHOD, USING A THRESHOLD VALUE OF 56,000 AF.	81
FIGURE 67. TIME SERIES OF HISTORICAL AND SIMULATED OUTFLOWS FROM THE GRIZZLY VALLEY DAM, USING RESULTS FROM THE SIMULATION USING THE THRESHOLD METHOD, AND HAVING A 56,000 AF THRESHOLD VALUE.	81
FIGURE 68. PLOT OF THE SIMULATED END-OF-MONTH STORAGE VALUES FOR GRIZZLY VALLEY DAM, ALONG WITH THE AMOUNTS AND TIMINGS OF THE SHORTAGES AND SURPLUSES OCCURRING OVER THE HISTORICAL PERIOD.	82
FIGURE 69. PLOT OF THE SIMULATED END-OF-MONTH STORAGE VALUES FOR GRIZZLY VALLEY DAM, ALONG WITH THE AMOUNTS AND TIMINGS OF THE SHORTAGES AND SURPLUSES OCCURRING OVER THE HISTORICAL PERIOD. SIMULATION WAS DONE USING THE THRESHOLD METHOD USING A THRESHOLD VALUE OF 36,000 AF.	83
FIGURE 70. ANNUAL BASIN AVERAGE PRECIPITATION PROJECTED OVER THE LAKE DAVIS BASIN AS PROJECTED BY THE 13 DIFFERENT GCM SCENARIOS. THE ENSEMBLE MEAN AND TRENDLINE ARE SHOWN BY THE BLACK BOLD AND RED DASHED LINES, RESPECTIVELY.	84
FIGURE 71. ANNUAL MEAN BASIN AVERAGE TEMPERATURE OVER THE LAKE DAVIS BASIN AS PROJECTED BY THE 13 DIFFERENT GCM SCENARIOS. THE ENSEMBLE MEAN AND TRENDLINE ARE SHOWN BY THE BLACK BOLD AND RED DASHED LINES, RESPECTIVELY.	85
FIGURE 72. PLOT OF THE SIMULATED END-OF-MONTH STORAGE VALUES FOR GRIZZLY VALLEY DAM, ALONG WITH THE AMOUNTS AND TIMINGS OF THE SHORTAGES AND SURPLUSES OCCURRING OVER THE FUTURE PERIOD BY USING PROJECTIONS FROM THE EH5 GCM. THRESHOLD VALUE USED: 56,000 AF (CONTINUED BELOW).....	89
FIGURE 73. PLOT OF THE SIMULATED END-OF-MONTH STORAGE VALUES FOR GRIZZLY VALLEY DAM, ALONG WITH THE AMOUNTS AND TIMINGS OF THE SHORTAGES AND SURPLUSES OCCURRING OVER THE FUTURE PERIOD BY USING PROJECTIONS FROM THE CCSM3 GCM. THRESHOLD VALUE USED: 56,000 AF (CONTINUED BELOW).....	92
FIGURE 74. SUMMARY OF GRIZZLY VALLEY DAM RESERVOIR SIMULATION RESULTS FOR THE 13 FUTURE PROJECTIONS, SHOWING SHORTAGES, SURPLUSES, AND MINIMUM RESERVOIR STORAGE VALUES OVER THE PERIOD FROM 2010 TO 2100. SIMULATION WAS RUN USING THRESHOLD METHOD, WITH A THRESHOLD VALUE OF 56,000 AF.....	94
FIGURE 75. PLOT OF THE SIMULATED END-OF-MONTH STORAGE VALUES FOR GRIZZLY VALLEY DAM, ALONG WITH THE AMOUNTS AND TIMINGS OF THE SHORTAGES AND SURPLUSES OCCURRING OVER THE FUTURE PERIOD BY USING PROJECTIONS FROM THE EH5 GCM. THRESHOLD VALUE USED: 62,000 AF (CONTINUED BELOW).....	97
FIGURE 76. PLOT OF THE SIMULATED END-OF-MONTH STORAGE VALUES FOR GRIZZLY VALLEY DAM, ALONG WITH THE AMOUNTS AND TIMINGS OF THE SHORTAGES AND SURPLUSES OCCURRING OVER THE FUTURE PERIOD BY USING PROJECTIONS FROM THE CCSM3 GCM. THRESHOLD VALUE USED: 62,000 AF (CONTINUED BELOW).....	100
FIGURE 77. SUMMARY OF GRIZZLY VALLEY DAM RESERVOIR SIMULATION RESULTS FOR THE 13 FUTURE PROJECTIONS, SHOWING SHORTAGES, SURPLUSES, AND MINIMUM RESERVOIR STORAGE VALUES OVER THE PERIOD FROM 2010 TO 2100. SIMULATION WAS RUN USING THRESHOLD METHOD, WITH A THRESHOLD VALUE OF 62,000 AF.	102
FIGURE 78. COMPARISON OF PLOTS OF THE SIMULATED END-OF-MONTH STORAGE VALUES FOR GRIZZLY VALLEY DAM (WITH SHORTAGES AND SURPLUSES) OVER THE FUTURE PERIOD (2010-2100) FOR THE EH5-B1-3 SCENARIO. SIMULATION WAS DONE USING THE THRESHOLD METHOD BY USING A THRESHOLD VALUE OF (A) 56,000 AF, AND (B) 62,000 AF.	104
FIGURE 79. PLOT OF THE SIMULATED END-OF-MONTH STORAGE VALUES FOR GRIZZLY VALLEY DAM, ALONG WITH THE AMOUNTS AND TIMINGS OF THE SHORTAGES AND SURPLUSES OCCURRING OVER THE FUTURE PERIOD BY USING PROJECTIONS FROM THE EH5 GCM. RESULTS PROVIDED FOR AN ASSUMED 10% INCREASE IN STORAGE CAPACITY. THRESHOLD VALUE USED: 56,000 AF (CONTINUED BELOW).....	105

FIGURE 80. PLOT OF THE SIMULATED END-OF-MONTH STORAGE VALUES FOR GRIZZLY VALLEY DAM, ALONG WITH THE AMOUNTS AND TIMINGS OF THE SHORTAGES AND SURPLUSES OCCURRING OVER THE FUTURE PERIOD BY USING PROJECTIONS FROM THE CCSM3 GCM. RESULTS PROVIDED FOR AN ASSUMED 10% INCREASE IN STORAGE CAPACITY. THRESHOLD VALUE USED: 56,000 AF (CONTINUED BELOW)	108
FIGURE 81. SUMMARY OF GRIZZLY VALLEY DAM RESERVOIR SIMULATION RESULTS FOR THE 13 FUTURE PROJECTIONS, SHOWING SHORTAGES, SURPLUSES, AND MINIMUM RESERVOIR STORAGE VALUES OVER THE PERIOD FROM 2010 TO 2100. SIMULATION WAS RUN USING THRESHOLD METHOD, WITH A THRESHOLD VALUE OF 56,000 AF AND A 10% ASSUMED INCREASE IN RESERVOIR CAPACITY.	110
FIGURE 82. LOCATION OF SIERRA VALLEY BASIN AS A SUBREGION OF THE UPPER MIDDLE FORK WATERSHED (UPPER FIGURE); DIGITAL ELEVATION MODEL (DEM) OF THE SIERRA VALLEY BASIN AND SIERRA VALLEY AQUIFER (LOWER FIGURE).....	113
FIGURE 83. GROUNDWATER LEVEL OBSERVATION LOCATIONS OVER THE SIERRA VALLEY OBTAINED FROM CASGEM DATABASE.	115
FIGURE 84. LOCATION OF SELECTED SNOW FIELD OBSERVATION STATION.	116
FIGURE 85. TIME SERIES OF THE OBSERVED AND MODEL-SIMULATED SNOW WATER EQUIVALENT (SWE) AT THE SELECTED FIELD OBSERVATION SITE FROM OCTOBER 2005 THROUGH SEPTEMBER 2006 (CALIBRATION PERIOD).	117
FIGURE 86. TIME SERIES OF THE OBSERVED AND MODEL-SIMULATED SNOW WATER EQUIVALENT (SWE) AT THE SELECTED FIELD OBSERVATION SITES FROM OCTOBER 2000 THROUGH SEPTEMBER 2010 (VALIDATION PERIOD).	118
FIGURE 87. MODEL-SIMULATED SNOW WATER EXTENT AND THE OBSERVED SNOW COVER PERCENT (MODIS) FOR THE MONTH OF APRIL FOR EACH OF 2008, 2009, AND 2010 OVER THE SIERRA VALLEY WATERSHED (WITHIN THE VALIDATION PERIOD).....	119
FIGURE 88. DIGITAL ELEVATION MODEL (DEM) FROM NATIONAL ELEVATION DATASET (NED) OVER THE SIERRA VALLEY BASIN.....	120
FIGURE 89. SURFACE SLOPE OVER THE SIERRA VALLEY BASIN.	121
FIGURE 90. LAND COVER TYPES FROM CALIFORNIA SPATIAL INFORMATION LIBRARY (CALSIL) AT 100-M RESOLUTION OVER THE SIERRA VALLEY BASIN.	121
FIGURE 91. SPATIAL SOIL MAP BASED ON SSURGO DATA FROM CALIFORNIA NRCS OVER THE SIERRA VALLEY BASIN.	122
FIGURE 92. DISCRETIZATION OF THE SV BASIN INTO 77 STREAM REACHES AND 154 MODEL COMPUTATIONAL UNITS, AND LOCATION OF THE CDEC MFP STREAM GAUGE.	123
FIGURE 93. MODIS MONTHLY LEAF AREA INDEX (LAI) OVER THE SIERRA VALLEY WATERSHED.	124
FIGURE 94. SAMPLE OF DISTRIBUTED LAND SURFACE PARAMETERS FROM DATABASE OVER THE SIERRA VALLEY WATERSHED.	124
FIGURE 95. SAMPLES OF DISTRIBUTED SOIL HYDRAULIC PARAMETERS FROM DATABASE OVER THE SIERRA VALLEY WATERSHED (CONTINUED BELOW).....	125
FIGURE 96. SCHEMATIC ILLUSTRATION OF THE PROCESSES MODELED IN IWFM (DOGRUL, 2014).....	127
FIGURE 97. MAJOR AND MINOR STREAM REACHES FLOWING INTO THE SIERRA VALLEY.	129
FIGURE 98. RESULTS OF THE STEREOGRAPHIC AERIAL PHOTO SURVEY. SOLID RED LINES REPRESENT THE STRIKE-SLIP MOTION FAULTS WHILE DASHED RED LINES REPRESENT NORMAL FAULT MOVEMENTS. YELLOW LINE IS THE BOUNDARY ESTIMATE FOR THE SV GROUNDWATER SYSTEM IMPLIED BY THE FAULTS.	131
FIGURE 99. THE TABLES AND RELATIONSHIPS OF THE MICROSOFT ACCESS DATABASE CREATED TO STORE THE WELL DRILLING LOGS.	132
FIGURE 100. WELL DRILLING LOGS STORED IN THE WELL LOG DATABASE. THE NUMBER INSIDE EACH MTRS GRID SHOWS THE NUMBER OF WELL LOGS AT THE CORRESPONDING 1 SQ-MI AREA. CROSS SECTION WELLS AND CROSS SECTIONS WERE TAKEN FROM THE PREVIOUS HYDROGEOLOGIC STUDIES OF THE VALLEY (KENNETH D. SCHMIDT, 2003, 2005 AND 2012).	133
FIGURE 101. UPDATED BEDROCK SHAPE FOR THE SIERRA VALLEY AQUIFER: TOP VIEW AND OBLIQUE VIEW. THE RED POINTS SHOW THE REFERENCE POINTS FOR DEPTH TO BEDROCK INFORMATION GATHERED FROM WELL LOGS. THE GREEN LINES SHOW STRIKE-SLIP AND NORMAL MOTION FAULTS.	134
FIGURE 102. AQUIFER DELINEATION OF THE SIERRA VALLEY AQUIFER. THE FORMATIONS ARE DIVIDED INTO THREE: SEDIMENTS (SED), SEDIMENTARY ROCKS (SRO) AND IGNEOUS ROCKS (IGN). EACH OF THESE IS THEN CATEGORIZED INTO FIVE GROUPS WITH RESPECT TO THE TYPICAL HYDRAULIC CONDUCTIVITY VALUES FOUND IN THE LITERATURE (1: HIGHEST HYDRAULIC CONDUCTIVITY, TO 5: LOWEST HYDRAULIC CONDUCTIVITY).	135
FIGURE 103. FINITE ELEMENT MESH GENERATED BY THE IWFM MESH GENERATOR.	136
FIGURE 104. BOUNDARY CONDITIONS ASSIGNED TO THE MODEL DOMAIN.	137
FIGURE 105. MAP SHOWING THE DECREED DIVERSIONS AND THE SCHEDULING AREAS IN SIERRA VALLEY.	138
FIGURE 106. PUMPING LOCATIONS OF MAJOR GROUNDWATER USERS IN SIERRA VALLEY AS REPORTED IN THE PREVIOUS HYDROGEOLOGIC STUDY REPORTS (KENNETH D. SCHMIDT, 2003, 2005 AND 2012).	139
FIGURE 107. POTENTIAL EVAPOTRANSPIRATION AND LIQUID WATER FOR THE WATER YEARS 2001-2010.	140
FIGURE 108. SOIL DATA FROM SSURGO DATABASE ON THE MODEL MESH: REPRESENTATIVE SATURATED HYDRAULIC CONDUCTIVITY (LEFT) AND PORE SIZE DISTRIBUTION INDEX (RIGHT).....	141

FIGURE 109. CROP DATA FROM CROPSCAPE DATABASE ON THE MODEL MESH.....	142
FIGURE 110. PARAMETRIC GRID USED TO DEFINE THE AQUIFER HYDRAULIC PROPERTIES.	145
FIGURE 111. MFP STREAM GAUGE STATION AND THE GROUNDWATER LEVEL OBSERVATION POINTS FROM THE CASGEM DATABASE. ...	146
FIGURE 112. THE CALIBRATION (TOP) AND VALIDATION (BOTTOM) RESULTS FOR THE MONTHLY STREAM FLOWRATES AT THE MFP STATION.	147
FIGURE 113. GROUNDWATER LEVEL RESULTS FOR THE CALIBRATION AND VALIDATION PERIODS FOR VARIOUS GROUNDWATER OBSERVATION WELLS.....	148
FIGURE 114. OBSERVED VERSUS SIMULATED PIEZOMETRIC SURFACES FOR OCTOBER 2010.	149
FIGURE 115. HISTORICAL MEAN MONTHLY RESULTS FOR SIERRA VALLEY FOR THE WATER YEARS 2000-2010: ROOTZONE COMPONENTS AS PERCENTAGES OF THE TOTAL INPUT (LEFT AXIS) AND VOLUMES IN AC-FT. (RIGHT AXIS).	152
FIGURE 116. HISTORICAL MEAN MONTHLY RESULTS FOR SIERRA VALLEY FOR THE WATER YEARS 2000-2010: LQW, IRRIGATION, INFILTRATION AND DEEP PERCOLATION.	153
FIGURE 117. HISTORICAL MEAN MONTHLY RESULTS FOR SIERRA VALLEY FOR THE WATER YEARS 2000-2010: POTENTIAL AND ACTUAL EVAPOTRANSPIRATIONS.	153
FIGURE 118. HISTORICAL MEAN MONTHLY RESULTS FOR SIERRA VALLEY FOR THE WATER YEARS 2000-2010: POTENTIAL AND ACTUAL EVAPOTRANSPIRATION AMOUNTS FOR IRRIGATED CROPS.	154
FIGURE 119. HISTORICAL MEAN MONTHLY RESULTS FOR SIERRA VALLEY FOR THE WATER YEARS 2000-2010: ROOT ZONE WATER BUDGET FOR THE AGRICULTURAL LANDS.	154
FIGURE 120. HISTORICAL MEAN MONTHLY RESULTS FOR SIERRA VALLEY FOR THE WATER YEARS 2000-2010: SOIL MOISTURE STORAGE.	155
FIGURE 121. HISTORICAL MEAN MONTHLY RESULTS FOR SIERRA VALLEY FOR THE WATER YEARS 2000-2010: GROUNDWATER STORAGE.	156
FIGURE 122. HISTORICAL MEAN MONTHLY RESULTS FOR SIERRA VALLEY FOR THE WATER YEARS 2000-2010: GROUNDWATER BUDGET COMPONENTS.....	156
FIGURE 123. SIMULATION RESULTS OF THE ANNUAL LIQUID WATER FOR THE 13 PROJECTED CLIMATE SCENARIOS.	158
FIGURE 124. SIMULATION RESULTS OF THE ANNUAL INFILTRATION FOR THE 13 PROJECTED CLIMATE SCENARIOS.	160
FIGURE 125. SIMULATION RESULTS OF THE ANNUAL DIRECT RUNOFF FOR THE 13 PROJECTED CLIMATE SCENARIOS.	162
FIGURE 126. SIMULATION RESULTS OF THE ANNUAL DEEP PERCOLATION FOR THE 13 PROJECTED CLIMATE SCENARIOS.	164
FIGURE 127. SIMULATION RESULTS OF THE ANNUAL POTENTIAL EVAPOTRANSPIRATION FOR THE 13 PROJECTED CLIMATE SCENARIOS.	166
FIGURE 128. SIMULATION RESULTS OF THE ANNUAL ACTUAL EVAPOTRANSPIRATION FOR THE 13 PROJECTED CLIMATE SCENARIOS.	168
FIGURE 129. SIMULATION RESULTS OF THE ANNUAL ACTUAL EVAPOTRANSPIRATION OF THE AGRICULTURAL CROPS FOR THE 13 PROJECTED CLIMATE SCENARIOS.....	170
FIGURE 130. SIMULATION RESULTS OF THE ANNUAL ACTUAL EVAPOTRANSPIRATION OF THE NATIVE AND RIPARIAN VEGETATION FOR THE 13 PROJECTED CLIMATE SCENARIOS.	170
FIGURE 131. SIMULATION RESULTS OF THE ANNUAL APPLIED PRIME WATER FOR THE 13 PROJECTED CLIMATE SCENARIOS.	173
FIGURE 132. SIMULATION RESULTS OF THE ANNUAL GROUNDWATER PUMPING FOR THE 13 PROJECTED CLIMATE SCENARIOS.	175
FIGURE 133. SIMULATION RESULTS OF THE ANNUAL NET GAIN FROM STREAMS FOR THE 13 PROJECTED CLIMATE SCENARIOS. NEGATIVE VALUES INDICATE THAT THE GROUNDWATER IS RECHARGING THE STREAMS.	177
FIGURE 134. SIMULATION RESULTS OF THE GROUNDWATER LEVELS AT NINE DIFFERENT LOCATIONS (CONTINUED BELOW).....	181
FIGURE 135. SIMULATED ENSEMBLE MEAN PIEZOMETRIC SURFACES FOR THE END OF EACH DECADE BETWEEN 2010 AND 2100.	184

List of Tables

TABLE 1. LOCATION INFORMATION AND DATA SOURCES OF THE USEFUL GROUND OBSERVATION STATIONS USED FOR THIS UMF PROJECT. .8

TABLE 2. STATISTICAL TEST VALUES OF THE BASIN AVERAGE MM5-SIMULATED PRECIPITATION (BASED ON NCEP/NCAR REANALYSIS DATA) AND PRISM PRECIPITATION DURING THE OCTOBER 1950 – SEPTEMBER 1999 PERIOD.18

TABLE 3. HISTORICAL AND FUTURE PERIODS OF CLIMATE SIMULATIONS FOR EACH OF THE TWO GCMs SELECTED FOR THIS STUDY (CCSM3 AND ECHAM5).19

TABLE 4. STATISTICAL TEST VALUES OF THE SIMULATED AND OBSERVED SNOW WATER EQUIVALENT FROM THE SELECTED OBSERVATION STATIONS (GRZ, FOR, BKL, AND PLP) DURING THE CALIBRATION PERIOD (OCTOBER 2005 THROUGH SEPTEMBER 2006). OBS: OBSERVED; SIM: SIMULATED; STDEV: STANDARD DEVIATION; RMSE: ROOT-MEAN-SQUARE ERROR; NASH: NASH-SUTCLIFFE EFFICIENCY.26

TABLE 5. STATISTICAL TEST VALUES OF THE SIMULATED AND OBSERVED SNOW WATER EQUIVALENT FROM THE SELECTED OBSERVATION STATIONS (GRZ, FOR, BKL, AND PLP) DURING THE VALIDATION PERIOD (OCTOBER 2000 THROUGH SEPTEMBER 2010). OBS: OBSERVED; SIM: SIMULATED; STDEV: STANDARD DEVIATION; RMSE: ROOT-MEAN-SQUARE ERROR; NASH: NASH-SUTCLIFFE EFFICIENCY.28

TABLE 6. STATISTICAL TEST VALUES OF SIMULATED AND OBSERVED DAILY FLOW VALUES AT THE MER STATION DURING THE CALIBRATION PERIOD (OCTOBER 1996 THROUGH SEPTEMBER 1997). OBS: OBSERVED; SIM: SIMULATED; STDEV: STANDARD DEVIATION; RMSE: ROOT-MEAN-SQUARE ERROR; NASH: NASH-SUTCLIFFE EFFICIENCY.39

TABLE 7. STATISTICAL TEST VALUES OF SIMULATED AND OBSERVED DAILY FLOW DISCHARGE VALUES AT THE MER STATION DURING THE VALIDATION PERIOD (OCTOBER 1979 THROUGH SEPTEMBER 2010). OBS: OBSERVED; SIM: SIMULATED; STDEV: STANDARD DEVIATION; RMSE: ROOT-MEAN-SQUARE ERROR; NASH: NASH-SUTCLIFFE EFFICIENCY.40

TABLE 8. AVERAGE FUTURE PROJECTED FLOWS AT THE UMF OUTLET OVER THE PERIOD SPANNING THE YEARS FROM 2010 TO 2100.51

TABLE 9. SLOPE (CMS/YR) OF THE TREND LINE OF ANNUAL MEAN OUTFLOW FROM UPPER MIDDLE FORK FOR THE 13 DIFFERENT FUTURE PROJECTIONS, AS WELL AS FOR THE ENSEMBLE OF CCSM3, EH5, AND ALL PROJECTIONS. SIGNIFICANCE OF THE TREND WAS DETERMINED USING THE MANN-KENDALL STATISTICAL TEST. *P* VALUES ARE GIVEN IN PARENTHESES; *P* VALUES THAT SHOW A SIGNIFICANT CHANGE ($P < 0.05$) ARE SHOWN IN BOLD.56

TABLE 10. MAGNITUDES OF FLOODS FOR DIFFERENT RETURN PERIODS OVER THE UMF WATERSHED DURING YEARS 2010-2100.60

TABLE 11. STATISTICAL TEST VALUES OF SIMULATED AND OBSERVED SNOW WATER EQUIVALENT FROM THE SELECTED OBSERVATION STATION (GRZ) DURING THE CALIBRATION PERIOD (OCTOBER 2005 THROUGH SEPTEMBER 2006). STDEV: STANDARD DEVIATION; RMSE: ROOT-MEAN-SQUARE ERROR; NASH: NASH-SUTCLIFFE EFFICIENCY.65

TABLE 12. STATISTICAL TEST VALUES OF SIMULATED AND OBSERVED SNOW WATER EQUIVALENT FROM THE SELECTED OBSERVATION STATION (GRZ) DURING THE VALIDATION PERIOD (OCTOBER 2000 THROUGH SEPTEMBER 2010). STDEV: STANDARD DEVIATION; RMSE: ROOT-MEAN-SQUARE ERROR; NASH: NASH-SUTCLIFFE EFFICIENCY.66

TABLE 13. STATISTICAL TEST VALUES OF SIMULATED AND OBSERVED MONTHLY FLOW VALUES AT THE DAV STATION DURING THE CALIBRATION PERIOD (OCTOBER 1985 THROUGH SEPTEMBER 1986). STDEV: STANDARD DEVIATION; RMSE: ROOT-MEAN-SQUARE ERROR; NASH: NASH-SUTCLIFFE EFFICIENCY.73

TABLE 14. STATISTICAL TEST VALUES OF SIMULATED AND OBSERVED MONTHLY FLOW DISCHARGE VALUES AT THE DAV STATION DURING THE VALIDATION PERIOD (OCTOBER 1985 THROUGH SEPTEMBER 1995). STDEV: STANDARD DEVIATION; RMSE: ROOT-MEAN-SQUARE ERROR; NASH: NASH-SUTCLIFFE EFFICIENCY.74

TABLE 15. AVERAGE FUTURE PROJECTED INFLOWS INTO THE GRIZZLY VALLEY DAM OVER THE PERIOD SPANNING THE YEARS FROM 2010 TO 2100.86

TABLE 16. SLOPE (CMS/YR) OF THE TREND LINE OF ANNUAL MEAN DAM INFLOW FOR GRIZZLY VALLEY DAM FOR THE 13 DIFFERENT FUTURE PROJECTIONS, AS WELL AS FOR THE ENSEMBLE OF CCSM3, EH5, AND ALL PROJECTIONS. SIGNIFICANCE OF THE TREND WAS DETERMINED USING THE MANN-KENDALL STATISTICAL TEST. *P* VALUES ARE GIVEN IN PARENTHESES; *P* VALUES THAT SHOW A SIGNIFICANT CHANGE ($P < 0.05$) ARE SHOWN IN BOLD.87

TABLE 17. STATISTICAL TEST VALUES OF SIMULATED AND OBSERVED SNOW WATER EQUIVALENT FROM THE SELECTED OBSERVATION STATION (GRZ) DURING THE CALIBRATION PERIOD (OCTOBER 2005 TO SEPTEMBER 2006).117

TABLE 18. STATISTICAL TEST VALUES OF SIMULATED AND OBSERVED SNOW WATER EQUIVALENT FROM THE SELECTED OBSERVATION STATION (GRZ) DURING THE VALIDATION PERIOD (OCTOBER 2000 TO SEPTEMBER 2010).118

TABLE 19. STATISTICAL TEST VALUES OF SIMULATED AND OBSERVED MONTHLY STREAM FLOWRATES AT THE MFP STATION DURING THE CALIBRATION AND VALIDATION PERIODS. OBS: OBSERVED; SIM: SIMULATED; STDEV: STANDARD DEVIATION; RMSE: ROOT-MEAN-SQUARE ERROR; NASH: NASH-SUTCLIFFE EFFICIENCY.147

TABLE 20. WATER BUDGET COMPONENTS FOR THE SIERRA VALLEY AS ESTIMATED BY THE IWFM AND WEHY MODELS.	150
TABLE 21. RESULTS OF THE TREND ANALYSIS FOR LIQUID WATER. SLOPE (ACFT/YR) OF THE TREND LINE OF ANNUAL LIQUID WATER ON THE SIERRA VALLEY FOR THE 13 DIFFERENT FUTURE PROJECTIONS. SIGNIFICANCE OF THE TREND WAS DETERMINED USING THE MANN-KENDALL STATISTICAL TEST. P VALUES ARE GIVEN IN PARENTHESES.	159
TABLE 22. RESULTS OF THE TREND ANALYSIS FOR INFILTRATION. SLOPE (ACFT/YR) OF THE TREND LINE OF ANNUAL INFILTRATION FOR THE 13 DIFFERENT FUTURE PROJECTIONS. SIGNIFICANCE OF THE TREND WAS DETERMINED USING THE MANN-KENDALL STATISTICAL TEST. P VALUES ARE GIVEN IN PARENTHESES.	161
TABLE 23. RESULTS OF THE TREND ANALYSIS FOR DIRECT RUNOFF. SLOPE (ACFT/YR) OF THE TREND LINE OF ANNUAL DIRECT RUNOFF ON THE SIERRA VALLEY FOR THE 13 DIFFERENT FUTURE PROJECTIONS. SIGNIFICANCE OF THE TREND WAS DETERMINED USING THE MANN-KENDALL STATISTICAL TEST. P VALUES ARE GIVEN IN PARENTHESES.	163
TABLE 24. RESULTS OF THE TREND ANALYSIS FOR DEEP PERCOLATION. SLOPE (ACFT/YR) OF THE TREND LINE OF ANNUAL DEEP PERCOLATION ON THE SIERRA VALLEY FOR THE 13 DIFFERENT FUTURE PROJECTIONS. SIGNIFICANCE OF THE TREND WAS DETERMINED USING THE MANN-KENDALL STATISTICAL TEST. P VALUES ARE GIVEN IN PARENTHESES.	165
TABLE 25. RESULTS OF THE TREND ANALYSIS FOR POTENTIAL EVAPOTRANSPIRATION. SLOPE (ACFT/YR) OF THE TREND LINE OF ANNUAL POTENTIAL EVAPOTRANSPIRATION ON THE SIERRA VALLEY FOR THE 13 DIFFERENT FUTURE PROJECTIONS. SIGNIFICANCE OF THE TREND WAS DETERMINED USING THE MANN-KENDALL STATISTICAL TEST. P VALUES ARE GIVEN IN PARENTHESES.	167
TABLE 26. RESULTS OF THE TREND ANALYSIS FOR ACTUAL EVAPOTRANSPIRATION. SLOPE (ACFT/YR) OF THE TREND LINE OF ANNUAL ACTUAL EVAPOTRANSPIRATION ON THE SIERRA VALLEY FOR THE 13 DIFFERENT FUTURE PROJECTIONS. SIGNIFICANCE OF THE TREND WAS DETERMINED USING THE MANN-KENDALL STATISTICAL TEST. P VALUES ARE GIVEN IN PARENTHESES.	169
TABLE 27. RESULTS OF THE TREND ANALYSIS FOR ACTUAL EVAPOTRANSPIRATION OF THE AGRICULTURAL CROPS. SLOPE (ACFT/YR) OF THE TREND LINE OF ANNUAL ACTUAL EVAPOTRANSPIRATION OF THE AGRICULTURAL CROPS ON THE SIERRA VALLEY FOR THE 13 DIFFERENT FUTURE PROJECTIONS. SIGNIFICANCE OF THE TREND WAS DETERMINED USING THE MANN-KENDALL STATISTICAL TEST. P VALUES ARE GIVEN IN PARENTHESES.	171
TABLE 28. RESULTS OF THE TREND ANALYSIS FOR ACTUAL EVAPOTRANSPIRATION OF THE NATIVE AND RIPARIAN VEGETATION. SLOPE (ACFT/YR) OF THE TREND LINE OF ANNUAL ACTUAL EVAPOTRANSPIRATION OF THE NATIVE AND RIPARIAN VEGETATION ON THE SIERRA VALLEY FOR THE 13 DIFFERENT FUTURE PROJECTIONS. SIGNIFICANCE OF THE TREND WAS DETERMINED USING THE MANN-KENDALL STATISTICAL TEST. P VALUES ARE GIVEN IN PARENTHESES.	172
TABLE 29. RESULTS OF THE TREND ANALYSIS FOR APPLIED PRIME WATER. SLOPE (ACFT/YR) OF THE TREND LINE OF ANNUAL APPLIED PRIME WATER ON THE SIERRA VALLEY FOR THE 13 DIFFERENT FUTURE PROJECTIONS. SIGNIFICANCE OF THE TREND WAS DETERMINED USING THE MANN-KENDALL STATISTICAL TEST. P VALUES ARE GIVEN IN PARENTHESES.	174
TABLE 30. RESULTS OF THE TREND ANALYSIS FOR GROUNDWATER PUMPING. SLOPE (ACFT/YR) OF THE TREND LINE OF ANNUAL GROUNDWATER PUMPING ON THE SIERRA VALLEY FOR THE 13 DIFFERENT FUTURE PROJECTIONS. SIGNIFICANCE OF THE TREND WAS DETERMINED USING THE MANN-KENDALL STATISTICAL TEST. P VALUES ARE GIVEN IN PARENTHESES.	176
TABLE 31. RESULTS OF THE TREND ANALYSIS FOR NET GAIN FROM STREAMS. SLOPE (ACFT/YR) OF THE TREND LINE OF ANNUAL NET GAIN FROM STREAMS ON THE SIERRA VALLEY FOR THE 13 DIFFERENT FUTURE PROJECTIONS. SIGNIFICANCE OF THE TREND WAS DETERMINED USING THE MANN-KENDALL STATISTICAL TEST. P VALUES ARE GIVEN IN PARENTHESES.	178
TABLE 33. RESULTS OF THE TREND ANALYSIS FOR THE GROUNDWATER LEVELS AT NINE DIFFERENT LOCATIONS. SLOPE (FT/YR) OF THE TREND LINE OF THE GROUNDWATER LEVEL AT NINE DIFFERENT LOCATIONS FOR ENSEMBLE AVERAGE OF THE 13 DIFFERENT FUTURE PROJECTIONS. SIGNIFICANCE OF THE TREND WAS DETERMINED USING THE MANN-KENDALL STATISTICAL TEST. P VALUES ARE GIVEN IN PARENTHESES.	180

I. SUMMARY AND OBJECTIVES OF STUDY

The Upper Middle Fork Project (UMF) project pilots coordinated implementation by two of the IRWM Plan signatories. Plumas County and the Sierra Valley Groundwater Management District each manage significant portions of the project area. The Upper Middle Fork project pilots the integration of local water management knowledge, local land and water use authorities, and the best available science to further the capacity to practice sustainable resource stewardship at the regional scale.

The goals of this project are:

- 1) to investigate climate scenarios and their effect on groundwater storage levels, summer base flows, and flood flows within the Upper Middle Fork watershed;
- 2) to develop a surface water/groundwater water budget that can be utilized to help coordinate the future management actions of the local organizations on the Upper Middle Fork watershed land/water resources.

The tasks to be implemented for this study consist of:

1. Reconstruction of historical climate data and projections of future climate data under climate change scenarios.
2. Development of a Geographic Information System (GIS) database on the local land and geologic features and historical climate conditions of the basin:
 - Collect spatially distributed soil survey data, land use/land cover data, vegetation data, groundwater data, and other water related geo-referenced data in order to establish the GIS database for the UMF area.
 - Locate and accumulate all existing hydrologic and hydraulic reports and data pertinent to the project, including, but not limited to precipitation, temperature, snow cover, stream flow, and groundwater data.
 - Perform field visits to document the visible hydrologic and hydraulic conditions of the watershed for model parameters.

3. Estimation of the parameters of the Watershed Environmental Hydrology (WEHY) model over the study watershed.
4. Implementation of a reservoir operation model for the Grizzly Valley Dam for the simulation of the reservoir re-operations within the basin under future climate scenarios.
5. Field Monitoring and Field work:
 - Conduct isotope water signature work at the headwaters of the Middle Fork canyon to identify aquifer-stream interactions and possible recharge areas.
 - Conduct analyses of existing groundwater data/records within the basin.
 - Coordinate the work to setup the weather stations that provide measurements of the local evapotranspiration, precipitation, temperature, relative humidity, wind speed, and etc.
 - Conduct intensive storm event monitoring, as needed.
 - Prepare quarterly reports detailing monitoring activities and results.
6. Implementation and use of a snow model for the simulation of snow conditions in the basin.
7. Calibration of the WEHY model by historical hydrologic data observed in the Upper Middle Fork (UMF) basin.
8. Validation of the WEHY model by historical hydrologic data at the UMF basin.
9. Flood, stormwater recharge, and baseflow discharge modeling using the WEHY model.
10. Simulation of the reconstructed future climate scenarios by the calibrated/validated model in order to quantify their surface water/groundwater balances.
11. Model installation and training.

II. UPPER MIDDLE FORK WATERSHED

1. Overview of the Project Site

Located in California's northern Sierra Nevada (**Figure 1**), the Upper Feather River (UFR) watershed covers 8,345 square kilometers (3,222 square miles) of land and drains west from the northern Sierra Nevada into the Sacramento River (George et al., 2007). The Upper Feather River (UFR) has four branches, namely the North Fork, Middle Fork, South Fork, and West Branch (SRWP, 2010). Originating from the mountains above Sierra Valley, the Middle Fork Feather River flows in a westerly direction until it reaches Lake Oroville (SRWP, 2010). Therefore, the watershed of this project, referred to as the Upper Middle Fork (UMF) watershed, is a subwatershed of UFR, comprising around 33% of its area, i.e., around 2,750 square kilometers (1,062 square miles) (**Figure 1**).

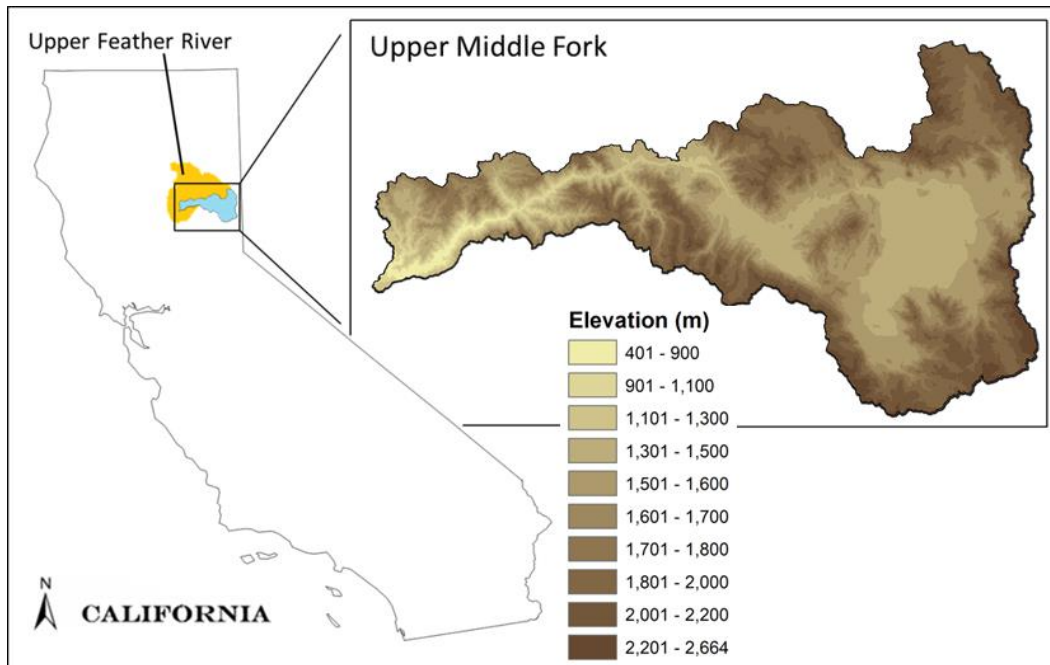


Figure 1. Location of Upper Feather River (UFR) and Upper Middle Fork (UMF) watersheds within California. The zoomed-in figure reveals elevations inside the UMF watershed. [Elevation data source: Digital Elevation Model (DEM) from the National Elevation Dataset (NED): <http://ned.usgs.gov/>].

Elevations within the UMF watershed are found to vary greatly, ranging from as low as 490 m (1,607 ft.) over some parts of the western portion of the watershed, and quickly increasing to over 1,000 m (3,281 ft.) within Sierra Valley (eastern portion) and the adjacent lands. At the

mountains bounding the watershed and surrounding Sierra Valley, elevations are found to exceed 2,000 m (6,562 ft.), increasing until they reach as high as 2,664 m (8,740 ft.) (**Figure 1**). Along with the wide range of elevations, the UMF watershed contains a diversity of vegetation (**Figure 2**), emphasizing its geophysical and biological heterogeneity. The western and middle portions of UMF are dominated with forested land (evergreen needleleaf/broadleaf and deciduous broadleaf), whereas a large area of irrigated cropland and pasture is found in the Sierra Valley portion of the watershed, surrounded by some shrubland.

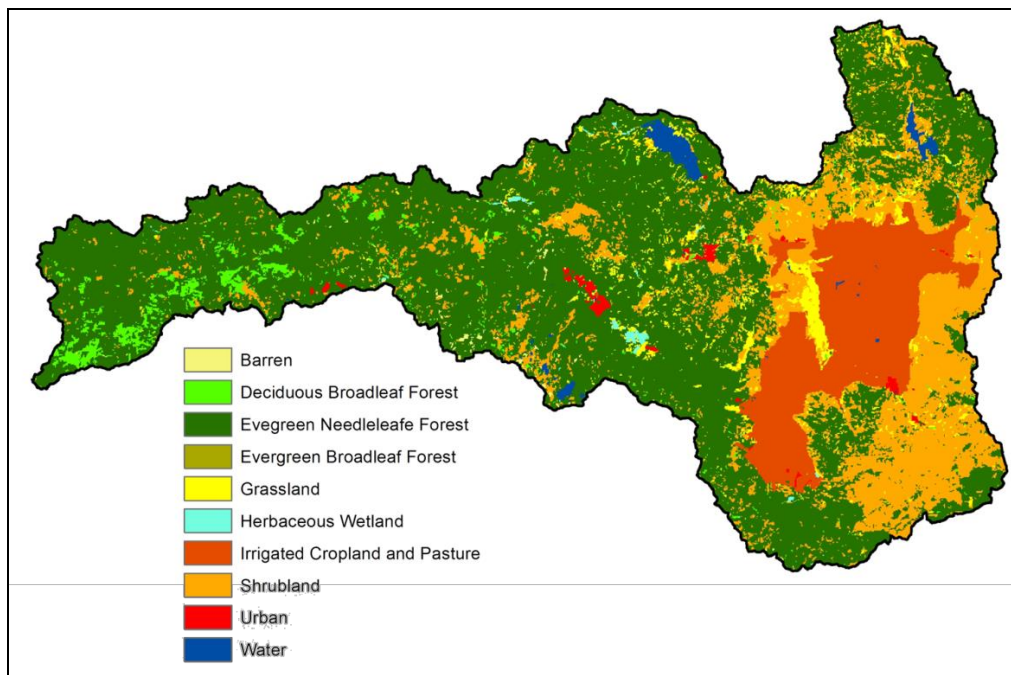


Figure 2. Vegetation and land-cover types at 100-m (328-ft) resolution over the Upper Middle Fork watershed.

2. Methodology

In order to correctly simulate the surface flows of the Upper Middle Fork (UMF) watershed under differing climate conditions, all the hydrologic processes in the watershed must be properly modeled. As such, hydroclimate modeling was implemented in this study through the coupling of a land hydrologic model with a regional climate model (RCM). Therefore, the model used for this study was the Watershed Environmental Hydrology Hydro-Climate Model (WEHY-HCM), which was developed by Kavvas et al. (2012) and Kure et al. (2012) as a physically-based distributed hydroclimate model. The fifth generation Mesoscale Atmospheric Model (MM5) (Grell et al. 1994) was used in this study as the RCM of the WHEY-HCM, and

will be discussed in details in a subsequent section. On the other hand, the Watershed Environmental Hydrology (WEHY) model was used as the hydrologic model of the WEHY-HCM. The WEHY model was developed by Kavvas et al. (2004) as a physically-based watershed hydrologic model which accounts for the effects of heterogeneity within natural watersheds. The model works by subdividing a watershed into several Model Computation Units (MCUs) or hillslopes. The physically-based (or process-based) modeling approach for the hydrological processes is essential in order to simulate the river stream discharge at ungauged or sparsely gauged basins, such as the UMF watershed. A simplified, generalized model flow chart for the steps needed for running the WEHY-HCM for a watershed is provided in **Figure 3**.

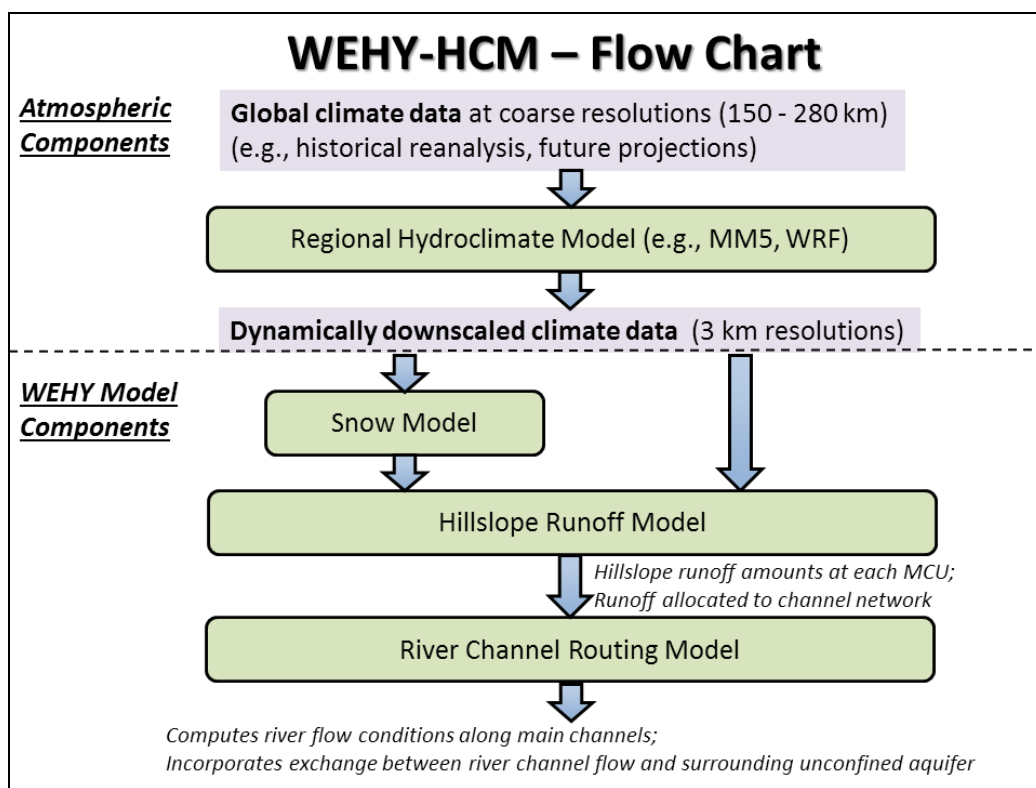


Figure 3. A simplified, generalized flow chart of the steps used for running the WEHY-HCM over a watershed. MCU: model computational unit – the computational unit used by the WEHY model to undergo the simulation; it is equivalent to the hillslope.

From the steps provided in **Figure 3**, simulating the WEHY-HCM model over a watershed involves, first, obtaining global climate data. Such data is usually available at coarse resolutions such as 150 – 280 km grids (93 – 174 mi.), and may include historical reanalysis data and/or future projections. This coarse global climate data is then fed into a regional climate model (e.g., MM5 or WRF) to be dynamically downscaled to much finer resolutions, i.e., to the

watershed scale (as low as 3 km or 1.86 mi.). This data then enters as input either into the snow model (if the watershed is snow-dominated) or directly into the hillslope runoff model. The hillslope runoff model calculates hillslope runoff amounts at every MCU which are then allocated to the channel network of that watershed. The river channel routing model computes the river flow conditions along the main channels of the network. It also incorporates the exchange between the river channel flow and the surrounding unconfined aquifer under meadow land.

Therefore, for this project, several model layers were organized and implemented: a regional hydroclimate model, a snow accumulation and melting model, a hillslope process model, and a river channel routing model. At every modeling step, the modeled hydrologic quantities were calibrated and validated by the available ground observation data.

3. Ground Observation Data Collection

To achieve an effective calibration and validation process for any model, historical records of hydrologic ground observation data are indispensable. As such, various data sources were searched in order to collect publicly available information on historical atmospheric data within the Upper Middle Fork (UMF) watershed, including precipitation, snow, and streamflow discharge data. Such data sources included California Data Exchange Center (CDEC), National Climatic Data Center (NCDC), U.S. Geological Survey (USGS), Feather River Coordinated Resource Management (FRCRM), and California Environmental Data Exchange Network (CEDEN).

Several precipitation stations (18) were found from the California Data Exchange Center (CDEC) within and around the UMF watershed, eleven of which were located inside the watershed and the remaining 7 were in the vicinity of the watershed. However, not all of the stations were useful for modeling purposes due to the duration and frequency (hourly, daily, or monthly) of the data being collected at those stations. As a result, with a criteria of hourly time intervals of data being collected for a long historical time period (~20 years), the list of precipitation stations was reduced to a total of 7, the locations of which are presented in **Figure 4**. A similar search for snow stations showed a total of 11 stations within the watershed, only four of which were deemed useful for the modeling process (**Figure 4**). As for the streamflow

discharge, information from several of the above-mentioned data sources was used to find nine different locations where the streamflow has been recorded. However, only two stations had frequenting and long-term data usable for this project’s modeling purposes (**Figure 4**). Finally, a search for meteorological stations provided four stations that were recording air temperature, solar radiation, and wind speed data. Only one of them was located inside the UMF watershed; however, it had no long-term data records.

A summary of the useful ground observation stations within the UMF watershed and their information is provided in **Table 1**; a plot of those stations is provided in **Figure 4**.

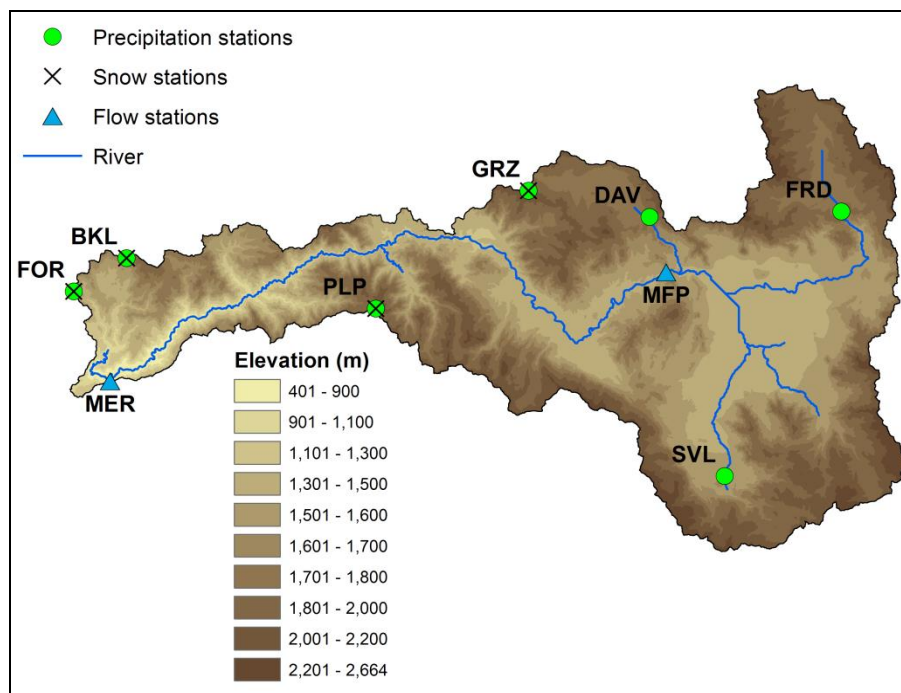


Figure 4. Locations of useful fine-interval, long-term precipitation, snow, and flow stations used for this UMF project.

From **Figure 4**, it is clear that there is a lack of useful observation data in some locations within the UMF watershed, especially in the Sierra Valley region. Useful precipitation data seem to be located closer to the watershed boundaries than to the middle, with a clear lack within the Sierra Valley region. Useful snow data also seems to be more concentrated at the watershed boundaries, and mainly in the western portion of UMF, leaving the eastern part as well as the Sierra Valley region void of useful snow observation data. Moreover, useful meteorological data are clearly lacking within the UMF watershed in general, and in the Sierra Valley region in

specific, which provided the incentive for placing additional weather stations within and around the Sierra Valley as part of this project, as will be discussed in more detail later in this report.

Table 1. Location information and data sources of the useful ground observation stations used for this UMF project.

Station ID	Station Name	Longitude	Latitude	Elevation (m)	Data Source	Data*
BKL	BUCKS LAKE	-121.2420	39.8500	1753	CDEC	P, S
DAV	LAKE DAVIS (DWR)	-120.4670	39.8830	1758	CDEC	P
FOR	FOUR TREES	-121.3210	39.8130	1570	CDEC	P, S
FRD	FRENCHMAN DAM	-120.1830	39.8830	1682	CDEC	P
GRZ	GRIZZLY RIDGE	-120.6450	39.9170	2103	CDEC	P, S
MER	FEATHER RIVER AT MERRIMAC	-121.2700	39.7090	475	CDEC/U SGS	F
MFP	MIDDLE FORK FEATHER RIVER NEAR PORTOLA	-120.4449	39.8190	1478	CDEC/U SGS	F
PLP	PILOT PEAK (DWR)	-120.8750	39.7860	2073	CDEC	P, S
SVL	SIERRAVILLE (DWR)	-120.3670	39.5830	1516	CDEC	P

*P: precipitation; S: snow; F: streamflow discharge

4. Development of a Geographic Information System (GIS) Database for the Upper Middle Fork Watershed

In order to effectively use the hydrologic model set for this project, it is important to set up a geographic information system (GIS) database over the Upper Middle Fork (UMF) watershed. All useful geo-referenced data from various sources, including spatially distributed data and point data, were downloaded and processed to form this database. Note that the Universal Transverse Mercator (UTM) coordinate system was selected as the standard GIS coordinate system for this project. The Universal Transverse Mercator Coordinate system divides the world into 60 zones, each being 6 degrees longitude wide, and extending from 80 degrees south latitude to 84 degrees north latitude (USGS, 2004). The UTM Zone 10 projection is used for the project. If any of the original collected digital maps mentioned below were not in the selected coordinate system, they were re-projected to the UTM Zone 10 coordinates. The GIS database consisted of the following spatial digital data maps.

A. Digital Elevation Model (DEM) Data

The Digital Elevation Model (DEM) data were obtained from the National Elevation Dataset (NED) at a 1 arc-second resolution (~30 m or 98.5 ft.) in geographic projection.

B. Land Use/Land Cover and Vegetation Data

The land use/land cover and vegetation data were obtained from the California Fire Resource and Assessment Program (FRAP) at 100-m (328-ft.) resolution in NAD27 projection. These provided a description of the different vegetation types available over the UMF watershed (see **Figure 2**). Moreover, the Leaf Area Index (LAI) data were obtained from Moderate Resolution Imaging Spectroradiometer (MODIS) satellite driven data at 1-km (0.62-mi.) spatial resolution provided by NASA.

C. Soil Survey Data

The county scale soil database (Soil Survey Geographic Database [SSURGO]) was obtained from the United States Department of Agriculture - California Natural Resources Conservation Service (USDA-NRCS) at 100-m (328-ft.) resolution. The USDA-NRCS has the finest available spatial resolution over the project area. A plot of the spatial soil map based on the SSURGO database is shown in **Figure 5**.

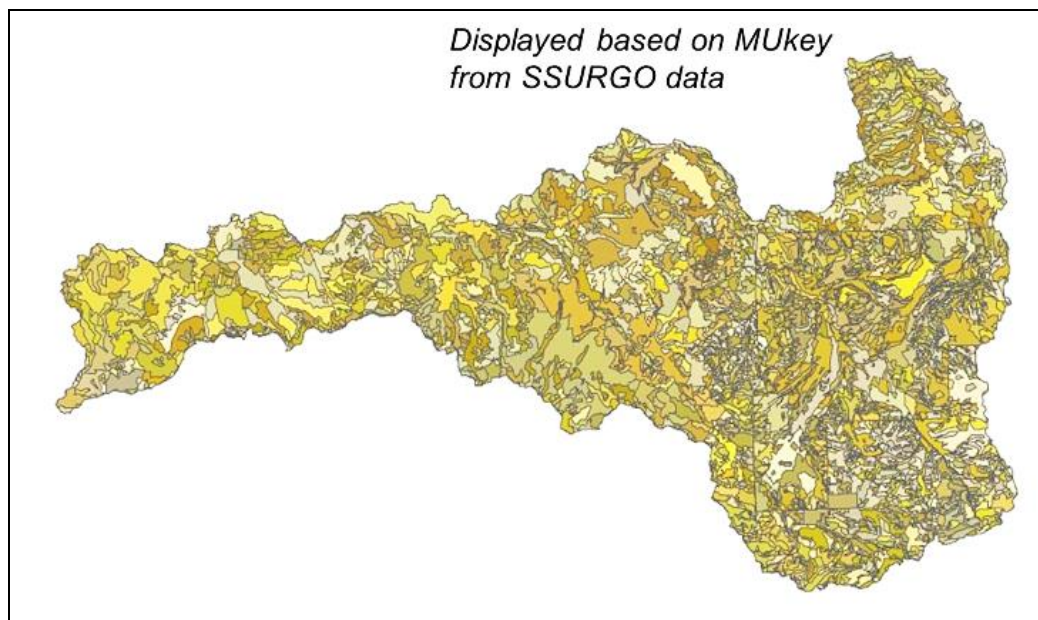


Figure 5. Spatial soil map based on SSURGO data from California USDA-NRCS over the UMF watershed.

In addition to the above data, the river channel network and large watershed boundaries were obtained from the National Hydrography Dataset (NHD), and the road network, aerial photos, county borders, and other digital maps were obtained from the California Spatial Information Library (CaSIL). All of the above-described spatial data maps were acquired and compiled into a GIS platform.

5. Reconstruction of Historical Hydro-climate Data over the Upper Middle Fork Watershed

As discussed previously, there is a lack of useful ground observation data in some portions of the Upper Middle Fork (UMF) watershed, and even with the useful stations, there is not enough spatial distribution among them. As such, it should be emphasized that the importance of the spatial variability of precipitation on the runoff hydrograph has been long recognized, and that the orographic precipitation is a well-known and common phenomenon in Sierra Nevada. Hence, the effects of the spatial distribution of the precipitation due to the orographic characteristics need to be considered for the input precipitation data to the watershed models applied to high elevation areas.

For the physically-based, spatially-distributed land surface parameterization and snow accumulation and melting process modeling that will be performed over the UMF watershed, a lot of fine-interval spatially distributed hydro-meteorologic data such as precipitation, air temperature, relative humidity, wind speed, as well as short and long wave radiation are required. Such data would be essential for the UMF's hydrologic modeling, and indispensable for the calibration and validation of the hydrologic model. However, under the lack of such spatially variable available data within UMF, the required fine-interval spatially distributed atmospheric data over UMF can be attained through a reconstruction of the historical atmospheric data, undergone during the historical period at hourly intervals and at a 3-km (1.86-mi.) resolution over the whole watershed. This can be achieved by using a regional climate model. Because regional climate models employed for the dynamical downscaling can simulate the physical atmospheric processes locally, the regional climate features such as orographic precipitation and extreme climate events can be simulated by these models. For this reason, we utilized in this

project the WEHY-HCM, which was developed by coupling a hydrology model (WEHY) with a regional climate model, as explained previously.

A. Using a Regional Climate Model to Reconstruct the Atmospheric Data over UMF

The first step in the reconstruction of the atmospheric variables at the scale of the UMF watershed is to obtain the NCEP/NCAR global reanalysis data. The data, which is from 1948 to the present, come as a result of the cooperation of the National Centers for Environmental Prediction (NCEP) and National Center for Atmospheric Research (NCAR) to aid the research community (Kistler et al., 2001). Land surface, ship, rawinsonde, pibal, aircraft, and satellite data (Kistler et al., 2001) are assimilated into a global circulation model in order to get a temporally and spatially uniform global atmospheric database that is consistent with the observations (Kalnay et al., 1996). The resulting database of reanalysis data is obtained on a 210 x 210 km (130.5 x 130.5 mi.) regular grid (Kistler et al., 2001) with data for pressure, winds, relative and specific humidity, temperature, and potential temperature at 6-hr intervals, all of which are available over the whole globe.

After obtaining the reanalysis data discussed above, the data can be used as initial and boundary conditions in a regional climate model. One such model is the fifth-generation Penn State/NCAR Mesoscale Model (MM5) (Anthes & Warner, 1978; Grell et al., 1994), a community model that is maintained by the NCAR and Penn State University (PSU). This model is a “limited-area, nonhydrostatic or hydrostatic, terrain-following sigma-coordinate model designed to simulate or predict mesoscale and regional-scale atmospheric circulation” (UCAR, 2003). MM5 contains a wide range of physical process routines to model advection, diffusion, radiation, boundary layer processes, surface layer processes, moisture dynamics, and cumulus convection. In its nonhydrostatic mode, the MM5 model can simulate the full vertical momentum equation and, as such, can satisfactorily describe the air motions over steep mountainous terrains at small grid scales (such as a few kilometers) suitable for atmospheric inputs into a watershed model. Therefore, MM5 can be used to downscale atmospheric data to as low as 1-km spatial resolutions, and as such, it is able to capture the impact of steep topography and land surface/land use conditions of watersheds on the local atmospheric conditions.

In addition, MM5 has multiple nesting capabilities, which either lack feedback (one-way nesting) or include feedback (two-way nesting) between the coarse-resolution domain and its

corresponding finer-resolution nest (Ganev, 2011). Due to its nesting capabilities, MM5 may either be coupled with other models of larger grid scales (e.g., simulation data of General Circulation Models), or with atmospheric data (e.g., NCEP/NCAR reanalysis data). Also note that MM5 has a variable grid size, and thus can provide atmospheric process simulations at any resolution. The model has already been used at various watersheds in the world, and has been tested and validated over those watersheds by the UC Davis group (Anderson et al., 2007; Ohara et al., 2007; Yoshitani et al., 2009; Jang et al., 2010; Ishida et al., 2014; Trinh et al., 2016).

For the purpose of this project, MM5 was employed as the atmospheric component of WEHY-HCM together with the NCEP/NCAR reanalysis data (i.e., large-resolution historical atmospheric data) in order to reconstruct the atmospheric data (precipitation, temperature, radiation, etc.) to a scale suitable for use in hydrologic modeling studies, i.e., to a significantly finer spatial resolution. The dynamical downscaling process downscaled the data from a resolution of 210 x 210 km (130.5 x 130.5 mi.) to a 3 x 3 km (1.86 x 1.86 mi.) resolution over the UMF watershed. This was done by using two-way nesting of four grids, each nest being one-third of its corresponding coarser parent grid, thus giving nested domains of the following resolutions: 81 km (50.3 mi.), 27 km (16.8 mi.), 9 km (5.6 mi.), and 3 km (1.86 mi.) (**Figure 6**). The 1/3 ratio between a nested grid and its parent grid is recommended in the user documentation for MM5 (Grell et al., 1994). Note that having a series of nested grids provides a more economical downscaling of the large-scale atmospheric data to the desired resolution. However, the number of domains is generally limited to four or less due to reasons of practicability, numerical stability, and computational power (Ganev, 2011).

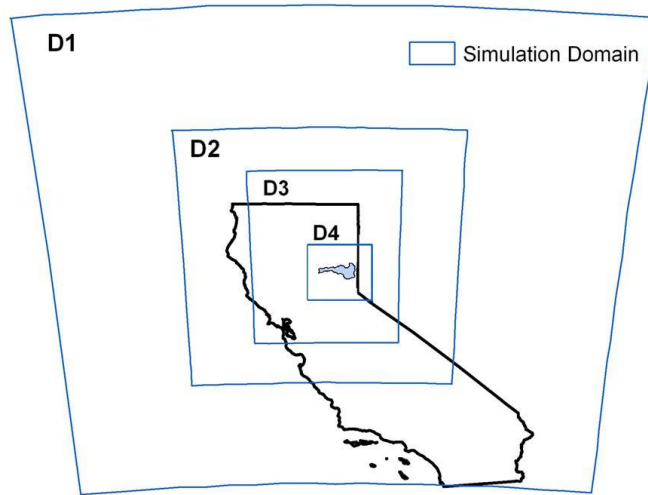


Figure 6. Spatial extent of the four nested grids for atmospheric data reconstruction by MM5. D1: 81 x 81 km (50.3 x 50.3 mi.), D2: 27 x 27 km (16.8 x 16.8 mi.), D3: 9 x 9 km (5.6 x 5.6 mi.), D4: 3 x 3 km (1.86 x 1.86 mi.).

B. Validation of the Reconstructed Historical Climate

In order to gain confidence in the performance of MM5 and the reconstructed historical climate variables, these climate variables were compared against ground observations as well as PRISM (Parameter-elevation Relationships on Independent Slopes Model) fine-scale historical climate data, mainly over the second half of the 20th century.

Starting with comparisons against ground observations, three CDEC ground observation stations were selected for the validation of MM5-simulated precipitation. The CDEC stations were selected based on their record length of observational data as well as the time interval of data provided. The selected stations are shown in **Figure 7**. Not that these stations were not represented in **Figure 4** since they do not have a fine time-interval (e.g., hourly). In fact, these stations have monthly precipitation data, but their long time period allows their comparison with the simulated MM5-NCEP monthly precipitation over the period from October 1951 through September 1999. The results in **Figure 8** show that the MM5-NCEP simulated monthly precipitation matches the corresponding monthly precipitation observations very well over the three selected stations for the whole historical period.

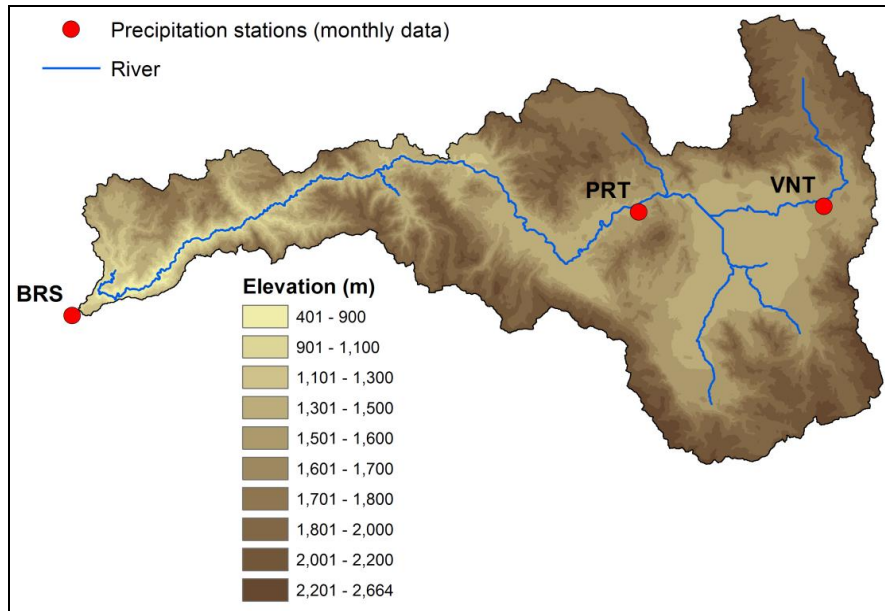


Figure 7. Locations of selected monthly, long-term ground precipitation stations for use in comparison against MM5-NCEP simulated results.

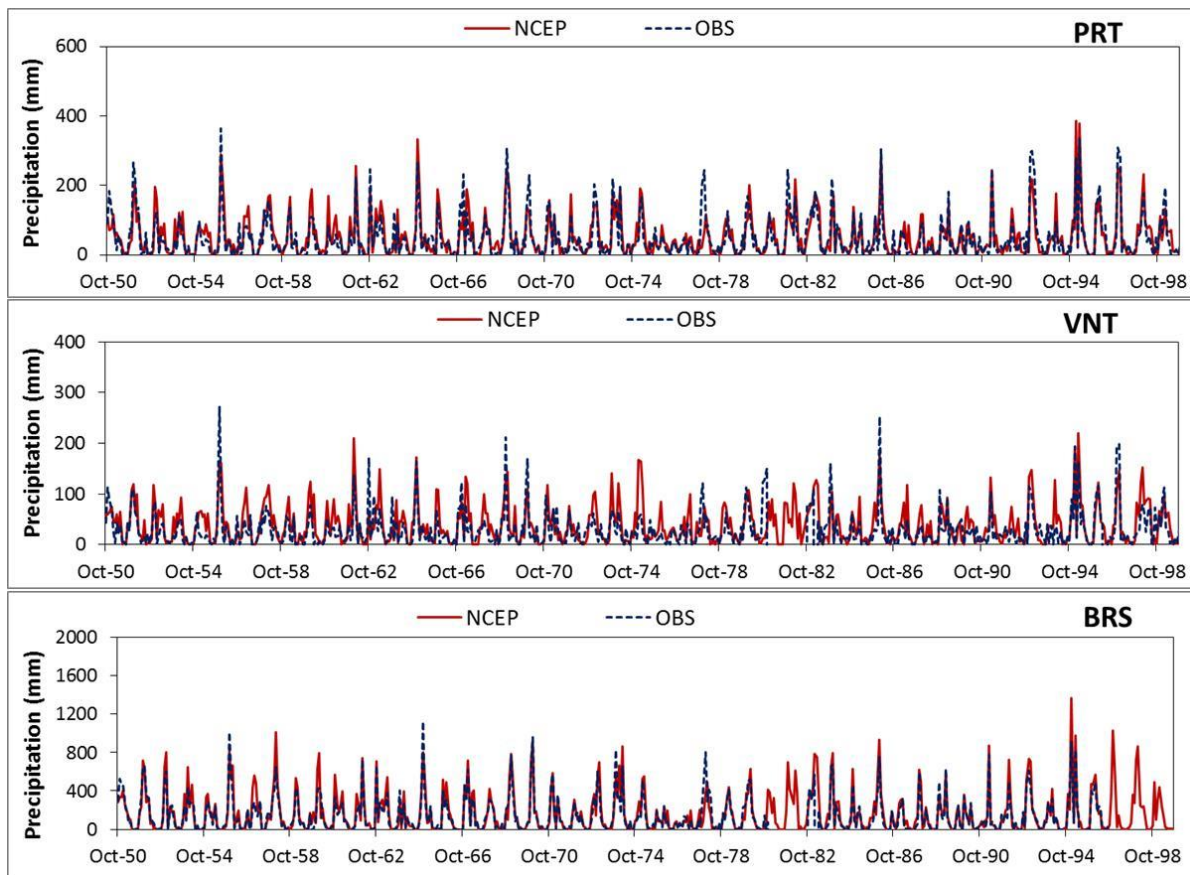


Figure 8. Time-series comparisons of monthly precipitation between ground observations and MM5-NCEP simulated values. No bias correction was applied.

The next validation step was to compare the MM5-NCEP reconstructed precipitation to PRISM (Parameter-elevation Relationships on Independent Slopes Model) data. Developed by Oregon State University, PRISM datasets span from 1895 to the present, and have a 4-km spatial resolution with a monthly time interval over the United States of America (NACSE, 2013). PRISM data are considered to be one of the most reliable and comparable datasets for model calibration or validation, and thus are important for validating the reconstructed precipitation and spatial fields of precipitation over the UMF watershed.

Figure 9 shows the comparisons of precipitation fields between MM5-simulated mean monthly precipitation, based on NCEP/NCAR reanalysis data, and the corresponding PRISM data during the period from water year 1951 to water year 1999 over the UMF watershed. In general, the heavy precipitation fields are found at the downstream of the watershed (from northwest to south), located in the snow-dominated, densely vegetated and high elevation mountain regions. Meanwhile, the light precipitation fields are found at the upstream sector of the watershed, located in the agricultural lands. These spatial patterns are found in both PRISM precipitation fields and MM5-simulated precipitation fields.

The magnitudes of the precipitation fields from MM5-NCEP simulations are slightly higher than the corresponding PRISM precipitation fields, especially around high elevation regions. It is noted that many physiographic and climatic effects were dictated for generating PRISM precipitation. However, the basic assumption in PRISM is that, given some topography information, climate can be predicted through a moving-window regression function that utilizes a linear relationship with elevation. The precipitation generated by PRISM depends on the ground observations that are located in similar physiographic and climatic areas (Daly et al., 2008). This may be the main reason for the difference in precipitation magnitudes. Thus, since PRISM data are based on a limited number of observations at low elevations, comparisons of the precipitation magnitudes between PRISM and MM5 simulations may not necessarily be appropriate at the high-elevation areas of the UMF watershed.

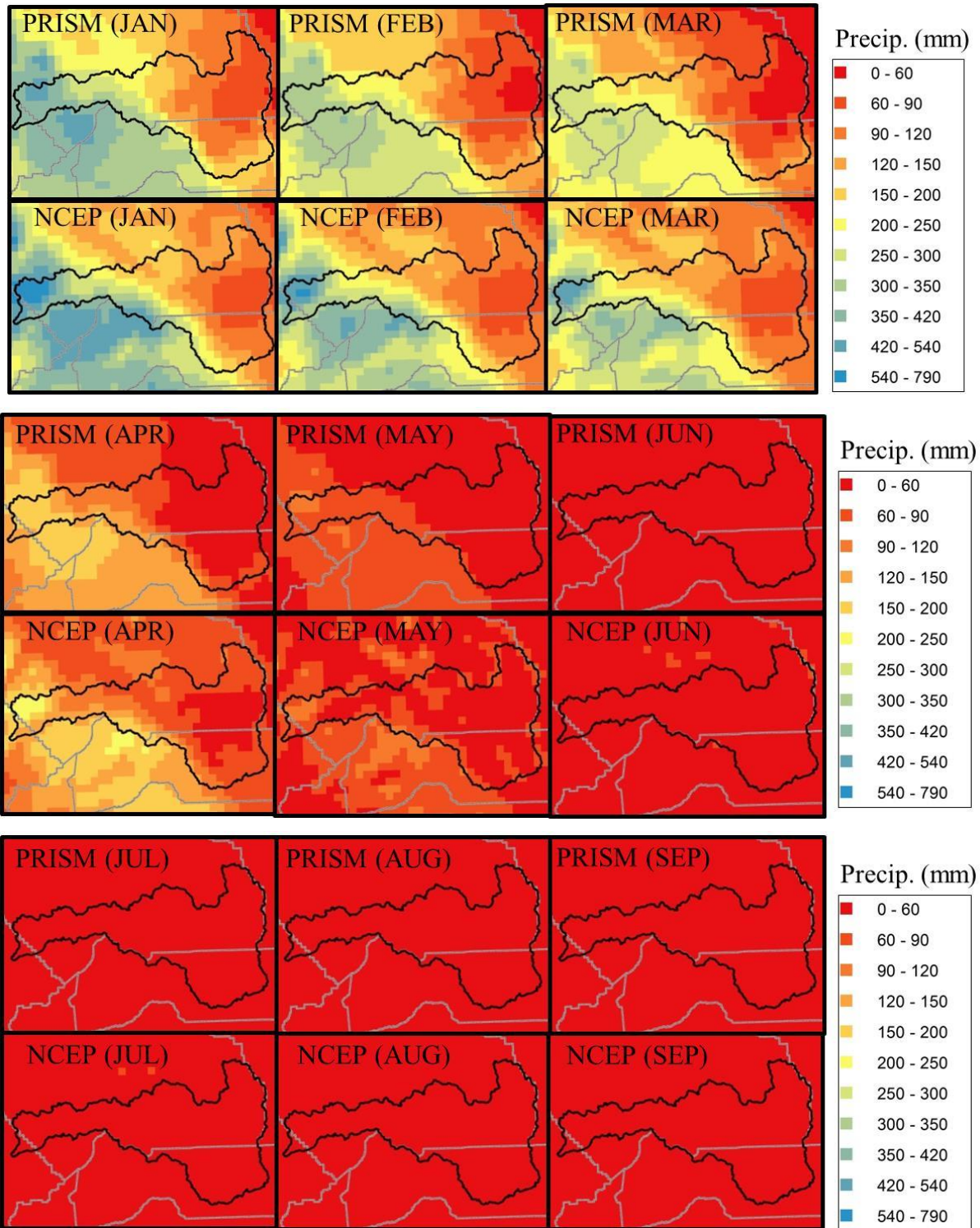


Figure 9. Mean monthly comparisons of simulated precipitation fields (based on MM5 downscaling of NCEP/NCAR reanalysis historical data) and PRISM data during the period spanning from water year 1951 to water year 1999 over the UMF watershed (continued below).

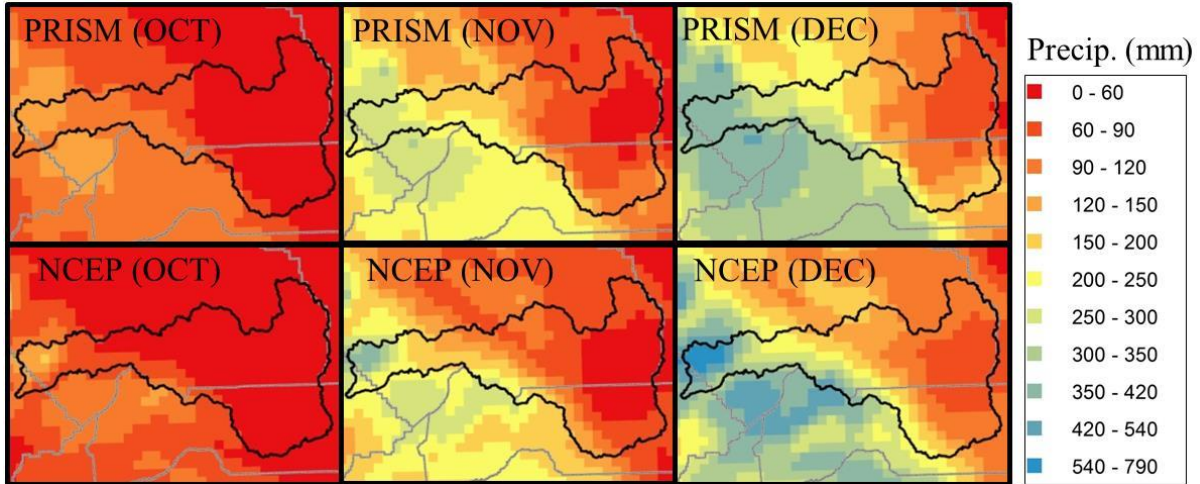


Figure 9 (continued). Mean monthly comparisons of simulated precipitation fields (based on MM5 downscaling of NCEP/NCAR reanalysis historical data) and PRISM data during the period spanning from water year 1951 to water year 1999 over the UMF watershed.

Figure 10 shows the monthly comparisons of the model-simulated (MM5-NCEP) and PRISM monthly precipitation for the basin-average values over the UMF watershed. From this figure, it is clear that the modeled values match the PRISM basin-averaged monthly precipitation quite well for both the timing and the magnitude of the monthly precipitation.

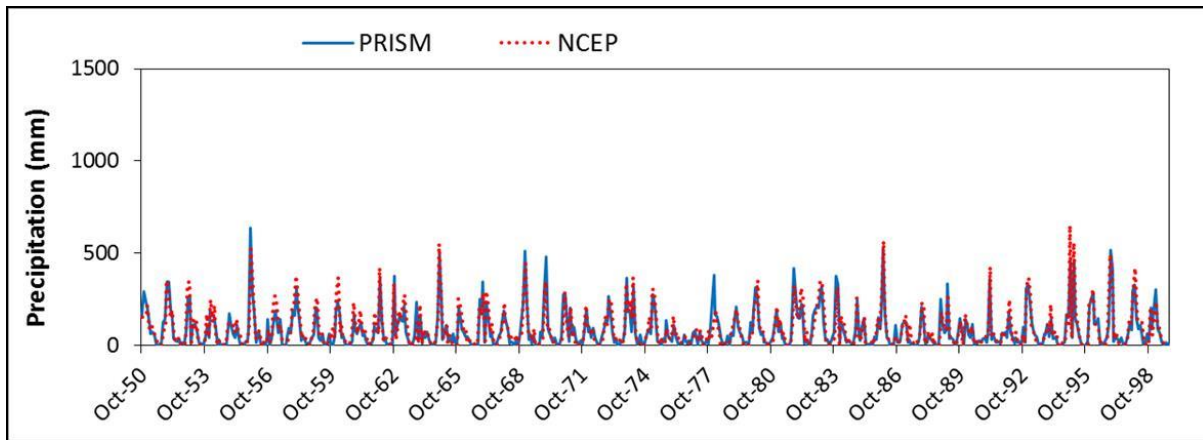


Figure 10. Time-series comparisons of the UMF watershed-average monthly precipitation between MM5-simulated and PRISM values. No bias correction was applied.

Table 2 shows the results of the statistical tests between the PRISM monthly precipitation and the model-simulated (MM5-NCEP) basin average monthly precipitation during the period from October 1950 through September 1999. The mean and the standard deviation of the simulated precipitation are similar to those of the PRISM precipitation, and the root mean

square error is relatively small. Furthermore, high values for the Correlation Coefficient and Nash-Sutcliffe Efficiency were computed at the basin scale.

Therefore, all of the above results related to the dynamical downscaling of NCAR/NCEP reanalysis data are quite encouraging for the watershed modeling of UMF. Accordingly, from these results it may be inferred that the dynamical downscaling method (MM5), which was applied in this project, is a plausible method for downscaling the GCM future climate projections to the study region.

Table 2. Statistical test values of the basin average MM5-simulated precipitation (based on NCEP/NCAR reanalysis data) and PRISM precipitation during the October 1950 – September 1999 period.

	PRISM	NCEP
Mean (mm)	83.98	90.12
Standard Deviation (mm)	100.49	105.44
Root Mean Square Error (mm)		37.28
Nash–Sutcliffe Efficiency		0.86
Correlation Coefficient		0.9372

6. Global Climate Models and the Reconstruction of their Historical and Projection of their Future Climate Simulations

As reported above, the NCEP/NCAR reanalysis data-based precipitation estimates, reconstructed by the MM5 regional climate model, were quite satisfactory and provided the justification for using the regional atmospheric model MM5 for dynamically downscaling the coarse spatial resolution global climate data to a fine spatial resolution over the modeling domain. However, the future climate projections over the Upper Middle Fork (UMF) watershed will be simulated and will be assessed based on the future climate projections obtained from Global Climate Models (GCM). Therefore, it is also important to validate the MM5-downscaled estimates of the GCM historical climate simulations over UMF in order to gain confidence in their use for simulations of future flows. This validation will be discussed below, following a brief discussion on GCMs first.

A. Discussion on Global Climate Models

Global climate models (GCMs) are models that attempt to incorporate as many physical processes as possible in order to simulate as closely as possible the observed climate. They usually provide outputs of temperature, precipitation, humidity, pressure, and several other climate variables provided on 2-dimensional or 3-dimensional grid cells over the globe and given over a period of time (NECIA, 2006). The two GCMs whose results will be used in this project are: (1) the Community Climate System Model Version 3 (CCSM3) (Collins et al., 2006), (2) and the aerosol-climate model ECHAM5-HAM (or simply ECHAM5) (Stier et al., 2005).

CCSM3 provides realistic atmospheric simulations by incorporating components representing each of land, atmosphere, ocean, and sea ice (Collins et al., 2006). ECHAM5 acknowledges the important role of aerosol particles in future climate dynamics in its simulations, and is reported to be the fifth generation of the atmospheric general circulation model, ECHAM (Stier et al., 2005). The aforementioned GCMs have climate simulations both in historical periods (control runs) as well as future periods (future projections). **Table 3** shows the time periods of the simulations of each of the GCMs.

Table 3. Historical and future periods of climate simulations for each of the two GCMs selected for this study (CCSM3 and ECHAM5).

	CCSM3	ECHAM5
Control runs	1901 – 1999	1901 – 2000
Future Projections	2000 – 2100	2001 – 2100

Future projections of GCMs are dependent on emission scenarios as their driving force. An emission scenario is a single future pathway along which atmospheric CO₂ concentrations might progress, based on certain assumptions regarding demographic, economic, social, technological, and environmental developments (IPCC, 2000). Hence, each scenario can be seen as an alternative route that might be followed in the coming years (NECIP, 2006). Accordingly, the Intergovernmental Panel on Climate Change (IPCC) developed a set of 40 different future emissions scenarios described in the Special Report on Emissions Scenarios (SRES) (IPCC, 2000). These scenarios were grouped into four different families (or storylines) based on the underlying assumptions regarding demographic, economic and technological developments; the storylines are: A1, A2, B1, and B2 (IPCC, 2000).

The A1 storyline describes a world with very rapid economic growth, rapid introduction of new and more efficient technological advancements, and an increasing global population that peaks by the middle of the 21st century and then declines (IPCC, 2007). The A1 storyline is further divided into three groups with different assumptions regarding technological development and energy resources: fossil intensive (A1FI), non-fossil intensive energy resources (A1T), and a balance across all sources (A1B) (IPCC, 2000).

The B1 family has the same global population growth assumptions as A1 and a high economic growth with rapid changes in economic structures toward a service and information economy; however, this storyline predicts that the world will shift to less fossil-fuel intensive industries and will introduce clean and resource-efficient technologies (NECIA, 2006).

The A2 storyline describes a very heterogeneous world, with a continuously increasing (and high) global population along with slower and more fragmented economic and technological growth (IPCC, 2000).

Finally, the B2 family also describes a world with a continuously increasing global population (but at a rate lower than that of A2), an intermediate economic growth, and less rapid and more diverse technological development (as compared to A1 and B1), along with an emphasis on local solutions to economic, social, and environmental sustainability (IPCC, 2007). Therefore, the development of these SRES scenarios provided numerous predictions of future CO₂ emissions that try to encompass the different possible pathways that the world may follow in future years.

For the future analyses involved in this study, 13 different future climate projections were used. Four of these projections were simulated by CCSM3 (A1B, A1FI, A2, and B1), and nine of them were simulated by ECHAM5 (A1B1, A1B2, A1B3, A2-1, A2-2, A2-3, B1-1, B1-2, and B1-3). Note that the atmospheric results used from ECHAM5 simulations are obtained from scenarios that are realizations of a major storyline with different initial conditions (e.g., A2-1 being a realization of A2 with different initial conditions, etc.).

B. Validation of GCM-based Precipitation Estimates Simulated by MM5

To gain confidence in using the regional atmospheric model MM5 for the projection of future climate conditions over UMF by downscaling the GCM projections of the future climate

conditions, the GCM-based historical precipitation simulation values, downscaled by the regional climate model MM5 during 1950 to 2000 from the GCM historical climate simulations, were compared against the PRISM precipitation values by means of graphical comparisons and precipitation trends.

Figure 11 shows the monthly comparisons for the UMF watershed average values of the model-simulated precipitation (MM5-CCSM3 and MM5-ECHAM5) versus PRISM monthly precipitation. The modeled values match the PRISM basin-averaged monthly precipitation values generally well with respect to both the timing and the magnitude of monthly precipitation. Long-term precipitation trends were also investigated based on the 10-year moving average of annual precipitation comparison between GCM-based MM5 simulations and PRISM values during 1900 to 2000 (see **Figure 12**). In general, the MM5-simulated precipitation trends are similar to the corresponding precipitation trends from PRISM.

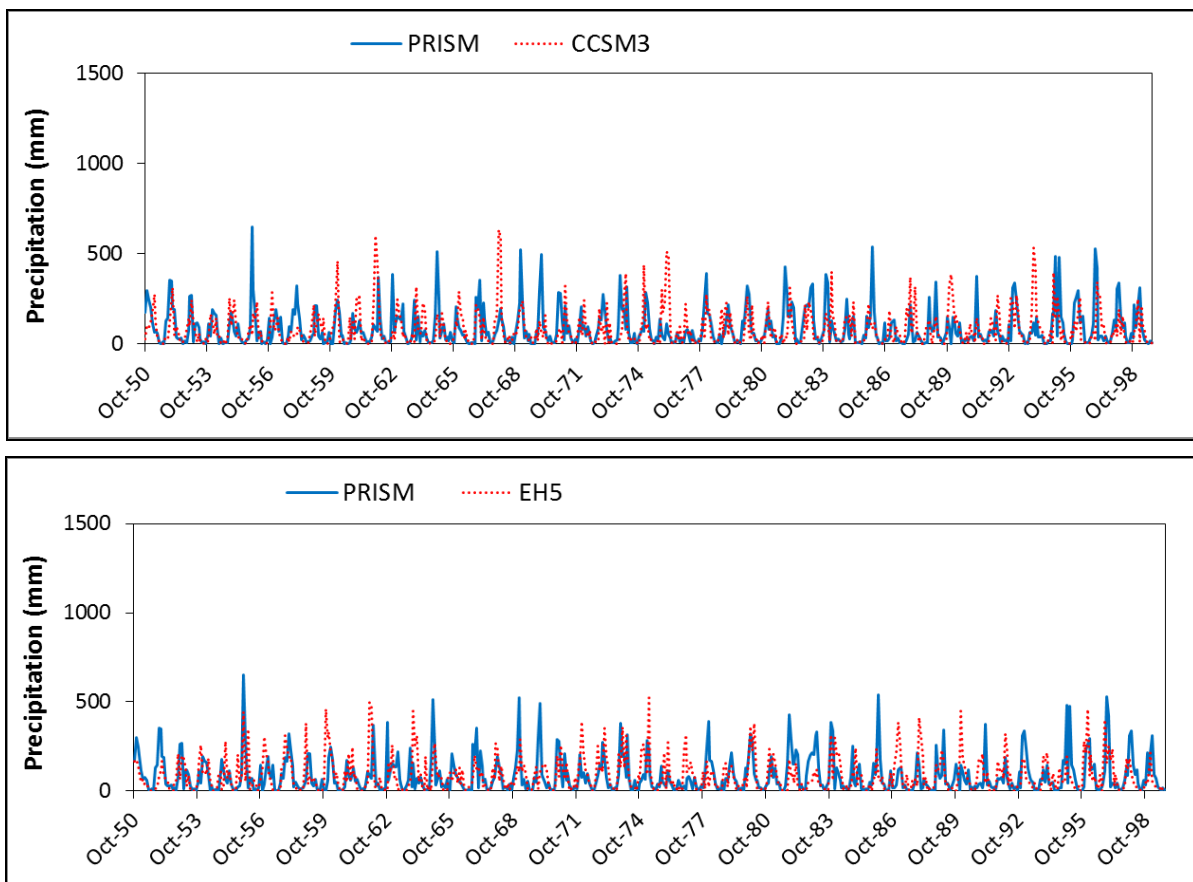


Figure 11. Time-series comparisons of UMF average monthly precipitation between GCM (CCSM3 and ECHAM5)-based estimates and PRISM values. Note: ECHAM5 is abbreviated as EH5 in the above figure.

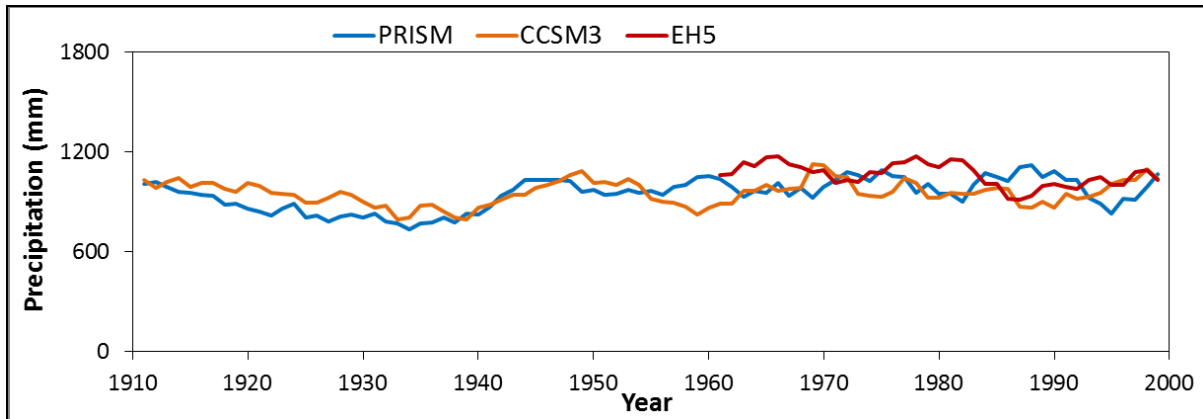


Figure 12. Precipitation trends based on the 10-year basin average annual precipitation from GCM (CCSM3 and ECHAM5)-based estimates and PRISM values. Note: ECHAM5 is abbreviated as EH5 in the above figure.

Unlike the NCEP/NCAR reanalysis data-based MM5 simulation results, the GCM-based MM5 simulation results may not be suitable for comparison to the time-series of observed precipitation because the GCM simulations focus on the climatology of the specified period. It is more important whether the distribution of the GCM-based MM5 simulation results is comparable to the corresponding distribution of observations. The quartile-quartile plot is a good method to see whether the distribution of the model-simulated values deviate from the distribution of the observed values.

Figure 13 and **Figure 14** show the comparison of the quartile-quartile plot for the UMF watershed average monthly precipitation between MM5-simulated precipitation (based on GCM historical simulations) and PRISM precipitation, during 1950 to 2000. As shown in **Figure 13** and **Figure 14**, the MM5-simulated precipitation values, which were estimated by downscaling the historical climate simulations of the GCMs, compare very well against the PRISM precipitation values. From these results it may be inferred that the dynamical downscaling method (by means of the regional climate model MM5) which was applied in this project, seems plausible for downscaling the GCM future climate projections for the UMF watershed.

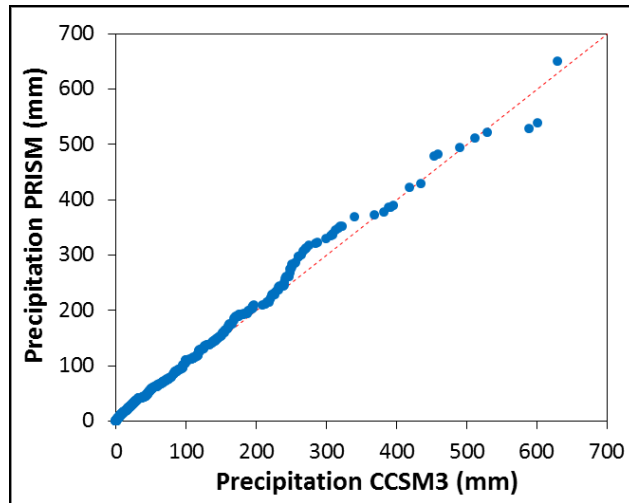


Figure 13. Comparison of the quartile-quartile plot between CCSM3-based simulated values and PRISM monthly precipitation values.

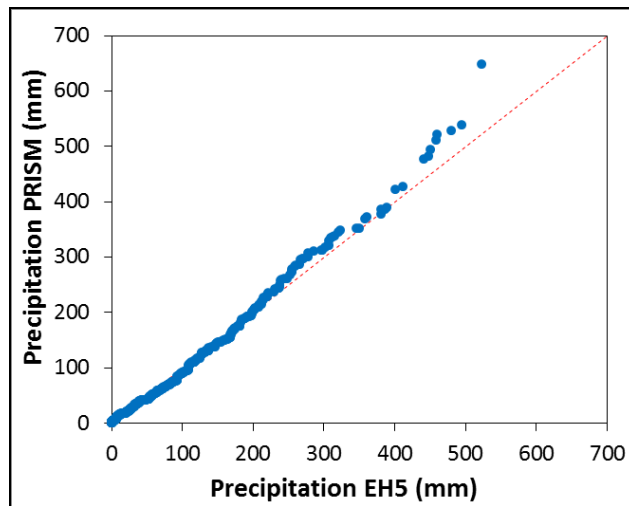


Figure 14. Comparison of the quartile-quartile plot between ECHAM5-based simulated values and PRISM monthly precipitation values. Note: ECHAM5 is abbreviated as EH5 in the above figure.

7. Hydrologic Modeling of the Upper Middle Fork Watershed

The watershed hydrologic model implemented for this project is the Watershed Environmental Hydrology (WEHY) model (Kavvas *et al.*, 2004), which is the hydrologic component of WEHY-HCM. WEHY is a watershed hydrologic model that utilizes upscaled hydrologic conservation equations through their ensemble-averaged forms and analyzes the formation of hydrologic processes within a watershed temporally and spatially by taking the heterogeneity of the watershed into account. The WEHY model is a physically-based model that

uses the conservation of mass, momentum, and/or energy equations of water flow in surface and subsurface flow domains of a watershed.

The emerging parameters in the WEHY model are areal averages and areal variances/covariances of the original point-scale parameter values. It is possible to implement and use the WEHY model at any ungauged or sparsely gauged watershed since its parameters are estimated directly from the land features of the watershed. The WEHY model can be used either for event-based runoff prediction, or for long-term continuous-time runoff prediction. Detailed descriptions of the WEHY model have been given previously elsewhere (Kavvas et al., 2004; Chen et al., 2004a, b; Kavvas et al., 2006). In order to validate the model's applicability and reliability over a certain watershed, the model must be calibrated and validated appropriately, as will be discussed in the following sections.

A. Implementation and Use of the WEHY Snow Module over Upper Middle Fork

A snow module is an important component of any watershed hydrology model that is to be applied over snow-dominated watersheds. This is because in such watersheds, large portions of the precipitation may fall as snow and may be stored in the snowpack of the mountainous areas, thus affecting the hydrologic regime in such regions. With the high-elevation regions present within the Upper Middle Fork (UMF) watershed, which is usually snow-covered in the winter seasons, it is crucial to take into account the snow accumulation and melting processes during the modeling procedure in order to accurately estimate the runoff process within this watershed. This was taken into account by implementing the WEHY snow module over the UMF watershed.

The snow module component of the WEHY model is a spatially distributed, physically-based energy budget model. It incorporates the effect of topography-modified solar radiation on the spatial distribution of snow melt, snow temperature, and snow depth, explicitly, by using depth-averaged energy balance equations (Horne & Kavvas, 1997; Ohara & Kavvas, 2006). The snow module models the amount of precipitation water kept in the snowpack and the released water from the snowpack in time. Some of the inputs to the snow module include precipitation, air temperature, relative humidity, and wind speed, whereas the module provides several output variables including snow depth and snow water equivalent. A schematic description of the WEHY snow module can be seen in **Figure 15** and **Figure 16**. **Figure 16** depicts how the

module divides the snowpack vertically into three layers: a skin layer, a top active layer, and a lower inactive layer.

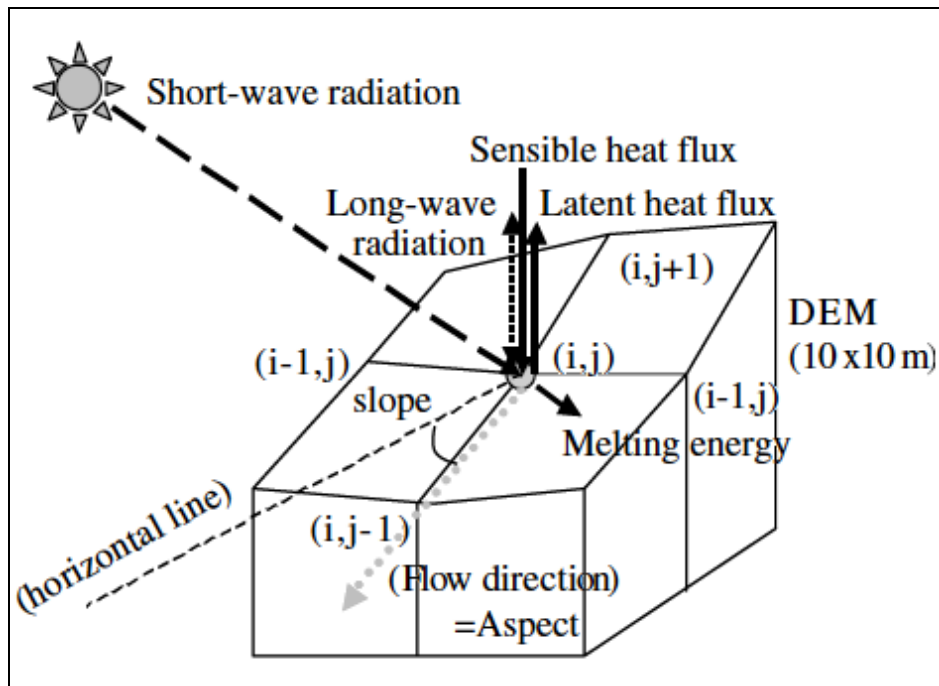


Figure 15. Sketch of the spatially distributed snow model. Source: Ohara & Kavvas (2006).

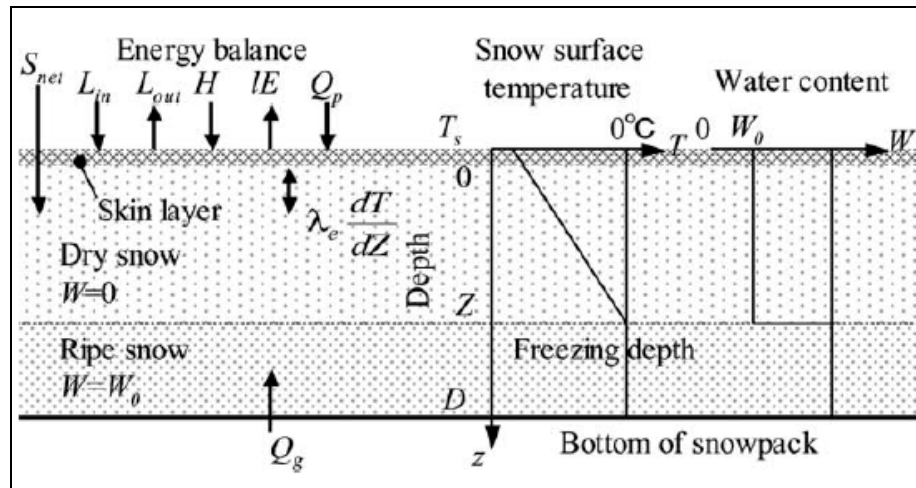


Figure 16. Illustration of the approximation of snow temperature vertical profile. Source: Ohara & Kavvas (2006).

The snow module simulations were run over UMF by using the reconstructed, mean monthly bias-corrected NCAR/NCEP global reanalysis hydro-climate data that were dynamically-downscaled to a spatial resolution of 3 km (1.86 mi.), as discussed previously. Constants and model parameters required for the snow module were determined from the

literature (Ohara & Kavvas, 2006). The snow module simulation results needed to be calibrated and validated to ensure the proper use of the snow module over the UMF watershed. The calibration and validation of the snow module made use of comparisons of the simulated results with observations in order to test the module’s performance. Observations were obtained from the four CDEC (California Data Exchange Center) field observation snow stations selected based on the availability of the required data and the preferred time intervals of the provided data. These useful snow observation stations have already been discussed previously and were shown in **Figure 4**.

Calibration of the snow module was conducted for water year 2006 (i.e., October 2005 through September 2006) by comparing the snow water equivalent (SWE) of the simulated results versus the observed hourly data for the selected four observation stations. The calibration results at the selected stations are depicted in **Figure 17** and their statistical results are shown in **Table 4**.

Table 4. Statistical test values of the simulated and observed snow water equivalent from the selected observation stations (GRZ, FOR, BKL, and PLP) during the calibration period (October 2005 through September 2006). Obs: observed; Sim: simulated; STDEV: standard deviation; RMSE: root-mean-square error; Nash: Nash-Sutcliffe Efficiency.

Parameter	GRZ		FOR		BKL		PLP	
	Obs	Sim	Obs	Sim	Obs	Sim	Obs	Sim
Mean (m)	0.28	0.38	0.24	0.21	0.40	0.27	0.41	0.48
STDEV (m)	0.32	0.36	0.35	0.27	0.49	0.37	0.46	0.38
RMSE (m)	0.14		0.10		0.21		0.15	
Nash	0.80		0.92		0.82		0.89	
Correlation Coefficient	0.96		0.98		0.97		0.96	

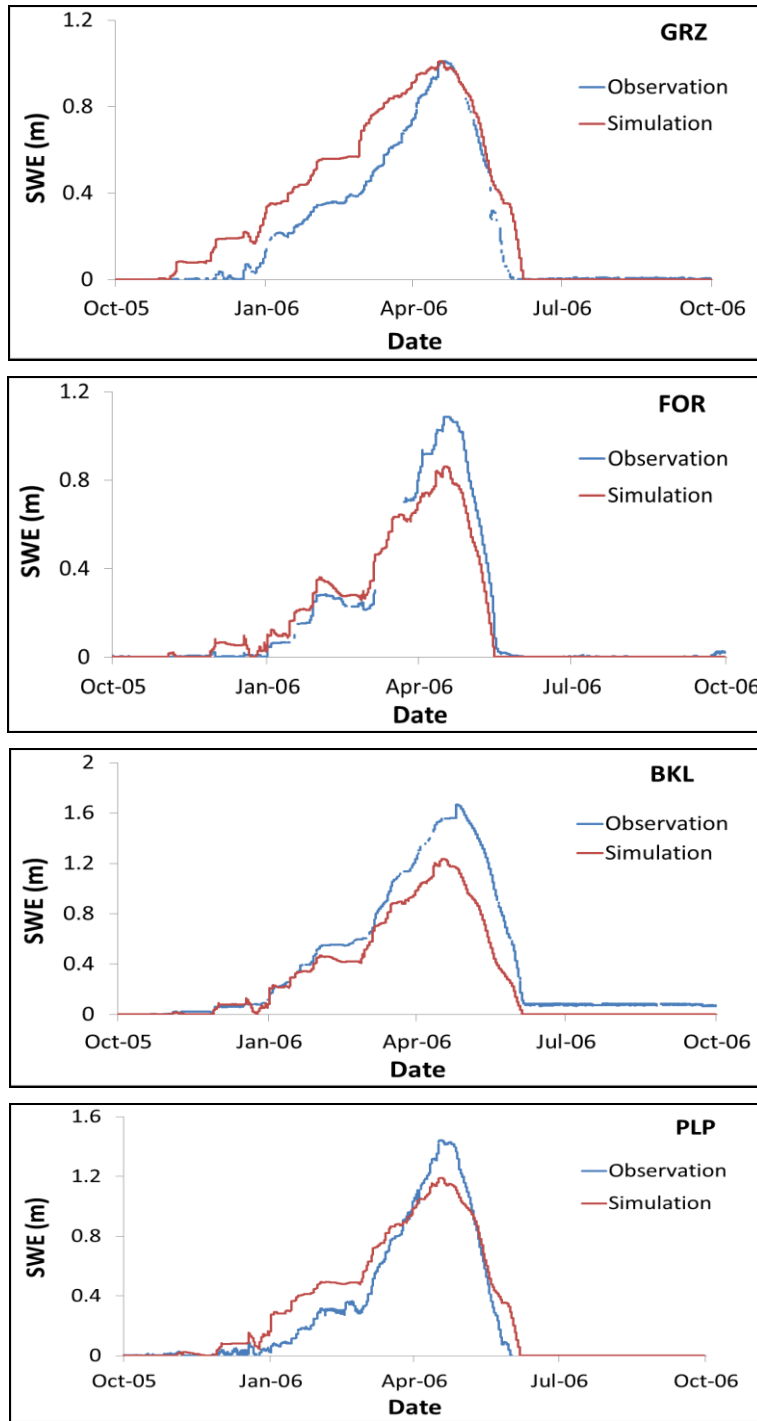


Figure 17. Time series of the observed and simulated snow water equivalent (SWE) at the selected field observation sites from October 2005 through September 2006 (calibration period).

From **Figure 17** and **Table 4**, one can see that the simulated SWE values are similar to their corresponding observed values, while the statistical test results show the performance of the

WEHY snow module with high values of correlation coefficient and Nash-Sutcliffe Efficiency (Nash).

While calibration is an important step for any model, validation provides the confidence needed in the simulated results of the model at hand. The validation period for the WEHY snow module was chosen to extend for a period of 10 years, from October 1, 2000 through September 30, 2010. Again, the SWE results simulated by the snow module over the validation period were compared against the observed results obtained from the observation stations, over the same period. The comparison results were plotted as shown in **Figure 18** and the results of the statistical tests are shown in **Table 5**.

Table 5. Statistical test values of the simulated and observed snow water equivalent from the selected observation stations (GRZ, FOR, BKL, and PLP) during the validation period (October 2000 through September 2010). Obs: observed; Sim: simulated; STDEV: standard deviation; RMSE: root-mean-square error; Nash: Nash-Sutcliffe Efficiency.

Parameter	GRZ		FOR		BKL		PLP	
	Obs	Sim	Obs	Sim	Obs	Sim	Obs	Sim
Mean (m)	0.25	0.28	0.22	0.17	0.51	0.36	0.29	0.33
STDEV (m)	0.25	0.27	0.30	0.24	0.51	0.38	0.34	0.35
RMSE (m)	0.08		0.13		0.27		0.10	
Nash	0.91		0.80		0.72		0.91	
Correlation Coefficient	0.96		0.92		0.91		0.96	

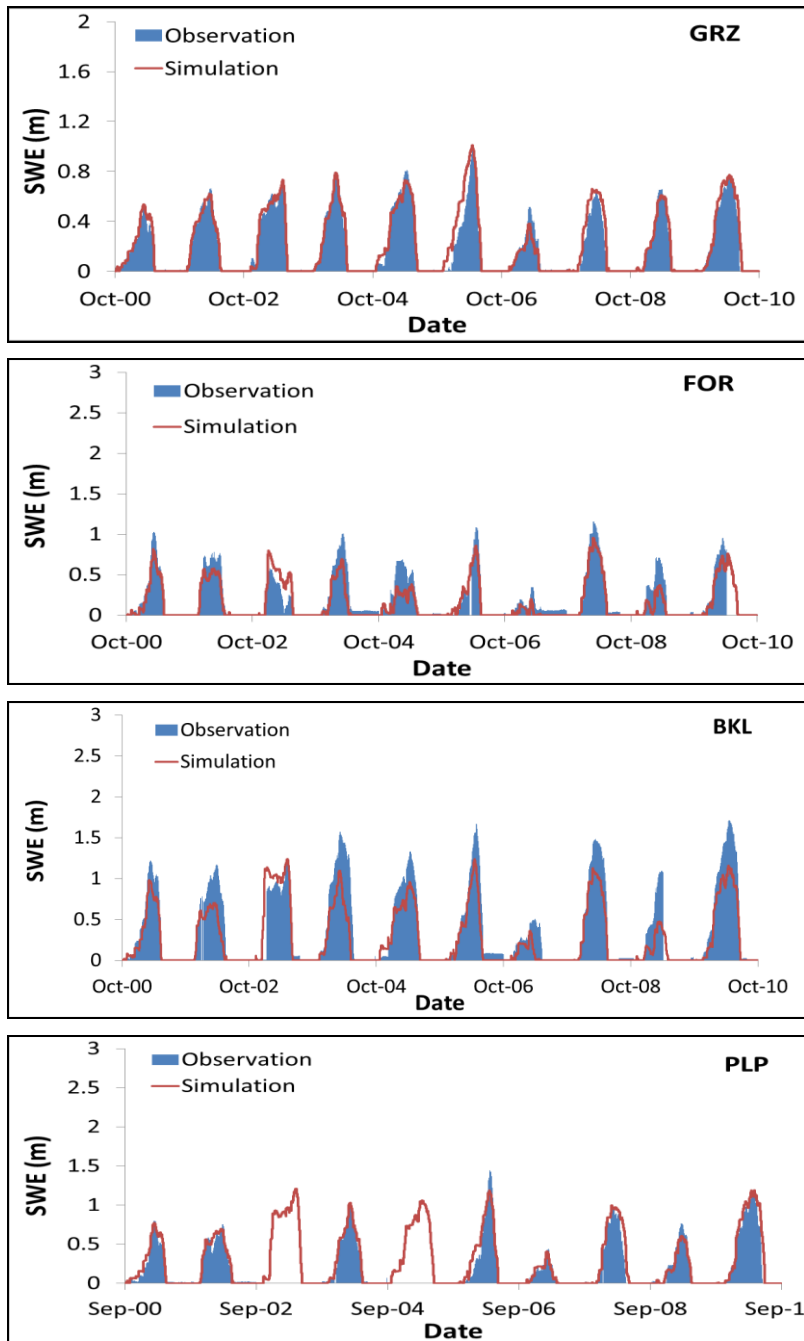


Figure 18. Time series of the observed and simulated snow water equivalent (SWE) at the selected field observation sites from October 2000 through September 2010 (validation period). Water years 2003 and 2005 were neglected from the analysis of PLP due to obvious erroneous data for these years.

As shown in **Figure 18**, one can see that the simulated SWE values are closely distributed along the time-series observed values from all four ground observation stations.

Table 5 shows that the mean and standard deviation between the observed and simulated values are close for most stations. The high values of the correlation coefficient (> 0.91) and Nash-Sutcliffe Efficiency (>0.72) indicate a reliability of performance of the WEHY snow module in its snow simulations over the UMF watershed. Furthermore, the spatial distribution of the WEHY snow module simulation results was evaluated against the observed snow cover obtained from MODIS (Moderate-Resolution Imaging Spectroradiometer) satellite driven data for the month of April in each 2008, 2009 and 2010 (**Figure 19**). As shown in **Figure 19**, the simulated snow spatial distributions almost perfectly match their corresponding observed spatial distributions from MODIS satellite driven data.

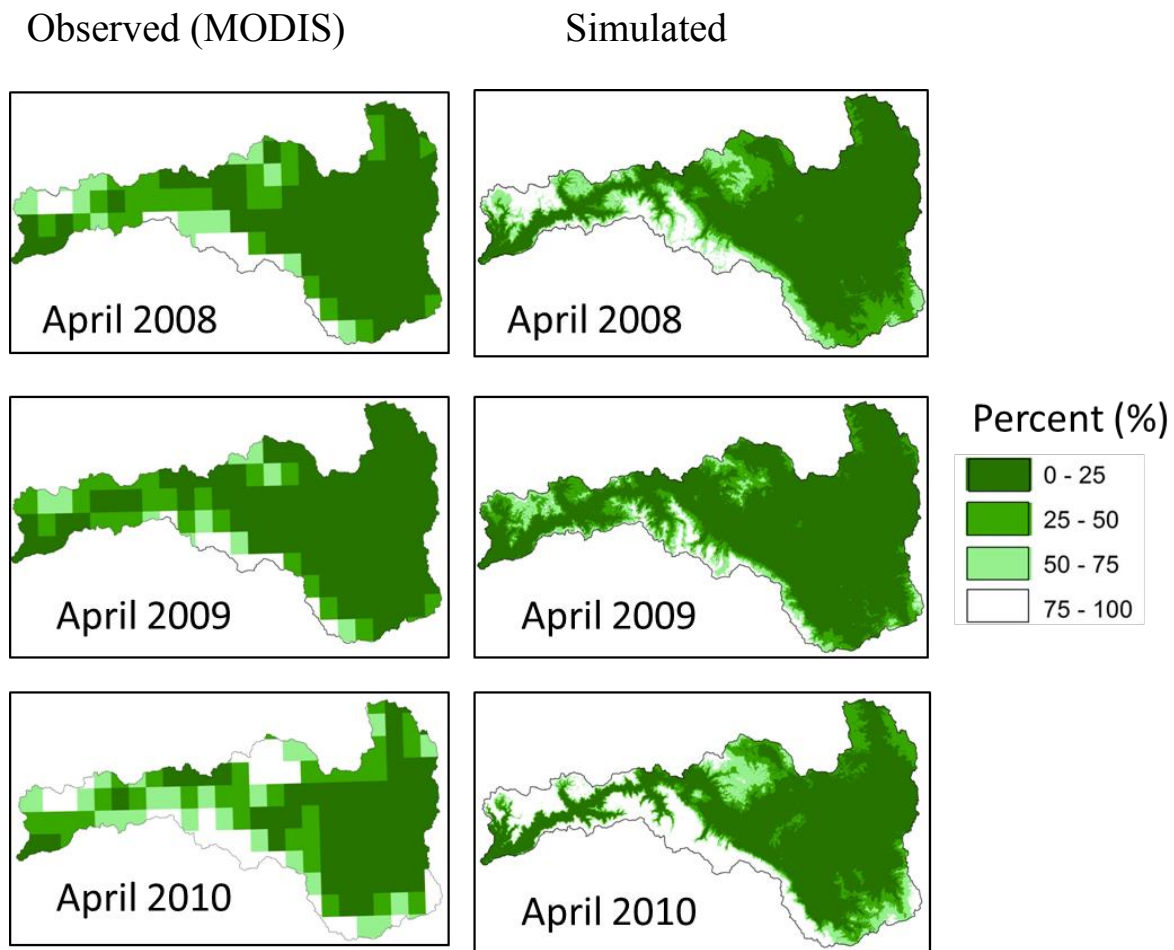


Figure 19. Model-simulated snow water extent and their corresponding observed snow cover percent (MODIS) for the month of April for each of 2008, 2009, and 2010 (within the validation period).

Therefore, the results from **Figure 18**, **Figure 19** and **Table 5** show that WEHY snow module can perform temporally and spatially well compared to the corresponding observations,

and they indicate the possibility and capability of the WEHY snow module to be applied with confidence to the UMF watershed.

B. Implementation and Use of the Hydrologic Module of the WEHY Model over Upper Middle Fork

Recall that the WEHY model is a spatially distributed watershed hydrology model that utilizes upscaled hydrologic conservation equations to account for the effect of heterogeneity within natural watersheds. WEHY divides a watershed into several model computational units (MCUs) based on the digital elevation map (DEM). These MCUs are either individual hillslopes or first-order watersheds. The WEHY model computes the surface and subsurface hillslope hydrologic processes that take place at these MCUs, in parallel and simultaneously. These computations yield the flow discharges to the stream network and the underlying unconfined groundwater aquifer of the watershed that are in dynamic interaction, both with the surface and subsurface hillslope processes at MCUs as well as with each other (as seen in **Figure 20** and **Figure 21**). These discharged flows are then routed by means of the stream network and the unconfined groundwater aquifer routing (Kavvas et al., 2004). A schematic description of the WEHY model is shown in **Figure 20**. A structural description of the WEHY model is shown in **Figure 21**.

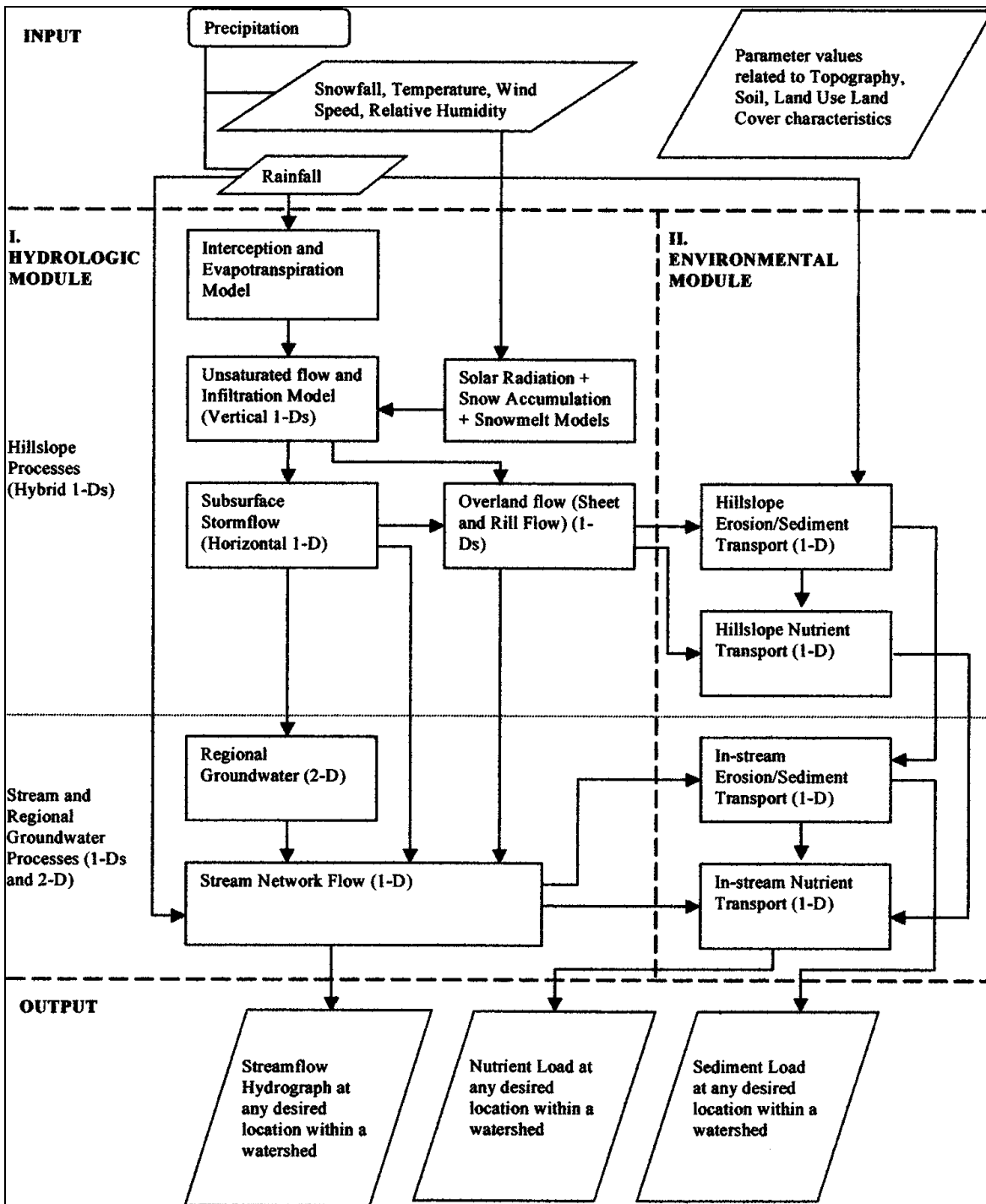


Figure 20. Schematic description of the WEHY model. Source: Kavvas et al. (2004).

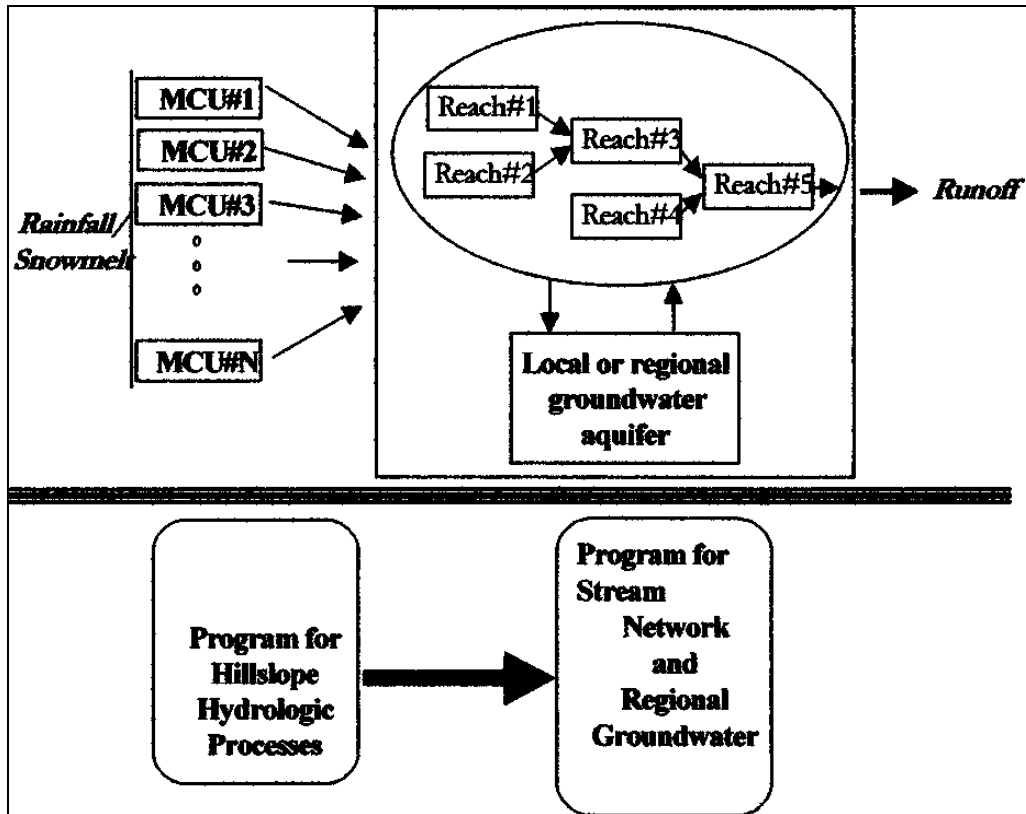


Figure 21. Structural description of the WEHY model. Source: Kavvas et al. (2004).

In a previous section, the Geographic Information System (GIS) database was shown to be set up and completed over the UMF watershed, including spatial information regarding elevations, soil types, and land use/land covers. The land use/land cover dataset (**Figure 2**) and the soil survey dataset (**Figure 5**) were processed and analyzed for their land surface and soil physical parameters and for quality control purposes. A set of lookup tables was established for the land cover types and soil map units that cover the UMF watershed. Moreover, from the 1 arc-second Digital Elevation Model (DEM), an aspect map, a slope map, and a preliminary river channel network were obtained for the areas that cover the UMF watershed. **Figure 22** and **Figure 23** show the sample spatial maps of the DEM and slope, respectively, for the UMF watershed.

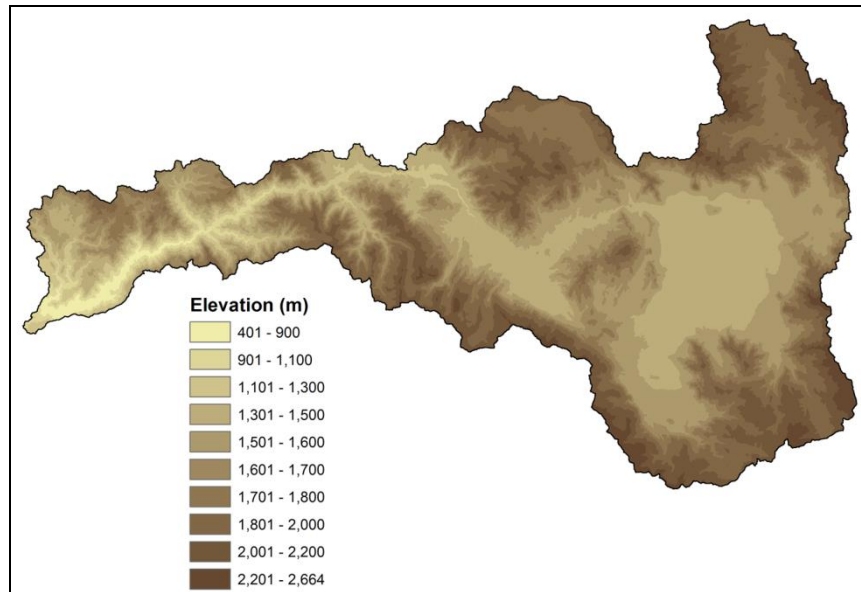


Figure 22. Digital Elevation Model (DEM) from the National Elevation Dataset (NED) over the UMF watershed.

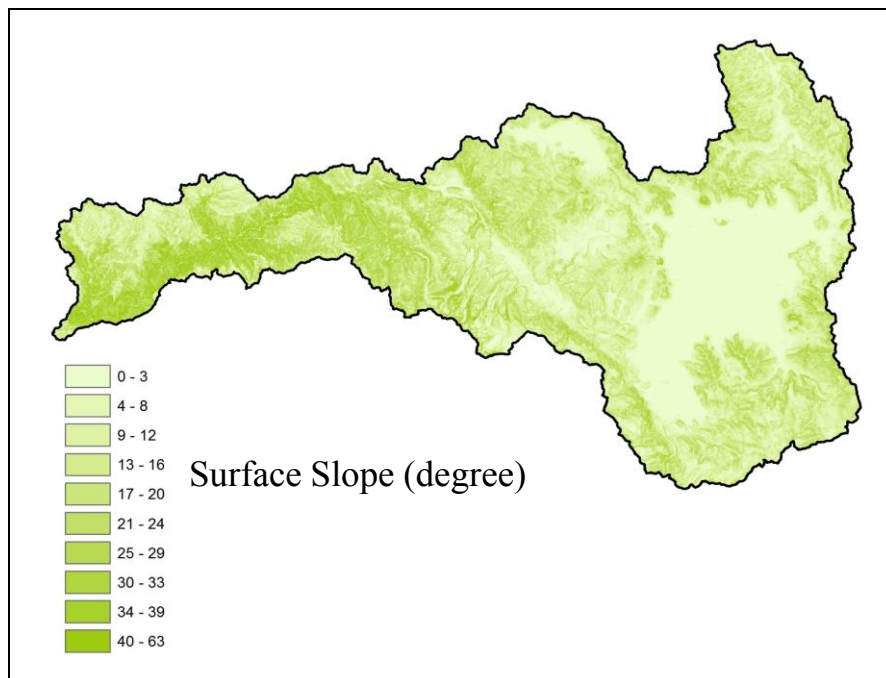


Figure 23. Surface slope over the UMF watershed.

While having such detailed information over the whole UMF watershed is required, it is also important to estimate parameters for each stream reach and MCU, in order to be used for computational purposes. These parameters were estimated directly from the prepared GIS database. Estimation of the geomorphologic, soil hydraulic, and vegetation parameters for the

MCUs of the WEHY model, as was described by Chen et al. (2004a) in detail, was performed by first overlaying the boundaries of the MCUs on the DEM map, the soil class map, and the vegetation class map. Then all of the parameters of an MCU were retrieved from the GIS data associated with the grid cells inside the boundary of that MCU. Note that the WEHY model requires that the land surface parameters (leaf area index, roughness height, albedo, emissivity and vegetation root depth) and soil hydraulic parameters (saturated hydraulic conductivity, soil depth, soil porosity and bubbling pressure) be estimated with a time and spatial variability in order to account for the heterogeneity within the watershed. However, as explained in the paper by Chen et al. (2004a), stationary heterogeneity of parameters within a hillslope was assumed. Consequently, the same mean and variance values of the parameters at the hillslope scale were used for all transects within that hillslope.

Starting with the land surface/vegetation parameters, the monthly mean Leaf Area Index (LAI) values were developed from Moderate Resolution Imaging Spectroradiometer (MODIS) satellite driven data which has 1 km spatial resolution; results over UMF are shown in **Figure 24**. Other land surface parameters such as vegetation root depth, roughness height, surface albedo, and emissivity were estimated based on the multi-source land cover data in **Figure 2** by means of California Wildlife Habitat Relationships (CWHR) and reference information from Asner et al. (2003) and Canadell et al. (1996). These vegetation parameters are important to calculate the evapotranspiration and snow accumulation and melting in the land surface processes. The samples of the vegetation root depth and the roughness height are shown in **Figure 25**.

Finally, soil parameters such as average soil depth, mean total porosity, mean residual saturation, mean bubbling pressure, mean pore size index, soil erodibility factor, mean hydraulic conductivity, and variance of hydraulic conductivity were estimated based on the Soil Survey Geographic (SSURGO) Database (Natural Resources Conservation Service, NRCS) in **Figure 5** by means of reference information from Gale and Grigal (1987), Canadell et al. (1996), McCuen et al. (1981), Rawls et al. (1982) and Yoshitani et al. (2002). The samples of the estimated soil parameters are shown in **Figure 26** (a-h).

The estimated geomorphologic, soil hydraulic, and vegetation/land surface parameters were all stored in the GIS database for this project. Furthermore, the geomorphologic parameter

file for the hydrologic module of the WEHY over the Upper Middle Fork watershed model was obtained by means of the estimated parameters.

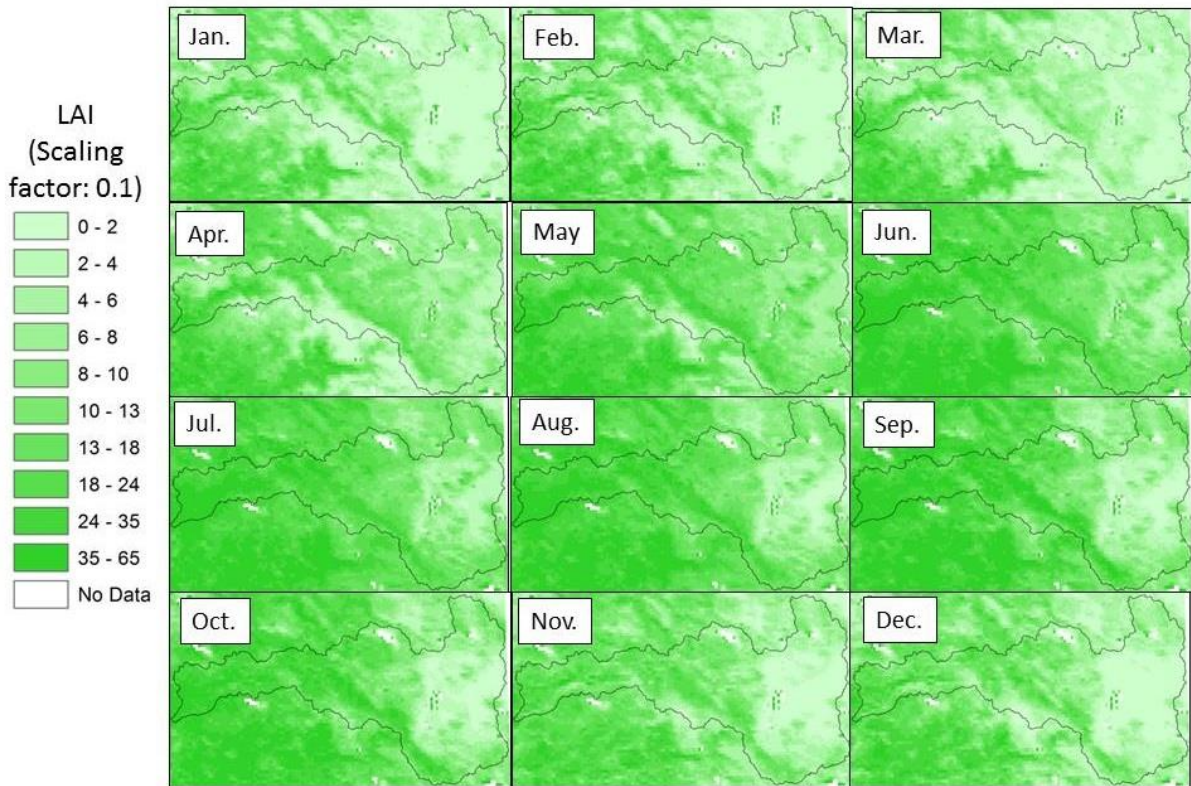


Figure 24. MODIS monthly leaf area index (LAI) over the Upper Middle Fork watershed.

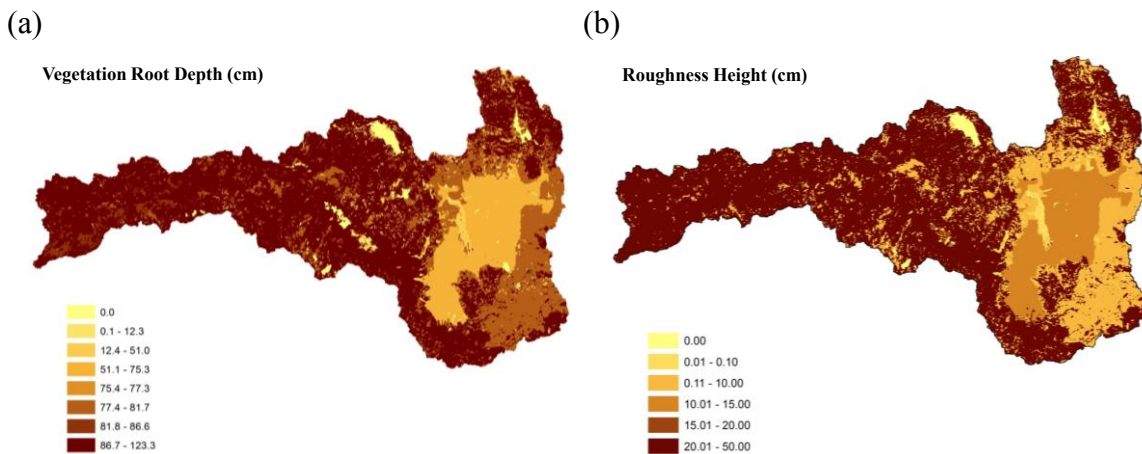


Figure 25. Sample of distributed land surface parameters from database over the Upper Middle Fork watershed.

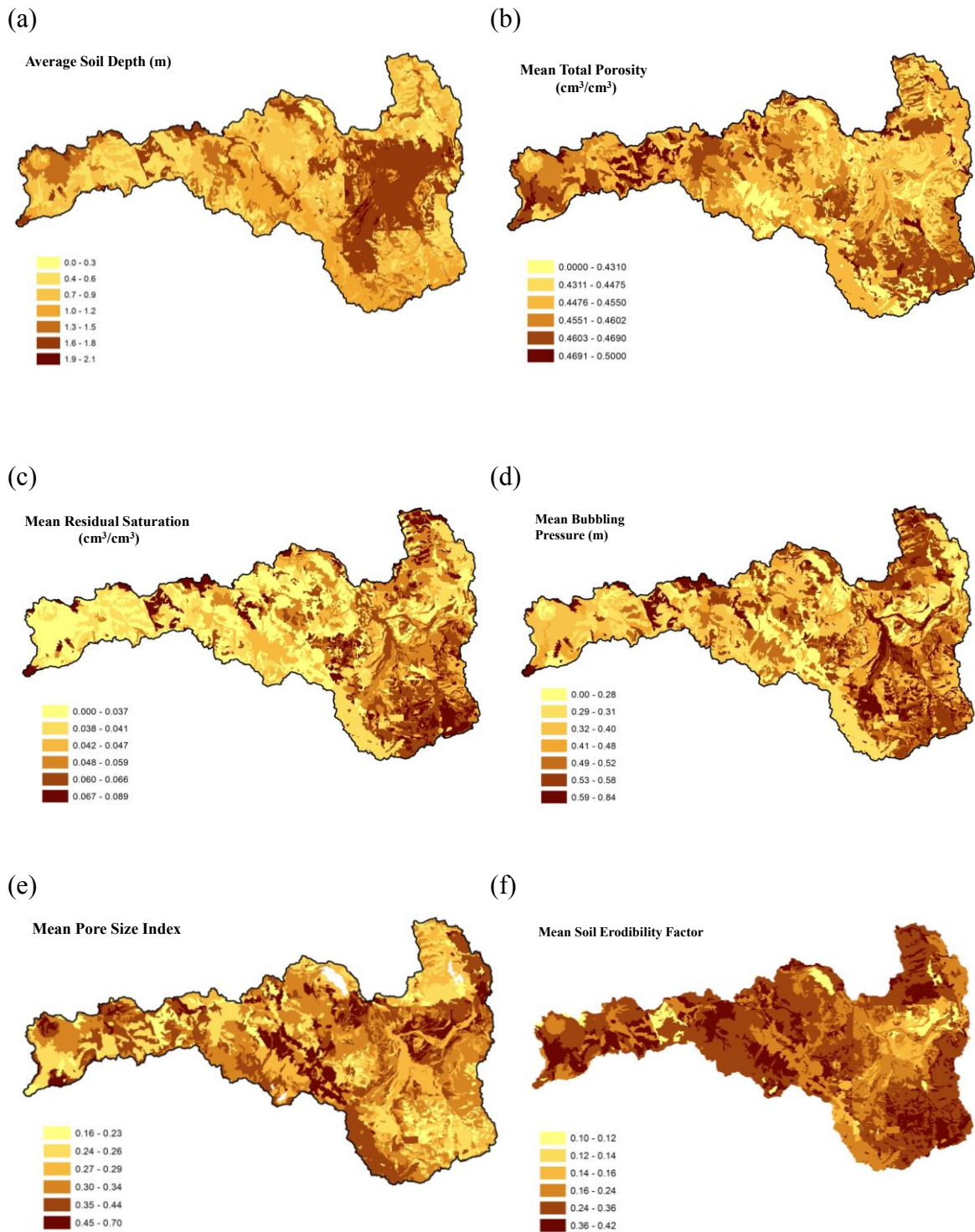


Figure 26. Samples of distributed soil hydraulic parameters from database over the Upper Middle Fork watershed (continued below).

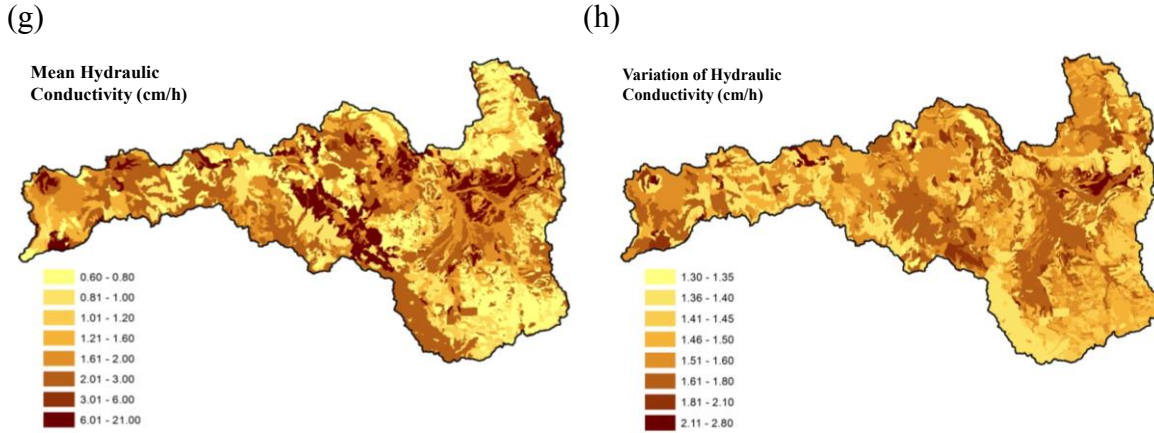


Figure 26 (continued). Samples of distributed soil hydraulic parameters from database over the Upper Middle Fork watershed.

Just as the WEHY snow module was calibrated and validated, the calibration and validation of the WEHY model is also an essential step to ensure its proper use for the proposed project area, UMF. In this regard, simulations of the WEHY model were run by using the reconstructed, mean monthly bias-corrected hydro-climate data at a spatial resolution of 3 km over the watershed, based on the dynamical downscaling of NCAR/NCEP global reanalysis data. Outputs from the previously calibrated and validated snow simulations were used as inputs to the WEHY model. The calibration and validation of the WEHY model made use of comparisons of the simulation results of flow discharge with observed flow values in order to test the model's performance. Observations were obtained from one of the two CDEC (California Data Exchange Center) field observation station selected based on the availability of the required data and the length of the provided data (**Figure 4**). This station is the outlet of the watershed, and is called *Feather River at Merrimac* (or alternatively, MER) and is shown in **Figure 4**. Note that this station is also found in the U. S. Geological Survey (USGS) website with an ID of 11394500.

Calibration of the WEHY model was carried out for water year 1997 (October 1996 through September 1997) by comparing the simulated daily flow discharges from the watershed's outlet against the observed data at the MER station. The results of the calibration are depicted in **Figure 27** and their statistical properties are shown in **Table 6**.

From **Figure 27**, one can see that the simulated flow values are similar to their corresponding observed values. Moreover, **Table 6** shows the statistical test results that reveal a

good performance of the WEHY model, which shows relatively close mean and standard deviation values, as well as a high correlation coefficient and Nash-Sutcliffe Efficiency.

Taking the calibration year as an example for the following discussion, note that some observed values in January of 1997, specifically January 1st and 2nd, are missing due to the high peak flows occurring during that period. This may come as a result of the inability of the gaging instruments to read large flow values that may occur during such periods of peak flows. As a result, such missing data may cause the observed mean to be lower than what it actually should be, and will show a lower peak value than the actual value when plotted.

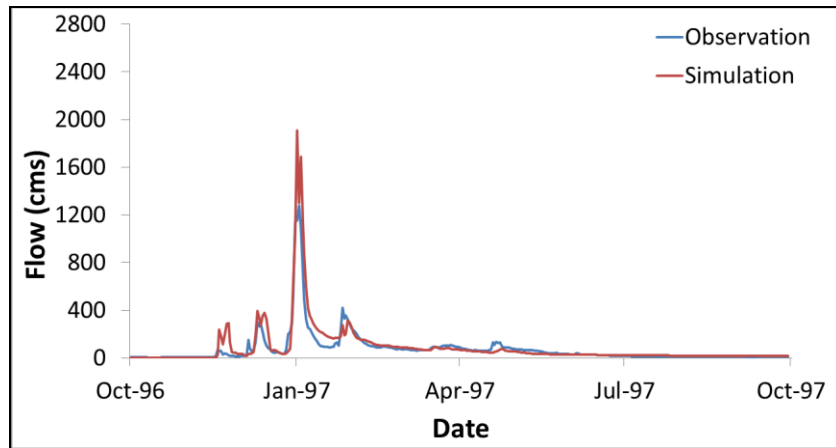


Figure 27. Time series of the observed and model-simulated daily flow discharges at the MER station from October 1996 through September 1997.

Table 6. Statistical test values of simulated and observed daily flow values at the MER station during the calibration period (October 1996 through September 1997). Obs: observed; Sim: simulated; STDEV: standard deviation; RMSE: root-mean-square error; Nash: Nash-Sutcliffe Efficiency.

Parameter	Obs	Sim
Mean (cms)	75.53	87.19
STDEV (cms)	142.56	188.88
RMSE	77.21	
Nash	0.71	
Correlation Coefficient	0.94	

Validation of the WEHY model was done over a 31-year period, extending from water year 1980 to water year 2010 (i.e., from October 1979 through September 2010). The simulation results obtained over this period were plotted against the observed values at the MER station, as shown in **Figure 28**, and their statistical properties are shown in **Table 7**.

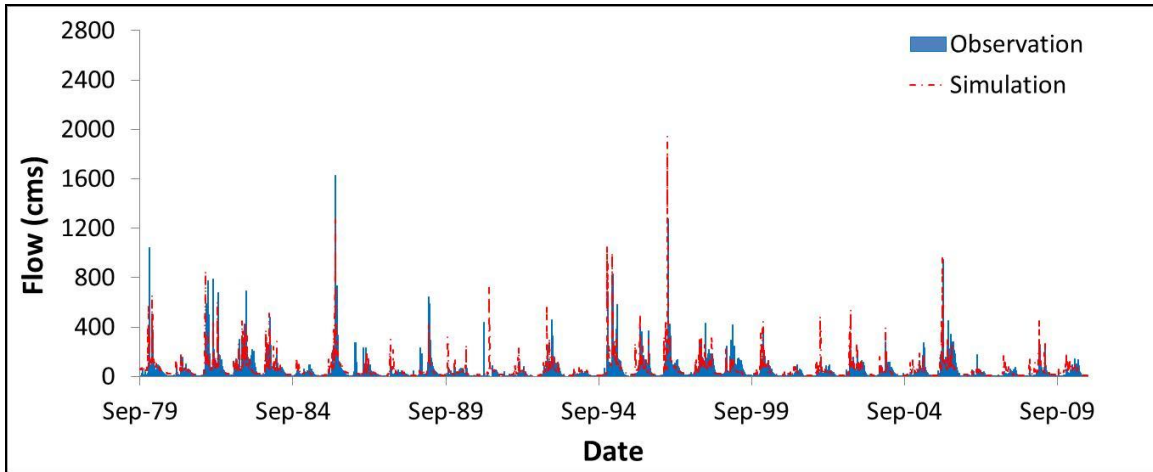


Figure 28. Time series of the observed and model-simulated daily flow discharges at the MER station from October 1979 through September 2010 (validation period).

Table 7. Statistical test values of simulated and observed daily flow discharge values at the MER station during the validation period (October 1979 through September 2010). Obs: observed; Sim: simulated; STDEV: standard deviation; RMSE: root-mean-square error; Nash: Nash-Sutcliffe Efficiency.

Parameter	Obs	Sim
Mean (cms)	42.71	48.85
STDEV (cms)	71.77	77.66
RMSE	49.81	
Nash	0.52	
Correlation Coefficient	0.79	

Figure 28 shows that the simulated flow discharge values are closely distributed along the time-series values of the MER observation station. Moreover, **Table 7** shows that the mean and standard deviation between the observed and simulated values are relatively close, while the Nash-Sutcliffe Efficiency and the high correlation coefficient indicate an acceptable reliable performance for the WEHY model.

However, note again that such a large period of flow comparisons may have missing values of observed peak data as a result of high flows which were not possible to record on the field. Accordingly, the observed peaks of some years may not be as high as the actual ones were. This reason, along with the relatively small size of the UMF watershed, would eventually render it more challenging to obtain high Nash values in the comparison of observed and simulated flows. Nevertheless, the above-discussed results show that the WEHY model can perform well temporally when compared to the corresponding observations, thus revealing its capability and providing confidence in its proper application to the UMF watershed. It is also concluded that the presented dynamical downscaling along with the physically-based distributed hydrology model employed in the project works quite well, and it can be a very useful tool for the future flow prediction and watershed modeling in ungauged or sparsely gauged basins generally, and in the UMF watershed specifically.

8. Simulating Historical Conditions and Future Projections of WEHY using Atmospheric Inputs from Global Climate Models

Following the successful calibration and validation of the Watershed Environmental Hydrology (WEHY) model, as discussed in the previous section, the WEHY model was run over the Upper Middle Fork (UMF) watershed, by using atmospheric results for control runs and future projections from two global climate models (GCMs): CCSM3 and ECHAM5. Simulations were done for the UMF watershed over the simulation periods shown in **Table 3**, using atmospheric results from the CCSM3 and ECHAM5 GCMs. Future simulations used GCM atmospheric results from the previously discussed 13 climate projections.

A sample of the GCM atmospheric results for the future period over the UMF watershed can be seen in **Figure 29**. This figure shows the projected annual precipitation averaged over the UMF basin for each of the 13 different future scenarios, along with their ensemble average and general trendline. The figure shows large variability in the projections for future precipitation over the UMF, but with a subtle negative trend over the future years. Another sample of the GCM atmospheric results can be seen in **Figure 30**, which shows the future projected annual mean basin average temperature over the UMF watershed. Similarly, this figure shows the results for all 13 different projections, as well as the ensemble average of all projections as well

as their trend. While **Figure 30** also shows large variability in the temperature values for the future period, it shows a much clearer trend in the temperature as a function of time during the 21st century. Moreover, the expected trend can be clearly seen to be positive, increasing the temperature over the course of the years along the future period. Additional analysis figures of precipitation and temperature projections over the UMF watershed can be found in Appendix A.

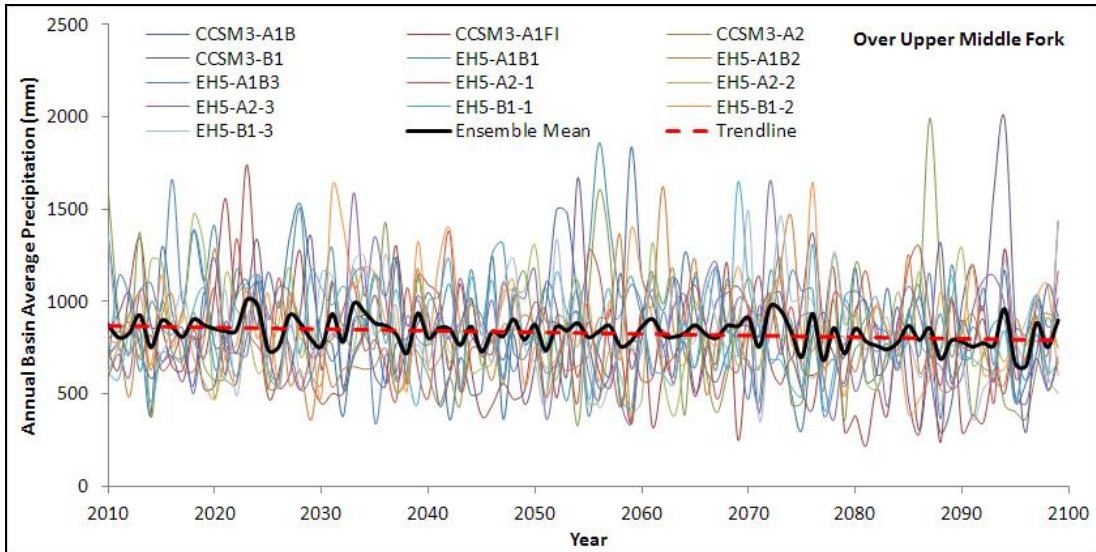


Figure 29. Annual basin average precipitation projected over the UMF watershed as projected by the 13 different GCM scenarios. The ensemble mean and trendline are shown by the black bold and red dashed lines, respectively.

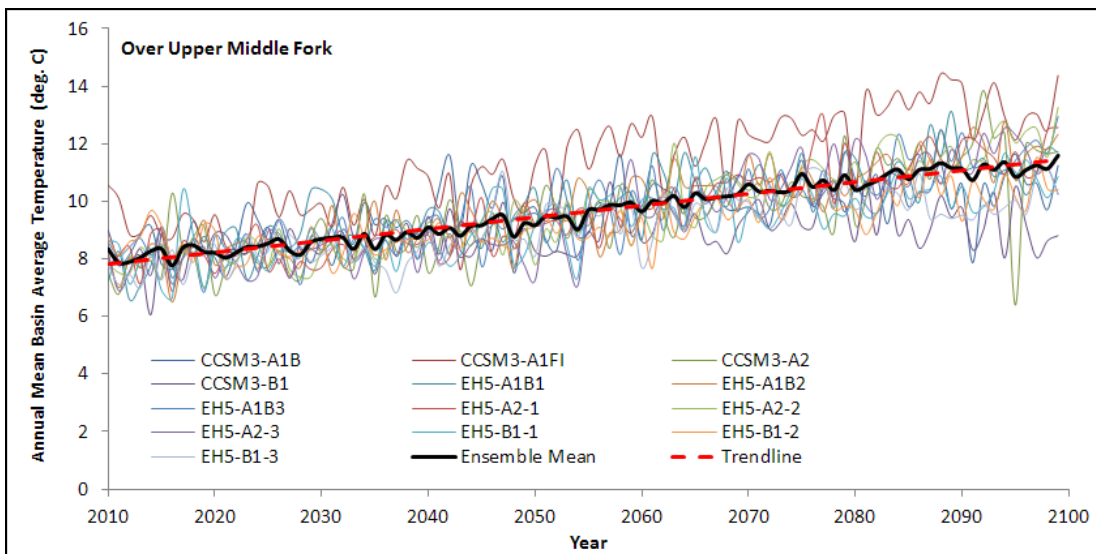


Figure 30. Annual mean basin average temperature over the UMF watershed as projected by the 13 different GCM scenarios. The ensemble mean and trendline are shown by the black bold and red dashed lines, respectively.

Using the GCM future period atmospheric parameters similar to those mentioned above to run the WEHY snow module over the UMF watershed, one would get results of snow parameters over the UMF watershed for the whole future period of the 21st century. An example of the results obtained is the snow depth over the watershed, as shown in **Figure 31** to **Figure 33**. These figures show the snow depth for the ensemble average of all of the 13 projections for three different months: January, March, and May. The snow depth values shown are monthly means and the figures show these monthly means averaged over 10-yr periods throughout the rest of the 21st century. As such, for the month of January for example, **Figure 31** shows 9 plots, each one showing the monthly mean snow depths over the UMF watershed for a certain decade of the 21st century. Therefore, using such figures, one can compare how the snow depth changes on average through the decades as time progresses to reach of the end of this century. One thing that is clear and common among the three figures (**Figure 31**, **Figure 32**, and **Figure 33**) is that the snow depth is projected to be decreasing on average with time. In fact, when comparing the first decade (2010-2020) and last decade (2090-2100) plots of each of the three figures, one can see a clear difference in the amount of the snow depth and its distribution over the watershed. For example, for the month of January, the last plot (2090-2100) of **Figure 31** shows how the snow depth reduces significantly for almost the entire UMF watershed as compared to the first plot (2010-2020). The figures for the months of March and May show a similar significant reduction in snow depth at the end of the century, but being more severe along the middle and eastern portions of the UMF watershed. Projected increases in temperatures as shown in **Figure 30** may have been an important factor in such expected reductions in the snow depth over the 21st century. For completion, please find in Appendix C the comparisons of such snow depth changes over the different decades for the remaining 9 months. Also note that for an even more detailed comparison, Appendix C also provides similar plots for each one of the 13 different projections, and for each of the 12 months. With such figures, it would be possible to analyze how the different projections independently affect the snow depth and distribution for each month over each of the decades within the rest of the 21st century. Figures of other corresponding variables are provided in Appendix D.

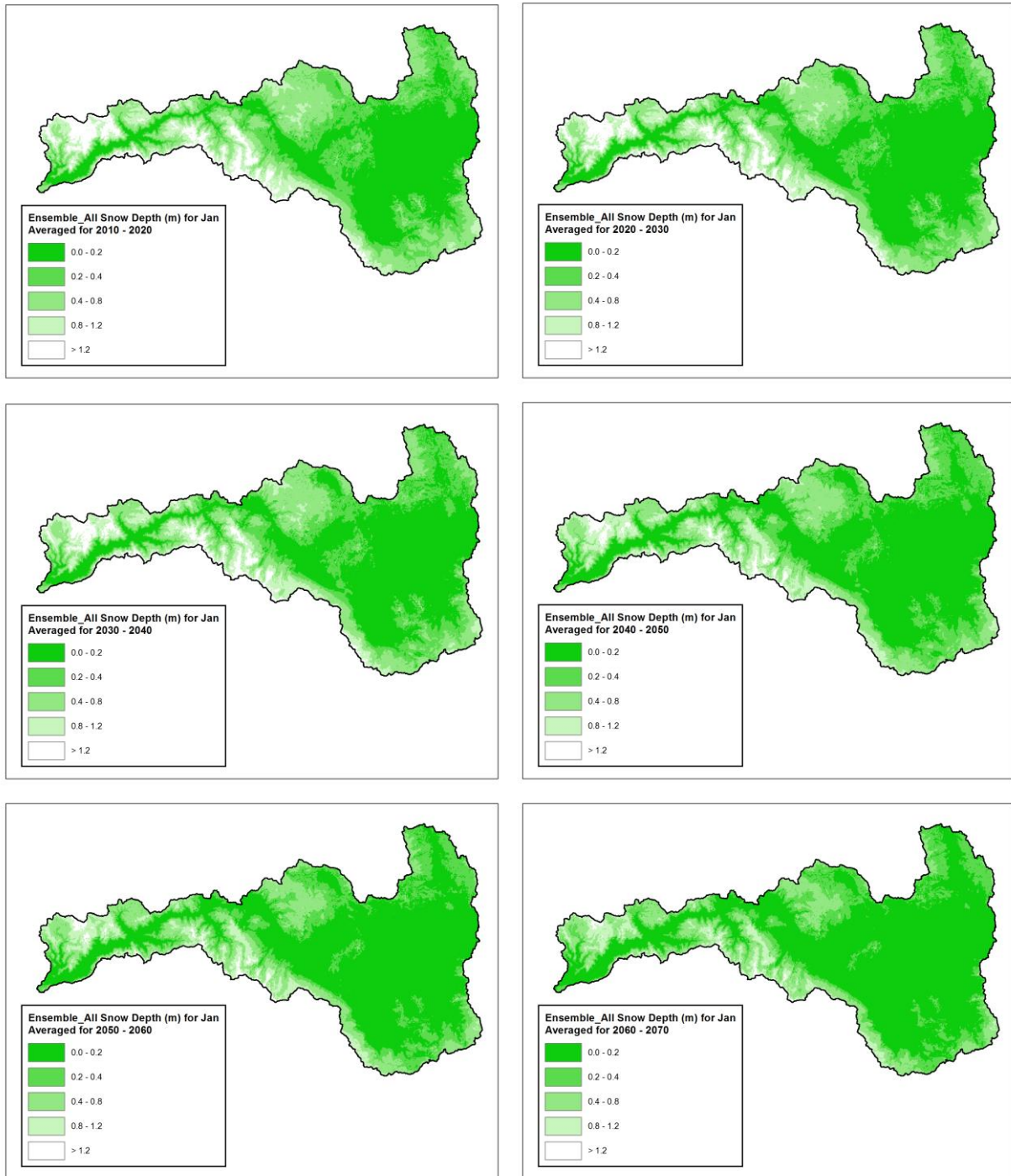


Figure 31. Spatial maps showing the ensemble average snow depth of all projections for the month of January, averaged over 10-yr periods throughout the future 21st century (continued below).

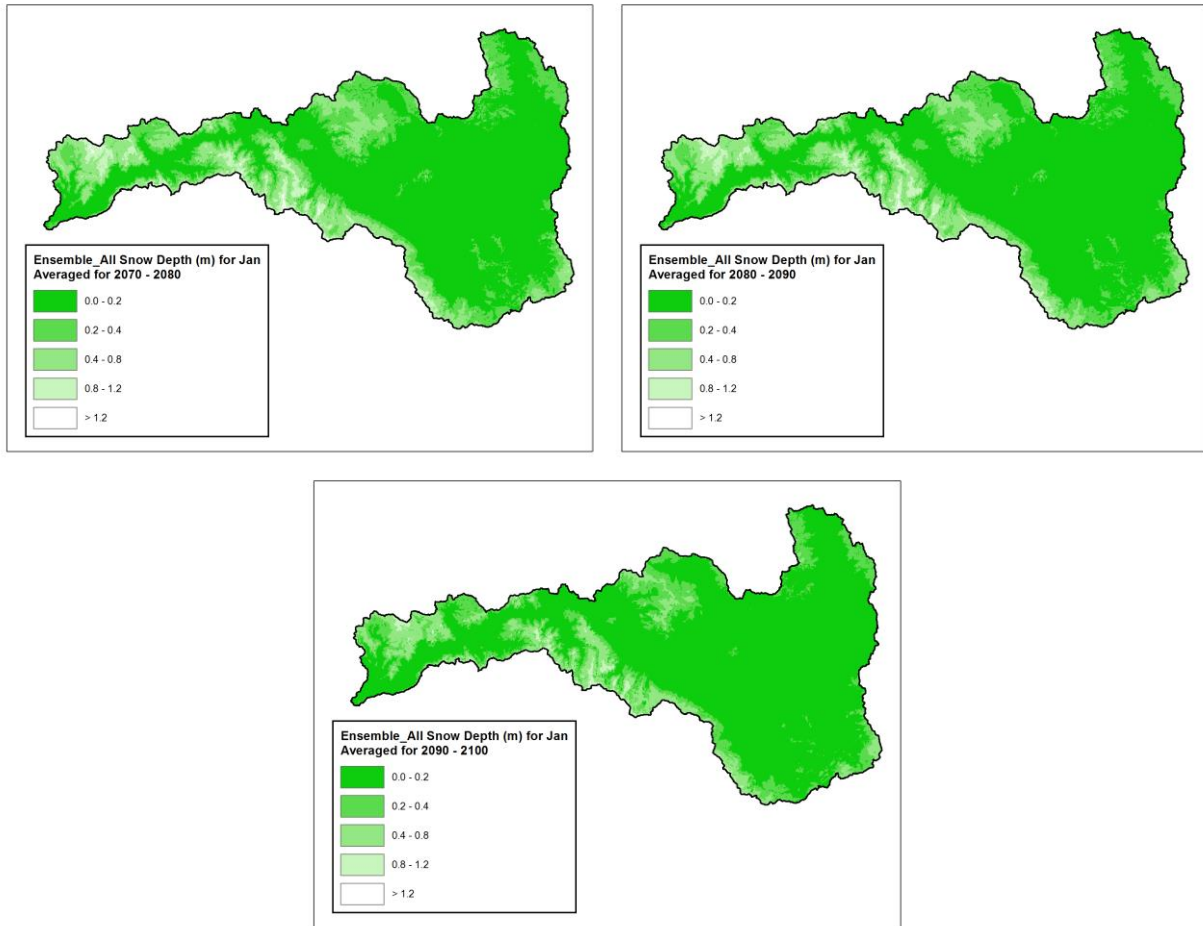


Figure 31 (continued). Spatial maps showing the ensemble average snow depth of all projections for the month of January, averaged over 10-yr periods throughout the future 21st century.

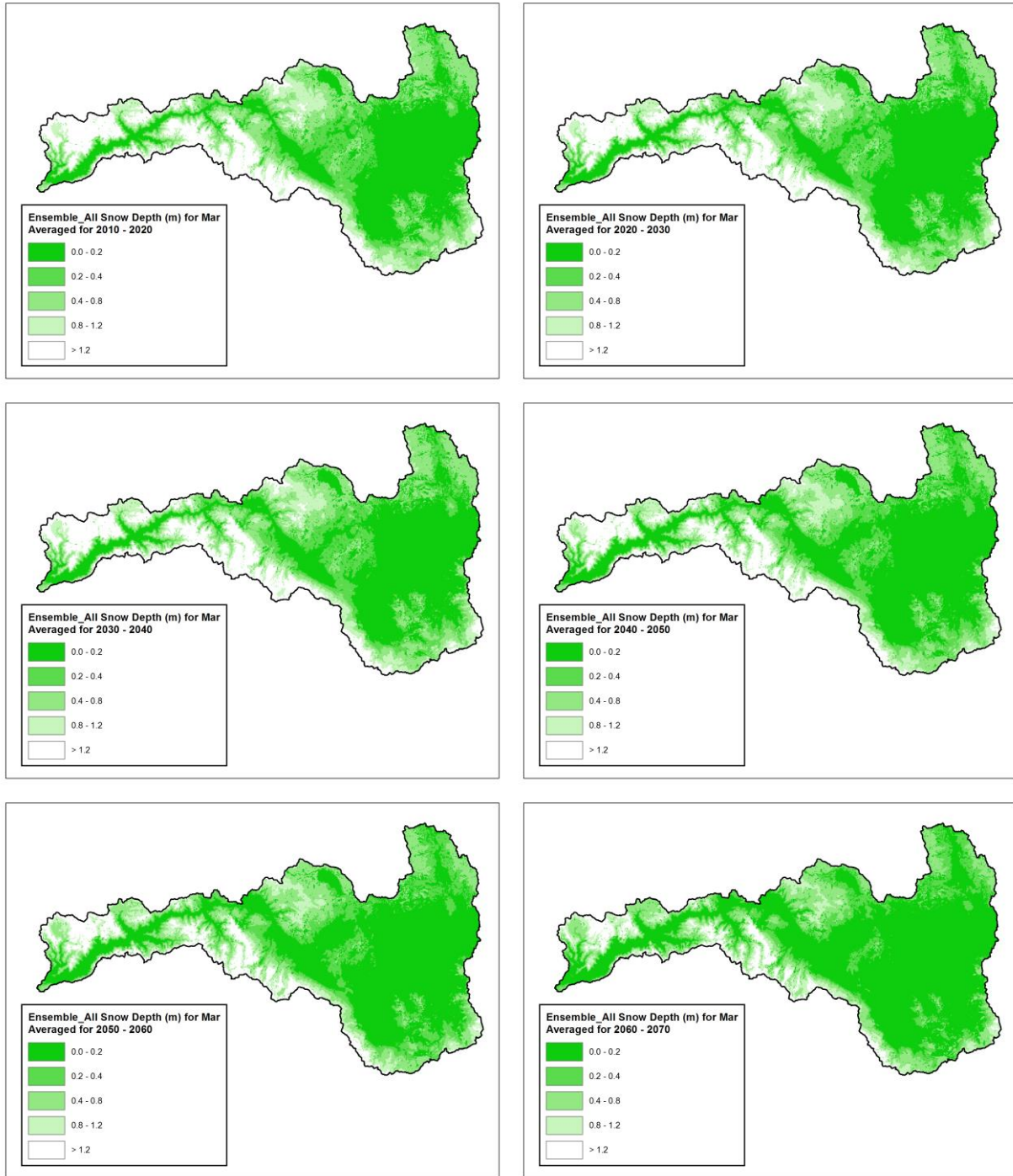


Figure 32. Spatial maps showing the ensemble average snow depth of all projections for the month of March, averaged over 10-yr periods throughout the future 21st century (continued below).

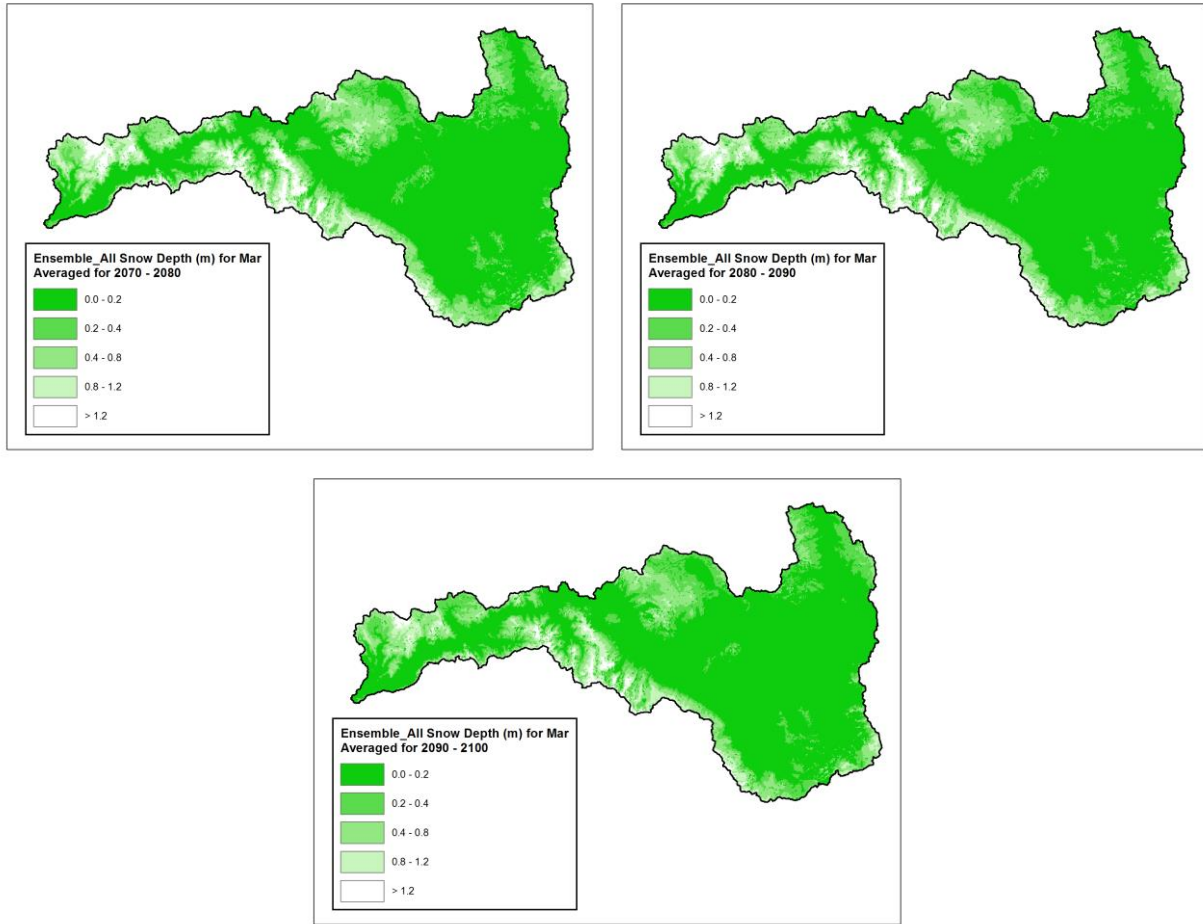


Figure 32 (continued). Spatial maps showing the ensemble average snow depth of all projections for the month of March, averaged over 10-yr periods throughout the future 21st century.

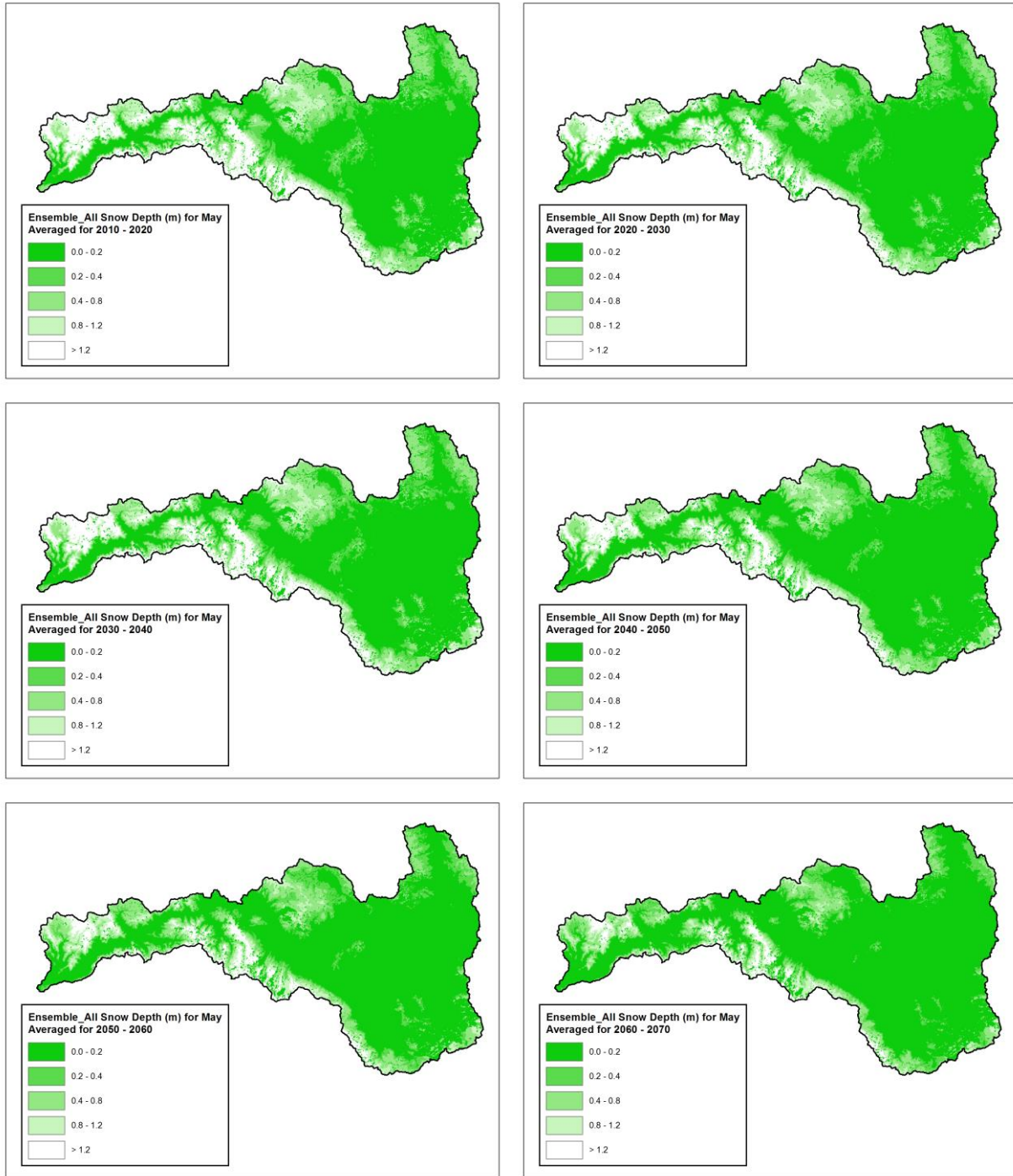


Figure 33. Spatial maps showing the ensemble average snow depth of all projections for the month of May, averaged over 10-yr periods throughout the future 21st century (continued below).

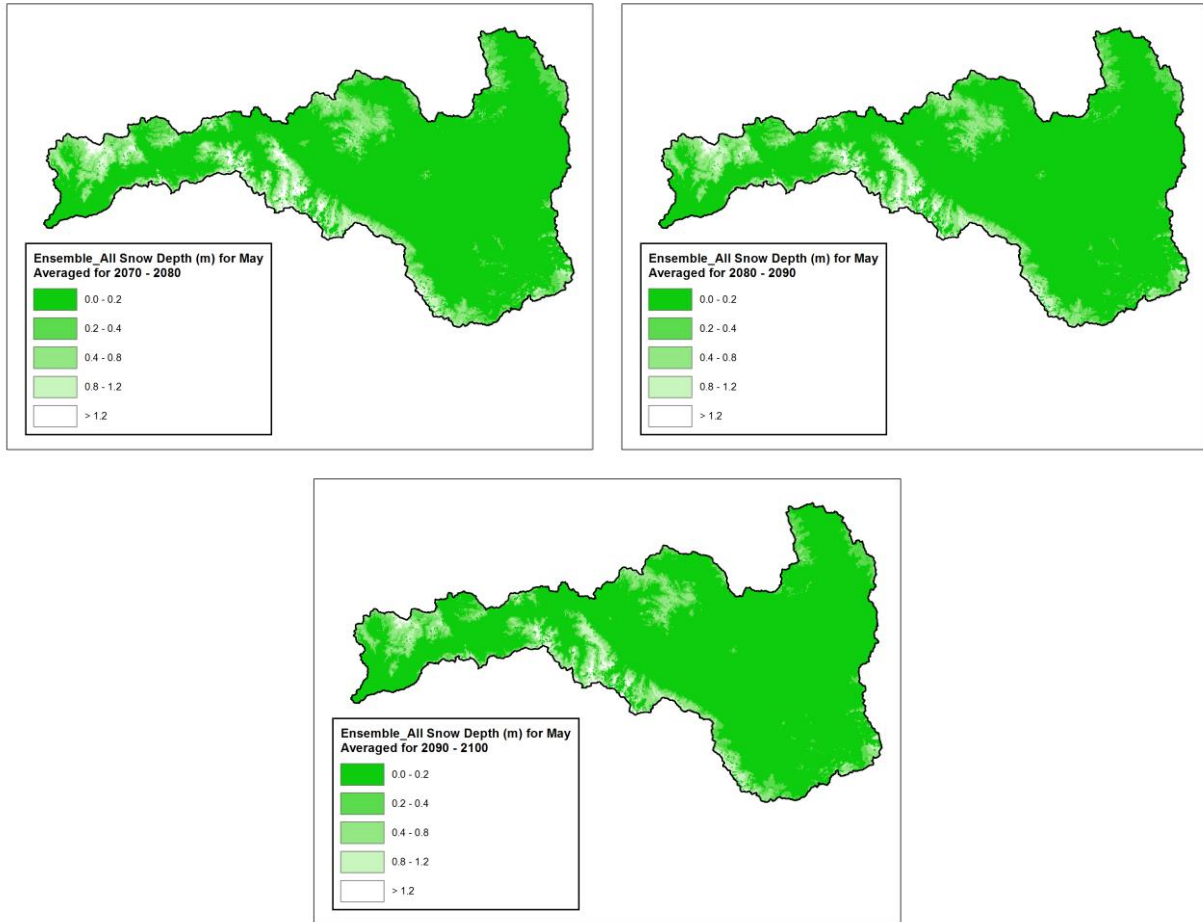


Figure 33 (continued). Spatial maps showing the ensemble average snow depth of all projections for the month of May, averaged over 10-yr periods throughout the future 21st century.

A. Comparison of Future Projected Flows at the Upper Middle Fork Watershed

WEHY simulation results were obtained in hourly increments, but also converted to daily and monthly intervals. **Figure 34** shows the WEHY-simulated future flow results at the watershed outlet (MER station in **Figure 4**) for each of the 13 climate projections in hourly intervals. **Figure 35** shows the hourly average flow among results obtained using the CCSM3-based projections (**Figure 35a**) and the ECHAM5-based projections (**Figure 35b**). The outlet is located at a station called *Feather River at Merrimac* (or alternatively, MER) (**Figure 4**). Note that this station is also found in the U. S. Geological Survey (USGS) website with an ID of 11394500.

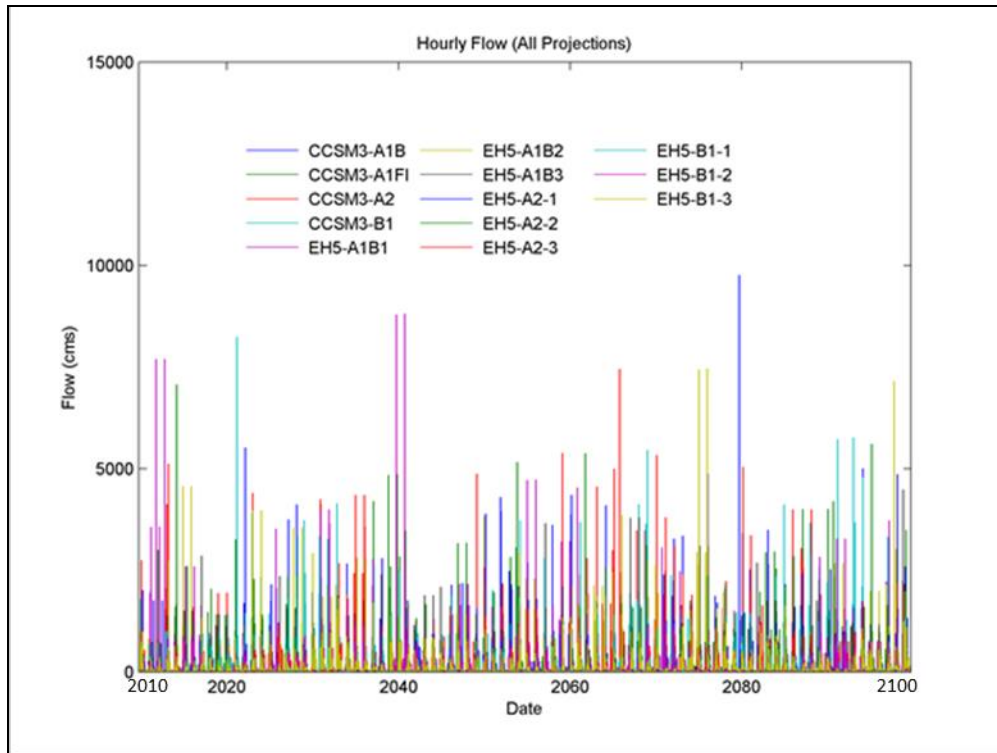


Figure 34. Hourly flow projections at the UMF outlet for years 2010 to 2100, using the 13 different climate projections from the two GCMs (CCSM3 and ECHAM5). Note: ECHAM5 is abbreviated as EH5 in the above figure.

Figure 34 shows that even though some peak flows are projected to fall within 5,000 cms and 10,000 cms (1.77×10^5 cfs to 3.54×10^5 cfs where cfs is cubic feet per second), most peak flows fall below 5,000 cms (1.77×10^5 cfs), compared to the historical peak of around 2,040 cms (0.72×10^5 cfs) that occurred in 1986. Among the WEHY simulations obtained from the four CCSM3 projections, the average flow discharge values over the whole period (2010 to 2100) show very close results for the four projections, with a minimum of around 58.2 cms (for A2; 2.05×10^3 cfs) and a maximum of around 62.5 cms (for A1B; 2.21×10^3 cfs) (**Table 8**). The range, however, is much larger among the ECHAM5 (EH5) results, with the maximum being around 59.4 cms (A1B1; 2.10×10^3 cfs) and the minimum as low as 50.6 cms (B1-1; 1.79×10^3 cfs). Therefore, **Table 8** shows that the highest average of flow discharges within the years 2010 to 2100 is projected by the CCSM3-A1B and the lowest is projected by ECHAM5-B1-1. It also shows that the average of the future flows in general is larger for CCSM3 compared to ECHAM5 simulations.

Table 8. Average future projected flows at the UMF outlet over the period spanning the years from 2010 to 2100.

GCM-Scenario	Flow (cms)
<i>CCSM3-A1B</i>	62.50
<i>CCSM3-A1FI</i>	60.23
<i>CCSM3-A2</i>	58.21
<i>CCSM3-B1</i>	58.73
<i>EH5-A1B1</i>	59.36
<i>EH5-A1B2</i>	51.47
<i>EH5-A1B3</i>	56.46
<i>EH5-A2-1</i>	53.90
<i>EH5-A2-2</i>	54.50
<i>EH5-A2-3</i>	53.56
<i>EH5-B1-1</i>	50.59
<i>EH5-B1-2</i>	58.16
<i>EH5-B1-3</i>	55.30

Figure 35 enforces the above conclusion, since one can see that the ensemble average of the WEHY-simulated flow discharges following the CCSM3 atmospheric simulations (**Figure 35a**) are larger than the ensemble average of the results obtained using the EHCAM5 atmospheric results (**Figure 35b**). In fact, the former reveals several projected hourly outlet flow discharges that exceed 1,000 cms (0.35×10^5 cfs) and may even cross the 2,000 cms (0.71×10^5 cfs) line, while the latter shows almost all projected flow discharges being below the 1,000 cms line. Moreover, averaging the results of all the 13 projections (**Figure 36**) shows hourly outlet flow discharges that fall within the range of historical observed data, which show only a few high flows (exceeding 1,000 cms or 0.35×10^5 cfs), while most of the rest being less than 550 cms (0.19×10^5 cfs). In **Figure 36**, the simulated flows are within that range of the historical values, being mostly less than 600 cms (0.21×10^5 cfs) but having a few instances that exceed this limit.

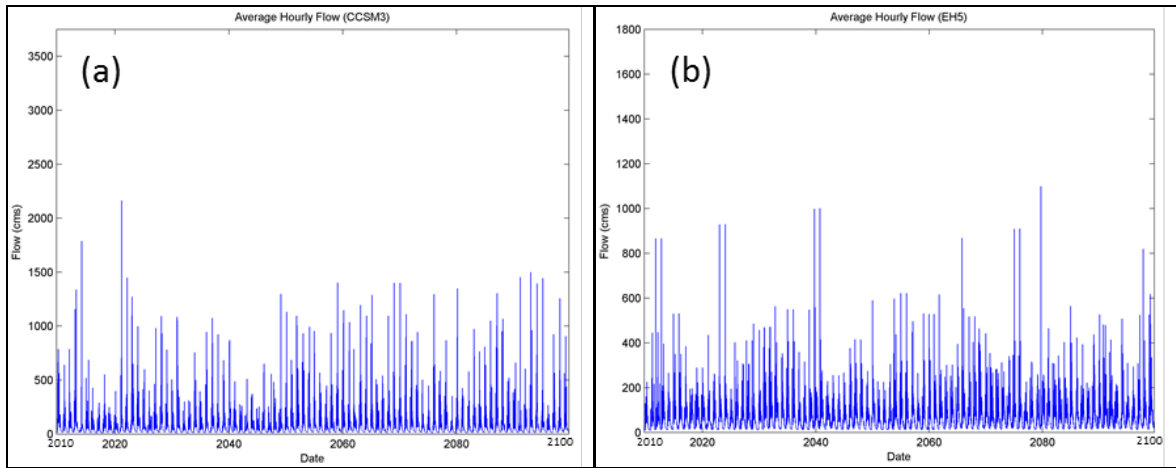


Figure 35. Ensemble average hourly flow projections at the UMF outlet for the period 2010 to 2100 for each of the climate projections of (a) CCSM3 and (b) ECHAM5. Note: ECHAM5 is abbreviated as EH5 in the above figure.

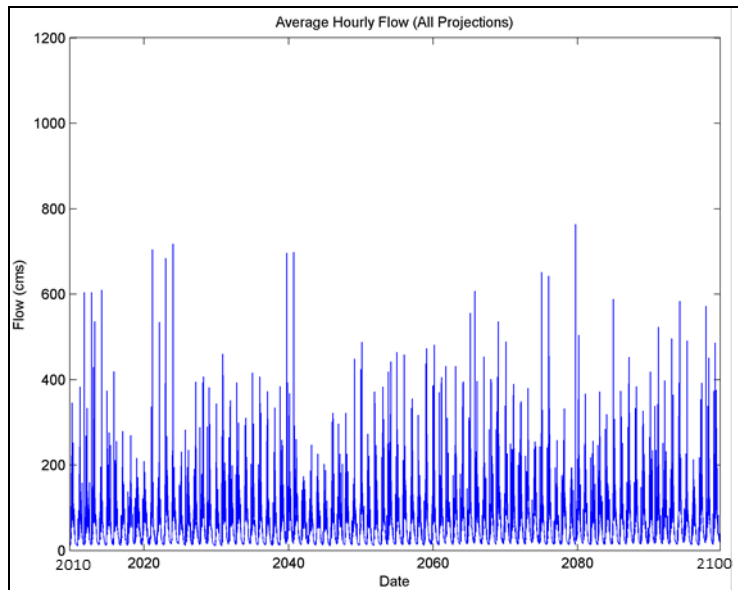


Figure 36. Ensemble average hourly flow projections at the UMF outlet for the years 2010 to 2100 for all 13 projections (i.e., results from both CCSM3 and ECHAM5).

Looking at the daily mean flow results (**Figure 37**), one can see that most peak values are below 2,000 cms (0.71×10^5 cfs), with only a few instances that exceed it, which compares well to historical data, showing a few high peaks close to 1,400 cms (0.49×10^5 cfs). Similarly to the above discussion, the greatest average daily flow contribution is seen to come from CCSM3, when compared to the flow results of EH5 (**Figure 38**). Finally, when taking the average of all 13 projections (**Figure 39**), one can see that most flows are below 300 cms (0.11×10^5 cfs), with a

few exceeding 300-400 cms ($0.11-0.14 \times 10^5$ cfs), which falls within the range of historical daily flows, most of which fall below 500 cms (0.18×10^5 cfs), but have a few high peaks as well.

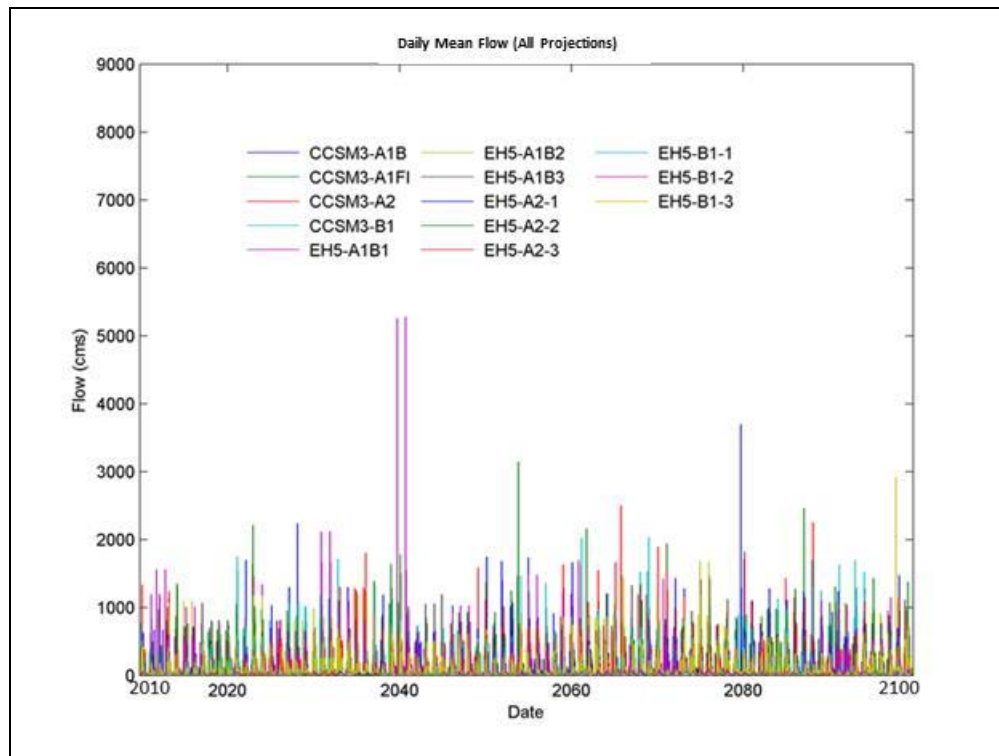


Figure 37. Daily mean flow projections at the UMF outlet for the years 2010 to 2100, using the 13 different climate projections from the two GCMs (CCSM3 and ECHAM5). Note: ECHAM5 is abbreviated as EH5 in the above figure.

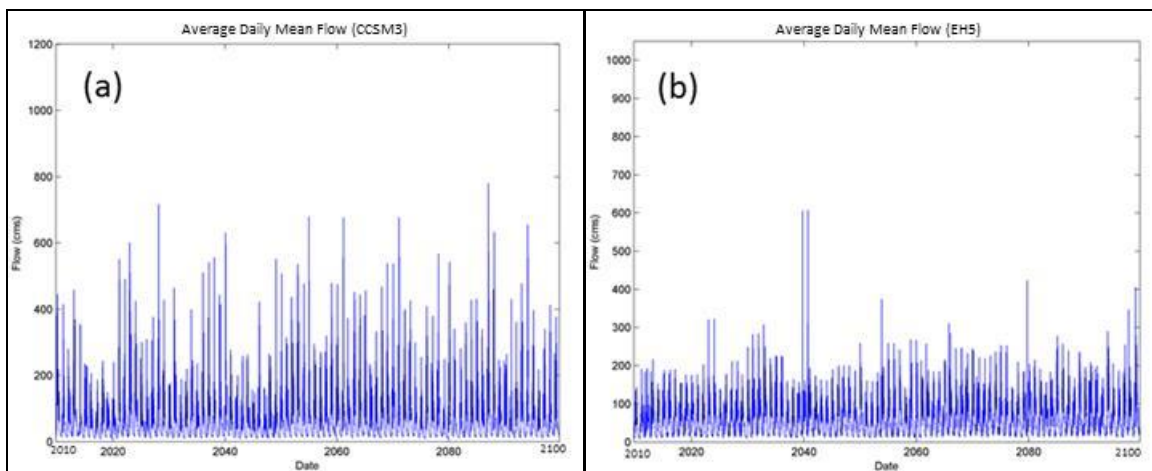


Figure 38. Ensemble average daily mean flow projections at the UMF outlet for the years 2010 to 2100 for each of the climate projections of (a) CCSM3 and (b) ECHAM5. Note: ECHAM5 is abbreviated as EH5 in the above figure.

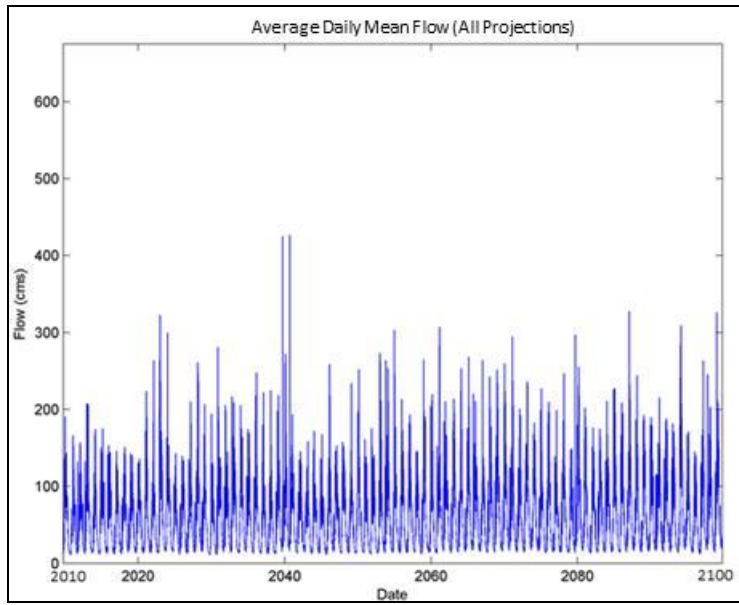


Figure 39. Ensemble average daily mean flow projections at the UMF outlet for the years 2010 to 2100 for all 13 projections (i.e., from both CCSM3 and ECHAM5).

Note that while the future projections discussed above span the years from 2010 to 2100, the simulated WEHY flows include projections for the years from 2000 (or 2001) to 2010. As a result, it is possible to plot these flows along with the available observed values in order to compare these projected flows to the observations. **Figure 40** does that by plotting all of the 13 projections along with the observations (in black). From this figure, it is clear that the projected flow values at the watershed outlet from 2000 to 2010 encompass the observed values, the latter falling within the range of possible flows provided by these projections. **Figure 41**, on the other hand, plots the observations along with the ensemble average of those 13 projections, from which one may notice that the ensemble average can be considered to be quite similar to, and within the range of, the observed values.

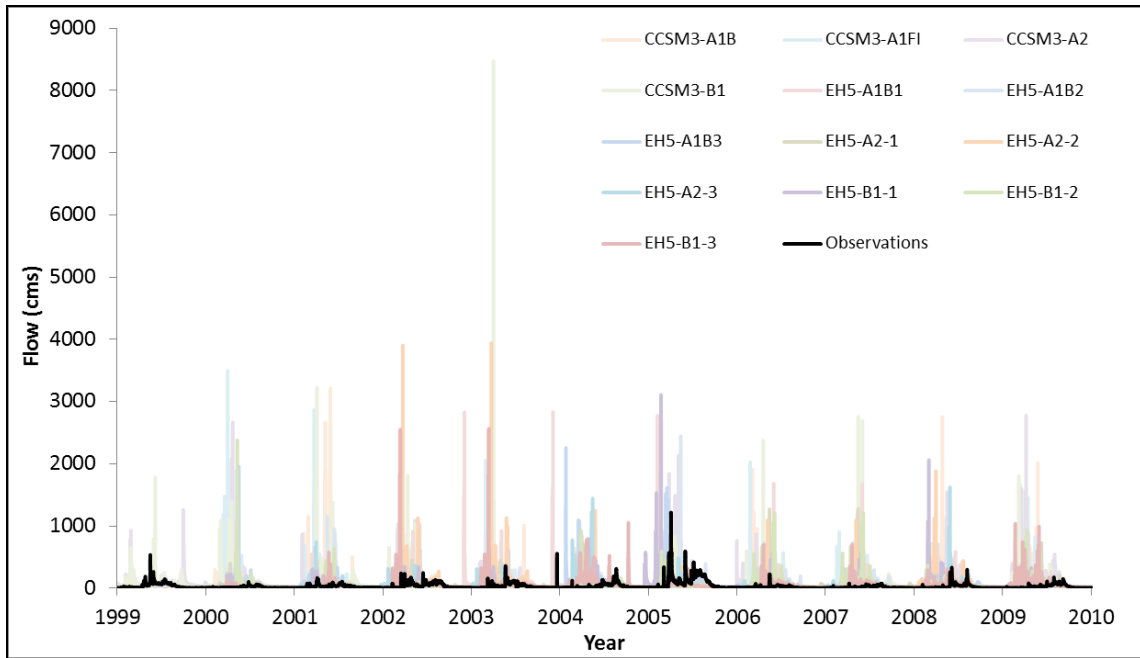


Figure 40. Hourly flow projections at the UMF outlet for the years 2000 to 2010 for all 13 projections (i.e., from both CCSM3 and ECHAM5), compared to corresponding observed flows.

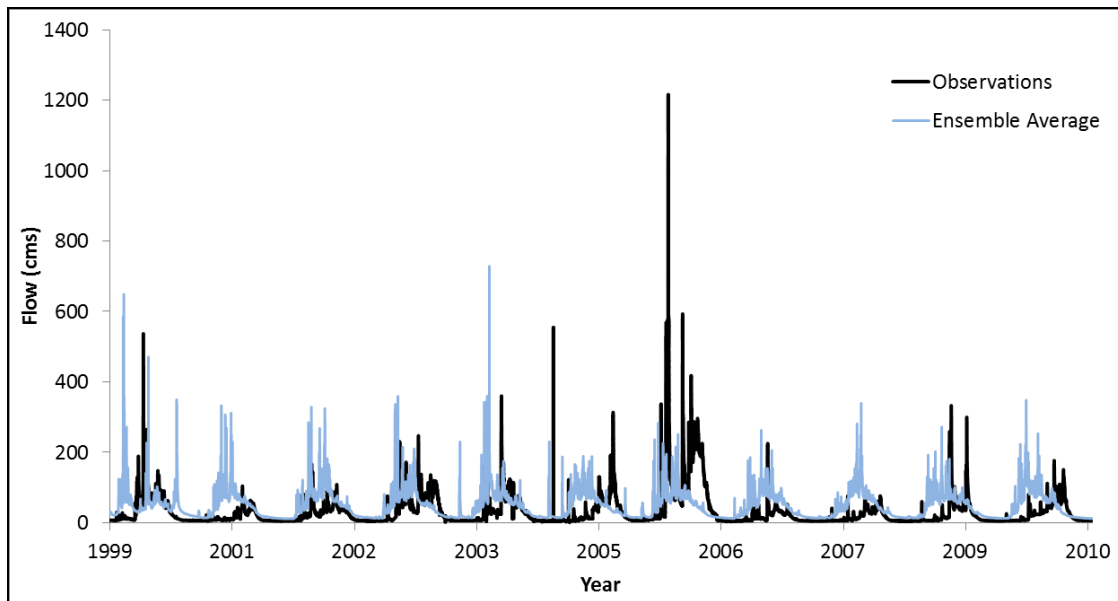


Figure 41. Ensemble average hourly flow projections at the UMF outlet for the years 2000 to 2010 from all 13 projections (i.e., from both CCSM3 and ECHAM5), compared to corresponding observed flows.

B. Trend Analysis of the Future Projected Flows at the Upper Middle Fork Watershed

To see if any of the projected future flows at the outlet of the UMF watershed has a significant trend, the non-parametric Mann-Kendall statistical test was used with a significance

level, α , of 0.05. The benefit of using this test is that it does not require the data to follow any type of distribution, it is less affected than other tests by the presence of outliers, and it can be used even with data sets showing non-linear trends (Önöz & Bayazit, 2003). This test was done for the 13 projections over the whole period from 2010 to 2100, as well as over three subdivisions of the period: 2010-2040, 2040-2070, and 2070-2100. In addition to that, the test was also applied to the ensemble of CCSM3 projections, the ensemble of ECHAM5 projections, and the ensemble of all 13 projections. The results of the test are shown in **Table 9**.

Table 9. Slope (cms/yr) of the trend line of annual mean outflow from Upper Middle Fork for the 13 different future projections, as well as for the ensemble of CCSM3, EH5, and all projections. Significance of the trend was determined using the Mann-Kendall statistical test. p values are given in parentheses; p values that show a significant change ($p < 0.05$) are shown in bold.

GCM-Projection	Water years 2010 – 2040	Water years 2040 – 2070	Water years 2070 - 2100	Water years 2010 - 2100
CCSM3-A1B	-0.063 (0.915)	0.474 (0.498)	-0.305 (0.568)	-0.021 (0.873)
CCSM3-A1FI	-0.233 (0.669)	-0.333 (0.568)	-0.172 (0.858)	-0.136 (0.223)
CCSM3-A2	0.013 (0.972)	1.433 (0.054)	-0.691 (0.354)	0.204 (0.046)
CCSM3-B1	0.348 (0.412)	1.102 (0.046)	0.273 (0.592)	0.245 (0.020)
EH5-A1B1	0.007 (0.986)	0.155 (0.748)	1.433 (0.001)	0.020 (0.845)
EH5-A1B2	-0.270 (0.318)	0.718 (0.108)	0.277 (0.372)	0.367 (<0.001)
EH5-A1B3	-0.654 (0.175)	0.461 (0.269)	0.144 (0.830)	0.215 (0.003)
EH5-A2-1	-0.242 (0.318)	-0.269 (0.592)	0.158 (0.748)	0.285 (<0.001)
EH5-A2-2	-1.058 (0.059)	-0.921 (0.046)	0.173 (0.721)	0.017 (0.867)
EH5-A2-3	0.857 (0.038)	0.931 (0.054)	-0.625 (0.432)	0.277 (0.004)
EH5-B1-1	0.821 (0.101)	0.298 (0.592)	-0.555 (0.164)	0.030 (0.733)
EH5-B1-2	0.948 (0.080)	-0.318 (0.568)	0.101 (0.803)	-0.083 (0.354)
EH5-B1-3	0.939 (0.025)	0.551 (0.301)	-1.299 (0.116)	0.167 (0.055)
Ensemble (CCSM3)	0.219 (0.592)	0.718 (0.007)	-0.158 (0.568)	0.123 (0.045)
Ensemble (EH5)	0.388 (0.050)	0.313 (0.116)	0.126 (0.498)	0.147 (<0.001)
Ensemble All Projections	0.189 (0.164)	0.427 (0.001)	0.073 (0.721)	0.132 (<0.001)

Table 9 shows the slopes of the trend lines of the annual mean outflows from UMF, along with the p value that helps determine if the trend is statistically significant or not. From this table, it is clear that most of the trends tested for the three subdivision periods within the 21st century are not significant. In fact, only four of those 39 (3x13) options show a statistically significant trend. However, when one considers the trends over the whole period from 2010 to

2100, the statistical test showed a statistically significant positive trend for 6 out of the 13 projections, two from CCSM3 (A2 and B1), and five from ECHAM5 (A1B2, A1B3, A2-1, A2-3), with average annual increases ranging from 0.204 cms/yr to 0.367 cms/yr (7.20 cfs/yr to 12.96 cfs/yr). Moreover, the Mann-Kendall test showed that the ensemble of CCSM3, EH5, and of the 13 projections combined all showed statistically significant positive trends.

Therefore, since all of the significant trends over the whole future period (2010-2100) are positive, and since the trend for the ensemble of all projections is a significant positive trend, an increase in the annual mean flows within the UMF watershed may be expected for the future years. This positive trend of the ensemble average of all 13 projections may be seen in **Figure 42**, by observing the general trend of the bold black line, as well as the linear trendline shown by the dashed red line. Moreover, **Figure 42** shows the wide ranges of flow values that can be attained due to the different future projections, and thus reinforces the level of variability regarding the future flows.

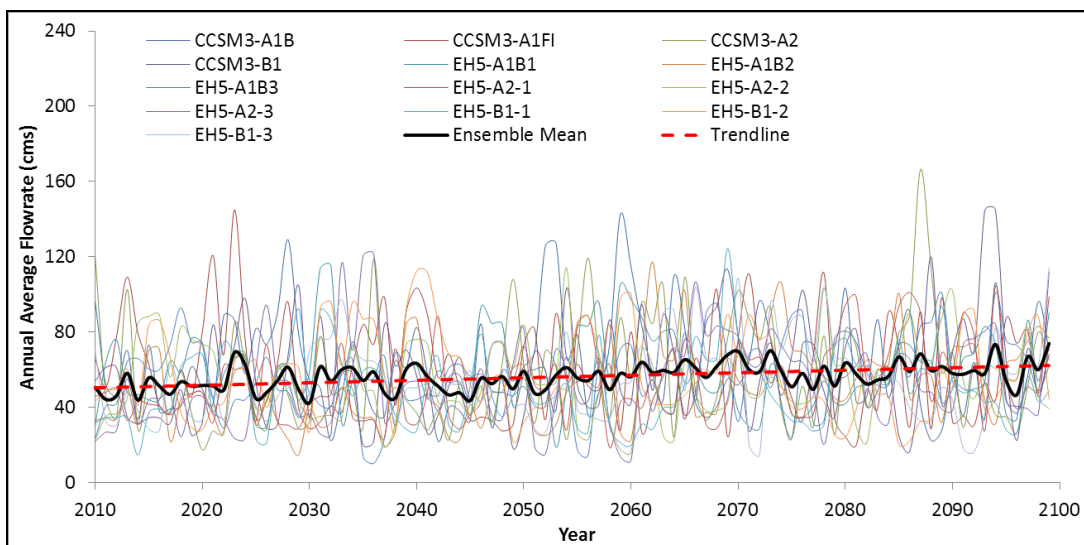


Figure 42. Annual average flowrates from the outlet of the UMF watershed. Flowrates are provided for each of the 13 future projections, as well as for the ensemble average of all projections. A linear trendline is also plotted to show the general trend of the ensemble average.

C. Flood Frequency Analysis for Future Projected Flows over the Upper Middle Fork Watershed

In addition to the above trend analysis, it is important to discuss the probability of hydrologic events over a watershed in order to have additional information regarding planning

for the future and the risks involved. As a result, a flood frequency analysis was done over the Upper Middle Fork (UMF) watershed for the future period.

First, the annual flood series for each of the 13 projections was prepared by taking the highest instantaneous flow rate during each year at the UMF outlet for the years from 2010 to 2100. This provides 90 data points for each projection, and thus a total of 1170 data points for all 13 projections combined. Using the above series of annual flow peaks, a frequency histogram was constructed (**Figure 43a**), as well as an integrated histogram (**Figure 43b**), both of which provide an idea of how the flood intensities are expected to be distributed. For example, the integrated histogram shows that around 230 out of the 1170 annual flood peaks (or ~20% of the peaks) are equal to or greater than 2,000 cms (0.71×10^5 cfs), while the frequency histogram shows that the highest frequency of the annual floods is occurring around the value of 1,000 cms (0.35×10^5 cfs).

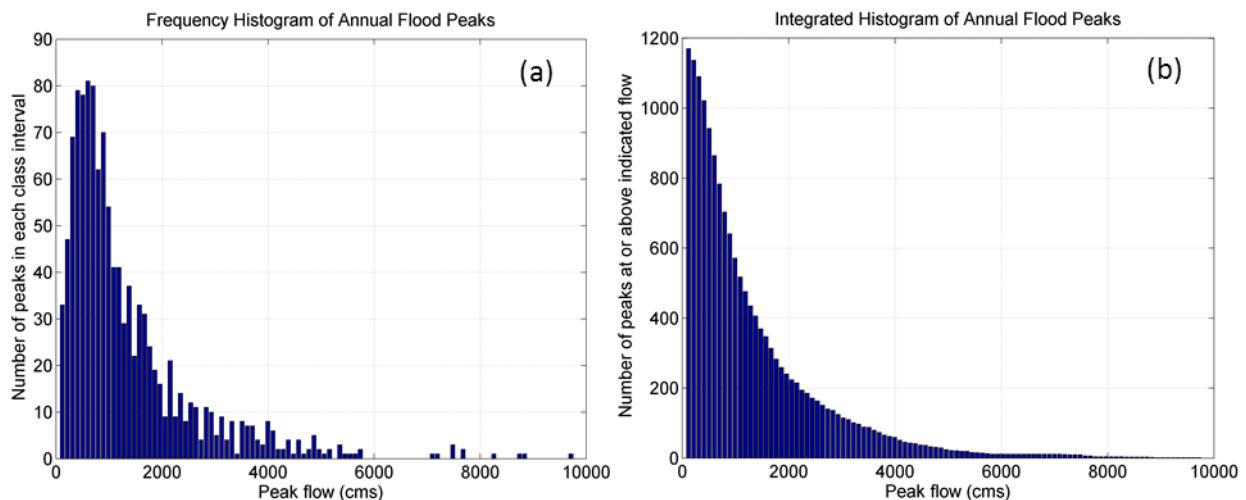


Figure 43. (a) Frequency histogram of annual flood peaks, and (b) integrated histogram of annual flood peaks over the UMF watershed using data from all 13 projections (2010-2100).

Another important computation is the return period of a flood, also known as the recurrence interval. The return period is an average interval (in years) between the occurrence of a flood of a certain magnitude and the occurrence of an equal or larger flood. Hence, it helps one get an idea of how frequently a certain flood would be expected to occur, and its probability of occurring within a certain number of years. Computing those return periods allows the plotting of the frequency curve of annual floods, as shown in **Figure 44**. From this figure, one can estimate that for the future period of the 21st century, a 3,000 cms (1.06×10^5 cfs) flood has

around a 10-yr average return period, a 4,000 cms (1.41×10^5 cfs) flood has around a 20-yr average return period, and a 5,750 cms (2.03×10^5 cfs) flood has a 100-yr average return period.

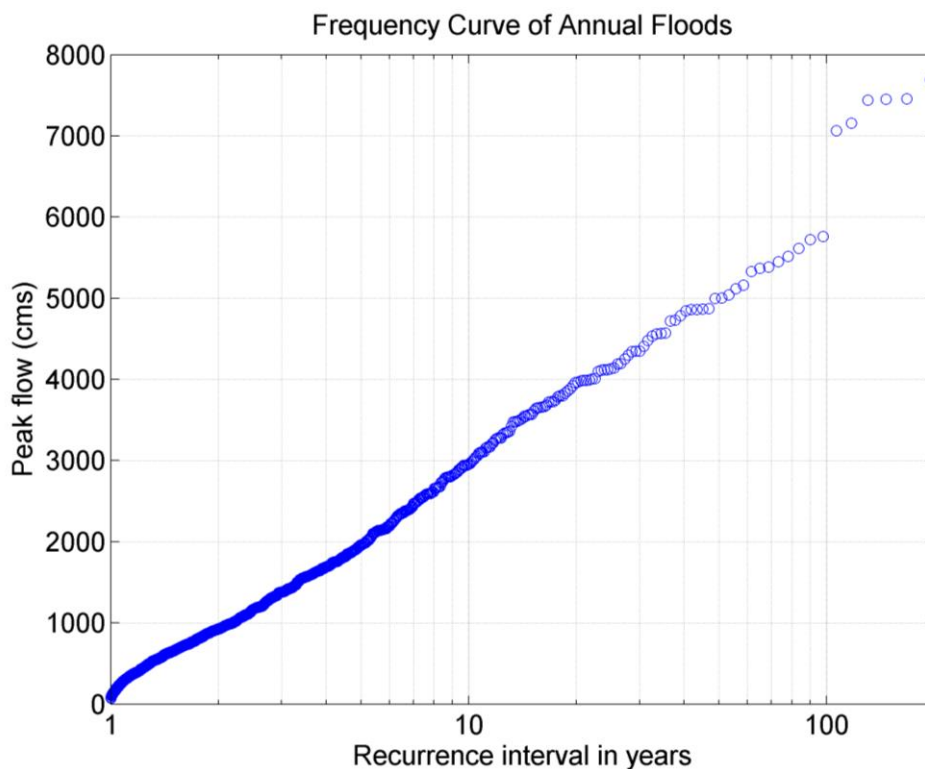


Figure 44. Frequency curve of annual floods for the UMF watershed (2010-2100).

While the information from **Figure 44** is crucial, it is important to remember that the figure is obtained from plots of data points. In such a case, there will be a low number of data points corresponding to the very large floods and a larger number of points for the lower-intensity floods. As a result, the figure would provide a good estimate of the flood intensity of low return periods; however, as the return period increases, the uncertainty in its corresponding flood magnitude increases as well. This is clear from **Figure 44**, which shows a much lower number of data points after the 50-year interval, and also shows a divergence of the plotted data points at very high recurrence intervals.

Accordingly, a different approach must be used in order to estimate the frequency of rare events. One such approach would be fitting the data to a certain standard frequency distribution. Since the log Pearson Type III distribution is a standard set by the U.S. Water Resources Council for use by federal agencies, the available data was fitted to that distribution. Both the Chi-squared test and the Kolmogorov-Smirnov test showed that the log Pearson Type III data is a

good fit for the available data. As a result, it was then possible to easily compute the flood magnitudes for different return periods by using the fitted distribution. The results are shown in **Table 10**.

Table 10. Magnitudes of floods for different return periods over the UMF watershed during years 2010-2100.

Return Period	Flood Magnitude (cms) (estimated using Log Pearson Type III)
2-yr flood	955 cms (0.34×10^5 cfs)
10-yr flood	2,811 cms (0.99×10^5 cfs)
25-yr flood	4,147 cms (1.46×10^5 cfs)
50-yr flood	5,321 cms (1.87×10^5 cfs)
100-yr flood	6,646 cms (2.35×10^5 cfs)
200-yr flood	8,147 cms (2.88×10^5 cfs)

The results of **Table 10** show flood magnitudes that are mostly in accordance with the results of **Figure 44**, especially for the lower return periods. However, as mentioned previously, the flood magnitudes in **Table 10** of the higher return periods (e.g., 50, 100, and 200 years) begin to deviate from their corresponding values in the plot of **Figure 44**. Having the well-fit log Pearson Type III distribution is, thus, important for estimating the flood magnitudes of the rare events with more confidence over the future period.

Therefore, the above discussion and analysis of the future flow projections over the UMF watershed revealed that the CCSM3 projections estimated larger flow discharges within the future period as compared to the ECHAM5 (EH5) projections. Moreover, the trend analysis of the projected future flows at the outlet of the UMF watershed showed a statistically significant positive trend for the ensemble of all 13 projections over the whole future period, thus suggesting, on average, an expected increase in the annual mean flows within the UMF watershed during the future period. Nonetheless, the presence of 13 different projections provided a wide range of flow values that can be attained, thus reinforcing a level of variability regarding those increasing future flows. Furthermore, the flood frequency analysis over UMF for the future period of the 21st century showed that about 20% of the annual flood peaks are expected to be equal to or greater than 2,000 cms (0.71×10^5 cfs), while the highest frequency of the annual floods is expected to occur at the value of around 1,000 cms (0.35×10^5 cfs). Finally, the information provided from all the future projections was used to get estimates of the flood magnitudes for

different return periods over the future period of the 21st century as shown in **Figure 44** and **Table 10**.

III. LAKE DAVIS BASIN

During the project period in which the HRL group was working on the Upper Middle Fork (UMF) watershed, Plumas County representatives informed the HRL group of their desire to undergo a study of the Lake Davis basin and its corresponding dam, Grizzly Valley Dam, in view of the ongoing drought befalling California in the current years. Thus, an independent modeling of the Lake Davis basin was undergone.

1. Overview of the Project Site

The Lake Davis Basin is a subwatershed of the Upper Middle Fork (UMF) watershed (**Figure 45**). It covers an area of around 114 square kilometers (44 square miles), which is the drainage area of the dam located at the outlet of that basin, the Grizzly Valley Dam.

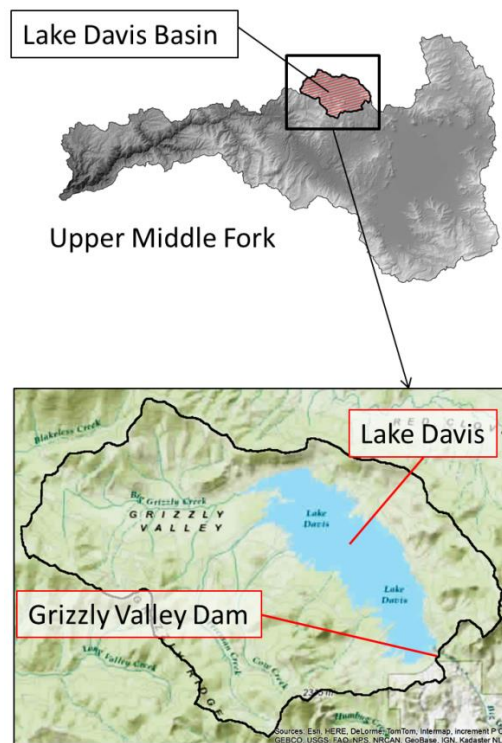


Figure 45. Location of Lake Davis Basin as a portion of the Upper Middle Fork watershed (upper figure); location of Lake Davis and Grizzly Valley Dam within the Lake Davis Basin (lower figure).

Grizzly Valley Dam is an earth and rockfill dam, located on Big Grizzly Creek (a tributary of the Middle Fork Feather River) just downstream of Lake Davis (**Figure 45**), which is the largest of the three Upper Feather River lakes. The dam was completed in 1966 and is

operated by California Department of Water Resources (DWR, 2013). With a maximum storage capacity of 84,371 acre-ft, the reservoir mainly serves the purpose of supplying water to the city of Portola, while also providing fish and wildlife enhancement, streamflow enhancement, as well as serving recreational purposes (Rischbieter, 2000).

The methodology, data collection, GIS database preparation, and reconstruction of the historical and future climates were all similar to what was done for the UMF watershed. Accordingly, the reader is referred to the previous chapter about the UMF watershed for details and discussions regarding these topics. Below, the implementation of the snow module and the WEHY model over the Lake Davis Basin will be discussed.

2. Hydrologic Modeling of the Lake Davis Basin

A. Implementation and Use of the WEHY Snow Module over the Lake Davis Basin

Simulations of the WEHY snow module were run by using the MM5-reconstructed, mean monthly hydro-climate data at a spatial resolution of 3 km over the watershed, based on the dynamical downscaling of NCAR/NCEP global reanalysis data as input. Constants and model parameters required were determined from the literature (Ohara & Kavvas, 2006). The calibration and validation of the snow model made use of comparisons of the simulation results with observations in order to test the model's performance. Observations were obtained from one CDEC (California Data Exchange Center) field observation station selected based on the availability of the required data and the preferred time intervals of the provided data; the station (called GRZ) is shown in **Figure 46**.

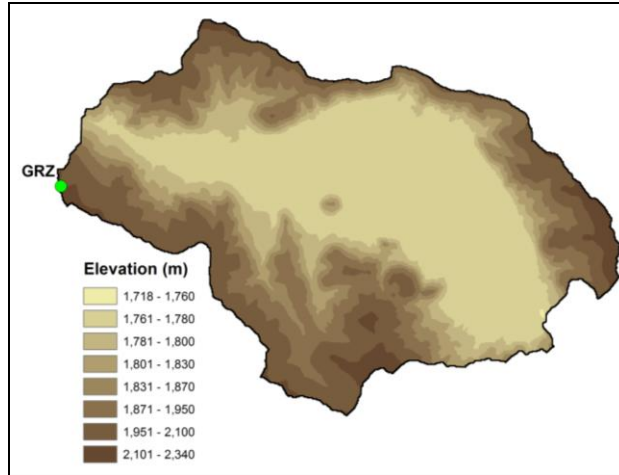


Figure 46. Location of the selected snow field observation station (GRZ) within the Lake Davis basin.

Calibration of the snow module was conducted for water year 2006 (October 2005 through September 2006) by comparing the snow water equivalent of the simulated results versus the observed hourly data for the selected observation station. The calibration results at the selected station are depicted in **Figure 47** and their statistical results are shown in **Table 11**.

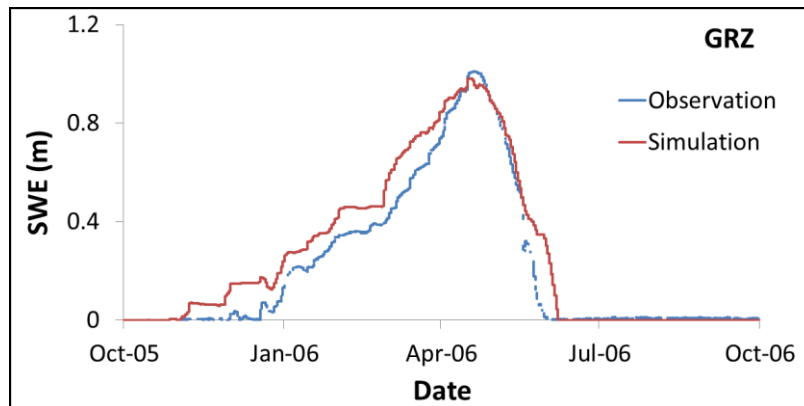


Figure 47. Time series of the observed and model-simulated snow water equivalent (SWE) at the selected field observation site from October 2005 through September 2006 (calibration period).

Table 11. Statistical test values of simulated and observed snow water equivalent from the selected observation station (GRZ) during the calibration period (October 2005 through September 2006). STDEV: standard deviation; RMSE: root-mean-square error; Nash: Nash-Sutcliffe Efficiency.

Parameter	GRZ	
	Observed	Simulated
Mean (m)	0.28	0.34
STDEV (m)	0.32	0.33
RMSE	0.09	
Nash	0.91	
Correlation Coefficient	0.98	

From **Figure 47** and **Table 11**, one can see that the simulated snow water equivalent values are similar to their corresponding observed values, while the statistical test results show a very good performance of the WEHY snow model, with high values of the correlation coefficient and the Nash-Sutcliffe Efficiency.

As for the validation period, it was chosen to be for a whole 10 years, ranging from October 1, 2000 through September 30, 2010. The results obtained were plotted as shown in **Figure 48** and the results of the statistical tests are shown in **Table 12**.

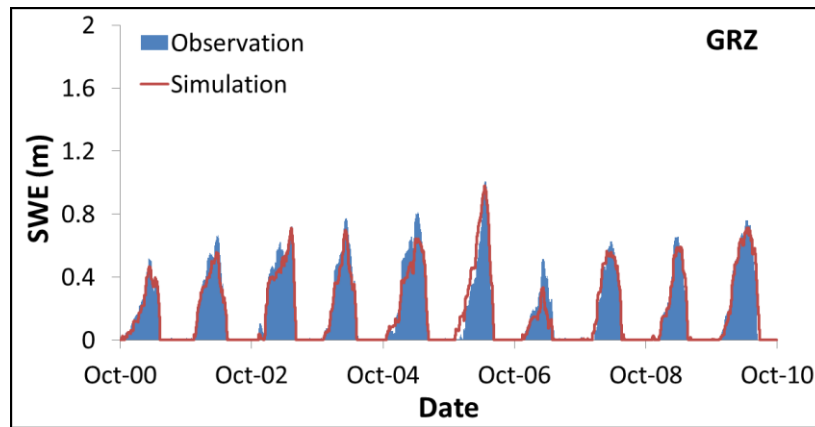


Figure 48. Time series of the observed and model-simulated snow water equivalent (SWE) at the selected field observation site from October 2000 through September 2010 (validation period).

Table 12. Statistical test values of simulated and observed snow water equivalent from the selected observation station (GRZ) during the validation period (October 2000 through September 2010). STDEV: standard deviation; RMSE: root-mean-square error; Nash: Nash-Sutcliffe Efficiency.

Parameter	GRZ	
	Observed	Simulated
Mean (m)	0.25	0.24
STDEV (m)	0.25	0.24
RMSE	0.07	
Nash	0.92	
Correlation Coefficient	0.96	

As shown in **Figure 48**, one can see that the simulated snow water equivalent values are closely distributed along the time-series observed values of the GRZ observation station. **Table 12** shows that the mean and standard deviation between the observed and simulated values are very close for the GRZ station. Moreover, the high values of the correlation coefficient (0.92) and the Nash-Sutcliffe Efficiency (0.96) indicate a reliability of the performance of the WEHY snow module, and reveal a high goodness of fit between the simulated and observed values.

Thus, the results from **Figure 48** and **Table 12** show that the WEHY snow module can perform temporally and spatially well compared to the corresponding observations, and indicate the possibility and capability of the WEHY snow module to be applied confidently to the Lake Davis watershed.

B. Implementation and Use of the Hydrologic Part of the WEHY Model over the Lake Davis Basin

Similarly to what was done for the Upper Middle Fork (UMF) watershed, a Geographic Information System (GIS) database was set up and completed over the Lake Davis watershed, including spatial information regarding elevations, soil types, and land use/land covers, all from the same sources as discussed for UMF in the previous chapter. The land use/land cover dataset (**Figure 49**) and the soil survey dataset (**Figure 50**) were processed and analyzed for their land surface and soil physical parameters and for quality control purposes. A set of lookup tables was

established for the land cover types and soil map units that cover the Lake Davis watershed. Moreover, from the 1 arc-second Digital Elevation Model (DEM), an aspect map, a slope map, and a preliminary river channel network were obtained for the areas that cover the UMF watershed. **Figure 51** and **Figure 52** show the sample spatial maps of the DEM and slope, respectively, for the Lake Davis watershed.

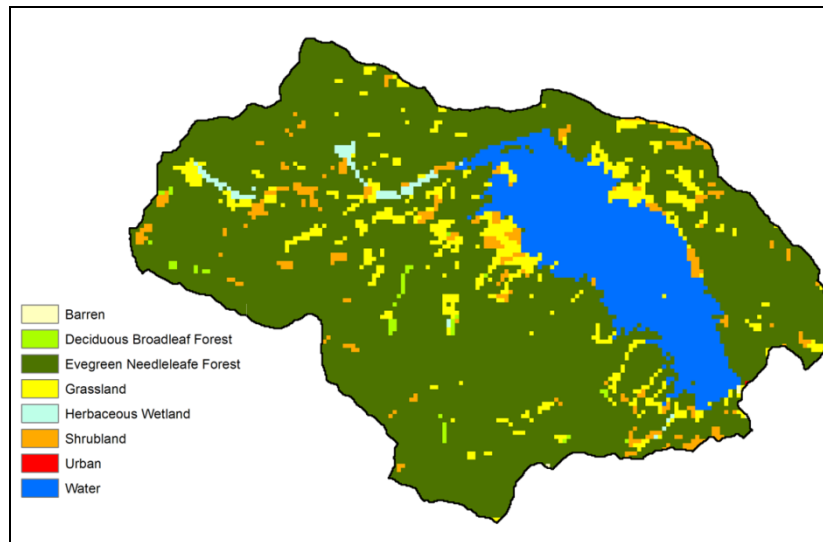


Figure 49. Vegetation and land-cover types over the Lake Davis watershed.

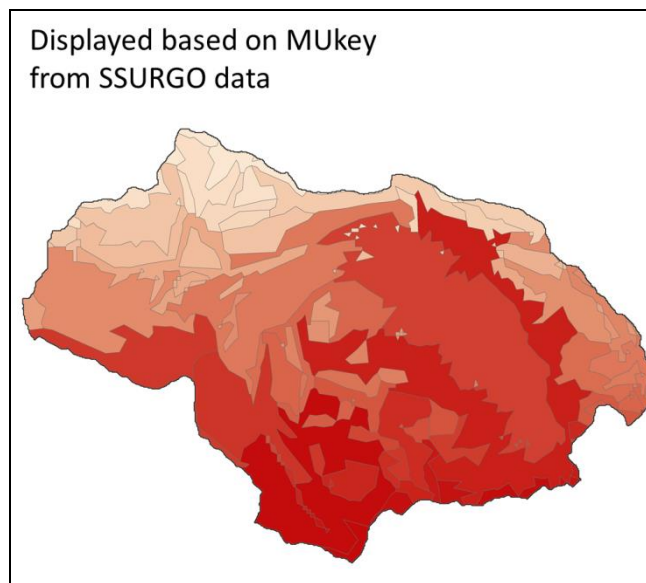


Figure 50. Spatial soil map based on SSURGO data from California USDA-NRCS over the Lake Davis watershed.

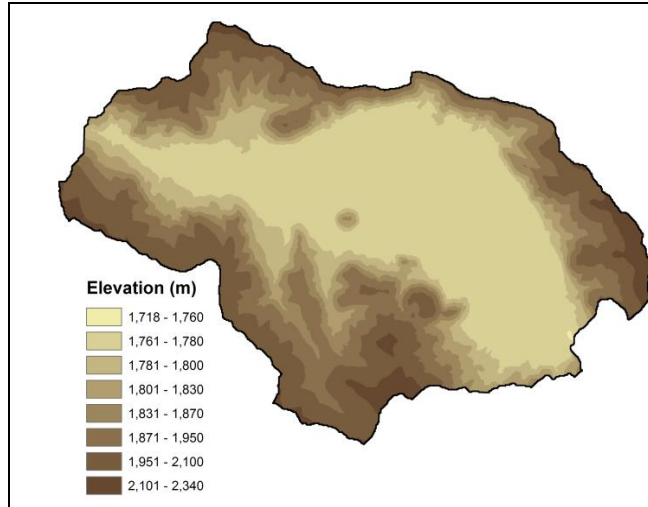


Figure 51. Digital Elevation Model (DEM) from the National Elevation Dataset (NED) over the Lake Davis watershed.

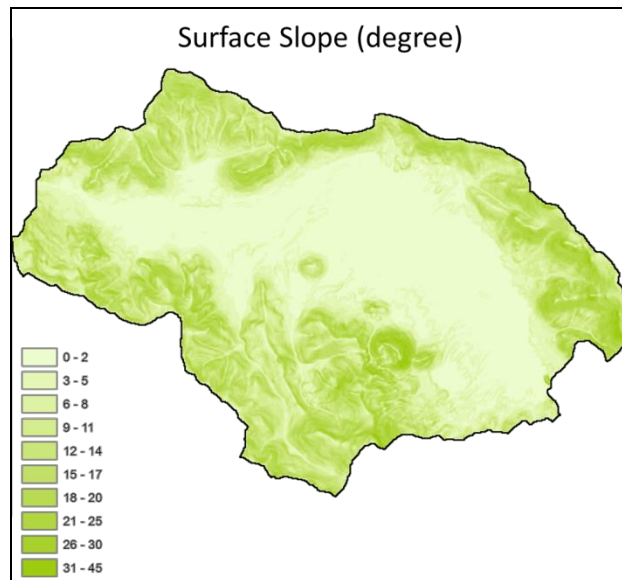


Figure 52. Surface slope over the Lake Davis watershed.

Estimation of the geomorphologic, soil hydraulic, and vegetation parameters for the delineated Model Computational Units (MCUs) of the WEHY model over the Lake Davis watershed were performed as was described by Chen et al. (2004a). Starting with the land surface/vegetation parameters, the monthly mean Leaf Area Index (LAI) values were developed from Moderate Resolution Imaging Spectroradiometer (MODIS) satellite driven data which has 1 km spatial resolution; results over the Lake Davis watershed are shown in **Figure 53**. Other land surface parameters such as vegetation root depth, roughness height, surface albedo, and emissivity were estimated based on the multi-source land cover data in **Figure 49** by means of

California Wildlife Habitat Relationships (CWHR) and reference information from Asner et al. (2003) and Canadell et al. (1996). These vegetation parameters are important to calculate the evapotranspiration and snow accumulation and melting in the land surface processes. The samples of the vegetation root depth and the roughness height are shown in **Figure 54**.

Finally, soil parameters such as average soil depth, mean total porosity, mean residual saturation, mean bubbling pressure, mean pore size index, soil erodibility factor, mean hydraulic conductivity, and variance of hydraulic conductivity were estimated based on the Soil Survey Geographic (SSURGO) Database (Natural Resources Conservation Service, NRCS) in **Figure 50** by means of reference information from Gale and Grigal (1987), Canadell et al. (1996), McCuen et al. (1981), Rawls et al. (1982) and Yoshitani et al. (2002). The samples of the estimated soil parameters are shown in **Figure 55** (a-h).

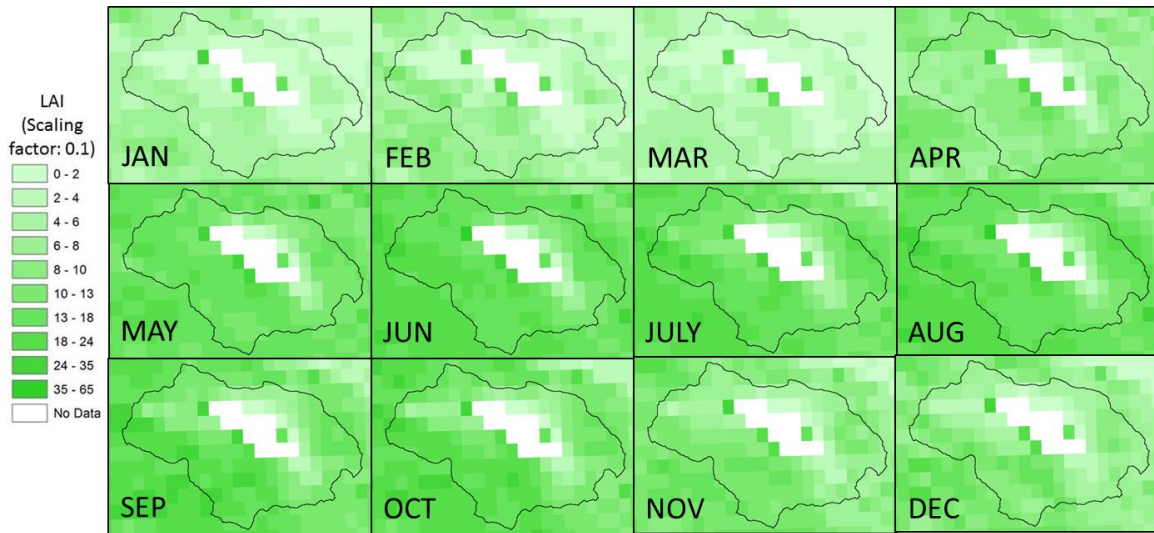


Figure 53. MODIS average monthly leaf area index (LAI) over the Lake Davis watershed.

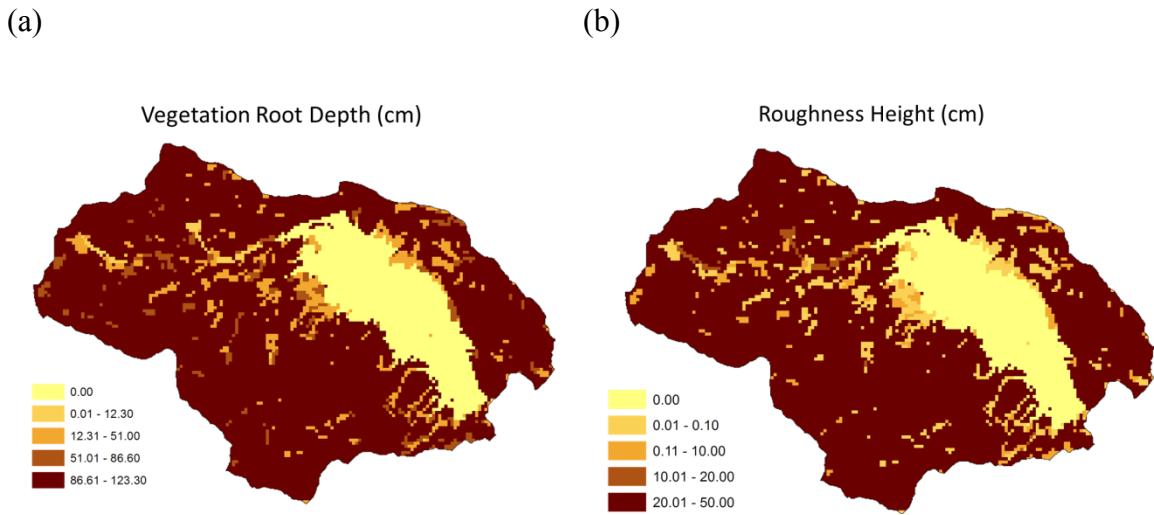


Figure 54. Samples of distributed land surface parameters from database over the Lake Davis watershed.

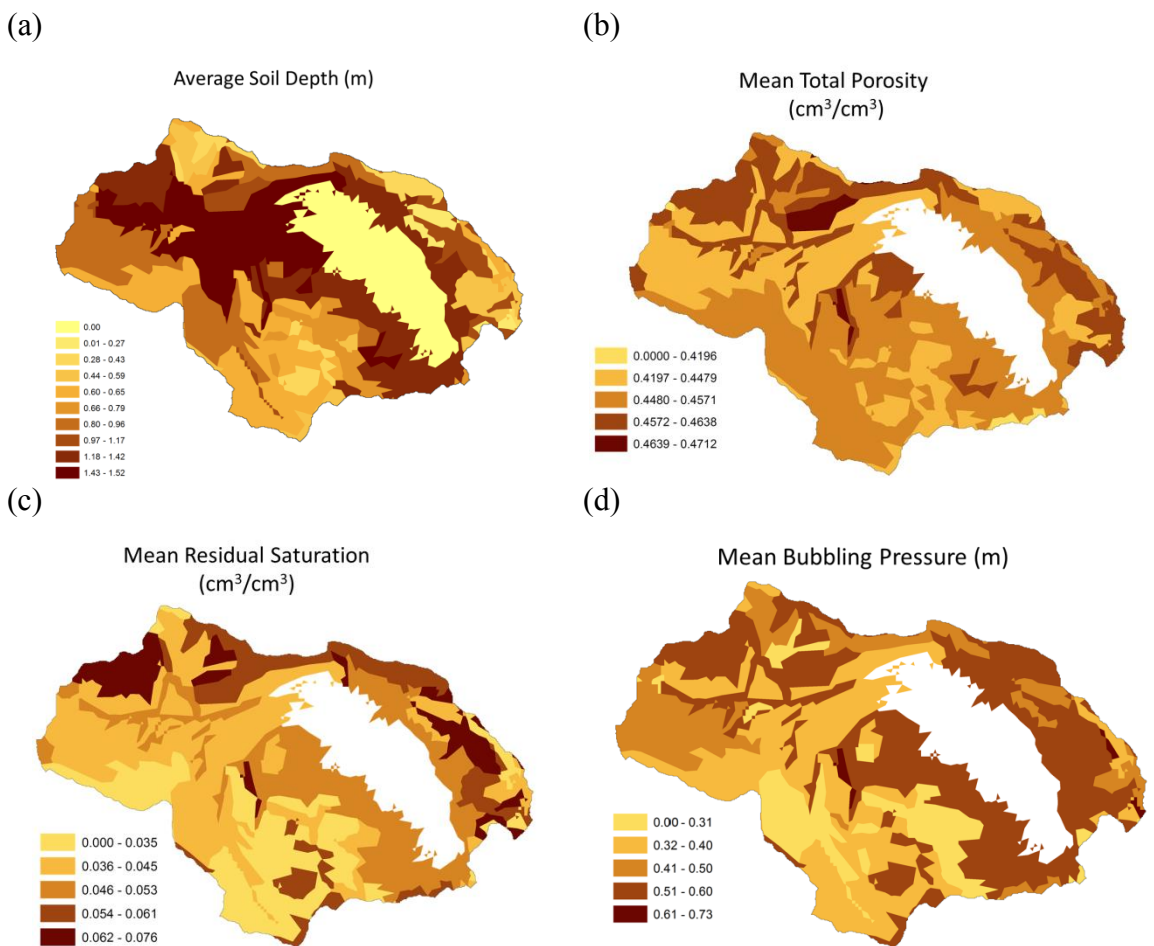


Figure 55. Samples of distributed soil hydraulic parameters from the database over the Lake Davis watershed (continued below).

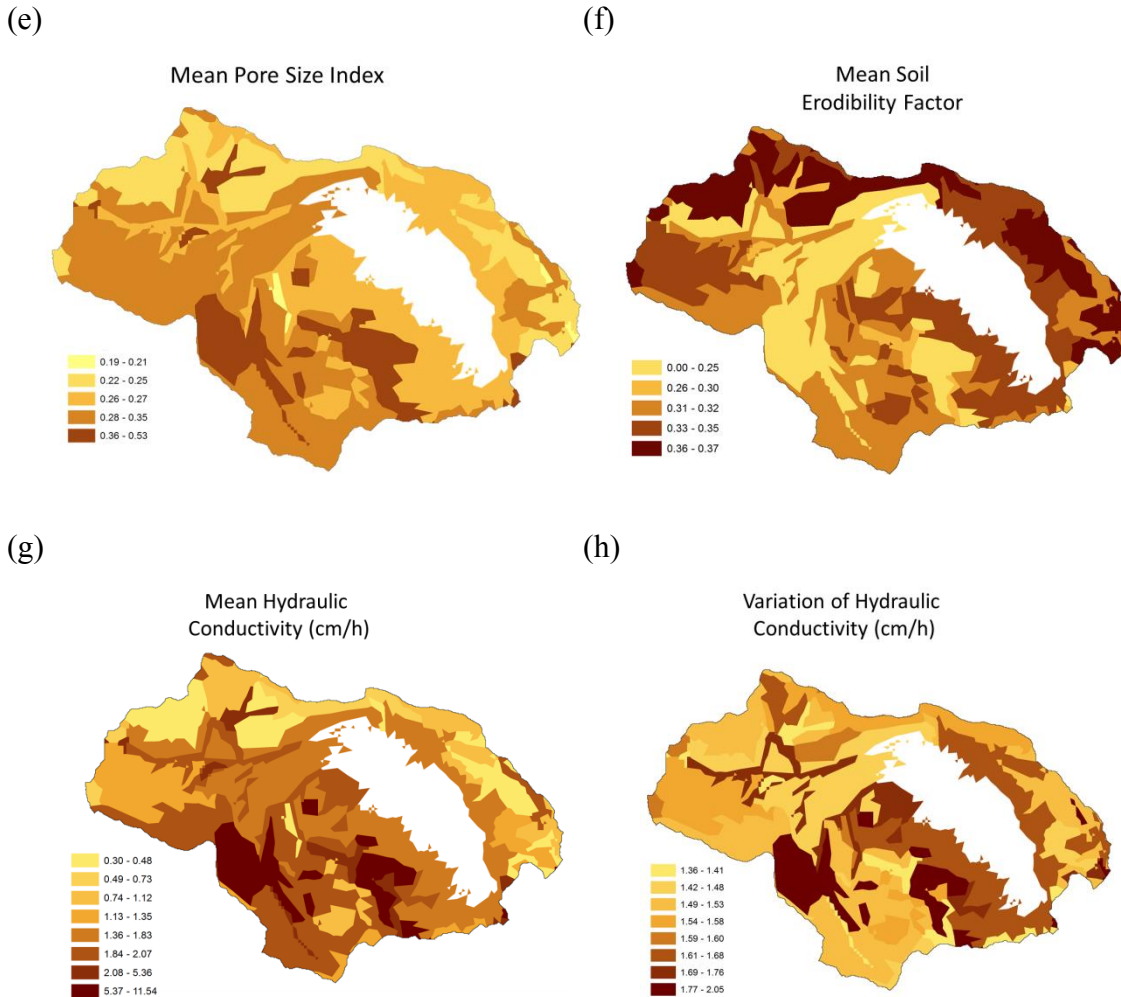


Figure 55 (continued). Samples of distributed soil hydraulic parameters from the database over the Lake Davis watershed.

Just as the WEHY snow module was calibrated and validated over the Lake Davis watershed, the calibration and validation of the WEHY model is also an essential step to ensure its proper use for the Lake Davis basin. In this regard, simulations of the model were run by using the reconstructed, mean monthly bias-corrected hydro-climate data at a spatial resolution of 3 km over the watershed, based on the dynamical downscaling of NCAR/NCEP global reanalysis data. Outputs from the previously calibrated and validated snow simulations were used as inputs to the WEHY model.

The calibration and validation of the WEHY model over the Lake Davis watershed made use of comparisons of the simulation results of flow discharge with observed flow values in order to test the model's performance. Observations were obtained from one CDEC (California

Data Exchange Center) field observation station selected based on the availability of the required data and the length of the provided record. This station is at the outlet of the watershed, and is called *Lake Davis* station (having an ID of DAV). The station is shown in **Figure 56**, and is located at Grizzly Valley Dam. Note that this station provides manually-entered monthly full natural flow data, which is defined as flow that has been reconstructed by removing the effects of any manmade alterations that may cause impairment to the natural flow. As a result, the reconstructed data from DAV station can be considered as the inflow into Grizzly Valley Dam, or in other words, the unimpaired outflow from the Lake Davis basin.

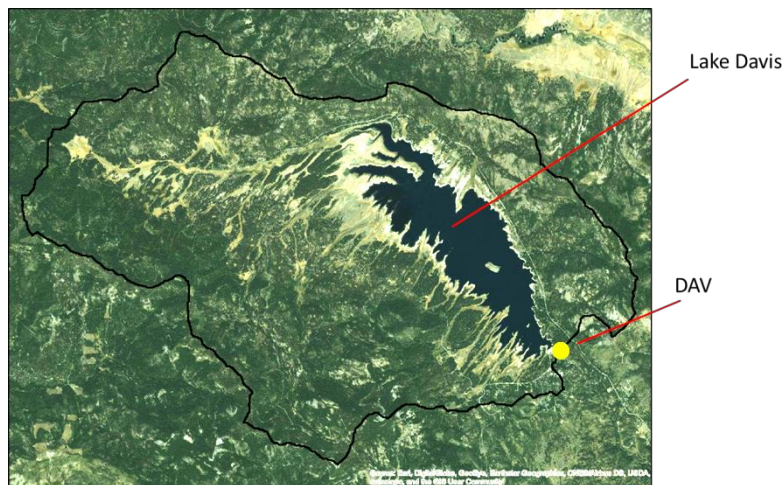


Figure 56. Location of the selected flow field observation station (DAV) in the Lake Davis watershed (delineated by the black boundary).

Calibration of the WEHY model was carried out for water year 1986 (October 1985 through September 1986) by comparing the simulated monthly flow discharges from the watershed’s outlet against the observed dam inflow (Full Natural Flow) data at the DAV station. The results of the calibration are depicted in **Figure 57** and their statistical properties are shown in **Table 13**.

From **Figure 57**, one can see that, for most of the months, the simulated flow values are similar to their corresponding observed values. Moreover, **Table 13** shows the statistical test results that reveal a good performance of the WEHY model, which shows relatively close mean and standard deviation values, as well as a high correlation coefficient and Nash-Sutcliffe efficiency.

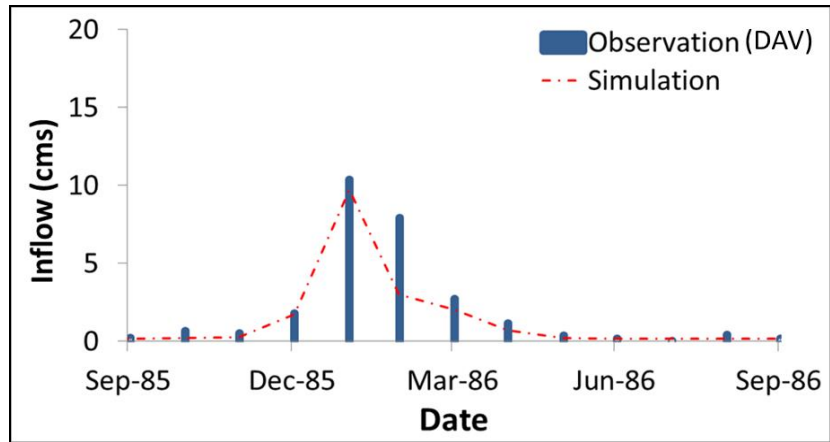


Figure 57. Time series of the observed and model-simulated monthly flow discharges at the DAV station from October 1985 through September 1986.

Table 13. Statistical test values of simulated and observed monthly flow values at the DAV station during the calibration period (October 1985 through September 1986). STDEV: standard deviation; RMSE: root-mean-square error; Nash: Nash-Sutcliffe Efficiency.

Parameter	Observed	Simulated
Mean (cms)	1.16	1.55
STDEV (cms)	3.38	2.75
RMSE	1.47	
Nash	0.81	
Correlation Coefficient	0.92	

Validation of the WEHY model was done over a 10-year period, extending from water year 1986 to water year 1995 (i.e., from October 1985 through September 1995). The simulation results obtained over this period were plotted against the observed values at the DAV station, as shown in **Figure 58**, and their statistical properties are shown in **Table 14**.

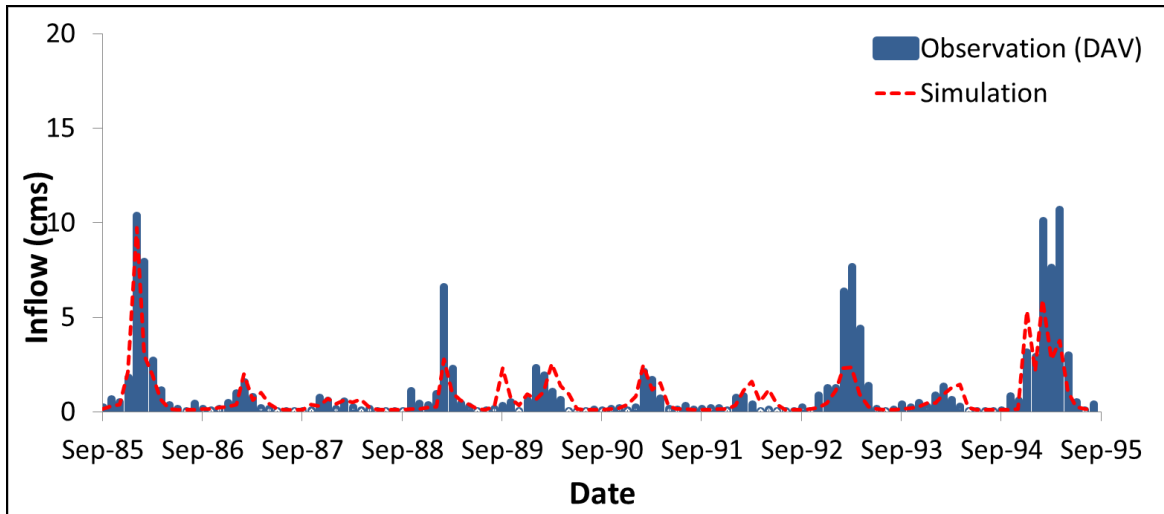


Figure 58. Time series of the observed and model-simulated monthly flow discharges at the DAV station from October 1985 through September 1995 (validation period).

Table 14. Statistical test values of simulated and observed monthly flow discharge values at the DAV station during the validation period (October 1985 through September 1995). STDEV: standard deviation; RMSE: root-mean-square error; Nash: Nash-Sutcliffe Efficiency.

Parameter	Observed	Simulated
Mean (cms)	1.11	0.80
STDEV (cms)	2.15	1.29
RMSE	1.36	
Nash	0.59	
Correlation Coefficient	0.81	

Figure 58 reveals that the simulated flow discharge values show a good match with the observation values for most of the months. The differences appearing for some of the months may result due to the small size of the Lake Davis basin. As a result of that, the coarseness of the climate data relative to the size of the watershed may adversely affect the results over the basin, with the position of one precipitation cell, for example, greatly affecting the peak runoff from the watershed. However, **Table 14** shows that the model is capable of replicating the amount of flow on average in a good manner over the validation period. Moreover, the Nash-Sutcliffe efficiency and the high correlation coefficient in **Table 14** indicate an acceptable reliable performance for the WEHY model. Thus, the above-discussed results show that the WEHY model can perform

well temporally when compared to the corresponding observations, thus revealing its capability in its proper application to the Lake Davis watershed.

3. Historical Analysis of the Grizzly Valley Dam

With the WEHY model being calibrated and validated successfully, it can now be used to simulate the flows in the stream network, thus eventually getting the inflows into Grizzly Valley Dam. When the global climate data used as an input are historical reanalysis data, then the WEHY outputs will provide reconstructed historical inflows into the dam. These inflows can be used, along with the demands, in order to analyze the historical operations of the reservoir (through a mass curve analysis), thus finding the amounts of shortages, surpluses, as well as the operations that would have reduced the historical shortages.

One method for such a mass curve analysis is the mass curve method, which was originally introduced by Rippl (1883) as a graphical technique to determine the reservoir storage capacity (Klemes, 1979), but may also be used to determine release rates from a reservoir with a specified storage capacity (Raghunath, 2006). In general, this method uses historical inflow records and demands that are usually given as a time series (hourly, daily, or monthly) (**Figure 59**). It then uses such time series in order to plot the inflow and demand mass curves (**Figure 60**). An inflow mass curve is a plot of the *cumulative* inflow to the reservoir as a function of time. The inflow rate into the reservoir at some time t is the slope of the mass curve at that particular time. In a similar form, the cumulative demand (draft) may be plotted as a function of time, and the demand rate at some time t is the slope of this curve at that particular time. These curves may then be used for analysis purposes, including storage capacities, releases from reservoir, and others.

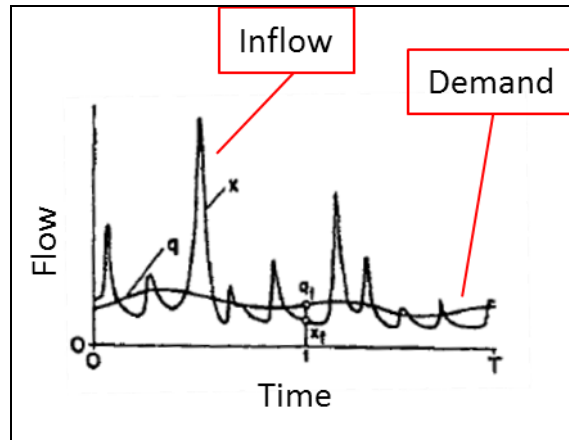


Figure 59. Sample plot of inflow and demand time series for a dam. [Source: Klemes (1979)].

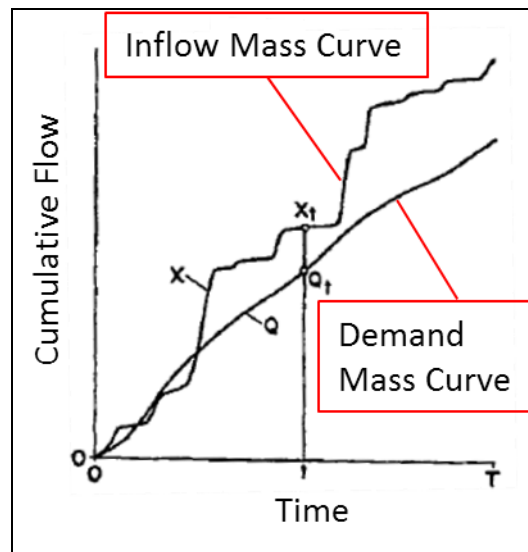


Figure 60. Sample plot of inflow and demand mass curves. [Source: Klemes (1979)].

For the case of the Grizzly Valley Dam, the full natural flows (inflows) and storages, given at a monthly time scale, were found to be provided online at the CDEC (California Data Exchange Center) field observation station called DAV (location shown in **Figure 56**). It was decided to use the data from water years 1968 to 2009 for the following historical analysis, which was done at a monthly time scale.

From this available data, it was possible to determine the historical monthly outflows (including evaporation and seepage losses) from the Grizzly Valley Dam by using the mass balance equation. This equation states that the inflow for a certain month minus the change in storage during that month is equal to any outflow (and losses) during that specific month. Averaging the outflows (plus losses) of each month over the historical period gave the mean

monthly historical outflow (and loss) for each month (i.e., a total of 12 values, each one being the average of its corresponding month). In order to determine how much of those outflows are in the form of losses, the monthly estimated evaporation and seepage losses were obtained from the monthly State Water Project Operations Data Reports, which are available online starting from January 1990 (<http://www.water.ca.gov/swp/operationscontrol/monthly.cfm>). Then, the data over each month was averaged in order to get an estimate of the average monthly loss rate from the dam.

With the average historical outflows and losses in hand, the historical operations of the reservoir can be analyzed. First, note that the DWR Bulletin No. 117-3 of July 1965 provides a schedule of flow releases downstream of Lake Davis (**Figure 61**). This release schedule defines the minimum flow releases to be provided within different periods of the year, based on the initial storage of the lake on May 1.

Lake storage on May 1, in acre-feet	Minimum flow release, in cubic feet per second		
	5/1 - 6/15	6/16 - 3/15	3/16 - 4/30
83,000	18	8	18
75,500 to 83,000	16	6	16
65,000 to 75,500	15	5	15
below 65,000	14	4	14

Figure 61. Minimum flow release schedule for Lake Davis. [Source: DWR Bulletin No. 117-3 of July 1965].

In addition to the release schedule, a historical rule curve, was attempted to be determined as follows. Looking at the annual inflows to the reservoir (**Figure 62**), some years were specified as dry (1976, 1977, 1987, 1988, 1992, 2001) and others as wet (1969, 1971, 1974, 1982, 1983, 1986, 1995, 2006). Then the storage for each month was averaged over the years in each period (the dry years alone, wet years alone, and all the years in historical record together). This provides the results in **Figure 63**, which show the average storage at Lake Davis at the beginning of every month for three cases: dry years, wet years, and all the years in the historical record. Such curves are usually called rule curves, and may be used to guide operations of reservoirs. Accordingly, the derived rule curves were tested by using them, along with the given release schedule, to run the reservoir simulation for Grizzly Valley Dam and perform a mass curve analysis for the historical period.

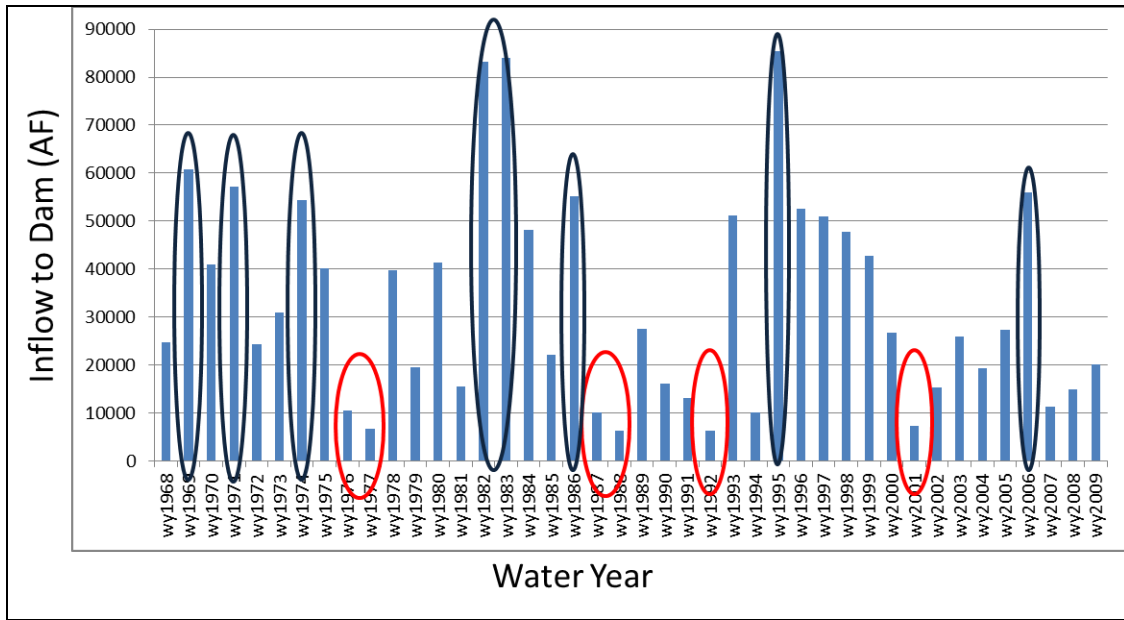


Figure 62. Historical annual inflows to Grizzly Valley Dam. Black ovals: wet years; red ovals: dry years.

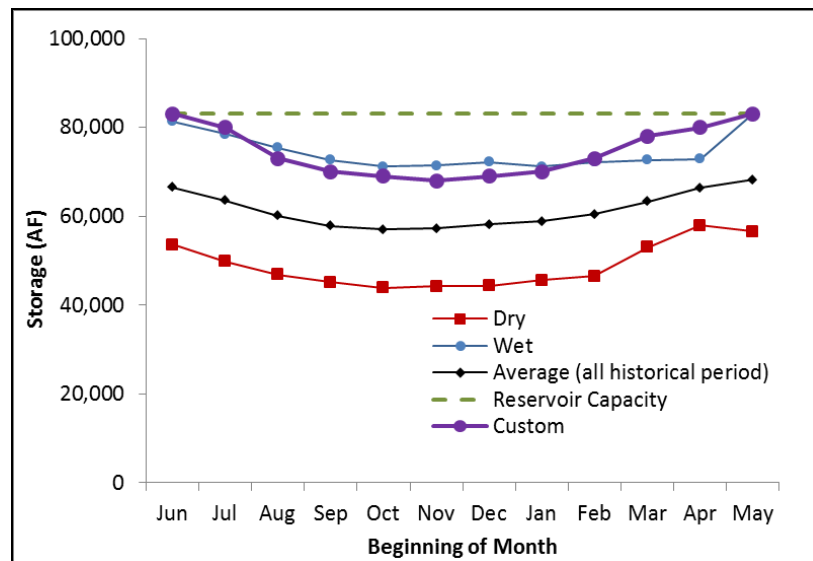


Figure 63. Rule curves derived from historical records for Grizzly Valley Dam: wet years, dry years, and all the years of the historical period. A user-defined custom rule curve is also plotted.

First, the reservoir simulations were done by using the wet rule curve and the release schedule. All runs were made on a monthly time interval. From **Figure 64a**, one can see that the simulated EoM (End of Month) storage is similar to the historical storage in the first portion of the historical period, but then retains slightly higher values than the historical storages for the second portion. Running the simulations for the dry (**Figure 64b**) and average (**Figure 64c**) rule curves do not provide a better fit to the historical storage values. As a result, attempts were made

to change the rule curve in order to get results as close as possible to the historical values. The custom rule curve that gave the closest results to the historical values is plotted in **Figure 63**. Running the reservoir simulation by using the custom rule curve, as well as the release schedule, provided the results in **Figure 64d**, which still show some discrepancies between the simulated and observed storages over the second half of the historical period.

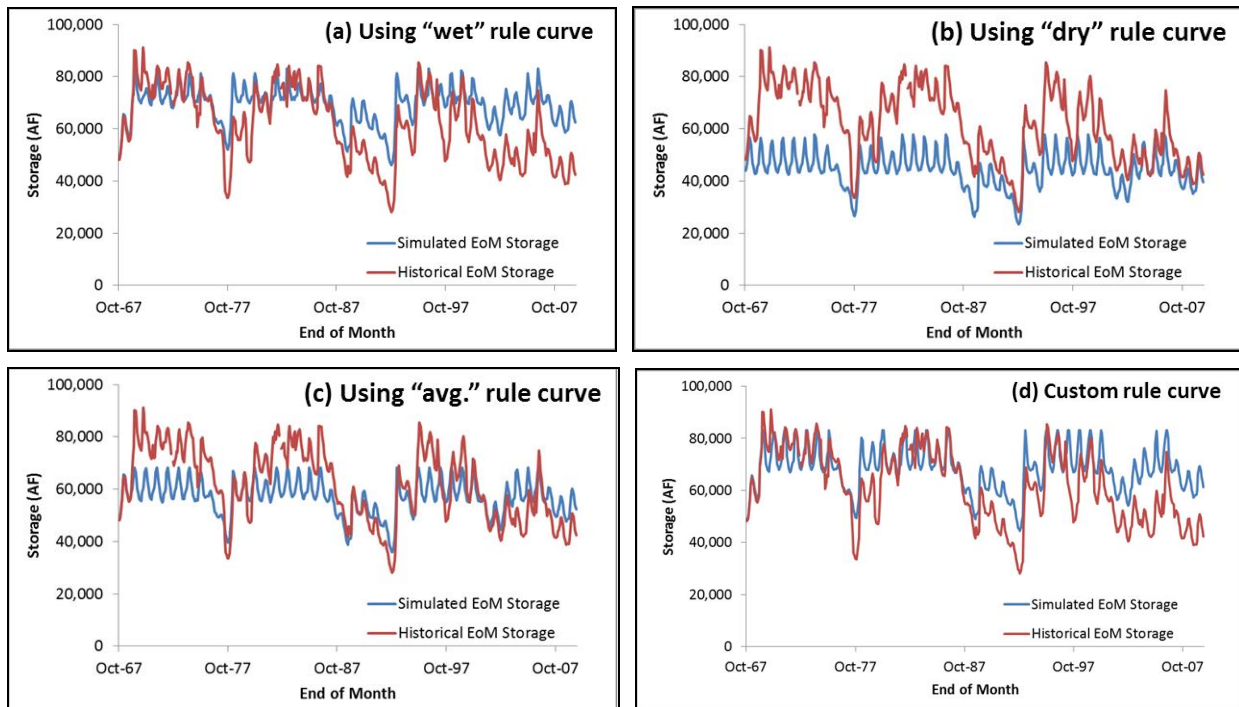


Figure 64. Time series of simulated and observed reservoir storages for Grizzly Valley Dam over the historical period. The simulations were run using: (a) the derived "wet" rule curve, (b) the derived "dry" rule curve, (c) the derived "average" rule curve; and (d) the custom rule curve. EoM: end of month.

Seeing that all of the above attempts did not provide a completely satisfactory simulation of the Grizzly Valley Dam storage time series as compared to the observed values, a different approach was then attempted. This approach involved running the reservoir simulations with no operation rules, and then plotting the simulated storage values against their historical counterparts. The results are shown in **Figure 65**. It is clear from this figure that the simulated and historical results begin in a similar manner at first, until they start to deviate from each other eventually. It was noticed that the major deviations start to occur when the lake storage values go under a certain threshold storage value (dotted line), at which the differences start to become more obvious (see vertical arrows).

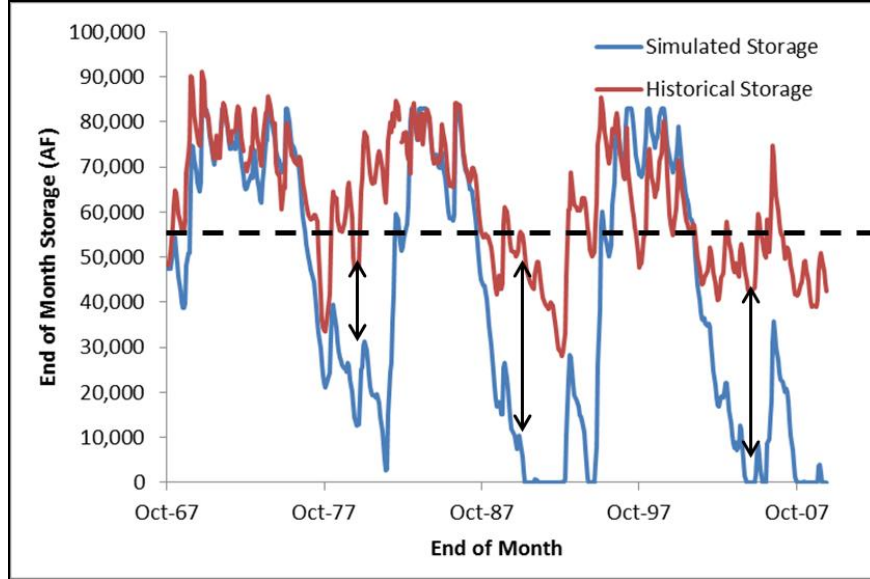


Figure 65. Time series simulated and observed reservoir storages for Grizzly Valley Dam over the historical period. The simulations were run with no rule curve. Vertical arrows emphasize the differences between historical and simulated values.

As a result, new reservoir simulations were run, but this time without the use of any rule curves. Instead of the rule curves, the simulations incorporated a user-defined threshold storage value below which the release of water from the dam was minimized, while still following the minimum release schedule provided in **Figure 61**. Hereafter, this method will be referred to as the threshold method.

After several attempts of the threshold method, a threshold storage value of 56,000 AF was found to provide the best fit results compared to the historical values (**Figure 66**). The results of this simulation produced dam outflow values similar to the historical values (**Figure 67**), with only a 2.3% difference in the sum of these outflows (see inset table in **Figure 67**).

A simple way to represent the results of the reservoir simulation in one figure is shown in **Figure 68**. This figure shows the simulated end-of-month storage values for the reservoir (black line with orange dots). Moreover, it shows the amounts and time-positions of any shortages (red bars) or surpluses (blue bars) faced during the simulation period. Note that for the purpose of this study, a shortage occurs when the demand for a certain period is not fully met; the value of the shortage is the amount of water still required in order to meet the demand. A surplus, on the other hand, occurs when there is excess water in the dam that would cause it to overflow and

spill; the surplus value is the amount of water that spills over the dam and cannot be stored. These values can be easily seen in a figure such as **Figure 68**.

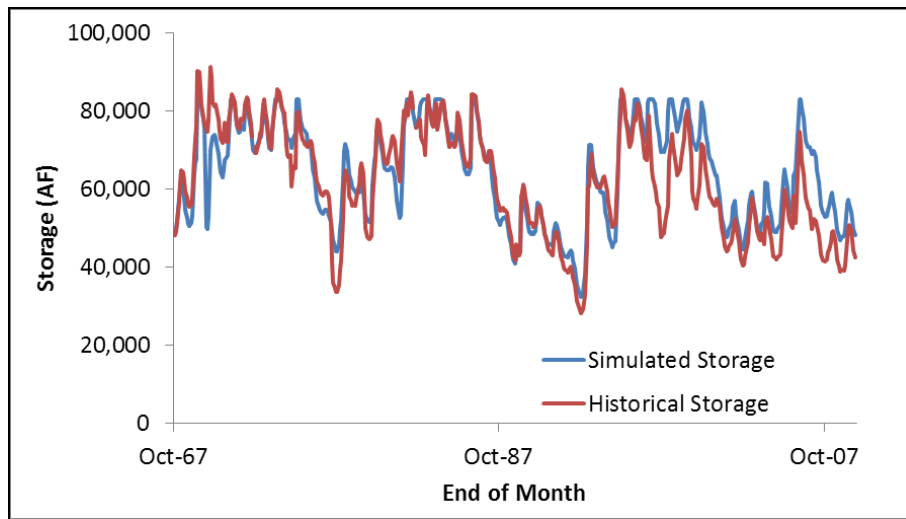


Figure 66. Time series of simulated and observed reservoir storages for Grizzly Valley Dam over the historical period. The simulations were run using the threshold method, using a threshold value of 56,000 AF.

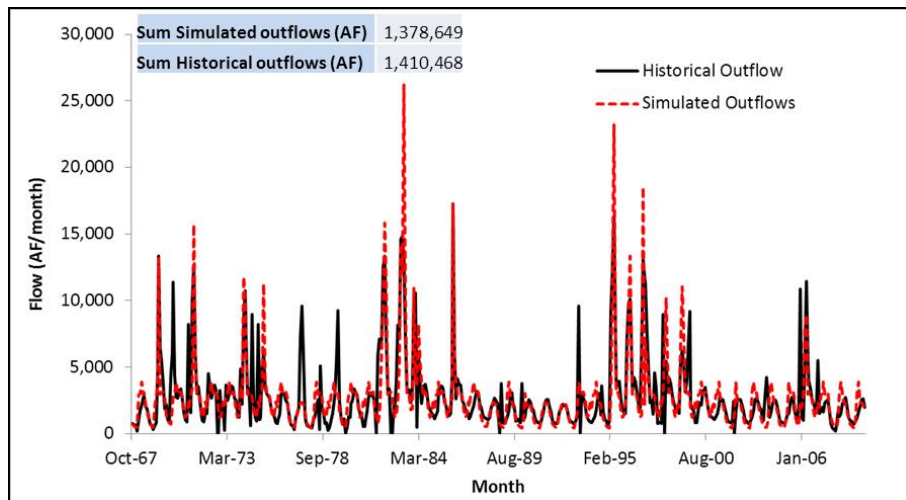


Figure 67. Time series of historical and simulated outflows from the Grizzly Valley Dam, using results from the simulation using the threshold method, and having a 56,000 AF threshold value.

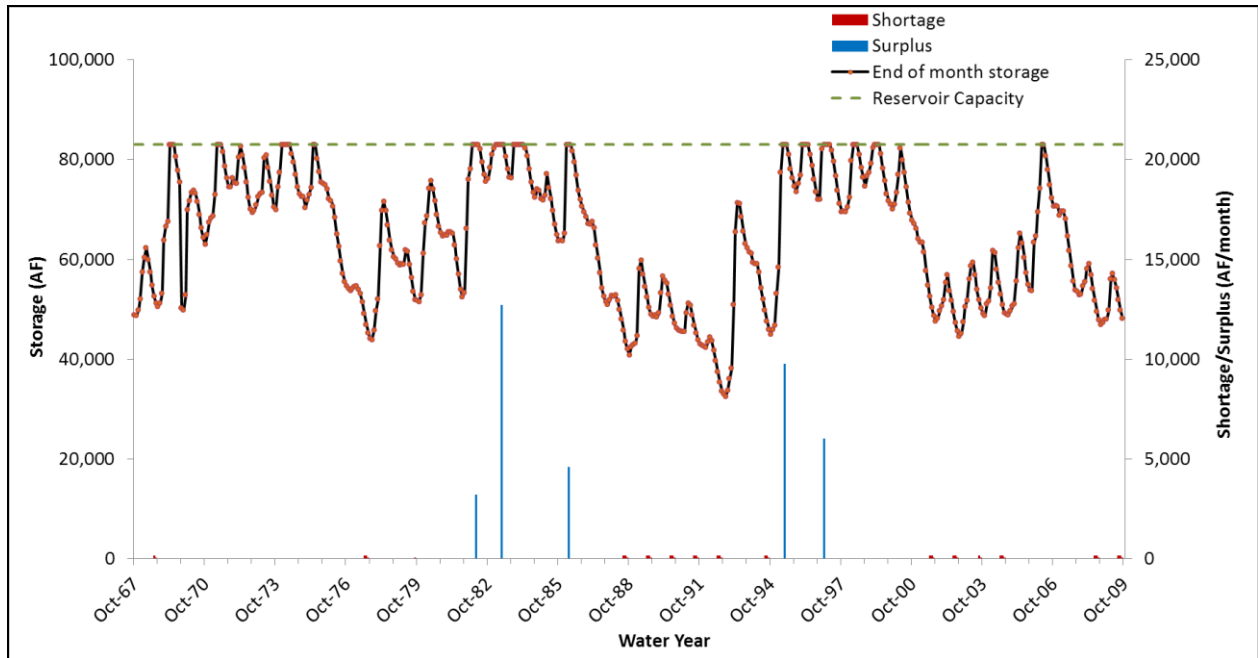


Figure 68. Plot of the simulated end-of-month storage values for Grizzly Valley Dam, along with the amounts and timings of the shortages and surpluses occurring over the historical period.

While **Figure 68** shows that shortages are barely visible and are almost negligible during this historical period, it also shows that the dam had reached maximum capacity several times during its historical period. During a few of those times, a few spills may have occurred, as can be seen from the blue bars in the figure; the estimated total amount of spills over the whole historical period is 36,294 AF.

Recall that the above results are obtained for the simulation using the threshold method that had the best fit the historical values (**Figure 66**), which used a threshold value of 56,000 AF. However, it is possible to adjust the storage threshold value to analyze how the sum of the spills would have been affected. In fact, reducing the threshold value to around half the storage capacity (42,000 AF) provides a 19.8% reduction in the estimated quantity of the amount of spills within the historical period, while a reduction of the threshold value to 36,000 AF provides an estimated 35.7% reduction in the estimated amounts of spills (**Figure 69**). However, comparing **Figure 69** to **Figure 68**, it is clear that this reduction in the amount of spills comes at the expense of having much lower storage values during some time periods, hence increasing the risk of having shortages in case the reservoir is subjected to dry years.

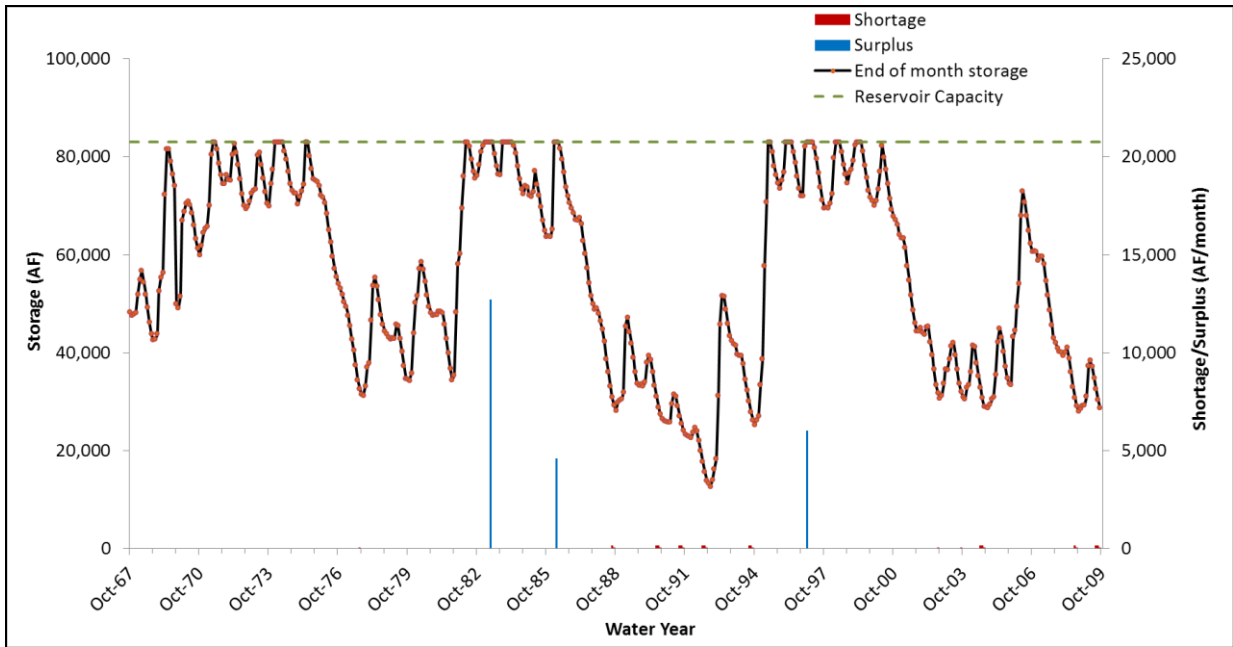


Figure 69. Plot of the simulated end-of-month storage values for Grizzly Valley Dam, along with the amounts and timings of the shortages and surpluses occurring over the historical period. Simulation was done using the threshold method using a threshold value of 36,000 AF.

Therefore, the above discussions show that the threshold method seems to be well representing the historical operations of the Grizzly Valley Dam, and they imply that a possible reduction in the total months and quantity of surpluses would have been possible during the historical period had the reservoir been operated by following the threshold method with a threshold less than 56,000 AF.

4. Future Analysis of the Grizzly Valley Dam

While the above analysis of the Grizzly Valley Dam was done for the historical period, similar analyses for future periods would be of great value for future reservoir operation and management. Global climate projections already exist, as explained in the previous chapter about the Upper Middle Fork (UMF) watershed. Such projections include GCM atmospheric results that show considerable uncertainty between the different future scenarios. The significance of the WEHY model is, thus, shown through the possibility of using those projected GCM atmospheric results as inputs into the model, which will provide the future inflows into the dam as its outputs, one inflow series for each projection.

A sample of the GCM atmospheric results for the future period over the Lake Davis basin can be seen in **Figure 70**. This figure shows the projected annual precipitation averaged over the Lake Davis basin for each of the 13 different future scenarios, along with their ensemble average and general trendline. The figure shows large variability in the projections for future precipitation over the Lake Davis basin, but with an extremely small, almost nonexistent, positive trend over the future years. Another sample of the GCM atmospheric results can be seen in **Figure 71**, which shows the future projected annual mean basin average temperature over the Lake Davis basin. Similarly, this figure shows the results for all 13 different projections, as well as the ensemble average of all projections as well as their trend. While **Figure 71** also shows large variability in the temperature values for the future period, it shows a much clearer trend in the temperature as a function of time during the 21st century. Moreover, the expected trend can be clearly seen to be positive, increasing the temperature over the course of the years along the future period. Additional analysis figures of precipitation and temperature projections over the Lake Davis basin can be found in Appendix B.

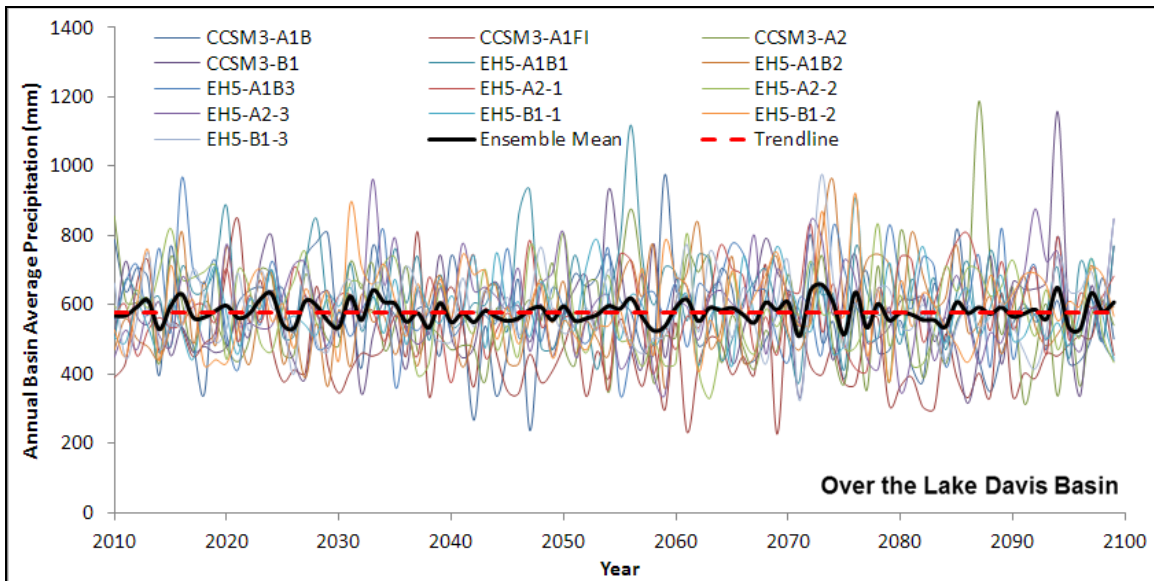


Figure 70. Annual basin average precipitation projected over the Lake Davis basin as projected by the 13 different GCM scenarios. The ensemble mean and trendline are shown by the black bold and red dashed lines, respectively.

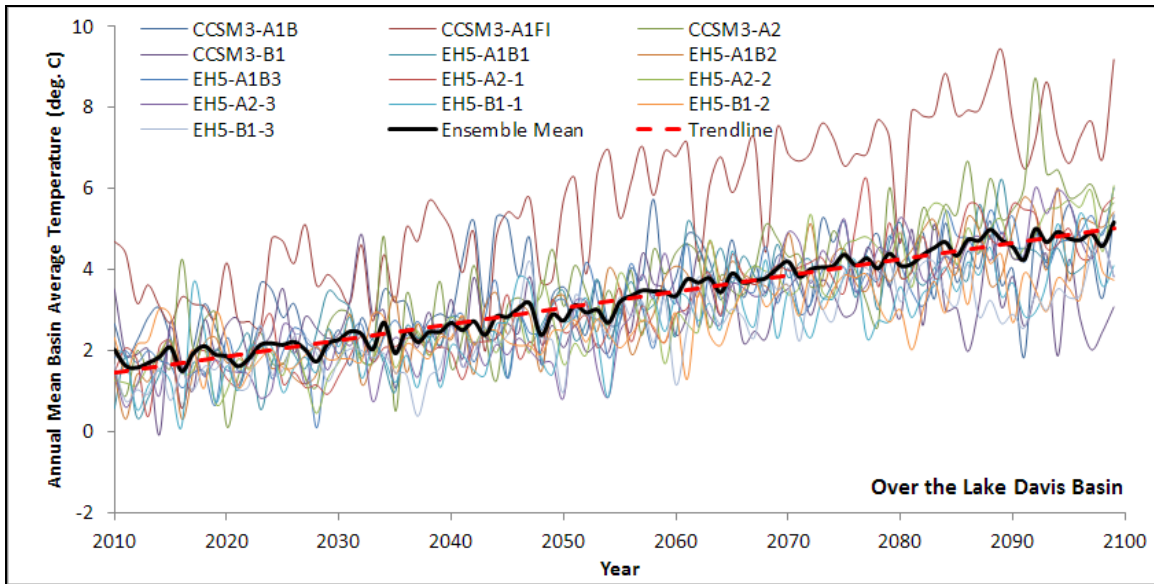


Figure 71. Annual mean basin average temperature over the Lake Davis basin as projected by the 13 different GCM scenarios. The ensemble mean and trendline are shown by the black bold and red dashed lines, respectively.

A. Comparison of Future Projected Inflows into the Grizzly Valley Dam

Future simulations over the Lake Davis watershed used Global Climate Model (GCM) atmospheric results from the previously-discussed 13 climate projections coming from the two GCMs: CCSM3 and ECHAM5. Among the WEHY simulations obtained from the four CCSM3 projections, the average flow discharge values into the Grizzly Valley Dam over the whole period (2010 to 2100) show very close results for the four projections, with a minimum of around 1.11 cms (for A2; 28,297 AF/yr) and a maximum of around 1.19 cms (for A1B; 30,534 AF/yr) (**Table 15**). The range, however, is much larger among the ECHAM5 (EH5) results, with the maximum being around 1.04 cms (B1-2; 26,702 AF/yr) and the minimum as low as 0.87 cms (B1-1; 22,242 AF/yr). Therefore, **Table 15** shows that the highest average of flow discharges within the years 2010 to 2100 is projected by CCSM3-A1B and the lowest is projected by ECHAM5-B1-1. It also shows that the average of the future flows in general is larger for CCSM3 compared to ECHAM5 simulations.

Table 15. Average future projected inflows into the Grizzly Valley Dam over the period spanning the years from 2010 to 2100.

GCM-Scenario	Flow (cms)	Flow (AF/yr)
<i>CCSM3-A1B</i>	1.19	30,534
<i>CCSM3-A1FI</i>	1.15	29,332
<i>CCSM3-A2</i>	1.11	28,297
<i>CCSM3-B1</i>	1.14	29,194
<i>EH5-A1B1</i>	1.03	26,440
<i>EH5-A1B2</i>	0.89	22,655
<i>EH5-A1B3</i>	1.00	25,556
<i>EH5-A2-1</i>	0.99	25,382
<i>EH5-A2-2</i>	0.95	24,341
<i>EH5-A2-3</i>	0.93	23,886
<i>EH5-B1-1</i>	0.87	22,242
<i>EH5-B1-2</i>	1.04	26,702
<i>EH5-B1-3</i>	0.96	24,464

B. Trend Analysis of the Future Projected Inflows into the Grizzly Valley Dam

To get a better idea of the projected future inflows into the dam, a trend analysis was undergone. The non-parametric Mann-Kendall statistical test was used with a significance level, α , of 0.05 to determine whether the trend, if any, can be described as being significant. The benefit of using this test is that it does not require the data to follow any type of distribution, it is less affected than other tests by the presence of outliers, and it can be used even with data sets showing non-linear trends (Önöz & Bayazit, 2003). This test was done for the 13 projections over the whole period from 2010 to 2100, as well as over three subdivisions of the period: 2010-2040, 2040-2070, and 2070-2100. In addition to that, the test was also applied to the ensemble of CCSM3 projections, the ensemble of ECHAM5 projections, and the ensemble of all 13 projections. The results of the test are shown in **Table 16**.

Table 16. Slope (cms/yr) of the trend line of annual mean dam inflow for Grizzly Valley Dam for the 13 different future projections, as well as for the ensemble of CCSM3, EH5, and all projections. Significance of the trend was determined using the Mann-Kendall statistical test. p values are given in parentheses; p values that show a significant change ($p < 0.05$) are shown in bold.

GCM-Projection	Water years 2010 – 2040	Water years 2040 – 2070	Water years 2070 - 2100	Water years 2010 - 2100
CCSM3-A1B	-4.84E-03 (0.544)	+1.54E-02 (0.475)	-9.94E-03 (0.475)	-2.21E-03 (0.354)
CCSM3-A1FI	-8.76E-03 (0.803)	-1.24E-02 (0.521)	-3.08E-03 (0.943)	-3.21E-03 (0.296)
CCSM3-A2	-5.49E-03 (0.433)	+2.57E-02 (0.094)	-1.88E-02 (0.318)	+3.12E-03 (0.229)
CCSM3-B1	+1.23E-02 (0.239)	+3.48E-02 (0.013)	+1.21E-02 (0.669)	+7.61E-03 (0.003)
EH5-A1B1	+6.32E-03 (0.254)	+5.16E-03 (0.695)	+3.83E-02 (0.002)	+3.07E-03 (0.195)
EH5-A1B2	-6.68E-04 (0.915)	+1.44E-02 (0.144)	-2.66E-02 (0.915)	+9.02E-03 (<0.001)
EH5-A1B3	-1.33E-02 (0.069)	+1.47E-02 (0.101)	+6.44E-03 (0.544)	+5.53E-03 (0.002)
EH5-A2-1	-2.07E-03 (0.748)	-4.89E-03 (0.568)	+1.27E-02 (0.372)	+7.24E-03 (<0.001)
EH5-A2-2	-2.32E-02 (0.154)	-1.68E-02 (0.187)	+1.09E-02 (0.475)	+1.72E-03 (0.387)
EH5-A2-3	+1.60E-02 (0.164)	+1.94E-02 (0.212)	-5.71E-03 (0.544)	+5.74E-03 (0.019)
EH5-B1-1	+1.25E-02 (0.225)	+8.95E-04 (0.844)	-1.35E-02 (0.094)	+1.35E-03 (0.409)
EH5-B1-2	+3.09E-02 (0.025)	-6.77E-03 (0.775)	+4.71E-03 (0.617)	-9.77E-04 (0.631)
EH5-B1-3	+1.42E-02 (0.059)	+7.64E-03 (0.372)	-1.38E-02 (0.354)	+4.47E-03 (0.041)
Ensemble (CCSM3)	+3.33E-03 (0.669)	+1.81E-02 (0.006)	-2.90E-03 (0.748)	+2.72E-03 (0.057)
Ensemble (EH5)	+9.13E-03 (0.052)	+5.71E-03 (0.212)	+4.44E-03 (0.187)	+4.24E-03 (<0.001)
Ensemble All Projections	+5.86E-03 (0.059)	+8.38E-03 (0.008)	+3.94E-03 (0.284)	+3.44E-03 (<0.001)

Table 16 shows the slopes of the trend lines of the annual mean inflow into the dam, along with the p value that helps determine if the trend is statistically significant or not. From this table, it is clear that for the three subdivision periods within the 21st century, there are only three that show statistically significant trends out of the 39 (3x13). These statistically significant ones are positive trends for EH5-B1-2, CCSM3-B1, and EH5-A1B1 in the early, mid, and late 21st century, respectively. However, looking at the whole period from 2010 to 2100, the statistical test showed a significant positive trend in 6 out of the 13 projections, one from CCSM3 (B1), and five from ECHAM5 (A1B2, A1B3, A2-1, A2-3, and B1-3), with average annual increases (slopes) ranging from 4.47×10^{-3} cms/yr to 9.02×10^{-3} cms/yr (122 AF/yr/yr to 231 AF/yr/yr). Finally, while the ensemble of CCSM3 did not show any significant trend for the

21st century, the ensemble of ECHAM5 and of all the projections both showed significant positive trends.

Therefore, since all of the significant trends in **Table 16** are positive, and since the trend for the ensemble of all projections is a significant positive trend, an increase in the annual mean inflows into the Grizzly Valley Dam for the future years would be the most likely scenario. While that may be a welcomed scenario, one must not disregard the distribution of the inflows with time into the dam, since that would also be of great importance to the dam operation. Hence, an analysis of the reservoir under these future projections would provide an understanding of the effects of such inflow changes to the dam storage, as well as any surplus or shortage that may occur.

C. Analysis of Reservoir Operations under Future Projected Inflows into the Grizzly Valley Dam

The analysis of the Grizzly Valley Dam for the future projections was done in a similar way to the historical analysis undergone in the previous section. In such analyses, it is important to observe how the reservoir storage, shortages, and surpluses change in order to assess the risk of running the reservoir using the current operation procedures and to decide if different procedures may produce better results for the future period.

First, the reservoir simulations were run for all of the 13 different projections by using the threshold method, with a threshold value of 56,000 AF (the one yielding results closest to historical values as discussed in the previous section). The detailed results for all of the 13 different projections are provided in **Figure 72** (for EH5) and in **Figure 73** (for CCSM3).

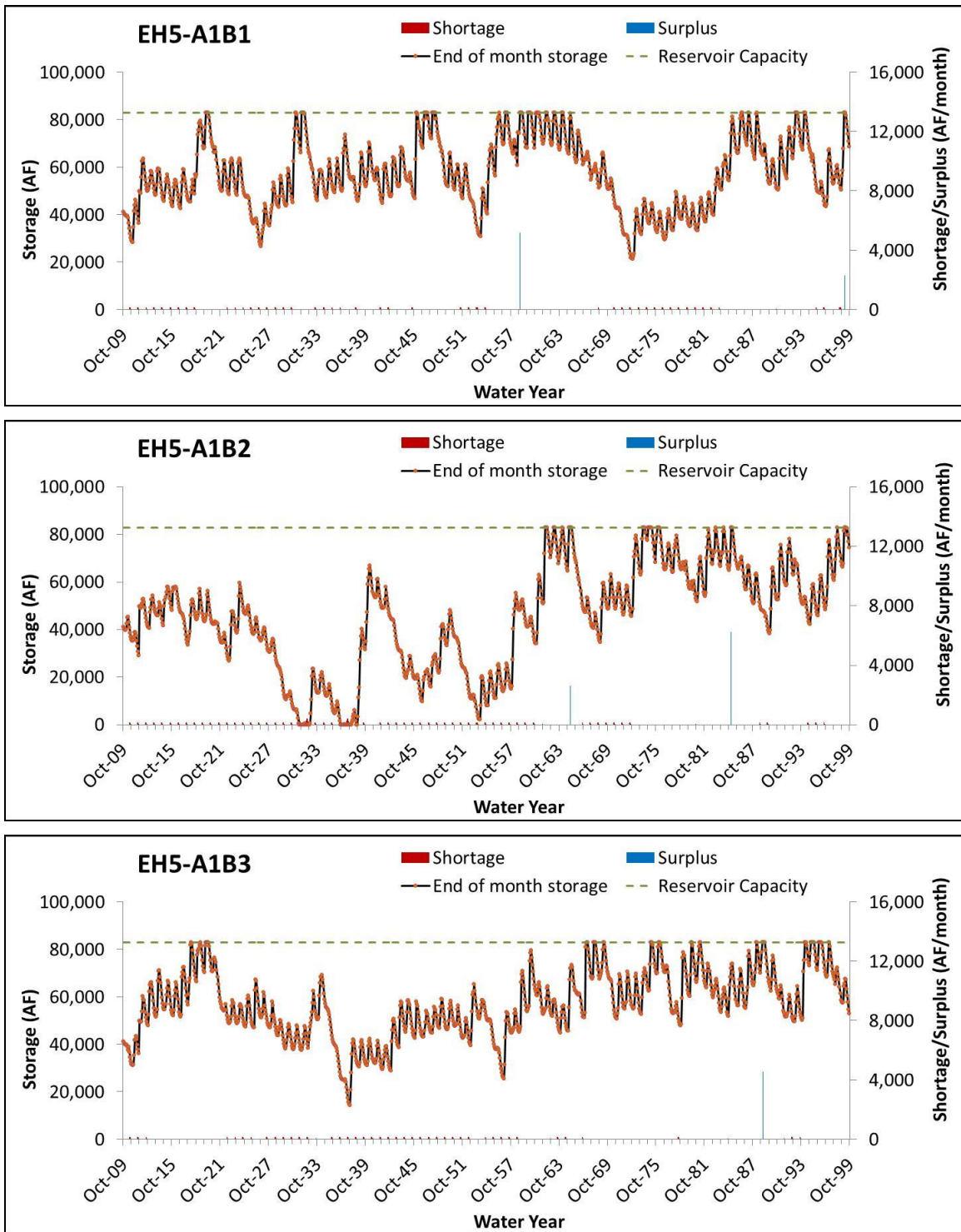


Figure 72. Plot of the simulated end-of-month storage values for Grizzly Valley Dam, along with the amounts and timings of the shortages and surpluses occurring over the future period by using projections from the EH5 GCM. Threshold value used: 56,000 AF (continued below).

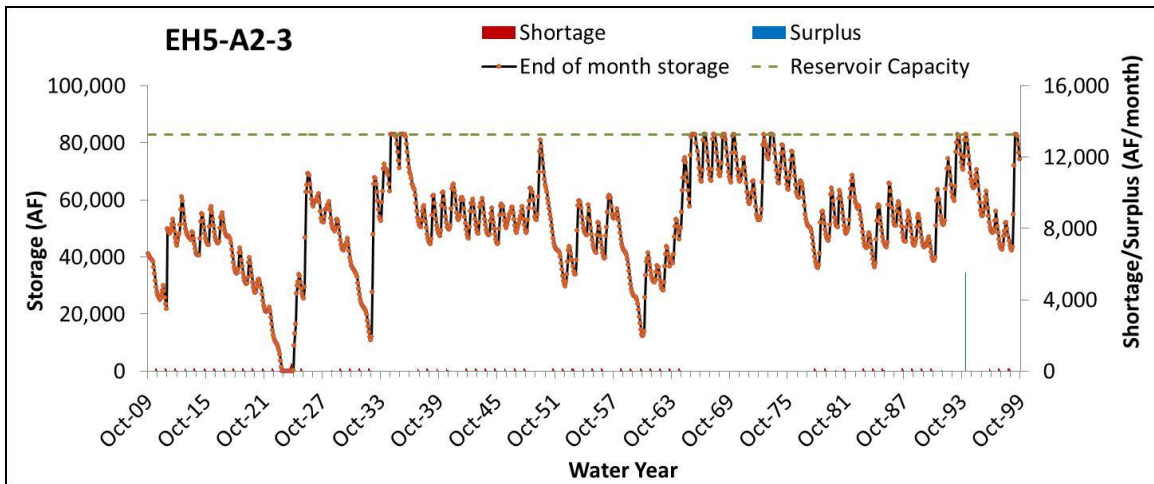
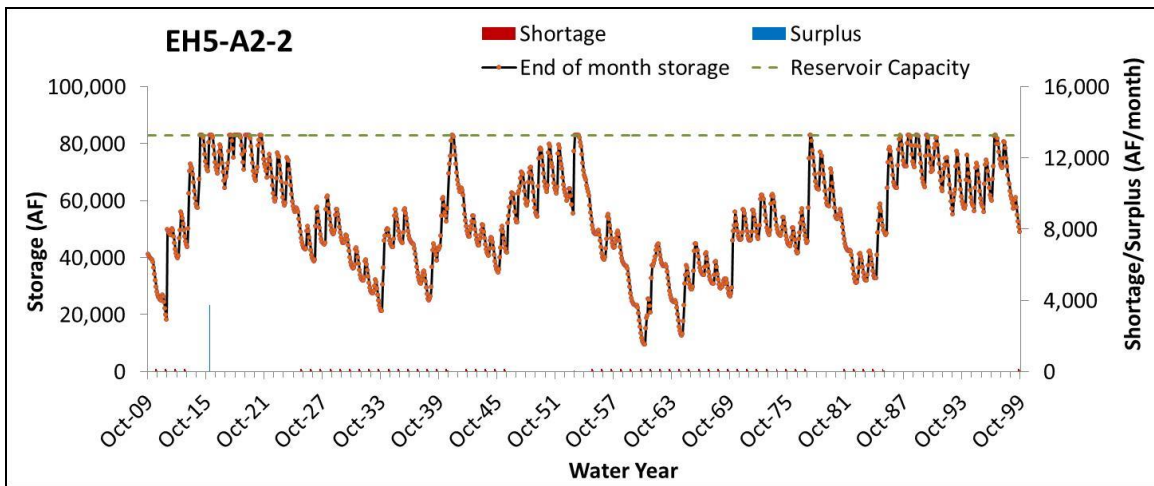
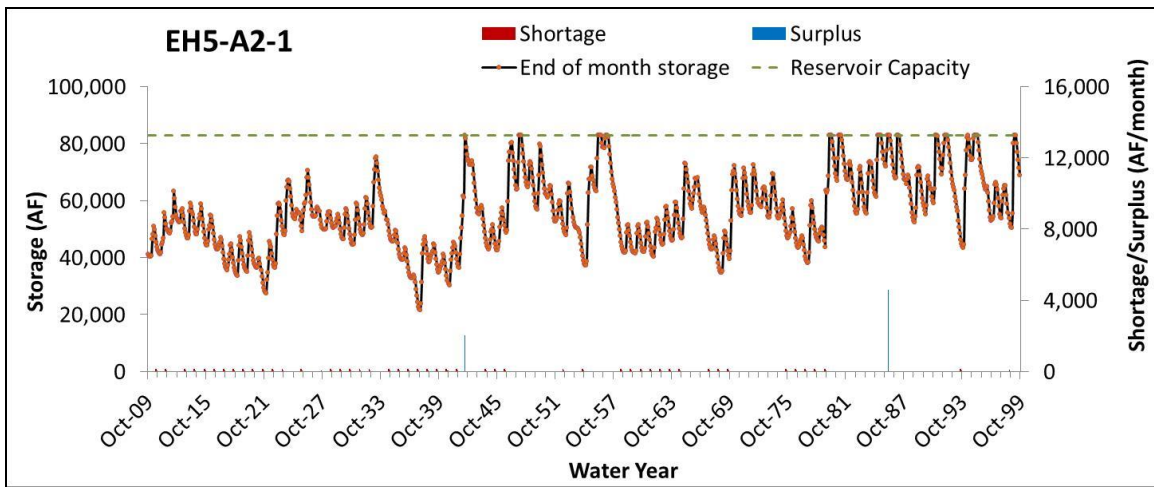


Figure 72 (continued). Plot of the simulated end-of-month storage values for Grizzly Valley Dam, along with the amounts and timings of the shortages and surpluses occurring over the future period by using projections from the EH5 GCM. Threshold value used: 56,000 AF (continued below).

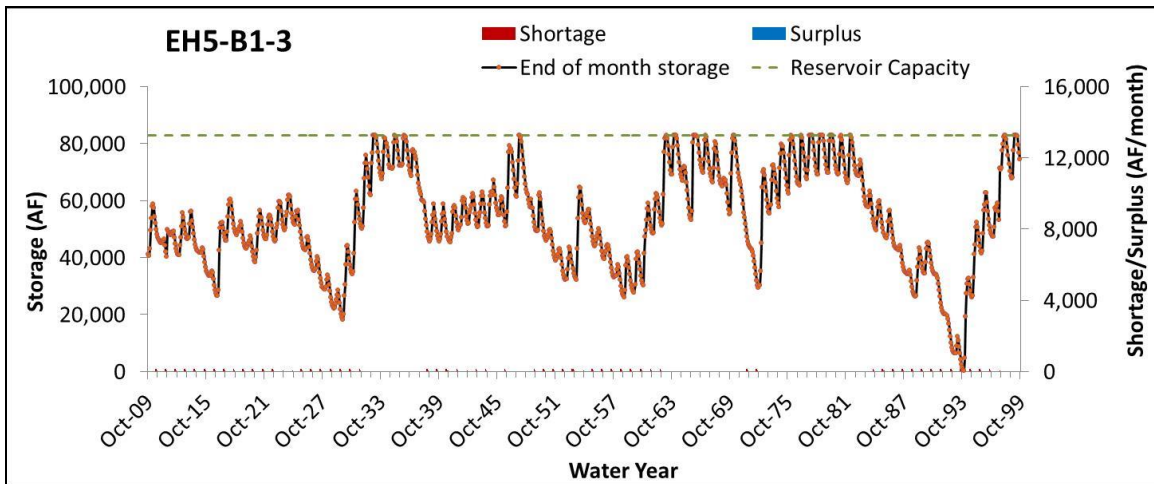
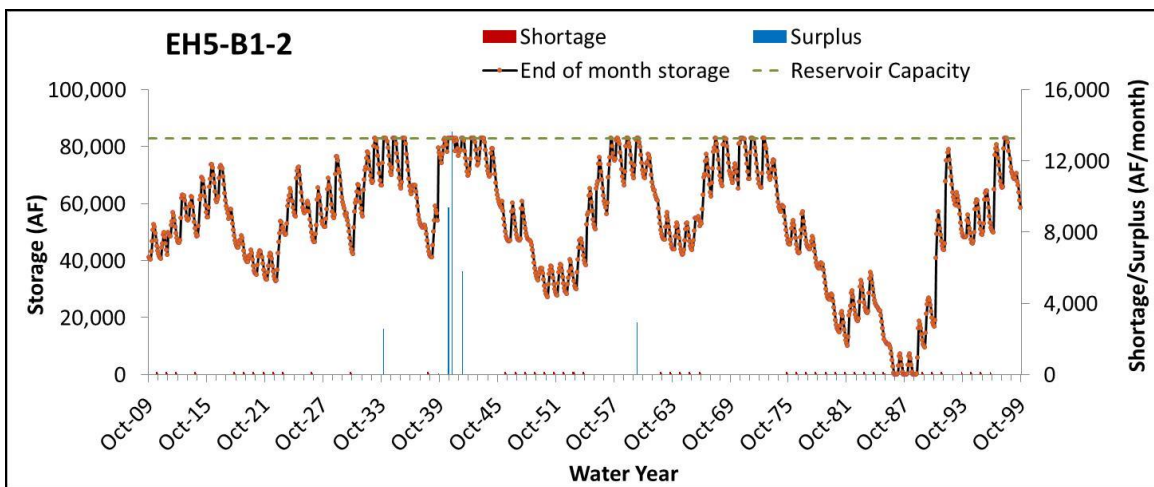
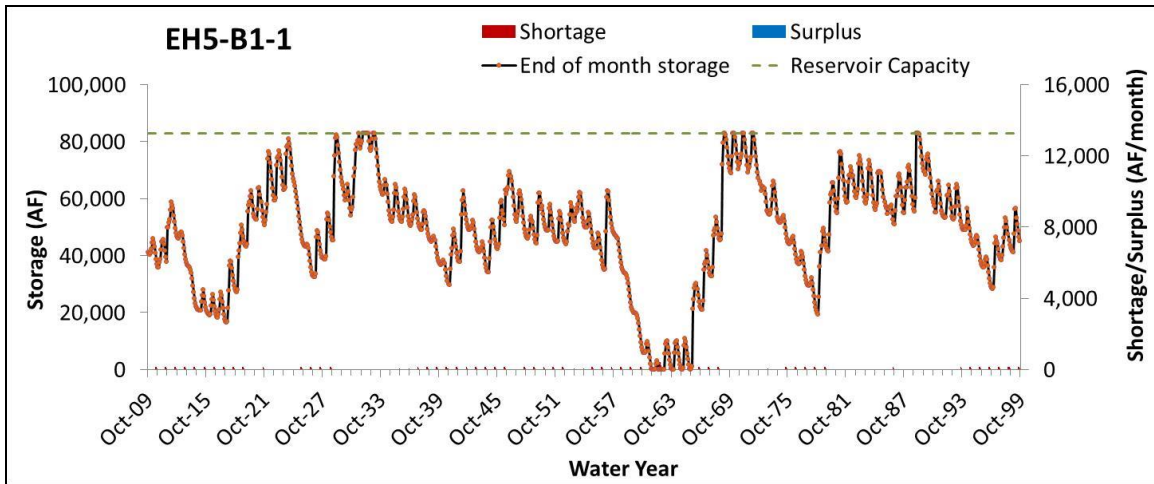


Figure 72 (continued). Plot of the simulated end-of-month storage values for Grizzly Valley Dam, along with the amounts and timings of the shortages and surpluses occurring over the future period by using projections from the EH5 GCM. Threshold value used: 56,000 AF.

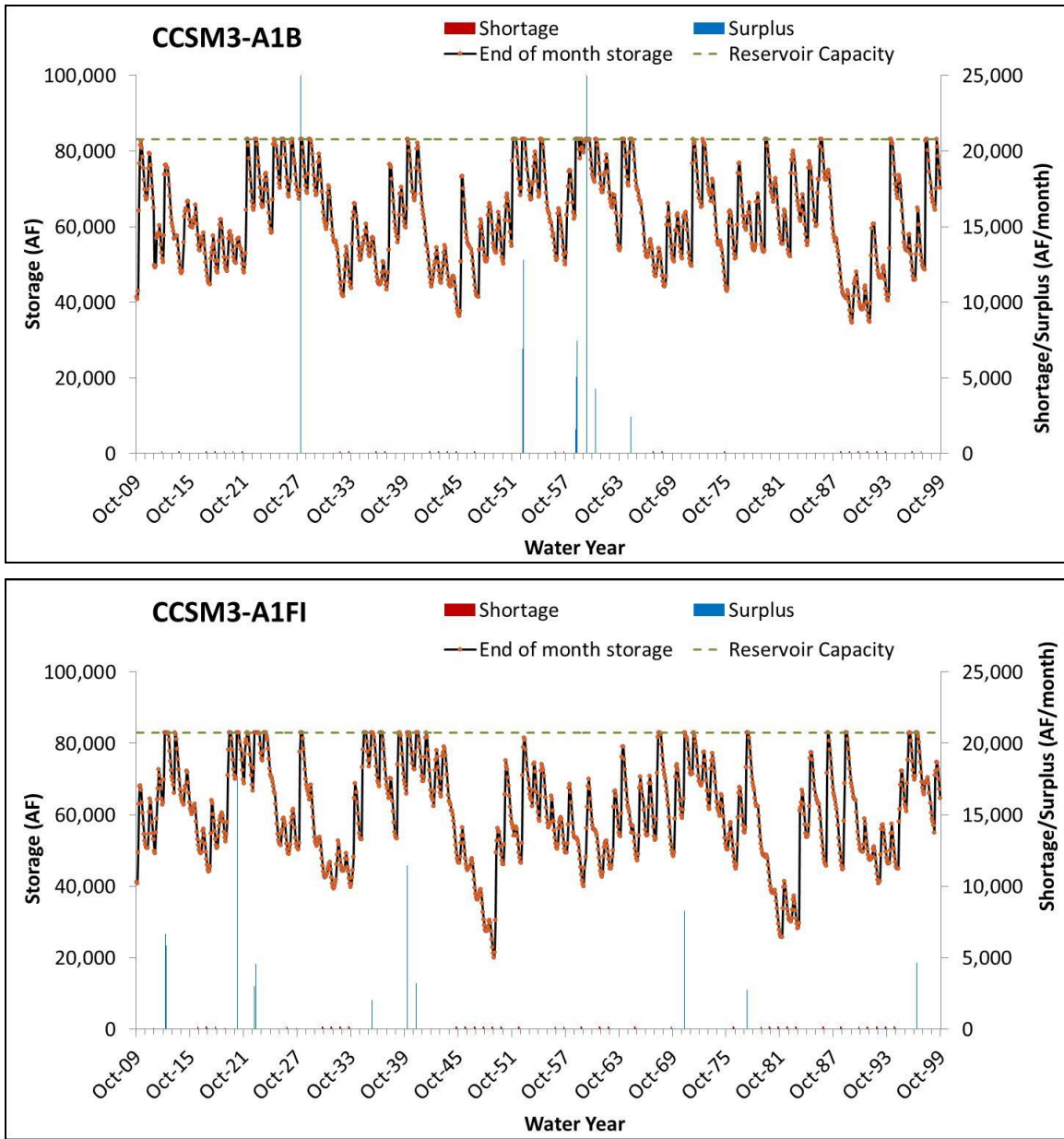


Figure 73. Plot of the simulated end-of-month storage values for Grizzly Valley Dam, along with the amounts and timings of the shortages and surpluses occurring over the future period by using projections from the CCSM3 GCM. Threshold value used: 56,000 AF (continued below).

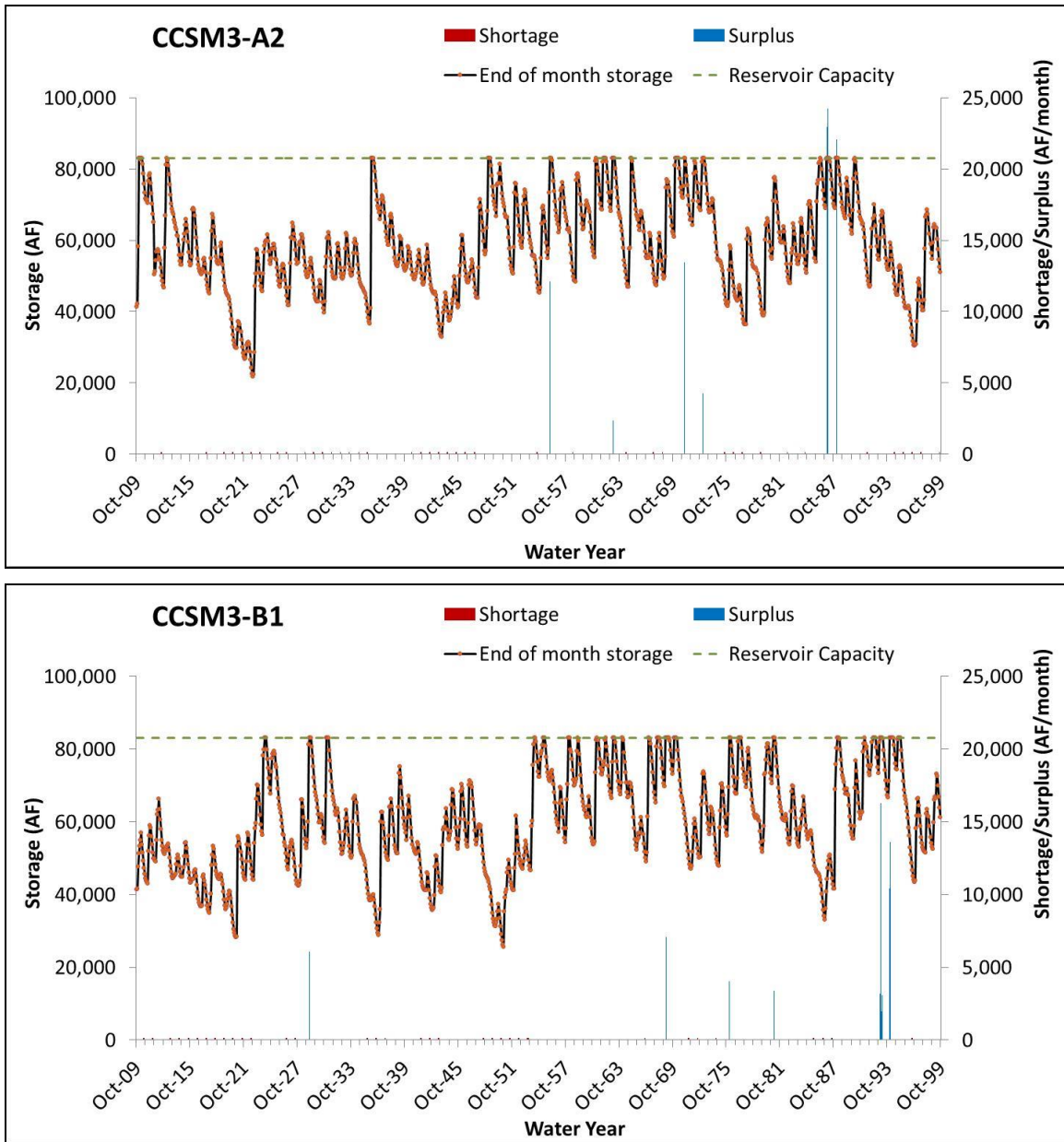


Figure 73 (continued). Plot of the simulated end-of-month storage values for Grizzly Valley Dam, along with the amounts and timings of the shortages and surpluses occurring over the future period by using projections from the CCSM3 GCM. Threshold value used: 56,000 AF.

In addition to plotting the above figures for each of the 13 future scenarios, the main results of all 13 scenarios can be summarized in a simplified figure, as shown in **Figure 74**. In this figure, one can see the average annual shortage and average annual surplus for each projection. Moreover, the figure also shows the lowest simulated reservoir storage during the simulation period from 2010 to 2100. As such, **Figure 74** provides a simplified summary of

Figure 72 and Figure 73 so that one can easily compare the dam operation results between the 13 different future scenarios.

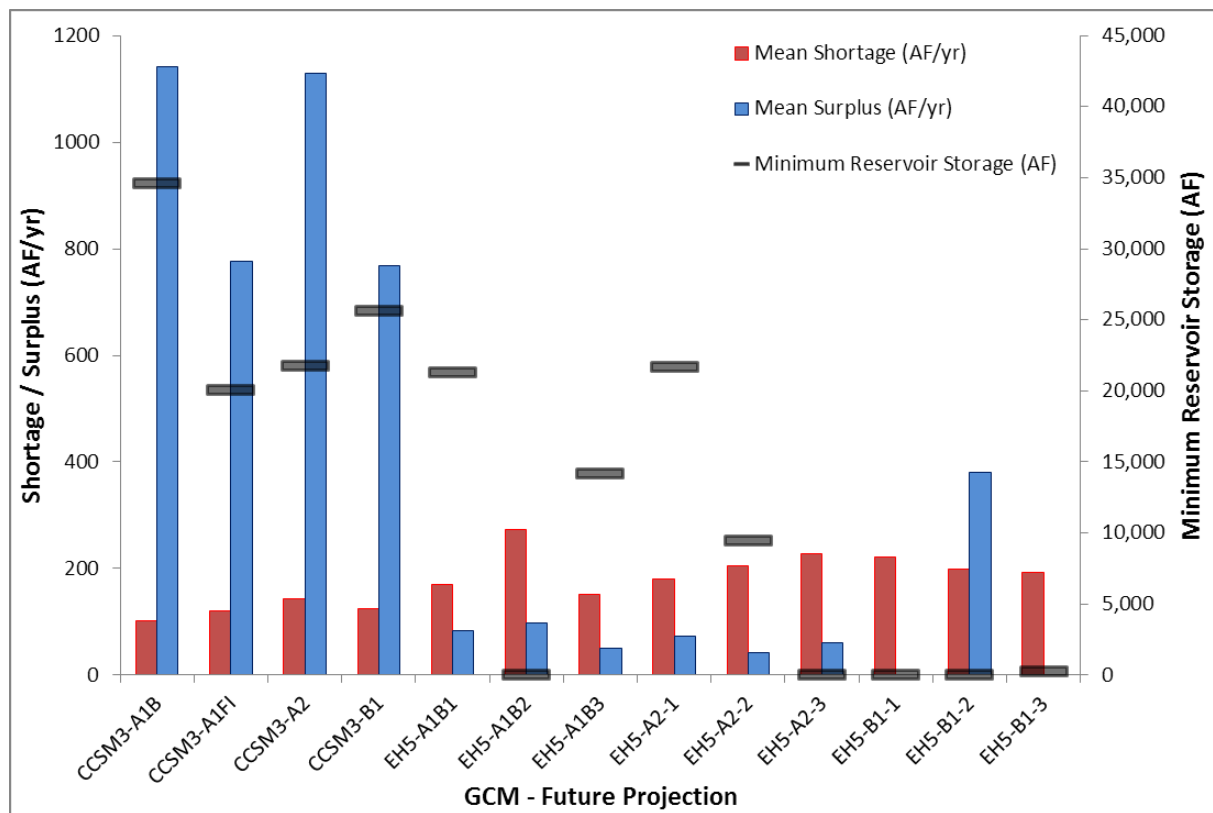


Figure 74. Summary of Grizzly Valley Dam reservoir simulation results for the 13 future projections, showing shortages, surpluses, and minimum reservoir storage values over the period from 2010 to 2100. Simulation was run using threshold method, with a threshold value of 56,000 AF.

Figure 74 shows that all future projections seem to project the presence of shortages and surpluses; however, some vary significantly in their values. In fact, it is clear that the CCSM3 projections provide the largest expected surpluses, whereas the expected shortages for the EH5 projections are slightly higher than those of CCSM3. The highest expected average annual shortage was found for the EH5-A1B2 projection, with a value of around 273 AF/yr. It is interesting to note that the EH5-A1B2 projection was shown to have a statistically significant positive trend during the 21st century period (Table 16). However, as stated previously, that would not necessarily be the only factor affecting the results. In fact, the time series of the inflow, as well as the variation within the flow values (e.g., presence of high maximums) would have an impact on the final results of the dam operation. Actually, looking at the plot for EH5-A1B2 from Figure 72, one can clearly see how the reservoir storage is projected to be relatively low

within the first half of the 21st century, even reaching zero a few times during that period. As such, this scenario shows the highest number of shortages (a total of 205) among all the other scenarios which add up to make this scenario the one with the highest average annual shortage (**Figure 74**).

As for the projected surpluses (or spills) from the Grizzly Valley Dam, it is clear from **Figure 74** that the highest surpluses are expected to occur for the CCSM3-A1B and CCSM3-A2 scenarios. This can also be seen by comparing the corresponding plots of these two scenarios in **Figure 73**, which not only show a large number of surpluses over the future period, but also reveal high values for each of those surpluses. The other two CCSM3 scenarios show lower surpluses than the former two, but all surpluses projected by the CCSM3 scenarios are significantly higher than those projected by the EH5 scenarios (**Figure 74**).

Another important observation for the dam operations would be the minimum storage that the reservoir attains during the simulation period. From **Figure 72** and **Figure 73**, one can see the detailed end-of-month time series of the reservoir storage over the future simulation period for all of the 13 scenarios. The summary figure, **Figure 74**, also provides an idea of such values by showing the minimum reservoir storage that was attained at any time during the simulation period. From all these figures, it is clear that some future scenarios may lead to the depletion of the reservoir storage under the current operating procedures. These scenarios are all from the ECHAM5 (EH5) GCM, specifically A1B2, A2-3, B1-1, B1-2 and B1-3 (**Figure 74**). However, it is important to note that the number of times the reservoir reaches depletion and the period at which that depletion occurs differ significantly among those five projections. Looking at the corresponding plots of **Figure 72**, one can see that the reservoir in the EH5-B1-3 scenario is projected to experience depletion at one month (one point) occurring near the end of the 21st century, whereas the EH5-B1-2 scenario is projected to experience depletion at a similar time but over a longer period. Moreover, the depletion period of EH5-B1-1 is seen to be even longer than the former two while occurring closer to the middle of the 21st century. Finally, the depletion occurring in EH5-A1B2 and EH5-A2-3 is expected to be in the first part of the 21st century. Therefore, different scenarios can be seen to provide different period lengths and timings for the occurrence of reservoir storage depletion.

While it is certainly critical not to deplete the reservoir storage during its operating life, it has also been mentioned to the UC Davis project team by Plumas County representatives that it would be recommended to maintain the release from the Grizzly Valley Dam from the top two outlets only, but not from the lowest one. Hence, it would be recommended for the reservoir storage not to decline below the second outlet elevation (5,740 ft), which translates into a storage value of around 5,595 AF. With this criterion in mind, one can see that 5 of the 13 projections attain minimum storage values less than 5,595 AF (**Figure 74**), and thus violate the recommended storage requirements.

One way to tackle the above problem is by changing the threshold value used for the reservoir operation. As stated previously, the above simulation runs that were done for the future projections used a threshold value of 56,000 AF, which is the threshold value that was found during the previously-discussed historical analysis. However, changing that threshold value may affect the results obtained. For this particular case of tackling the reservoir storage depletion, a higher threshold value may be preferred. Using a higher threshold means that switching to the minimum release schedule will occur earlier, i.e., it will occur when the reservoir hits a higher minimum threshold storage limit. For example, using a threshold value of 62,000 AF means that the releases from the reservoir will follow the minimum release schedule as soon as the end-of-month reservoir storage falls below 62,000 AF (as opposed to waiting until it falls below 56,000 AF). The results of such a change for all 13 future projections are shown in **Figure 75** (for EH5) and **Figure 76** (for CCSM3), with the summary results plotted in **Figure 77**.

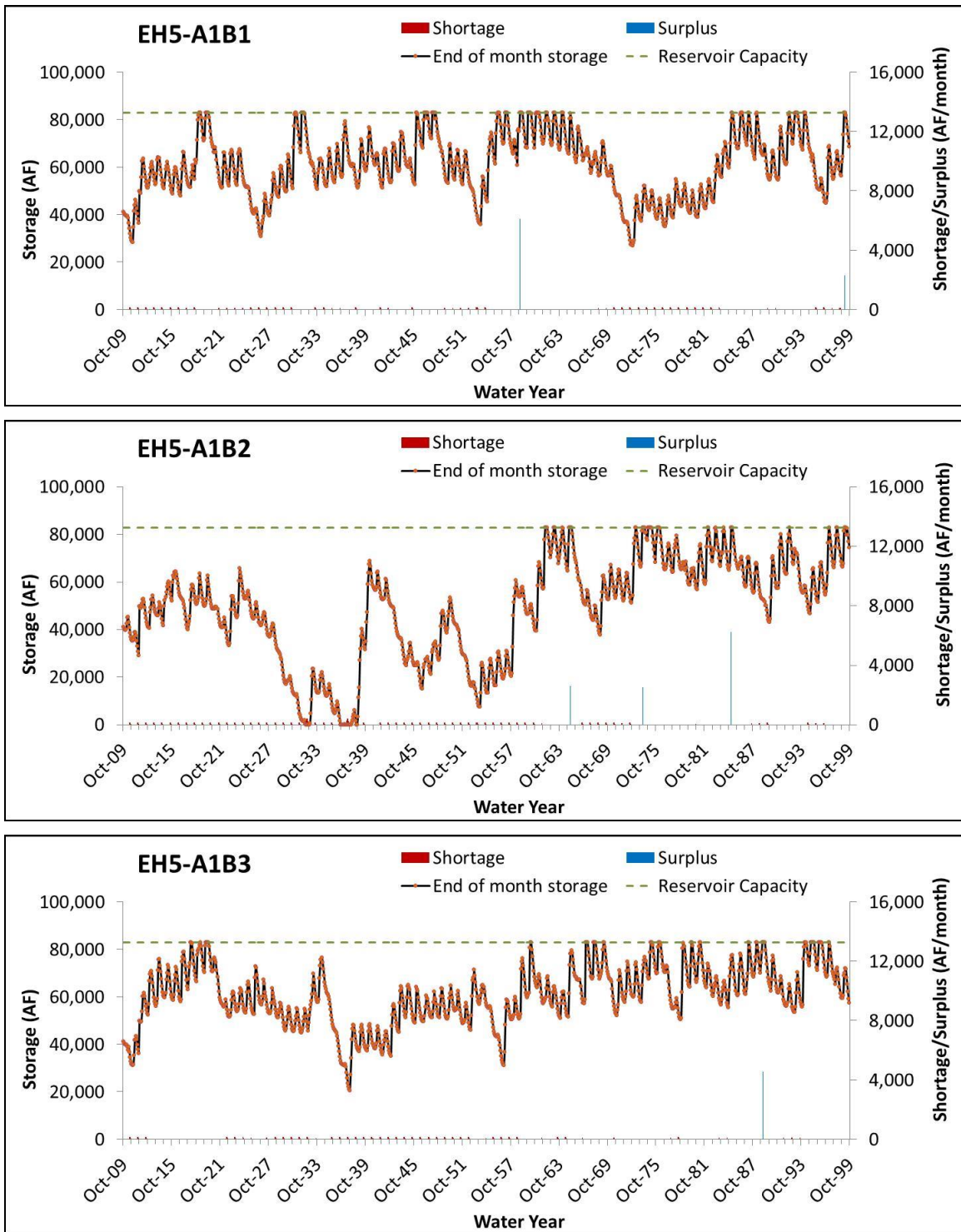


Figure 75. Plot of the simulated end-of-month storage values for Grizzly Valley Dam, along with the amounts and timings of the shortages and surpluses occurring over the future period by using projections from the EH5 GCM. Threshold value used: 62,000 AF (continued below).

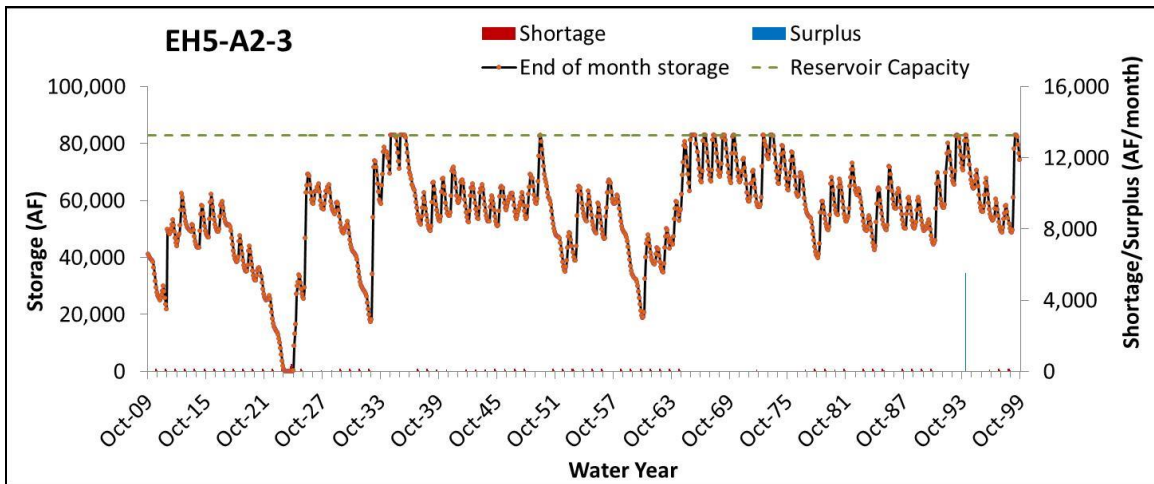
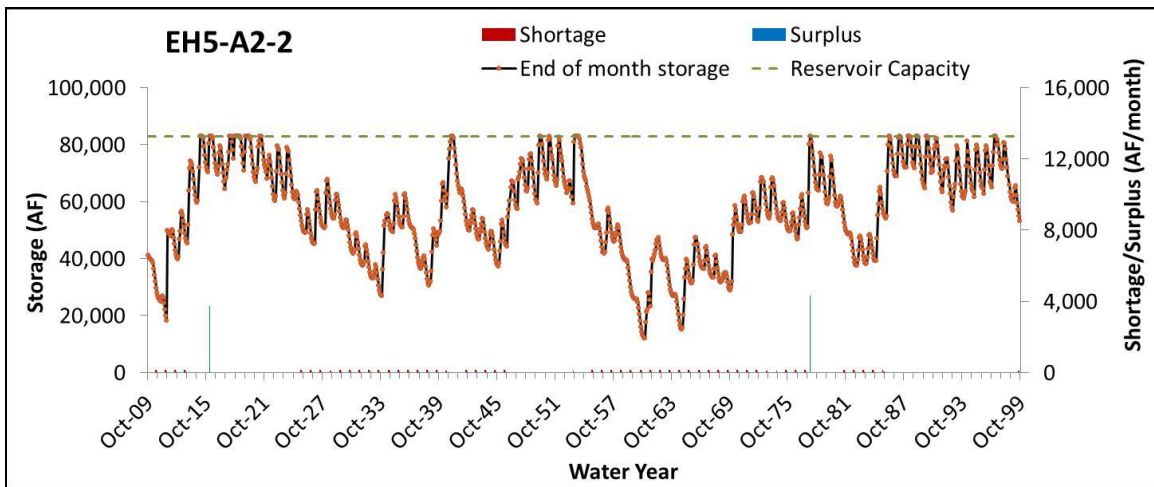
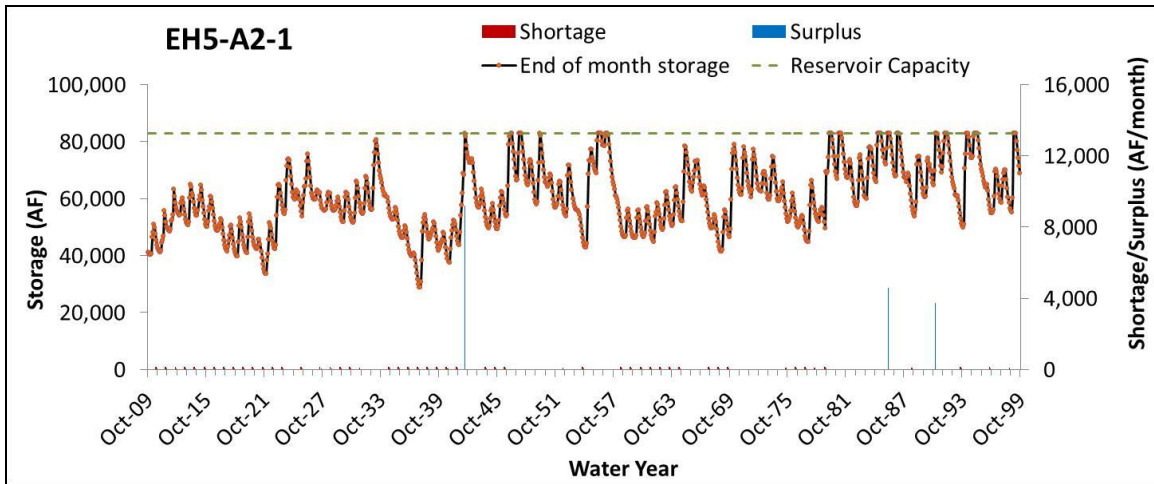


Figure 75 (continued). Plot of the simulated end-of-month storage values for Grizzly Valley Dam, along with the amounts and timings of the shortages and surpluses occurring over the future period by using projections from the EH5 GCM. Threshold value used: 62,000 AF (continued below).

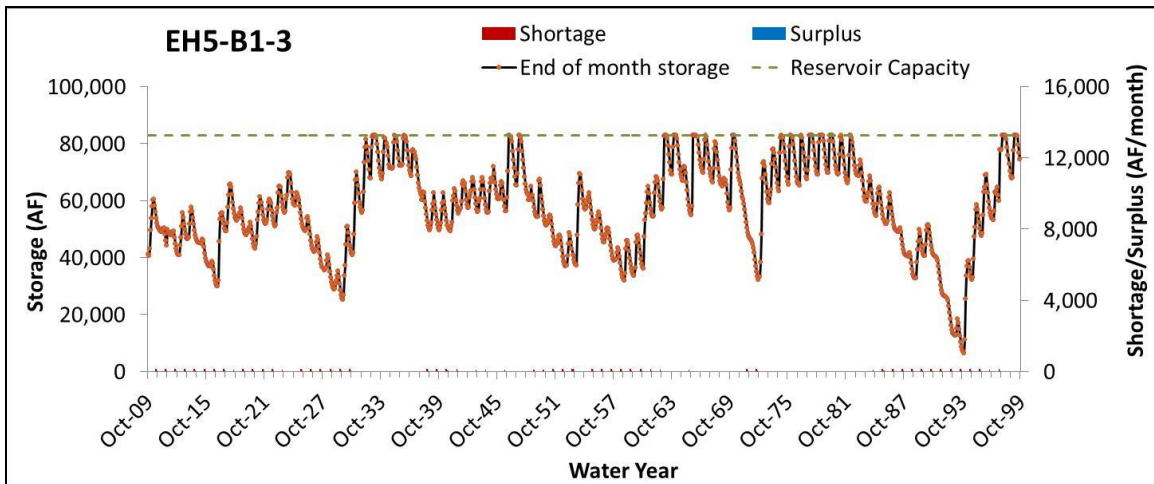
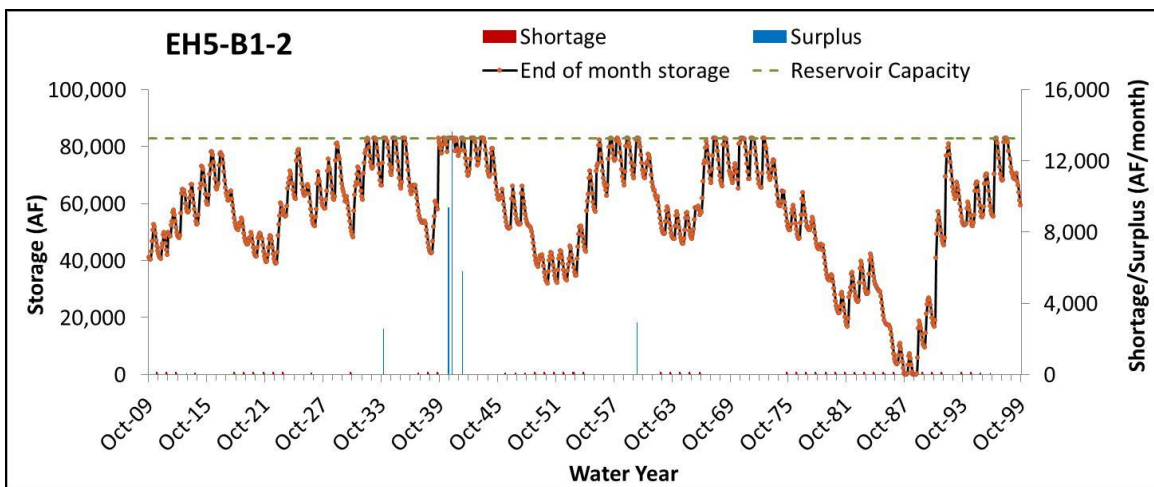
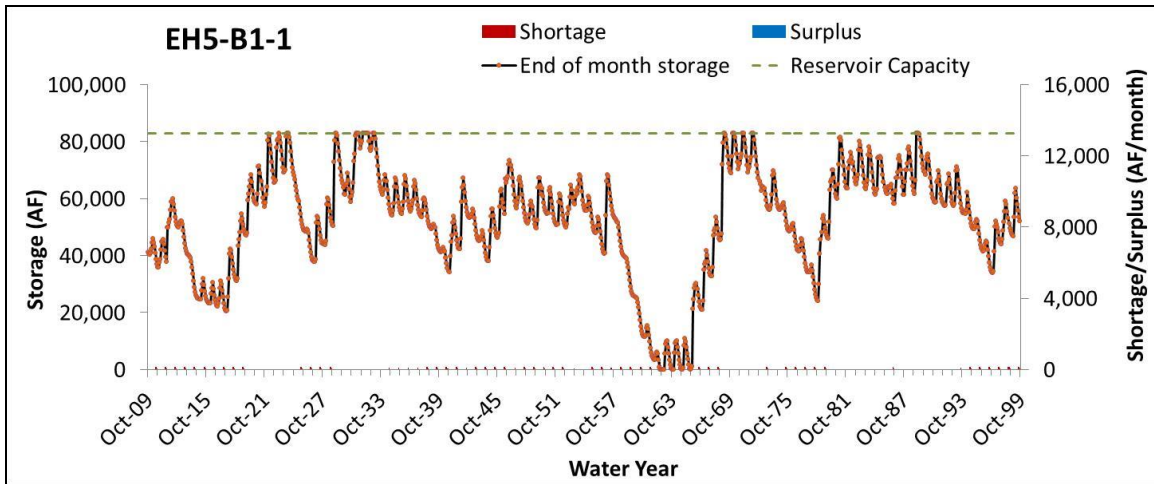


Figure 75 (continued). Plot of the simulated end-of-month storage values for Grizzly Valley Dam, along with the amounts and timings of the shortages and surpluses occurring over the future period by using projections from the EH5 GCM. Threshold value used: 62,000 AF.

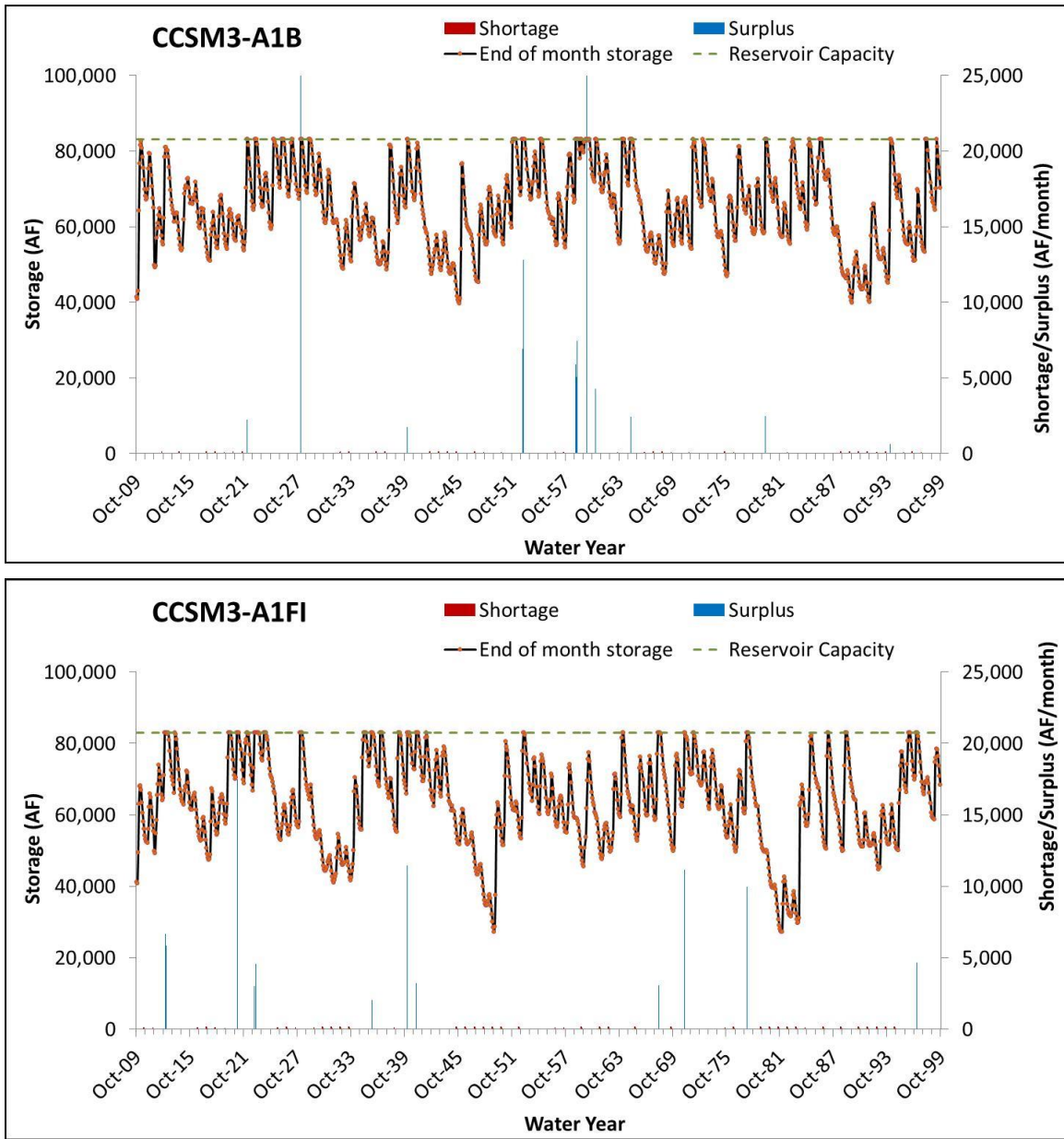


Figure 76. Plot of the simulated end-of-month storage values for Grizzly Valley Dam, along with the amounts and timings of the shortages and surpluses occurring over the future period by using projections from the CCSM3 GCM. Threshold value used: 62,000 AF (continued below).

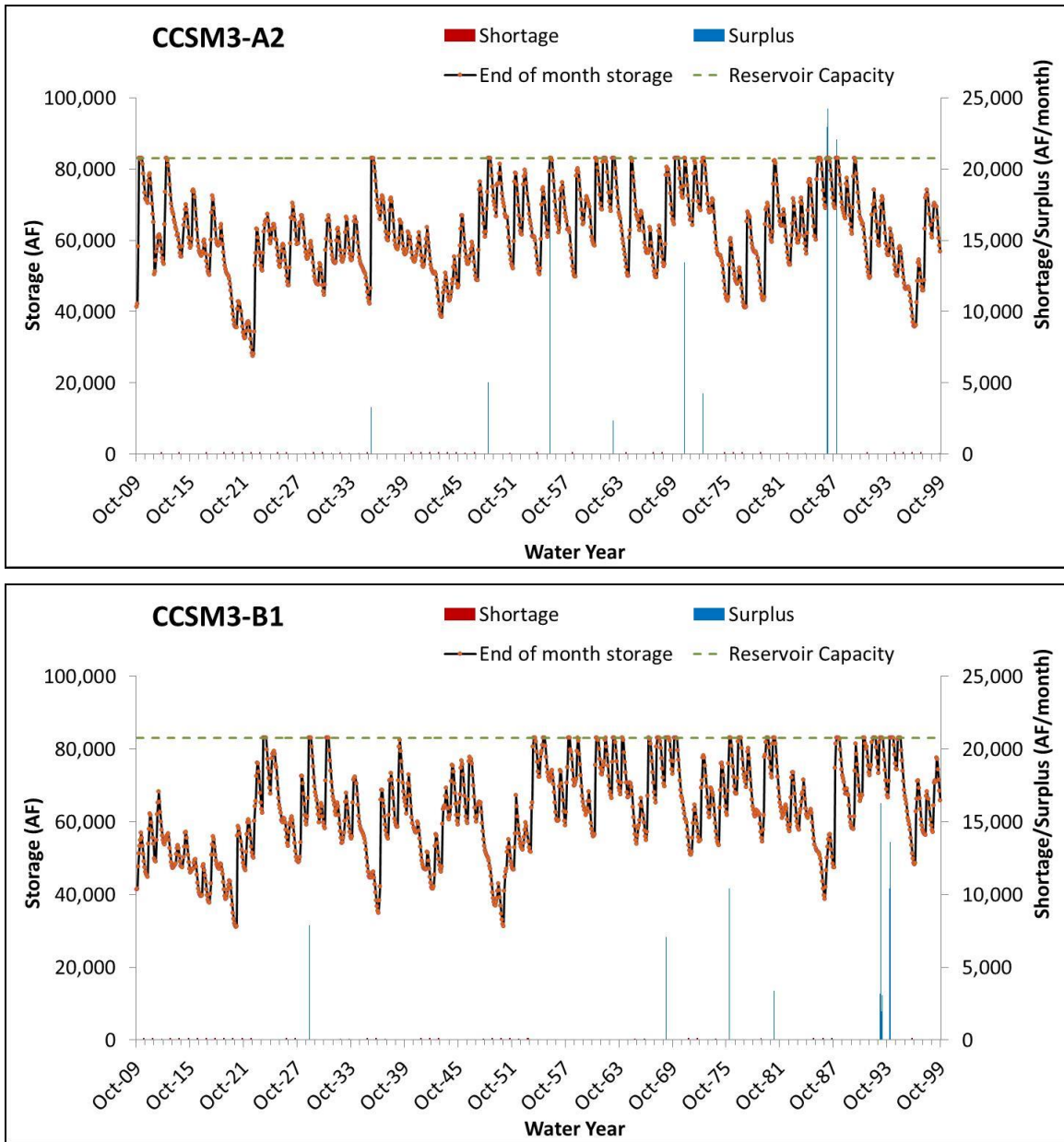


Figure 76 (continued). Plot of the simulated end-of-month storage values for Grizzly Valley Dam, along with the amounts and timings of the shortages and surpluses occurring over the future period by using projections from the CCSM3 GCM. Threshold value used: 62,000 AF.

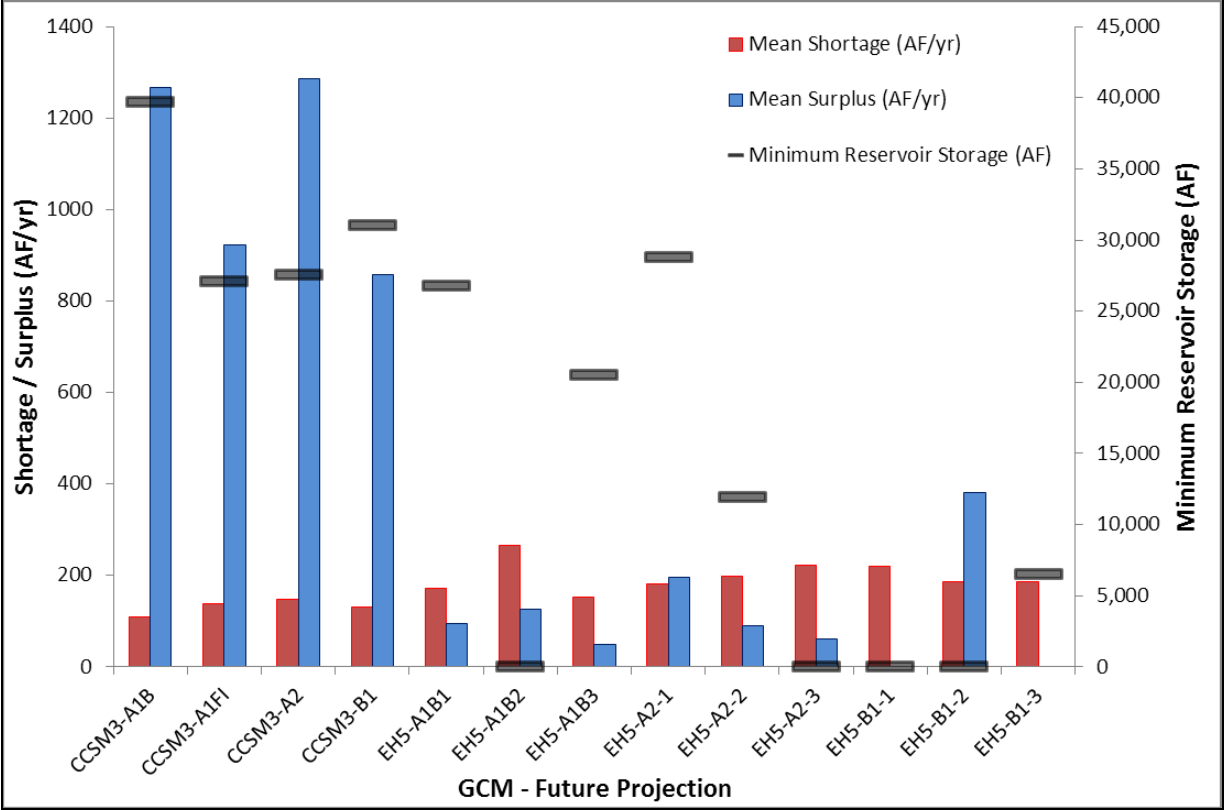


Figure 77. Summary of Grizzly Valley Dam reservoir simulation results for the 13 future projections, showing shortages, surpluses, and minimum reservoir storage values over the period from 2010 to 2100. Simulation was run using threshold method, with a threshold value of 62,000 AF.

The main result of switching to the higher threshold value was the slight shifting-up of the end-of-month storage values for all of the plots in **Figure 75** and **Figure 76**. This shows slightly higher reservoir storage values in general within the same future period. While this change did not cause a significant change in the number and amounts of shortages occurring over the future period, it caused an increase in the number of surpluses and the amount of surpluses by about 20% and 16% on average, respectively. This can be seen by comparing **Figure 74** to **Figure 77**, the latter which shows that while the shortages of the 62,000 AF threshold value case stayed fairly similar to the 56,000 AF threshold value case, the surplus amounts increased for most of the future projections.

Another important result of this new threshold value is the minimum storage value attained by the reservoir for the EH5-B1-3 scenario. Recall that the change in the threshold value

was made as an attempt to tackle the problem of the depletion in the reservoir storages within the future period. Accordingly, from **Figure 77**, one can see that this change in the threshold value was found to raise the minimum storage for EH5-B1-3 to 6,533 AF during the 21st century, which is enough to pass the minimum-storage criterion of 5,595 AF discussed above. This result can also be seen by comparing the corresponding detailed end-of-month storage plot for the EH5-B1-3 scenario in **Figure 72** and **Figure 75**. For convenience, these plots for both threshold values are plotted again in **Figure 78**. It is clear from **Figure 78a** that the lowest reservoir storage occurs during 2093, specifically on December 2093. The projected inflows to the dam show that water years 2091 and 2092 would be extremely low, while those of water year 2093 would not be too high either. Therefore, it may be possible that such a predicted drought period during those water years would cause such a reduction in the reservoir storage under the current operational procedures (56,000 AF threshold value) that, if such procedures are followed, they may lead to the reduction of the reservoir storage leading to its depletion in December 2093. In fact, similar droughts or dry periods have led to the low minimum storages for the four other EH5 scenarios as well. However, under a threshold value of 62,000 AF, **Figure 78b** shows that the intensity of the dip in the reservoir storage during the 2091-2093 period would be reduced enough in order to prevent the reservoir storage from falling below the 5,595 AF limit in December 2093.

While raising the threshold value to 62,000 AF helped improve the storage for EH5-B1-3, notice that the other four cases that attain very low reservoir storage values at some point in the future period still suffer from reservoir levels lower than the second outlet (**Figure 77**), even with the threshold increase to 62,000 AF. One can also see this result by checking the corresponding detailed plots in **Figure 75** of these four EH5 scenarios: A1B2, A2-3, B1-1, and B1-2. Trying higher thresholds did not provide much difference in the minimum storage for those scenarios. In fact, only the minimum storage for EH5-B1-2 increased over the minimum limit when a threshold value of 82,500 AF was used for the simulations. However, operating the reservoir using such a high threshold limit would not be practical.

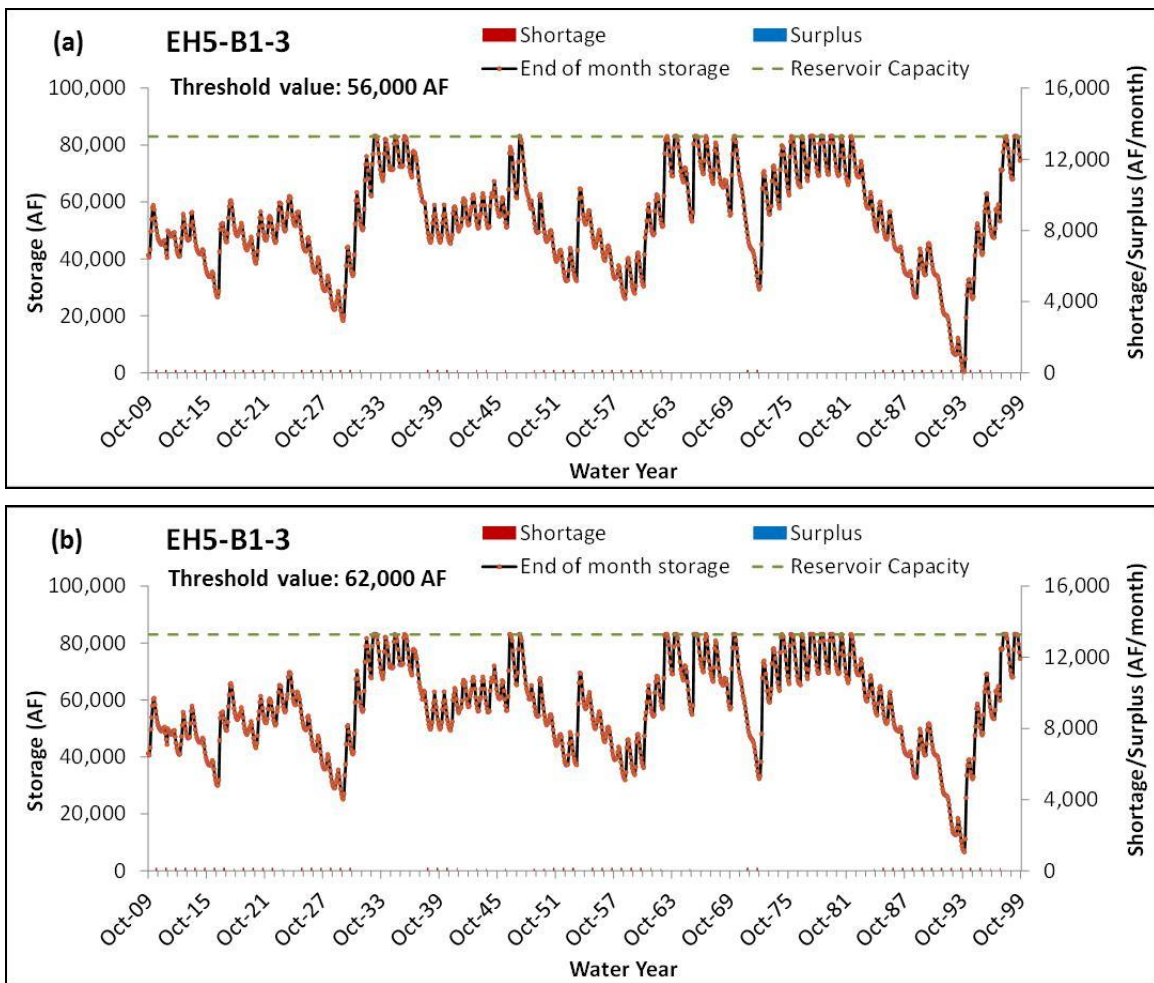


Figure 78. Comparison of plots of the simulated end-of-month storage values for Grizzly Valley Dam (with shortages and surpluses) over the future period (2010-2100) for the EH5-B1-3 scenario. Simulation was done using the threshold method by using a threshold value of (a) 56,000 AF, and (b) 62,000 AF.

Another approach to tackle this issue, not involving changing the threshold value, may include making changes to the reservoir itself, e.g., changing the reservoir capacity. If a change in the reservoir capacity would be at all possible, then one can assume a 10% increase in reservoir capacity and simulate the 13 different projections under the original reservoir operation of 56,000 AF threshold value in order to get the results shown in **Figure 79** and **Figure 80**, as well as the summarized results shown in **Figure 81**.

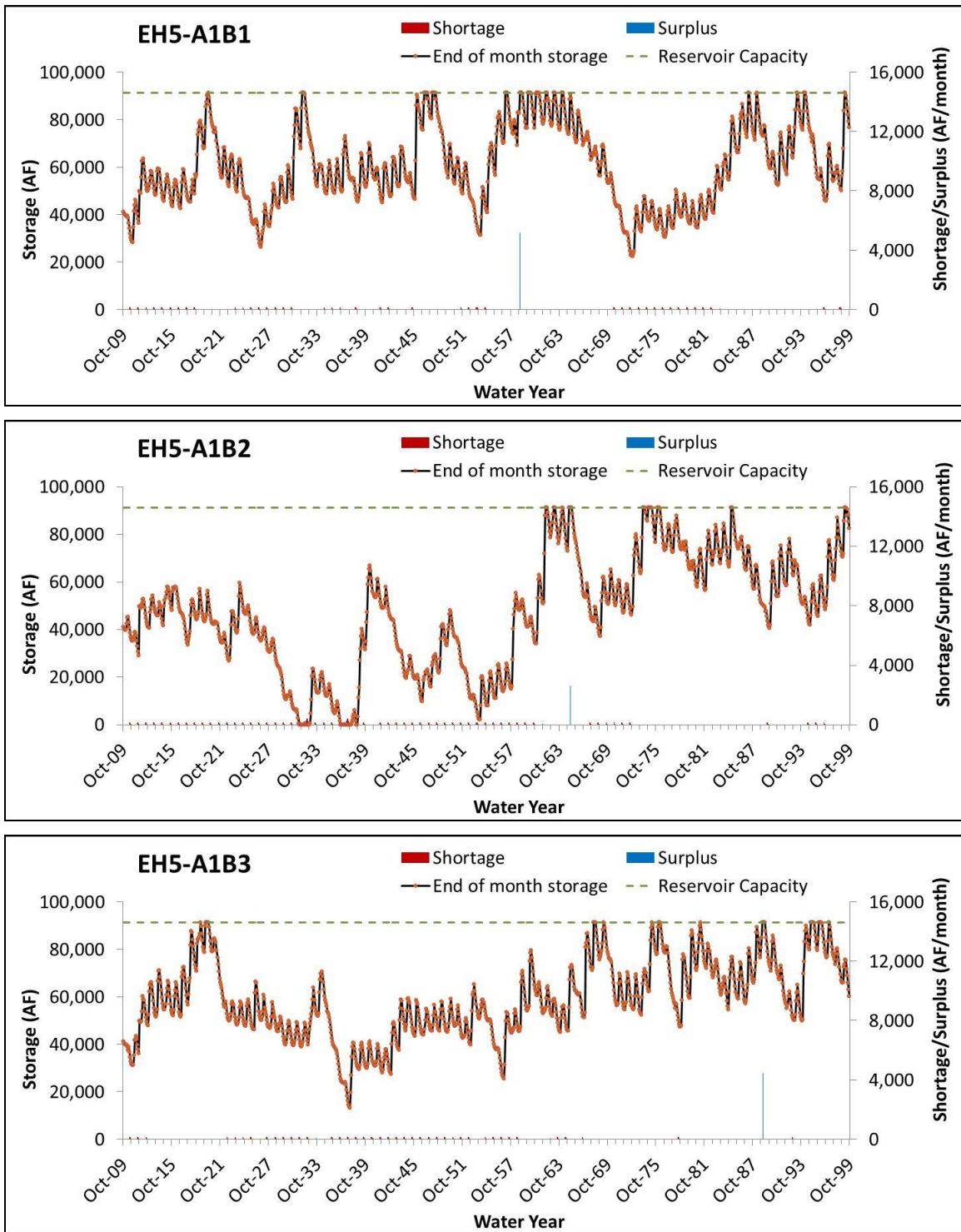


Figure 79. Plot of the simulated end-of-month storage values for Grizzly Valley Dam, along with the amounts and timings of the shortages and surpluses occurring over the future period by using projections from the EH5 GCM. Results provided for an assumed 10% increase in storage capacity. Threshold value used: 56,000 AF (continued below).

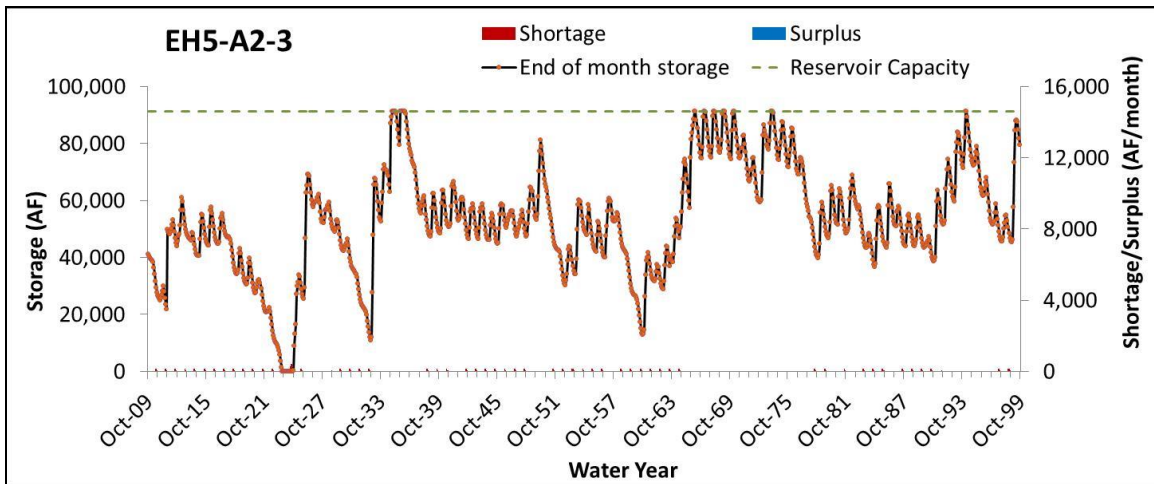
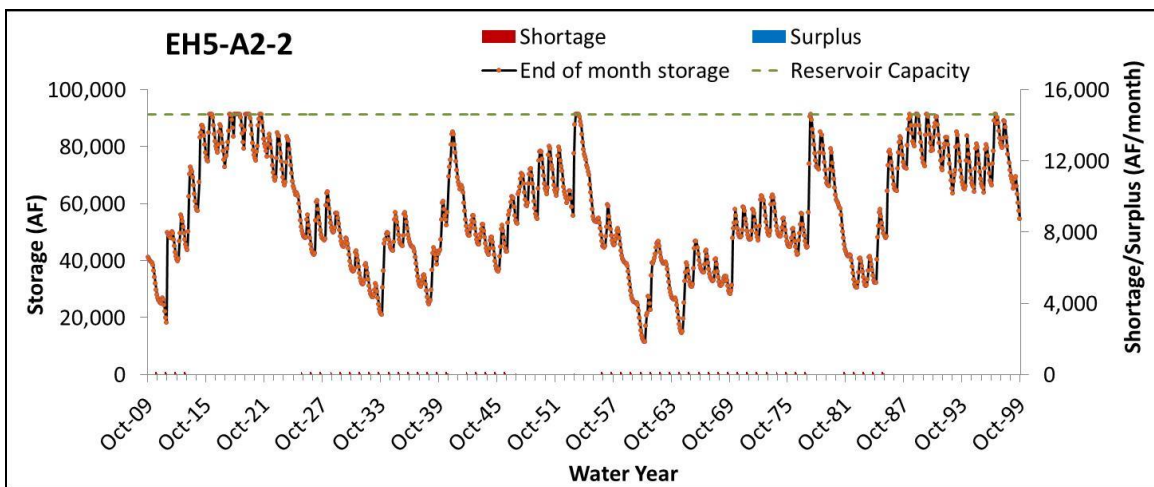
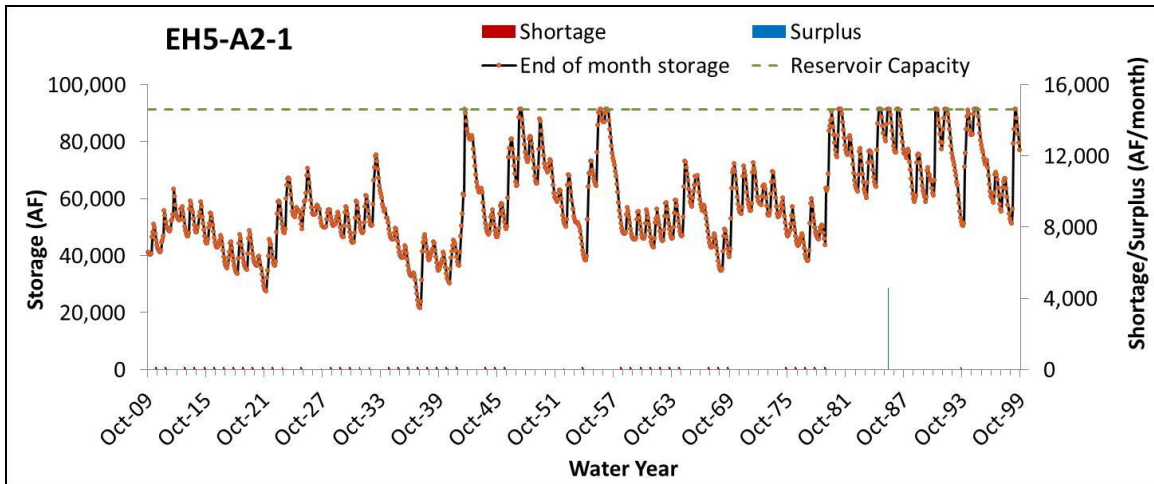


Figure 79 (continued). Plot of the simulated end-of-month storage values for Grizzly Valley Dam, along with the amounts and timings of the shortages and surpluses occurring over the future period by using projections from the EH5 GCM. Results provided for an assumed 10% increase in storage capacity. Threshold value used: 56,000 AF (continued below).

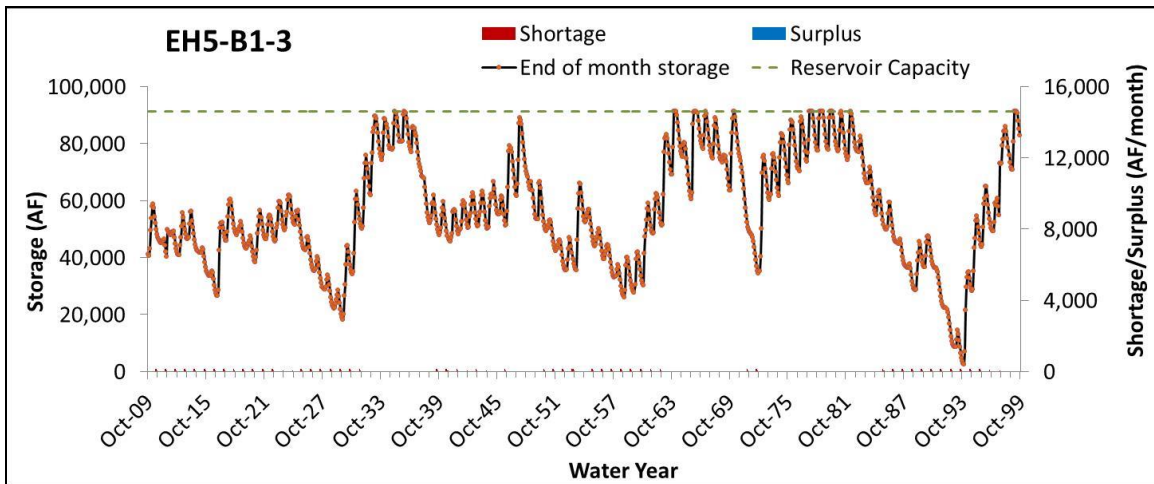
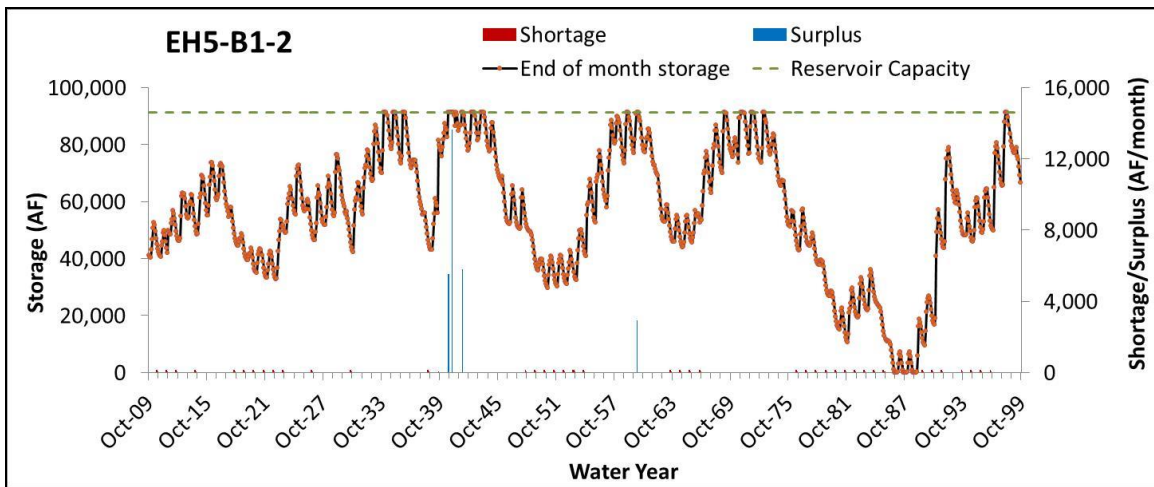
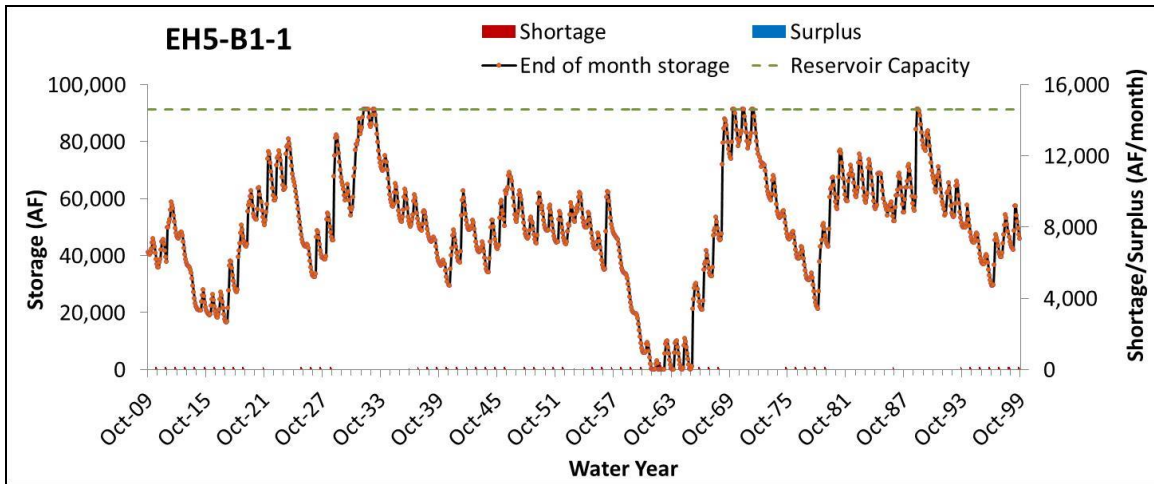


Figure 79 (continued). Plot of the simulated end-of-month storage values for Grizzly Valley Dam, along with the amounts and timings of the shortages and surpluses occurring over the future period by using projections from the EH5 GCM. Results provided for an assumed 10% increase in storage capacity. Threshold value used: 56,000 AF.

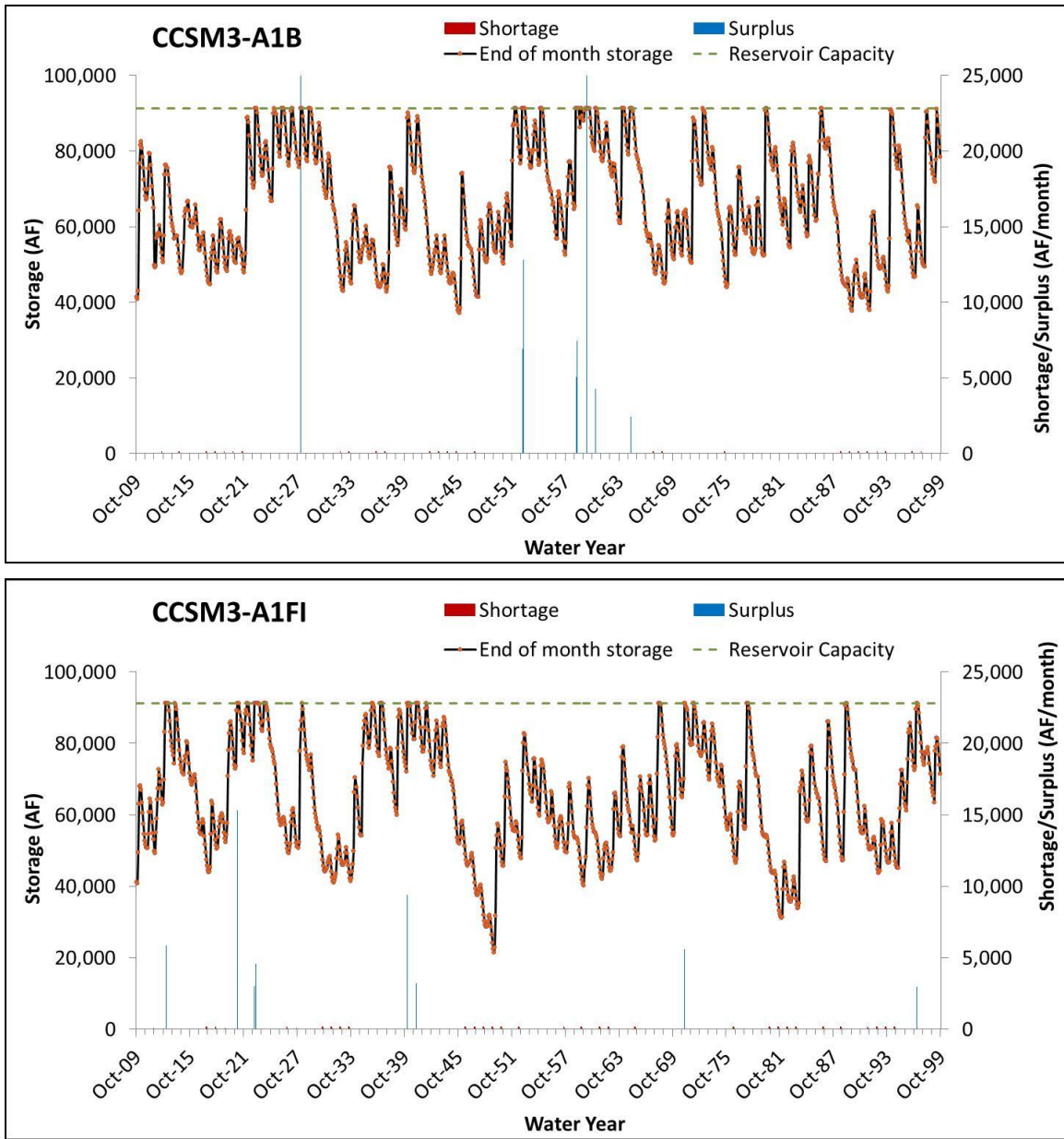


Figure 80. Plot of the simulated end-of-month storage values for Grizzly Valley Dam, along with the amounts and timings of the shortages and surpluses occurring over the future period by using projections from the CCSM3 GCM. Results provided for an assumed 10% increase in storage capacity. Threshold value used: 56,000 AF (continued below).

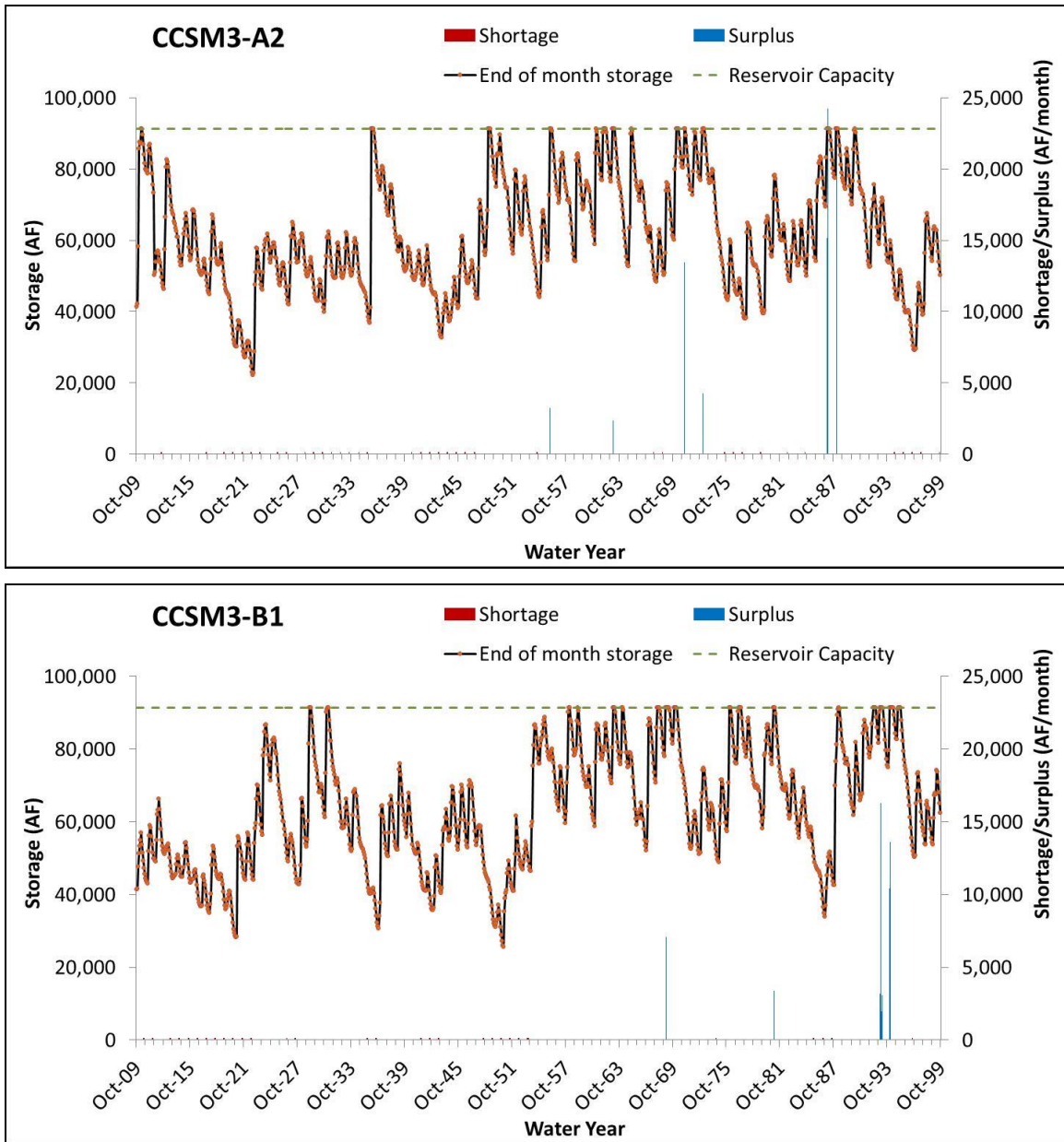


Figure 80 (continued). Plot of the simulated end-of-month storage values for Grizzly Valley Dam, along with the amounts and timings of the shortages and surpluses occurring over the future period by using projections from the CCSM3 GCM. Results provided for an assumed 10% increase in storage capacity. Threshold value used: 56,000 AF.

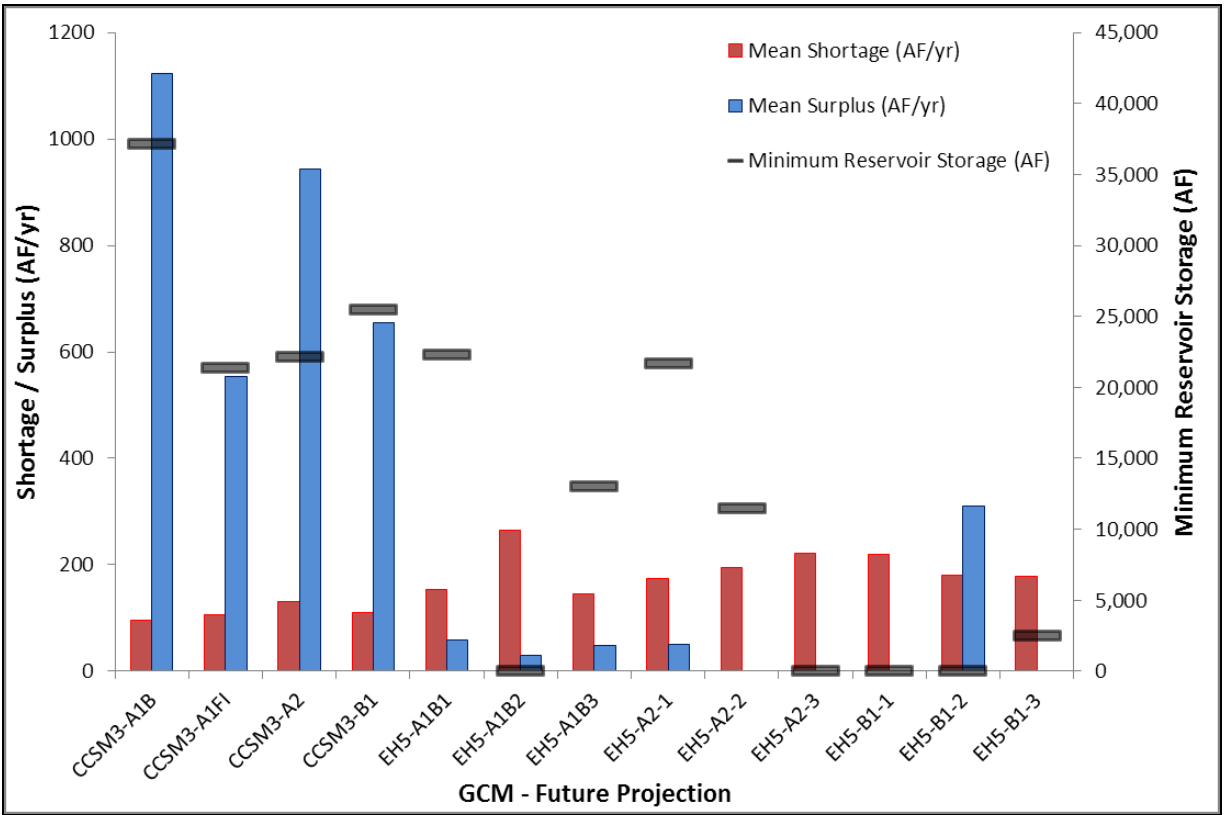


Figure 81. Summary of Grizzly Valley Dam reservoir simulation results for the 13 future projections, showing shortages, surpluses, and minimum reservoir storage values over the period from 2010 to 2100. Simulation was run using threshold method, with a threshold value of 56,000 AF and a 10% assumed increase in reservoir capacity.

Figure 79 and **Figure 81** show that the same five EH5 scenarios that had minimum storage values below the recommended minimum limit are still in the same situation even after the 10% assumed capacity increase; however, one can notice that the minimum storage for EH5-B1-3 is larger than that for the normal reservoir capacity (compare to **Figure 74**). While assuming an increase in reservoir capacity did not greatly affect the depletion of the reservoir storages in the five EH5 future scenarios, it had significant effects on the shortages and surpluses expected within the future time period. In fact, with this 10% capacity increase, the surpluses (or spills) are expected to reduce; some examples include CCSM3-A1FI (29% reduction), CCSM3-A2 (16.5% reduction) and CCSM3-B1 (14.6% reduction). Shortages are also expected to be reduced by up to 13.1% with this new assumed change. Note that a combination of both an

increase in reservoir capacity and a change in threshold value may provide a better opportunity in tackling the reservoir depletion that is expected to occur in some of the EH5 projections.

A final approach for tackling the reservoir minimum storage problem may involve the process of hedging. Hedging involves keeping water in storage and deliberately creating a shortage in the aim of saving water for the future. Therefore, the intent of hedging would be to reduce the risk and cost of large shortages, but at a cost of more frequent small shortages. As was mentioned previously, dry periods have been noticed to follow the very low minimum reservoir storage values expected in the 5 projections EH5-A1B2, EH5-A2-3, EH5-B1-1, EH5-B1-2, and EH5-B1-3. While increasing the threshold value to 62,000 AF helped improve the minimum storage of EH5-B1-3 during the critical period around the year 2093, **Figure 78** showed that such an increase in the threshold value may not be needed for the other years of the 21st century. In fact, **Figure 78a** shows that the reservoir storage performs well with the original threshold value of 56,000 AF, and does not reach unwanted low values except during the critical period that follows the dry period. As a result, a better solution for the reservoir depletion problem may be to keep the original threshold value (56,000 AF) for most of the years during the 21st century, but apply stricter hedging before reaching the critical period. In this case, water would be deliberately stored in the dam to reduce the risks of reservoir depletion in the following years.

Such a solution may be implemented in two ways. One way would be to use a threshold value of 56,000 AF for most of the 21st century but assign a higher threshold value for the period preceding the expected critical period. This will impose the use of the minimum release schedule (**Figure 61**) at an earlier stage, thus intensifying the applied hedging and storing more water in the reservoir. The threshold value can then be reduced back to the original value once the critical period has passed. Another way to implement such a solution would be to adjust the minimum release schedule (**Figure 61**) during the critical period so that the minimum release quantities would be lower during this critical period. This would lead to less water being released from the reservoir when following the minimum release schedule, thus allowing for more water to be stored as a buffer in order to be used later in the critical period. While such options may cause some shortages in the water during the hedging periods, they may be an important compromise to take in order to prevent the depletion of the reservoir storage during anticipated critical periods.

Therefore, the analysis of the Grizzly Valley Dam operations for the future period using future projections of the dam inflows have shown that some of the scenarios may lead to extremely low storage values during the 21st century. With the recommendation being to run the reservoir with the reservoir storage not decreasing below the second outlet (5,595 AF), it was clear that 5 of the scenarios violate this criterion. The above discussion showed that increasing the threshold value for the dam operation from 56,000 AF to 62,000 AF allowed one of the scenarios to improve its minimum reservoir storage over the required limit. However, such a change also caused increases in the expected spills and shortages during the 21st century. On the other hand, while a 10% assumed increase in dam capacity did not help much with the minimum storage values, it reduced the projected shortages and surpluses by up to 13.1% and 29%, respectively. Finally, disregarding the above changes in threshold and capacity, it was seen that another possible option would be to operate the reservoir normally during most of the 21st century, while applying strict hedging when nearing periods that are projected to be extremely dry, thus saving water and preventing the depletion of the reservoir storage during and after those excessively dry periods.

IV. SIERRA VALLEY GROUNDWATER SYSTEM

1. Overview of the Project Site

The Sierra Valley (SV) basin is located at the upstream of the Upper Middle Fork (UMF) watershed (**Figure 82**). It covers an area of around 590 square miles, which is the drainage area of the California Data Exchange Center (CDEC) station MFP (Middle Fork Feather River near Portola, CA / USGS 11392100). The central portion of the SV basin constitutes the Sierra Valley Aquifer, which is an important source of groundwater for agricultural water supply in the region.

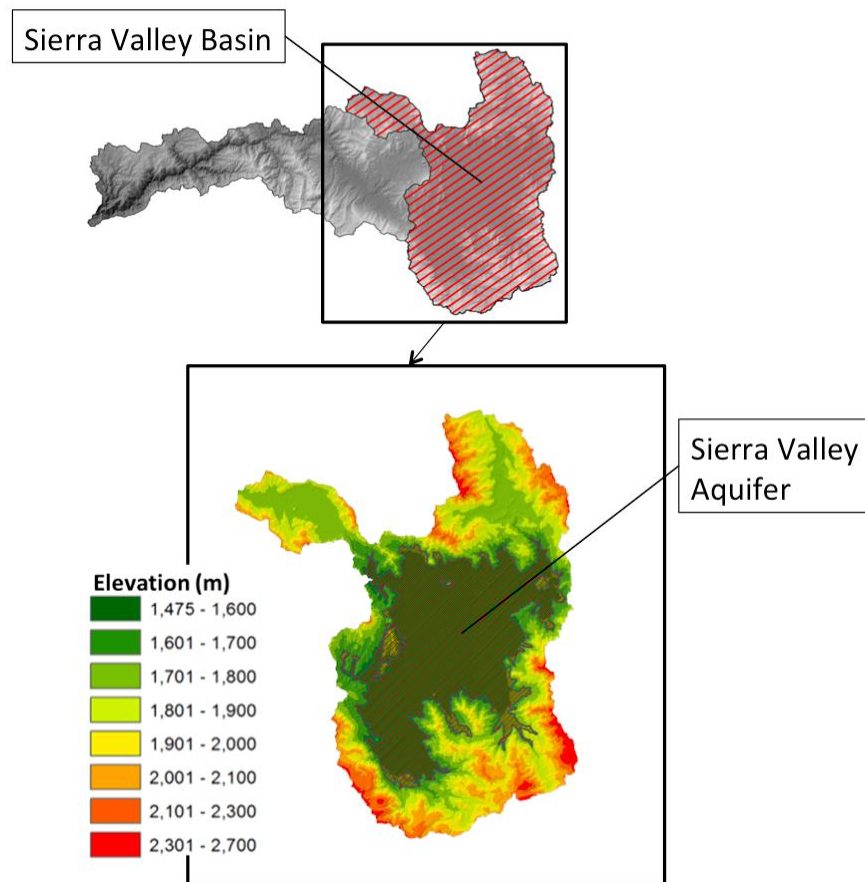


Figure 82. Location of Sierra Valley Basin as a subregion of the Upper Middle Fork watershed (upper figure); Digital Elevation Model (DEM) of the Sierra Valley Basin and Sierra Valley Aquifer (lower figure).

Sierra Valley Aquifer is a former lake basin filled with sediments during the ice ages of the Pleistocene epoch. It is bounded to the North by Miocene pyroclastic rocks of

Reconnaissance Peak, to the west by Miocene andesite of Beckwourth Peak, to the south and east by Tertiary andesite and to the east by Mesozoic granitic rocks (Saucedo, 1992). The main water bearing formations are Holocene sedimentary deposits, Pleistocene lake deposits and Pleistocene volcanic rocks (California Department of Water Resources (DWR), 1963 and 1983).

Annual precipitation changes from 13 inches in the valley to 29 inches in the upland areas to the south and west (DWR, 2004). The infiltration of surface water from the streams that drain the mountains and flow across the fans are believed to play an important role for the recharge of the groundwater (DWR, 1963 and 1983). Additionally, in the last decades, the return flow from the increased amount of irrigation is expected to contribute to the recharge.

Groundwater is pumped mainly for irrigation purposes. In a survey by DWR in 1997, the estimated annual agricultural and municipal/industrial uses were given as 3,400 and 100 acre-feet respectively (DWR, 2004). However, in the recent hydrogeologic studies the average annual pumping between 1989 and 2011 is reported as 7,000 acre-feet (Kenneth D. Schmidt, 2003, 2005 and 2012).

Increased groundwater development resulted in a decrease in the artesian flows and the lowering of the water table around the developed areas. Although an increase in groundwater levels were observed in low pumpage years, the overall trend shows decreasing water levels (Kenneth D. Schmidt, 2003, 2005 and 2012).

2. Methodology

Considering the increasing demand, the changing climate conditions, and the interaction of surface- and ground-waters in the SV, an integrated hydrologic modeling approach that combines the atmospheric, hydrologic and groundwater models is deemed necessary for the successful modeling of the SV groundwater system. In the Hydrologic Research Lab at UC Davis, our modeling approach consists of two steps: simulation of snow conditions over the SV Basin and surface water conditions over the SV foothill by the WEHY-HCM model with NCAR/NCEP global climate data, and the root zone and the groundwater flow simulation by the Integrated Water Flow Model (IWFM) (Dogrul, 2014) using the inflows provided by the WEHY-HCM model simulation.

3. Ground Observation Data Collection

For calibration and validation purposes, the CDEC MFP (USGS 11392100) stream gauge station, located at the outlet of the SV watershed has daily flow records for the water years 1969-1980 and 15-minute discharge records from 10/31/2006 to present. Those records were downloaded from CDEC and stored in a database.

Groundwater level data corresponding to 48 locations within the SV were obtained from the California Statewide Groundwater Elevation Monitoring (CASGEM) database (**Figure 83**). Groundwater level time series were plotted and studied to identify similar patterns and to construct the piezometric surface.

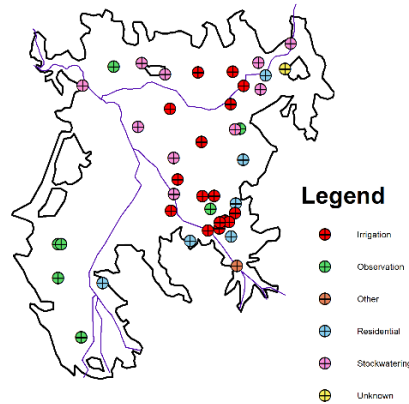


Figure 83. Groundwater level observation locations over the Sierra Valley obtained from CASGEM database.

The surface water usage for irrigation is highly developed in SV. The water in the streams and channels is diverted to irrigation ditches at hundreds of diversion points with respect to the decreed water rights and available water. Additionally, a significant amount of water is imported into SV from a nearby watershed via a system called “Ramelli Ditch”. Both the diversions and the Ramelli Ditch are monitored and flows are measured by the SV Watermaster. These data could not be obtained from the Watermaster. Locations of channels, diversions, ditches and irrigable land information were obtained from the DWR Red Bluff office. Information on decreed water rights was downloaded from the Sierra Valley Watermaster website and stored in a database.

4. Geohydrologic Modeling of the Sierra Valley Groundwater System

The geohydrologic modeling of the Sierra Valley includes the implementation and use of the hydrologic component of WEHY-HCM (WEHY Snow and Hydrologic Modules) and the IWFM over Sierra Valley Aquifer.

A. Implementation and Use of the WEHY Snow Module over the Sierra Valley Basin

The implementation and use of this WEHY snow module for the simulation of snow conditions were completed for the Sierra Valley (SV) basin. Snow simulation results were, then, calibrated and validated to ensure the snow model's proper use for the SV basin. In this regard, simulations of the snow model were run by using the reconstructed, mean monthly hydro-climate data at a spatial resolution of 3 km over the watershed, based on the dynamically downscaling of NCAR/NCEP global reanalysis data by means of the atmospheric component of the WEHY-HCM (MM5) as input. Constants and model parameters required were determined from the literature (Ohara, Kavvas, & Chen, 2006). The calibration and validation of the snow model made use of comparisons of the simulation results with observations in order to test the model's performance. Observations were obtained from one CDEC (California Data Exchange Center) field observation station selected based on the availability of the required data and the preferred time intervals of the provided data; the station is shown in **Figure 84**.

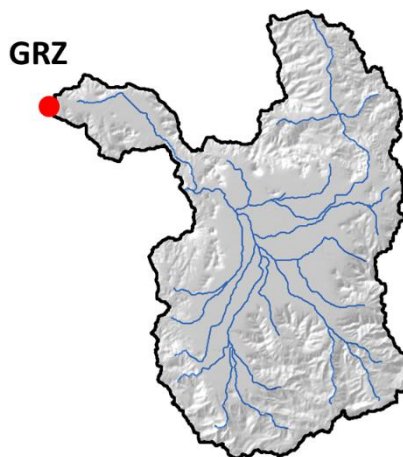


Figure 84. Location of selected snow field observation station.

Calibration of the model was first conducted for water year 2006 (October 2005 through September 2006) by comparing the snow water equivalent of the simulated results versus the observed hourly data for the selected observation station. The calibration results at the selected station are depicted in **Figure 85** and their statistical results are shown in **Table 17**.

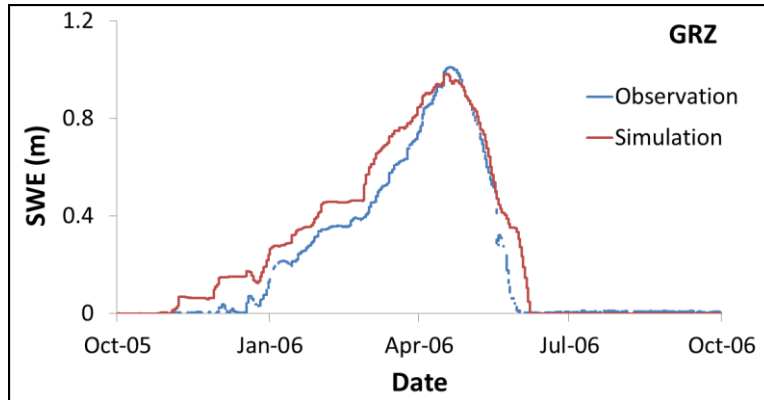


Figure 85. Time series of the observed and model-simulated snow water equivalent (SWE) at the selected field observation site from October 2005 through September 2006 (calibration period).

Table 17. Statistical test values of simulated and observed snow water equivalent from the selected observation station (GRZ) during the calibration period (October 2005 to September 2006).

Parameter	GRZ	
	Observed	Simulated
Mean (m)	0.28	0.34
STDEV (m)	0.32	0.33
RMSE	0.10	
Nash	0.91	
Correlation Coefficient	0.98	

From **Figure 85** and **Table 17**, one can see that the simulated snow water equivalent values are similar to corresponding observed values, while the statistical test results show the performance of the WEHY snow model with high values of the correlation coefficient and the Nash-Sutcliffe Efficiency (Nash).

As for the validation period, it is extended for a whole 10 years, ranging from October 1, 2000 through September 30, 2010. The results obtained were plotted as shown in **Figure 86** and the results of the statistical tests are shown in **Table 18**.

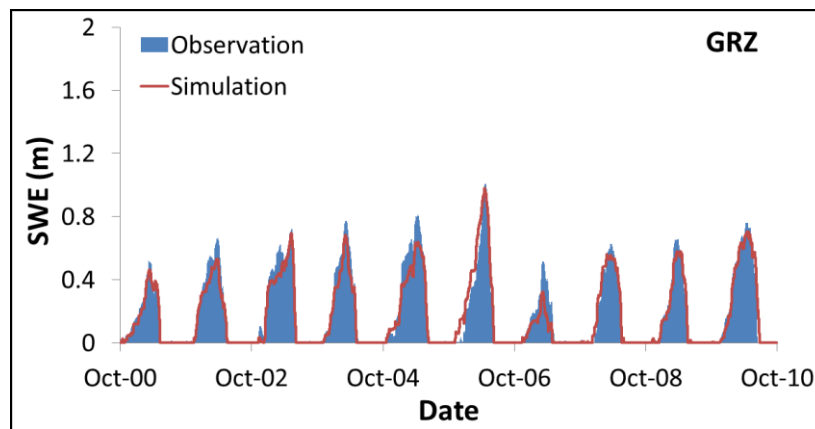


Figure 86. Time series of the observed and model-simulated snow water equivalent (SWE) at the selected field observation sites from October 2000 through September 2010 (validation period).

Table 18. Statistical test values of simulated and observed snow water equivalent from the selected observation station (GRZ) during the validation period (October 2000 to September 2010).

Parameter	GRZ	
	Observed	Simulated
Mean (m)	0.25	0.23
STDEV (m)	0.25	0.24
RMSE	0.08	
Nash	0.91	
Correlation Coefficient	0.96	

As shown in **Figure 86**, one can see that the simulated snow water equivalent values are closely distributed along the time-series values from the GRZ observation station. **Table 18** shows that the mean and standard deviation (STDEV) between observed and simulated values are very close for the GRZ station. Moreover, the high values of correlation coefficient (0.91) and Nash-Sutcliffe Efficiency (0.96) indicate a reliability of the performance of the WEHY snow model.

Furthermore, the spatial distribution of the WEHY snow simulation results were evaluated against the observed snow cover obtained from MODIS (Moderate-Resolution Imaging Spectroradiometer) satellite driven data for the month of April in each of 2008, 2009 and 2010 (see **Figure 87**). As shown in **Figure 87**, the WEHY snow simulated spatial distributions greatly match the corresponding observed spatial distributions from MODIS satellite driven data.

The results from **Figure 86**, **Figure 87** and **Table 18** show that WEHY snow model can perform temporally and spatially well compared to the corresponding observations and indicate the possibility and capability of the WEHY snow model to be applied to the Sierra Valley watershed.

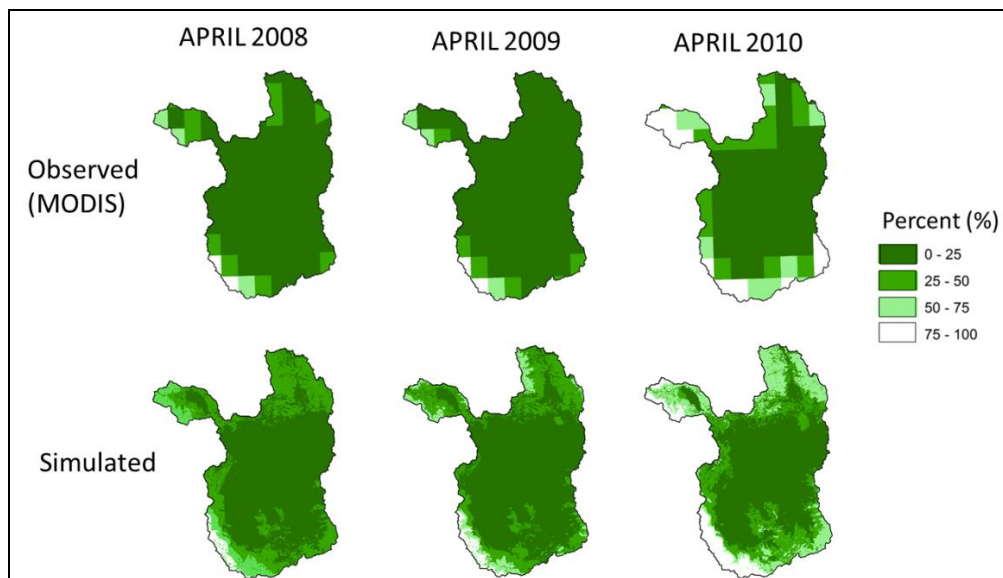


Figure 87. Model-simulated snow water extent and the observed snow cover percent (MODIS) for the month of April for each of 2008, 2009, and 2010 over the Sierra Valley watershed (within the validation period).

B. Implementation and Use of the Hydrologic Module of the WEHY Model over the Foothills Watersheds

The GIS database setup over the Sierra Valley (SV) consists of the county scale soil database, Soil Survey Geographic Database (SSURGO), from California Natural Resources Conservation Service (NRCS), the Digital Elevation Model (DEM) from National Elevation Dataset (NED) at 1 arc second resolution in Geographic projection, the Land Cover Data from California Fire Resource and Assessment Program (FRAP) at 100-m resolution in NAD27 projection, the river channel network and large watershed boundaries from National Hydrography Dataset (NHD), and the road network, aerial photos, county borders, and other digital maps from California Spatial Information Library (CalSIL). The collected digital maps were also projected to the same map projection (UTM Zone 10).

From the 1 arc second National Elevation Dataset (NED), an aspect map, a slope map, and a preliminary river channel network were obtained for the areas that cover the SV basin. **Figure 88** and **Figure 89** show the spatial map of DEM and slope, respectively, for the SV basin. The SSURGO and FRAP datasets (**Figure 90** and **Figure 91**) were processed and analyzed for their soil and land surface physical parameters and for quality control purposes. A set of lookup tables was established for the land cover types and soil map units that cover the SV basin.

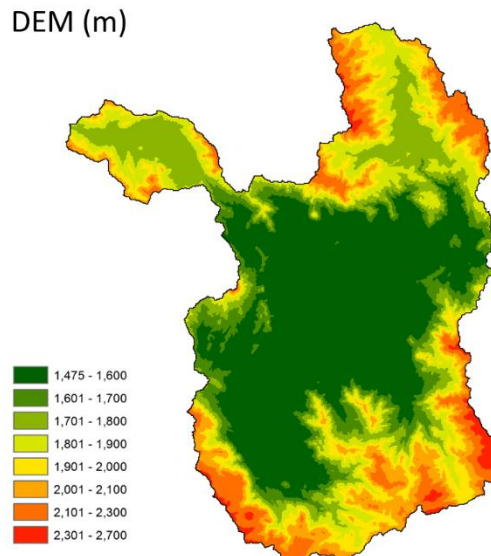


Figure 88. Digital Elevation Model (DEM) from National Elevation Dataset (NED) over the Sierra Valley basin.

Surface Slope (degree)

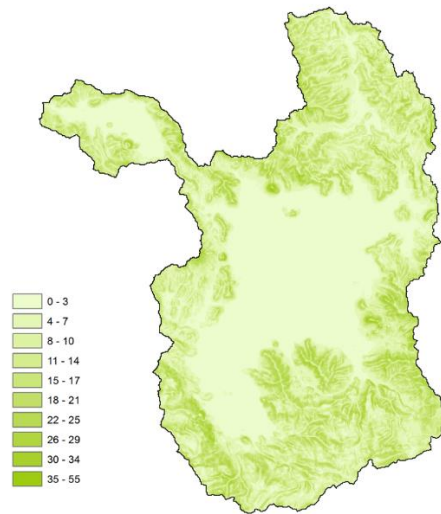


Figure 89. Surface slope over the Sierra Valley basin.

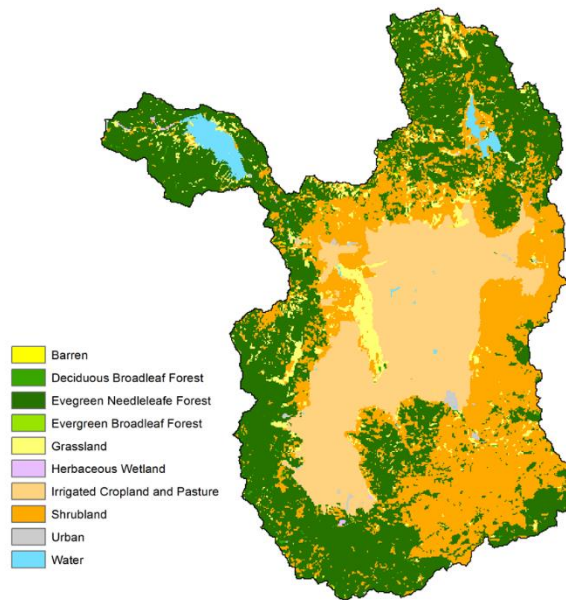


Figure 90. Land cover types from California Spatial Information Library (CalSIL) at 100-m resolution over the Sierra Valley basin.

Displayed based on MUkey
from SSURGO data

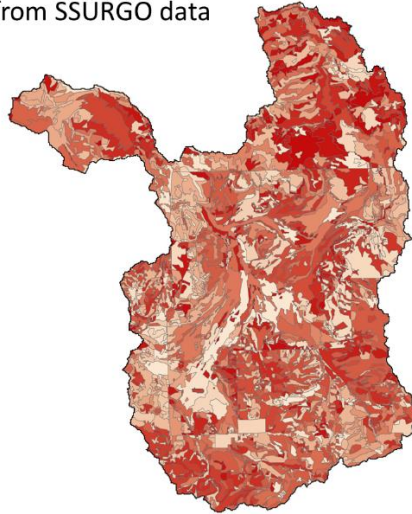


Figure 91. Spatial soil map based on SSURGO data from California NRCS over the Sierra Valley basin.

Geomorphologic parameters for the delineated stream reaches and model computational units (MCUs) in the hydrologic module of the WEHY model (Chen et al, 2004a; 2004b; Kavvas et al, 2004) for the target watershed were estimated from the prepared GIS database. These geomorphologic parameters define the flow domains and the configurations of rills and interrill areas for MCUs of the hydrologic module of the WEHY model for the Sierra Valley watershed.

Using the geomorphologic parameters from the GIS database, the stream network in the SV basin was divided into 77 stream reaches and 154 hillslopes or Model Computational Units (MCUs) as called in the WEHY model (**Figure 92**). Land surface and soil parameters were assigned to each MCU in order to account for the heterogeneity within the watershed (Chen et al., 2004a).

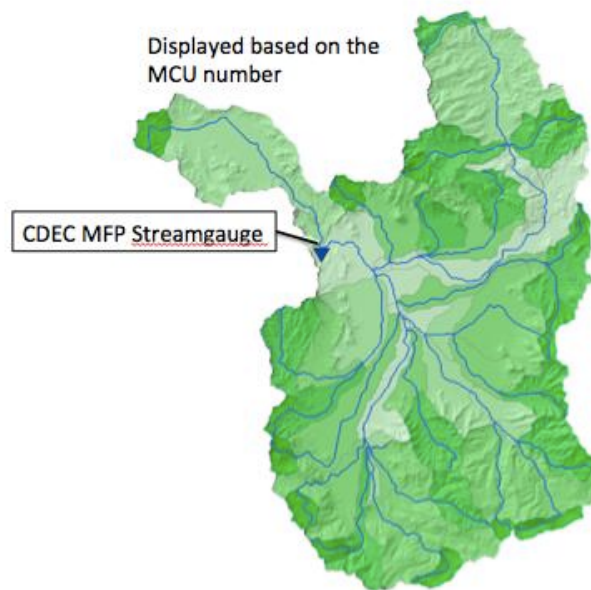


Figure 92. Discretization of the SV basin into 77 stream reaches and 154 Model Computational Units, and location of the CDEC MFP stream gauge.

The WEHY model requires land surface parameters (leaf area index, roughness height, albedo, emissivity, and vegetation root depth) and soil hydraulic parameters (saturated hydraulic conductivity, soil depth, soil porosity and bubbling pressure) with a temporal and spatial variability in order to account for the heterogeneity within the watershed.

Monthly mean Leaf Area Index (LAI) values were obtained from Moderate Resolution Imaging Spectroradiometer (MODIS) satellite driven data which has 1 km spatial resolution (**Figure 93**). The other land surface parameters such as vegetation root depth and roughness height were estimated based on the multi-source land cover data in **Figure 90** by means of California Wildlife Habitat Relationships (CWHR) and reference information from Asner et al. (2003), Scurlock et al. (2001) and Canadell et al. (1996). The samples of the vegetation root depth and the roughness height are shown in **Figure 94**.

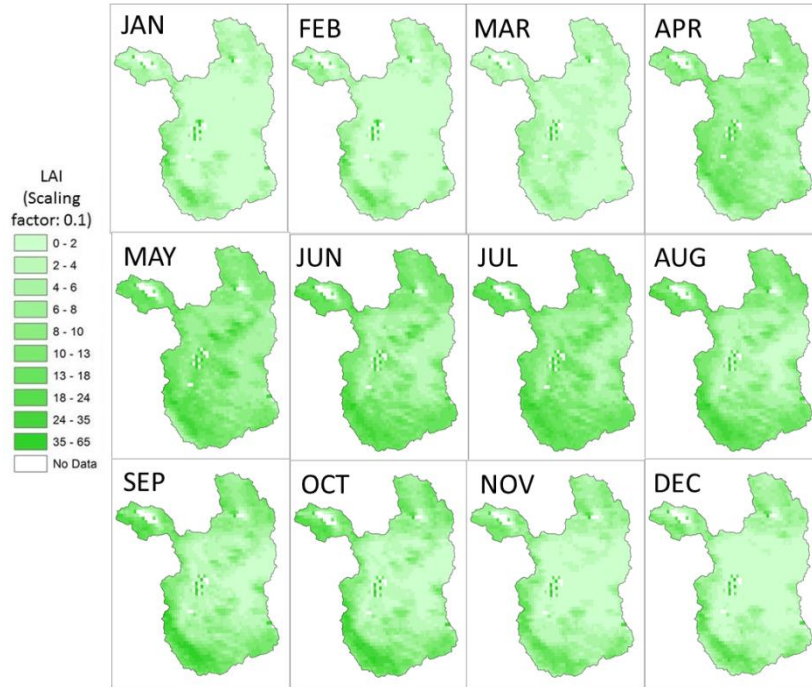


Figure 93. MODIS monthly leaf area index (LAI) over the Sierra Valley watershed.

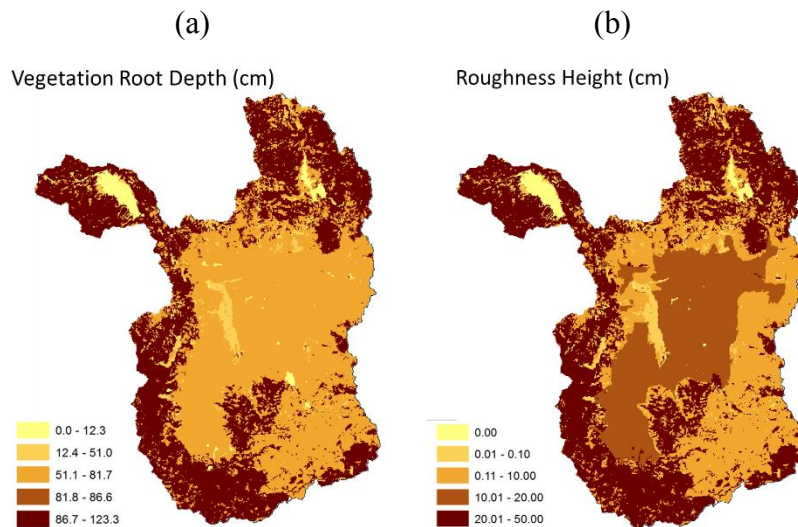


Figure 94. Sample of distributed land surface parameters from database over the Sierra Valley watershed.

The soil parameters such as average soil depth, mean total porosity, mean residual saturation, mean bubbling pressure, mean pore size index, soil erodibility factor, mean hydraulic conductivity, and variance of hydraulic conductivity were estimated based on the Soil Survey

Geographic (SSURGO) Database (Natural Resources Conservation Service, NRCS) in **Figure 91** by means of reference information from Gale and Grigal (1987), Canadell et al. (1996), McCuen et al. (1981), Rawls et al. (1982) and Yoshitani et al. (2002). The samples of the estimated soil parameters are shown in **Figure 95**.

These estimated parameters were also stored in the GIS database for this project. Furthermore, the geomorphologic parameter file for the hydrologic module of the WEHY over the Sierra Valley watershed model was obtained by means of the estimated parameters.

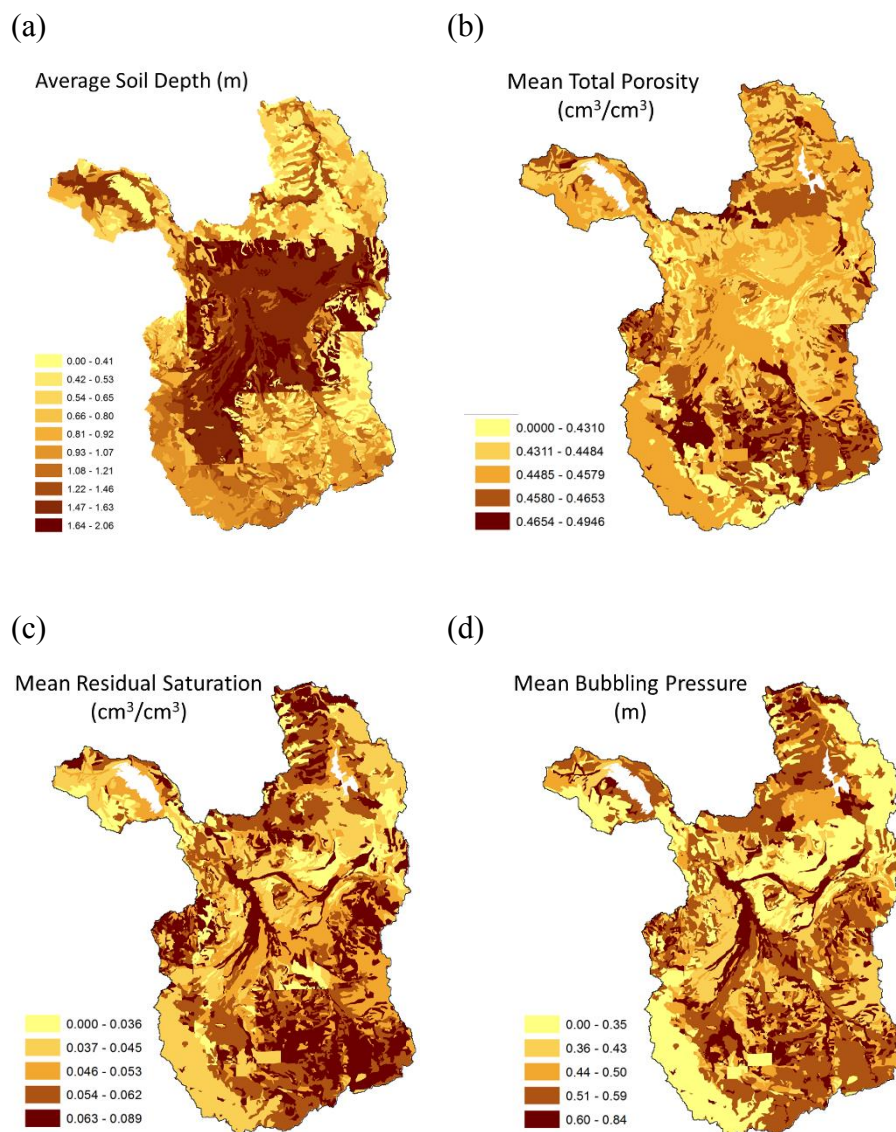


Figure 95. Samples of distributed soil hydraulic parameters from database over the Sierra Valley watershed (continued below).

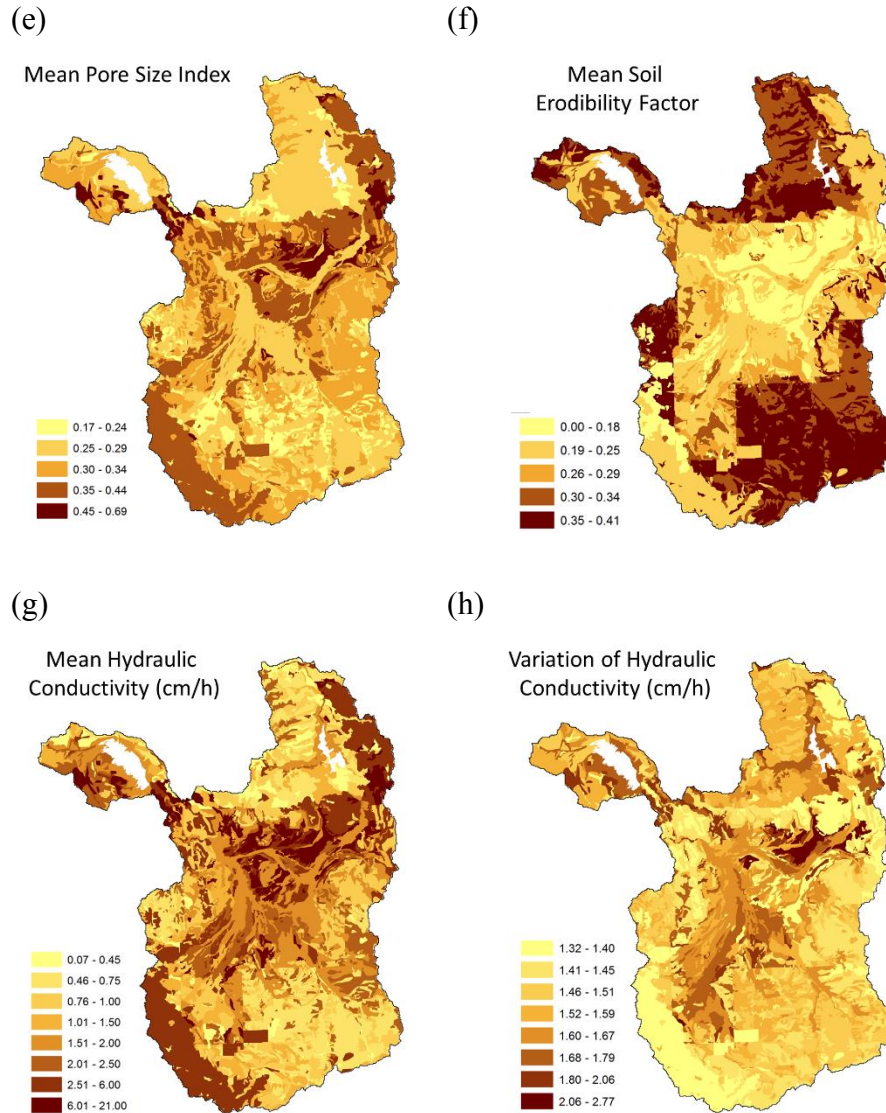
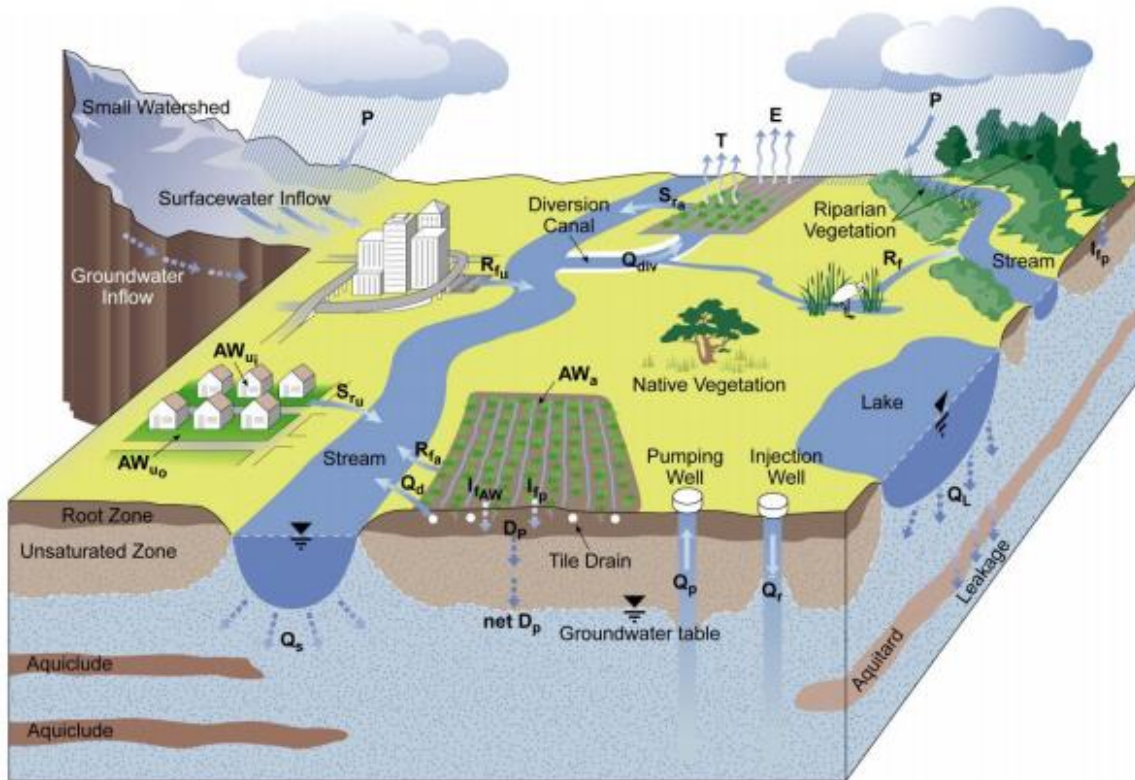


Figure 95 (continued). Samples of distributed soil hydraulic parameters from database over the Sierra Valley watershed.

C. Implementation and Use of the IWFM over the Sierra Valley Aquifer

The model implemented in this study for the simulation of the groundwater components over the Sierra Valley (SV) Aquifer is the quasi 3-D groundwater flow model IWFM (Integrated Water Flow Model) v2015 (Dogrul, 2014). IWFM integrates surface water, root zone processes as well as other components of the hydrologic cycle shown in **Figure 96** into groundwater modeling. This way, the interaction and mutual dependence between these components can be simulated. It also allows for the dynamic supply adjustment where the surface water diversion

and groundwater pumping amounts can be dynamically calculated within the model during simulation. This feature is very important for the historical simulations where the surface water diversion or groundwater pumping records are not available. Also, it allows the modelers to simulate future management scenarios without the need to specify the diversion and pumping rates.



LEGEND					
P.....	Precipitation	I_{fAW}	Infiltration of applied water	D_p	Deep percolation of water to the unsaturated zone
AW_a	Water applied to agricultural lands	Q_{div}	Surface water diversion	$net D_p$	Recharge to the groundwater aquifer
AW_{u_i}	Water applied to indoor urban lands	S_{r_a}	Agricultural runoff	Q_p	Pumping from groundwater aquifer
AW_{u_o}	Water applied to outdoor urban lands	S_{r_u}	Urban runoff	Q_r	Recharge to groundwater aquifer
E.....	Evaporation	R_f	Return flow	Q_s	Stream-groundwater interaction
T.....	Transpiration	R_{f_a}	Agricultural return flow	Q_L	Lake-groundwater interaction
I_{f_p}	Infiltration of precipitation	R_{f_u}	Urban return flow	Q_d	Tile drainage flow

Figure 96. Schematic illustration of the processes modeled in IWF (Dogrul, 2014)

As the first step of the implementation of the IWFM, a conceptual model for the Sierra Valley Aquifer was constructed. The conceptual model includes the identification of significant inflows and outflows to the system (boundary conditions) and the hydrogeological delineation of the aquifer.

Three main inflows were identified for the SV Aquifer:

- Infiltration from the stream reaches flowing into the valley from the foothills watersheds.
- Infiltration from the surface over the valley in terms of rainfall and snowmelt;
- Irrigation return flow from irrigated areas.

The stream network used in the IWFM implementation was simplified from the NHDPlus dataset (Horizon Systems Corporation, 2016). The simplified network is presented in **Figure 97**. Surface water flowrates on the hillslopes surrounding the SV were simulated by the Watershed Environmental Hydrology (WEHY) model (Kavvas, et al., 2004; Ohara, Kavvas, & Chen, 2006) as explained in the previous section. From the simulation results, 8 major stream reaches with significant flow rates were identified. These include the tributaries of Big Grizzly Creek, Little Last Chance Creek, Smithneck Creek and Cold Creek (**Figure 97**). The flows of the Big Grizzly Creek and the Little Last Chance Creek are regulated by Lake Davis and Frenchman Dam releases respectively. In personal communications with the SV Watermaster office, the project team were told that the released amounts from the two dams are rarely significant compared to the natural flows coming from the other streams. In addition, Big Grizzly Creek enters to SV at a location that is very close to the drainage point of SV. For these reasons, surface water inflow from the boundaries of these two streams were neglected in the model. For all other boundary reaches, the flowrates simulated by WEHY were assigned to the corresponding stream nodes on the groundwater model domain boundary in the IWFM.

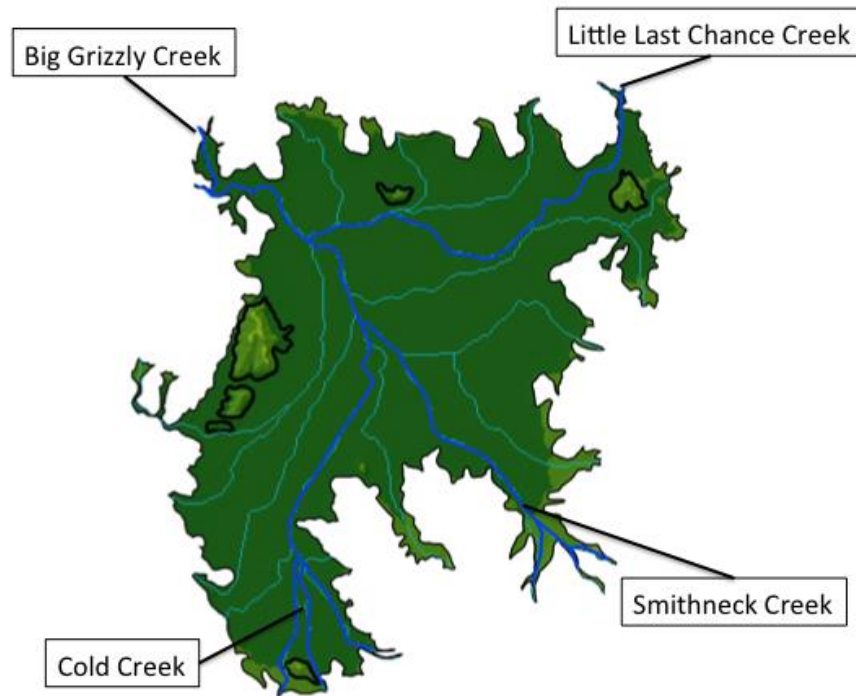


Figure 97. Major and minor stream reaches flowing into the Sierra Valley.

Temperature data measured at various wells and depths around the SV suggest that there is no typical geothermal waters discharge into SV. Most SV groundwater samples have temperatures between 60 and 85 °F; these are expected to be heated by conduction in the shallow crust. Additionally, the groundwater isotope samples from the deep basin do not show the O-18 shift characteristic for geothermal waters (Bohm, 2015).

As for the flows out of the SV aquifer, three main outflows were identified:

- Irrigation pumping from the agricultural wells around the valley;
- Baseflow to the stream network;
- Groundwater boundary flow to Mohawk Valley near the MFP stream gauge station.

Considering the population density in the area, the urban water consumption is assumed to be insignificant in comparison to the agricultural demand.

Hydrogeological Delineation:

A Stereographic Aerial Photo Survey study has been conducted to identify the fracture traces to support the hydrogeologic model of the Sierra Valley basin (Bohm, 2015). The results showed three consistent trends in NNW, NW and NE directions (**Figure 98**). The NW and NNW trending lineaments are interpreted to be associated mostly with a strike-slip (horizontal) fault motion component. This kind of motion is poorly suited to create enhanced permeability. NE striking lineaments are interpreted to be associated mostly with normal (vertical) fault movement. Opposite to the strike-slip motion components, the normal fault movements facilitate groundwater flow through enhanced permeability.

In the survey report (Bohm, 2015) it was explained that “The faults that define the SV periphery imply for all practical purposes impermeable boundaries and would most likely occupy that function in pumping tests conducted on nearby wells in the basin fill. On the other hand, wherever fault intersections may provide important avenues for groundwater entering the basin from the surrounding uplands. Such situations are evident wherever a perennial stream enters the basin.” The periphery defined by the faults is used for defining the domain of the IWFMM model.

Well construction logs of 810 wells from Plumas and Sierra Counties together with the hydrogeological cross-sections created in the previous hydrogeologic studies were digitized and organized in a Microsoft Access database for a systematic analysis (**Figure 99**). In the well construction logs, locations of the wells are given in the MTRS (Township, Range, Section) system in which each grid corresponds to a 1 sq-mi area (**Figure 100**).

Conceptual model construction approach of the Groundwater Modeling Software (GMS) (Aquaveo, 2015) was followed to delineate the SV Aquifer using drilling well logs. For this reason, the top layer was obtained from the ground surface elevations provided by the Digital Elevation Model. The bedrock layer at the bottom was constructed by using the bedrock information from the well logs, the structure and shape of the surrounding hill slopes, and considering the effect of faulting on the bedrock layer (**Figure 101**). Cross sections between the chosen well locations were created and edited. GMS algorithm then enumerated the top and bottom of each formation with a corresponding Horizon ID. All these information were then interpreted by the solid creation algorithm of the GMS and created the delineation shown in **Figure 102**.

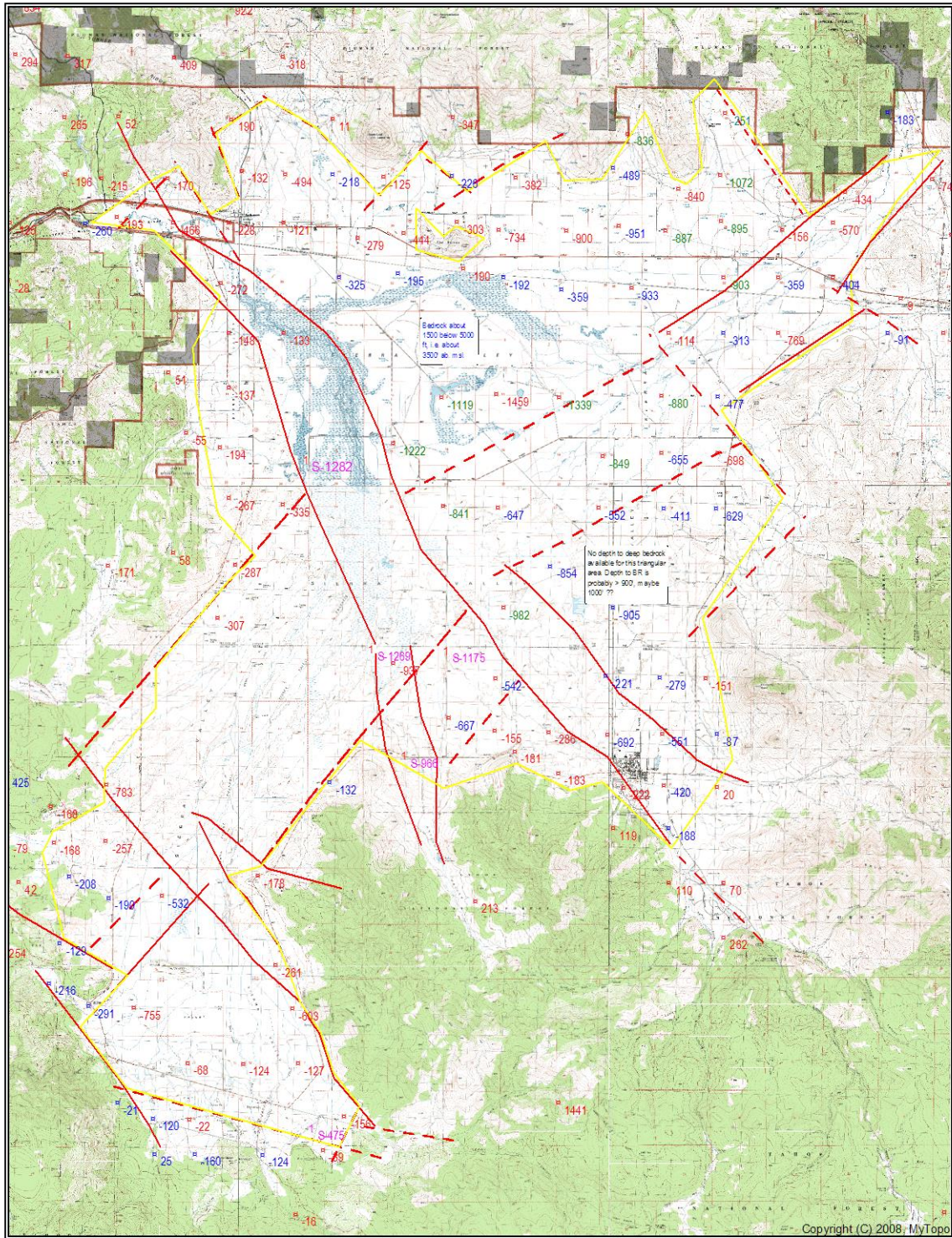


Figure 98. Results of the stereographic aerial photo survey. Solid red lines represent the strike-slip motion faults while dashed red lines represent normal fault movements. Yellow line is the boundary estimate for the SV groundwater system implied by the faults.

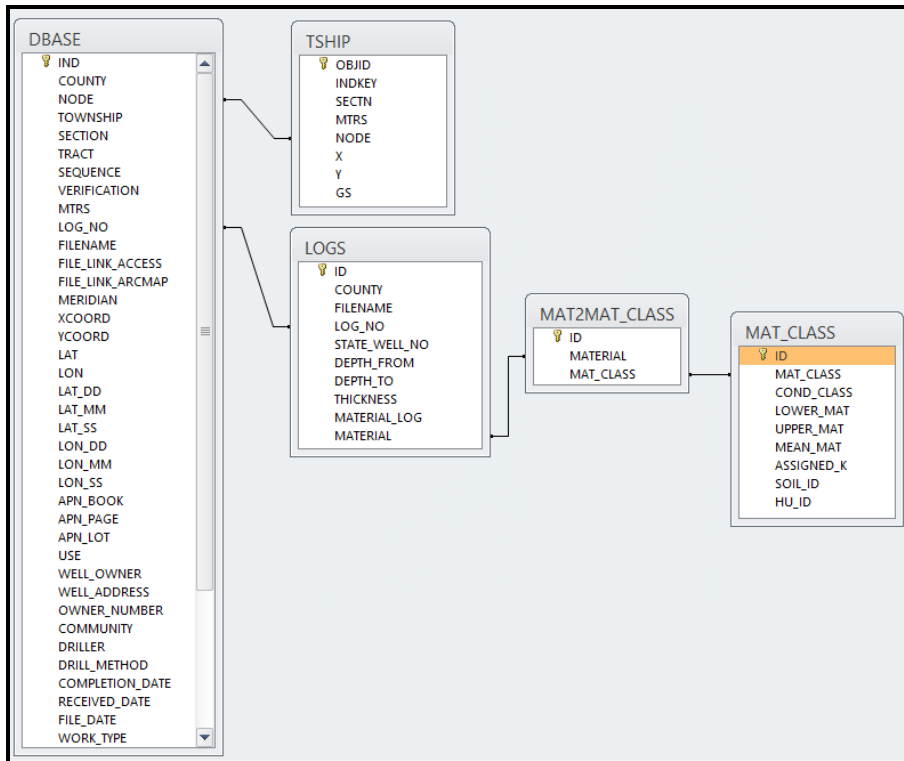


Figure 99. The tables and relationships of the Microsoft Access database created to store the well drilling logs.

This delineation (**Figure 102**) serves the purpose of giving a general conceptualization of the hydrogeologic formations under the SV rather than being an exact geological model of the area. It shows us that the SV Aquifer is made up of local confined and unconfined zones that are mostly interconnected. Most of the SV is covered by sediments with high and low hydraulic conductivities. Igneous rocks cover the Chilcoot basin.

However, there is no source of information to our knowledge that characterized the extent of these local hydrogeologic formations. Regional geologic maps covering the Sierra Valley consider the aquifer mostly as a single formation of lake deposits.

Characterizing the extent of these formations requires extensive analysis of the previously constructed wells as well as additional field studies. Therefore, it's not in the scope of this modeling study. To overcome this problem, the modeling team will parameterize the hydraulic part of the groundwater model in accordance with the suggestions of the project hydrogeologist in order to account for the aforementioned heterogeneity. It is expected that the

outcomes of this approach will provide suggestions for the areas that should be investigated in greater detail for the future studies.

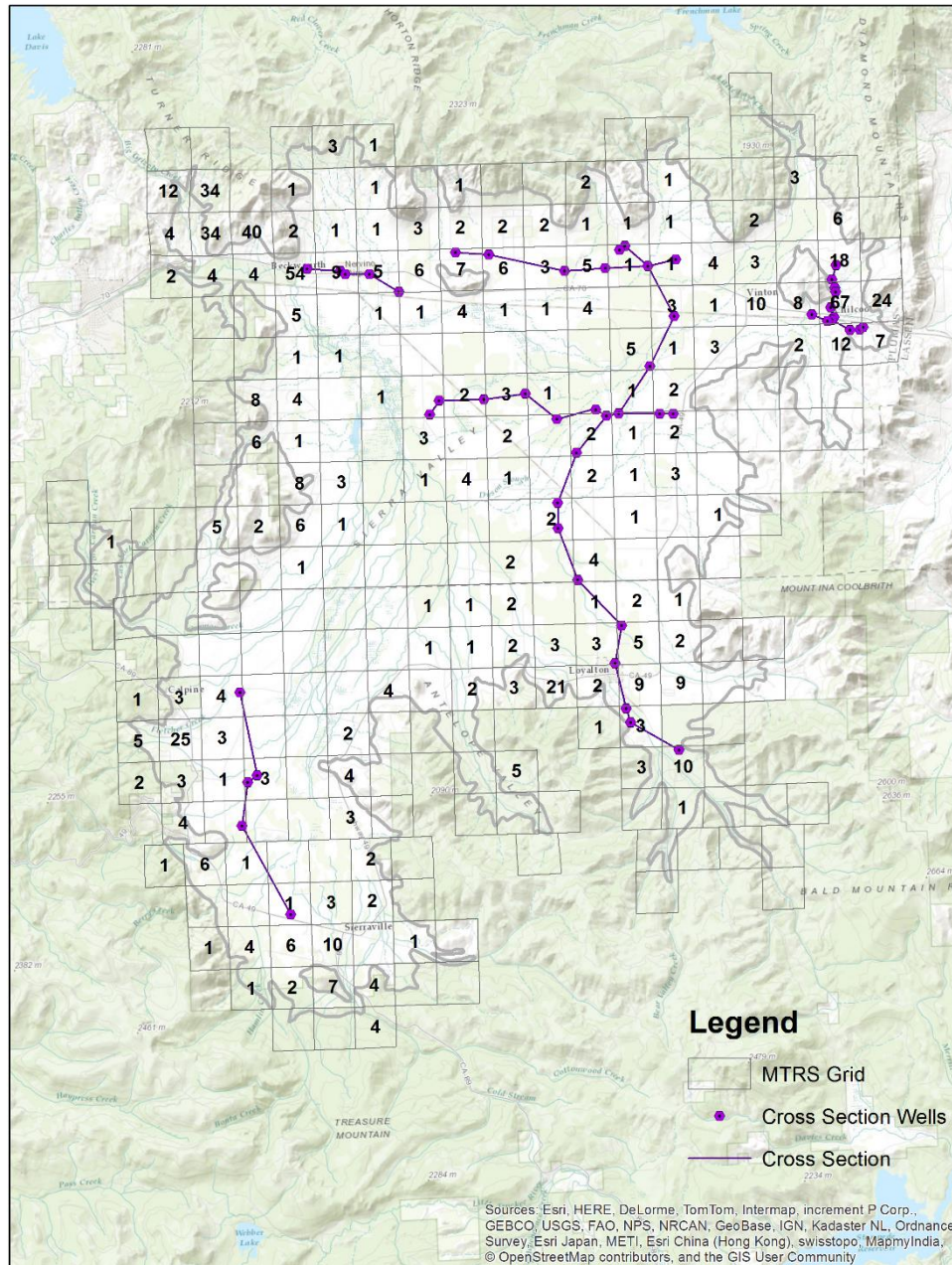


Figure 100. Well drilling logs stored in the well log database. The number inside each MTRS grid shows the number of well logs at the corresponding 1 sq-mi area. Cross section wells and cross sections were taken from the previous hydrogeologic studies of the Valley (Kenneth D. Schmidt, 2003, 2005 and 2012).

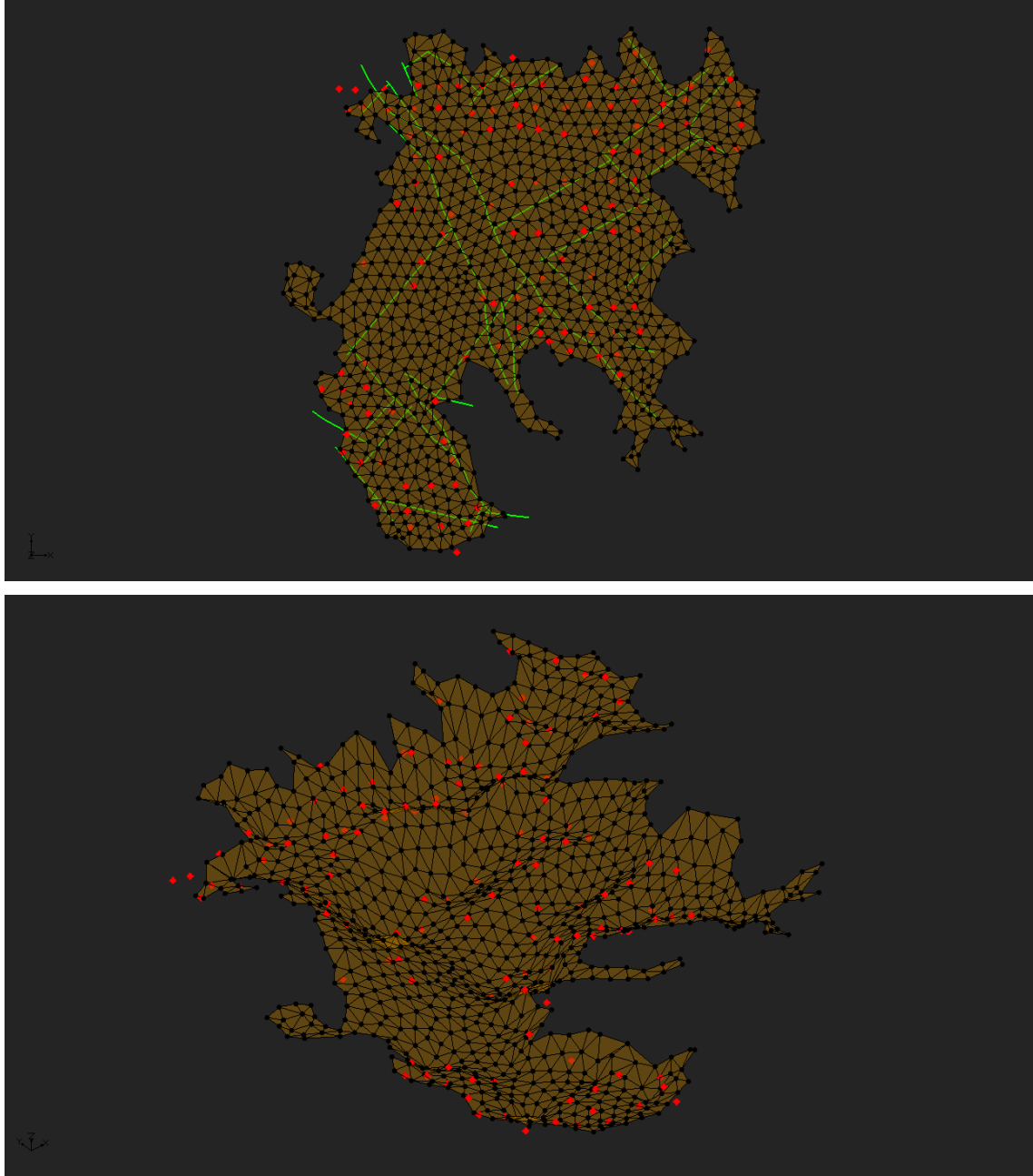


Figure 101. Updated bedrock shape for the Sierra Valley aquifer: Top view and oblique view. The red points show the reference points for depth to bedrock information gathered from well logs. The green lines show strike-slip and normal motion faults.

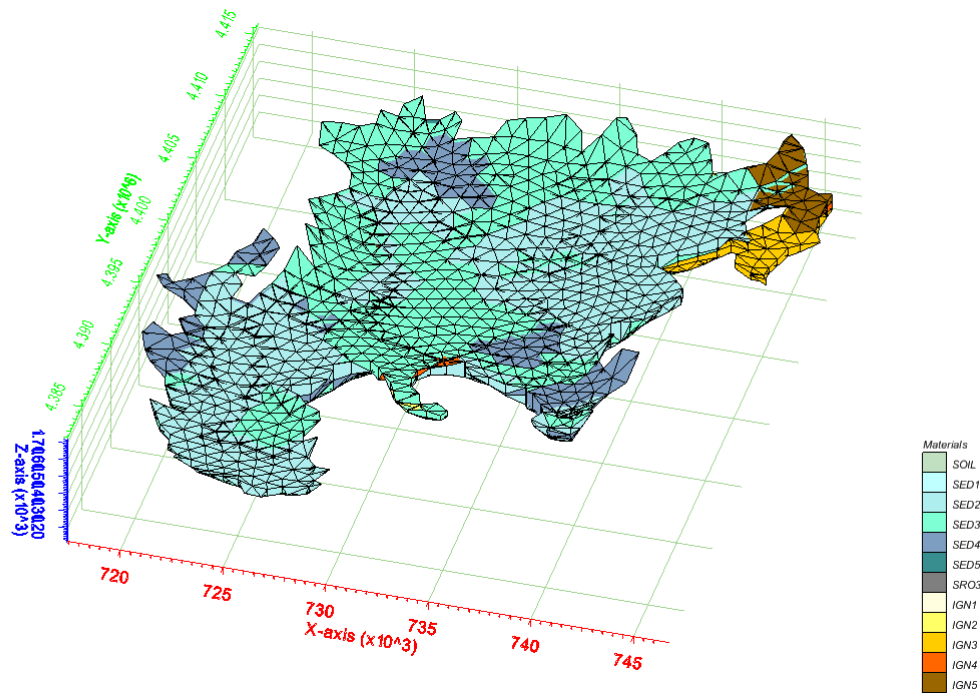


Figure 102. Aquifer delineation of the Sierra Valley Aquifer. The formations are divided into three: Sediments (SED), sedimentary rocks (SRO) and igneous rocks (IGN). Each of these is then categorized into five groups with respect to the typical hydraulic conductivity values found in the literature (1: highest hydraulic conductivity, to 5: lowest hydraulic conductivity).

Model Discretization

IWFM uses the finite element discretization to obtain the numerical solution for the differential equations of groundwater flow. A finite element mesh is generated for SV by using the IWFM Mesh Generator tool. At the surface, horizontal boundaries of the mesh were determined by intersecting the basin boundary and the strike-slip and normal fault lines given by (Bohm, 2015). Below the surface, the boundaries were defined by the bedrock surface shaped from the data recorded in well construction logs. The stream network and the pumping wells observed by SVGMD were forced into the mesh generation process. The mesh was further refined around the streams and pumping wells. The resulting mesh is presented in **Figure 103** and it has 8,700 elements and 4,560 nodes. The stream network was represented by 21 reaches at 566 nodes.

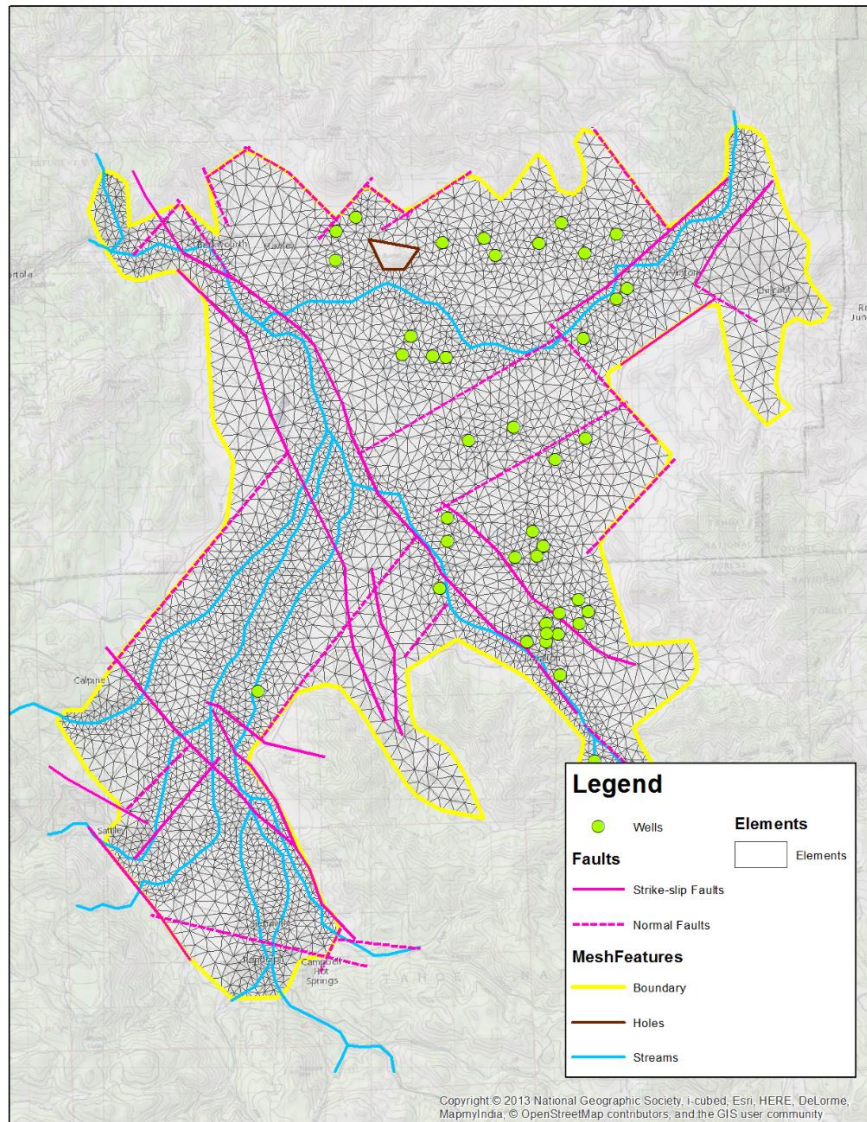


Figure 103. Finite Element Mesh generated by the IWFM Mesh Generator.

As recommended by the project hydrogeologist, the medium was discretized vertically into five layers. A shallow unconfined zone was created at the surface. Below the unconfined zone, there are two confined layers and two layers considered as the aquitards confining them. The depths of these layers were estimated from the filtering depths recorded in the well construction logs (Bohm, 2015).

Boundary Conditions:

Groundwater flow to Mohawk Valley near the MFP station are represented by a general head boundary condition. No flow boundary conditions were assumed for the other parts of the SV. **Figure 104** shows the no flow, and the general head boundaries assigned to the model domain. The boundary flow to Mohawk Valley is controlled by the geology around the MFP station, which is also uncertain due to the shape of the surrounding foothills and the intersection of the fault lines nearby. The properties of this general head boundary are considered as calibration parameters in the IWFEM.

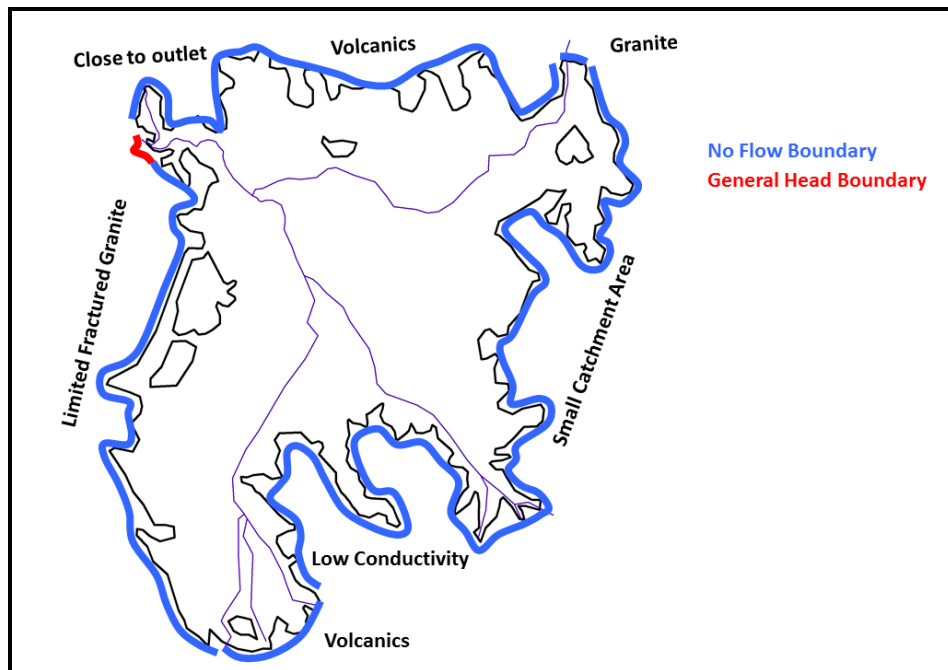


Figure 104. Boundary conditions assigned to the model domain.

Irrigation Water Use:

Surface water rights in Sierra Valley are defined by two decrees: Sierra Valley Decree 3095, 1940 (Superior Court of the State of California, 1940) and Little Last Chance Creek Decreed Water Rights, 1959 (Superior Court of the State of California, 1959). These two documents provide the amount to be diverted if water is available, the priorities, and the locations of the corresponding diversions. The exact locations of the diversions (274 diversions

in total), as provided in the DWR Maps, were digitized and stored in GIS database together with the decreed water rights. As presented in **Figure 105**, the diversions are located on three main streams:

- The Sierra Valley Channels starting on the southwest around Sierraville and flowing north on the west side of the Sierra Valley.
- The Smithneck Creek starting on the southeast of Loyalton and flowing northwest to the Sierra Valley Channels.
- The Little Last Chance Creek on the northeastern part, flowing from Frenchman Lake.

The relationship between the diversions and the irrigated fields is constructed with the DWR Tract areas. Each diversion is assumed to be supplying the irrigation demand for the DWR Tract area in which it is located.

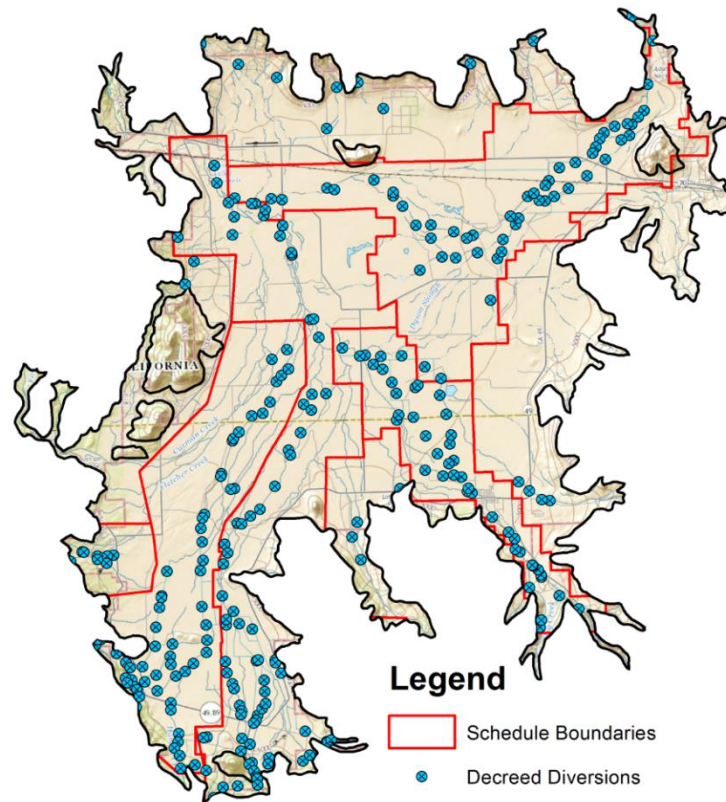


Figure 105. Map showing the decreed diversions and the scheduling areas in Sierra Valley.

In the Sierra Valley, the major groundwater wells are mostly used for the irrigation of the alfalfa fields. Sierra Valley Groundwater Management District (SVGMD) monitors and keeps records of the monthly pumping rates of the major groundwater users in the area (**Figure 106**) while the data is not available to the public. This information is summarized as the annual total pumping rates for each MTRS grid (1 sq-mi area), with the meter locations as reported in the previous hydrogeologic study reports (Kenneth D. Schmidt, 2003, 2005 and 2012). Major pumping well locations were digitized from the maps provided in these studies, however, since the state well identification numbers are not provided, the well properties such as the well diameter and the screened depths could not be identified.

In order to introduce the groundwater pumping wells to the model, well properties were estimated from the available well logs of the nearby wells and pumping rates were estimated by the IWFM to meet the irrigation water demand. Similar to the surface water diversions, the relationship between the groundwater pumping wells and the irrigated fields is constructed with the DWR Tract areas. Each groundwater pumping well is assumed to be supplying the irrigation demand for the DWR Tract area in which it is located.

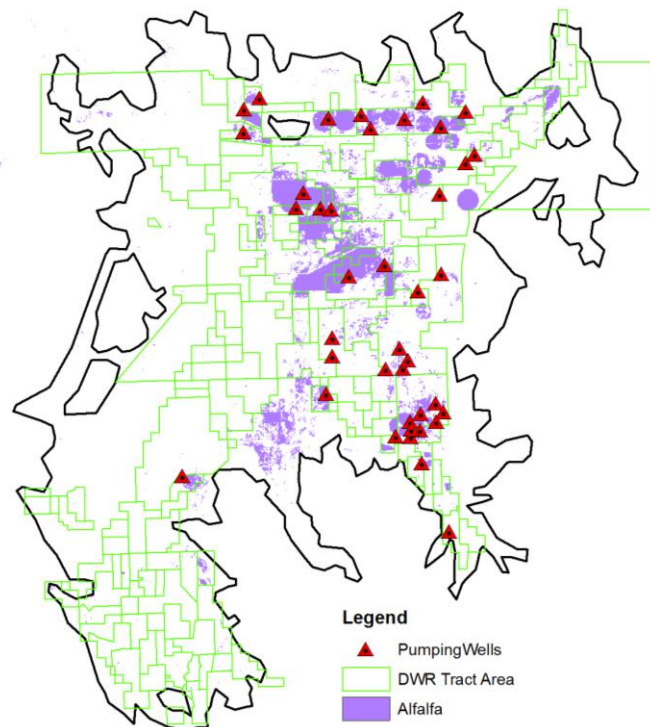


Figure 106. Pumping locations of major groundwater users in Sierra Valley as reported in the previous hydrogeologic study reports (Kenneth D. Schmidt, 2003, 2005 and 2012).

IWFM Demand Calculator (IDC):

The root zone processes and the water demand for supply adjustment are calculated with the IDC (California Department of Water Resources, 2016) component of the IWFM. IDC requires precipitation and crop evapotranspiration time series as well as soil properties, land use and agricultural data to calculate the water demand of agricultural, urban and native vegetation water demands.

For the precipitation input, the spatially distributed liquid water (LQW, rainfall + snowmelt) time series output from the Snow Module of the WEHY model was used. In this way, the snowfall and snowmelt processes were taken into account.

Crop evapotranspiration was calculated externally using the FAO56 Penman-Monteith method (Allen, Pereira, Raes, & Smith, 1998). In this method, climate variables such as the temperature and wind speed from the WEHY Snow Module output were used to calculate the reference evapotranspiration (ET_0) for each model computational unit (MCU). Then, the ET_0 was multiplied with the corresponding crop coefficients (Allen, Pereira, Raes, & Smith, 1998) to find the potential evapotranspiration rate for each crop, ET_c . The spatially averaged daily liquid water and potential evapotranspiration time series for the water years 2001-2010 is given in **Figure 107**.

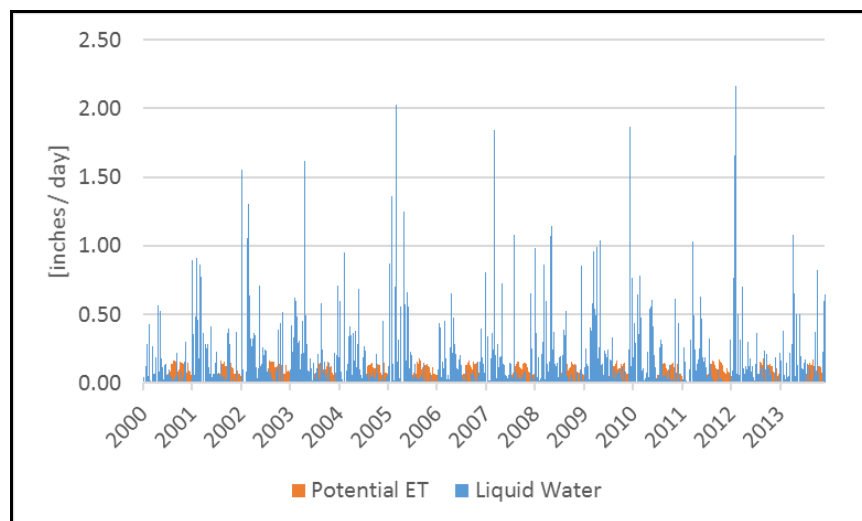


Figure 107. Potential evapotranspiration and liquid water for the water years 2001-2010.

The soil hydraulic parameters required by the IDC such as wilting point, field capacity, total porosity, pore size distribution index and saturated hydraulic conductivity to calculate the root zone processes were gathered from the SSURGO database. The representative values for the mentioned soil parameters for each element in the mesh were calculated by the IWFM Soil Data Builder GIS tool (California Department of Water Resources, 2016). Additionally, the representative soil group types to be used in surface runoff calculations by the curve number method were determined from the SSURGO database. **Figure 108** presents the two most sensitive soil hydraulic parameters, the representative saturated hydraulic conductivity and the pore size distribution index, over the Sierra Valley.

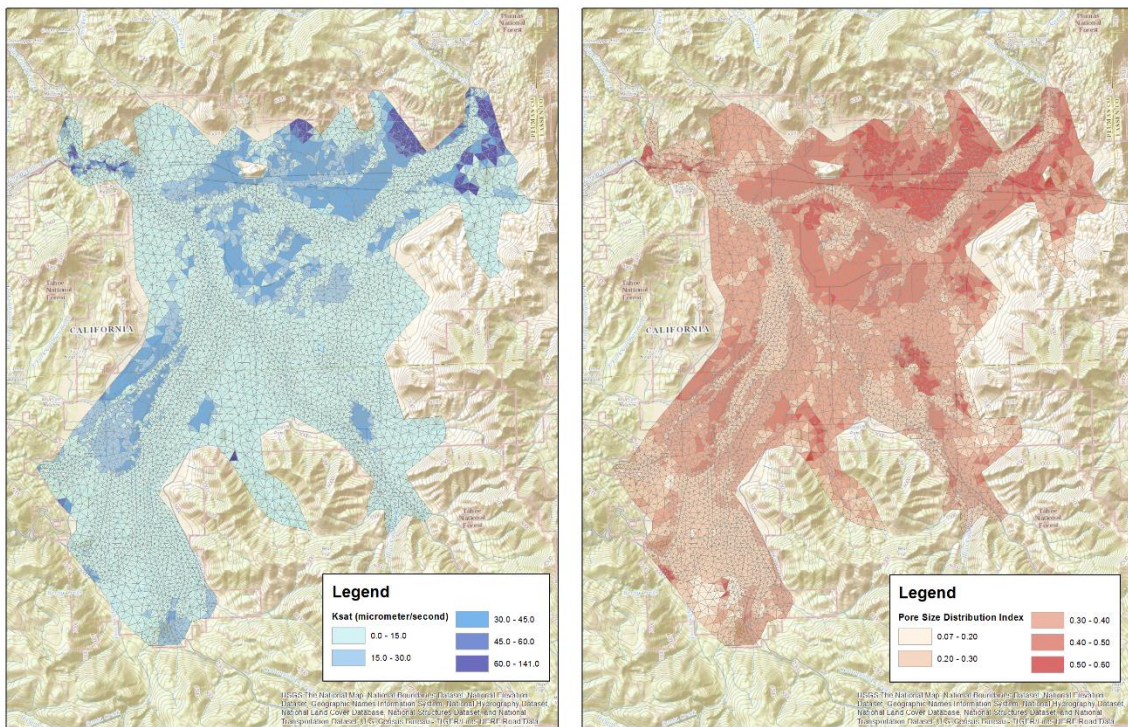


Figure 108. Soil data from SSURGO database on the model mesh: Representative saturated hydraulic conductivity (left) and pore size distribution index (right).

The Cropscape database was used to determine the main crop types and their spatial distribution. Cropscape database provides geo-referenced, crop-specific land cover data for the continental United States using satellite imagery and extensive agricultural ground truth (USDA, 2016). The four main crop types were identified in Sierra Valley as: Alfalfa, grass/pasture, herbaceous wetlands and shrubland. Shrubland and other minority classes are grouped together

as native vegetation in the IDC model and the other three crop types are given their individual classes. Note that alfalfa and grass/pasture zones are irrigated lands, while the remaining areas are not irrigated. The percentage area covered by crop types and their spatial distribution is presented in **Figure 109**.

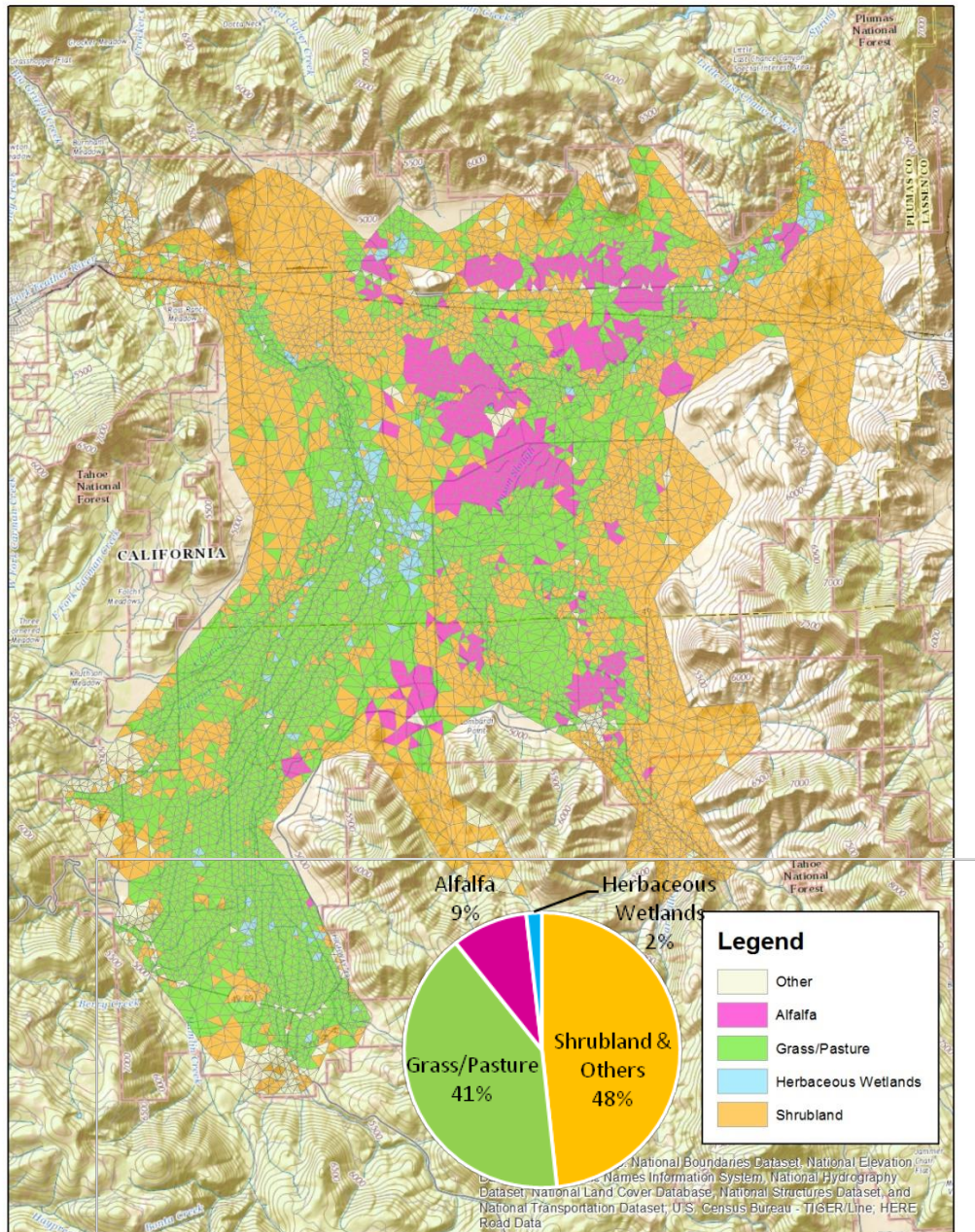


Figure 109. Crop data from Cropscape database on the model mesh.

Model Calibration and Validation:

In almost all cases, model calibration is necessary to represent the complex, heterogeneous disposition of physical properties that characterizes real-world environmental systems with a simplified parameter field that numerical models need. For this reason, the project team set up the model independent parameter estimation and uncertainty analysis software PEST (Doherty, Muffels, Rumbaugh, & Tonkin, 2016) to run and calibrate the IWFM for the Sierra Valley aquifer system.

PEST implements mathematical parameter estimation and inverse modeling techniques to estimate and simplify the parameter fields of any model while attaining maximum reasonableness. With the uncertainty analysis, it also helps the modeler to assess the uncertainty associated with model parameters and predictions as well as what data is needed to be gathered to most effectively reduce the model predictive uncertainty. Further information about PEST can be found in (Doherty, Muffels, Rumbaugh, & Tonkin, 2016).

With the provided information, PEST runs the model multiple times in an iterative manner to analyze how changes in parameters affect the results, and to come up with the best set of estimated parameter values that minimizes the differences between model outputs and provided observations.

For the problems in which limited information about the model parameters is available, the modeler should use the principle of parsimony to parameterize the system with the smallest number of parameters possible while ensuring the goodness of the model results. In our case, this parameterization was drafted initially when the conceptual model for the Sierra Valley aquifer was created. Following this principle, the modeling team revised the parameterization of the IWFM model for Sierra Valley between calibration runs to accommodate the heterogeneity in the area.

Regarding the aquifer hydraulic parameters, Sierra Valley was parameterized by the parametric grid approach of IWFM. In the parametric grid approach, one can use the nodes in a parametric mesh, which is different than the finite element mesh used for numerical discretization, to define the aquifer hydraulic properties. IWFM then interpolates these values based on their geographic location and assigns the interpolated values to individual finite element nodes. The parametric grid defining the aquifer hydraulic properties is illustrated in

Figure 110. The locations of the inside nodes are chosen to represent the heterogeneous formations identified during the hydrogeological delineation. Other calibration parameters include the mean streambed conductance, and conductance for the general head boundary. Initial values and boundaries for these parameters were identified from the previous analysis with well logs, SSURGO soil databases, available pumping test results, and field visits.

Observed values for the monthly stream flowrate at the MFP station and groundwater levels at various stations in the SV as well as the differential changes in annual mean groundwater levels were used for the calibration and validation of the IWFM (**Figure 111**).

The calibration period was chosen as the water years 2009 and 2010 after taking into consideration the availability of the stream flow observation records at the MFP station, and the groundwater level records in the CASGEM database. For that period, there are 730 daily streamflow records from the MFP station and 145 groundwater level observations (mostly biannual) at 47 different stations.

The validation period was chosen as the water years 2012 to 2014. For that period, there are 1,096 daily streamflow records from the MFP station and 298 groundwater level observations (mostly biannual) at 48 different stations.

Figure 112 presents the calibration and validation results for the stream flowrates at the MFP station. The statistical test results are summarized in **Table 19**. These show that the simulated monthly stream flowrates at the MFP station are similar to their corresponding observed values, both for the calibration and validation periods, while the statistical test results show a good performance of the IWFM model, with high values of the correlation coefficient and the Nash-Sutcliffe Efficiency.

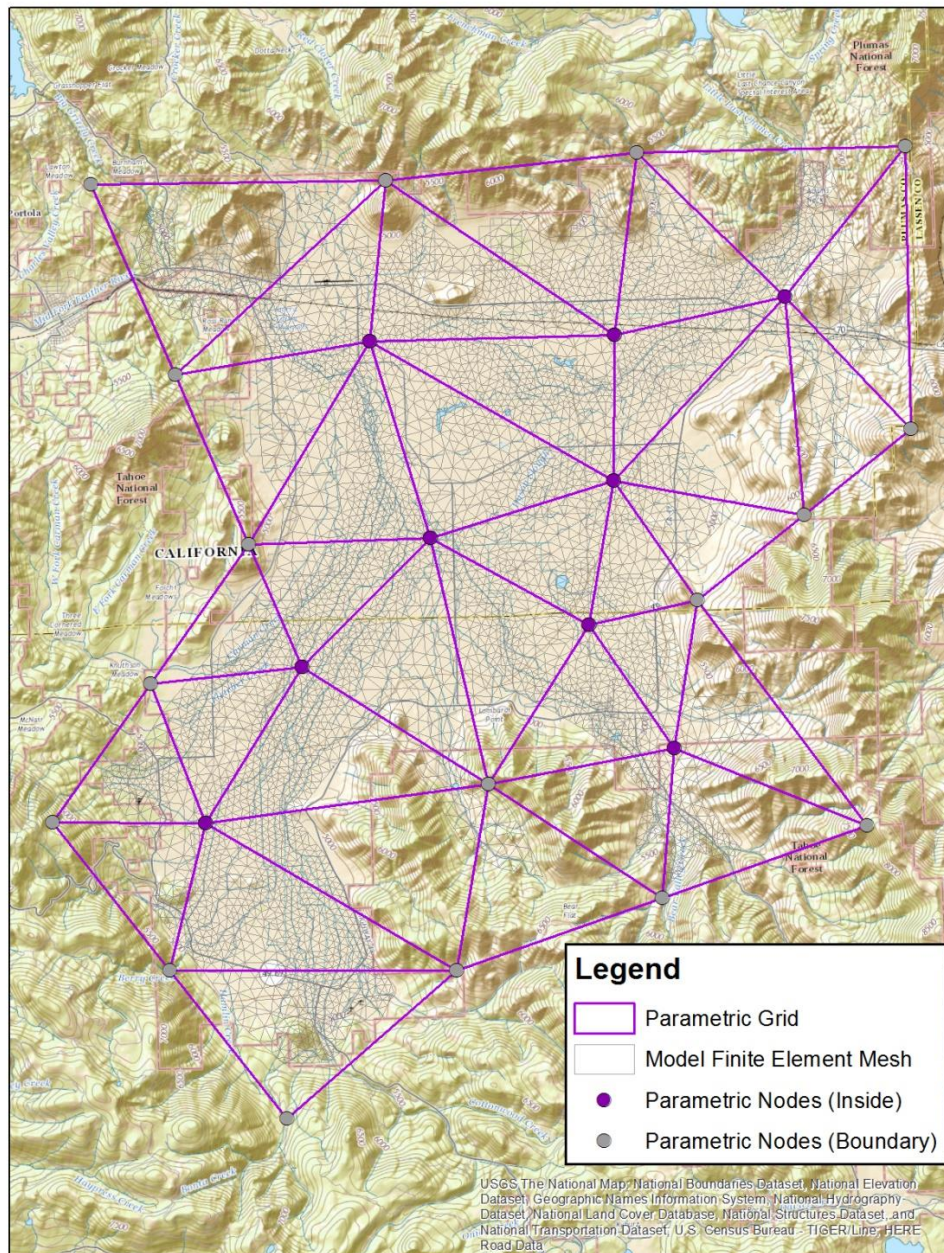


Figure 110. Parametric grid used to define the aquifer hydraulic properties.

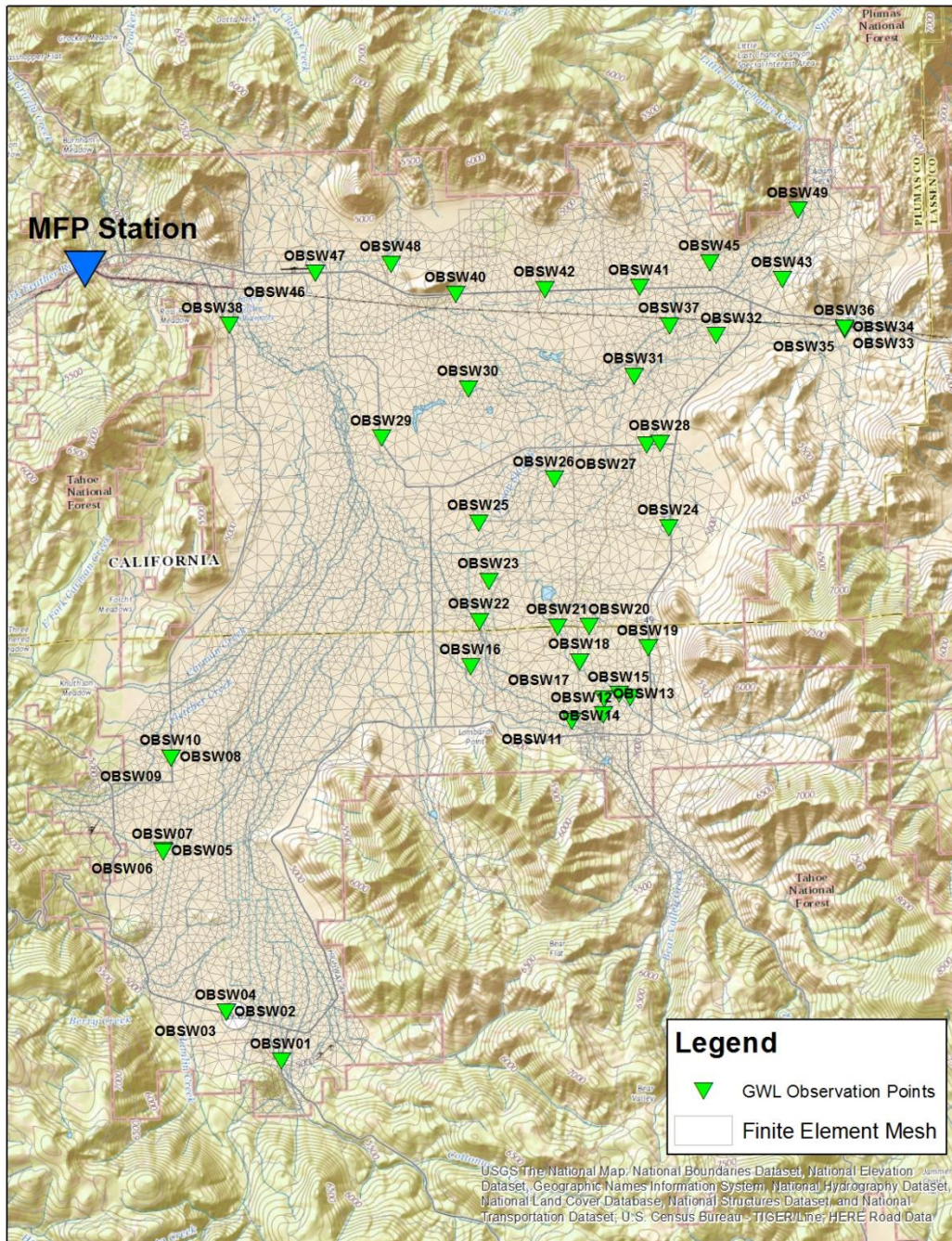


Figure 111. MFP stream gauge station and the groundwater level observation points from the CASGEM database.

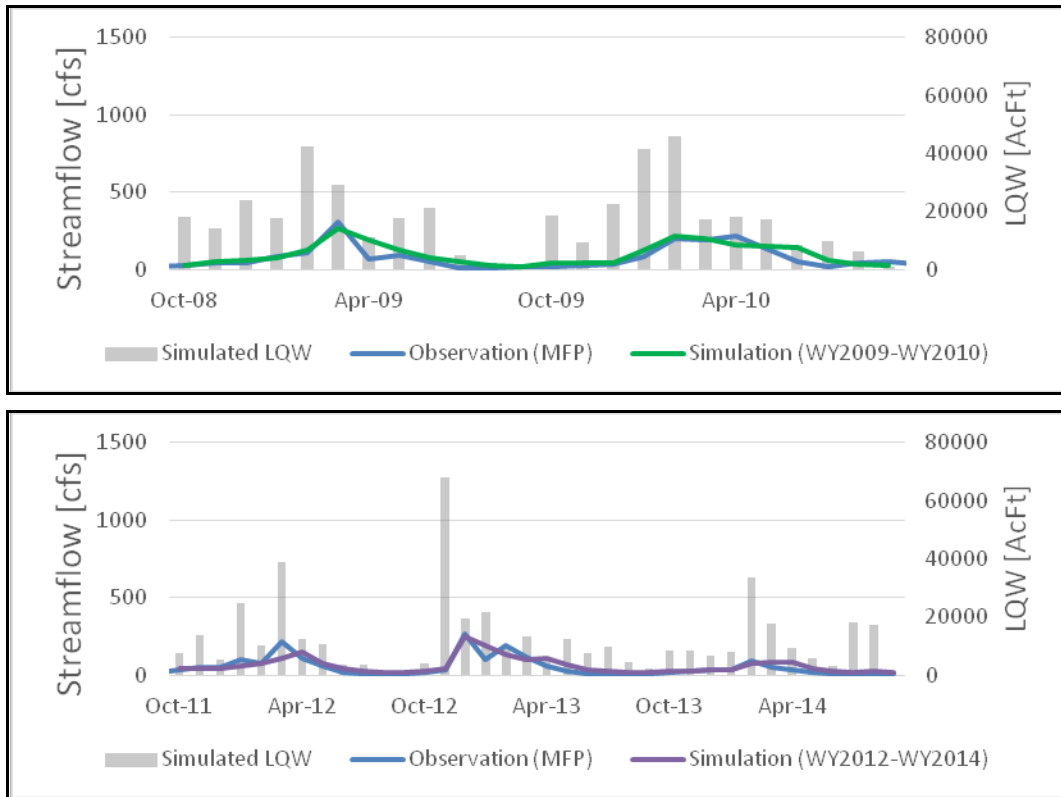


Figure 112. The calibration (top) and validation (bottom) results for the monthly stream flowrates at the MFP station.

Table 19. Statistical test values of simulated and observed monthly stream flowrates at the MFP station during the calibration and validation periods. Obs: observed; Sim: simulated; STDEV: standard deviation; RMSE: root-mean-square error; Nash: Nash-Sutcliffe Efficiency.

Parameter	Calibration (WY2009-WY2010)		Validation (WY2012-WY2014)	
	Obs	Sim	Obs	Sim
Mean (cfs)	78.61	96.03	53.08	60.38
STDEV (cfs)	77.52	70.52	61.73	53.82
RMSE	40.08		33.57	
Nash	0.72		0.70	
Correlation Coefficient	0.88		0.84	

Figure 113 presents the groundwater level simulation results for a selected group of the observation wells around the Sierra Valley for the water years 2000 to 2014 which include the calibration and validation periods. The results show acceptable match for the purpose of this study considering the limited information on the geologic formations and groundwater use.

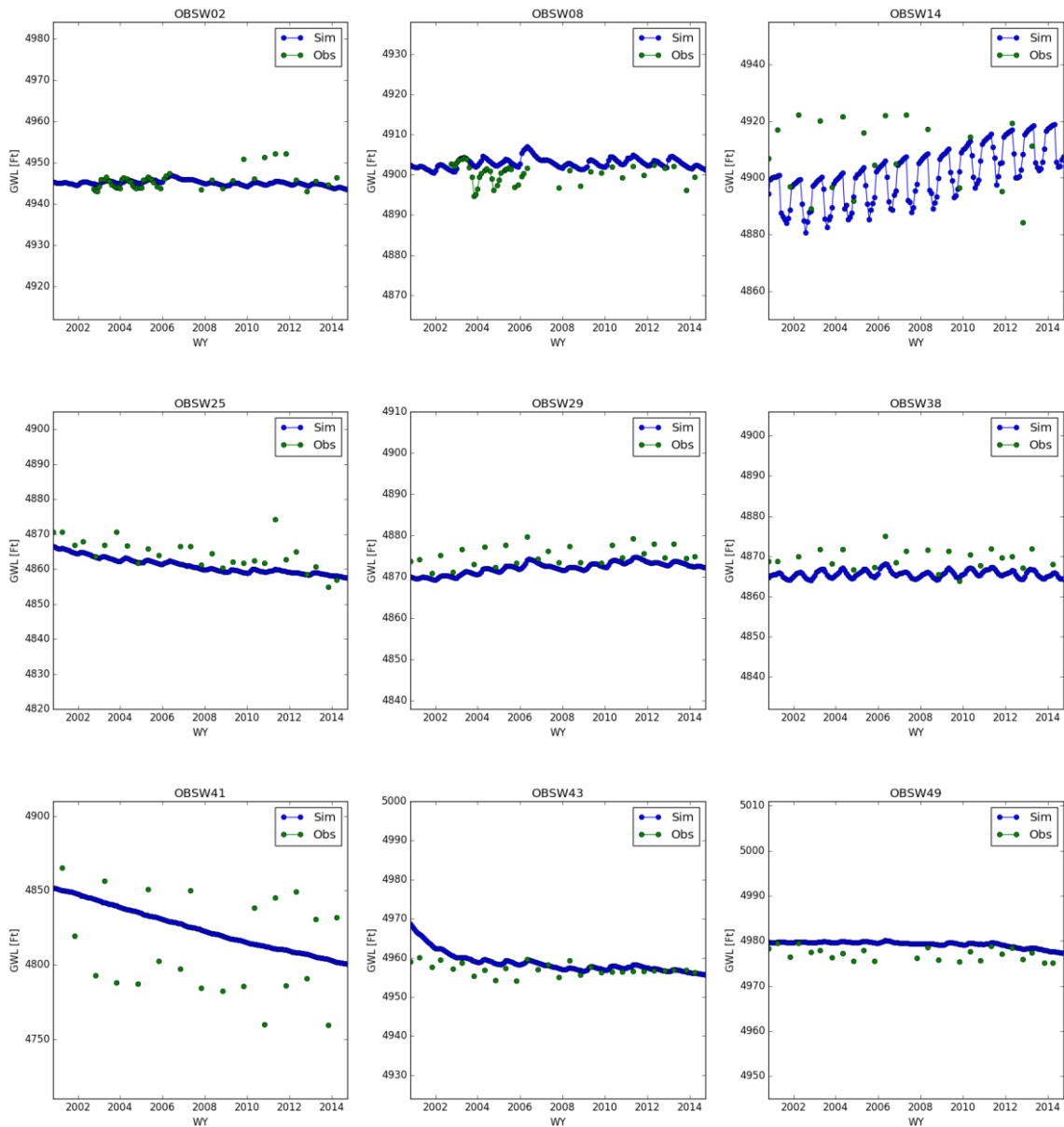


Figure 113. Groundwater level results for the calibration and validation periods for various groundwater observation wells.

Figure 114 presents the piezometric surfaces prepared from October 2010 observations and the corresponding simulation results. These figures confirm the model performance and conceptualization around the domain boundaries. Also, the model creates the cone of depression observed in the pumping intensive areas at the Northeast and Southeast of the Sierra Valley. Introduction of the detailed pumping information and a correct well inventory to the model are very important to improve the model performance and to decrease the uncertainty of the results.

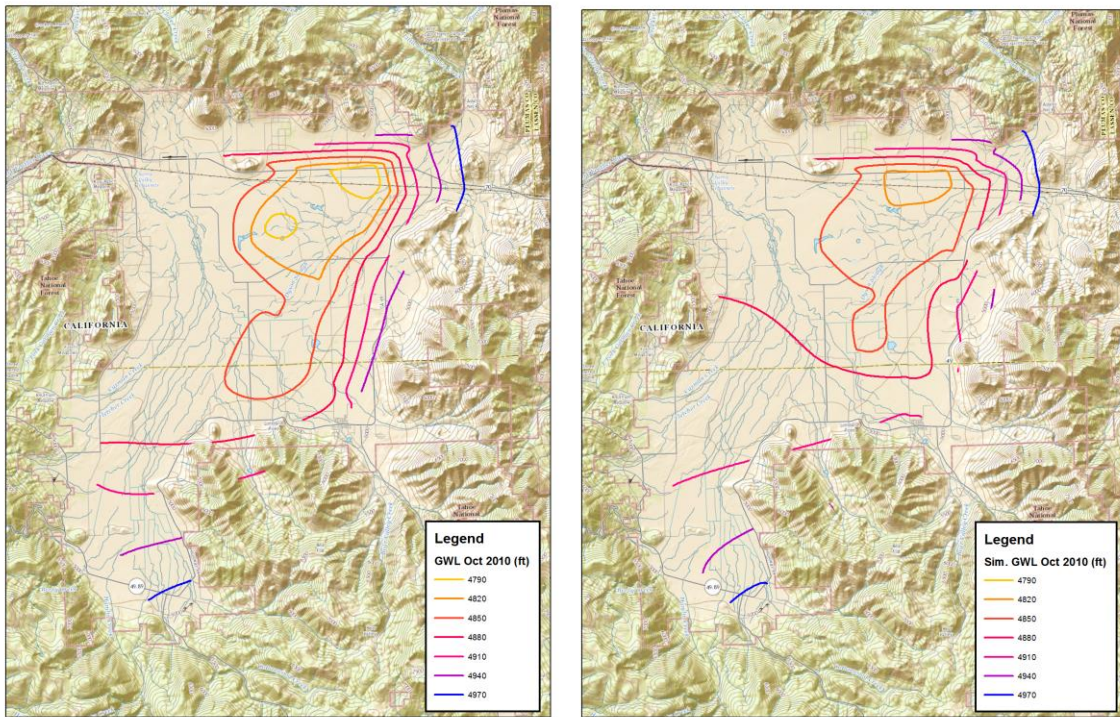


Figure 114. Observed versus simulated piezometric surfaces for October 2010.

5. Historical Analysis of the Sierra Valley Groundwater System

In order to create a baseline for the future scenario simulations and to determine the current water budget, the Sierra Valley groundwater system was simulated for the historical period of water years 2000-2010. The water budget components for an average water year from 2000 to 2010 are presented in **Table 20**. The different water budget components will be defined and discussed in the following paragraphs.

Table 20. Water budget components for the Sierra Valley as estimated by the IWFM and WEHY models.

Water budget component	Average Annual Volume [Ac Ft] 2000 - 2010
Liquid Water (LQW)	188,725
Prime Water	34,675
Total Input on the Ground Surface (LQW + Prime Water)	223,400
Direct Runoff	21,650
Infiltration	201,750
Potential Evapotranspiration	257,700
Actual Evapotranspiration	152,000
Deep Percolation	48,250
Streamflow in from foothills	38,000
Streamflow out at MFP	46,280

Liquid water (LQW) is water available at the ground surface in the liquid state and is defined as the sum of rainfall and snowmelt. These results suggest that annually almost 189,000 Ac-Ft (~20 inches) of liquid water is available on the grounds of the Sierra Valley.

Prime water is the amount of water applied to the agricultural and urban lands in addition to the liquid water, mainly for the purpose of irrigation. In IWFM, prime water can come from surface water diversions, from groundwater pumping wells or from an external source. In this study, no external sources are considered, urban lands were neglected and the automatic supply adjustment feature of IWFM was used. Therefore, prime water is dynamically calculated during the simulations depending on the water demand of the agricultural crops and available water at the surface water diversions and groundwater pumping wells. In addition to the liquid water,

about 34,700 Ac-Ft of irrigation water is applied annually to the valley to meet the water demand of the irrigated crops. These two components together make a little more than 223,000 Ac-Ft of water applied annually on the grounds of the Sierra Valley.

Direct runoff is defined as the amount of liquid water that does not enter into the soil but instead flows from the surface. Almost 10% of the total input becomes direct runoff and joins the streamflow, while the remaining 90% of the total input is estimated by IWFM to infiltrate into the soil as infiltration, which is the movement of water from the ground surface into the soil (Dogrul, 2014).

Evapotranspiration is the combination of the processes of evaporation and transpiration. The term represents the loss of liquid water as water vapor to the atmosphere by both direct evaporation from a surface and transpiration through plant tissues. Potential evapotranspiration is the amount of evapotranspiration under optimum conditions where the plant growth is not limited by the available amount of water as soil moisture or other management and environmental conditions. Actual evapotranspiration is the amount of evapotranspiration under the present management and environmental conditions that differ from the optimum conditions, such as the available soil moisture. According to IWFM results, 152,000 Ac-Ft of the infiltration, about 68% of the total input, leaves the root zone of the soil as evapotranspiration.

Deep percolation is defined as the moisture that travels down from the root zone and enters the unsaturated zone. This moisture travels downward through the unsaturated zone and eventually recharges groundwater. In this study, the unsaturated zone has not been simulated. Therefore, the deep percolation is considered to be equal to the groundwater recharge. The remaining 48,000 Ac-Ft (about 22% of the total input, about 5 inches) continues to infiltrate downwards as deep percolation and eventually becomes groundwater recharge.

The WEHY model simulation results show an average amount of 38,000 Ac-Ft of water flowing to Sierra Valley from the surrounding foothills via the major streams. IWFM results suggest that an average streamflow of 46,280 Ac-Ft is contributed to the flow measured at the MFP station annually. This results in an annual net stream recharge by the aquifer of 8,280 Ac-Ft (about 1 inch).

The monthly averages of some water budget components are presented in **Figure 115**. From this figure, it can be seen that the most important recharge months are from January to

April due to the high deep percolation in these months. Starting with May, liquid water starts to decrease, evapotranspiration starts to increase and the agricultural water demand is met with irrigation (prime water). Direct runoff is generated from November to March.

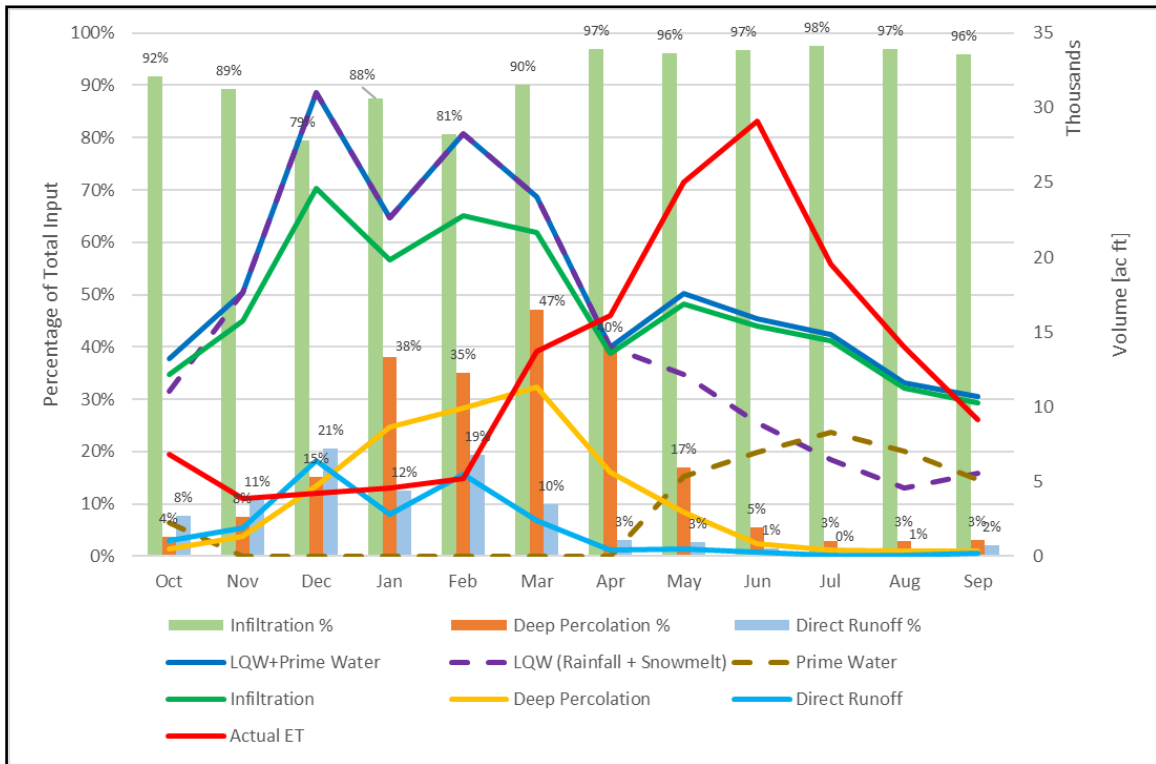


Figure 115. Historical mean monthly results for Sierra Valley for the water years 2000-2010: Rootzone components as percentages of the total input (left axis) and volumes in ac-ft. (right axis).

In **Figure 116**, the mean monthly values of the liquid water (rainfall + snowmelt) and agricultural irrigation water (prime water) are compared with total infiltration from ground surface to root zone and total deep percolation from the root zone into groundwater.

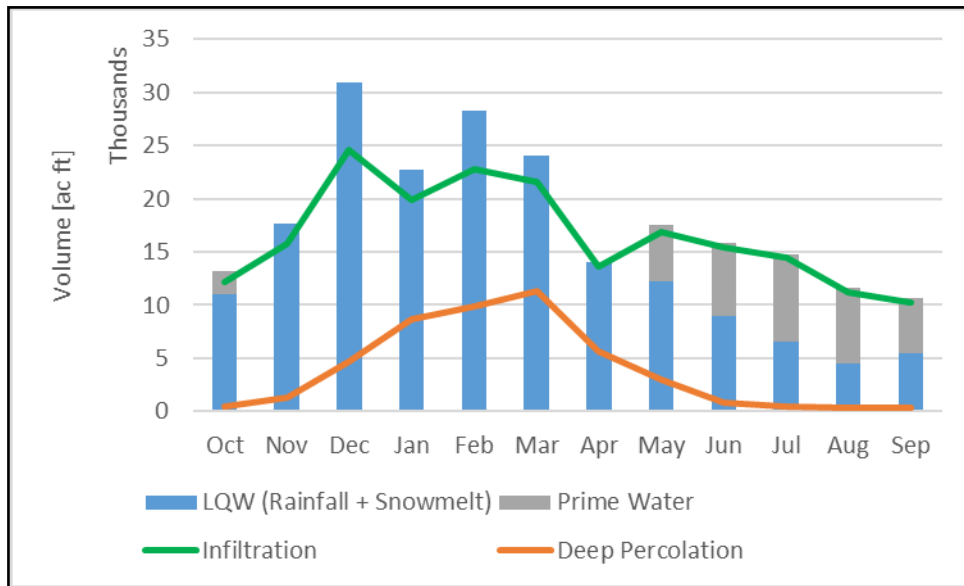


Figure 116. Historical mean monthly results for Sierra Valley for the water years 2000-2010: LQW, irrigation, infiltration and deep percolation.

In **Figure 117**, actual evapotranspiration rates are compared to the potential evapotranspiration. From July to the end of the irrigation season, agricultural evapotranspiration constitutes the major part of the total evapotranspiration.

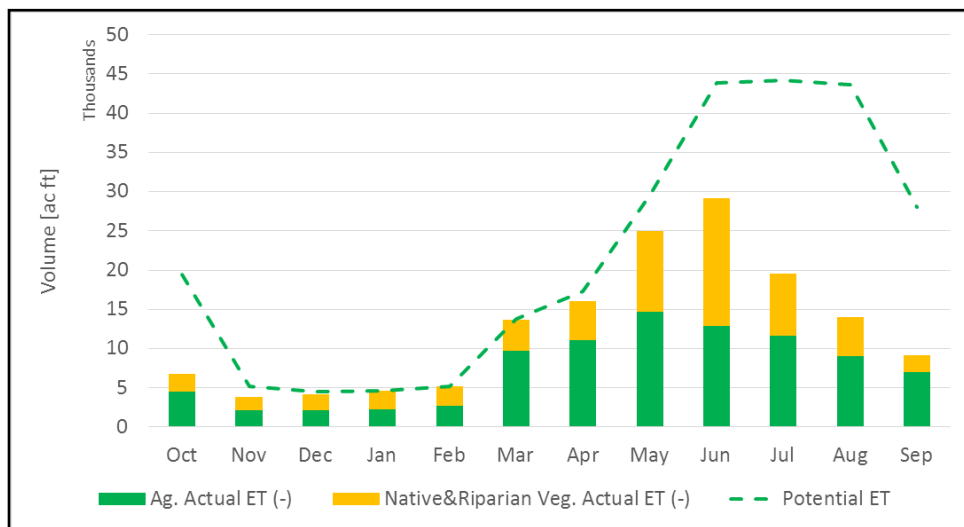


Figure 117. Historical mean monthly results for Sierra Valley for the water years 2000-2010: Potential and actual evapotranspirations.

Figure 118 compares the potential and actual evapotranspiration amounts of the irrigated crops alfalfa (AL) and pasture (PA). The evapotranspiration from the pastures are much larger than alfalfa because of the areal coverage. Starting from May until November, the difference between actual evapotranspiration and potential evapotranspiration increases, signifying that the conditions are not optimal for plant growth.

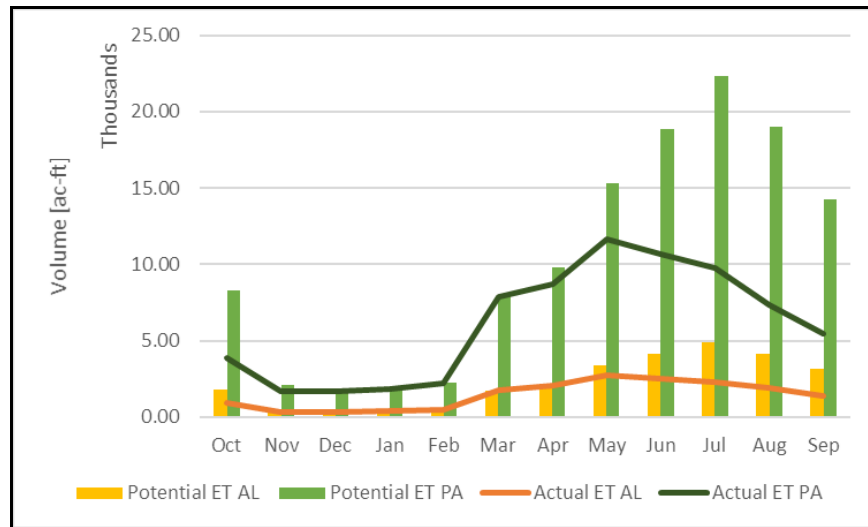


Figure 118. Historical mean monthly results for Sierra Valley for the water years 2000-2010: Potential and actual evapotranspiration amounts for irrigated crops.

Figure 119 summarizes the root zone components in the agricultural zones. It can be seen that the water deficit in summer months are supplied by the prime water (irrigation). Water leaves the root zone as either evapotranspiration or deep percolation.

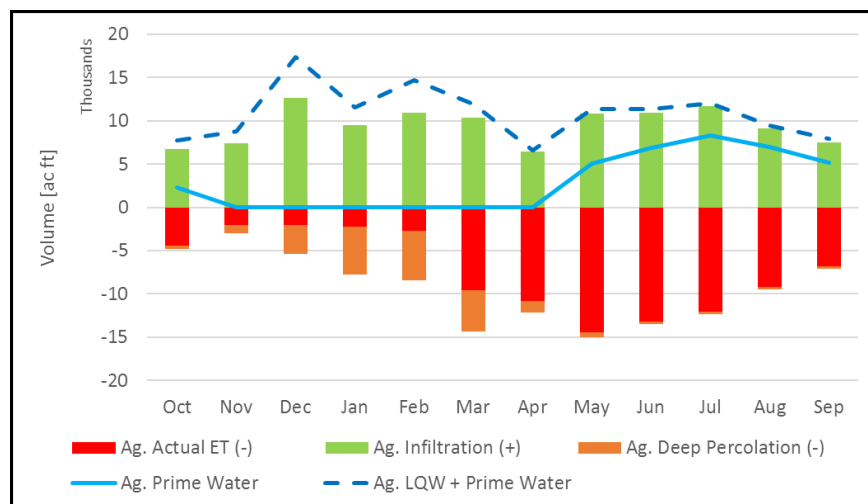


Figure 119. Historical mean monthly results for Sierra Valley for the water years 2000-2010: Root zone water budget for the agricultural lands.

One of the features of IWFM is its capability to account for soil moisture storage. **Figure 120** presents the change of soil moisture storage in an average year for the historical period. Between March and September, the soil moisture storage decreases continuously. During the months of November and December, the change in soil moisture storage is positive.

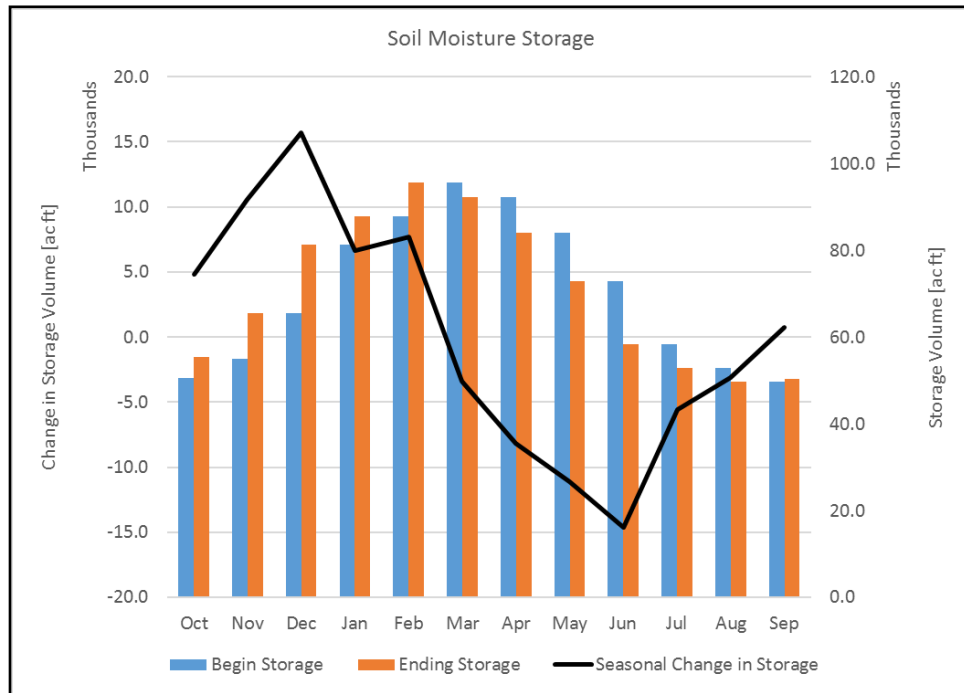


Figure 120. Historical mean monthly results for Sierra Valley for the water years 2000-2010: Soil moisture storage.

Figure 121 and **Figure 122** show the change of groundwater storage and the groundwater budget components within an average year. The period between November and March is when groundwater storage increases significantly due to the increasing percolation, stream gain and decreasing pumping. Starting from May, with the increasing groundwater use, the storage starts to decrease. Also groundwater recharges the streams during this time.

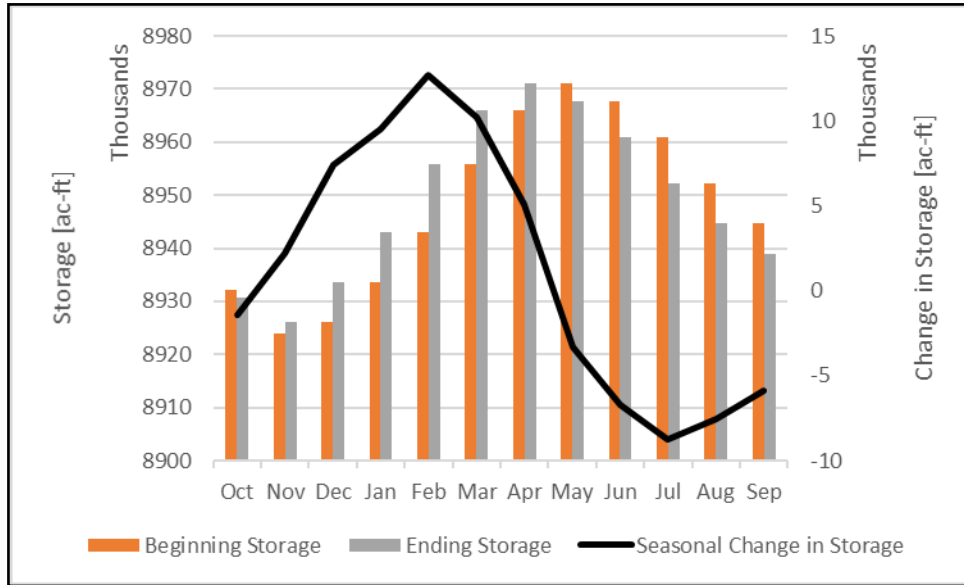


Figure 121. Historical mean monthly results for Sierra Valley for the water years 2000-2010: Groundwater storage.

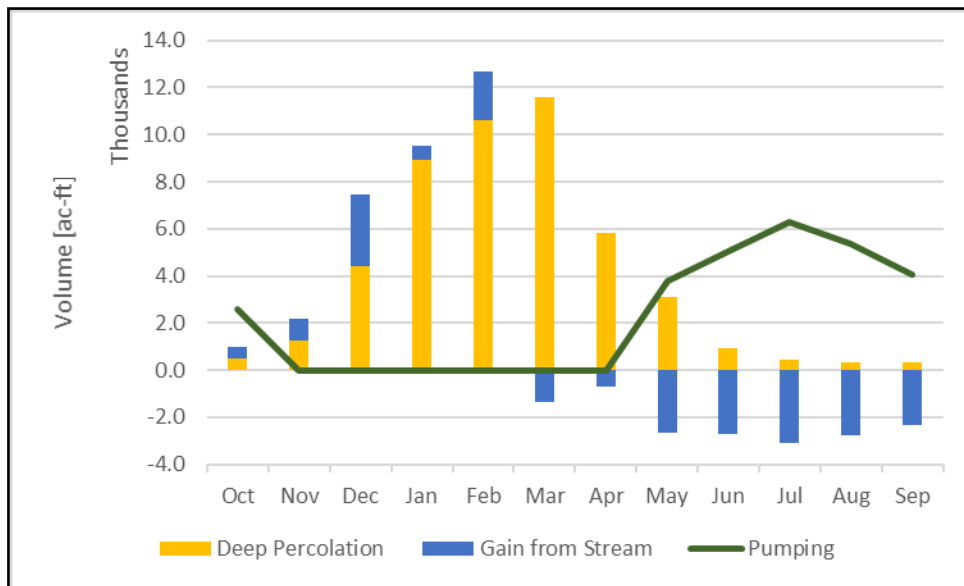


Figure 122. Historical mean monthly results for Sierra Valley for the water years 2000-2010: Groundwater budget components.

6. Future Analysis of the Sierra Valley Groundwater System

The above water balance analysis of the Sierra Valley aquifer that was done for the historical period of water years 2000-2010 is useful to understand the current conditions. Similar analyses for future periods would be of great value for future planning in Sierra Valley. Using the global climate projections explained previously, and the physically based models WEHY and IWFEM, it is possible to quantify the uncertainties of the water balance components for the future.

Future simulations over the Sierra Valley basin used Global Climate Model (GCM) atmospheric results from the previously-discussed 13 climate projections coming from the two GCMs, CCSM3 and ECHAM5 (denoted as EH5), as inputs for climate variables. As a result, the time series of the important water balance components such as liquid water (rainfall+snowmelt), infiltration, direct runoff, deep percolation, potential and actual evapotranspiration, applied irrigation water (prime water), groundwater pumping, and stream groundwater interaction for each of the projections were obtained.

To have a better understanding of the projected future climate conditions of the water balance components mentioned above, a trend analysis was undergone. Similar to the previous chapters, the non-parametric Mann-Kendall statistical test was used with a significance level, α , of 0.05 to determine whether the trend, if any, can be described as being significant. This test was done for the 13 projections over the whole period from 2010 to 2100, as well as over three subdivisions of the period: 2010-2040, 2040-2070, and 2070-2100. In addition to that, the test was also applied to the ensemble of all 13 projections.

Liquid Water

Figure 123 presents the simulation results of the annual liquid water (rainfall + snowmelt) available on the Sierra Valley for the 13 projected climate scenarios, as well as the ensemble average, the 20 year moving window average (MW(20)) and the trend line. The results of the trend analysis are presented in **Table 21**.

The trend analysis for the liquid water shows generally no significant trend for individual GCM projections. The ensemble average on the other hand shows a significant decreasing trend for the period 2010-2100 even though the ensemble trend has a positive slope in the first 60 years of simulation.

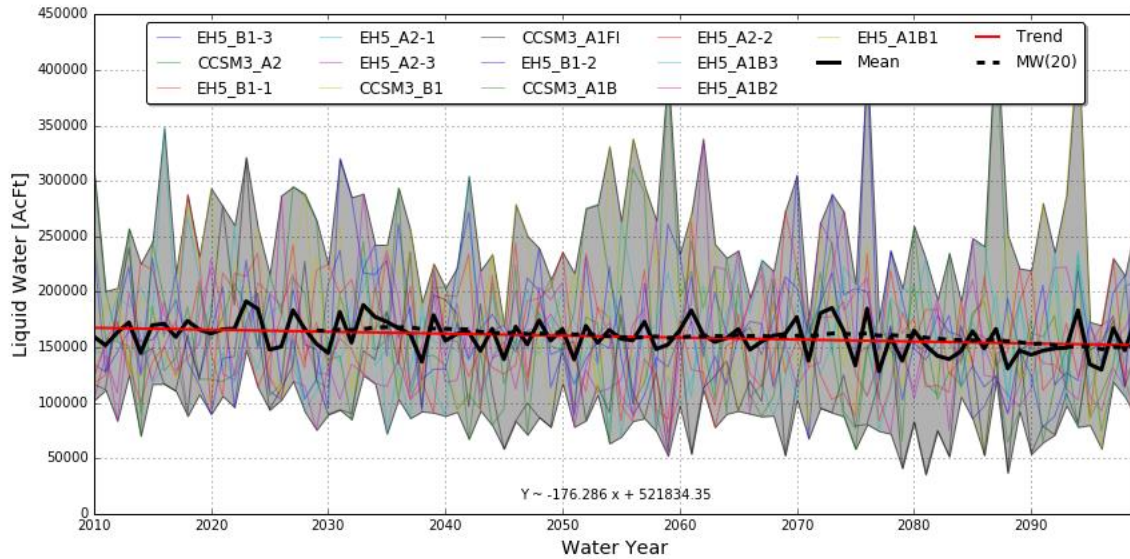


Figure 123. Simulation results of the annual liquid water for the 13 projected climate scenarios.

Table 21. Results of the trend analysis for liquid water. Slope (AcFt/yr) of the trend line of annual liquid water on the Sierra Valley for the 13 different future projections. Significance of the trend was determined using the Mann-Kendall statistical test. *p* values are given in parentheses.

GCM-Projection	Water years 2010 - 2040	Water years 2040 - 2070	Water years 2070 - 2100	Water years 2010 - 2100
CCSM3_A1B	-138.54 No Trend (1.000)	832.65 No Trend (0.668)	234.77 No Trend (1.000)	-361.46 No Trend (0.117)
CCSM3_A1FI	-353.47 No Trend (0.915)	-705.29 No Trend (0.617)	619.15 No Trend (0.592)	-769.01 Decreasing (0.001)
CCSM3_A2	-697.90 No Trend (0.544)	796.01 No Trend (0.592)	-1326.20 No Trend (0.253)	-236.79 No Trend (0.157)
CCSM3_B1	1328.13 No Trend (0.239)	1466.88 No Trend (0.253)	1745.66 No Trend (0.498)	392.69 No Trend (0.172)
EH5_A1B1	422.46 No Trend (0.475)	-773.96 No Trend (0.643)	447.52 No Trend (0.269)	-586.58 Decreasing (0.011)
EH5_A1B2	-639.77 No Trend (0.269)	2051.25 No Trend (0.069)	-581.93 No Trend (0.858)	169.50 No Trend (0.343)
EH5_A1B3	-2044.18 No Trend (0.116)	911.28 No Trend (0.284)	-323.68 No Trend (0.568)	-214.00 No Trend (0.415)
EH5_A2-1	-305.51 No Trend (0.617)	-1712.72 No Trend (0.164)	-141.39 No Trend (0.748)	153.54 No Trend (0.376)
EH5_A2-2	-932.24 No Trend (0.353)	-817.38 No Trend (0.239)	-565.30 No Trend (0.498)	-330.36 No Trend (0.084)
EH5_A2-3	1994.21 Increasing (0.042)	659.47 No Trend (0.353)	-1031.75 No Trend (0.412)	-50.33 No Trend (0.933)
EH5_B1-1	1280.97 No Trend (0.212)	-742.47 No Trend (0.372)	138.35 No Trend (0.915)	-140.57 No Trend (0.490)
EH5_B1-2	1518.27 No Trend (0.239)	-730.98 No Trend (0.521)	-1575.65 No Trend (0.269)	-208.66 No Trend (0.280)
EH5_B1-3	486.26 No Trend (0.617)	-140.86 No Trend (0.972)	-2172.14 Decreasing (0.042)	-109.69 No Trend (0.391)
Ensemble All Projections	147.59 No Trend (0.498)	84.14 No Trend (0.915)	-348.66 No Trend (0.643)	-176.29 Decreasing (0.004)

Infiltration

Figure 124 presents the simulation results of the annual infiltration for the 13 projected climate scenarios, as well as the ensemble average, the 20 year moving window average (MW(20)) and the trend line. The results of the trend analysis are presented in **Table 22**.

The trend analysis for infiltration shows generally no significant trend for individual GCM projections. When the ensemble average was analyzed there is again no significant trend for each of the 30 year periods. However, infiltration has a positive slope for the first 30 years, then it starts decreasing according to the ensemble average behavior. The overall trend of the ensemble average shows a significantly decreasing trend.

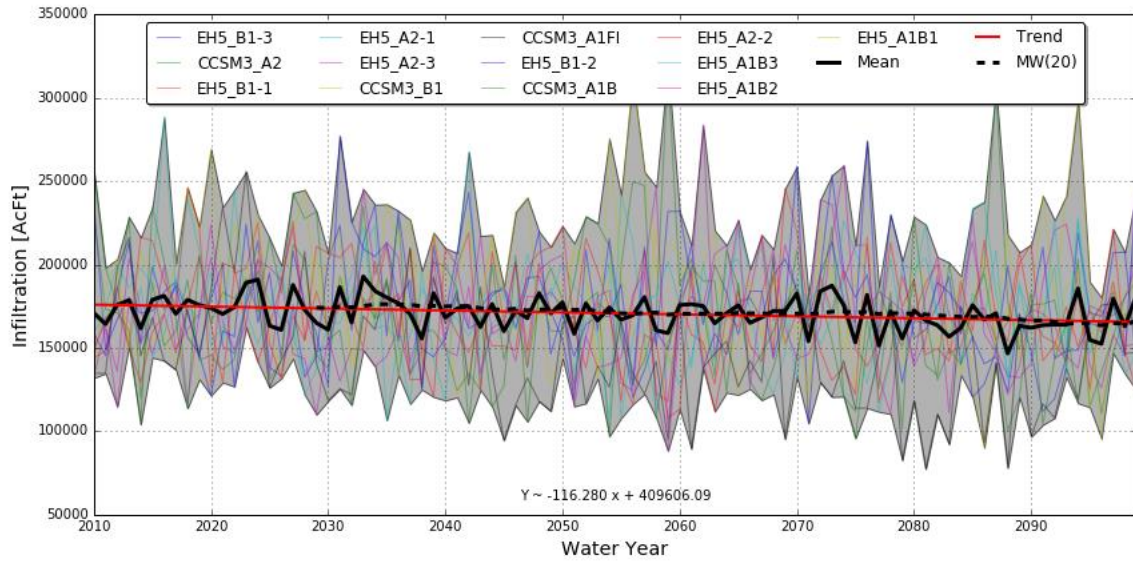


Figure 124. Simulation results of the annual infiltration for the 13 projected climate scenarios.

Table 22. Results of the trend analysis for infiltration. Slope (AcFt/yr) of the trend line of annual infiltration for the 13 different future projections. Significance of the trend was determined using the Mann-Kendall statistical test. *p* values are given in parentheses.

GCM-Projection	Water years 2010 - 2040	Water years 2040 - 2070	Water years 2070 - 2100	Water years 2010 - 2100
CCSM3_A1B	-237.78 No Trend (0.775)	618.25 No Trend (0.568)	161.33 No Trend (0.775)	-284.87 No Trend (0.057)
CCSM3_A1FI	-164.53 No Trend (0.915)	-275.05 No Trend (0.943)	426.76 No Trend (0.544)	-509.31 Decreasing (0.002)
CCSM3_A2	-452.02 No Trend (0.617)	270.64 No Trend (0.748)	-665.22 No Trend (0.454)	-193.47 No Trend (0.157)
CCSM3_B1	917.03 No Trend (0.108)	573.65 No Trend (0.392)	768.25 No Trend (0.592)	230.13 No Trend (0.101)
EH5_A1B1	284.94 No Trend (0.521)	-768.29 No Trend (0.335)	366.45 No Trend (0.318)	-431.14 Decreasing (0.002)
EH5_A1B2	-446.84 No Trend (0.153)	1256.26 No Trend (0.143)	-463.08 No Trend (0.830)	197.46 No Trend (0.170)
EH5_A1B3	-1247.07 No Trend (0.108)	577.70 No Trend (0.284)	-198.54 No Trend (0.643)	-123.39 No Trend (0.423)
EH5_A2-1	-275.17 No Trend (0.695)	-1084.44 No Trend (0.239)	55.43 No Trend (0.943)	91.22 No Trend (0.411)
EH5_A2-2	-524.07 No Trend (0.568)	-743.73 No Trend (0.225)	-408.80 No Trend (0.475)	-207.57 No Trend (0.099)
EH5_A2-3	1233.33 No Trend (0.069)	331.01 No Trend (0.392)	-626.27 No Trend (0.475)	6.11 No Trend (0.867)
EH5_B1-1	859.40 No Trend (0.108)	-516.45 No Trend (0.284)	104.48 No Trend (0.748)	-86.65 No Trend (0.512)
EH5_B1-2	1046.33 No Trend (0.175)	-344.05 No Trend (0.775)	-693.87 No Trend (0.253)	-108.20 No Trend (0.384)
EH5_B1-3	72.16 No Trend (0.943)	17.15 No Trend (0.858)	-1197.57 No Trend (0.080)	-91.94 No Trend (0.431)
Ensemble All Projections	81.98 No Trend (0.830)	-6.72 No Trend (0.915)	-182.36 No Trend (0.432)	-116.28 Decreasing (0.005)

Direct Runoff

Figure 125 presents the simulation results of the annual direct runoff for the 13 projected climate scenarios, as well as the ensemble average, the 20 year moving window average (MW(20)) and the trend line. The results of the trend analysis are presented in **Table 23**.

The trend analysis for direct runoff shows generally no significant trend for individual GCM projections as well as the ensemble average behavior even though the trend has a positive slope for the ensemble average in the first 60 years.

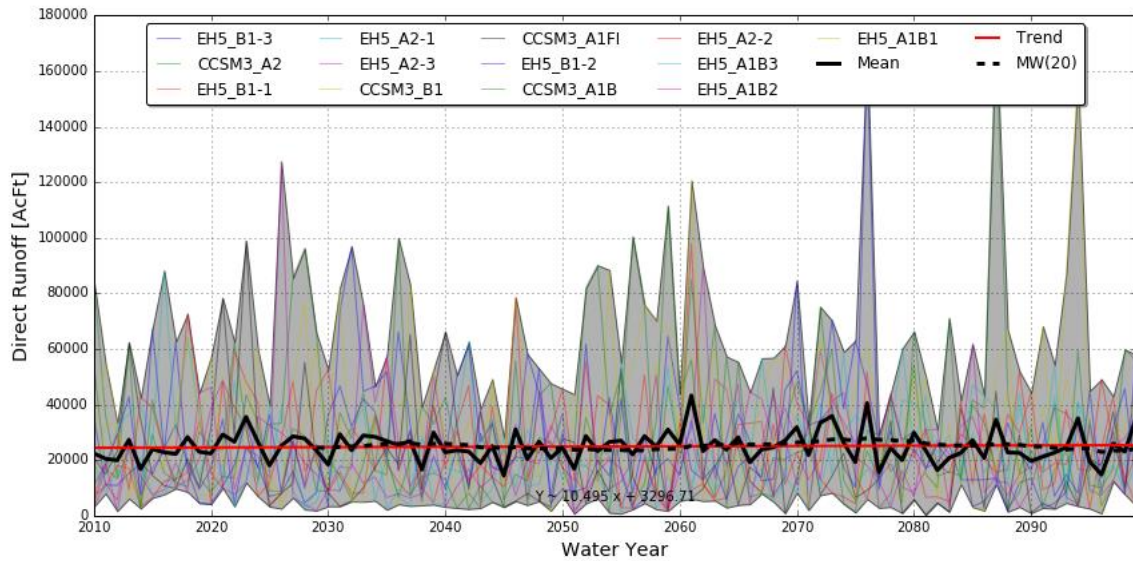


Figure 125. Simulation results of the annual direct runoff for the 13 projected climate scenarios.

Table 23. Results of the trend analysis for direct runoff. Slope (AcFt/yr) of the trend line of annual direct runoff on the Sierra Valley for the 13 different future projections. Significance of the trend was determined using the Mann-Kendall statistical test. *p* values are given in parentheses.

GCM-Projection	Water years 2010 - 2040	Water years 2040 - 2070	Water years 2070 - 2100	Water years 2010 - 2100
CCSM3_A1B	180.14 No Trend (0.544)	208.83 No Trend (0.617)	90.29 No Trend (0.972)	-25.89 No Trend (0.770)
CCSM3_A1FI	-134.62 No Trend (0.475)	-296.67 No Trend (0.568)	173.91 No Trend (0.830)	-174.26 Decreasing (0.016)
CCSM3_A2	-231.16 No Trend (0.592)	782.73 No Trend (0.187)	-482.13 No Trend (0.187)	71.06 No Trend (0.743)
CCSM3_B1	433.80 No Trend (0.643)	938.39 No Trend (0.059)	891.72 No Trend (0.353)	197.42 No Trend (0.233)
EH5_A1B1	346.48 No Trend (0.335)	142.41 No Trend (1.000)	148.10 No Trend (0.544)	-81.46 No Trend (0.280)
EH5_A1B2	-128.69 No Trend (0.432)	873.53 Increasing (0.012)	-18.61 No Trend (0.775)	58.89 Increasing (0.044)
EH5_A1B3	-741.09 No Trend (0.101)	384.52 No Trend (0.269)	-53.33 No Trend (0.915)	-27.85 No Trend (0.873)
EH5_A2-1	-21.57 No Trend (0.617)	-478.39 No Trend (0.175)	-116.89 No Trend (0.858)	152.72 Increasing (0.023)
EH5_A2-2	-358.37 No Trend (0.392)	-45.01 No Trend (0.454)	-9.92 No Trend (0.972)	-37.26 No Trend (0.691)
EH5_A2-3	869.75 Increasing (0.011)	420.20 No Trend (0.318)	-359.51 No Trend (0.253)	36.62 No Trend (0.495)
EH5_B1-1	505.21 No Trend (0.187)	-187.82 No Trend (0.592)	60.22 No Trend (0.721)	-2.47 No Trend (0.691)
EH5_B1-2	489.77 No Trend (0.412)	-398.31 No Trend (0.269)	-826.37 No Trend (0.199)	-61.30 No Trend (0.372)
EH5_B1-3	515.37 No Trend (0.253)	-106.93 No Trend (0.943)	-1099.32 Decreasing (0.007)	30.22 No Trend (0.944)
Ensemble All Projections	132.70 No Trend (0.054)	172.11 No Trend (0.074)	-123.22 No Trend (0.617)	10.50 No Trend (1.000)

Deep Percolation

Figure 126 presents the simulation results of the annual deep percolation for the 13 projected climate scenarios, as well as the ensemble average, the 20 year moving window average (MW(20)) and the trend line. The results of the trend analysis are presented in **Table 24**.

The trend analysis for deep percolation shows that the GCM projections CCSM3-A1FI, ECHAM5-A1B1, ECHAM5-A2-2 show a significantly decreasing trend while ECHAM5-A1B2 shows a significantly increasing trend. The ensemble average for deep percolation shows a significantly decreasing trend for the whole simulation period.

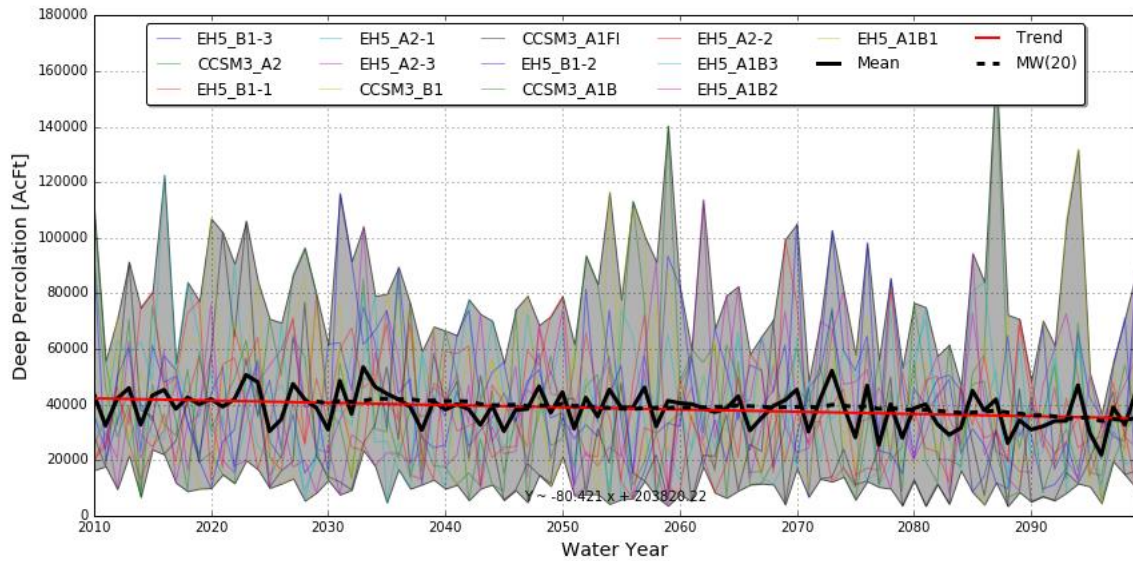


Figure 126. Simulation results of the annual deep percolation for the 13 projected climate scenarios.

Table 24. Results of the trend analysis for deep percolation. Slope (AcFt/yr) of the trend line of annual deep percolation on the Sierra Valley for the 13 different future projections. Significance of the trend was determined using the Mann-Kendall statistical test. *p* values are given in parentheses.

GCM-Projection	Water years 2010 - 2040	Water years 2040 - 2070	Water years 2070 - 2100	Water years 2010 - 2100
CCSM3_A1B	-288.93 No Trend (0.643)	166.10 No Trend (0.775)	4.31 No Trend (0.943)	-202.04 No Trend (0.058)
CCSM3_A1FI	-302.46 No Trend (0.568)	-157.29 No Trend (0.521)	-106.96 No Trend (0.915)	-327.74 Decreasing (0.000)
CCSM3_A2	-442.00 No Trend (0.432)	519.70 No Trend (0.199)	-489.94 No Trend (0.284)	-42.39 No Trend (0.582)
CCSM3_B1	533.77 No Trend (0.284)	467.68 No Trend (0.284)	529.09 No Trend (0.617)	177.80 No Trend (0.143)
EH5_A1B1	281.33 No Trend (0.412)	-361.19 No Trend (0.372)	288.09 No Trend (0.301)	-266.13 Decreasing (0.005)
EH5_A1B2	-199.32 No Trend (0.498)	952.84 No Trend (0.054)	-171.10 No Trend (0.943)	155.96 Increasing (0.035)
EH5_A1B3	-886.60 No Trend (0.116)	124.62 No Trend (0.915)	-362.04 No Trend (0.498)	-152.09 No Trend (0.143)
EH5_A2-1	-183.29 No Trend (0.284)	-615.83 No Trend (0.187)	32.94 No Trend (1.000)	37.62 No Trend (0.802)
EH5_A2-2	-604.73 No Trend (0.212)	-668.64 No Trend (0.080)	-162.77 No Trend (0.803)	-182.75 Decreasing (0.027)
EH5_A2-3	786.34 No Trend (0.064)	233.63 No Trend (0.668)	-68.23 No Trend (0.592)	-3.02 No Trend (0.950)
EH5_B1-1	699.19 No Trend (0.108)	-167.58 No Trend (0.475)	-223.14 No Trend (0.643)	-84.47 No Trend (0.286)
EH5_B1-2	655.68 No Trend (0.239)	-282.45 No Trend (0.432)	-413.73 No Trend (0.353)	-106.87 No Trend (0.168)
EH5_B1-3	85.21 No Trend (0.695)	170.96 No Trend (0.775)	-1078.99 Decreasing (0.046)	-49.35 No Trend (0.369)
Ensemble All Projections	10.32 No Trend (0.695)	29.43 No Trend (0.668)	-170.96 No Trend (0.392)	-80.42 Decreasing (0.002)

Potential Evapotranspiration

Figure 127 presents the simulation results of the annual potential evapotranspiration for the 13 projected climate scenarios, as well as the ensemble average, the 20 year moving window average (MW(20)) and the trend line. The results of the trend analysis are presented in **Table 25**.

The trend analysis shows a significantly increasing trend for all GCM projections as well as the ensemble average for the whole simulation period.

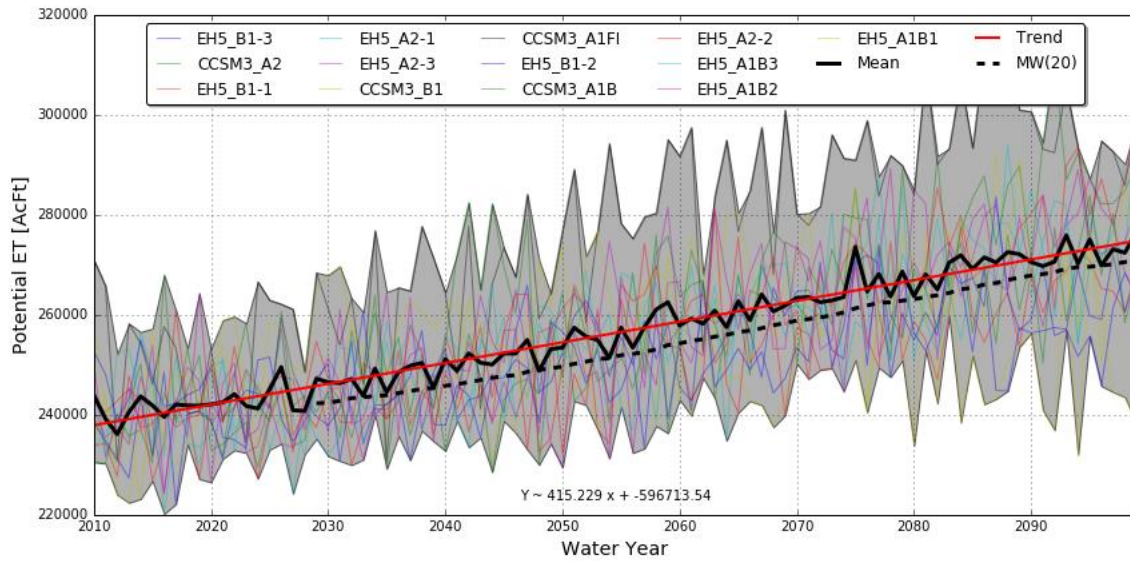


Figure 127. Simulation results of the annual potential evapotranspiration for the 13 projected climate scenarios.

Table 25. Results of the trend analysis for potential evapotranspiration. Slope (AcFt/yr) of the trend line of annual potential evapotranspiration on the Sierra Valley for the 13 different future projections. Significance of the trend was determined using the Mann-Kendall statistical test. *p* values are given in parentheses.

GCM-Projection	Water years 2010 - 2040	Water years 2040 - 2070	Water years 2070 - 2100	Water years 2010 - 2100
CCSM3_A1B	391.14 Increasing (0.032)	-184.88 No Trend (0.592)	151.63 No Trend (0.454)	343.95 Increasing (0.000)
CCSM3_A1FI	480.42 No Trend (0.093)	1006.99 Increasing (0.001)	299.30 No Trend (0.080)	633.62 Increasing (0.000)
CCSM3_A2	259.43 No Trend (0.069)	971.06 Increasing (0.000)	1015.51 Increasing (0.000)	642.23 Increasing (0.000)
CCSM3_B1	245.20 No Trend (0.074)	-23.37 No Trend (0.617)	-315.09 No Trend (0.199)	147.32 Increasing (0.002)
EH5_A1B1	870.63 Increasing (0.000)	403.21 No Trend (0.074)	271.59 No Trend (0.318)	319.55 Increasing (0.000)
EH5_A1B2	384.14 No Trend (0.087)	372.13 Increasing (0.038)	498.85 Increasing (0.011)	462.05 Increasing (0.000)
EH5_A1B3	339.26 No Trend (0.101)	432.43 Increasing (0.038)	661.23 Increasing (0.027)	412.37 Increasing (0.000)
EH5_A2-1	66.40 No Trend (0.284)	566.12 Increasing (0.005)	563.83 Increasing (0.003)	510.97 Increasing (0.000)
EH5_A2-2	254.36 No Trend (0.059)	494.22 No Trend (0.101)	944.17 Increasing (0.000)	542.01 Increasing (0.000)
EH5_A2-3	111.62 No Trend (0.475)	819.89 Increasing (0.000)	304.04 No Trend (0.253)	488.84 Increasing (0.000)
EH5_B1-1	148.38 No Trend (0.498)	379.65 No Trend (0.187)	457.66 Increasing (0.005)	319.30 Increasing (0.000)
EH5_B1-2	-19.49 No Trend (0.748)	198.18 No Trend (0.253)	239.54 No Trend (0.125)	281.85 Increasing (0.000)
EH5_B1-3	319.82 Increasing (0.046)	328.81 Increasing (0.032)	-196.92 No Trend (0.353)	293.91 Increasing (0.000)
Ensemble All Projections	296.25 Increasing (0.000)	443.42 Increasing (0.000)	376.56 Increasing (0.000)	415.23 Increasing (0.000)

Actual Evapotranspiration

Figure 128 presents the simulation results of the annual total actual evapotranspiration for the 13 projected climate scenarios, as well as the ensemble average, the 20-year moving window average (MW(20)) and the trend line. The results of the trend analysis are presented in **Table 26**.

The trend analysis for actual evapotranspiration shows generally no significant trends for individual GCM projections except the decreasing trend for the projections CCSM3-A1FI, CCSM3-A2, and ECHAM5-A1B1. The ensemble behavior has also no significant trend during the simulation period; however, it has a negative slope. When actual evapotranspiration is analyzed together with the increasing potential evapotranspiration, it can be concluded that the soil moisture availability keeps the actual evapotranspiration from increasing. Since the potential evapotranspiration represents the conditions for the optimal plant growth, the increasing demand of the plants with the limited soil moisture availability will increase the stress on the plants in time. For agricultural crops, this will result in an increase in the irrigation demands.

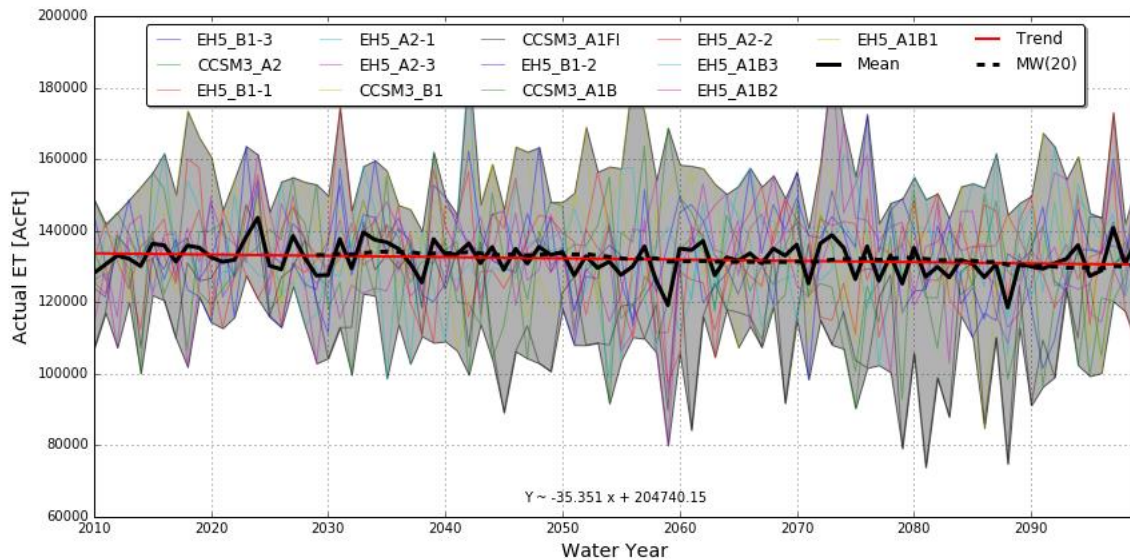


Figure 128. Simulation results of the annual actual evapotranspiration for the 13 projected climate scenarios.

Table 26. Results of the trend analysis for actual evapotranspiration. Slope (AcFt/yr) of the trend line of annual actual evapotranspiration on the Sierra Valley for the 13 different future projections. Significance of the trend was determined using the Mann-Kendall statistical test. *p* values are given in parentheses.

GCM-Projection	Water years 2010 - 2040	Water years 2040 - 2070	Water years 2070 - 2100	Water years 2010 - 2100
CCSM3_A1B	44.30 No Trend (0.943)	434.85 No Trend (0.269)	150.77 No Trend (0.617)	-82.10 No Trend (0.155)
CCSM3_A1FI	146.42 No Trend (0.521)	-115.63 No Trend (0.915)	538.12 No Trend (0.187)	-181.33 Decreasing (0.011)
CCSM3_A2	-88.69 No Trend (0.617)	-301.20 No Trend (0.239)	-173.83 No Trend (0.886)	-154.08 Decreasing (0.011)
CCSM3_B1	370.62 Increasing (0.050)	90.78 No Trend (0.721)	220.54 No Trend (0.353)	50.12 No Trend (0.153)
EH5_A1B1	9.32 No Trend (0.858)	-362.21 No Trend (0.318)	119.05 No Trend (0.269)	-159.83 Decreasing (0.008)
EH5_A1B2	-213.86 No Trend (0.199)	312.19 No Trend (0.187)	-278.57 No Trend (0.187)	44.83 No Trend (0.411)
EH5_A1B3	-337.74 No Trend (0.253)	494.29 Increasing (0.019)	234.24 No Trend (0.544)	34.33 No Trend (0.549)
EH5_A2-1	-63.74 No Trend (0.775)	-441.97 No Trend (0.498)	36.38 No Trend (1.000)	54.94 No Trend (0.170)
EH5_A2-2	-56.02 No Trend (0.886)	-154.00 No Trend (0.643)	-250.06 No Trend (0.392)	-30.68 No Trend (0.681)
EH5_A2-3	388.90 No Trend (0.212)	47.60 No Trend (0.617)	-537.33 No Trend (0.225)	11.40 No Trend (0.802)
EH5_B1-1	176.08 No Trend (0.475)	-310.81 No Trend (0.239)	321.46 No Trend (0.592)	-3.53 No Trend (0.928)
EH5_B1-2	313.16 No Trend (0.187)	-157.86 No Trend (0.695)	-275.00 No Trend (0.253)	0.17 No Trend (0.983)
EH5_B1-3	-3.23 No Trend (0.803)	-153.18 No Trend (0.544)	-140.81 No Trend (0.568)	-43.81 No Trend (0.517)
Ensemble All Projections	52.73 No Trend (0.695)	-47.47 No Trend (0.544)	-2.70 No Trend (0.886)	-35.35 No Trend (0.054)

Figure 129 and **Figure 130** present the actual evapotranspiration for the agricultural crops, and native and riparian vegetation respectively. The results of the corresponding trend analysis are given in **Table 27** and **Table 28**. These results show a statistically significant increase in the ensemble average of the actual evapotranspiration for the irrigated agricultural crops during the simulation period. On the other hand, for the native and riparian vegetation, which is not irrigated, the ensemble average of the actual evapotranspiration shows a statistically decreasing trend as a result of the decreasing soil moisture availability.

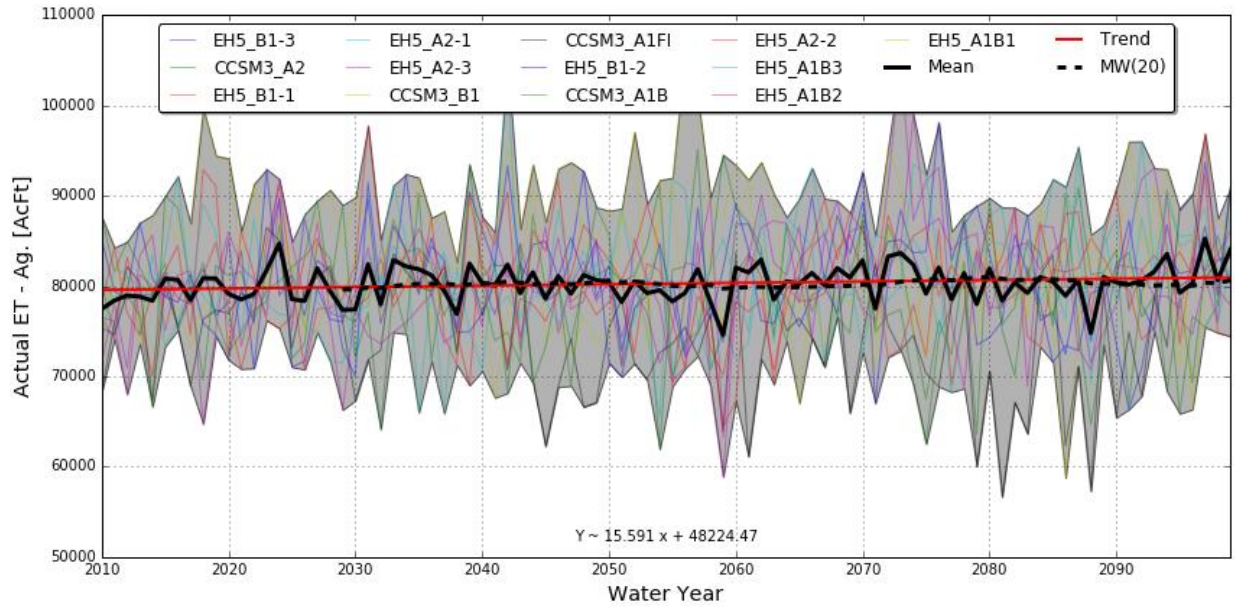


Figure 129. Simulation results of the annual actual evapotranspiration of the agricultural crops for the 13 projected climate scenarios.

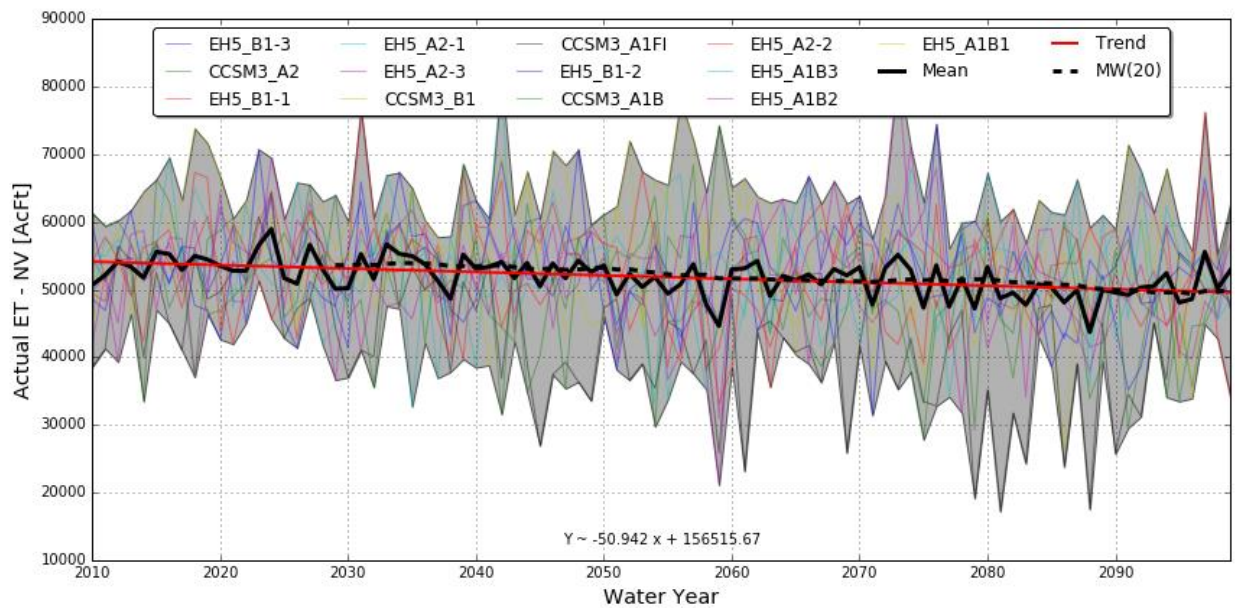


Figure 130. Simulation results of the annual actual evapotranspiration of the native and riparian vegetation for the 13 projected climate scenarios.

Table 27. Results of the trend analysis for actual evapotranspiration of the agricultural crops. Slope (AcFt/yr) of the trend line of annual actual evapotranspiration of the agricultural crops on the Sierra Valley for the 13 different future projections. Significance of the trend was determined using the Mann-Kendall statistical test. *p* values are given in parentheses.

GCM-Projection	Water years 2010 - 2040	Water years 2040 - 2070	Water years 2070 - 2100	Water years 2010 - 2100
CCSM3_A1B	49.08 No Trend (0.748)	194.85 No Trend (0.187)	72.12 No Trend (0.592)	-11.77 No Trend (0.867)
CCSM3_A1FI	135.69 No Trend (0.225)	23.85 No Trend (0.748)	278.60 No Trend (0.143)	-36.81 No Trend (0.212)
CCSM3_A2	-2.69 No Trend (0.943)	-67.32 No Trend (0.721)	1.35 No Trend (1.000)	-27.29 No Trend (0.358)
CCSM3_B1	191.58 Increasing (0.020)	28.34 No Trend (0.803)	109.17 No Trend (0.372)	41.16 Increasing (0.028)
EH5_A1B1	104.91 No Trend (0.372)	-143.35 No Trend (0.544)	55.33 No Trend (0.187)	-50.90 No Trend (0.064)
EH5_A1B2	-80.03 No Trend (0.318)	177.50 No Trend (0.069)	-123.15 No Trend (0.318)	57.54 Increasing (0.004)
EH5_A1B3	-111.20 No Trend (0.454)	263.46 Increasing (0.009)	159.24 No Trend (0.212)	46.10 Increasing (0.043)
EH5_A2-1	5.42 No Trend (0.568)	-152.44 No Trend (0.643)	63.94 No Trend (0.748)	67.42 Increasing (0.002)
EH5_A2-2	11.35 No Trend (0.886)	-29.79 No Trend (0.972)	-35.23 No Trend (0.858)	26.33 No Trend (0.147)
EH5_A2-3	196.51 No Trend (0.143)	61.03 No Trend (0.432)	-220.88 No Trend (0.225)	45.39 No Trend (0.125)
EH5_B1-1	90.17 No Trend (0.372)	-115.83 No Trend (0.498)	155.53 No Trend (0.521)	16.23 No Trend (0.447)
EH5_B1-2	180.83 No Trend (0.125)	-31.21 No Trend (0.886)	-111.76 No Trend (0.372)	23.03 No Trend (0.231)
EH5_B1-3	22.62 No Trend (0.943)	-41.20 No Trend (0.775)	-85.75 No Trend (0.372)	6.26 No Trend (0.650)
Ensemble All Projections	61.09 No Trend (0.134)	12.91 No Trend (0.668)	24.50 No Trend (0.748)	15.59 Increasing (0.038)

Table 28. Results of the trend analysis for actual evapotranspiration of the native and riparian vegetation. Slope (AcFt/yr) of the trend line of annual actual evapotranspiration of the native and riparian vegetation on the Sierra Valley for the 13 different future projections. Significance of the trend was determined using the Mann-Kendall statistical test. *p* values are given in parentheses.

GCM-Projection	Water years 2010 - 2040	Water years 2040 - 2070	Water years 2070 - 2100	Water years 2010 - 2100
CCSM3_A1B	-4.78 No Trend (0.721)	240.00 No Trend (0.372)	78.66 No Trend (0.721)	-70.34 Decreasing (0.018)
CCSM3_A1FI	10.73 No Trend (1.000)	-139.48 No Trend (0.617)	259.52 No Trend (0.239)	-144.52 Decreasing (0.000)
CCSM3_A2	-86.00 No Trend (0.392)	-233.88 No Trend (0.143)	-175.18 No Trend (0.353)	-126.79 Decreasing (0.000)
CCSM3_B1	179.03 No Trend (0.087)	62.44 No Trend (0.775)	111.37 No Trend (0.392)	8.97 No Trend (0.490)
EH5_A1B1	-95.59 No Trend (0.521)	-218.86 No Trend (0.284)	63.72 No Trend (0.498)	-108.93 Decreasing (0.002)
EH5_A1B2	-133.83 No Trend (0.301)	134.69 No Trend (0.318)	-155.42 No Trend (0.269)	-12.71 No Trend (0.490)
EH5_A1B3	-226.54 No Trend (0.175)	230.83 Increasing (0.032)	75.00 No Trend (0.830)	-11.77 No Trend (0.691)
EH5_A2-1	-69.16 No Trend (1.000)	-289.53 No Trend (0.372)	-27.56 No Trend (0.915)	-12.48 No Trend (0.780)
EH5_A2-2	-67.37 No Trend (0.830)	-124.21 No Trend (0.475)	-214.83 No Trend (0.134)	-57.01 Decreasing (0.049)
EH5_A2-3	192.40 No Trend (0.284)	-13.43 No Trend (0.748)	-316.46 No Trend (0.225)	-33.99 No Trend (0.468)
EH5_B1-1	85.91 No Trend (0.695)	-194.98 No Trend (0.153)	165.93 No Trend (0.643)	-19.75 No Trend (0.452)
EH5_B1-2	132.34 No Trend (0.225)	-126.65 No Trend (0.568)	-163.24 No Trend (0.199)	-22.85 No Trend (0.369)
EH5_B1-3	-25.85 No Trend (0.803)	-111.98 No Trend (0.301)	-55.06 No Trend (0.592)	-50.07 No Trend (0.112)
Ensemble All Projections	-8.36 No Trend (0.858)	-60.39 No Trend (0.143)	-27.20 No Trend (0.858)	-50.94 Decreasing (0.000)

Prime Water

Figure 131 presents the simulation results of the annual irrigation water (prime water) volumes supplied to the irrigated fields to meet the agricultural irrigation demand for the 13 projected climate scenarios, as well as the ensemble average, the 20-year moving window average (MW(20)) and the trend line. The results of the trend analysis are presented in **Table 29**.

The trend analysis for annual applied prime water shows a significantly increasing trend for each GCM projection as well as the ensemble average. This increase in the agricultural water demand is a result of the increasing trend in potential evapotranspiration. The ensemble average shows that the second 30-year period has the steepest slope.

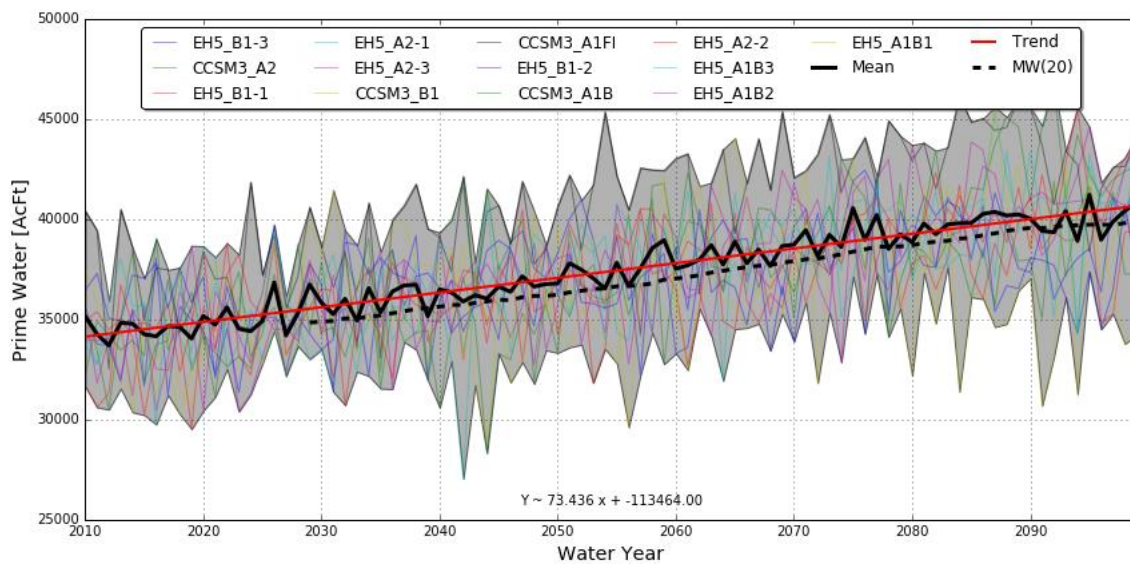


Figure 131. Simulation results of the annual applied prime water for the 13 projected climate scenarios.

Table 29. Results of the trend analysis for applied prime water. Slope (AcFt/yr) of the trend line of annual applied prime water on the Sierra Valley for the 13 different future projections. Significance of the trend was determined using the Mann-Kendall statistical test. *p* values are given in parentheses.

GCM-Projection	Water years 2010 - 2040	Water years 2040 - 2070	Water years 2070 - 2100	Water years 2010 - 2100
CCSM3_A1B	84.21 No Trend (0.093)	-5.80 No Trend (0.943)	17.58 No Trend (0.972)	52.81 Increasing (0.000)
CCSM3_A1FI	56.58 No Trend (0.301)	139.13 Increasing (0.003)	-19.25 No Trend (0.886)	88.99 Increasing (0.000)
CCSM3_A2	15.31 No Trend (0.521)	268.09 Increasing (0.000)	186.30 Increasing (0.002)	119.14 Increasing (0.000)
CCSM3_B1	23.62 No Trend (0.617)	47.05 No Trend (0.617)	-89.24 No Trend (0.074)	36.30 Increasing (0.001)
EH5_A1B1	217.65 Increasing (0.000)	154.26 Increasing (0.032)	69.82 No Trend (0.239)	77.05 Increasing (0.000)
EH5_A1B2	66.92 Increasing (0.050)	81.84 No Trend (0.093)	104.42 Increasing (0.027)	90.47 Increasing (0.000)
EH5_A1B3	58.36 No Trend (0.301)	53.04 No Trend (0.301)	74.80 No Trend (0.054)	65.37 Increasing (0.000)
EH5_A2-1	9.12 No Trend (0.643)	156.11 Increasing (0.005)	83.28 Increasing (0.027)	94.16 Increasing (0.000)
EH5_A2-2	51.87 No Trend (0.335)	29.82 No Trend (0.592)	152.67 Increasing (0.001)	89.08 Increasing (0.000)
EH5_A2-3	113.42 Increasing (0.020)	95.56 No Trend (0.093)	47.92 No Trend (0.475)	96.94 Increasing (0.000)
EH5_B1-1	87.12 Increasing (0.038)	39.75 No Trend (0.643)	27.44 No Trend (0.335)	53.60 Increasing (0.000)
EH5_B1-2	18.58 No Trend (0.372)	-11.82 No Trend (0.803)	57.70 No Trend (0.475)	40.80 Increasing (0.000)
EH5_B1-3	105.47 Increasing (0.038)	53.19 No Trend (0.175)	-129.95 Decreasing (0.005)	49.96 Increasing (0.000)
Ensemble All Projections	69.86 Increasing (0.000)	84.63 Increasing (0.000)	44.88 Increasing (0.002)	73.44 Increasing (0.000)

Groundwater Pumping

Groundwater pumping represents the part of the irrigation water in addition to the surface water diversions to meet the agricultural crop water demands. **Figure 132** presents the simulation results of the annual groundwater pumping volumes for the 13 projected climate scenarios, as well as the ensemble average, the 20 year moving window average (MW(20)) and the trend line. The results of the trend analysis are presented in **Table 30**.

Similar to prime water, the trend analysis for groundwater pumping shows a significantly increasing trend for each GCM projection except CCSM3-B1 as well as the ensemble average to meet the increasing agricultural water demand.

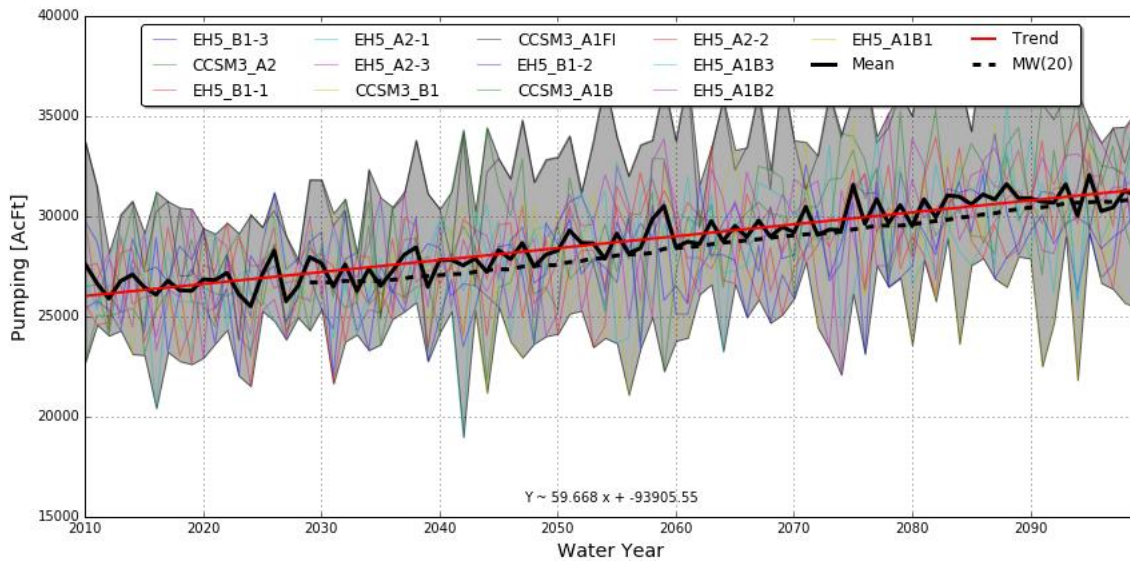


Figure 132. Simulation results of the annual groundwater pumping for the 13 projected climate scenarios.

Table 30. Results of the trend analysis for groundwater pumping. Slope (AcFt/yr) of the trend line of annual groundwater pumping on the Sierra Valley for the 13 different future projections. Significance of the trend was determined using the Mann-Kendall statistical test. *p* values are given in parentheses.

GCM-Projection	Water years 2010 - 2040	Water years 2040 - 2070	Water years 2070 - 2100	Water years 2010 - 2100
CCSM3_A1B	41.02 No Trend (0.498)	-54.68 No Trend (0.748)	16.70 No Trend (0.830)	52.27 Increasing (0.000)
CCSM3_A1FI	42.54 No Trend (0.284)	138.42 Increasing (0.022)	-12.33 No Trend (1.000)	92.35 Increasing (0.000)
CCSM3_A2	31.70 No Trend (0.269)	179.19 Increasing (0.003)	151.59 Increasing (0.019)	103.14 Increasing (0.000)
CCSM3_B1	-9.39 No Trend (0.668)	3.79 No Trend (0.803)	-81.84 No Trend (0.164)	16.01 No Trend (0.086)
EH5_A1B1	118.69 Increasing (0.007)	85.37 No Trend (0.125)	41.37 No Trend (0.392)	59.84 Increasing (0.000)
EH5_A1B2	68.09 No Trend (0.175)	33.88 No Trend (0.301)	108.20 Increasing (0.019)	62.27 Increasing (0.000)
EH5_A1B3	61.83 No Trend (0.199)	9.42 No Trend (0.721)	63.26 No Trend (0.225)	51.74 Increasing (0.000)
EH5_A2-1	-2.88 No Trend (0.886)	118.16 No Trend (0.064)	61.63 No Trend (0.134)	64.44 Increasing (0.000)
EH5_A2-2	31.05 No Trend (0.353)	65.18 No Trend (0.212)	134.18 Increasing (0.002)	76.57 Increasing (0.000)
EH5_A2-3	-15.98 No Trend (0.830)	109.75 Increasing (0.020)	96.65 No Trend (0.153)	67.85 Increasing (0.000)
EH5_B1-1	0.94 No Trend (0.886)	67.55 No Trend (0.353)	49.89 No Trend (0.134)	46.13 Increasing (0.000)
EH5_B1-2	-47.71 No Trend (0.412)	28.97 No Trend (0.617)	56.51 No Trend (0.617)	38.61 Increasing (0.000)
EH5_B1-3	51.72 No Trend (0.253)	58.23 No Trend (0.143)	-22.67 No Trend (0.748)	44.45 Increasing (0.000)
Ensemble All Projections	28.59 No Trend (0.108)	64.86 Increasing (0.000)	51.01 Increasing (0.003)	59.67 Increasing (0.000)

Net Gain from Stream

Stream-groundwater interaction is represented by the water balance component net gain from stream. It's the amount of water that flows from the streams to the aquifer. Negative values indicate that the water is leaving the aquifer and recharging the streams. **Figure 133** presents the simulation results of the annual total flow between the streams and the aquifer for the 13 projected climate scenarios, as well as the ensemble average, the 20 year moving window average (MW(20)) and the trend line. The results of the trend analysis is presented in **Table 31**.

An increasing trend for the negative values of net gain from stream means that the aquifer is recharging the streams in a decreasing rate. GCM projections CCSM3-A1B, CCSM3-A1FI, CCSM3-A2, ECHAM5-A1B1, ECHAM5-A1B3, ECHAM5-A2-2, and ECHAM5-B1-1 show such an increasing trend for the whole simulation period. On the other hand, CCSM3-B1, and ECHAM5-A1B2 show an opposite trend. When the ensemble average behavior is analyzed, the results show a significantly decreasing trend for the first 30 years, which means that the contribution to the stream flow rate from the aquifer will increase in the beginning. However, for the rest of the century, this trend changes and shows a significantly increasing trend for the second and third 30-year period.

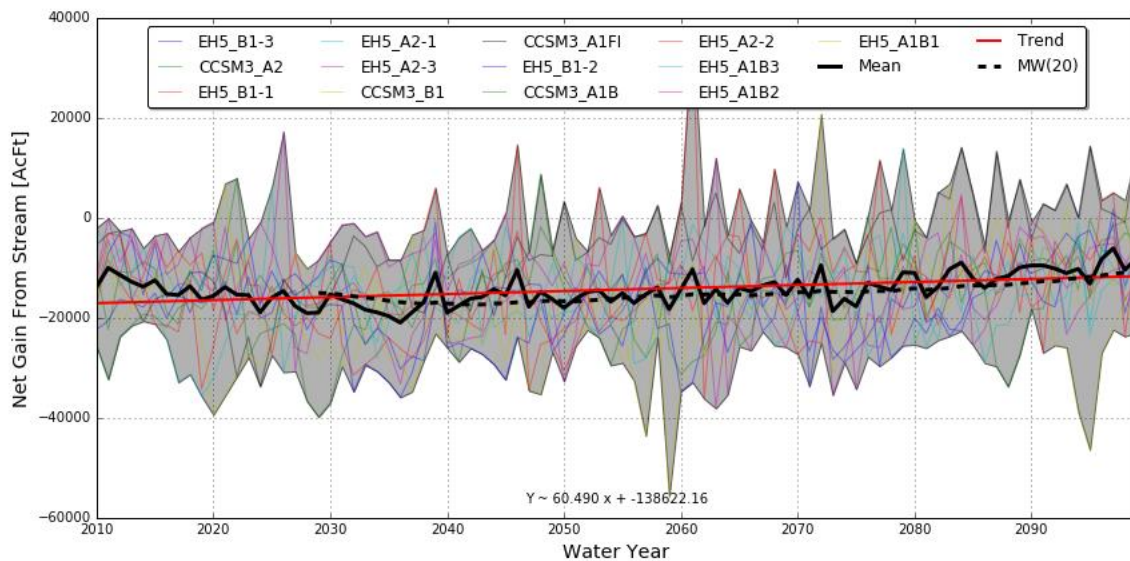


Figure 133. Simulation results of the annual net gain from streams for the 13 projected climate scenarios. Negative values indicate that the groundwater is recharging the streams.

Table 31. Results of the trend analysis for net gain from streams. Slope (AcFt/yr) of the trend line of annual net gain from streams on the Sierra Valley for the 13 different future projections. Significance of the trend was determined using the Mann-Kendall statistical test. *p* values are given in parentheses.

GCM-Projection	Water years 2010 - 2040	Water years 2040 - 2070	Water years 2070 - 2100	Water years 2010 - 2100
CCSM3_A1B	-282.21 No Trend (0.253)	-223.26 No Trend (0.239)	189.32 Increasing (0.029)	118.27 Increasing (0.000)
CCSM3_A1FI	-25.37 No Trend (0.972)	364.83 Increasing (0.005)	348.75 Increasing (0.022)	259.01 Increasing (0.000)
CCSM3_A2	201.18 No Trend (0.054)	-313.57 No Trend (0.074)	178.14 No Trend (0.125)	66.66 Increasing (0.003)
CCSM3_B1	-133.58 No Trend (0.372)	-18.53 No Trend (0.830)	-170.21 No Trend (0.915)	-94.87 Decreasing (0.006)
EH5_A1B1	-474.41 Decreasing (0.020)	26.45 No Trend (0.353)	89.83 No Trend (0.592)	174.58 Increasing (0.000)
EH5_A1B2	141.06 No Trend (0.199)	-412.45 Decreasing (0.012)	373.45 Increasing (0.007)	-69.14 Decreasing (0.016)
EH5_A1B3	119.15 No Trend (0.498)	3.34 No Trend (0.592)	226.74 No Trend (0.054)	79.97 Increasing (0.008)
EH5_A2-1	-199.84 No Trend (0.143)	135.87 No Trend (0.412)	-169.12 No Trend (0.568)	-9.38 No Trend (0.671)
EH5_A2-2	86.88 No Trend (0.972)	527.31 Increasing (0.046)	-125.10 No Trend (0.521)	128.53 Increasing (0.001)
EH5_A2-3	-556.64 Decreasing (0.001)	257.79 No Trend (0.064)	358.59 Increasing (0.032)	-8.01 No Trend (0.873)
EH5_B1-1	-598.27 Decreasing (0.003)	259.63 Increasing (0.012)	368.97 Increasing (0.035)	67.46 Increasing (0.024)
EH5_B1-2	-695.24 Decreasing (0.000)	411.85 Increasing (0.007)	445.73 Increasing (0.002)	27.13 No Trend (0.477)
EH5_B1-3	-180.27 No Trend (0.454)	-66.61 No Trend (0.803)	783.54 Increasing (0.000)	46.16 No Trend (0.107)
Ensemble All Projections	-199.81 Decreasing (0.000)	73.28 Increasing (0.035)	222.97 Increasing (0.000)	60.49 Increasing (0.000)

To better understand these changes on the groundwater levels, a similar analysis was conducted on the projected groundwater levels at nine observation wells. “OBSW02” and “OBSW08” are located on the Southwest of the valley. They are close to the boundary and some of the major stream reaches near Cold Creek. There is not much pumping nearby. “OBSW25” is located at the center of the Valley, on the Northwest of Loyalton and sits between the two pumping intensive areas of the Valley. “OBSW29” is located on the Western half of the Valley and close to the Sierra Valley Channels. “OBSW02” is located on the East of Vinton, close to the basin boundary between California and Nevada. “OBSW38” is the observation point that is closest to the drainage point near the MFP stream flow observation station and close to a stream bed. It’s also away from the major pumping wells. “OBSW42” is located near the alfalfa fields at the North of the Valley and therefore subject to high groundwater pumping from the nearby irrigation wells. Finally, “OBSW43” and “OBSW49” are located on the Northeast of the Valley near the Little Last Chance Creek.

Figure 134 shows the annual average groundwater level projections for nine different locations. Trend analysis for the ensemble averages are provided in **Table 32** below. OSBW02 and OBSW08 show statistically significant increasing groundwater levels for the whole simulation period. Since these locations are close to streambeds and the foothills, they are easily affected by the stream conditions. Even though it’s statistically significant, the increase is about 2.5 ft for OBSW02 and 1 ft for OBSW08 over a 100-year period and within the range of the historical oscillations. Even though some projections show larger changes for short terms, the levels recover back quickly. For the other wells away from the streambeds and foothills, the change is more drastic. For example, over the 100 years of simulation, the ensemble average behavior at OBSW42 shows a decrease of almost 100 feet in groundwater levels.

Contour plots of the piezometric surfaces created from the simulated ensemble average groundwater levels are shown in **Figure 135** for the end of each decade between 2010 and 2100. Similar plots of the piezometric surface for the end of each decade from 2010 to 2100 for each of the 13 climate projections, as well as the ensemble minimum and maximum are presented in Appendix E.

Table 32. Results of the trend analysis for the groundwater levels at nine different locations. Slope (Ft/yr) of the trend line of the groundwater level at nine different locations for ensemble average of the 13 different future projections. Significance of the trend was determined using the Mann-Kendall statistical test. *p* values are given in parentheses.

GCM- Projection	Water years 2010 - 2040	Water years 2040 - 2070	Water years 2070 - 2100	Water years 2010 - 2100
Ensemble for OBSW02	-0.00 No Trend (0.915)	0.05 Increasing (0.000)	-0.03 Decreasing (0.000)	0.02 Increasing (0.000)
Ensemble for OBSW08	0.03 Increasing (0.000)	0.03 Increasing (0.000)	-0.03 Decreasing (0.000)	0.01 Increasing (0.000)
Ensemble for OBSW25	-0.00 No Trend (0.175)	-0.06 Decreasing (0.000)	-0.13 Decreasing (0.000)	-0.06 Decreasing (0.000)
Ensemble for OBSW29	0.09 Increasing (0.000)	0.00 No Trend (0.915)	-0.05 Decreasing (0.000)	0.00 No Trend (0.583)
Ensemble for OBSW36	-0.49 Decreasing (0.000)	-0.25 Decreasing (0.000)	-0.21 Decreasing (0.000)	-0.29 Decreasing (0.000)
Ensemble for OBSW38	0.01 No Trend (0.059)	0.00 No Trend (0.335)	-0.01 Decreasing (0.027)	-0.00 No Trend (0.598)
Ensemble for OBSW42	-2.16 Decreasing (0.000)	-0.82 Decreasing (0.000)	-0.84 Decreasing (0.000)	-1.07 Decreasing (0.000)
Ensemble for OBSW43	-0.12 Decreasing (0.000)	-0.09 Decreasing (0.000)	-0.12 Decreasing (0.000)	-0.11 Decreasing (0.000)
Ensemble for OBSW49	-0.23 Decreasing (0.000)	-0.10 Decreasing (0.000)	-0.12 Decreasing (0.000)	-0.13 Decreasing (0.000)

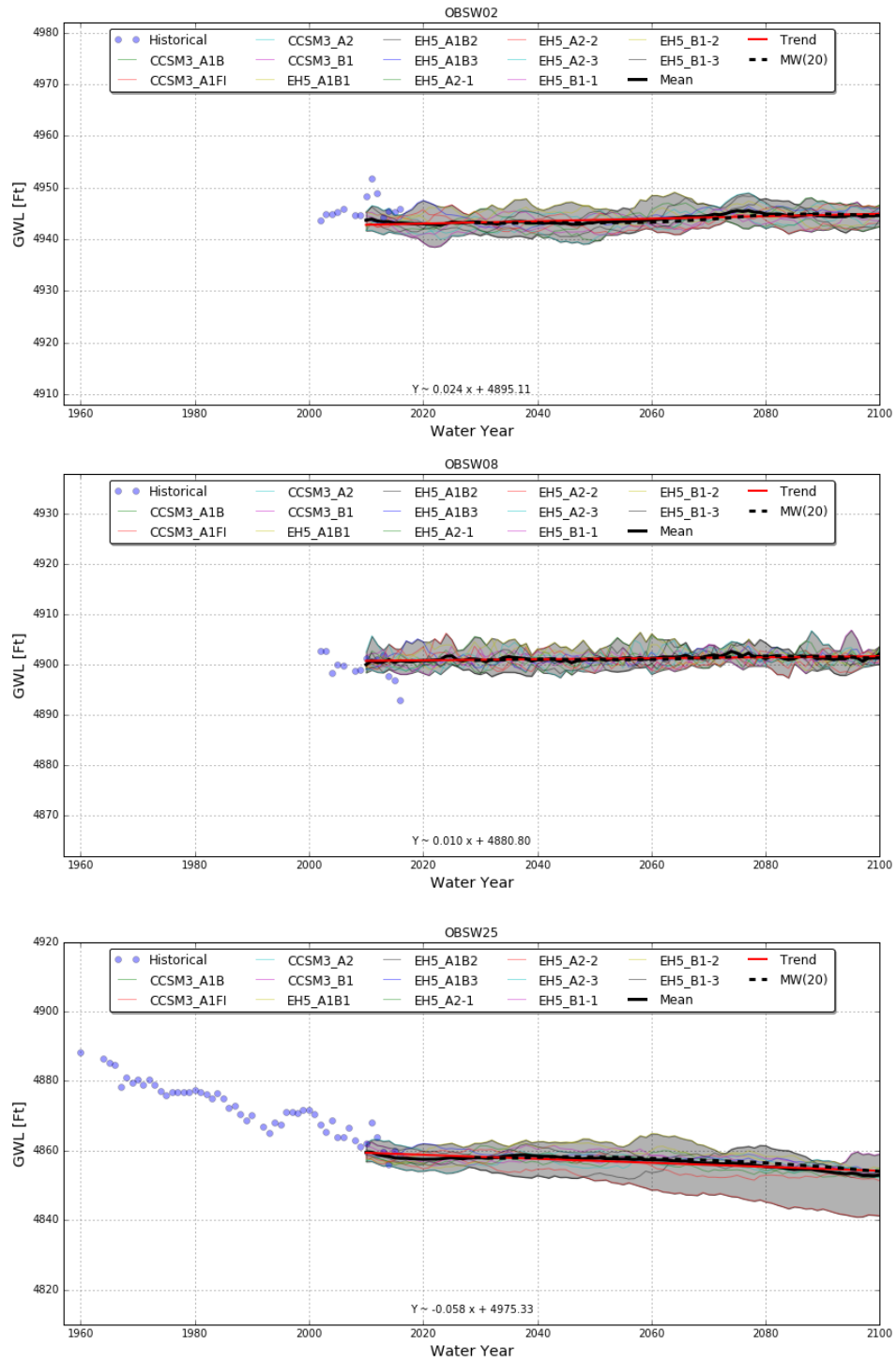


Figure 134. Simulation results of the groundwater levels at nine different locations (continued below).

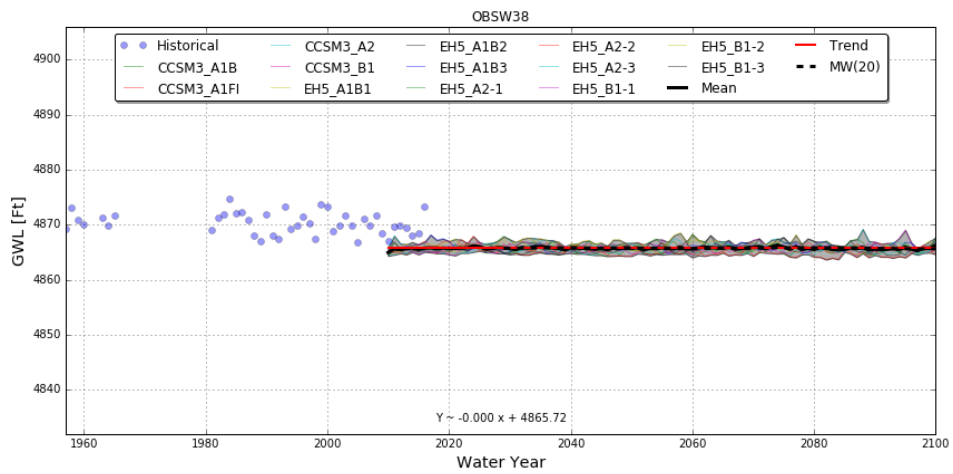
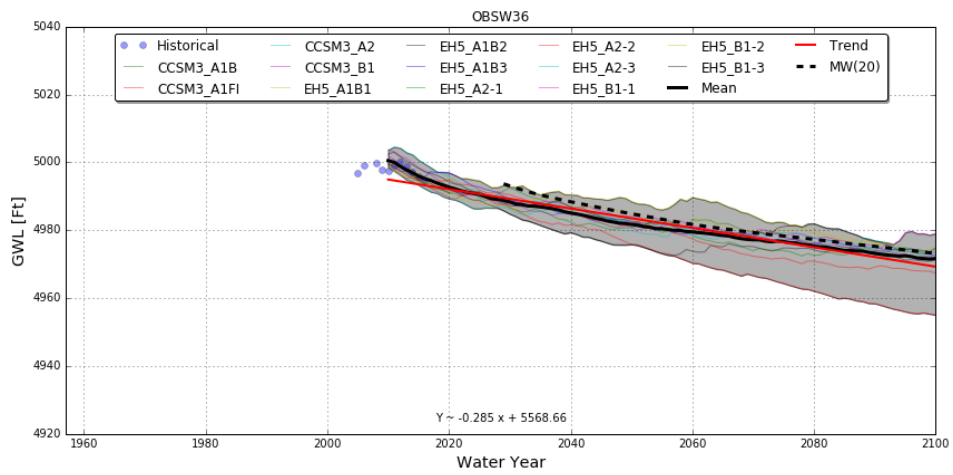
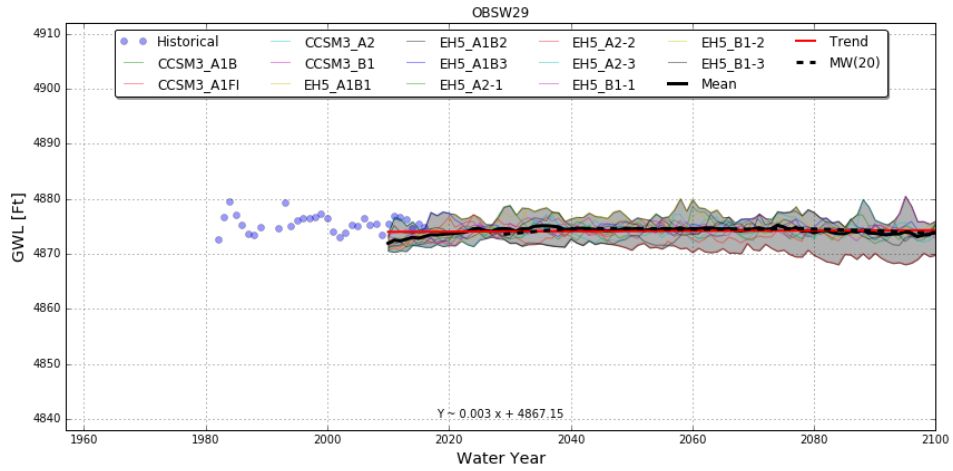


Figure 134 (continued). Simulation results of the groundwater levels at nine different locations (continued below).

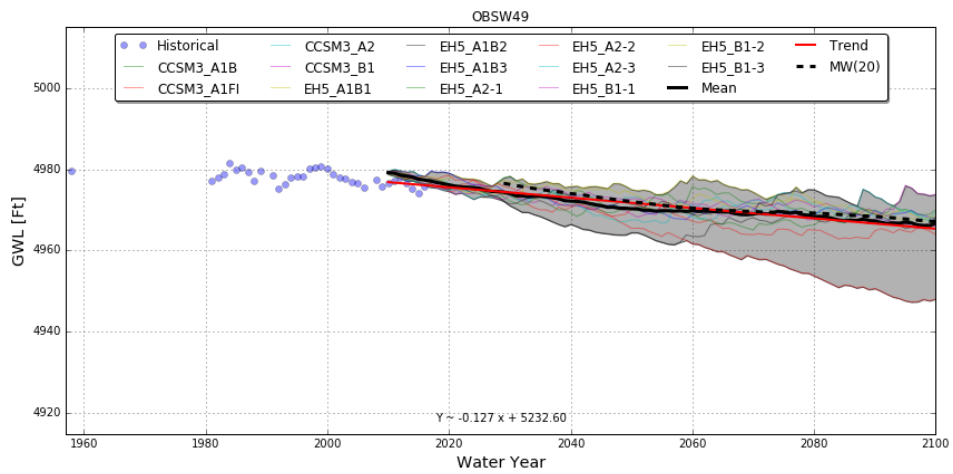
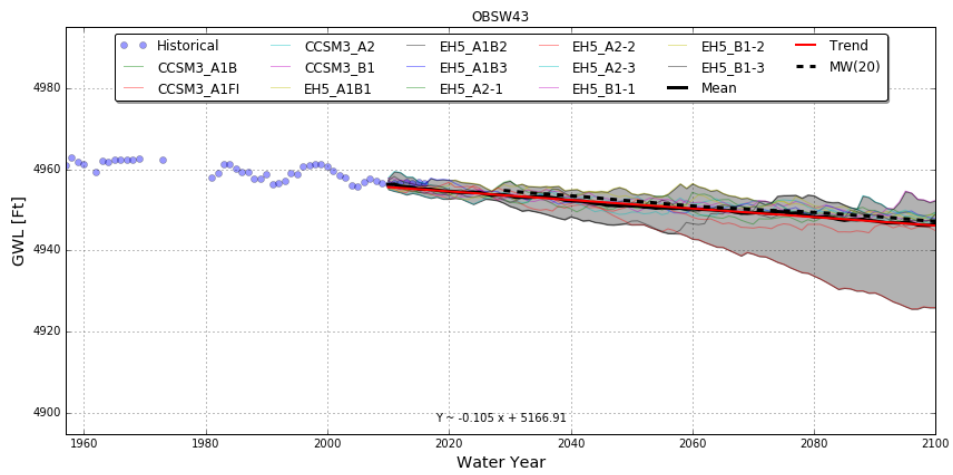
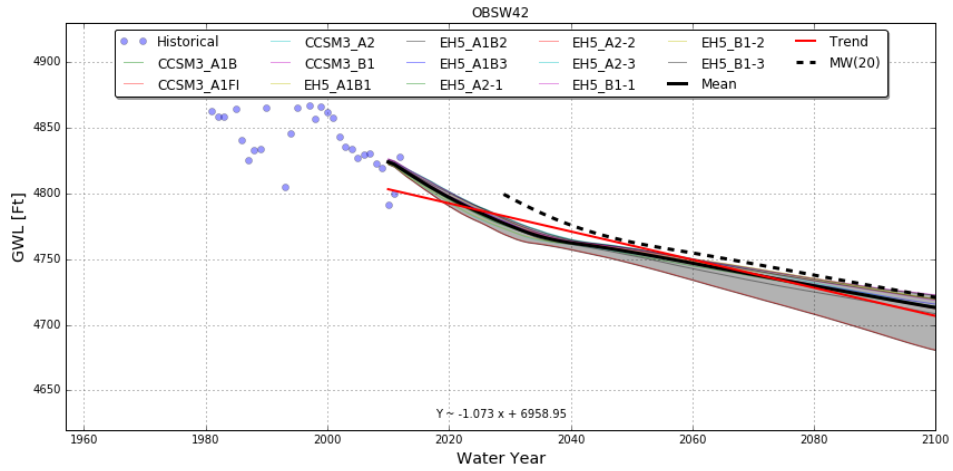


Figure 134 (continued). Simulation results of the groundwater levels at nine different locations.

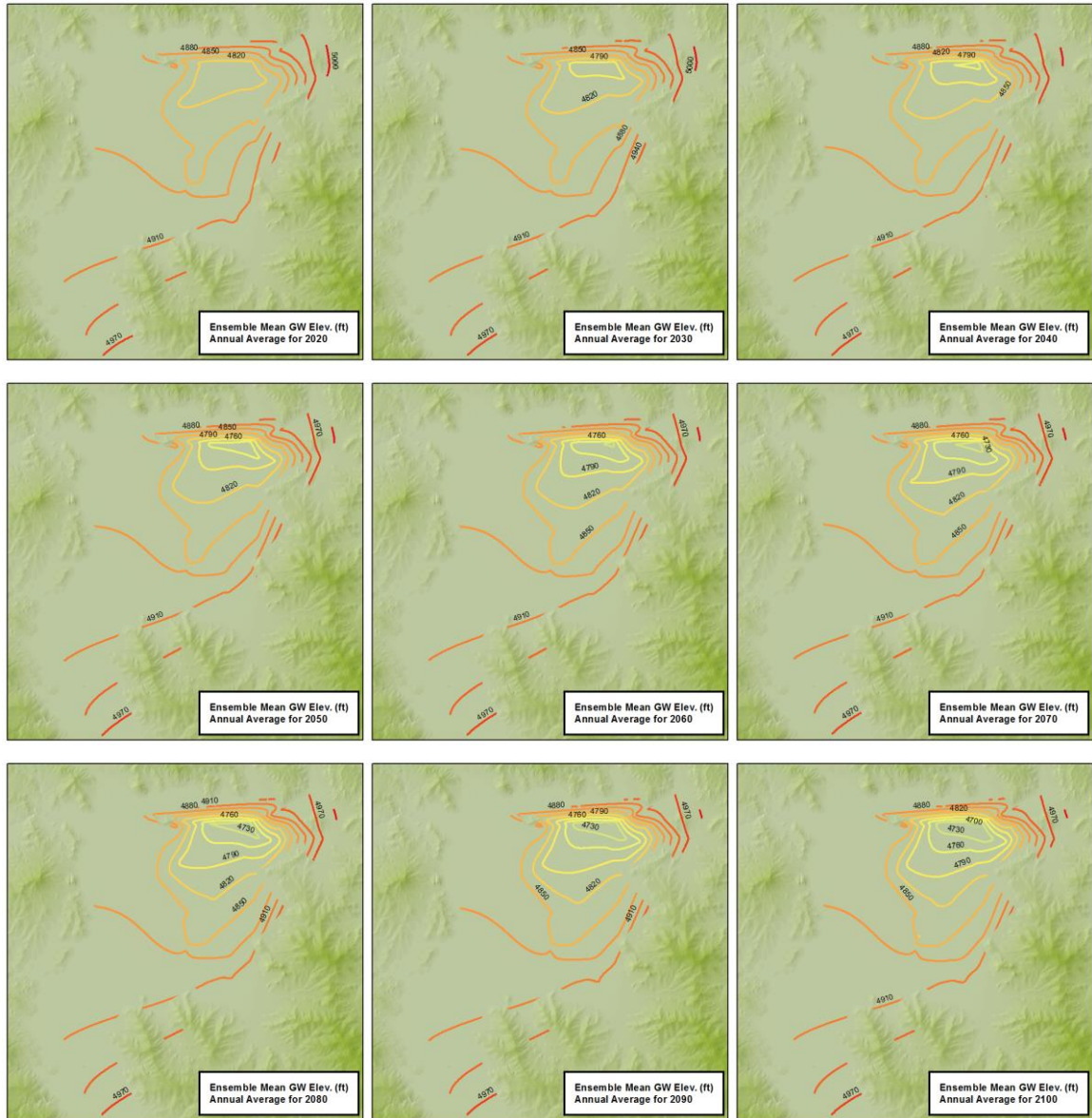


Figure 135. Simulated ensemble mean piezometric surfaces for the end of each decade between 2010 and 2100.

V. SUMMARY AND CONCLUSIONS

The objectives of this study were realized through the modeling of the study areas by the use of the Watershed Environmental Hydrology Hydro-Climate Model (WEHY-HCM) and the Integrated Water Flow Model (IWFM). The fifth generation Mesoscale Atmospheric Model (MM5) was used as the regional climate model (RCM) of the WEHY-HCM, the Watershed Environmental Hydrology (WEHY) model was used as the hydrologic part of the WEHY-HCM, while the IWFM was used for the groundwater analysis portion of this study. Successful calibration and validation of these models was presented in the previous chapters, revealing the capability of the models to perform well for simulating surface water and groundwater flows within the study region.

Working with the UMF watershed, historical records of hydrologic ground observation data were obtained from various data sources to ensure an effective calibration and validation process of the WEHY-HCM. Moreover, a Geographic Information System (GIS) database for the UMF watershed was set up to guarantee the effective use of the WEHY-HCM over the study watershed. The MM5 regional climate model was applied to reconstruct the historical hydro-climate data over the Upper Middle Fork (UMF) watershed, in which case this reconstructed data was later validated to ensure the plausibility of the downscaling method applied over the UMF. This provided confidence in the use of such a method for downscaling the future climate projections over the UMF watershed, which was done in this study for the 13 future projections obtained from the CCSM3 and ECHAM5 Global Climate Models (GCMs).

Likewise, for the analysis of the Lake Davis basin and the Sierra Valley basin, a similar set of steps were followed as above, including obtaining historical observation data, setting up a GIS database, as well as reconstructing and validating the historical hydro-climate over the areas of interest. For the Lake Davis basin, historical reservoir operations for the Grizzly Valley Dam were analyzed in detail, which allowed the estimation of the rules used for its operation within that period. As for the Sierra Valley basin, the conceptual model of the Sierra Valley aquifer based on the available data was explained in detail together with the implementation of the IWFM. Simulation results for the historical period were analyzed to quantify the water budget components over the Sierra Valley and to form a baseline for future simulations.

With the above-mentioned models set up over the required areas, the reconstructed future climate projections were used for running the above models for the different areas in order to get results for the future surface water and groundwater projections over the UMF watershed and the Sierra Valley aquifer.

The analysis of the future flow projections over the UMF watershed revealed that the average of the flow discharges within the future period is projected to be larger for simulations using the CCSM3 projections compared to the ones using the ECHAM5 (EH5) projections. The trend analysis of the flows at the outlet of the UMF watershed showed very few significant trends when considering the early-, mid-, and late-century periods separately for each of the 13 scenarios. However, when considering the ensemble of the flows of all 13 projections over the whole future period, a statistically significant positive trend was observed. This suggests, on average, an expected increase in the annual mean flows within the UMF watershed during the future period. Nonetheless, the presence of 13 different projections provides a wide range of flow values that can be attained, thus reinforcing a level of variability regarding those increasing future flows. In addition to the trend analysis of the future flows, a flood frequency analysis over UMF was performed for the future projected flows, from which a frequency histogram and an integrated histogram were constructed. These showed that in the simulated future period of the 21st century, about 20% of the annual flood peaks are expected to be equal to or greater than 2,000 cms (0.71×10^5 cfs), while the highest frequency of the annual floods is expected to occur at the value of around 1,000 cms (0.35×10^5 cfs). Finally, the information provided from all the future projections was used to get estimates of the flood magnitudes for different return periods. For example, one could estimate that for the future period of the 21st century, a 2,811 cms (0.99×10^5 cfs) flood has around a 10-yr average return period, a 5,321 cms (1.87×10^5 cfs) flood has around a 50-yr average return period, and a 6,646 cms (2.35×10^5 cfs) flood has a 100-yr average return period.

As for the Lake Davis basin, the analysis the future projections over this basin and the Grizzly Valley Dam have shown that some of the future scenarios may lead to extremely low storage values during the 21st century. With the recommendation being to run the reservoir with a reservoir storage not falling below the second outlet ($\sim 5,595$ AF), it was clear that 5 of the future scenarios violate this criterion, all being from the ECHAM5 (EH5) GCM. It was shown that increasing the threshold value for the dam operation from the original value of 56,000 AF to

62,000 AF allowed one of those five EH5 scenarios to improve its minimum reservoir storage during the critical period and pass the minimum recommended limit. However, such a change in the threshold value also caused increases in the projected spills and shortages during the 21st century. On the other hand, while a 10% assumed increase in dam capacity did not help much with preventing the reservoir storage depletion in these five scenarios, it reduced expected shortages and surpluses by up to 13.1% and 29%, respectively. Finally, disregarding the above changes in threshold and capacity, it was seen that another possible option would be to operate the reservoir normally during most of the 21st century, while applying strict hedging when nearing periods that are projected to be extremely dry, thus saving water and preventing the depletion of the reservoir storage during and after those excessively dry periods.

Regarding the Sierra Valley groundwater system, the analysis with the future climate projections quantifies the possible effects of the changing climate on the groundwater stresses. The results show an increase in the irrigation demand and therefore an increase in the groundwater pumping rates by around 25% until the end of the century. The increase in the irrigation demand is mainly caused by the increase in the potential evapotranspiration rates. As a result of the increasing demand and pumping amounts, the groundwater levels are forecasted to be decreasing in the pumping intensive areas of the valley.

The completed results discussed in this study, including the analyses of the historical data and the future projections, can provide great insight into the effect of future climate scenarios on groundwater storage and usage, flood flows, and reservoir operations (for Grizzly Valley Dam). They can be of great assistance for water managers in deciding on future management actions to protect the involved water users and ecosystems, as well as to appropriately manage the available water resources in the study area over the course of the 21st century.

References

- Allen, R. G., Pereira, L. S., Raes, D., & Smith, M. (1998). *Crop evapotranspiration - Guidelines for computing crop water requirements - FAO Irrigation and drainage paper 56*. Rome: FAO - Food and Agriculture Organization of the United Nations.
- Anderson, M.L., Chen, Z.Q., Kavvas, M.L., Yoon, J.Y. (2007). Reconstructed Historical Atmospheric Data by Dynamic Downscaling. *Journal of Hydrologic Engineering*, ASCE, 12(2), 156-162.
- Anthes, R. A., & Warner, T. T. (1978). Development of hydrodynamic models suitable for air pollution and other mesometeorological studies. *American Meteorological Society*, 106(8), 1045-1078.
- Aquaveo. (2015, September 17). *Groundwater Modeling Software (GMS)*. Retrieved from Aquaveo: <http://www.aquaveo.com/software/gms-groundwater-modeling-system-introduction>
- Asner, G.P., Scurlock, J.M.O., and Hicke, J.A (2003). Global Synthesis of Leaf Area Index Observations: Implications for Ecological and Remote Sensing Studies, *Global Ecology and Biogeography*, 12, 191-205.
- Bohm, B. (2015). *SVB Aquifer Delineation: Conceptual Models, Methodology and Results - DRAFT*. Graeagle: Plumas Geo-Hydrology.
- California Department of Water Resources. (1963). *Northeastern Counties Groundwater Investigation (Bulletin 98)*.
- California Department of Water Resources. (1983). *Sierra Valley Groundwater Study*.
- California Department of Water Resources, (2004). *Sierra Valley Groundwater Basin, Sierra Valley Groundwater Subbasin (Bulletin 118)*. Retrieved on September 17, 2015 from DWR: <http://www.water.ca.gov/groundwater/bulletin118/basindescriptions/5-12.01.pdf>
- California Department of Water Resources. (2013). Upper Feather River Lakes (Brochure). Retrieved on February 20, 2014, from DWR: http://www.water.ca.gov/recreation/brochures/pdf/UFRL_brochure_2013.pdf
- California Department of Water Resources. (2016). *IWFM Soil Data Buuilder with GIS (IWFM SDB-GIS) User's Manual Rev.31*. DWR, Bay-Delta Office, Integrated Hydrological Models Development Unit Modeling Support Branch.
- California Department of Water Resources. (2016, 03 10). *IWFM: Integrated Water Flow Model - Demand Calculator (IDC)*. Retrieved from CA Department of Water Resources Bay-Delta: http://baydeltaoffice.water.ca.gov/modeling/hydrology/IDC/index_IDC.cfm

- Canadell, J., Jackson, R.B., Ehleringer, J.R., Mooney, H.A., Sala, O.E., and Schulze, E.D. (1996). Maximum Rooting Depth of Vegetation Types at the Global Scale. *Oecologia*, 108, 583-595.
- Chen, Z.Q., Kavvas, M.L., Yoon, J.Y., Dogrul, E.C., Fukami, K., Yoshitani, J., Matsuura, T. (2004a). Geomorphologic and Soil Hydraulic Parameters for Watershed Environmental Hydrology (WEHY) Model, *Journal of Hydrologic Engineering*, ASCE, 9(6), 465-479.
- Chen, Z.Q., Kavvas, M.L., Fukami, K., Yoshitani, J., Matsuura, T. (2004b). Watershed Environmental Hydrology (WEHY) Model: Model Application, *Journal of Hydrologic Engineering*, ASCE, 9(6), 480-490.
- Collins, W.D., Bitz, C.M., Blackmon, M.L., Bonan, G.B., Bretherton, C.S., Carton, J.A., Chang, P., Doney, S.C., Hack, J.J., Henderson, T.B., Kiehl, J.T., Large, W.G., McKenna, D.S., Santer, B.D., & Smith, R.D. (2006). The Community Climate System Model Version 3 (CCSM3). *Journal of Climate*, 19(11), 2122-2143.
- Daly, C., Halbleib, M., Smith, J.I., Gibson, W.P., Doggett, M.K., Taylor, G.H., Curtis, J. & Pasteris, P.P. (2008) Physiographically sensitive mapping of climatological temperature and precipitation across the conterminous United States. *International Journal of Climatology*, 28, 2031–2064.
- Dogrul, E. C. (2014). *Integrated Water Flow Model Theoretical Documentation*. California Department of Water Resources.
- Doherty, J., Muffels, C., Rumbaugh, J., & Tonkin, M. (2016, Aug 25). Retrieved from PEST: Model-Independent Parameter Estimation and Uncertainty Analysis: <http://www.pesthomepage.org/Home.php>
- Gale, M.R., and D.F. Grigal. (1987). Vertical Root Distributions of Northern Rree Species in Relation to Successional Status. *Can. J. For. Res.*, 17, 829-834.
- Ganev, K. (2011). Air pollution. Pages 499-555 in S. E. Jorgensen, editor, *Handbook of Ecological Models used in Ecosystem and Environmental Management*. Florida: CRC Press.
- George, H., Lile, D., Childers, C., Noble, C., Oilar, A., Haworth, K., Schmidt, K., & Miller, G. (2007). *Upper Feather River Watershed Irrigation Discharge Management Program*. Retrieved December 20, 2014, from UCANR: <http://ucanr.org/sites/UCCE-Plumas-Sierra/files/13633.pdf>
- Grell, G. A., Dudhia, J., & Stauffer, D. R. (1994). A description of the fifth-generation Penn State/NCAR Mesoscale Model (MM5). NCAR Technical Note NCAR/TN-398+STR, DOI:10.5065/D60Z716B.

- Horizon Systems Corporation. (2016, 06 25). *NHDPlus Homepage*. Retrieved from NHD Plus: <http://www.horizon-systems.com/nhdplus/>
- Horne, F.E., & Kavvas, M.L. (1997). Physics of the spatially averaged snowmelt process. *J Hydrol*, 191, 179–207.
- IPCC. (2000). *Special Report on Emissions Scenarios: A Special Report of Working Group III of the Intergovernmental Panel on Climate Change*. Eds. Nebojsa Nakicenovic & Robert Swart. Retrieved December 1, 2014 from <http://www.ipcc.ch/pdf/special-reports/spm/sres-en.pdf>
- IPCC. (2007). *Climate Change 2007: Synthesis Report*. Eds. Rajendra K. Pachauri & Andy Reisinger. Retrieved December 1, 2014 from http://www.ipcc.ch/pdf/assessment-report/ar4/syr/ar4_syr.pdf
- Ishida, K., Kavvas, M., Jang, S., Chen, Z., Ohara, N., and Anderson, M. (2014). Physically Based Estimation of Maximum Precipitation over Three Watersheds in Northern California: Atmospheric Boundary Condition Shifting. *J. Hydrol. Eng.*, 10.1061/(ASCE)HE.1943-5584.0001026, 04014052.
- Jang, S. H., S. Kure, N. Ohara, and M.L. Kavvas. (2010). Hydrologic and Environmental Modeling for Upper Putah Creek Watershed Using Reconstructed Historical Atmospheric Data by Dynamical Downscaling. ASCE, World Environmental & Water Resources Congress 2010 in Rhode Island.
- Kalnay, E., Kanamitsu, M., Kistler, R., Collins, W., Deaven, D., Gandin, L., Iredell, M., Saha, S., White, G., Woollen, J., Zhu, Y., Chelliah, M., Ebisuzaki, W., Higgins, W., Janowiak, J., Mo, K. C., Ropelweski, C., Wang, J., Leetmaa, A., Reynolds, R., Jenne, R., & Joseph, D. (1996). The NCEP/NCAR 40-year reanalysis project. *Bulletin of the American Meteorological Society*, 77(3), 437-471.
- Kavvas, M.L., Chen, Z. Q., Dogrul, C., Yoon, J. Y., Ohara, N., Liang, L., Aksoy, H., Anderson, M. L., Yoshitani, J., Fukami, K & Matsuura, T. (2004). Watershed Environmental Hydrology (WEHY) model, based on upscaled conservation equations: Hydrologic module. *J. Hydrologic Eng.*, 9(6), 450–464.
- Kavvas, M.L., Yoon, J. Chen, Z.Q., Liang, L., Dogrul, E.C., Ohara, N., Aksoy, H., Anderson, M. L., Reuter, J. and Hackley, S. (2006). “Watershed Environmental Hydrology Model: Environmental Module and Its Application to a California Watershed”, *Journal of Hydrologic Engineering*, 11(3), 261-272.
- Kavvas, M., Kure, S., Chen, Z., Ohara, N., and Jang, S. (2012). “WEHYHCM for modeling interactive atmospheric-hydrologic processes at watershed scale. I: Model description.” *Journal of Hydrologic Engineering*, 18(10), 1262-1271.

- Kenneth D. Schmidt & Associates. (2003). *Technical Report on 1998-2003 Hydrogeologic Evaluation for Sierra Valley*. Sierra Valley Groundwater Management District.
- Kenneth D. Schmidt & Associates. (2005). *Technical Report on 2003-2005 Hydrogeological Evaluation for Sierra Valley*. Sierra Valley Groundwater Management District.
- Kenneth D. Schmidt & Associates. (2012). *Technical Report on 2005-2011 Hydrogeologic Evaluation for Sierra Valley*. Sierra Valley Groundwater Management District.
- Kistler, R., Kalnay, E., Collins, W., Saha, S., White, G., Woollen, J., Chelliah, M., Ebisuzaki, W., Kanamitsu, M., Kousky, V., van den Dool, H., Jenne, R., & Fiorino, M. (2001). The NCEP-NCAR 50-year reanalysis: Monthly means CD-ROM and documentation. *Bulletin of the American Meteorological Society*, 82(2), 247-267.
- Klemes, V. (1979). Storage mass-curve analysis in a system-analytic perspective. *Water Resources Research*, 15(2), 359-370.
- Kure, S., Jang, S., Ohara, N., Kavvas, M., and Chen, Z. (2012). “WEHYHCM for modeling interactive atmospheric-hydrologic processes at watershed scale. II: Model application to ungauged and sparsely gauged watersheds.” *Journal of Hydrologic Engineering*, 18(10), 1272-1281.
- McCuen, R.H., Rawls, W.J., and Brakensiek, D.L. (1981). Statistical analysis of the Brooks-Corey and the Green-Ampt parameters across soil textures. *Water Resour. Res.*, 2(4), 1005–1013.
- Northeast Climate Impacts Assessment (NECIA). (2006). Climate Change in the U.S. Northeast. Retrieved September 16, 2014 from http://www.ucsusa.org/assets/documents/global_warming/necia_climate_report_final.pdf
- Northwest Alliance for Computational Science and Engineering (NACSE). (2013). *Descriptions of PRISM spatial climate datasets for the conterminous United States*. Retrieved January 3, 2015, from http://www.prism.oregonstate.edu/documents/PRISM_datasets_aug2013.pdf
- Ohara, N., & Kavvas, M. L. (2006). “Field observations and numerical model experiments for the snowmelt process at a field site.” *Adv. Water Resour.*, Vol.29, No.2, 194-211.
- Ohara, N., Kavvas, M., Chen, Z., Anderson, M., Liang, L., Wilcox, J., and Mink, L. (2007) Estimation of ET Based on Reconstructed Atmospheric Conditions and Remotely Sensed Information Over Last Chance Creek Watershed, Feather River Basin, California. World Environmental and Water Resources Congress 2007: pp. 1-9.
- Önöz, B., & Bayazit, M. (2003). The power of statistical tests for trend detection. *Turkish Journal of Engineering and Environmental Sciences*, 27(4), 247-251.

- Raghunath, H. M. (2006). *Hydrology: Principles-Analysis-Design* (Rev. 2nd ed.). New Delhi: New Age International (P) Ltd.
- Rawls, W. J., D. L. Brakensiek, and K. E. Saxton. (1982). Estimation of soil water properties. *Transactions of the American Society of Agricultural Engineering*, 25, 1316-1320, 1328.
- Rippl, W. (1883). The capacity of storage-reservoirs for water-supply, *Minutes of proceedings of the Institution of Civil Engineers*, 71, 270-278.
- Rischbieter, D.B.C. (2000). "Structures to Prevent the Spread of Nuisance Fish from Lake Davis, California." *North American Journal of Fisheries Management*, 20(3), 784-790.
- Sacramento River Watershed Program (SRWP). (2010). *Upper Feather River Watershed (UFRW)*. Retrieved December 19, 2014, from Sacramento River Watershed Program: http://www.sacriver.org/files/documents/roadmap/report/Feather_UpperFeather.pdf
- Saucedo, G.J. and D.L. Wagner (1992). Geologic Map of the Chico Quadrangle, California, California Division of Mines and Geology.
- Stier, P., Feichter, J., Kinne, S., Kloster, S., Vignatti, E., Wilson, J., Ganzeveld, L., Tegen, I., Werner, M., Balkanski, Y., Schulz, M., Boucher, O., Minikin, A., & Petzold, A. (2005). The aerosol-climate model ECHAM5-HAM. *Atmospheric Chemistry and Physics*, 5(4), 1125-1156.
- Superior Court of the State of California. (1940). *ND, Service Areas, Sierra Valley*. Retrieved from CA Department of Water Resources: http://www.water.ca.gov/watermaster/ND_Watermasters/Decrees/SierraValley/SierraValleyDecree_3095_1940.pdf
- Superior Court of the State of California. (1959, December 1). *ND, Service Areas, Sierra Valley*. Retrieved from CA Department of Water Resources: http://www.water.ca.gov/watermaster/ND_Watermasters/Decrees/SierraValley/LittleLastChanceCreekDecreedWaterRights_1959.pdf
- Trinh, T., Ishida, K., Fischer, I., Jang, S., Darama, Y., Nosacka, J., Brown, K., and Kavvas, M. (2016). New Methodology to Develop Future Flood Frequency under Changing Climate by Means of Physically Based Numerical Atmospheric-Hydrologic Modeling. *J. Hydrol. Eng.*, 10.1061/(ASCE)HE.1943-5584.0001331, 04016001.
- United States Geological Survey (USGS). (2004, July 15). *The Universal Transverse Mercator (UTM) Grid*. Retrieved August 12, 2016, from USGS Online Publications Directory: <https://pubs.usgs.gov/fs/2001/0077/report.pdf>
- University Corporation for Atmospheric Research (UCAR). (2003). *MM5 modeling system overview*. Retrieved December 27, 2014 from <http://www2.mmm.ucar.edu/mm5/overview.html>

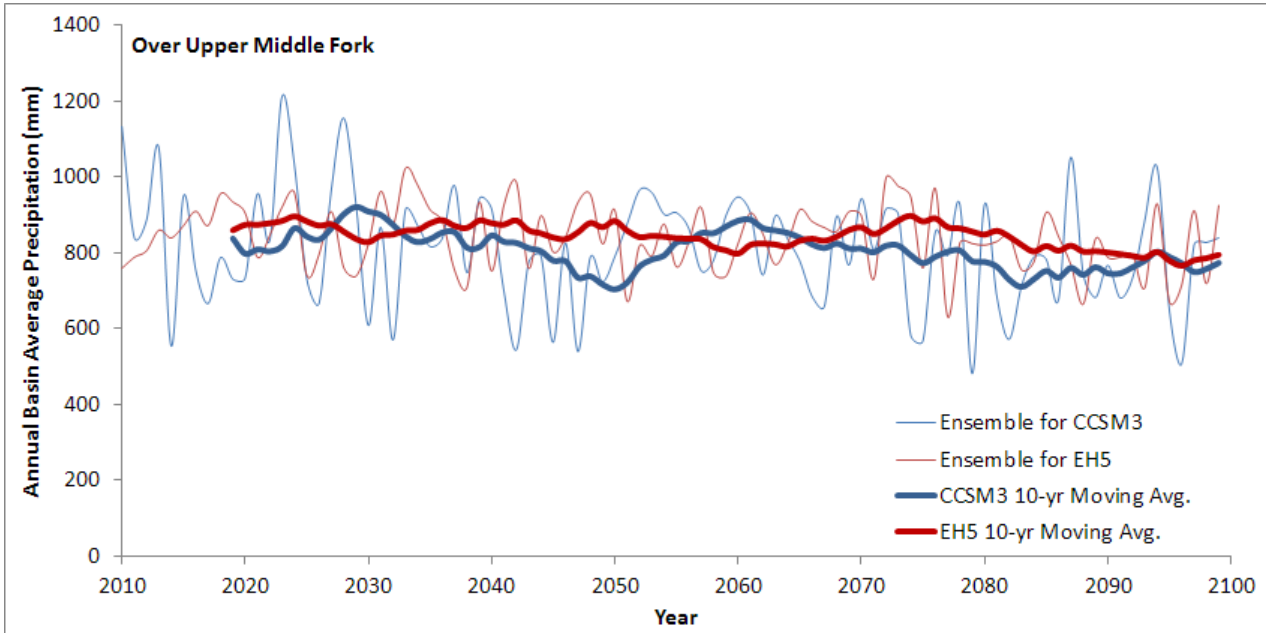
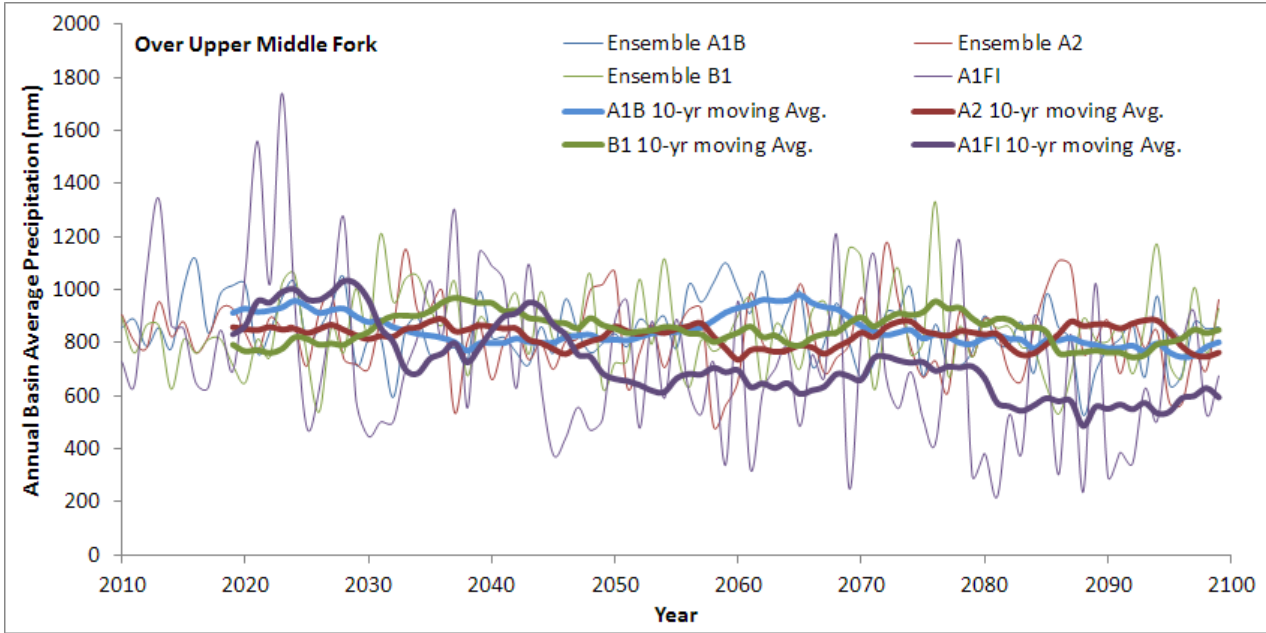
USDA. (2016, 03 25). *USDA - National Agricultural Statistics Service*. Retrieved from United States Department of Agriculture: http://www.nass.usda.gov/Research_and_Science/Cropland/SARS1a.php

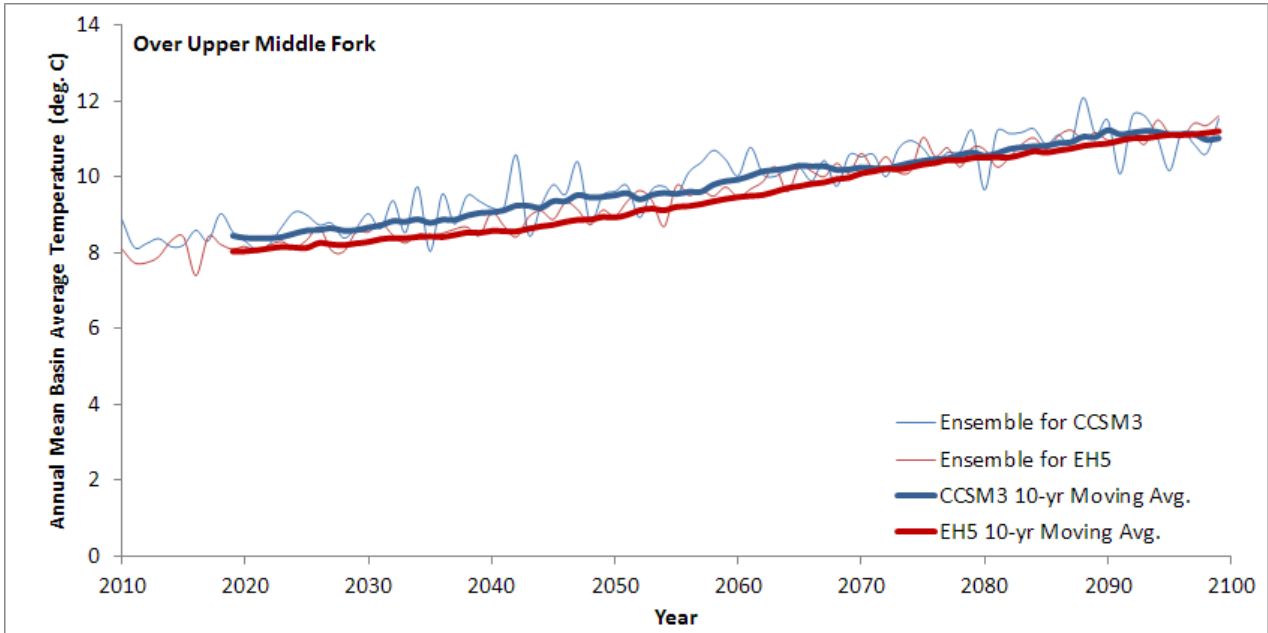
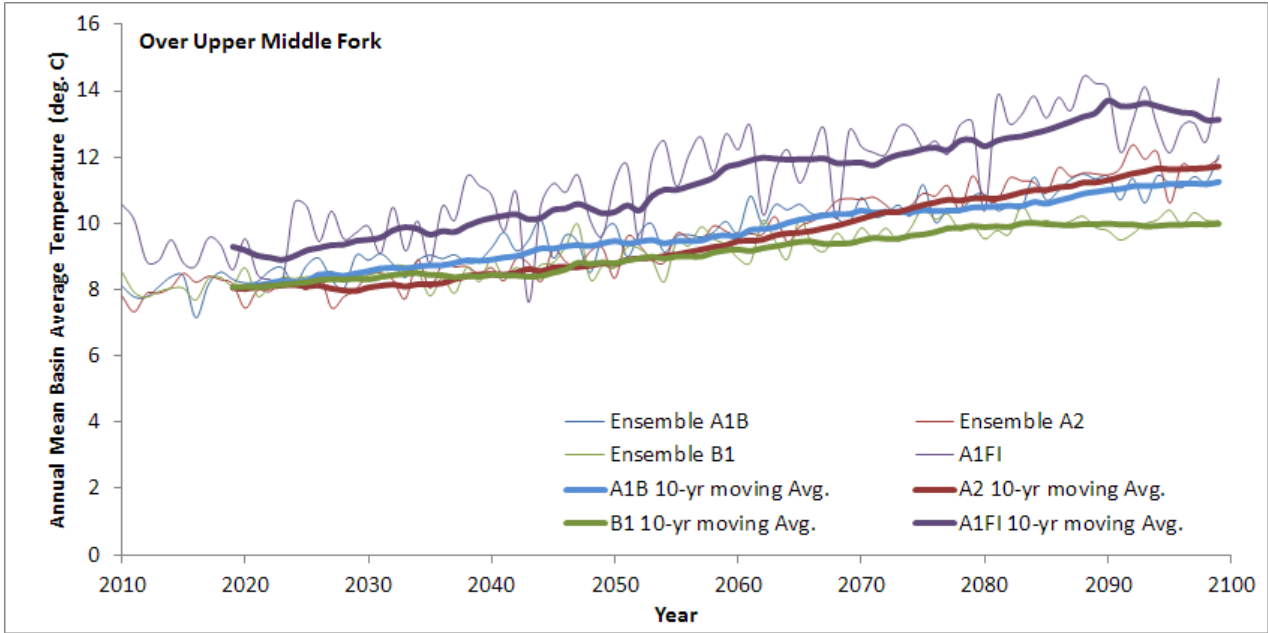
Yoshitani, J., Kavvas, M.L., and Chen, Z.Q. (2002). “Mathematical watershed models of large watershed hydrology: Chapter 7, Regional-Scale Hydroclimate Model .” Water Resources Publication, LLC.

Yoshitani, J., Kavvas, M. L., Chen, Z. Q., and Fukami K. (2009). Atmospheric Model-Based Streamflow Forecasting at Small, Mountainous Watersheds by a Distributed Hydrologic Model: Application to a Watershed in Japan. *J. Hydrol. Eng.*, 14(10), 1107-1118.

APPENDIX A

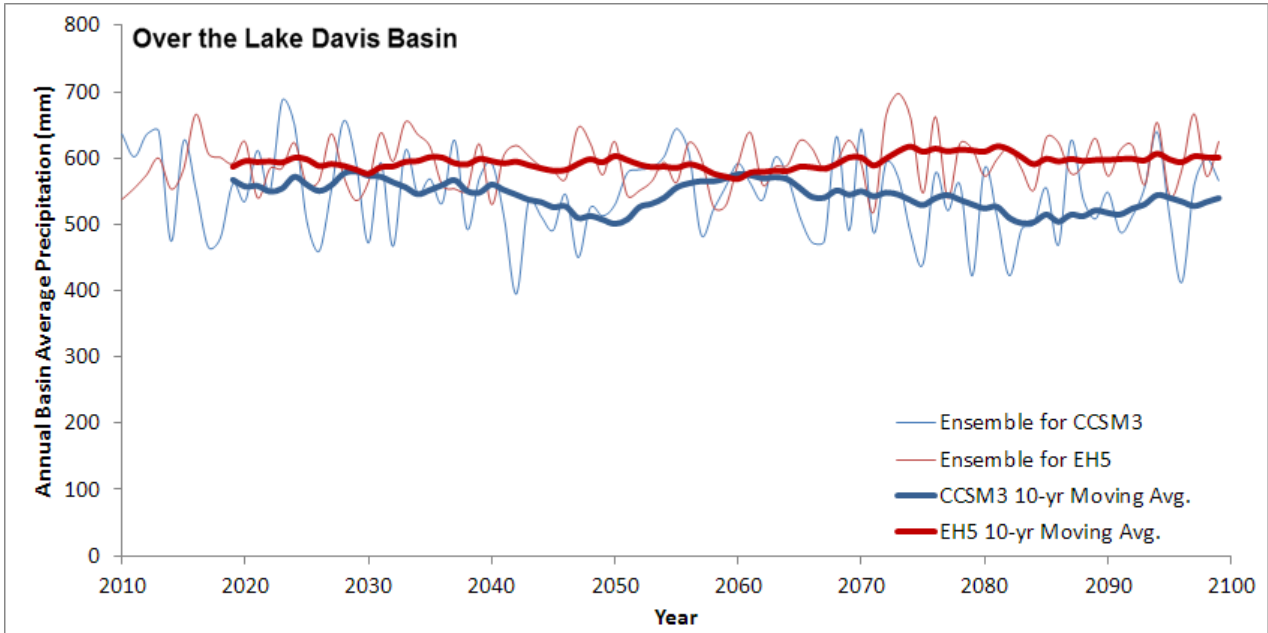
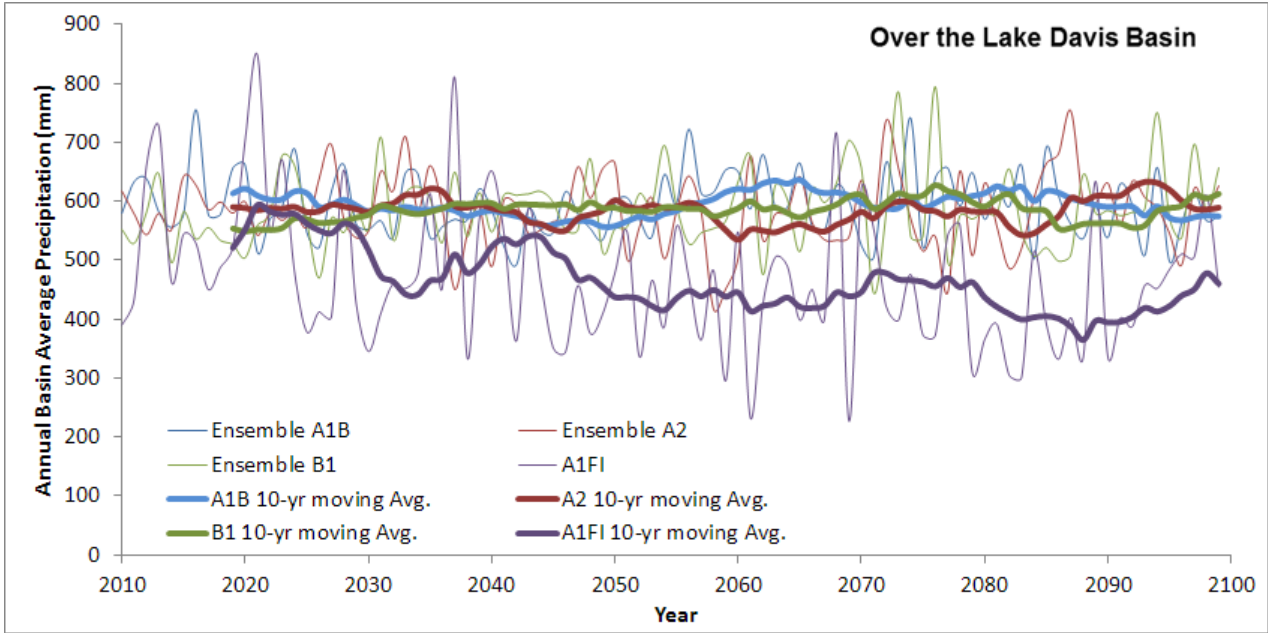
Projections of Basin Average Precipitation and Temperature
over the Upper Middle Fork Watershed for the 21st Century

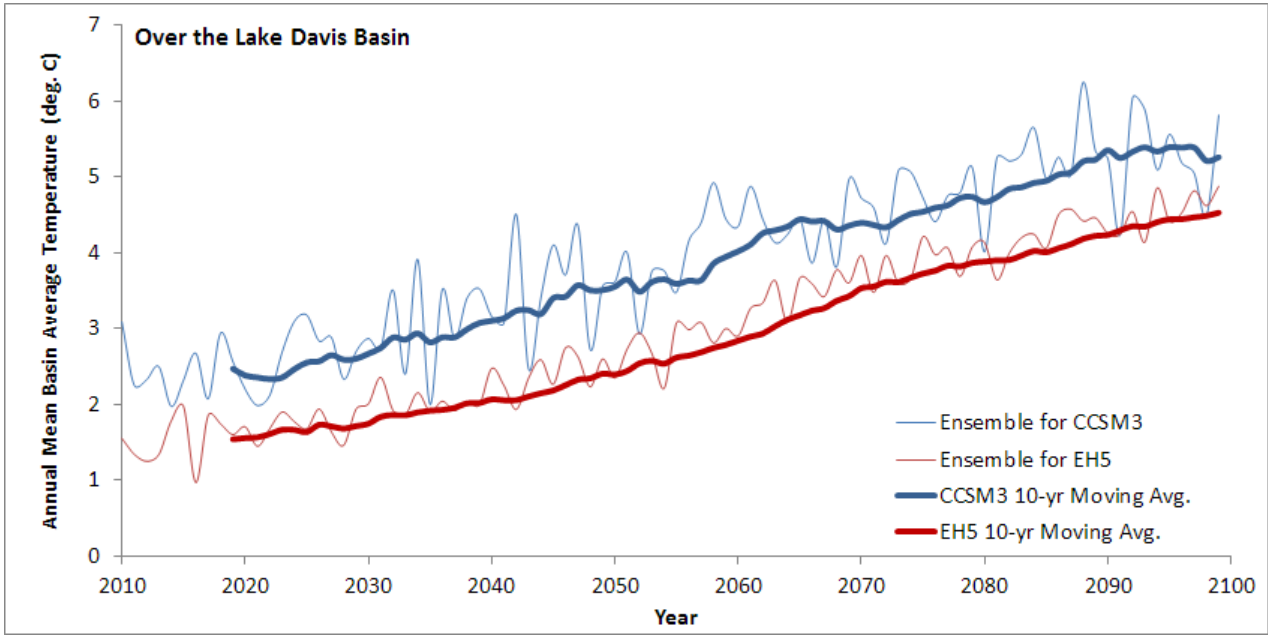
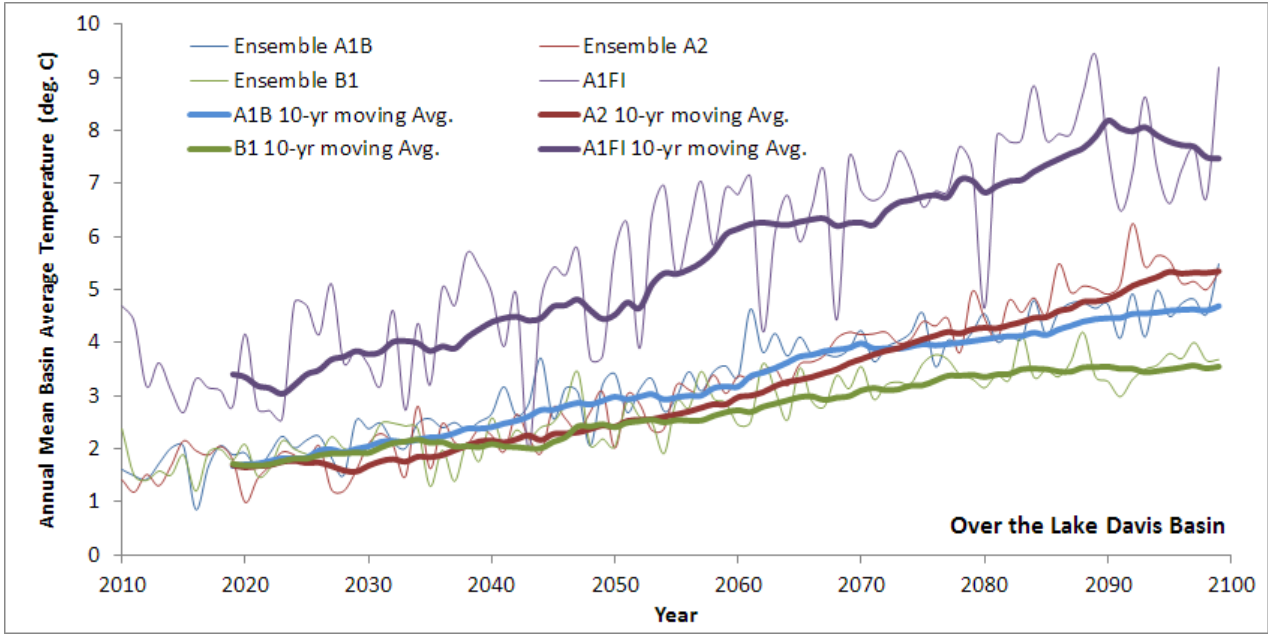




APPENDIX B

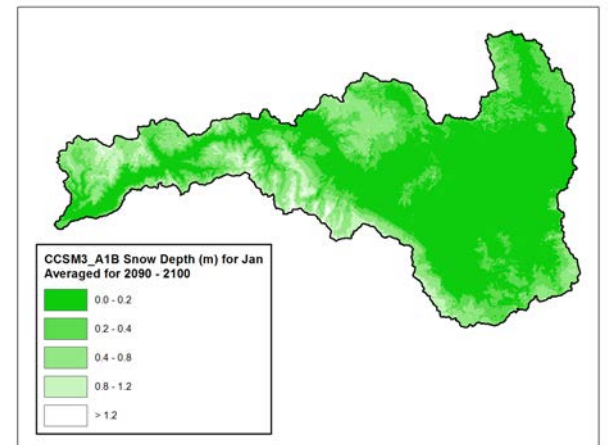
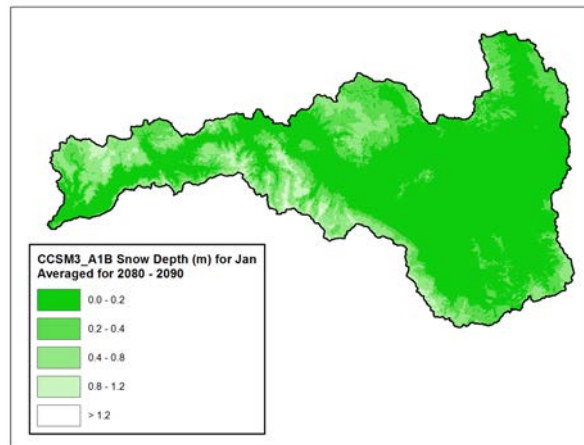
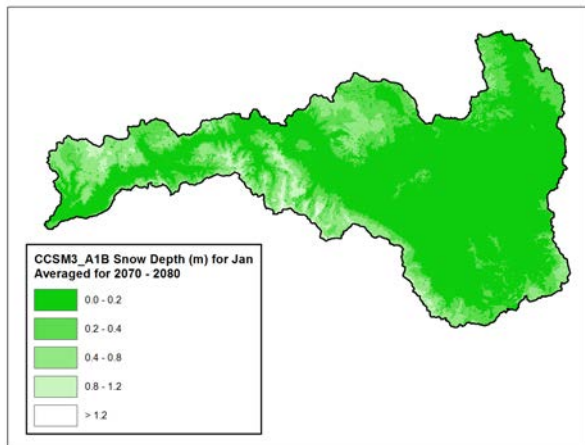
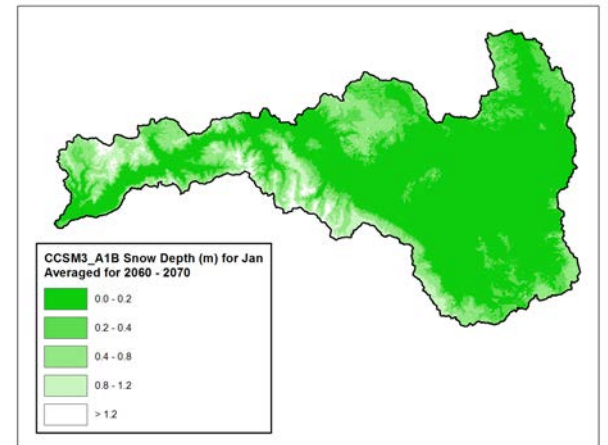
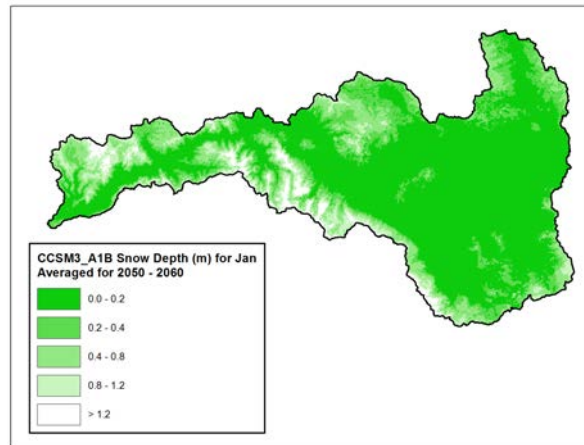
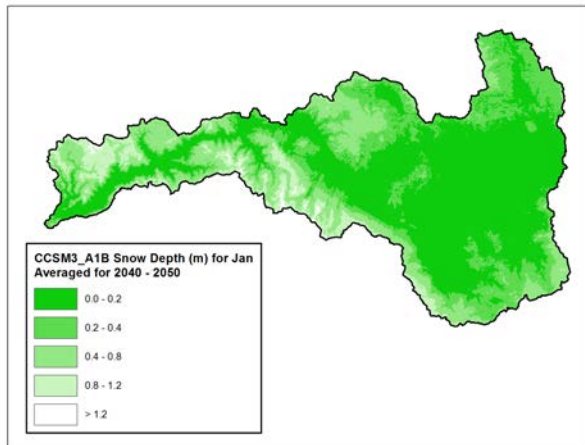
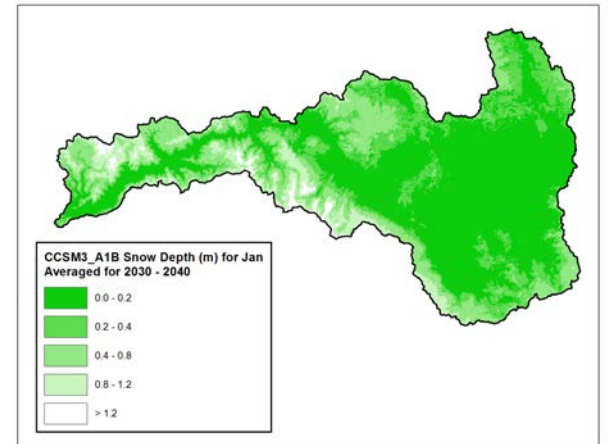
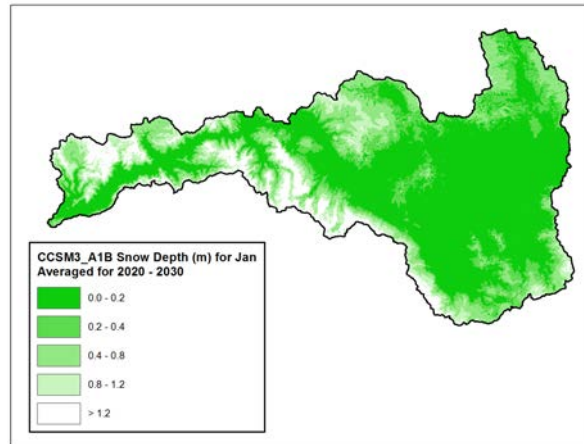
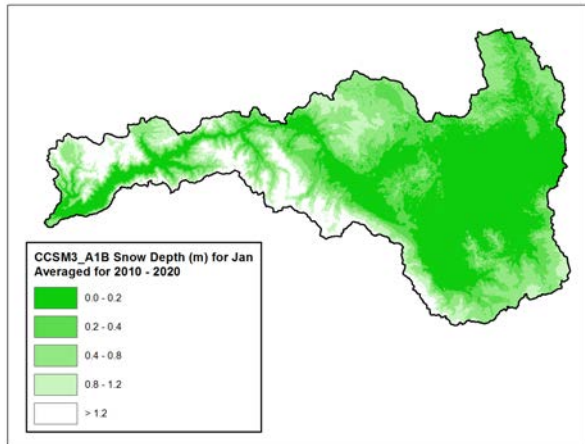
Projections of Basin Average Precipitation and Temperature
over the Lake Davis Basin for the 21st Century

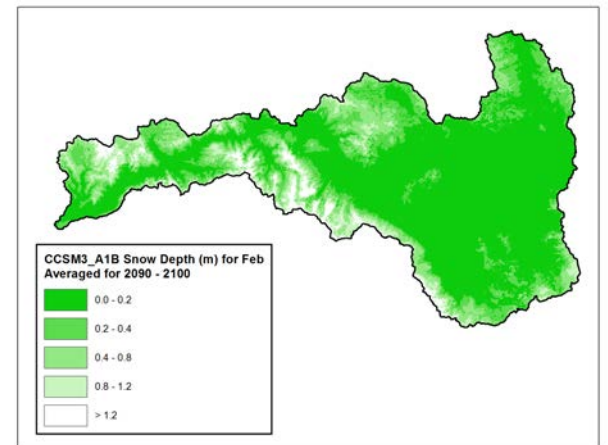
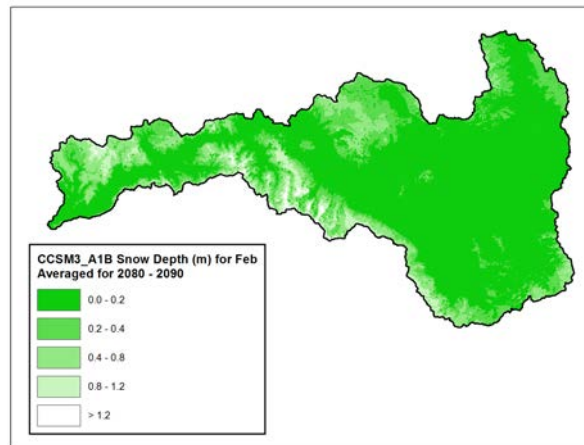
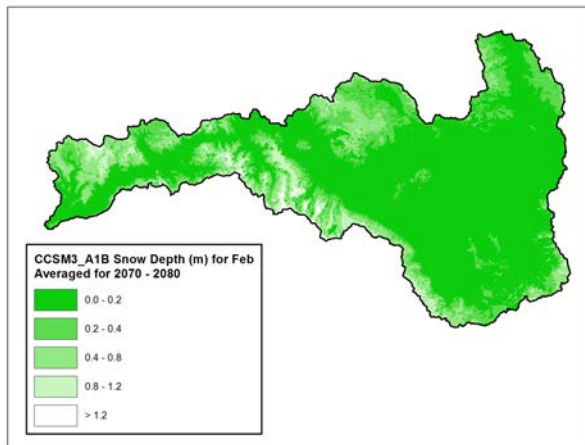
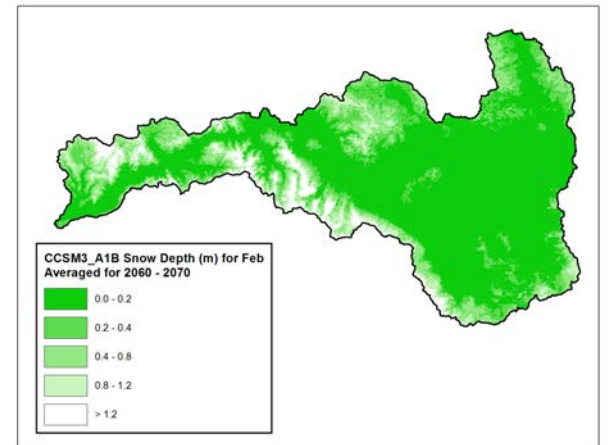
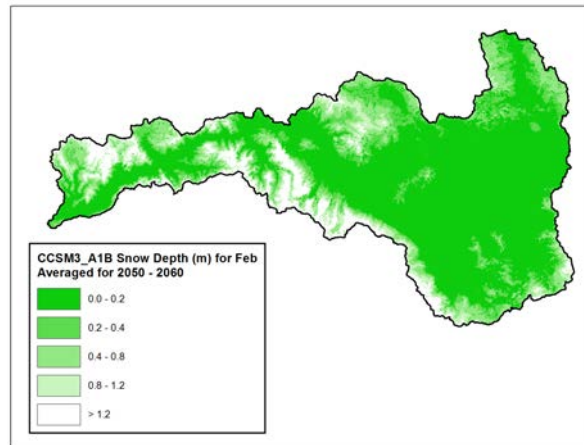
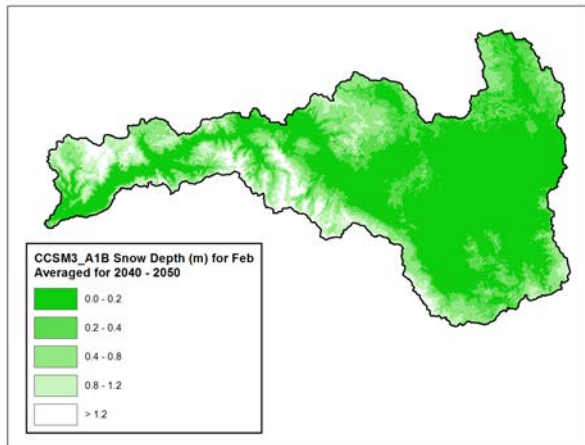
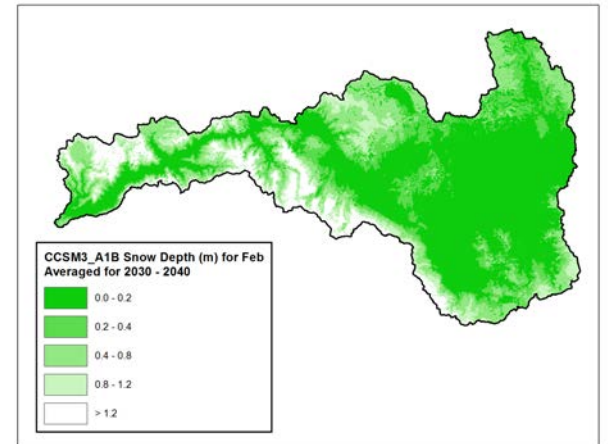
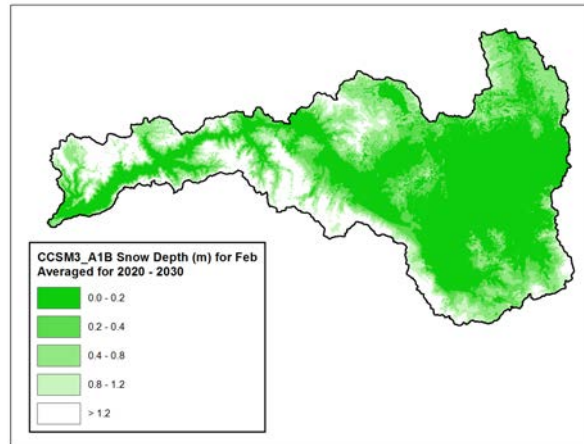
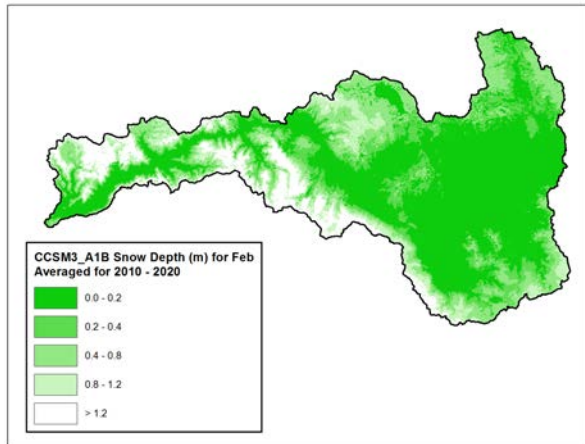


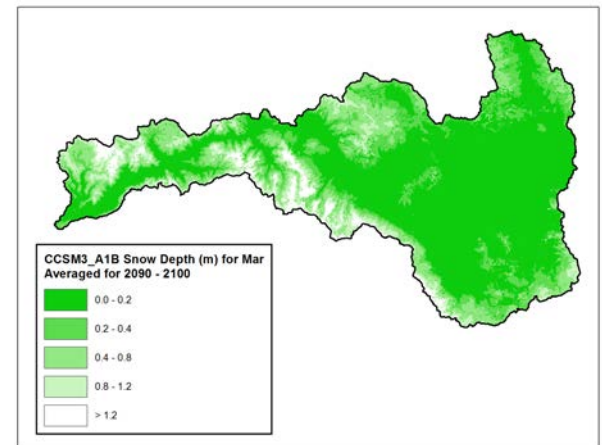
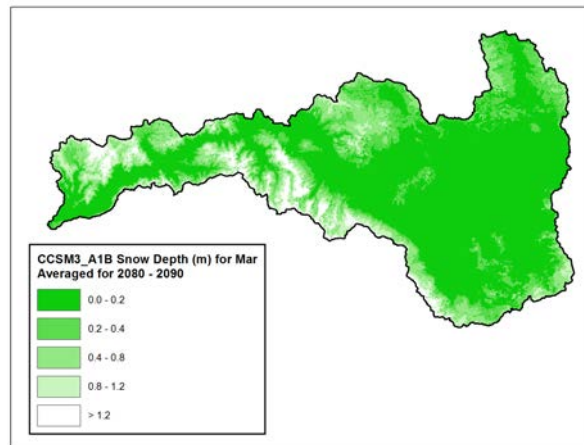
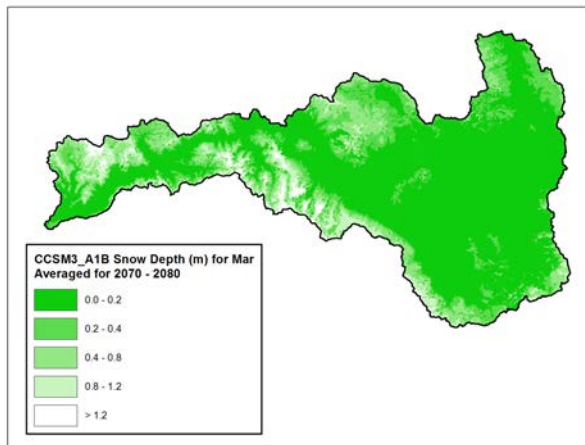
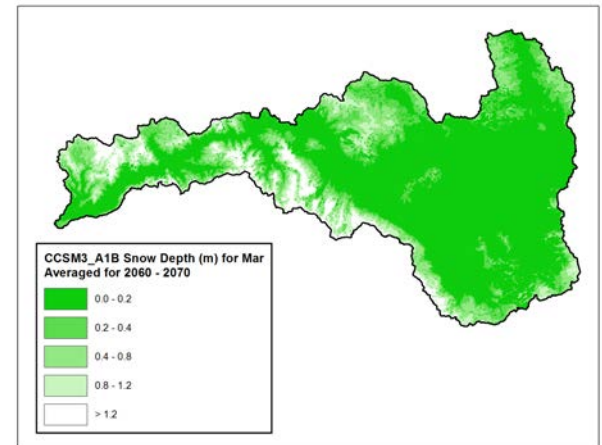
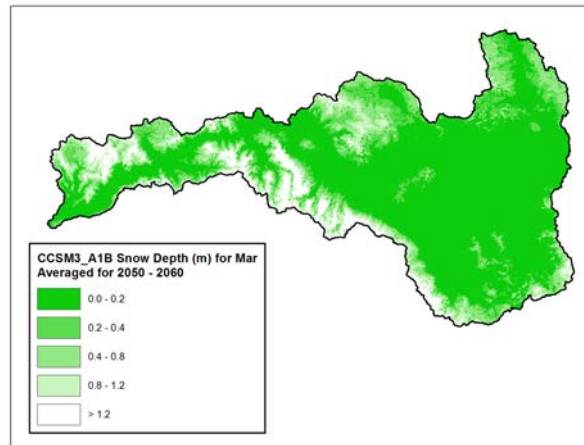
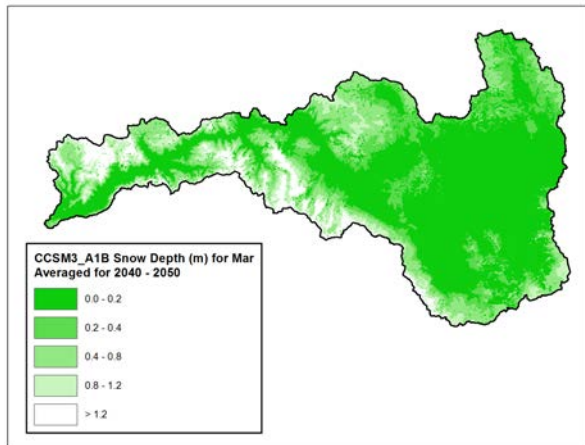
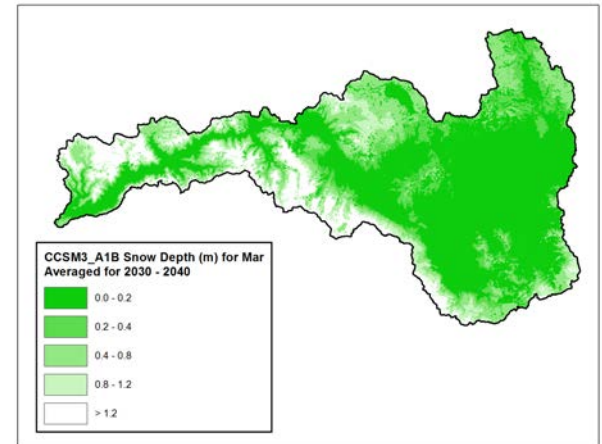
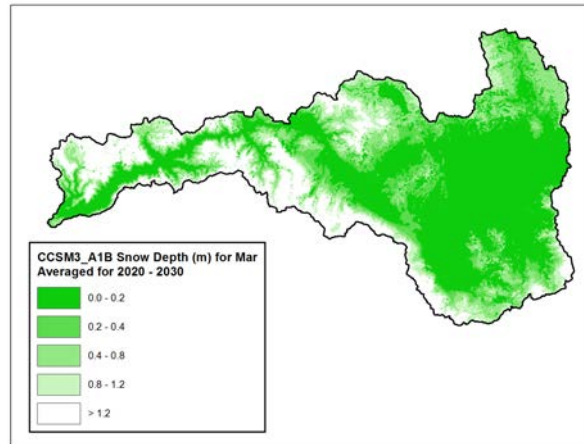
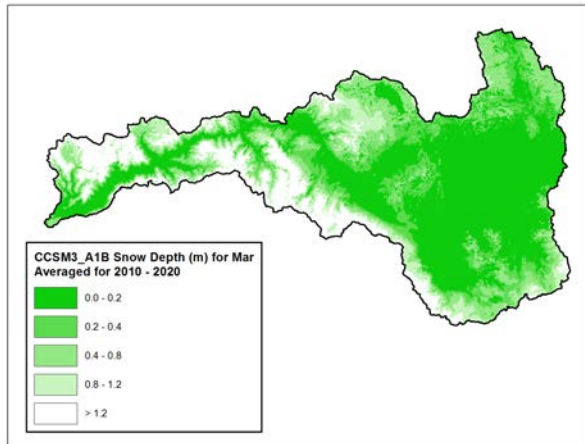


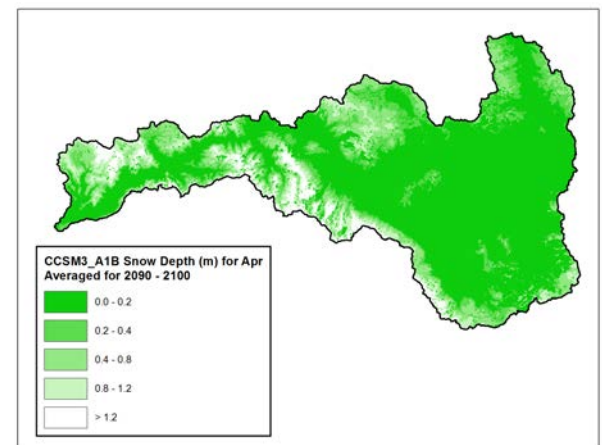
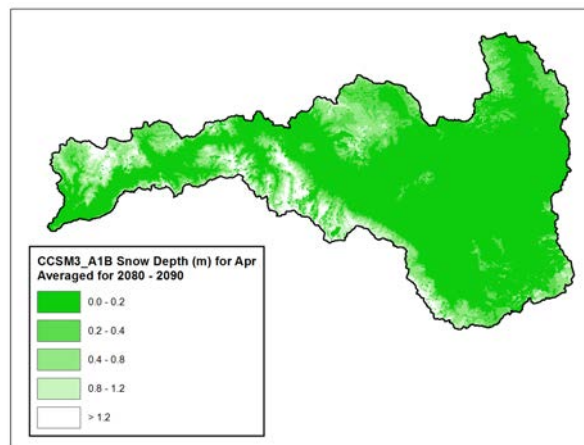
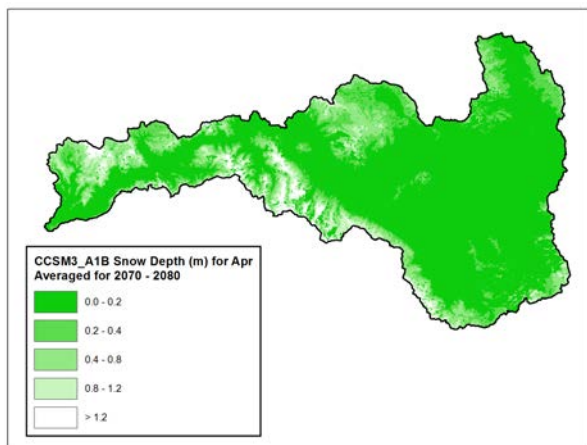
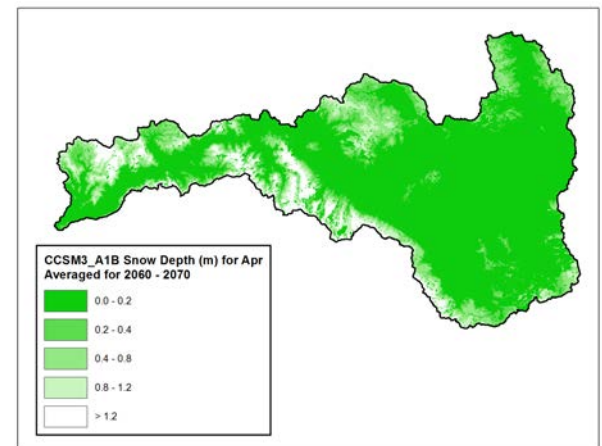
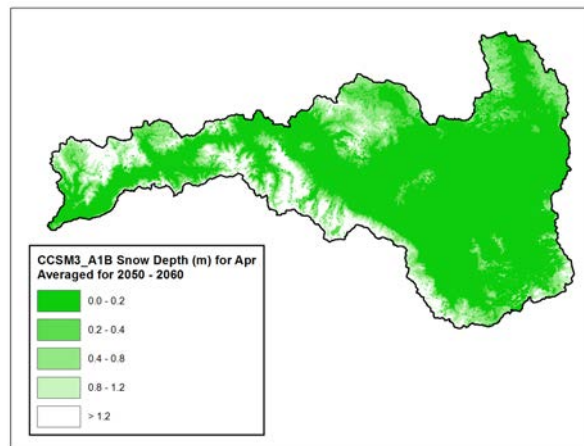
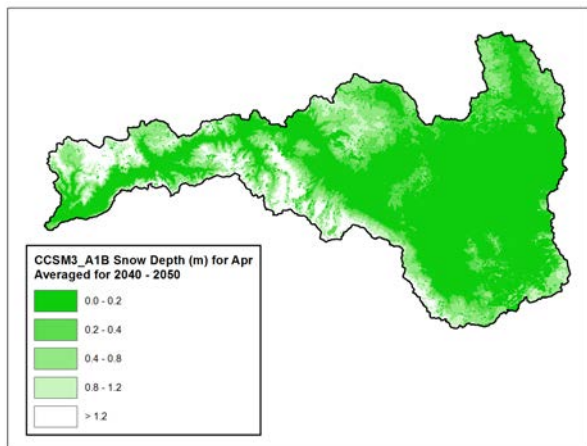
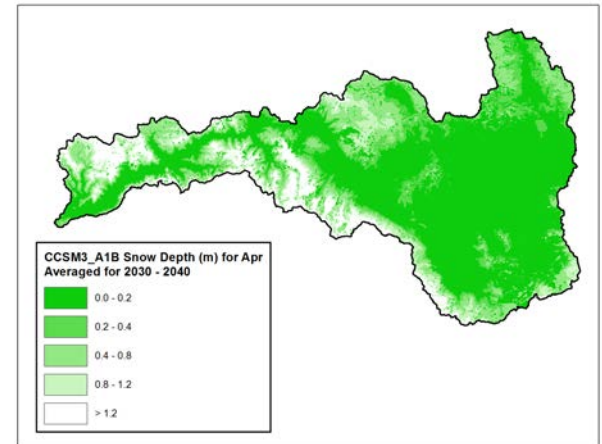
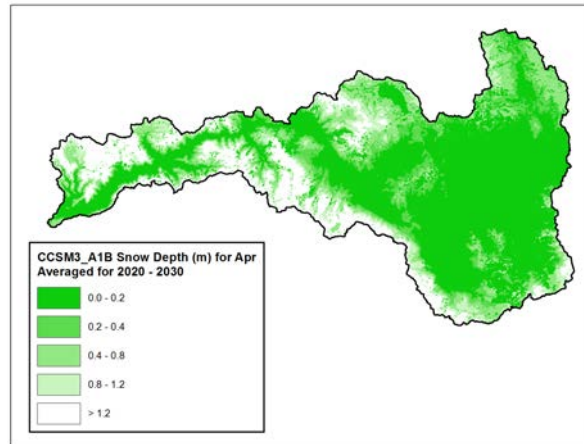
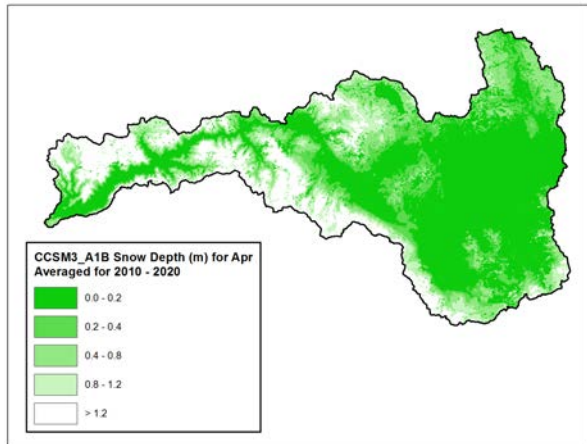
APPENDIX C

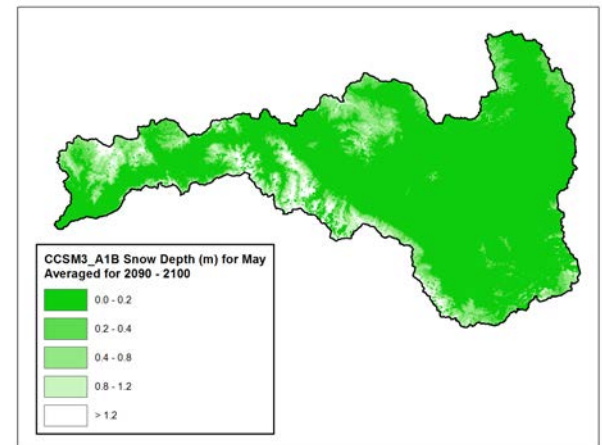
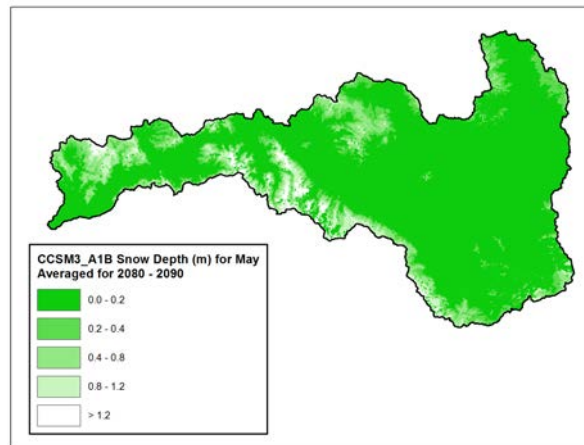
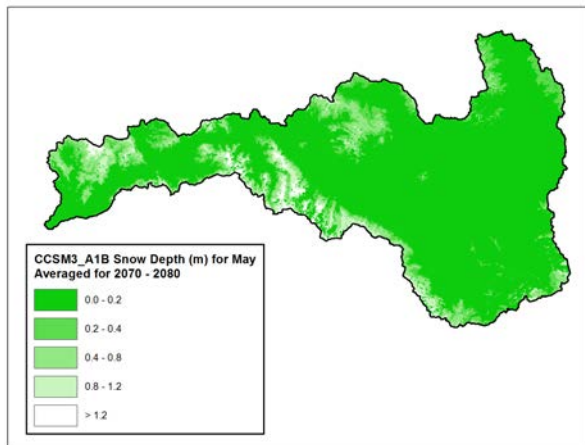
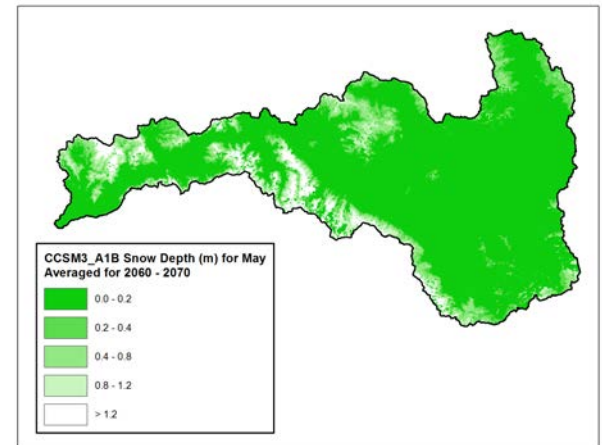
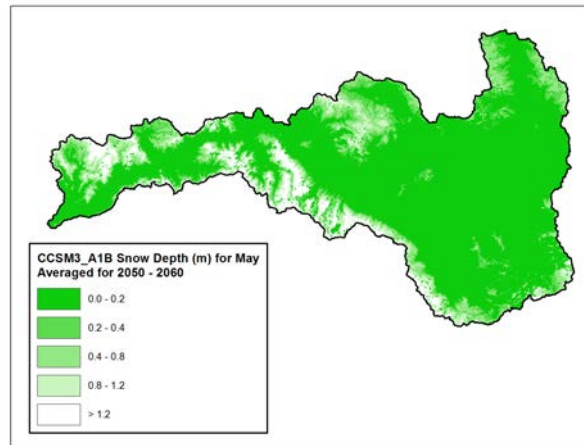
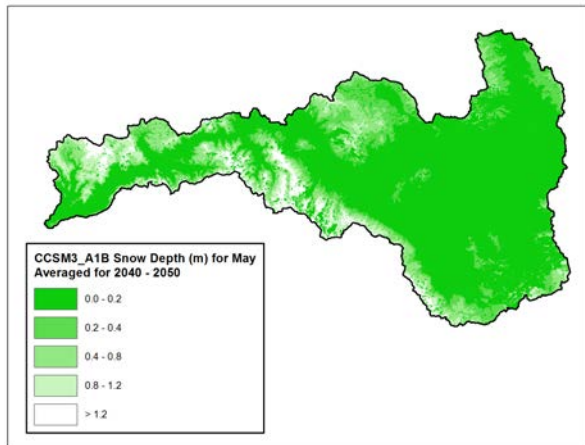
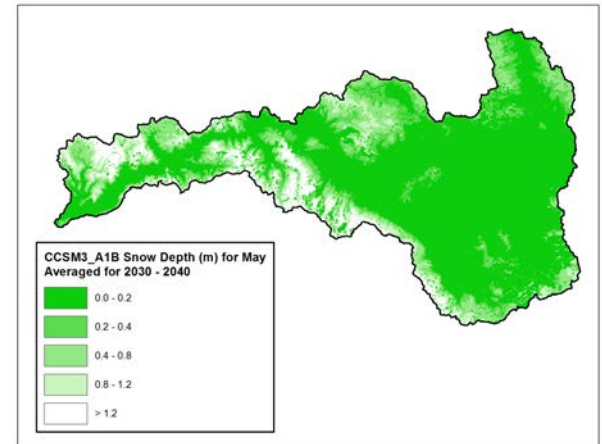
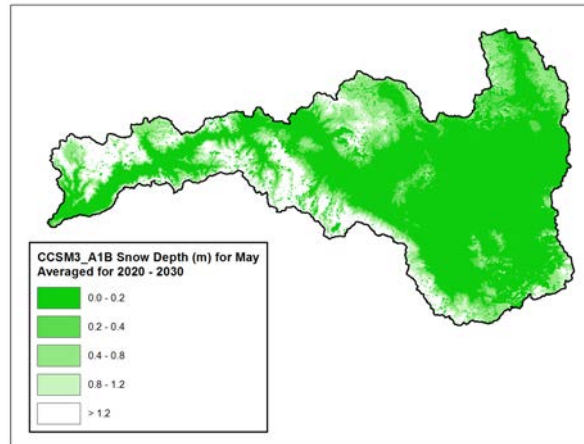
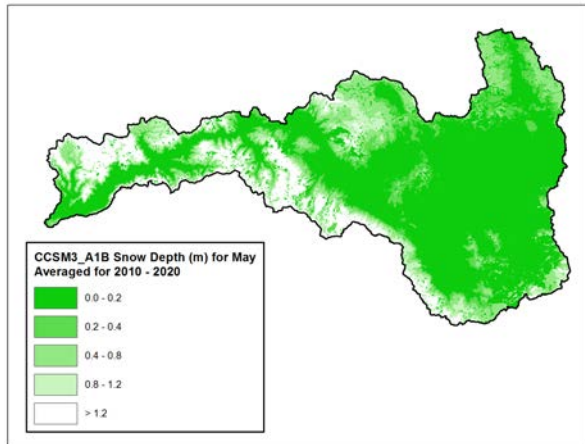
Spatial Distributions of Monthly Average Snow Depths over the Upper Middle Fork Watershed for all 13 Future Projections and their Ensemble Averages, Provided as an Average over Each Decade

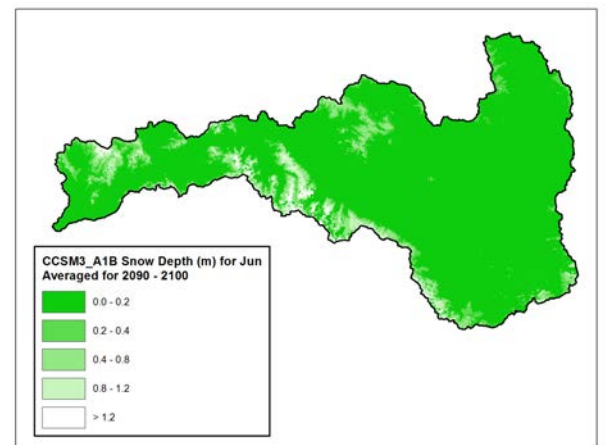
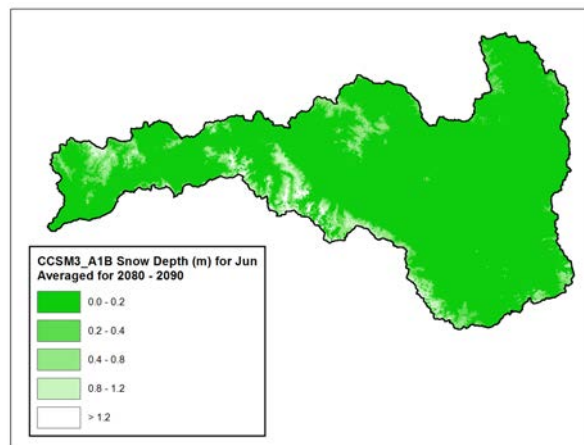
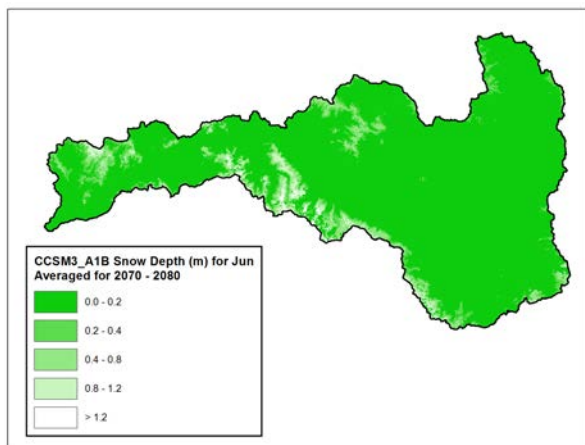
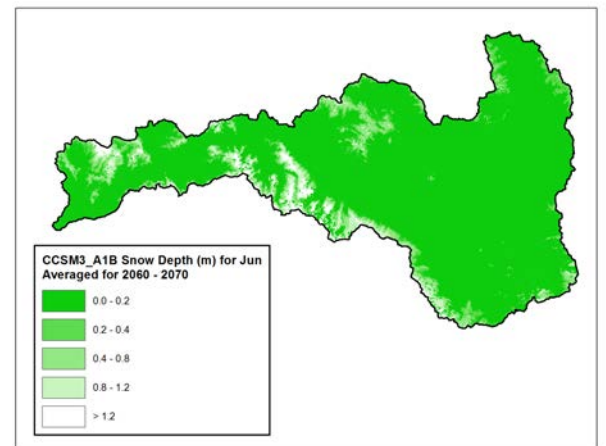
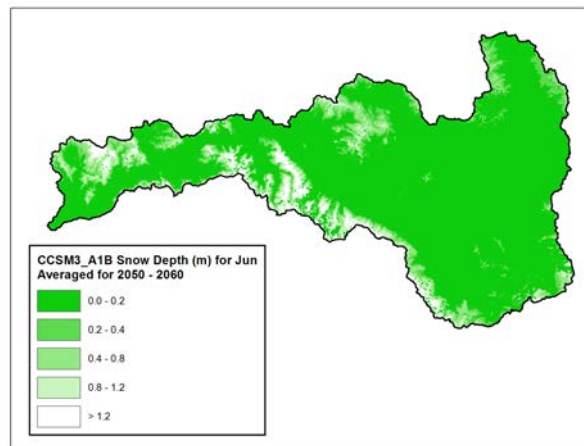
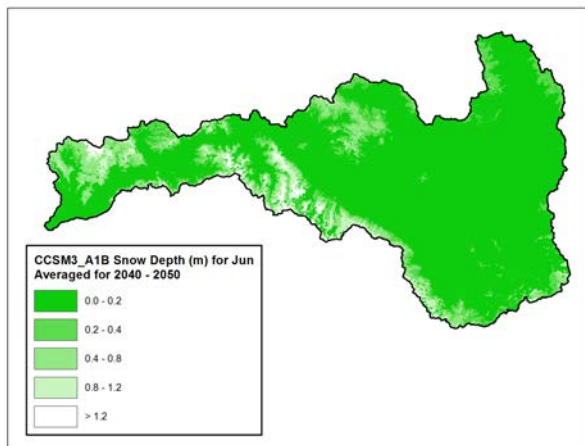
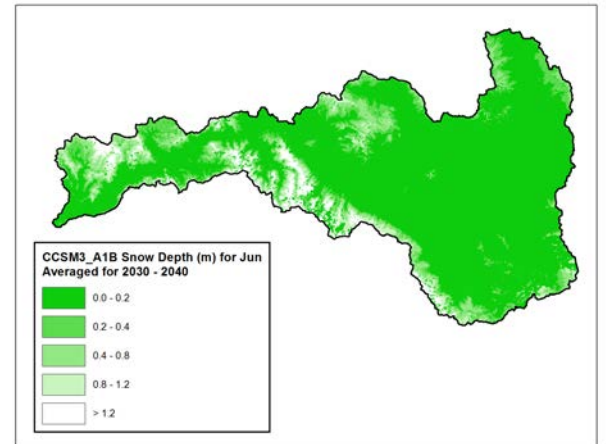
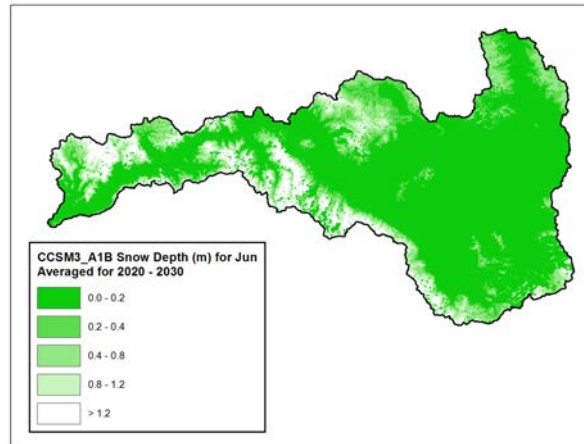
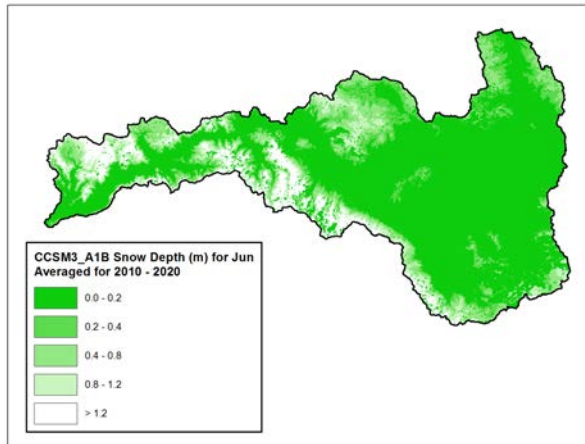


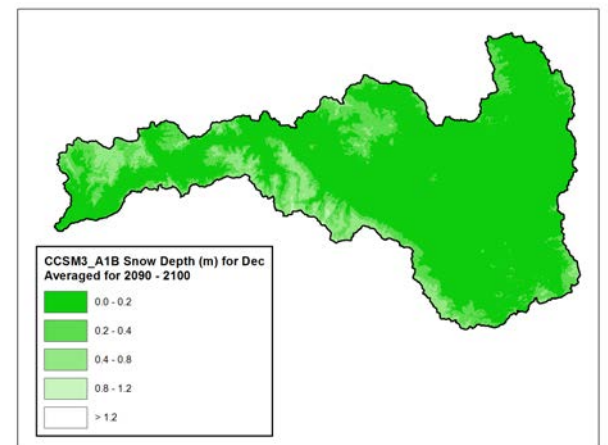
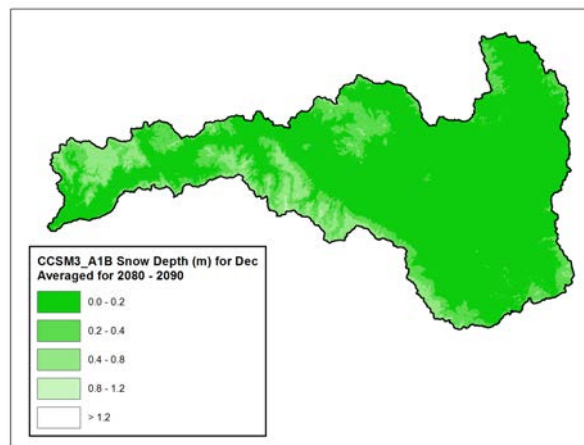
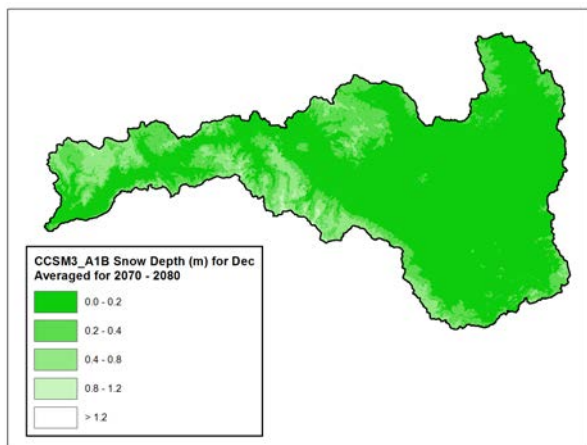
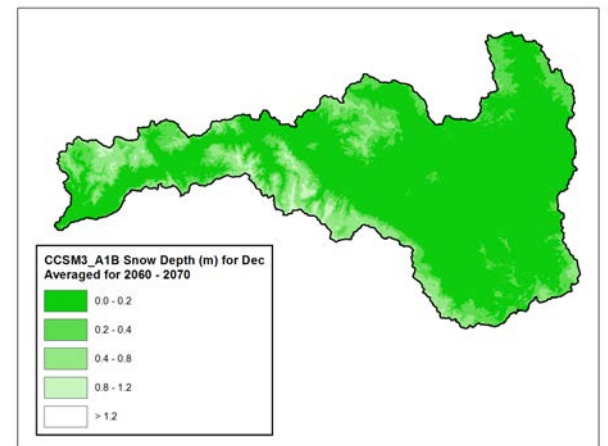
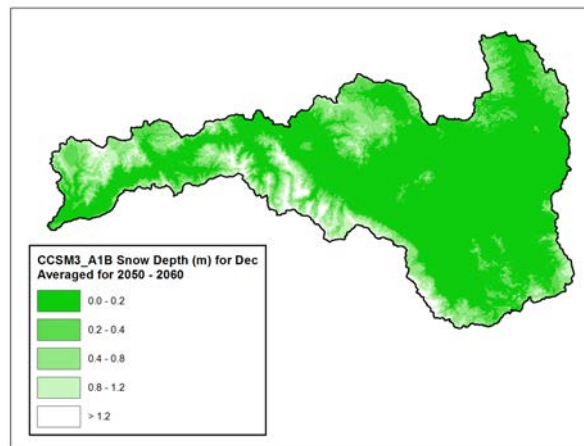
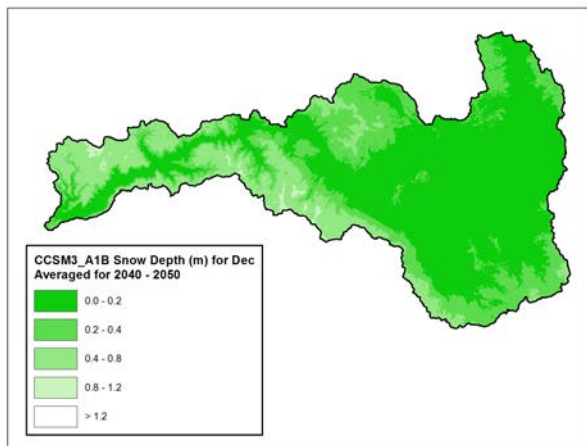
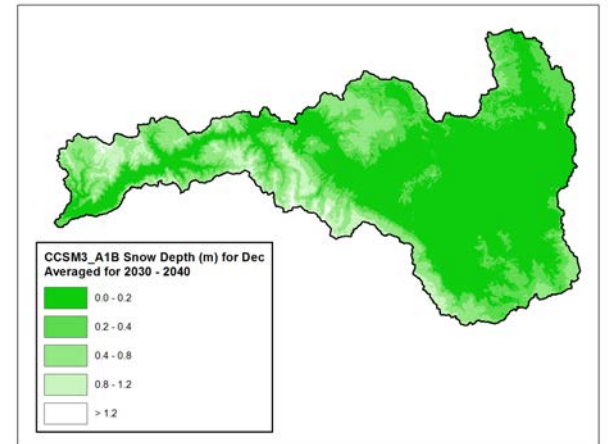
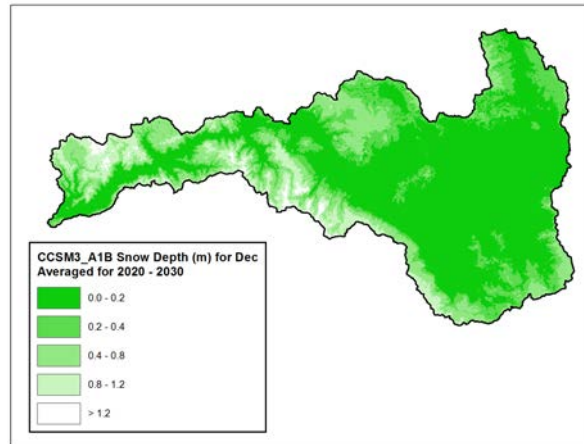
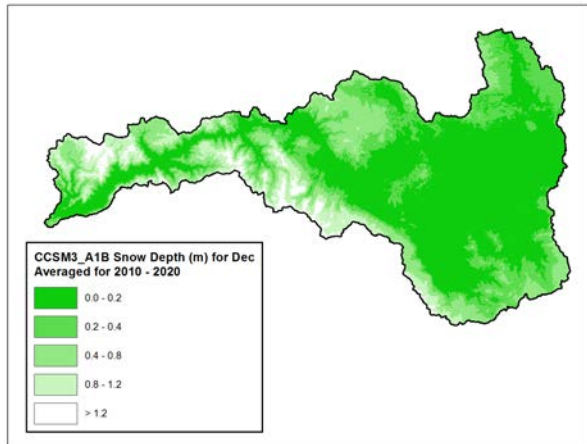


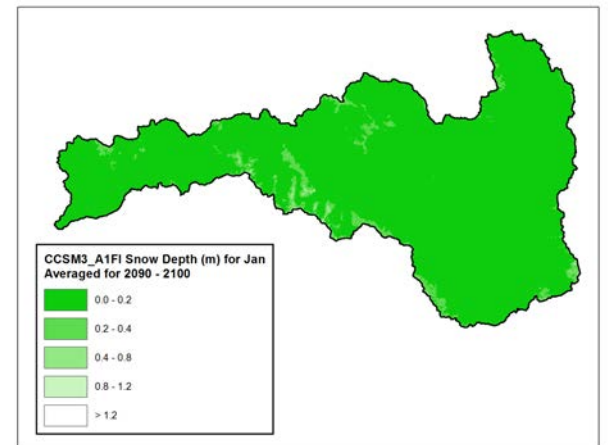
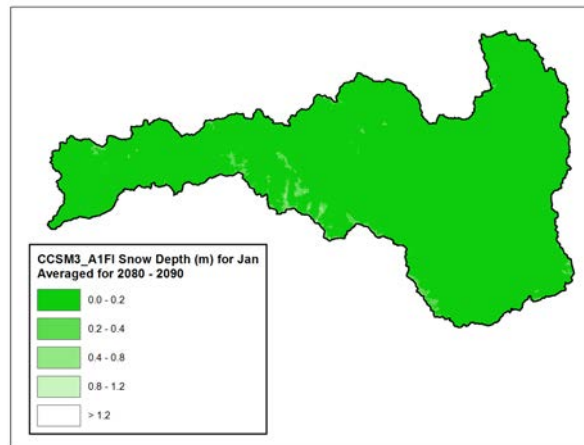
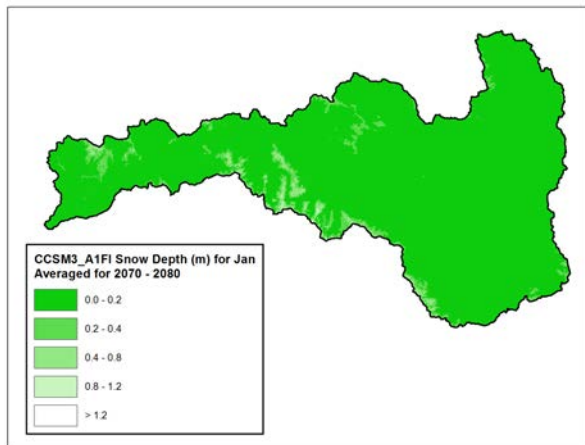
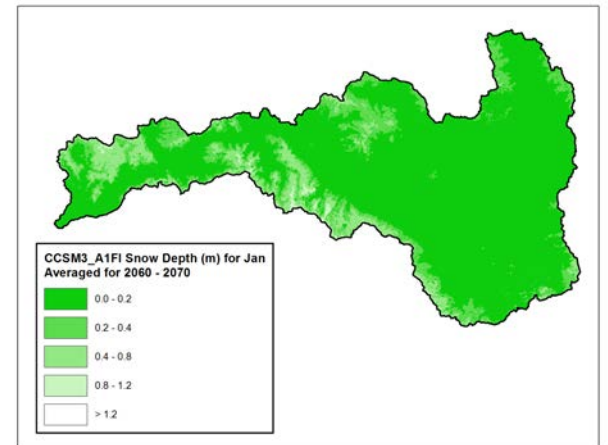
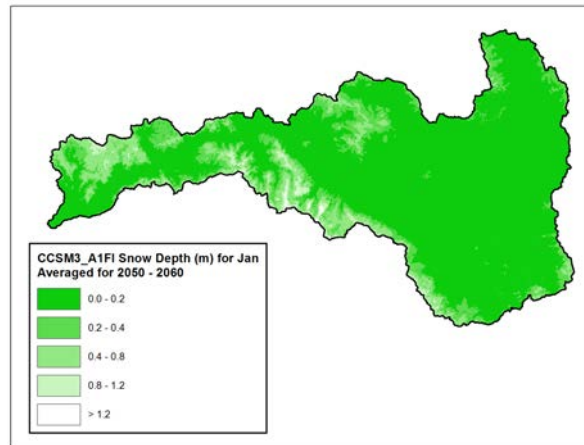
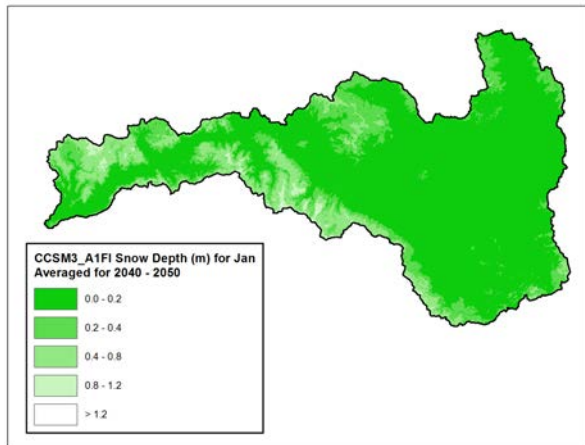
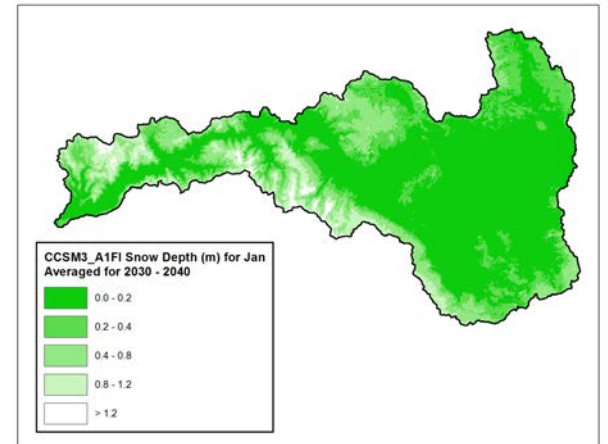
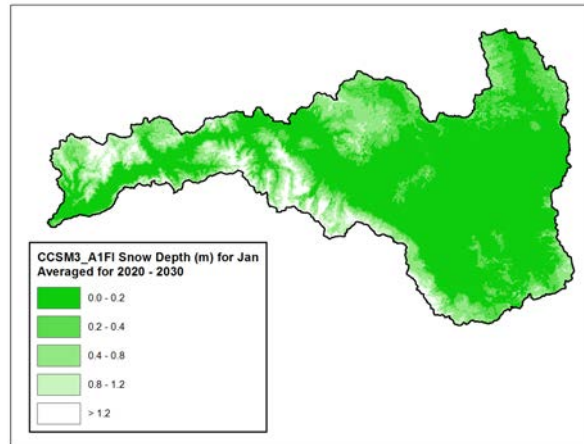
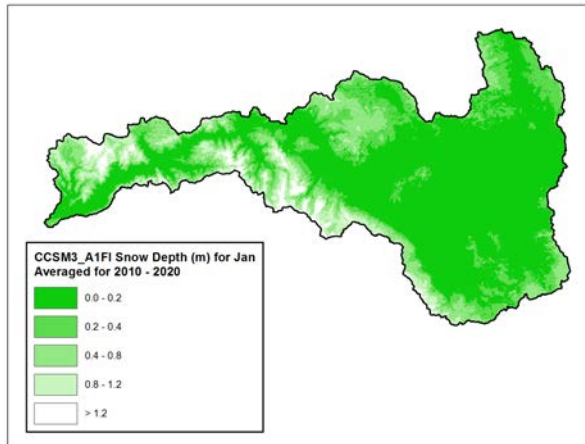


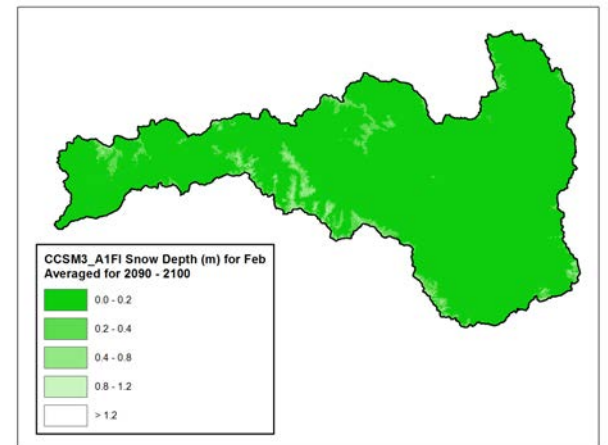
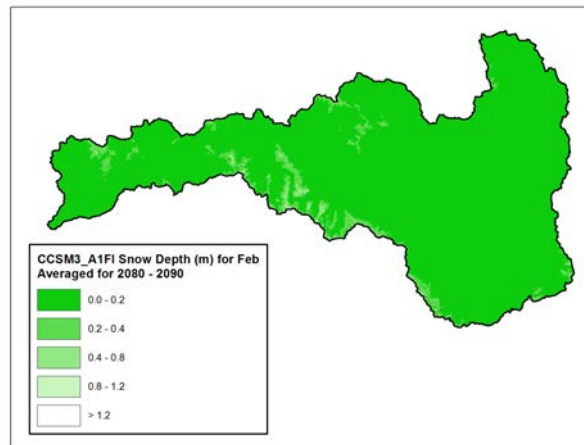
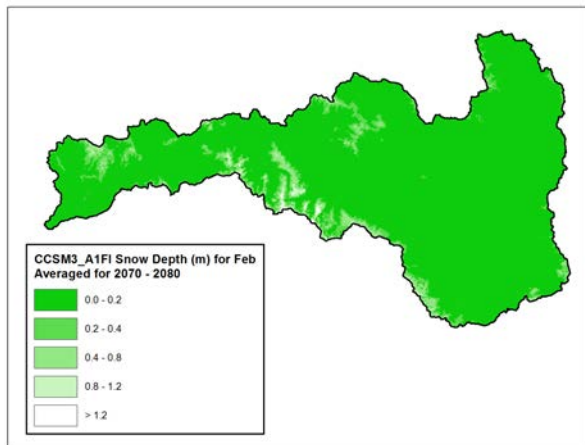
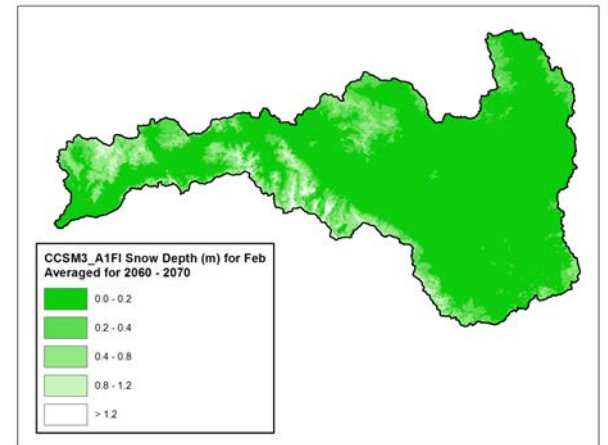
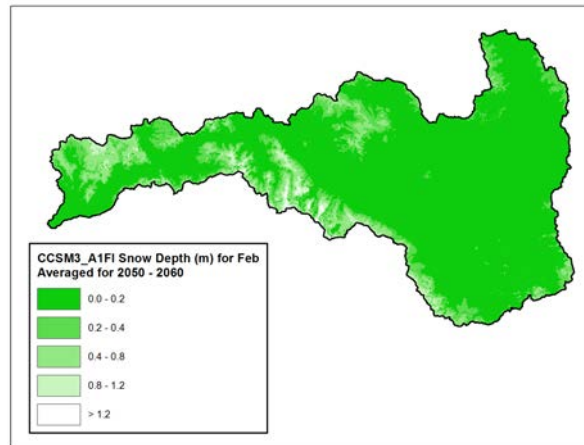
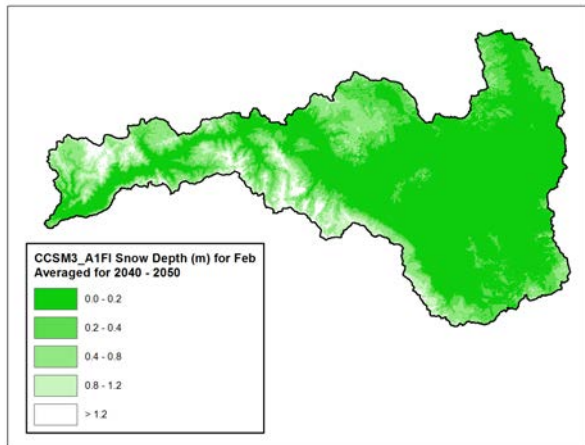
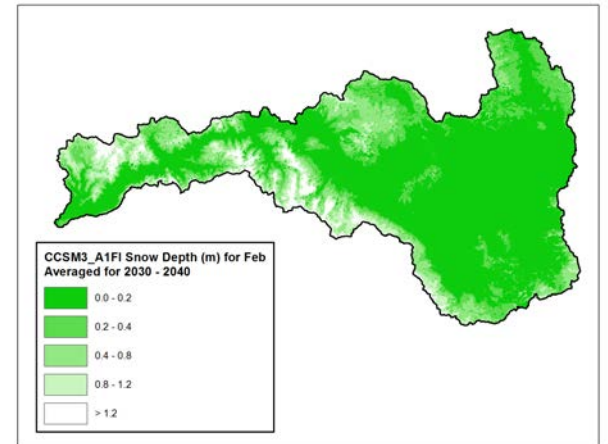
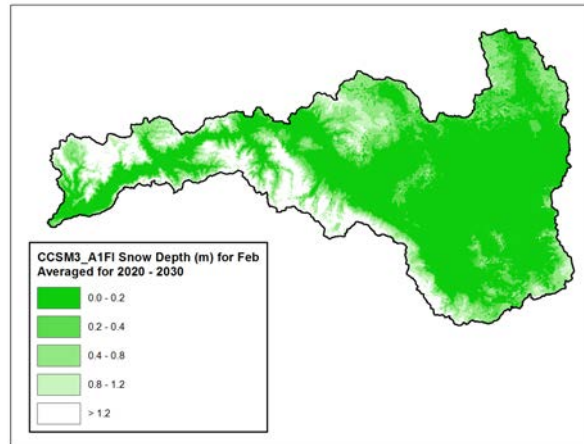
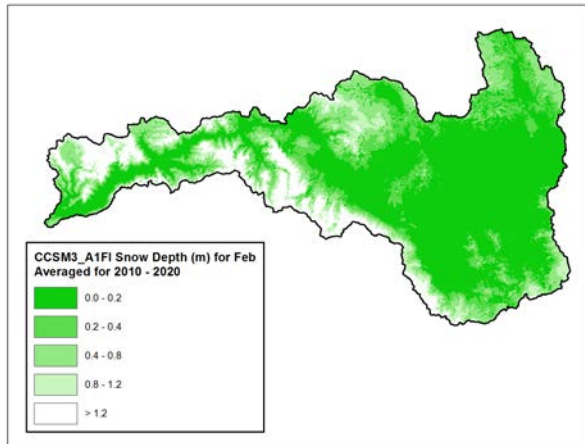


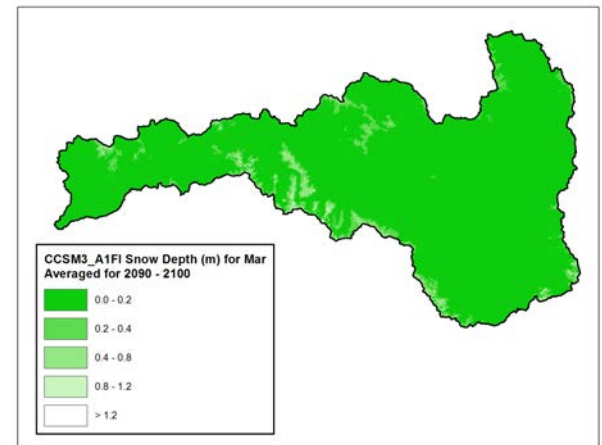
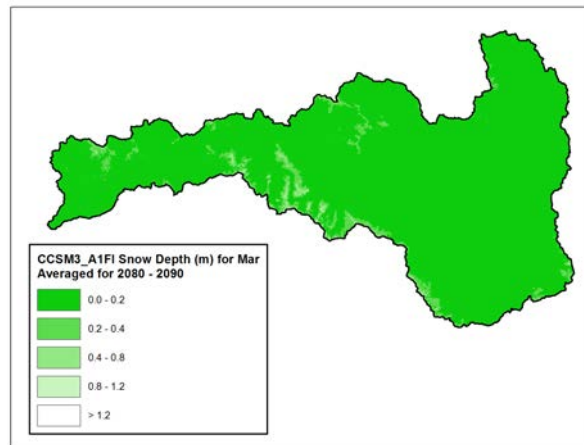
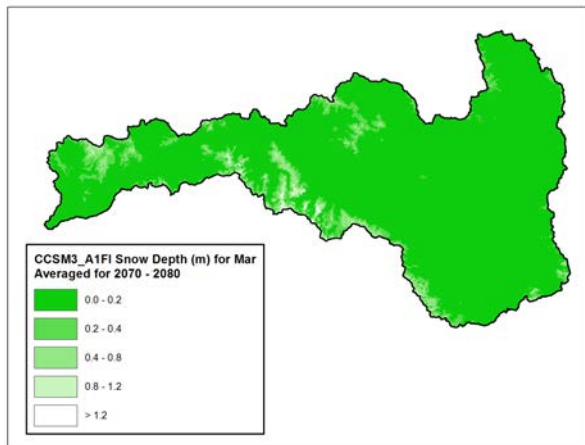
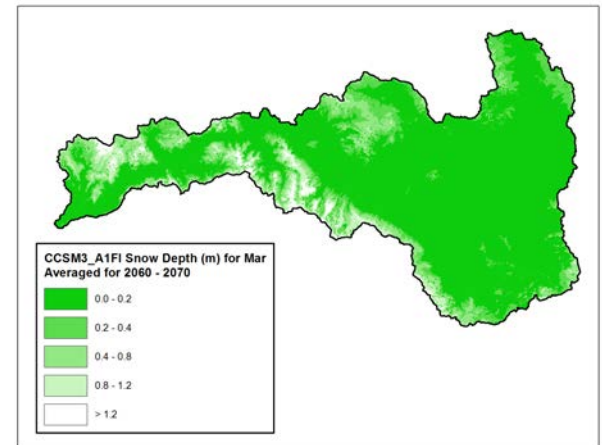
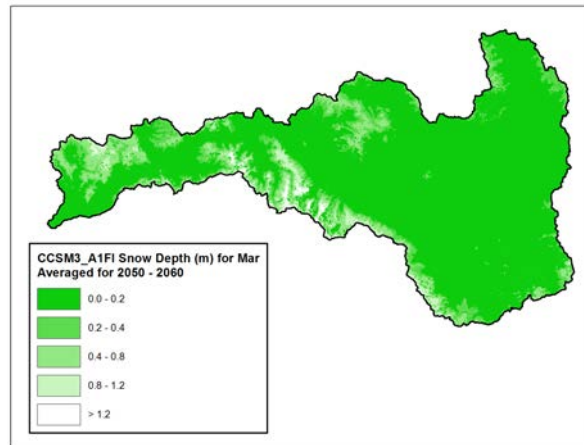
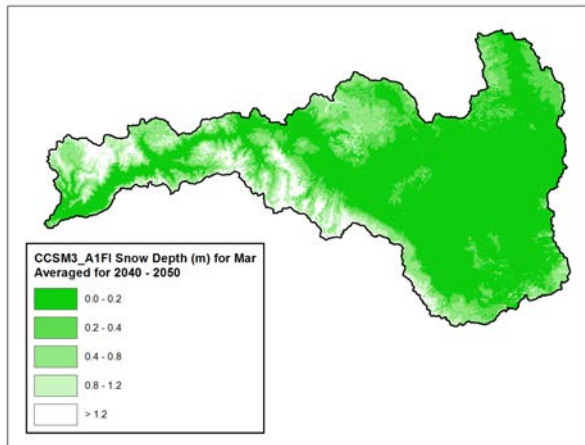
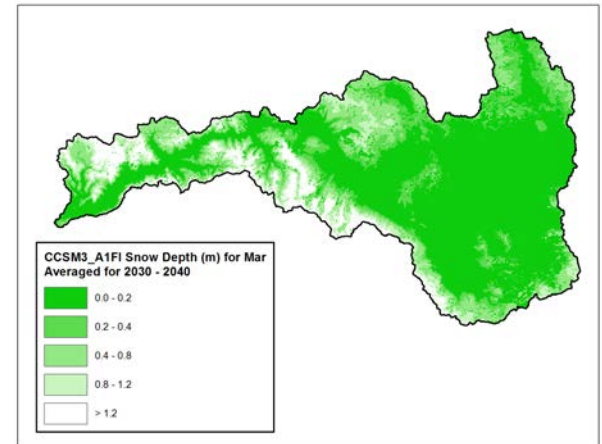
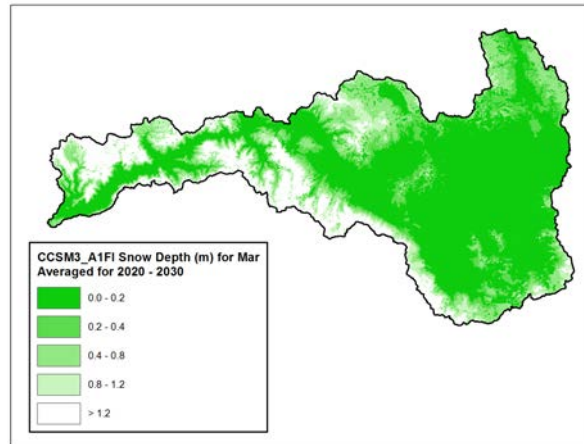
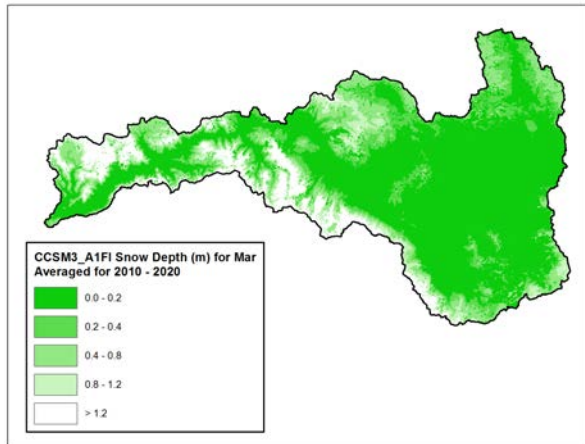


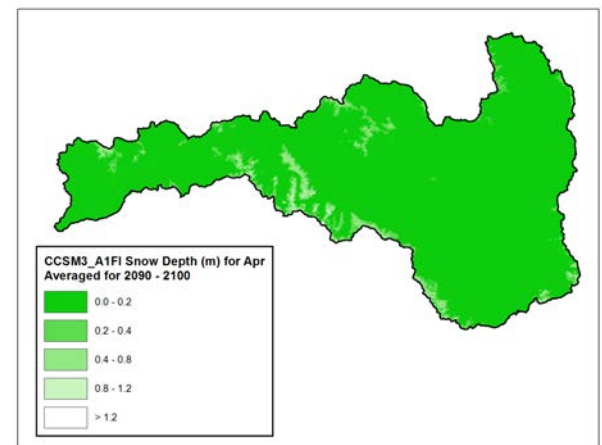
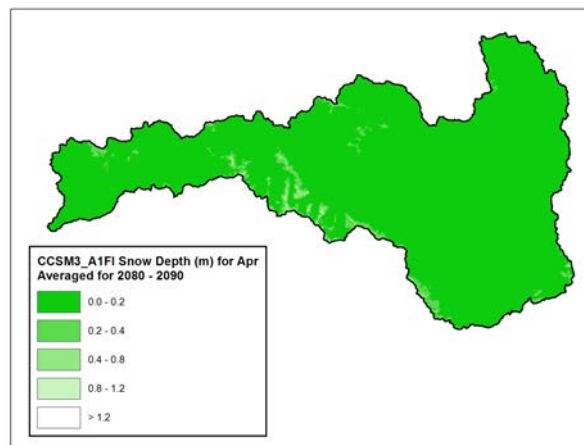
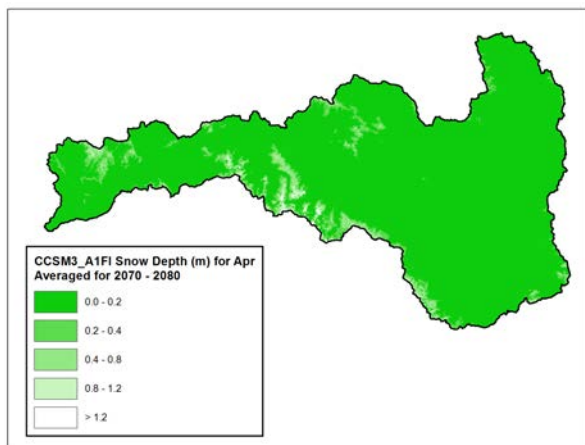
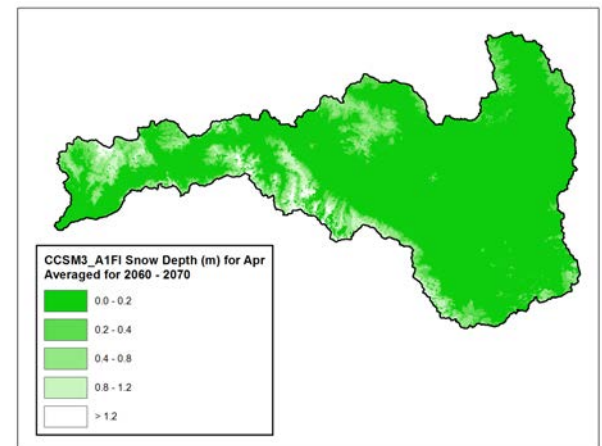
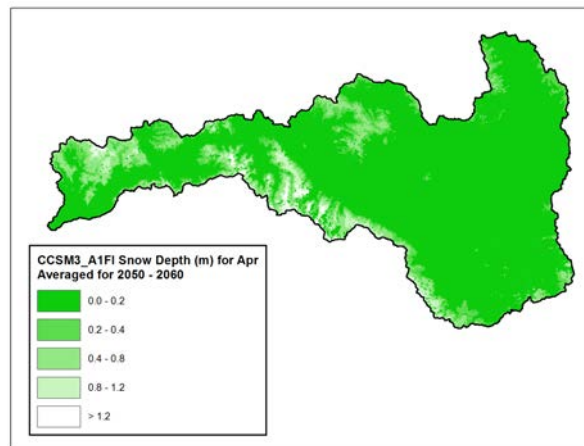
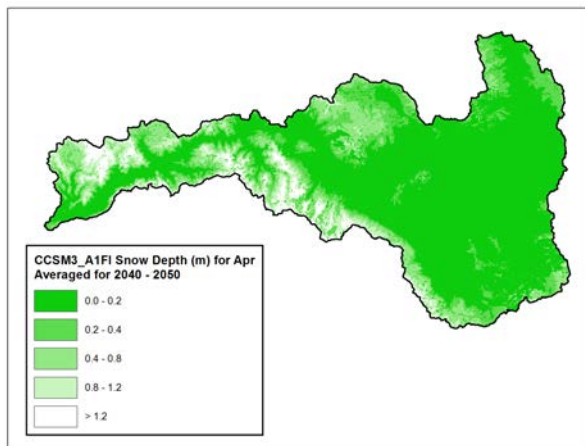
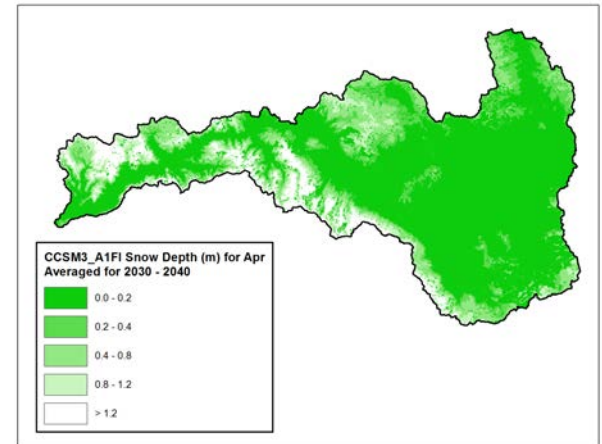
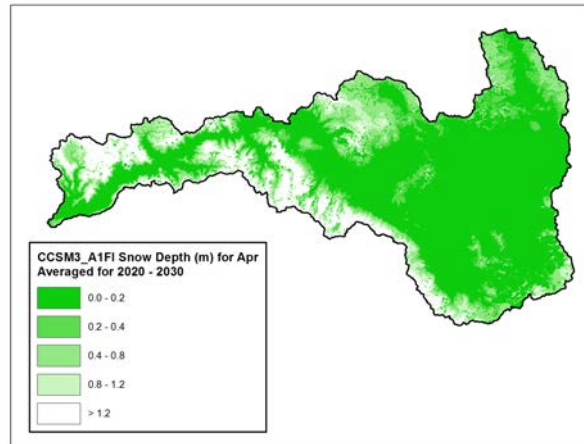
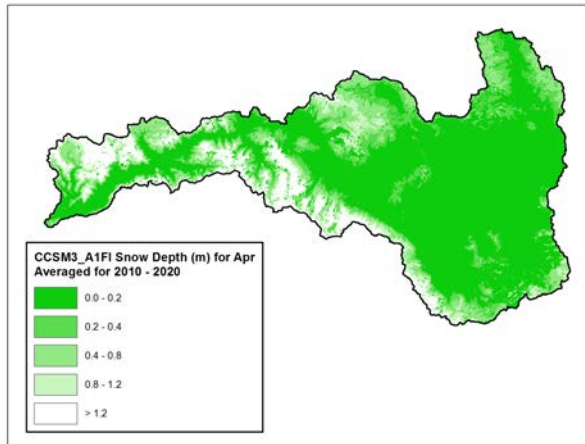


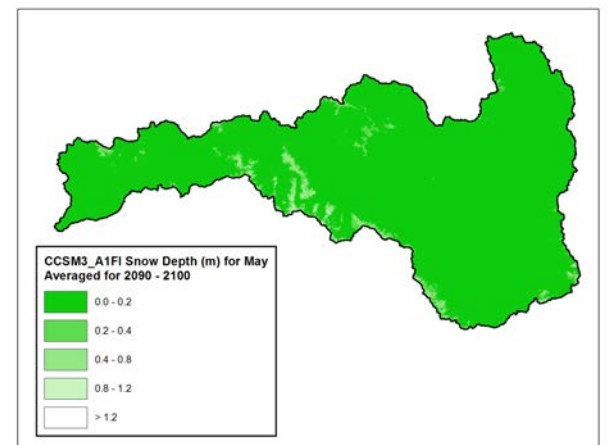
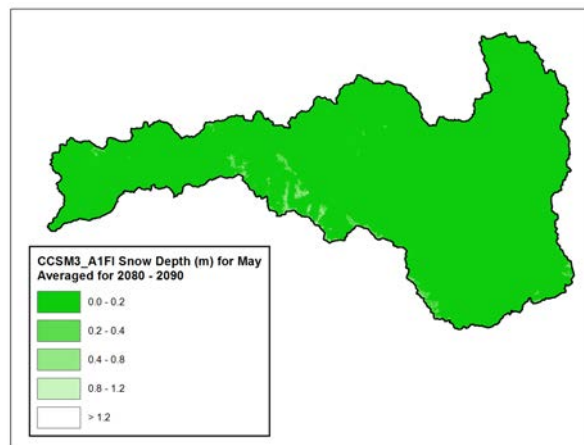
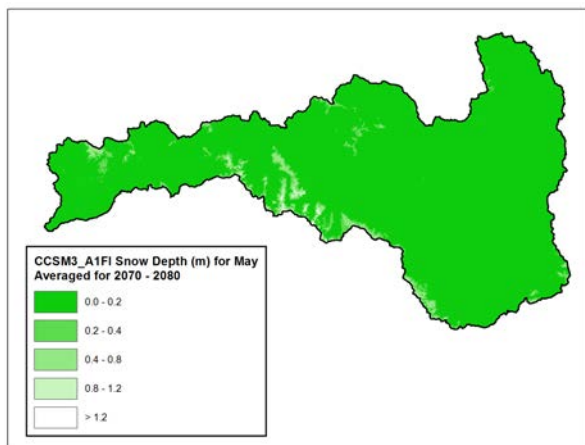
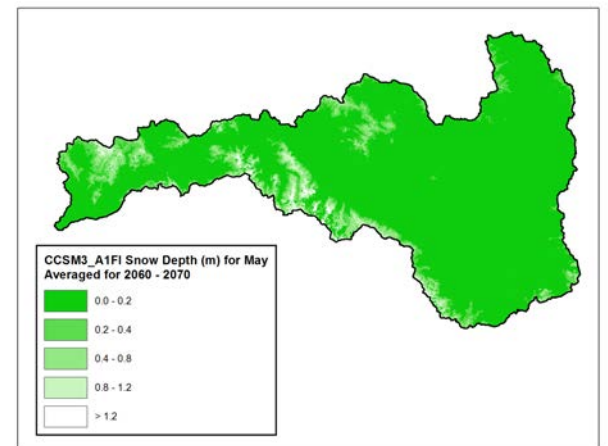
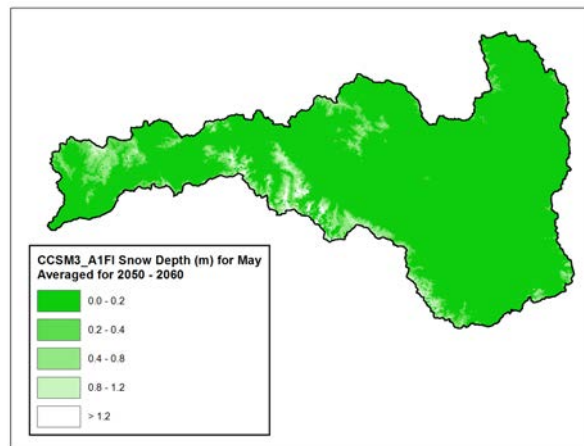
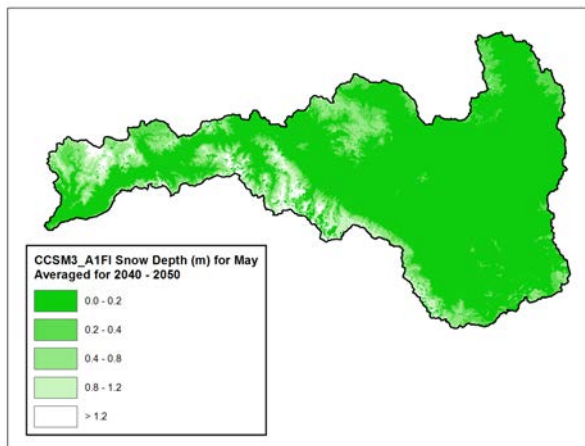
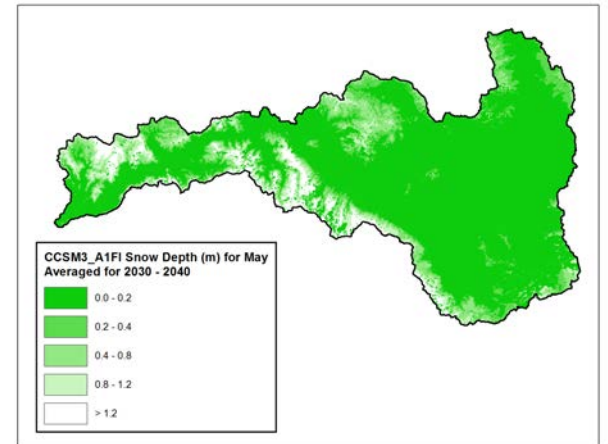
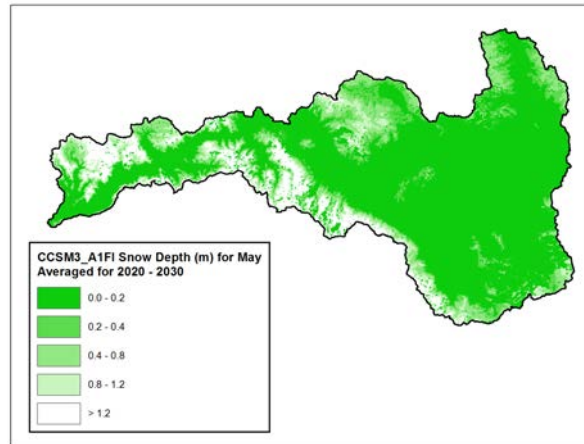
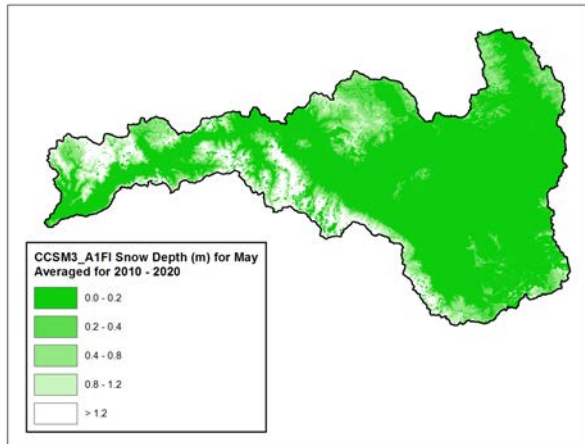


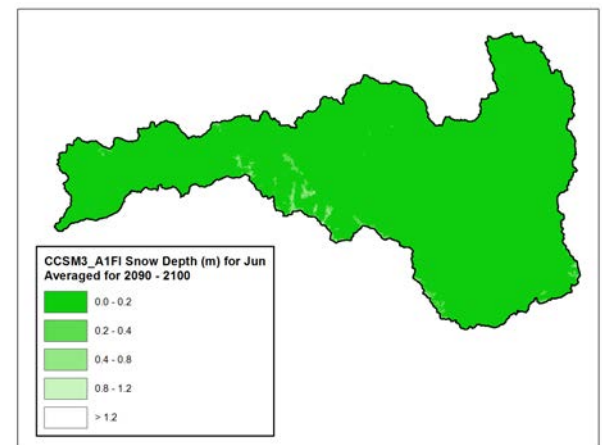
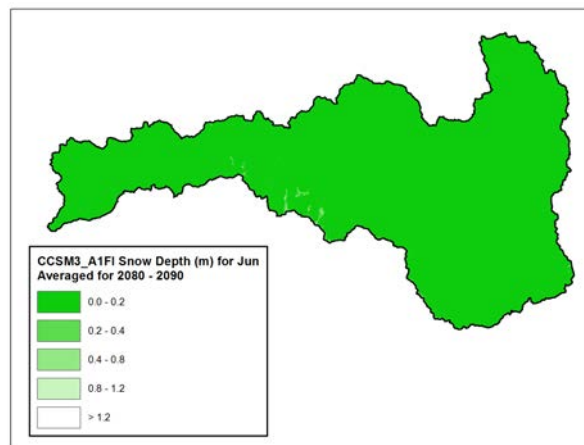
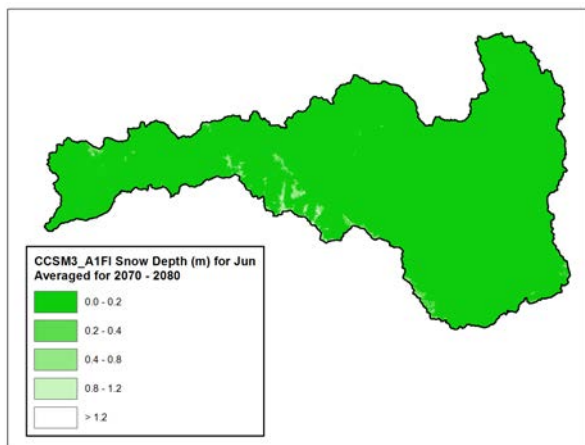
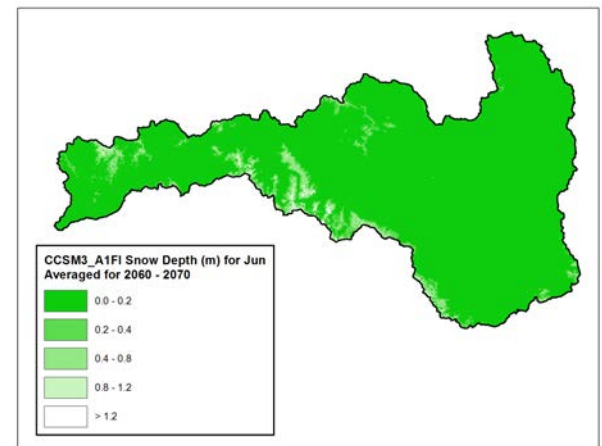
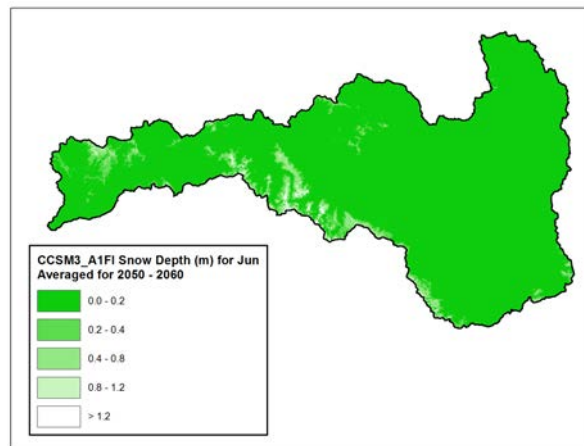
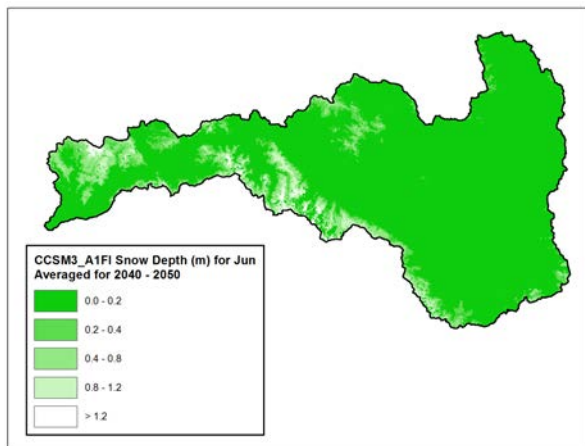
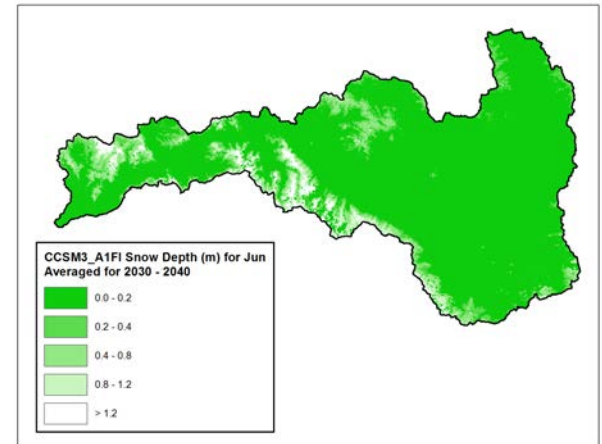
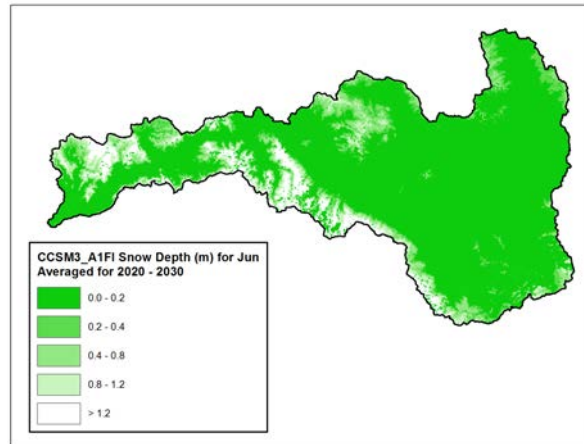
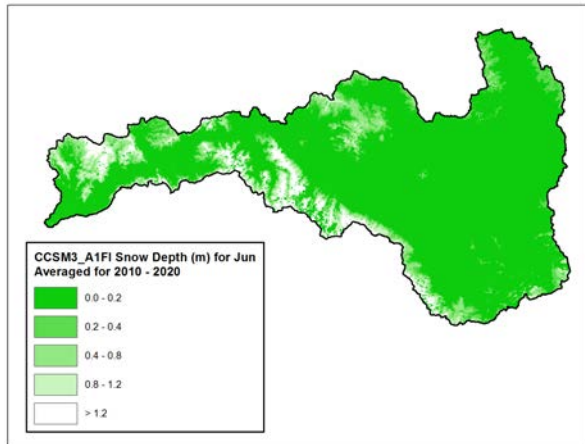


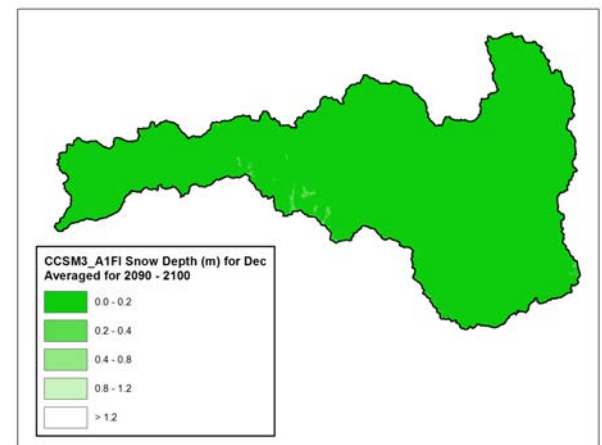
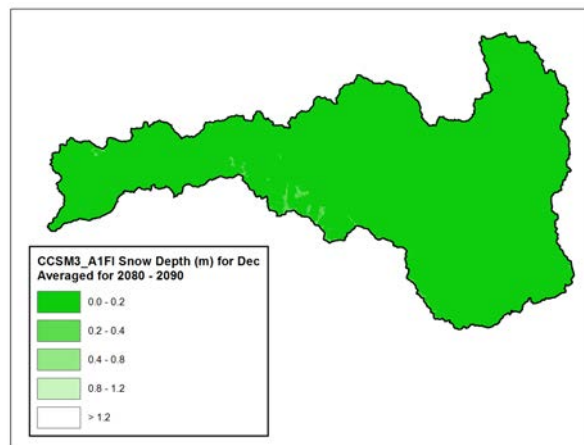
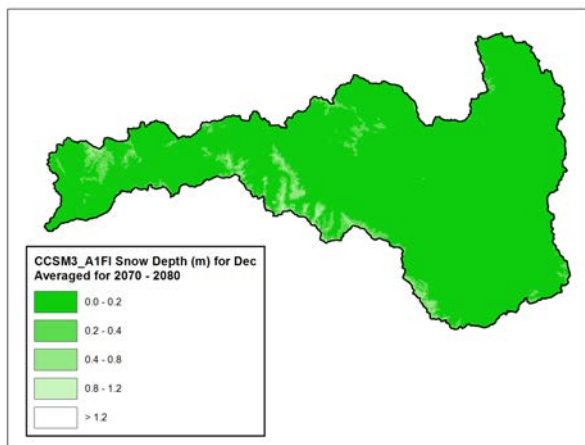
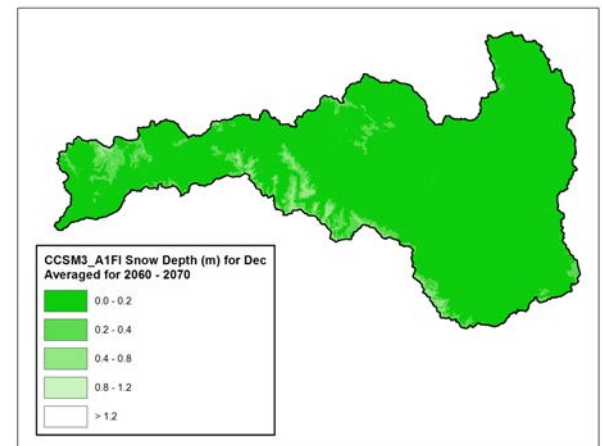
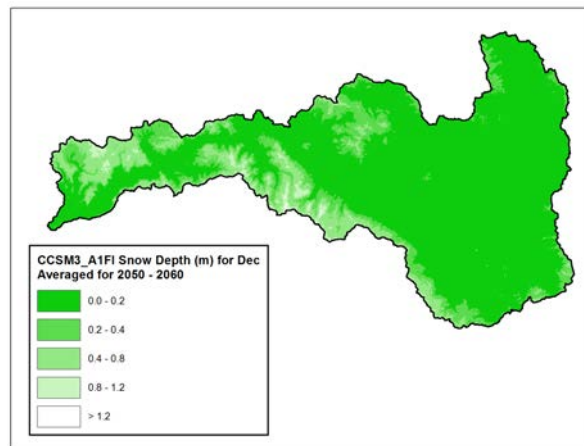
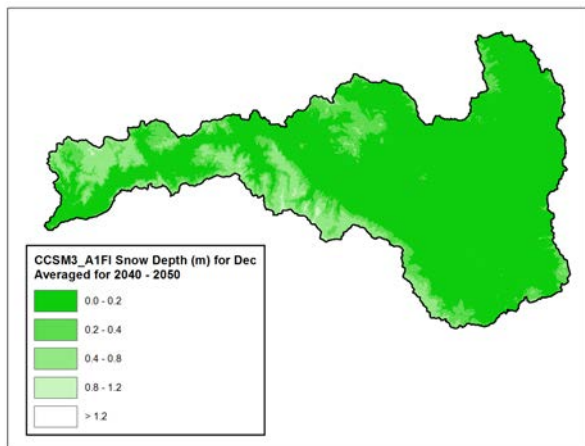
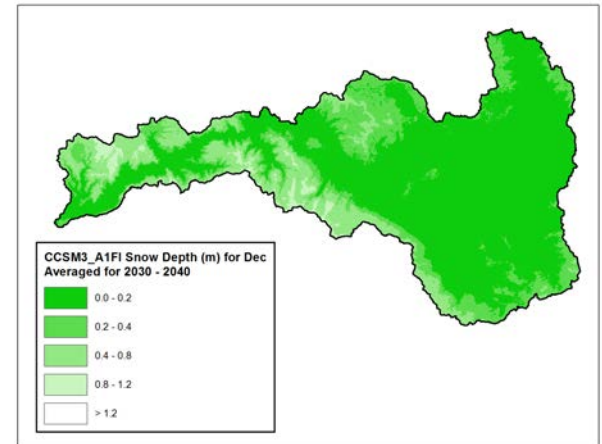
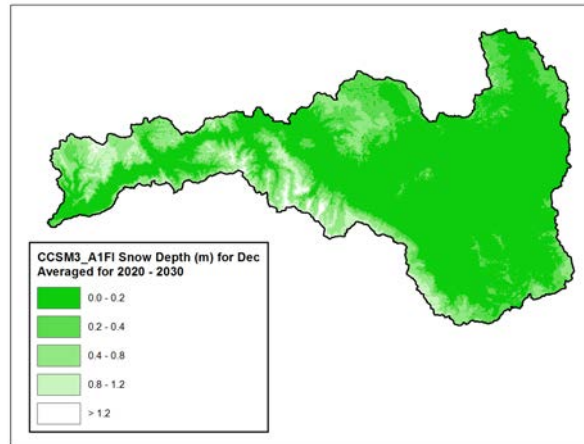
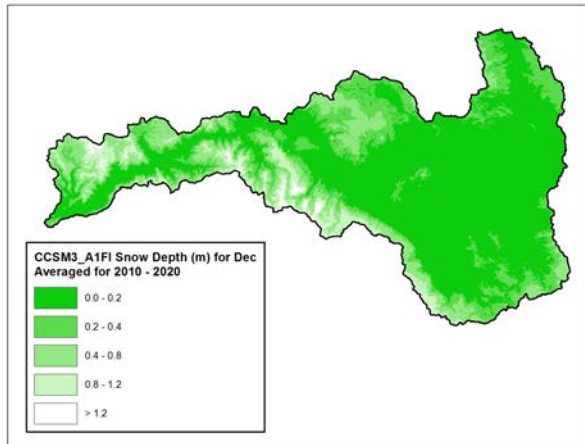


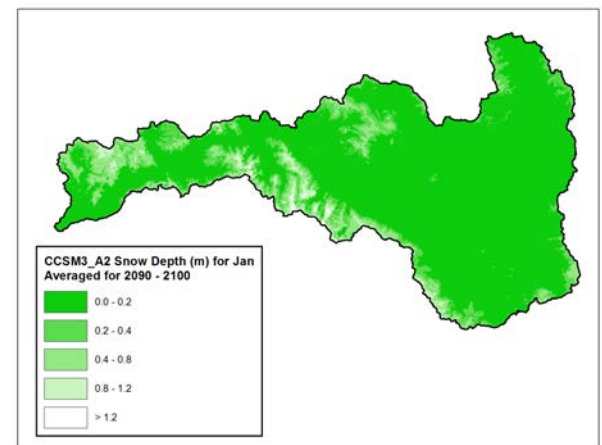
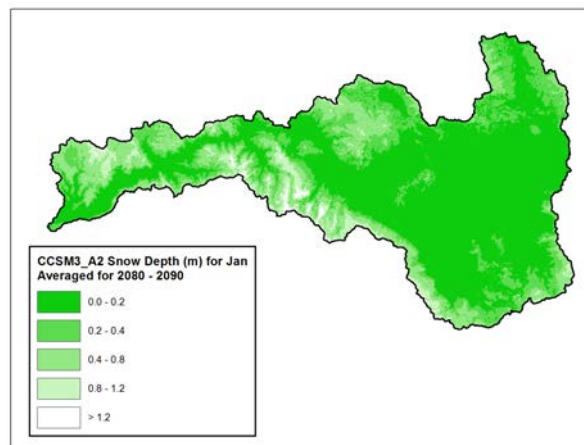
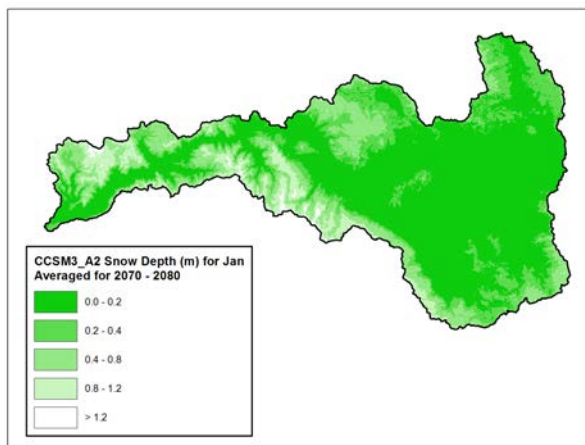
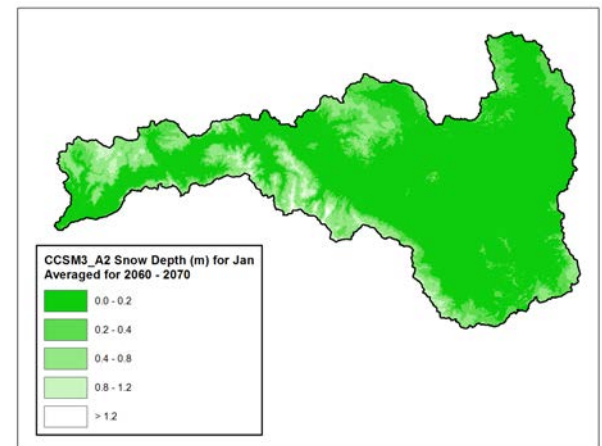
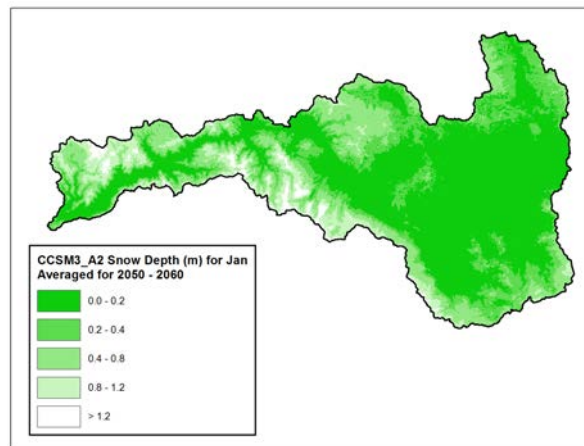
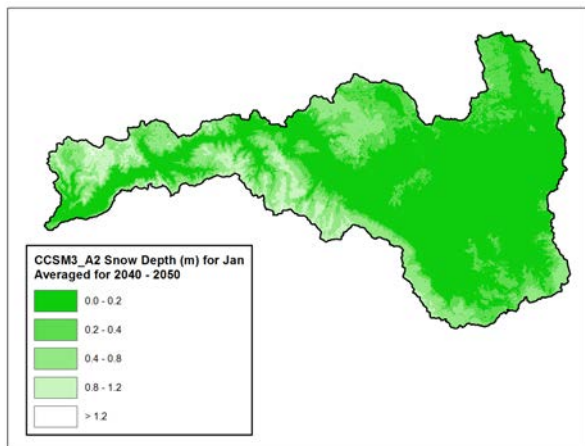
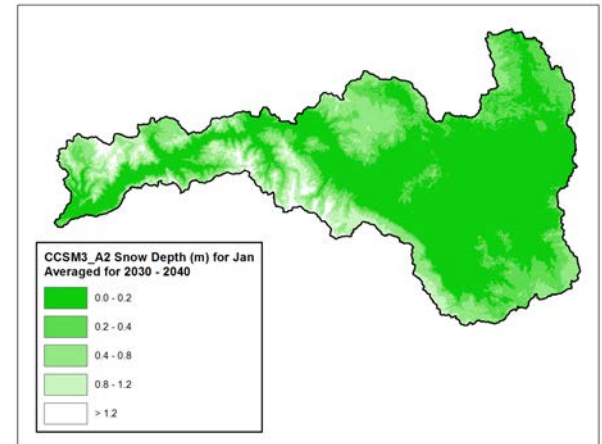
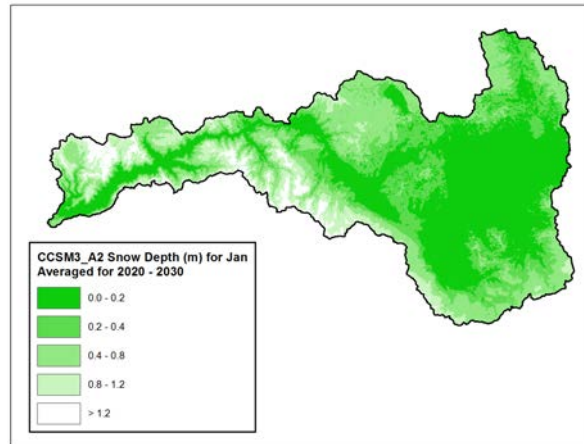
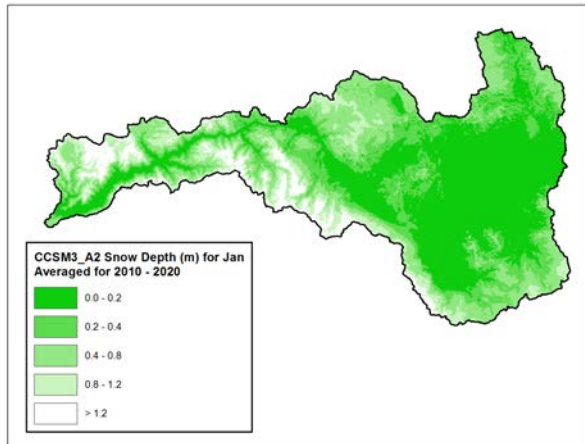


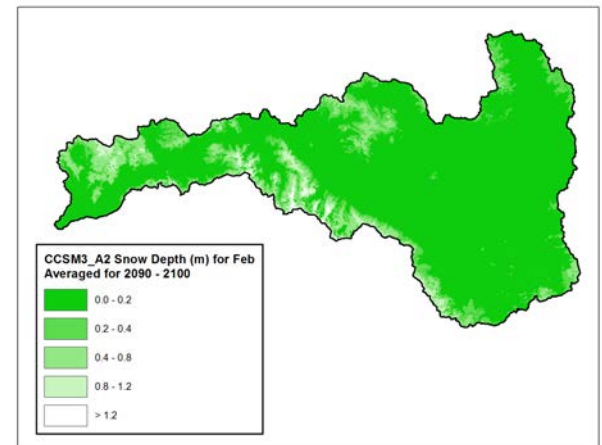
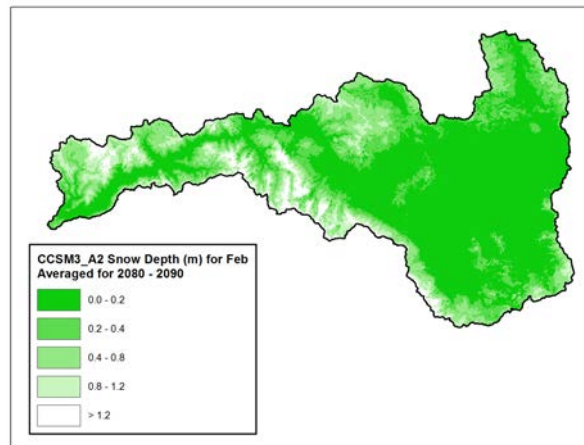
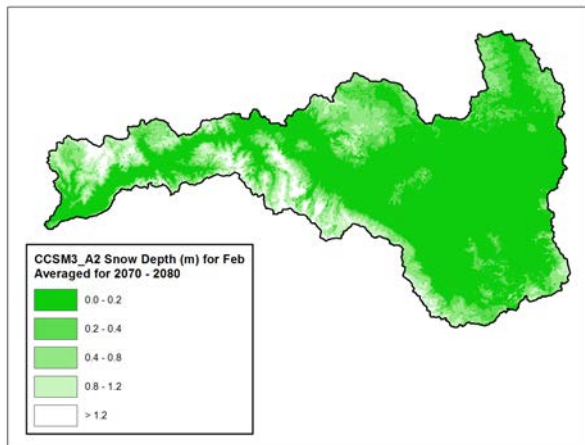
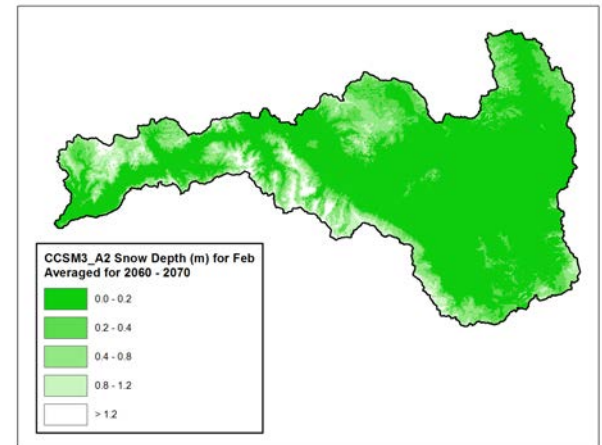
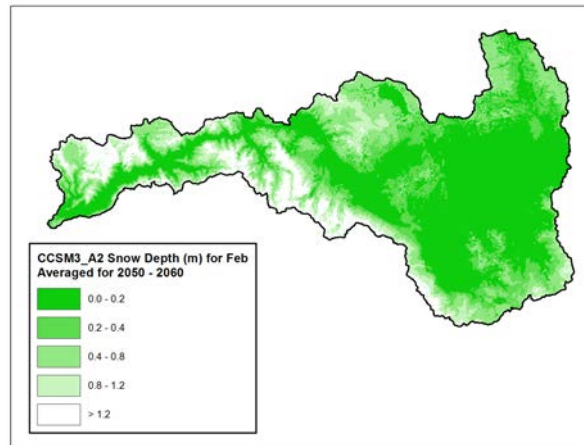
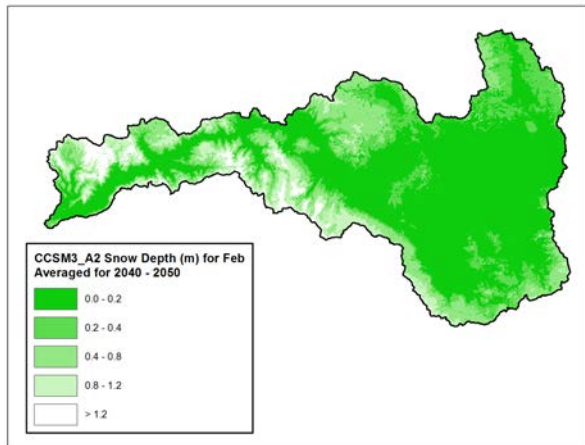
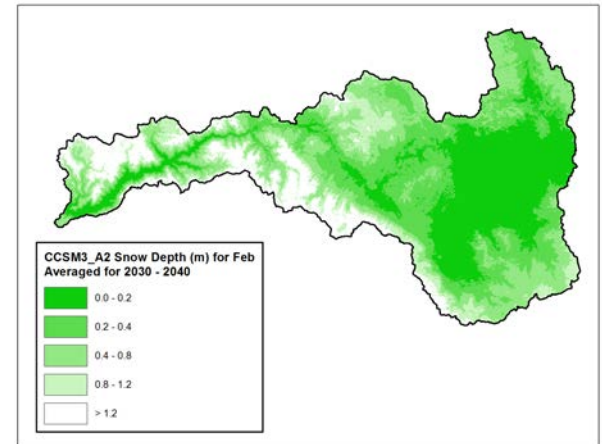
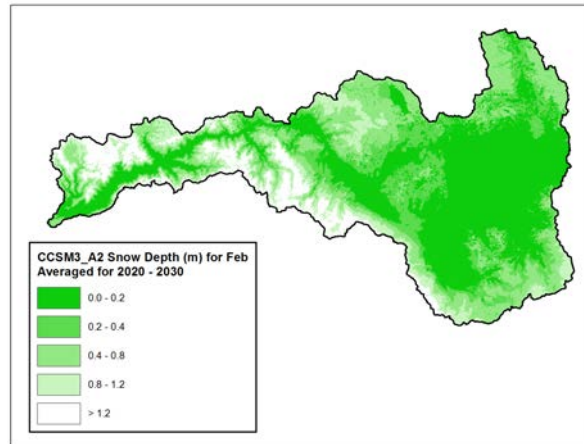
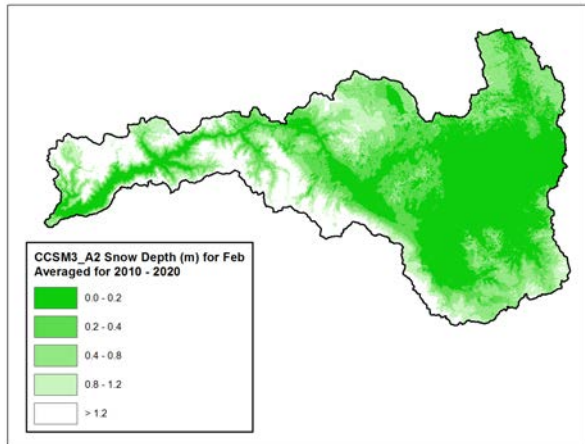


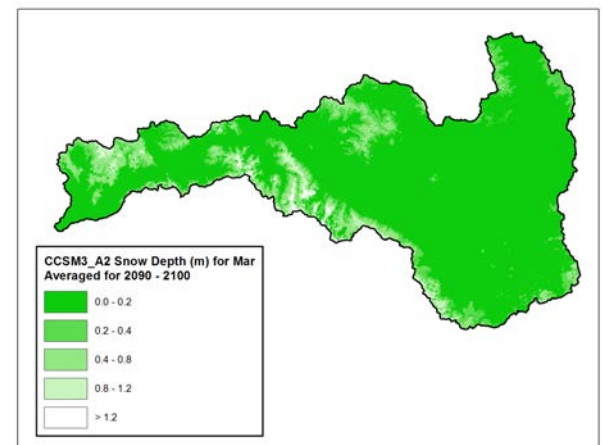
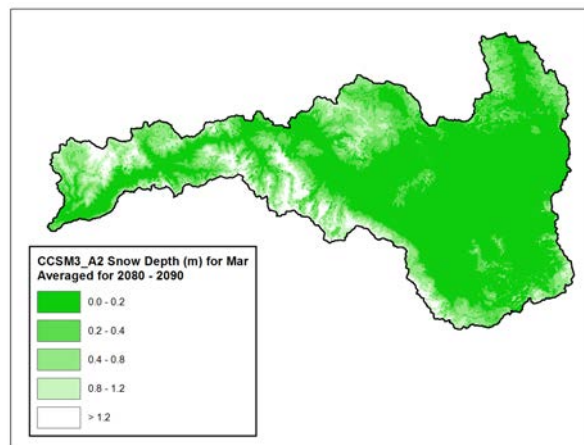
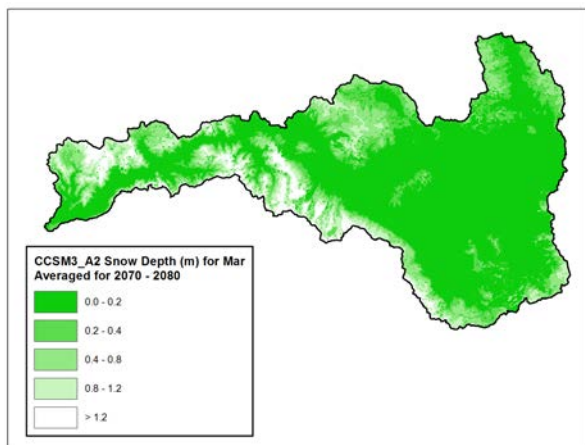
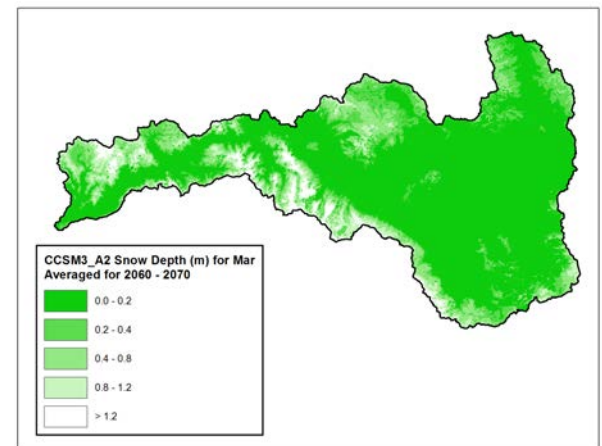
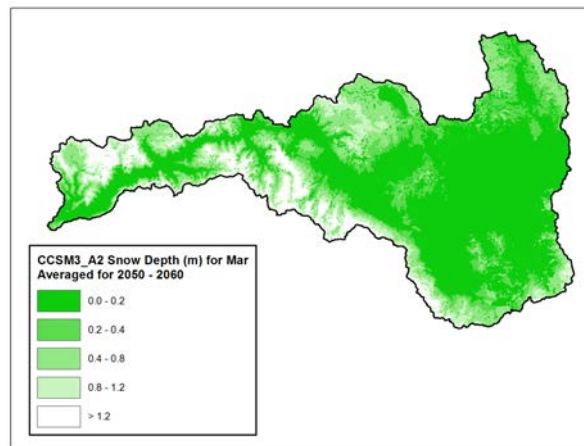
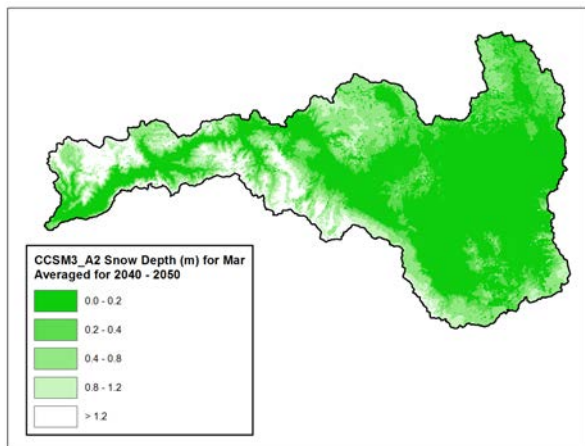
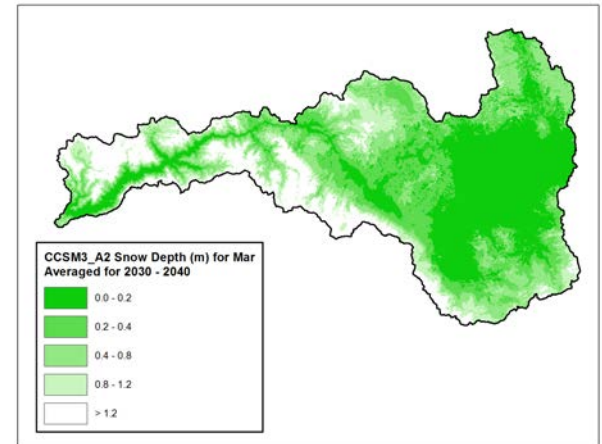
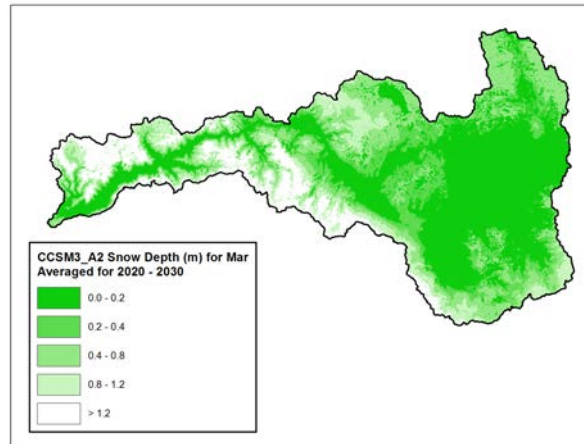
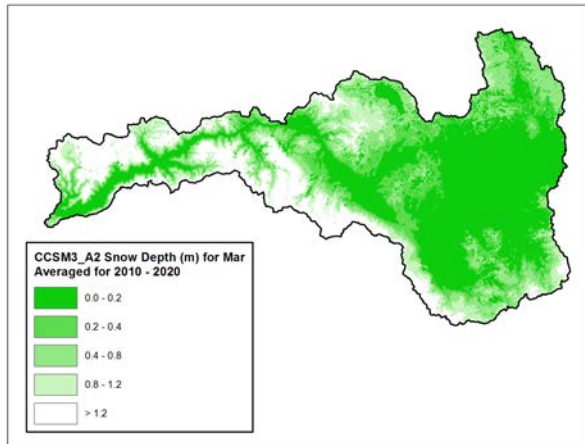


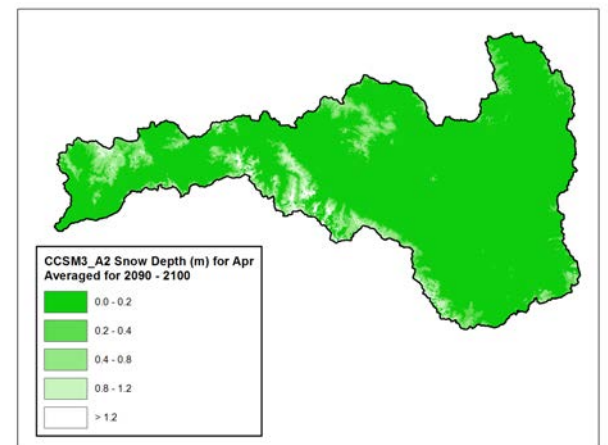
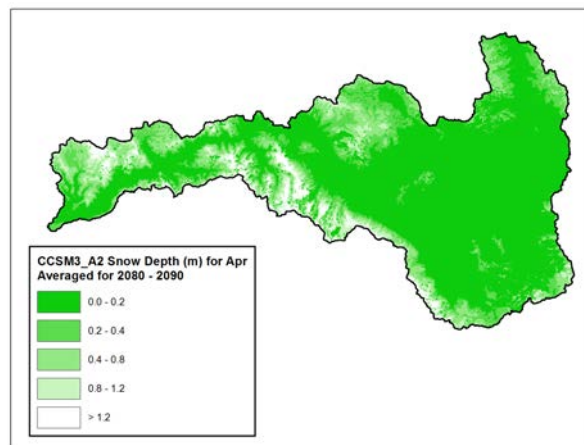
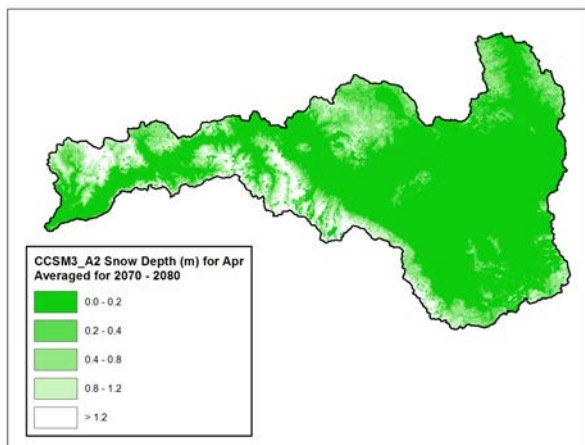
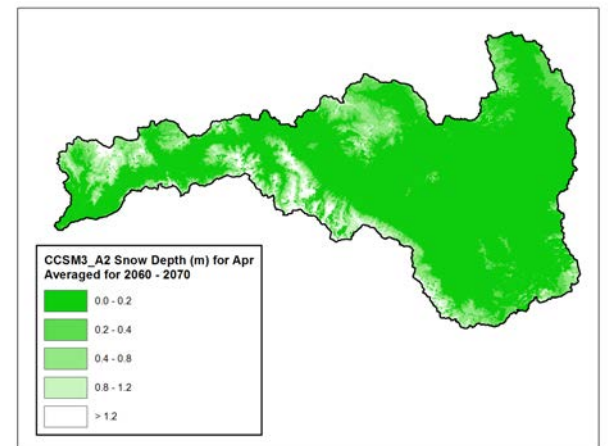
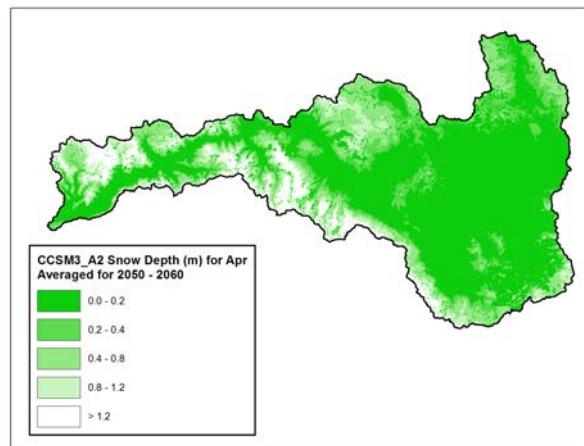
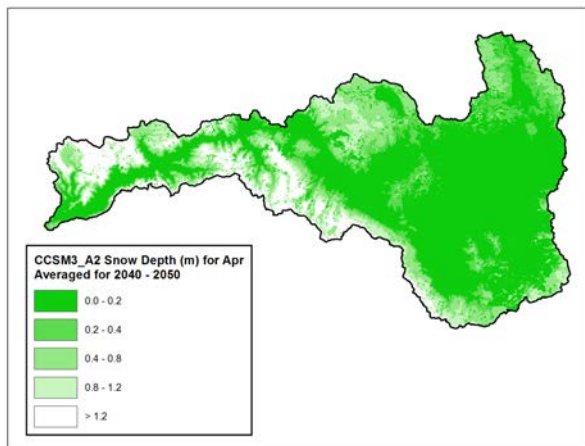
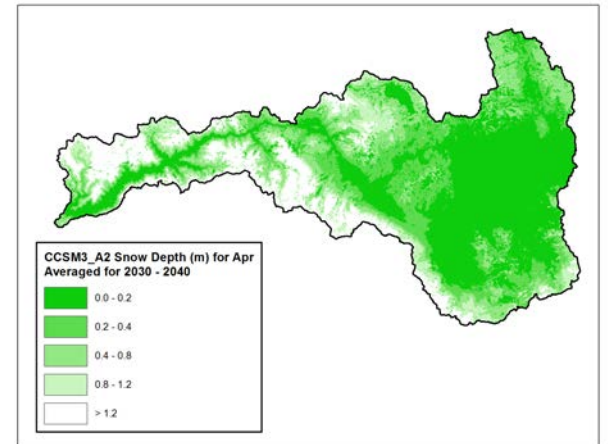
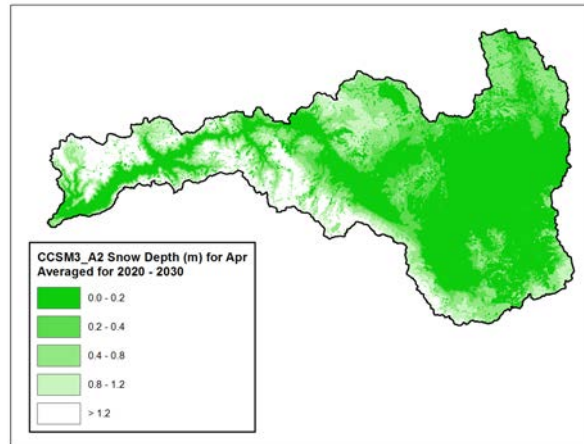
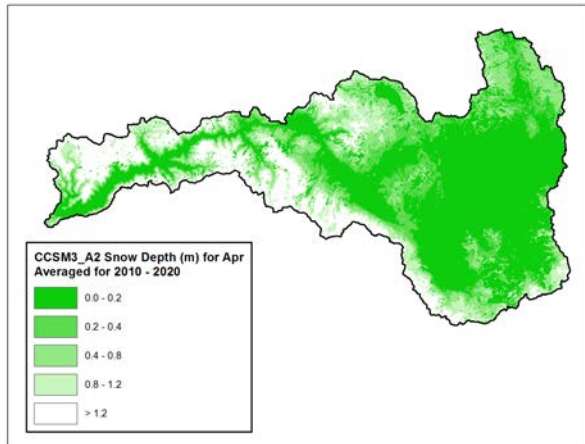


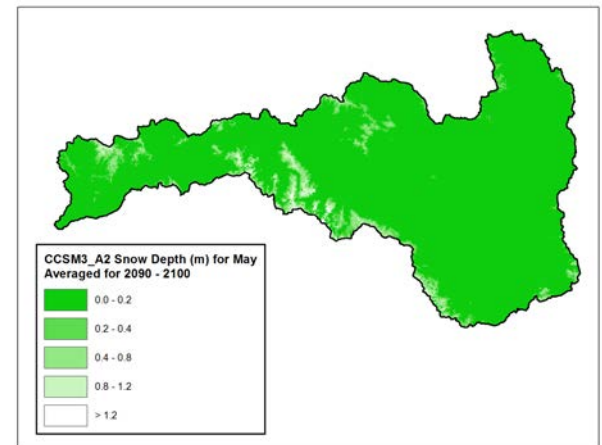
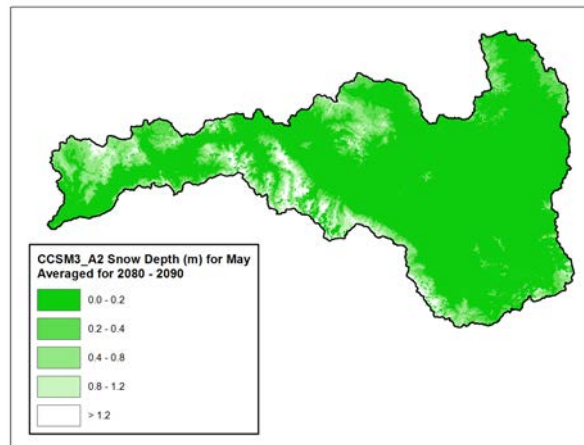
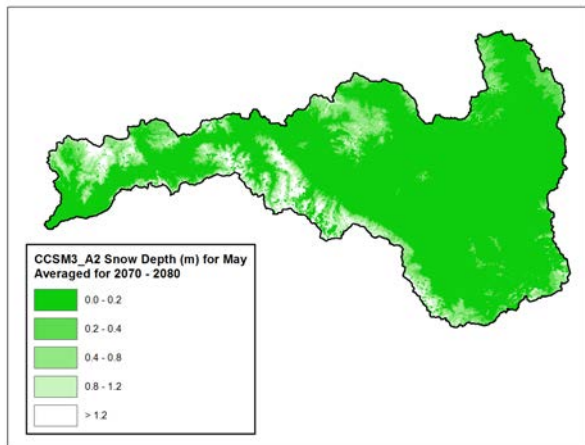
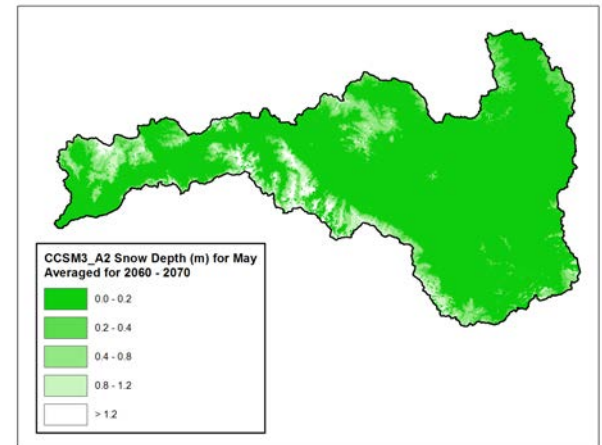
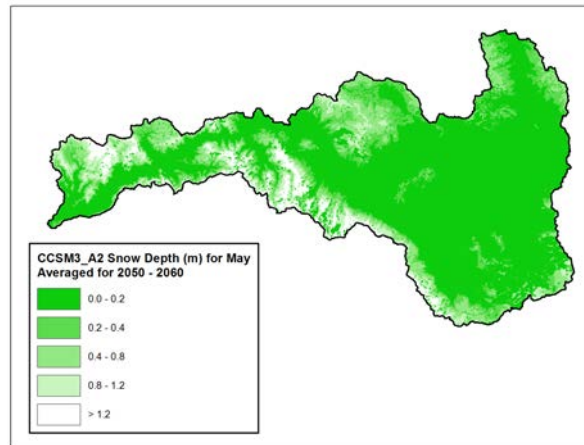
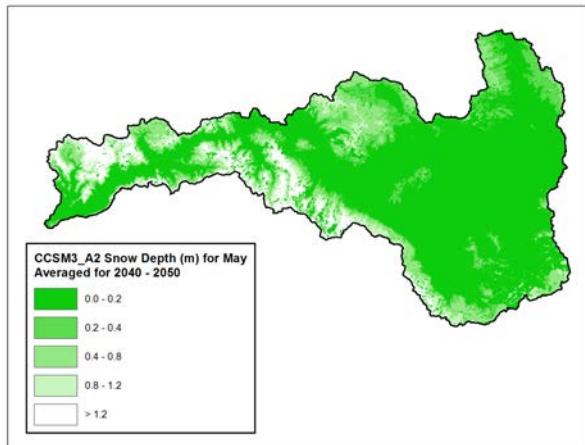
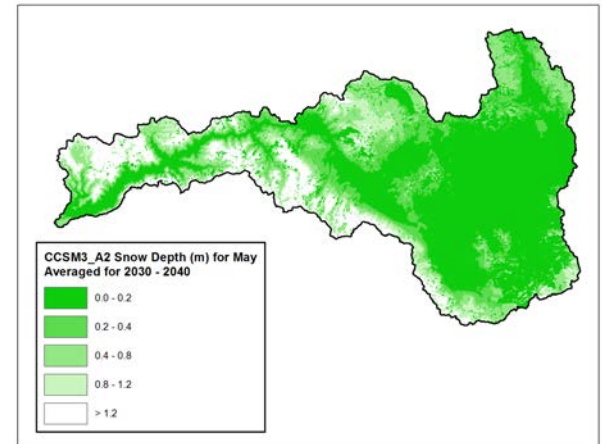
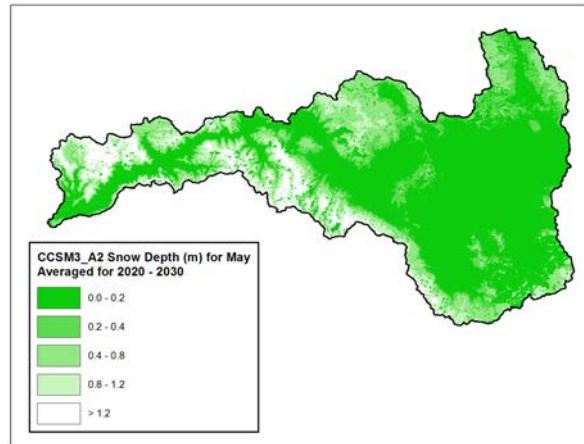
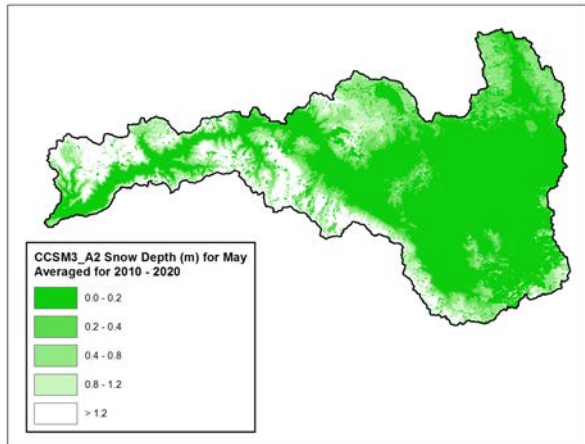


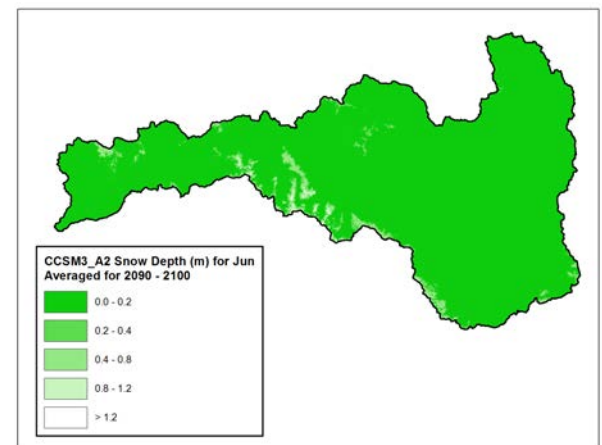
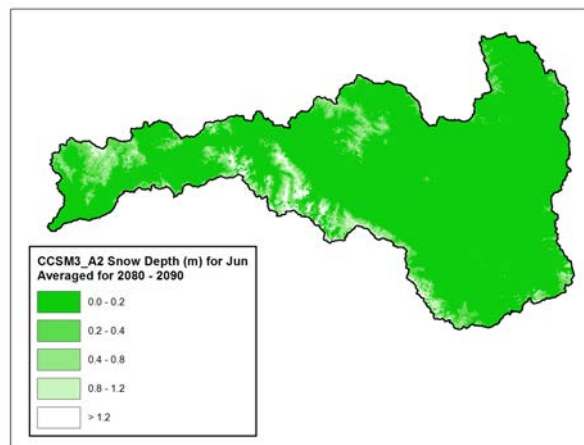
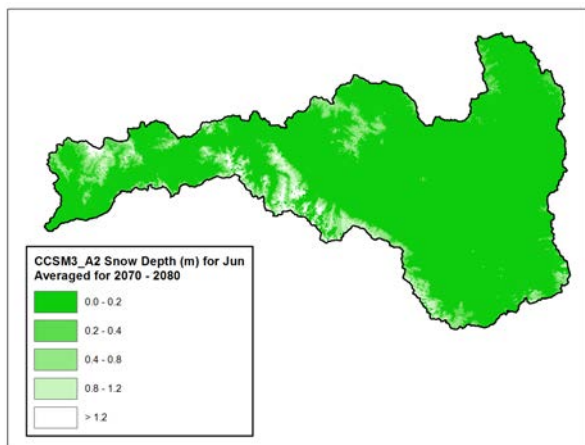
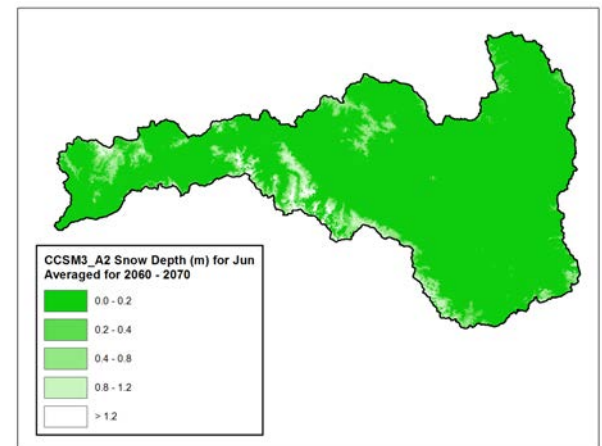
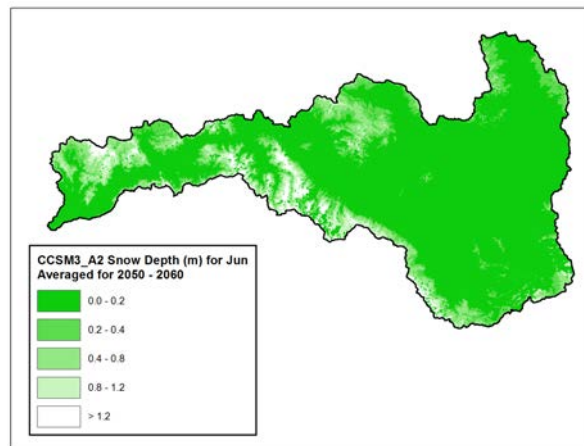
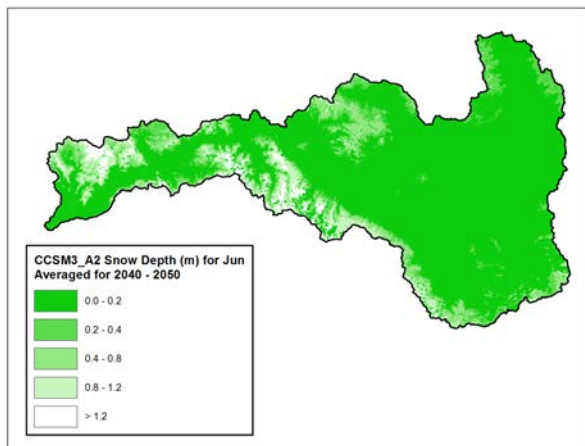
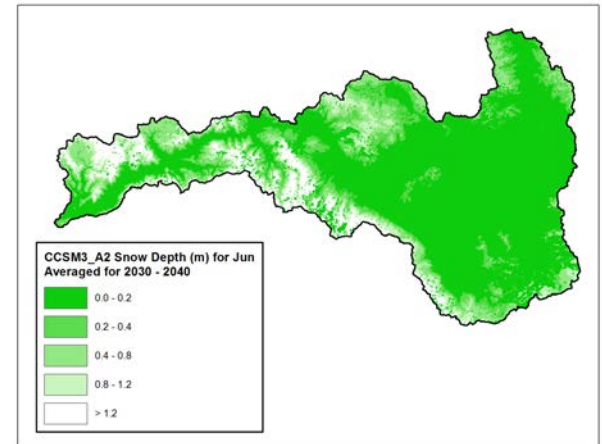
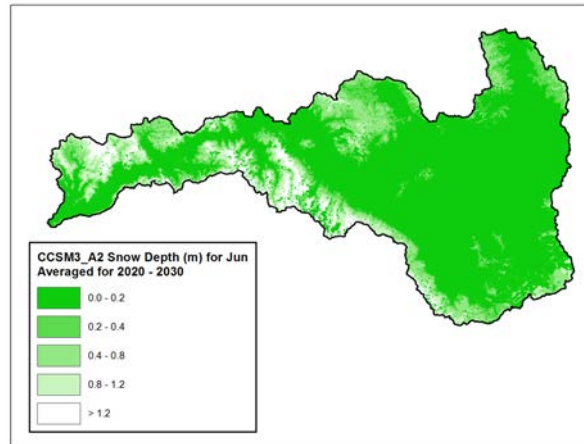
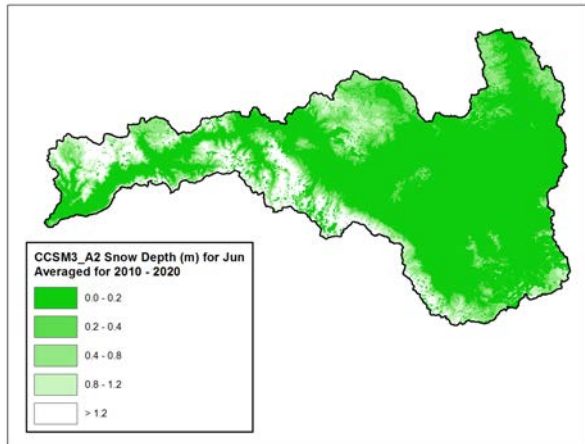


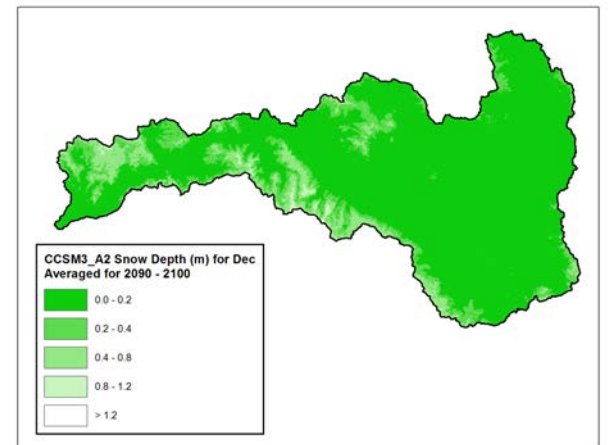
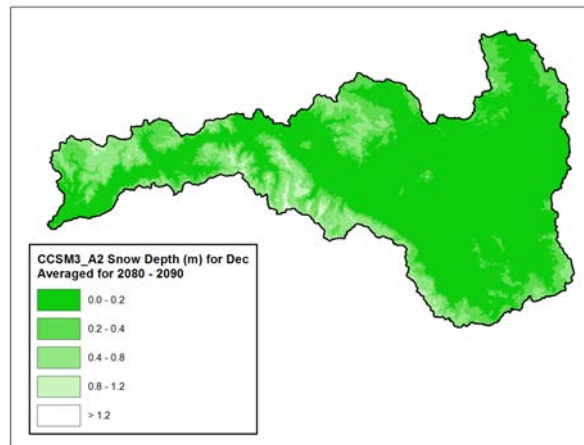
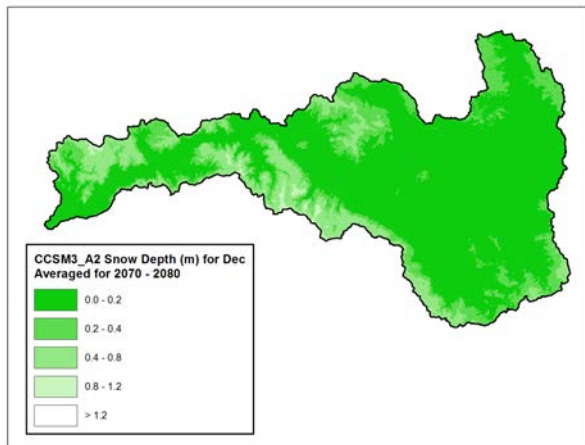
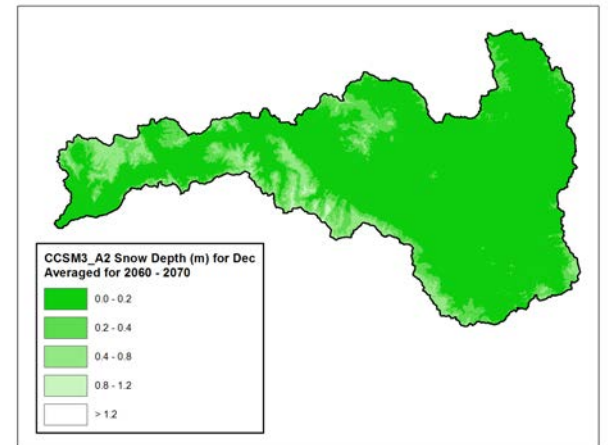
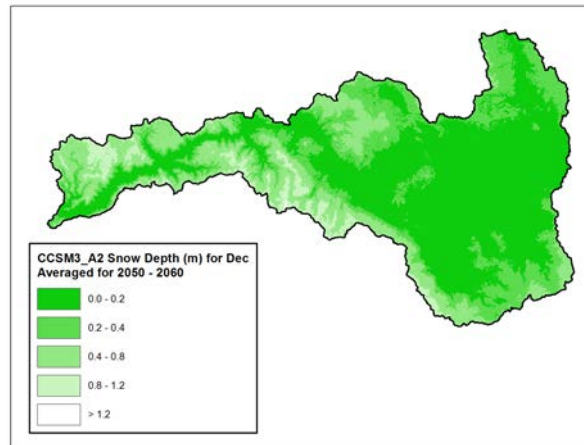
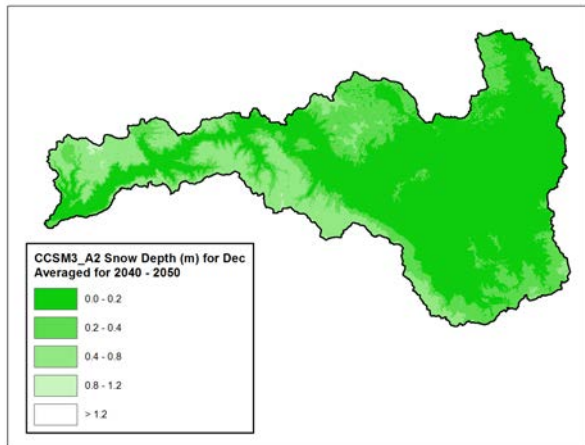
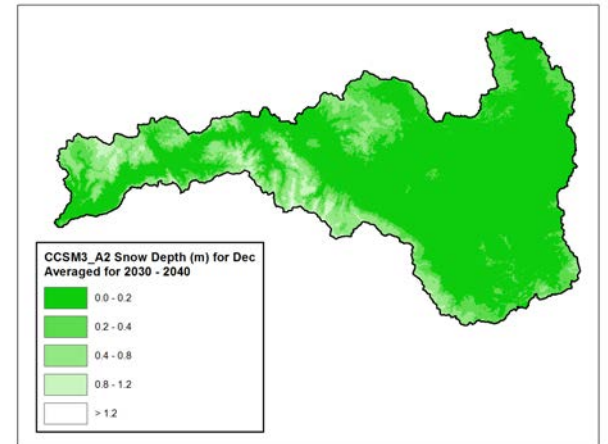
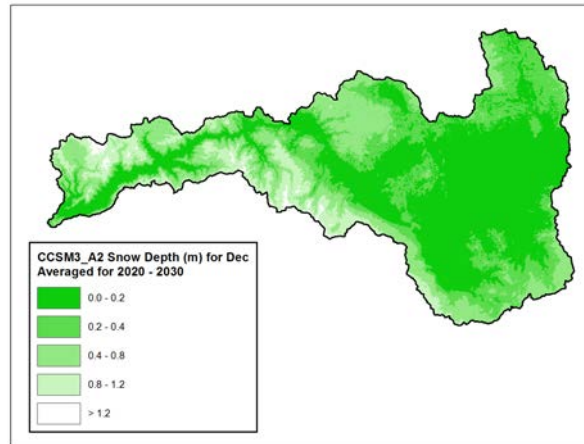
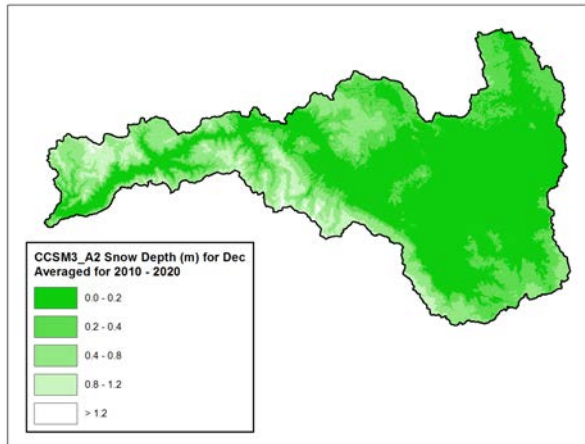


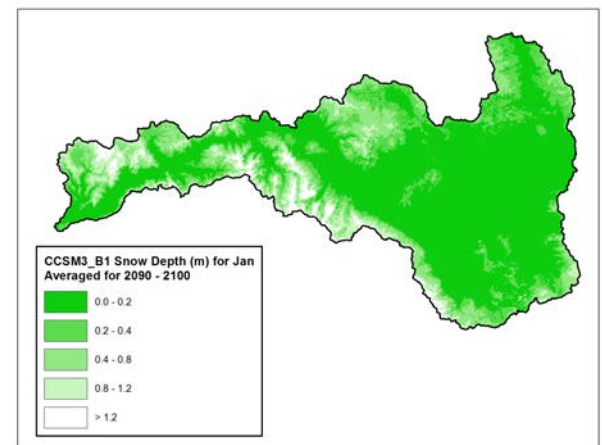
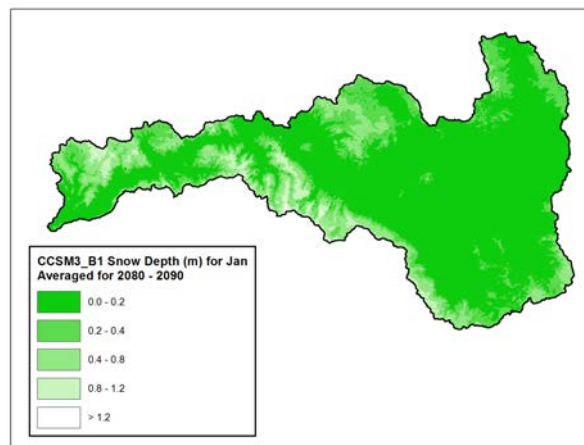
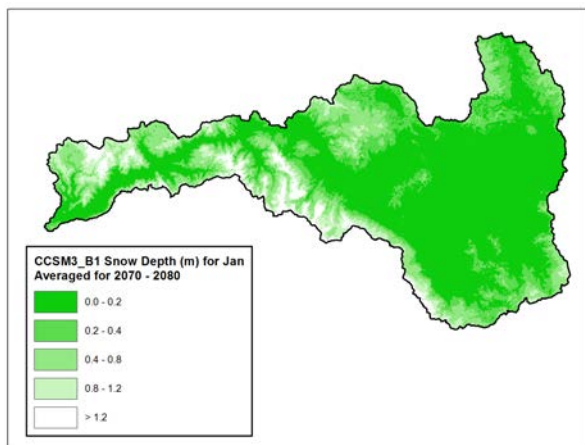
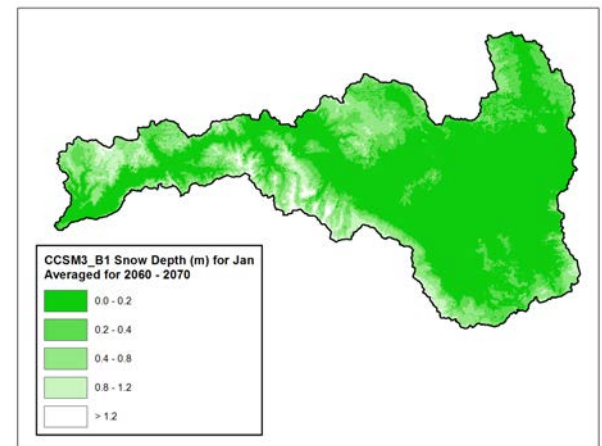
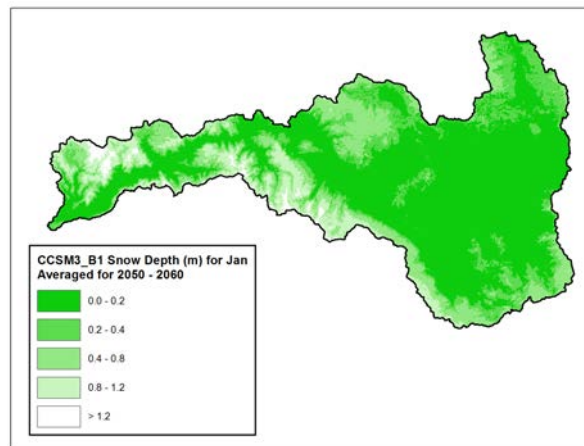
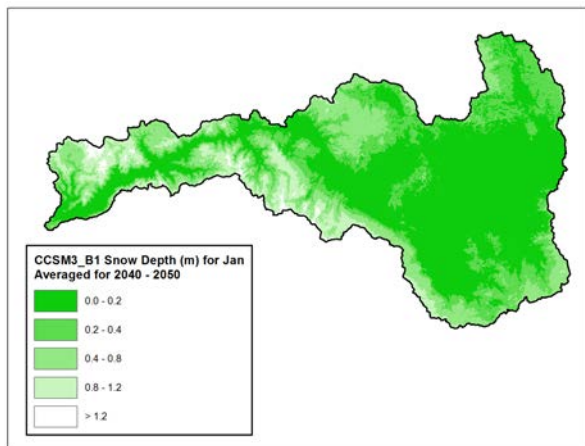
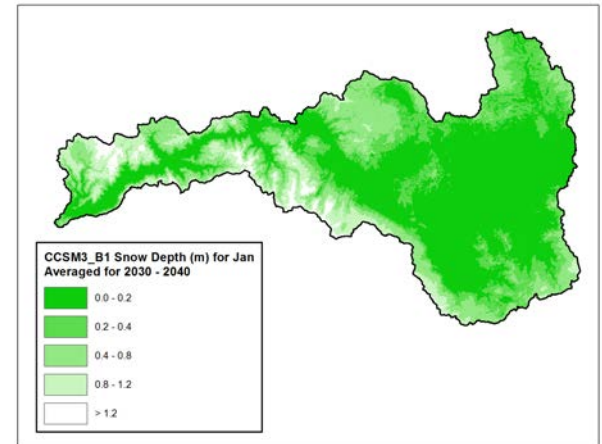
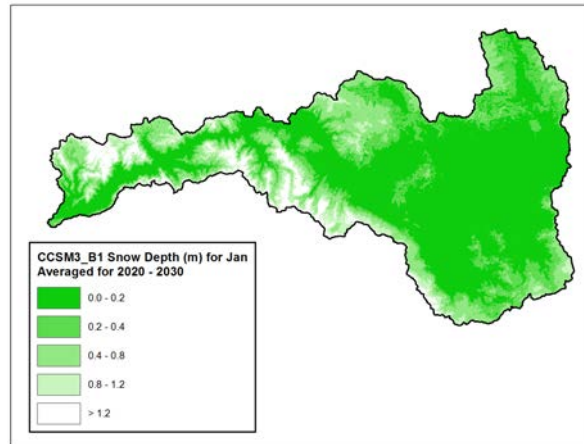
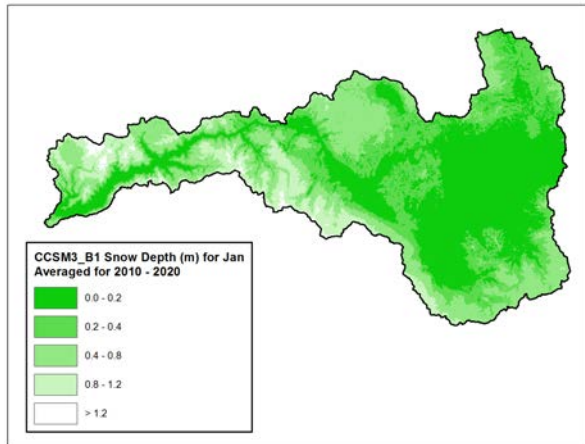


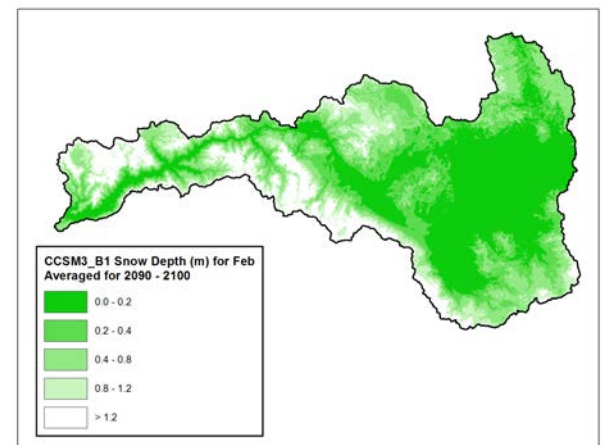
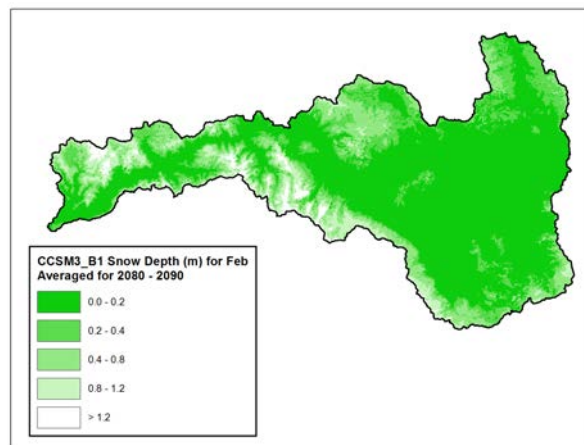
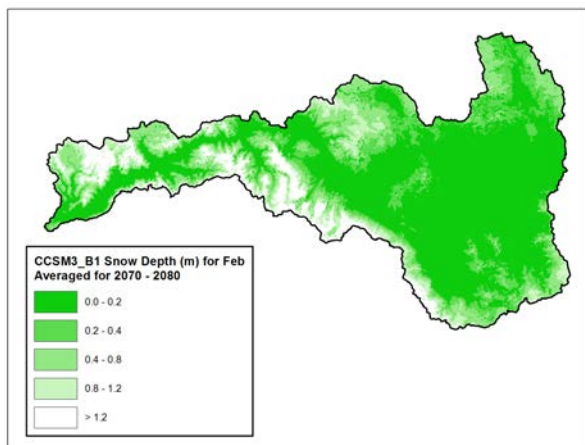
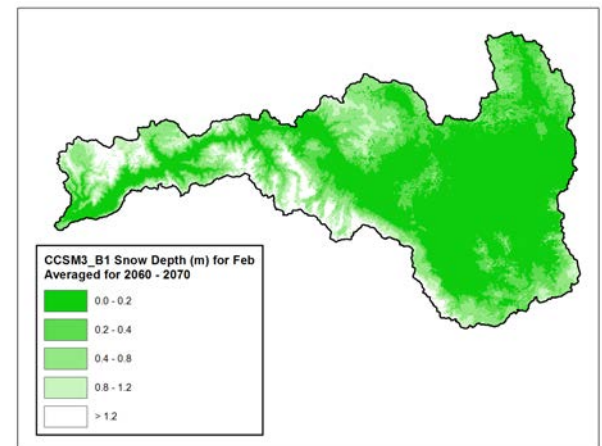
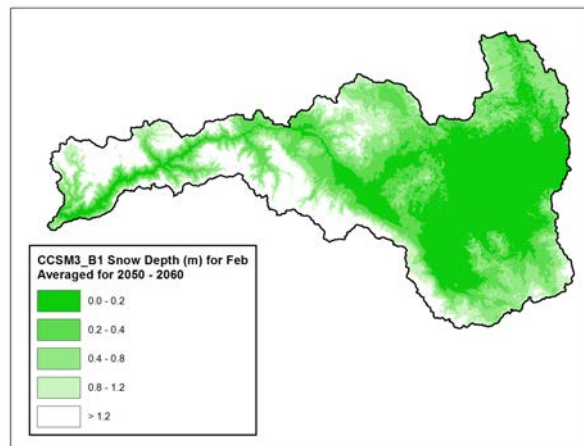
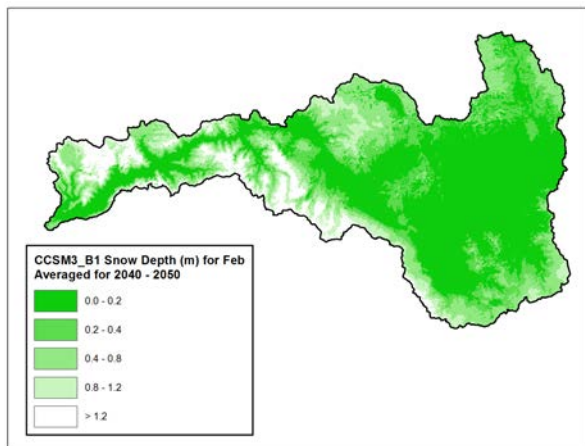
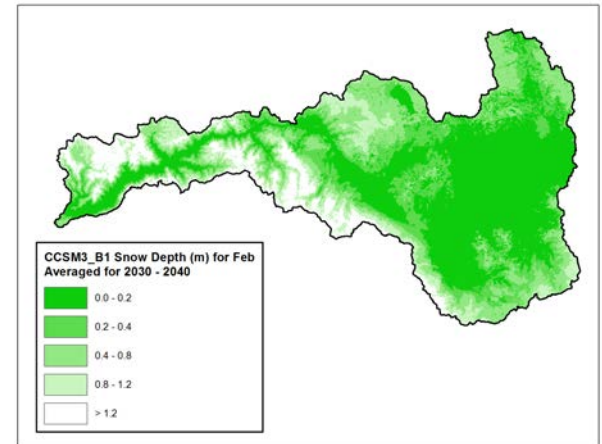
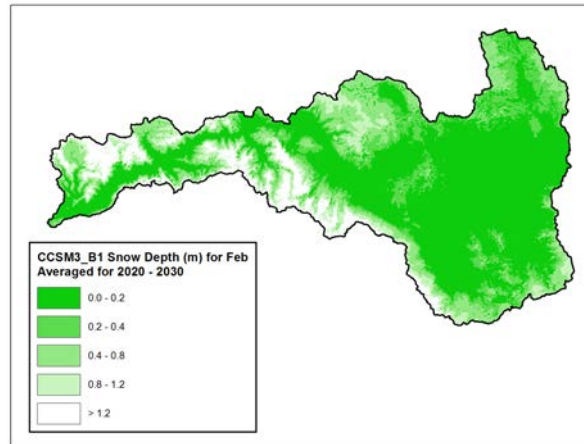
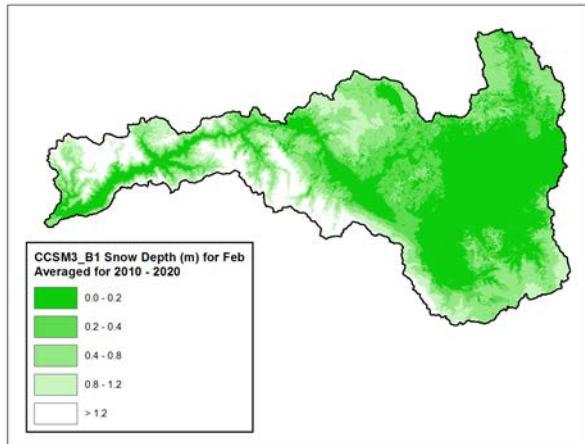


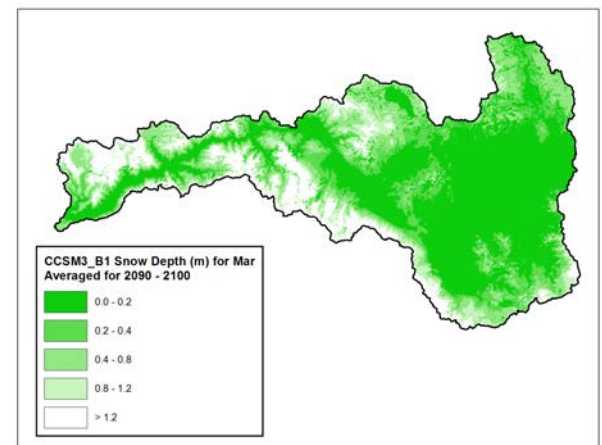
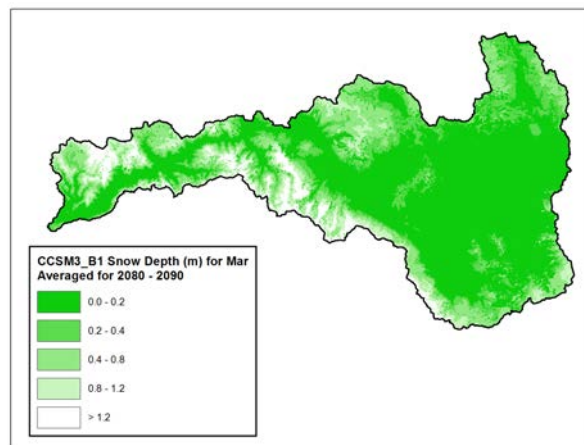
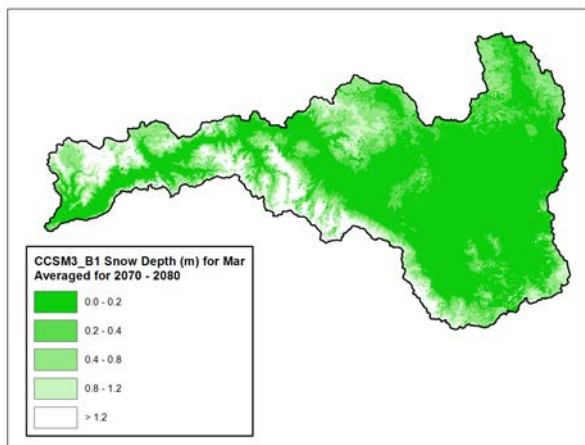
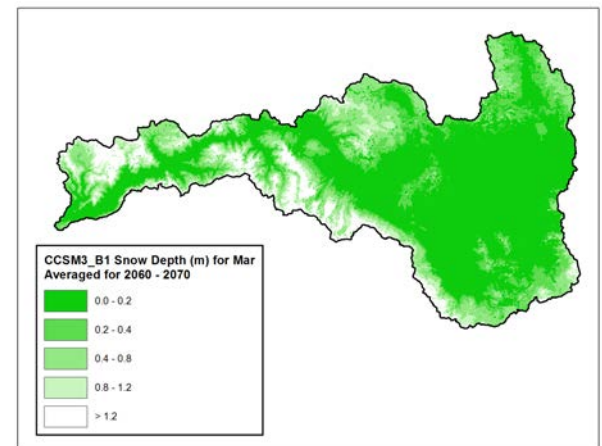
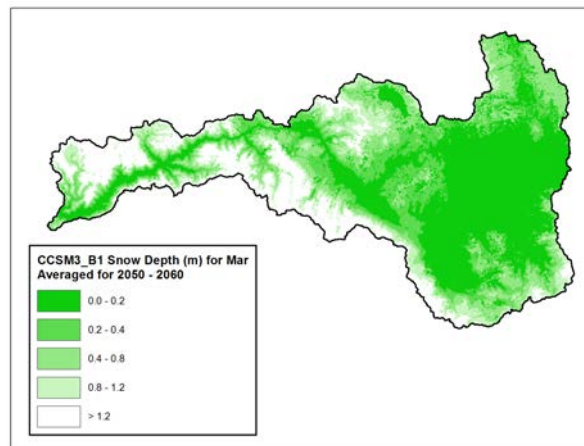
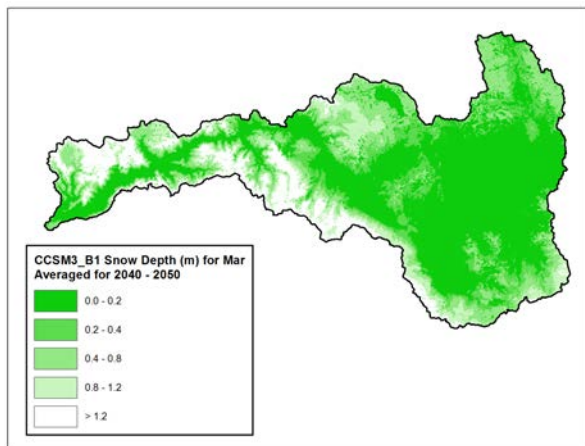
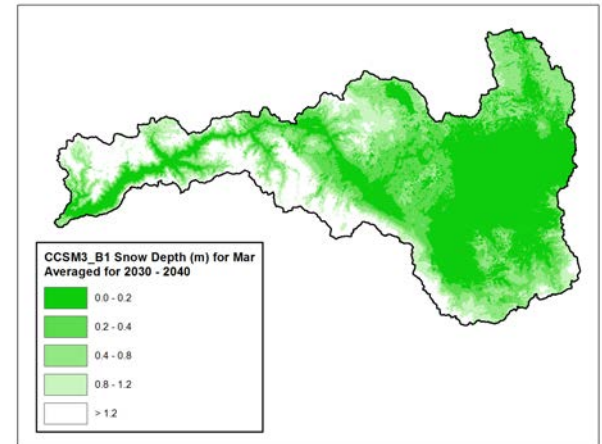
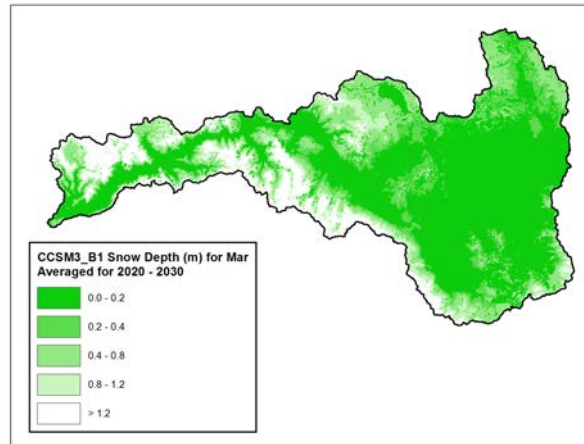
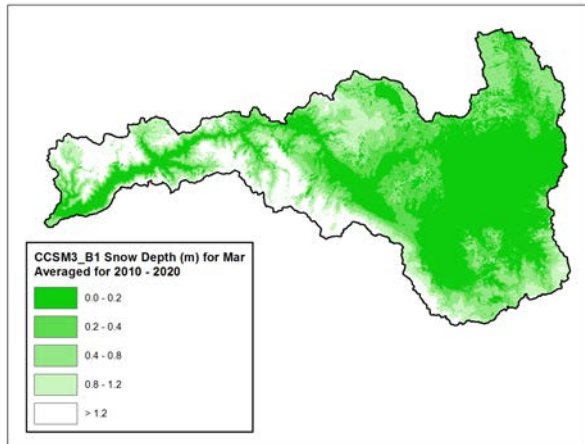


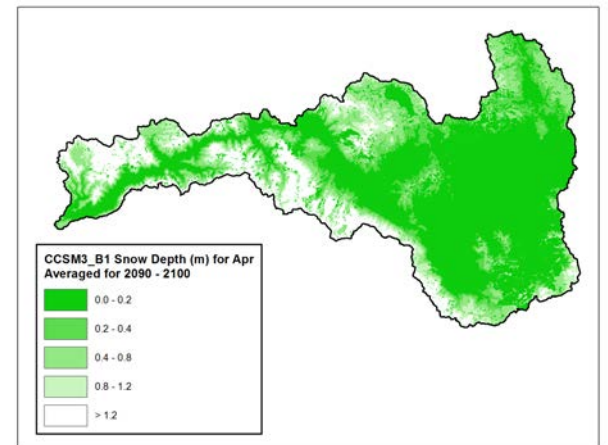
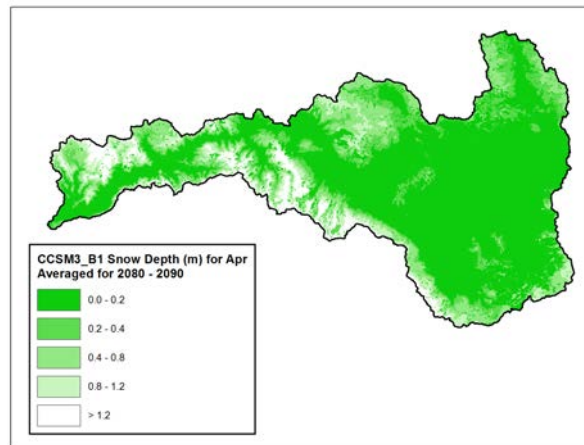
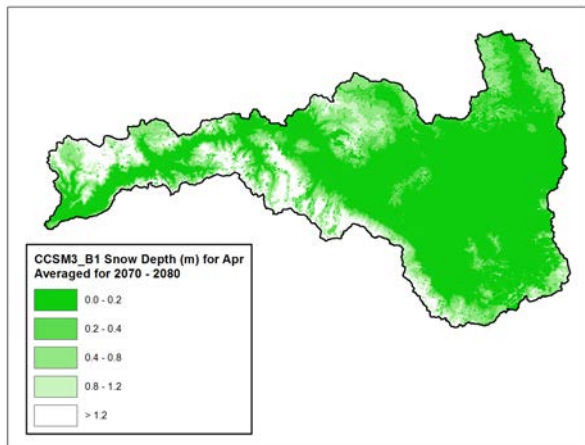
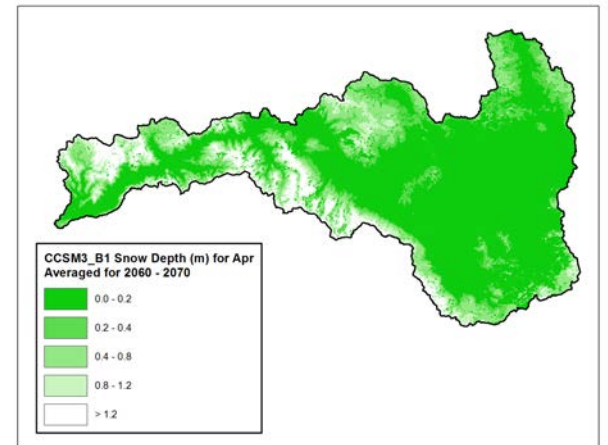
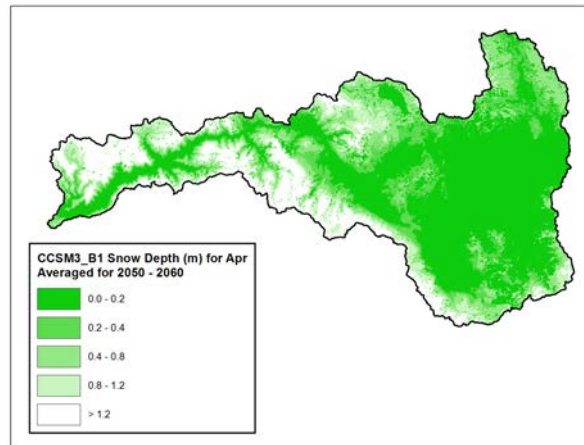
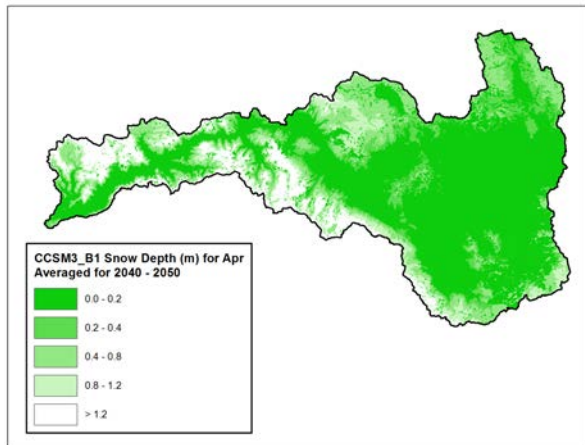
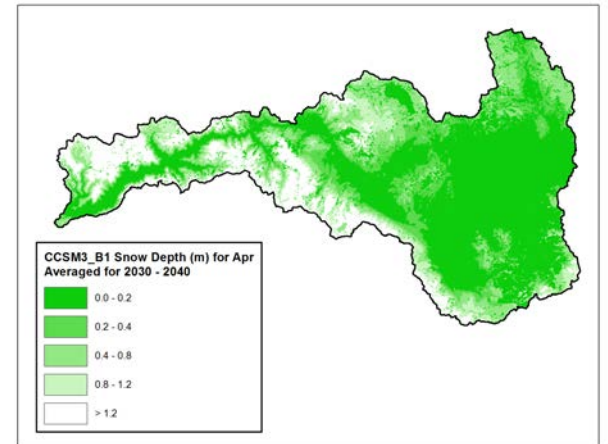
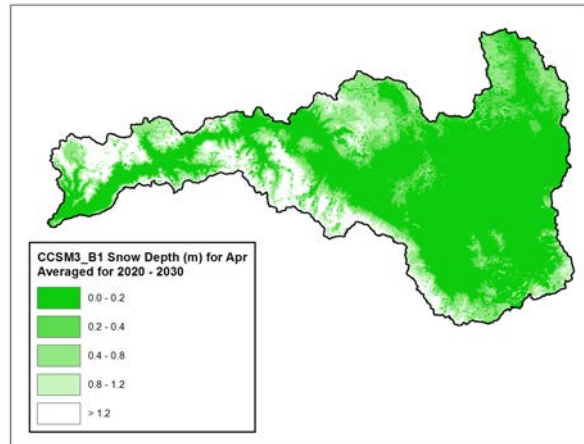
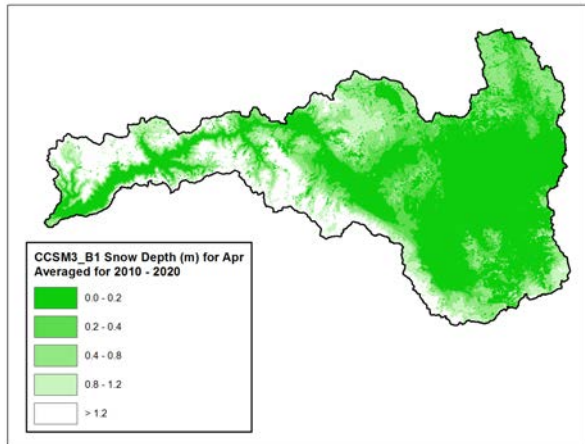


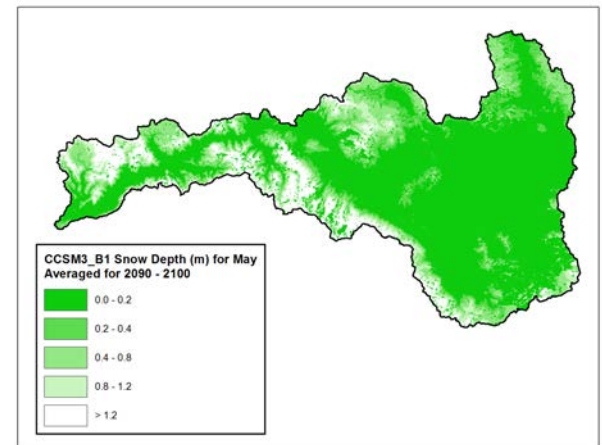
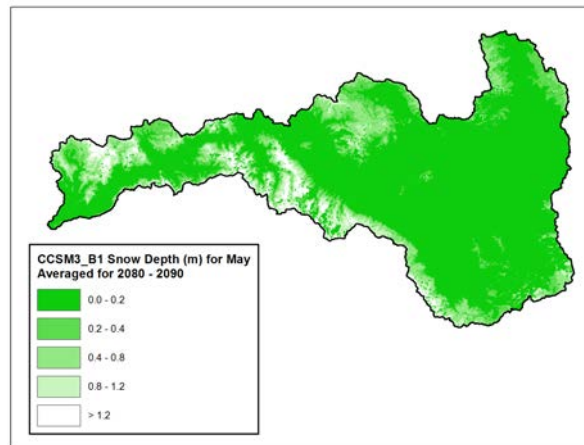
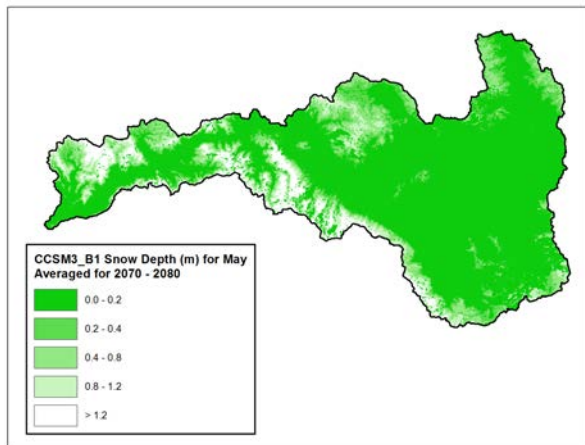
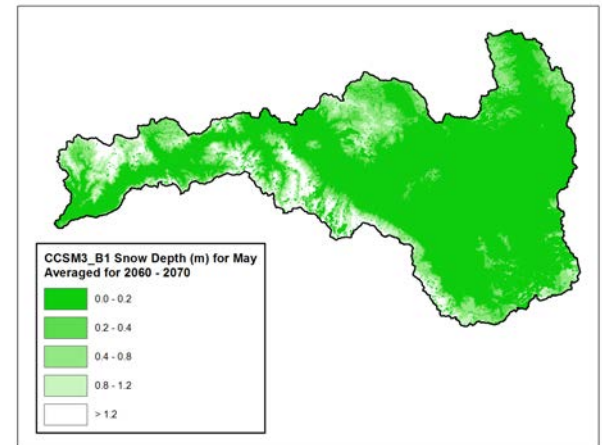
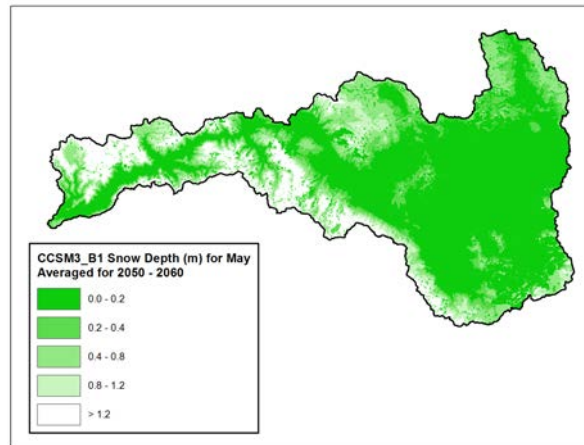
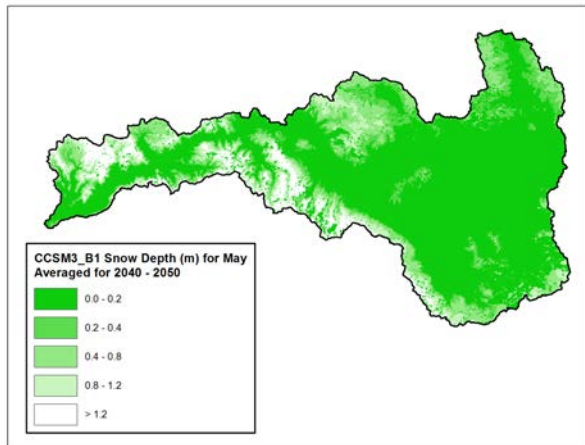
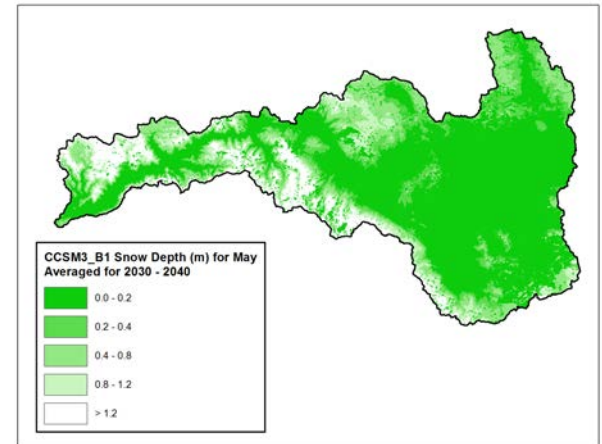
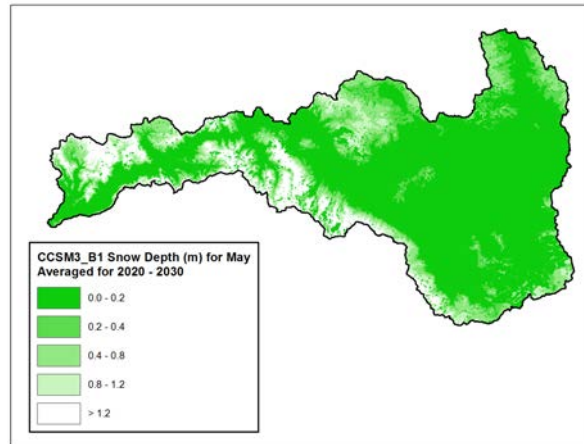
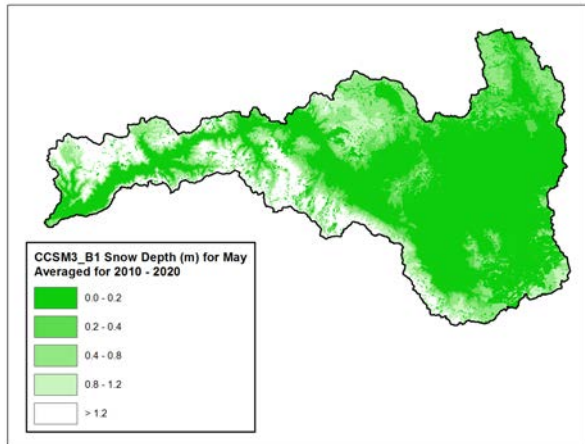


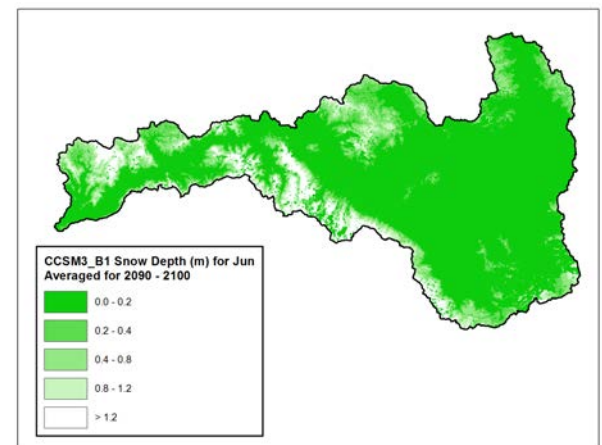
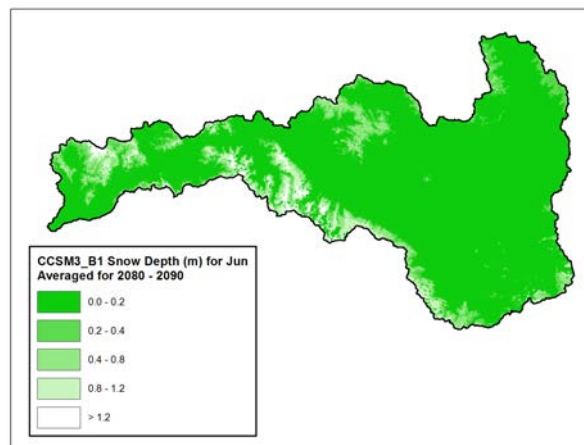
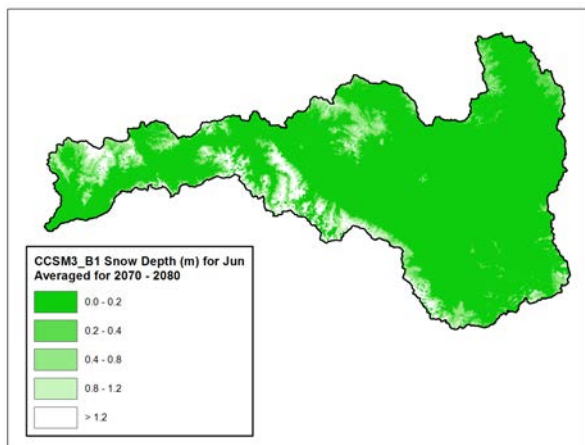
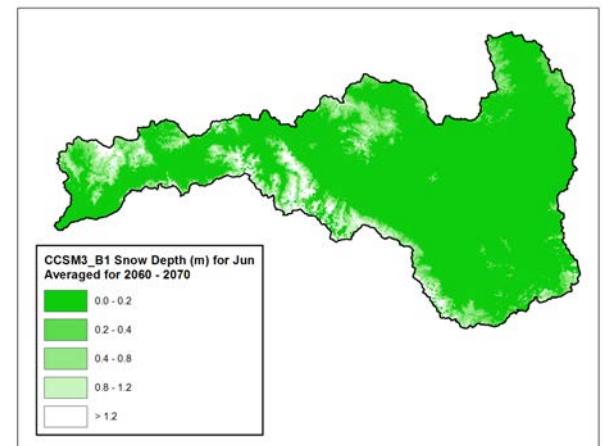
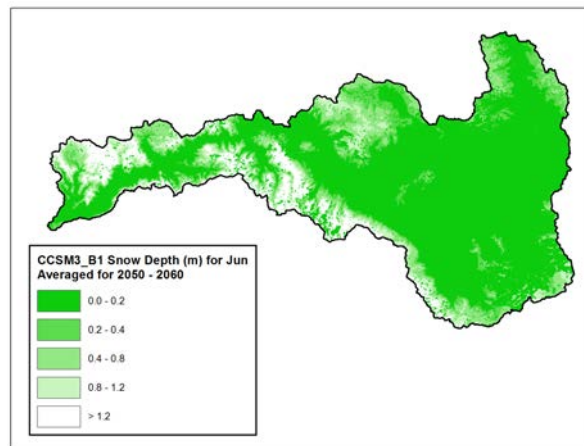
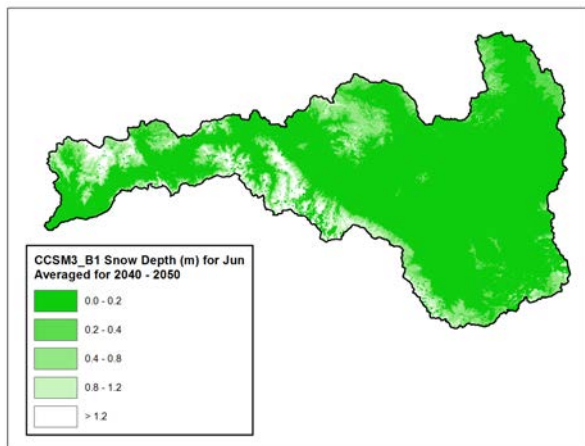
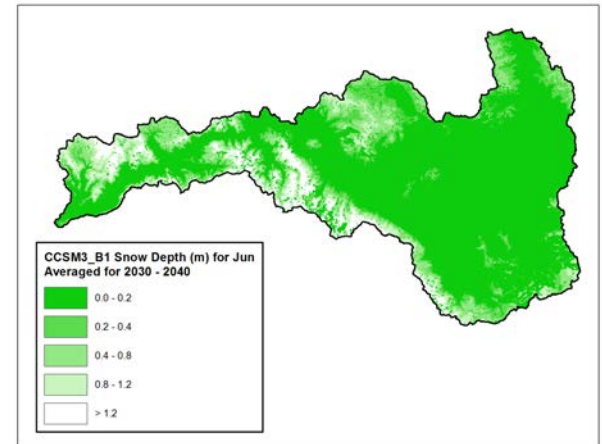
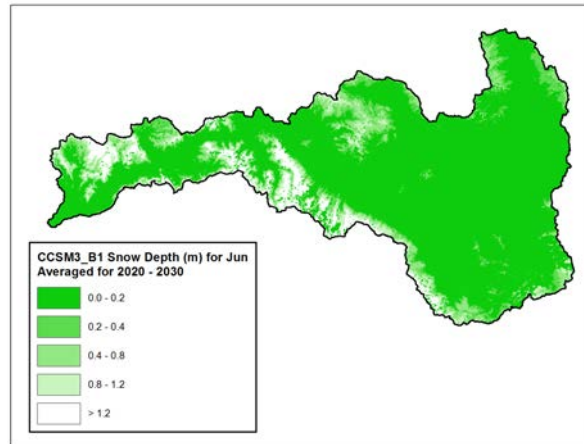
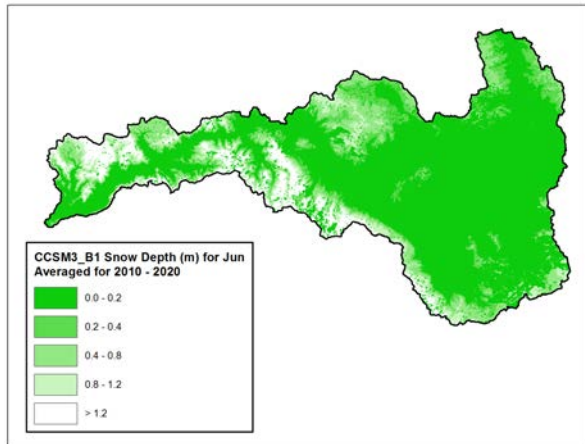


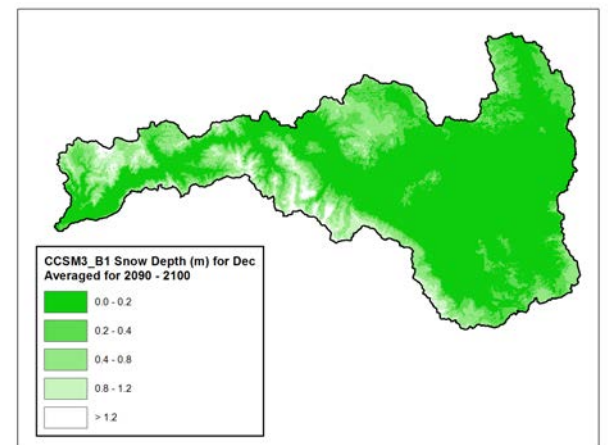
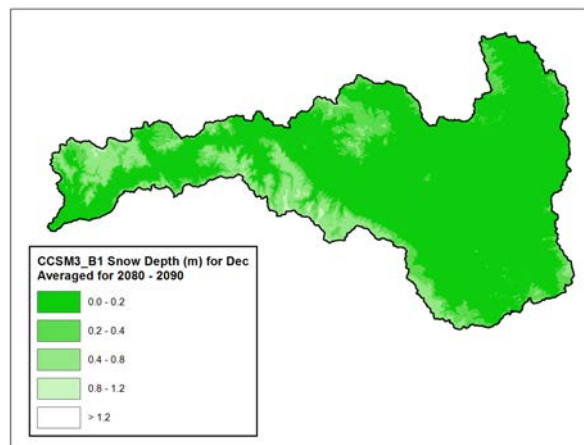
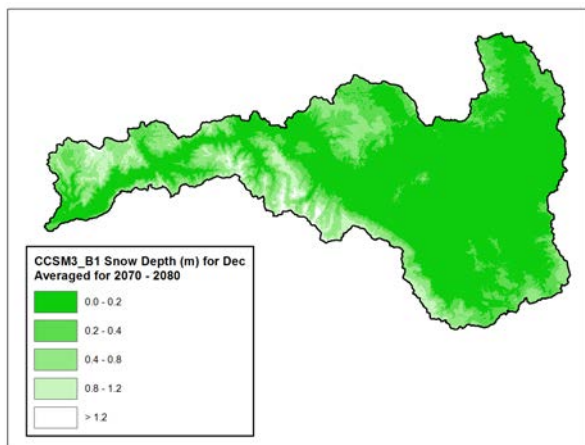
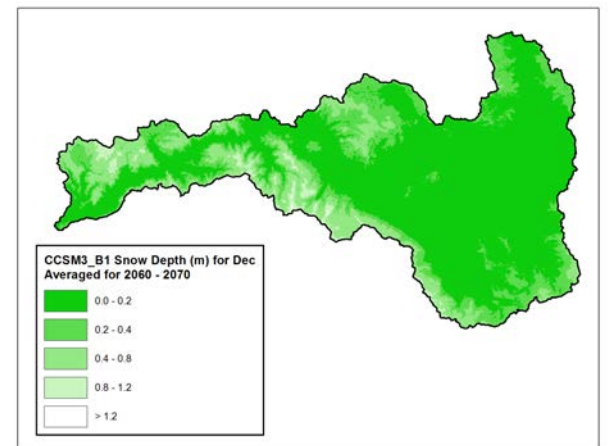
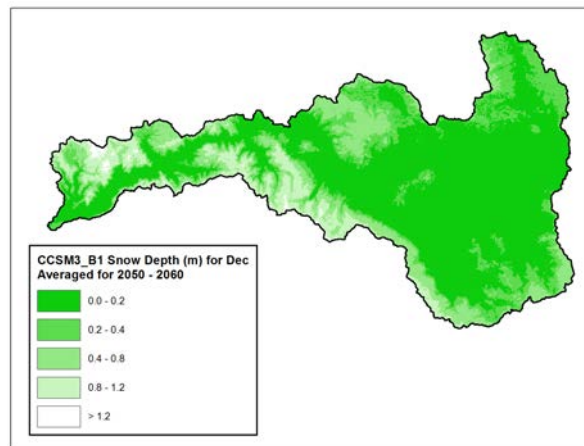
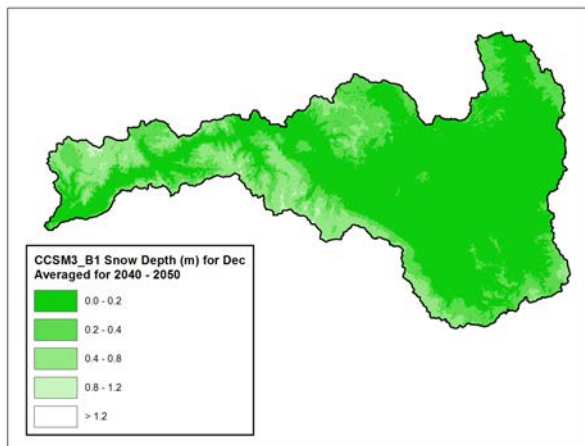
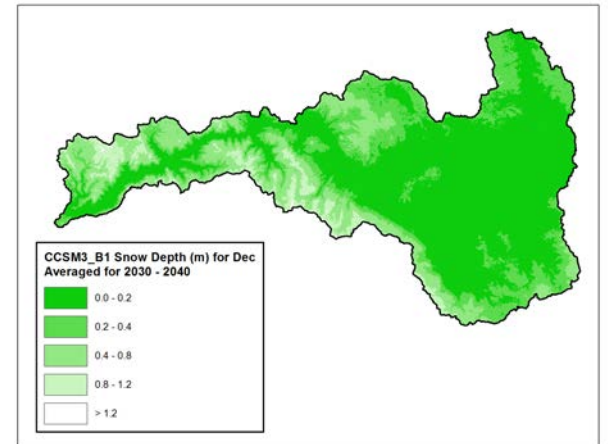
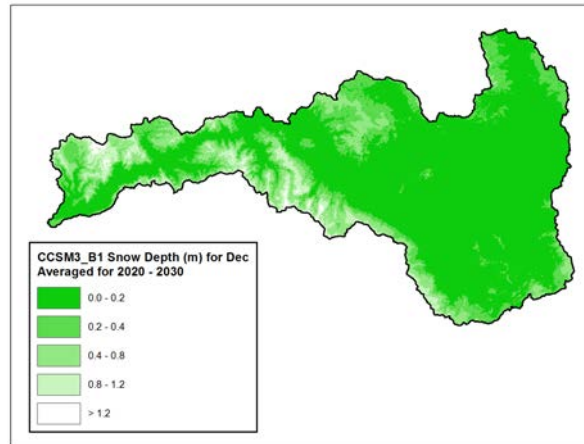
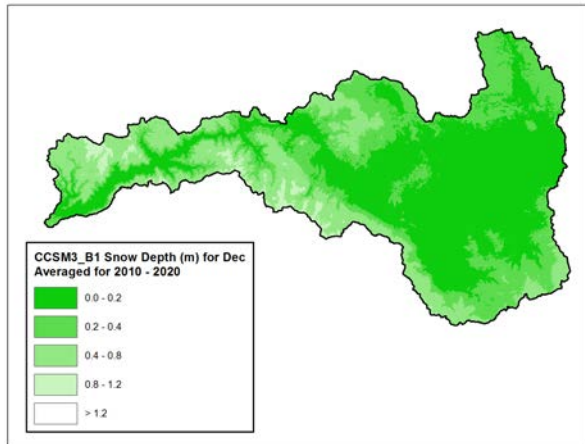


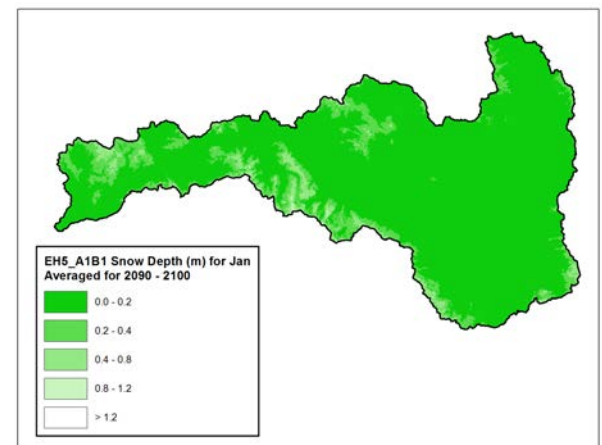
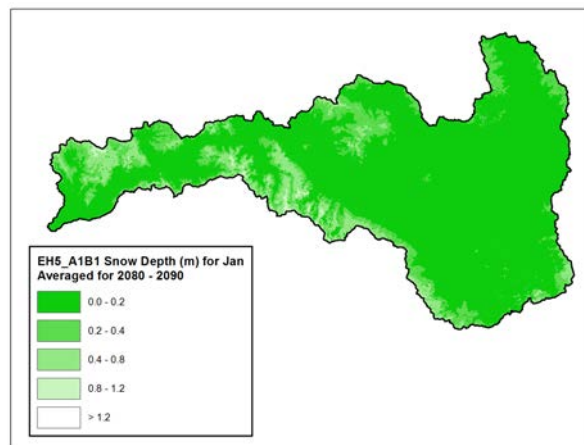
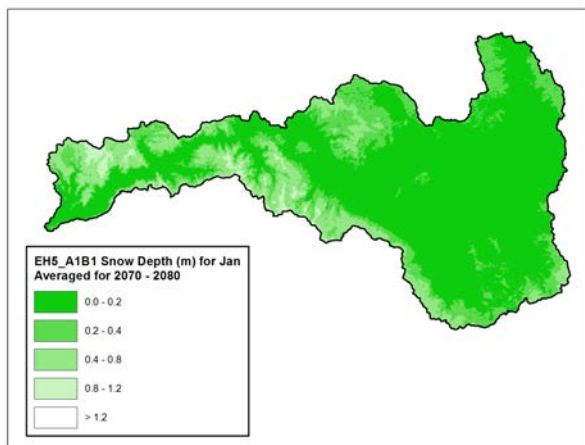
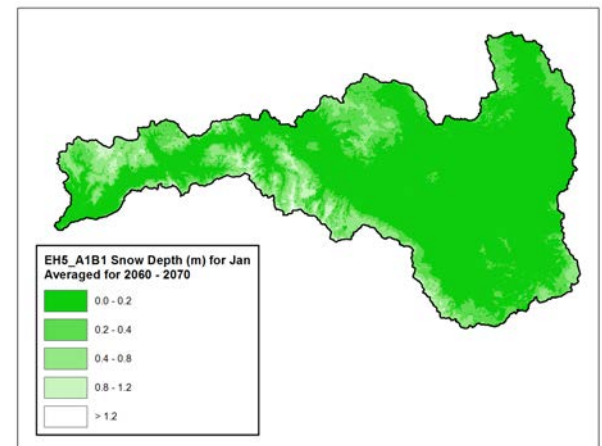
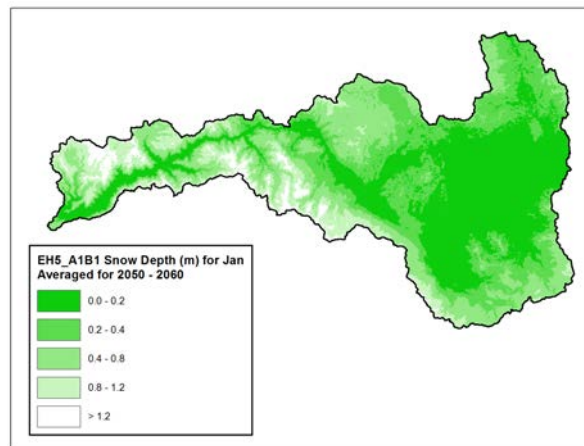
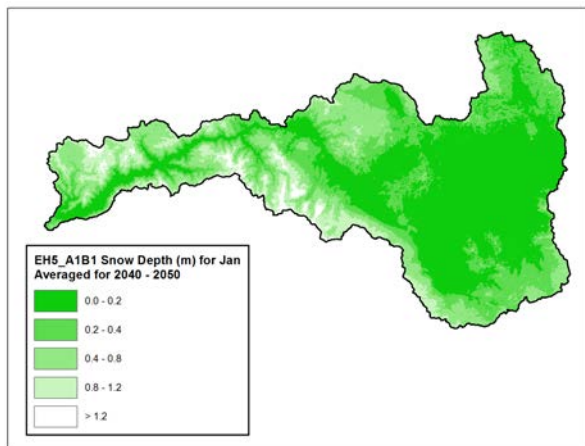
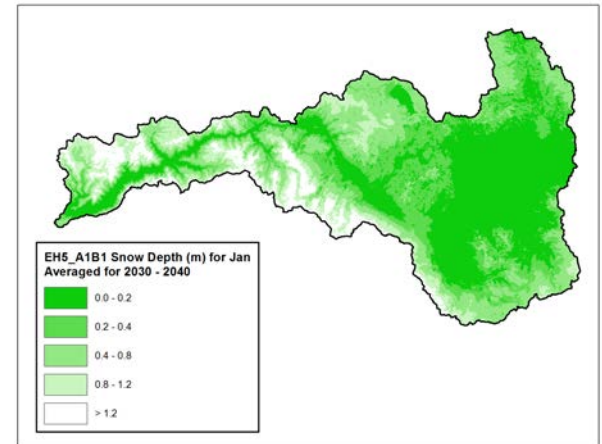
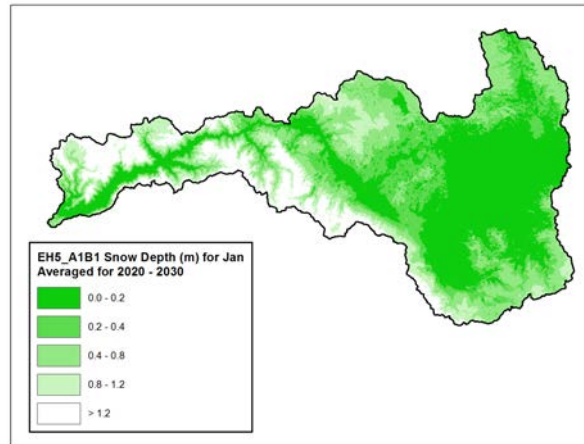
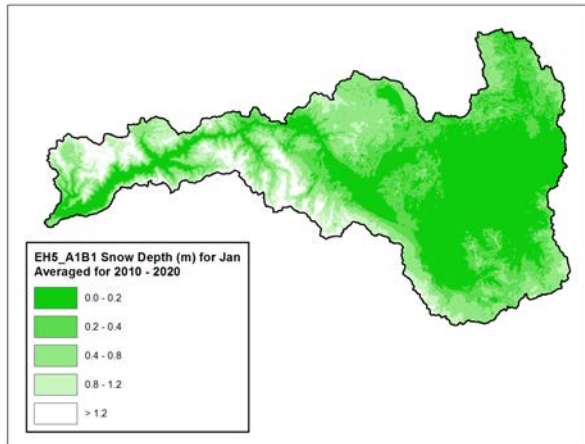


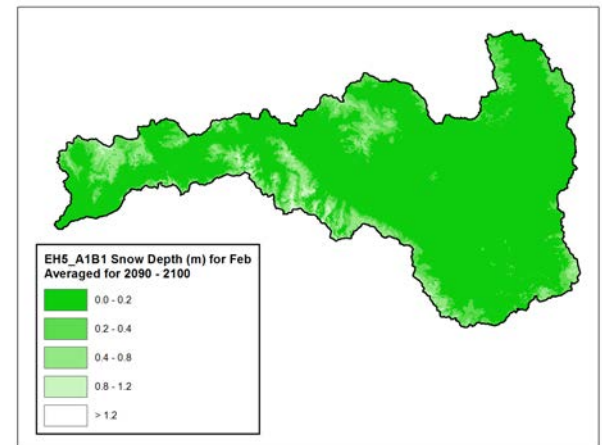
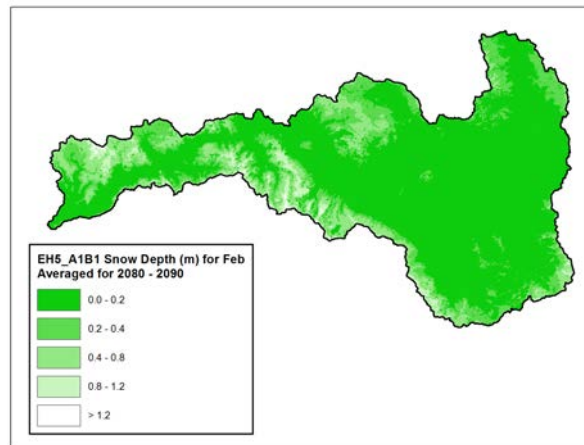
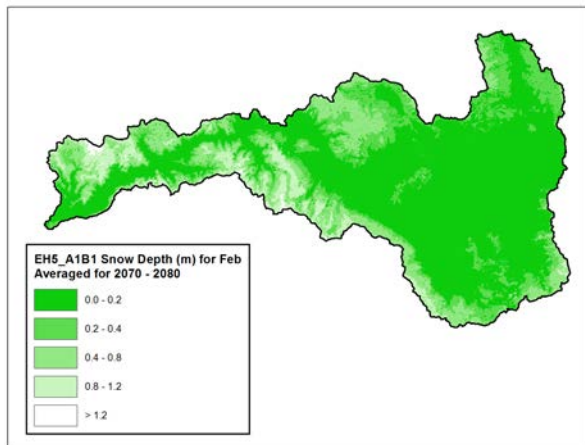
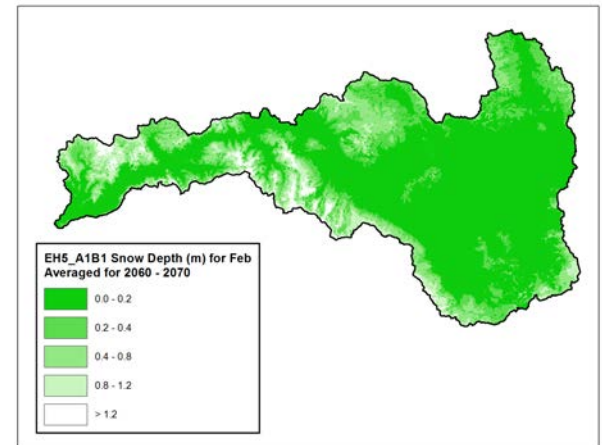
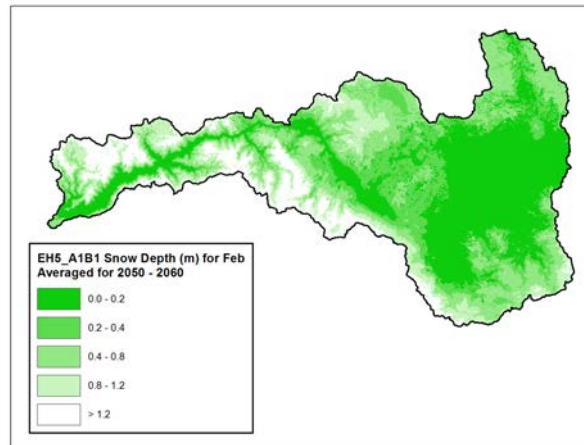
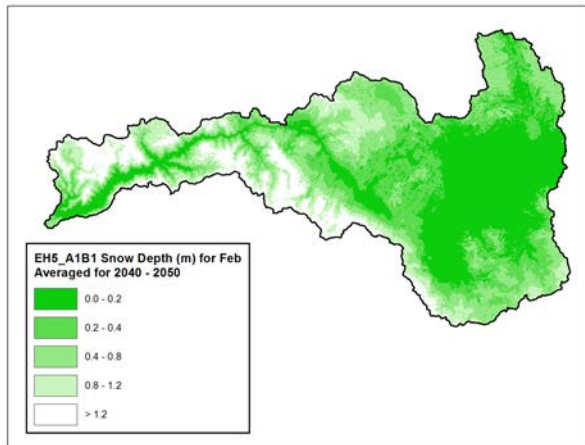
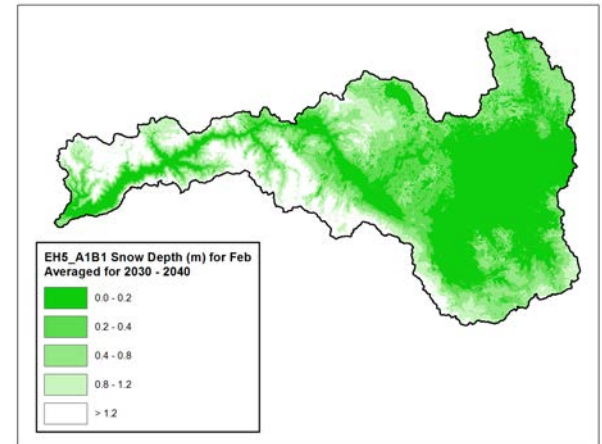
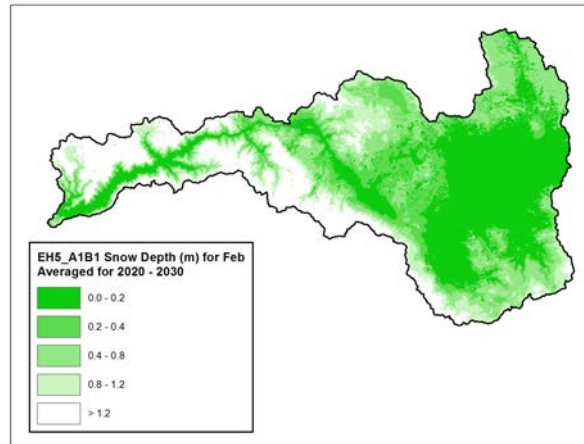
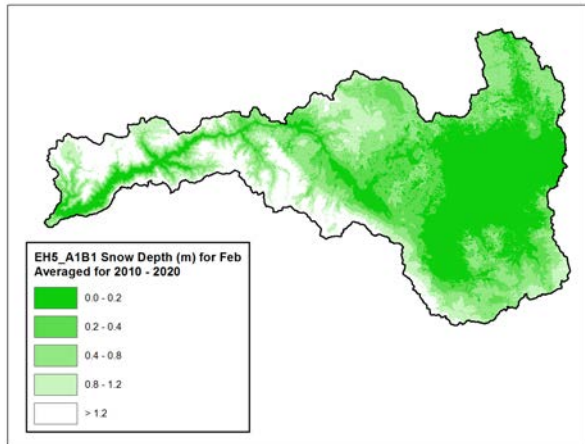


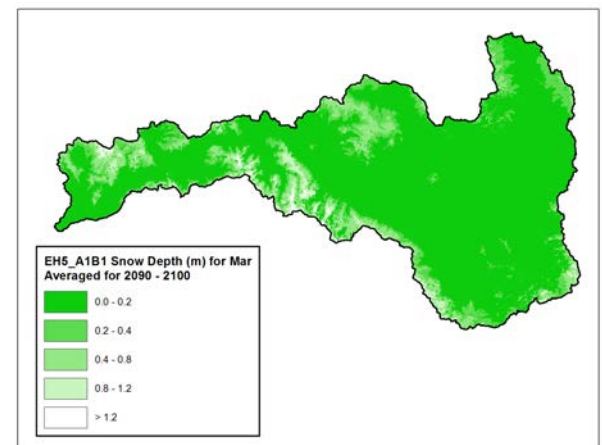
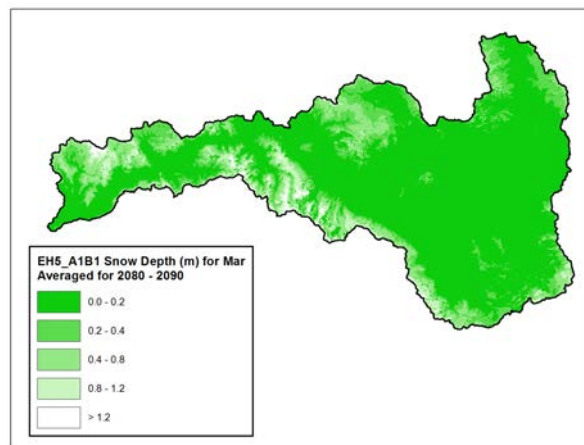
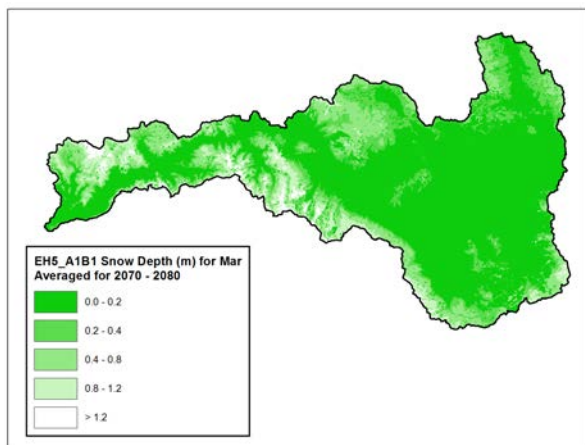
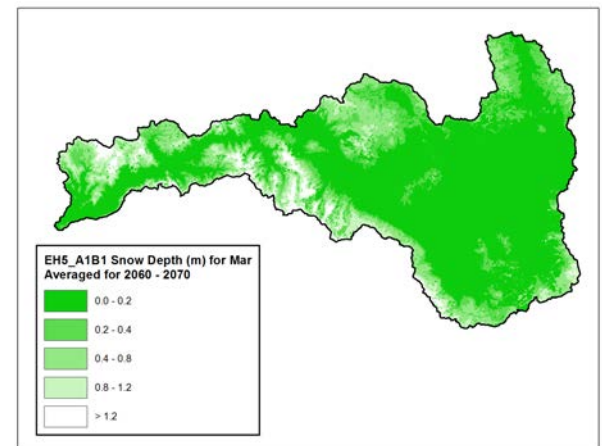
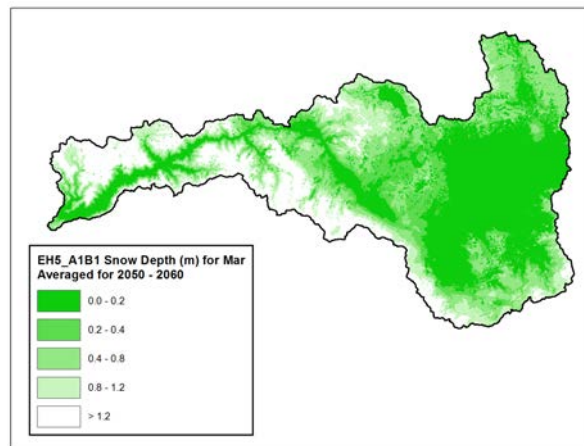
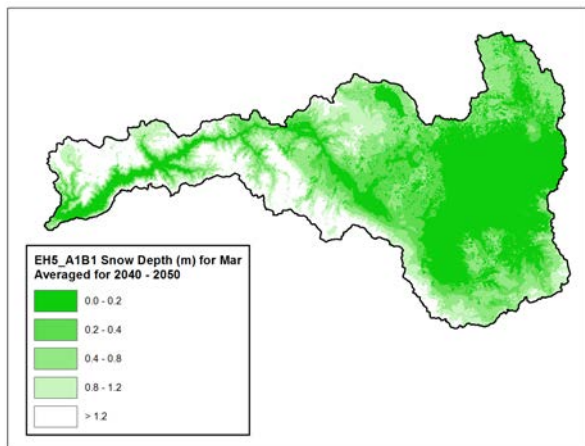
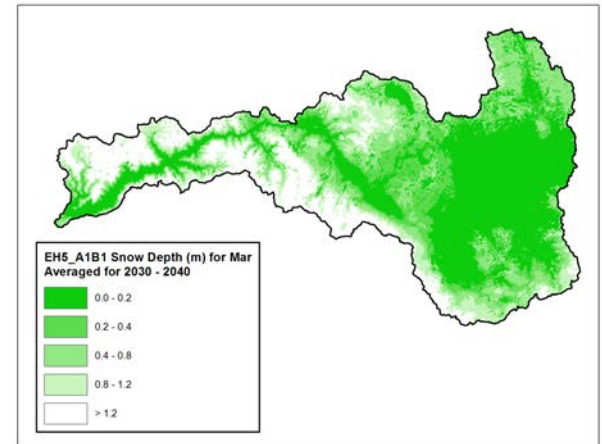
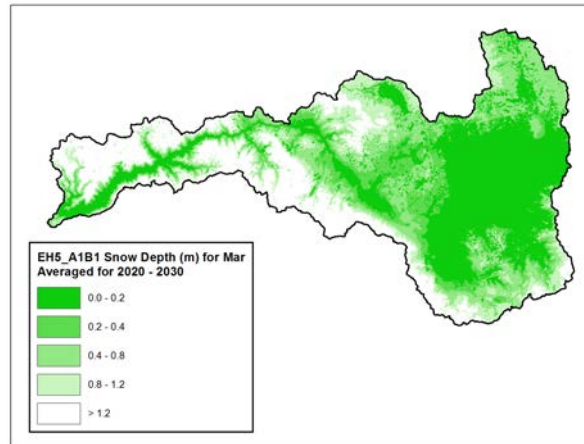
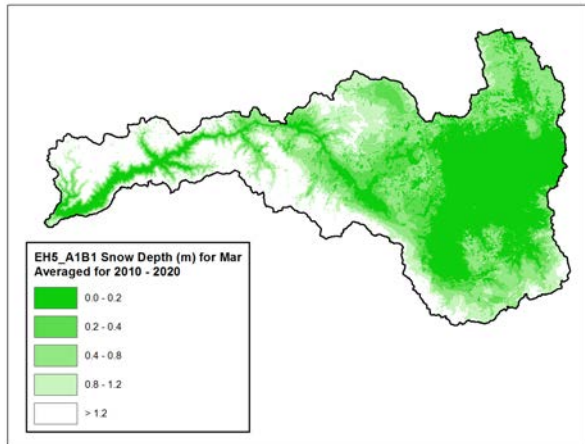


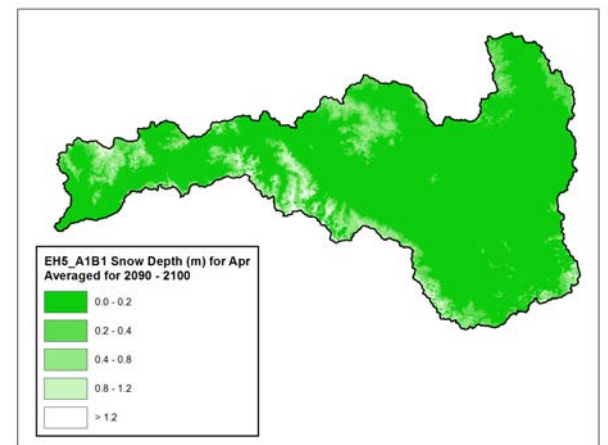
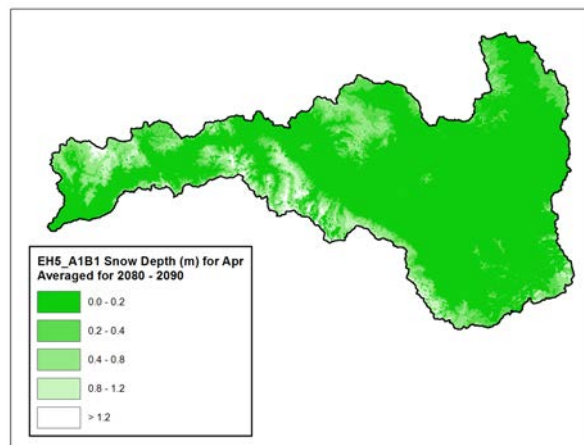
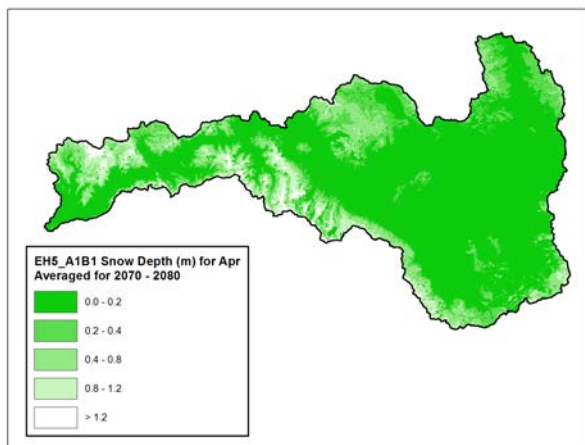
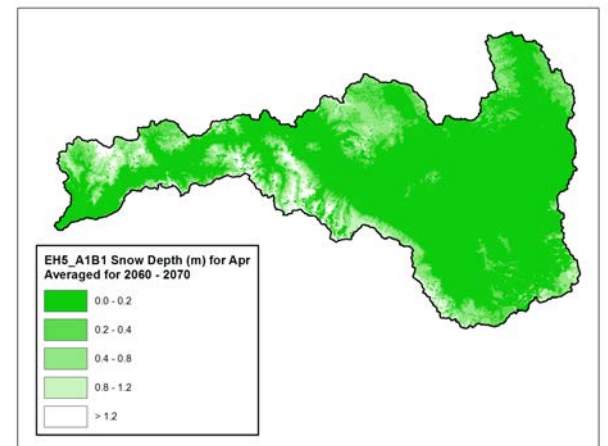
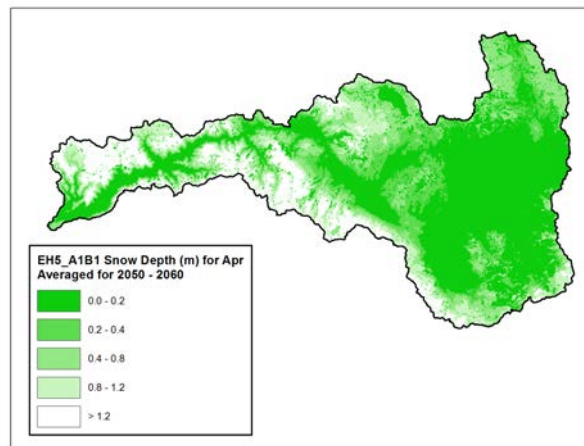
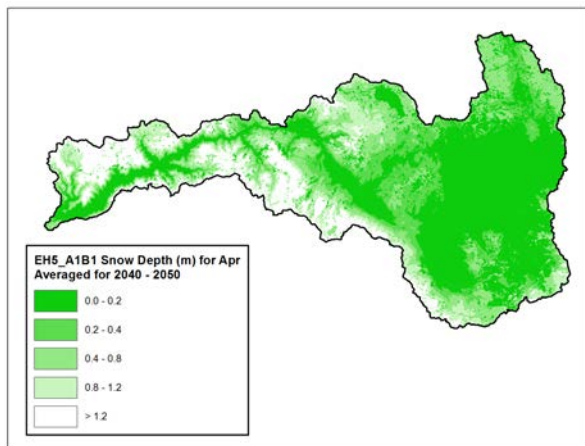
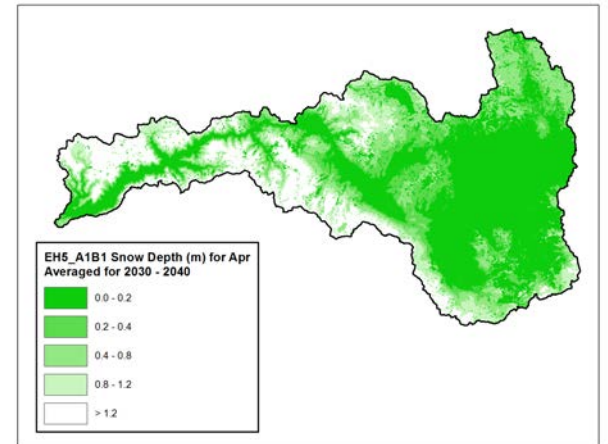
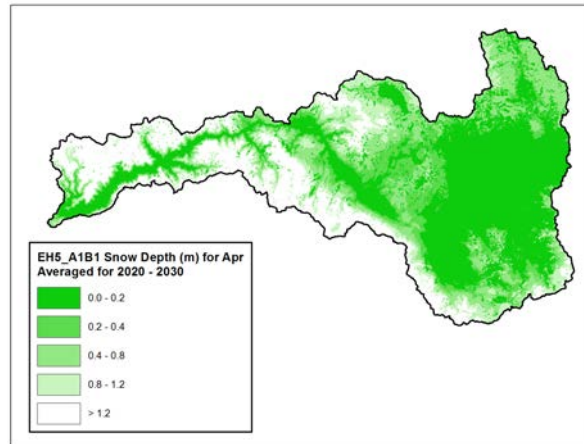
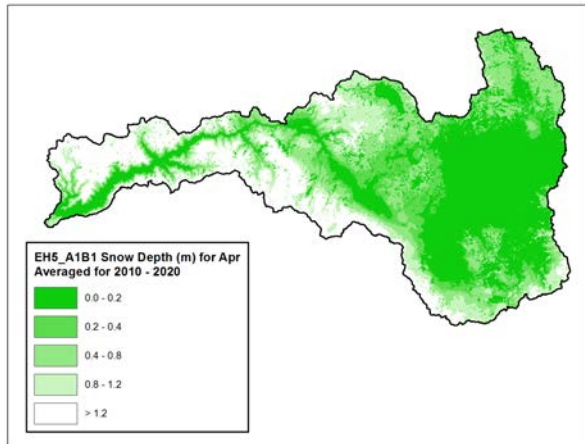


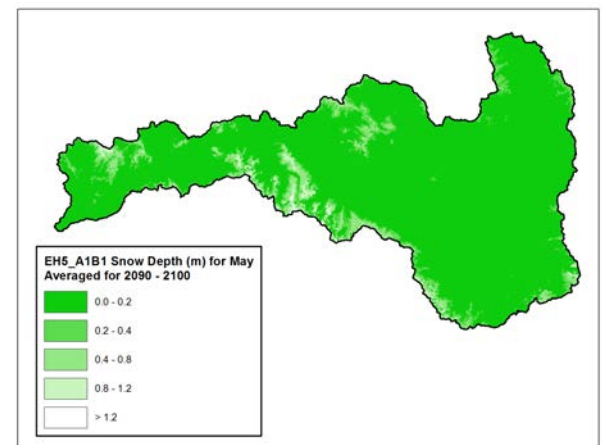
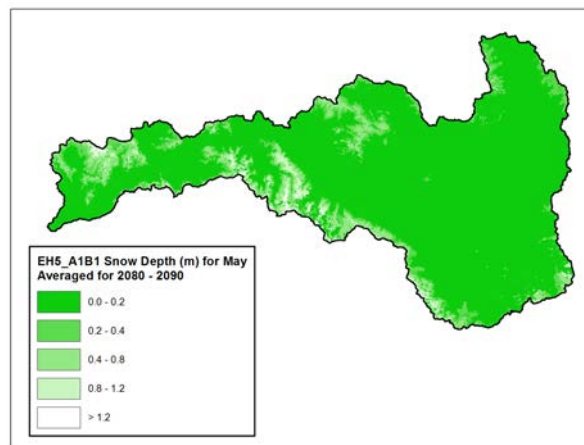
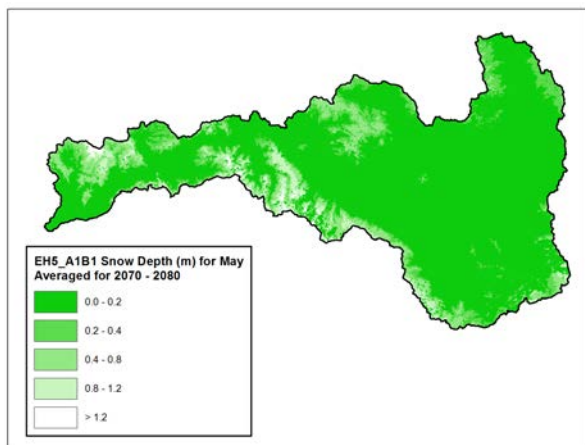
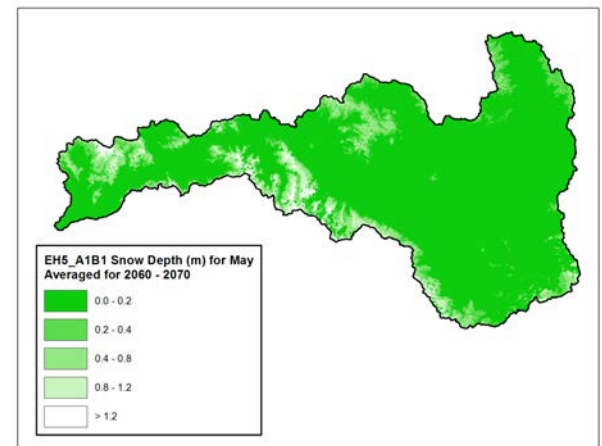
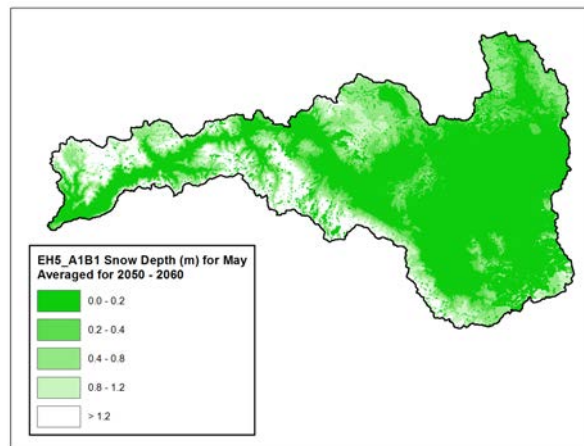
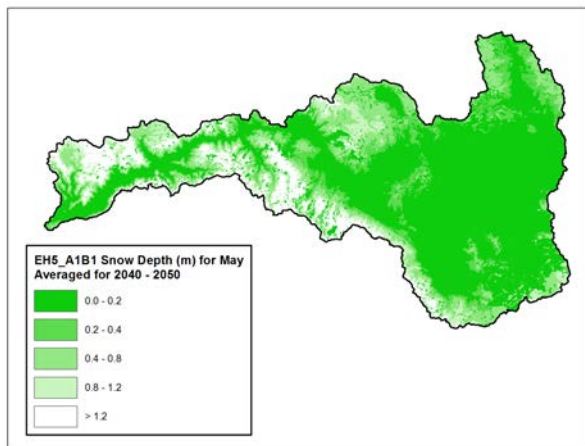
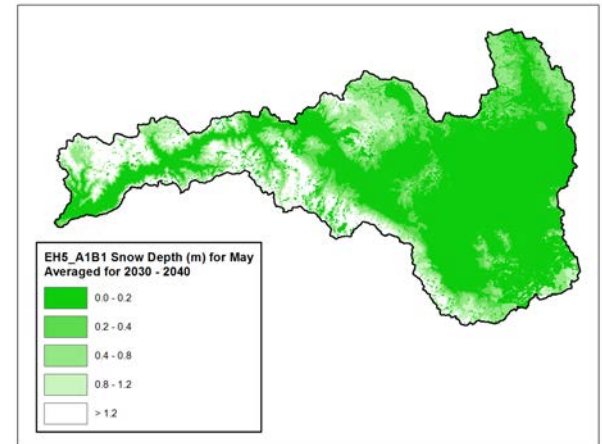
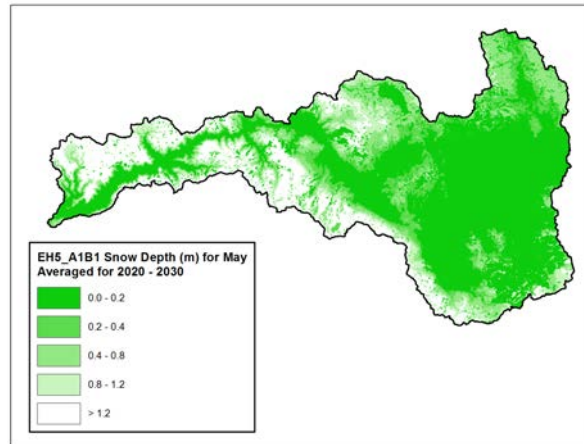
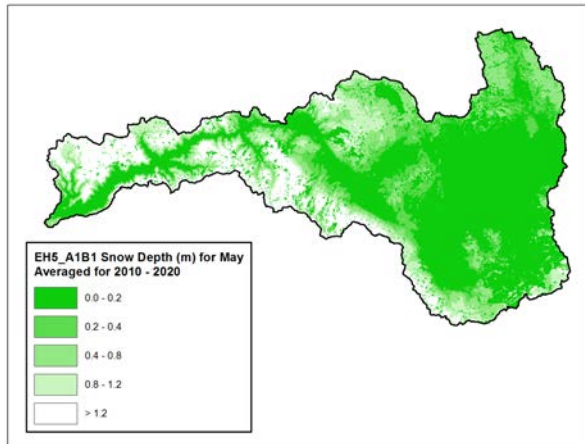


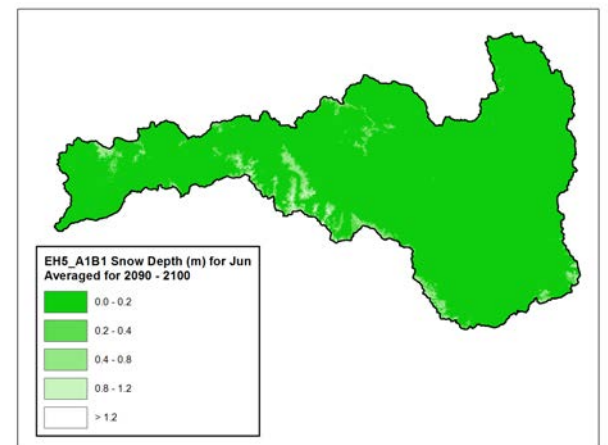
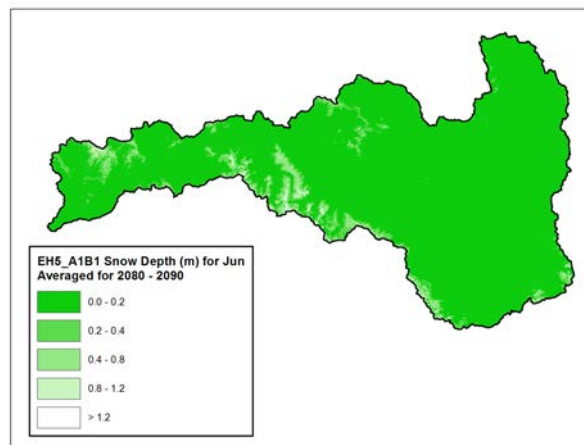
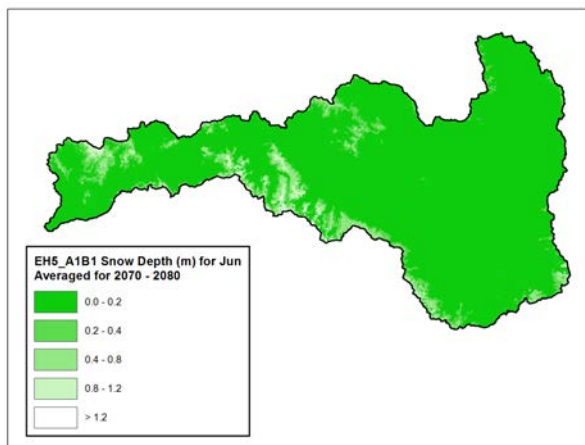
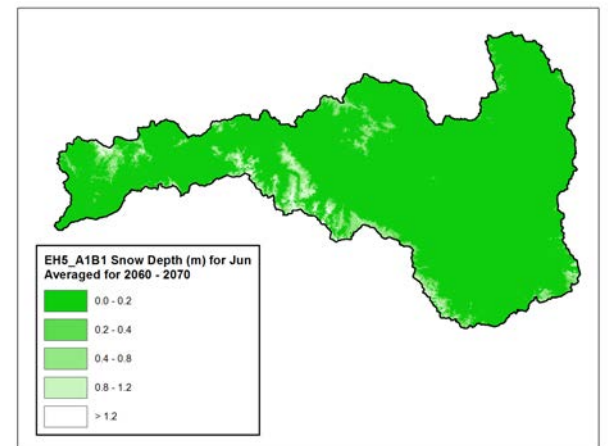
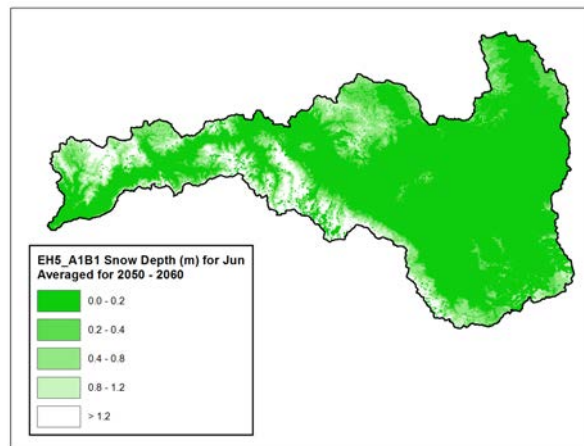
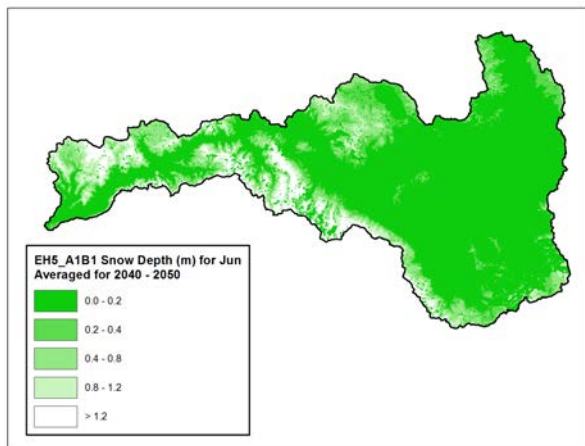
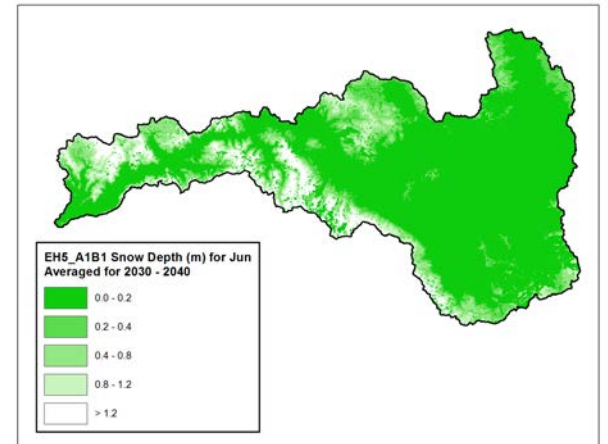
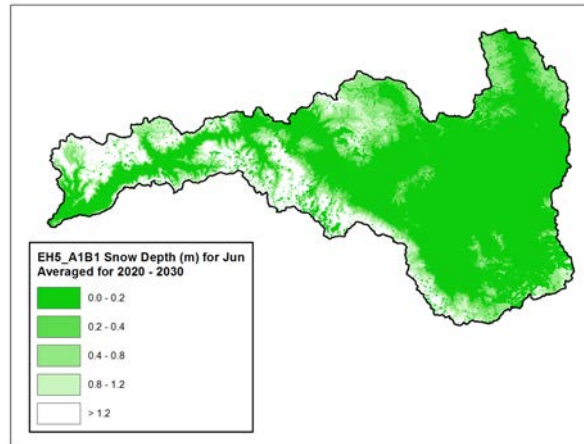
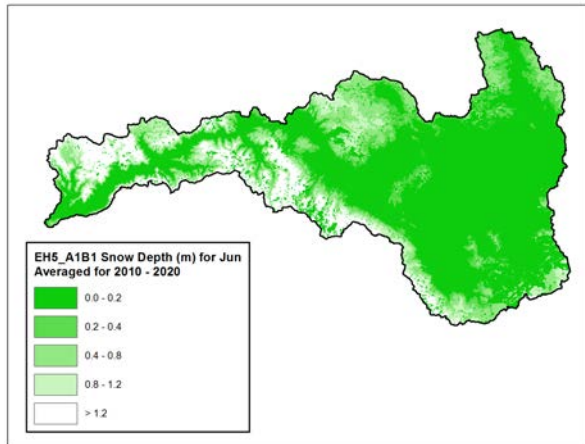


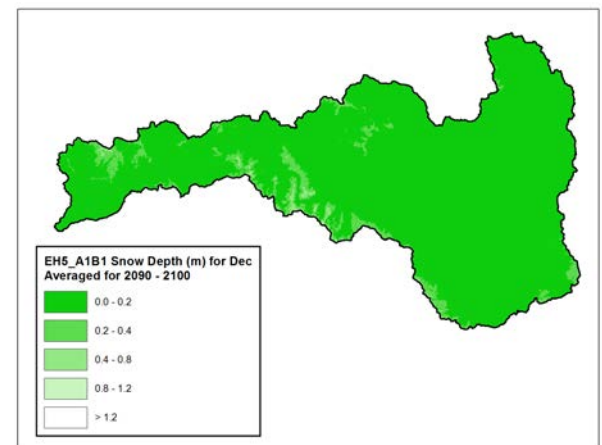
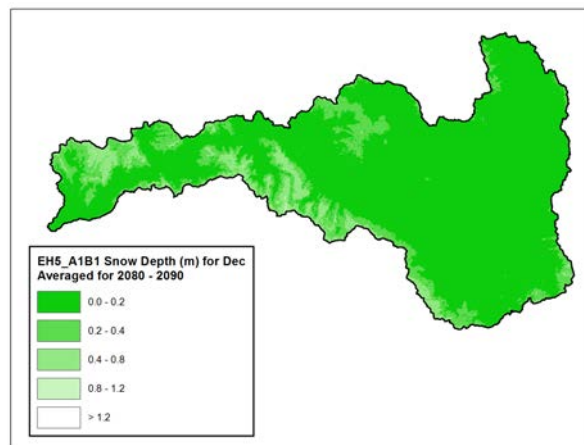
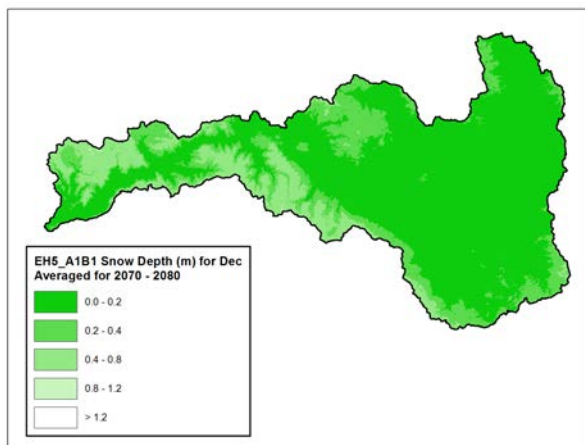
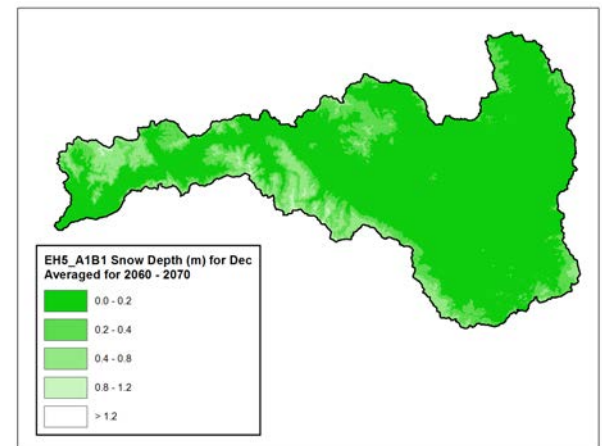
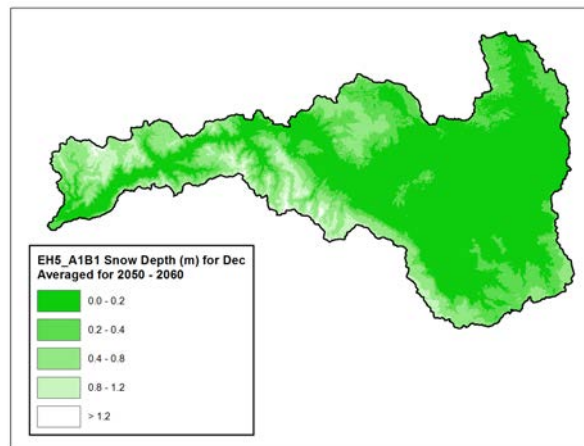
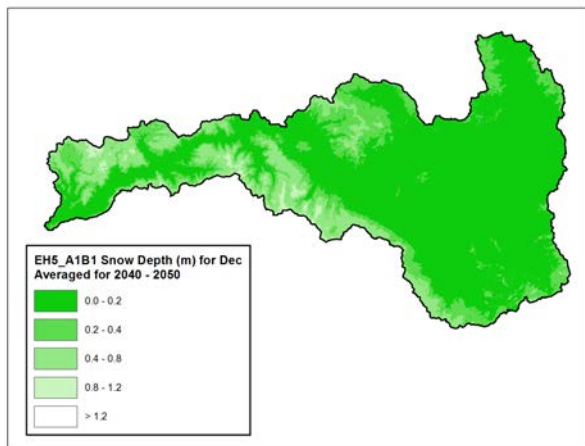
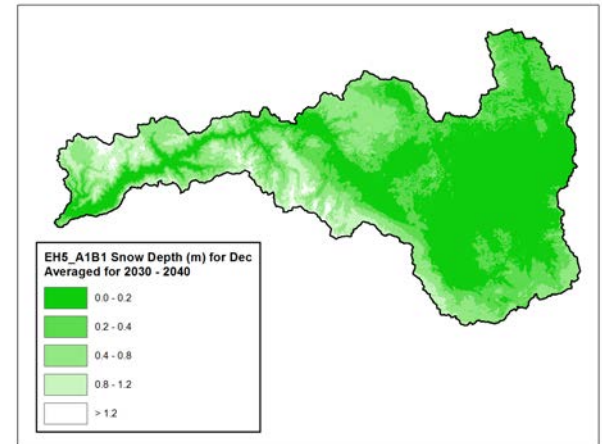
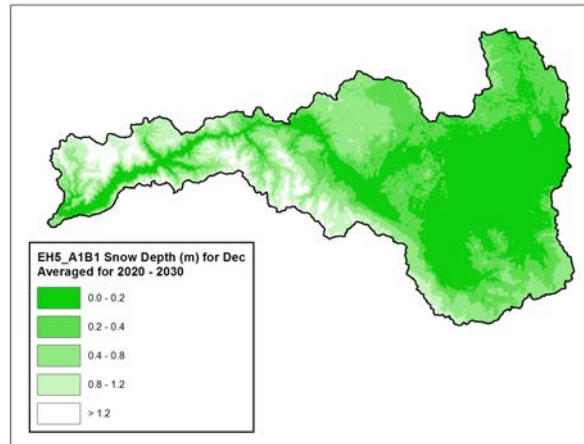
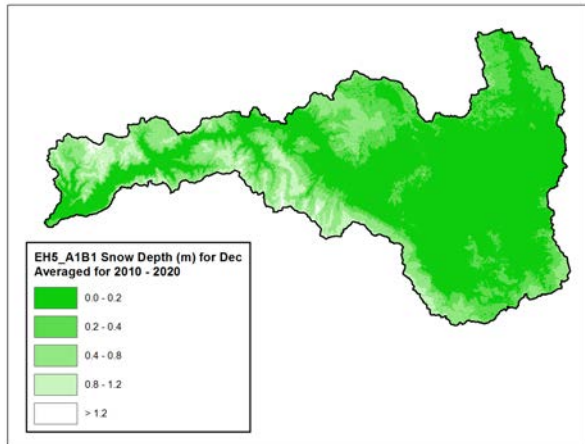


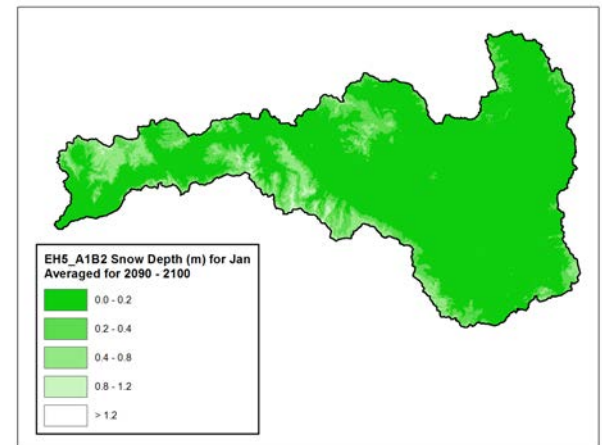
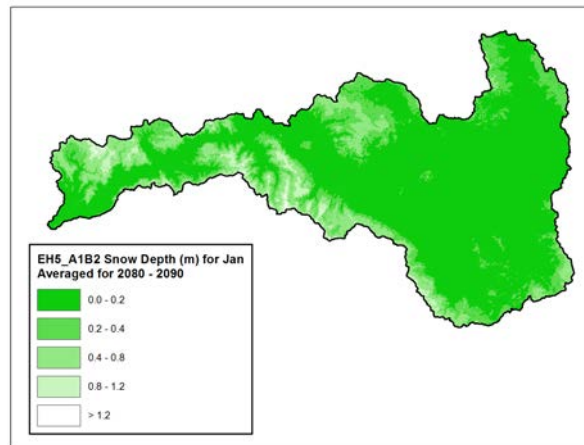
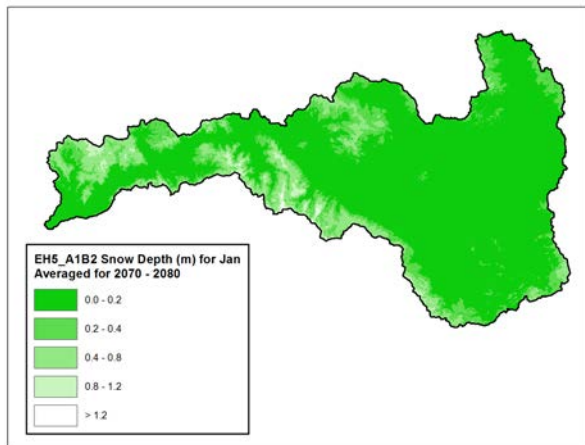
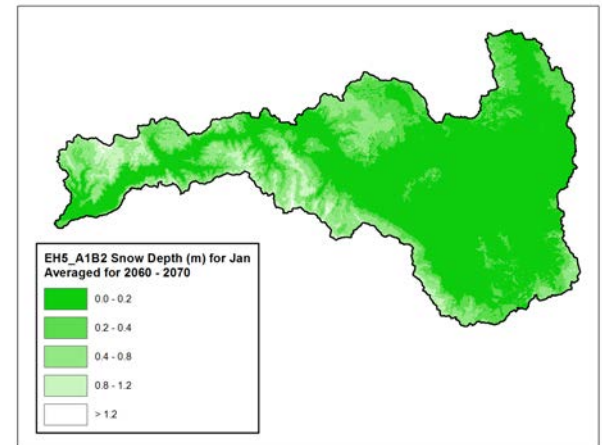
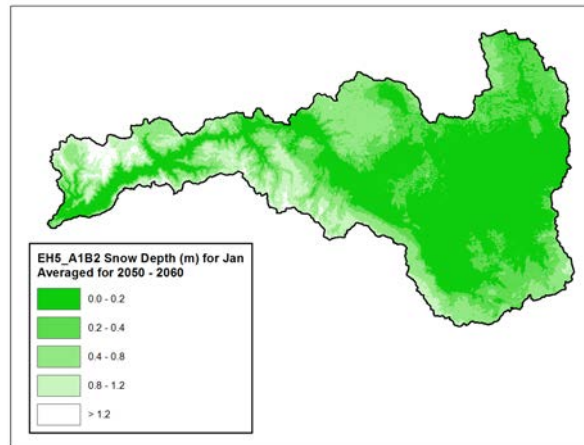
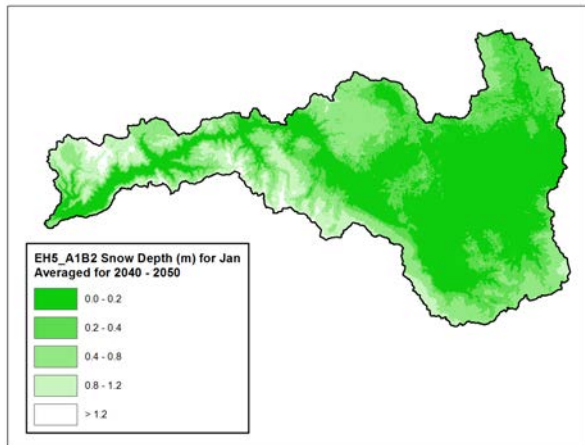
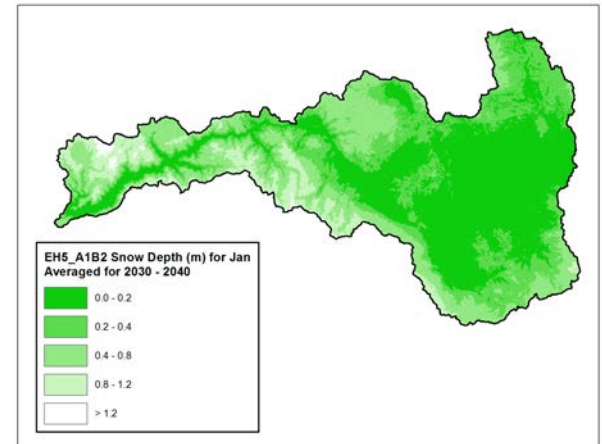
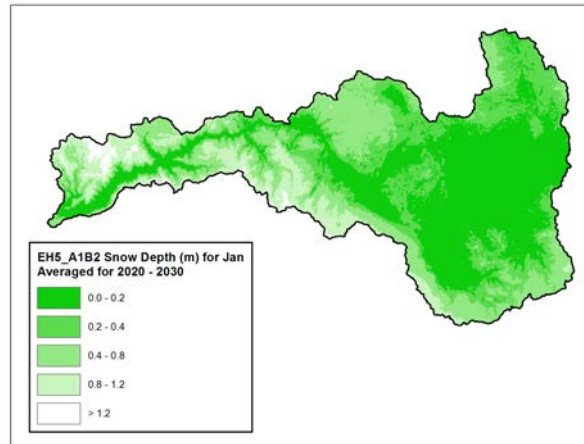
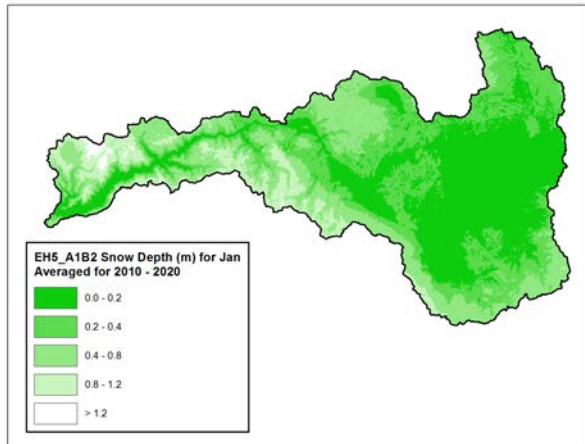


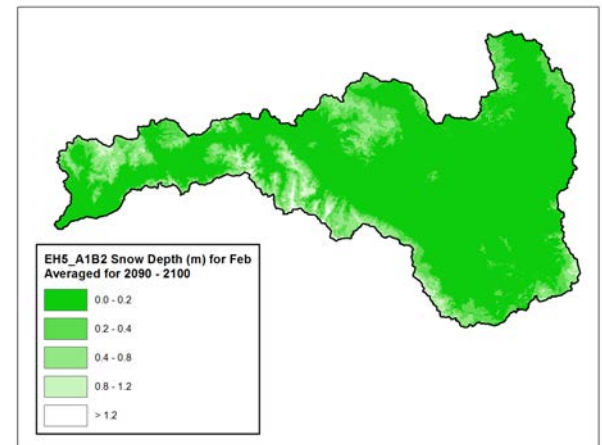
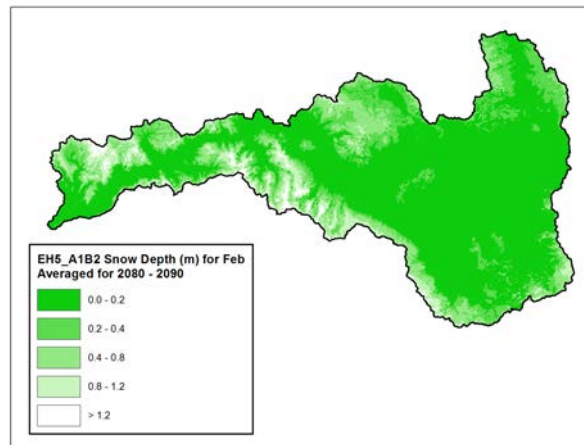
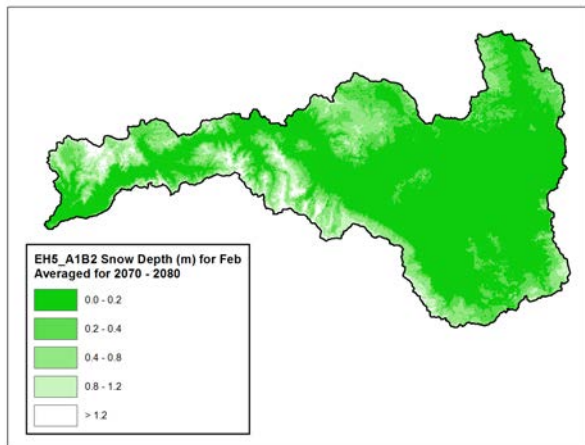
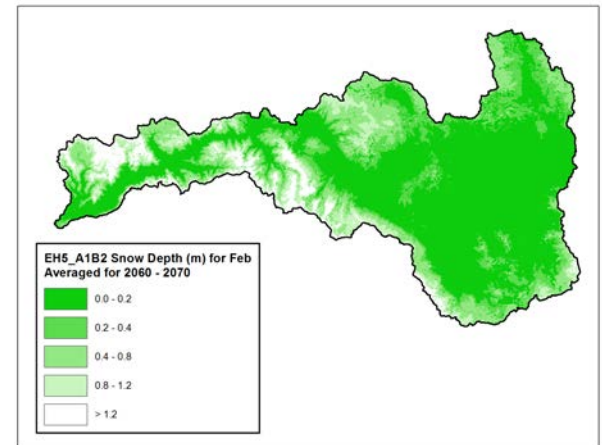
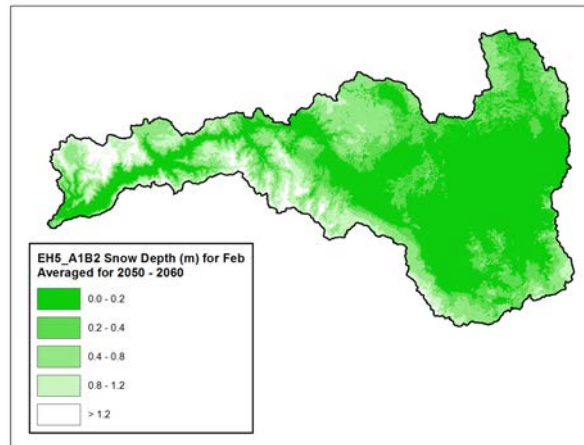
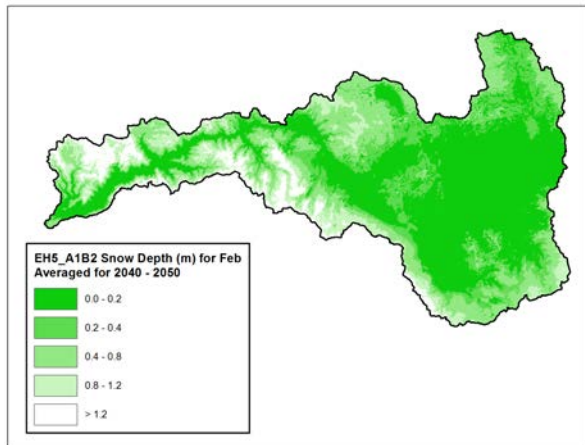
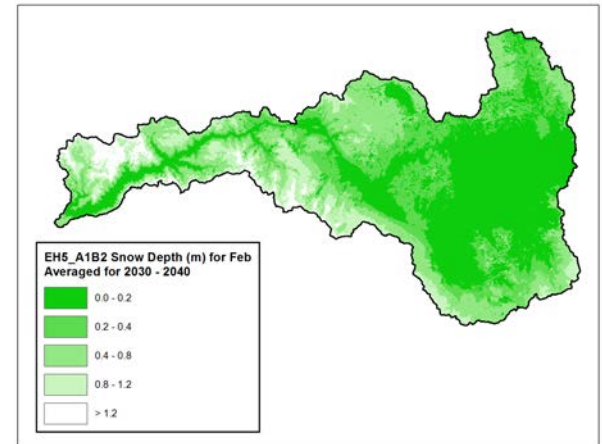
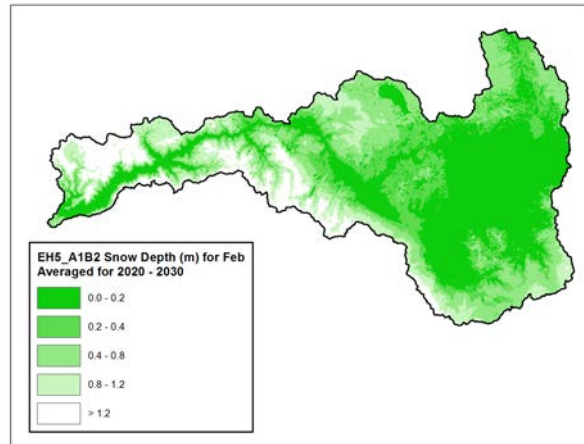
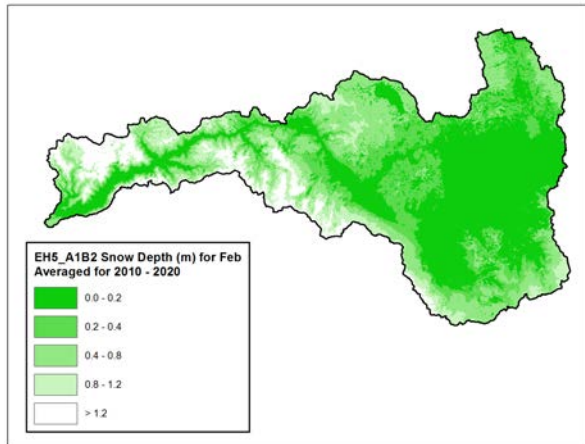


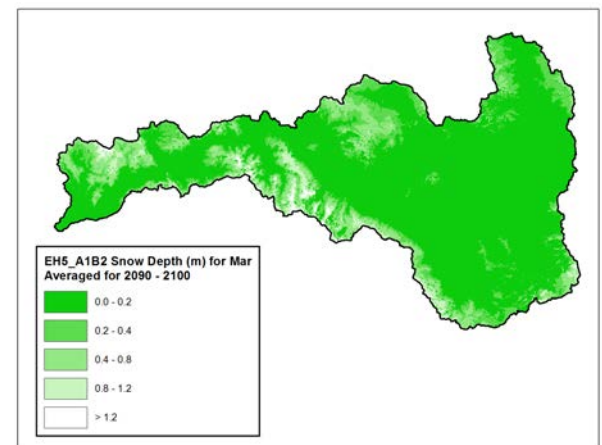
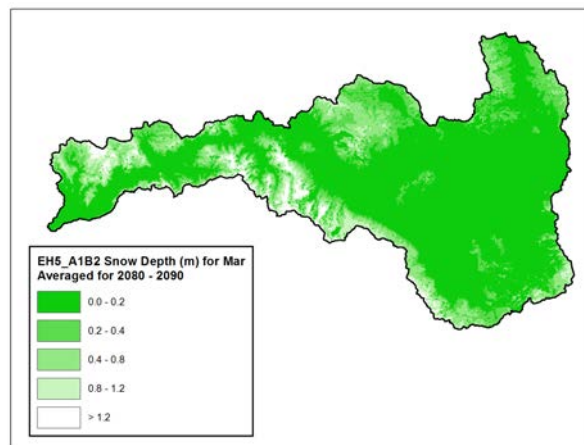
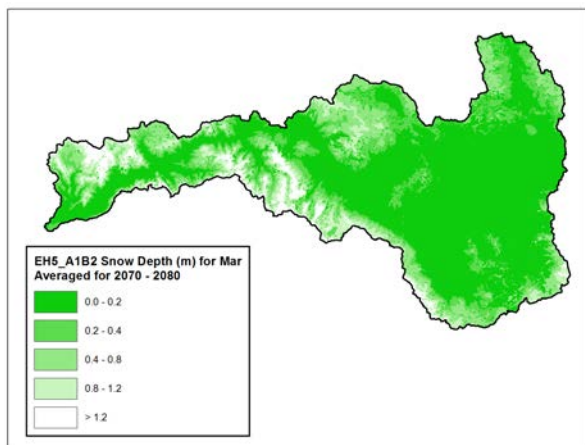
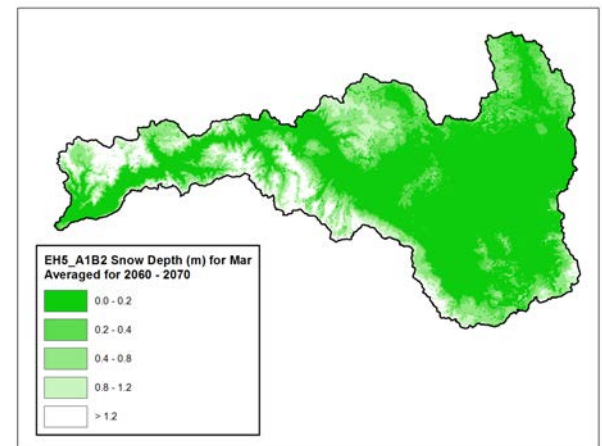
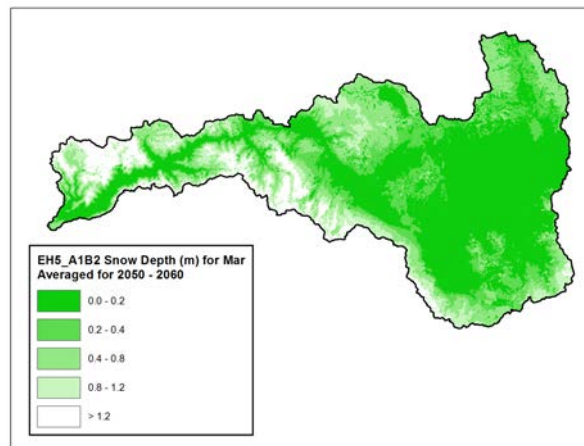
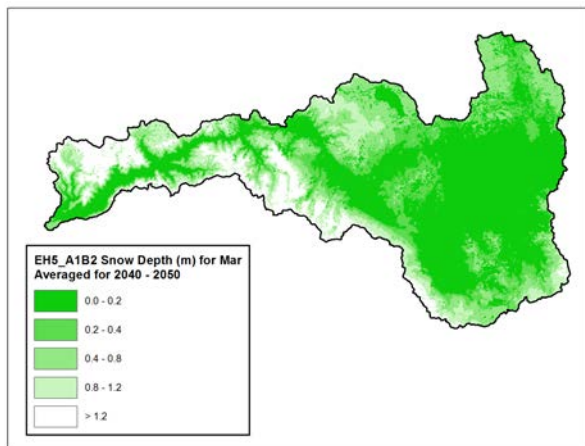
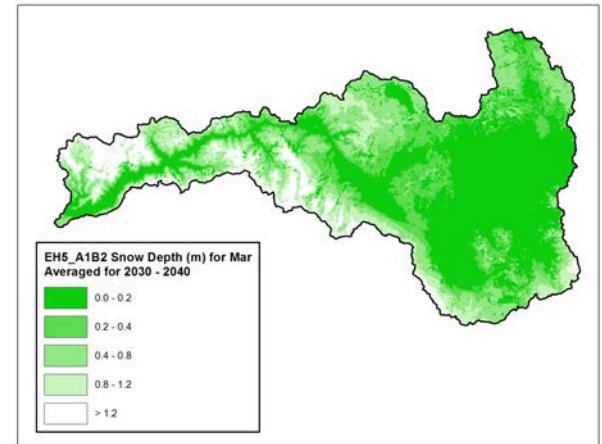
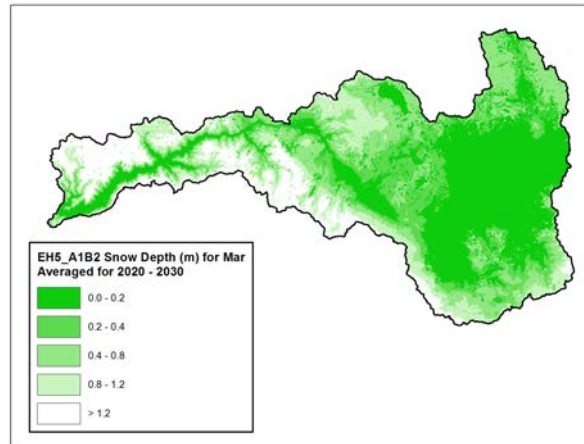
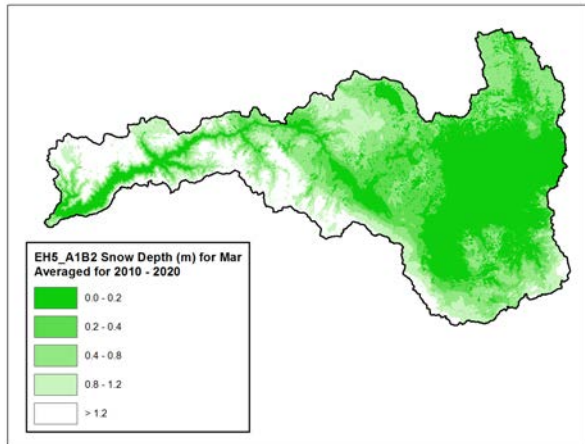


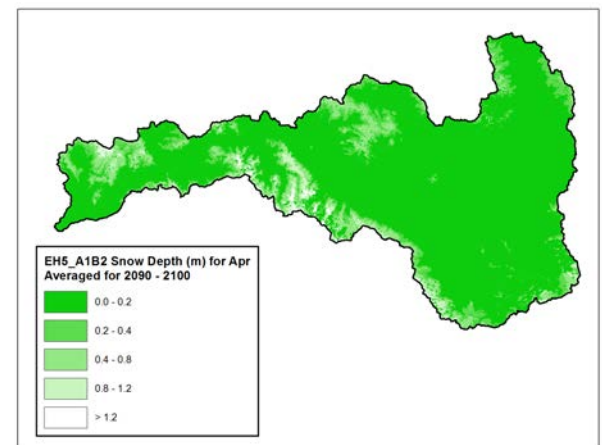
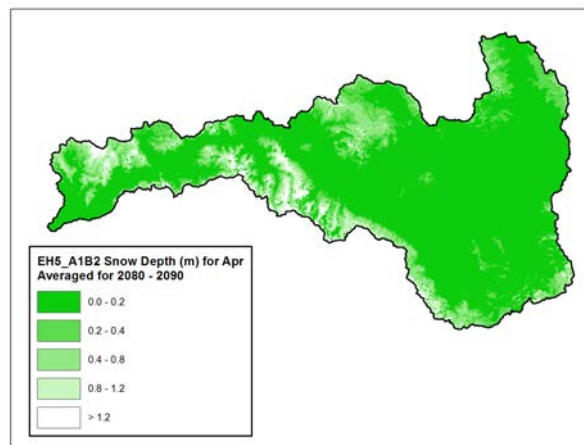
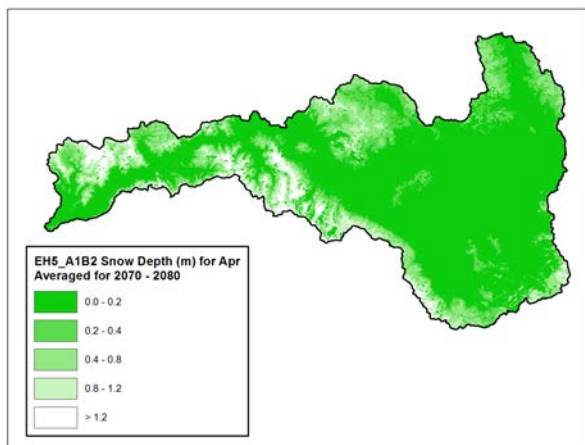
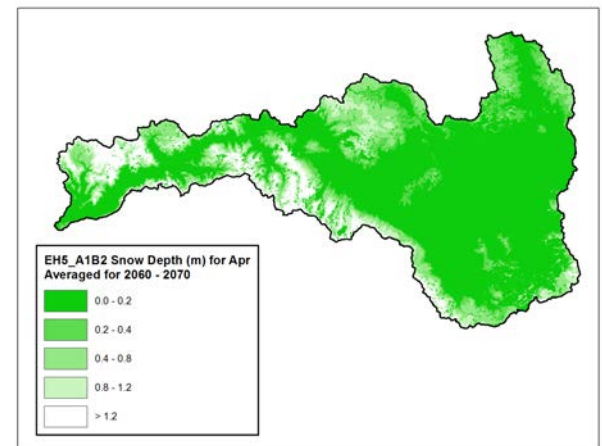
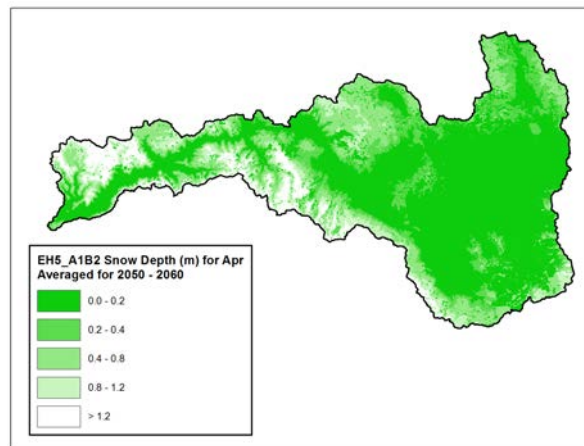
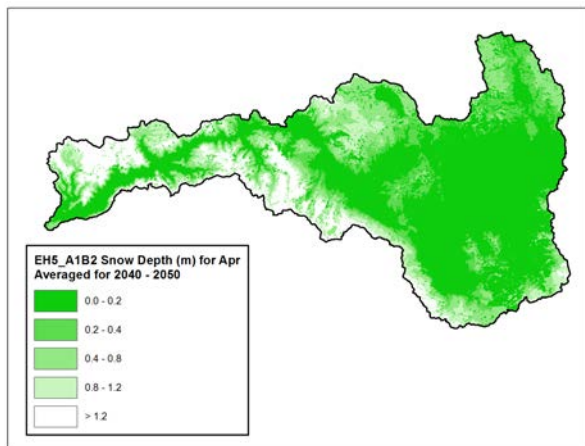
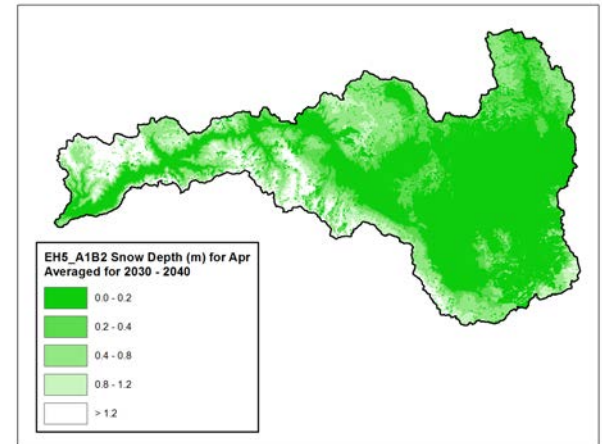
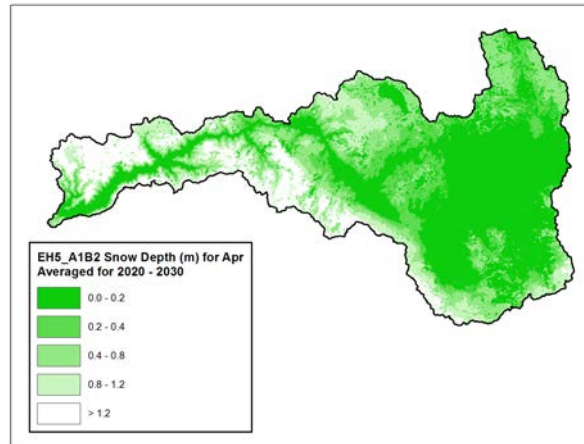
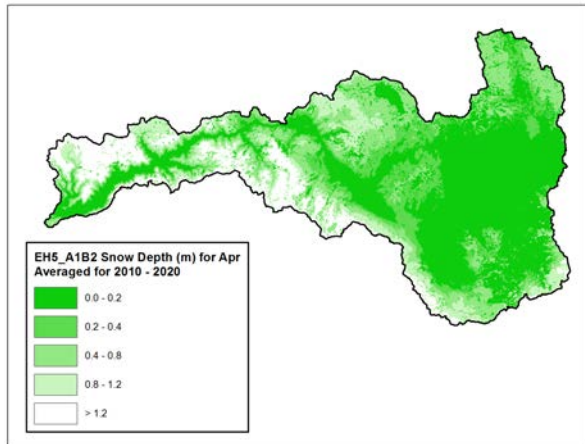


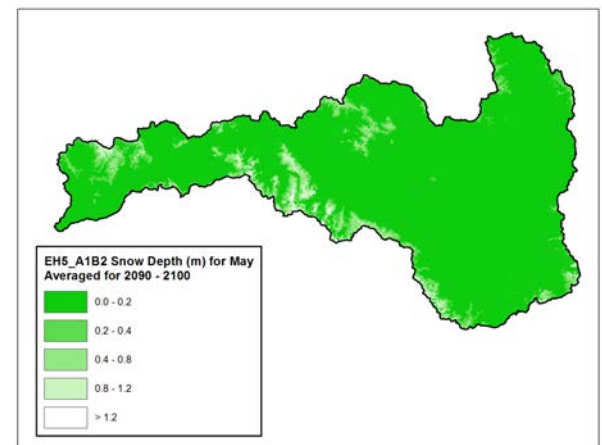
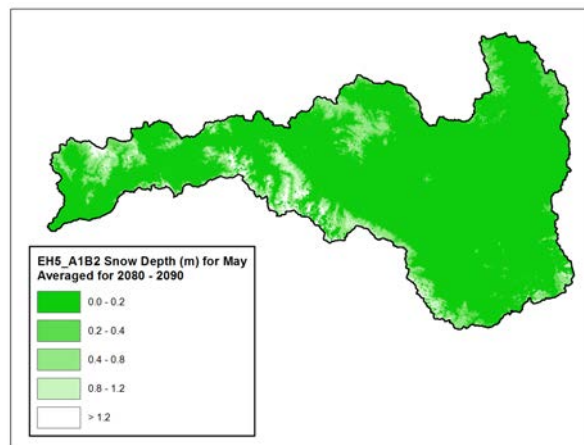
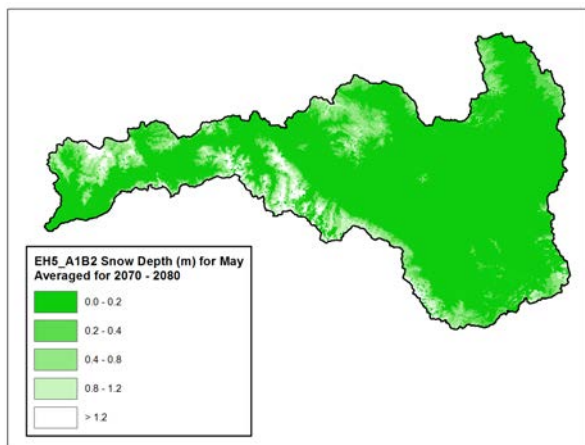
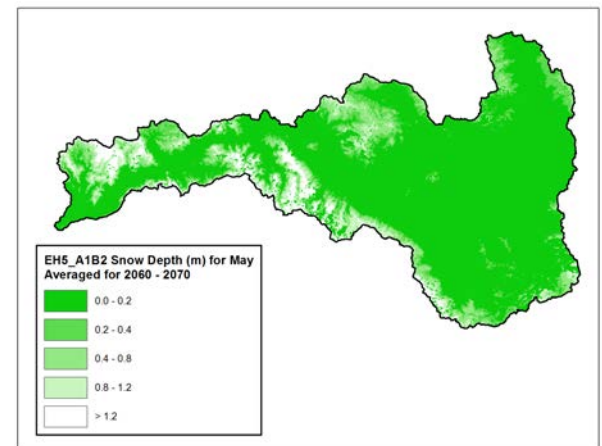
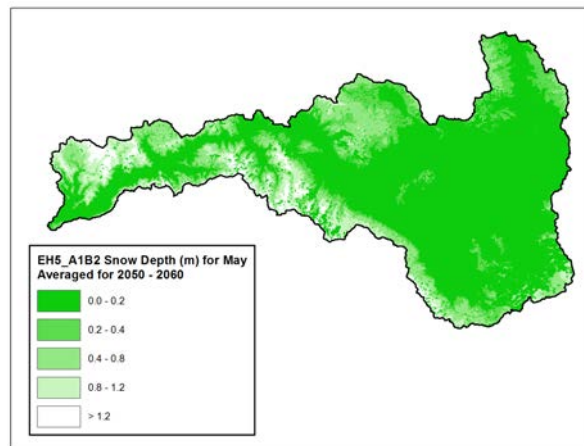
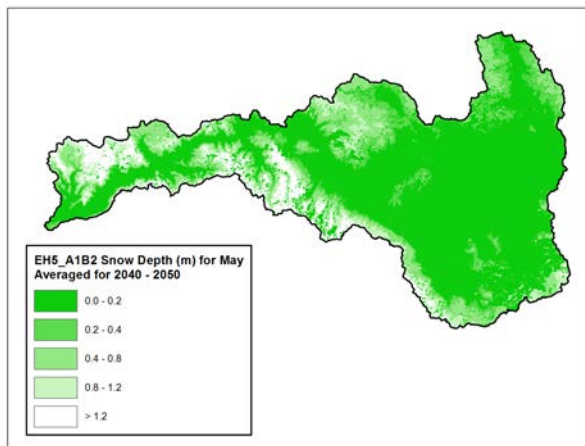
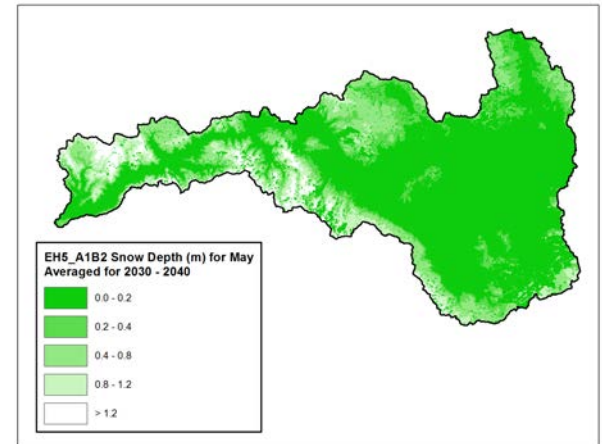
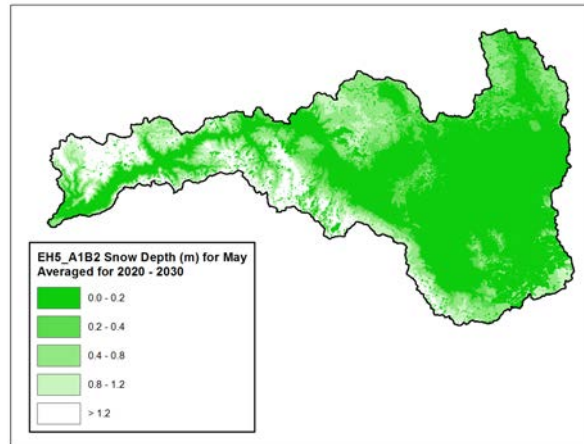
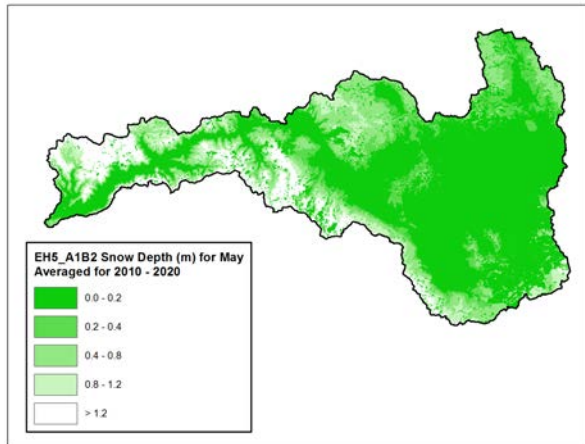


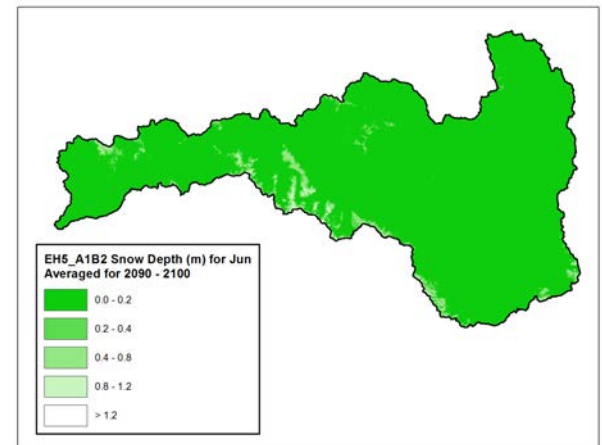
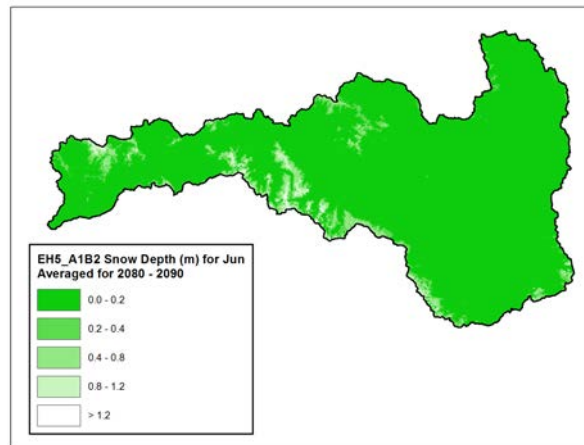
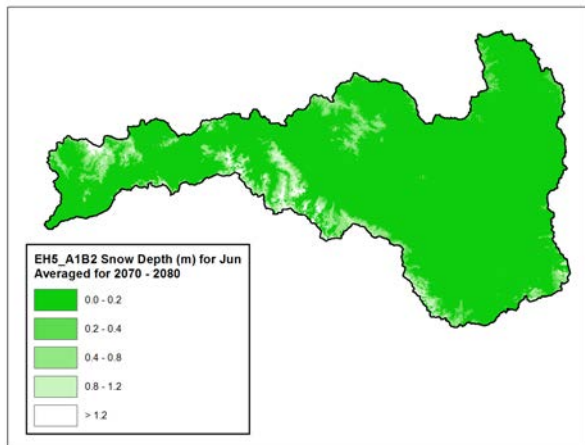
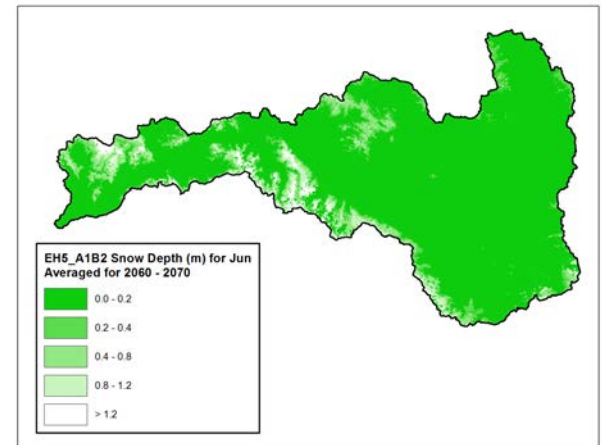
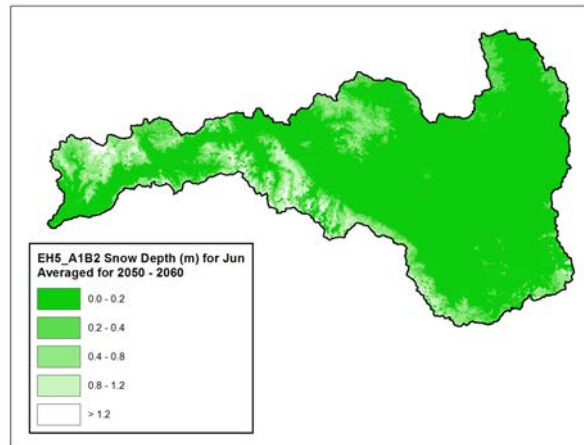
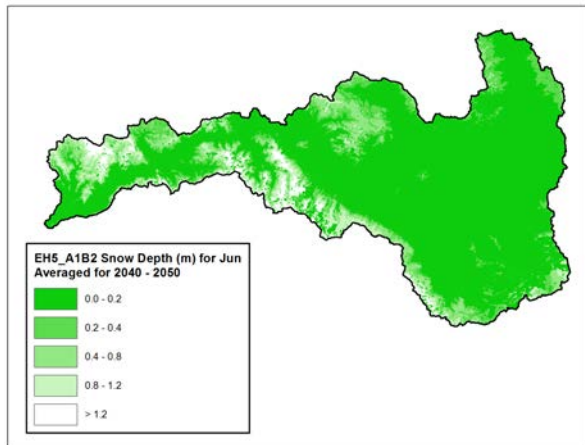
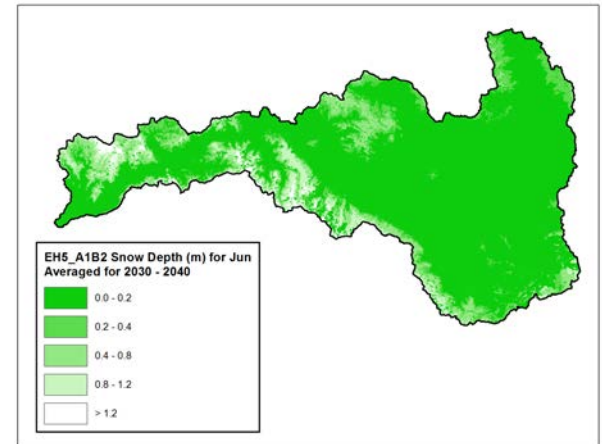
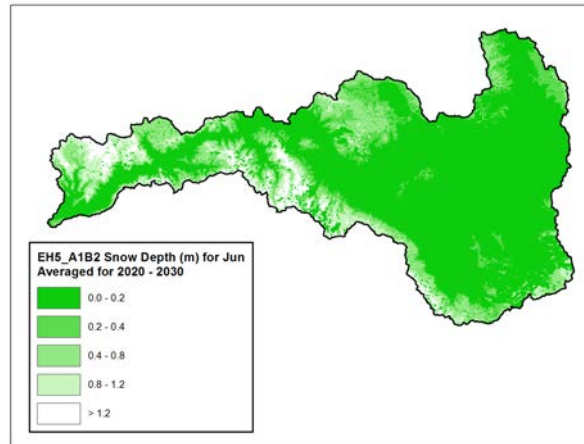
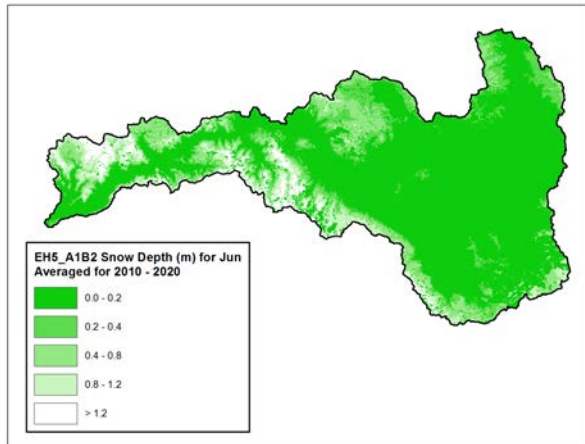


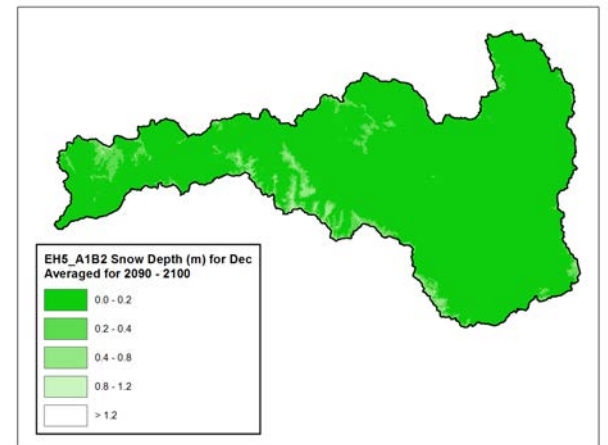
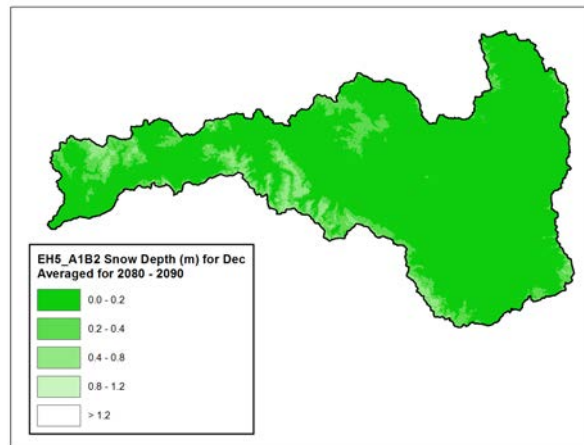
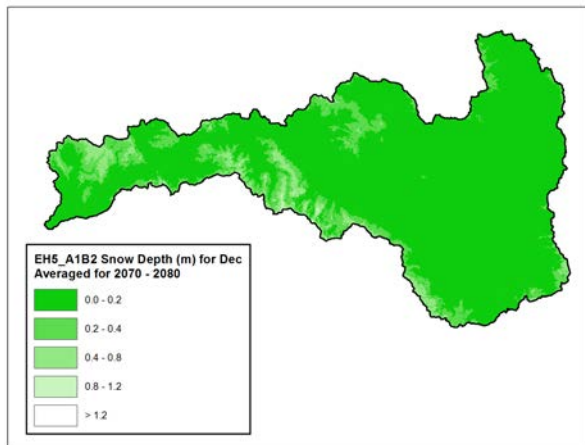
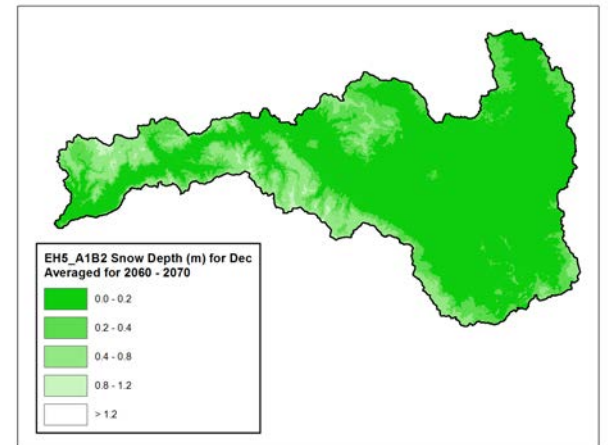
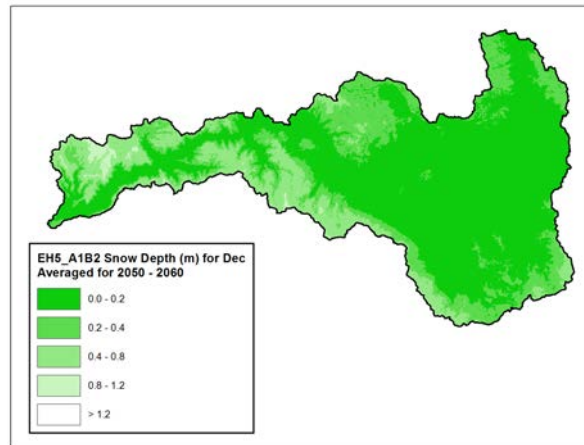
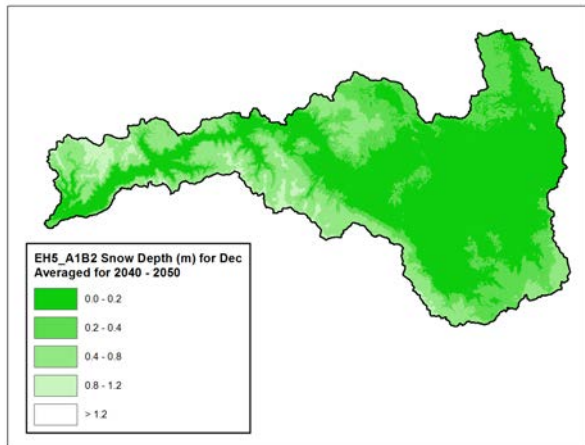
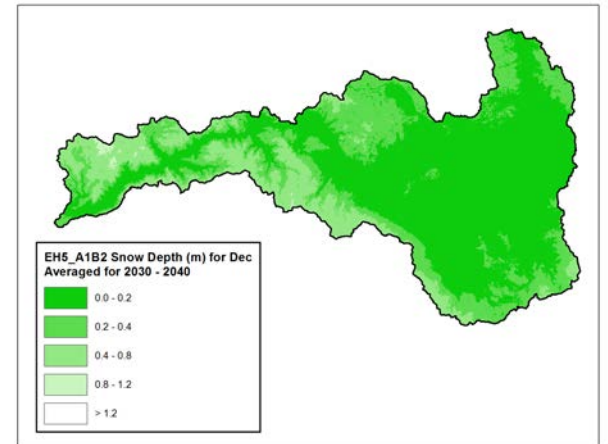
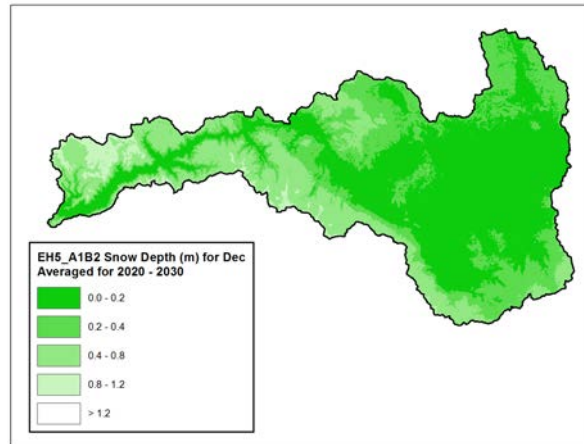
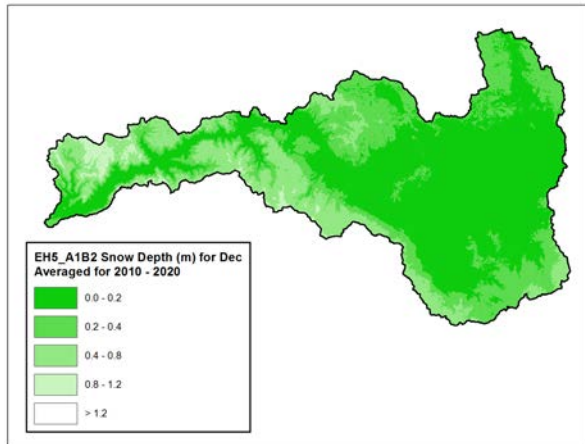


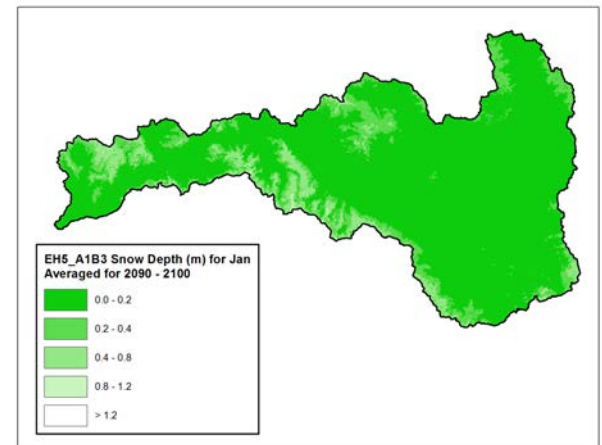
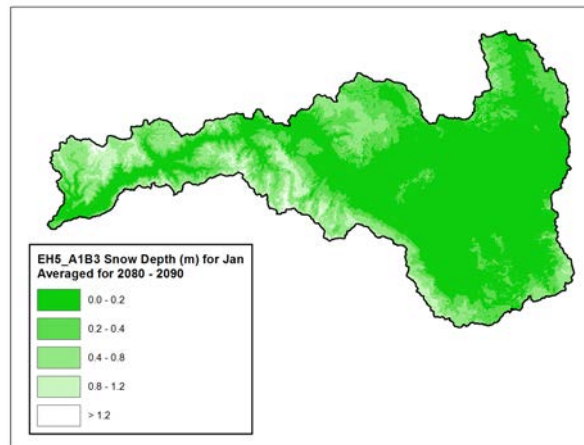
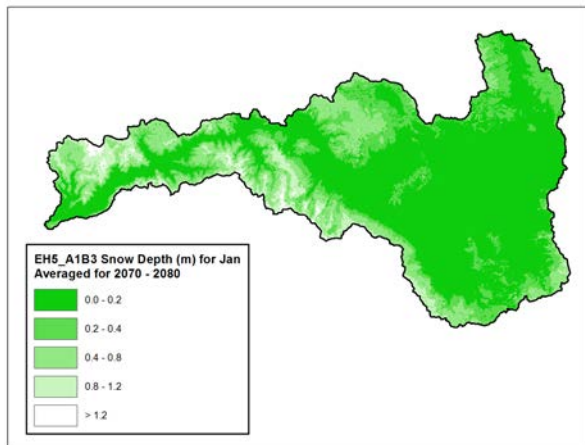
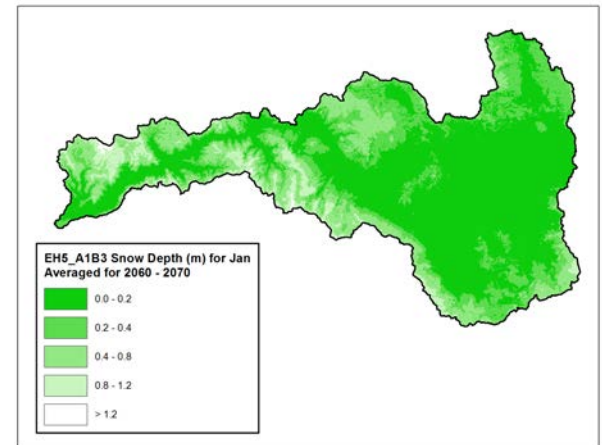
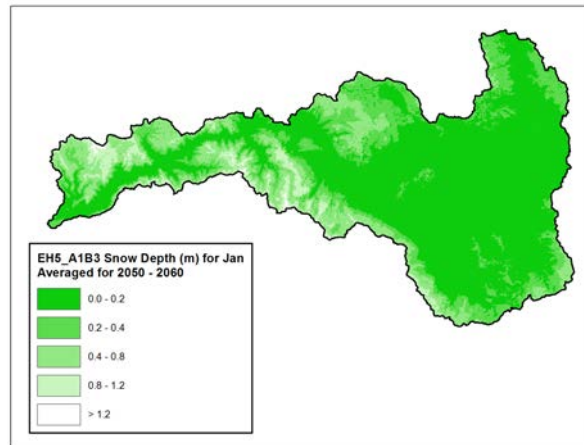
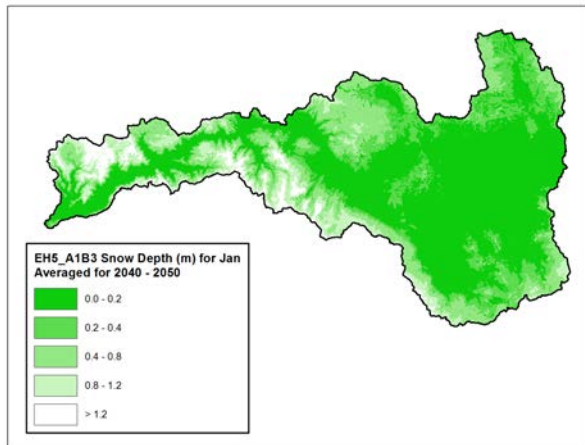
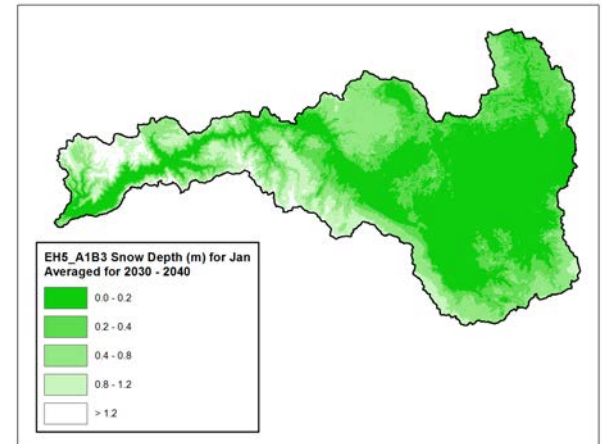
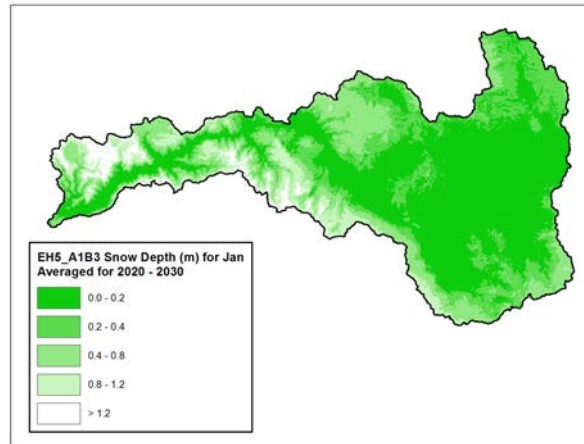
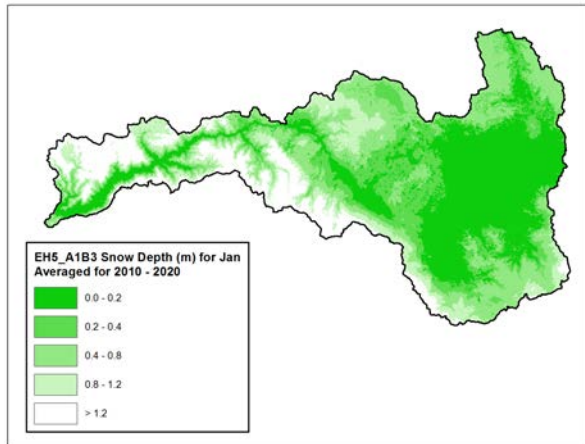


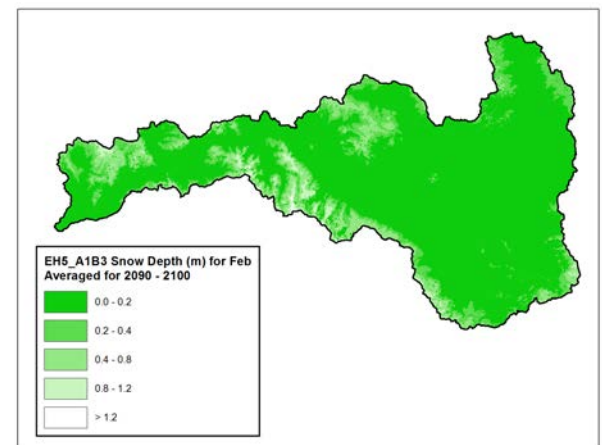
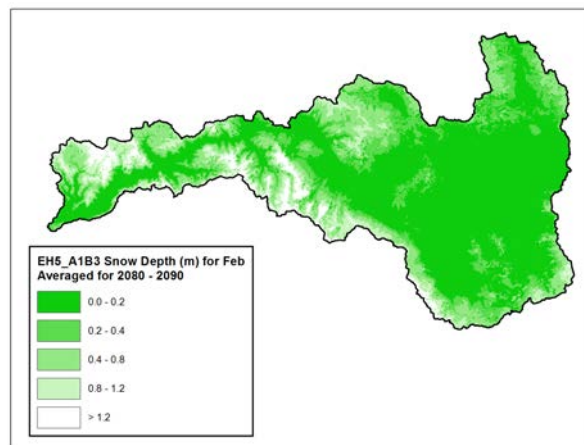
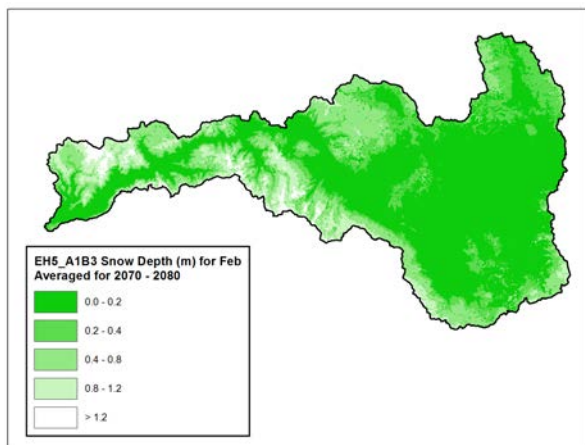
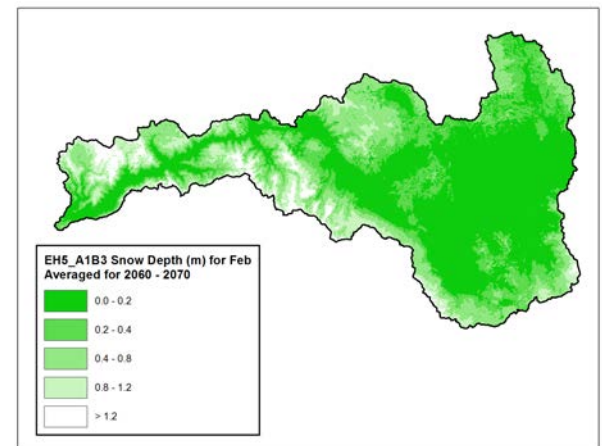
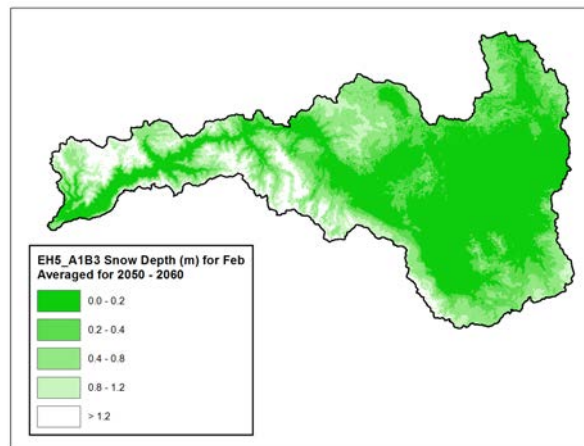
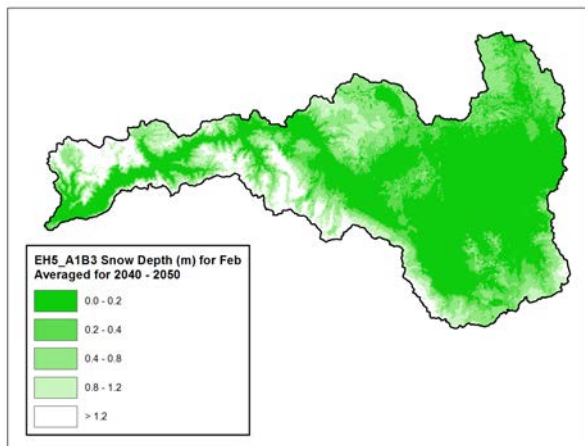
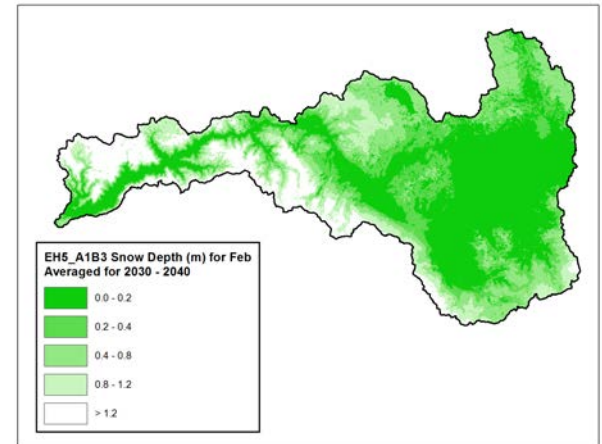
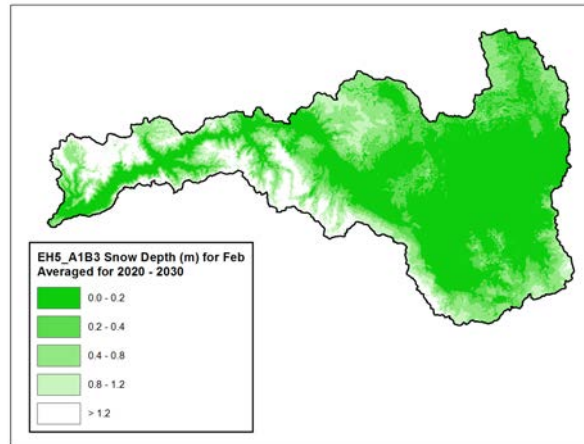
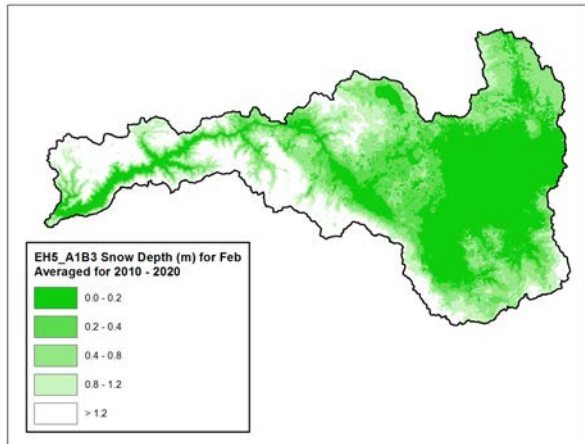


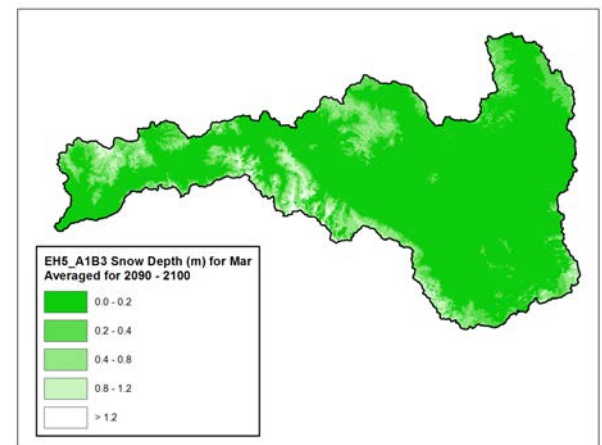
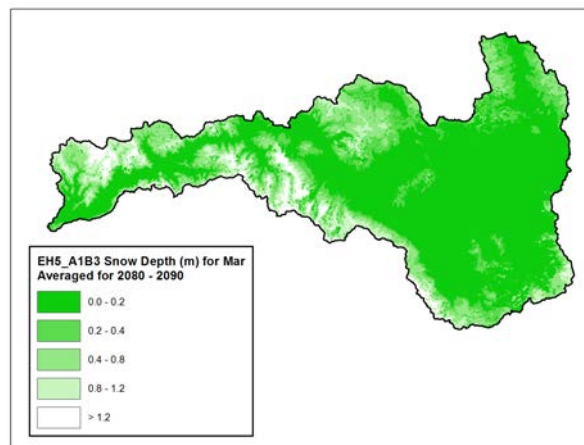
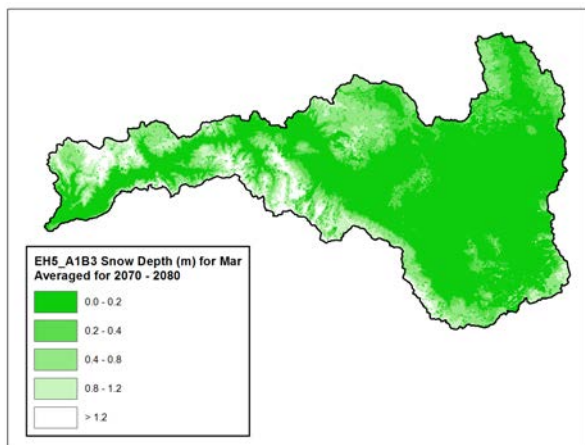
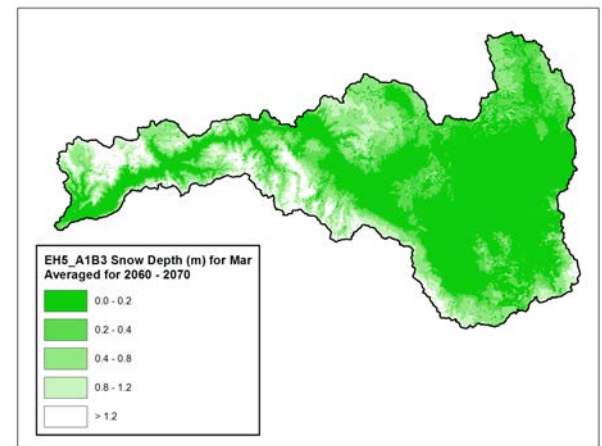
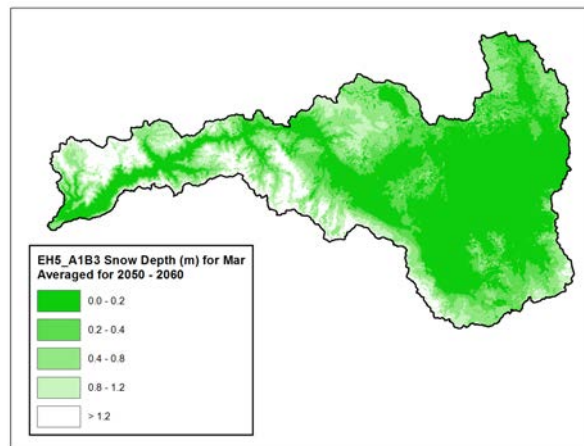
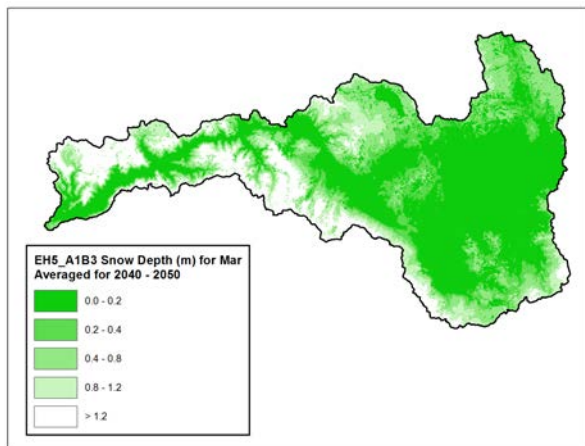
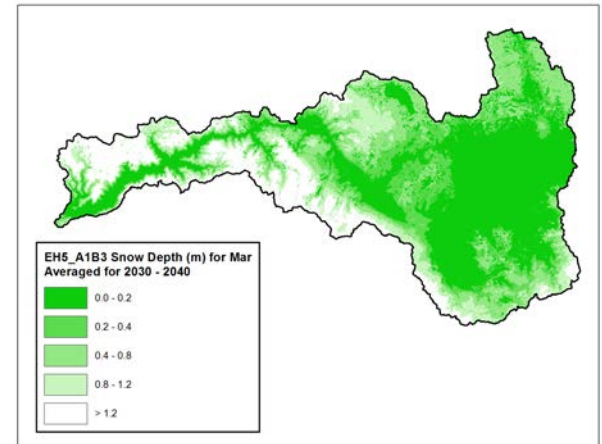
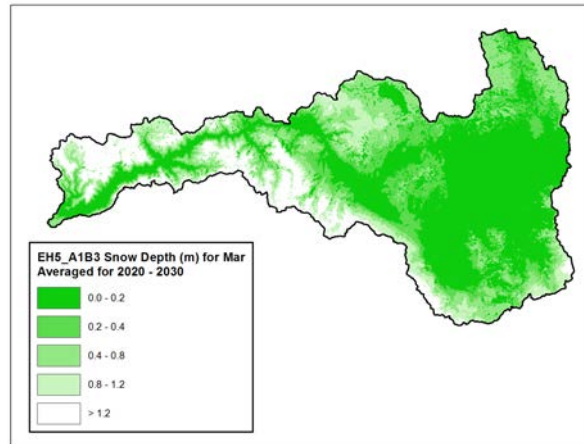
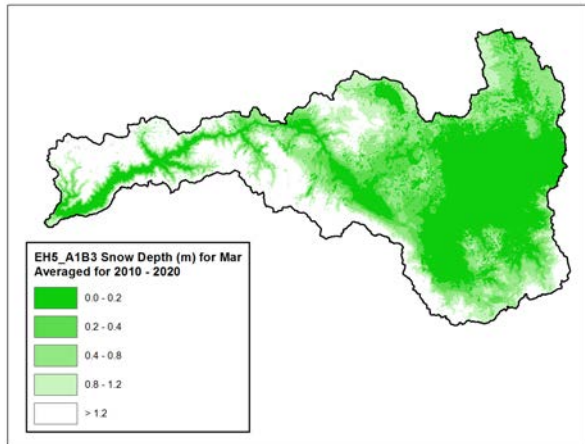


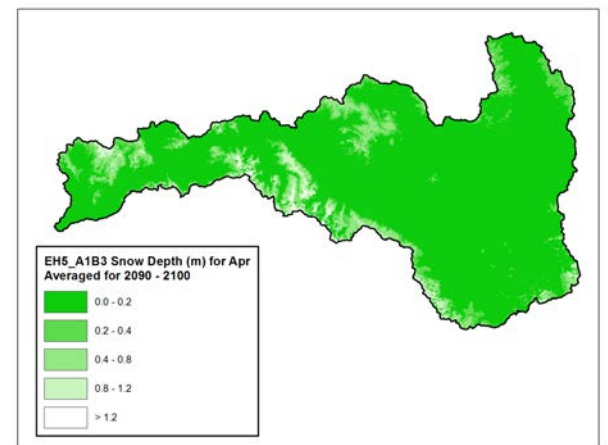
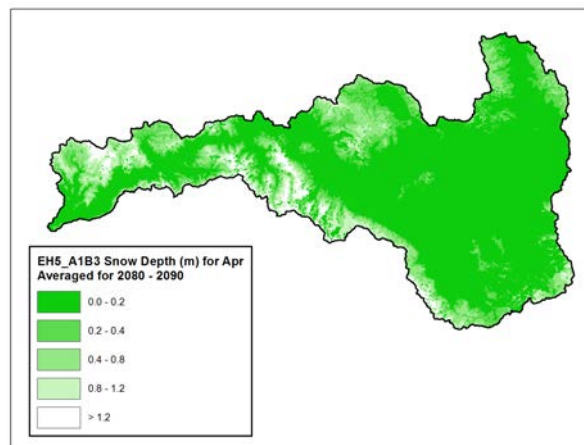
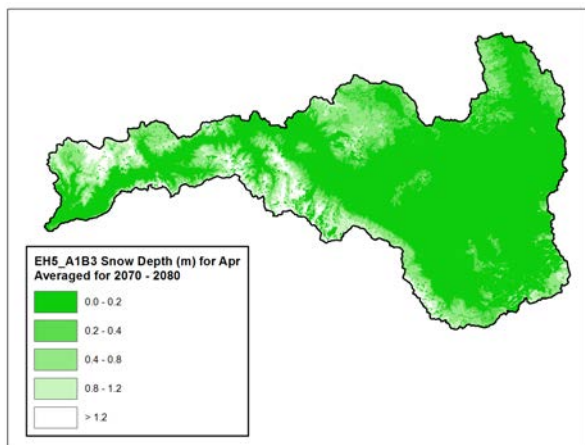
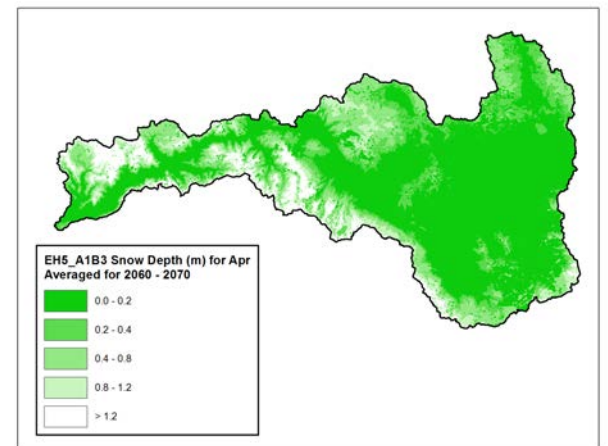
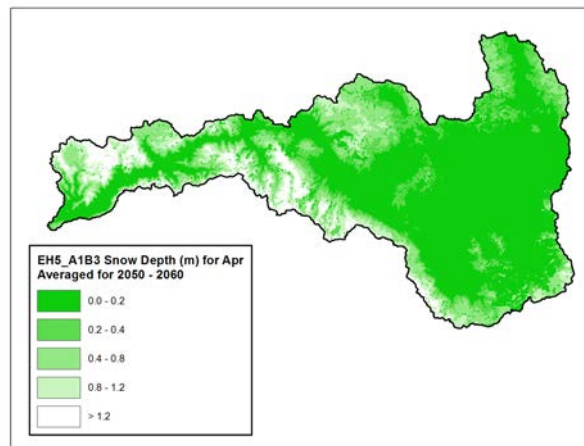
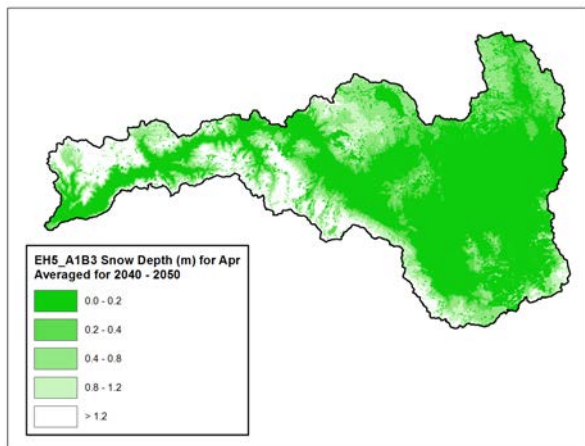
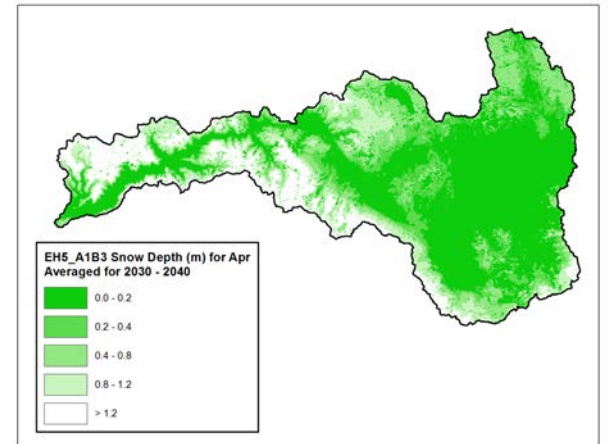
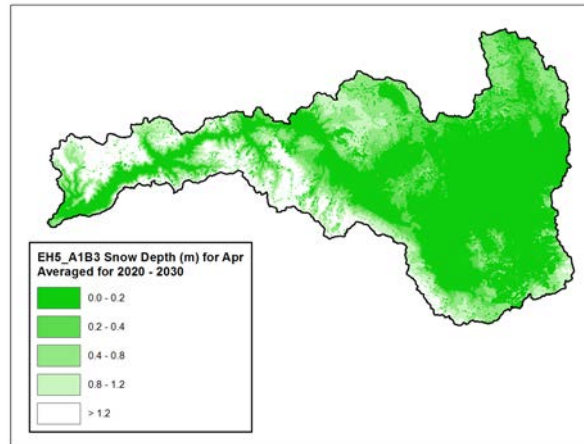
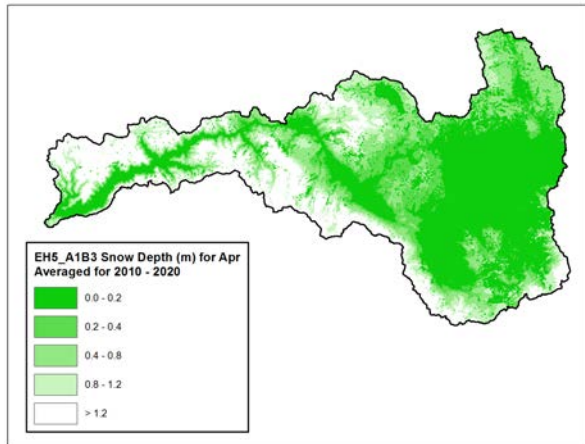


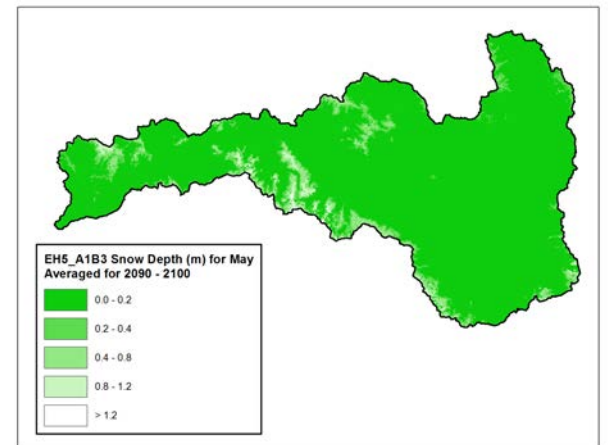
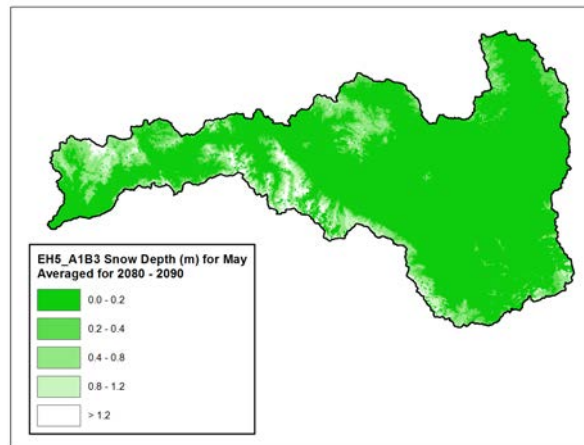
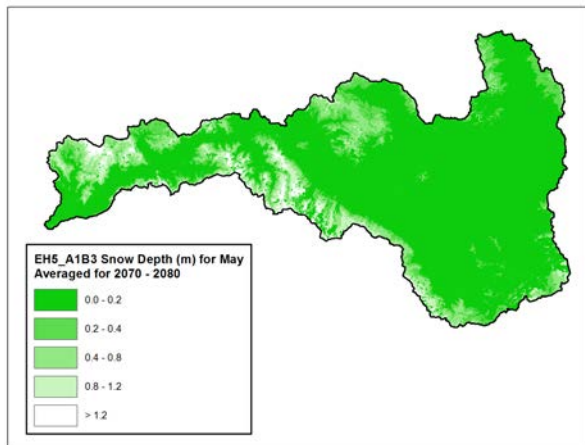
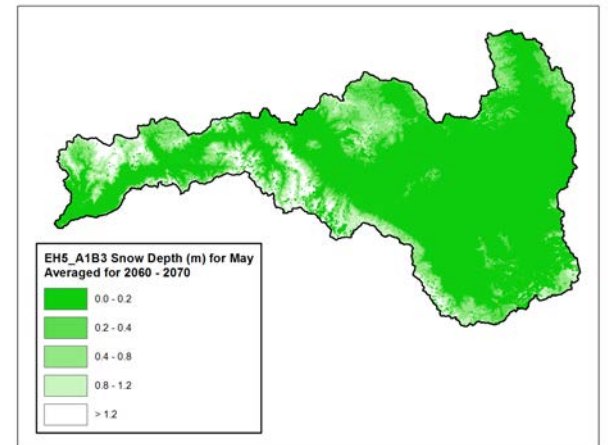
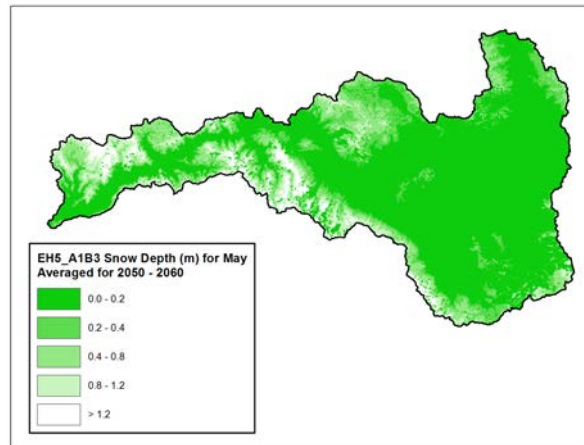
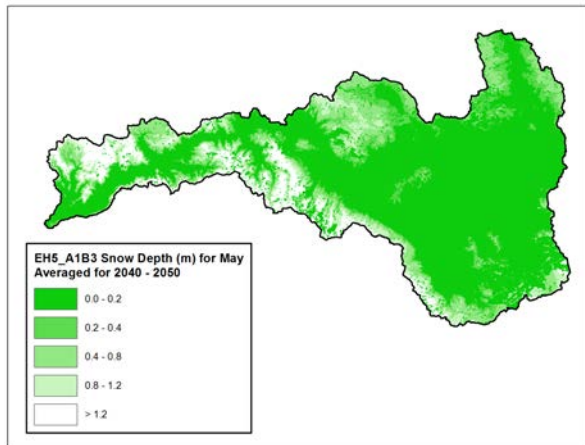
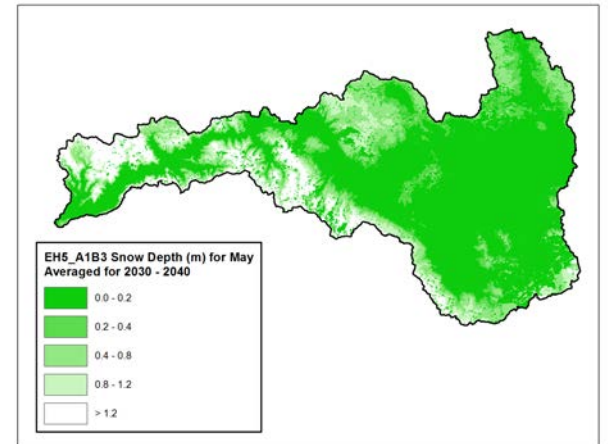
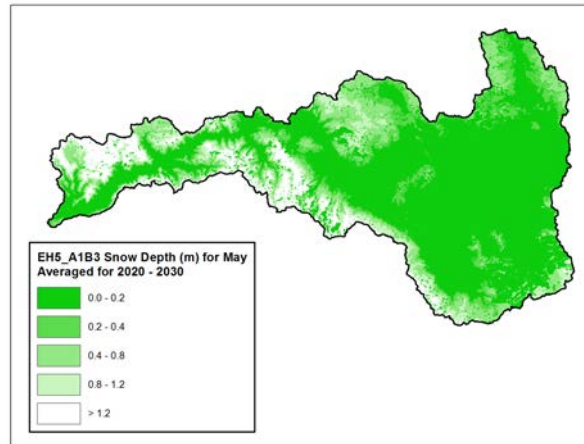
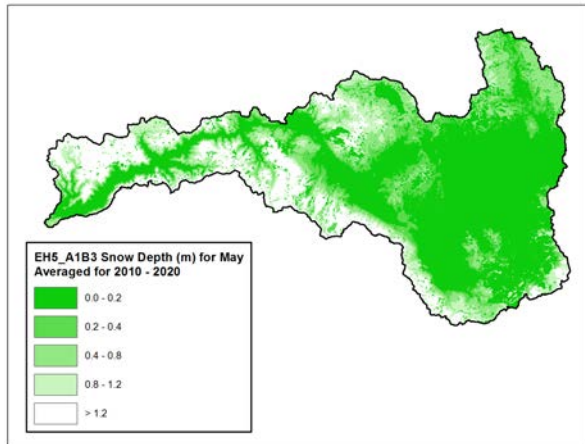


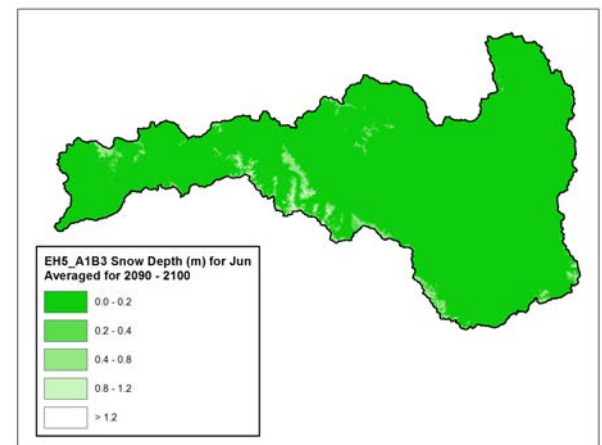
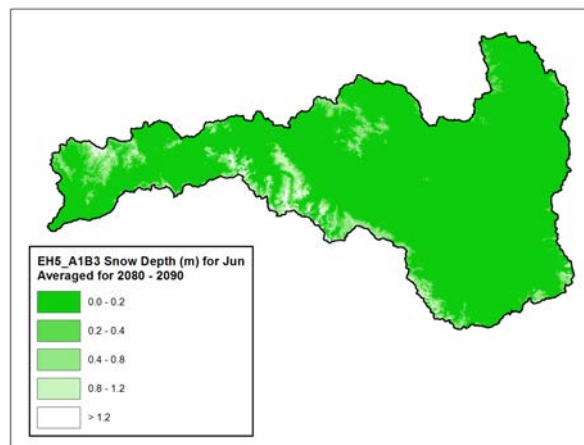
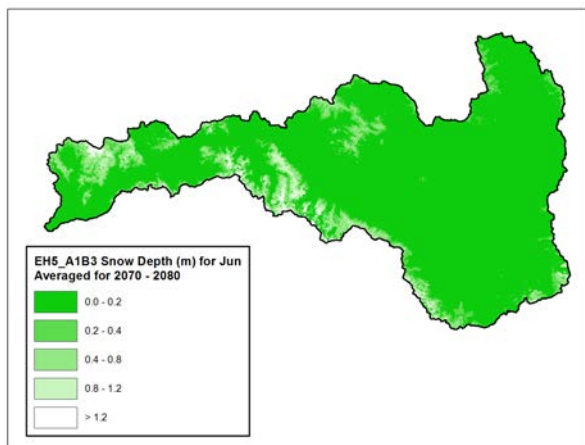
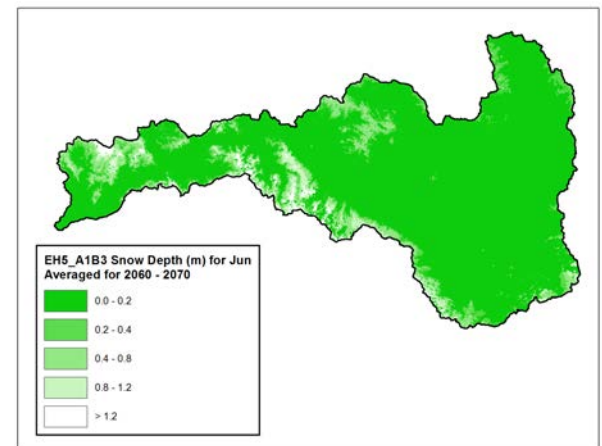
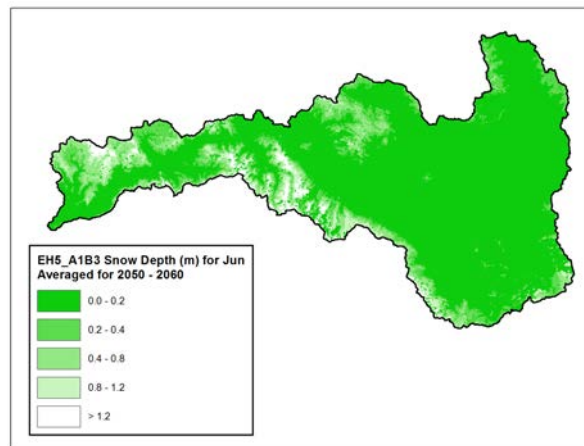
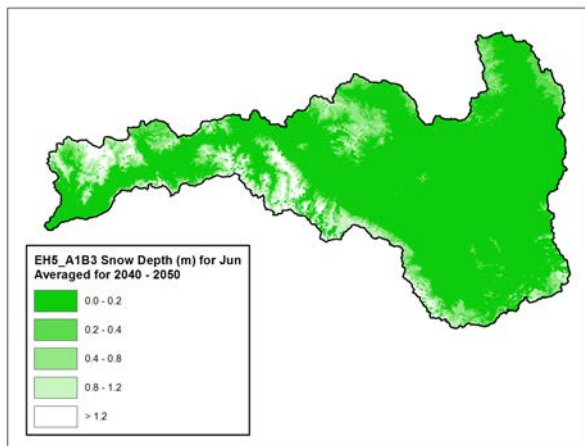
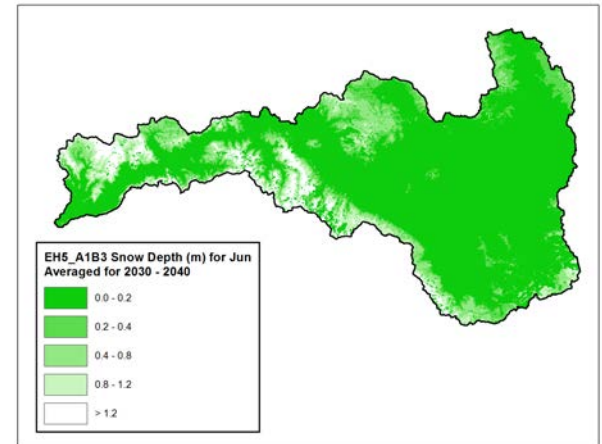
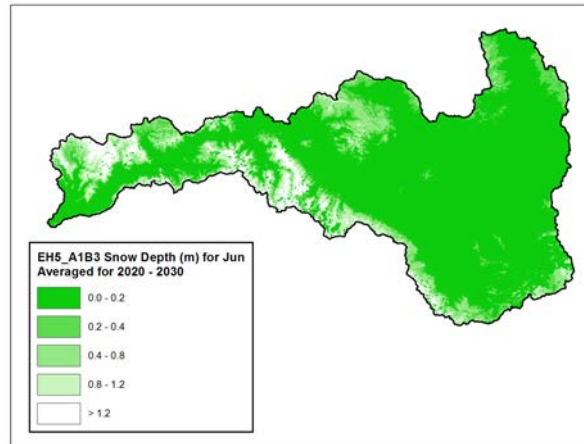
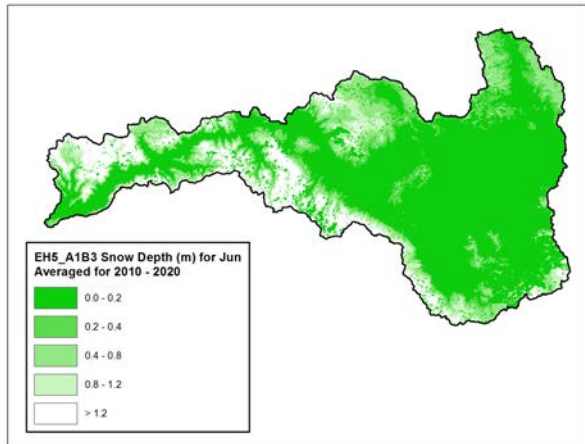


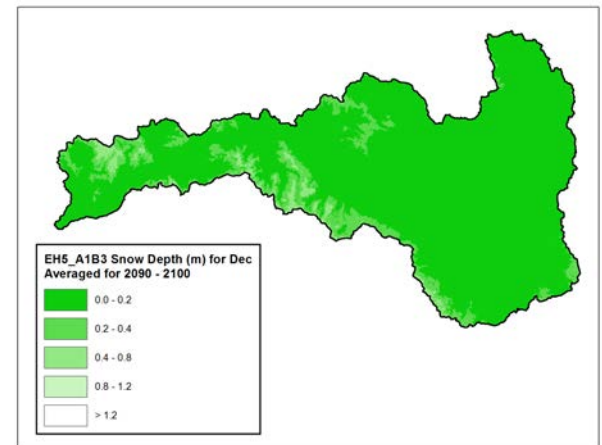
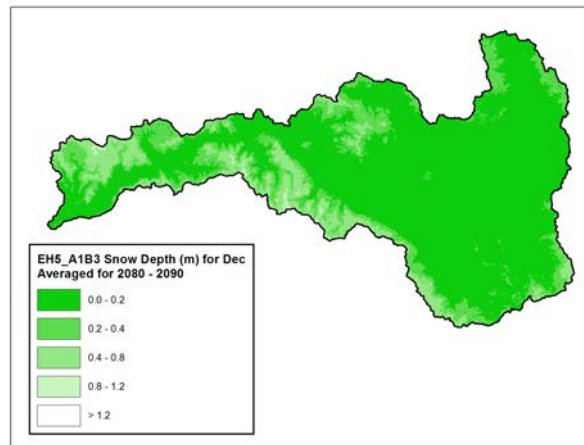
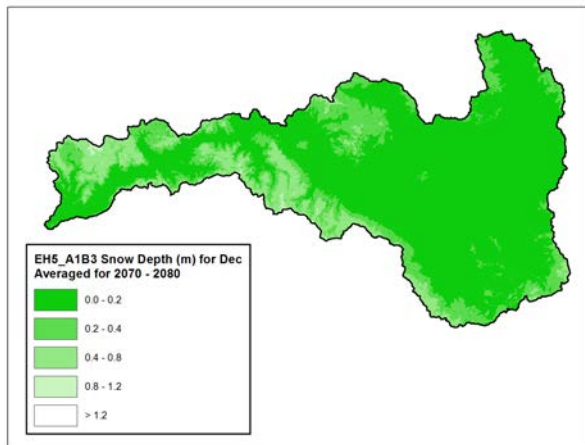
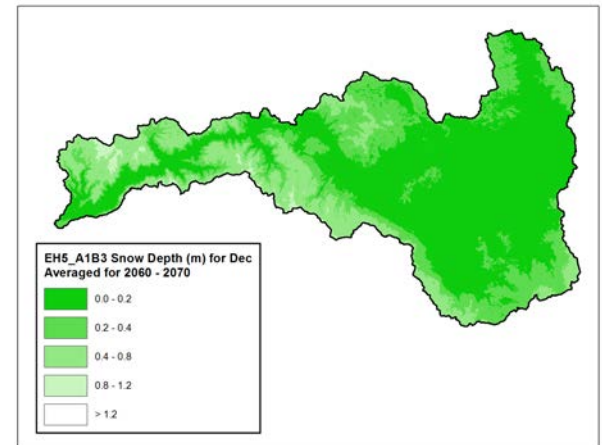
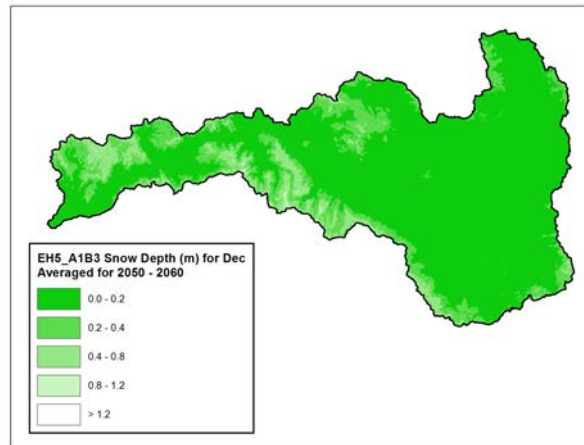
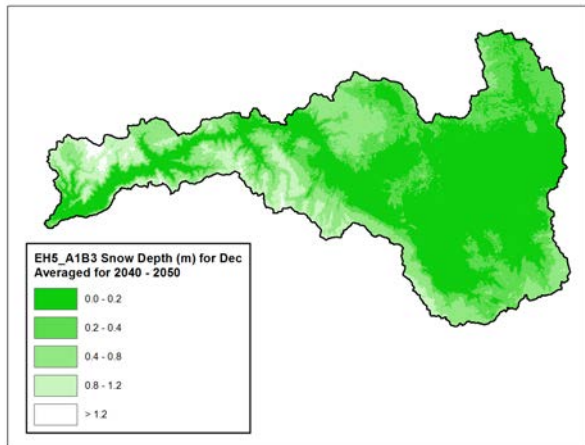
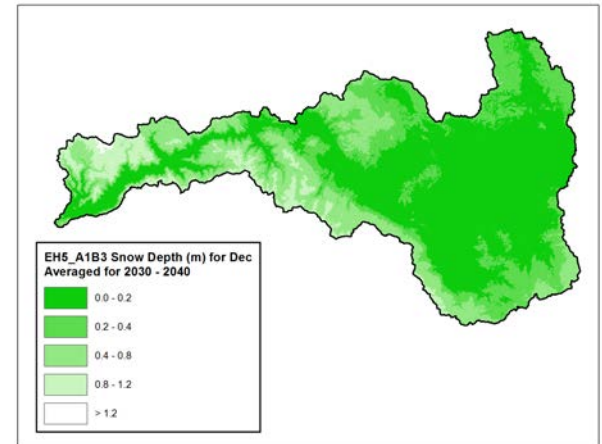
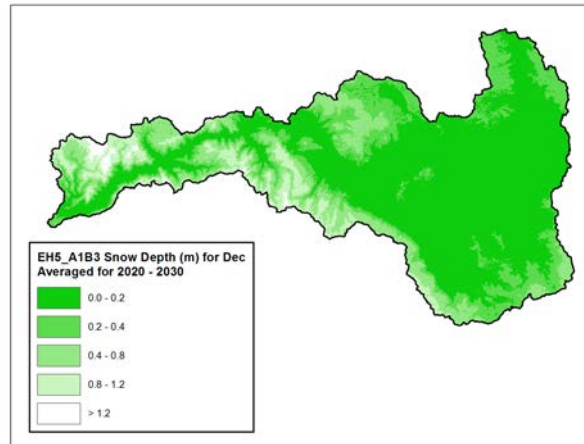
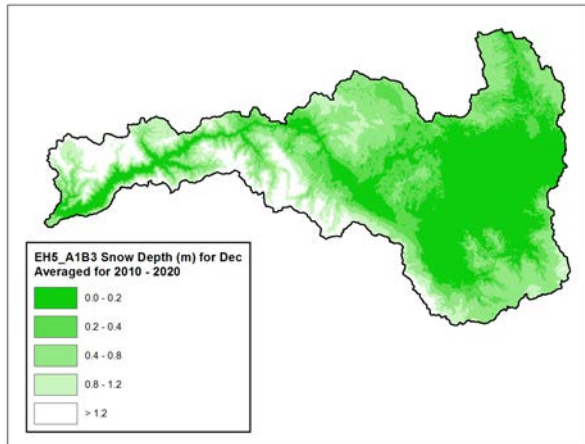


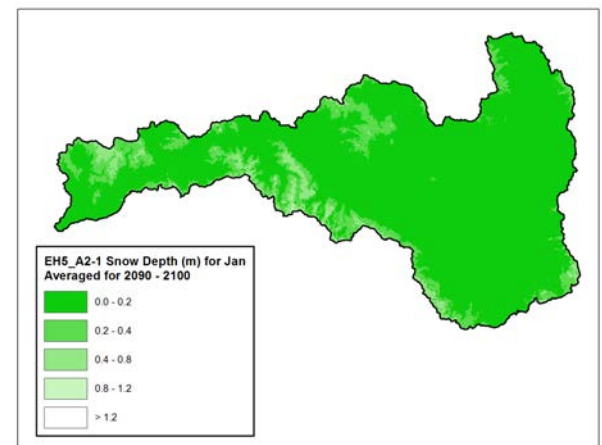
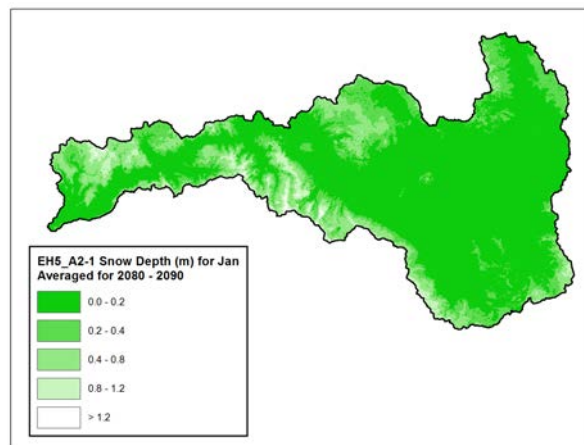
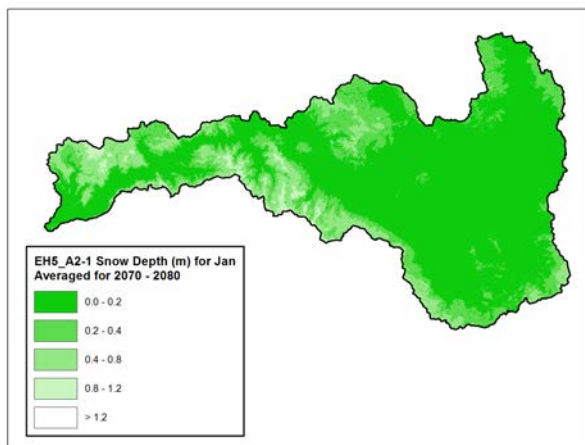
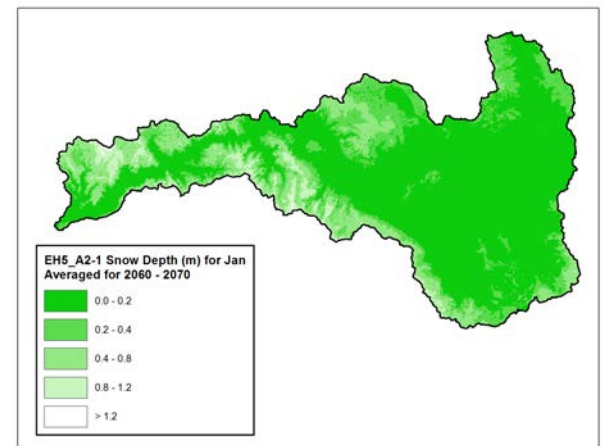
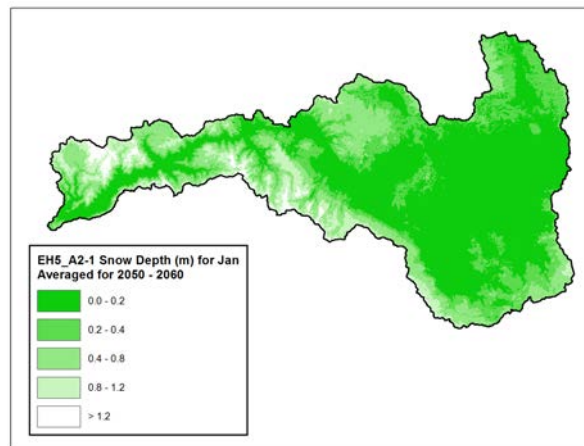
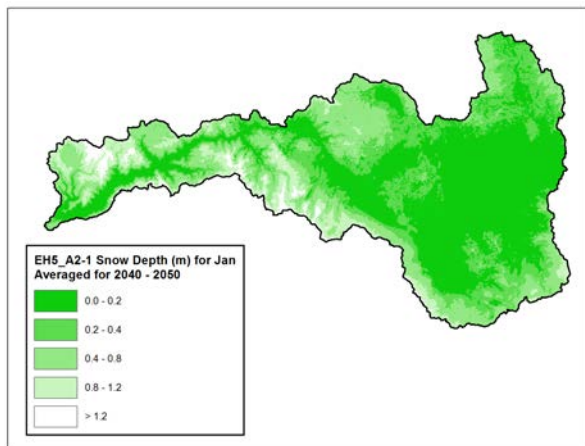
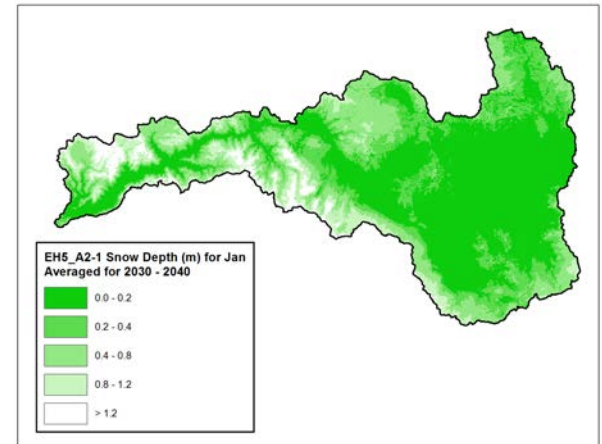
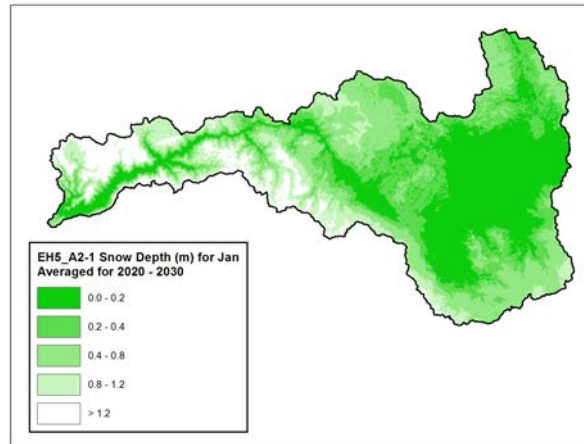
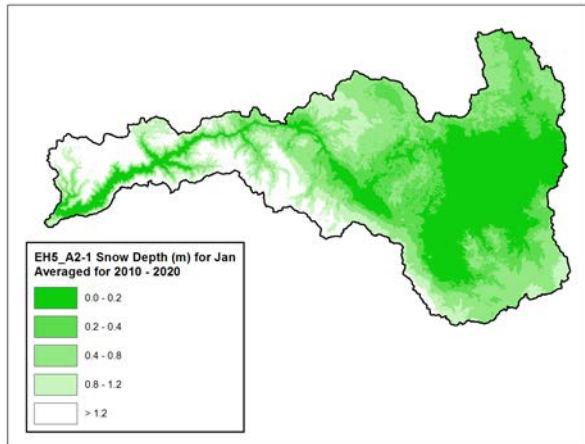


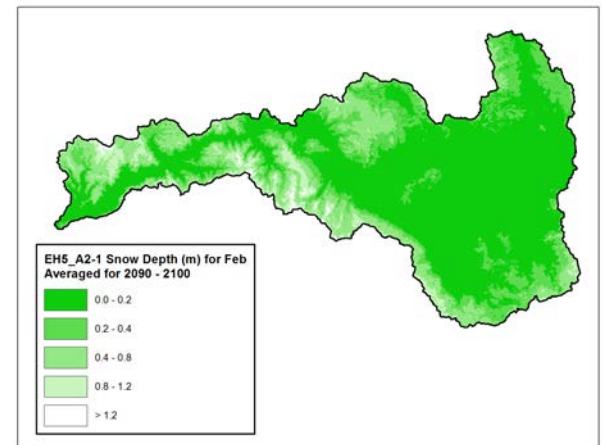
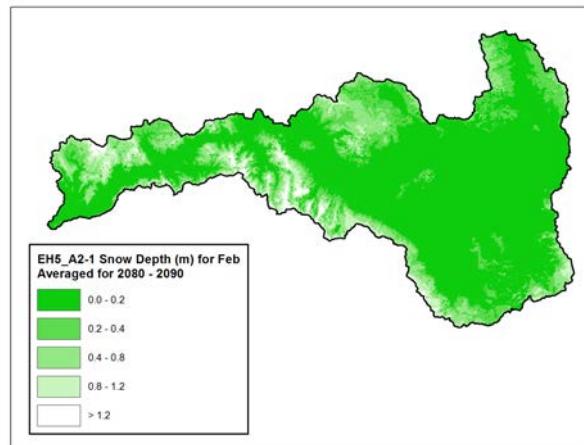
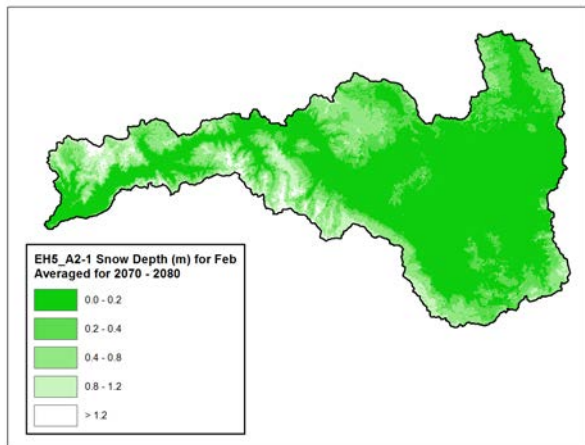
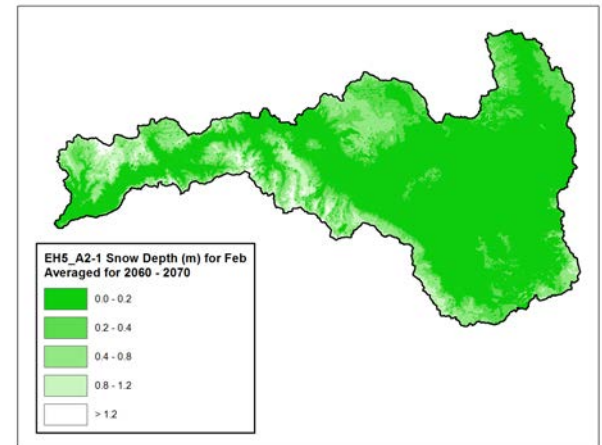
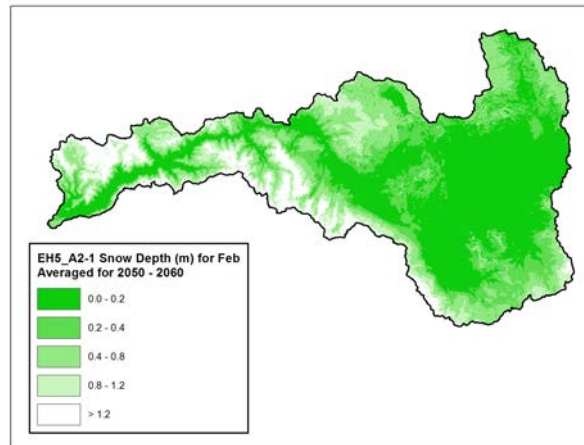
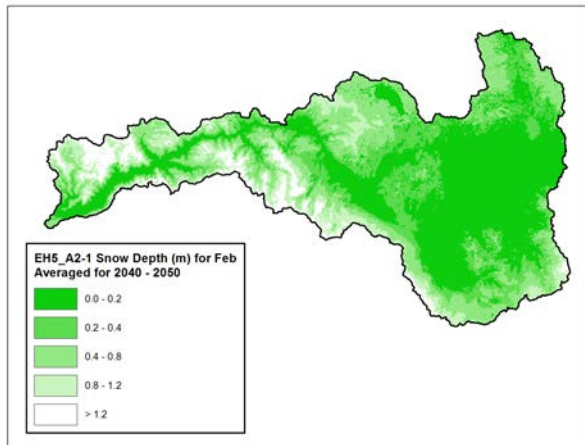
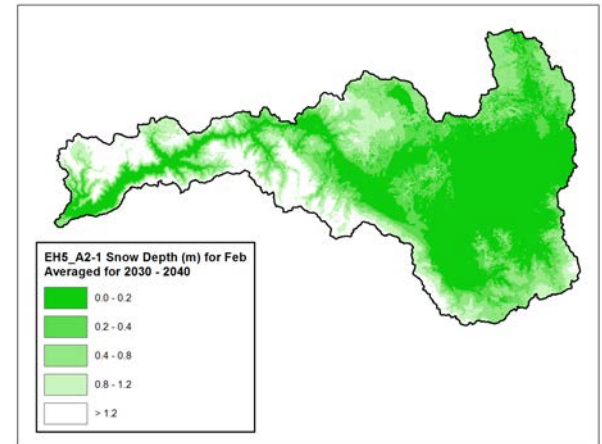
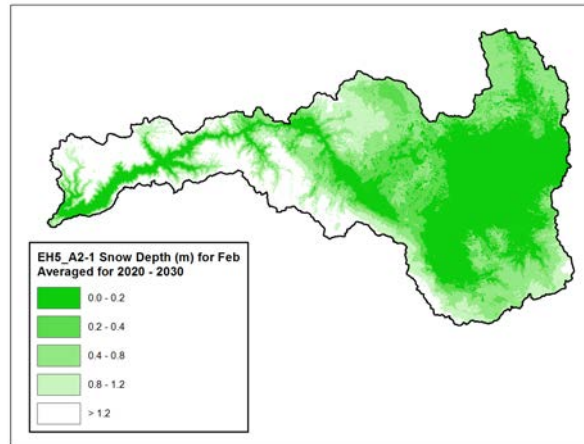
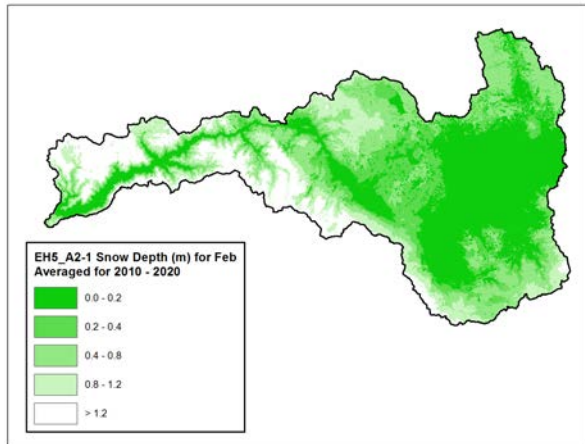


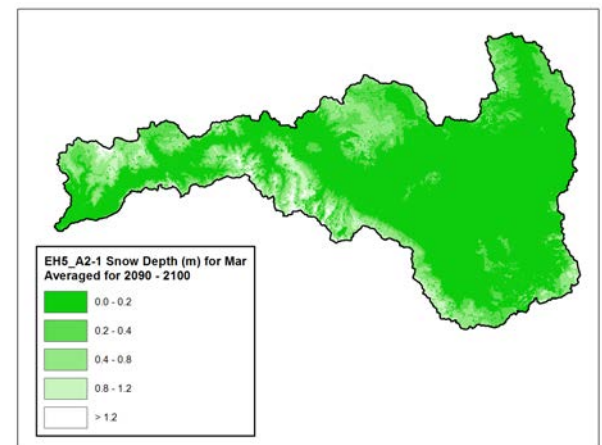
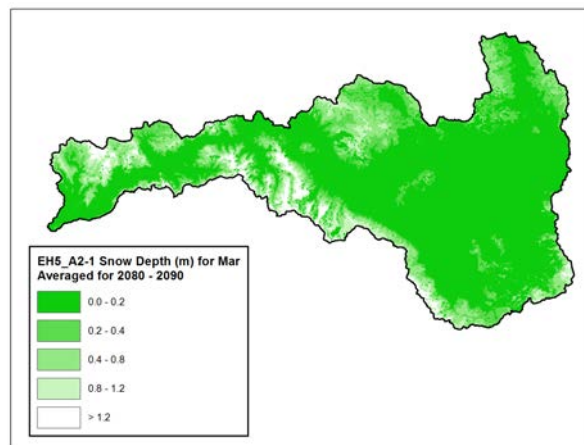
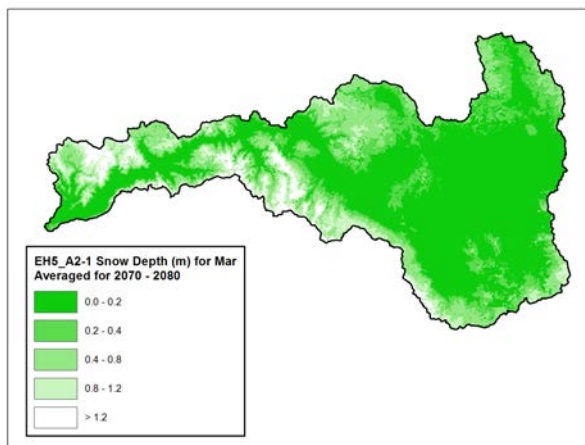
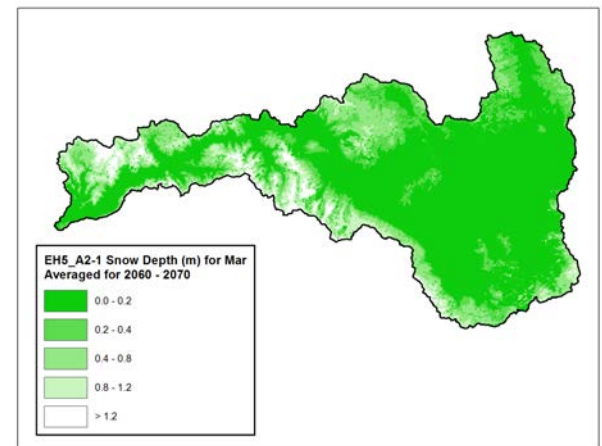
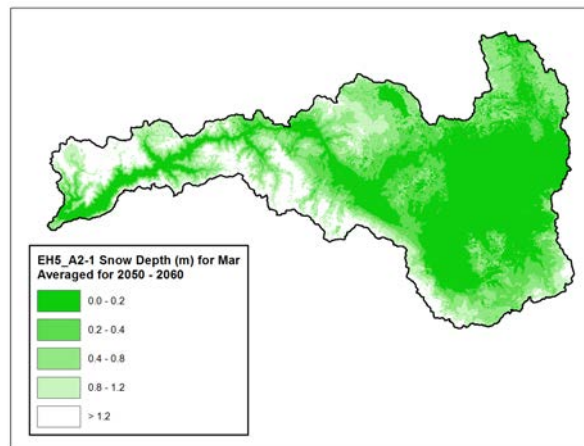
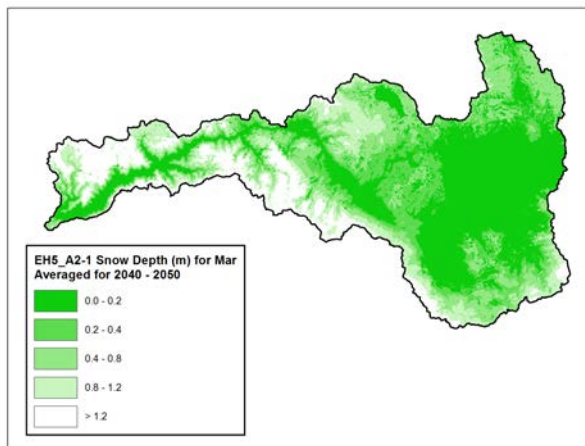
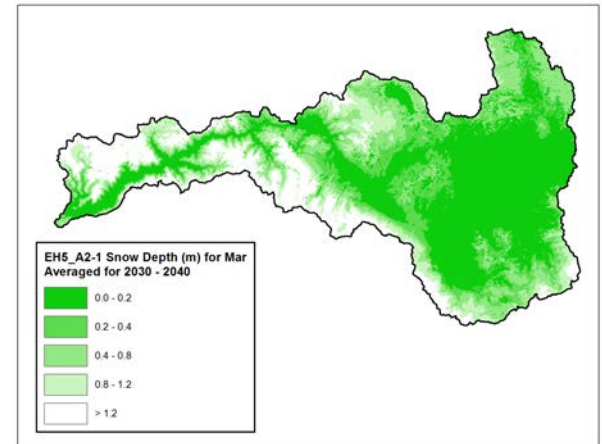
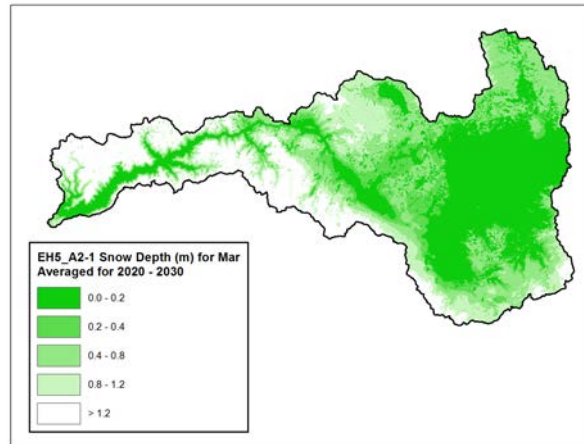
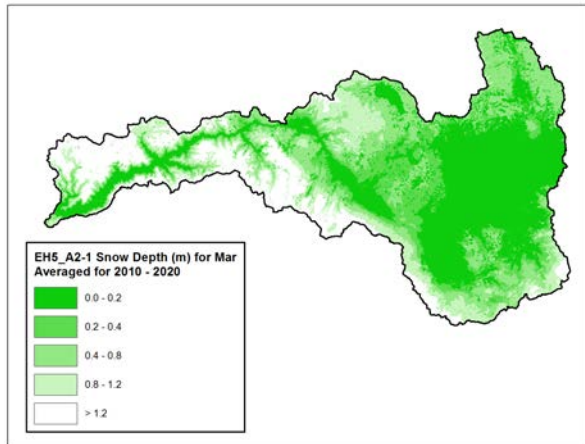


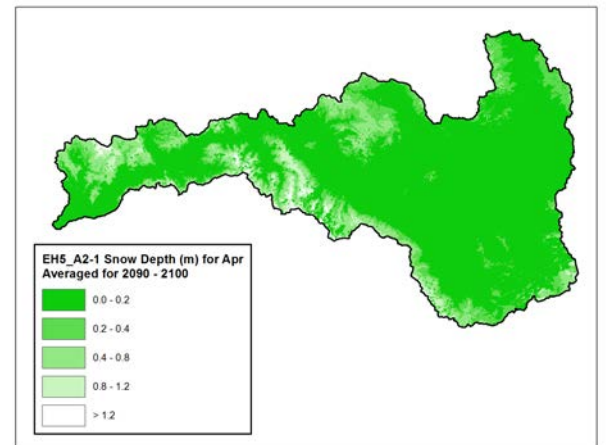
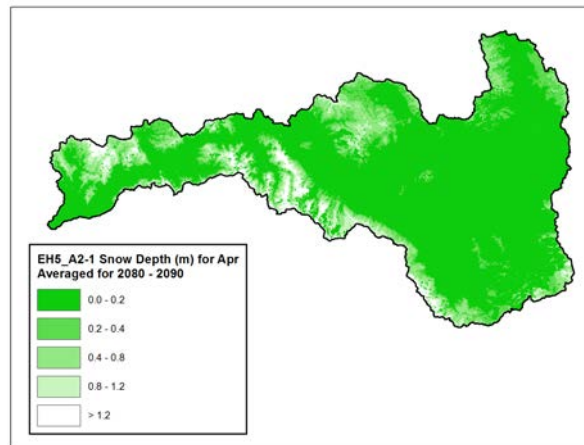
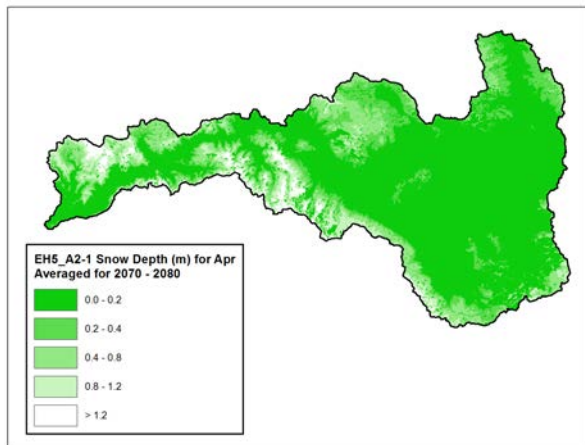
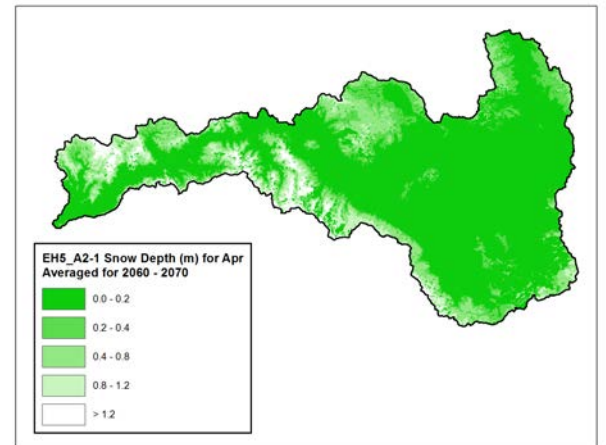
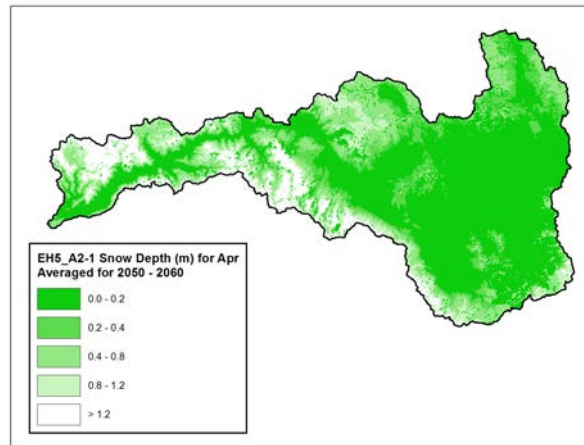
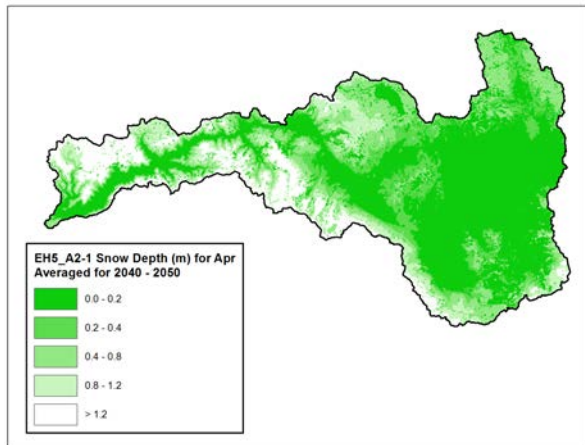
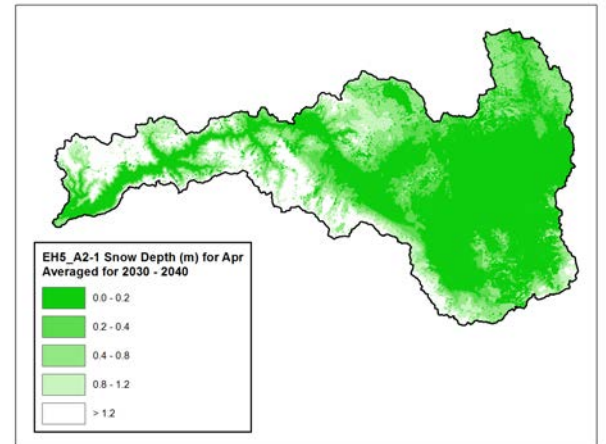
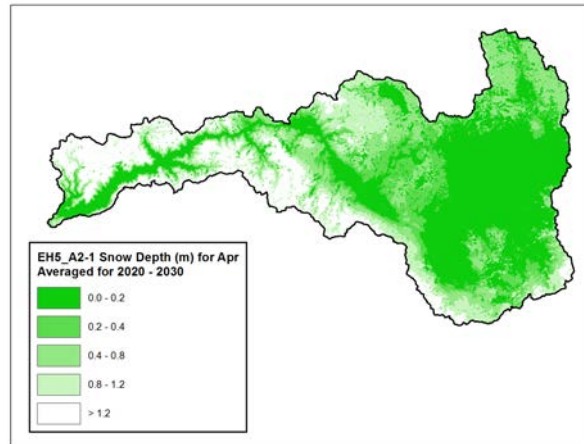
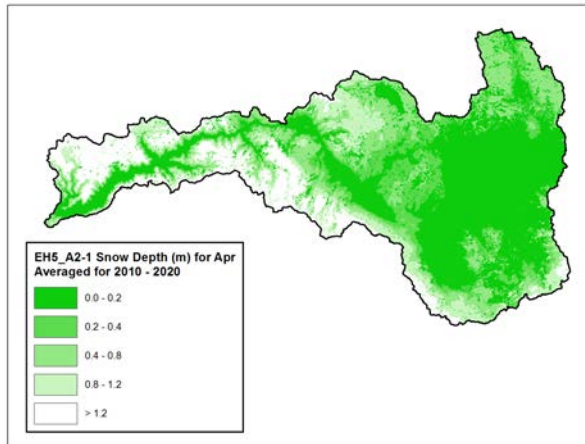


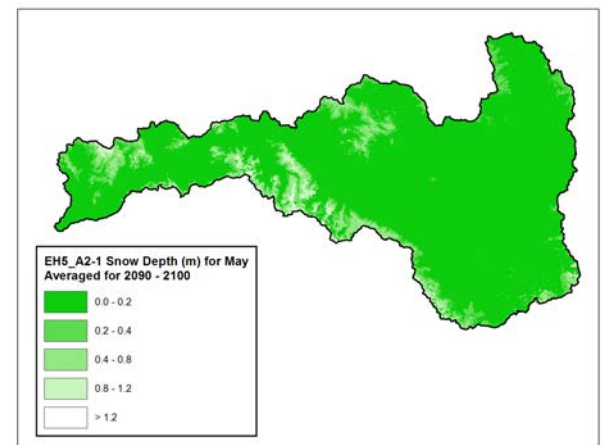
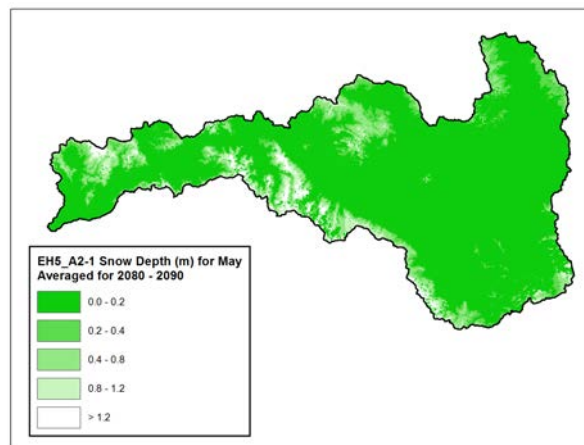
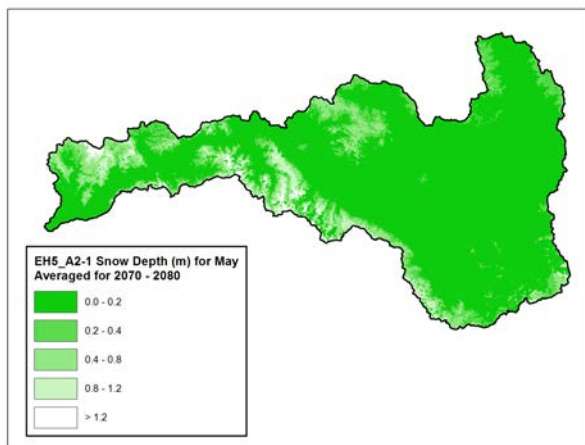
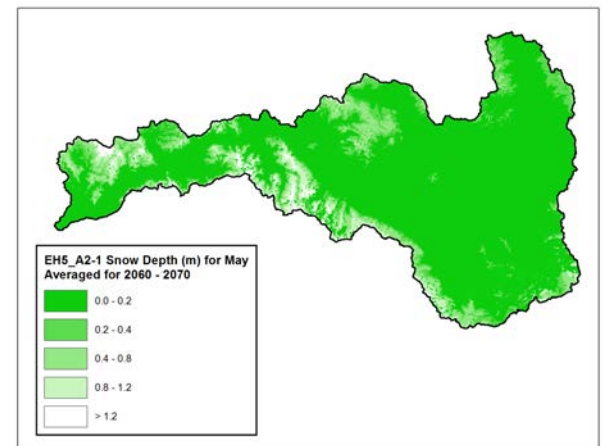
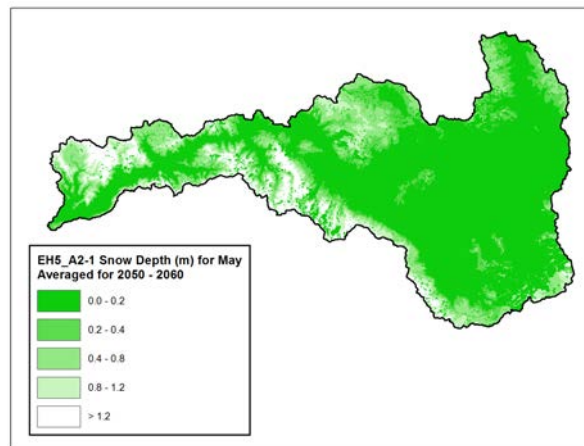
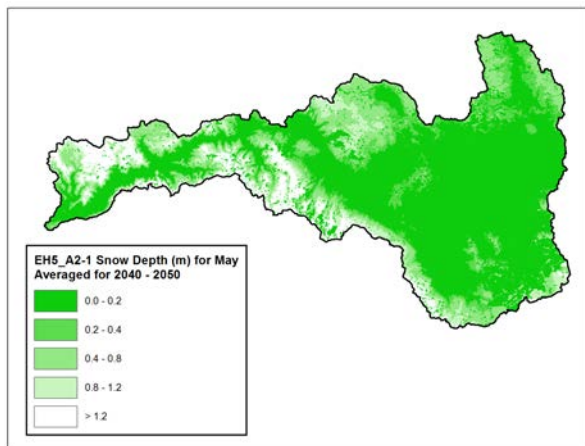
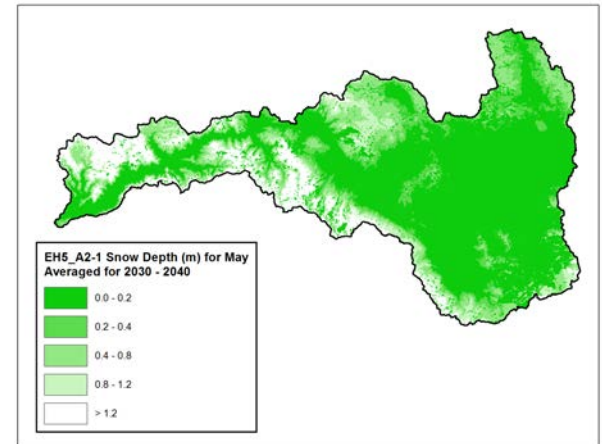
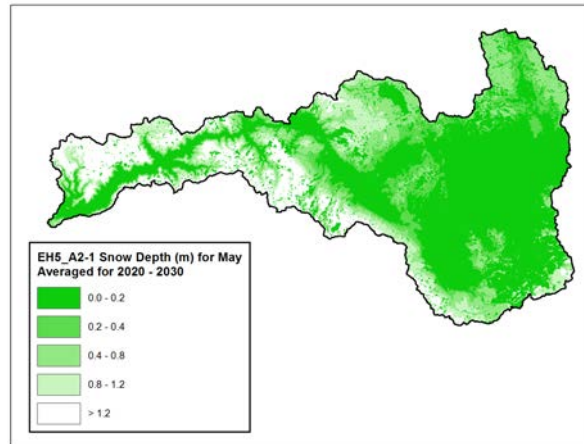
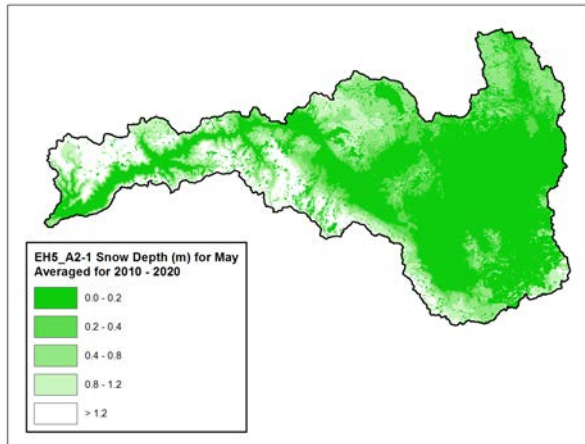


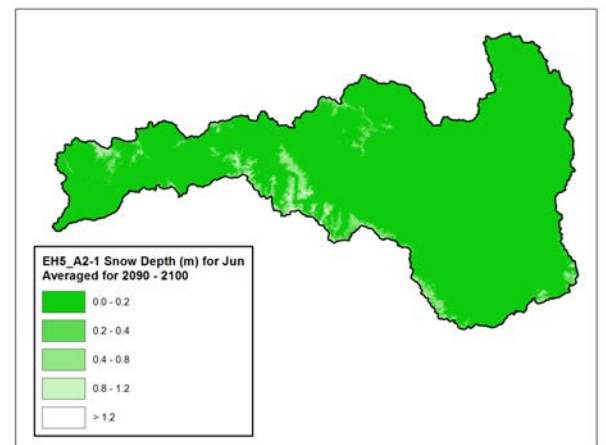
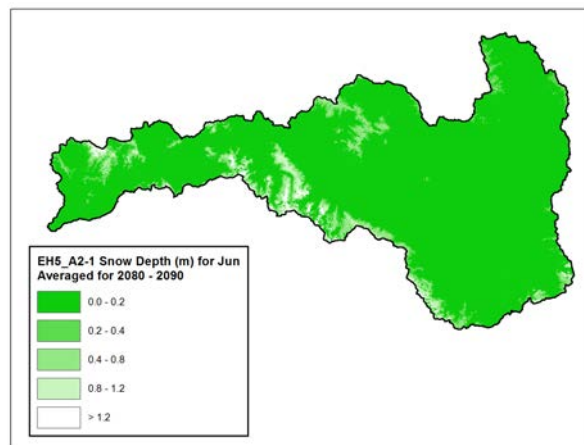
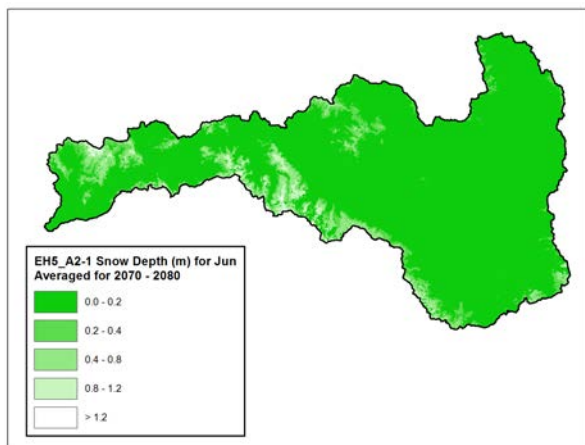
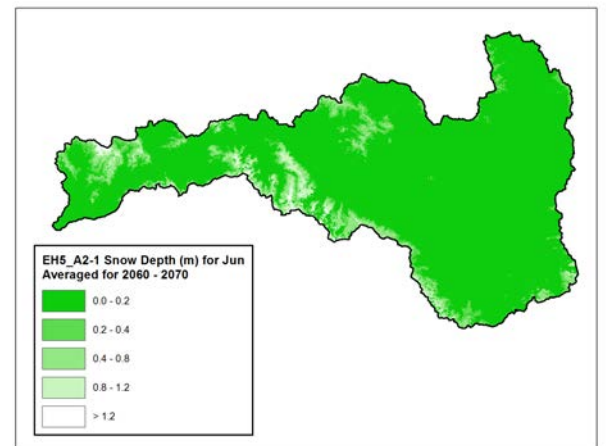
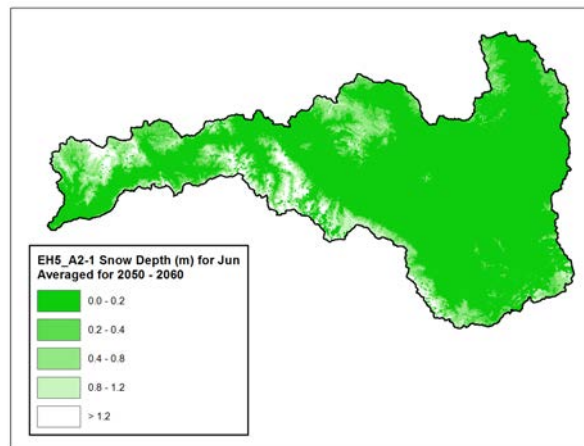
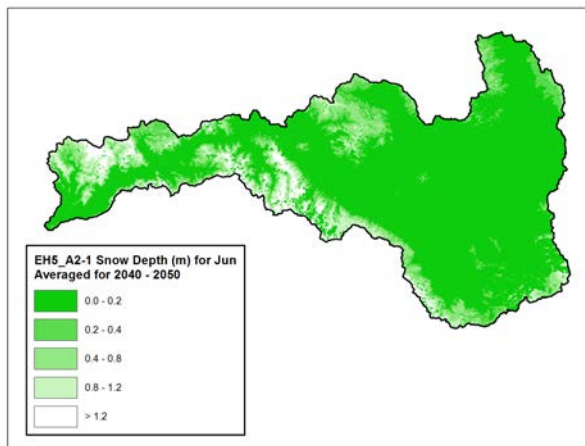
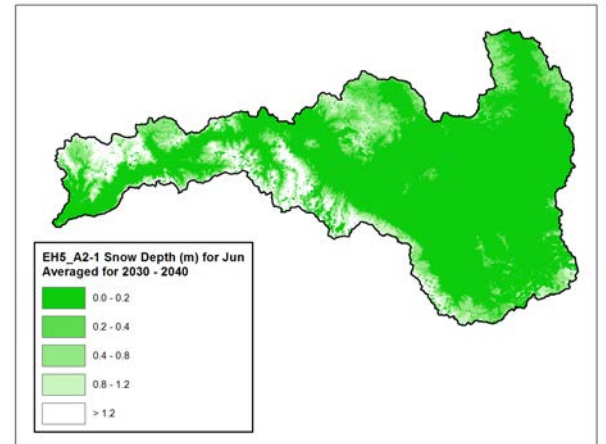
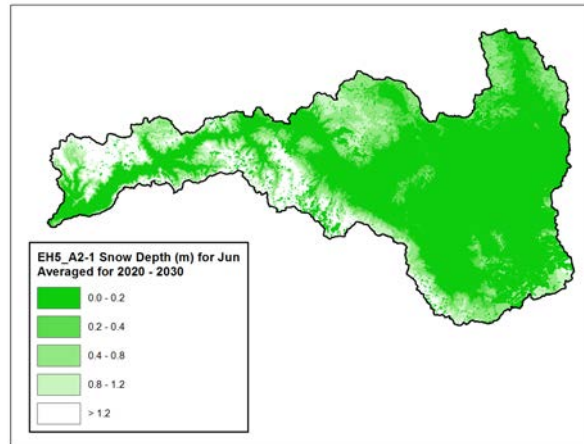
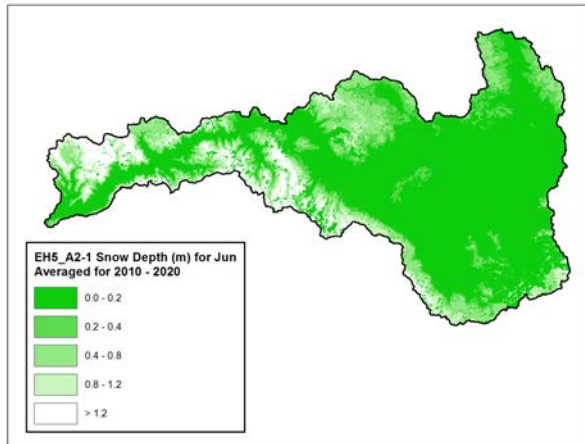


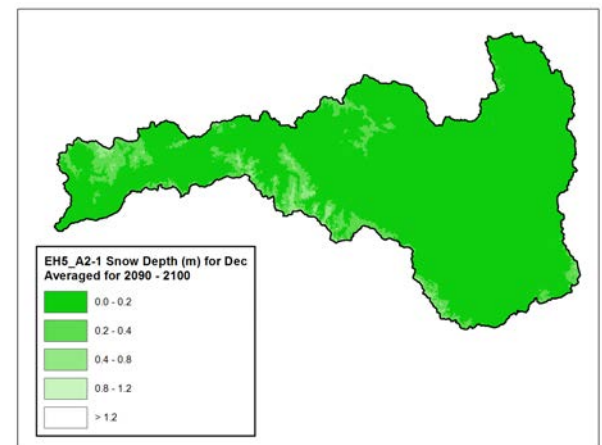
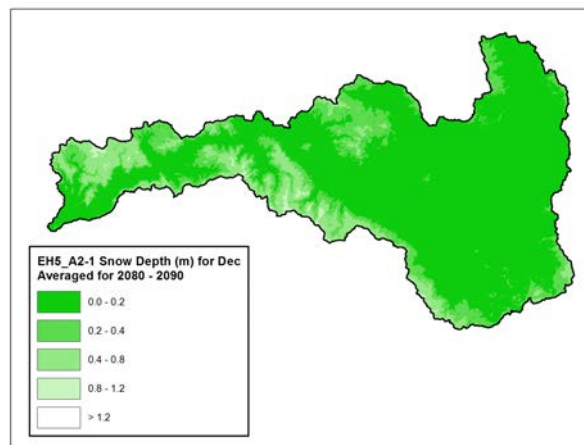
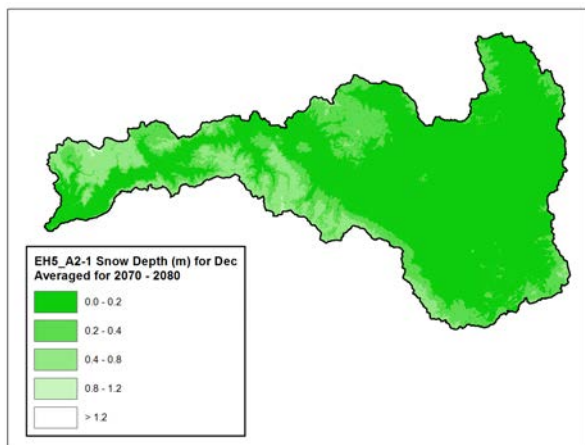
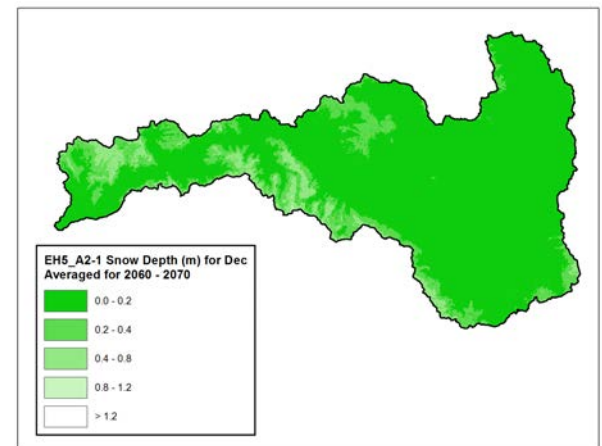
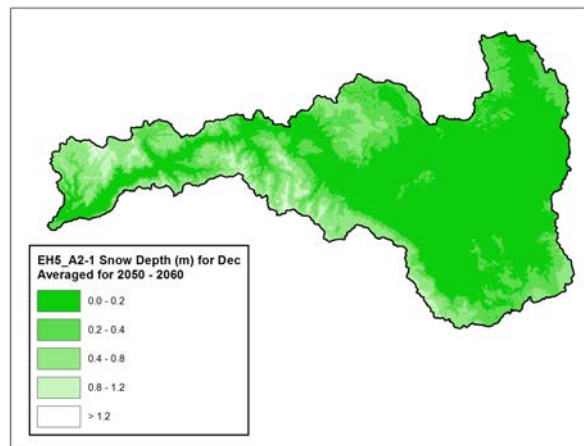
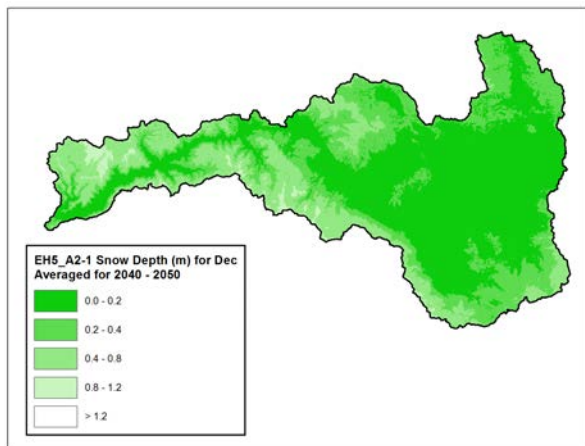
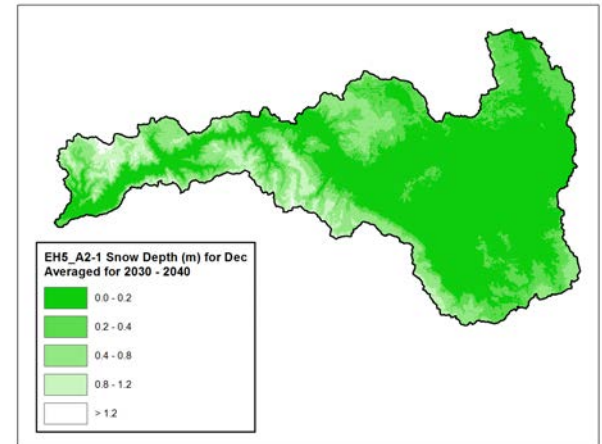
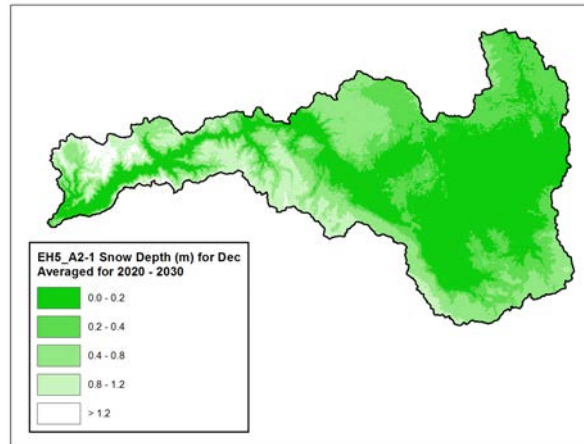
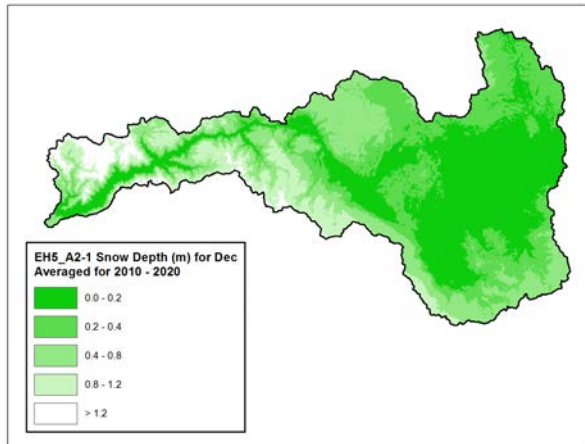


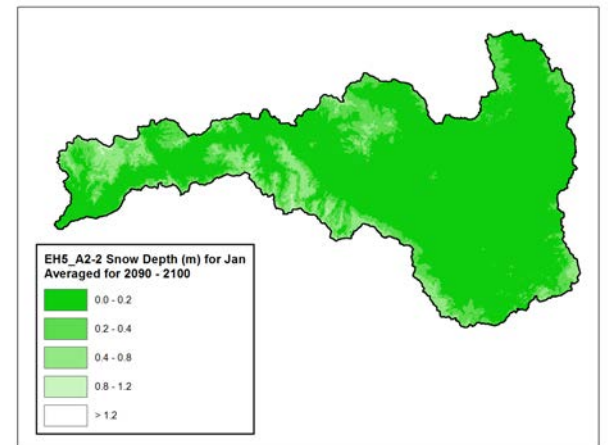
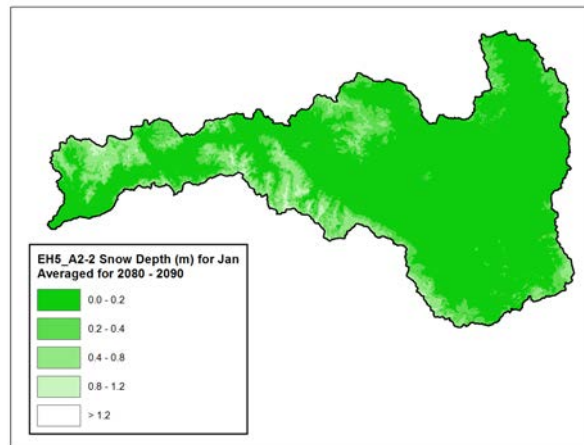
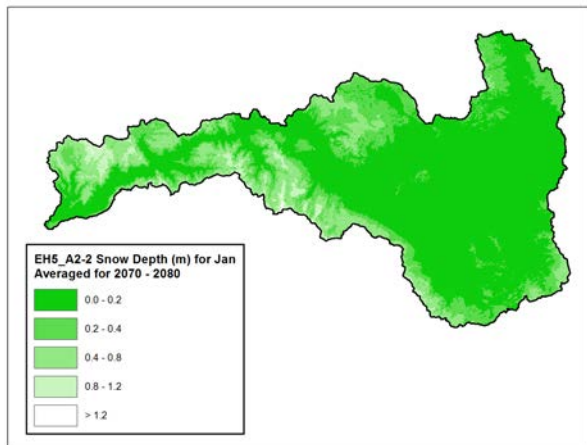
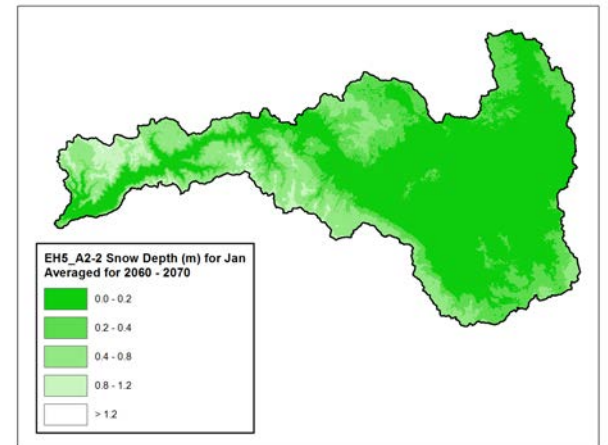
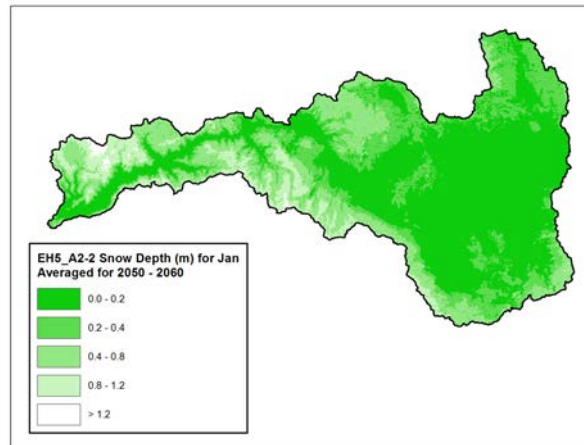
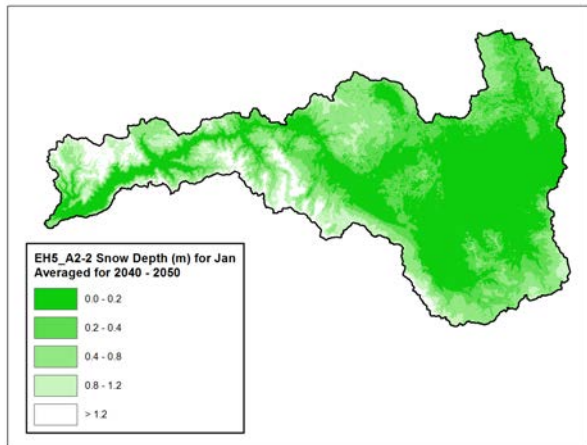
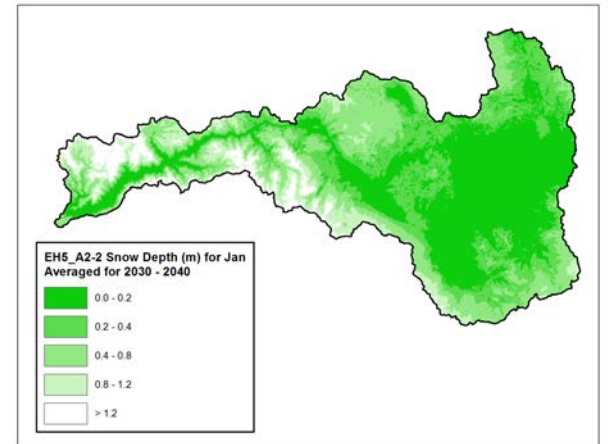
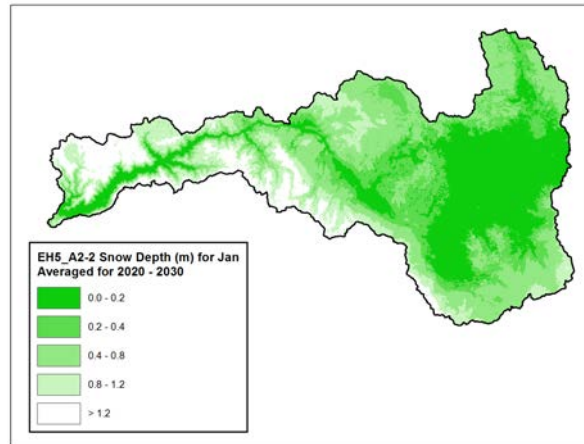
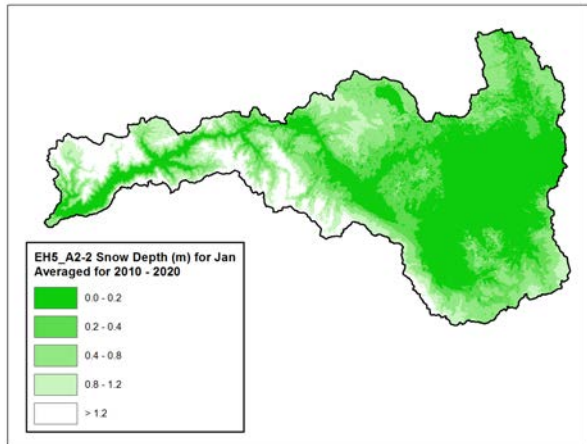


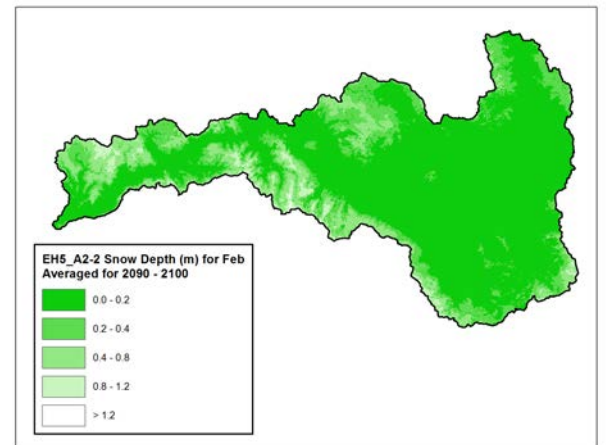
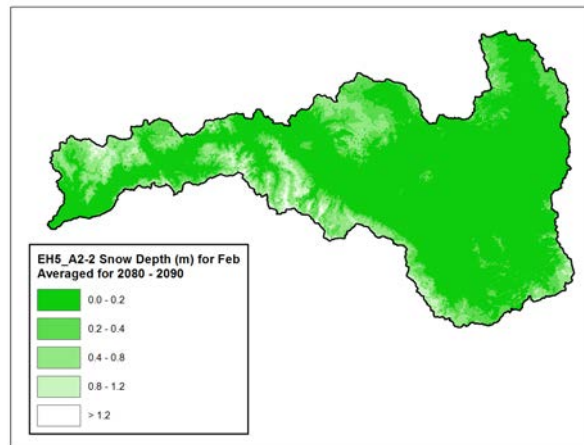
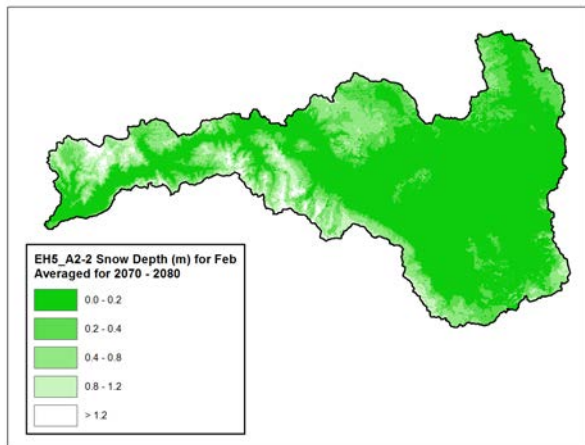
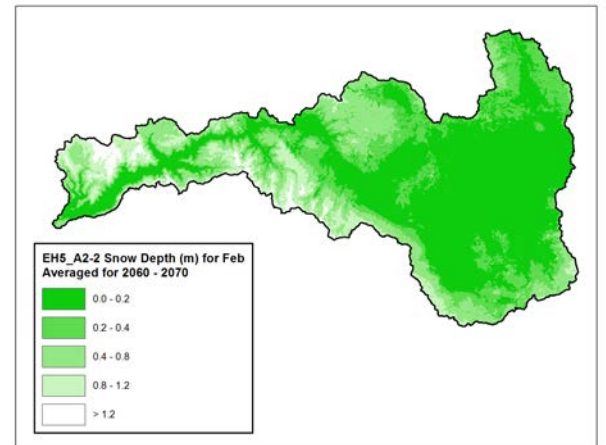
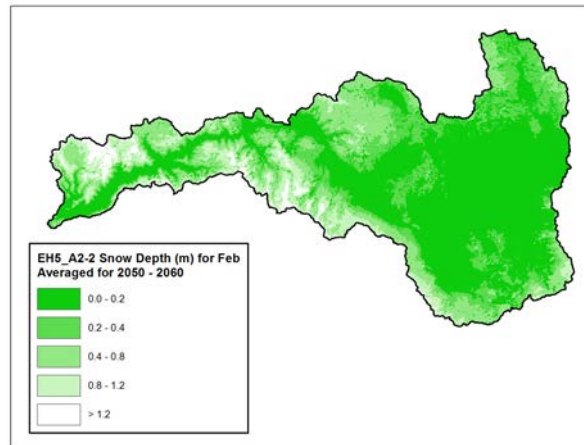
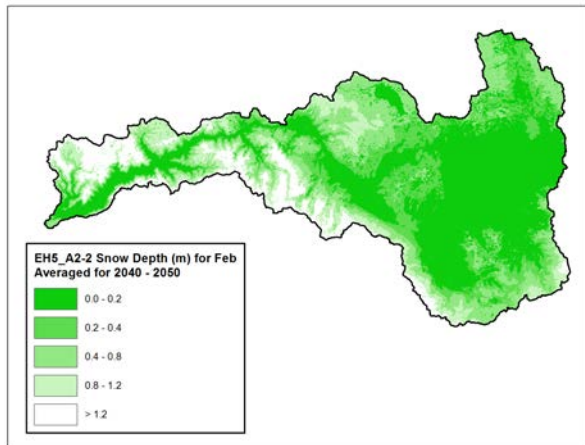
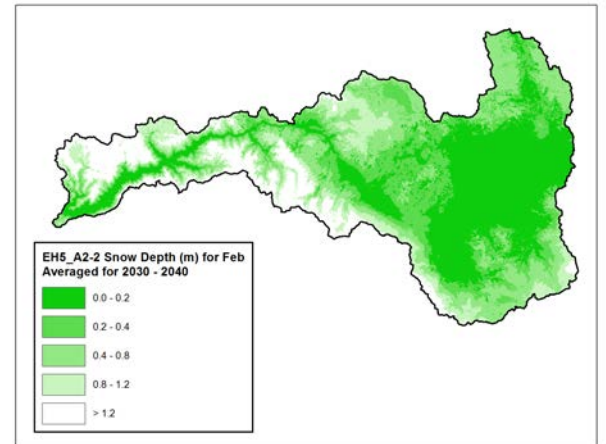
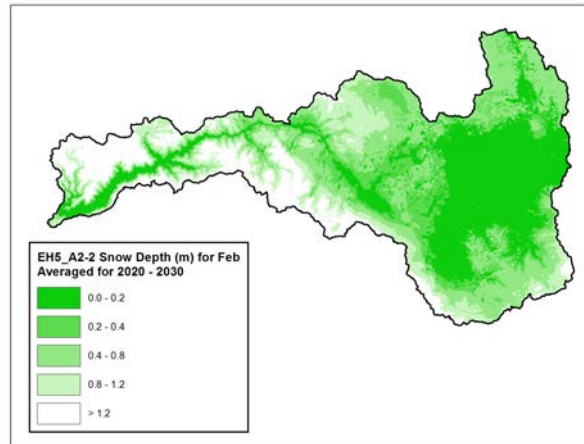
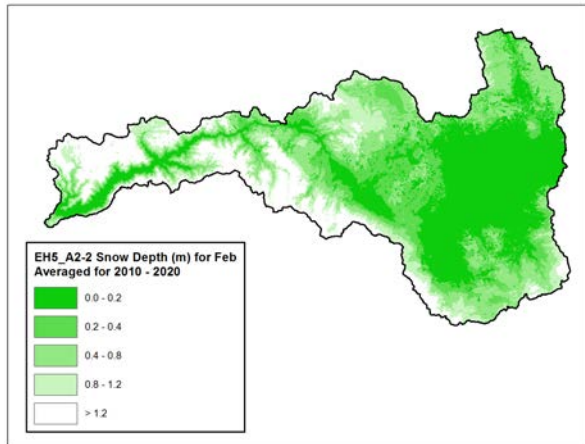


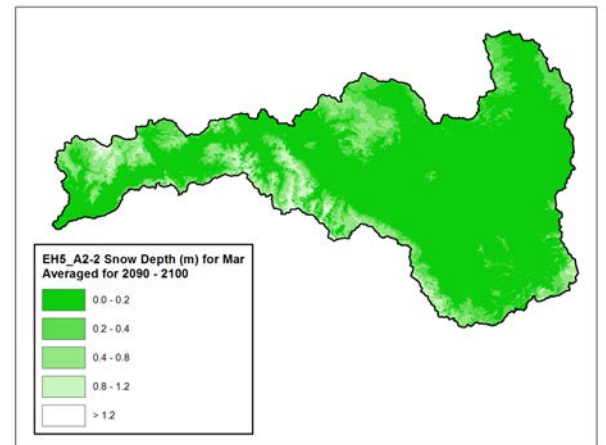
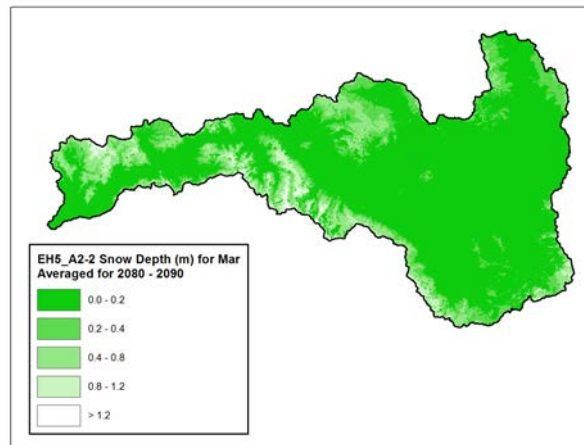
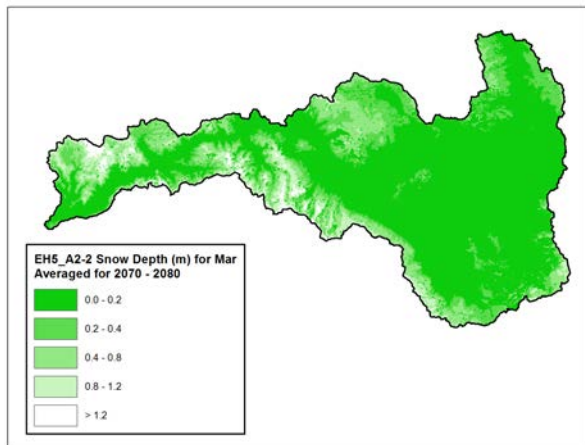
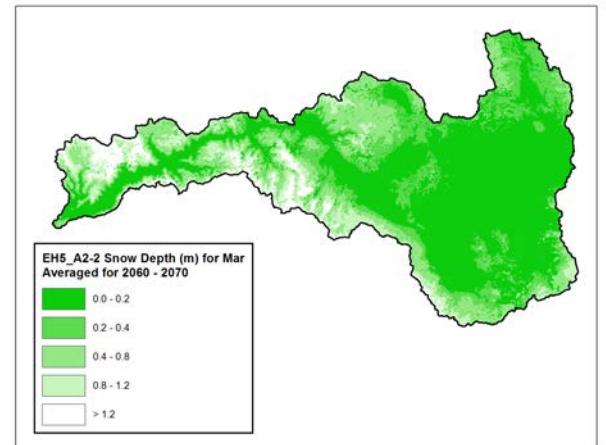
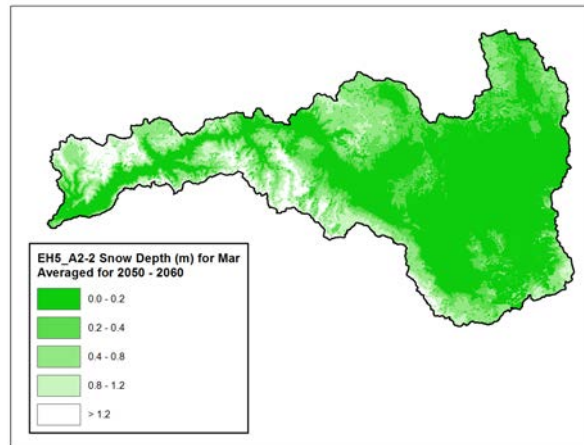
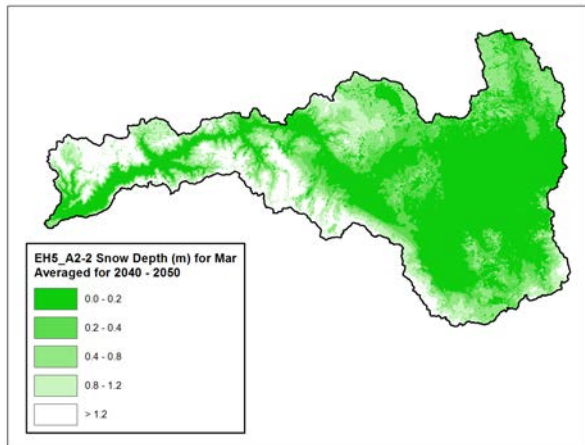
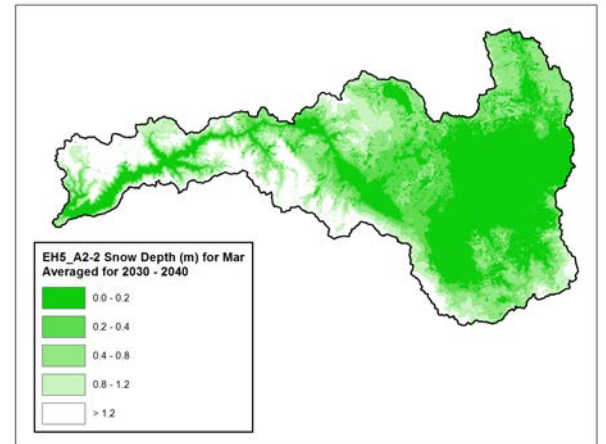
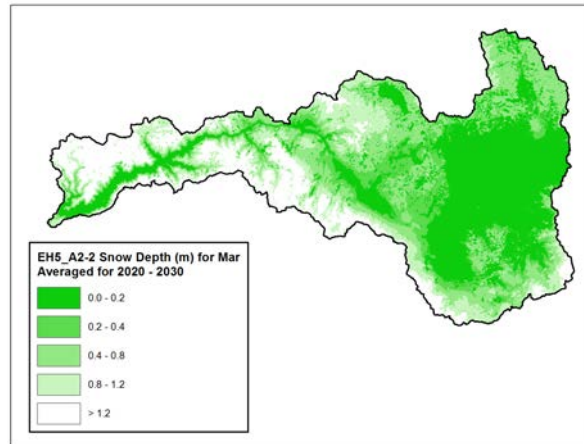
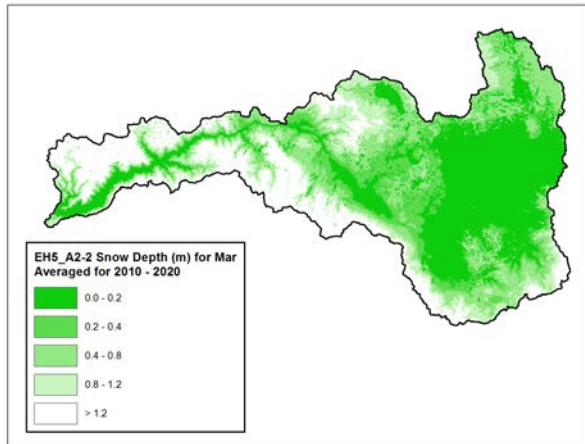


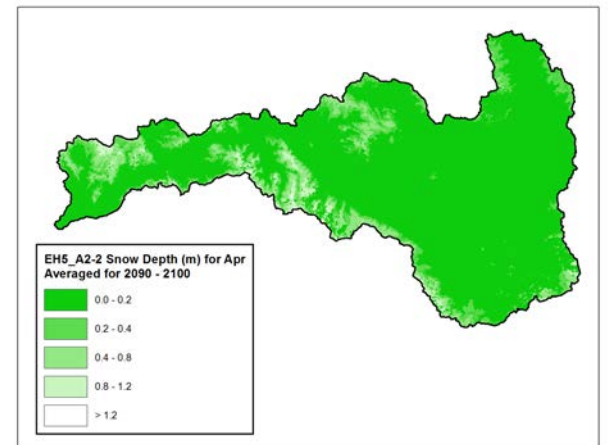
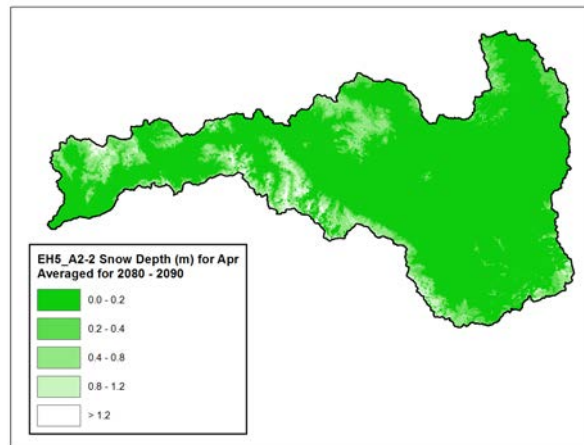
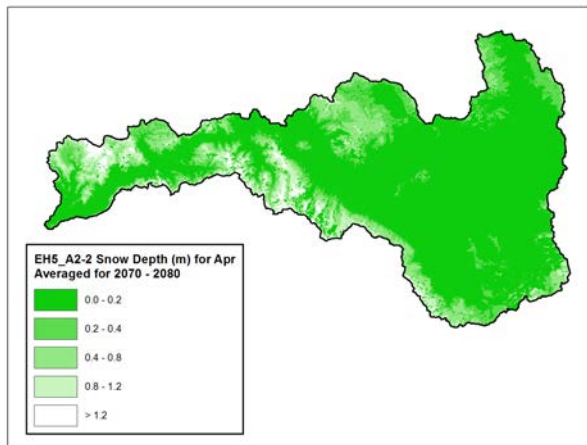
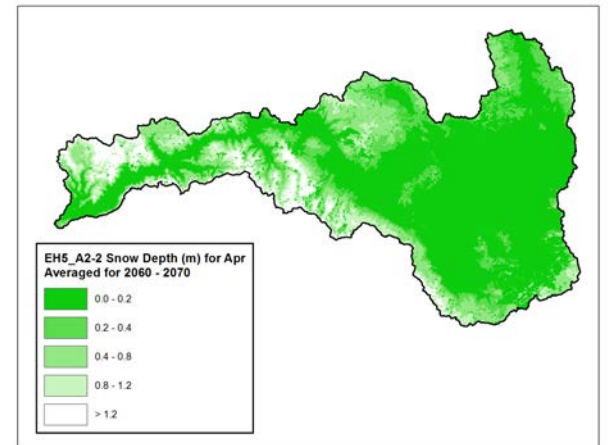
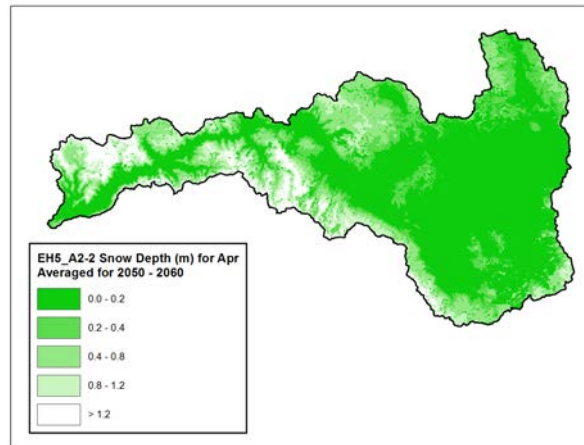
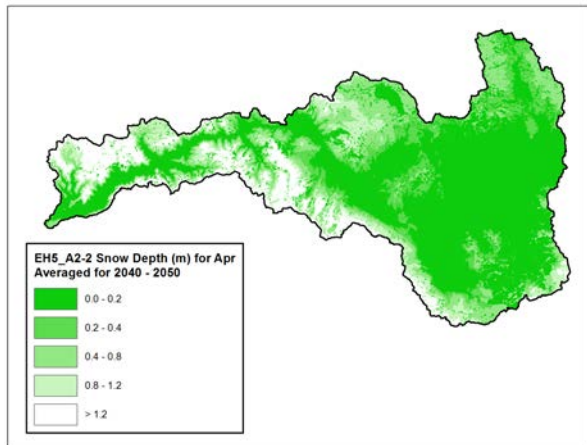
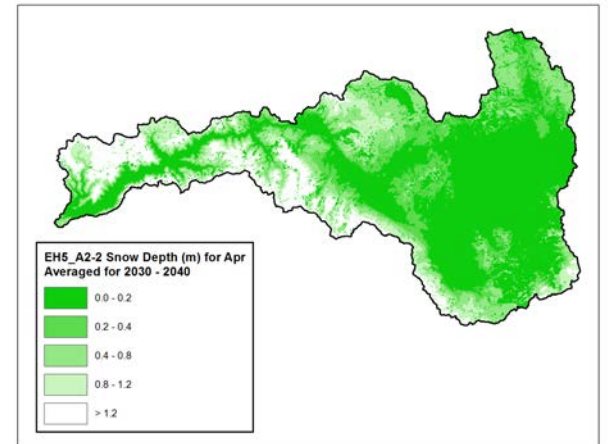
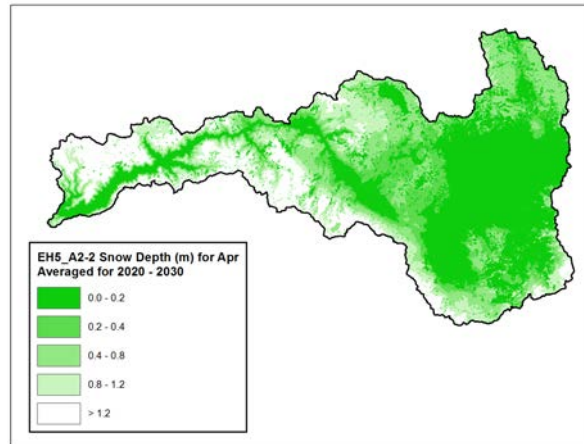
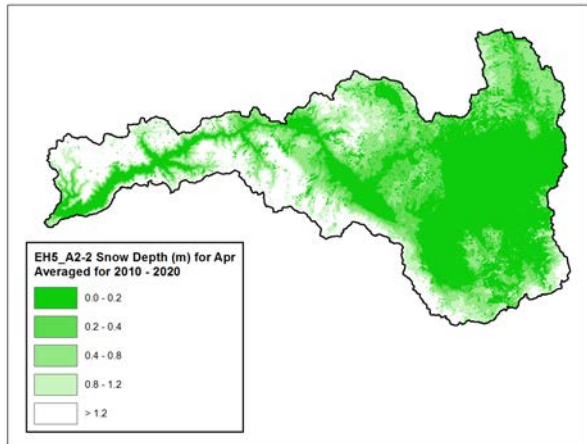


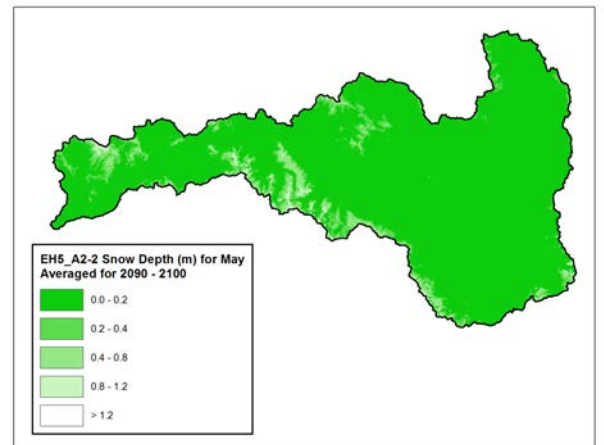
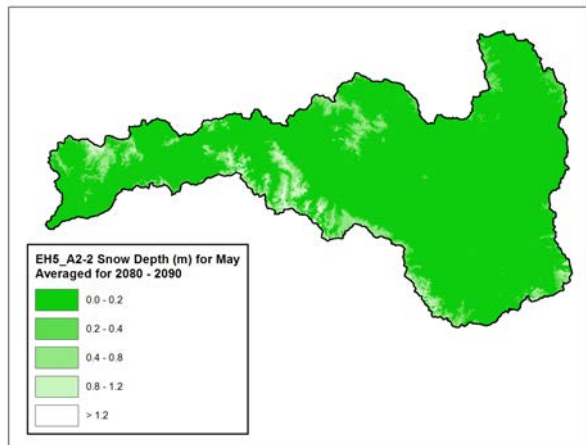
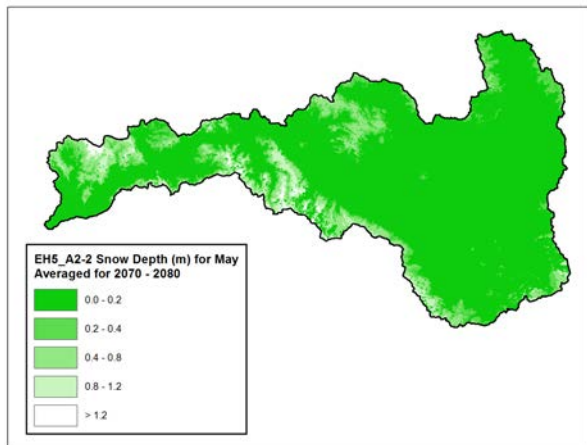
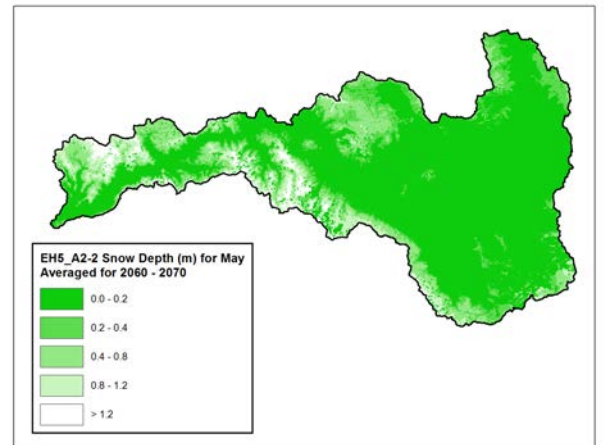
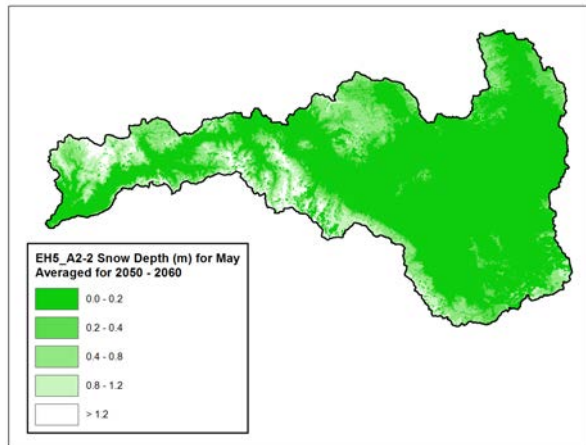
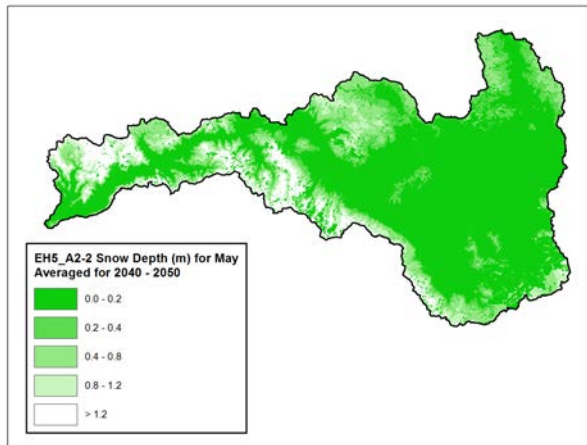
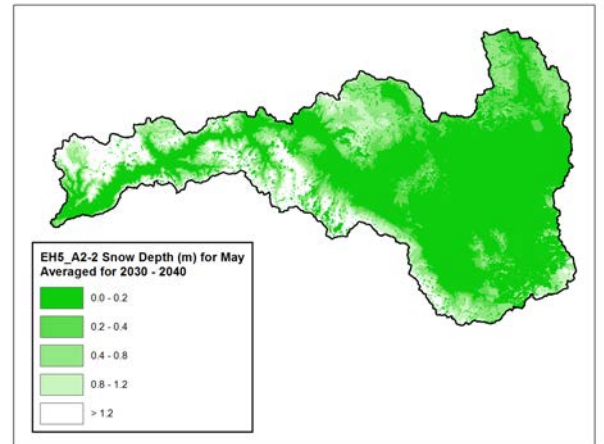
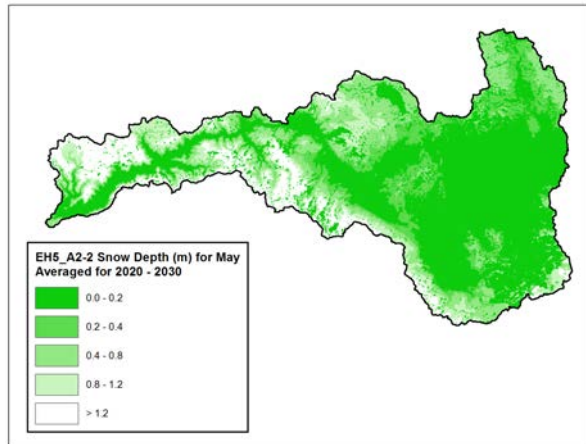
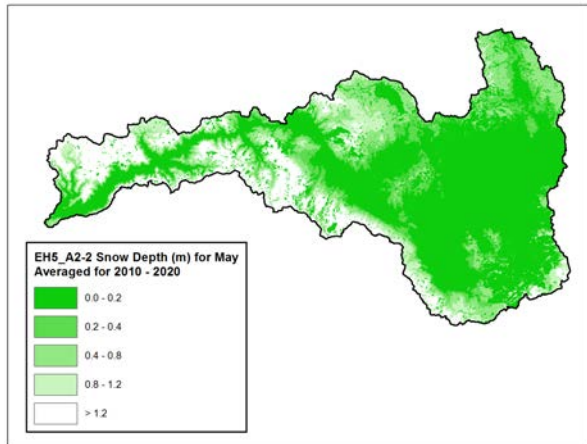


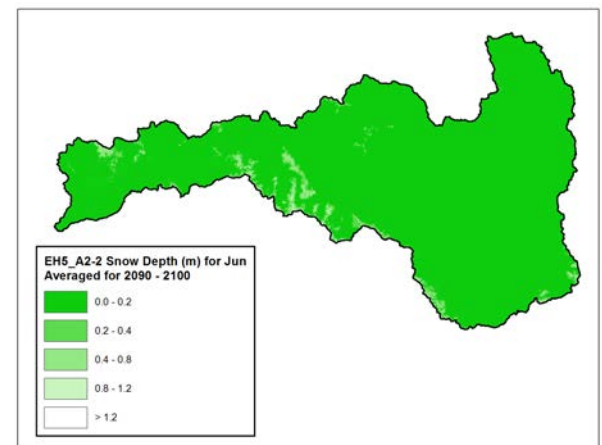
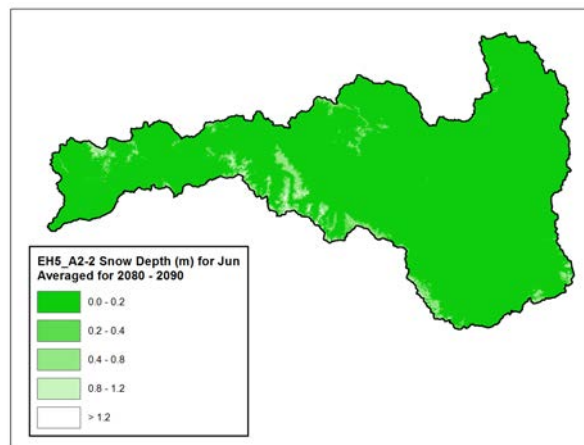
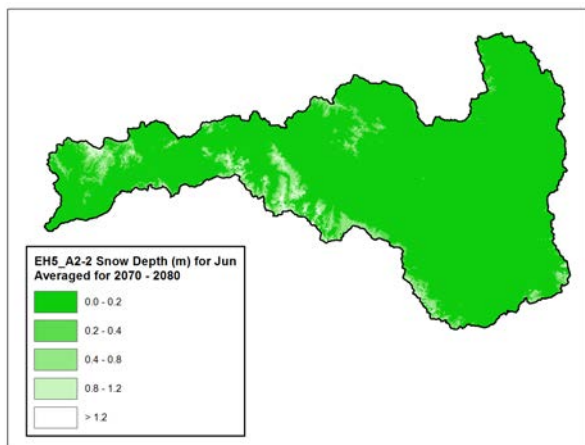
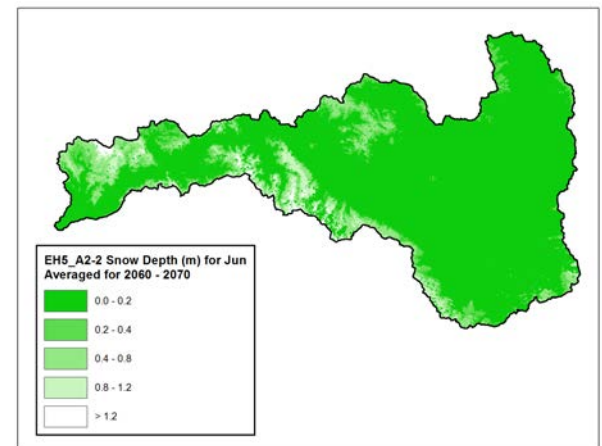
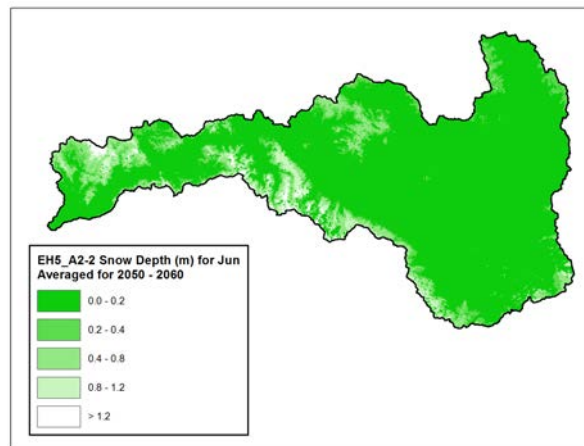
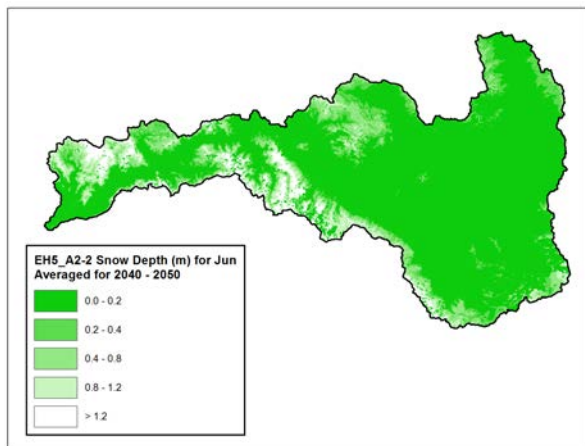
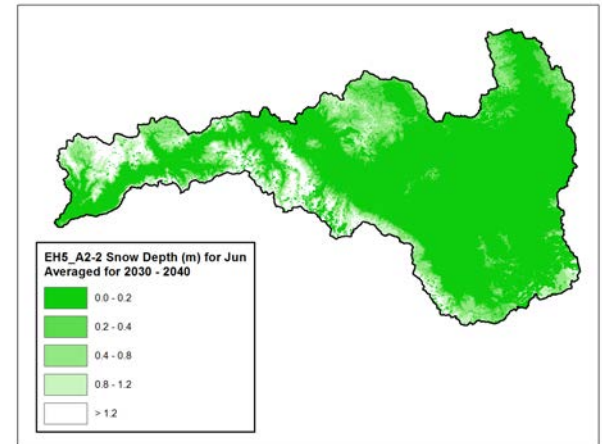
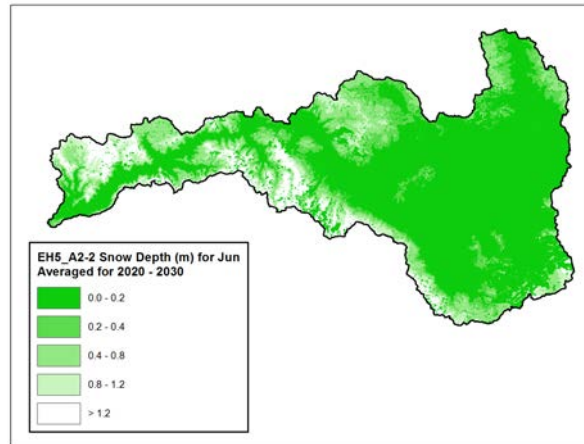
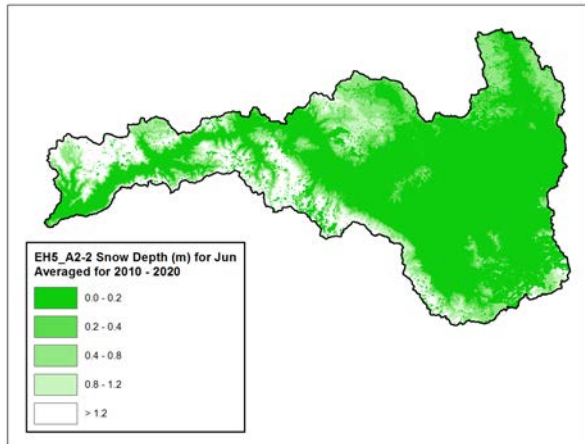


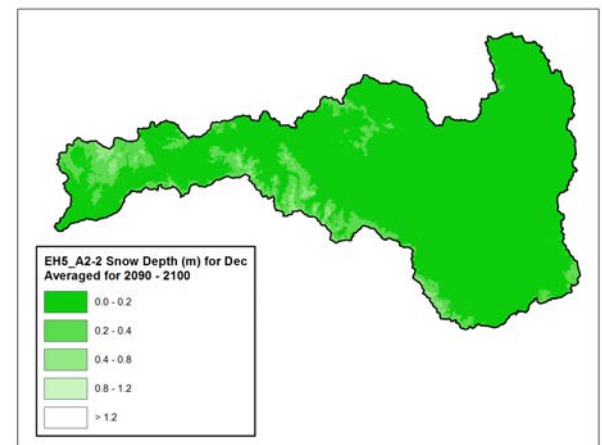
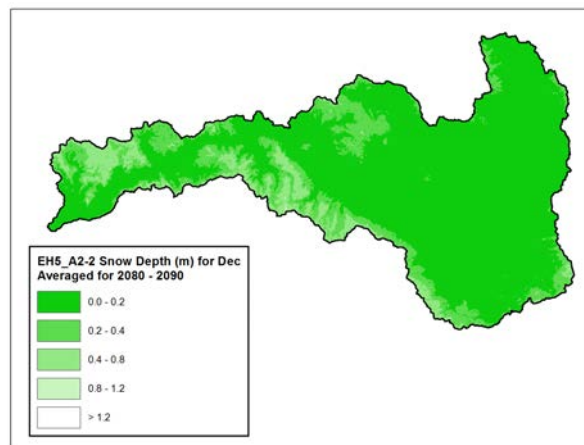
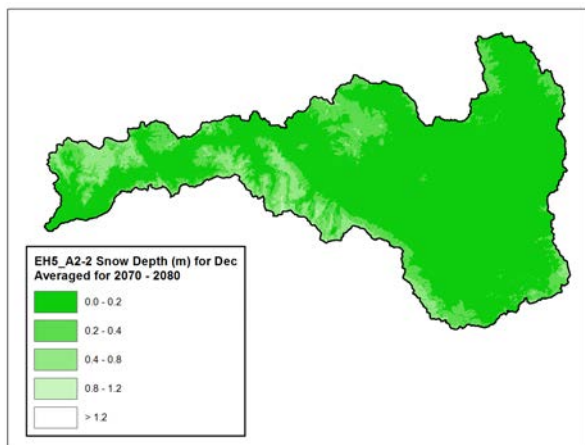
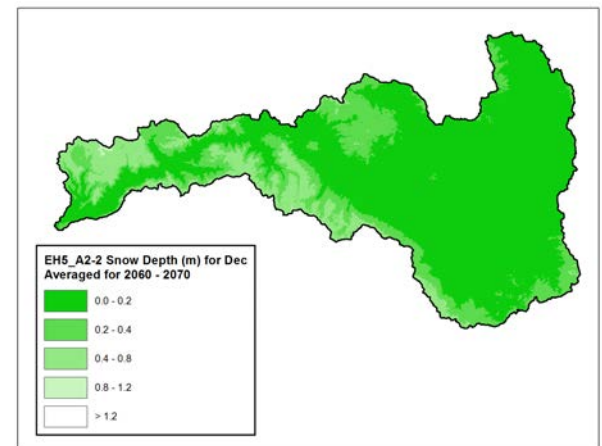
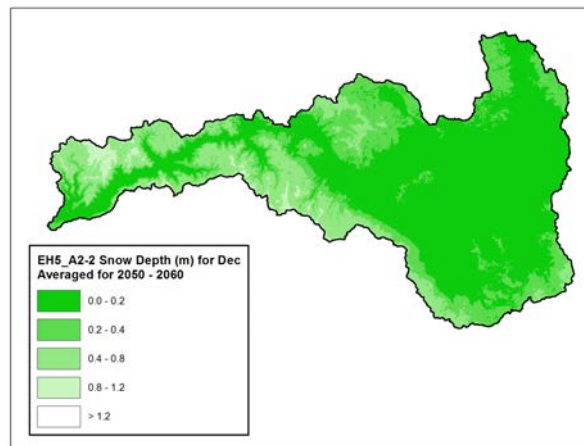
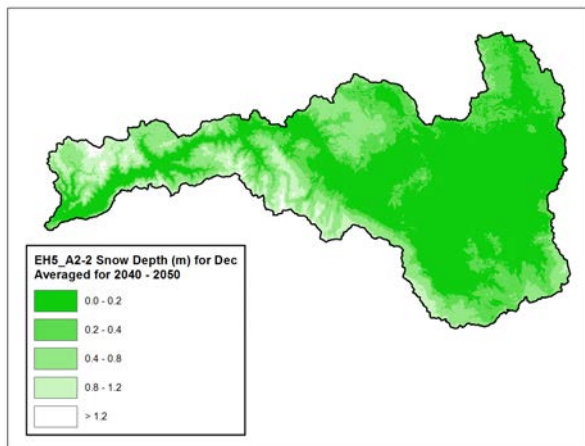
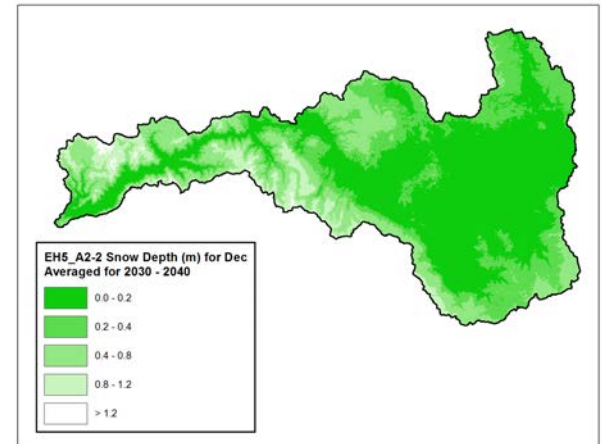
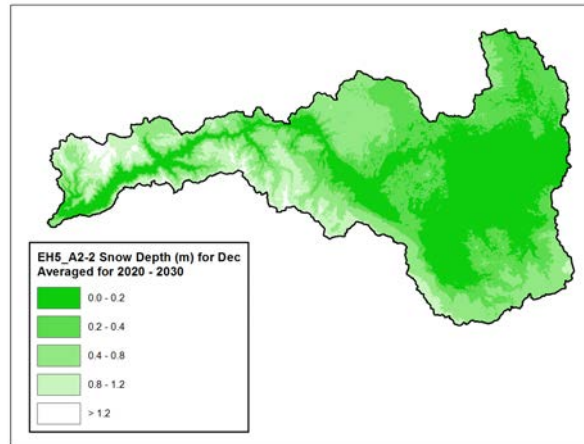
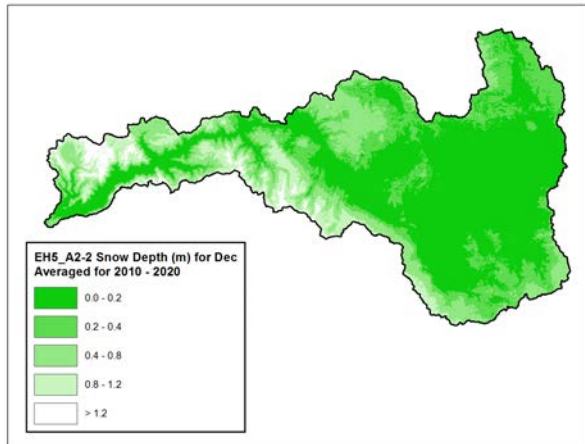


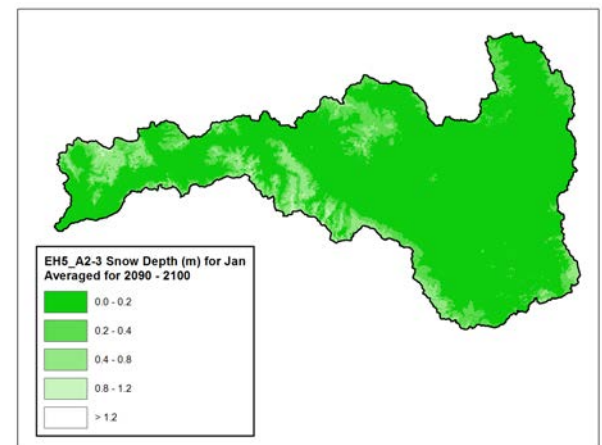
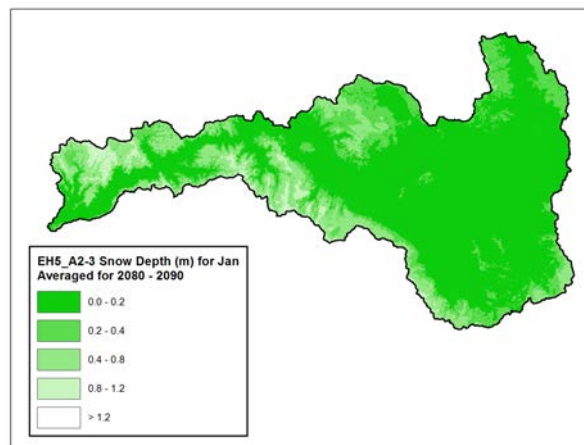
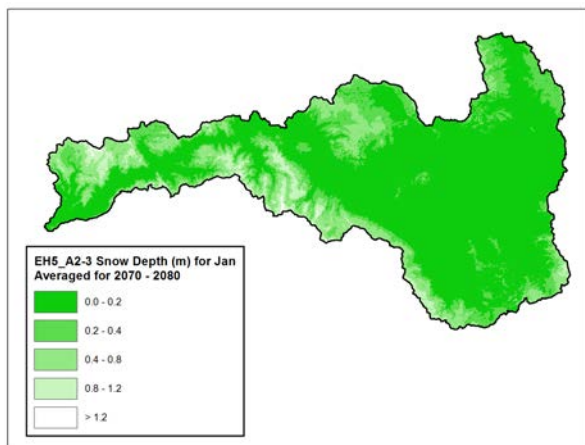
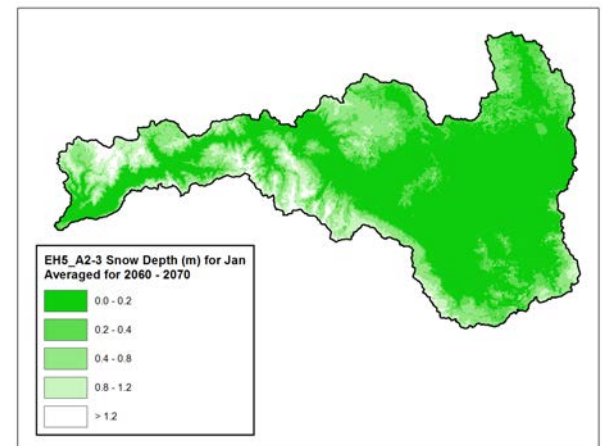
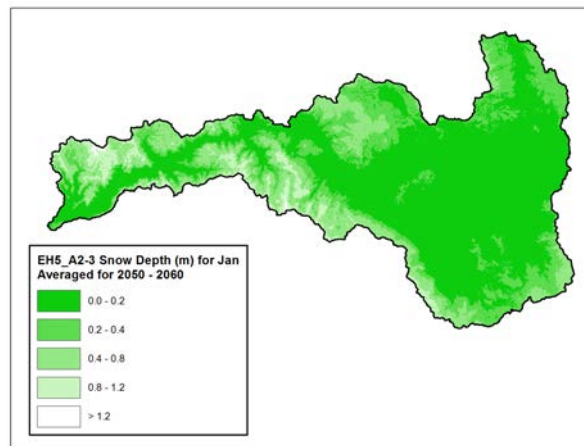
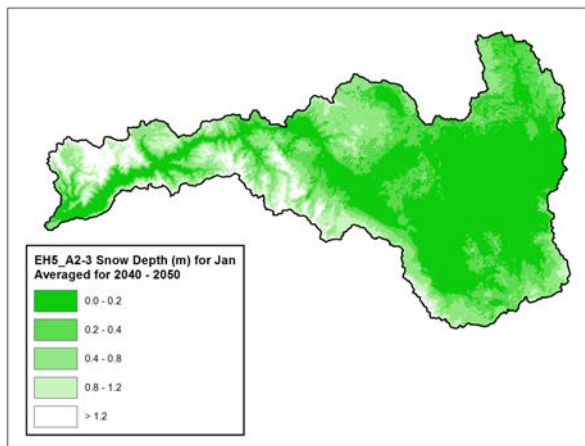
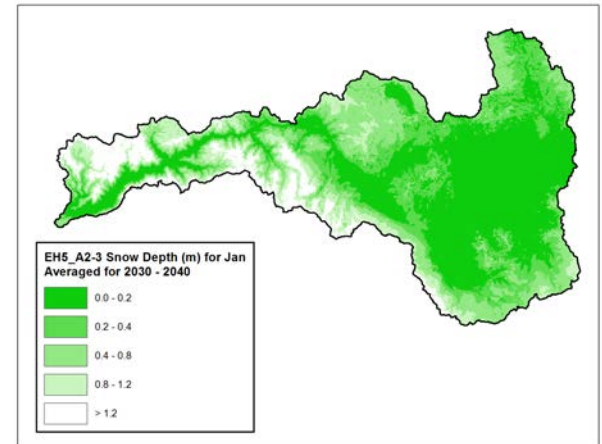
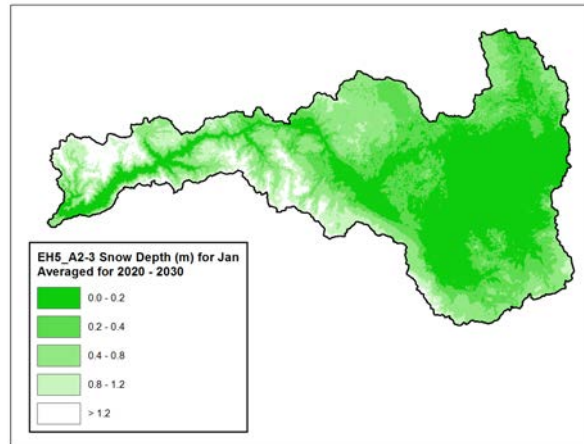
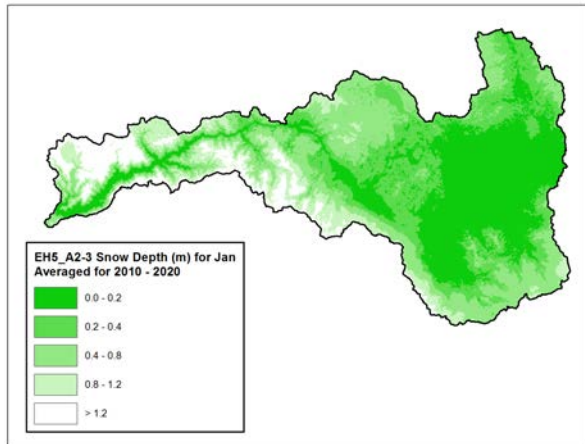


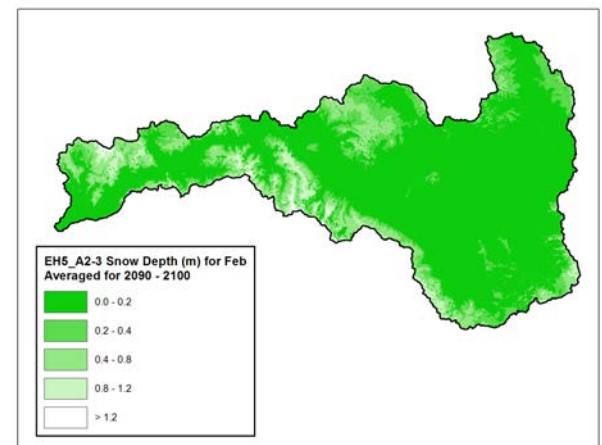
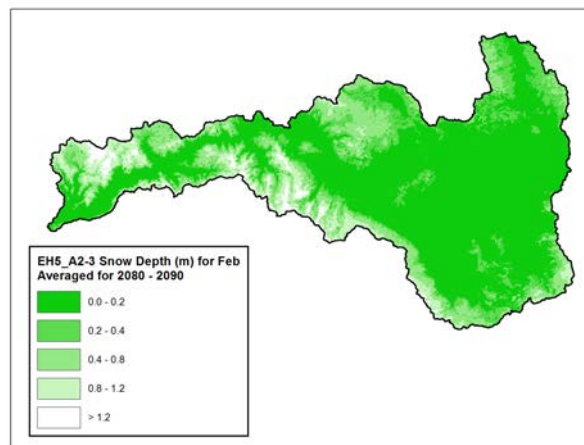
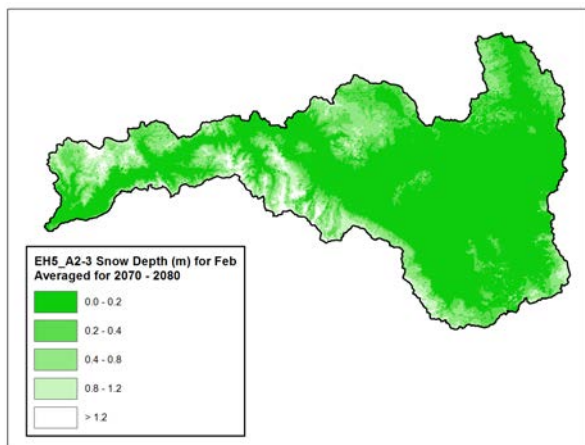
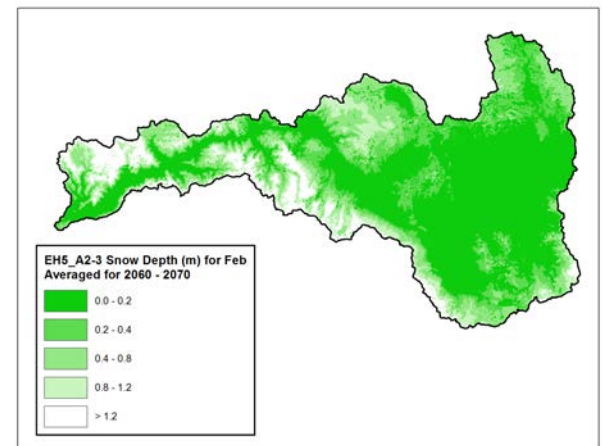
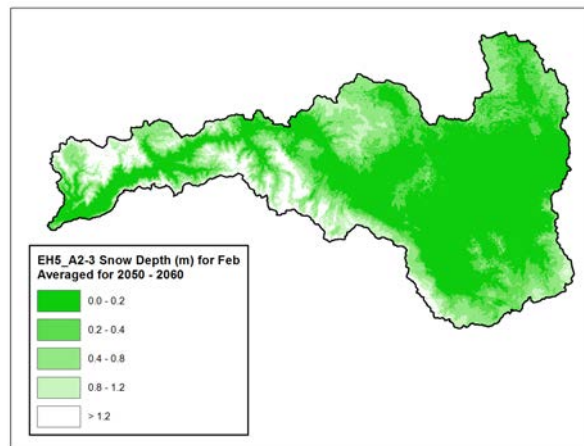
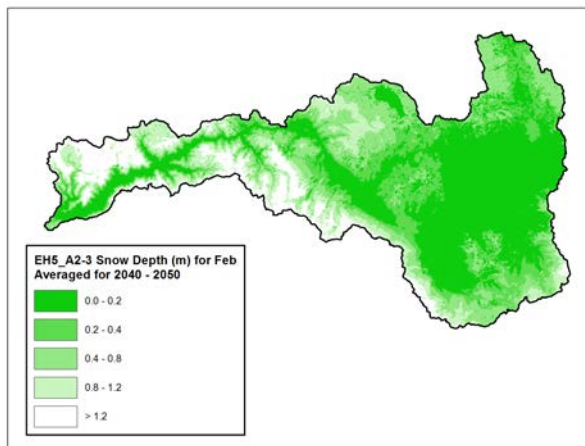
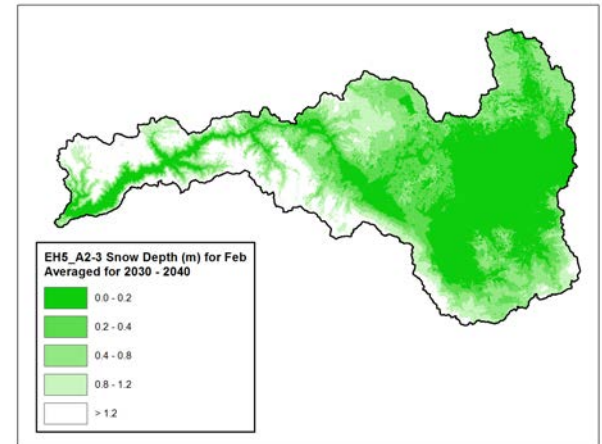
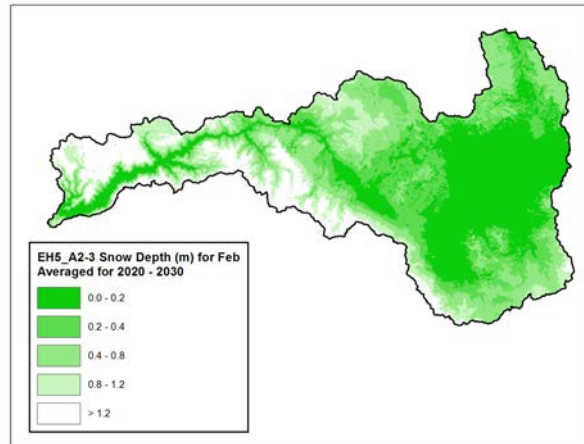
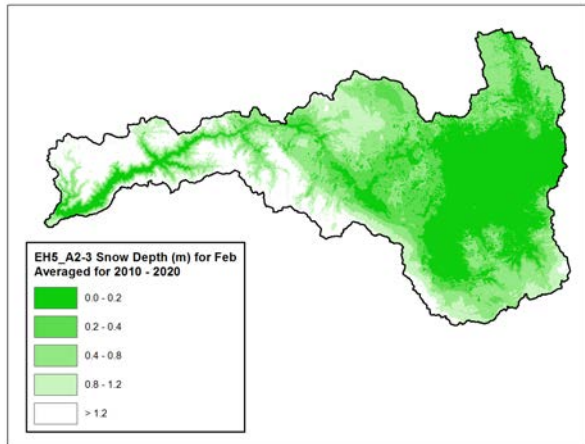


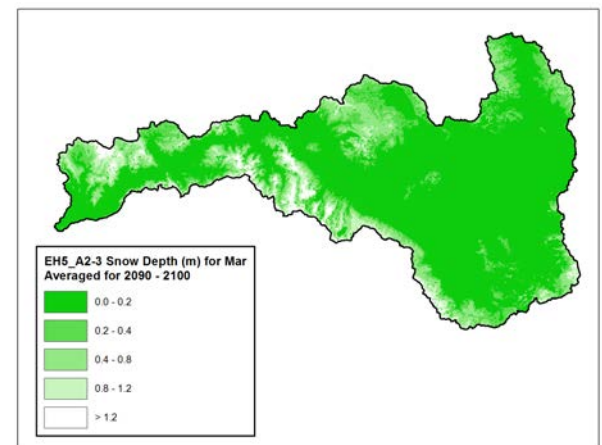
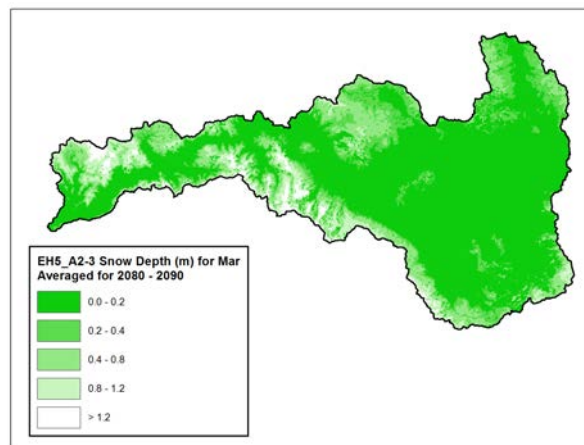
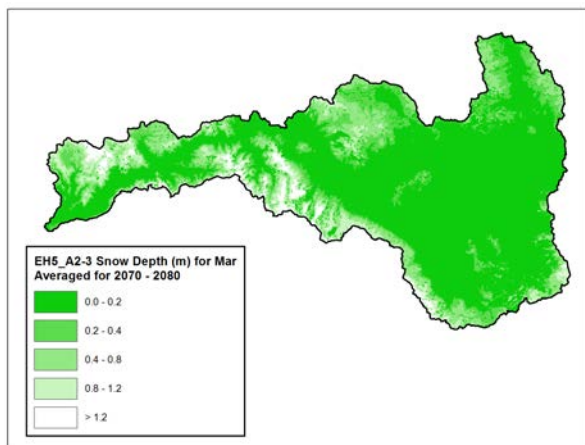
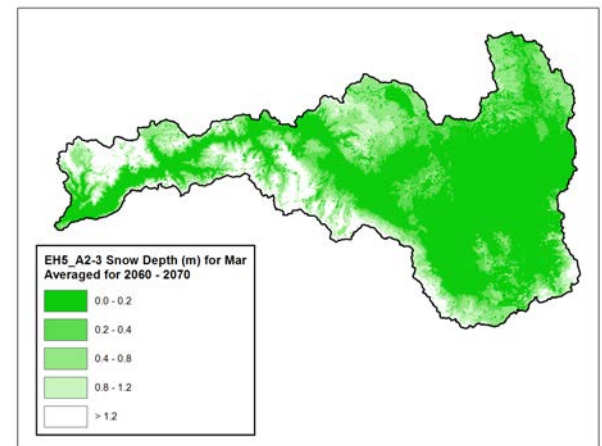
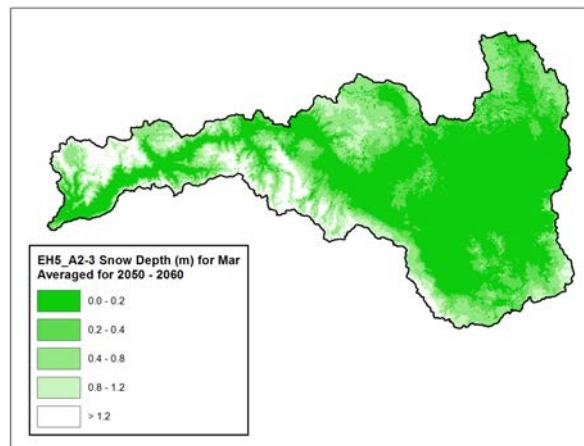
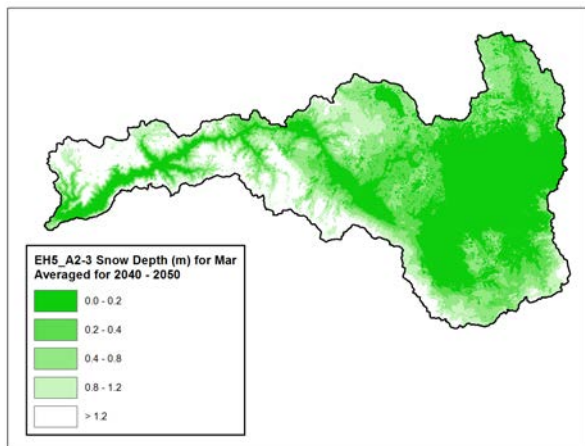
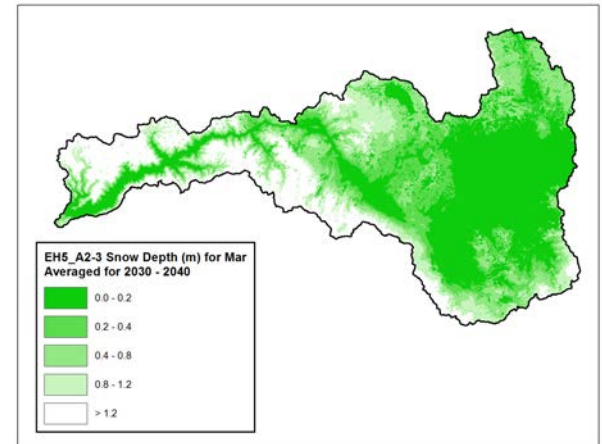
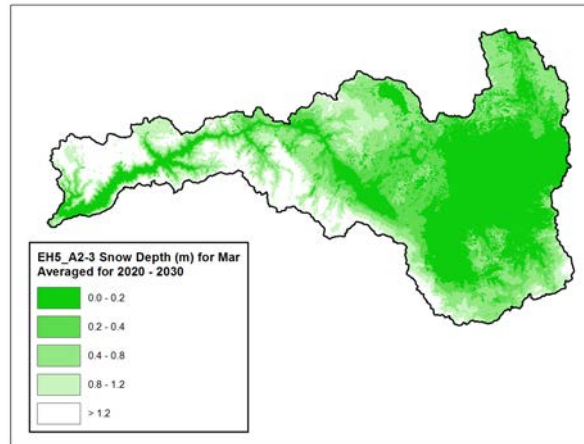
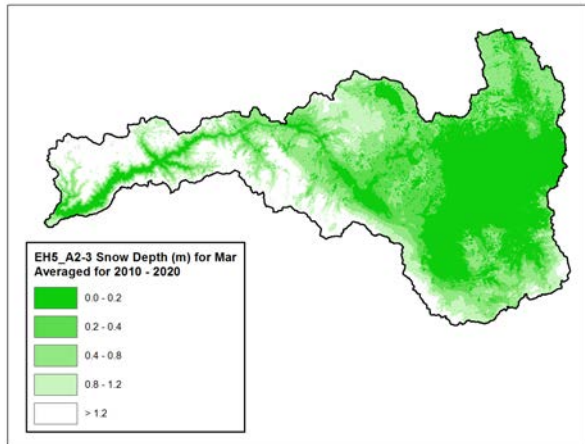


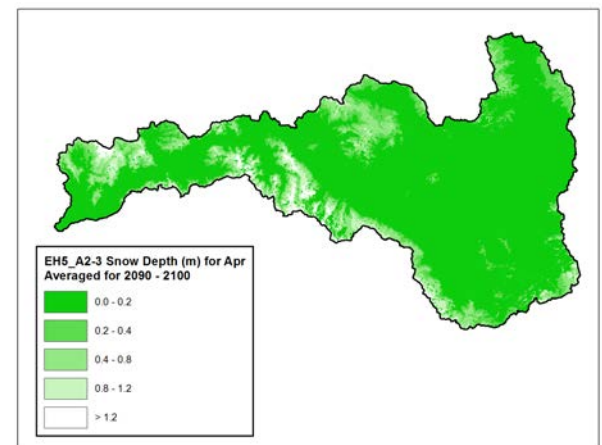
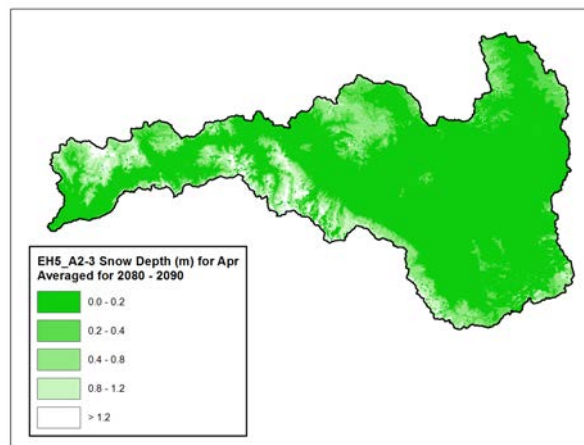
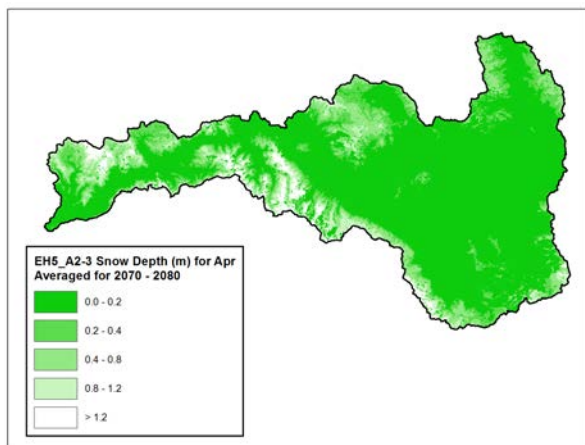
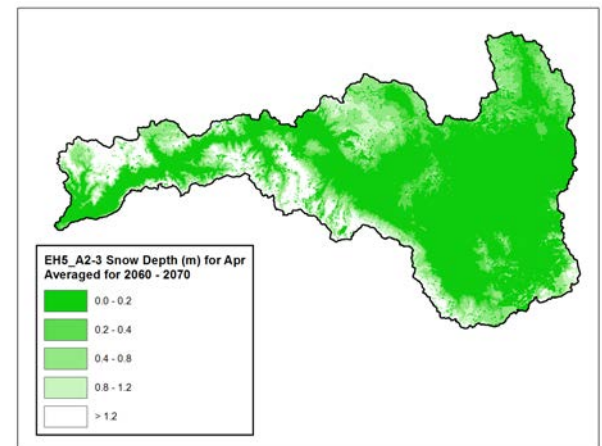
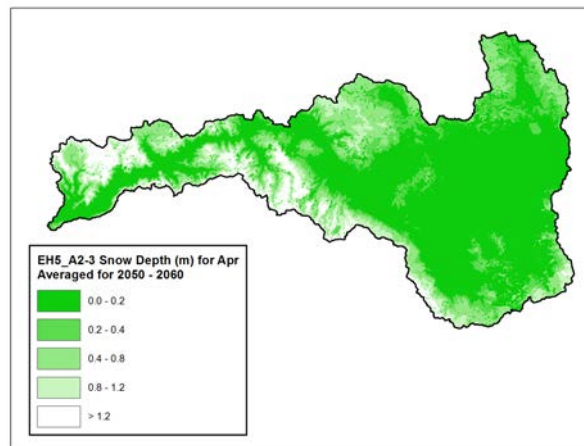
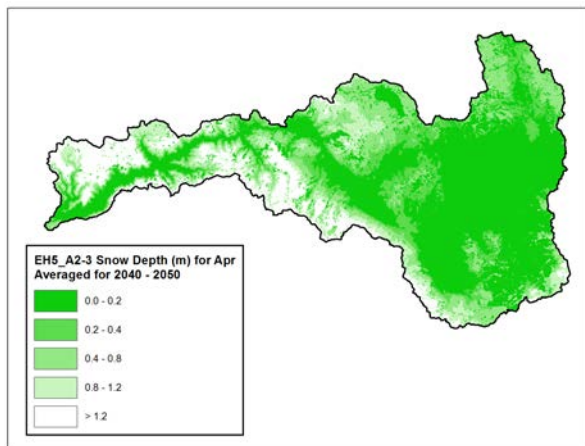
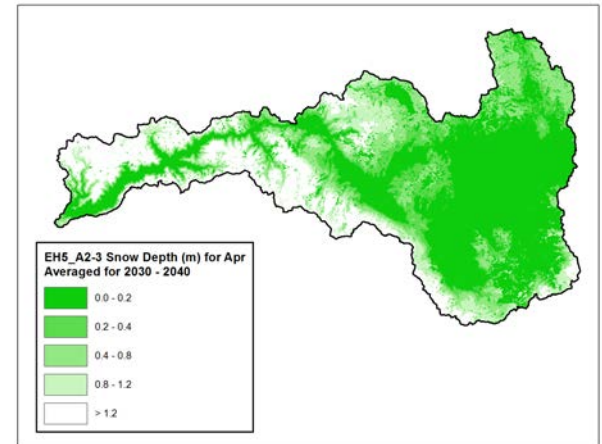
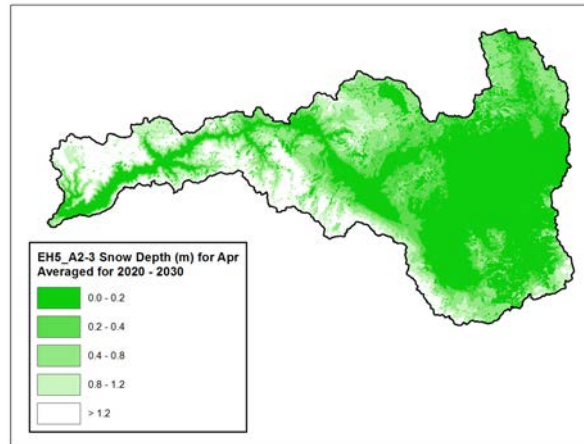
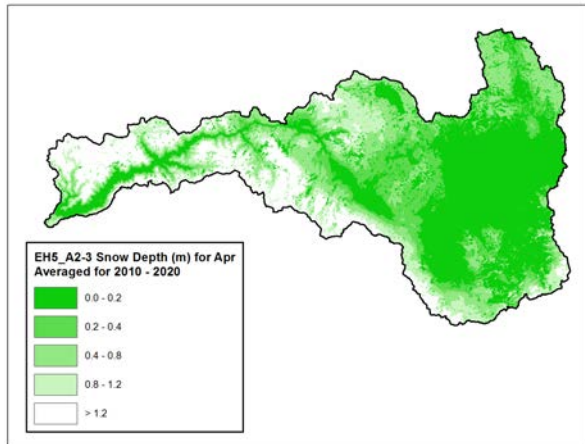


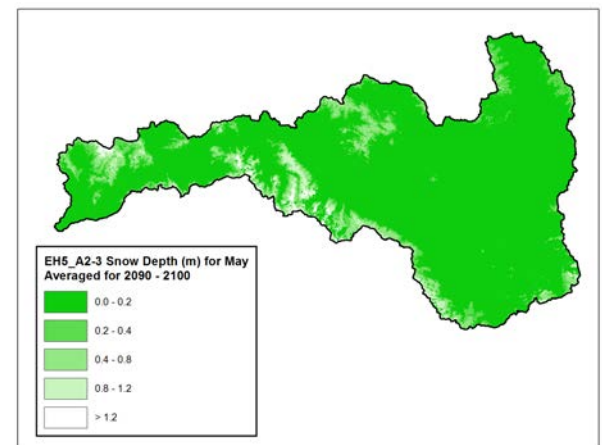
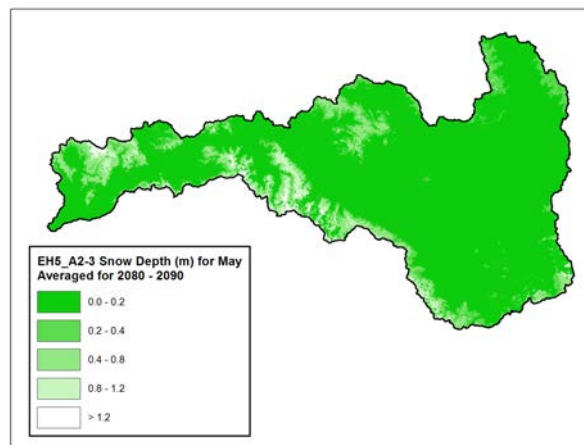
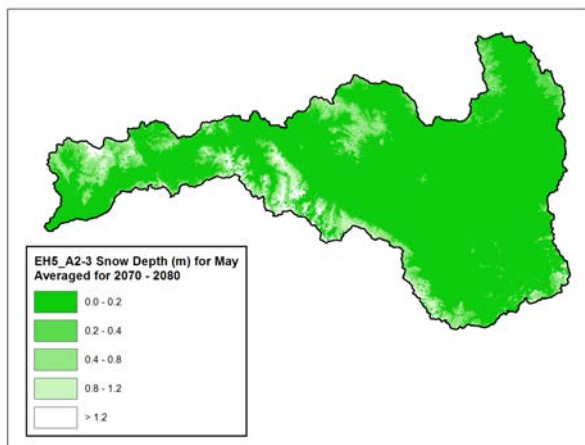
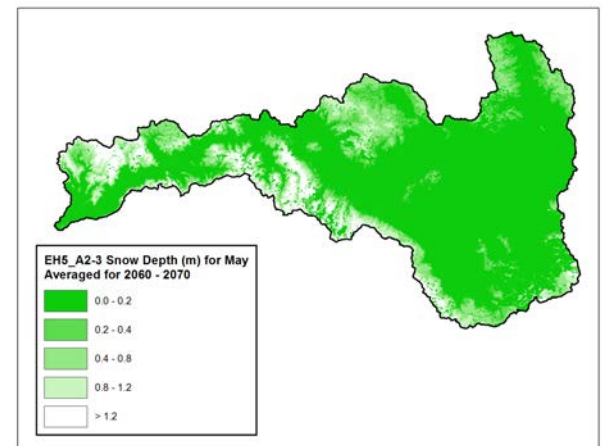
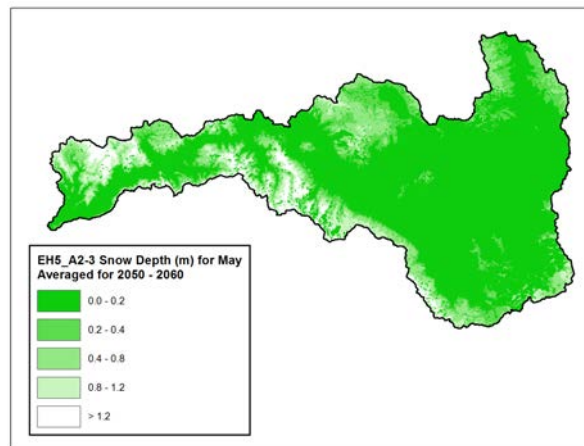
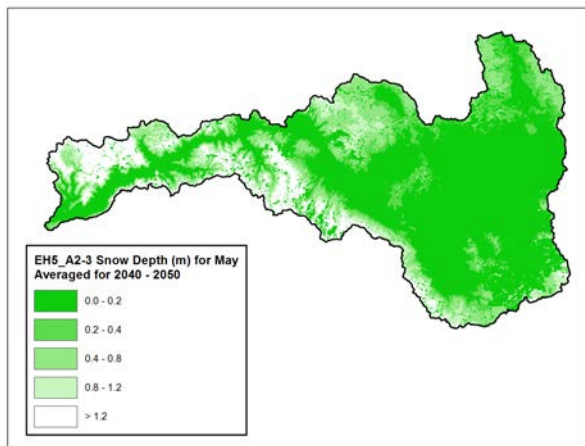
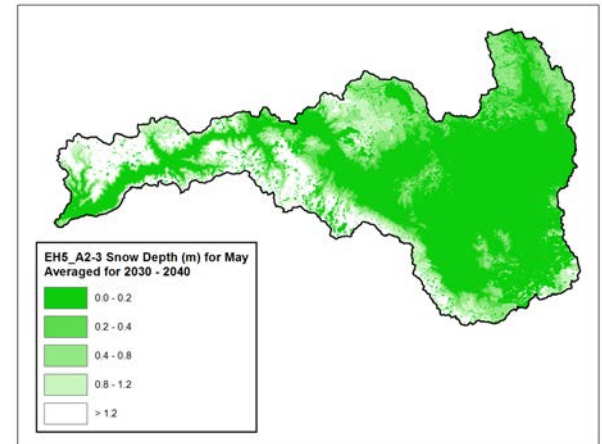
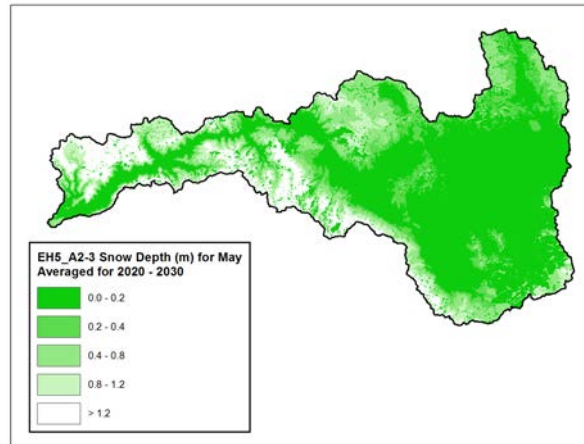
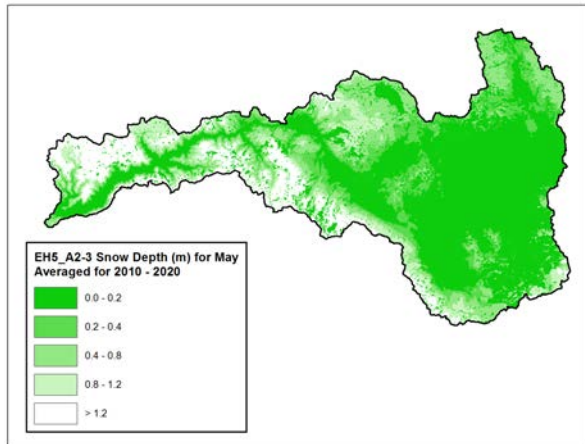


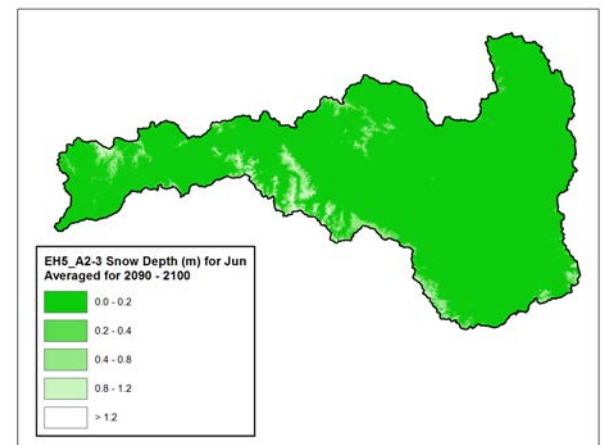
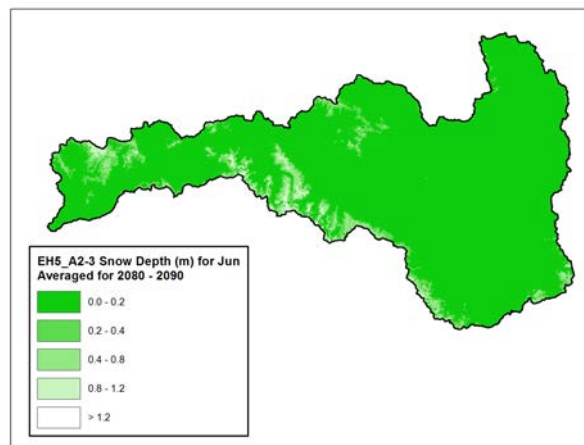
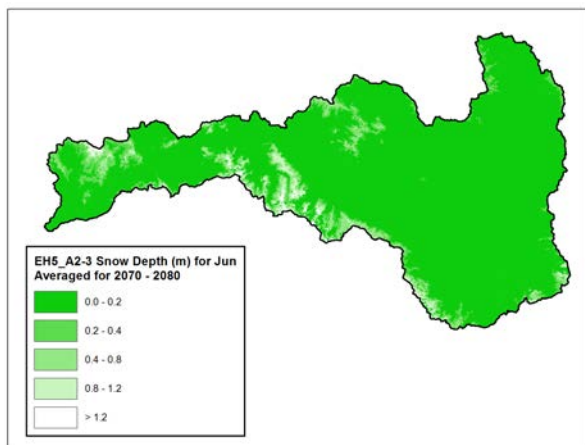
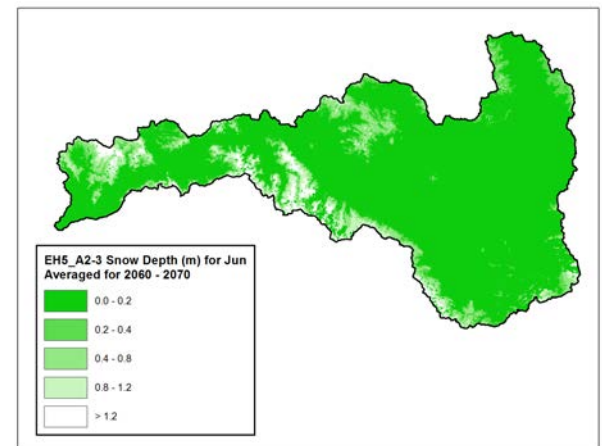
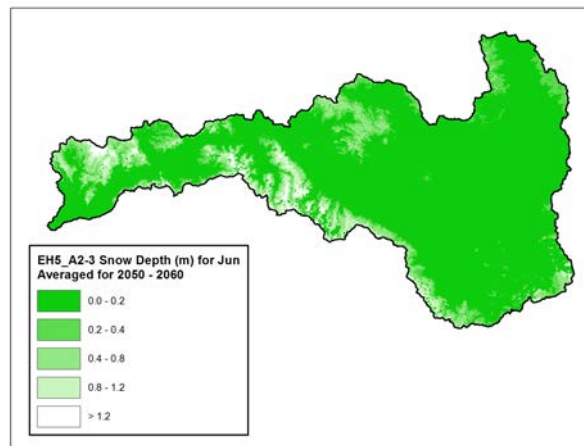
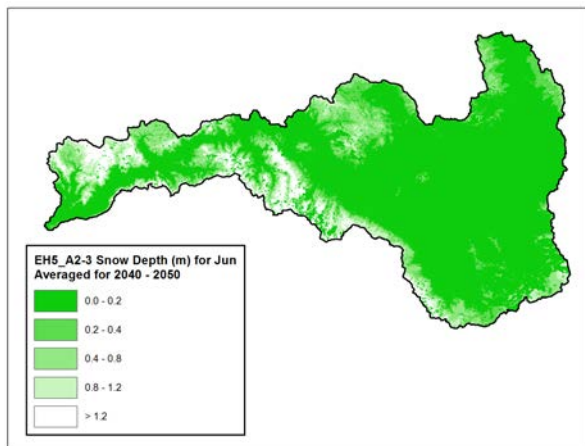
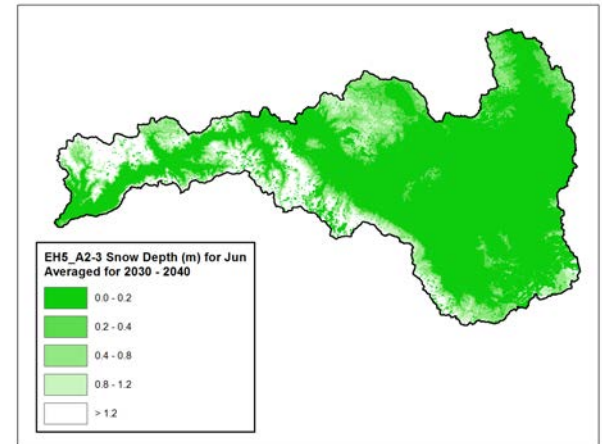
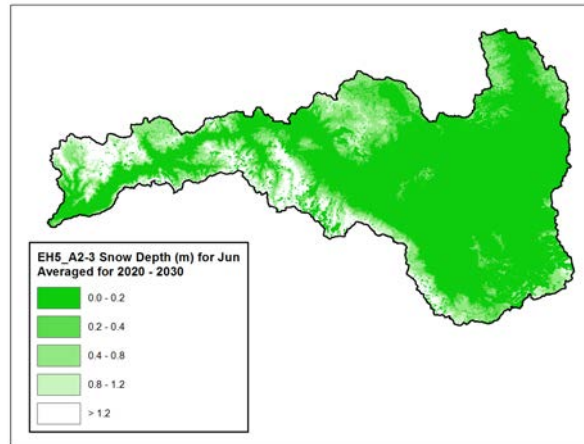
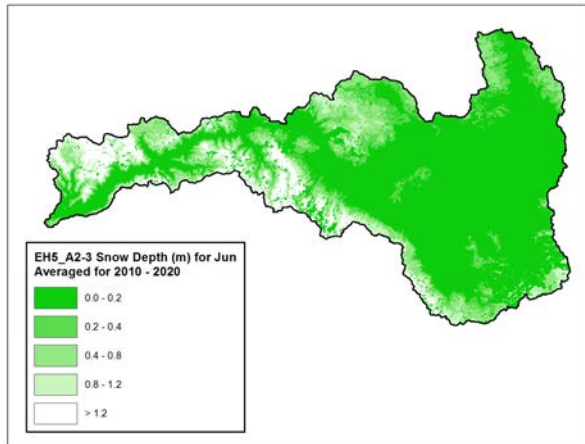


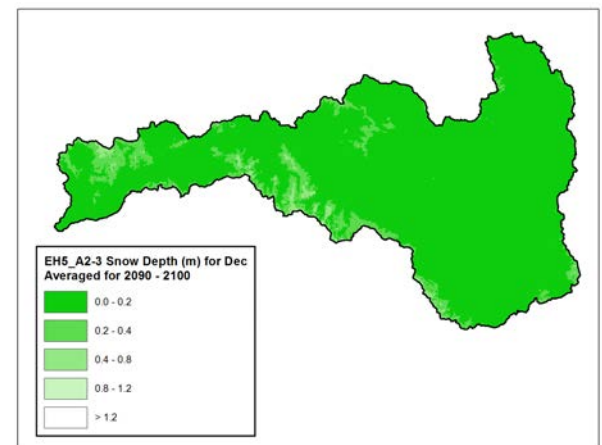
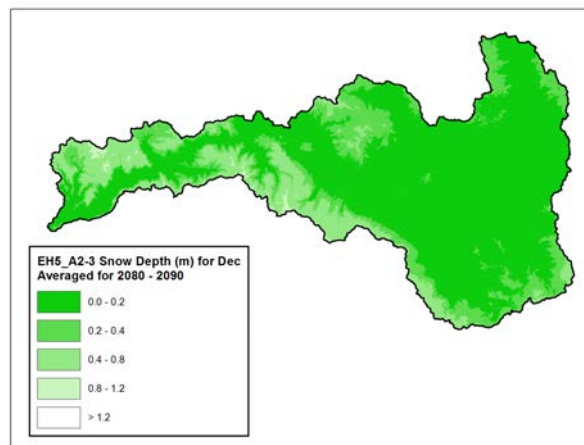
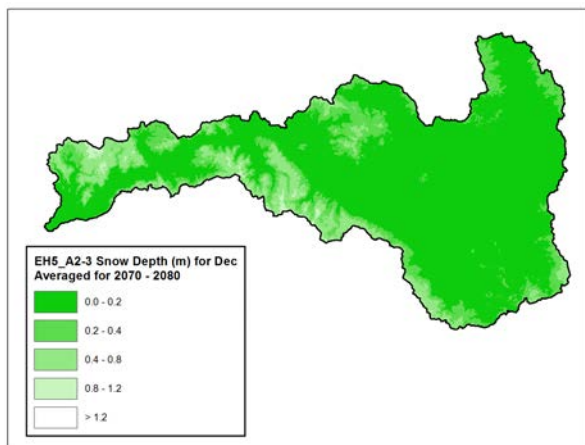
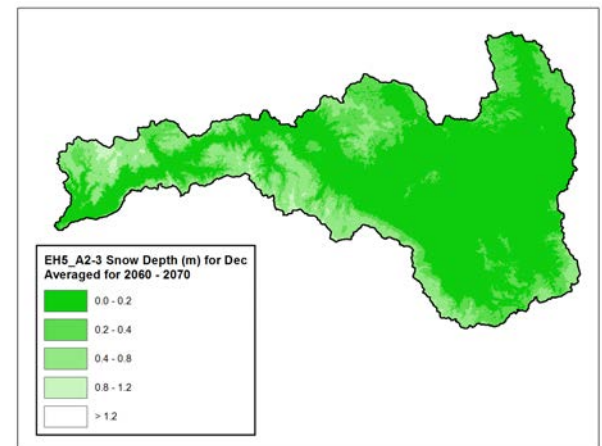
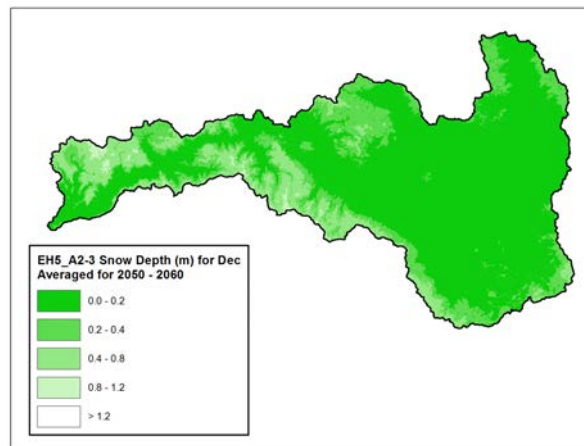
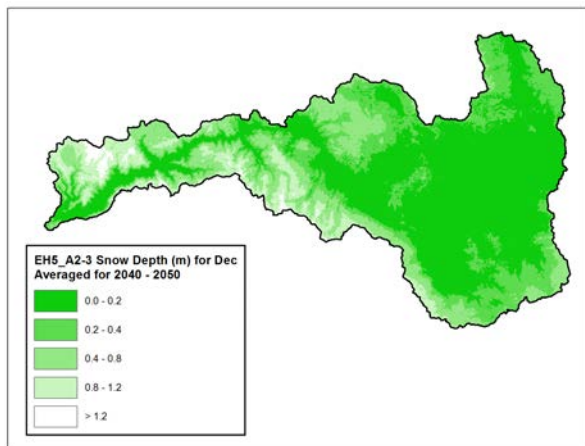
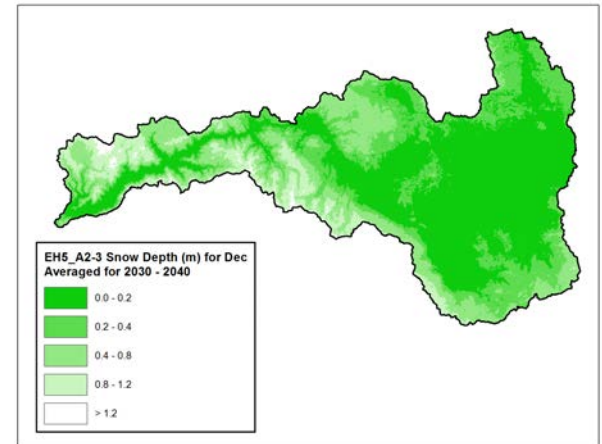
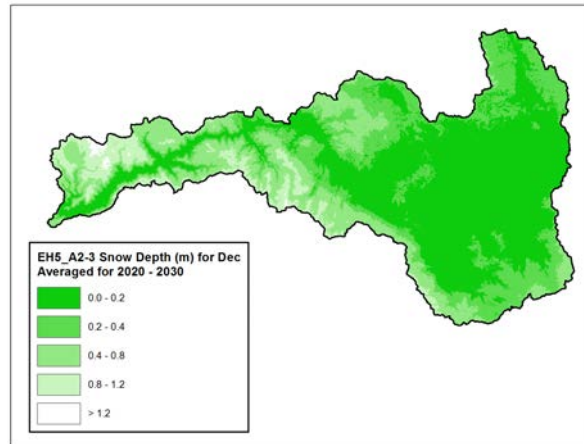
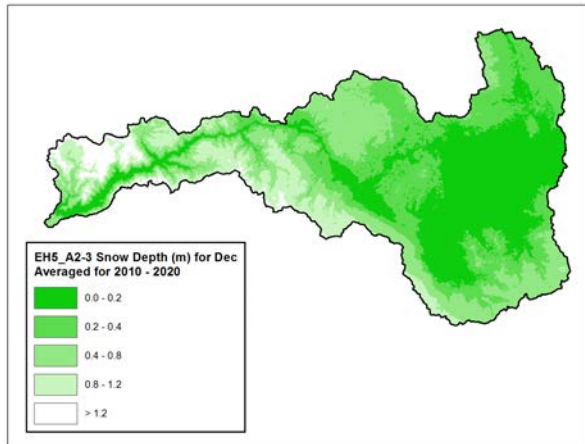


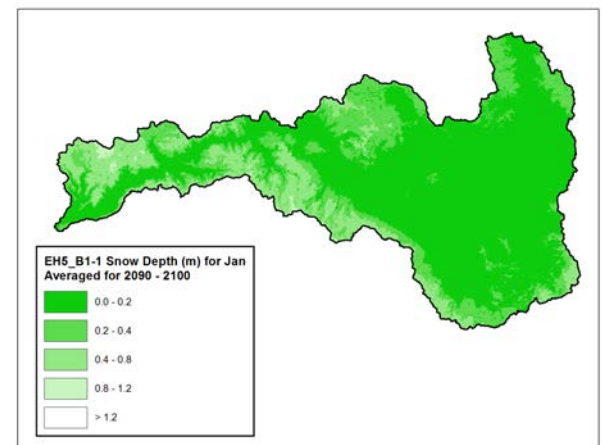
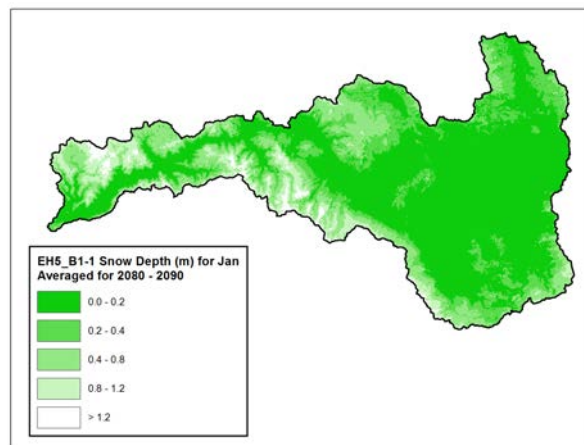
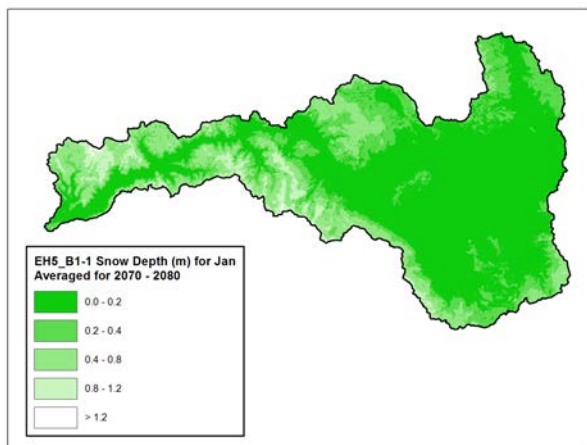
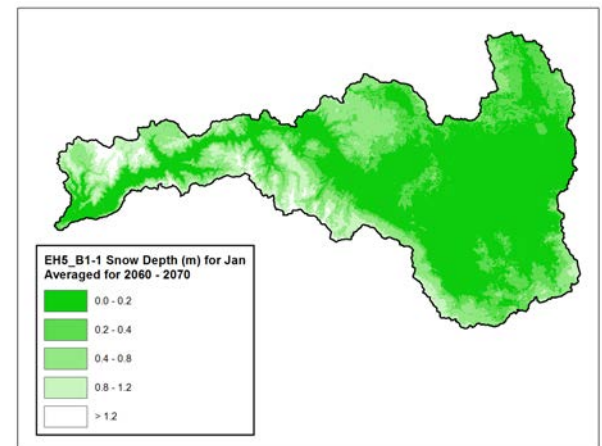
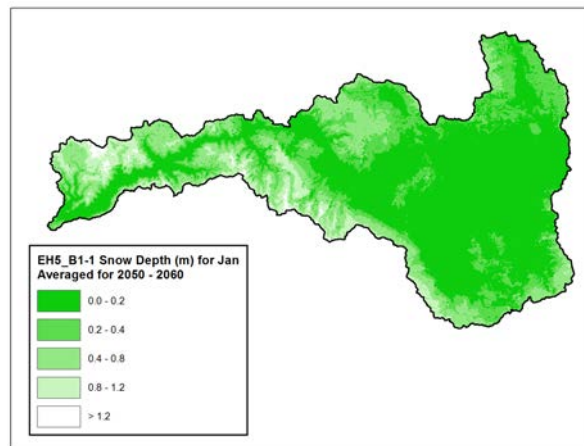
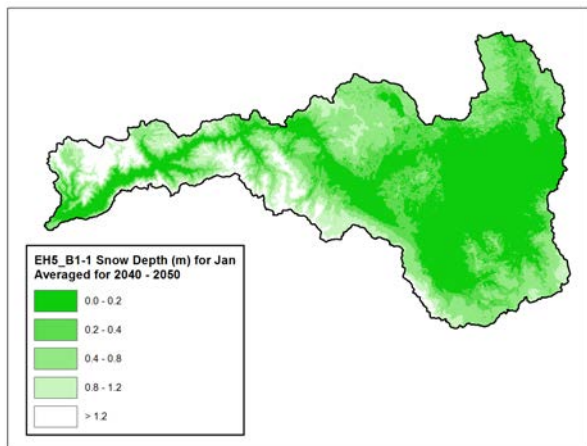
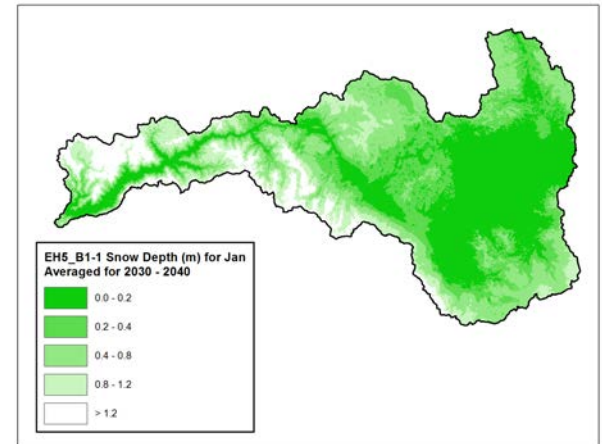
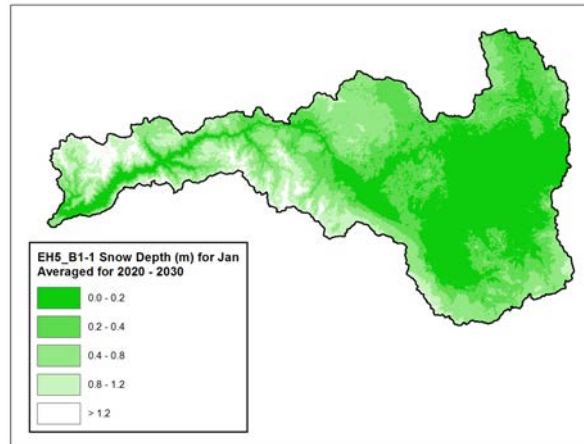
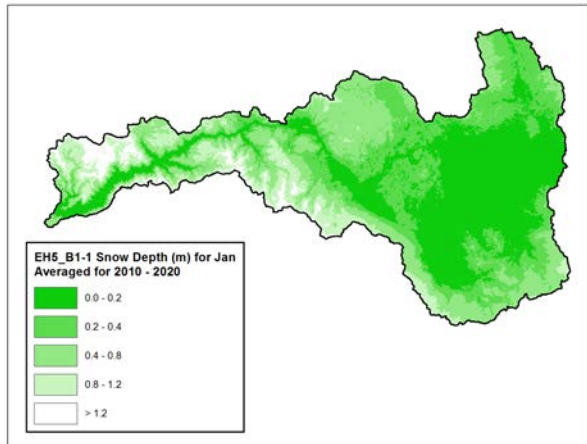


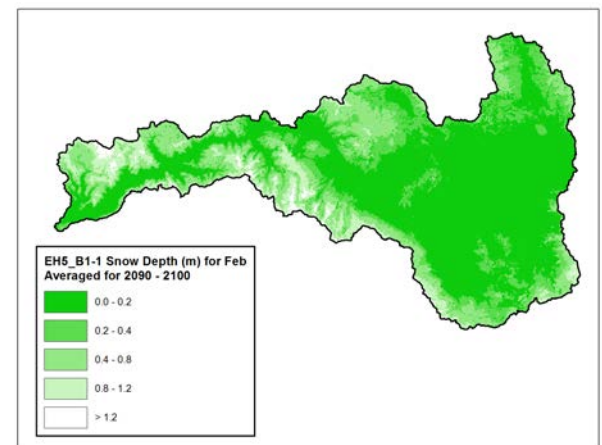
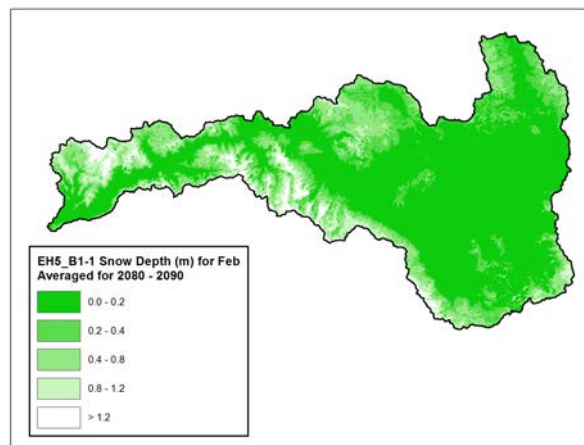
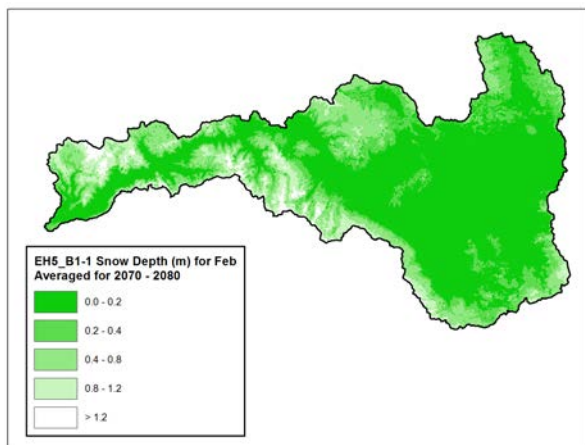
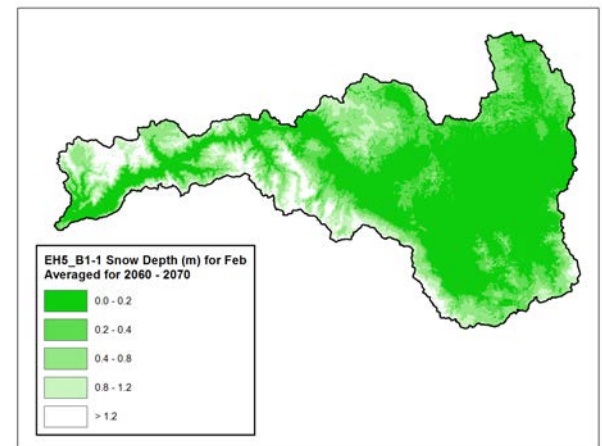
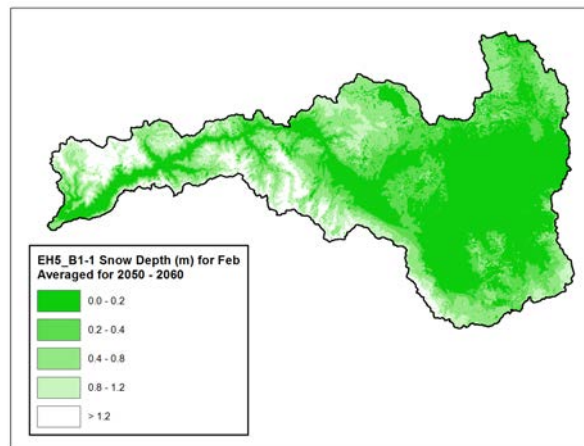
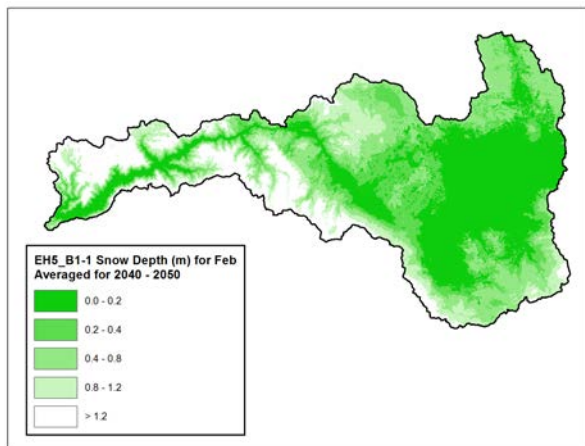
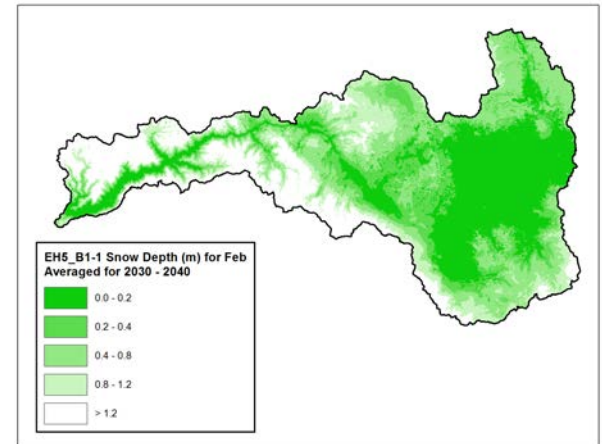
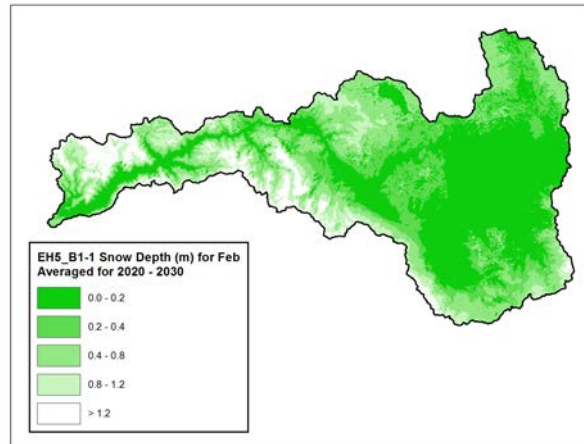
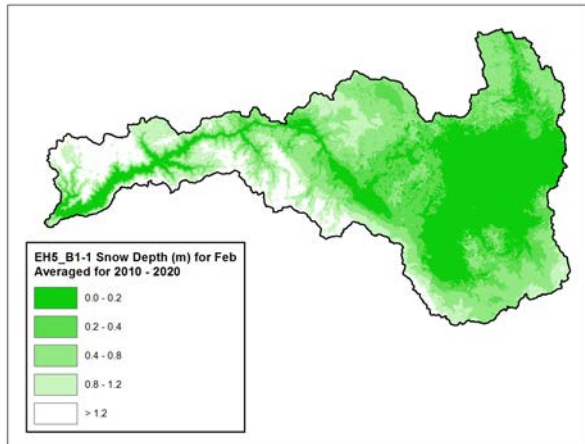


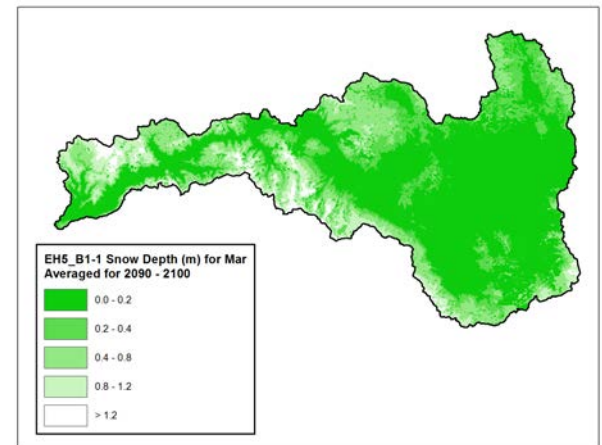
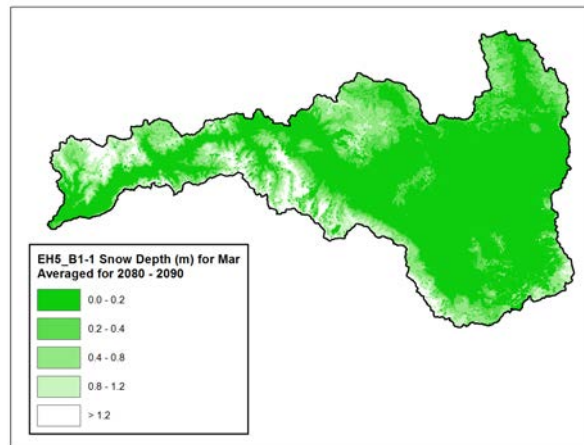
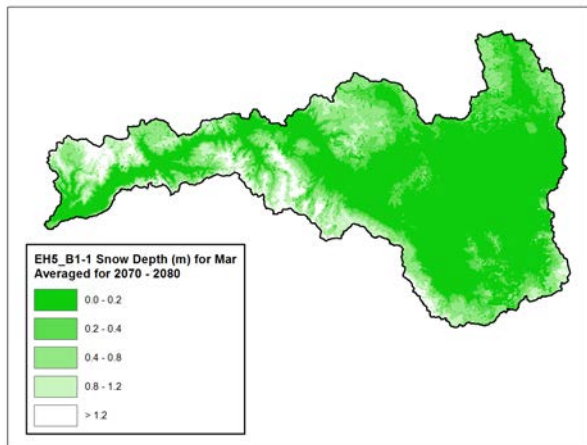
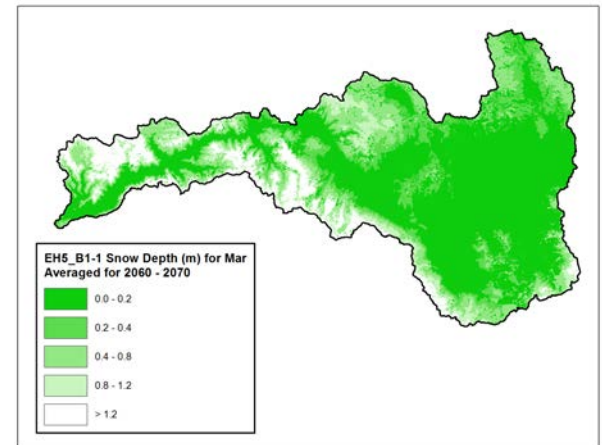
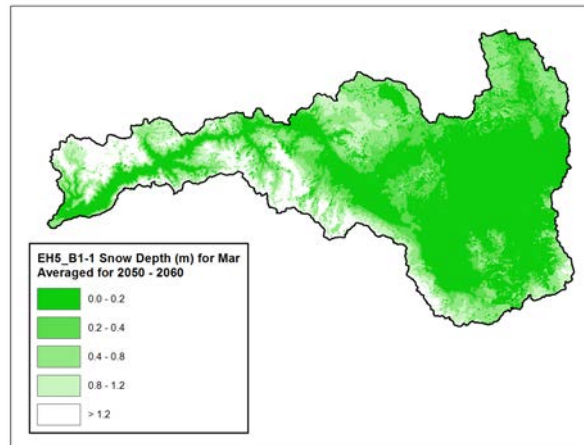
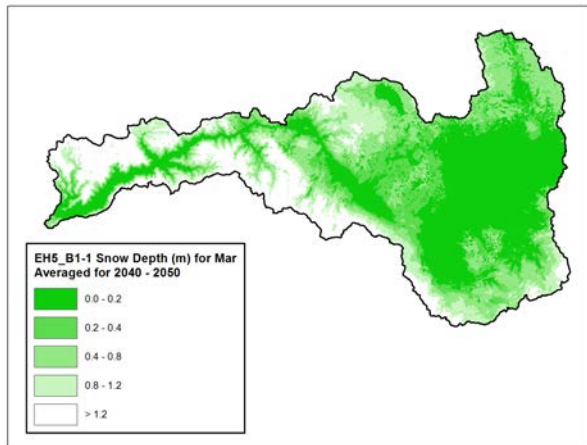
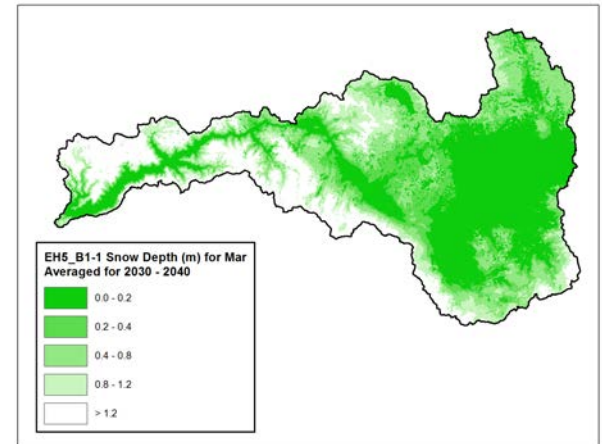
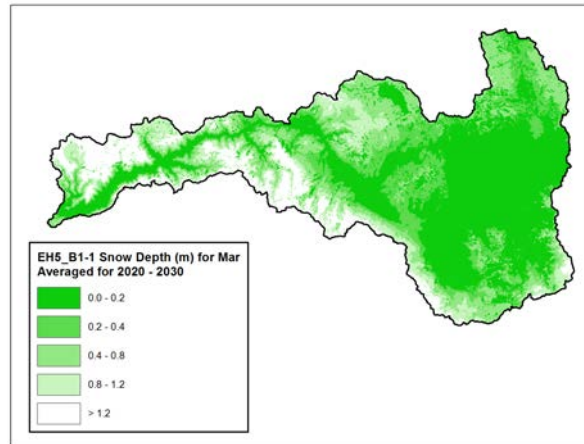
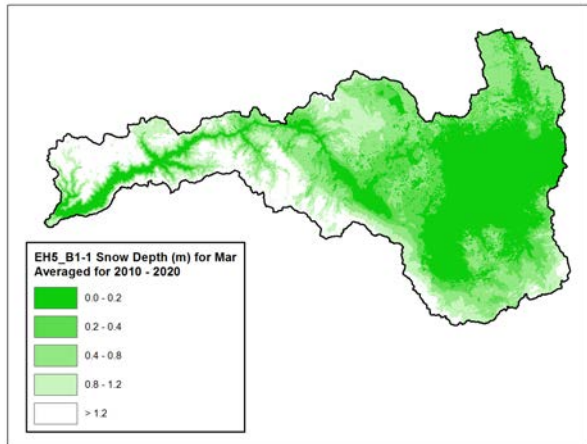


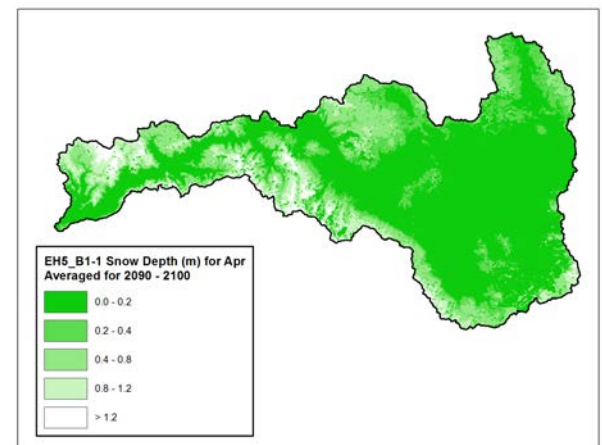
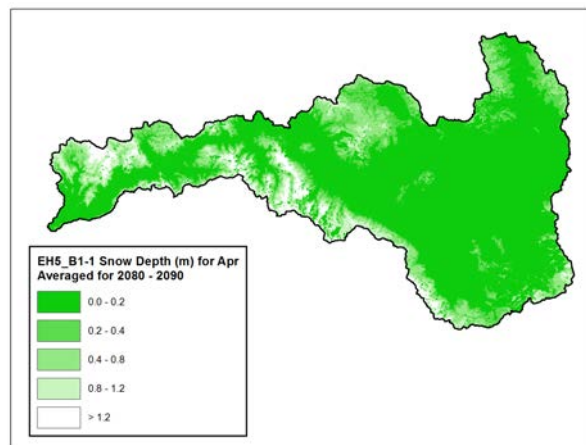
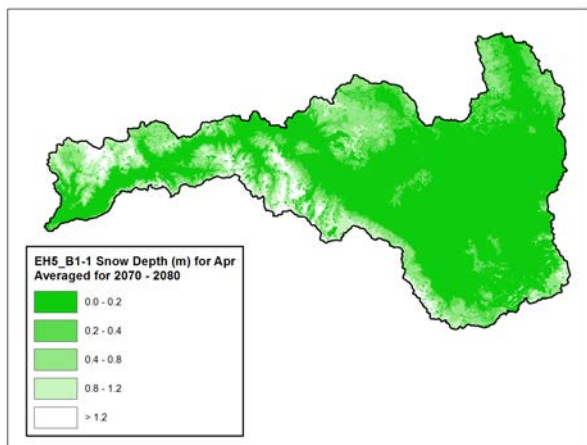
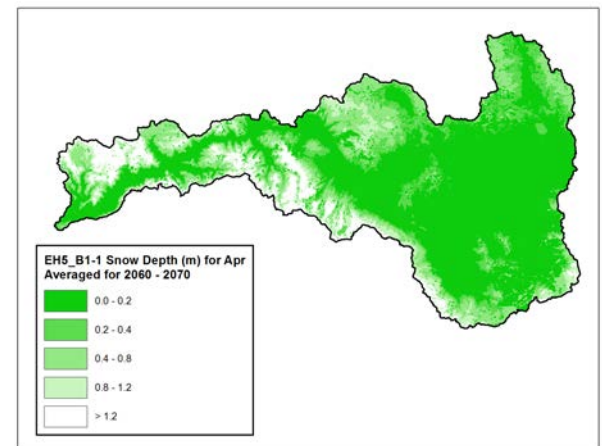
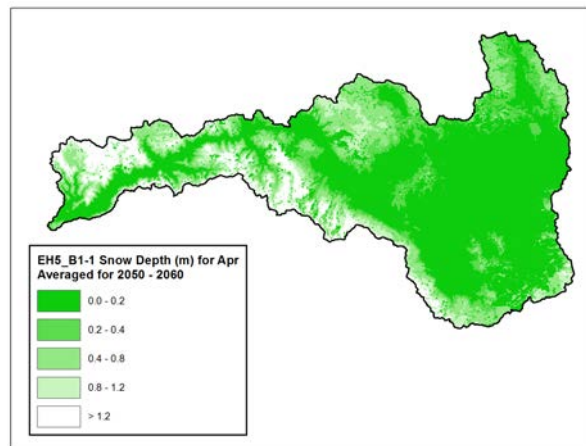
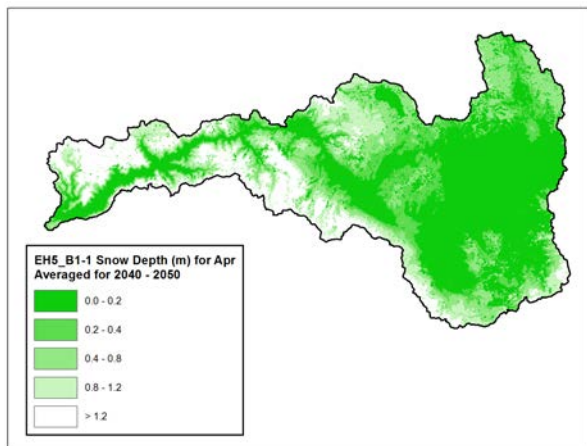
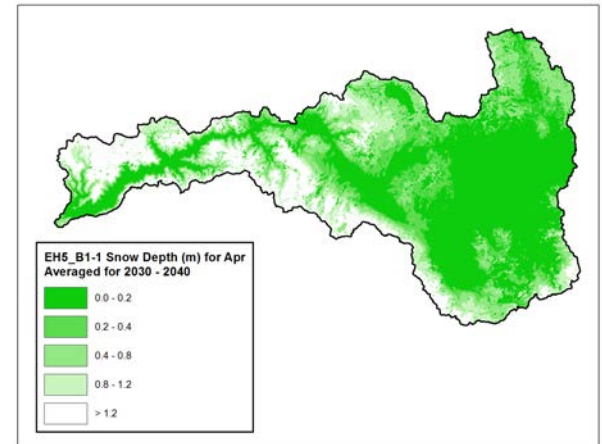
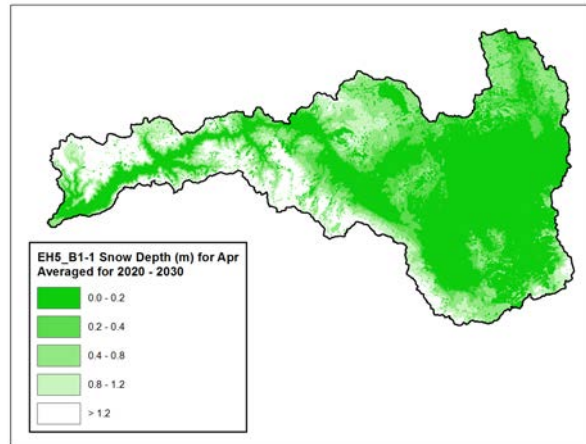
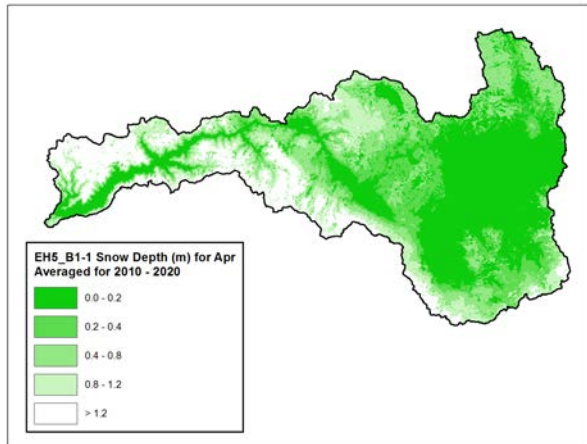


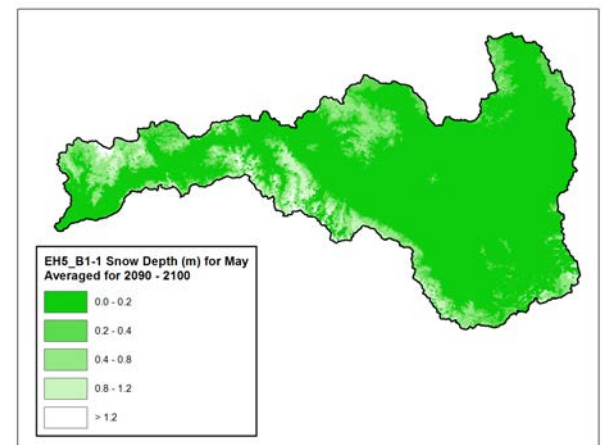
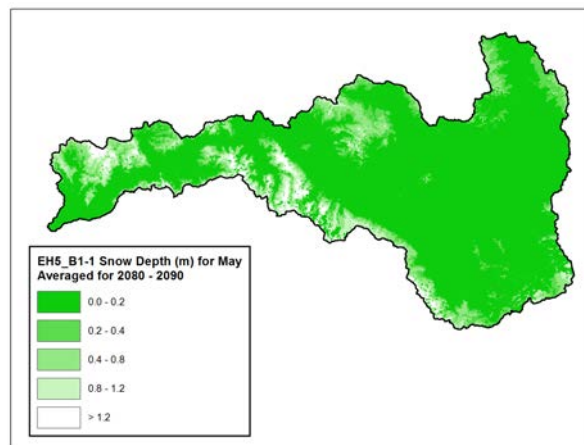
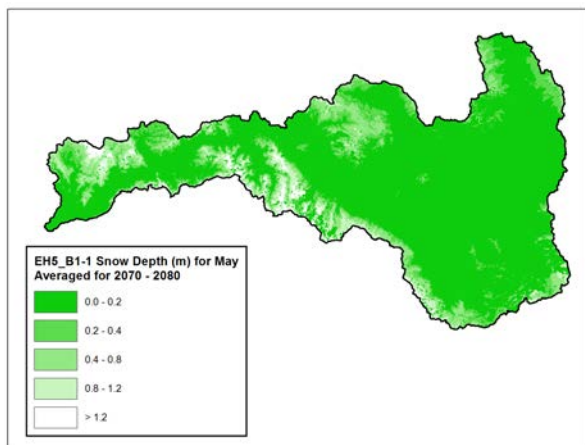
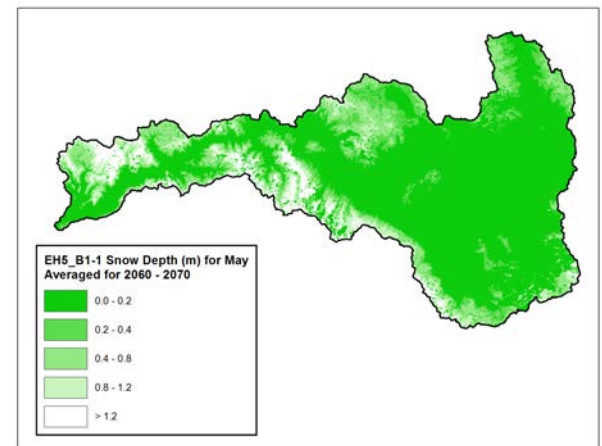
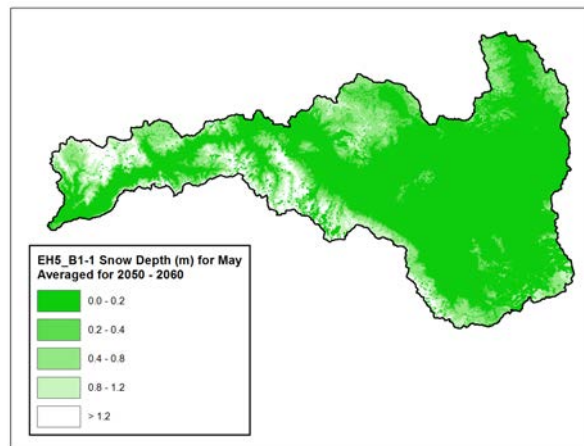
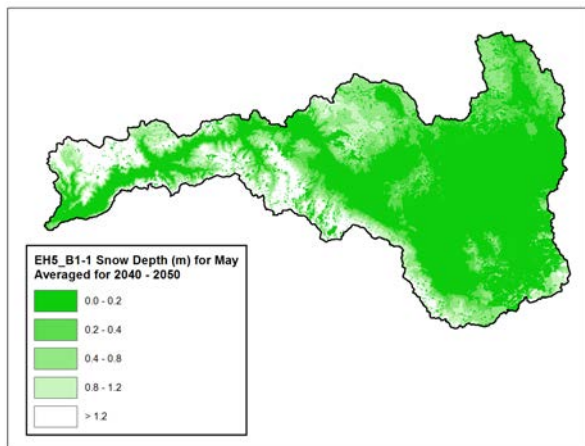
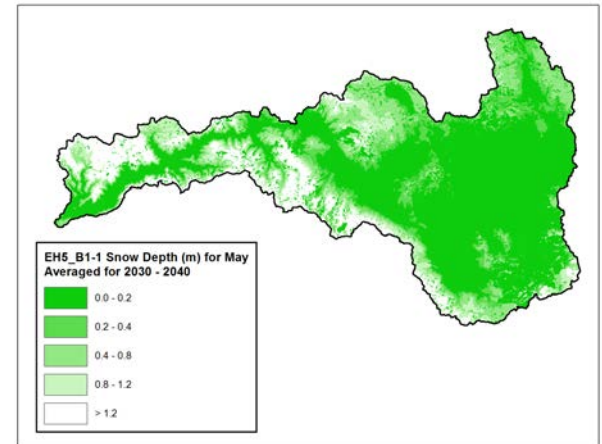
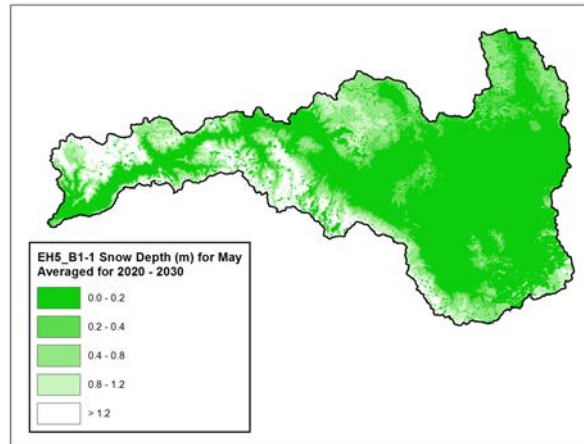
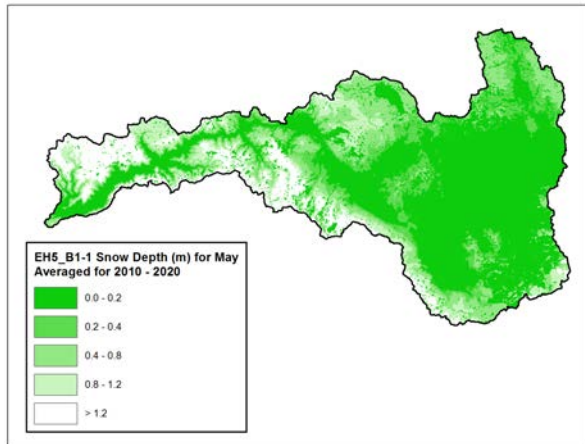


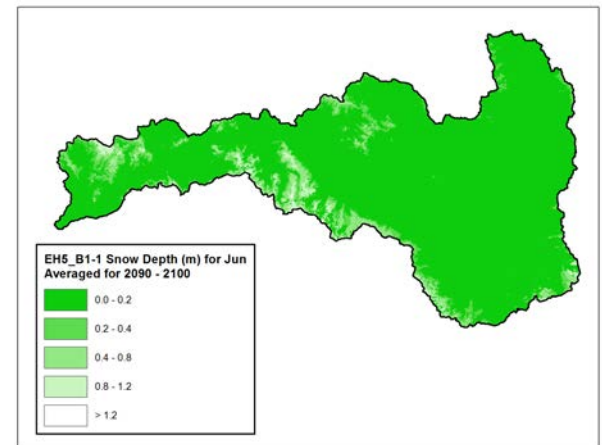
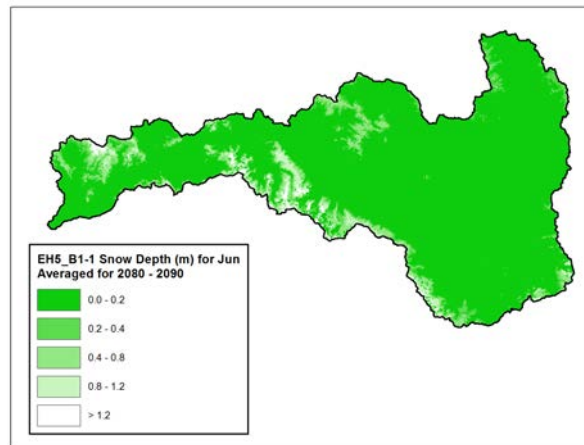
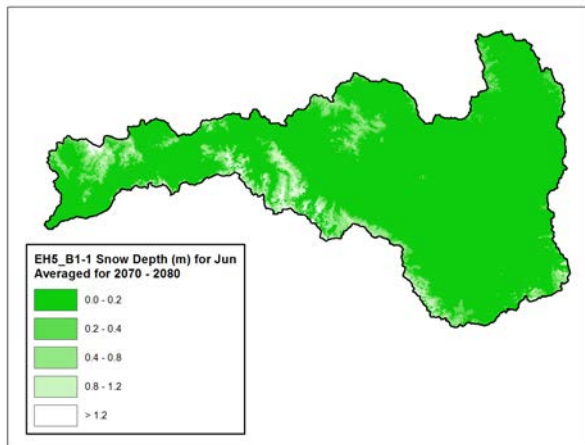
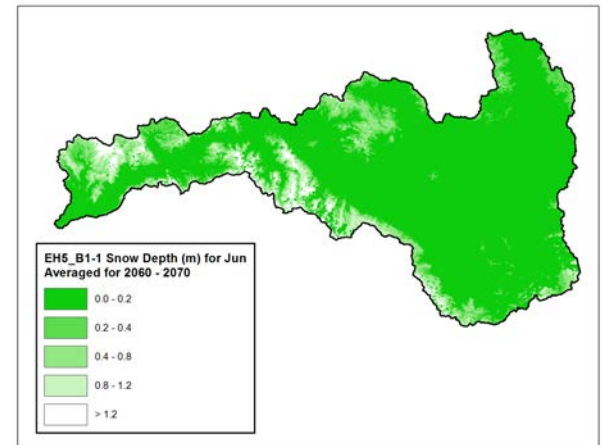
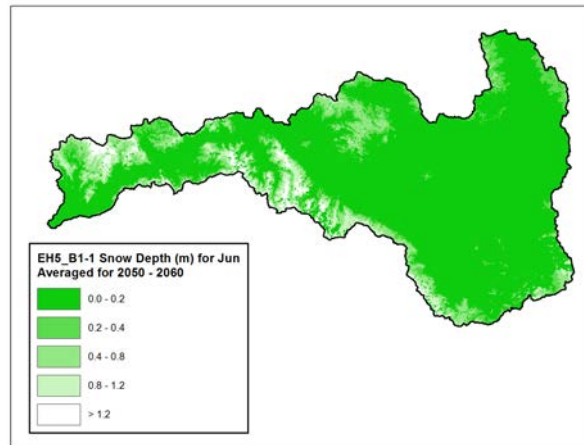
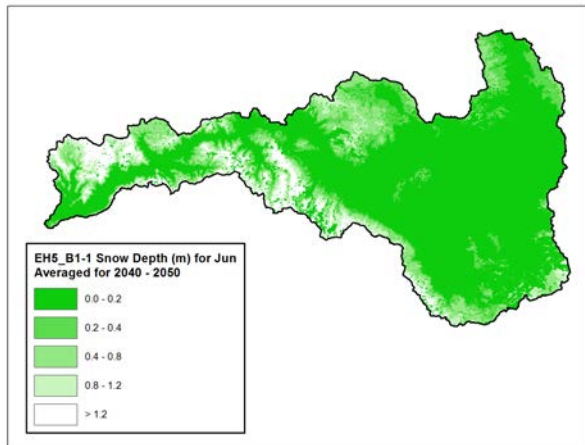
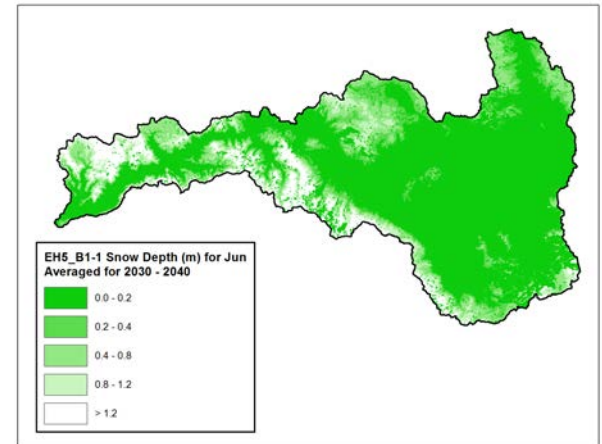
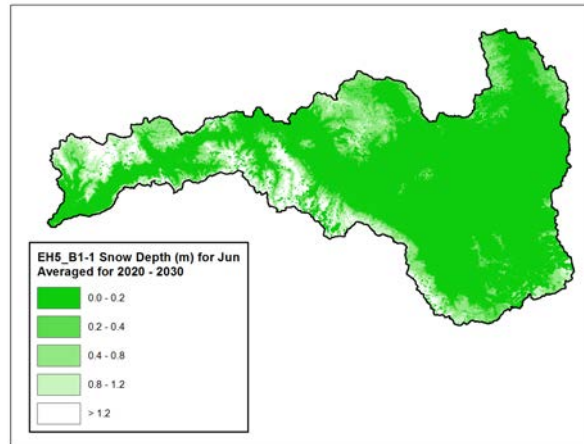
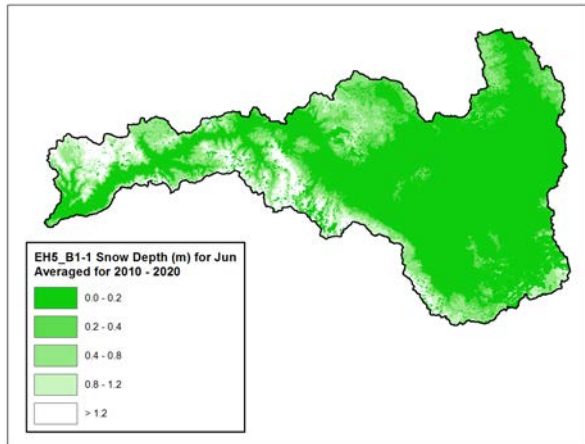


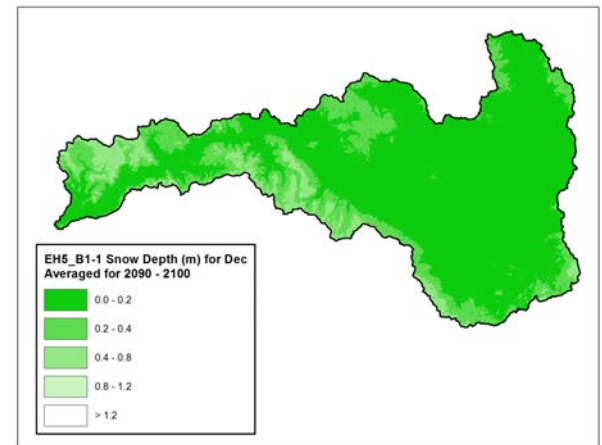
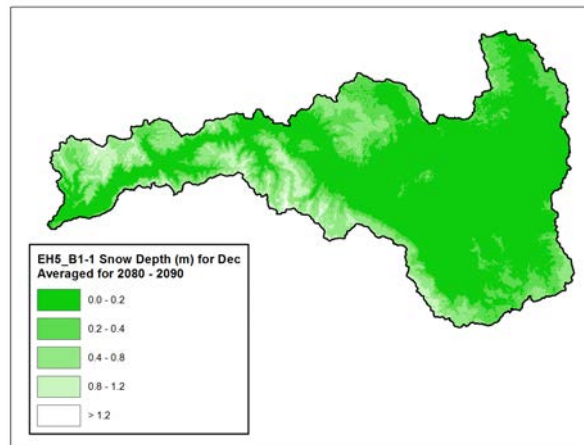
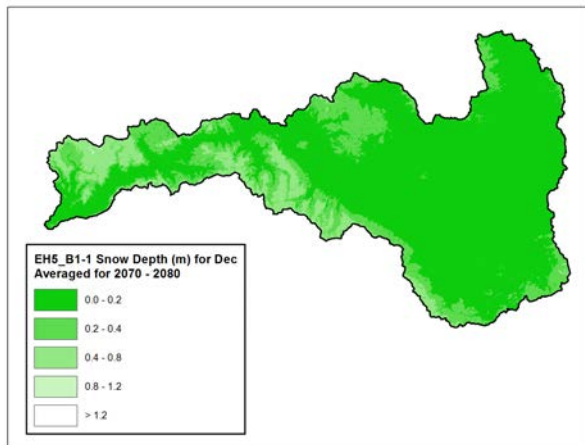
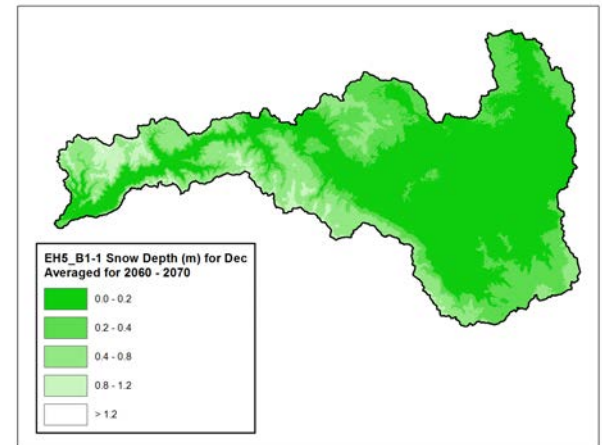
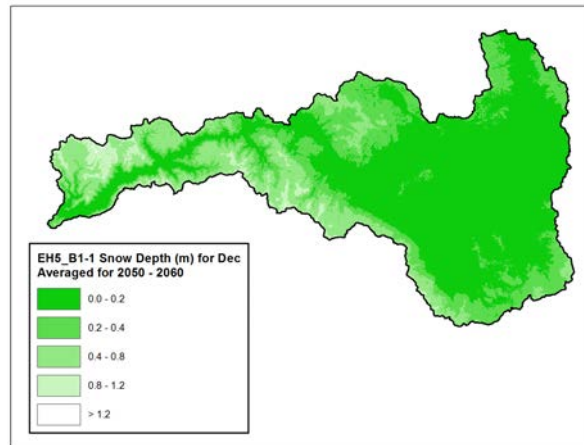
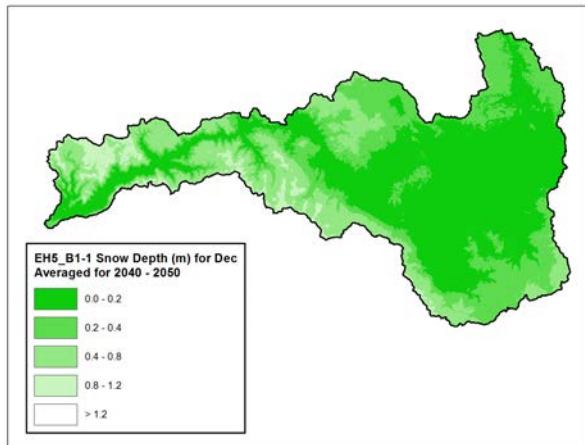
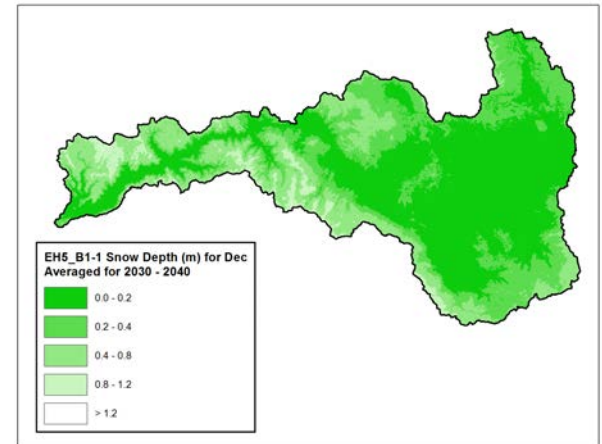
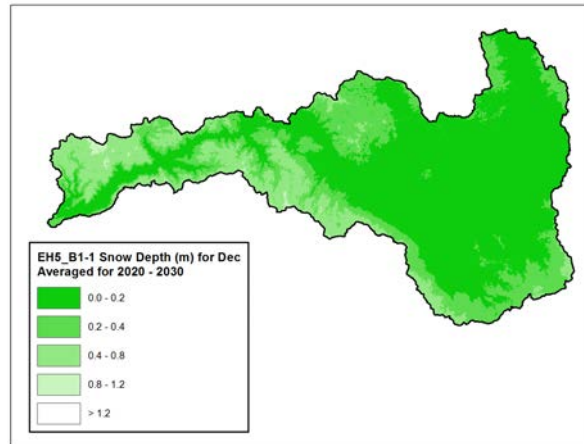
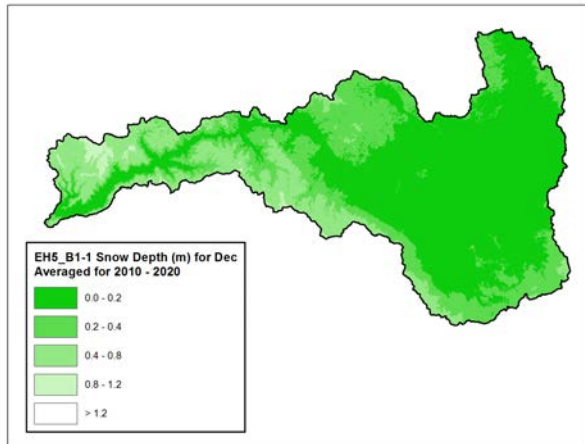


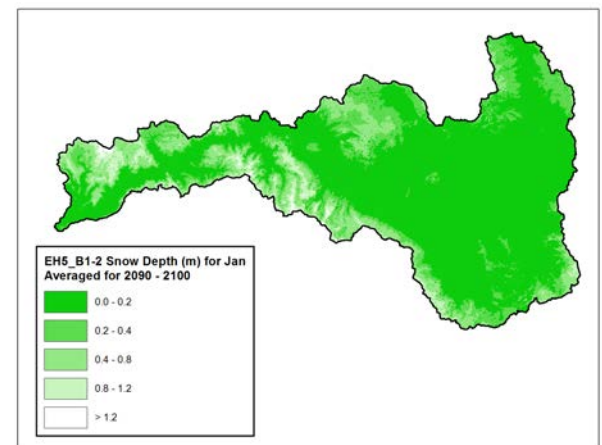
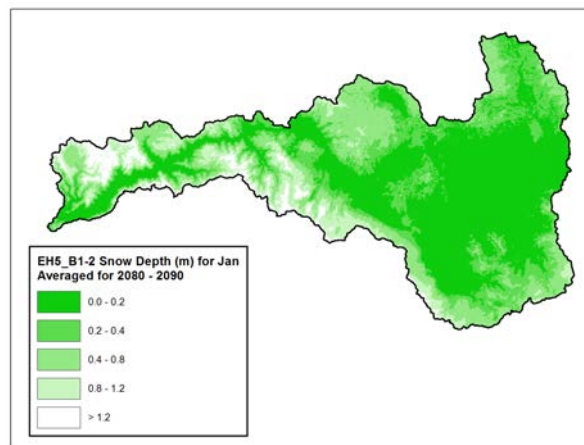
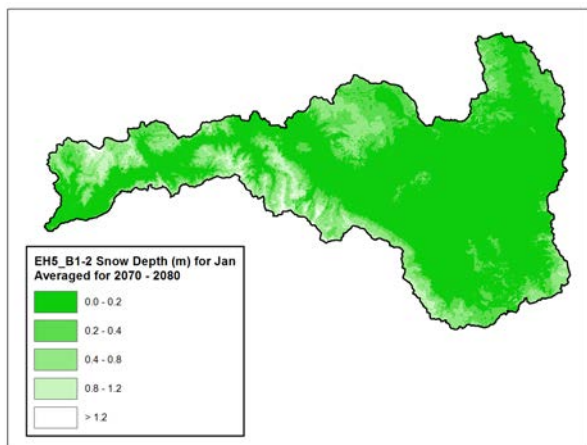
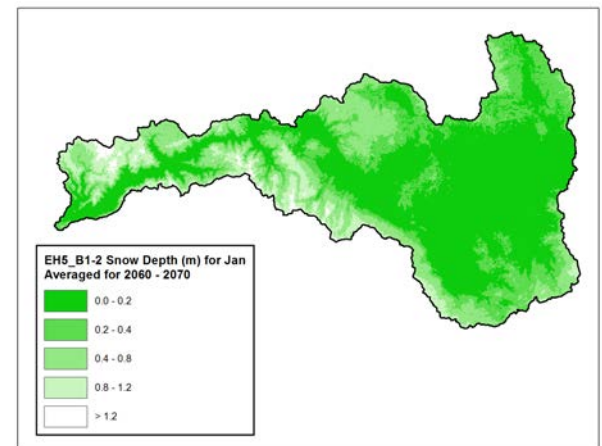
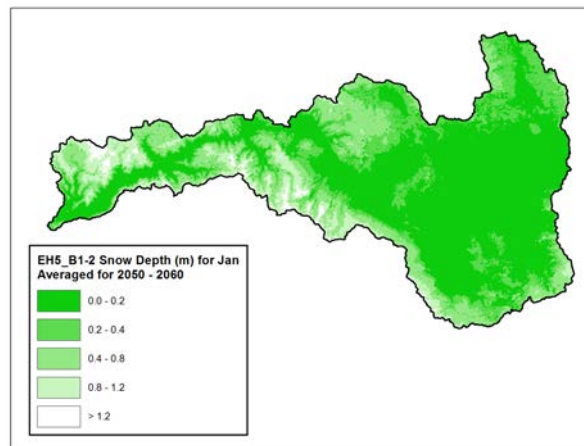
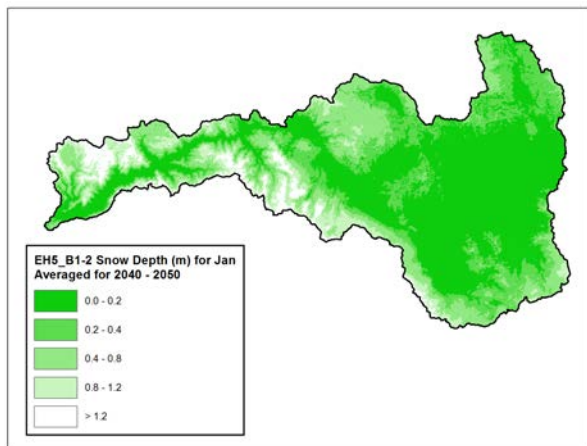
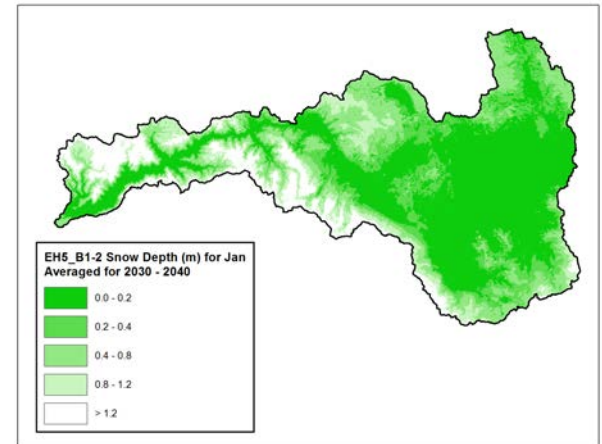
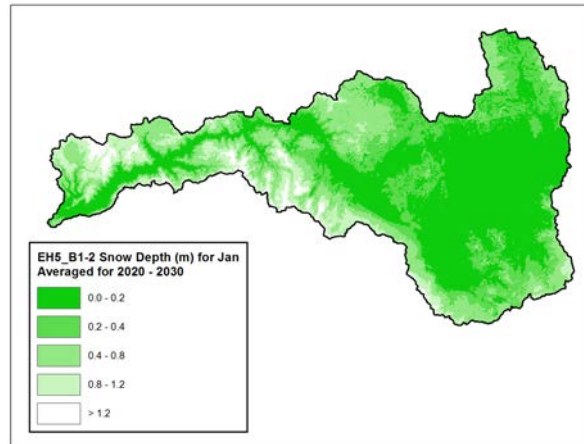
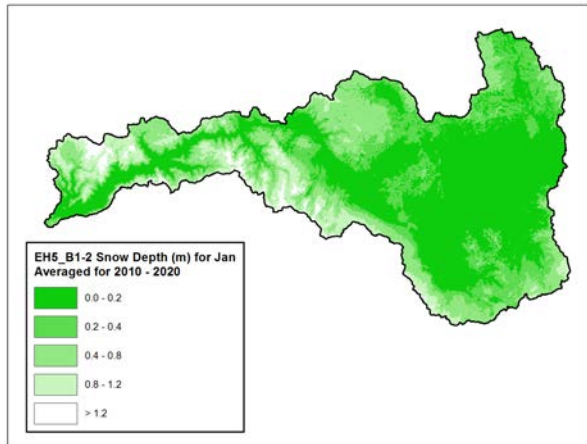


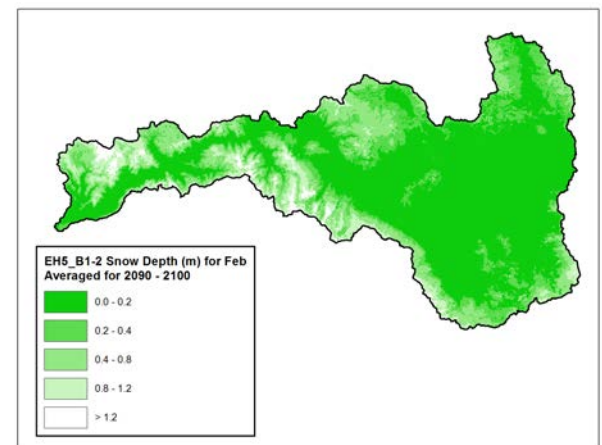
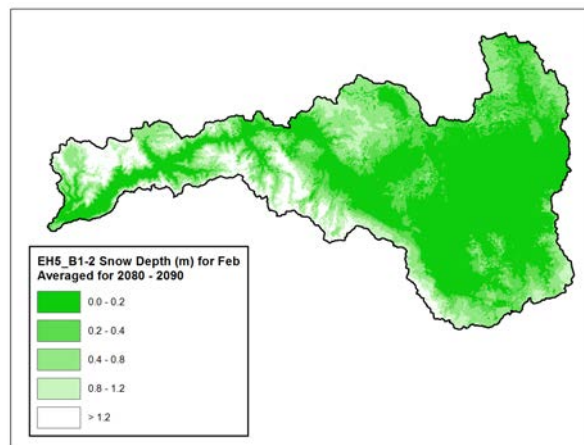
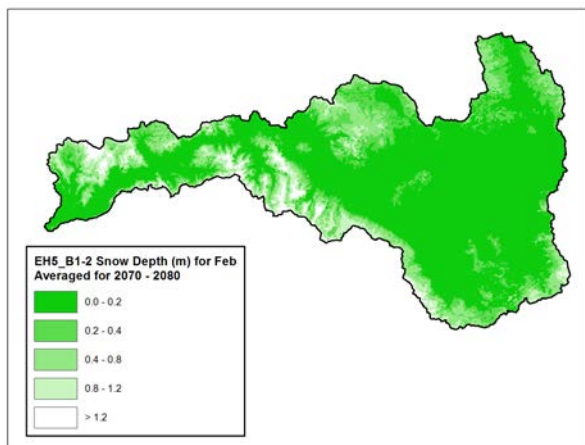
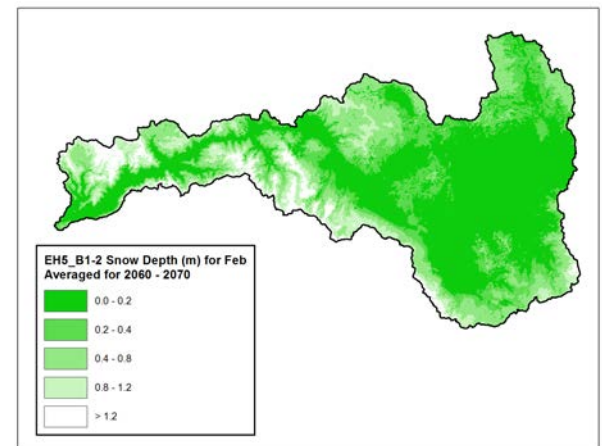
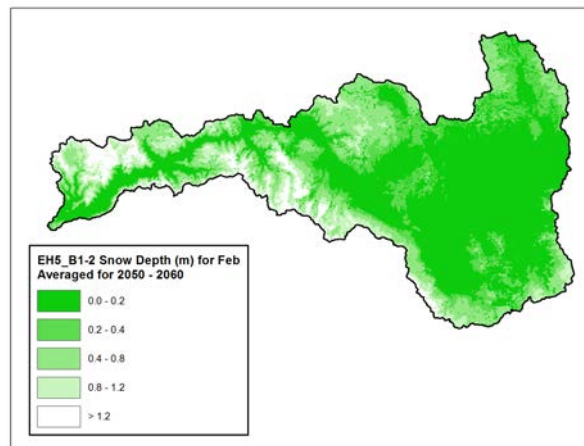
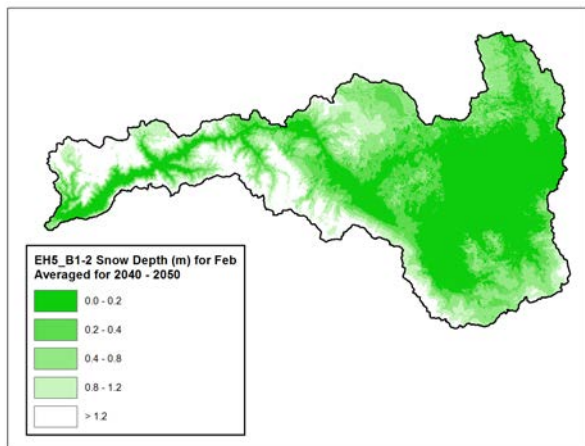
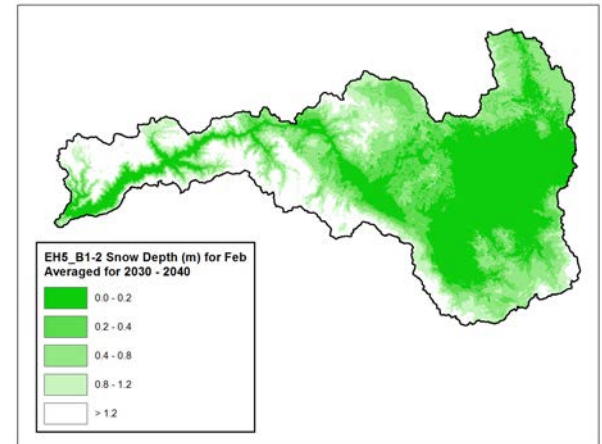
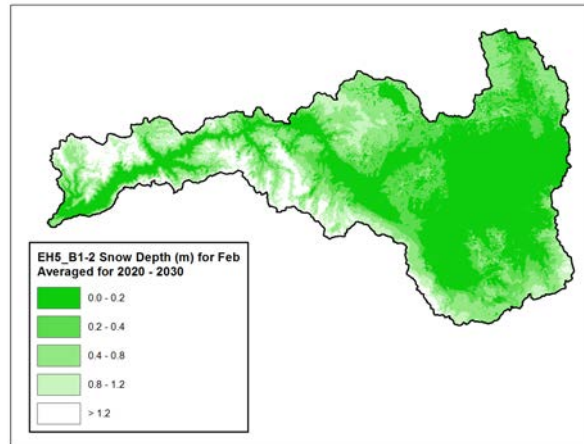
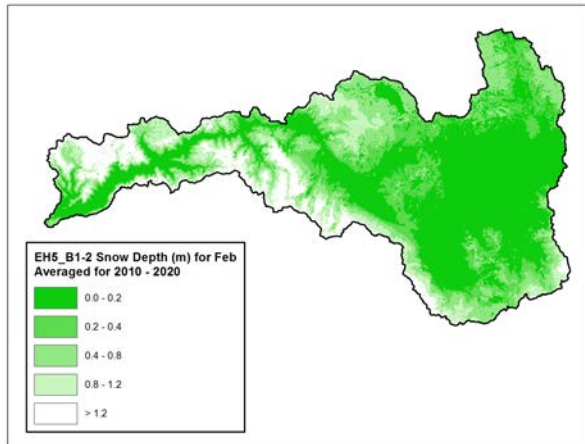


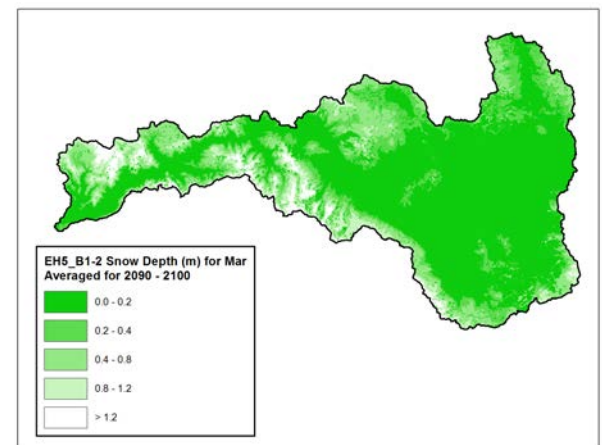
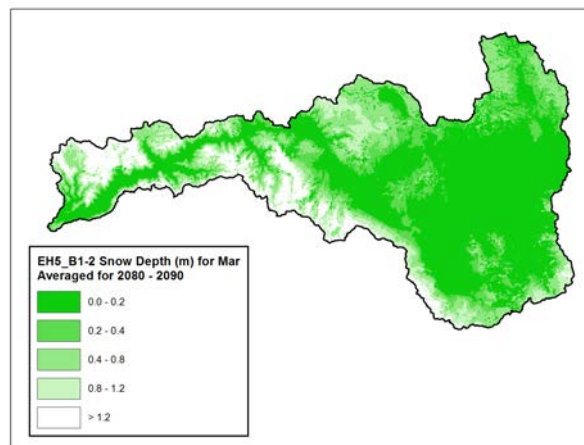
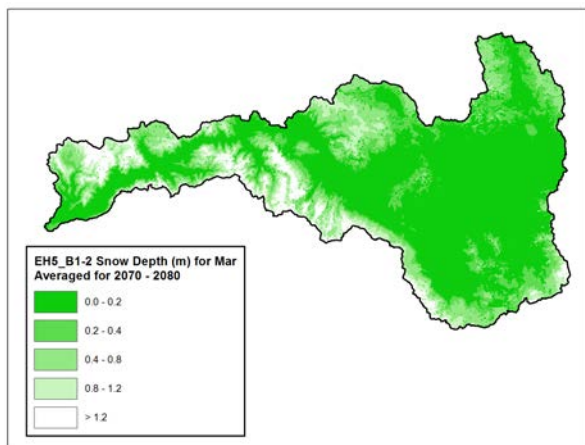
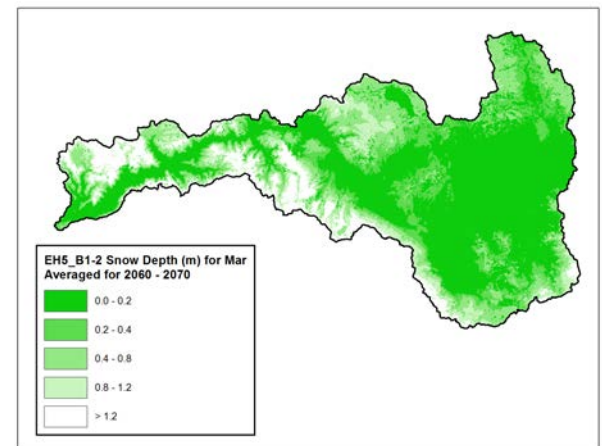
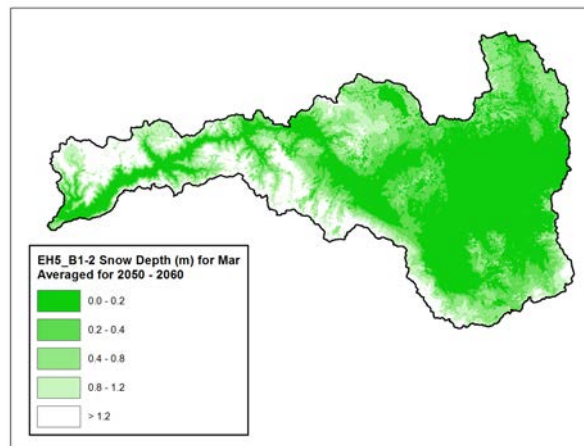
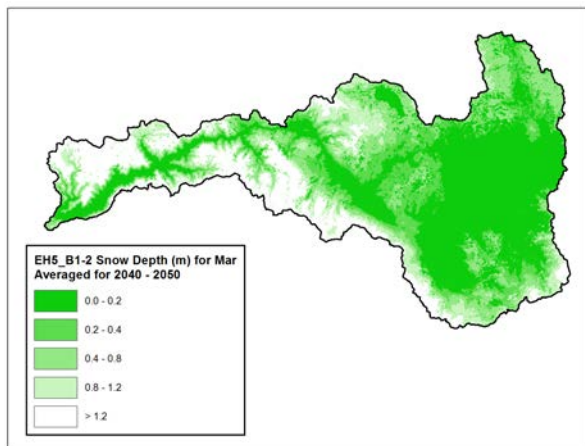
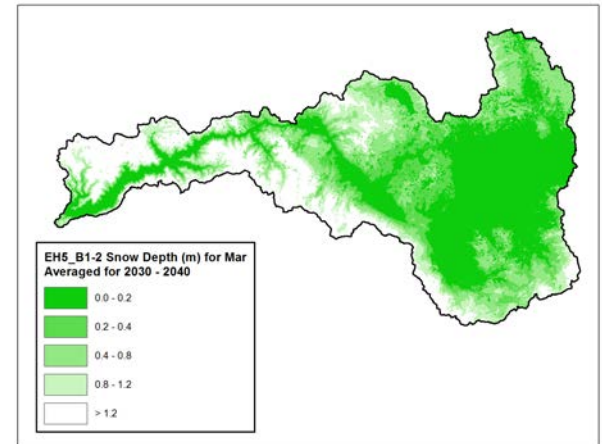
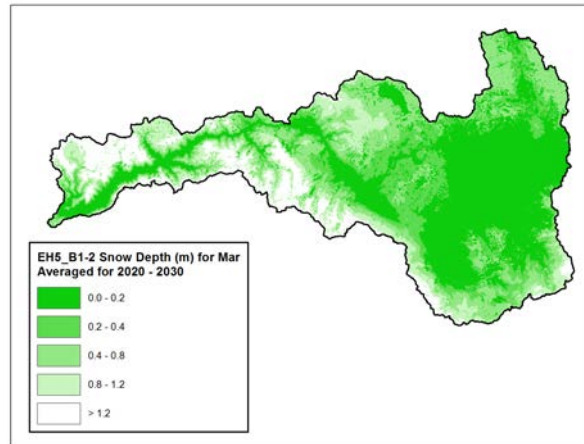
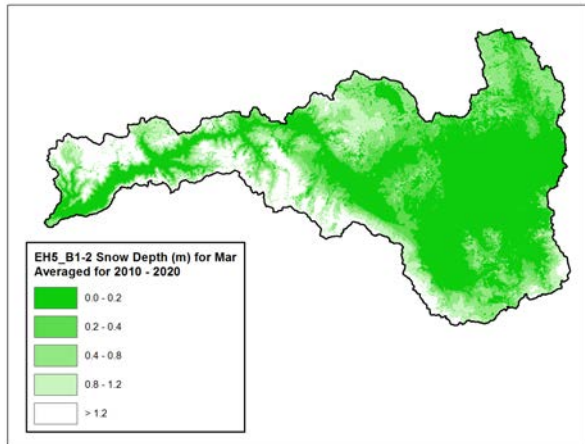


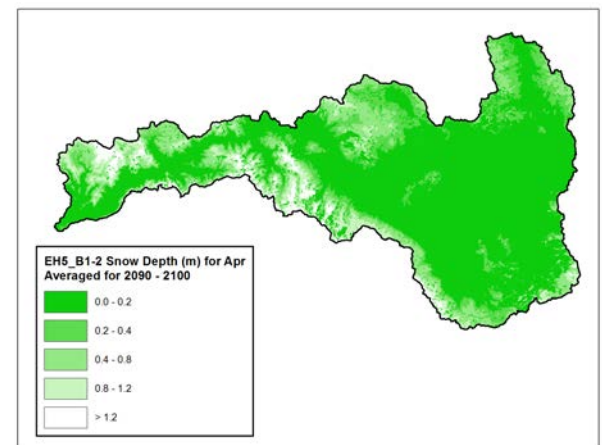
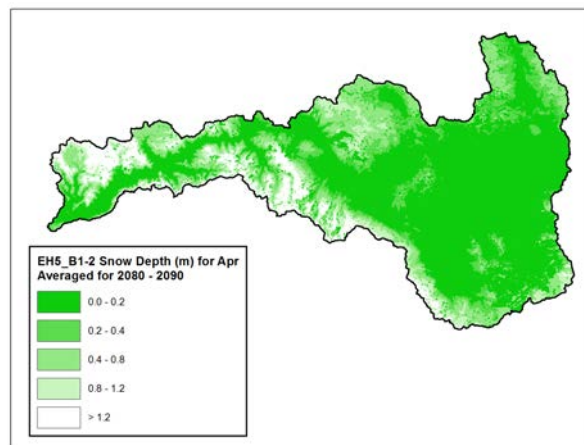
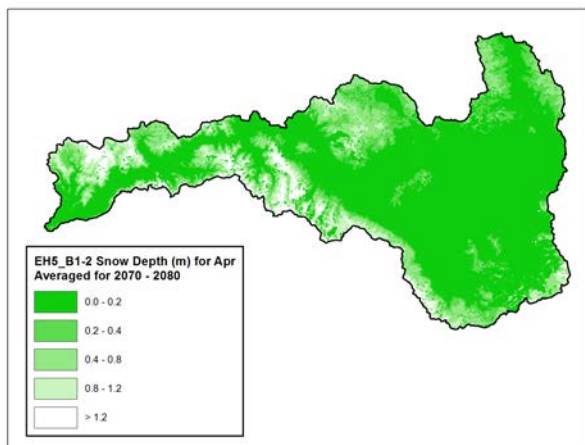
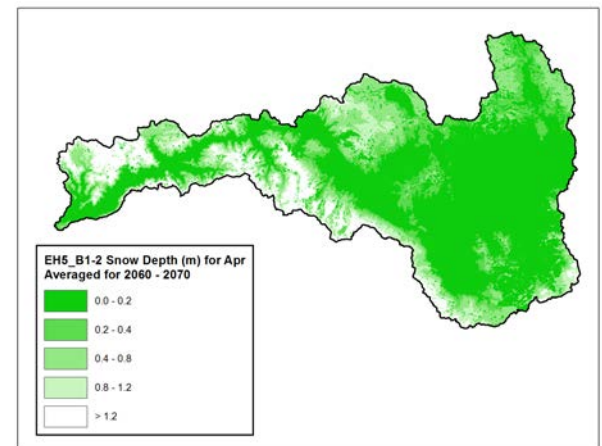
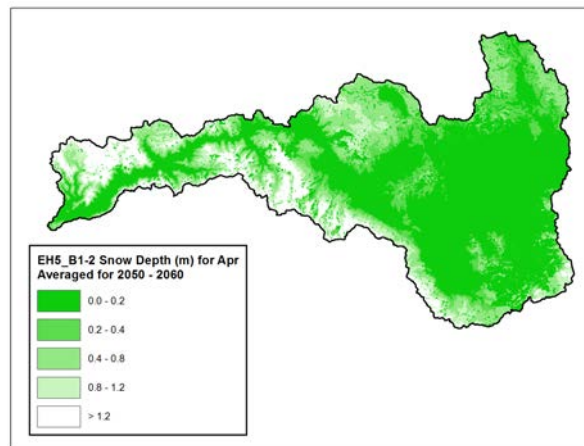
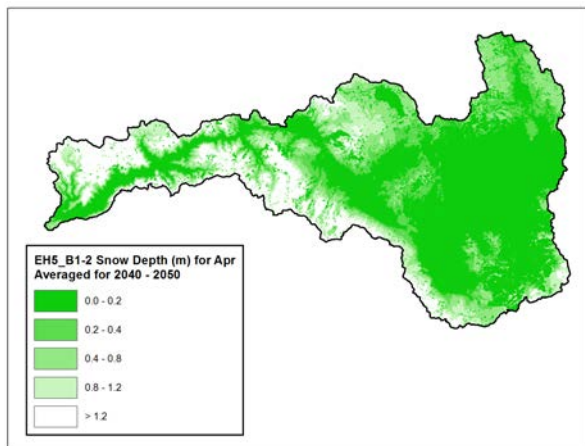
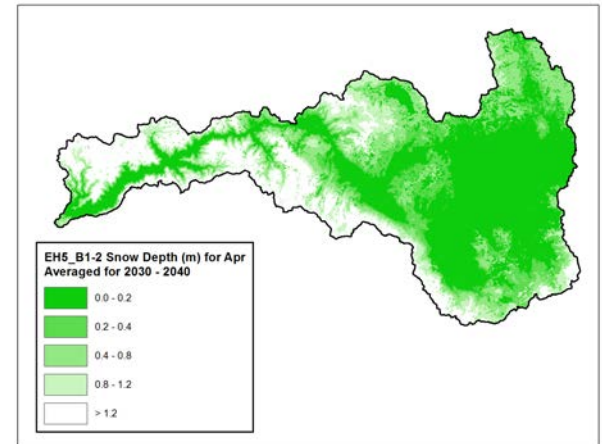
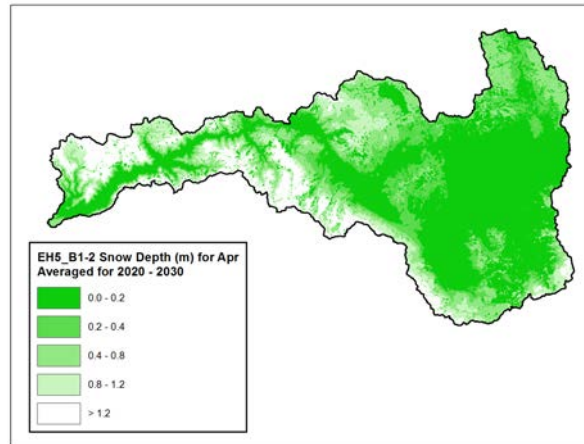
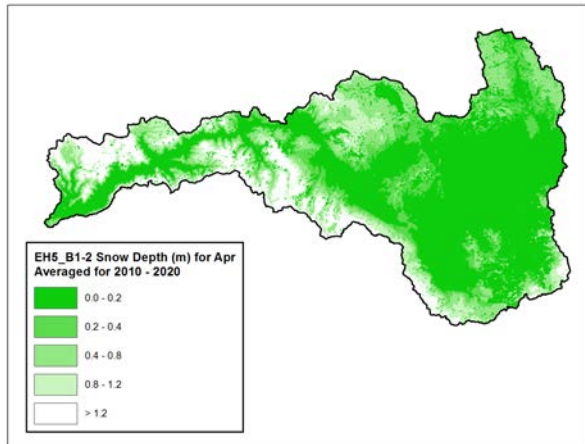


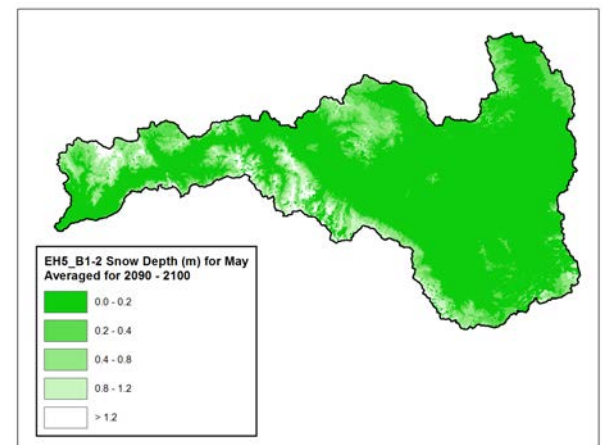
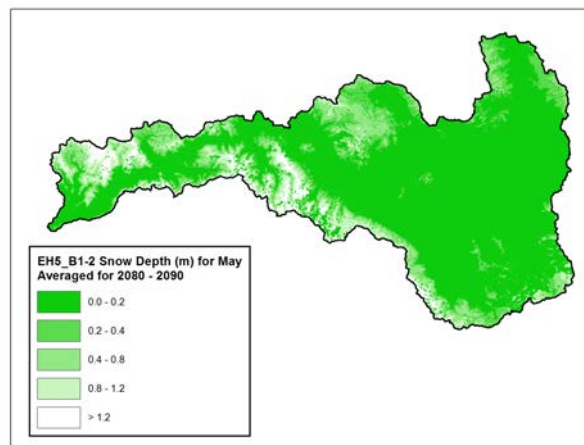
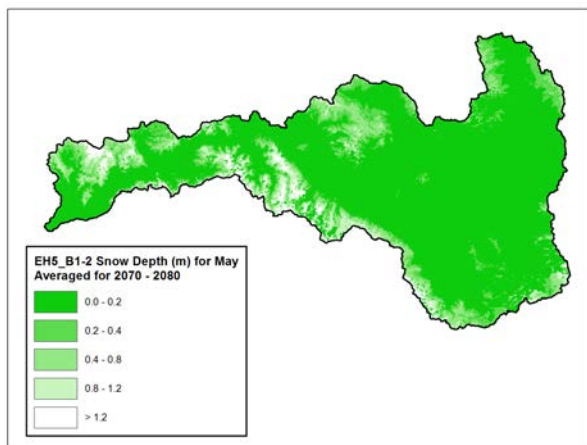
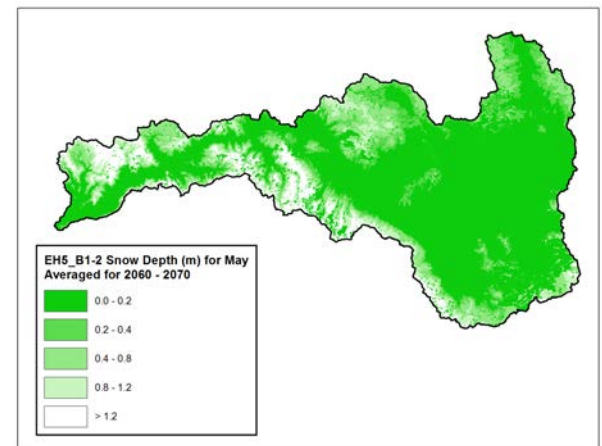
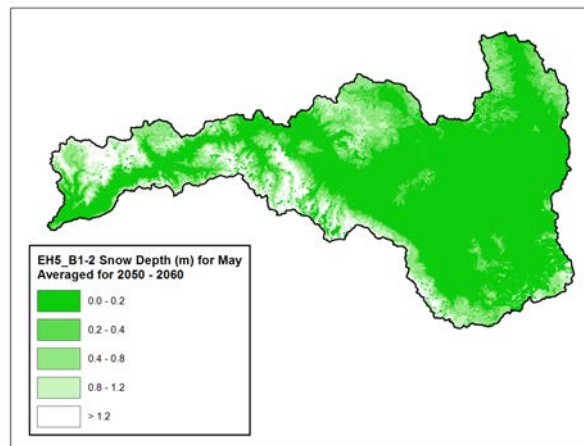
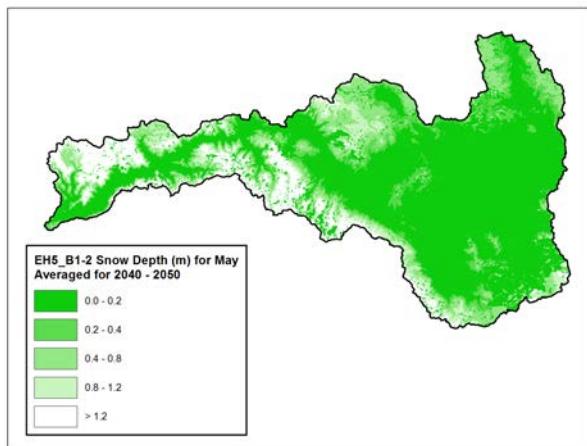
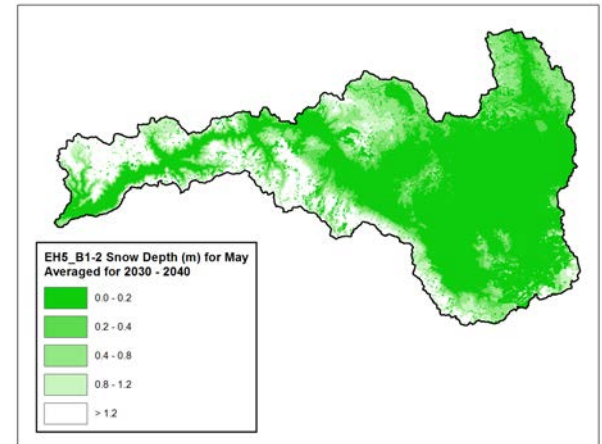
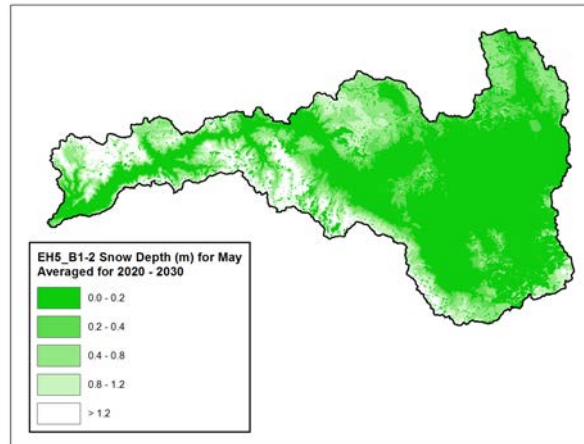
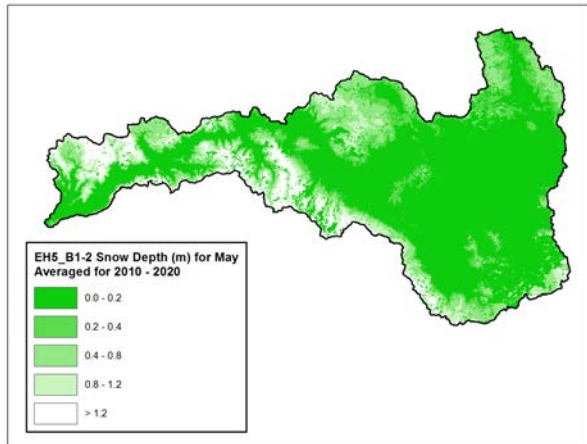


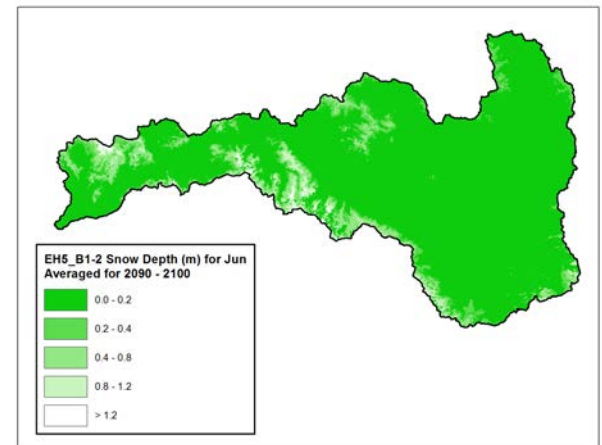
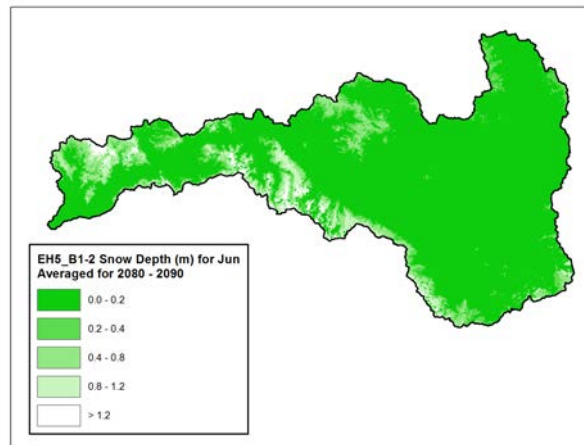
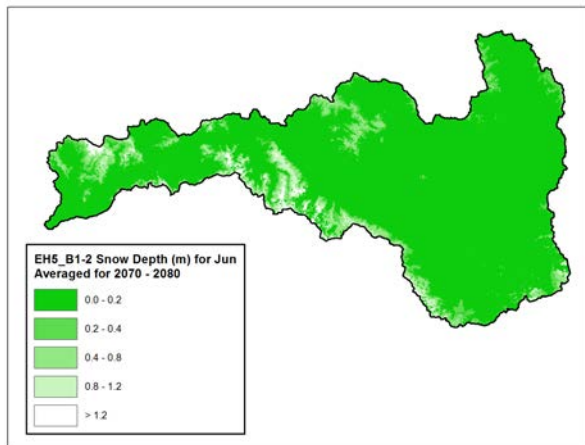
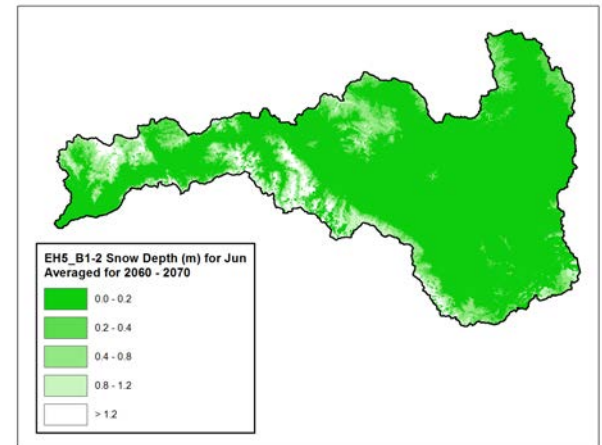
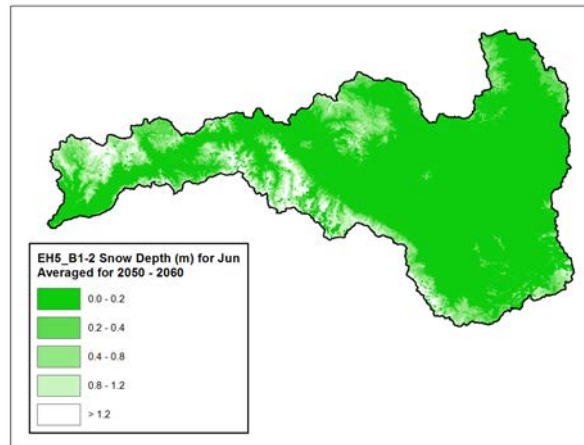
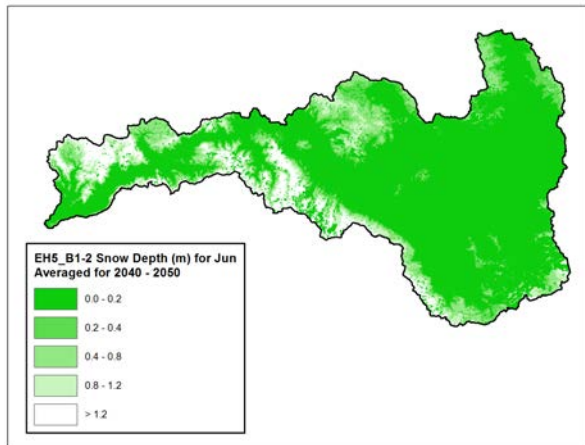
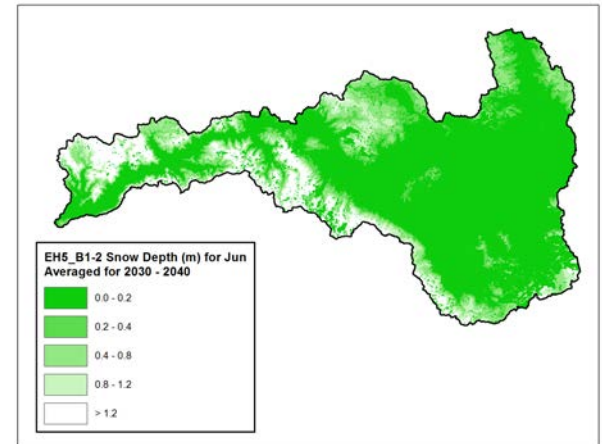
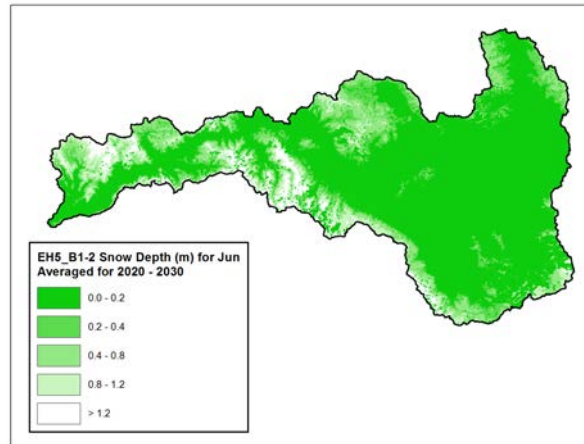
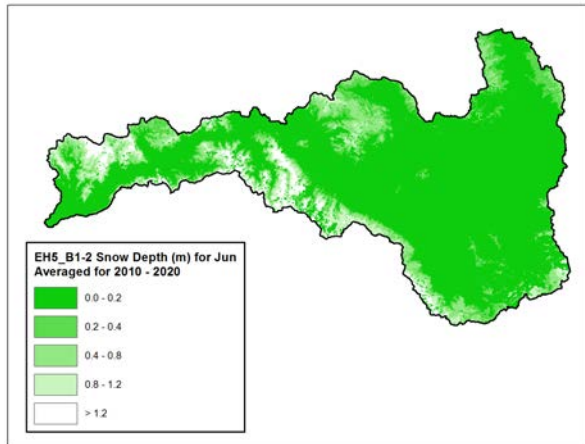


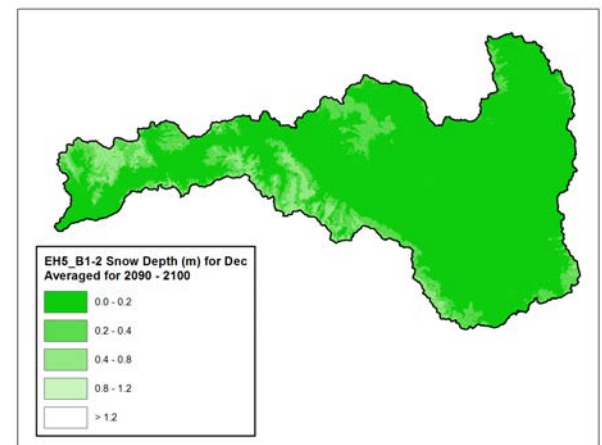
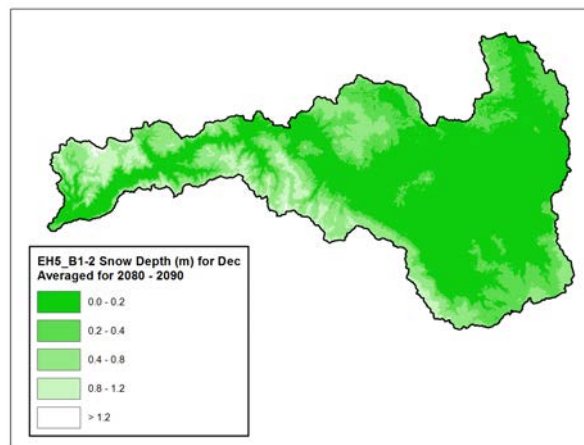
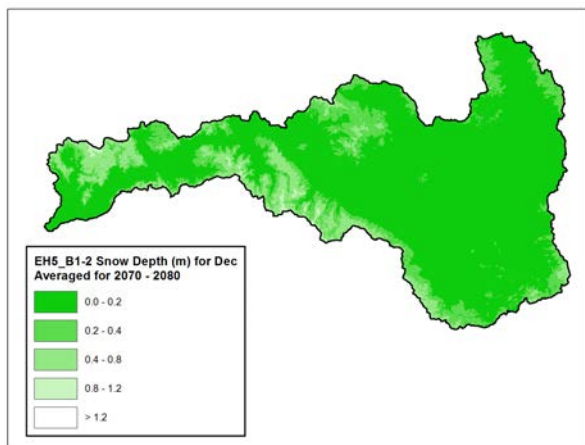
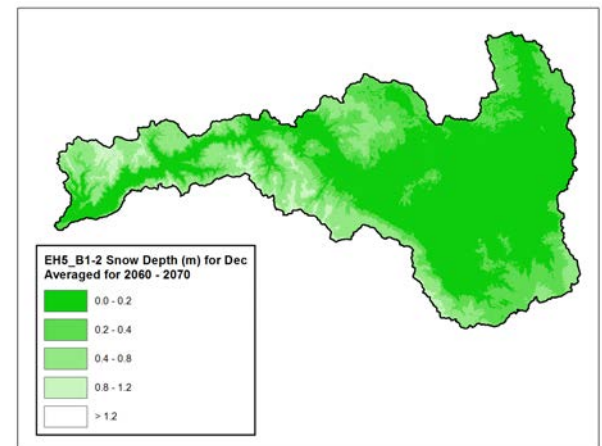
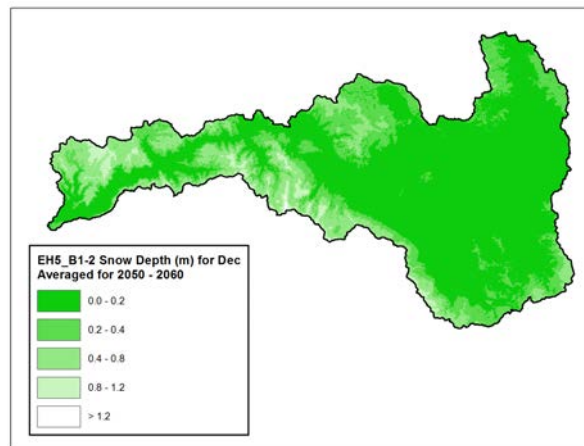
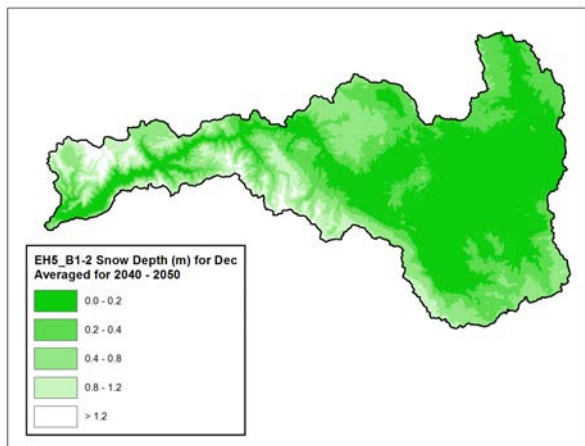
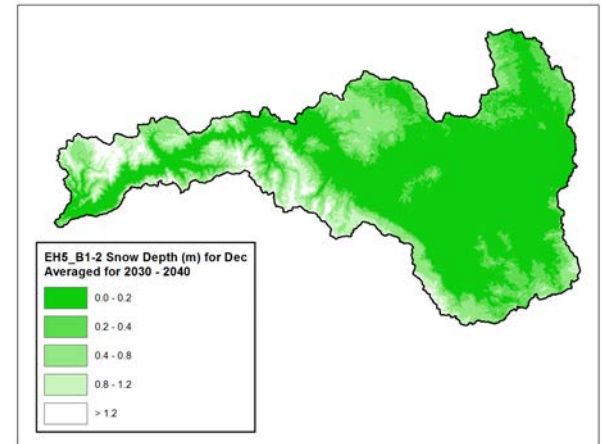
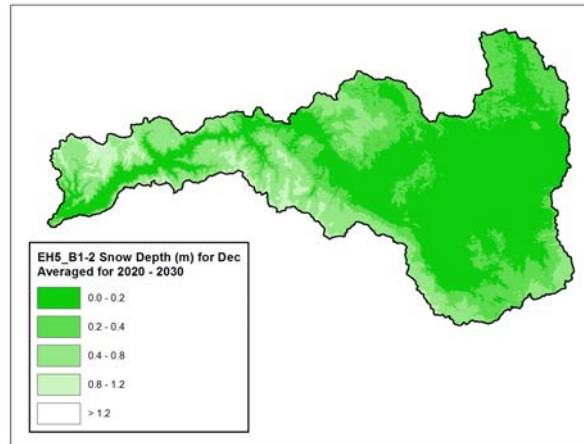
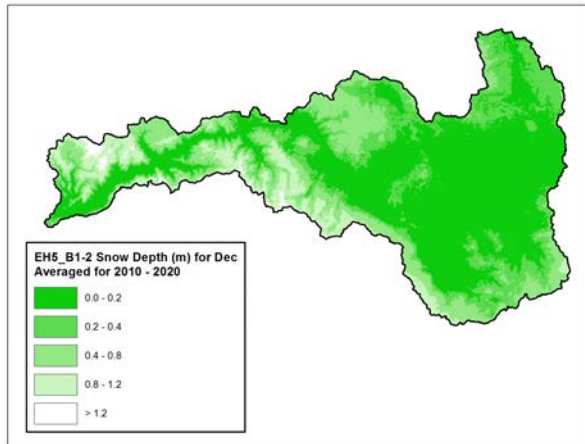


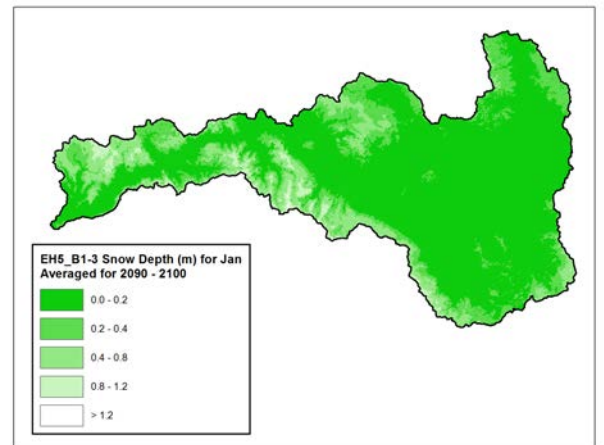
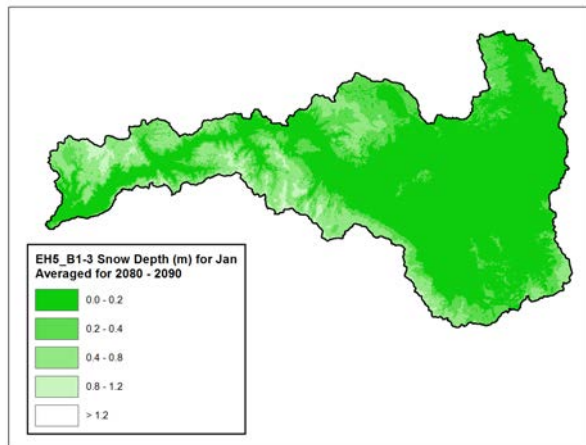
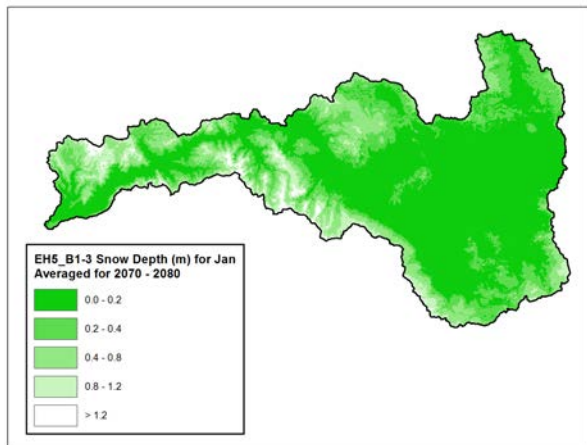
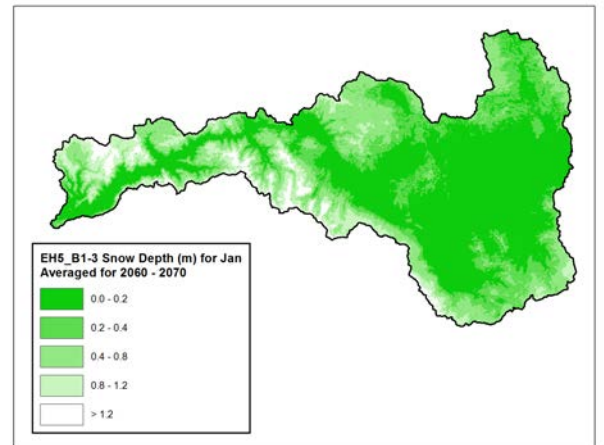
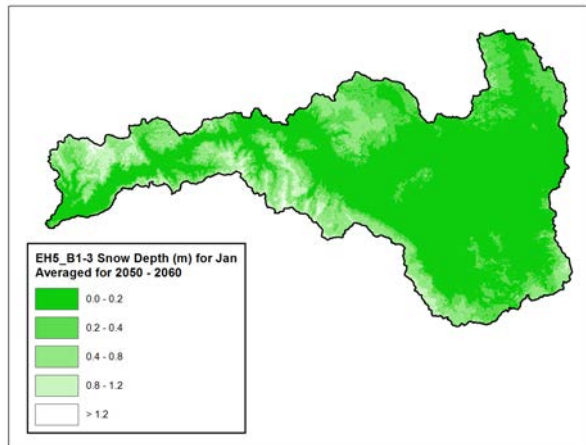
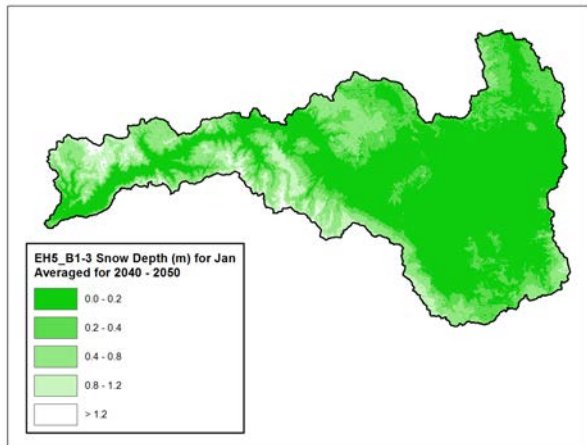
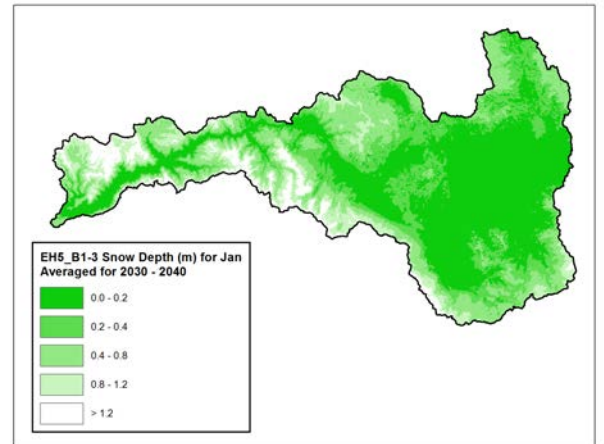
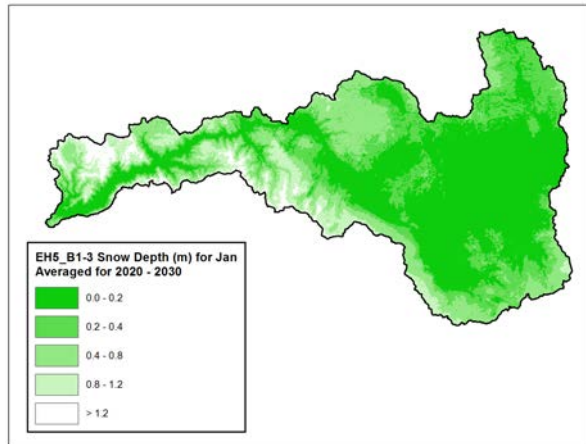
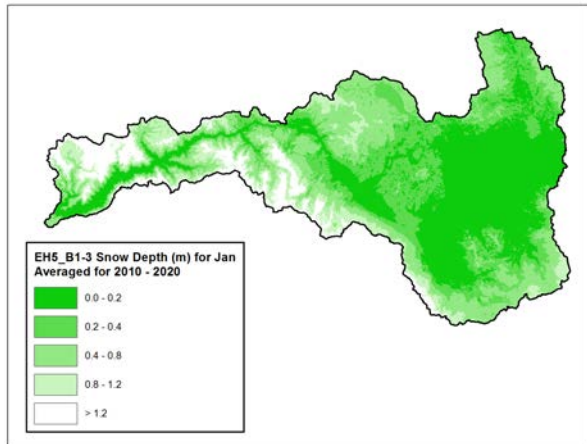


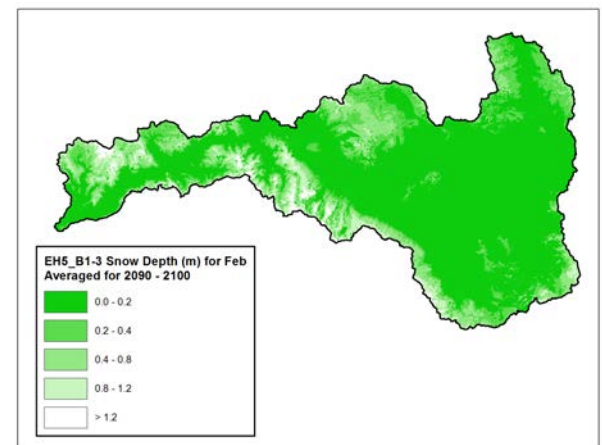
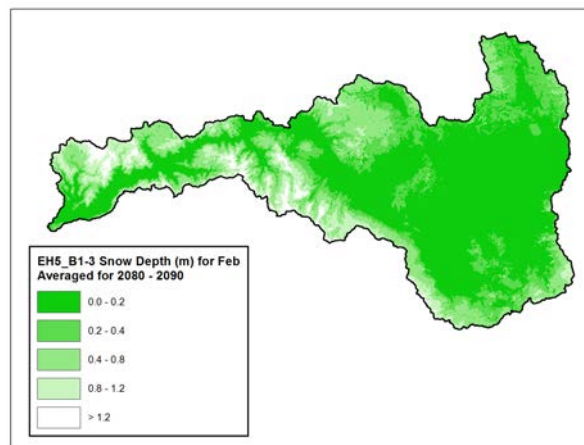
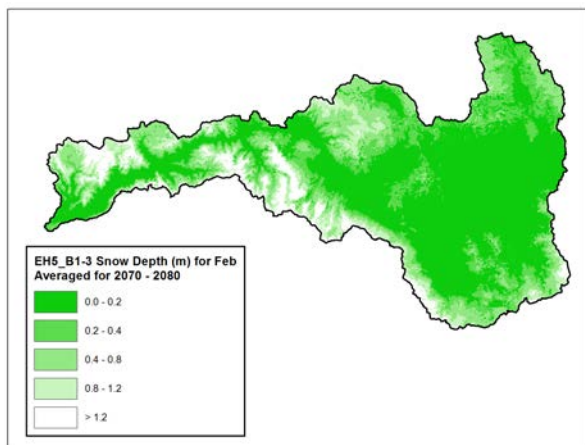
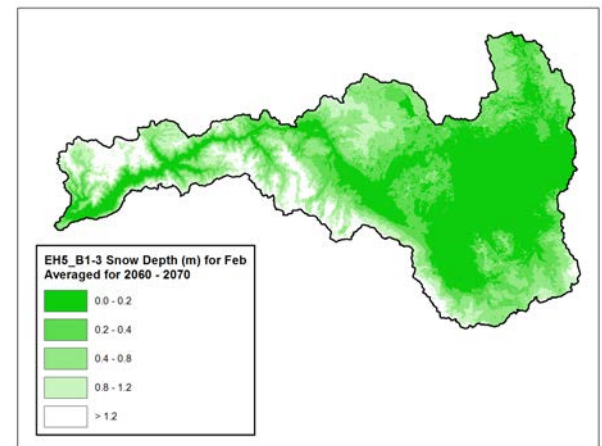
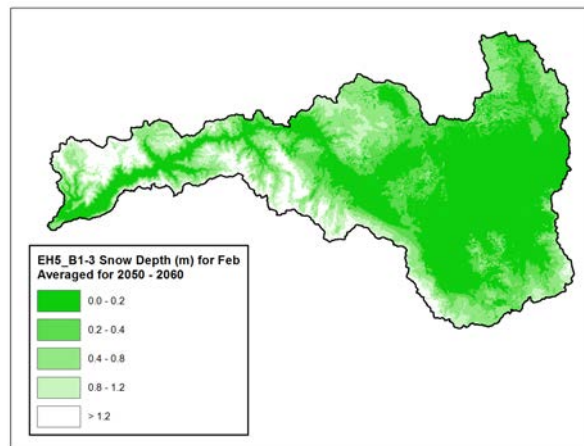
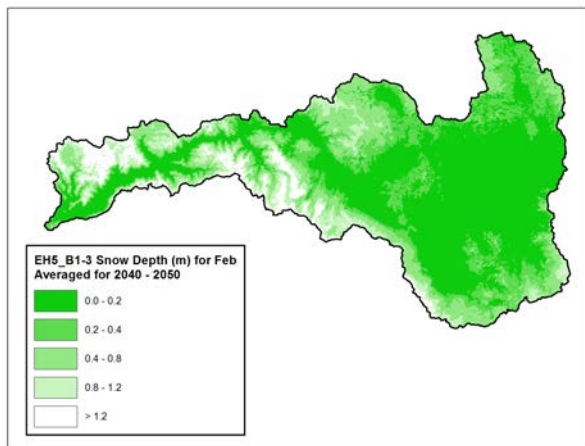
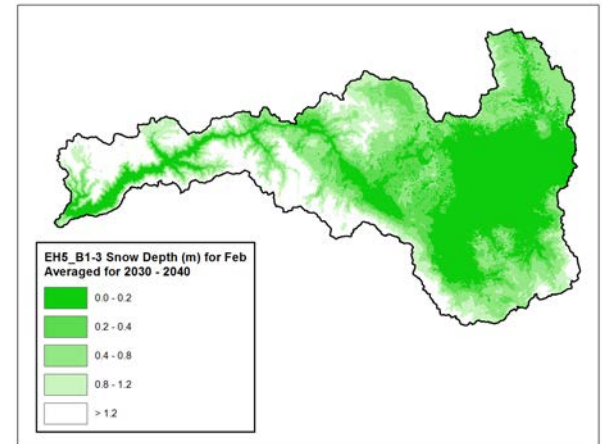
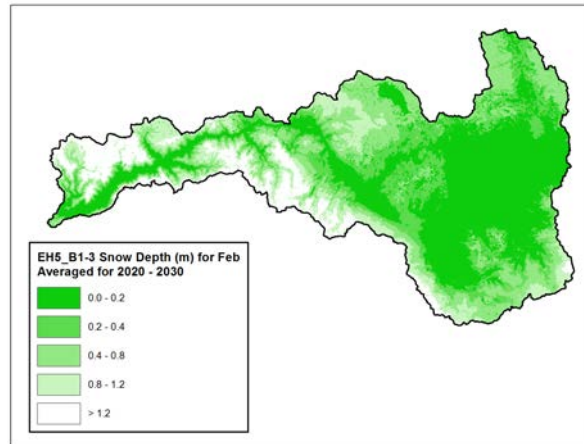
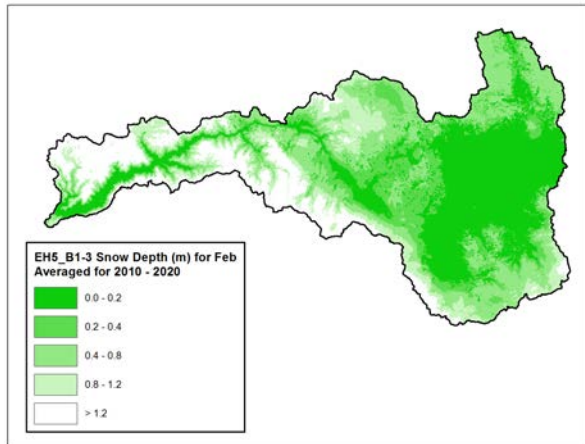


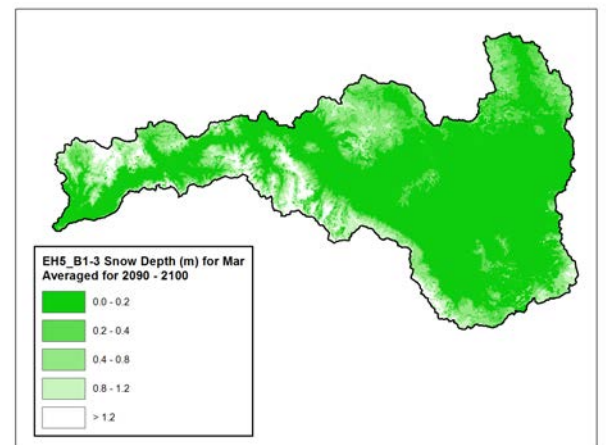
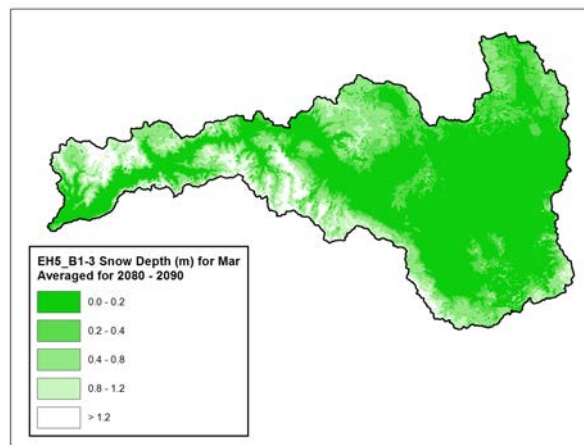
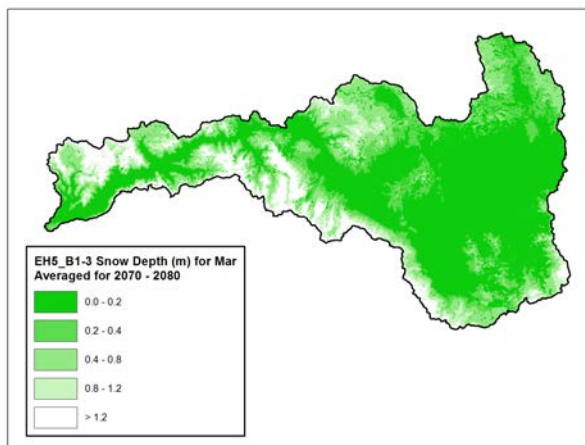
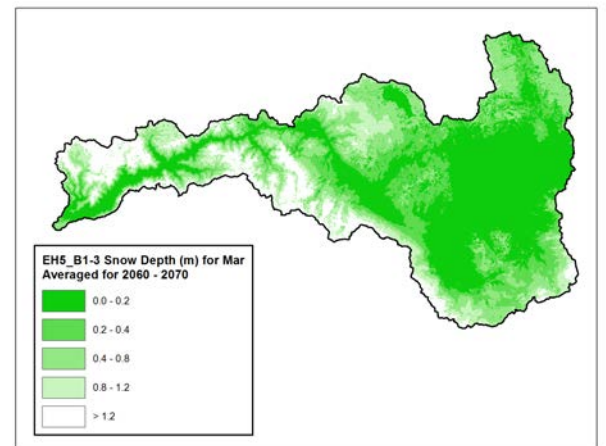
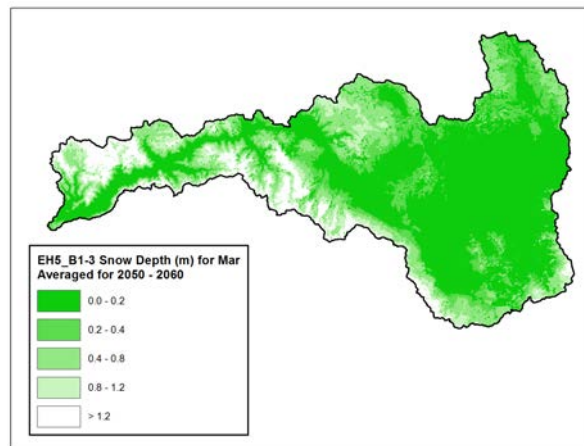
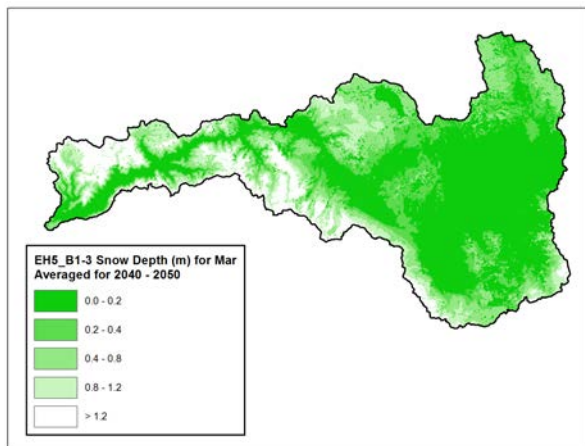
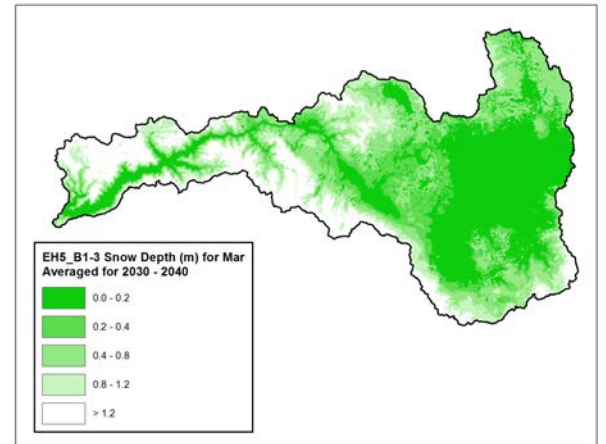
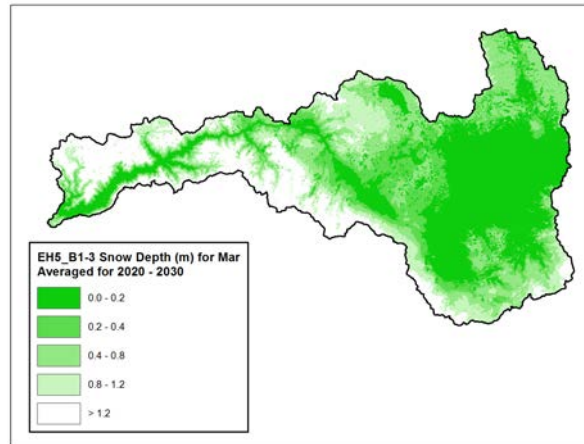
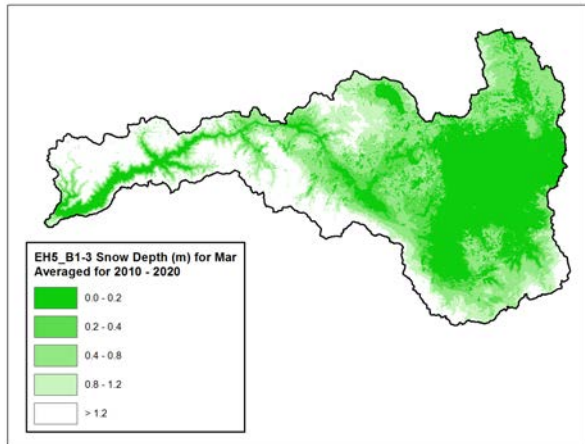


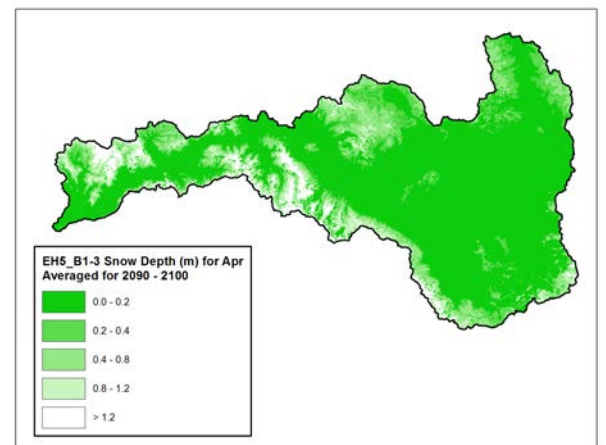
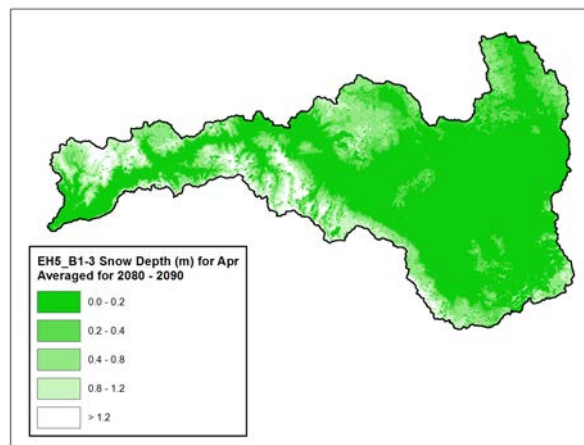
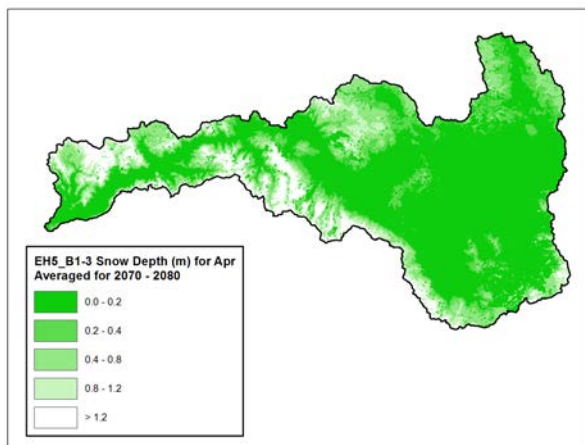
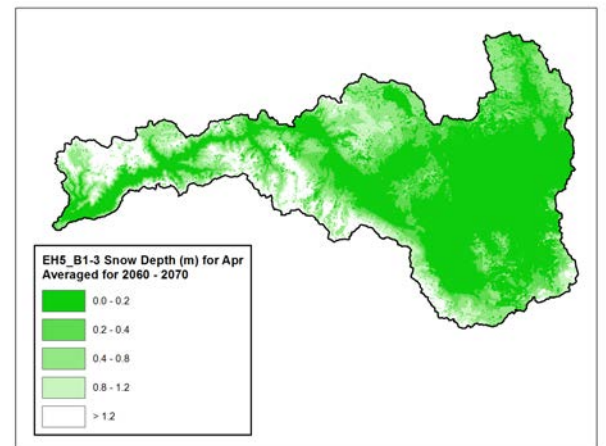
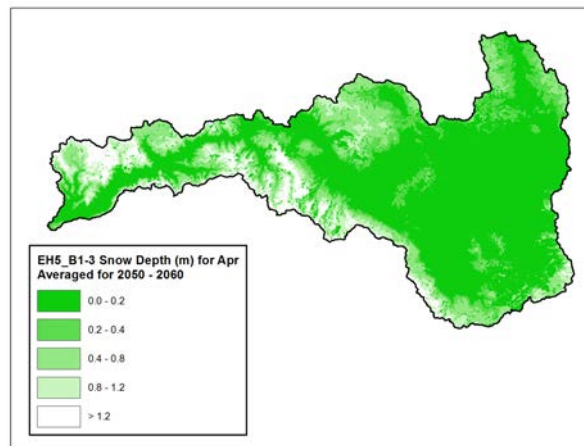
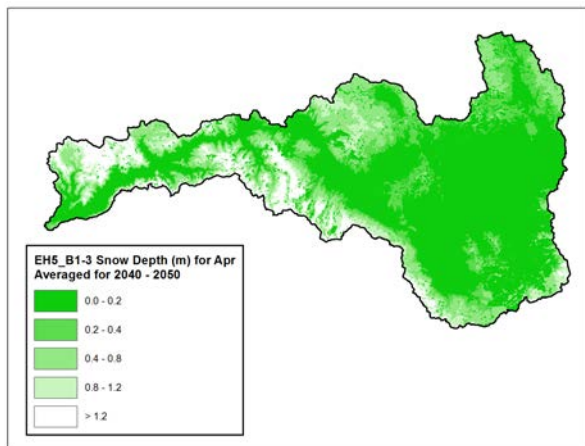
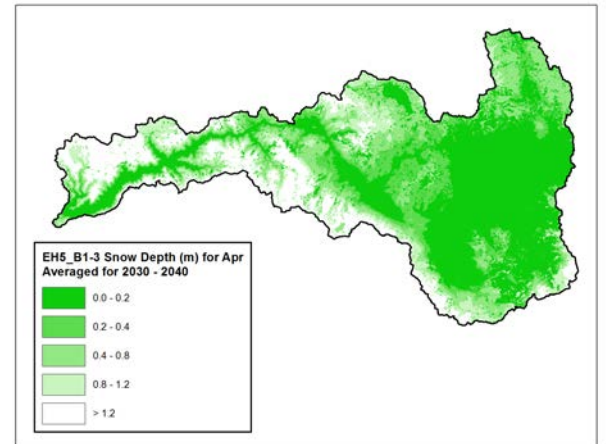
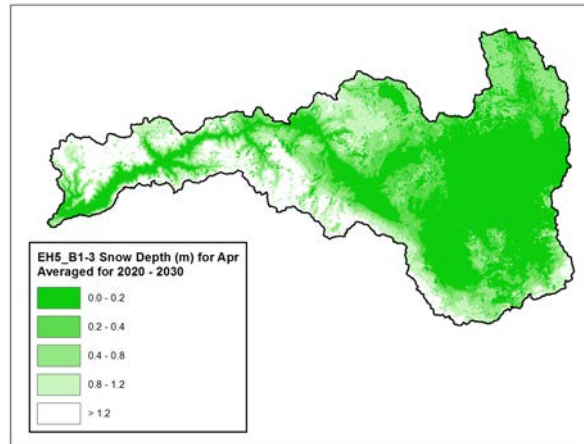
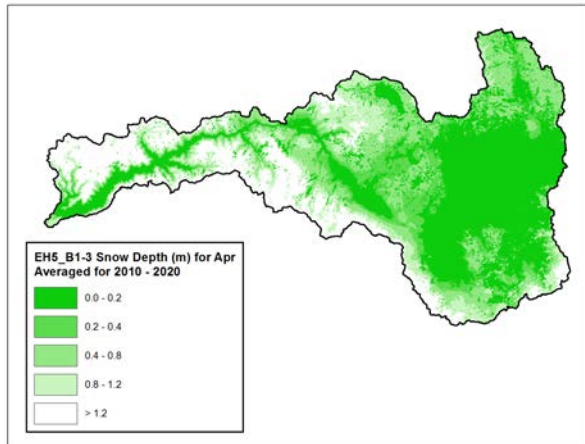


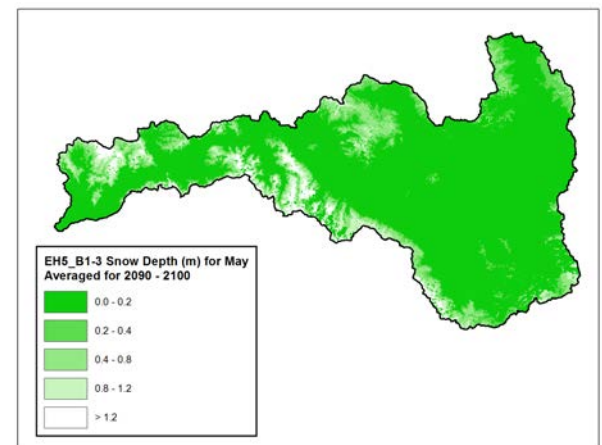
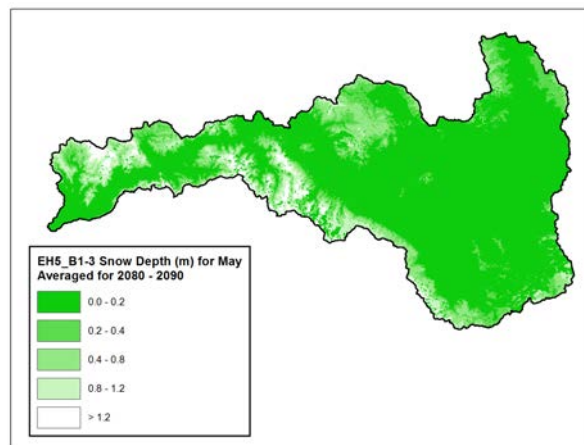
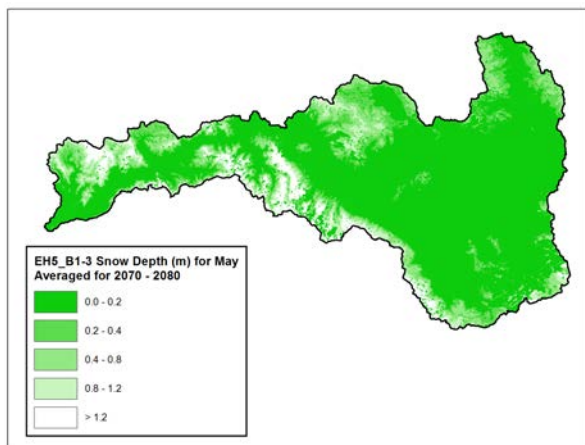
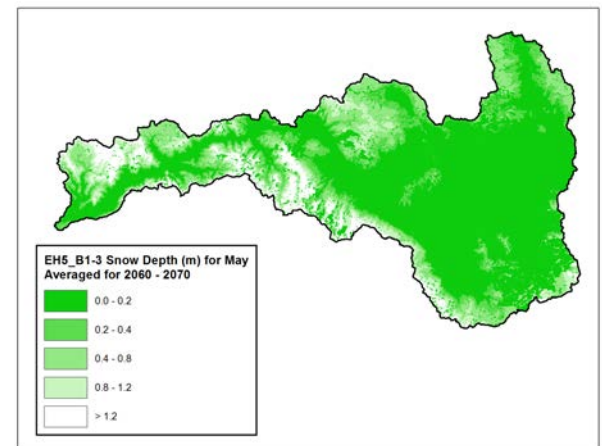
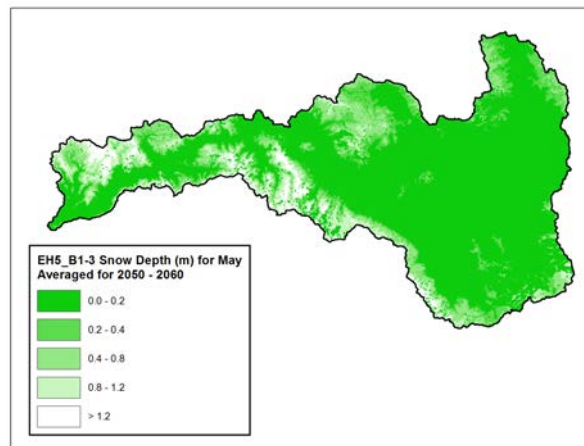
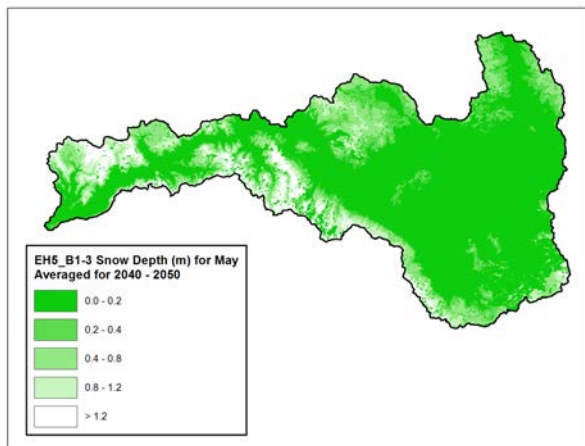
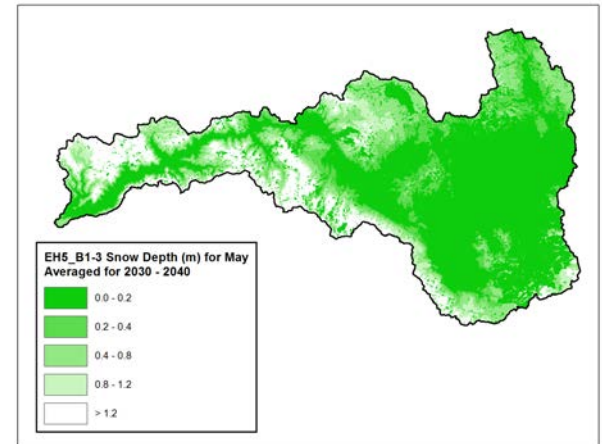
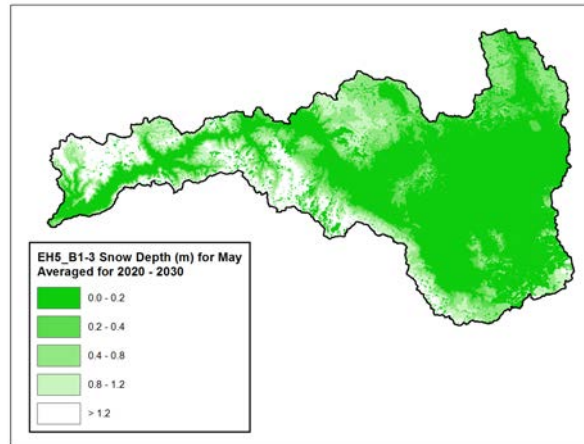
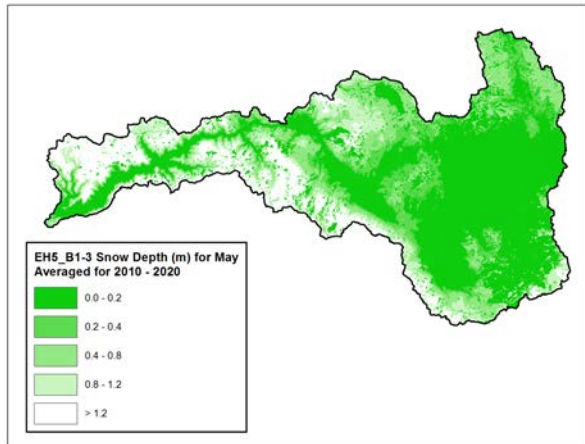


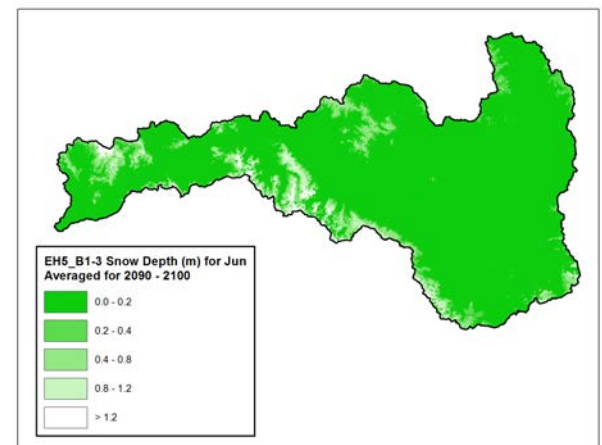
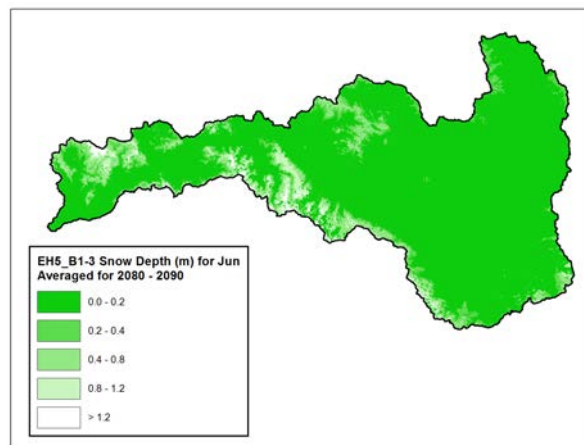
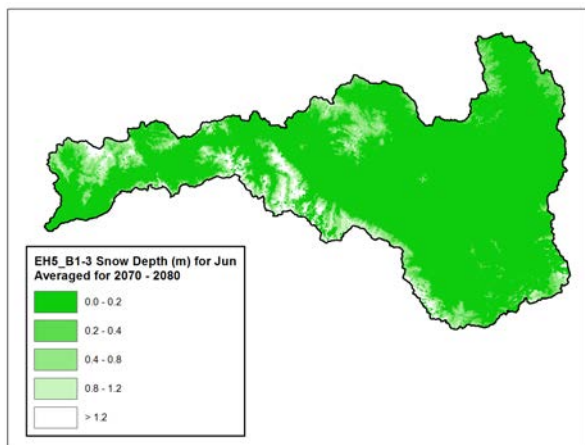
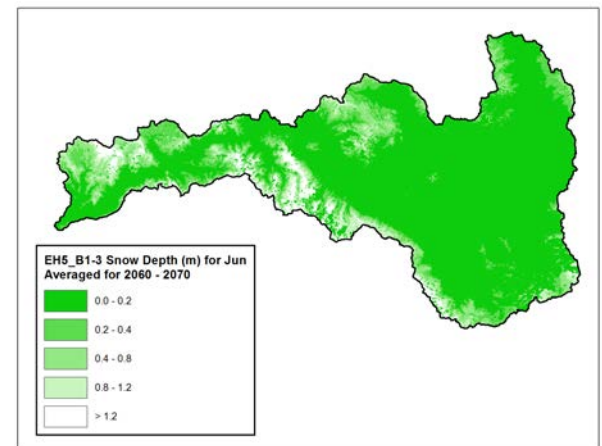
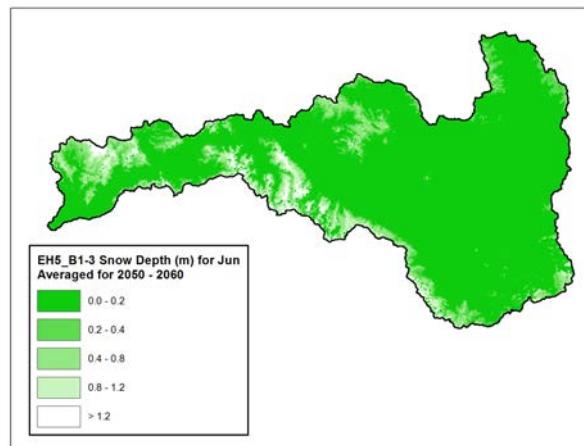
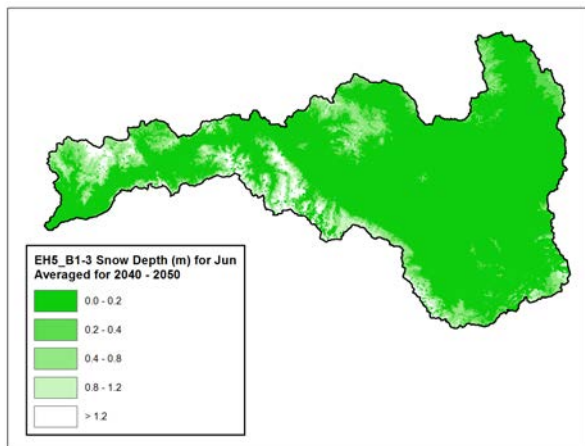
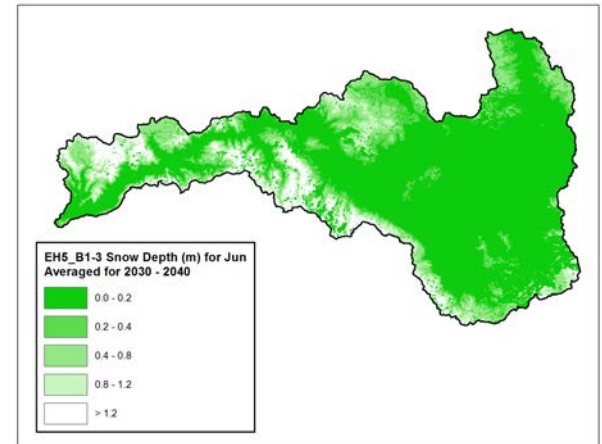
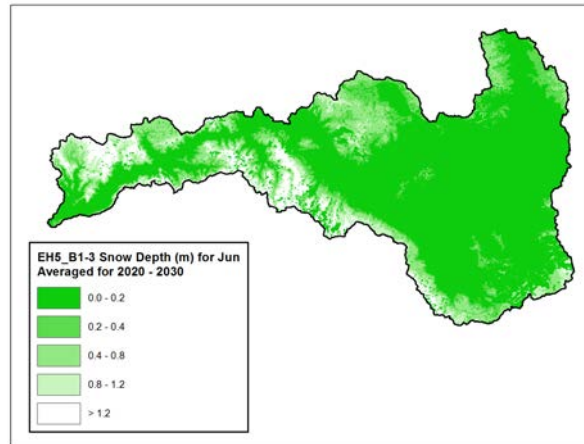
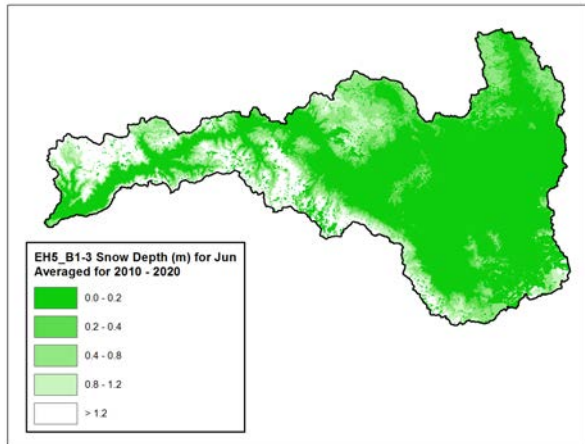


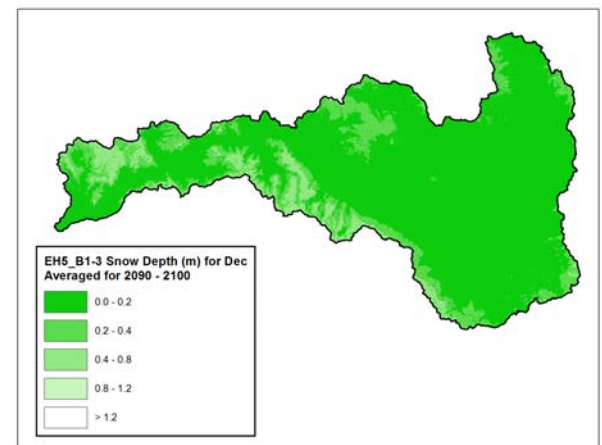
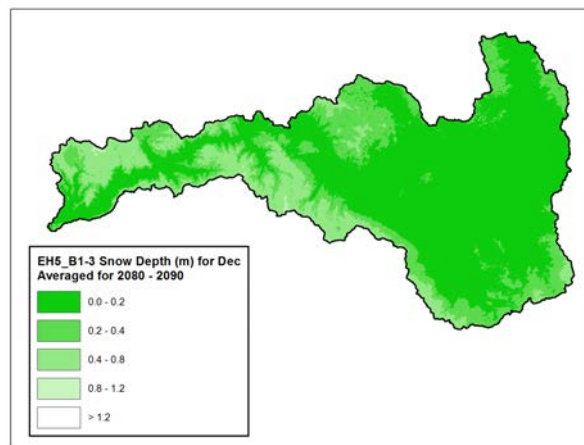
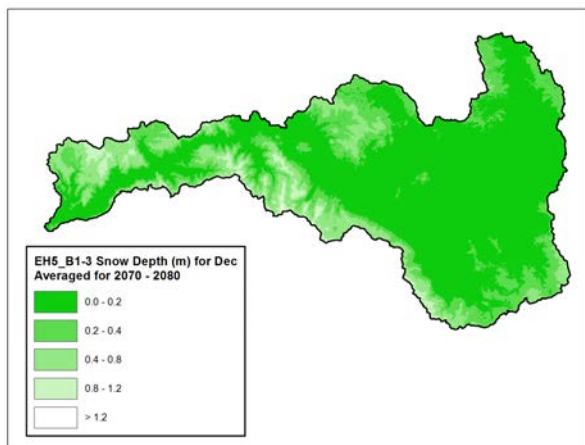
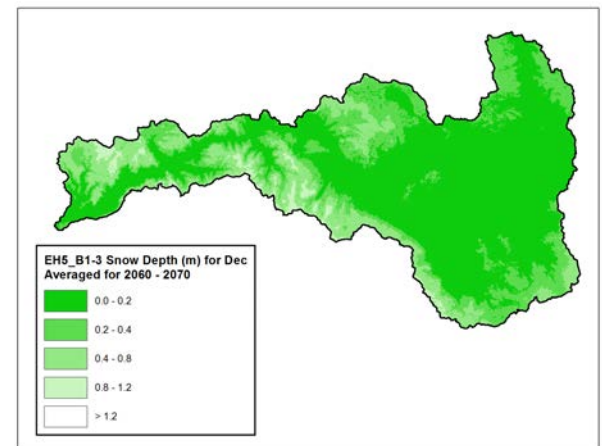
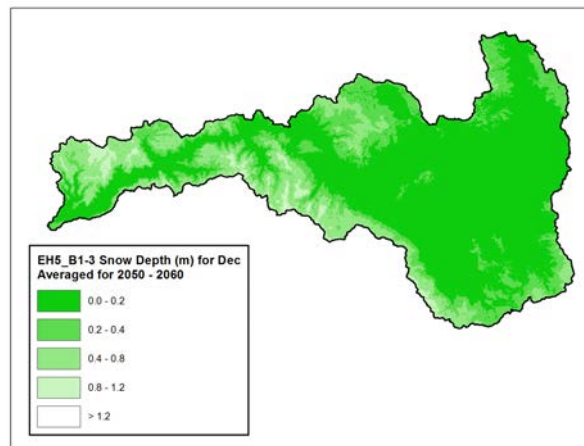
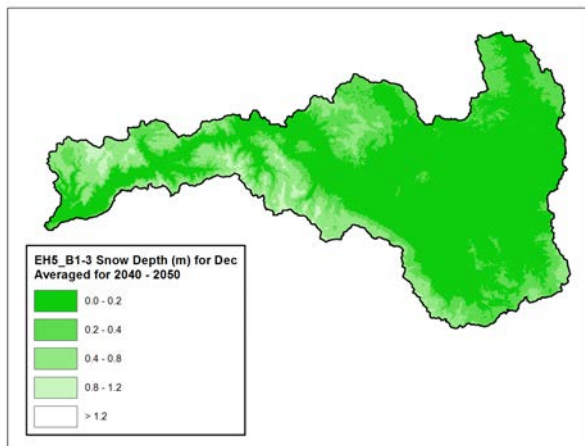
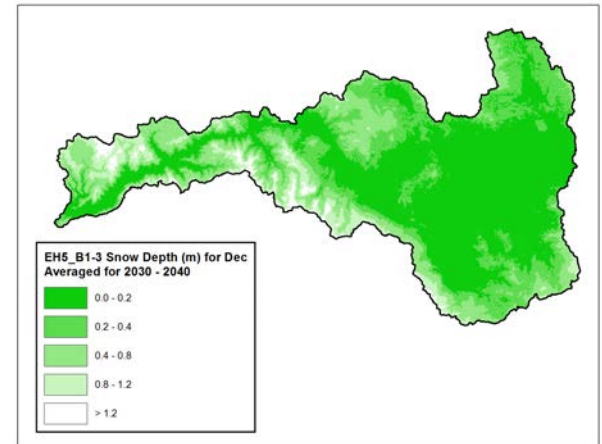
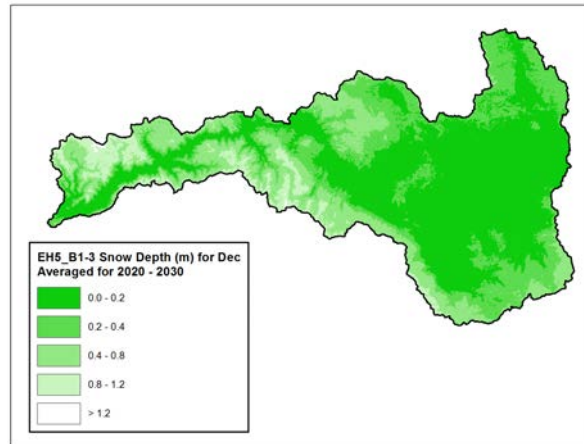
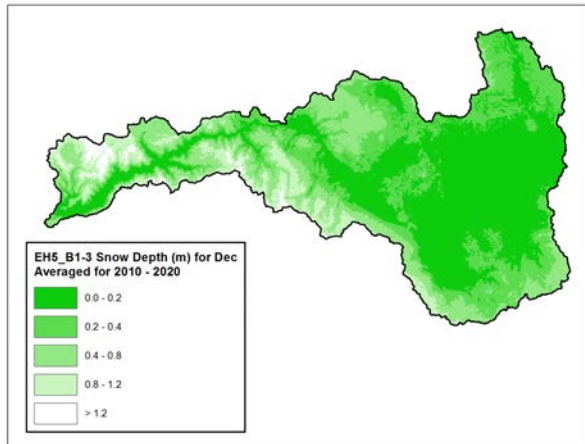


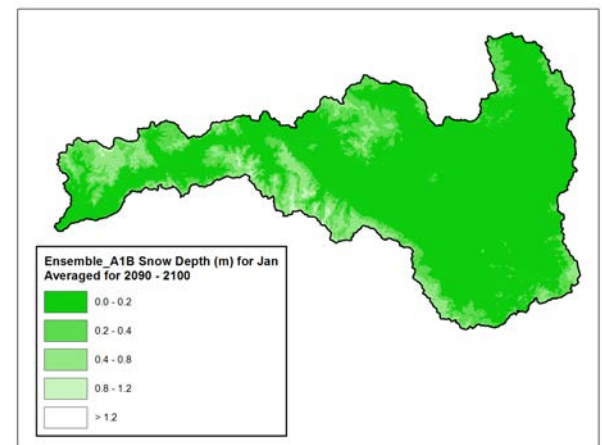
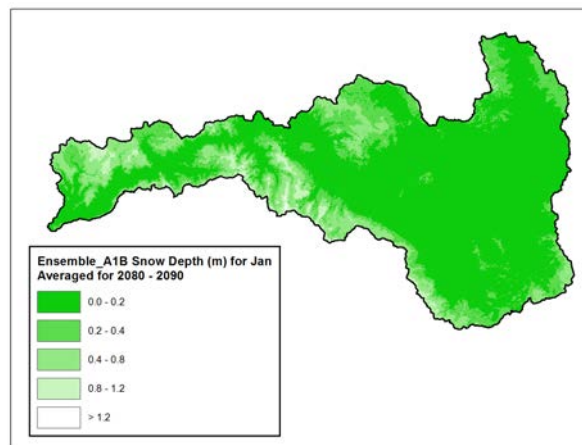
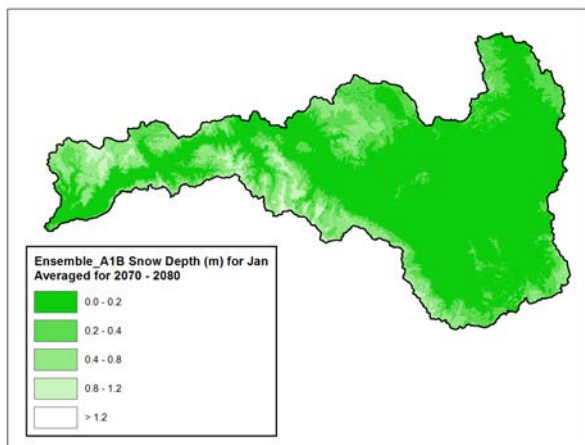
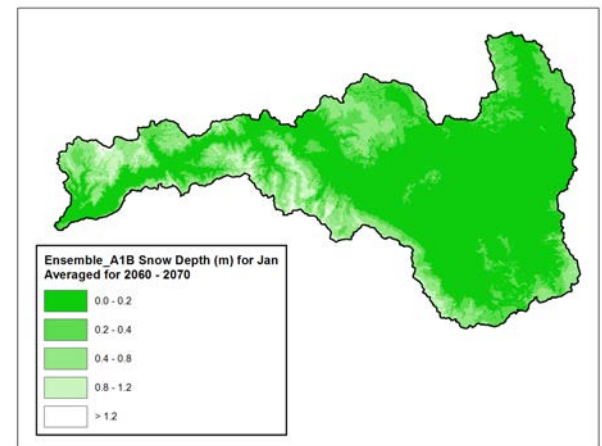
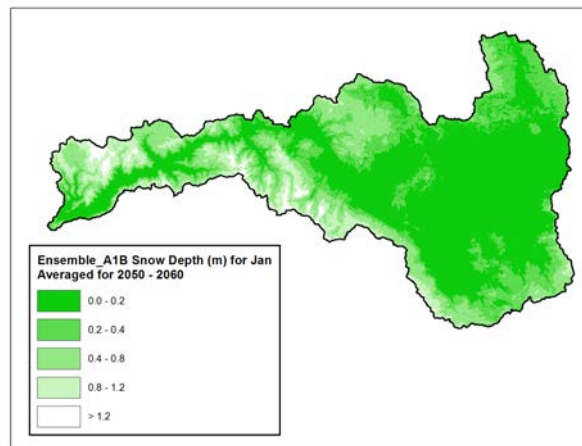
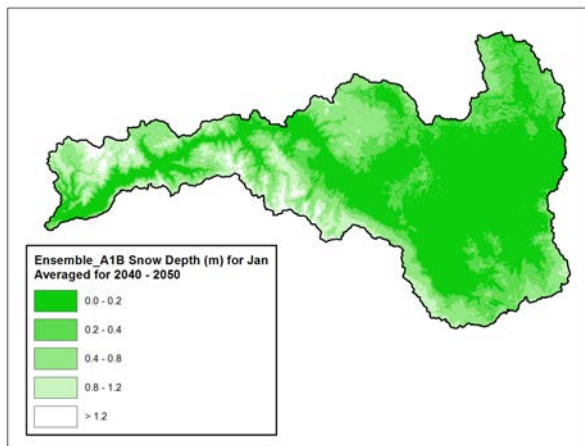
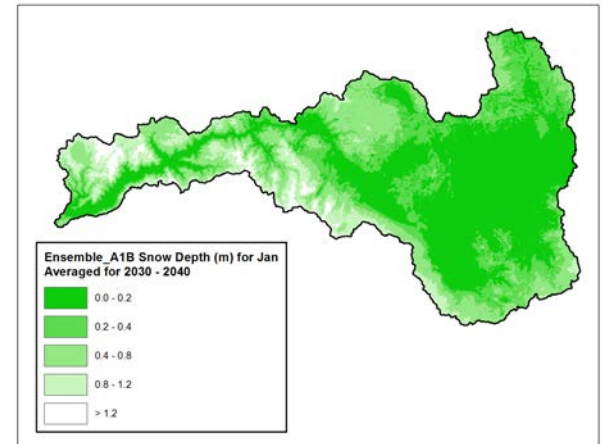
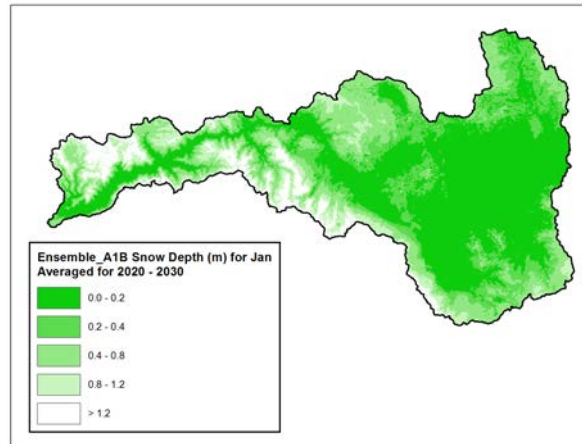
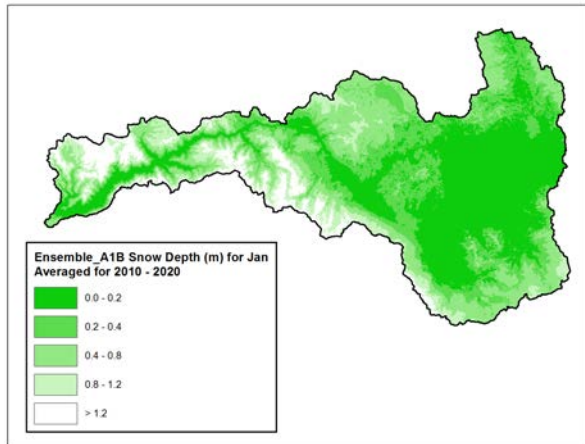


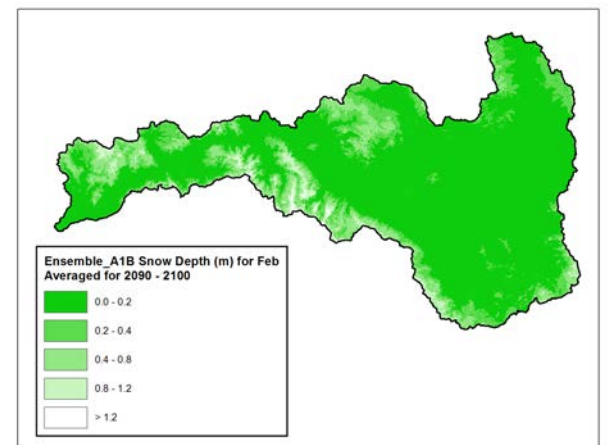
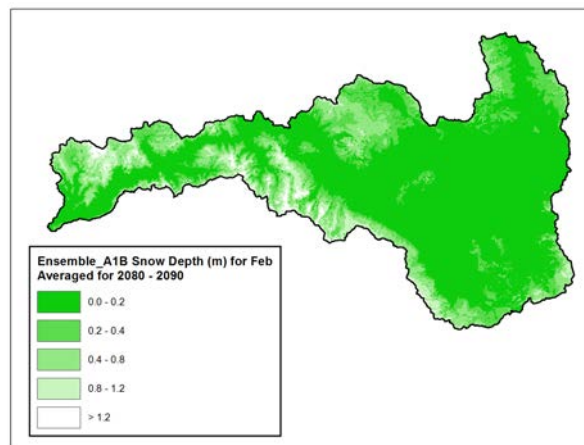
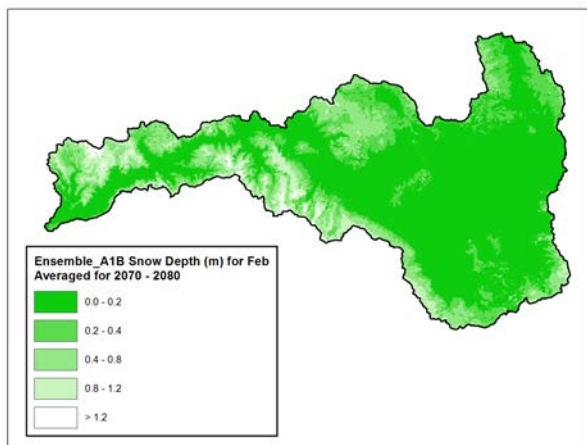
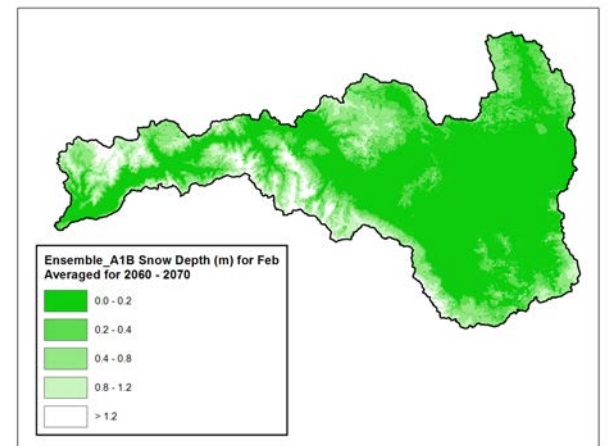
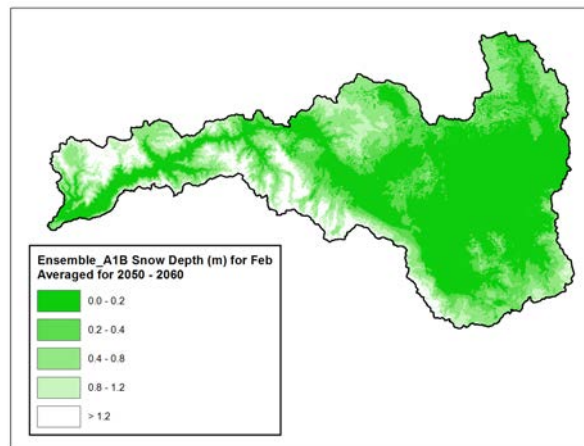
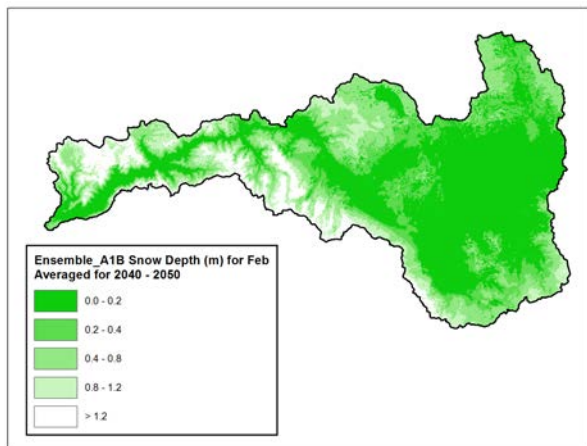
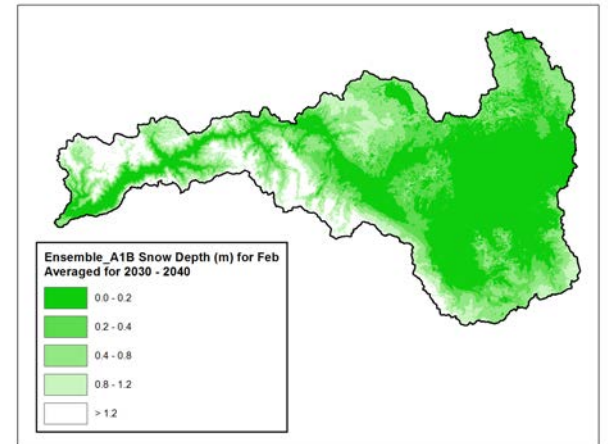
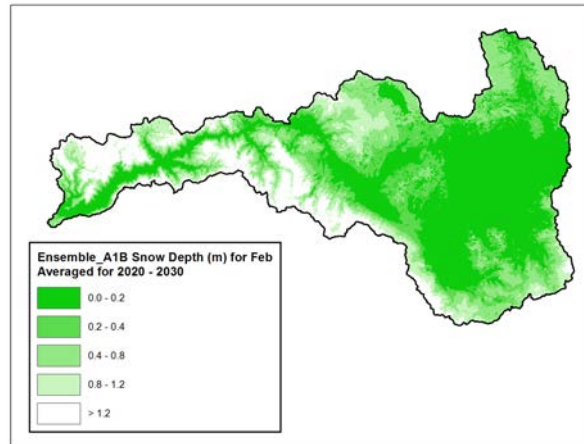
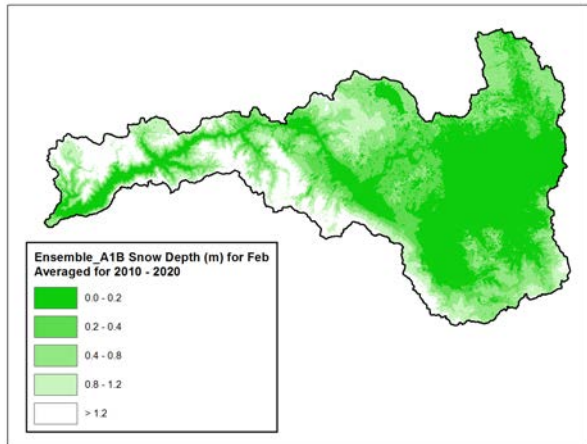


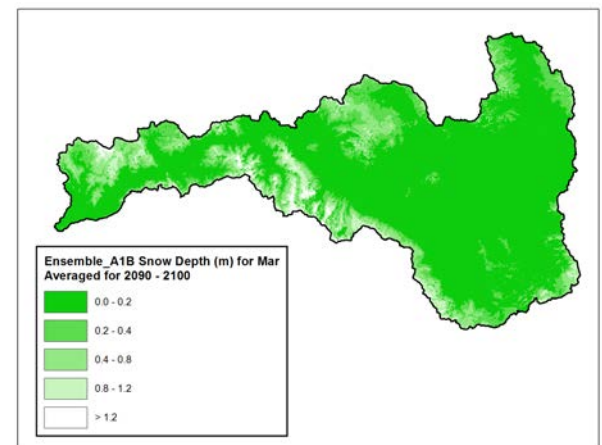
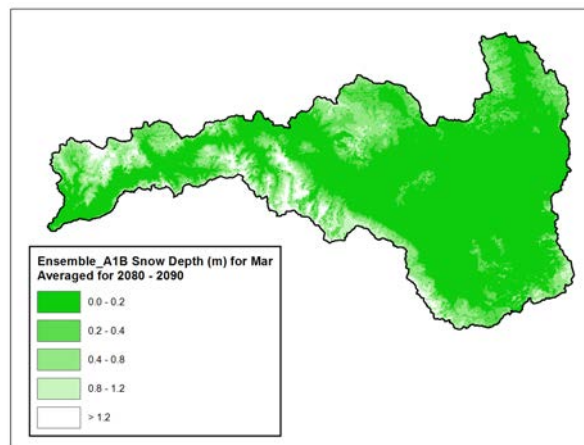
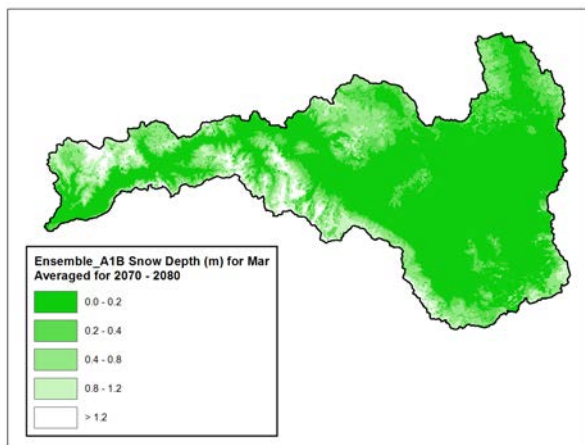
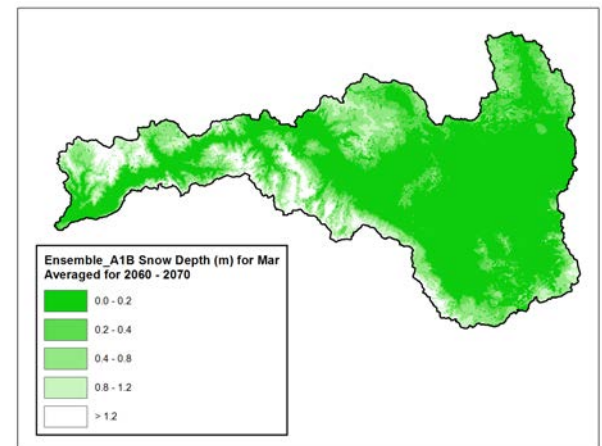
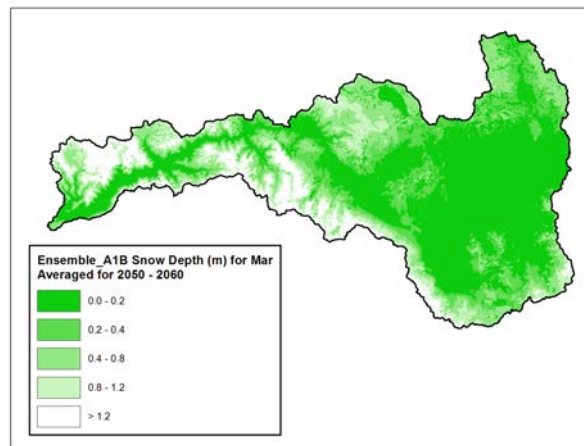
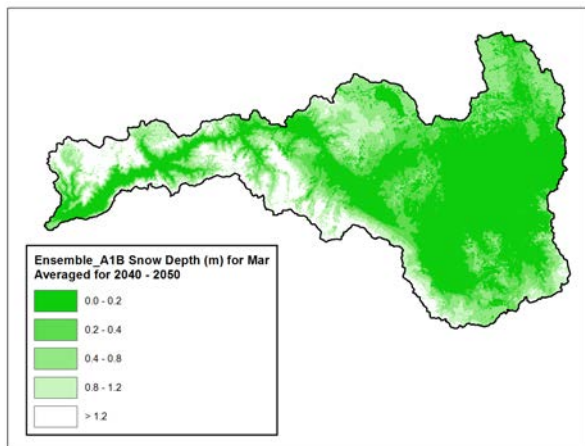
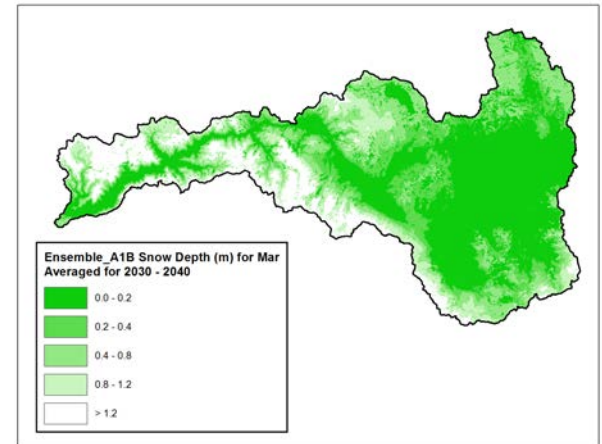
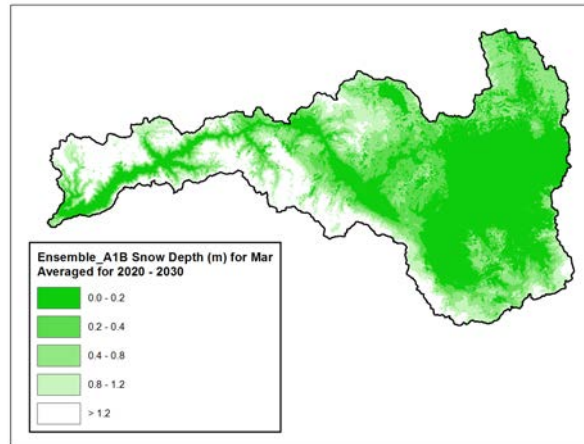
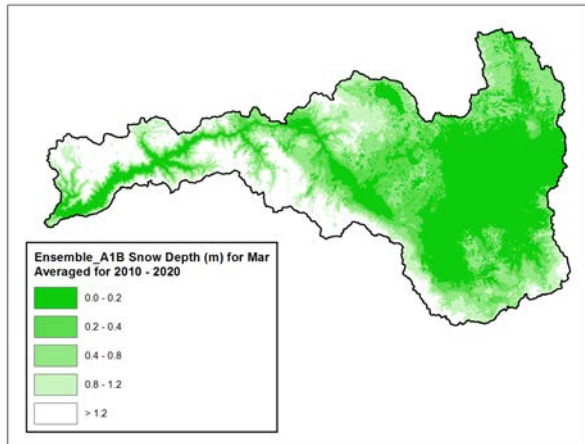


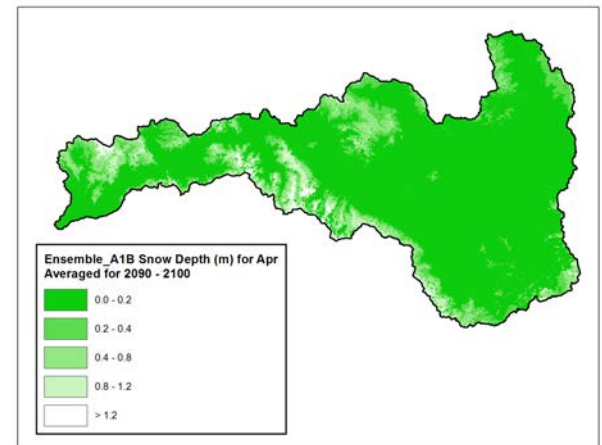
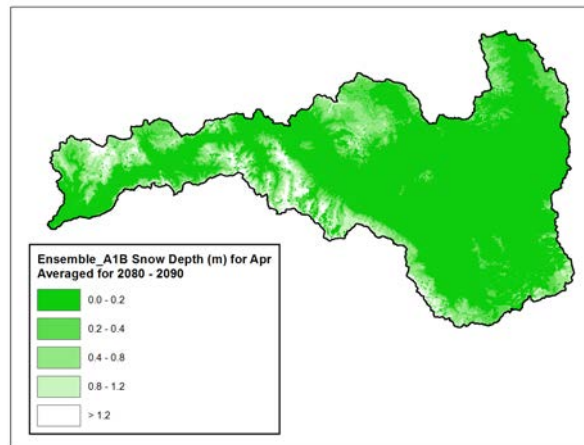
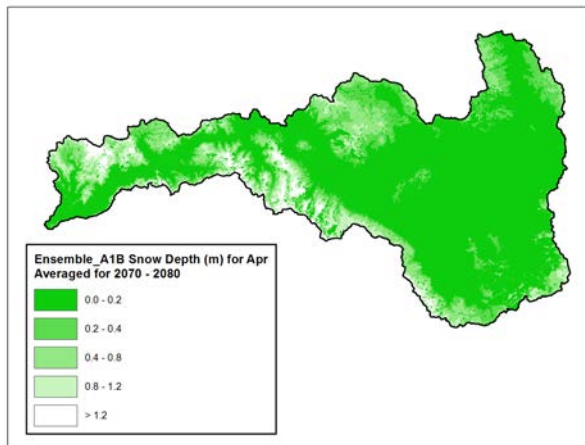
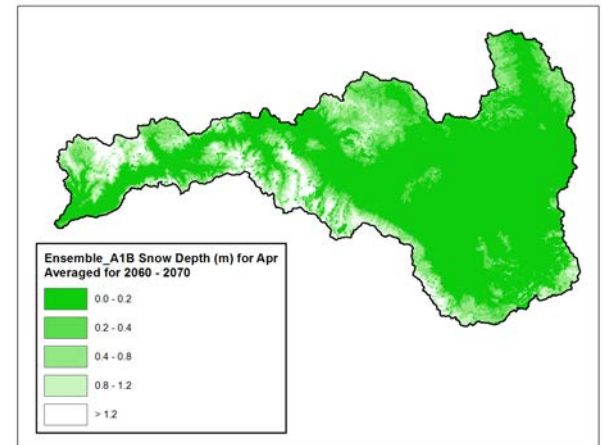
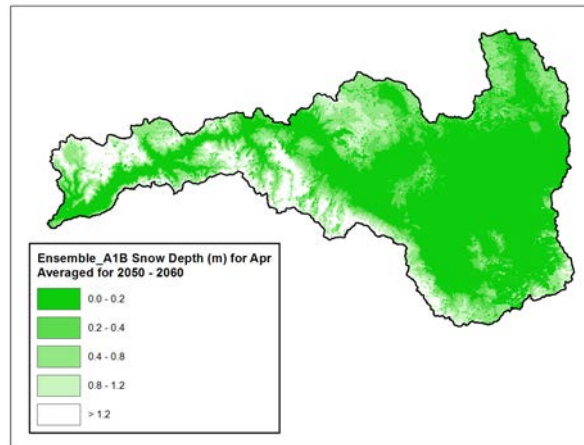
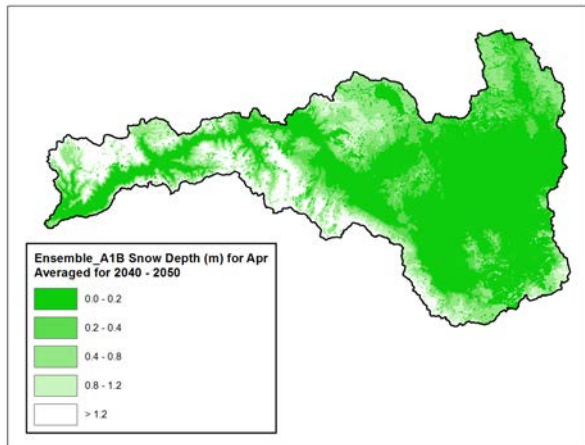
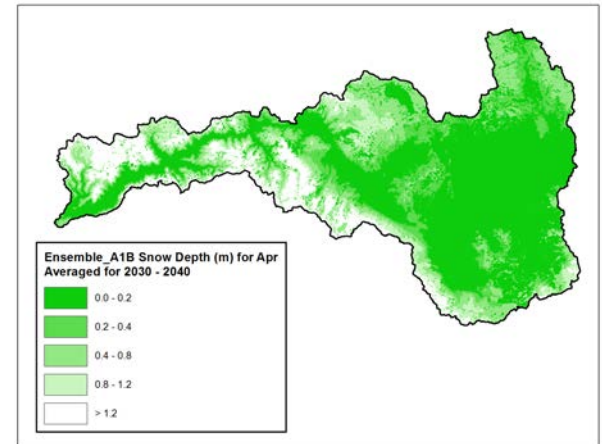
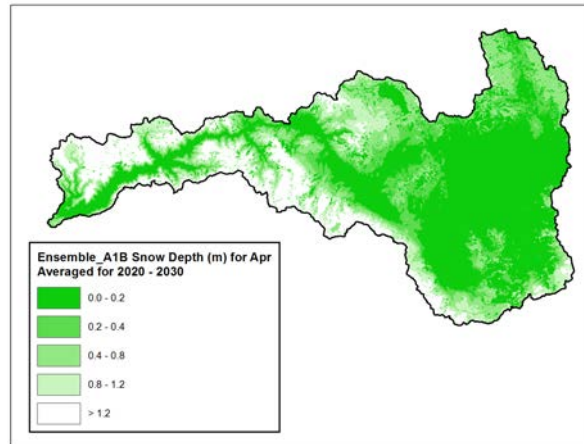
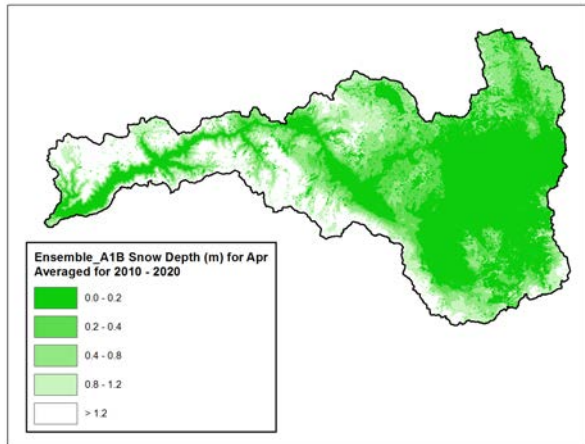


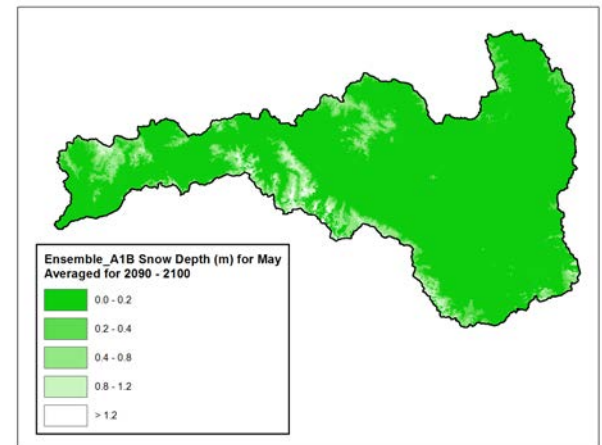
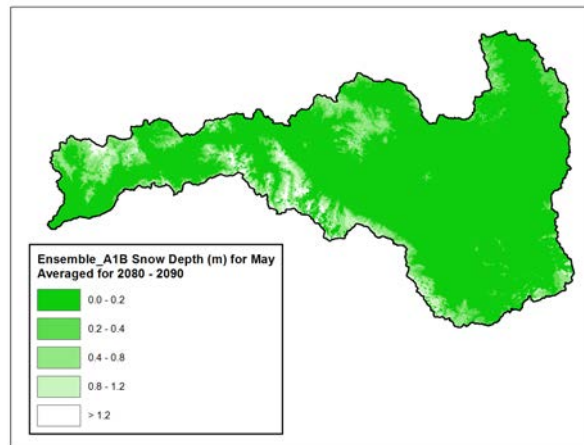
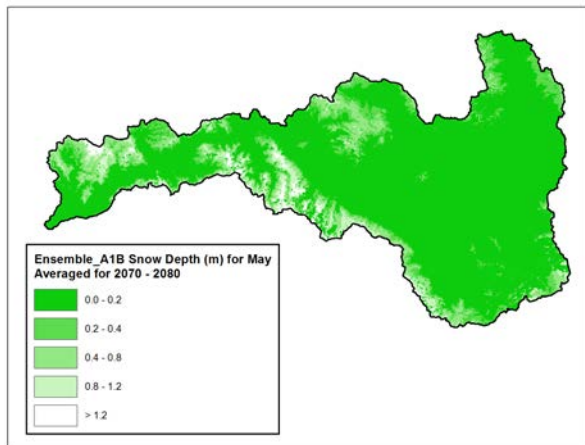
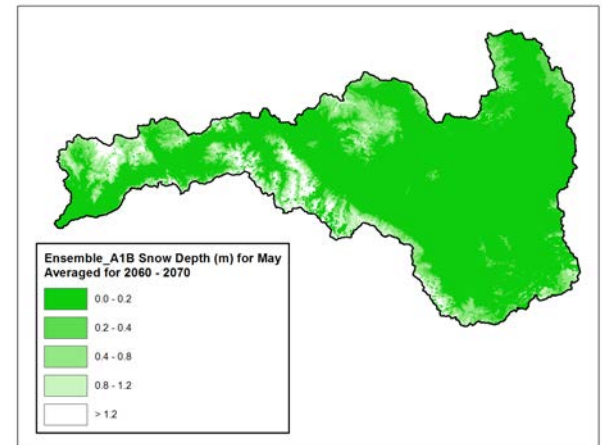
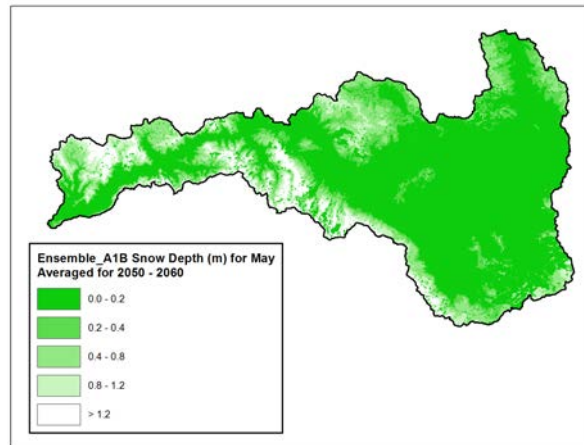
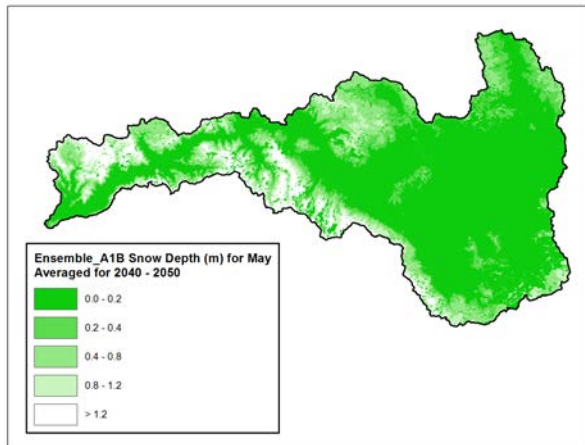
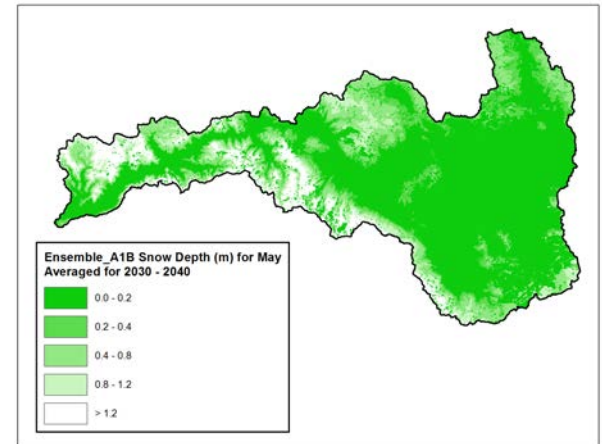
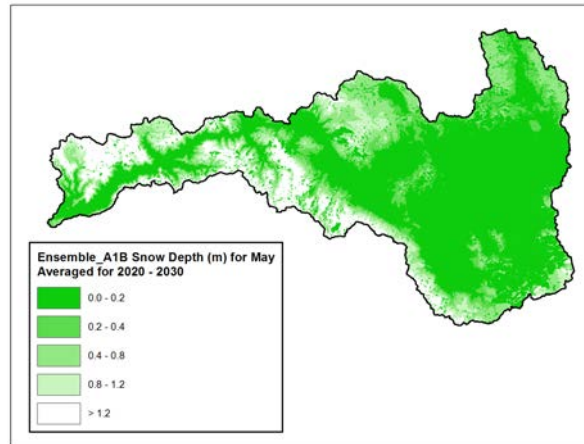
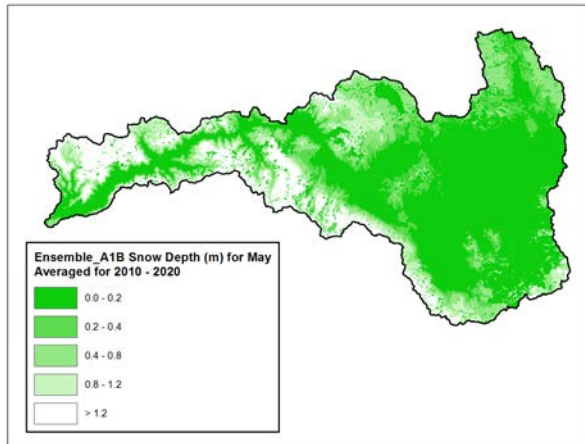


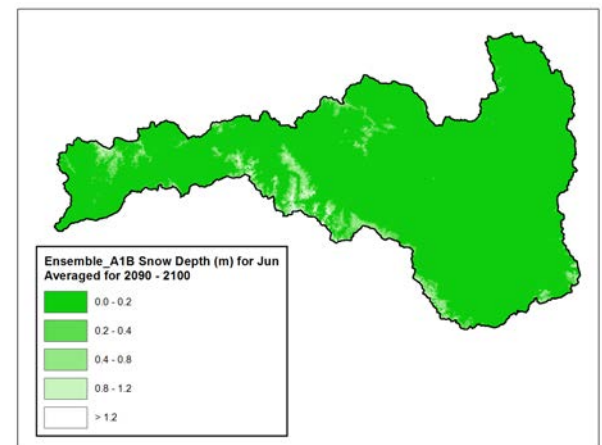
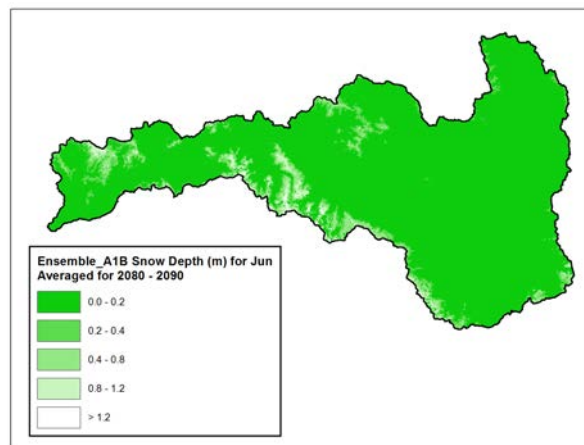
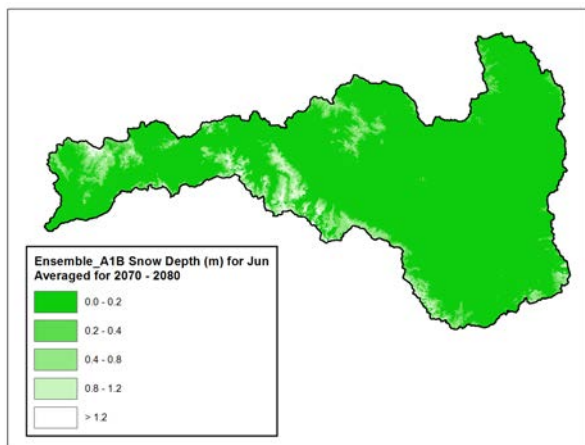
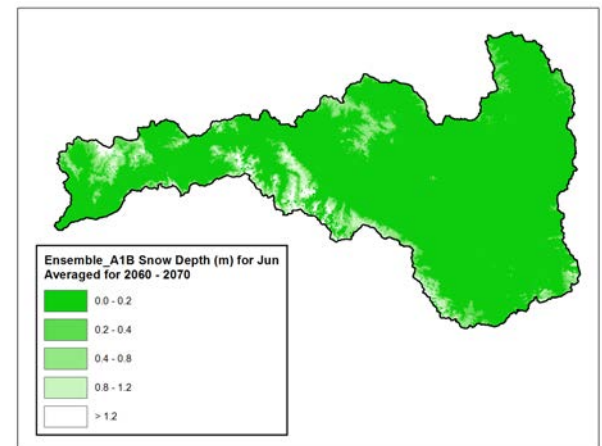
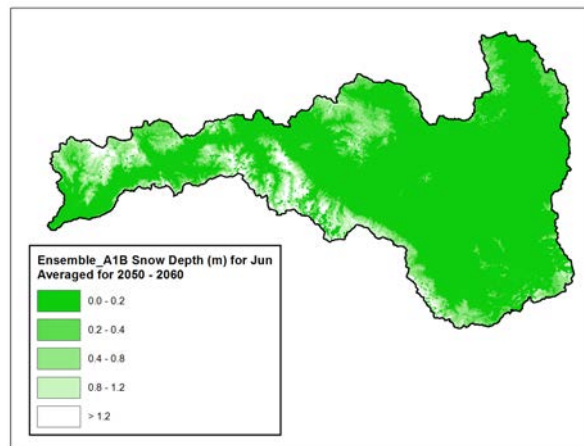
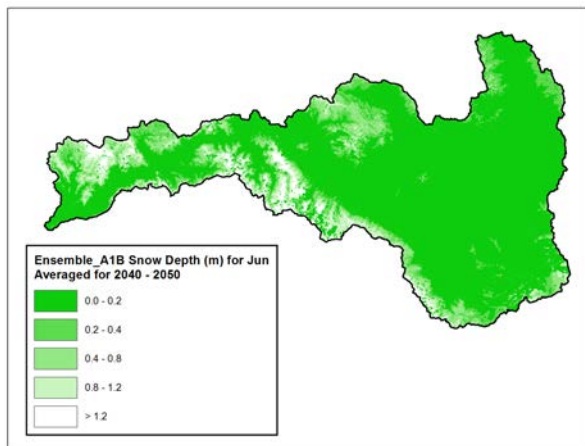
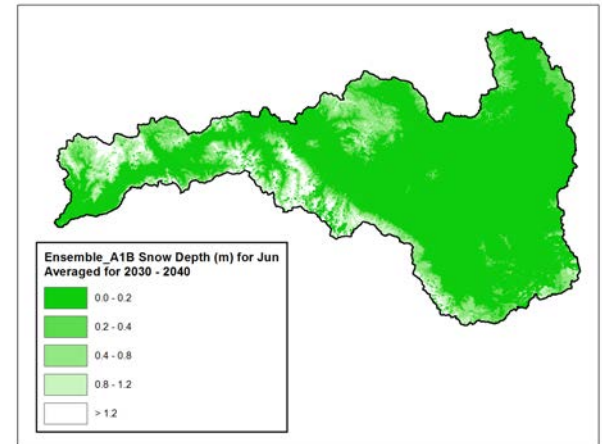
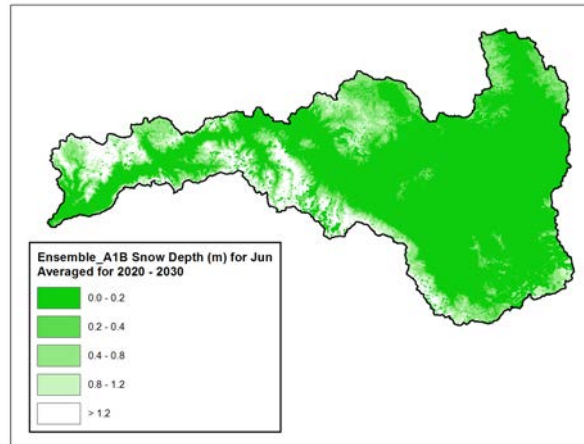
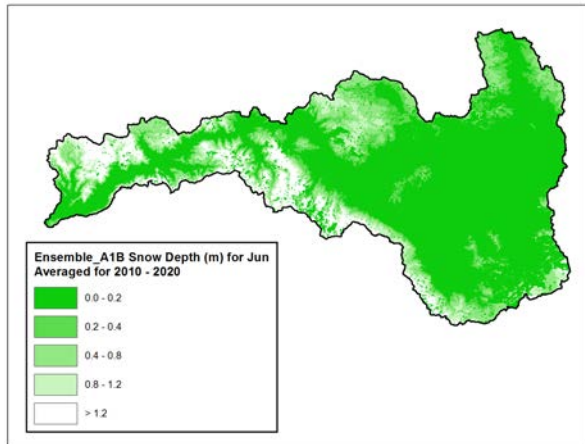


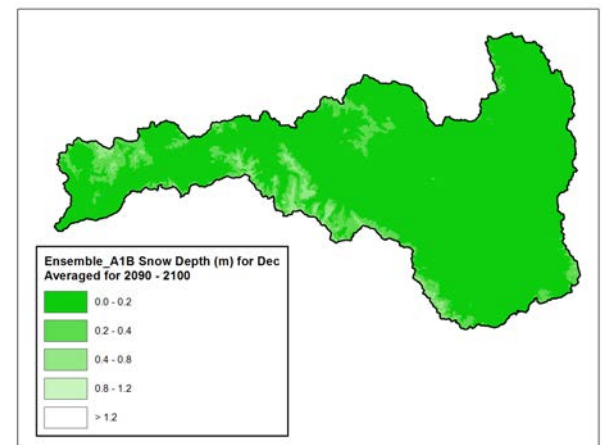
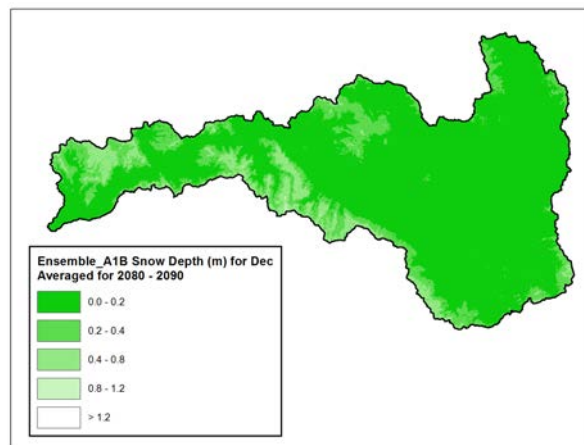
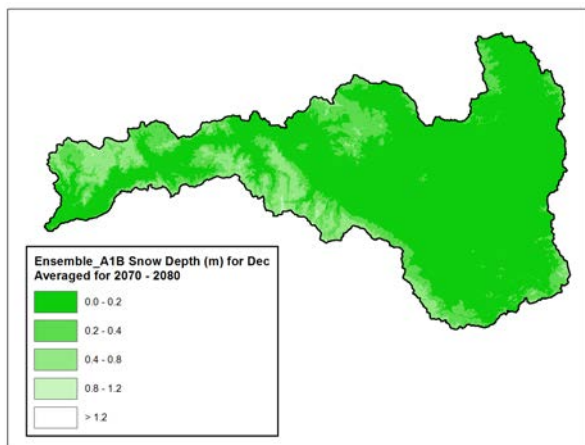
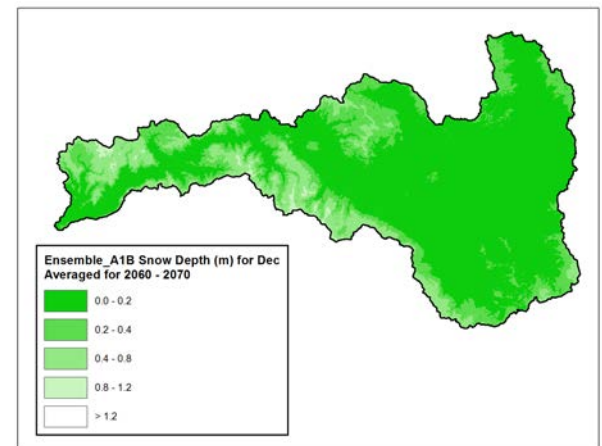
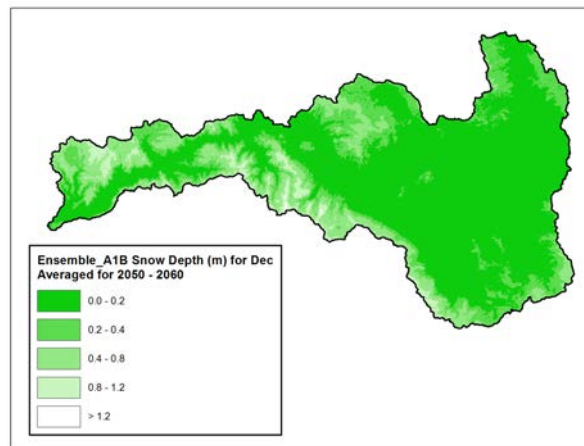
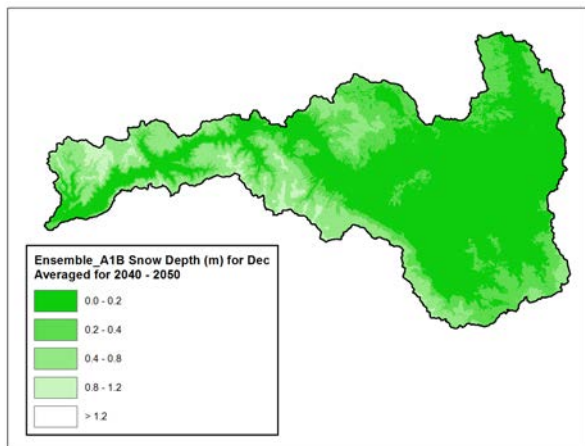
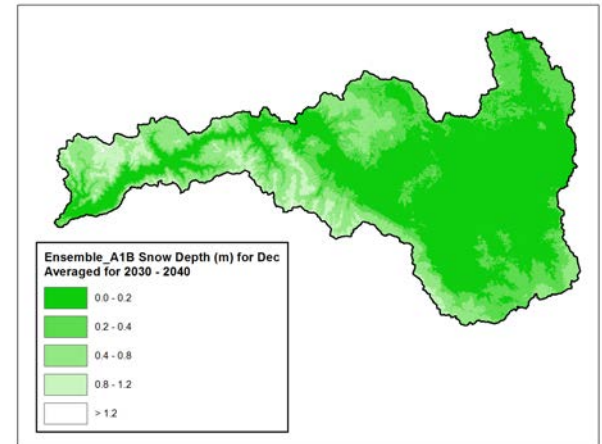
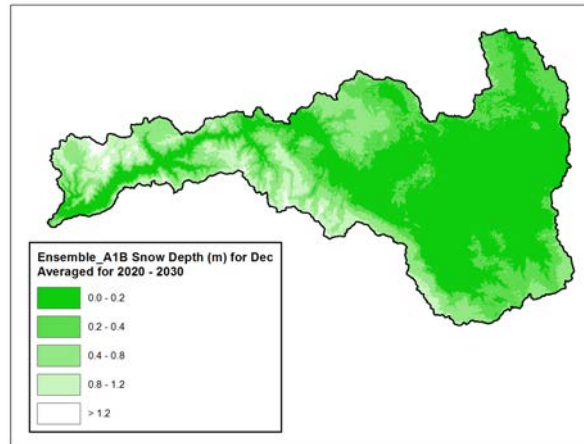
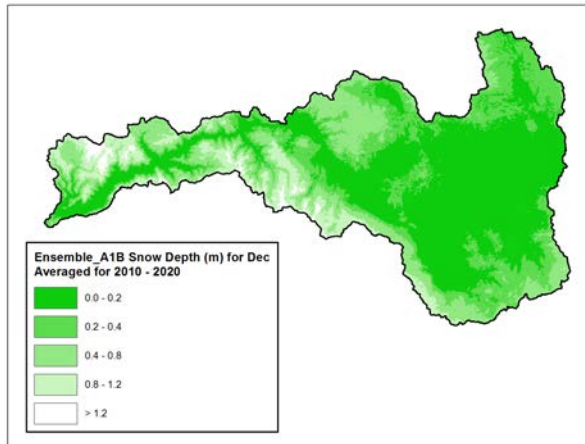


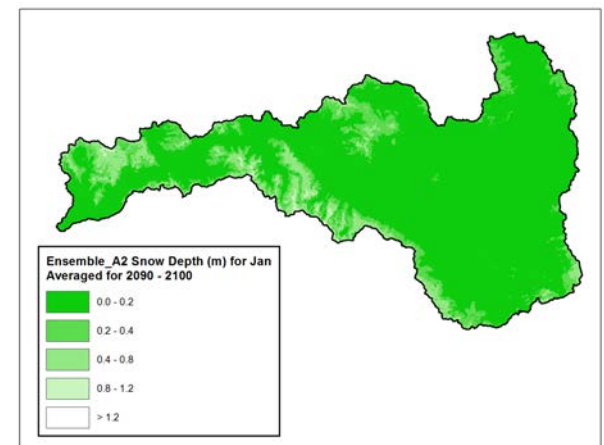
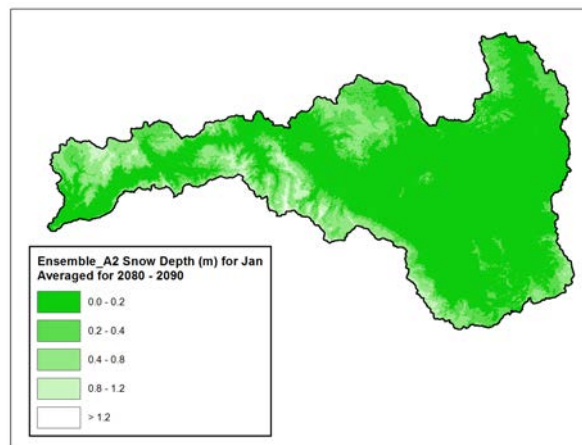
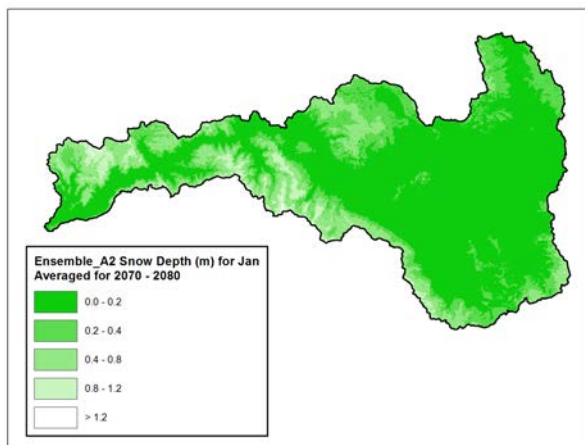
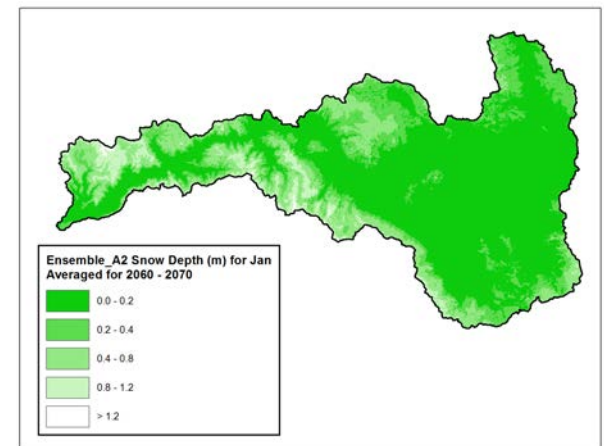
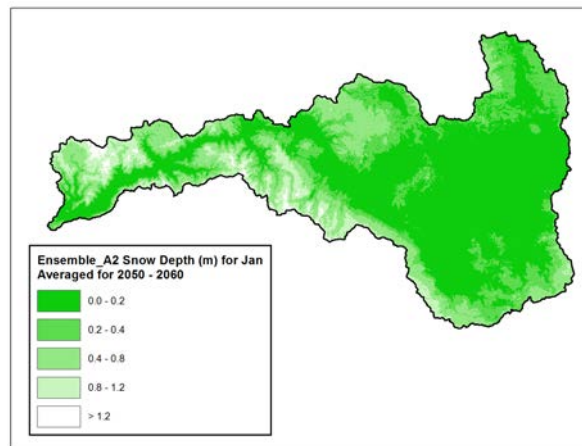
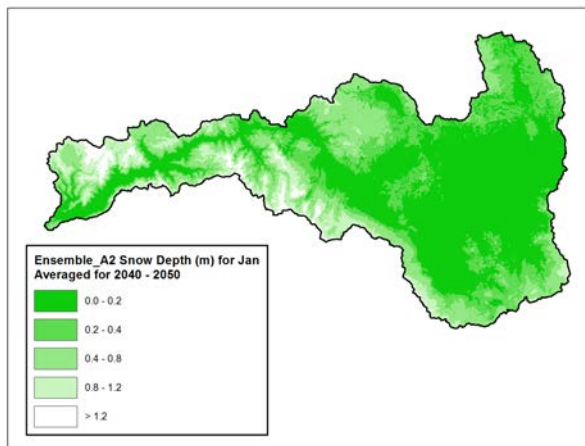
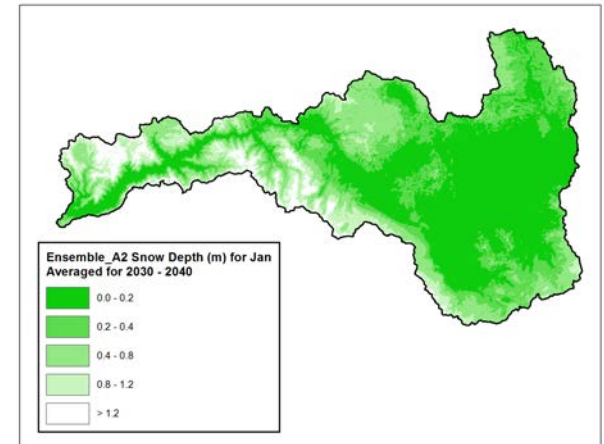
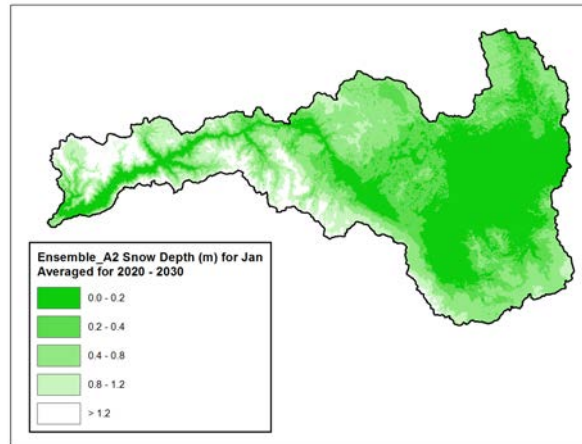
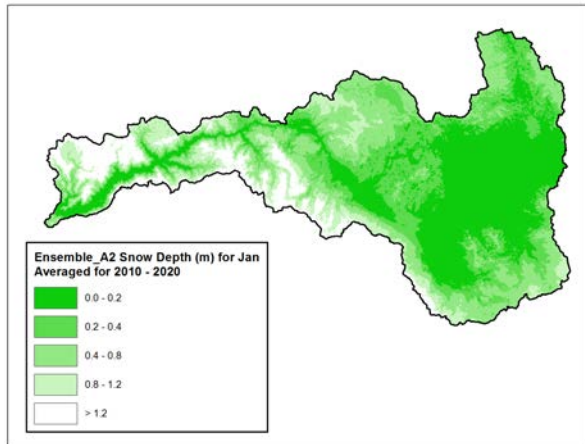


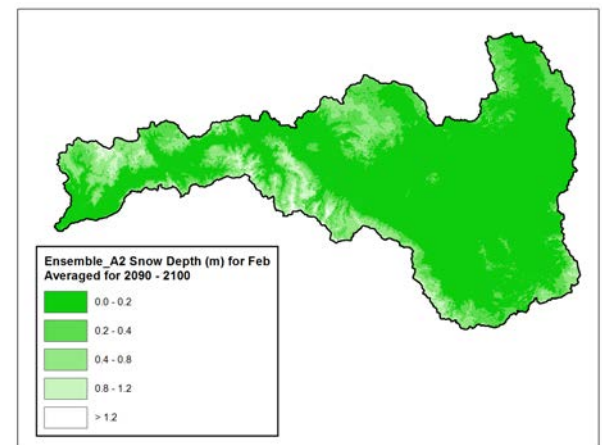
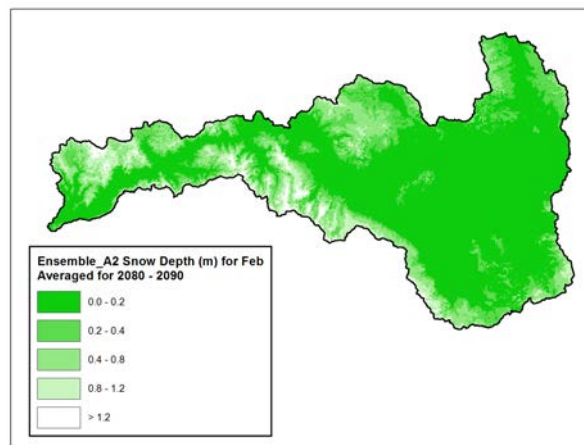
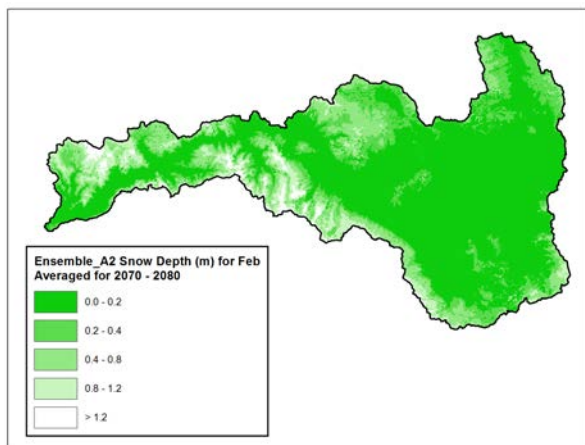
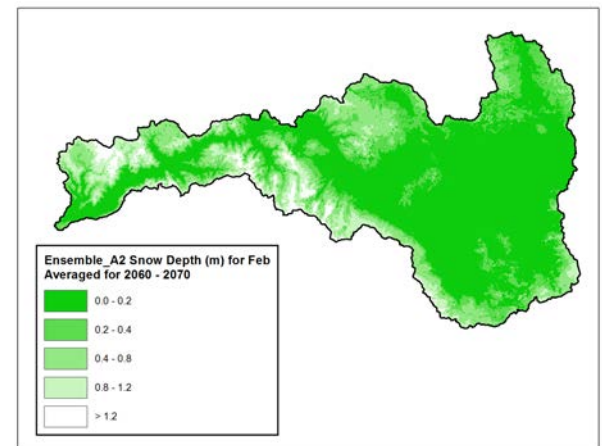
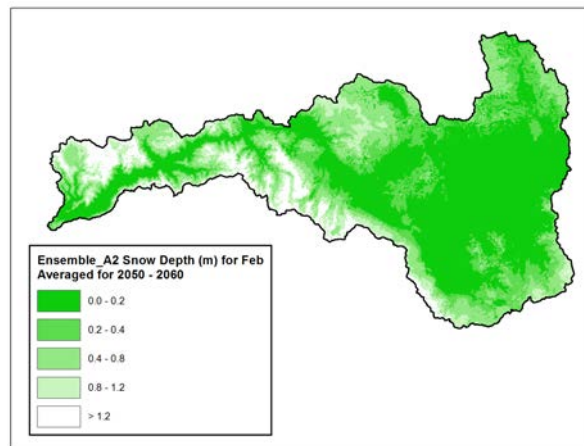
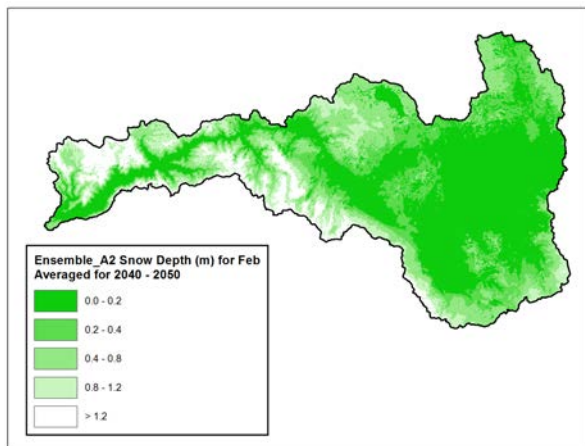
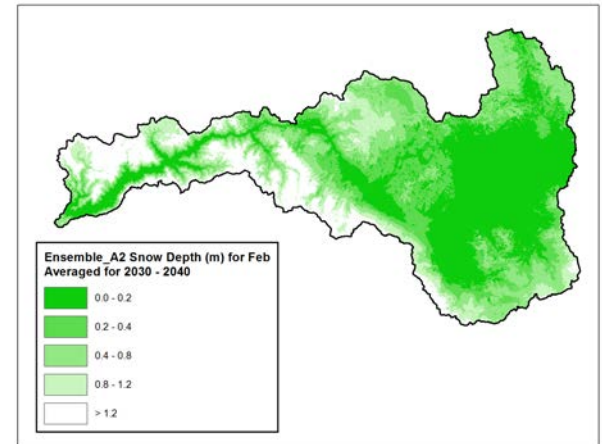
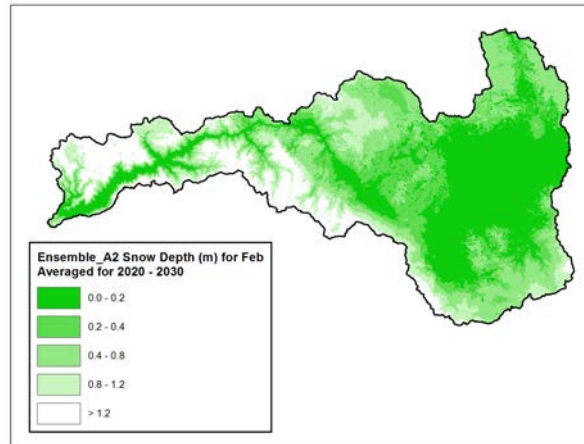
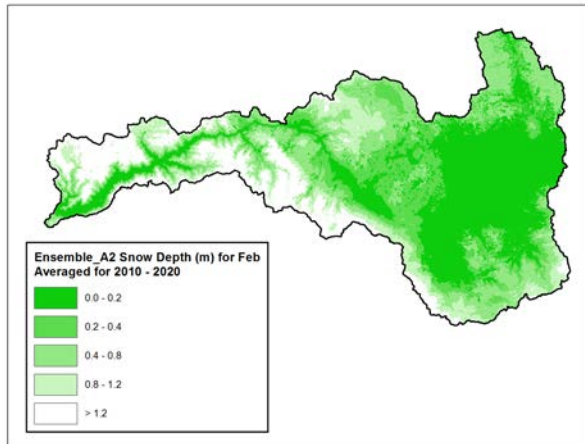


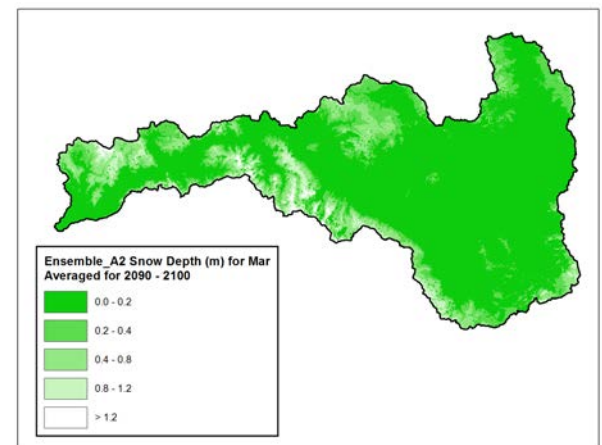
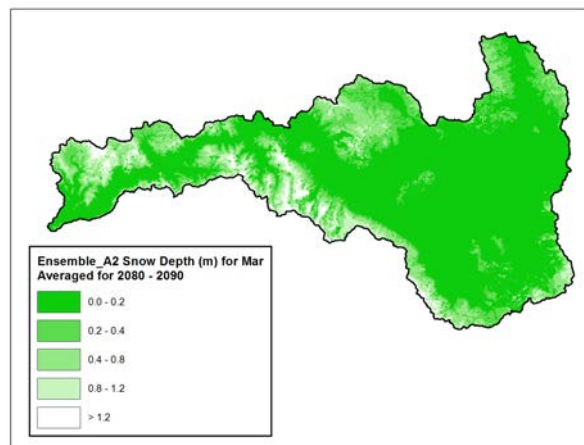
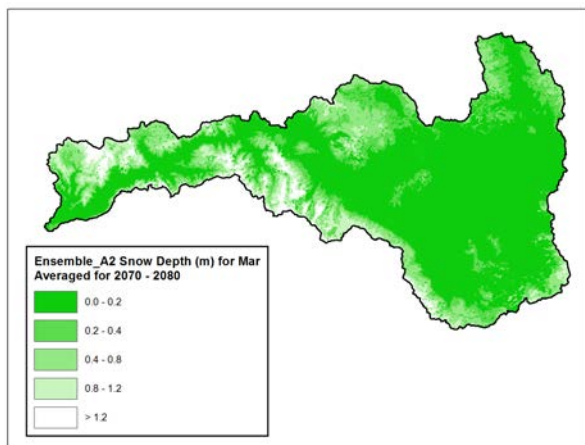
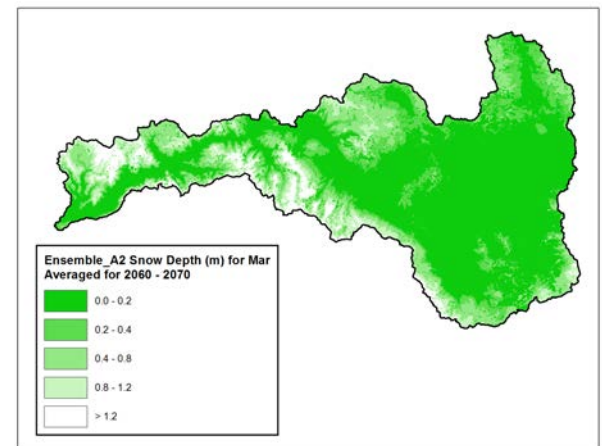
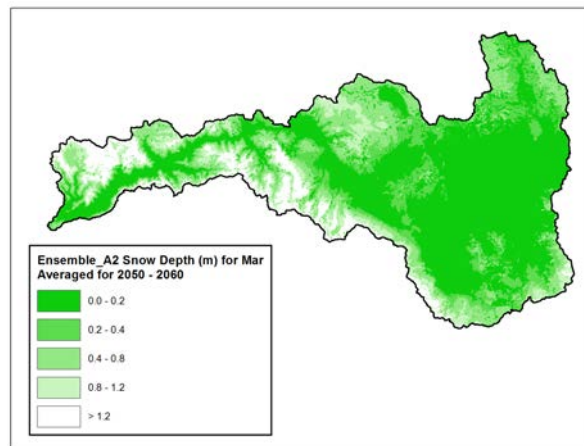
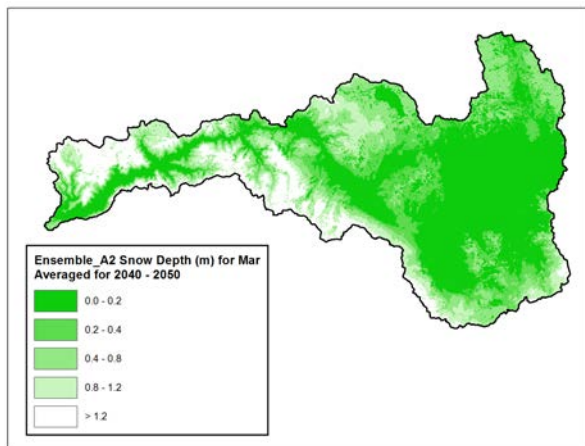
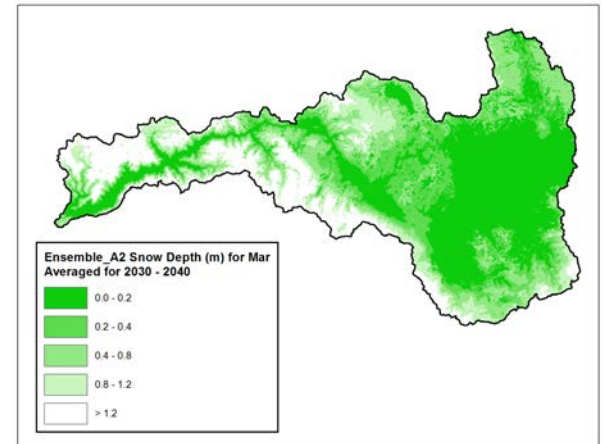
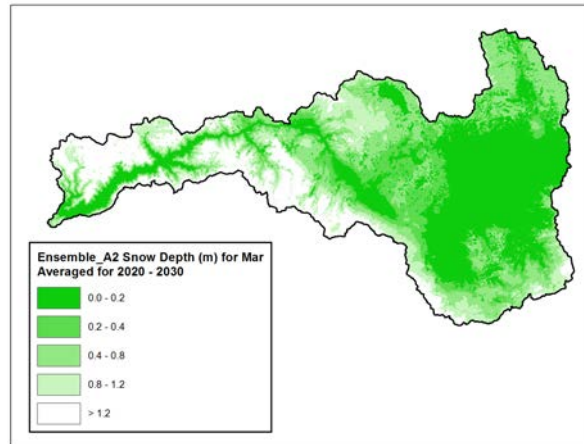
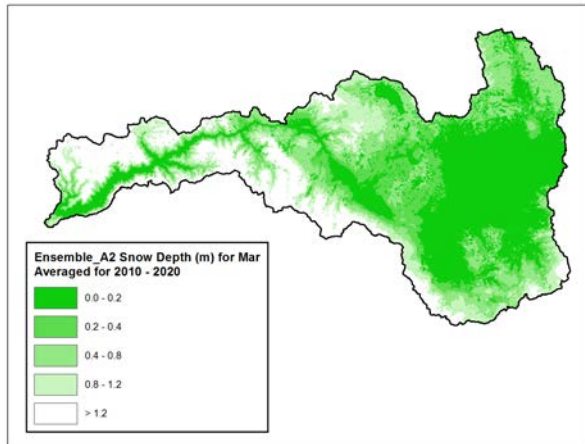


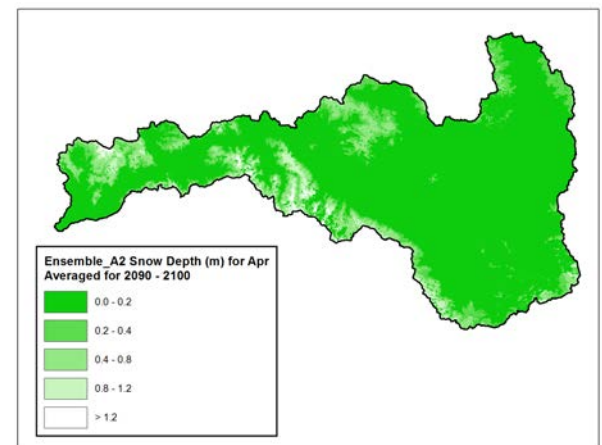
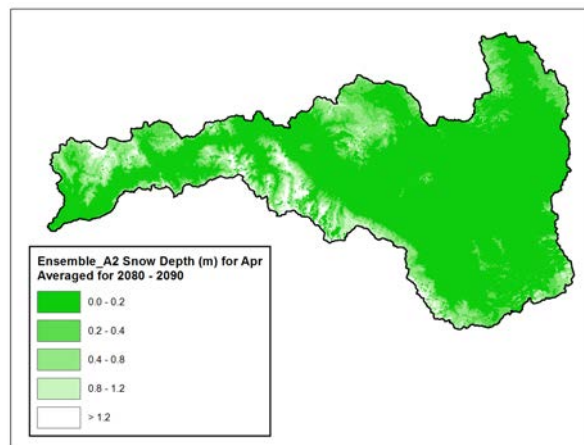
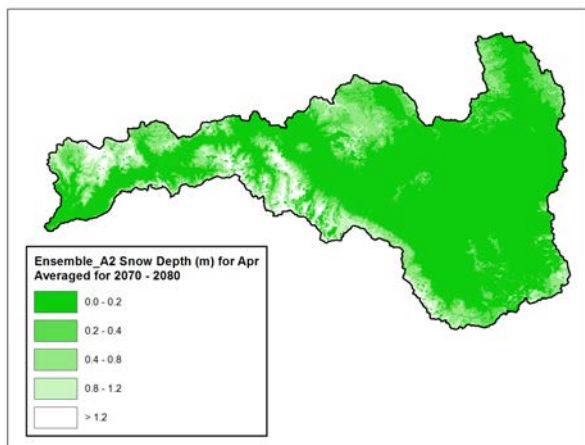
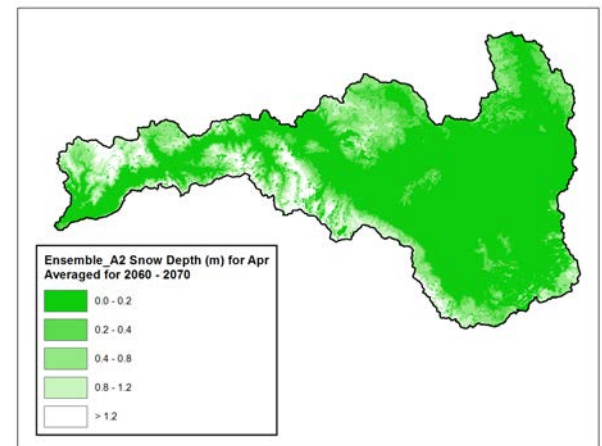
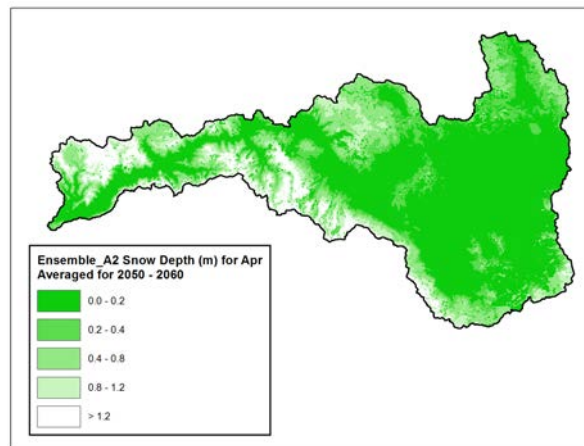
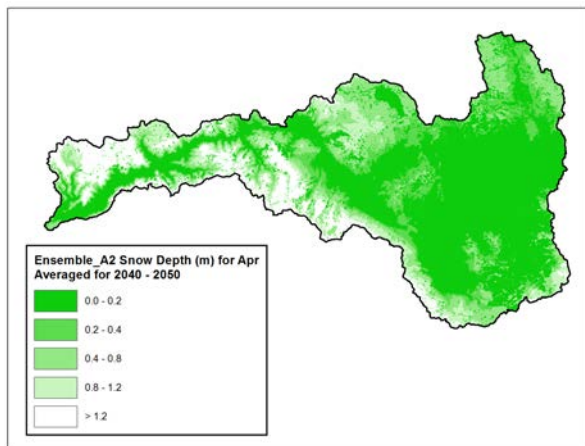
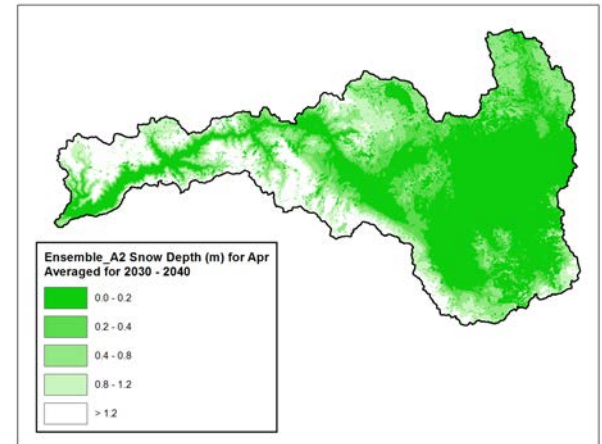
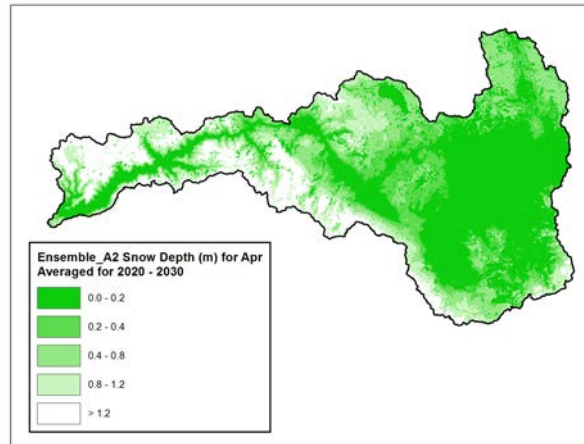
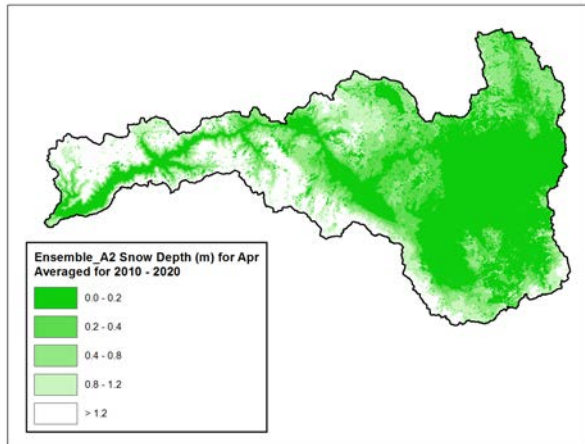


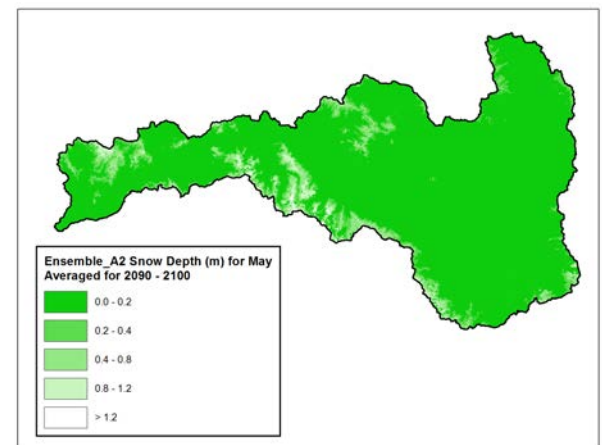
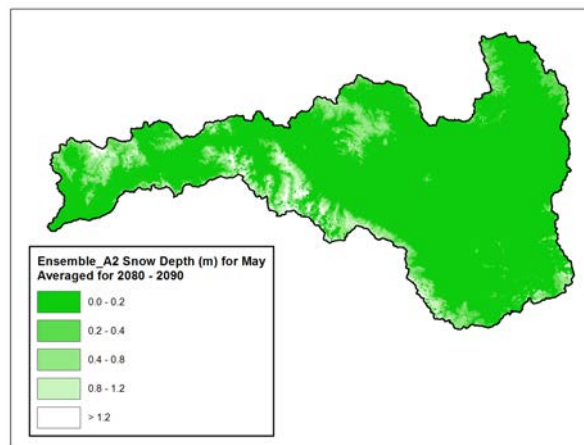
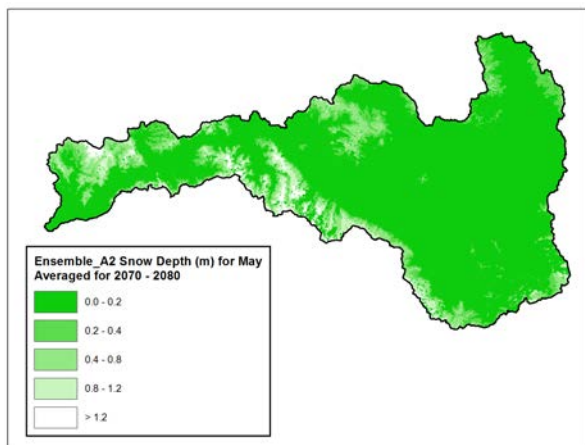
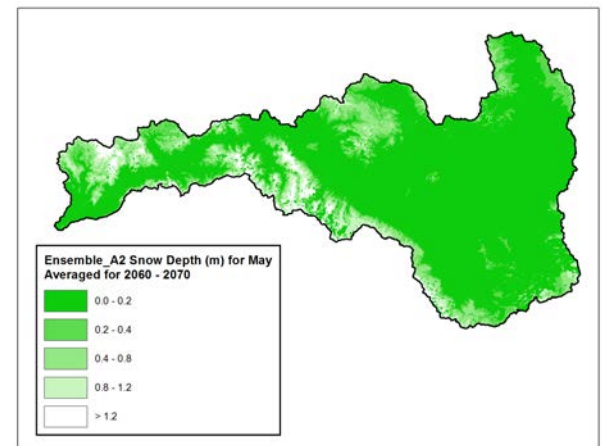
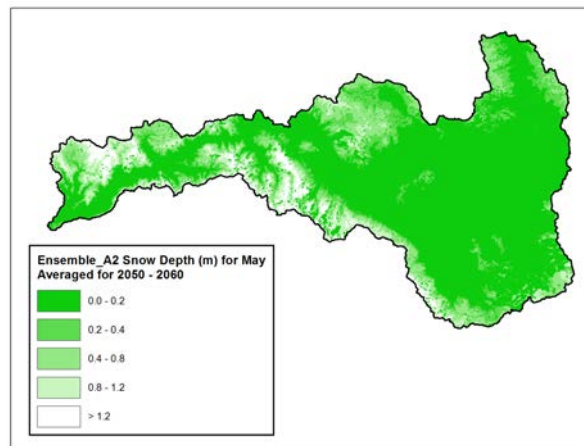
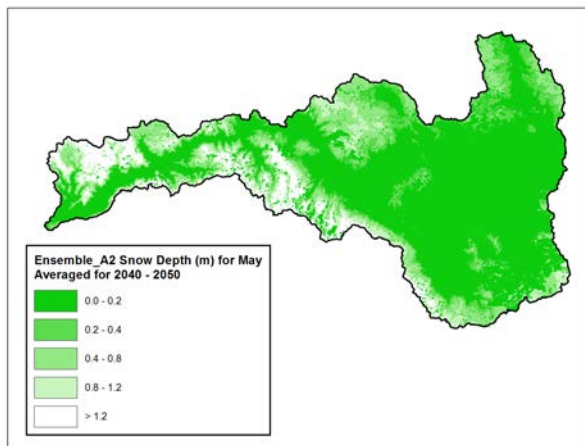
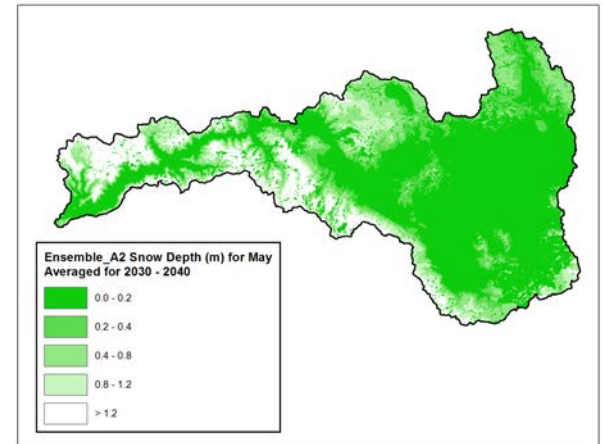
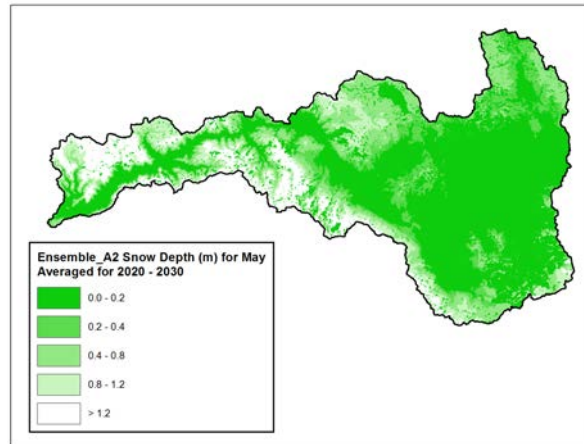
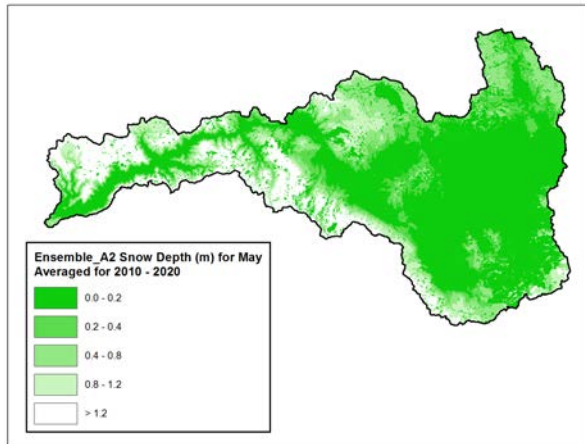


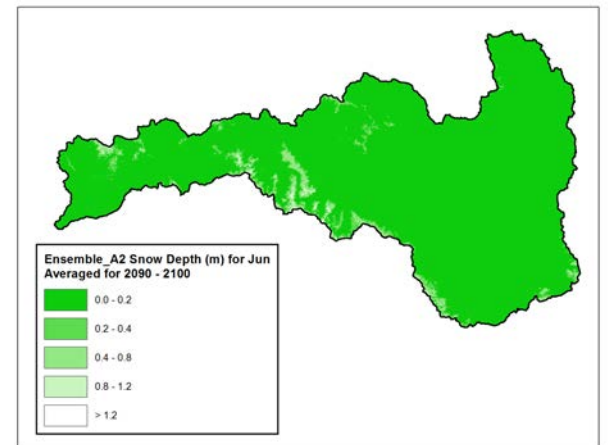
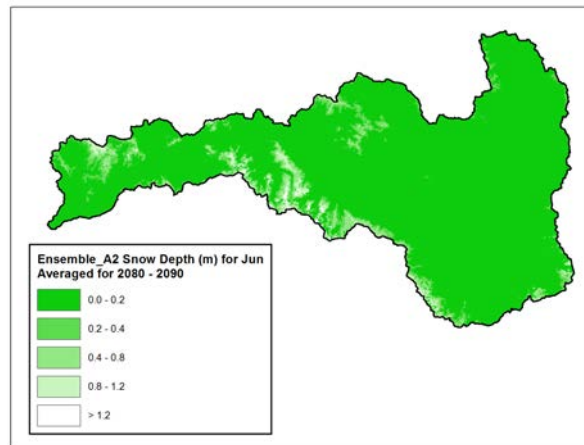
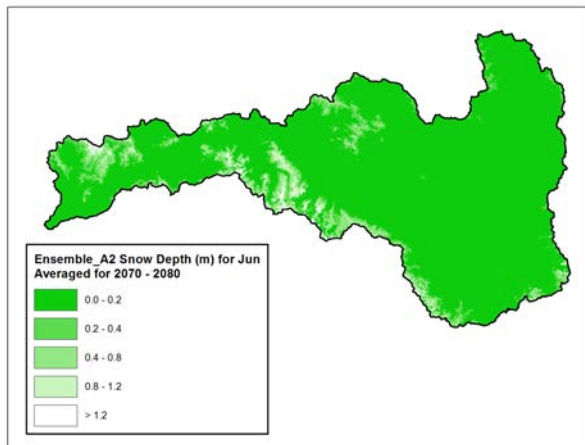
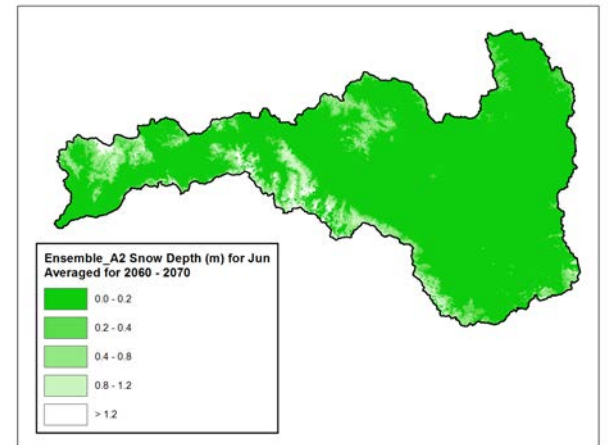
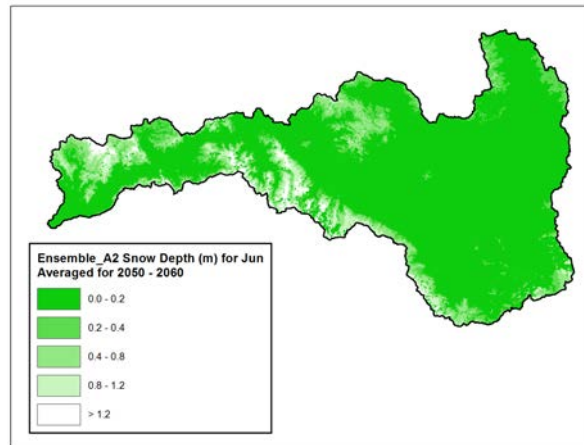
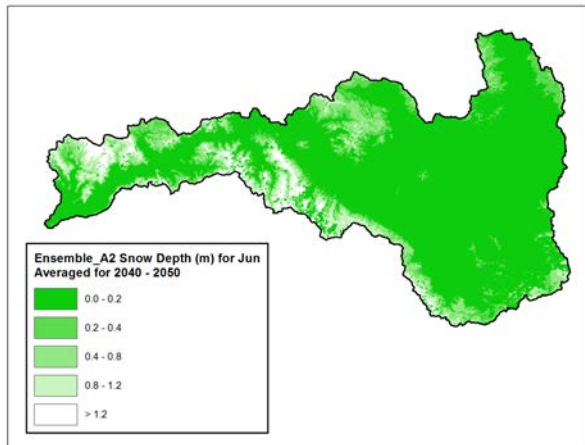
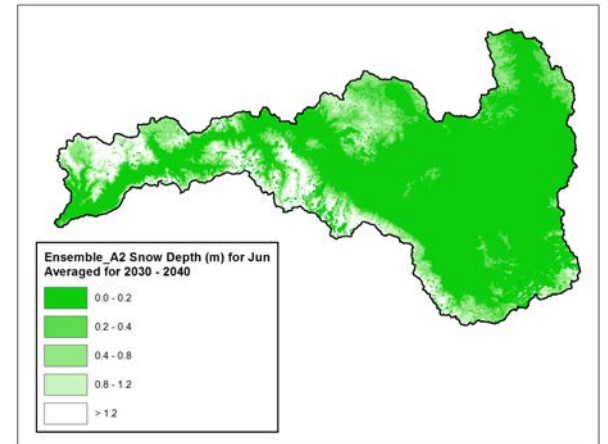
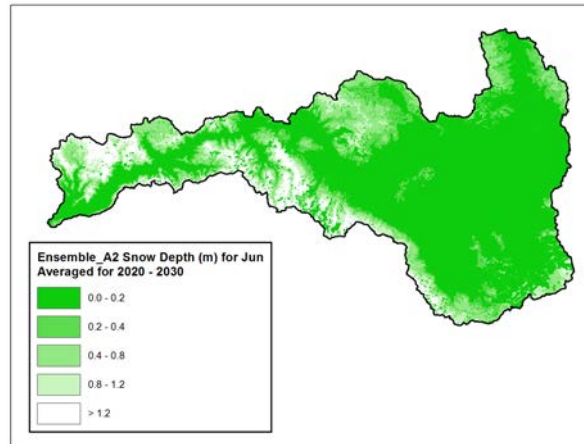
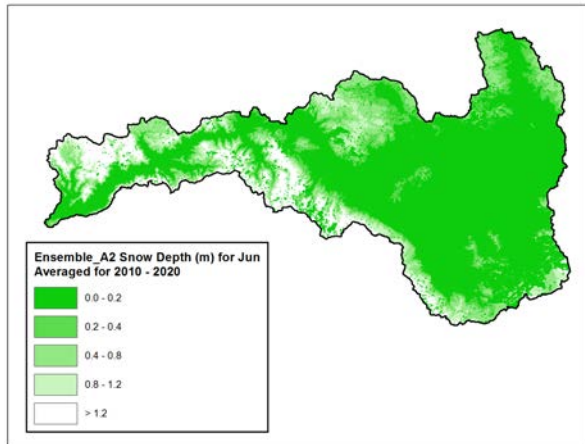


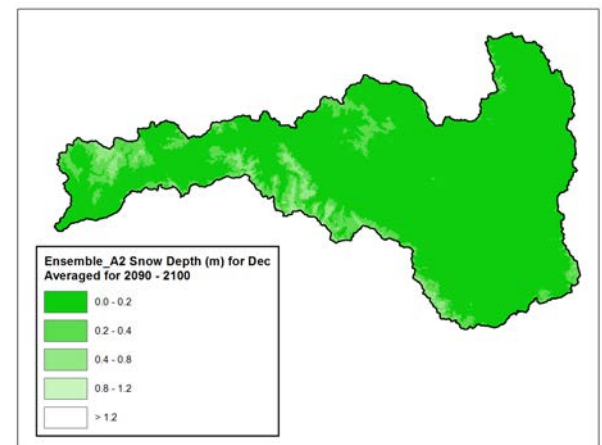
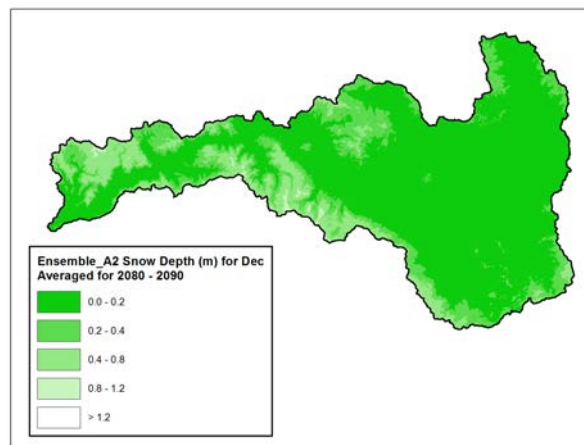
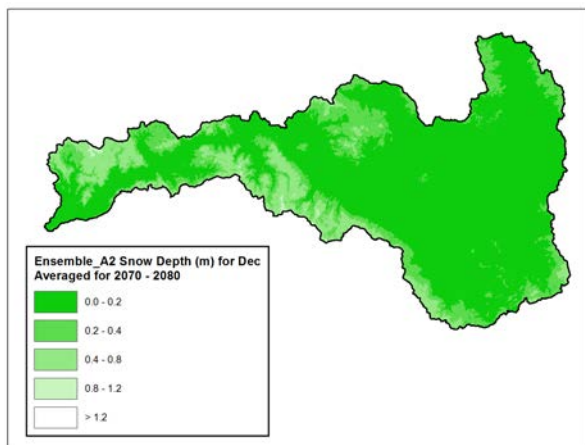
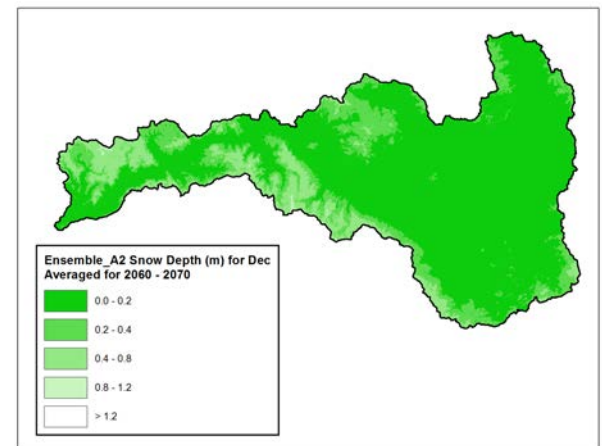
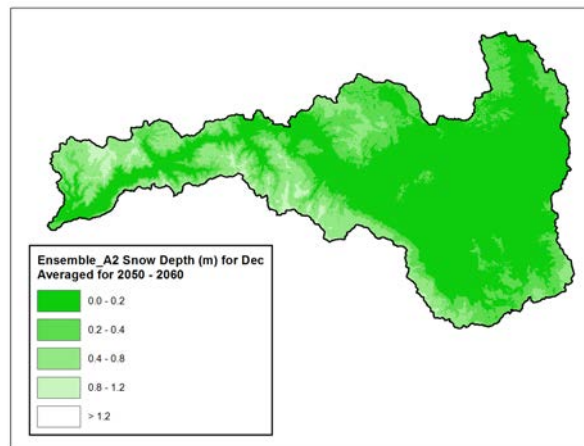
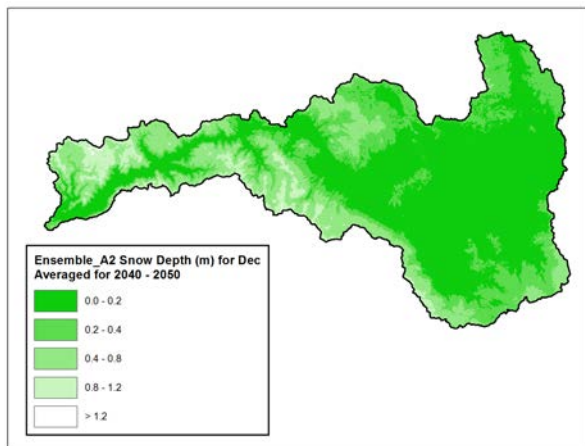
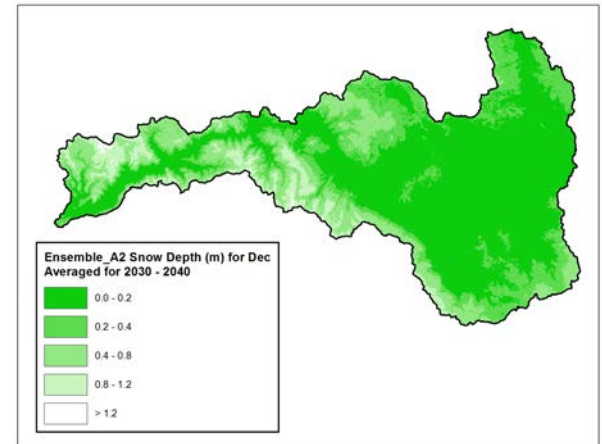
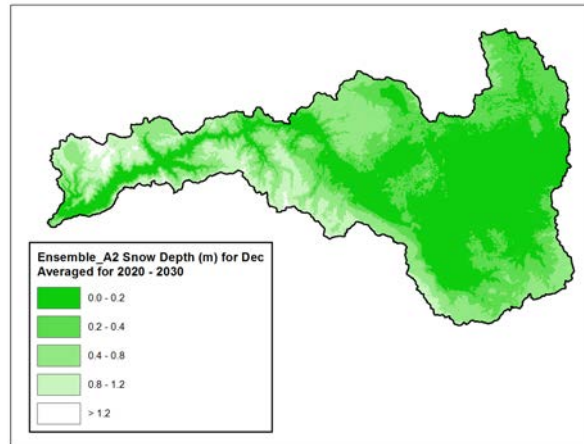
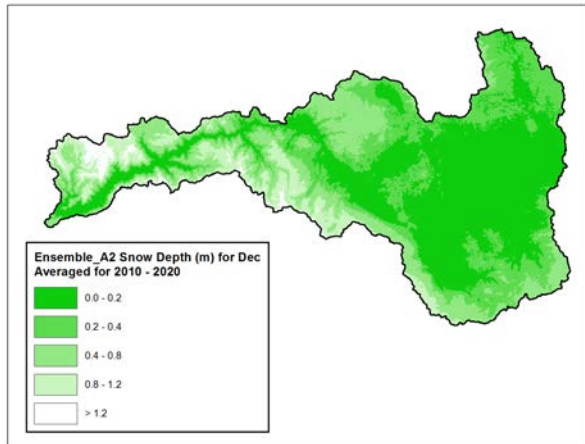


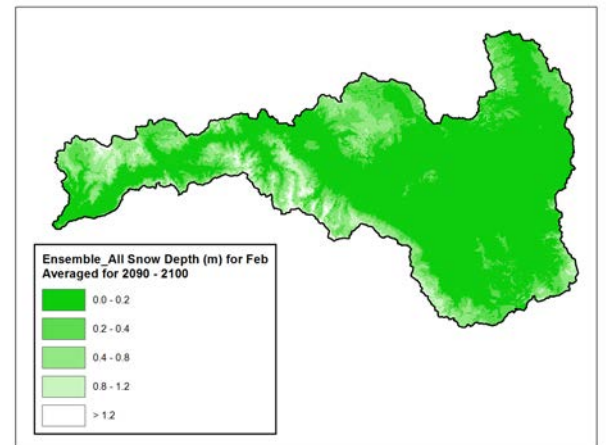
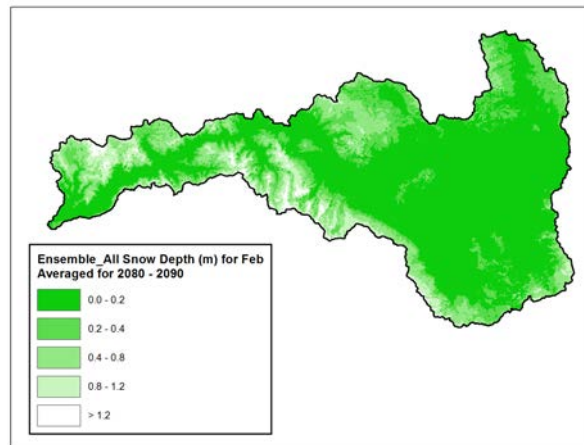
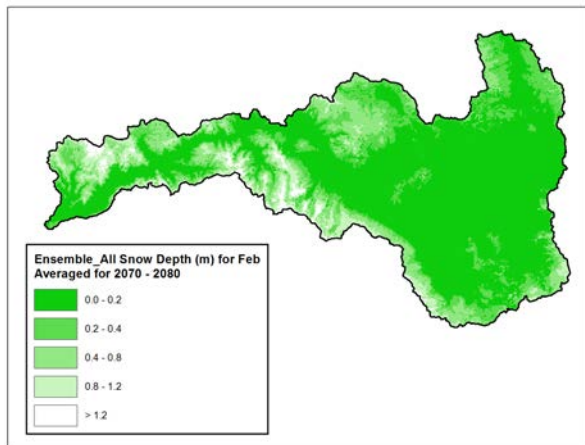
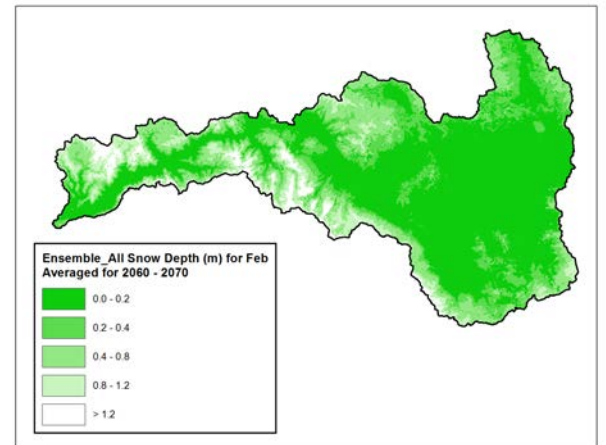
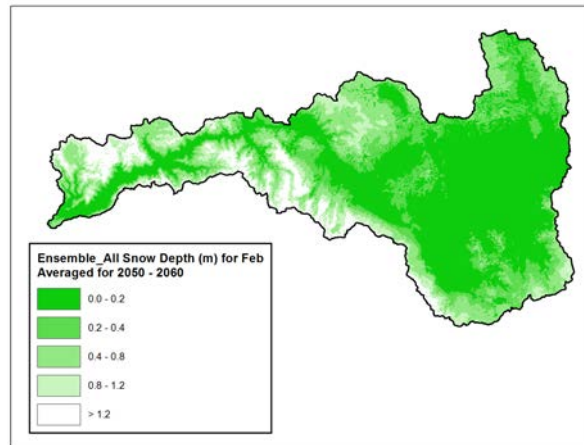
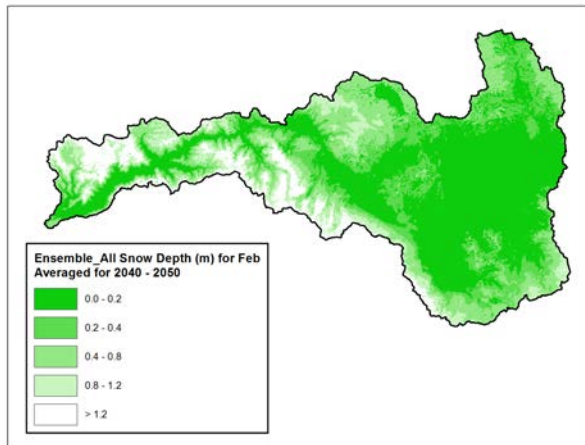
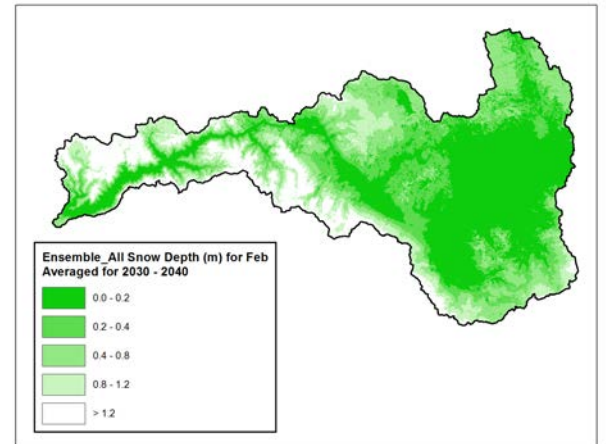
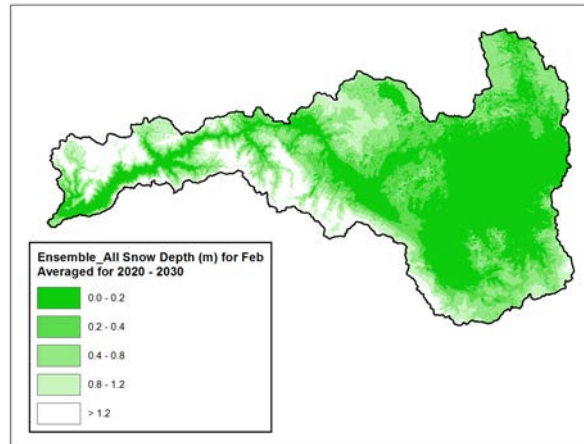
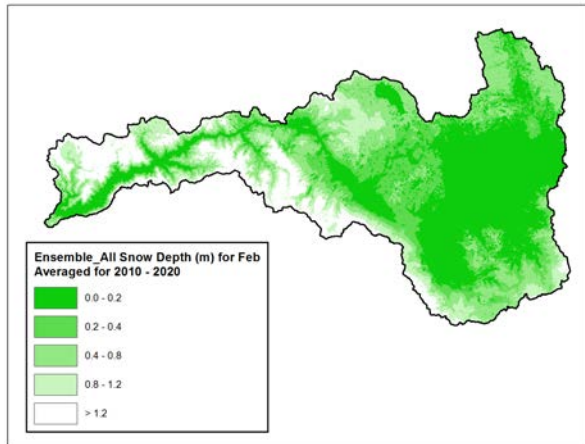


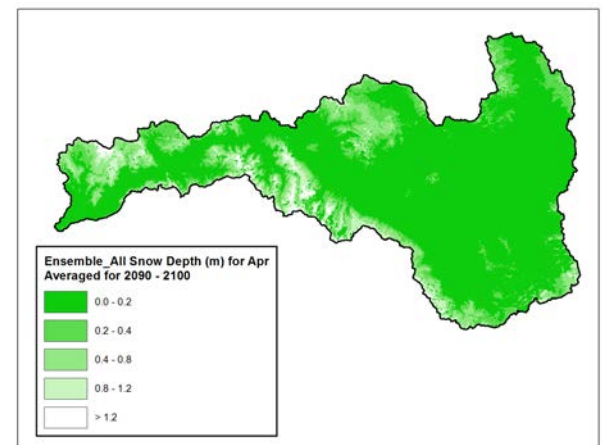
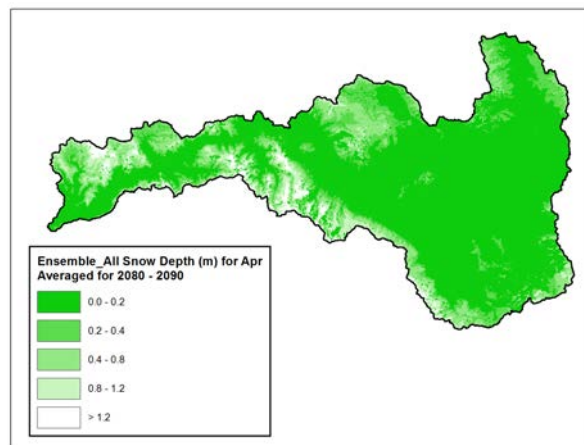
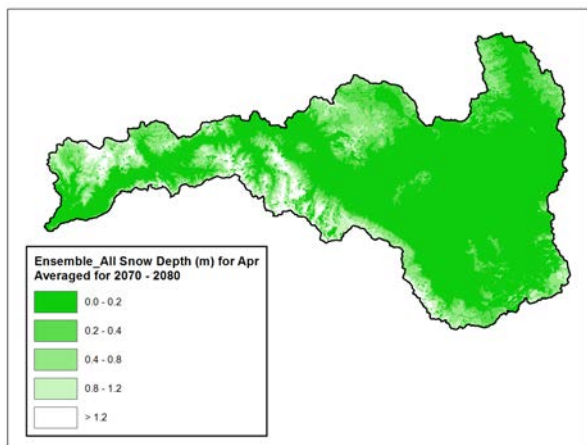
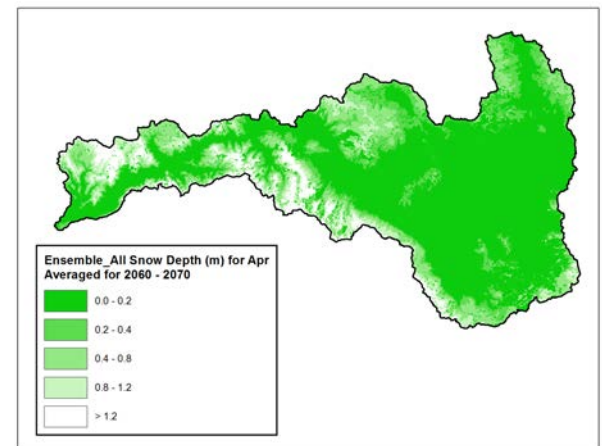
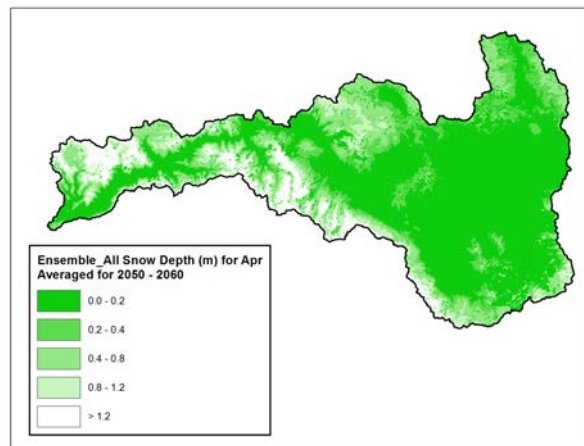
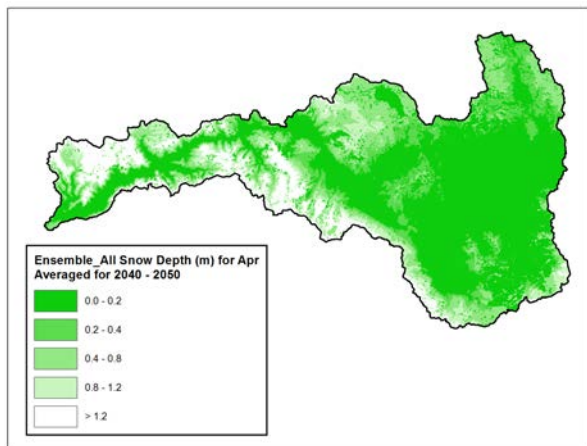
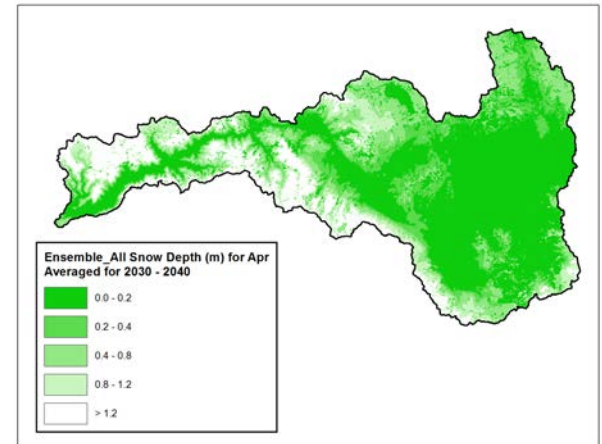
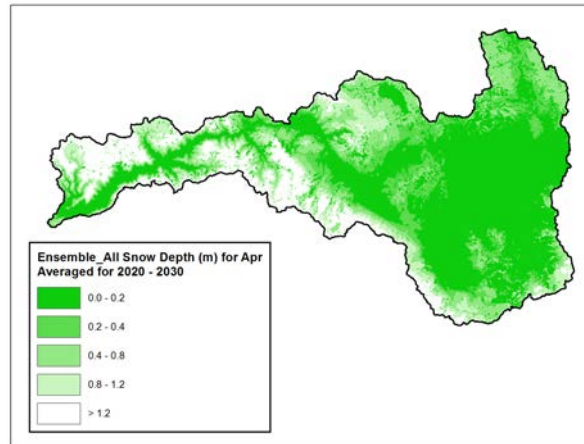
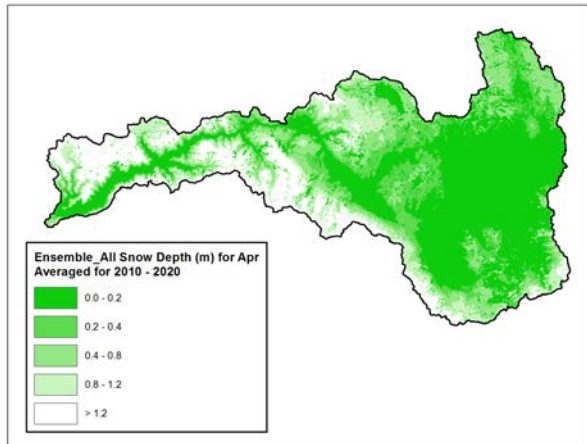


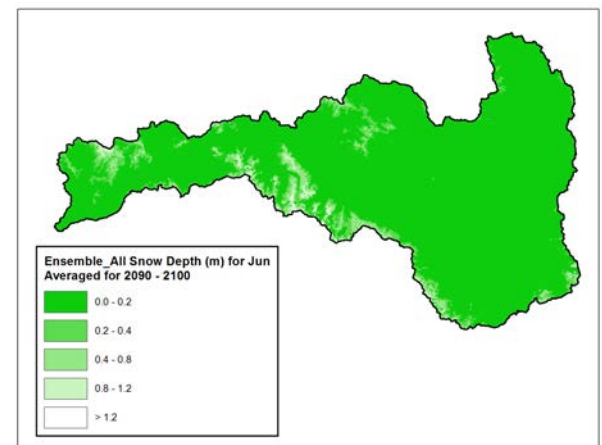
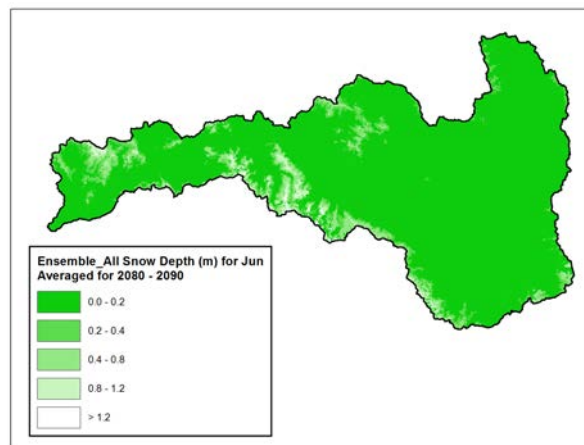
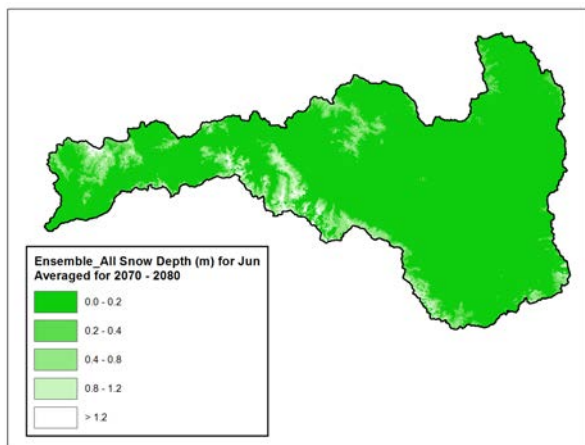
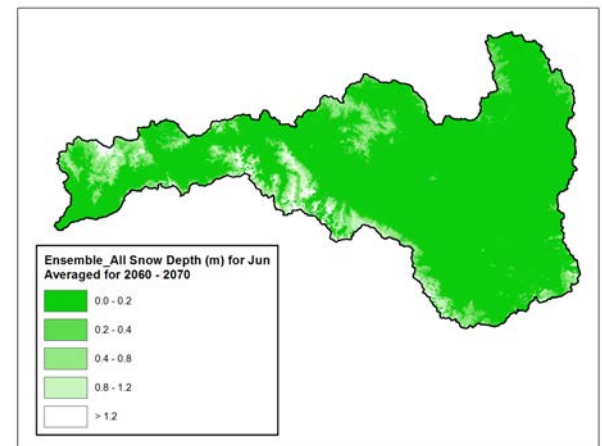
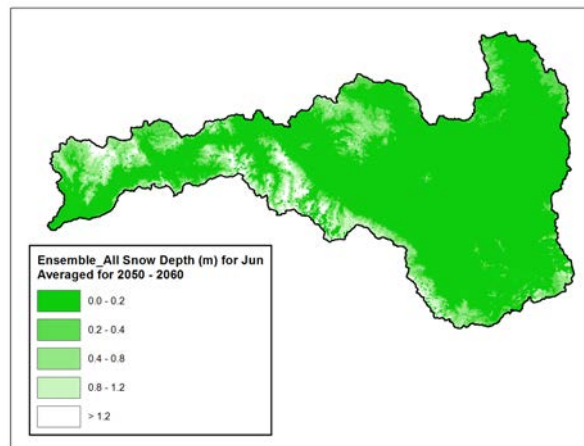
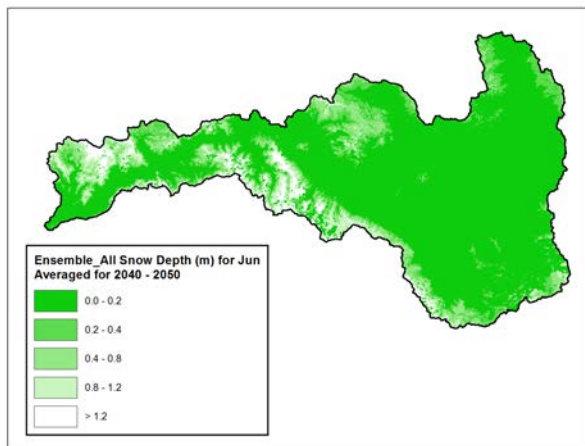
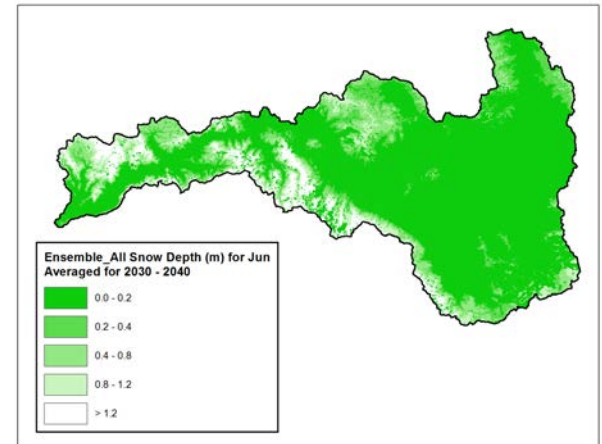
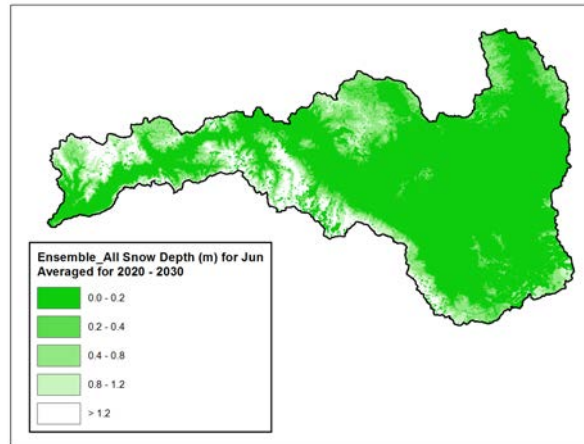
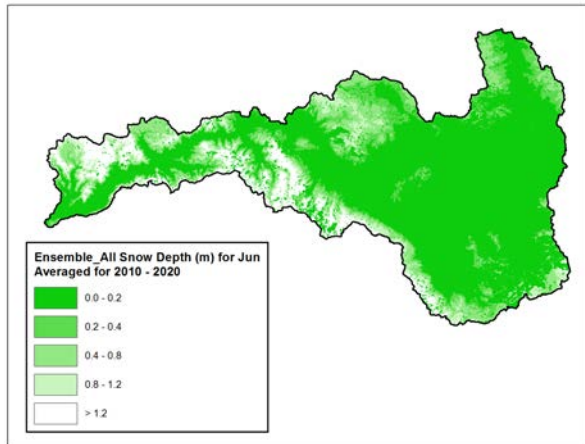


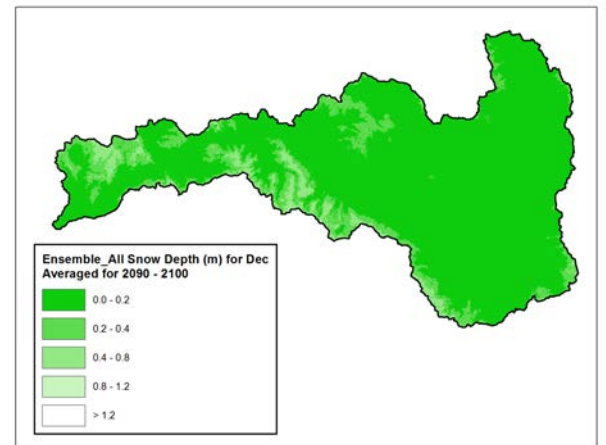
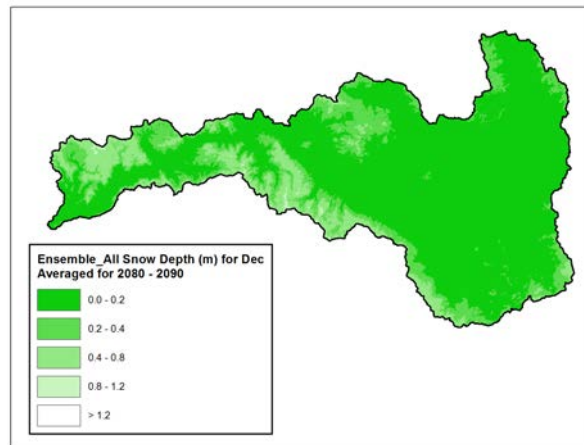
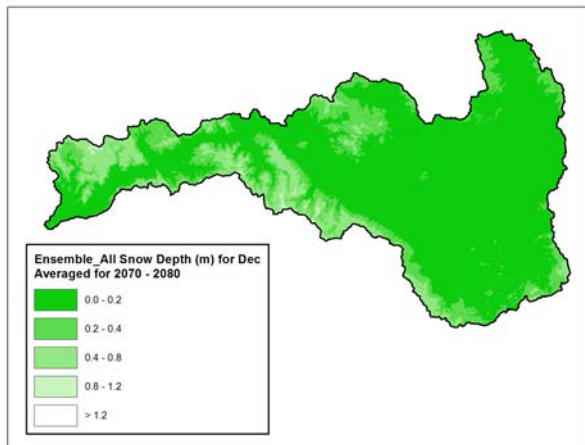
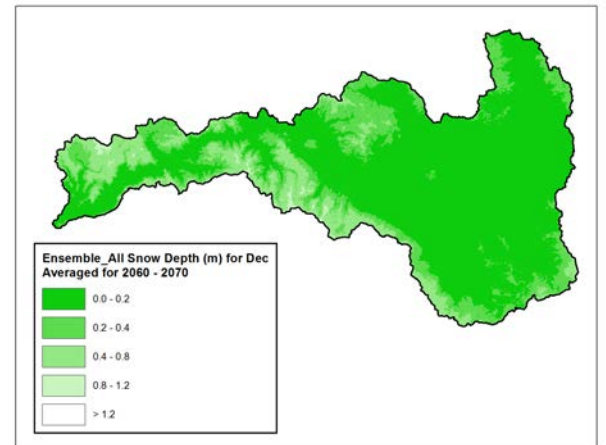
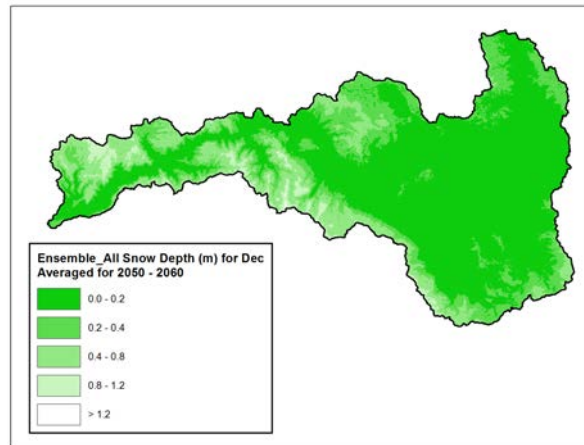
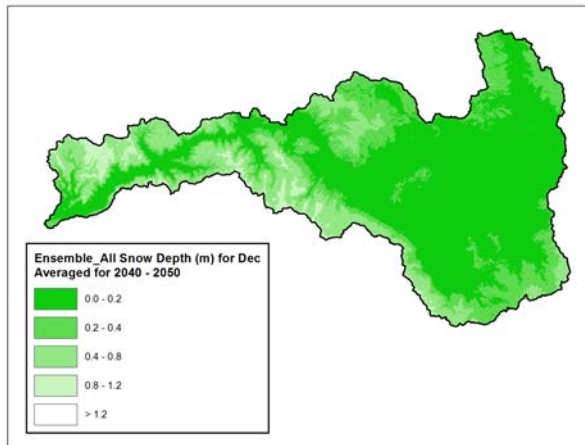
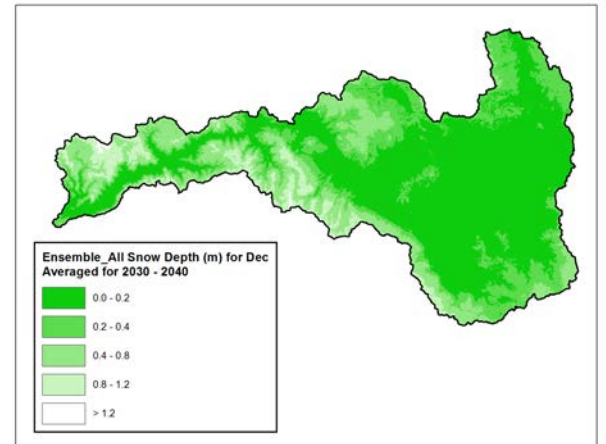
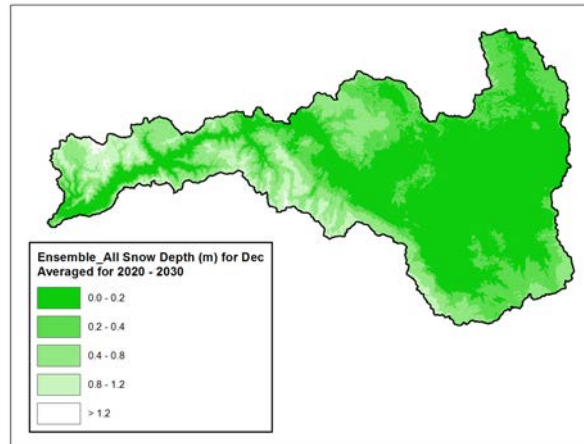
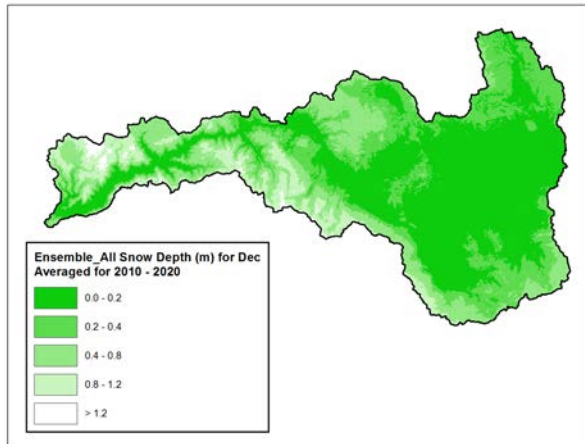


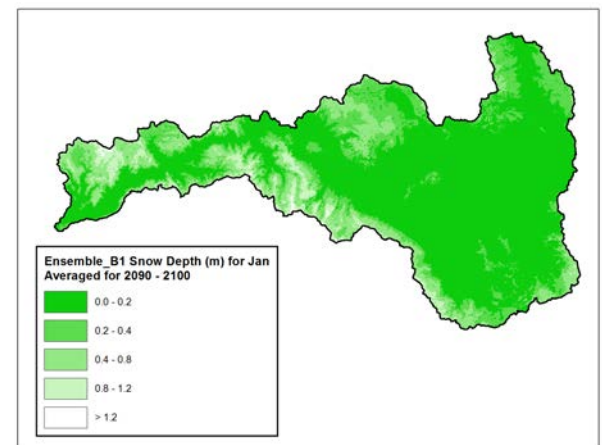
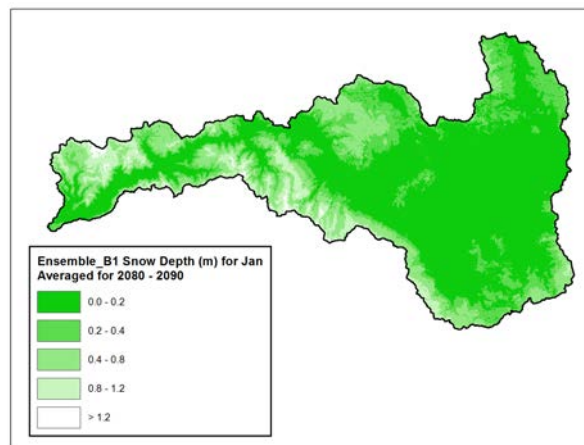
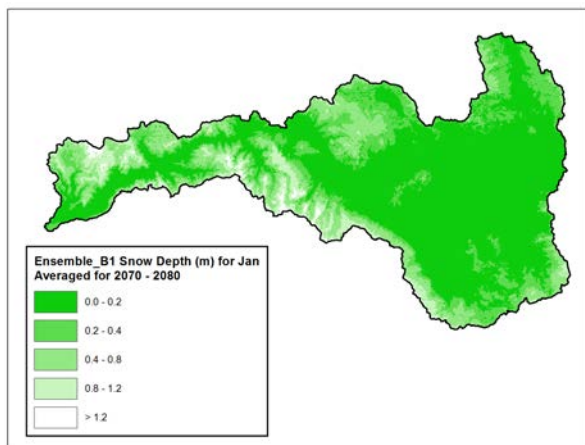
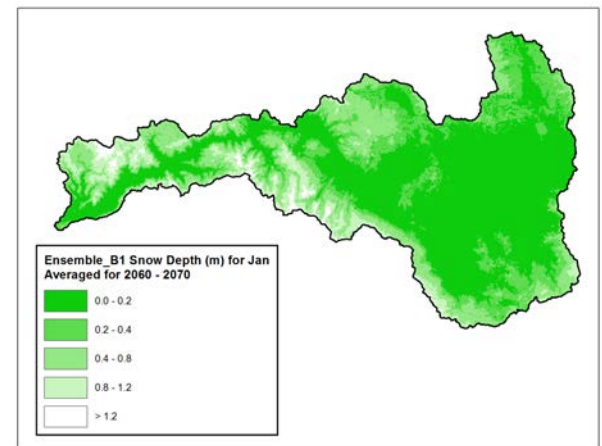
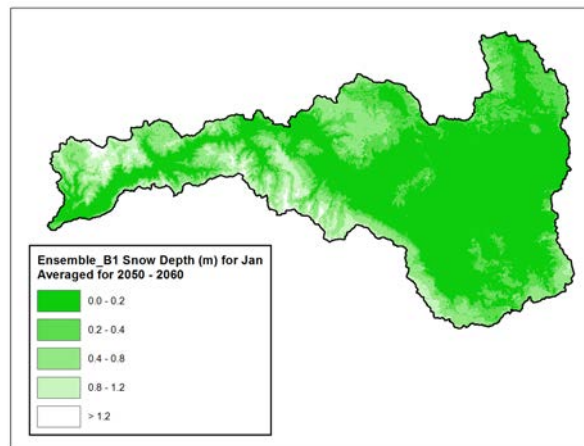
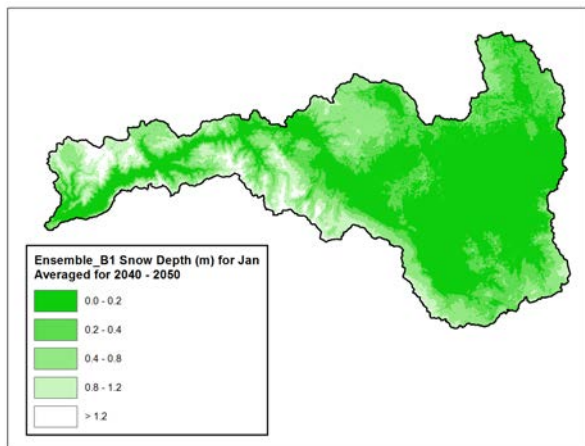
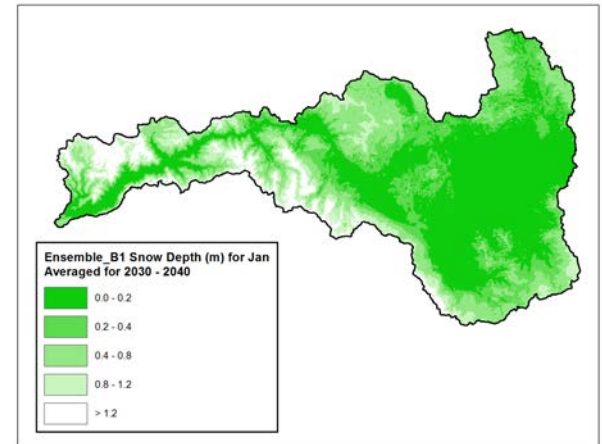
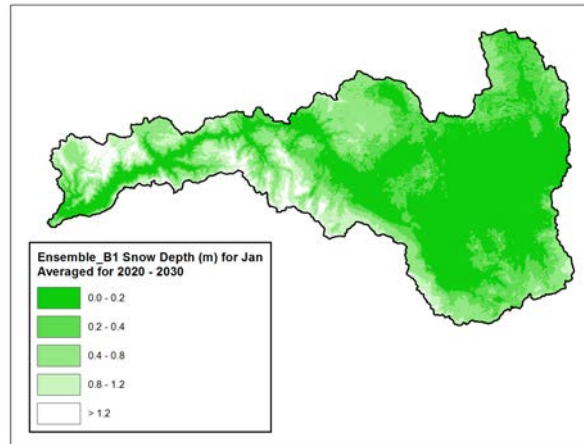
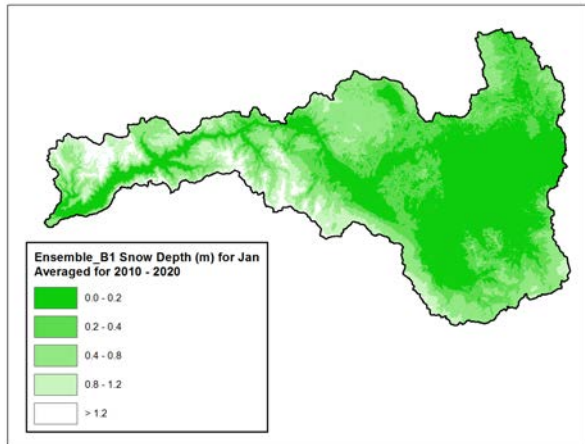


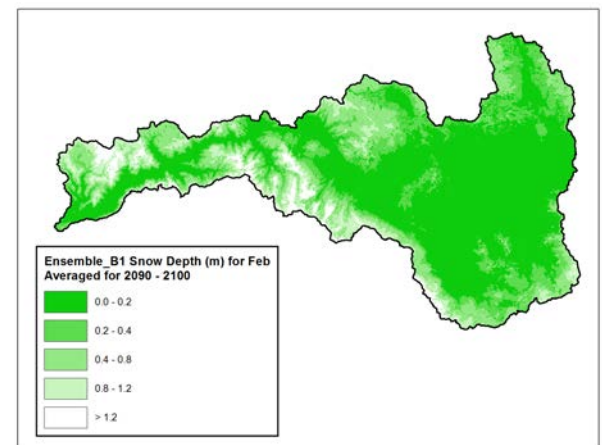
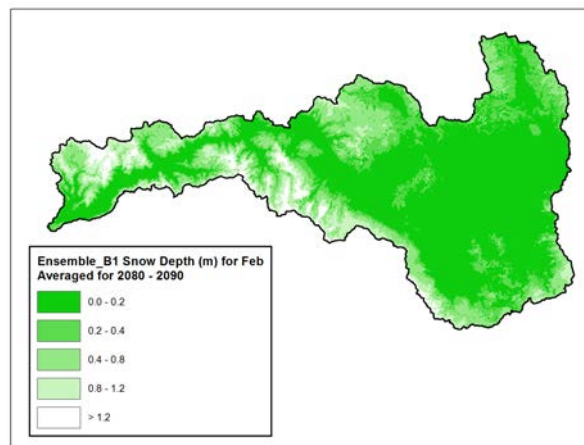
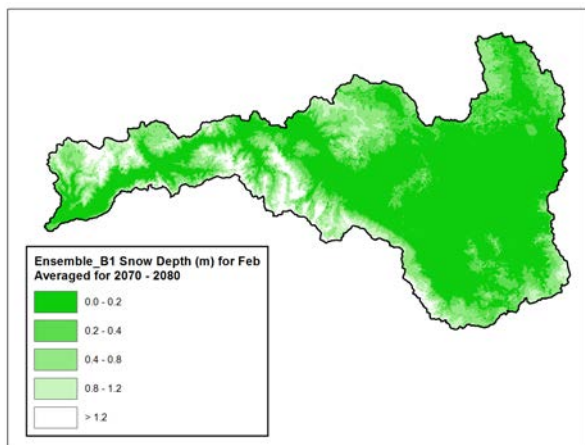
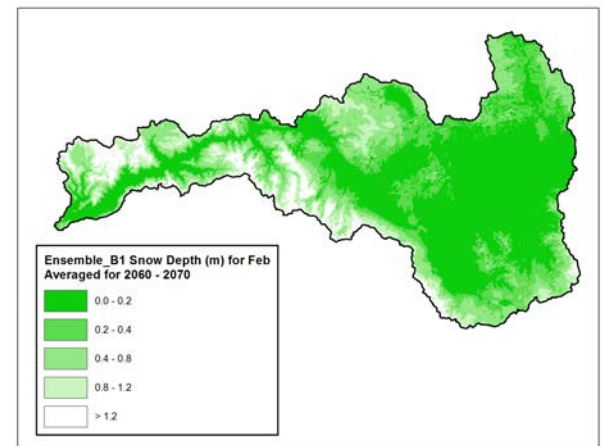
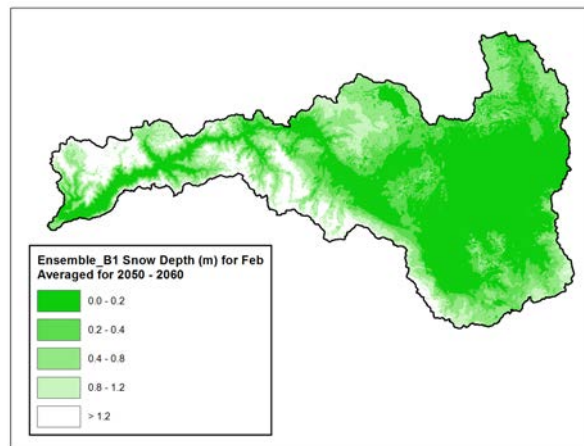
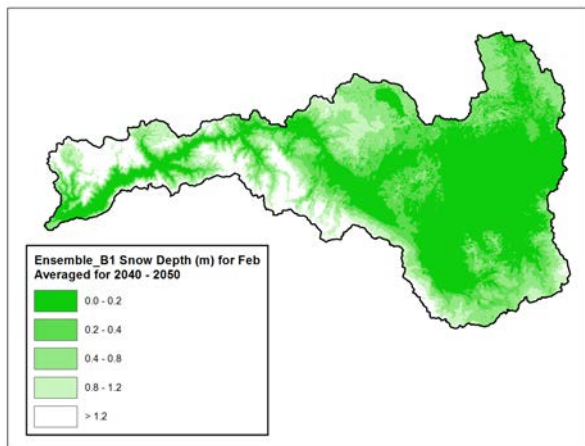
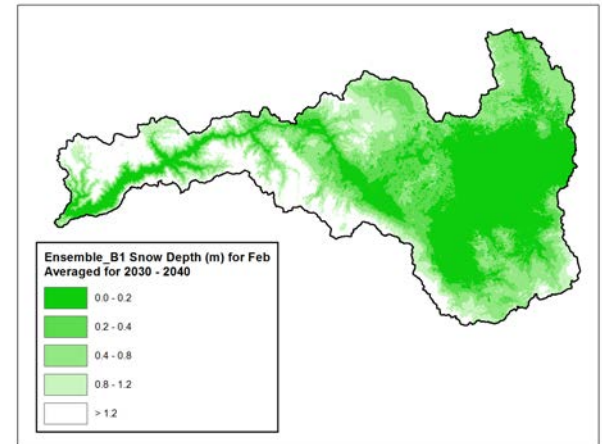
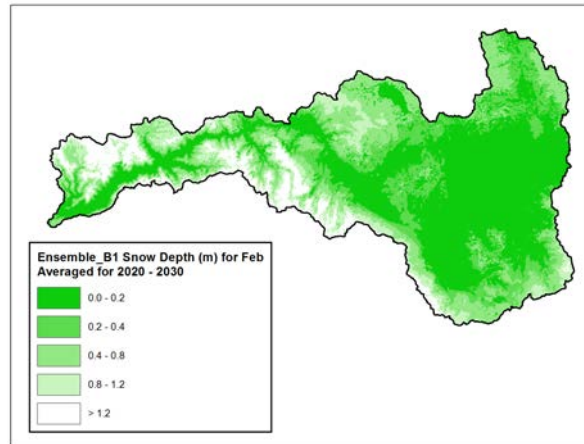
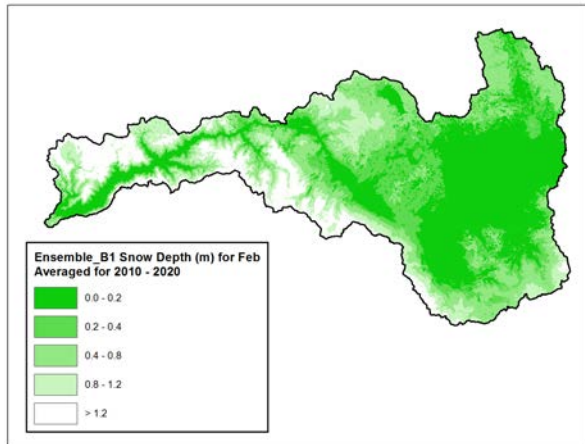


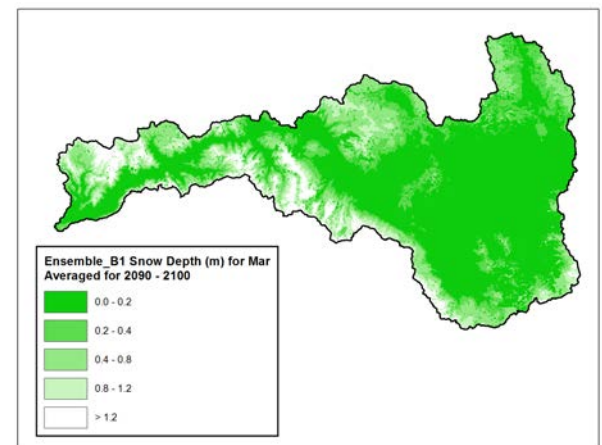
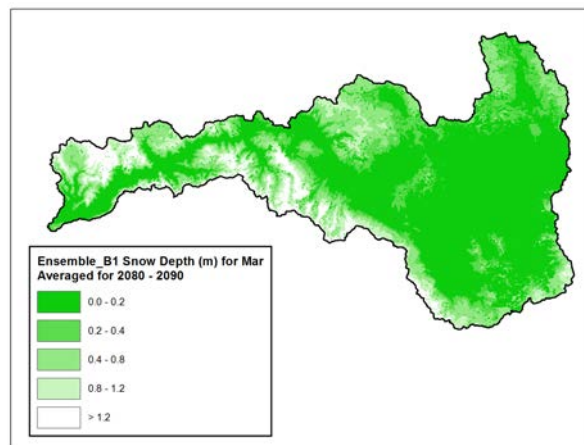
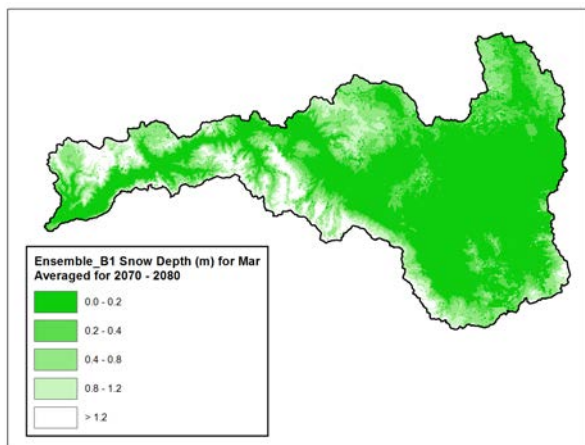
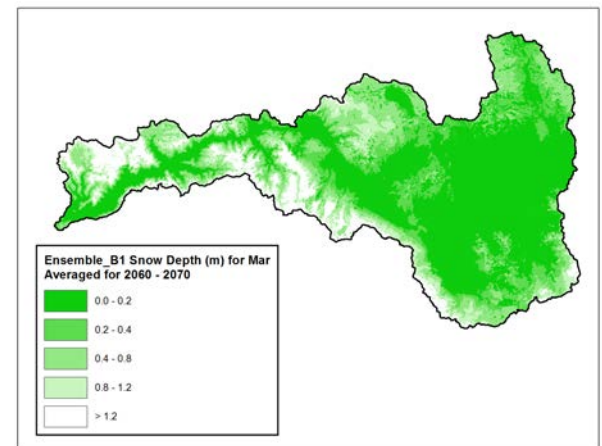
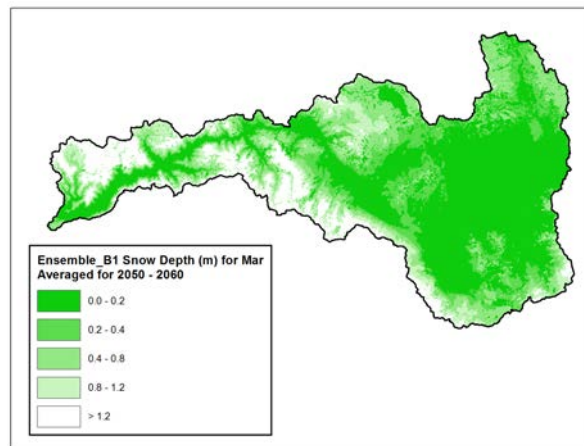
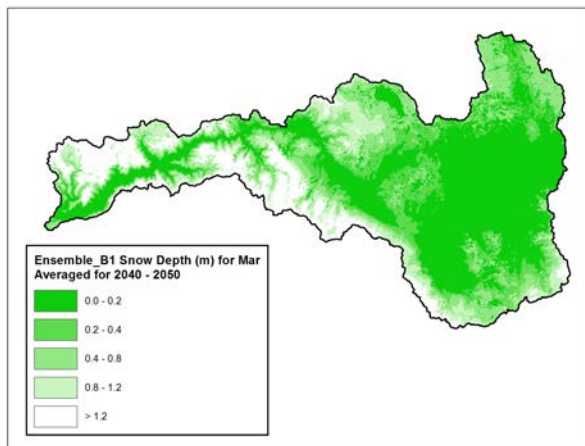
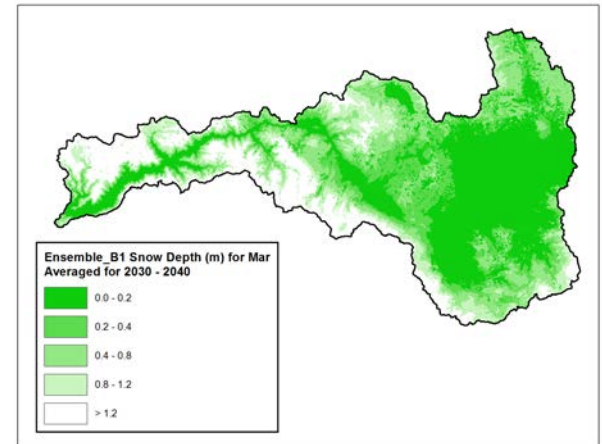
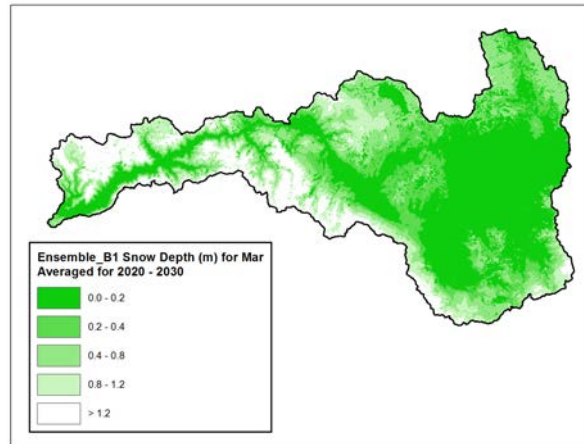
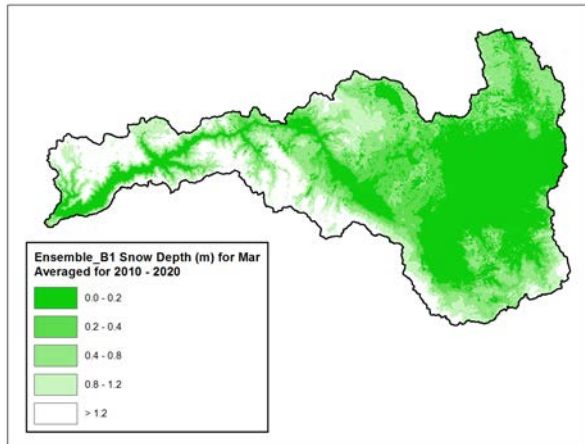


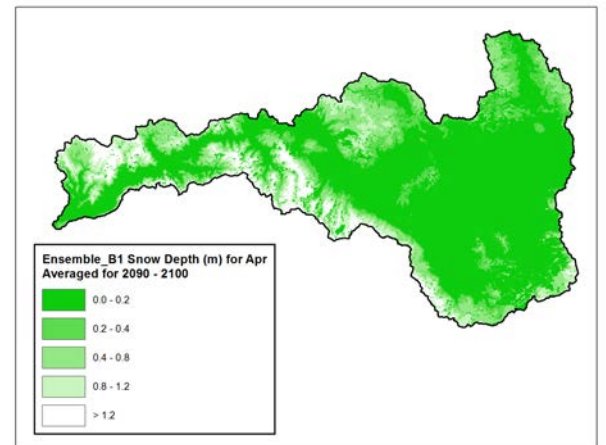
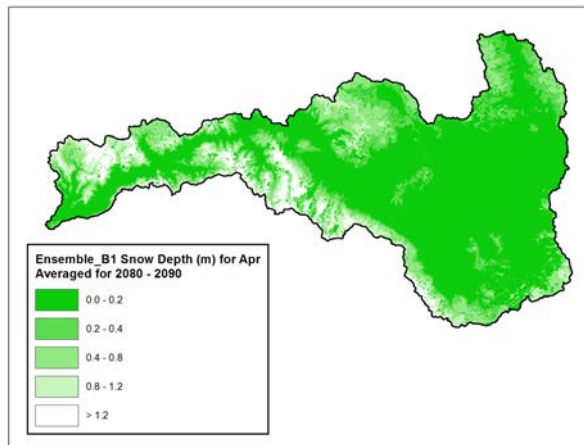
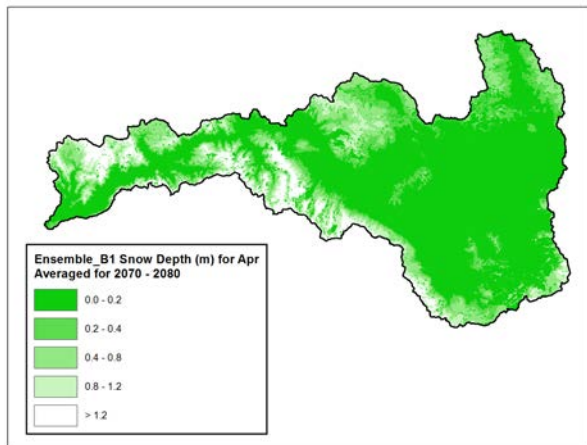
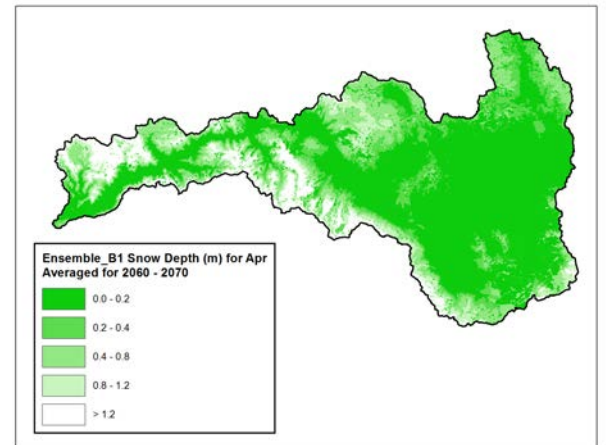
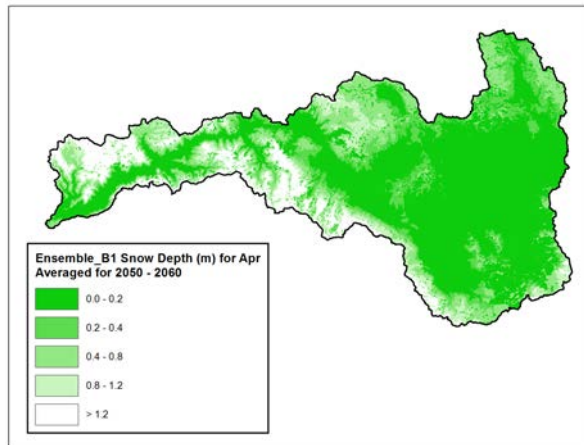
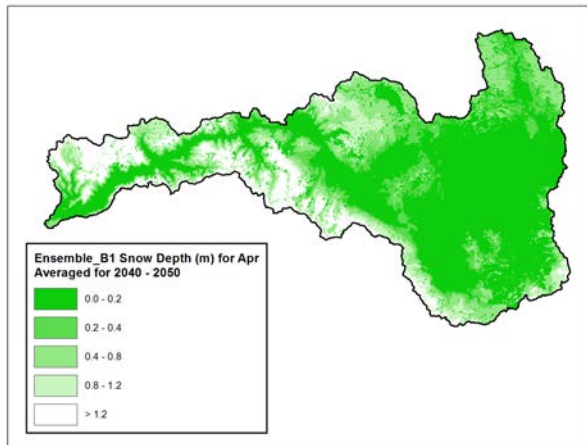
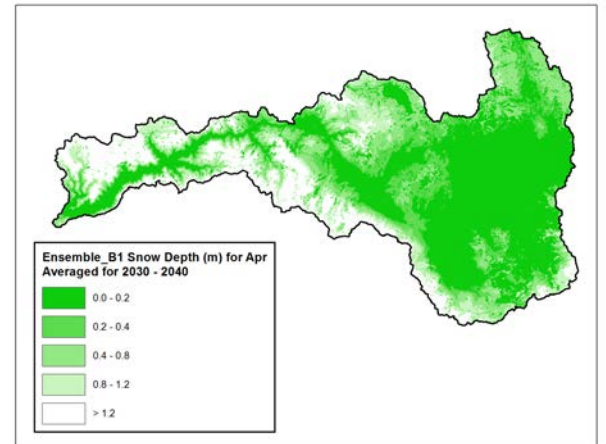
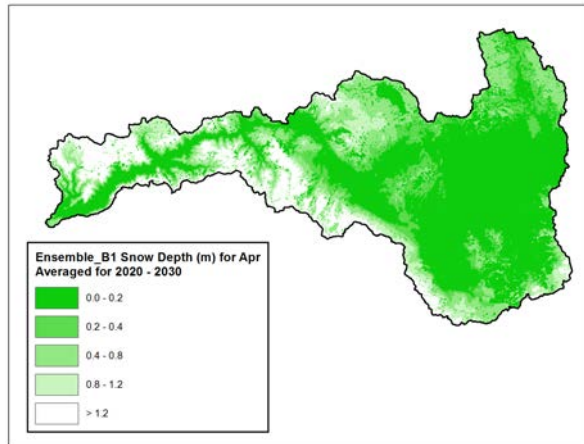
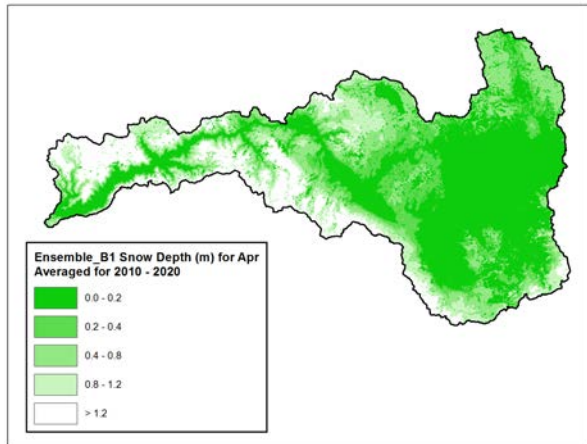


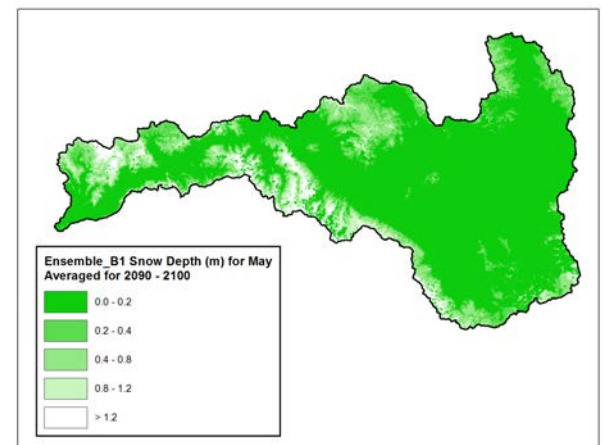
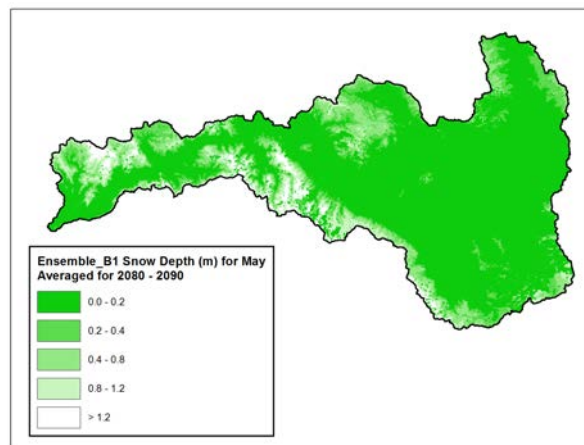
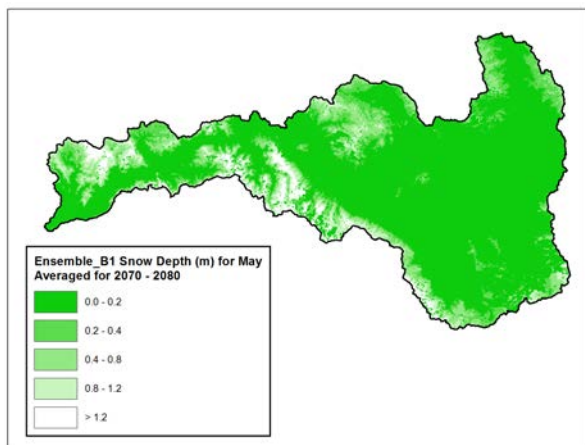
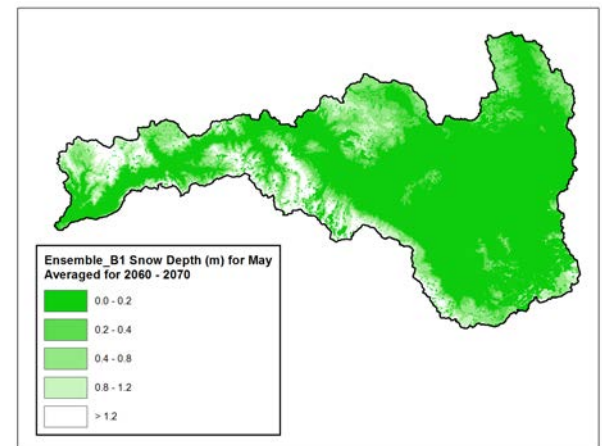
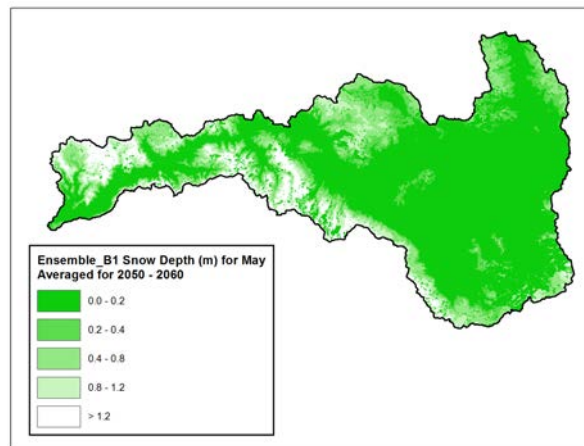
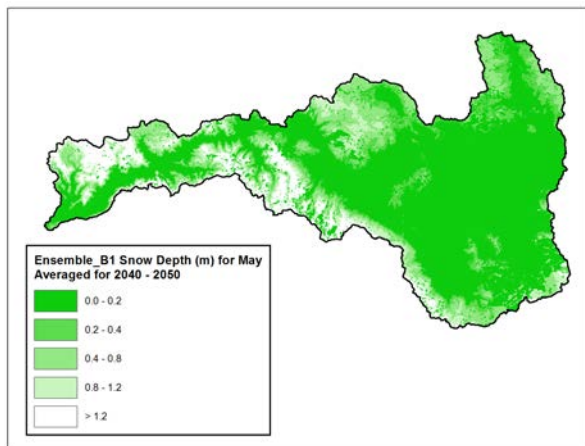
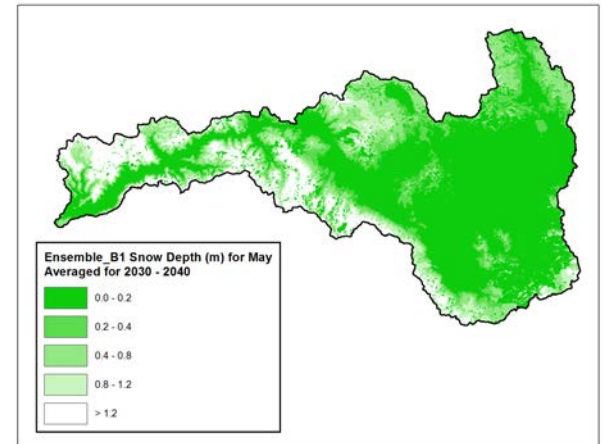
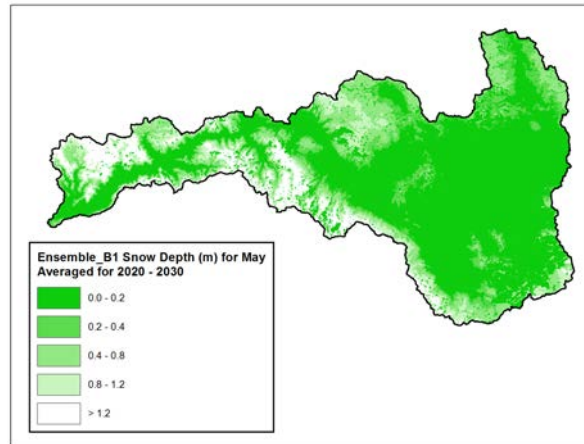
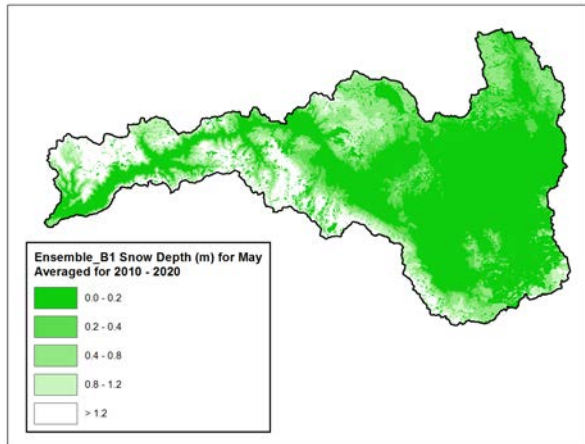


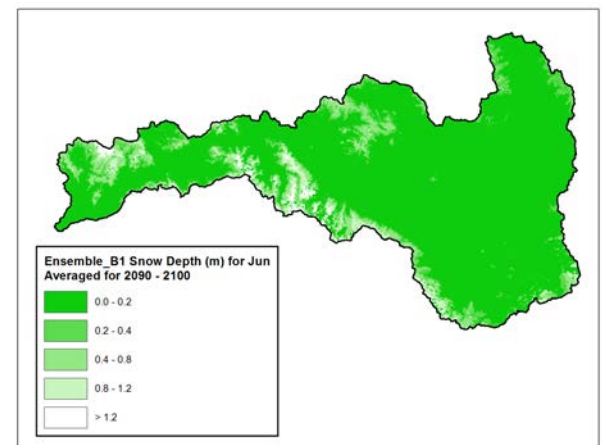
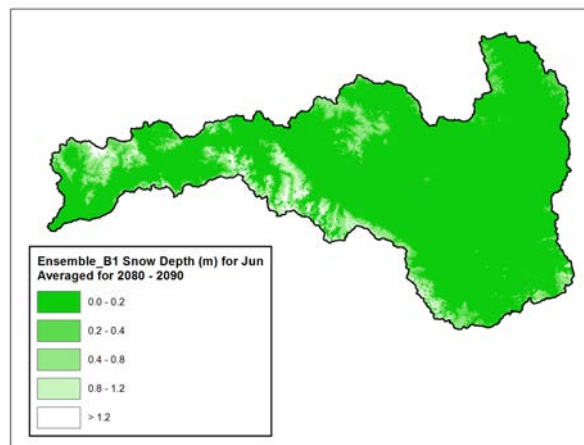
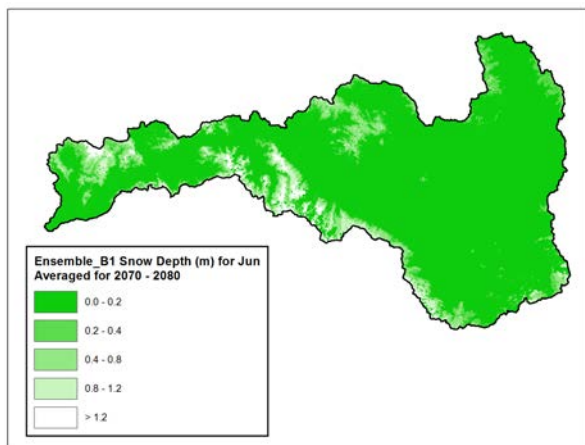
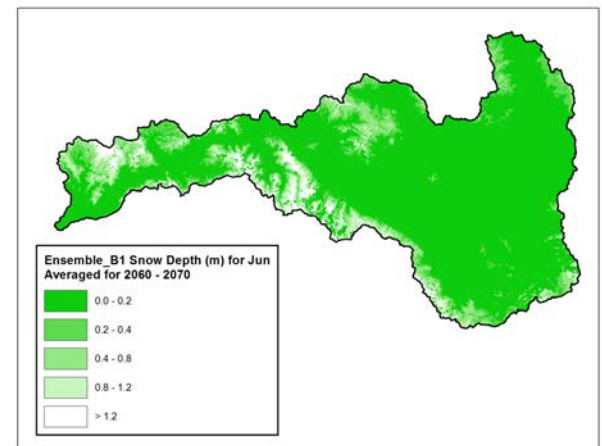
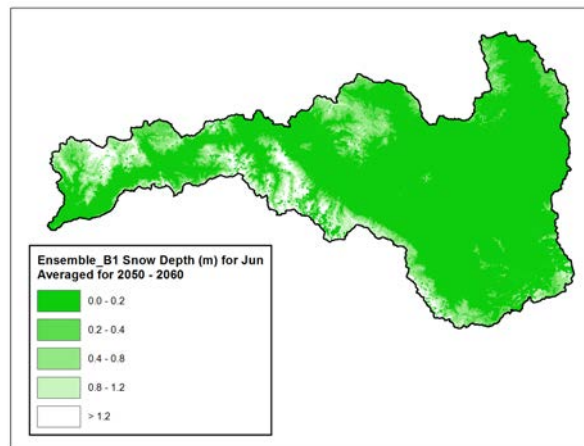
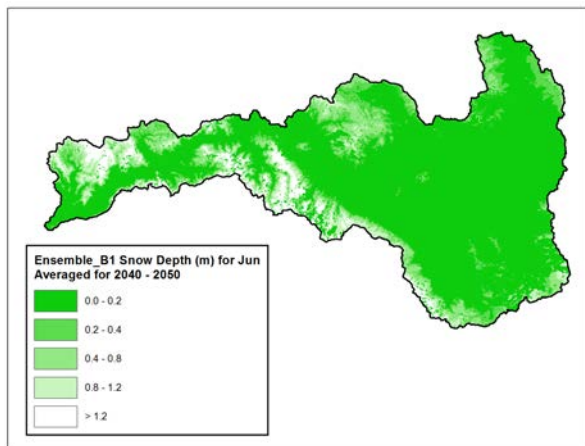
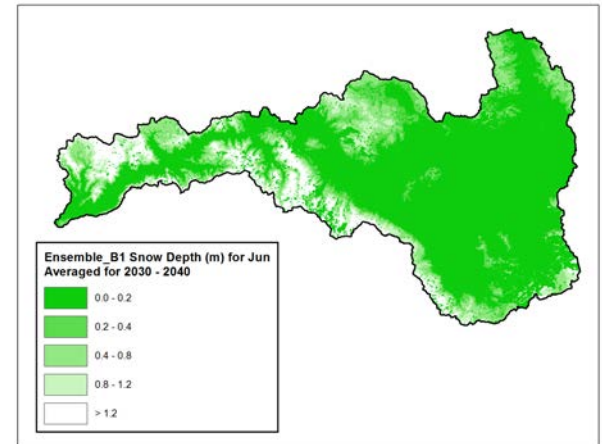
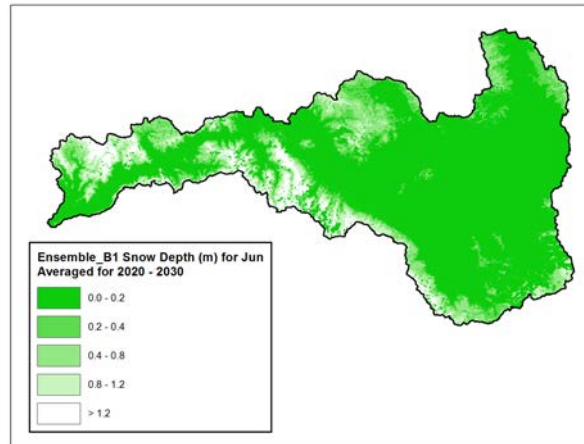
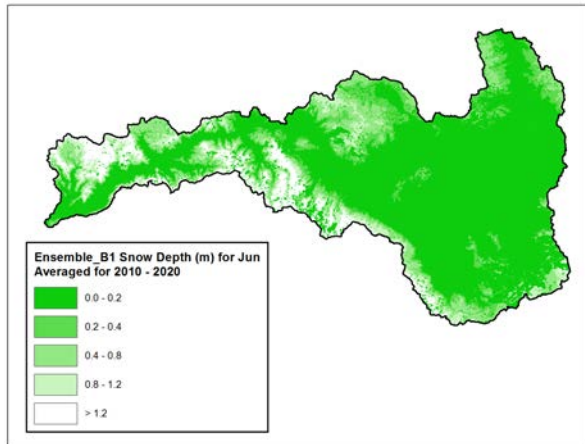


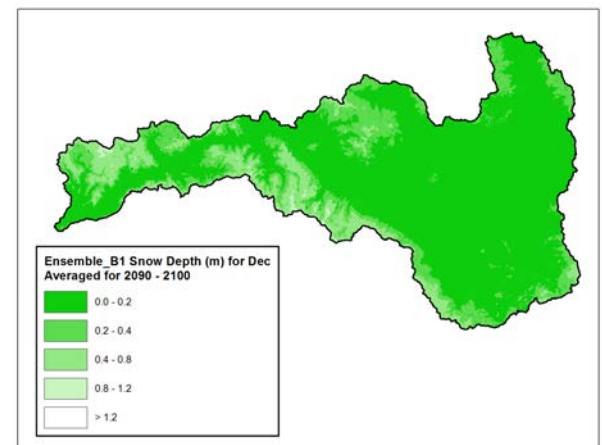
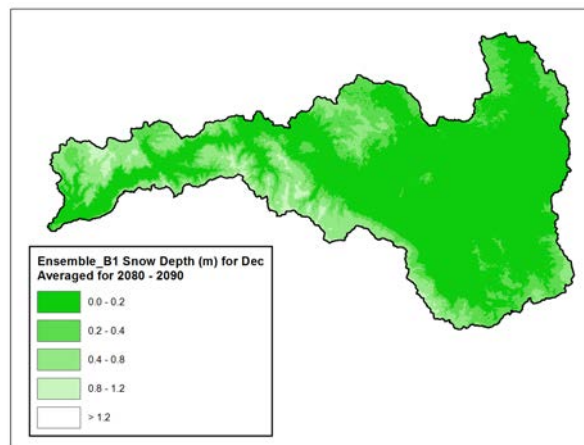
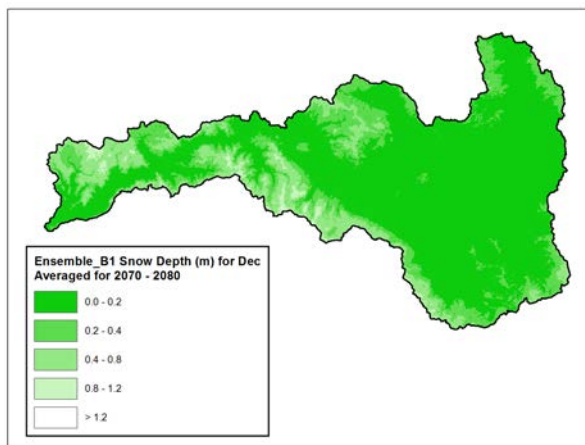
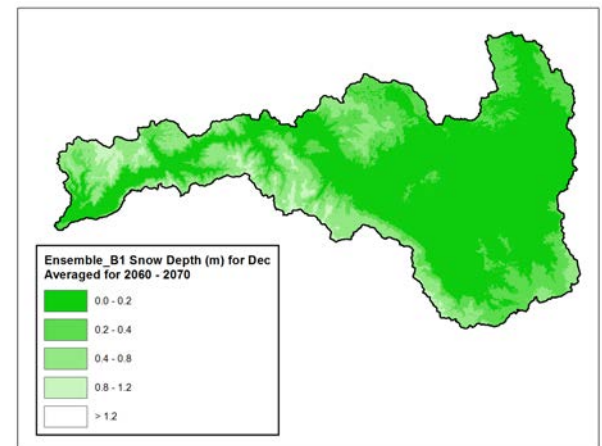
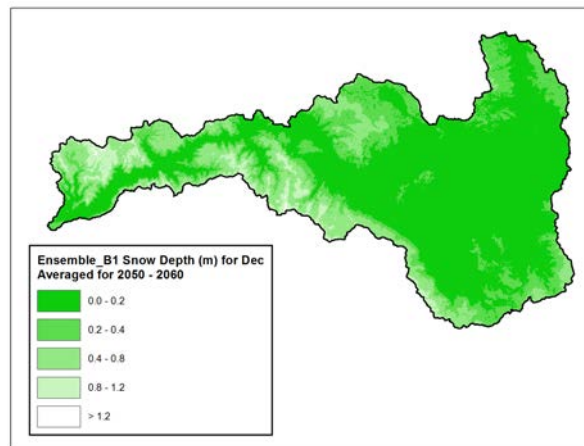
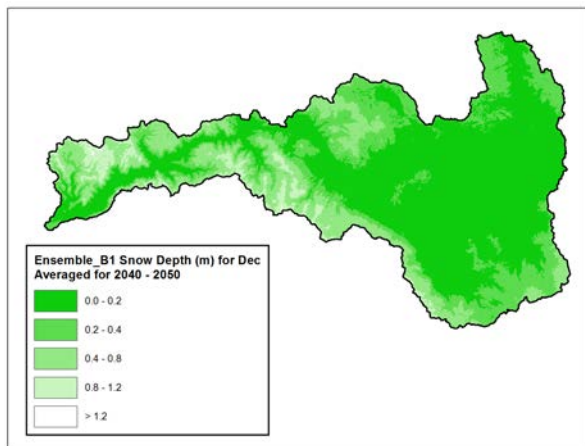
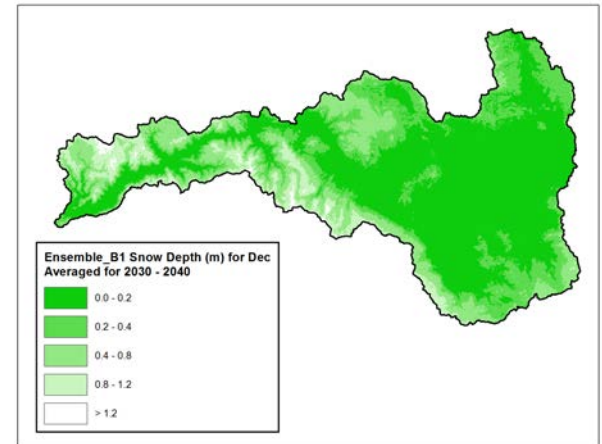
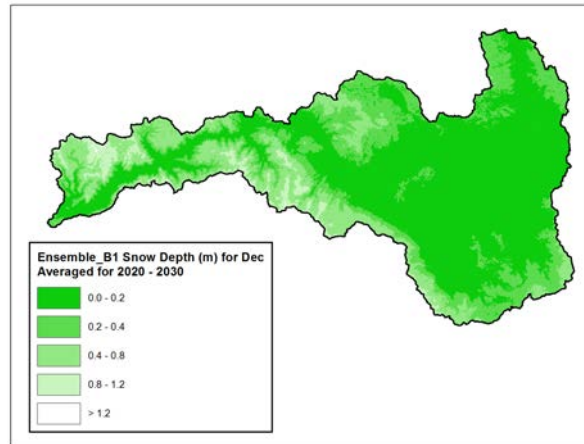
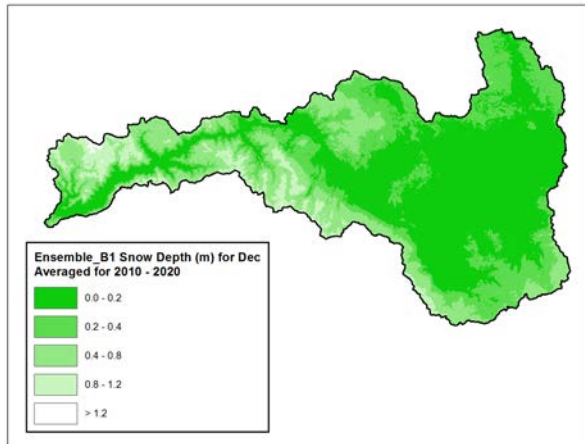


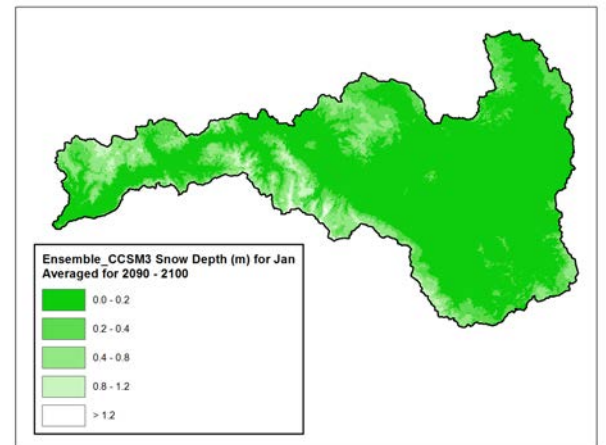
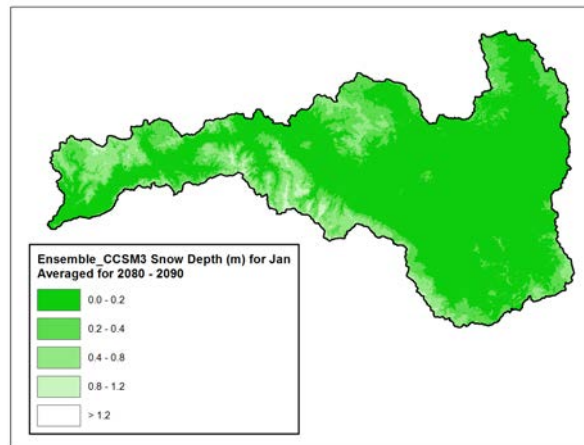
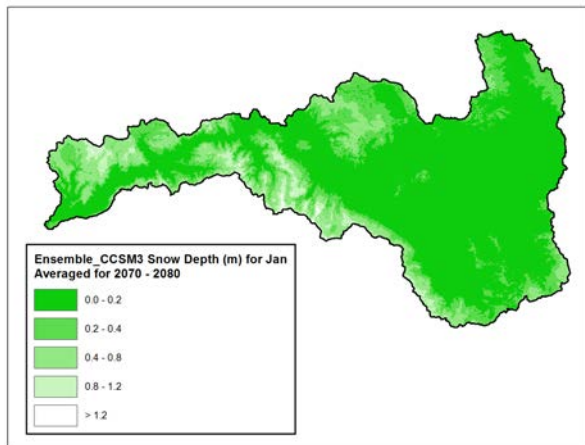
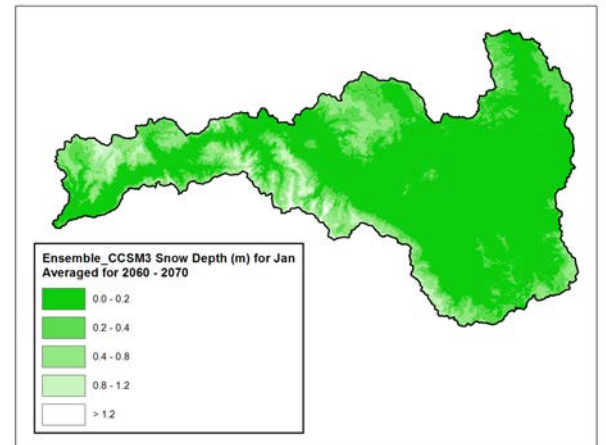
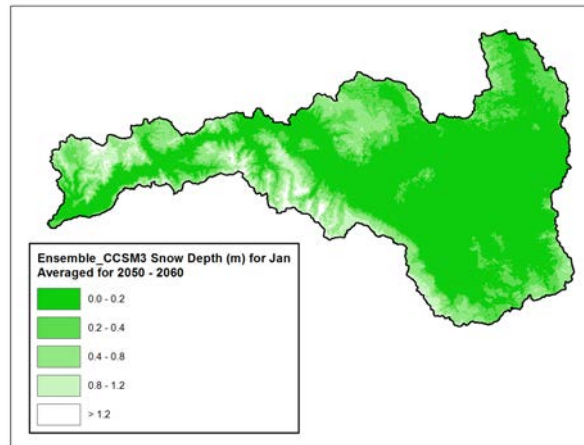
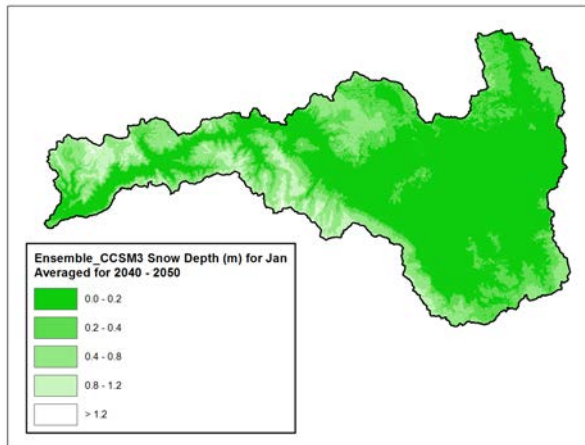
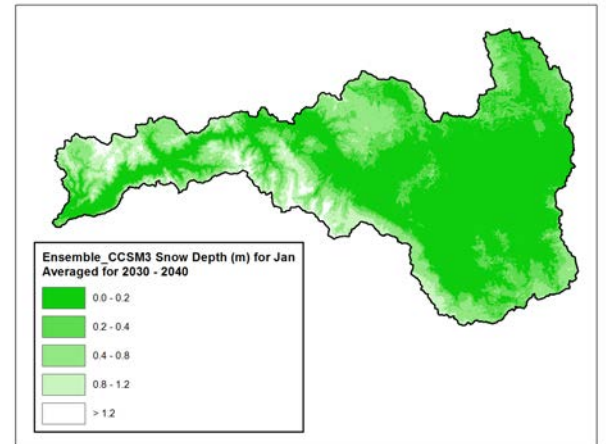
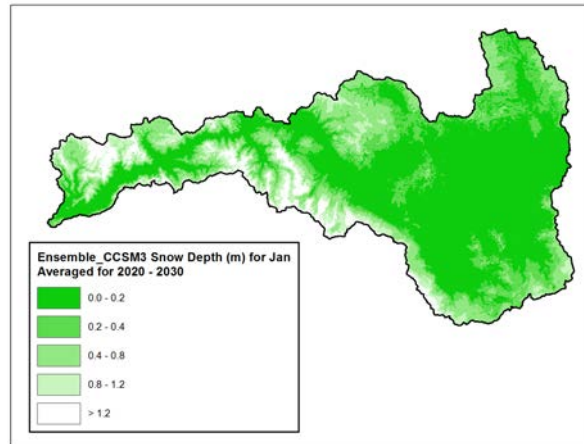
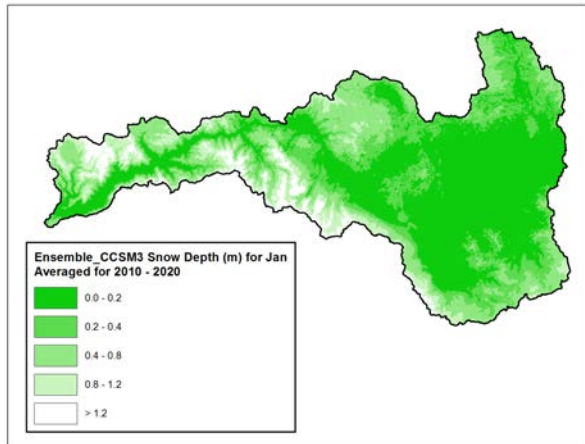


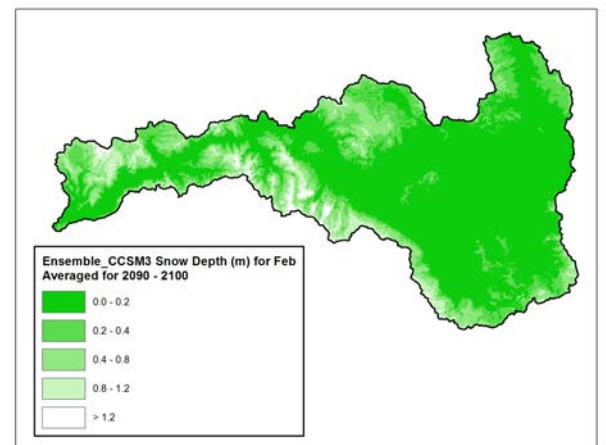
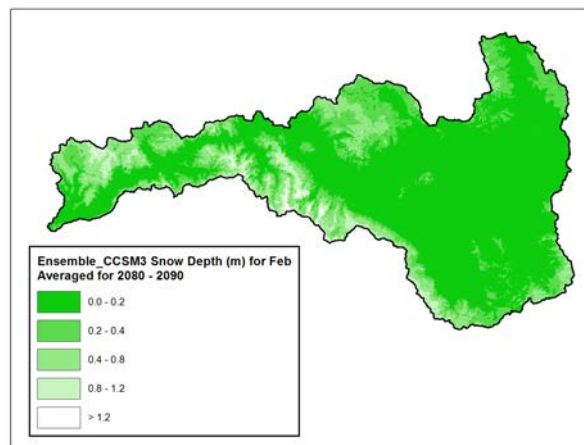
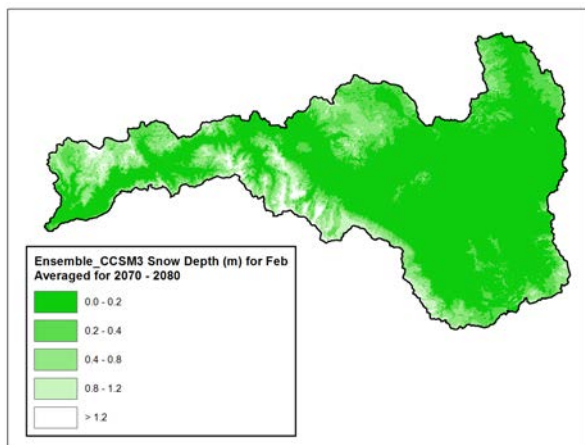
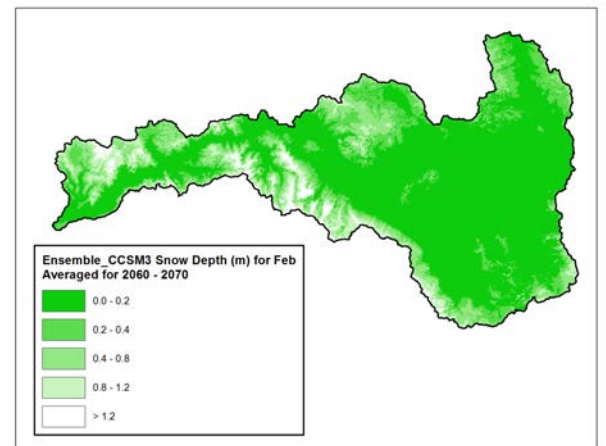
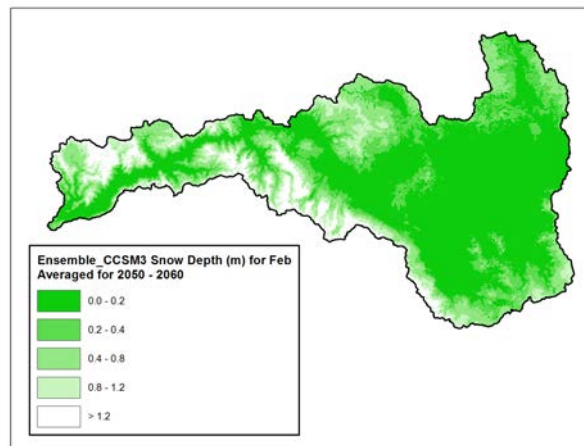
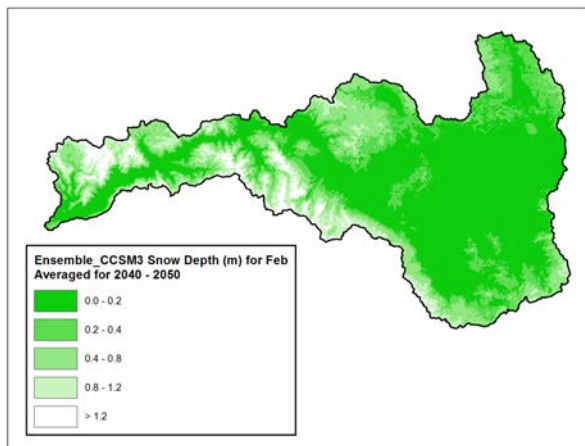
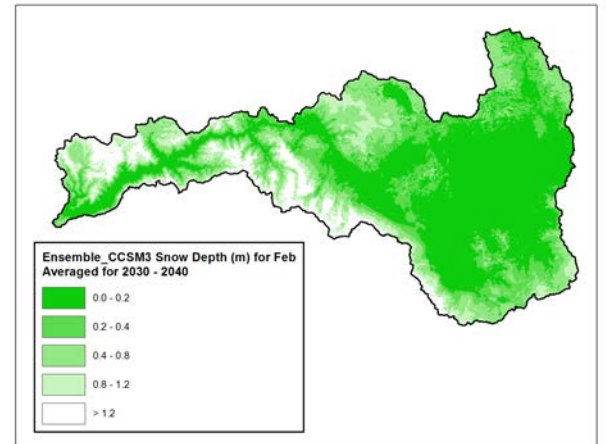
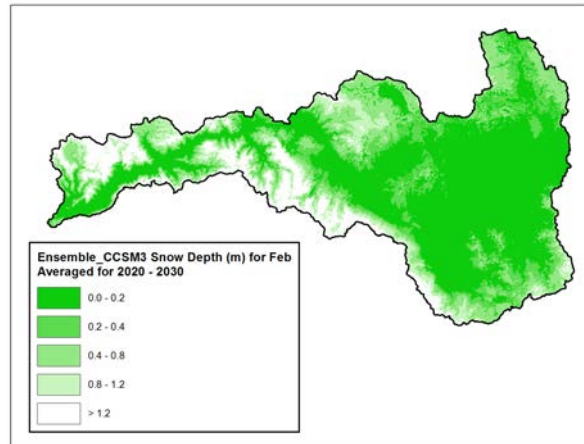
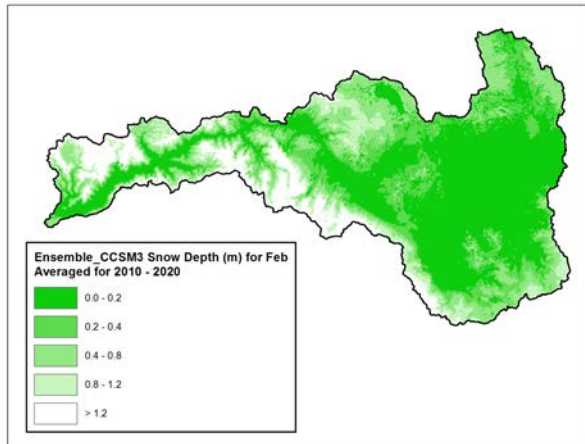


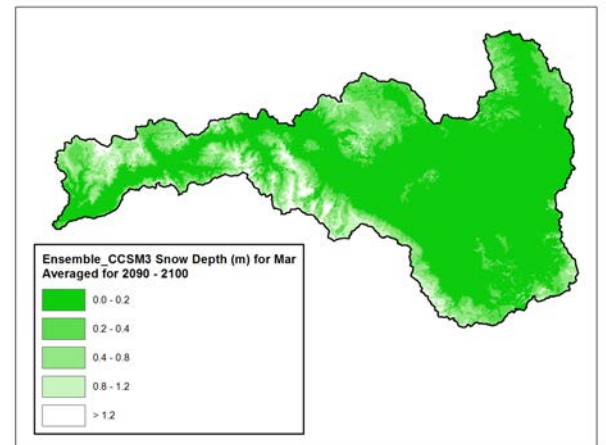
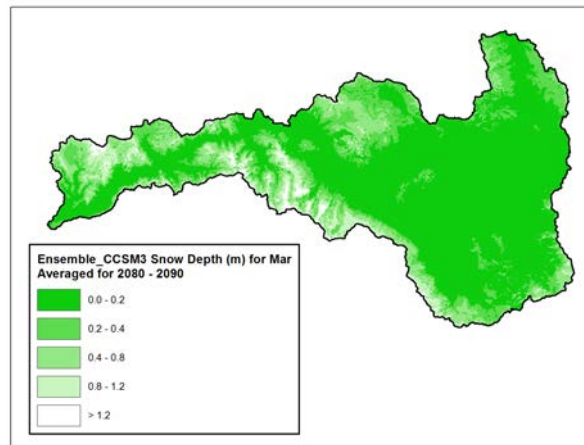
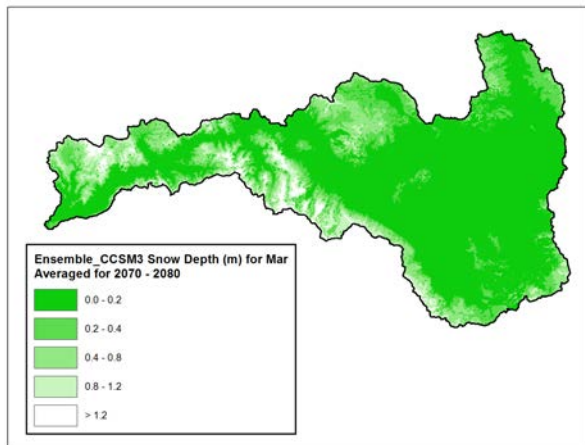
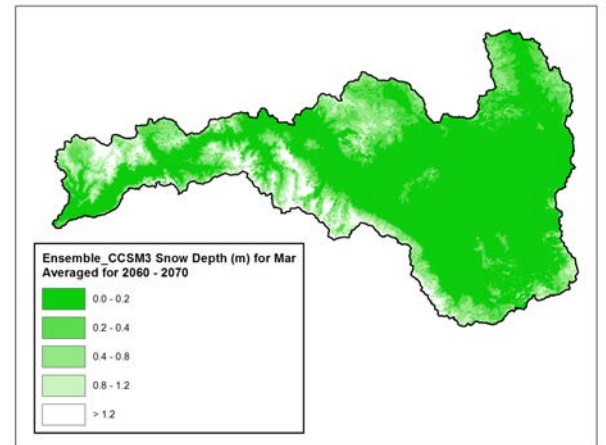
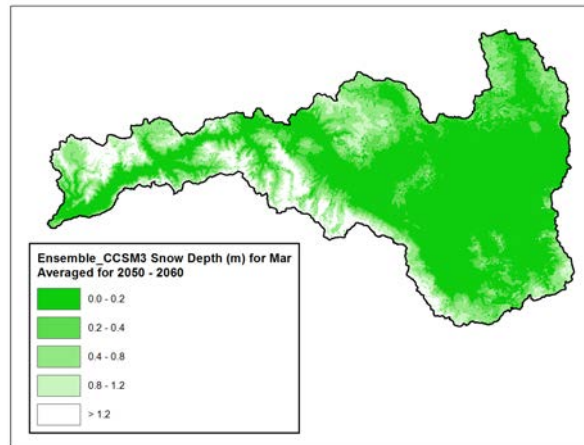
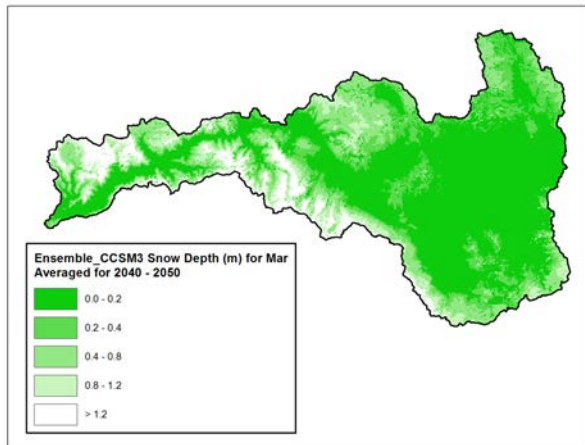
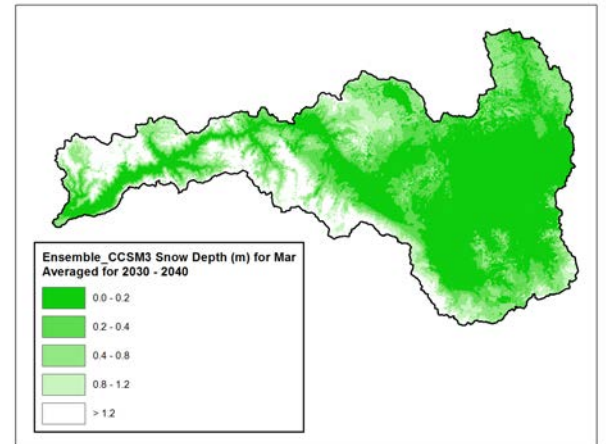
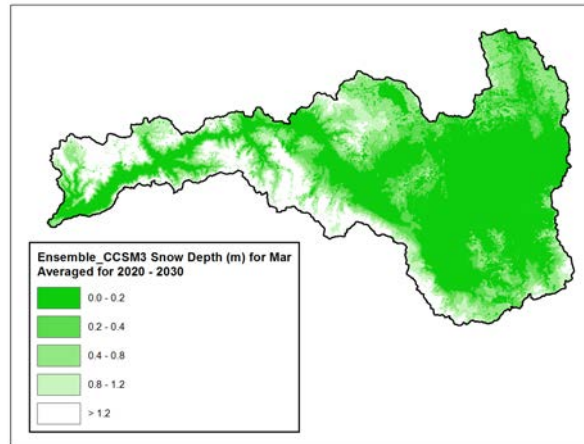
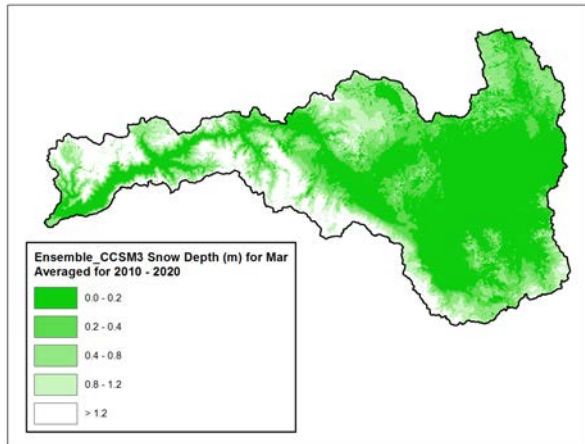


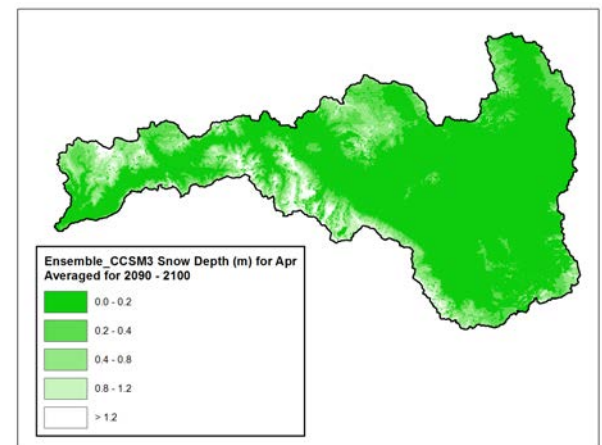
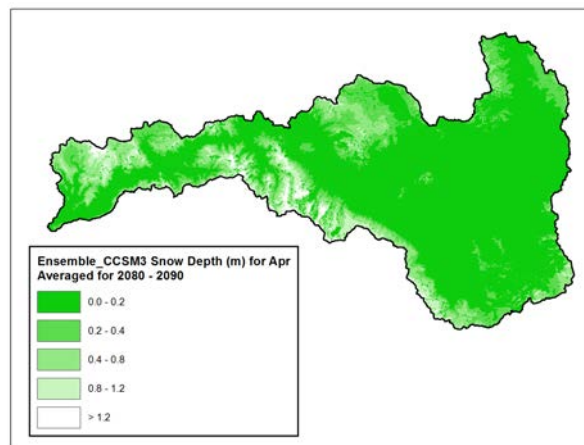
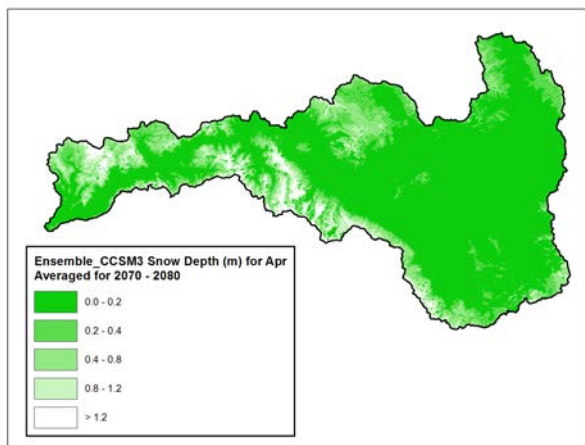
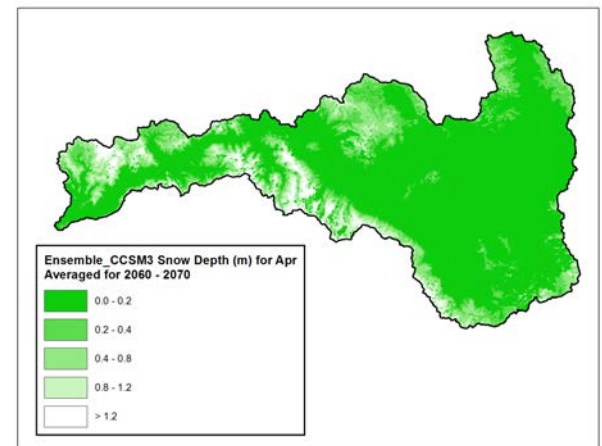
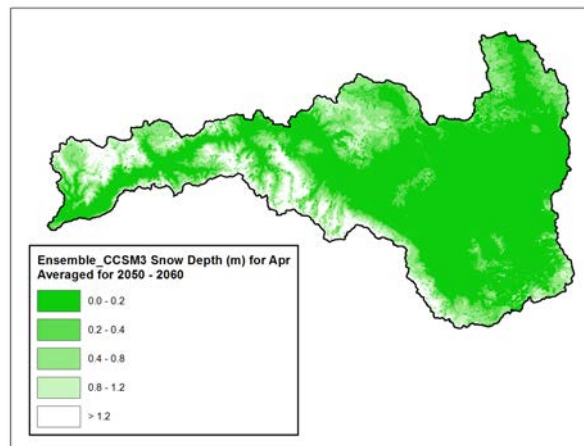
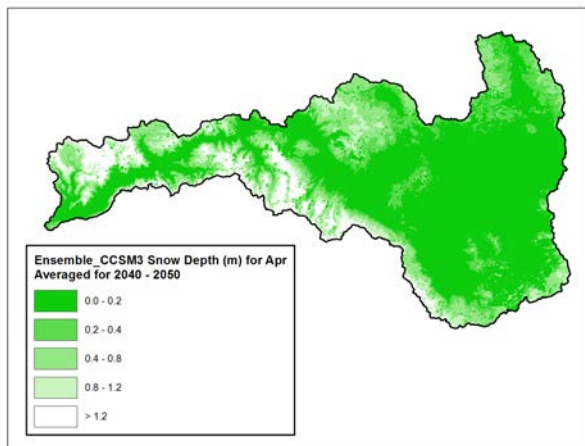
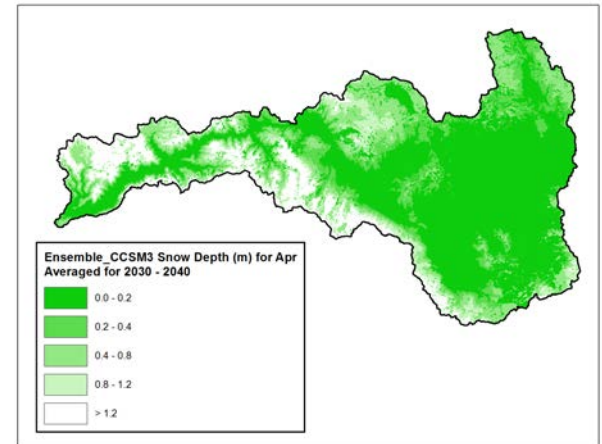
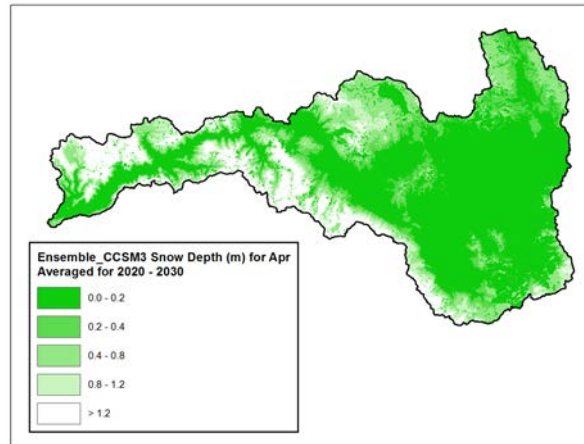
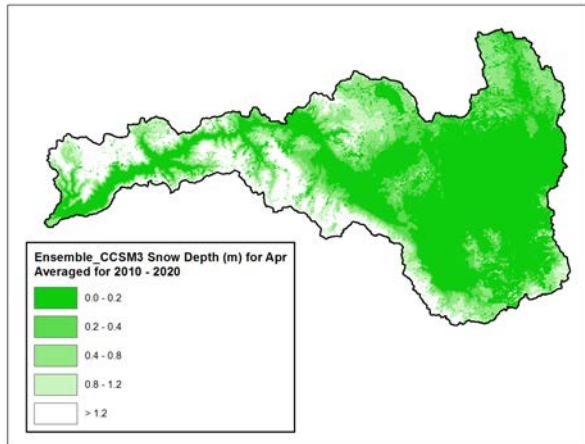


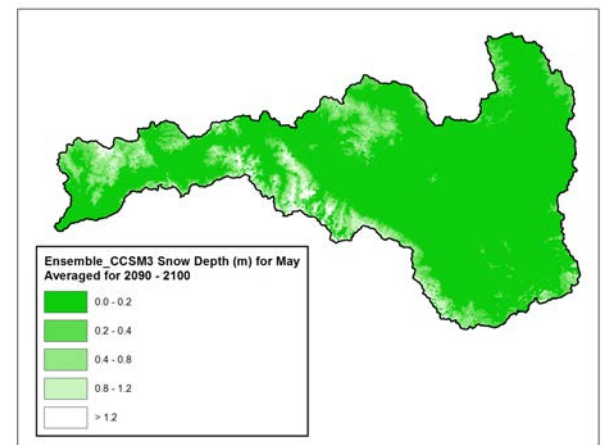
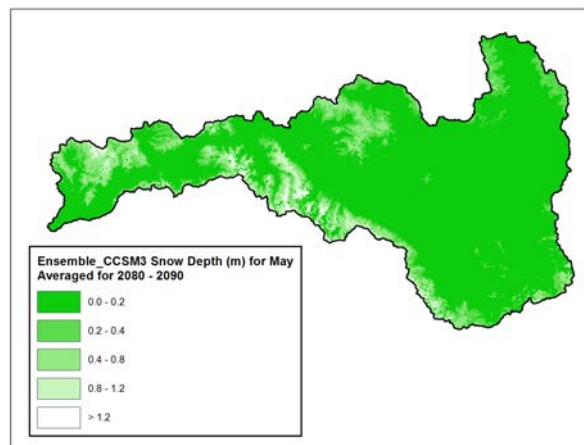
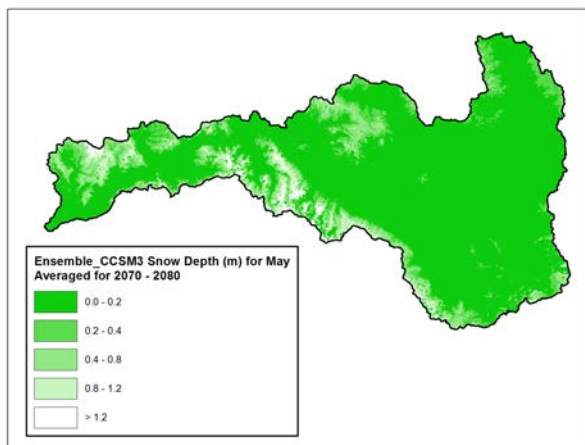
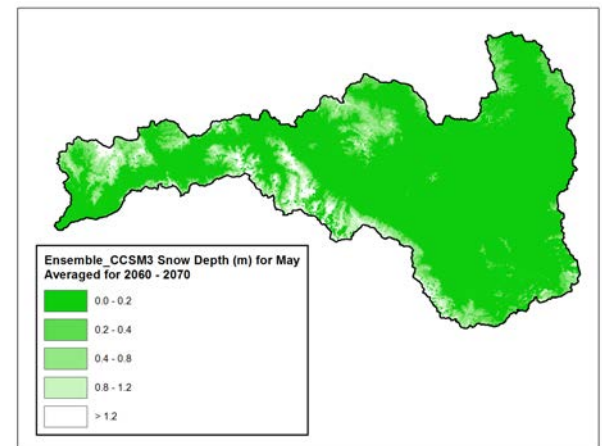
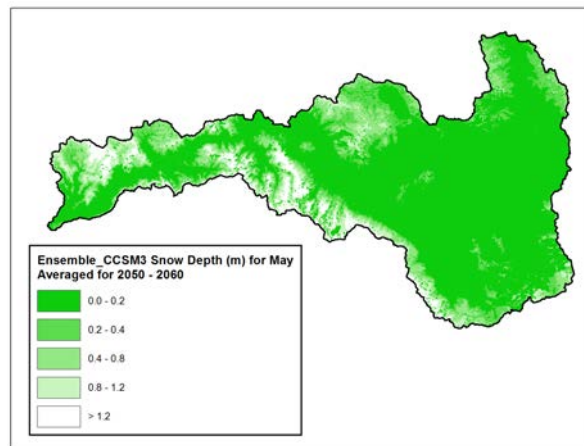
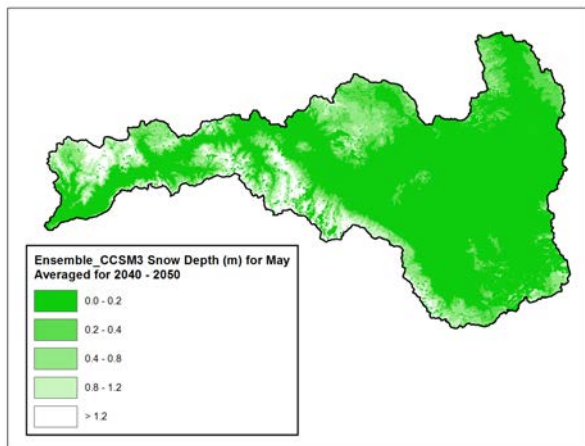
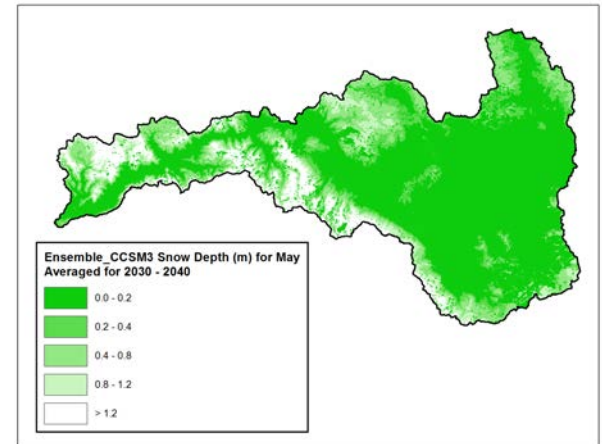
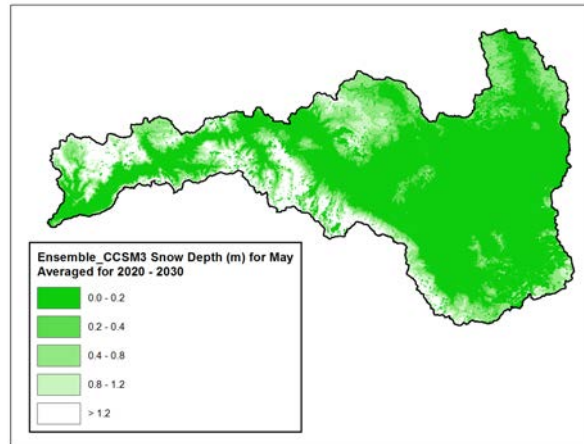
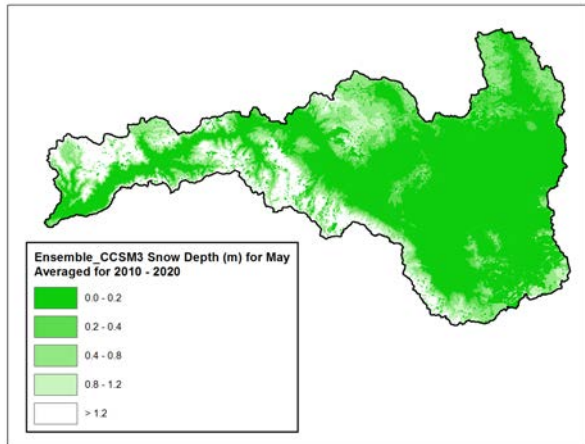


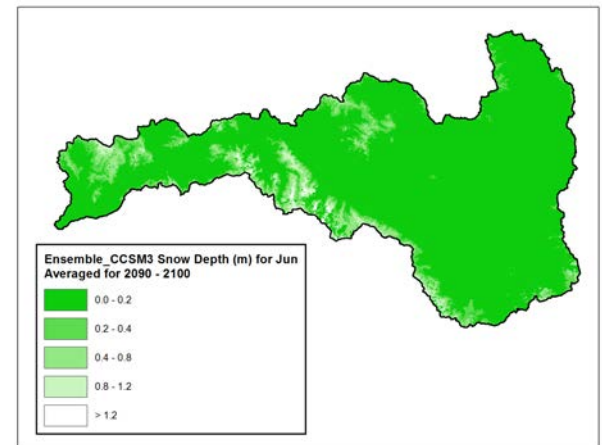
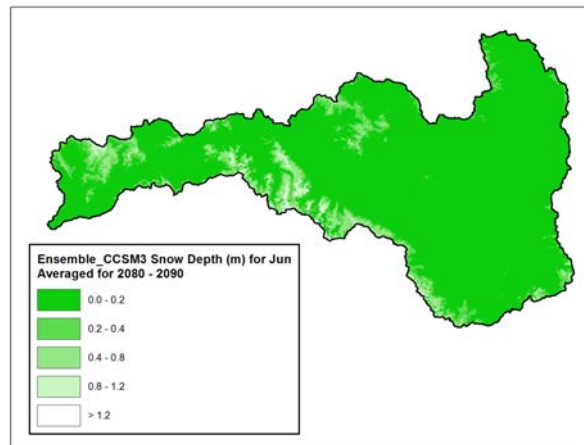
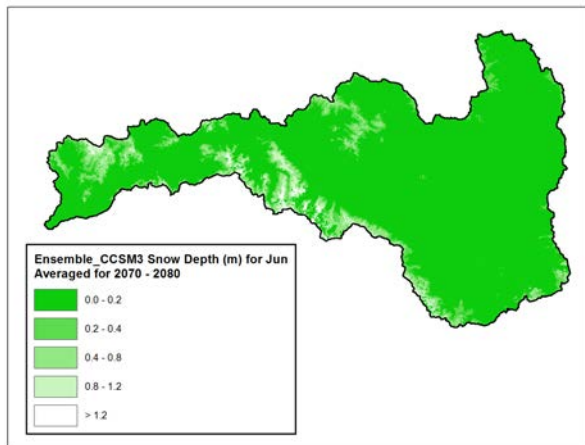
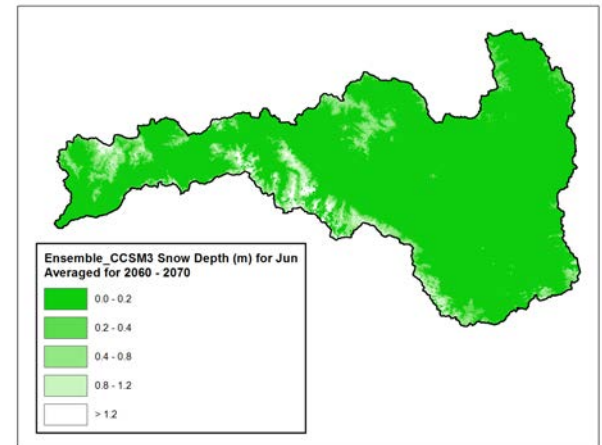
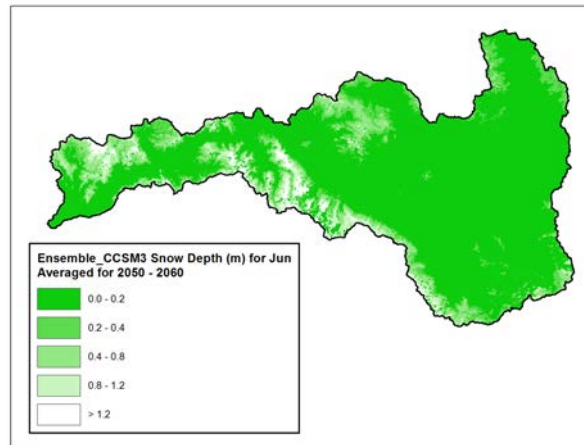
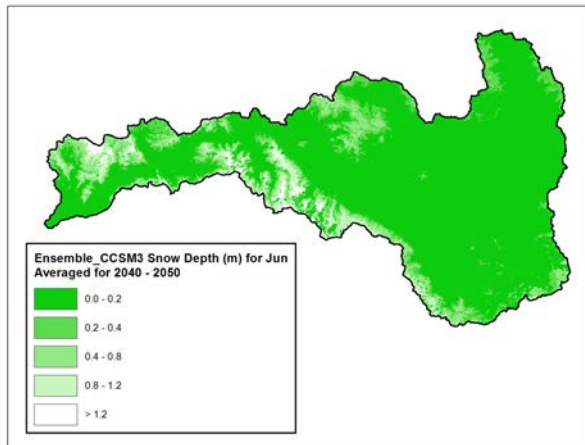
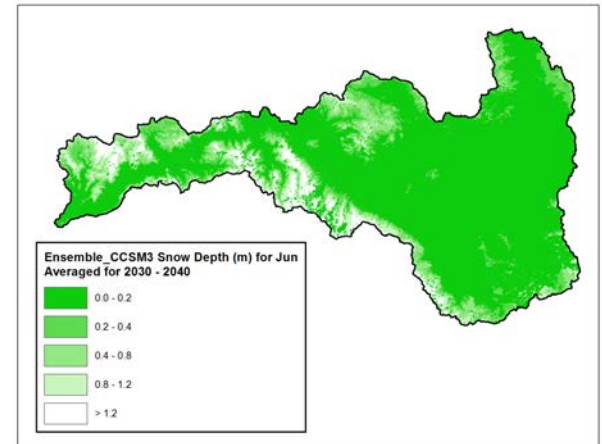
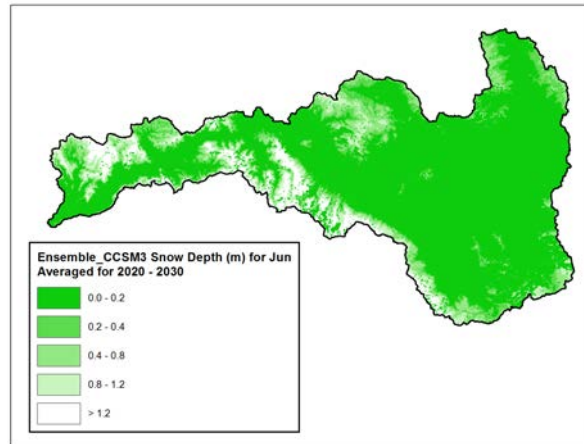
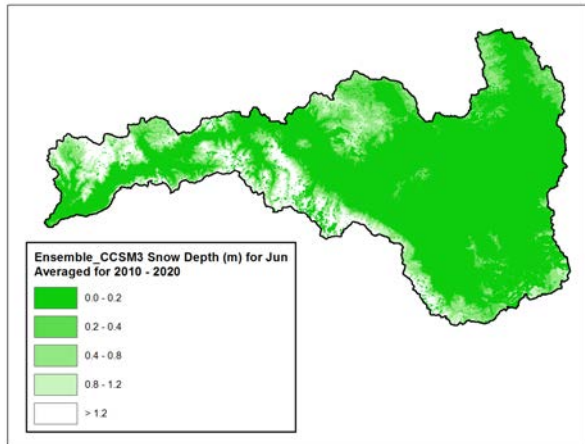


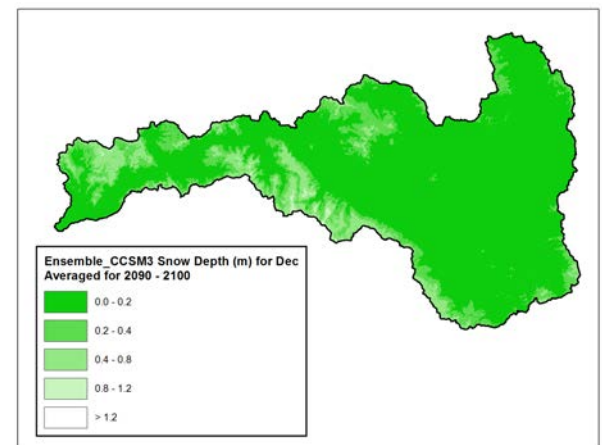
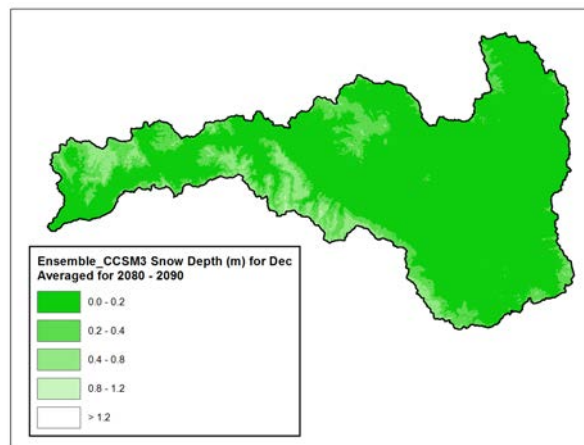
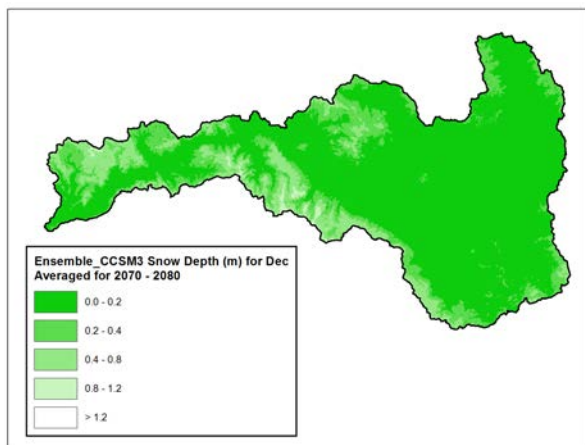
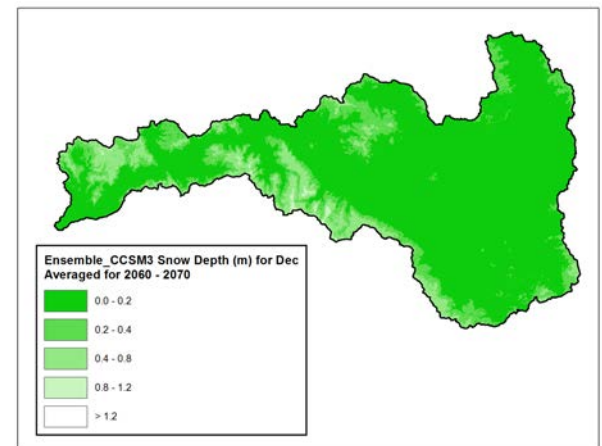
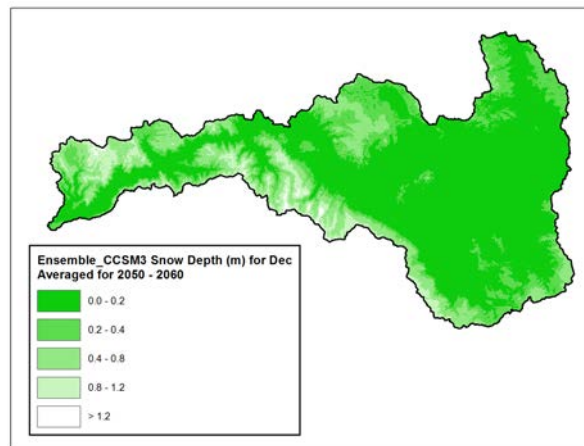
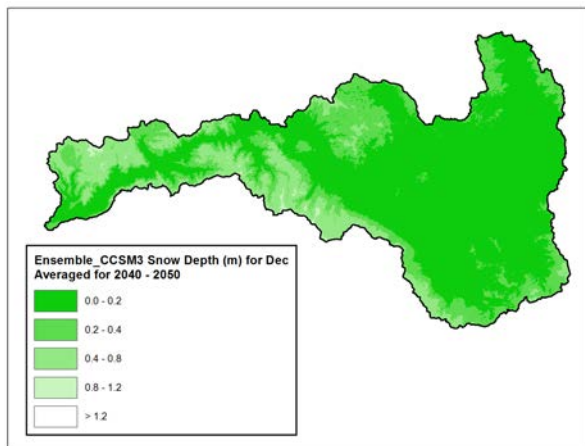
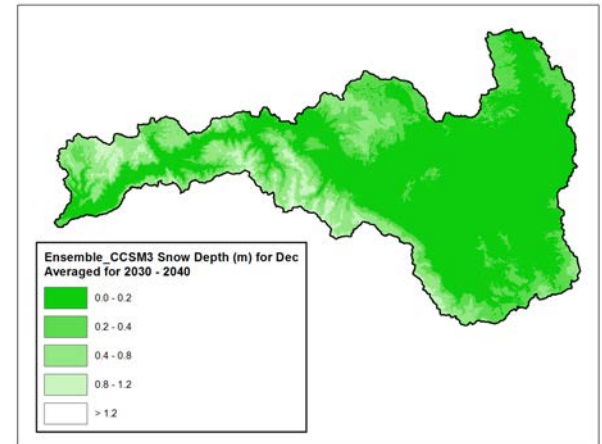
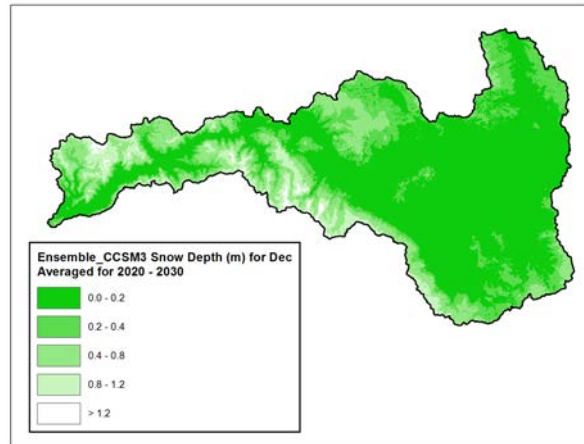
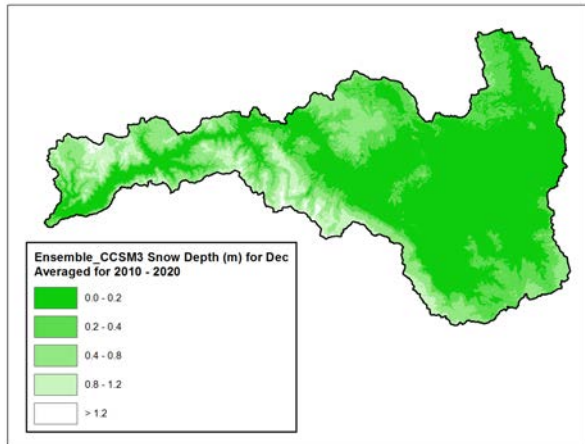


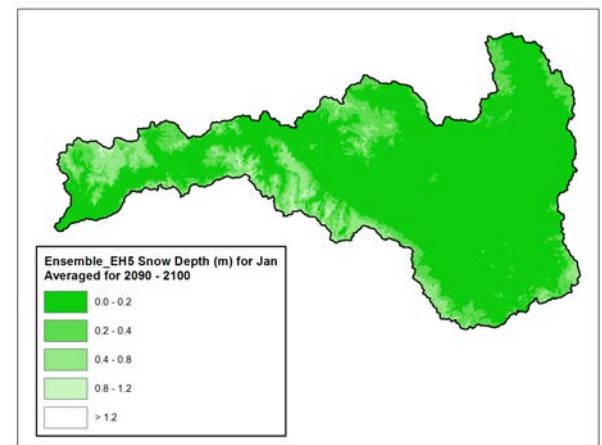
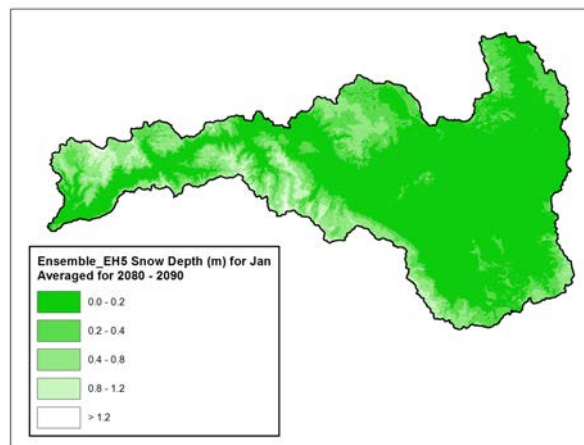
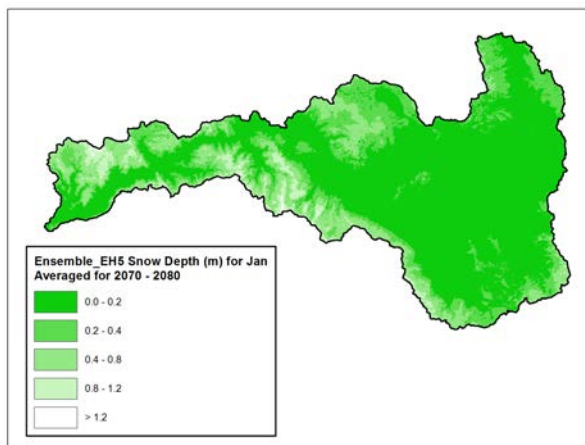
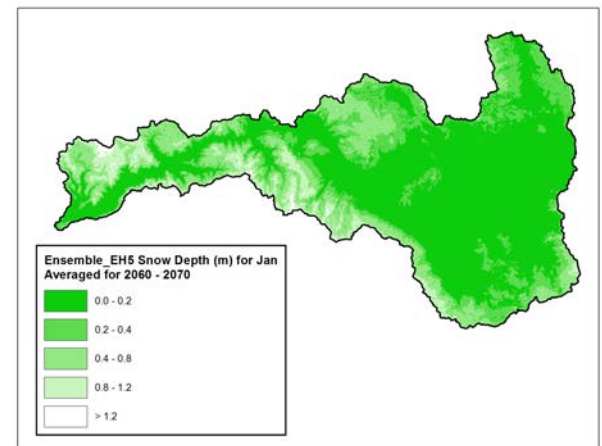
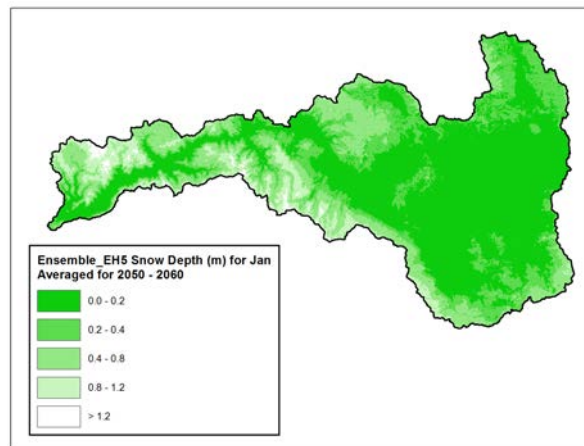
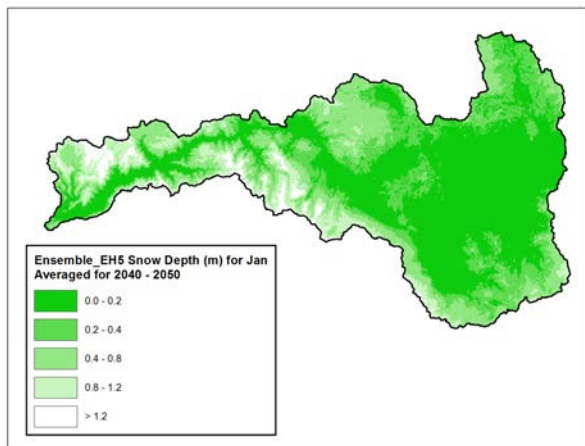
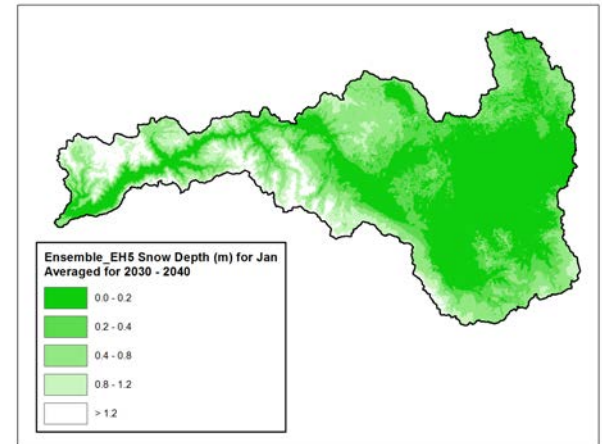
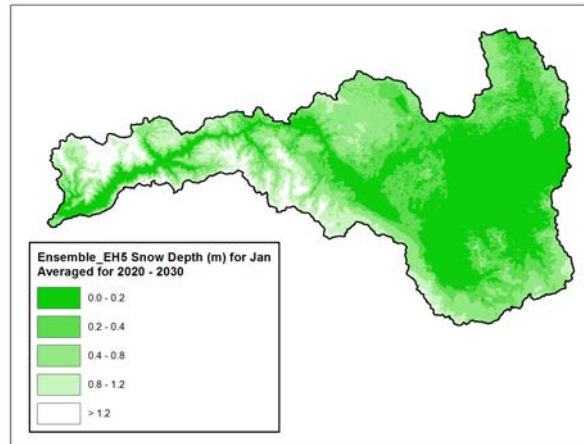
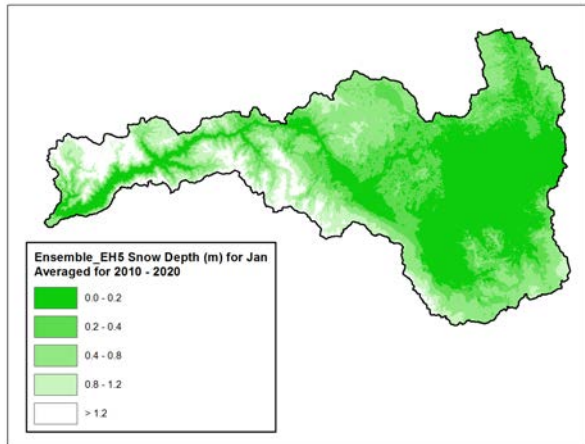


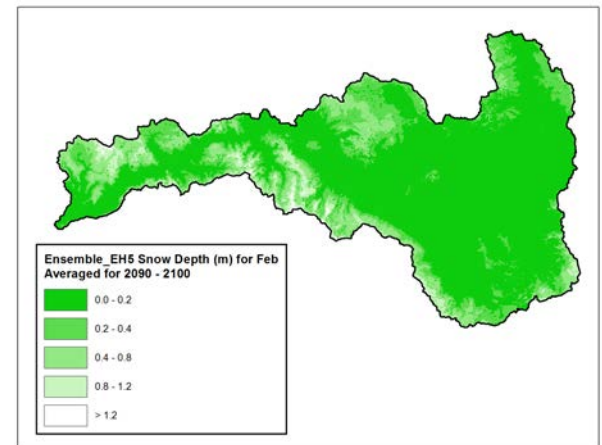
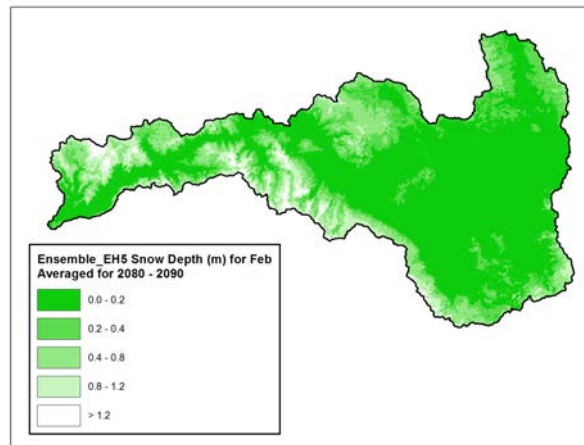
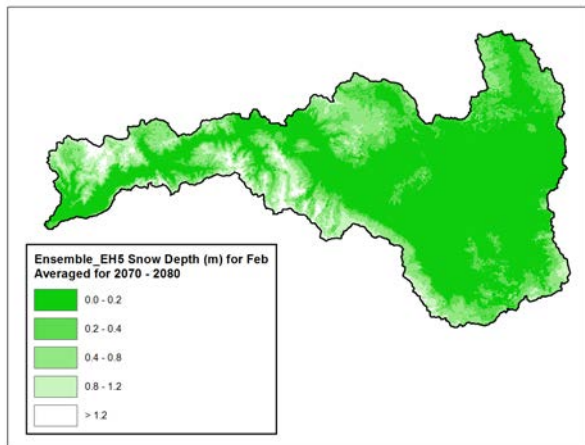
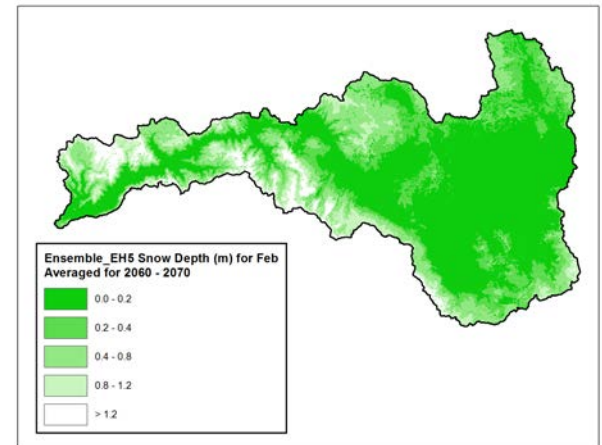
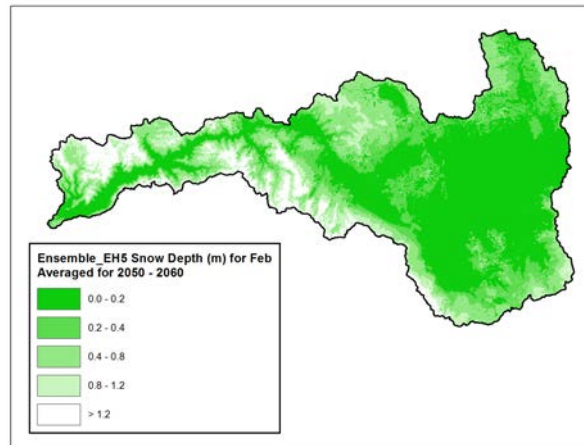
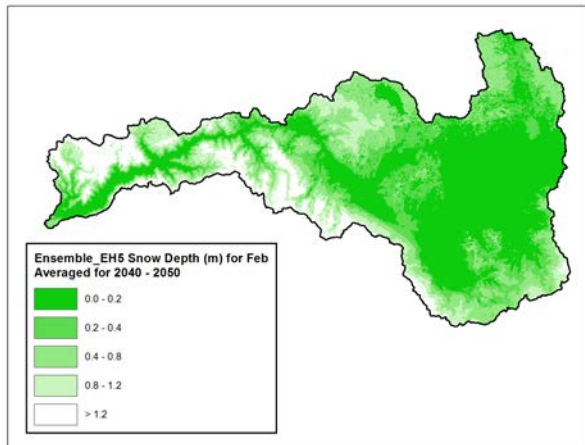
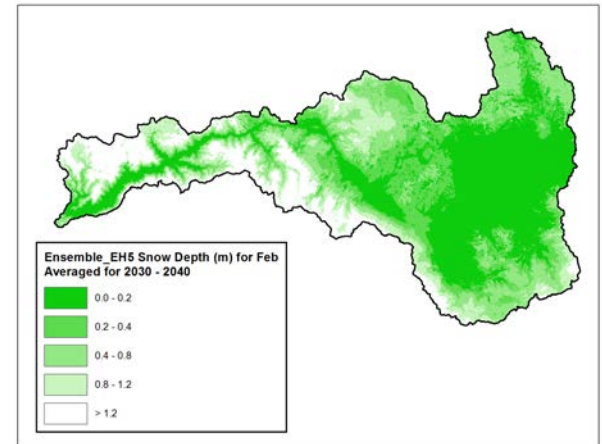
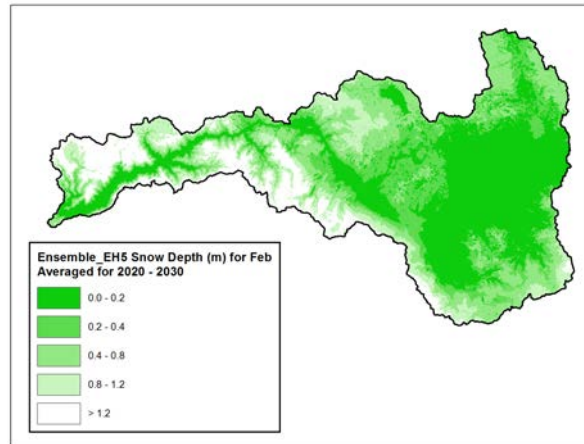
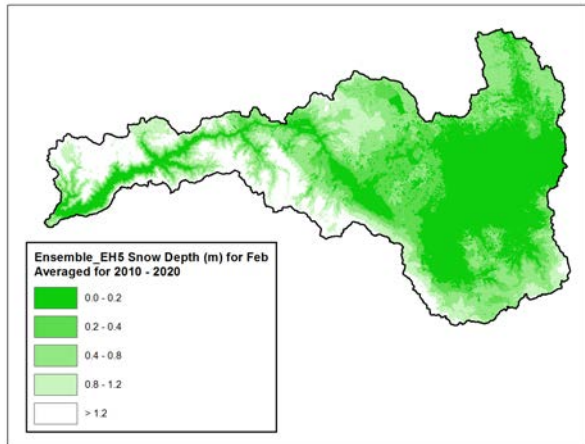


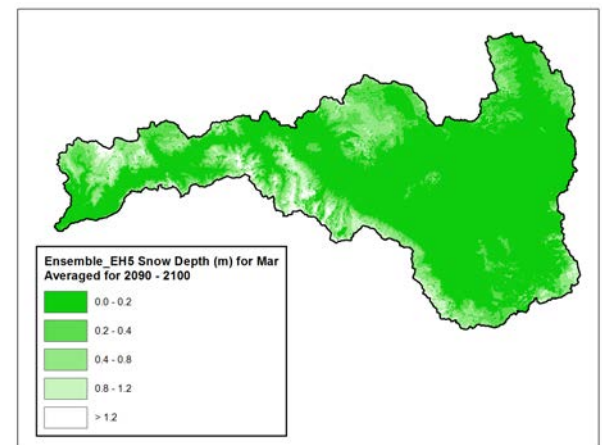
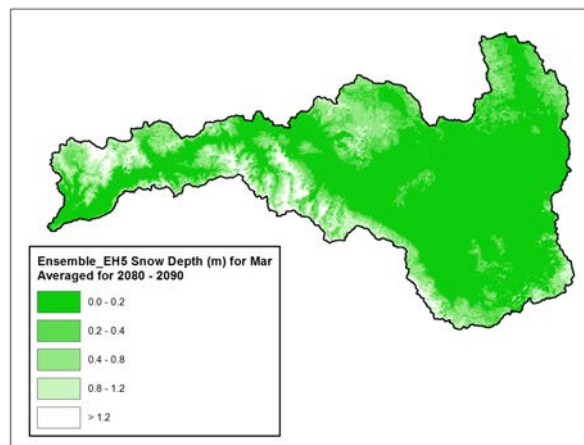
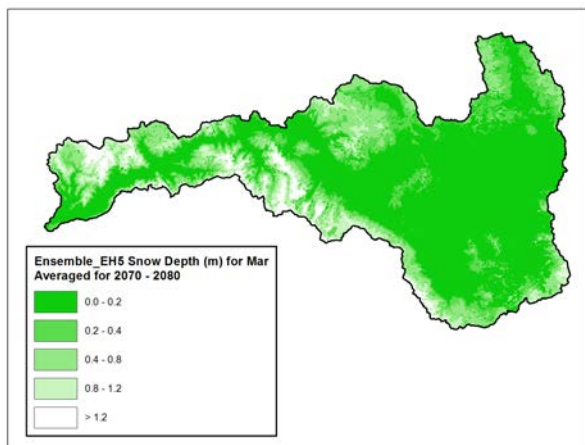
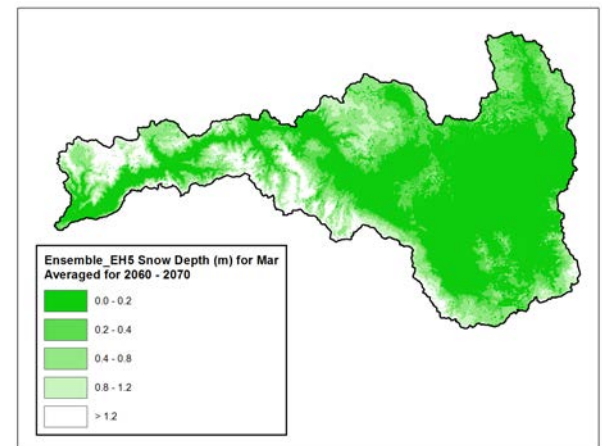
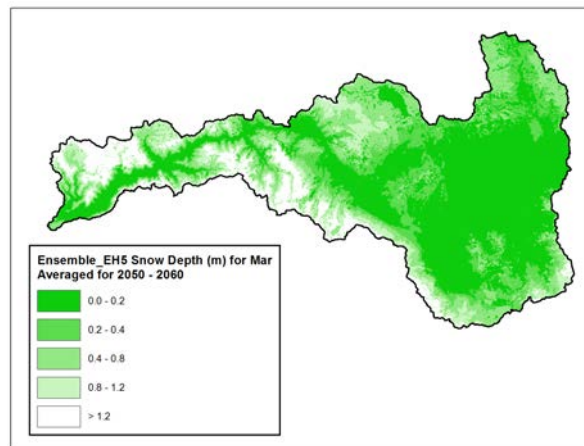
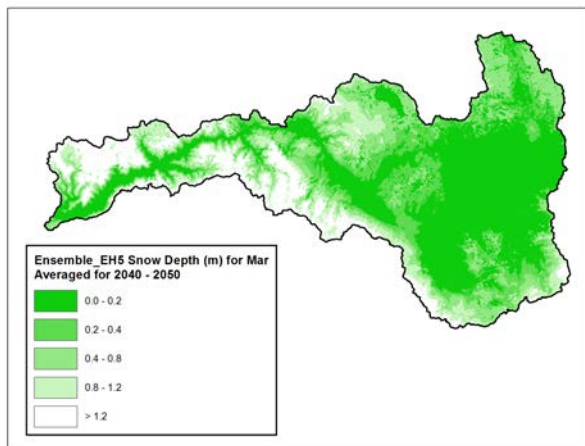
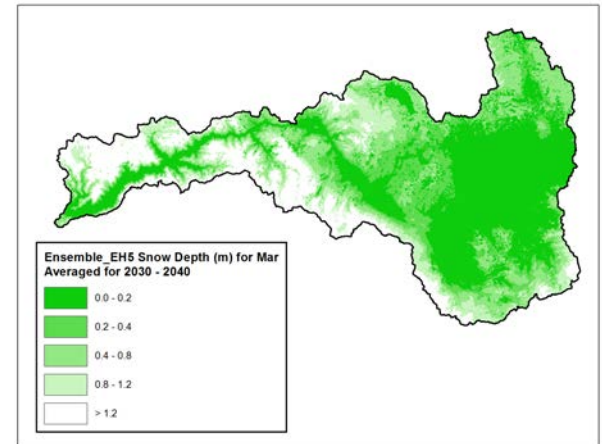
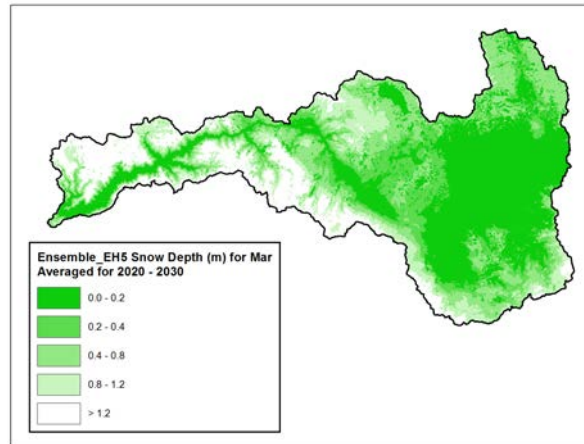
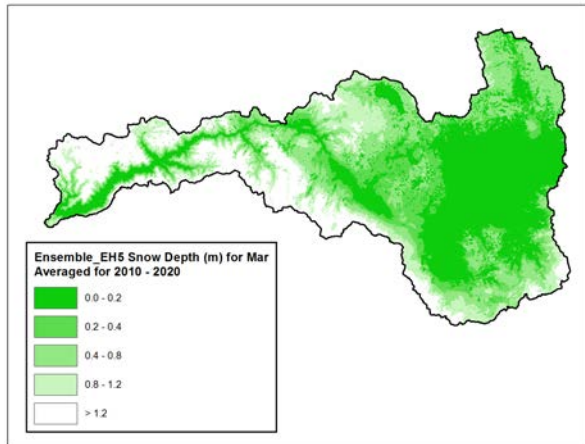


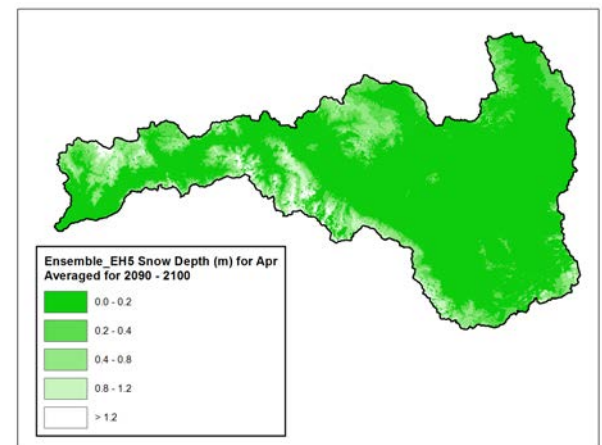
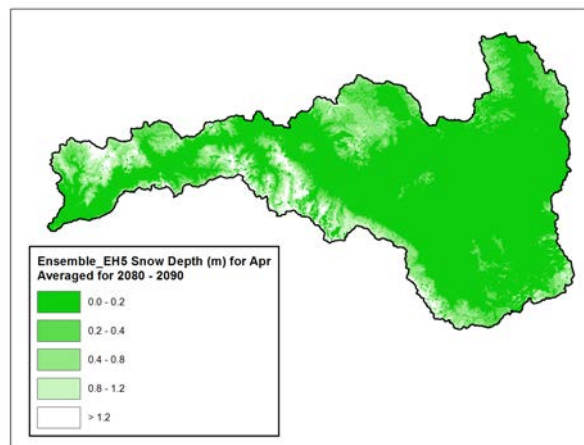
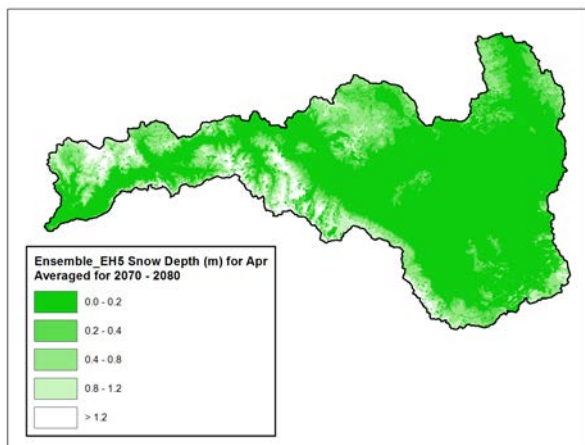
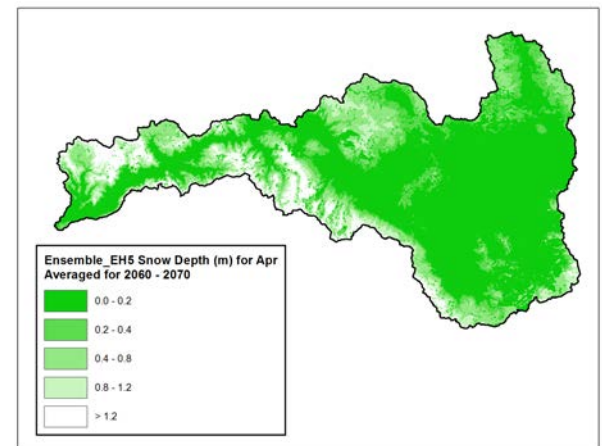
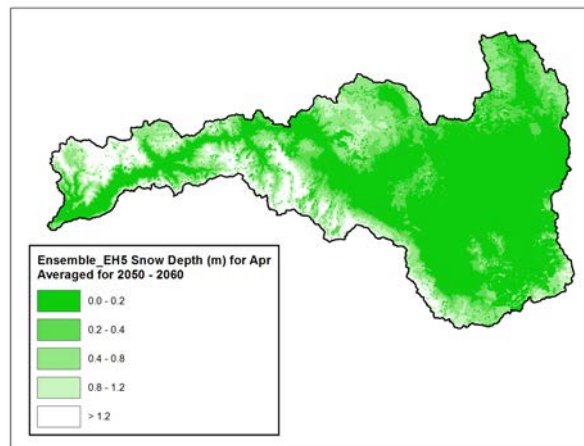
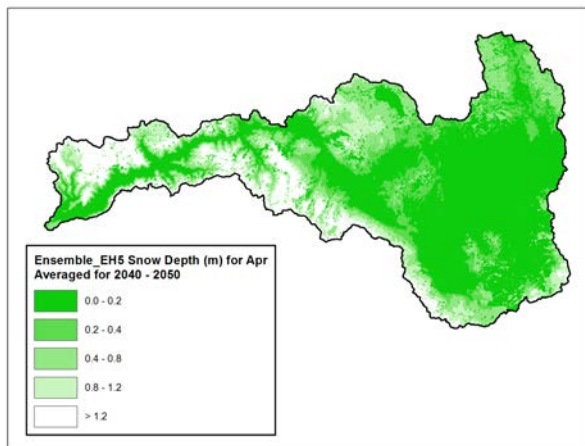
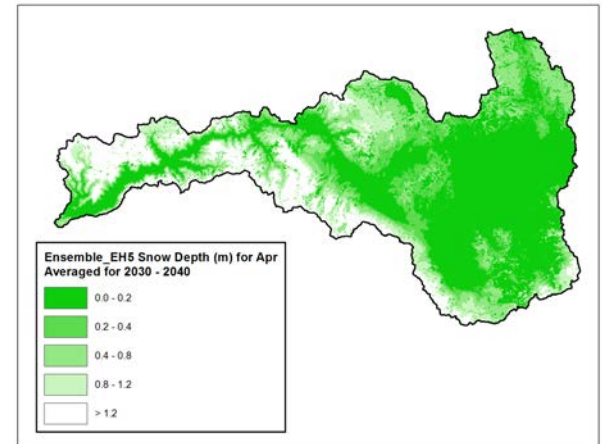
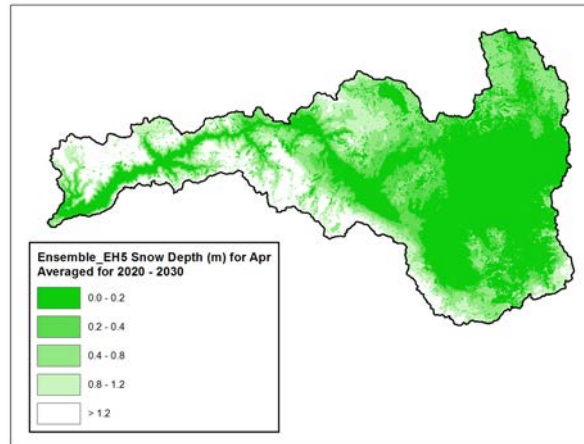
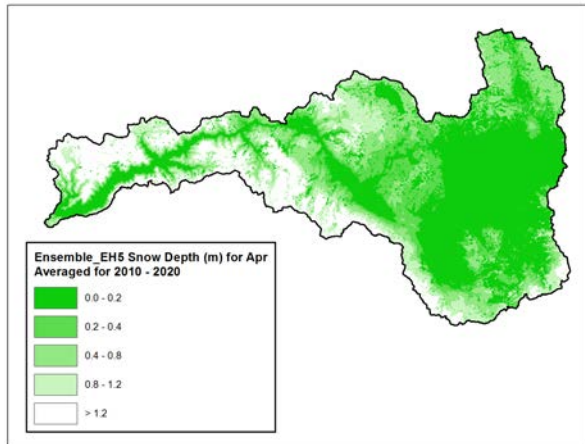


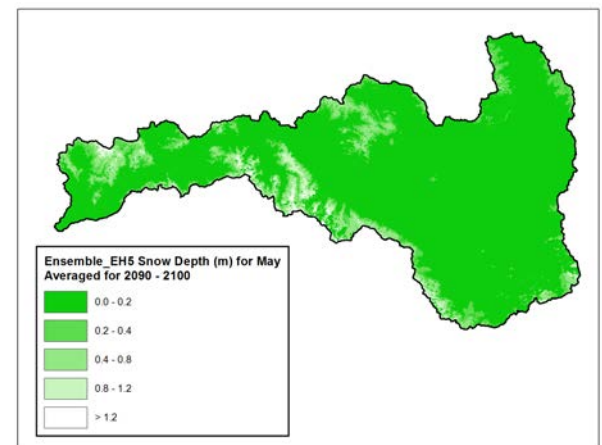
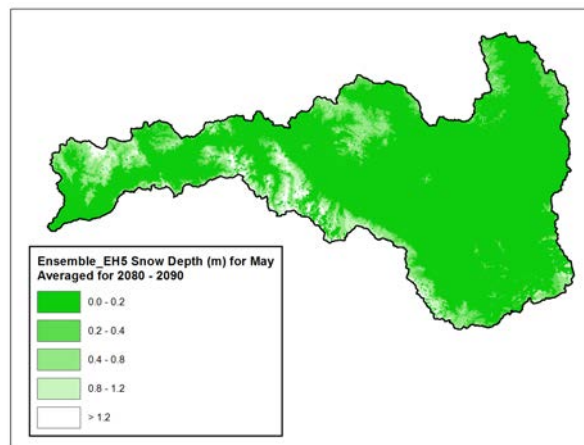
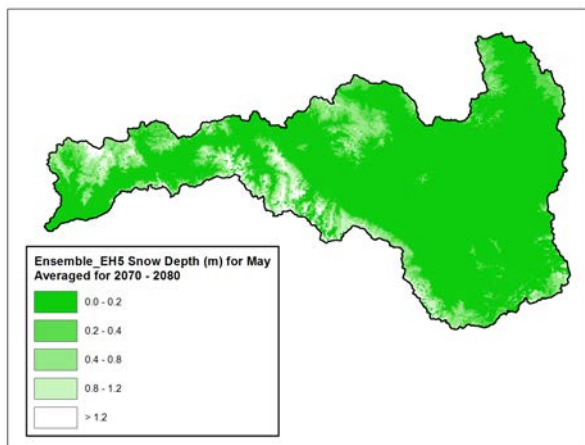
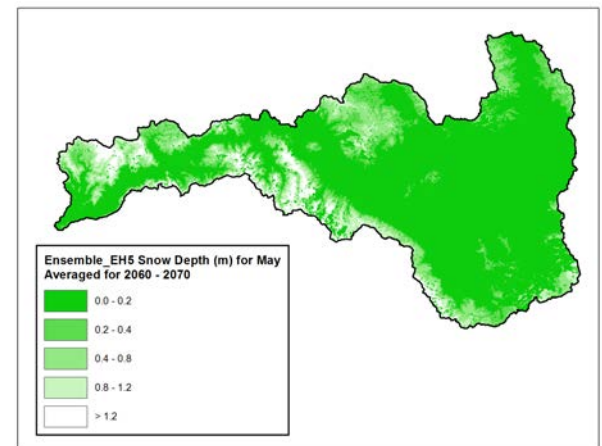
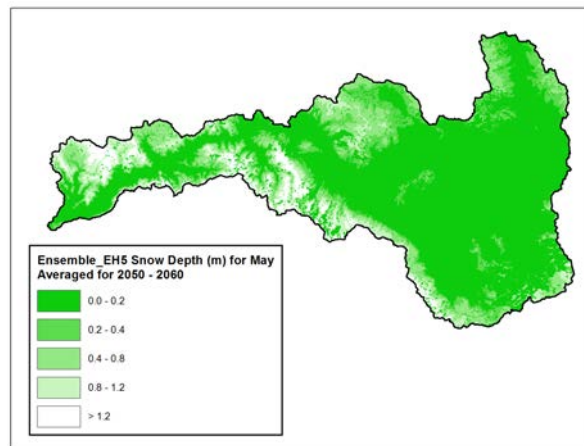
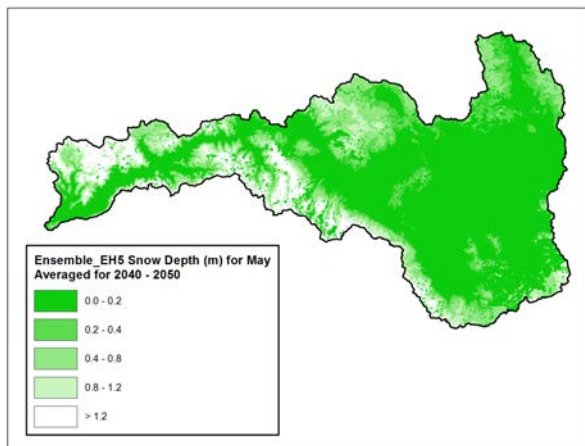
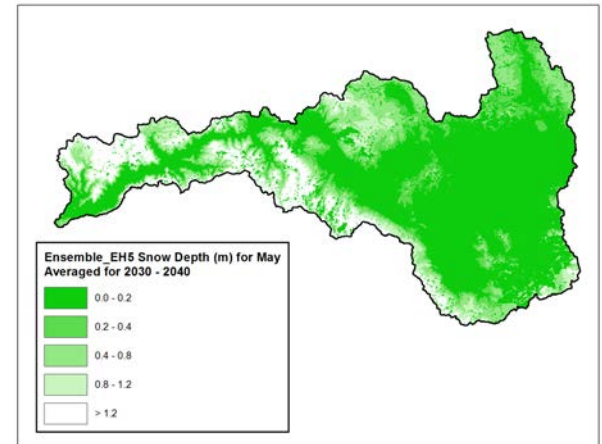
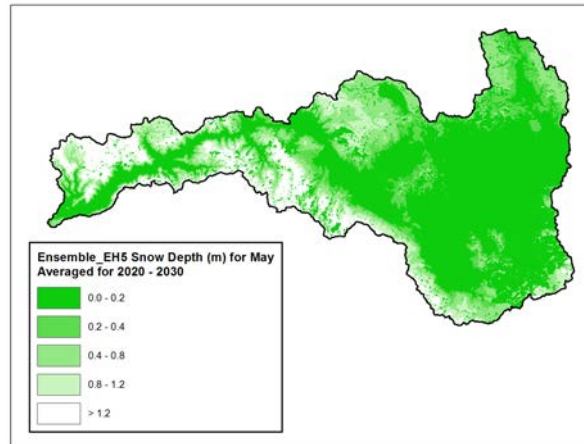
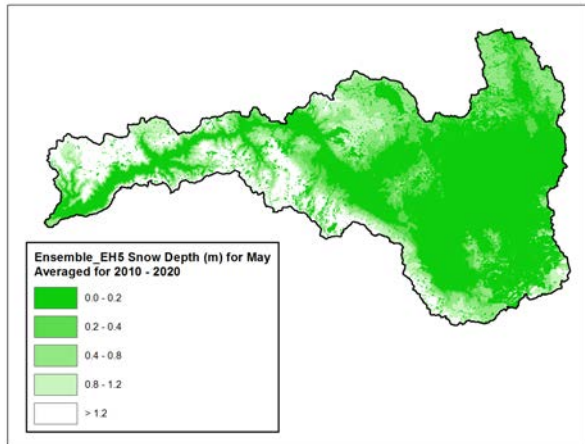


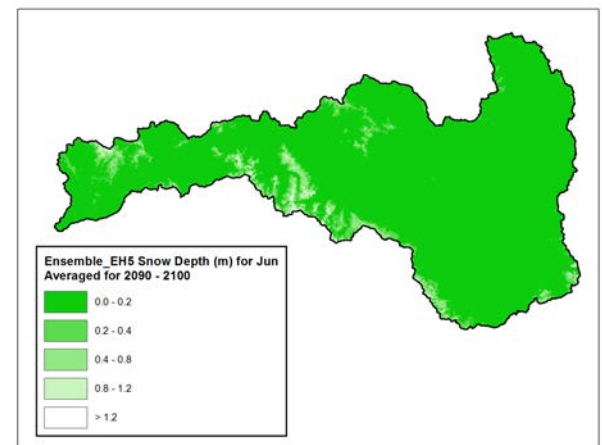
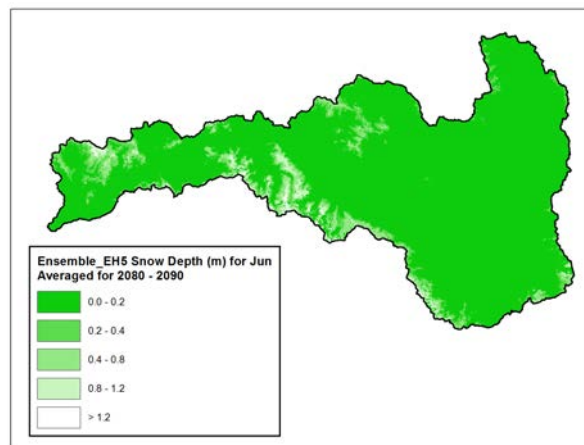
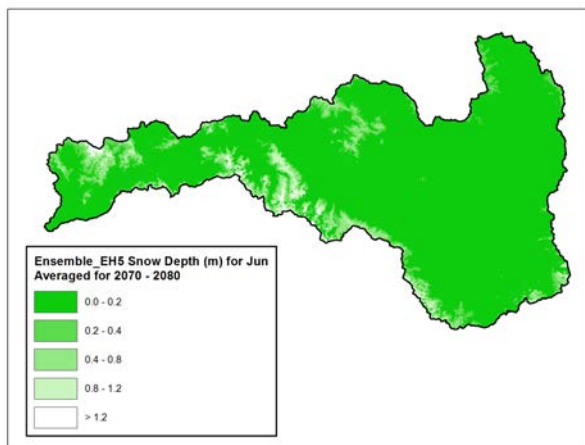
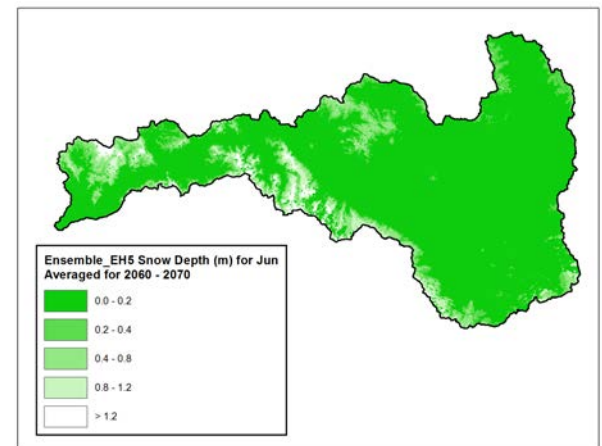
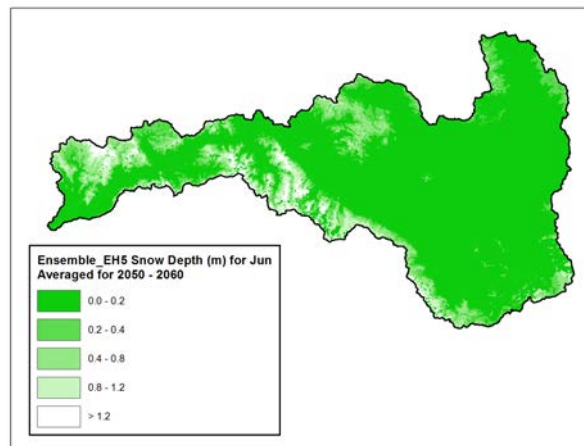
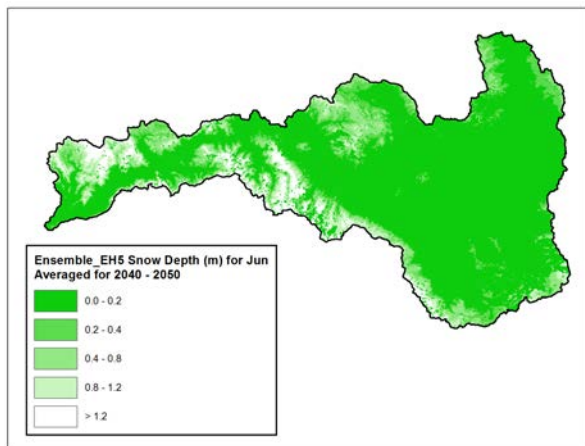
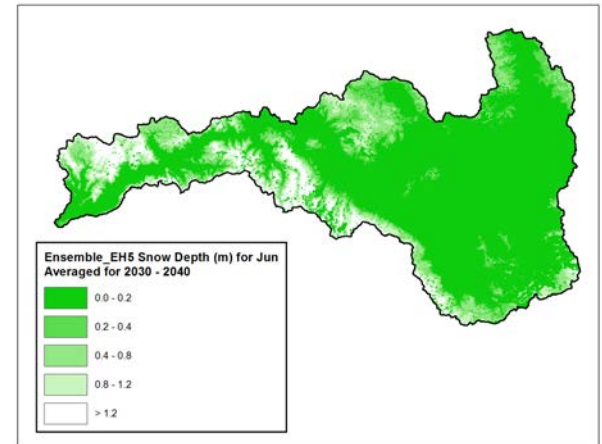
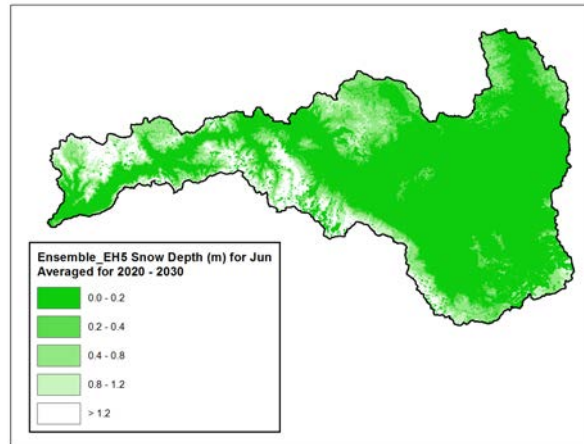
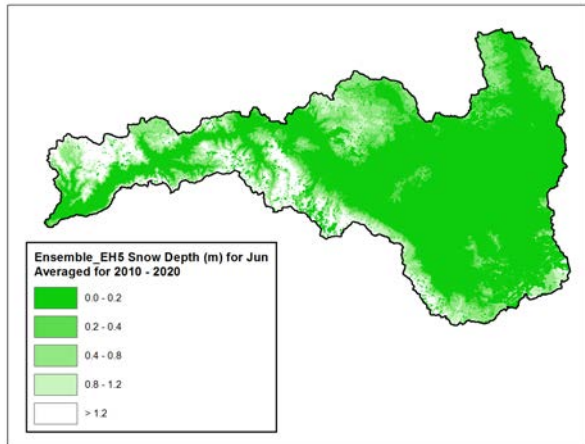


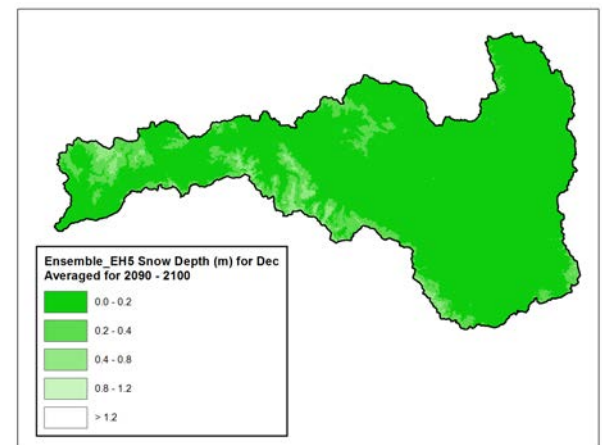
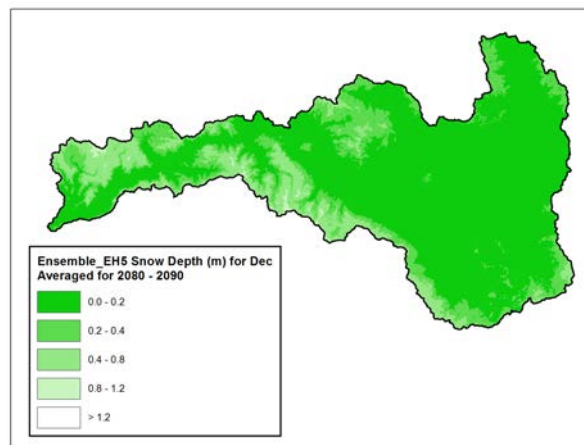
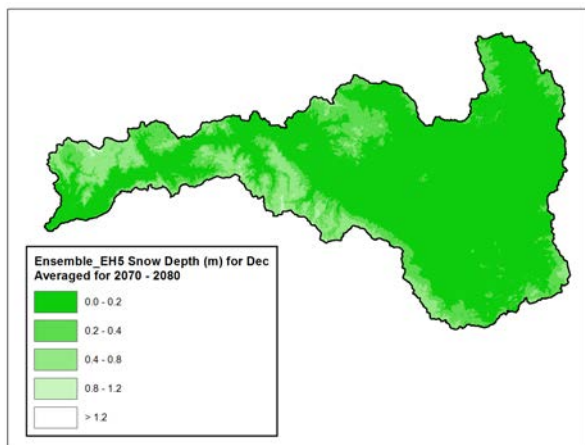
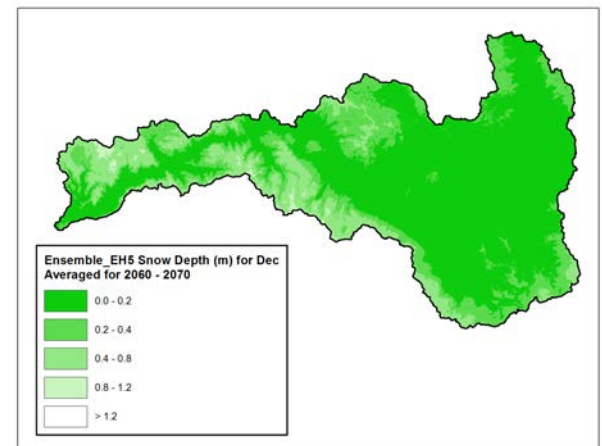
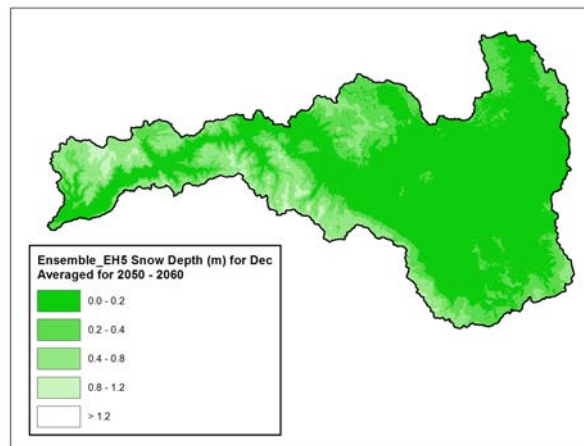
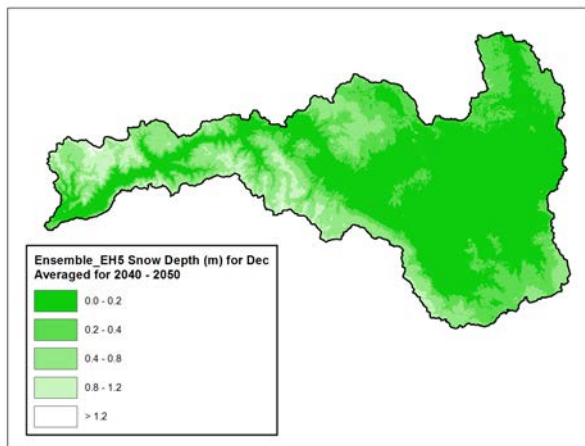
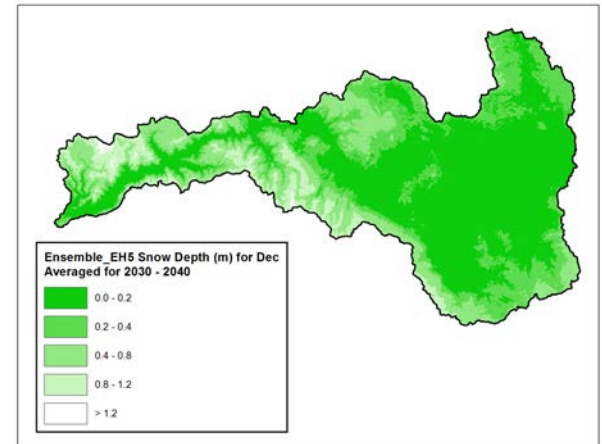
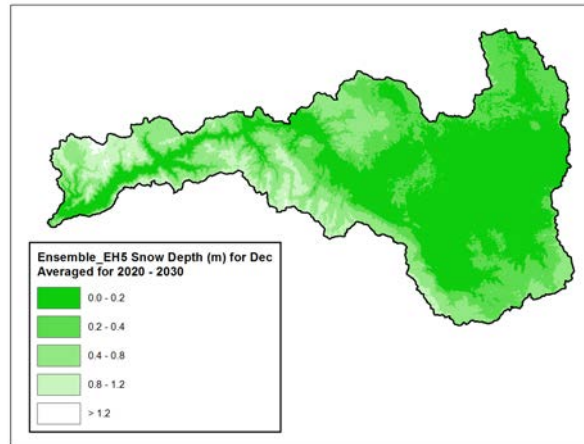
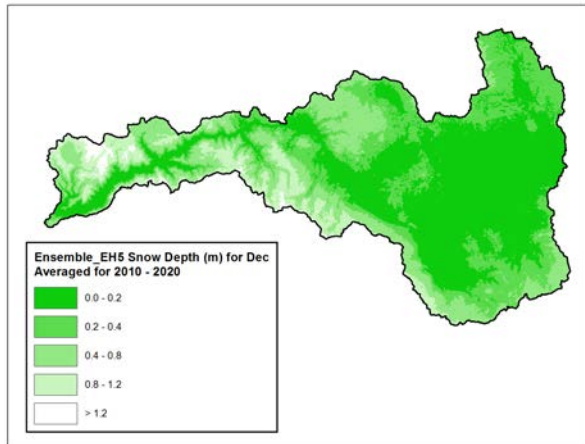








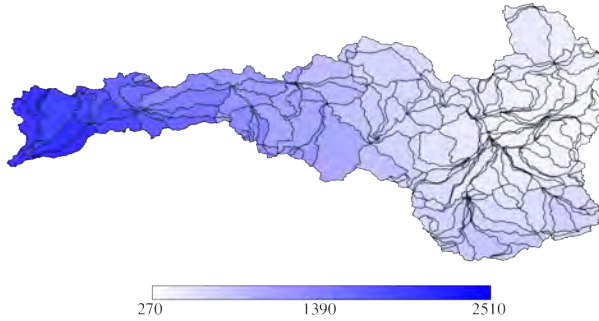




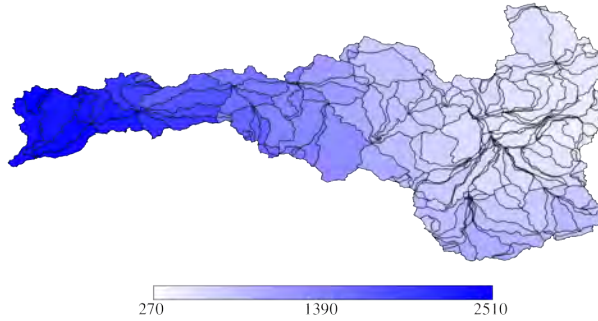
APPENDIX D

Spatial Distributions of Annual Average Liquid Water,
Precipitation, Short-wave Radiation, and Air Temperature over
the Upper Middle Fork Watershed for all 13 Future Projections,
Provided as an Average over Each Decade

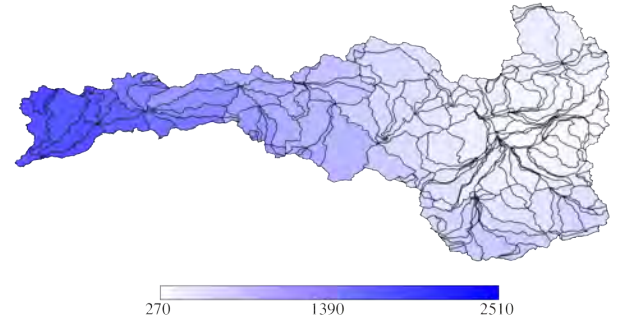
10-Year Average of Annual Liquid Water (mm)
CCSM3 A1B wy2010-wy2020



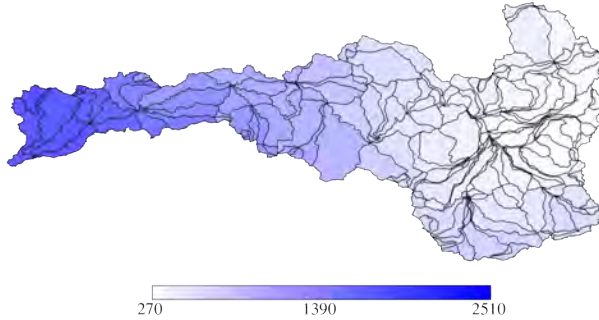
10-Year Average of Annual Liquid Water (mm)
CCSM3 A1B wy2020-wy2030



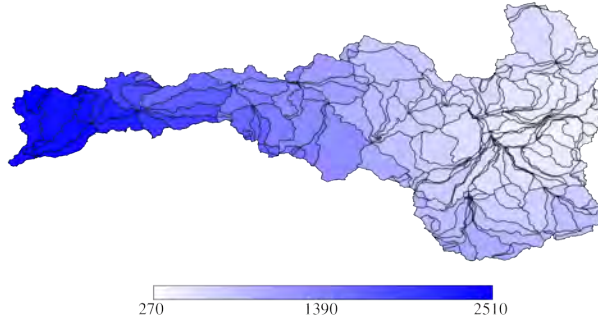
10-Year Average of Annual Liquid Water (mm)
CCSM3 A1B wy2030-wy2040



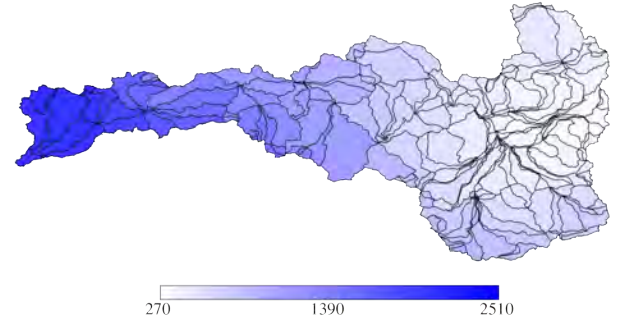
10-Year Average of Annual Liquid Water (mm)
CCSM3 A1B wy2040-wy2050



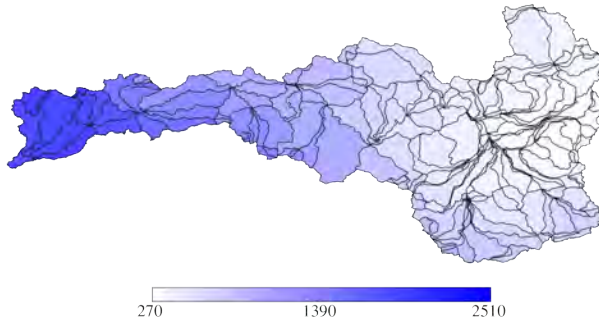
10-Year Average of Annual Liquid Water (mm)
CCSM3 A1B wy2050-wy2060



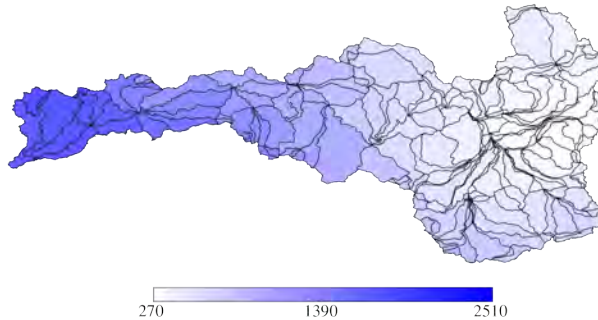
10-Year Average of Annual Liquid Water (mm)
CCSM3 A1B wy2060-wy2070



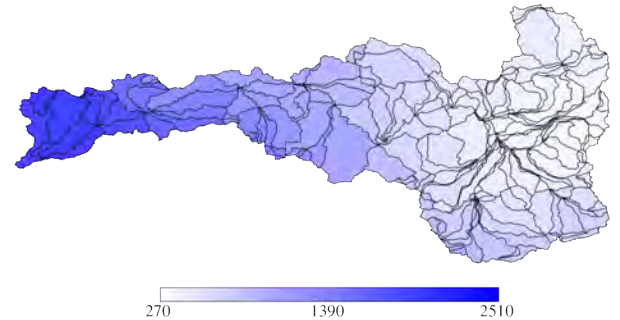
10-Year Average of Annual Liquid Water (mm)
CCSM3 A1B wy2070-wy2080



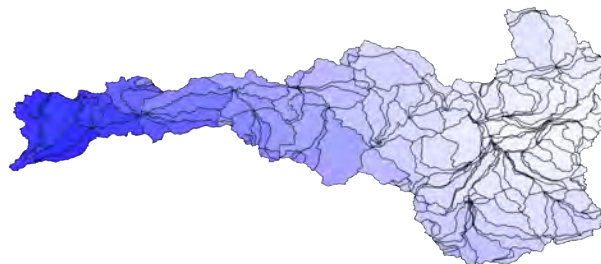
10-Year Average of Annual Liquid Water (mm)
CCSM3 A1B wy2080-wy2090



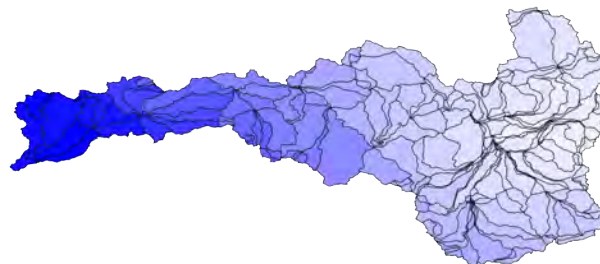
10-Year Average of Annual Liquid Water (mm)
CCSM3 A1B wy2090-wy2100



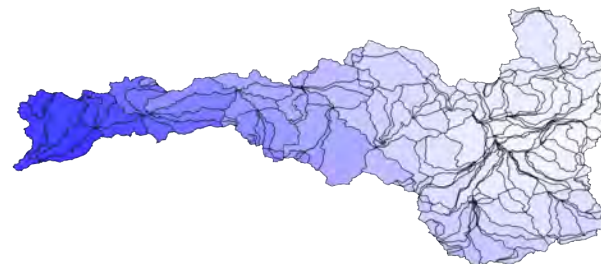
10-Year Average of Annual Liquid Water (mm)
CCSM3 A1FI wy2010-wy2020



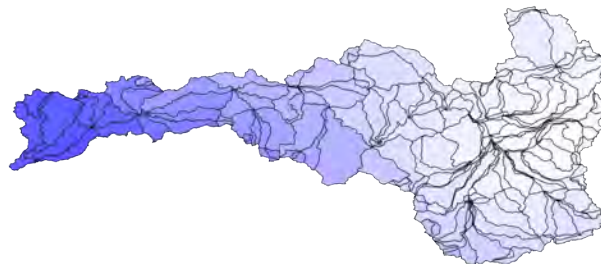
10-Year Average of Annual Liquid Water (mm)
CCSM3 A1FI wy2020-wy2030



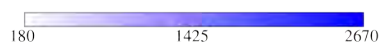
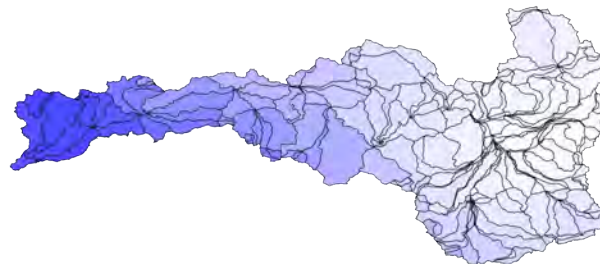
10-Year Average of Annual Liquid Water (mm)
CCSM3 A1FI wy2030-wy2040



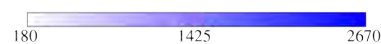
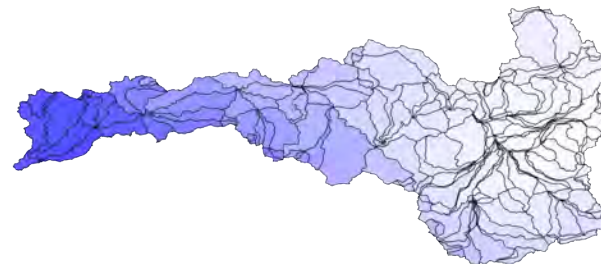
10-Year Average of Annual Liquid Water (mm)
CCSM3 A1FI wy2040-wy2050



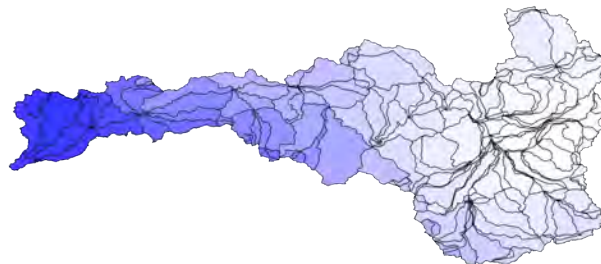
10-Year Average of Annual Liquid Water (mm)
CCSM3 A1FI wy2050-wy2060



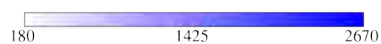
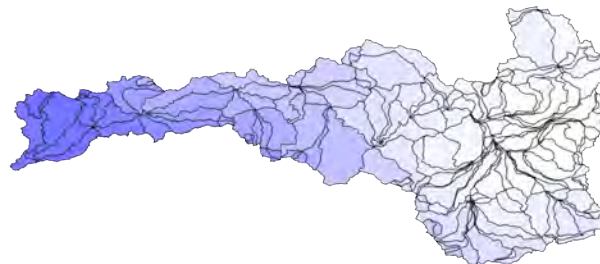
10-Year Average of Annual Liquid Water (mm)
CCSM3 A1FI wy2060-wy2070



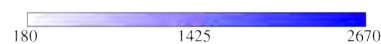
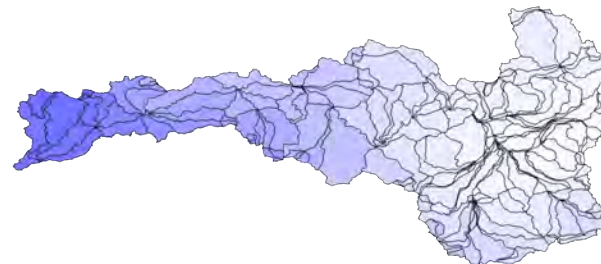
10-Year Average of Annual Liquid Water (mm)
CCSM3 A1FI wy2070-wy2080



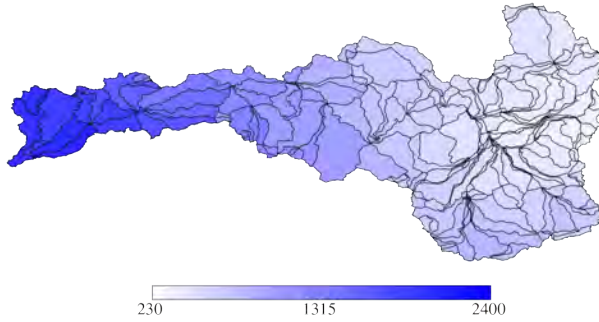
10-Year Average of Annual Liquid Water (mm)
CCSM3 A1FI wy2080-wy2090



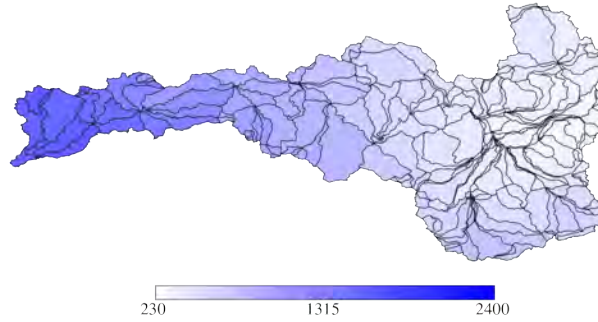
10-Year Average of Annual Liquid Water (mm)
CCSM3 A1FI wy2090-wy2100



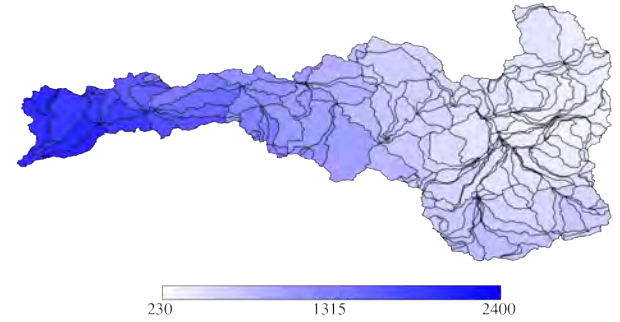
10-Year Average of Annual Liquid Water (mm)
CCSM3 A2 wy2010-wy2020



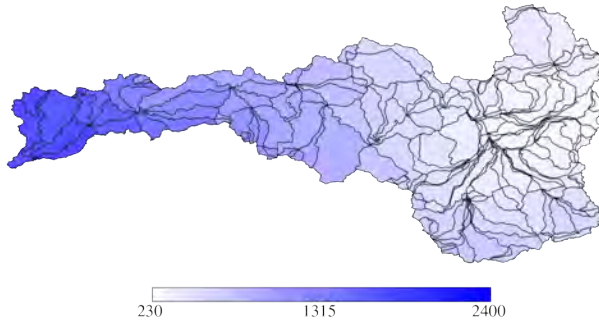
10-Year Average of Annual Liquid Water (mm)
CCSM3 A2 wy2020-wy2030



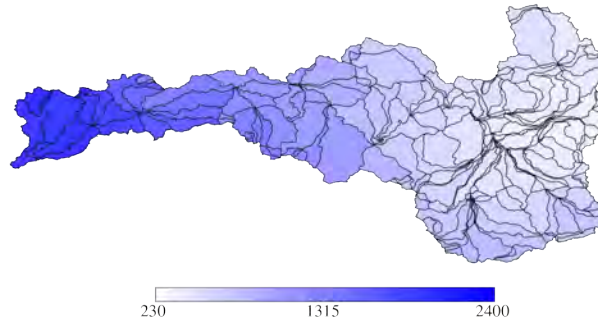
10-Year Average of Annual Liquid Water (mm)
CCSM3 A2 wy2030-wy2040



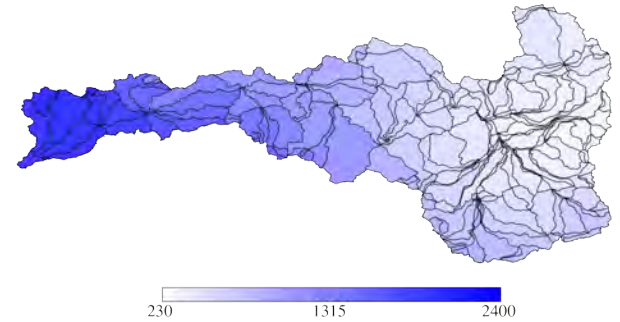
10-Year Average of Annual Liquid Water (mm)
CCSM3 A2 wy2040-wy2050



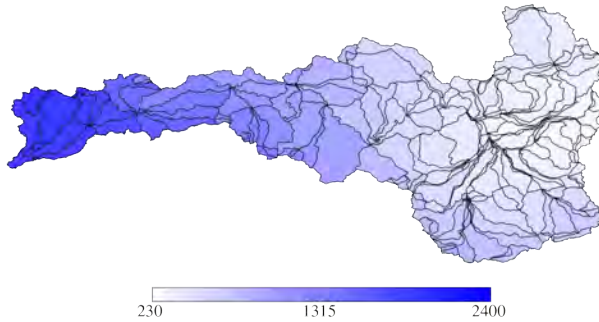
10-Year Average of Annual Liquid Water (mm)
CCSM3 A2 wy2050-wy2060



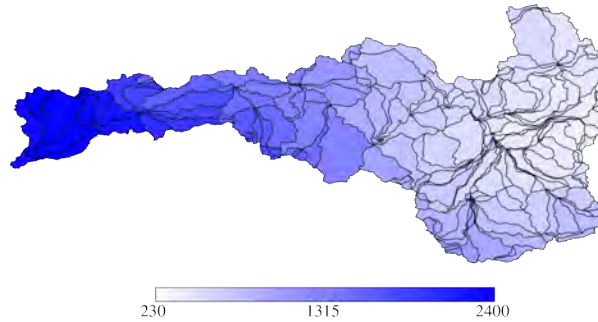
10-Year Average of Annual Liquid Water (mm)
CCSM3 A2 wy2060-wy2070



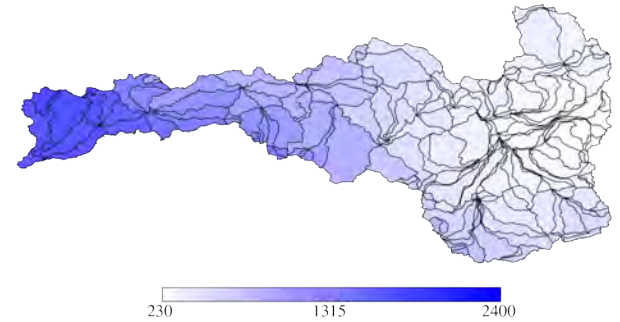
10-Year Average of Annual Liquid Water (mm)
CCSM3 A2 wy2070-wy2080



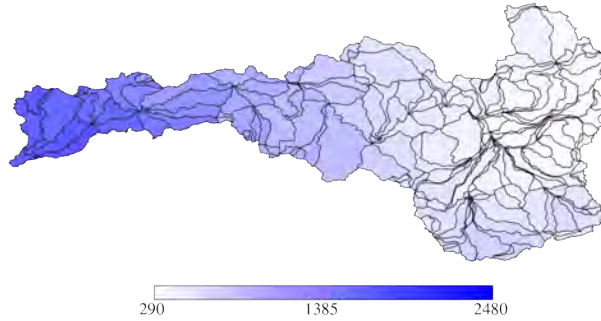
10-Year Average of Annual Liquid Water (mm)
CCSM3 A2 wy2080-wy2090



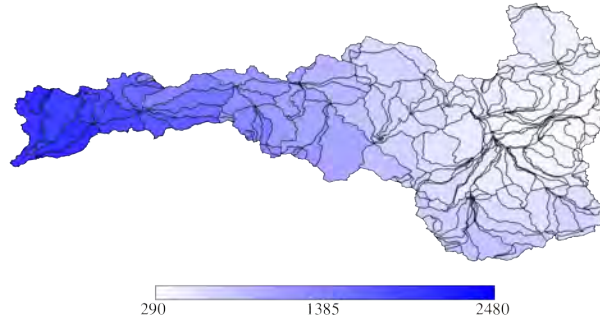
10-Year Average of Annual Liquid Water (mm)
CCSM3 A2 wy2090-wy2100



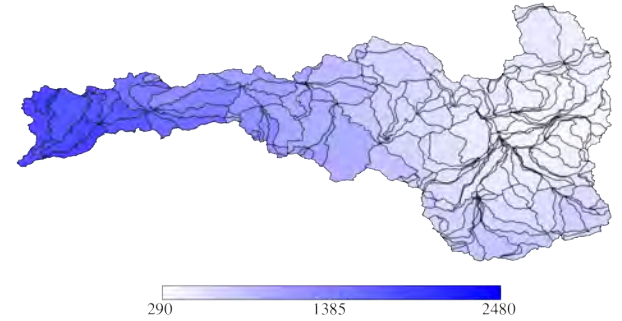
10-Year Average of Annual Liquid Water (mm)
CCSM3 B1 wy2010-wy2020



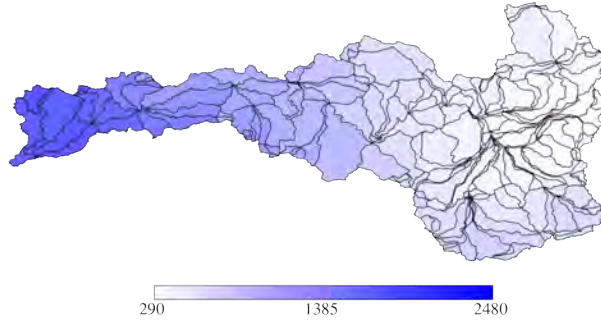
10-Year Average of Annual Liquid Water (mm)
CCSM3 B1 wy2020-wy2030



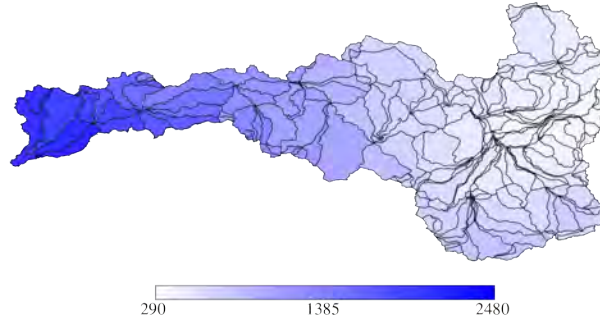
10-Year Average of Annual Liquid Water (mm)
CCSM3 B1 wy2030-wy2040



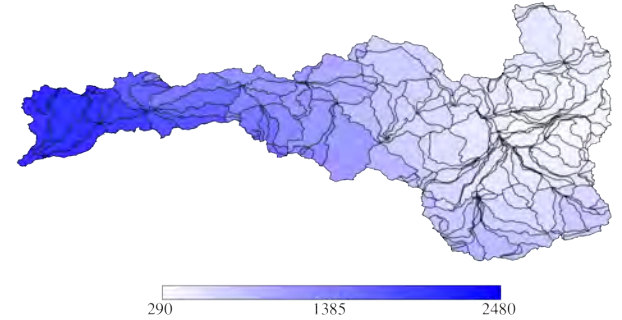
10-Year Average of Annual Liquid Water (mm)
CCSM3 B1 wy2040-wy2050



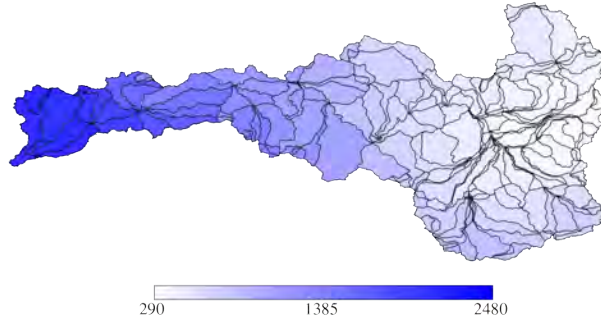
10-Year Average of Annual Liquid Water (mm)
CCSM3 B1 wy2050-wy2060



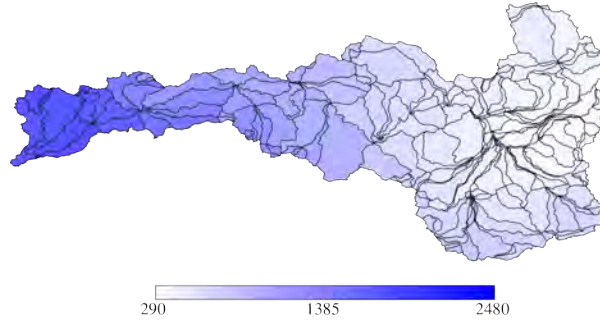
10-Year Average of Annual Liquid Water (mm)
CCSM3 B1 wy2060-wy2070



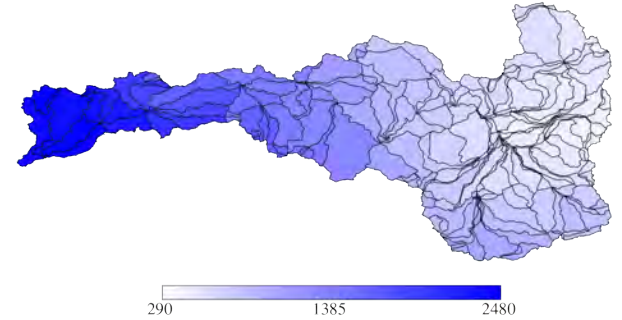
10-Year Average of Annual Liquid Water (mm)
CCSM3 B1 wy2070-wy2080



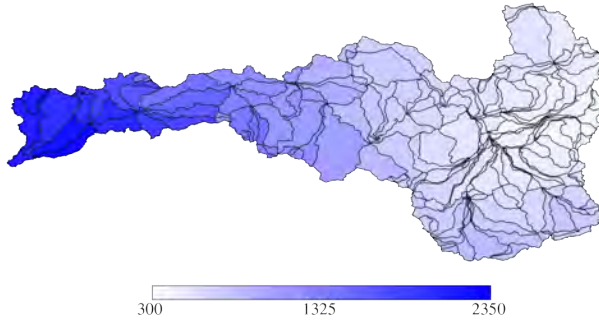
10-Year Average of Annual Liquid Water (mm)
CCSM3 B1 wy2080-wy2090



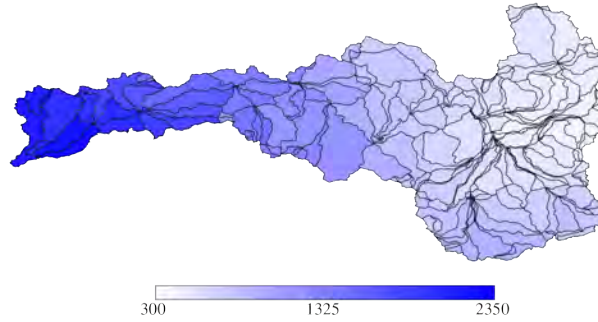
10-Year Average of Annual Liquid Water (mm)
CCSM3 B1 wy2090-wy2100



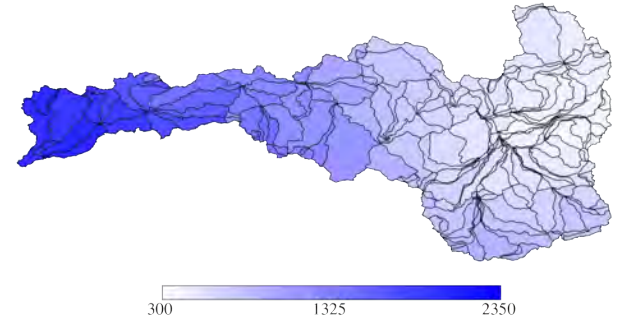
10-Year Average of Annual Liquid Water (mm)
ECHAM5 A1B1 wy2010-wy2020



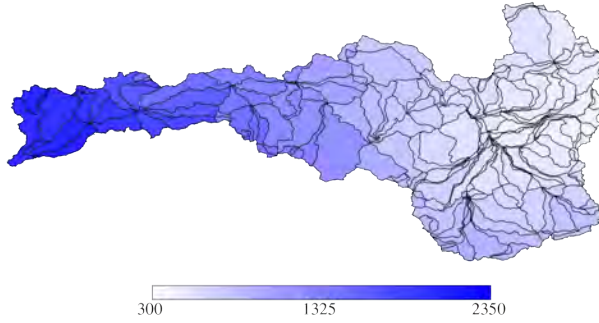
10-Year Average of Annual Liquid Water (mm)
ECHAM5 A1B1 wy2020-wy2030



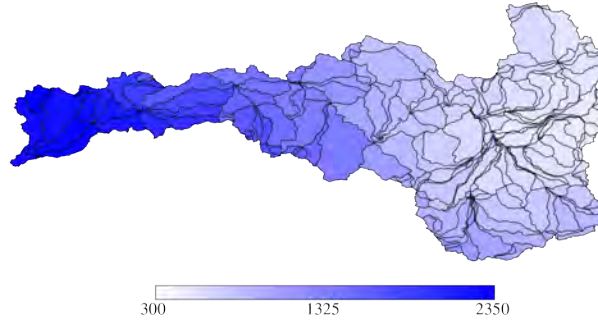
10-Year Average of Annual Liquid Water (mm)
ECHAM5 A1B1 wy2030-wy2040



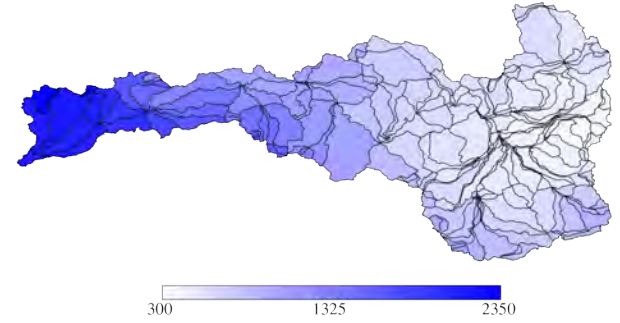
10-Year Average of Annual Liquid Water (mm)
ECHAM5 A1B1 wy2040-wy2050



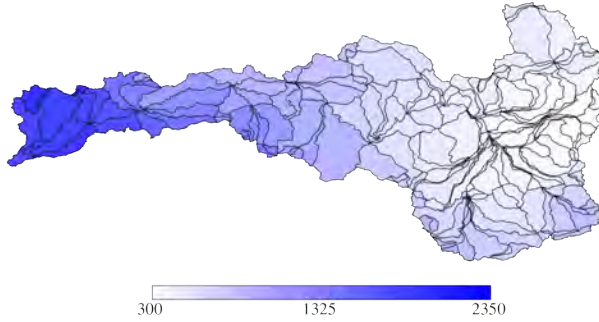
10-Year Average of Annual Liquid Water (mm)
ECHAM5 A1B1 wy2050-wy2060



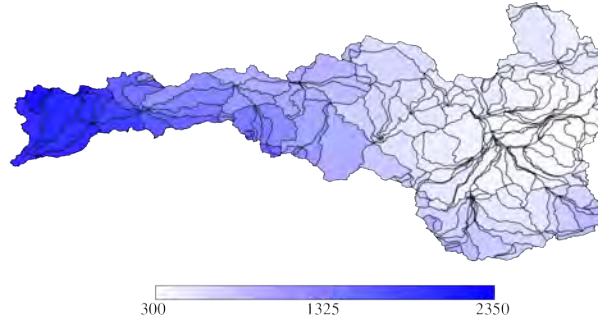
10-Year Average of Annual Liquid Water (mm)
ECHAM5 A1B1 wy2060-wy2070



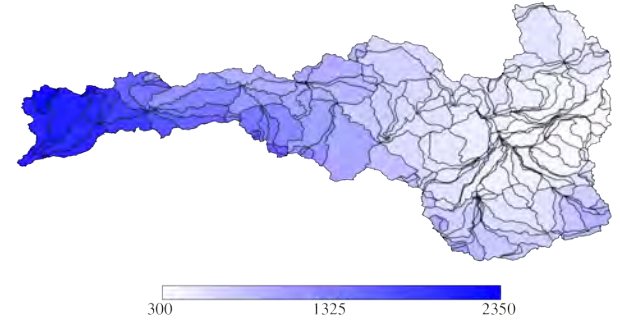
10-Year Average of Annual Liquid Water (mm)
ECHAM5 A1B1 wy2070-wy2080



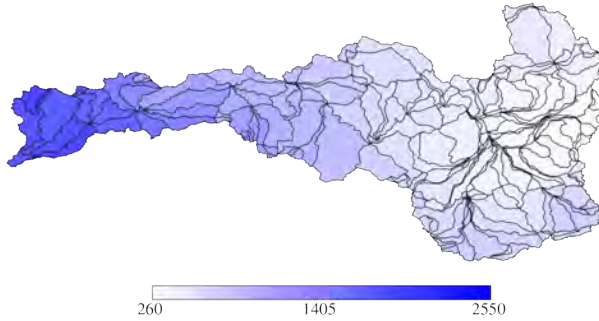
10-Year Average of Annual Liquid Water (mm)
ECHAM5 A1B1 wy2080-wy2090



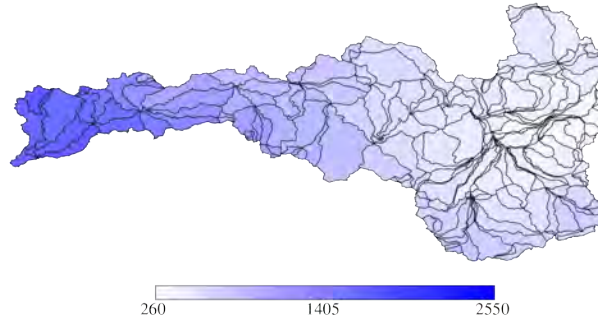
10-Year Average of Annual Liquid Water (mm)
ECHAM5 A1B1 wy2090-wy2100



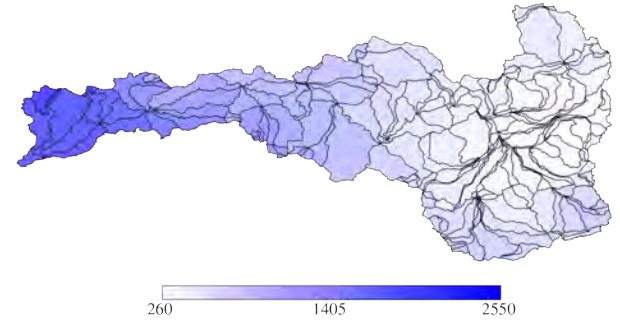
10-Year Average of Annual Liquid Water (mm)
ECHAM5 A1B2 wy2010-wy2020



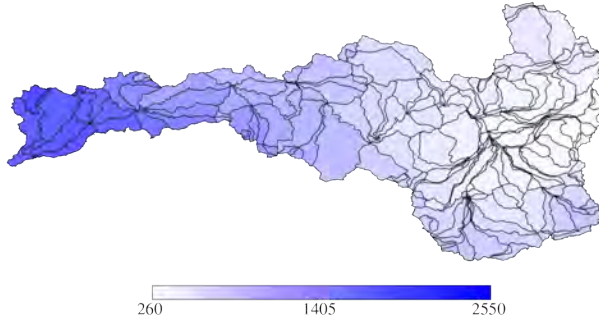
10-Year Average of Annual Liquid Water (mm)
ECHAM5 A1B2 wy2020-wy2030



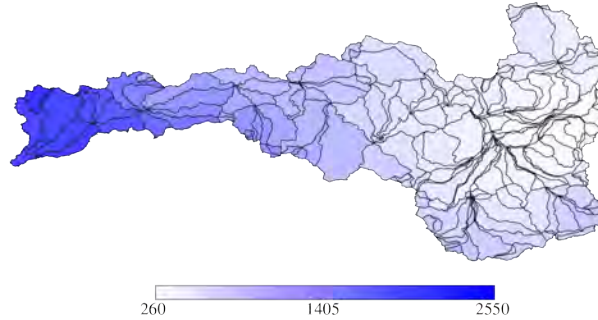
10-Year Average of Annual Liquid Water (mm)
ECHAM5 A1B2 wy2030-wy2040



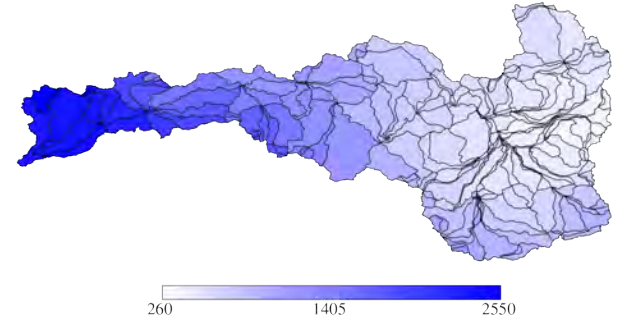
10-Year Average of Annual Liquid Water (mm)
ECHAM5 A1B2 wy2040-wy2050



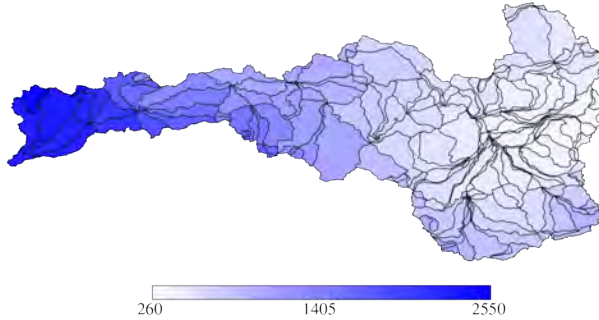
10-Year Average of Annual Liquid Water (mm)
ECHAM5 A1B2 wy2050-wy2060



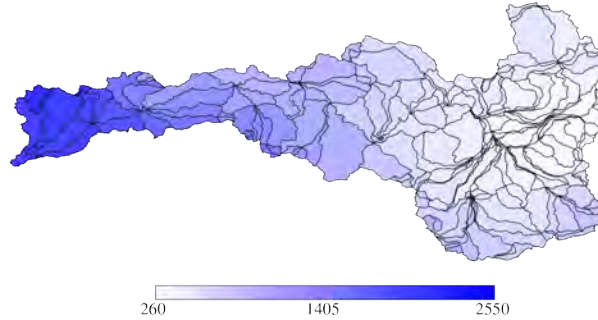
10-Year Average of Annual Liquid Water (mm)
ECHAM5 A1B2 wy2060-wy2070



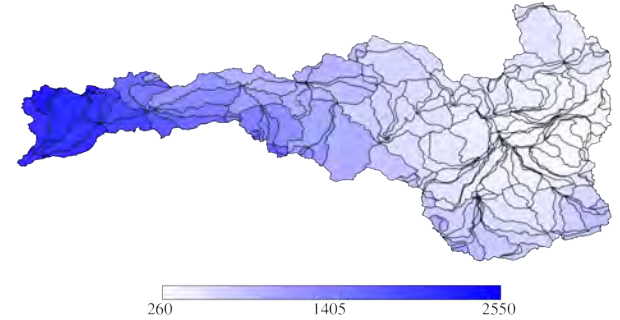
10-Year Average of Annual Liquid Water (mm)
ECHAM5 A1B2 wy2070-wy2080



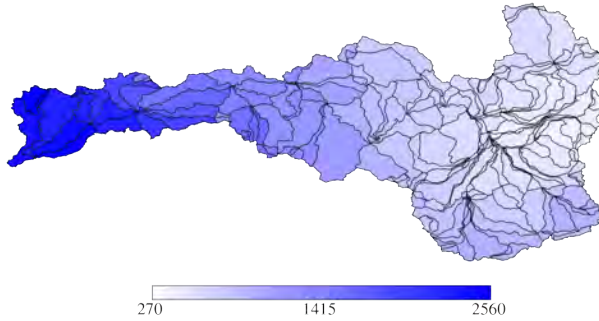
10-Year Average of Annual Liquid Water (mm)
ECHAM5 A1B2 wy2080-wy2090



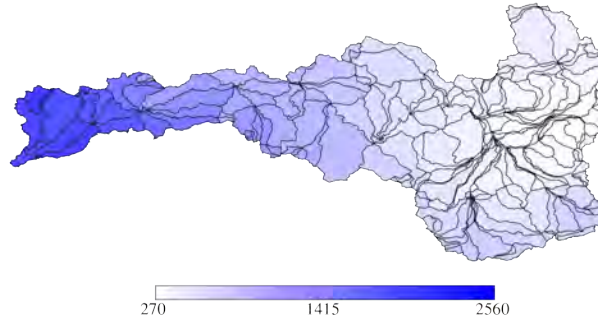
10-Year Average of Annual Liquid Water (mm)
ECHAM5 A1B2 wy2090-wy2100



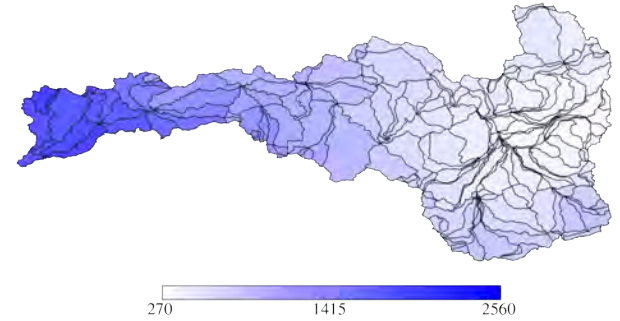
10-Year Average of Annual Liquid Water (mm)
ECHAM5 A1B3 wy2010-wy2020



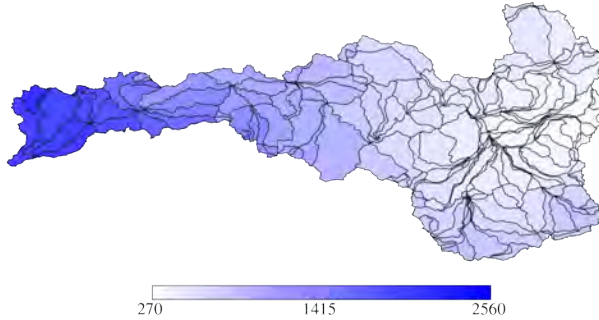
10-Year Average of Annual Liquid Water (mm)
ECHAM5 A1B3 wy2020-wy2030



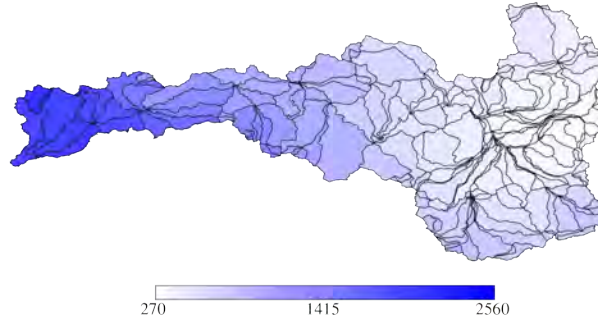
10-Year Average of Annual Liquid Water (mm)
ECHAM5 A1B3 wy2030-wy2040



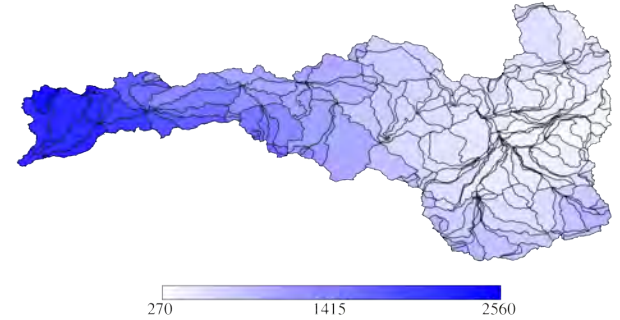
10-Year Average of Annual Liquid Water (mm)
ECHAM5 A1B3 wy2040-wy2050



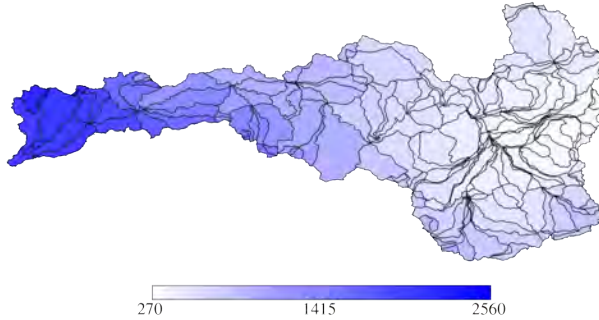
10-Year Average of Annual Liquid Water (mm)
ECHAM5 A1B3 wy2050-wy2060



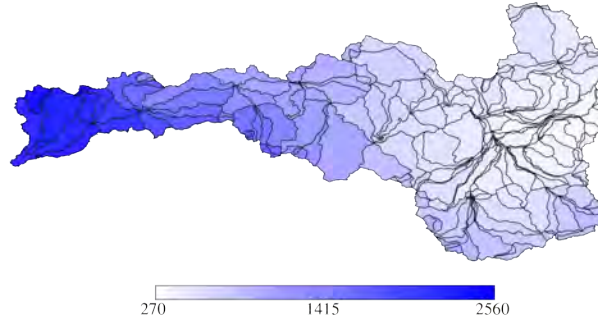
10-Year Average of Annual Liquid Water (mm)
ECHAM5 A1B3 wy2060-wy2070



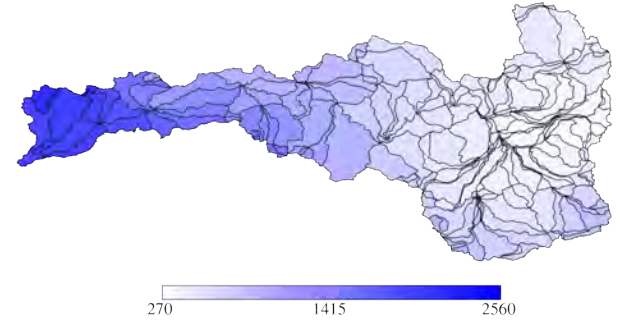
10-Year Average of Annual Liquid Water (mm)
ECHAM5 A1B3 wy2070-wy2080



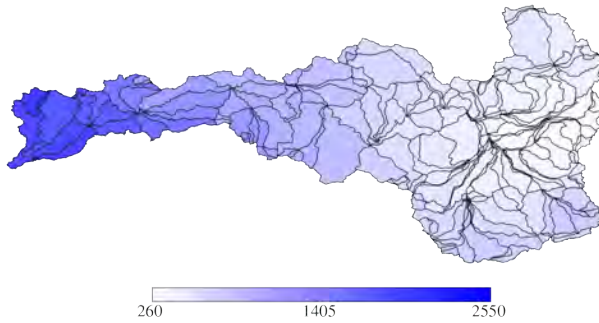
10-Year Average of Annual Liquid Water (mm)
ECHAM5 A1B3 wy2080-wy2090



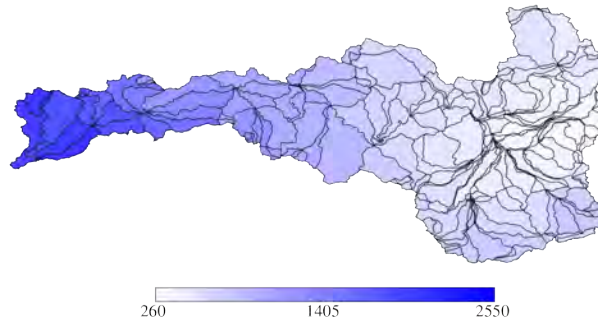
10-Year Average of Annual Liquid Water (mm)
ECHAM5 A1B3 wy2090-wy2100



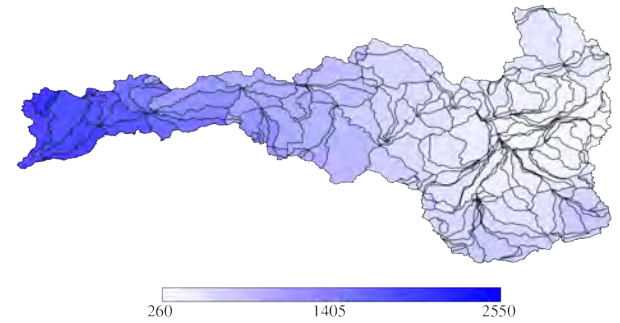
10-Year Average of Annual Liquid Water (mm)
ECHAM5 A2-1 wy2010-wy2020



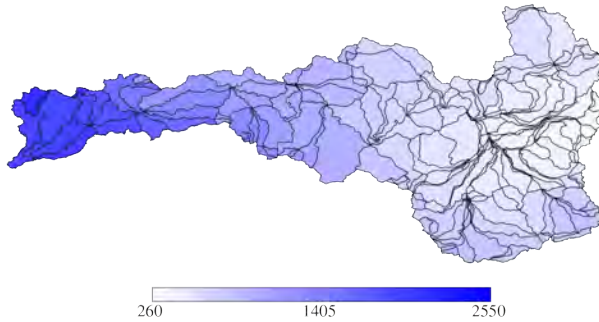
10-Year Average of Annual Liquid Water (mm)
ECHAM5 A2-1 wy2020-wy2030



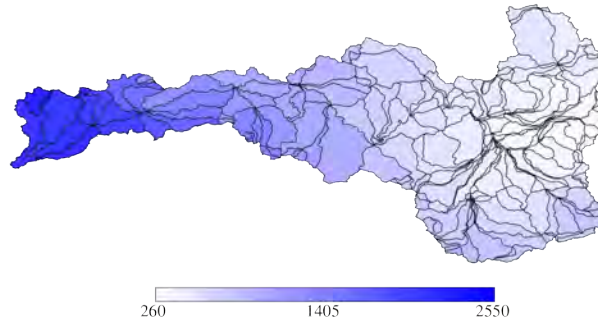
10-Year Average of Annual Liquid Water (mm)
ECHAM5 A2-1 wy2030-wy2040



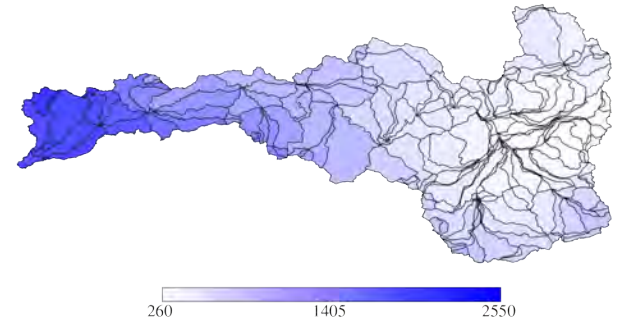
10-Year Average of Annual Liquid Water (mm)
ECHAM5 A2-1 wy2040-wy2050



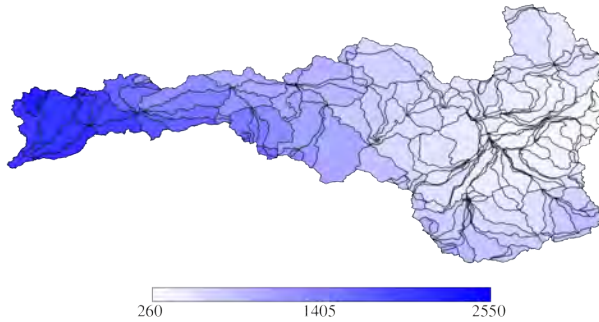
10-Year Average of Annual Liquid Water (mm)
ECHAM5 A2-1 wy2050-wy2060



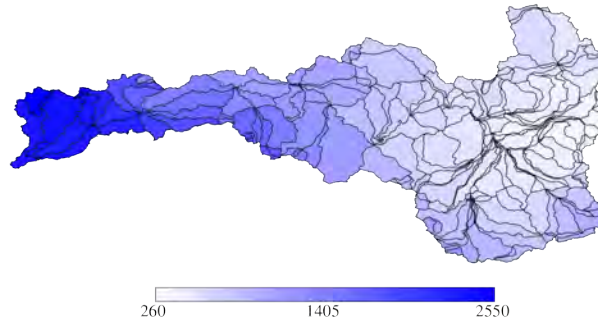
10-Year Average of Annual Liquid Water (mm)
ECHAM5 A2-1 wy2060-wy2070



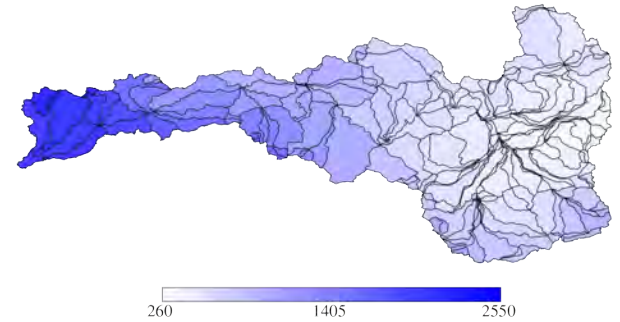
10-Year Average of Annual Liquid Water (mm)
ECHAM5 A2-1 wy2070-wy2080



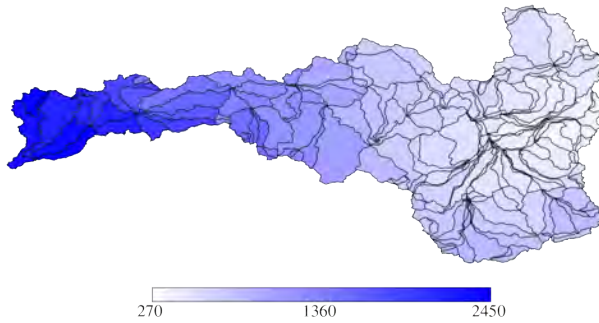
10-Year Average of Annual Liquid Water (mm)
ECHAM5 A2-1 wy2080-wy2090



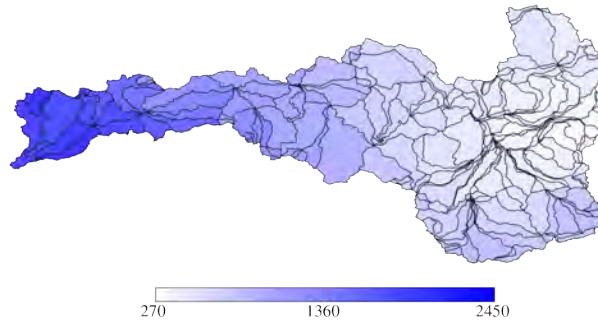
10-Year Average of Annual Liquid Water (mm)
ECHAM5 A2-1 wy2090-wy2100



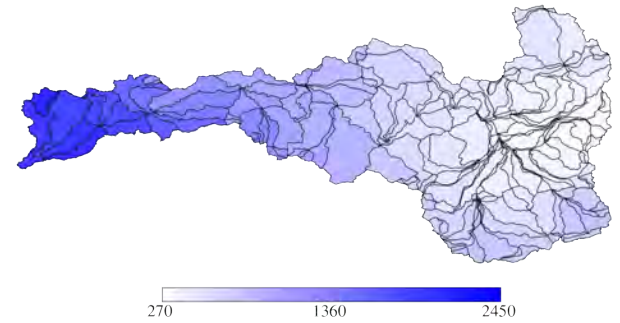
10-Year Average of Annual Liquid Water (mm)
ECHAM5 A2-2 wy2010-wy2020



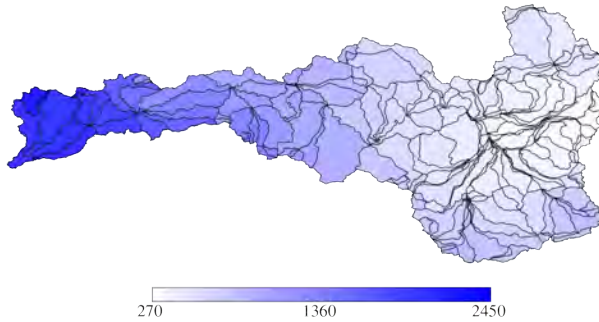
10-Year Average of Annual Liquid Water (mm)
ECHAM5 A2-2 wy2020-wy2030



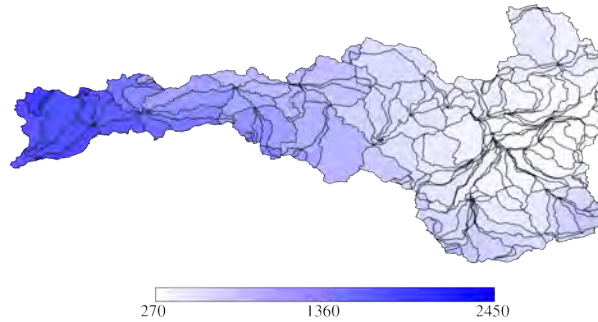
10-Year Average of Annual Liquid Water (mm)
ECHAM5 A2-2 wy2030-wy2040



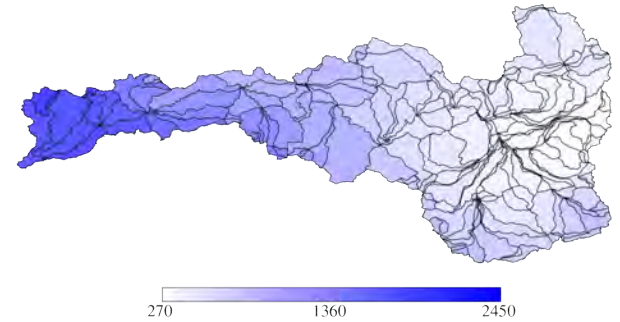
10-Year Average of Annual Liquid Water (mm)
ECHAM5 A2-2 wy2040-wy2050



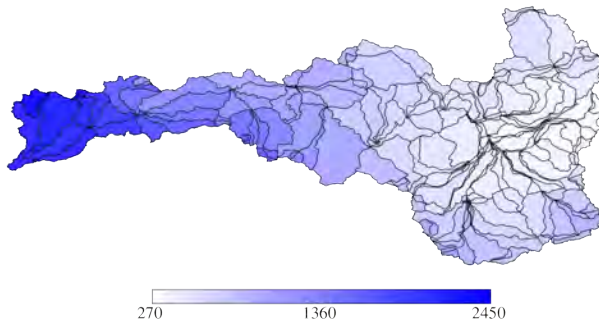
10-Year Average of Annual Liquid Water (mm)
ECHAM5 A2-2 wy2050-wy2060



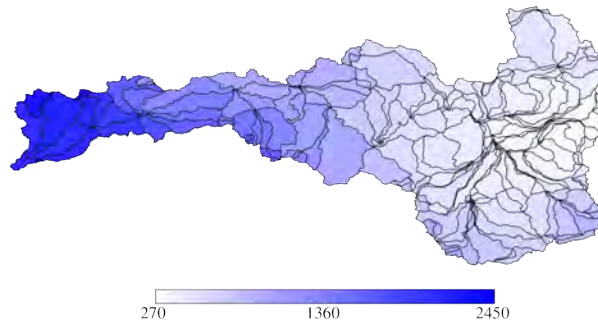
10-Year Average of Annual Liquid Water (mm)
ECHAM5 A2-2 wy2060-wy2070



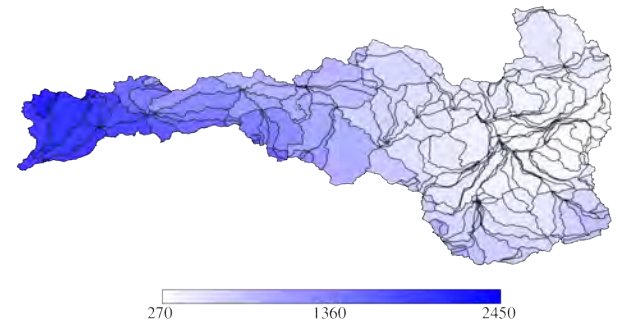
10-Year Average of Annual Liquid Water (mm)
ECHAM5 A2-2 wy2070-wy2080



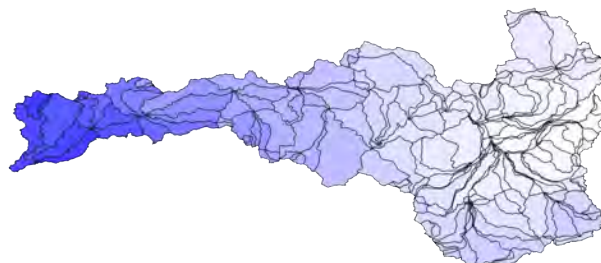
10-Year Average of Annual Liquid Water (mm)
ECHAM5 A2-2 wy2080-wy2090



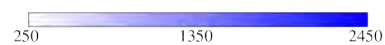
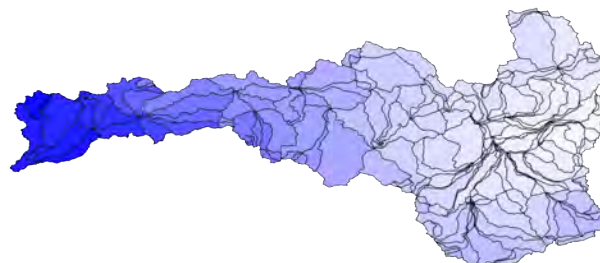
10-Year Average of Annual Liquid Water (mm)
ECHAM5 A2-2 wy2090-wy2100



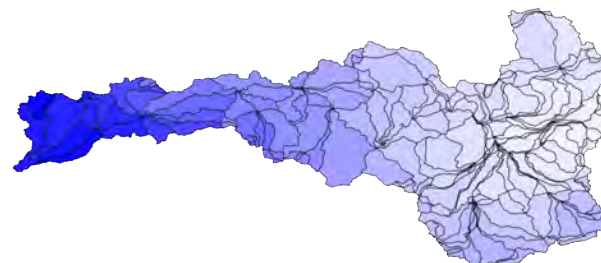
10-Year Average of Annual Liquid Water (mm)
ECHAM5 A2-3 wy2010-wy2020



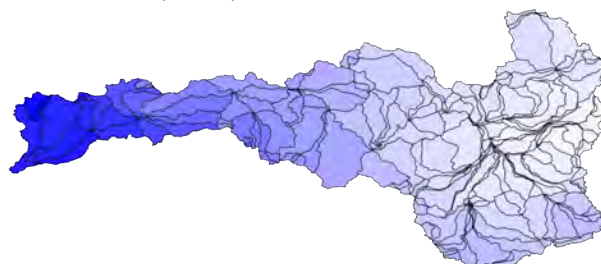
10-Year Average of Annual Liquid Water (mm)
ECHAM5 A2-3 wy2020-wy2030



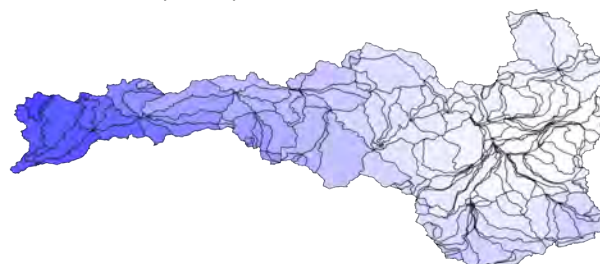
10-Year Average of Annual Liquid Water (mm)
ECHAM5 A2-3 wy2030-wy2040



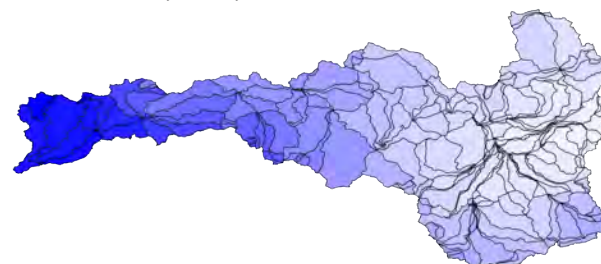
10-Year Average of Annual Liquid Water (mm)
ECHAM5 A2-3 wy2040-wy2050



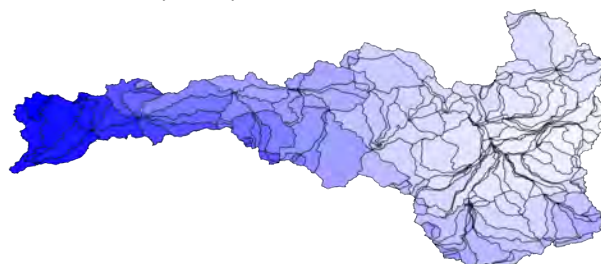
10-Year Average of Annual Liquid Water (mm)
ECHAM5 A2-3 wy2050-wy2060



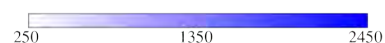
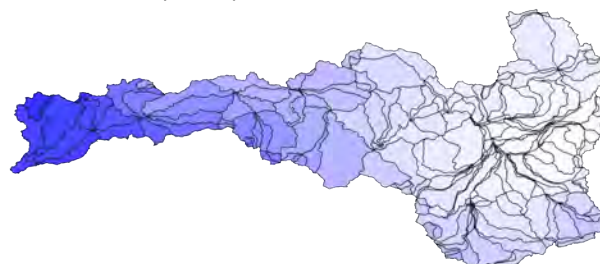
10-Year Average of Annual Liquid Water (mm)
ECHAM5 A2-3 wy2060-wy2070



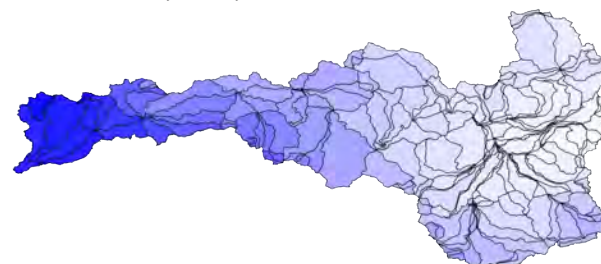
10-Year Average of Annual Liquid Water (mm)
ECHAM5 A2-3 wy2070-wy2080



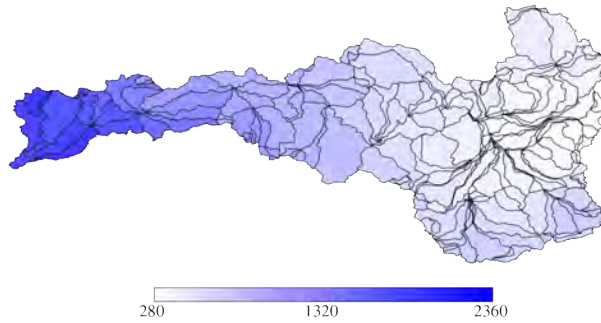
10-Year Average of Annual Liquid Water (mm)
ECHAM5 A2-3 wy2080-wy2090



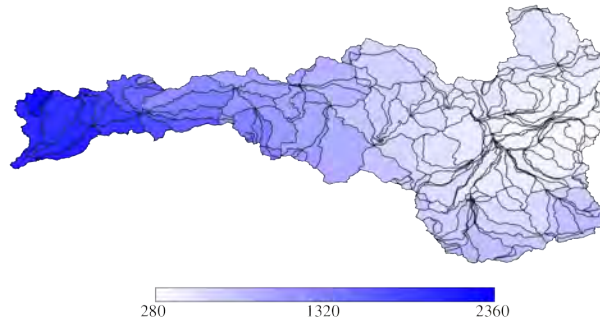
10-Year Average of Annual Liquid Water (mm)
ECHAM5 A2-3 wy2090-wy2100



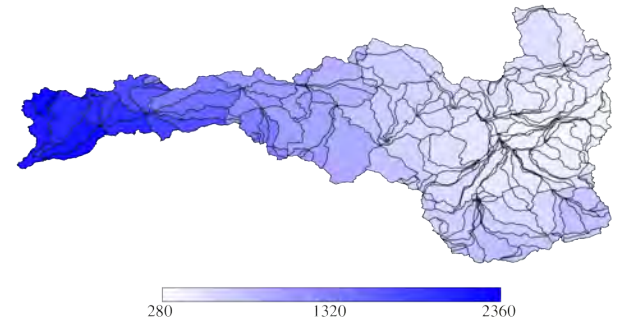
10-Year Average of Annual Liquid Water (mm)
ECHAM5 B1-1 wy2010-wy2020



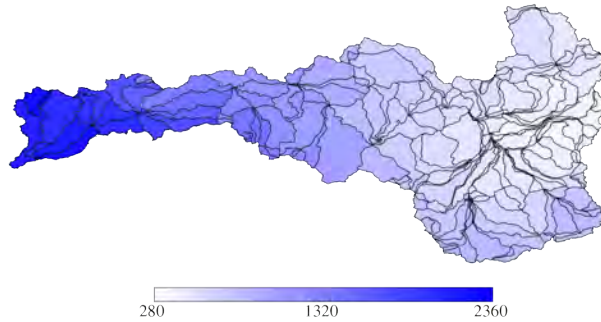
10-Year Average of Annual Liquid Water (mm)
ECHAM5 B1-1 wy2020-wy2030



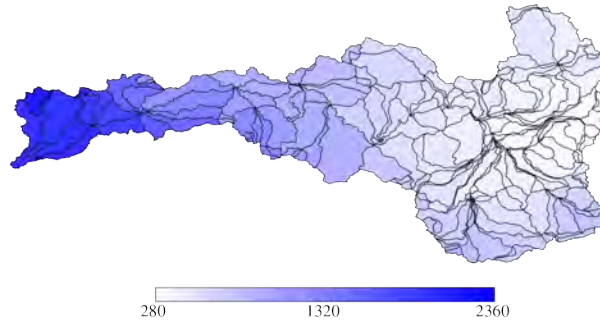
10-Year Average of Annual Liquid Water (mm)
ECHAM5 B1-1 wy2030-wy2040



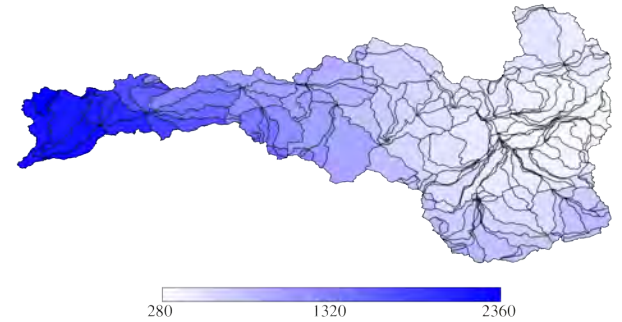
10-Year Average of Annual Liquid Water (mm)
ECHAM5 B1-1 wy2040-wy2050



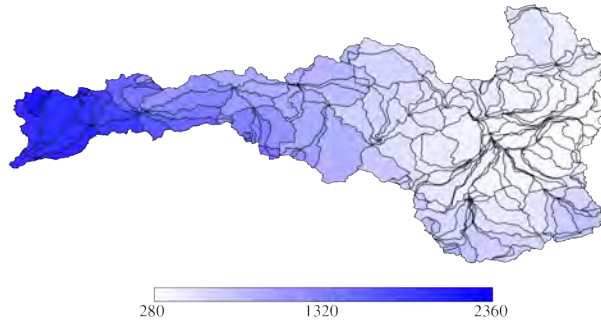
10-Year Average of Annual Liquid Water (mm)
ECHAM5 B1-1 wy2050-wy2060



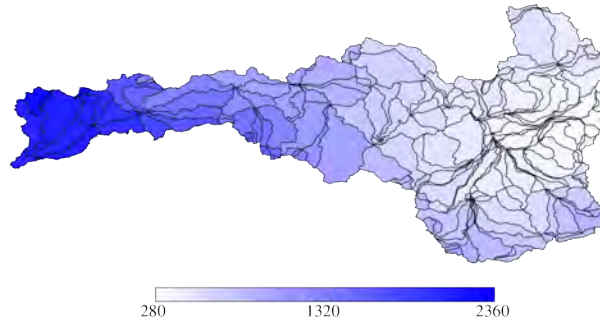
10-Year Average of Annual Liquid Water (mm)
ECHAM5 B1-1 wy2060-wy2070



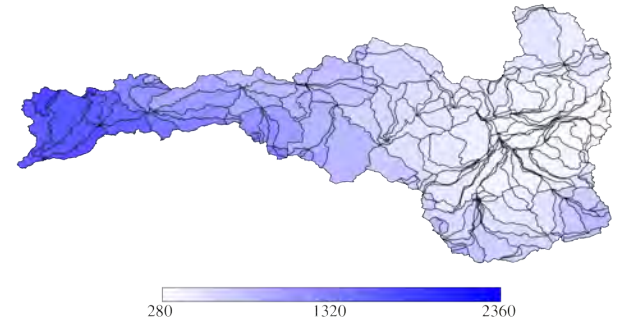
10-Year Average of Annual Liquid Water (mm)
ECHAM5 B1-1 wy2070-wy2080



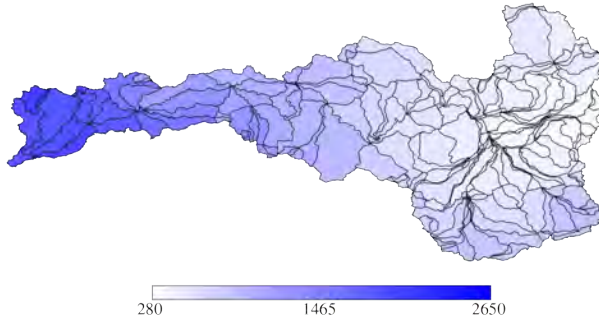
10-Year Average of Annual Liquid Water (mm)
ECHAM5 B1-1 wy2080-wy2090



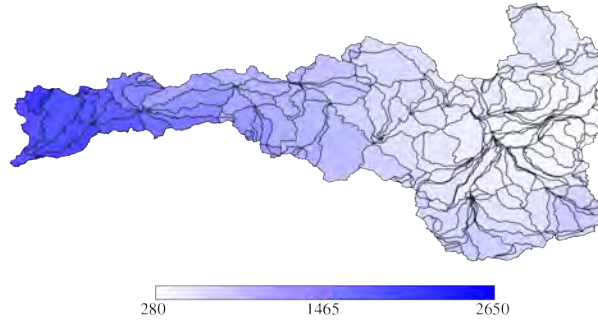
10-Year Average of Annual Liquid Water (mm)
ECHAM5 B1-1 wy2090-wy2100



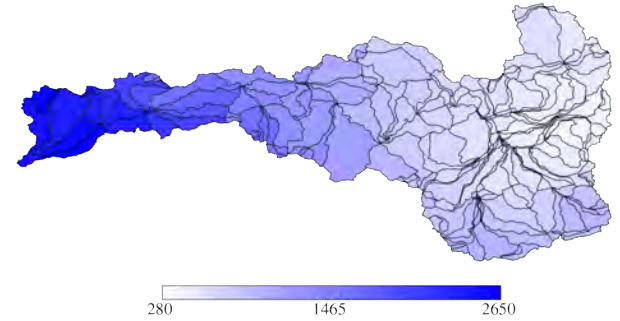
10-Year Average of Annual Liquid Water (mm)
ECHAM5 B1-2 wy2010-wy2020



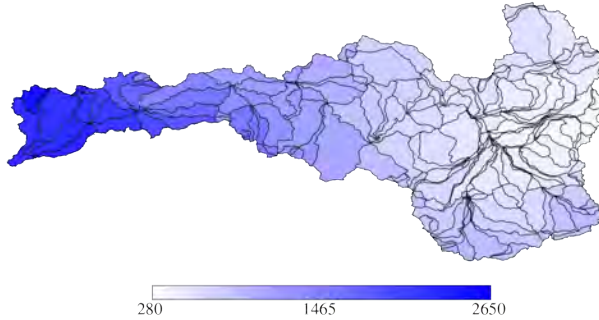
10-Year Average of Annual Liquid Water (mm)
ECHAM5 B1-2 wy2020-wy2030



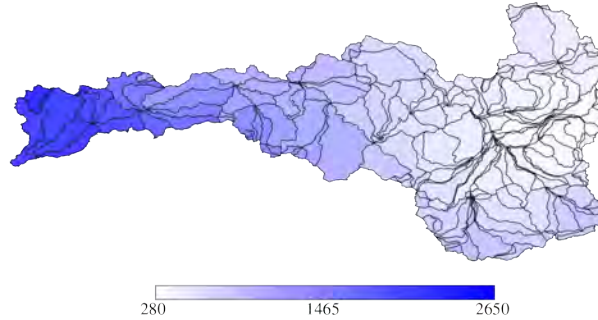
10-Year Average of Annual Liquid Water (mm)
ECHAM5 B1-2 wy2030-wy2040



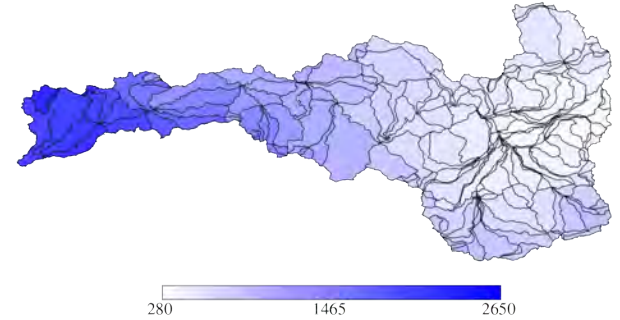
10-Year Average of Annual Liquid Water (mm)
ECHAM5 B1-2 wy2040-wy2050



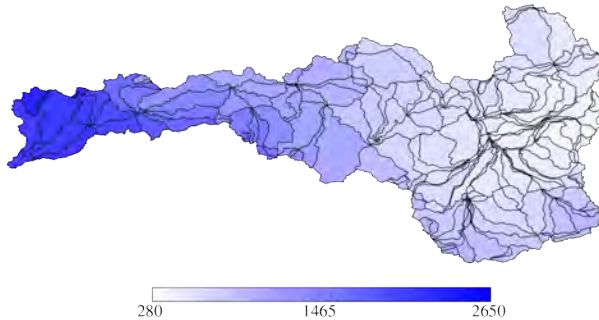
10-Year Average of Annual Liquid Water (mm)
ECHAM5 B1-2 wy2050-wy2060



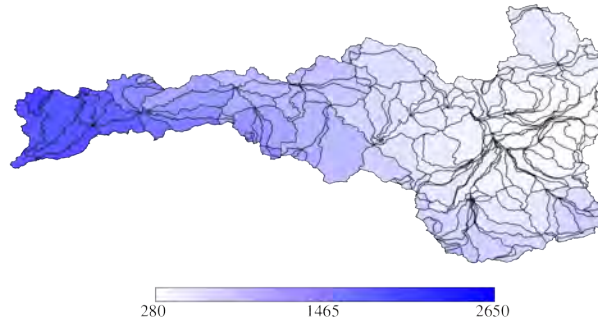
10-Year Average of Annual Liquid Water (mm)
ECHAM5 B1-2 wy2060-wy2070



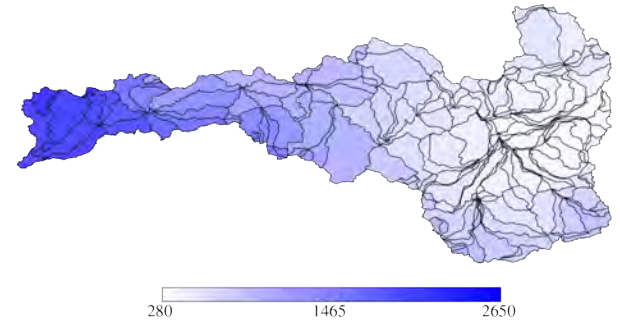
10-Year Average of Annual Liquid Water (mm)
ECHAM5 B1-2 wy2070-wy2080



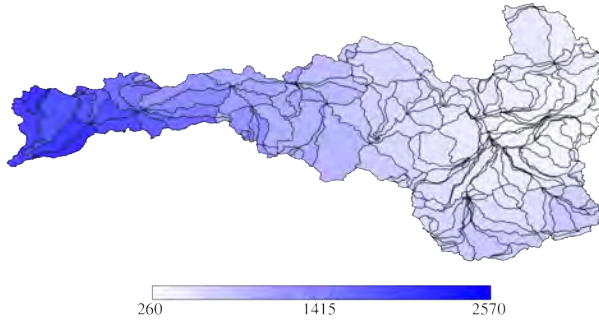
10-Year Average of Annual Liquid Water (mm)
ECHAM5 B1-2 wy2080-wy2090



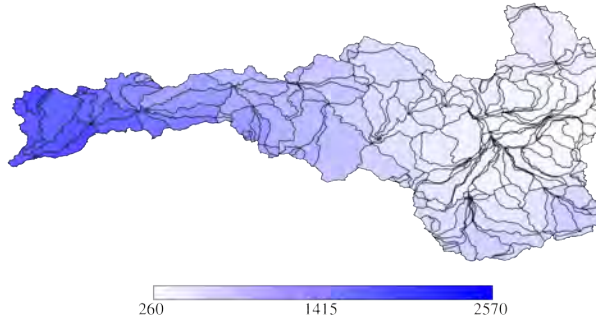
10-Year Average of Annual Liquid Water (mm)
ECHAM5 B1-2 wy2090-wy2100



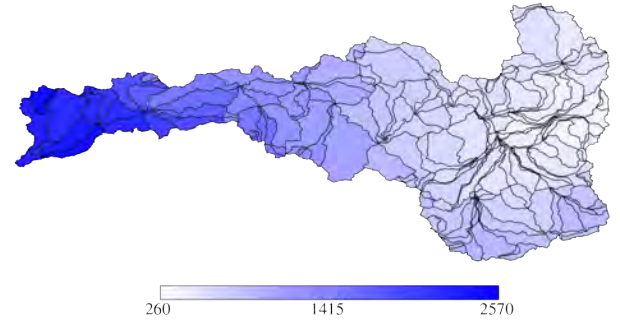
10-Year Average of Annual Liquid Water (mm)
ECHAM5 B1-3 wy2010-wy2020



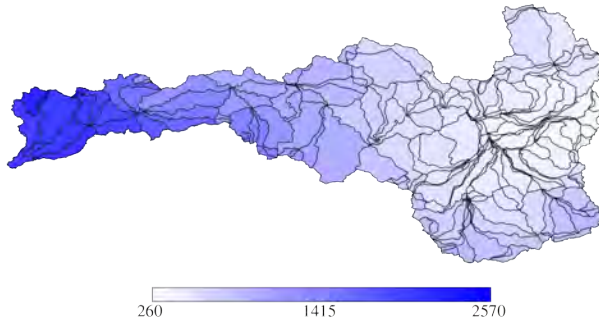
10-Year Average of Annual Liquid Water (mm)
ECHAM5 B1-3 wy2020-wy2030



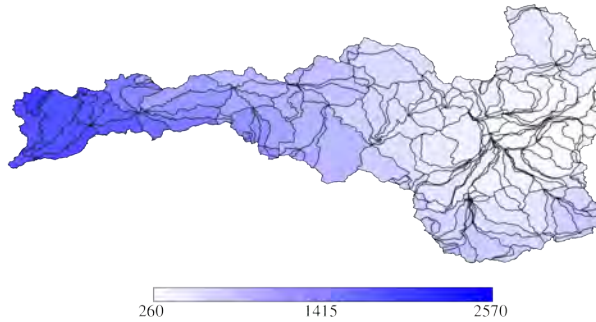
10-Year Average of Annual Liquid Water (mm)
ECHAM5 B1-3 wy2030-wy2040



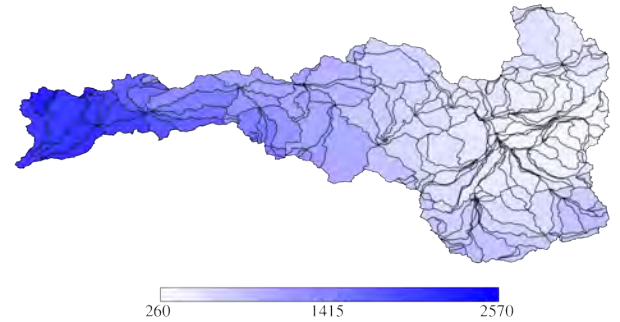
10-Year Average of Annual Liquid Water (mm)
ECHAM5 B1-3 wy2040-wy2050



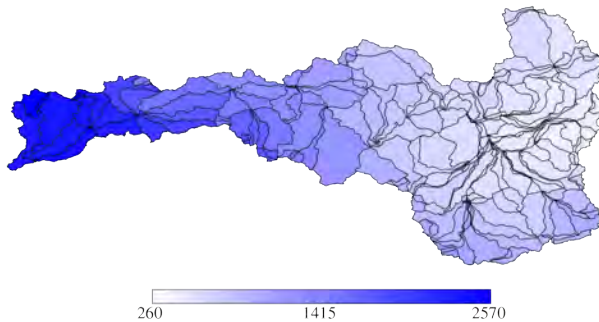
10-Year Average of Annual Liquid Water (mm)
ECHAM5 B1-3 wy2050-wy2060



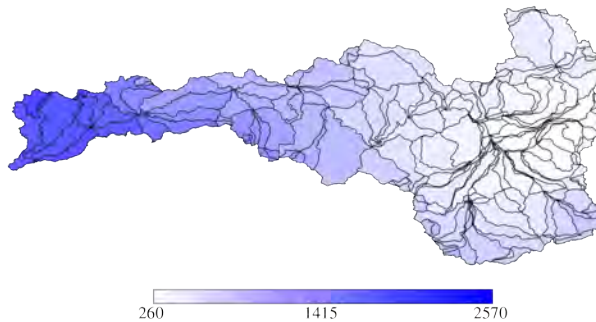
10-Year Average of Annual Liquid Water (mm)
ECHAM5 B1-3 wy2060-wy2070



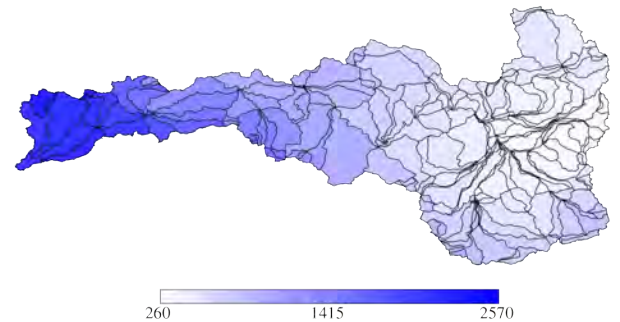
10-Year Average of Annual Liquid Water (mm)
ECHAM5 B1-3 wy2070-wy2080



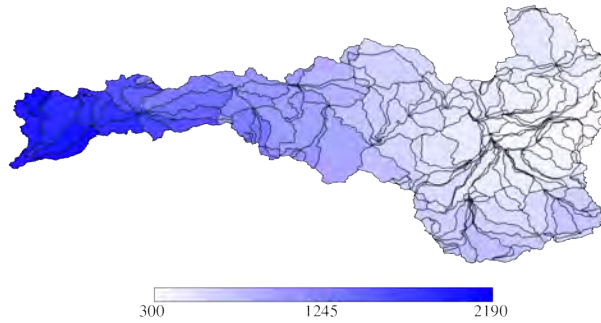
10-Year Average of Annual Liquid Water (mm)
ECHAM5 B1-3 wy2080-wy2090



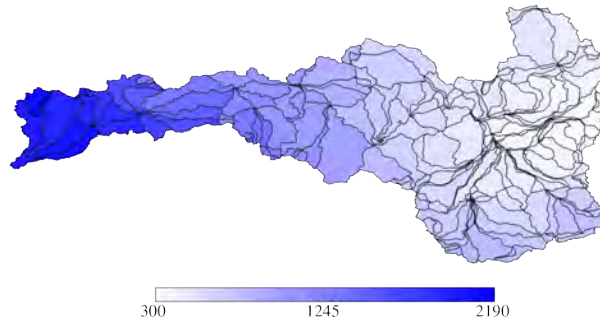
10-Year Average of Annual Liquid Water (mm)
ECHAM5 B1-3 wy2090-wy2100



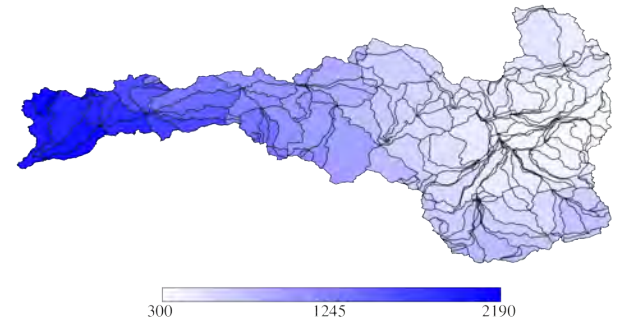
10-Year Average of Annual Liquid Water (mm)
Ensemble All wy2010-wy2020



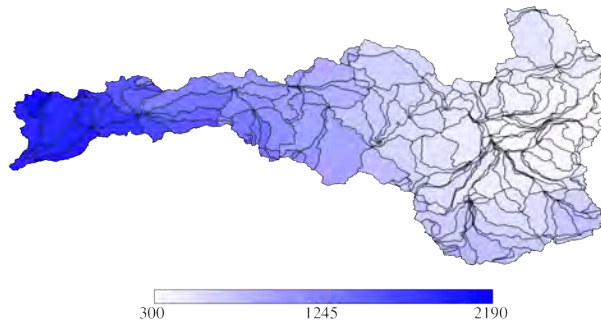
10-Year Average of Annual Liquid Water (mm)
Ensemble All wy2020-wy2030



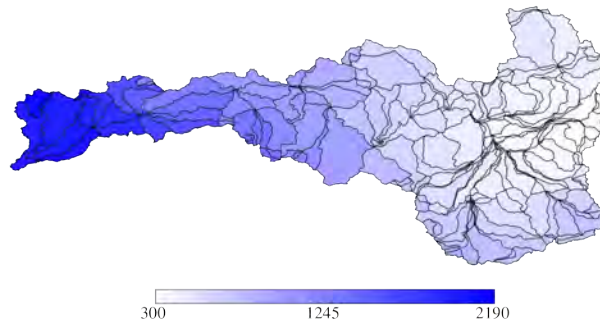
10-Year Average of Annual Liquid Water (mm)
Ensemble All wy2030-wy2040



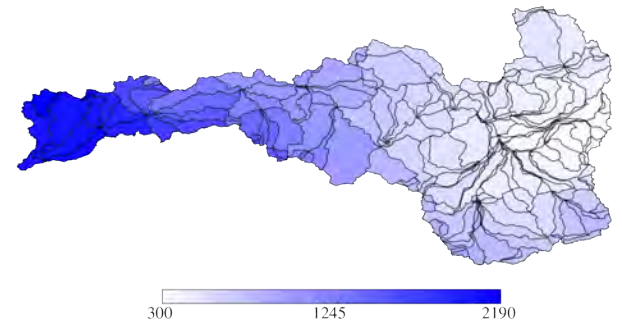
10-Year Average of Annual Liquid Water (mm)
Ensemble All wy2040-wy2050



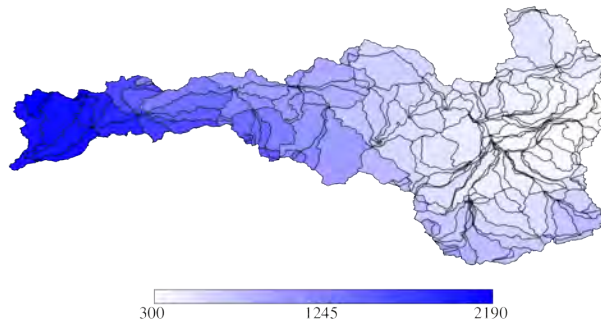
10-Year Average of Annual Liquid Water (mm)
Ensemble All wy2050-wy2060



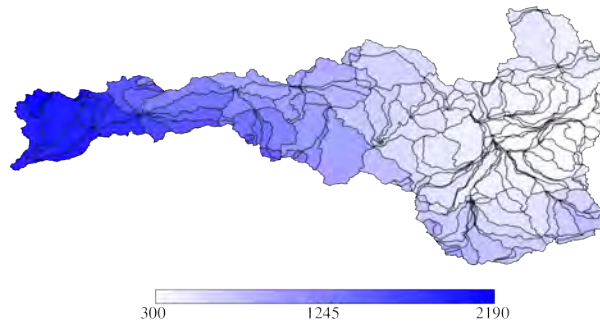
10-Year Average of Annual Liquid Water (mm)
Ensemble All wy2060-wy2070



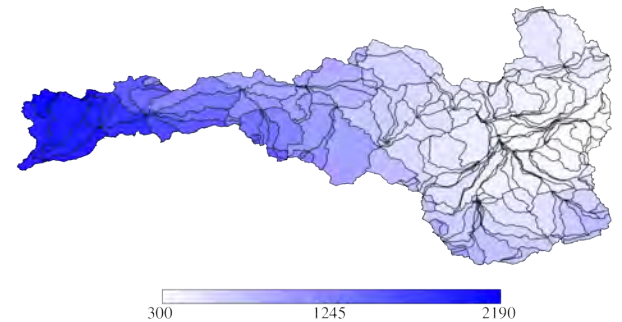
10-Year Average of Annual Liquid Water (mm)
Ensemble All wy2070-wy2080



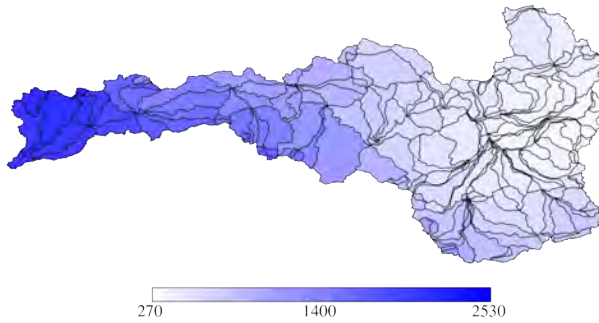
10-Year Average of Annual Liquid Water (mm)
Ensemble All wy2080-wy2090



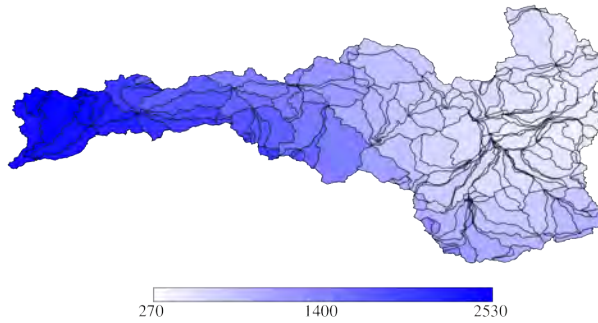
10-Year Average of Annual Liquid Water (mm)
Ensemble All wy2090-wy2100



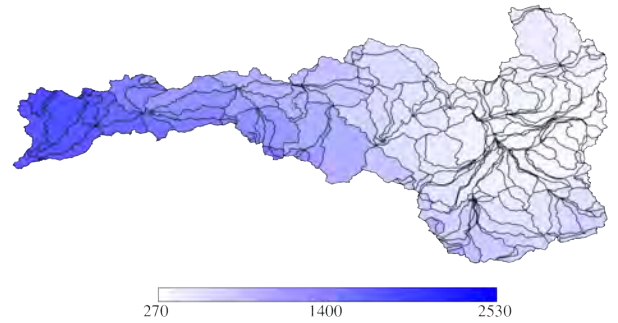
10-Year Average of Annual Precipitation (mm)
CCSM3 A1B wy2010-wy2020



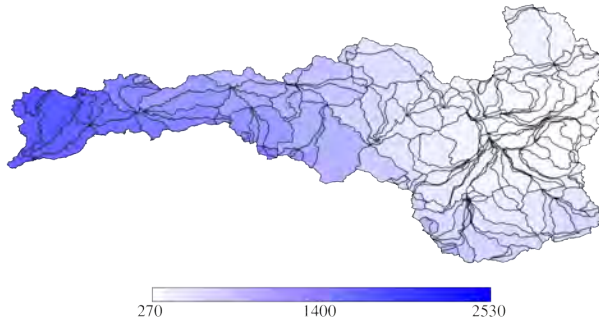
10-Year Average of Annual Precipitation (mm)
CCSM3 A1B wy2020-wy2030



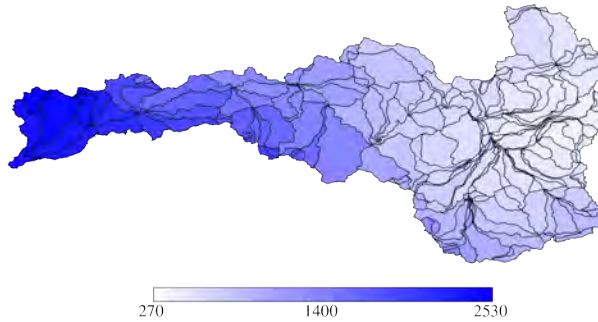
10-Year Average of Annual Precipitation (mm)
CCSM3 A1B wy2030-wy2040



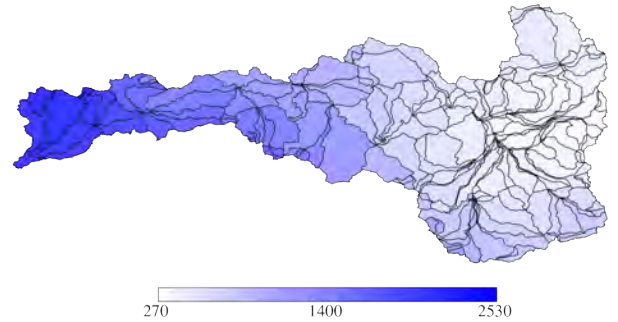
10-Year Average of Annual Precipitation (mm)
CCSM3 A1B wy2040-wy2050



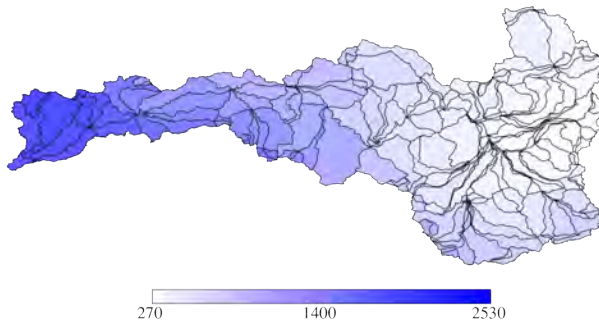
10-Year Average of Annual Precipitation (mm)
CCSM3 A1B wy2050-wy2060



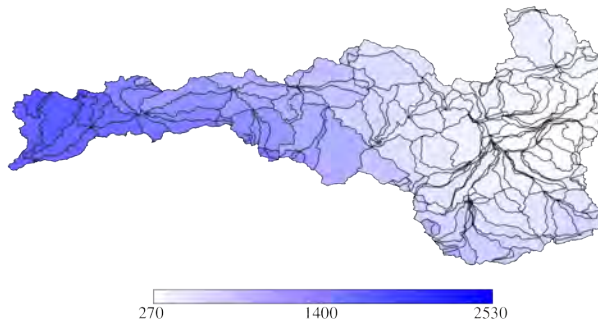
10-Year Average of Annual Precipitation (mm)
CCSM3 A1B wy2060-wy2070



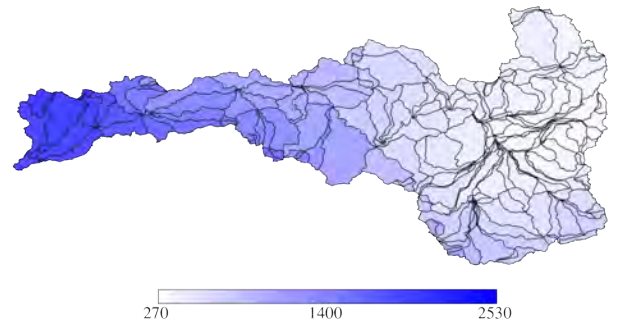
10-Year Average of Annual Precipitation (mm)
CCSM3 A1B wy2070-wy2080



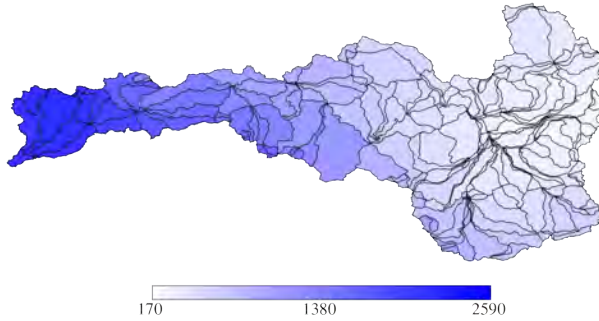
10-Year Average of Annual Precipitation (mm)
CCSM3 A1B wy2080-wy2090



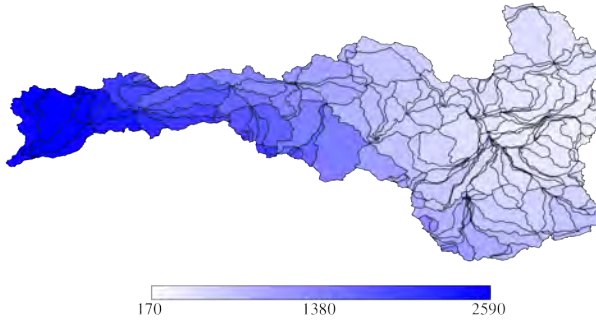
10-Year Average of Annual Precipitation (mm)
CCSM3 A1B wy2090-wy2100



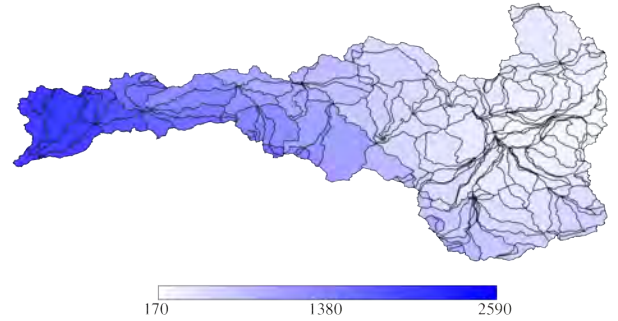
10-Year Average of Annual Precipitation (mm)
CCSM3 A1FI wy2010-wy2020



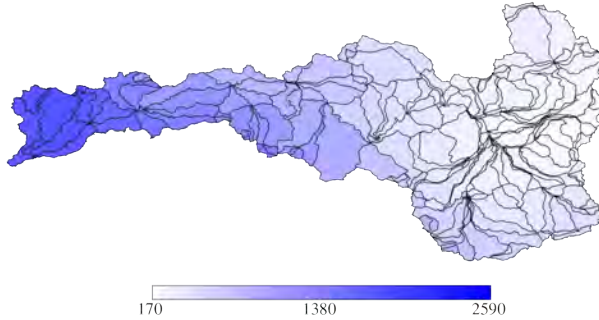
10-Year Average of Annual Precipitation (mm)
CCSM3 A1FI wy2020-wy2030



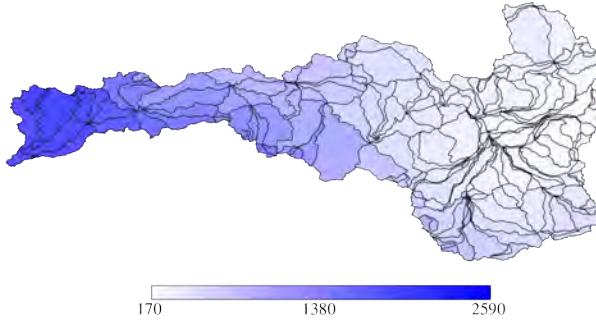
10-Year Average of Annual Precipitation (mm)
CCSM3 A1FI wy2030-wy2040



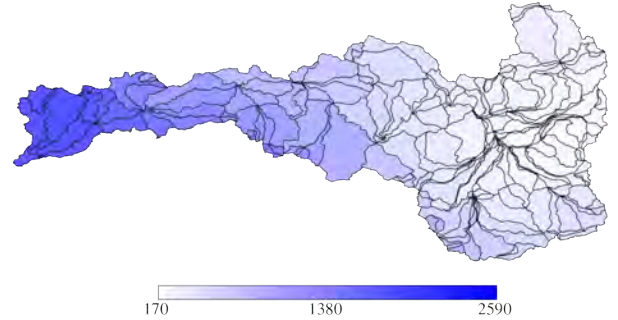
10-Year Average of Annual Precipitation (mm)
CCSM3 A1FI wy2040-wy2050



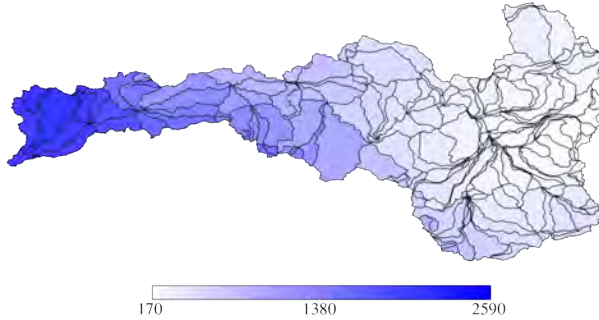
10-Year Average of Annual Precipitation (mm)
CCSM3 A1FI wy2050-wy2060



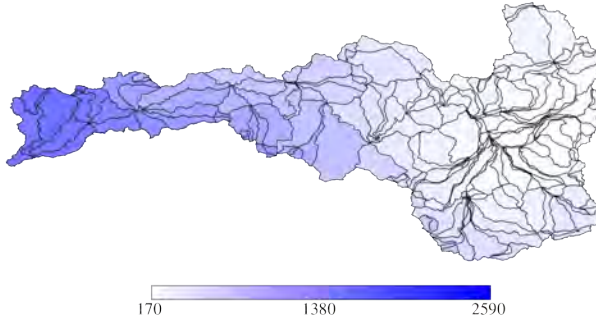
10-Year Average of Annual Precipitation (mm)
CCSM3 A1FI wy2060-wy2070



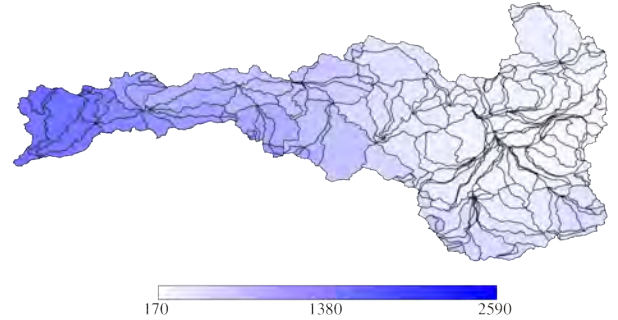
10-Year Average of Annual Precipitation (mm)
CCSM3 A1FI wy2070-wy2080



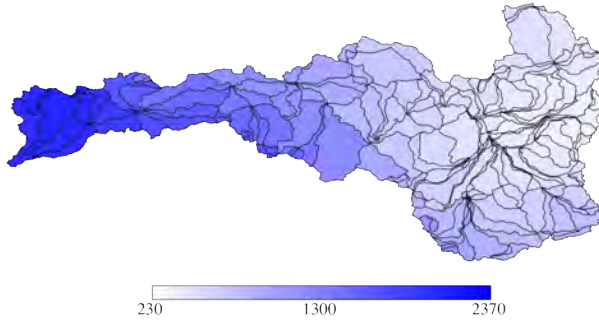
10-Year Average of Annual Precipitation (mm)
CCSM3 A1FI wy2080-wy2090



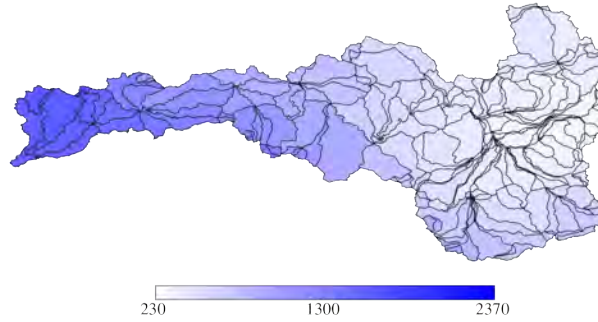
10-Year Average of Annual Precipitation (mm)
CCSM3 A1FI wy2090-wy2100



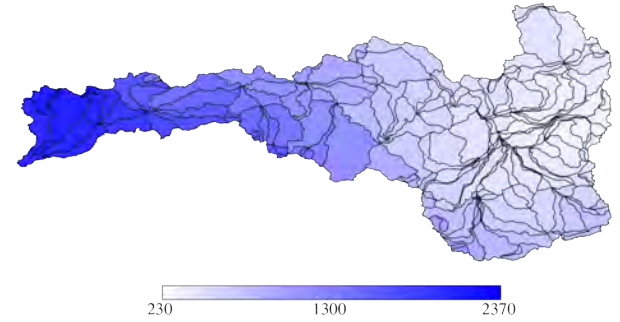
10-Year Average of Annual Precipitation (mm)
CCSM3 A2 wy2010-wy2020



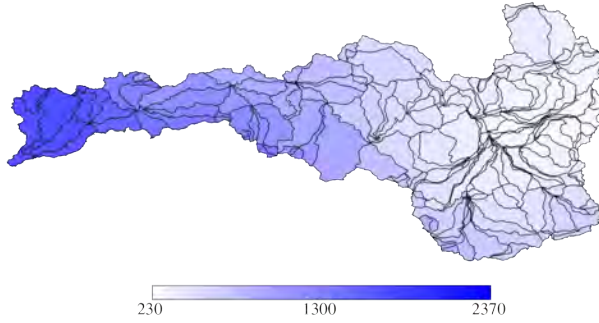
10-Year Average of Annual Precipitation (mm)
CCSM3 A2 wy2020-wy2030



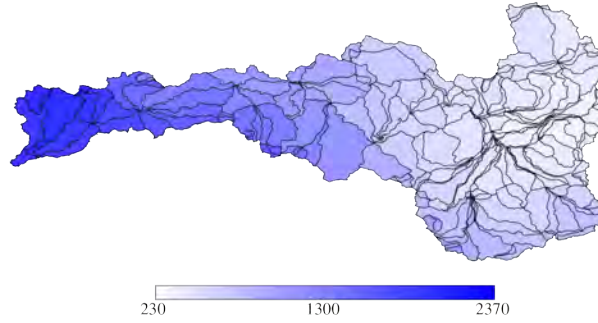
10-Year Average of Annual Precipitation (mm)
CCSM3 A2 wy2030-wy2040



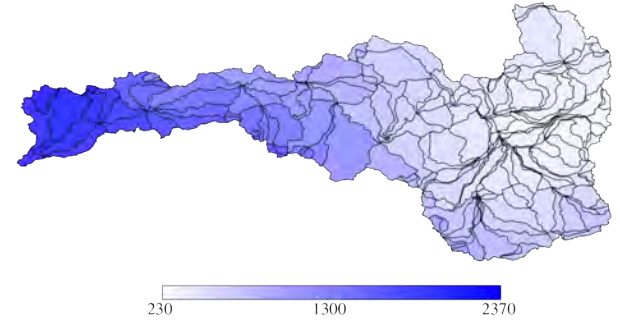
10-Year Average of Annual Precipitation (mm)
CCSM3 A2 wy2040-wy2050



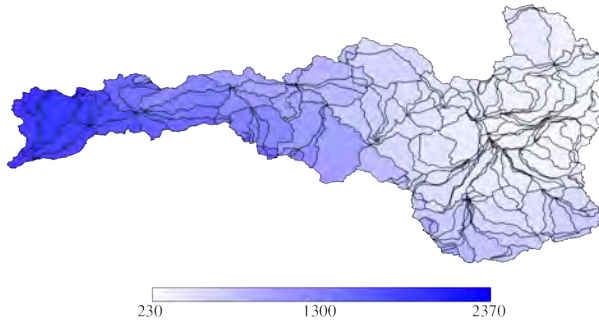
10-Year Average of Annual Precipitation (mm)
CCSM3 A2 wy2050-wy2060



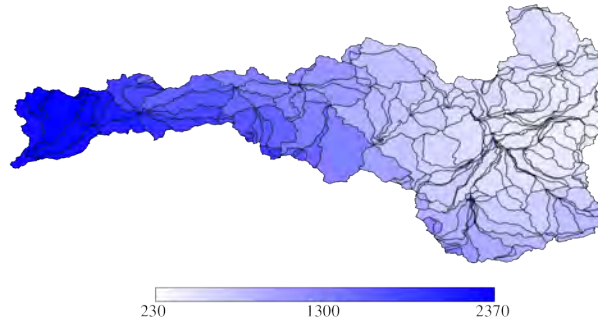
10-Year Average of Annual Precipitation (mm)
CCSM3 A2 wy2060-wy2070



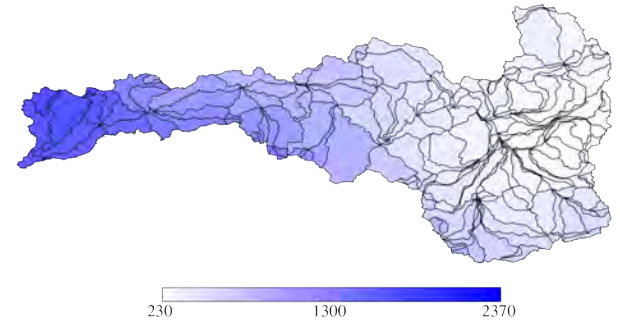
10-Year Average of Annual Precipitation (mm)
CCSM3 A2 wy2070-wy2080



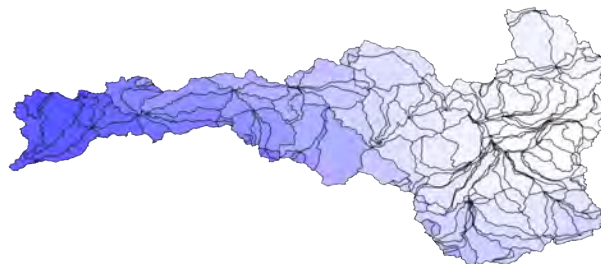
10-Year Average of Annual Precipitation (mm)
CCSM3 A2 wy2080-wy2090



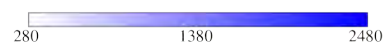
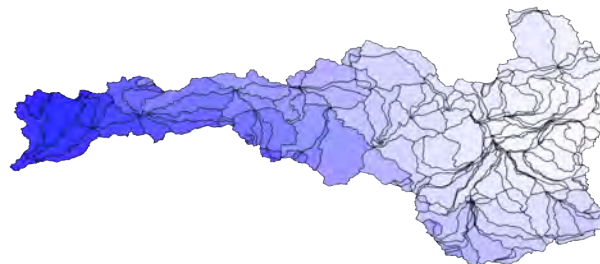
10-Year Average of Annual Precipitation (mm)
CCSM3 A2 wy2090-wy2100



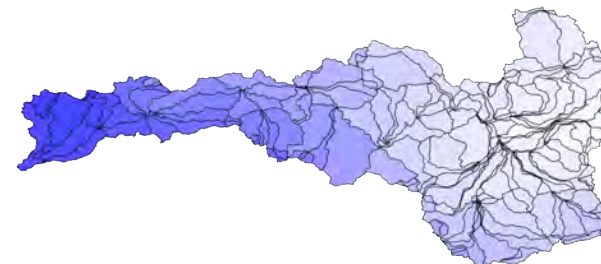
10-Year Average of Annual Precipitation (mm)
CCSM3 B1 wy2010-wy2020



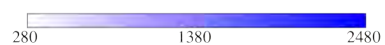
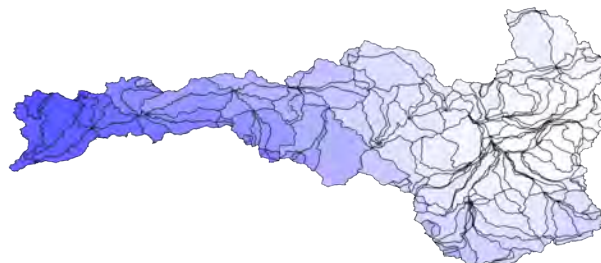
10-Year Average of Annual Precipitation (mm)
CCSM3 B1 wy2020-wy2030



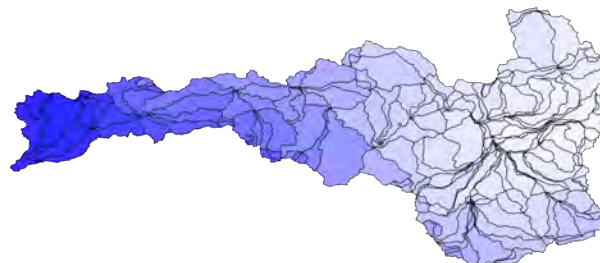
10-Year Average of Annual Precipitation (mm)
CCSM3 B1 wy2030-wy2040



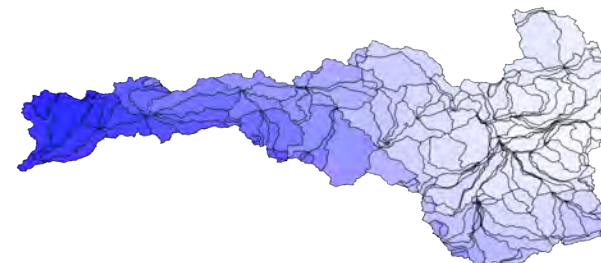
10-Year Average of Annual Precipitation (mm)
CCSM3 B1 wy2040-wy2050



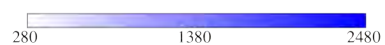
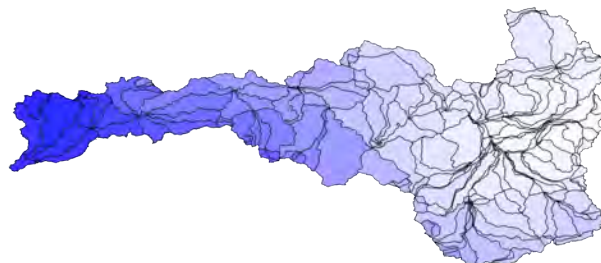
10-Year Average of Annual Precipitation (mm)
CCSM3 B1 wy2050-wy2060



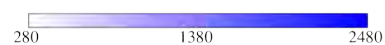
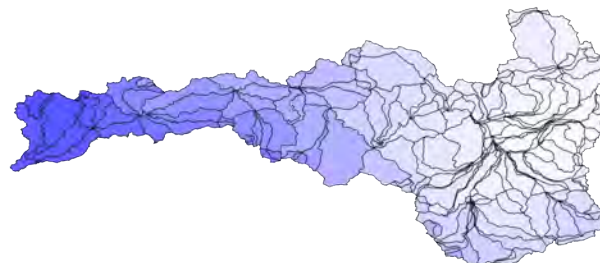
10-Year Average of Annual Precipitation (mm)
CCSM3 B1 wy2060-wy2070



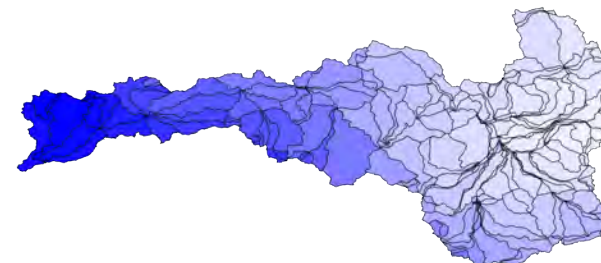
10-Year Average of Annual Precipitation (mm)
CCSM3 B1 wy2070-wy2080



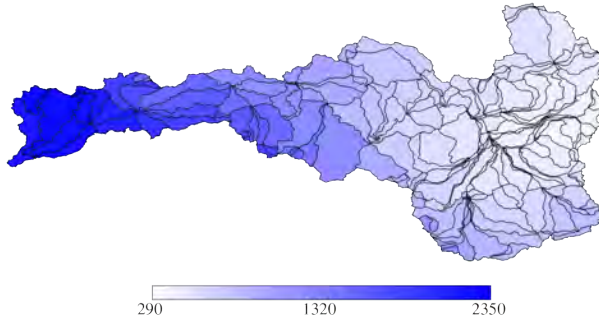
10-Year Average of Annual Precipitation (mm)
CCSM3 B1 wy2080-wy2090



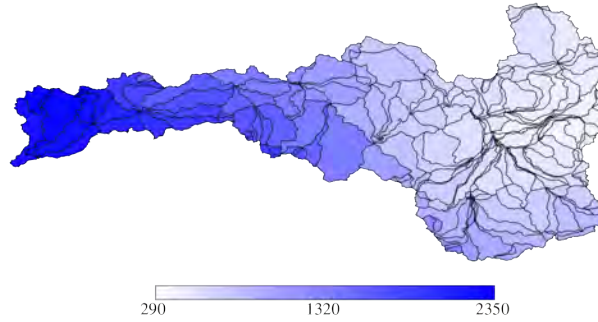
10-Year Average of Annual Precipitation (mm)
CCSM3 B1 wy2090-wy2100



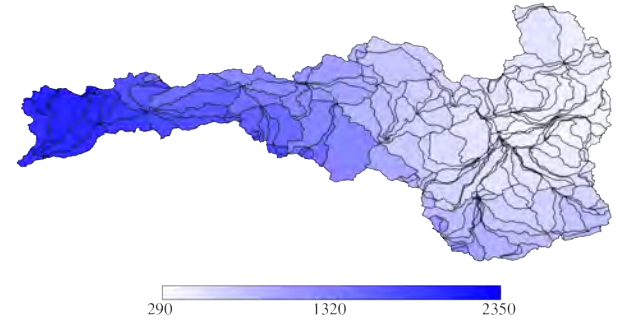
10-Year Average of Annual Precipitation (mm)
ECHAM5 A1B1 wy2010-wy2020



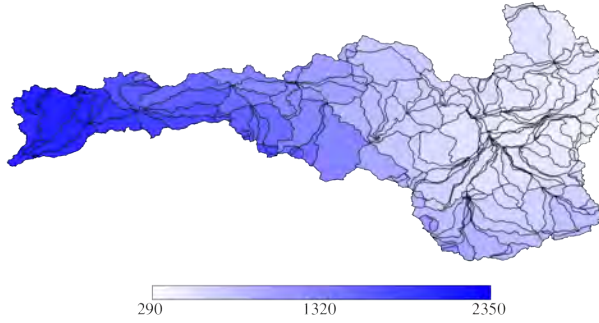
10-Year Average of Annual Precipitation (mm)
ECHAM5 A1B1 wy2020-wy2030



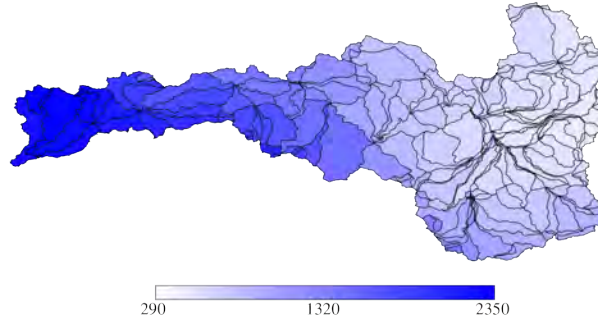
10-Year Average of Annual Precipitation (mm)
ECHAM5 A1B1 wy2030-wy2040



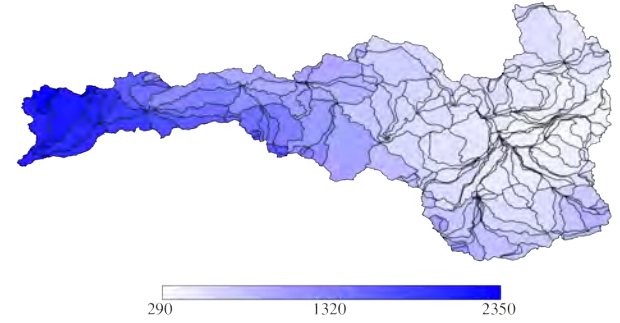
10-Year Average of Annual Precipitation (mm)
ECHAM5 A1B1 wy2040-wy2050



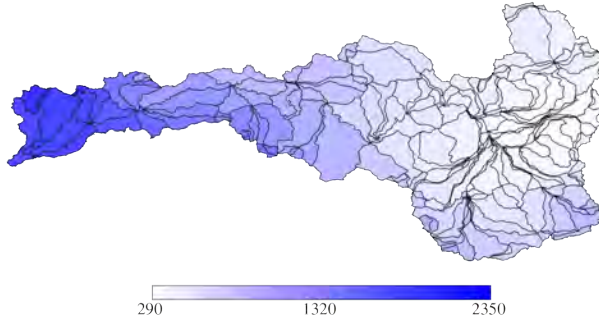
10-Year Average of Annual Precipitation (mm)
ECHAM5 A1B1 wy2050-wy2060



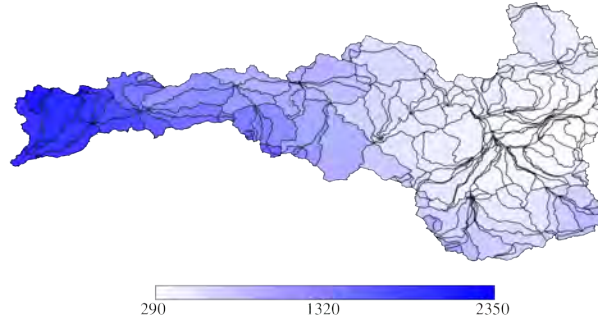
10-Year Average of Annual Precipitation (mm)
ECHAM5 A1B1 wy2060-wy2070



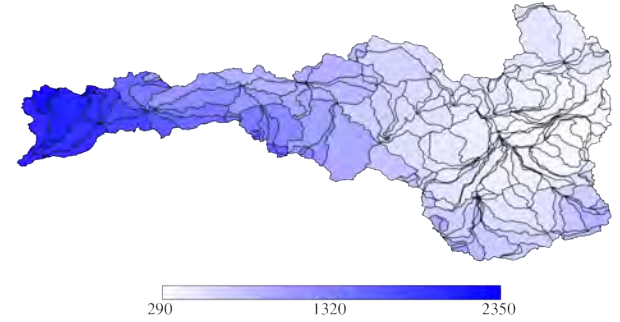
10-Year Average of Annual Precipitation (mm)
ECHAM5 A1B1 wy2070-wy2080



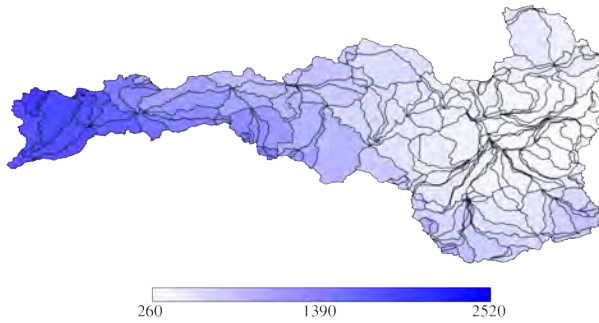
10-Year Average of Annual Precipitation (mm)
ECHAM5 A1B1 wy2080-wy2090



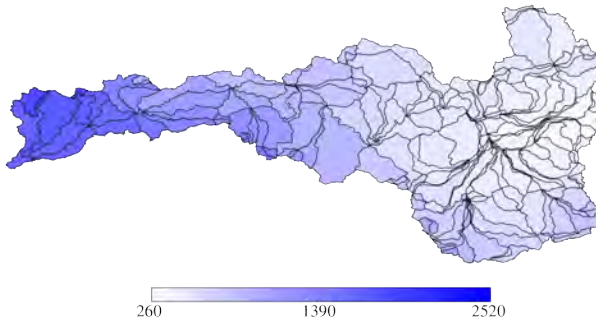
10-Year Average of Annual Precipitation (mm)
ECHAM5 A1B1 wy2090-wy2100



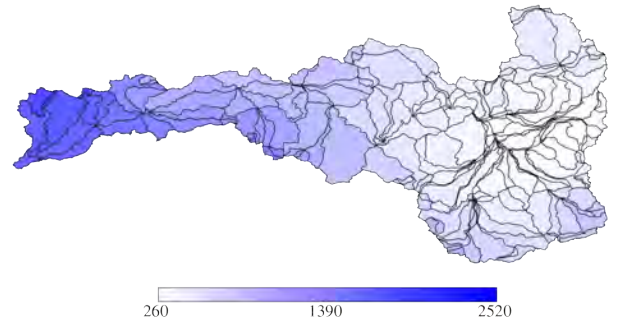
10-Year Average of Annual Precipitation (mm)
ECHAM5 A1B2 wy2010-wy2020



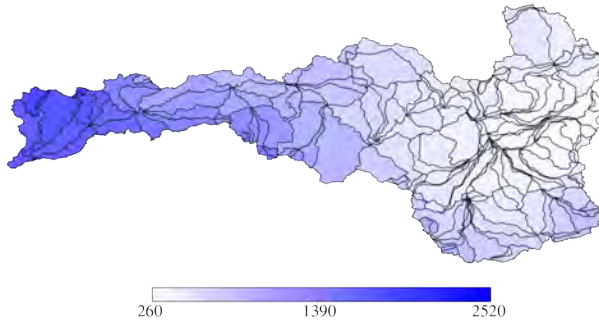
10-Year Average of Annual Precipitation (mm)
ECHAM5 A1B2 wy2020-wy2030



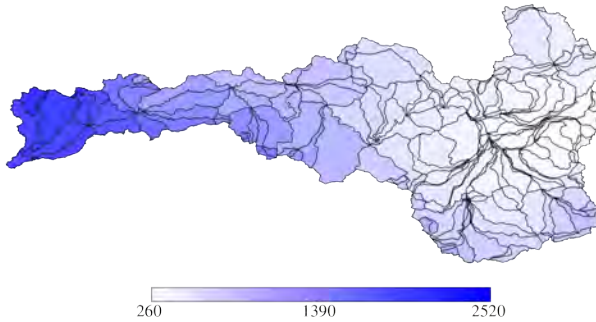
10-Year Average of Annual Precipitation (mm)
ECHAM5 A1B2 wy2030-wy2040



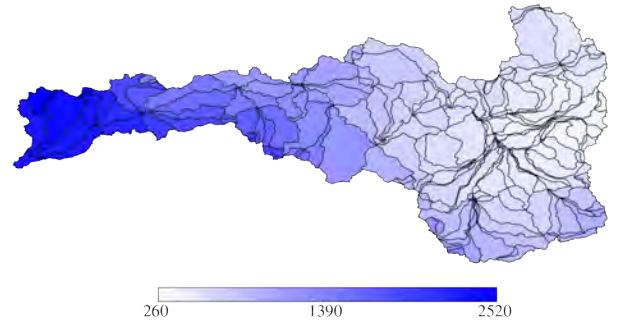
10-Year Average of Annual Precipitation (mm)
ECHAM5 A1B2 wy2040-wy2050



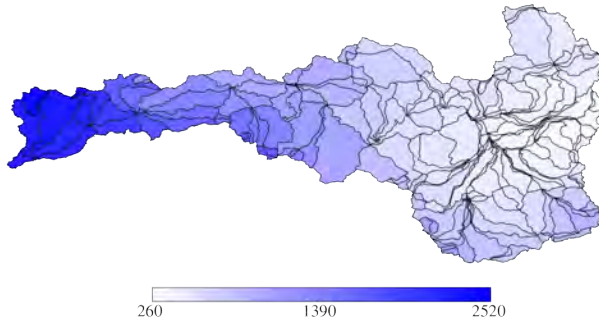
10-Year Average of Annual Precipitation (mm)
ECHAM5 A1B2 wy2050-wy2060



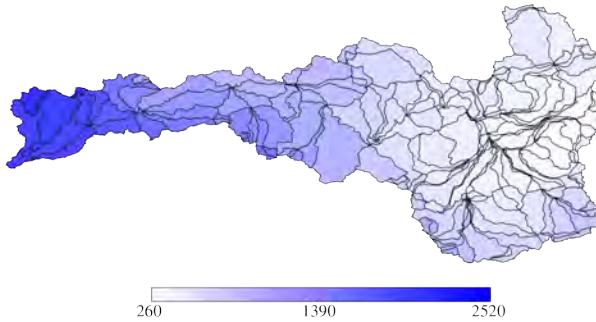
10-Year Average of Annual Precipitation (mm)
ECHAM5 A1B2 wy2060-wy2070



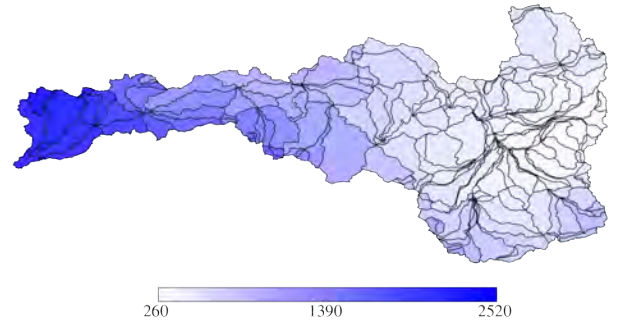
10-Year Average of Annual Precipitation (mm)
ECHAM5 A1B2 wy2070-wy2080



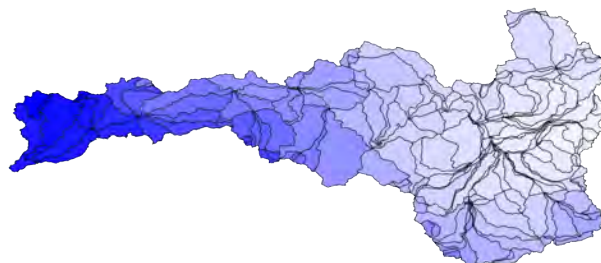
10-Year Average of Annual Precipitation (mm)
ECHAM5 A1B2 wy2080-wy2090



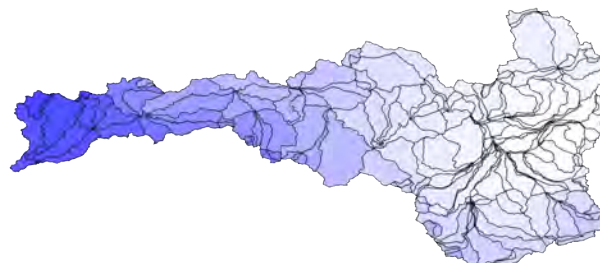
10-Year Average of Annual Precipitation (mm)
ECHAM5 A1B2 wy2090-wy2100



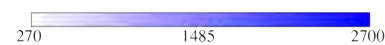
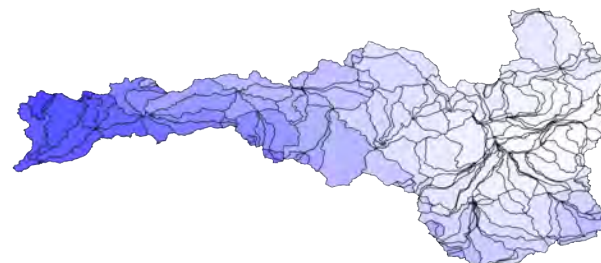
10-Year Average of Annual Precipitation (mm)
ECHAM5 A1B3 wy2010-wy2020



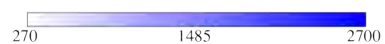
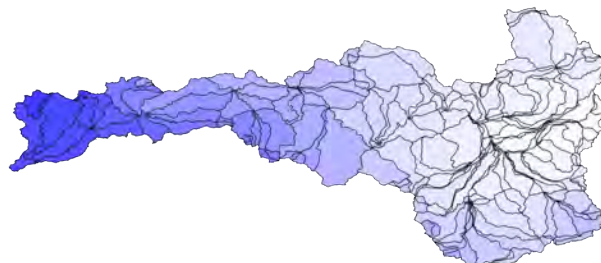
10-Year Average of Annual Precipitation (mm)
ECHAM5 A1B3 wy2020-wy2030



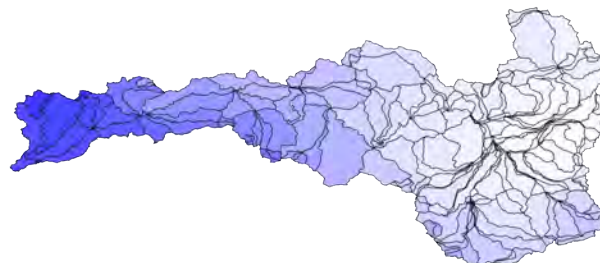
10-Year Average of Annual Precipitation (mm)
ECHAM5 A1B3 wy2030-wy2040



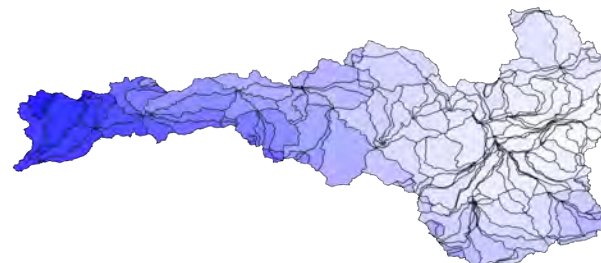
10-Year Average of Annual Precipitation (mm)
ECHAM5 A1B3 wy2040-wy2050



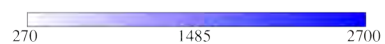
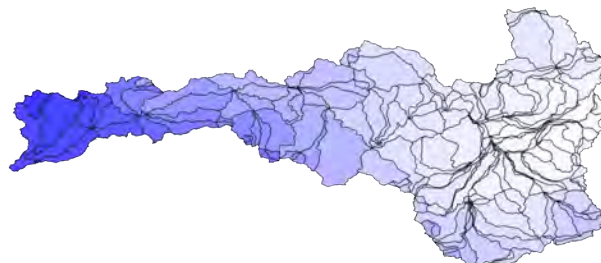
10-Year Average of Annual Precipitation (mm)
ECHAM5 A1B3 wy2050-wy2060



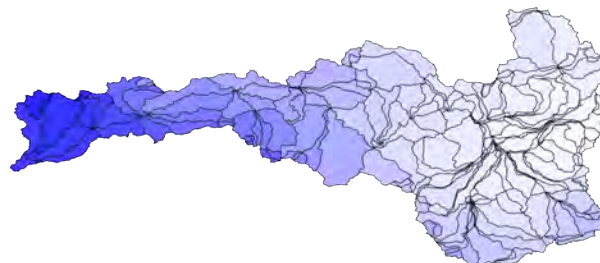
10-Year Average of Annual Precipitation (mm)
ECHAM5 A1B3 wy2060-wy2070



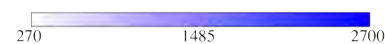
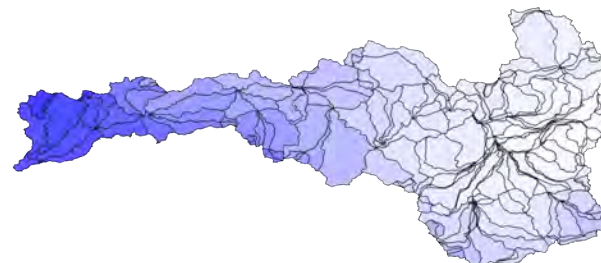
10-Year Average of Annual Precipitation (mm)
ECHAM5 A1B3 wy2070-wy2080



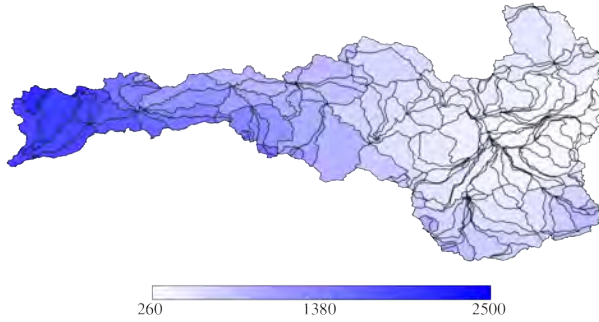
10-Year Average of Annual Precipitation (mm)
ECHAM5 A1B3 wy2080-wy2090



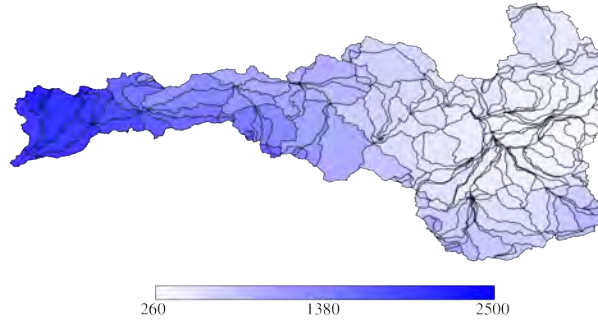
10-Year Average of Annual Precipitation (mm)
ECHAM5 A1B3 wy2090-wy2100



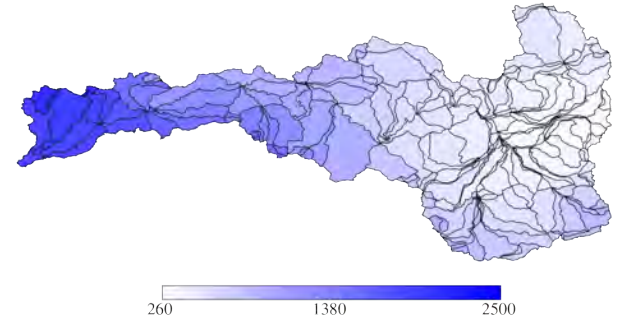
10-Year Average of Annual Precipitation (mm)
ECHAM5 A2-1 wy2010-wy2020



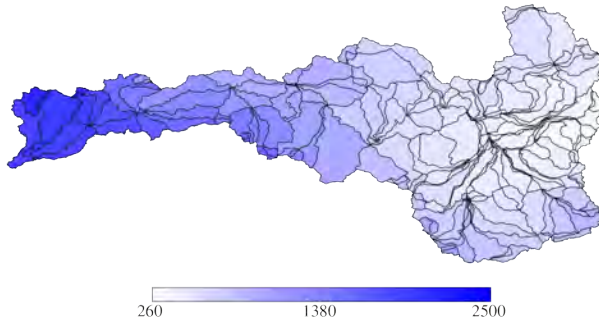
10-Year Average of Annual Precipitation (mm)
ECHAM5 A2-1 wy2020-wy2030



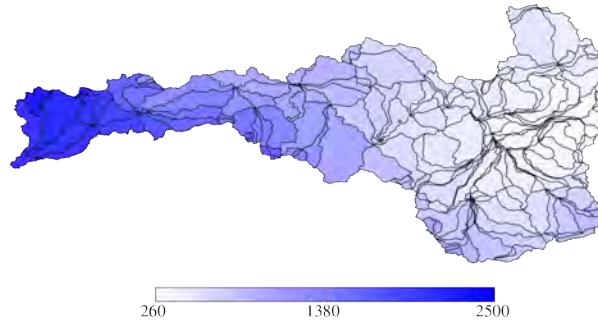
10-Year Average of Annual Precipitation (mm)
ECHAM5 A2-1 wy2030-wy2040



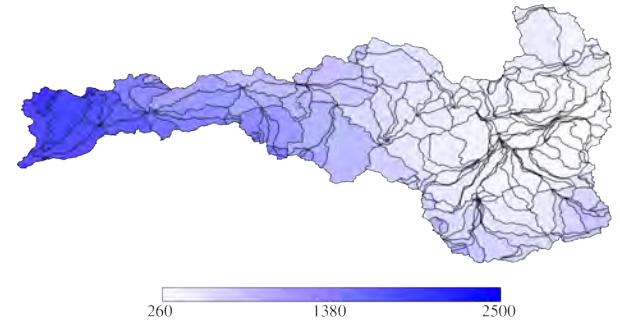
10-Year Average of Annual Precipitation (mm)
ECHAM5 A2-1 wy2040-wy2050



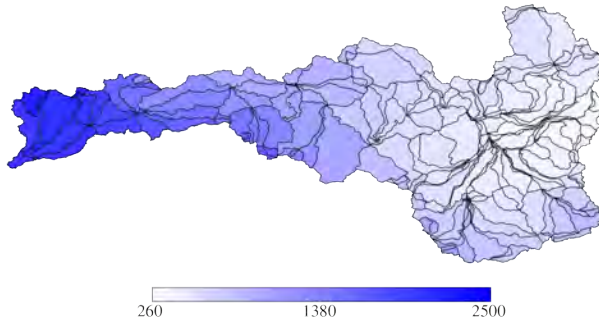
10-Year Average of Annual Precipitation (mm)
ECHAM5 A2-1 wy2050-wy2060



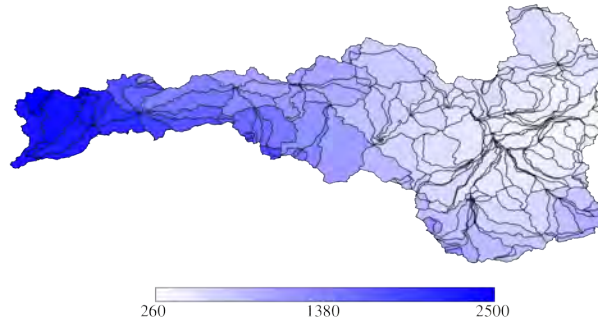
10-Year Average of Annual Precipitation (mm)
ECHAM5 A2-1 wy2060-wy2070



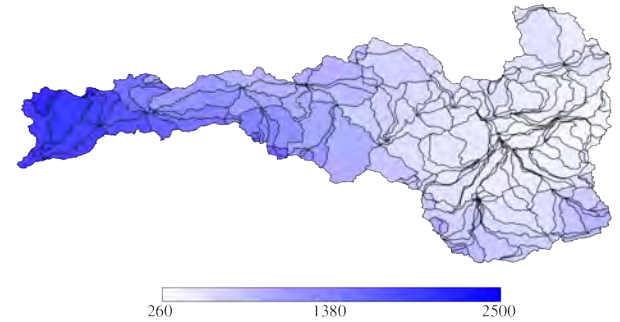
10-Year Average of Annual Precipitation (mm)
ECHAM5 A2-1 wy2070-wy2080



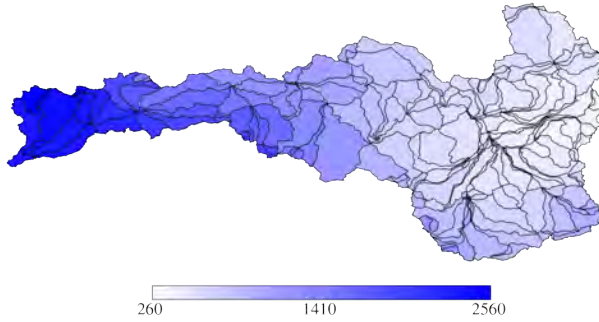
10-Year Average of Annual Precipitation (mm)
ECHAM5 A2-1 wy2080-wy2090



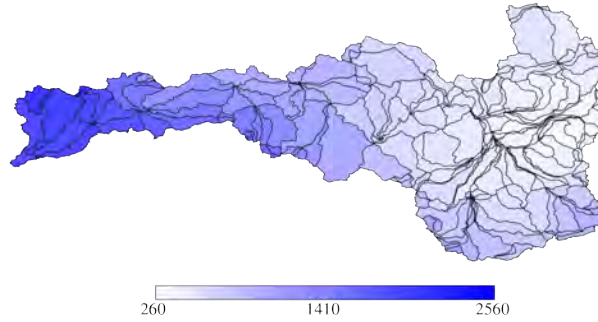
10-Year Average of Annual Precipitation (mm)
ECHAM5 A2-1 wy2090-wy2100



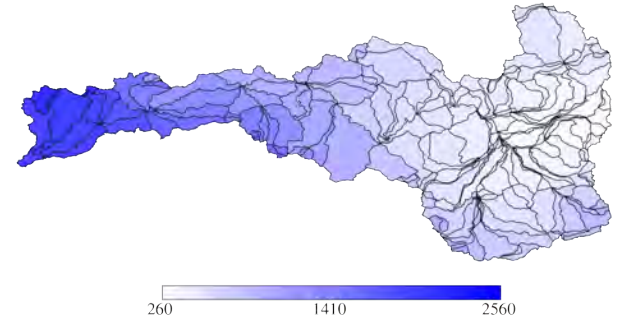
10-Year Average of Annual Precipitation (mm)
ECHAM5 A2-2 wy2010-wy2020



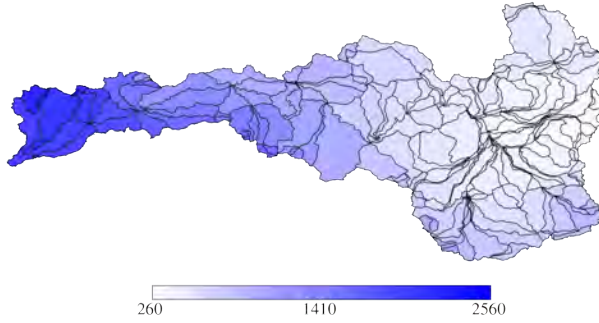
10-Year Average of Annual Precipitation (mm)
ECHAM5 A2-2 wy2020-wy2030



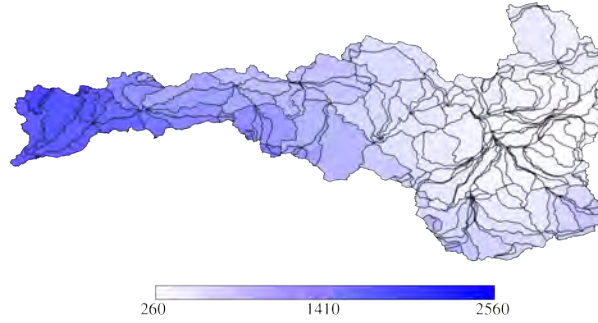
10-Year Average of Annual Precipitation (mm)
ECHAM5 A2-2 wy2030-wy2040



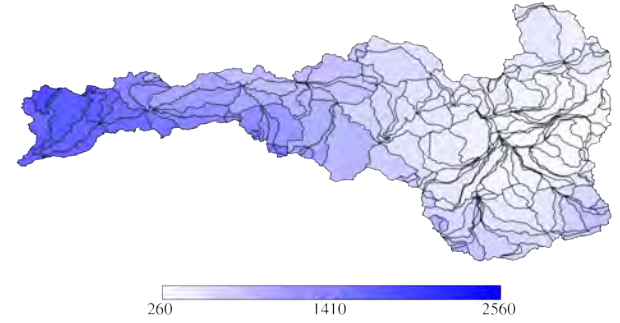
10-Year Average of Annual Precipitation (mm)
ECHAM5 A2-2 wy2040-wy2050



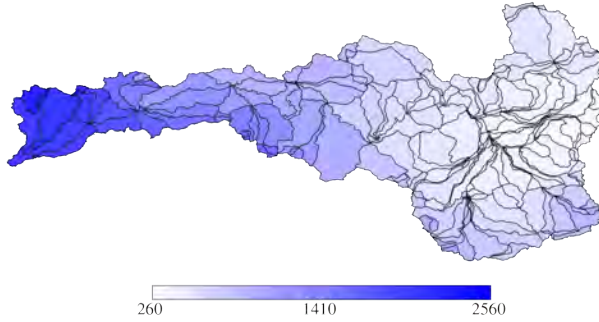
10-Year Average of Annual Precipitation (mm)
ECHAM5 A2-2 wy2050-wy2060



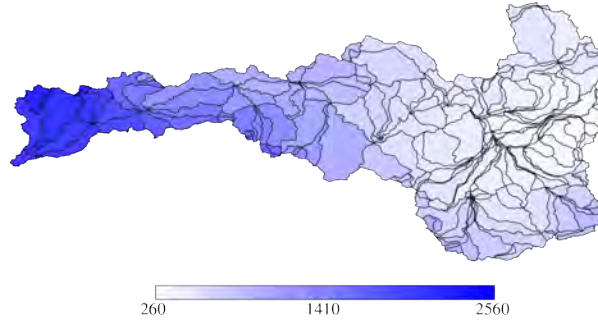
10-Year Average of Annual Precipitation (mm)
ECHAM5 A2-2 wy2060-wy2070



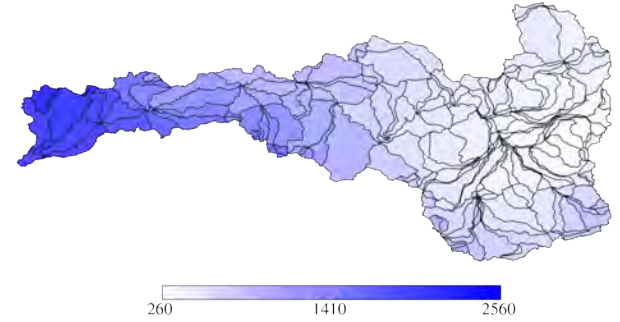
10-Year Average of Annual Precipitation (mm)
ECHAM5 A2-2 wy2070-wy2080



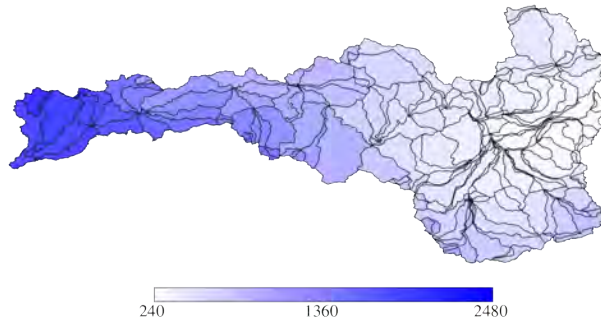
10-Year Average of Annual Precipitation (mm)
ECHAM5 A2-2 wy2080-wy2090



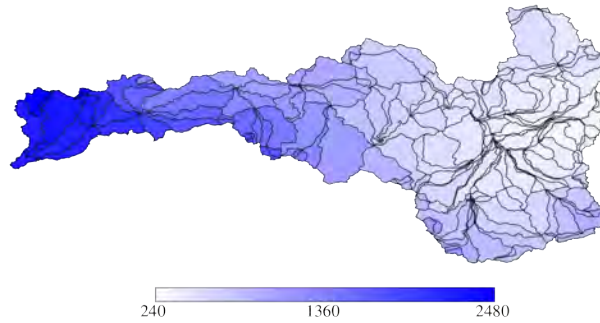
10-Year Average of Annual Precipitation (mm)
ECHAM5 A2-2 wy2090-wy2100



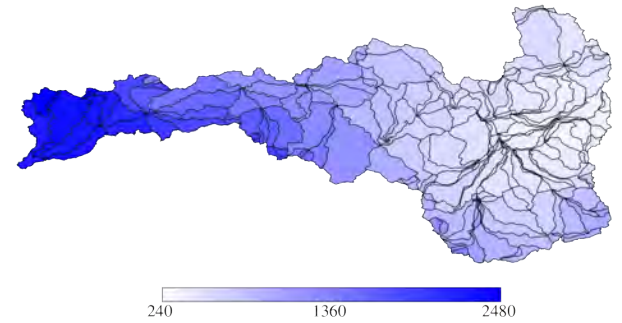
10-Year Average of Annual Precipitation (mm)
ECHAM5 A2-3 wy2010-wy2020



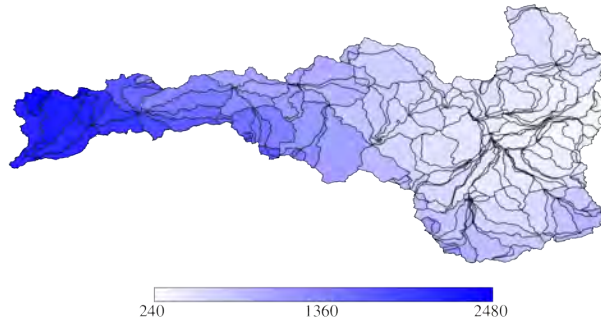
10-Year Average of Annual Precipitation (mm)
ECHAM5 A2-3 wy2020-wy2030



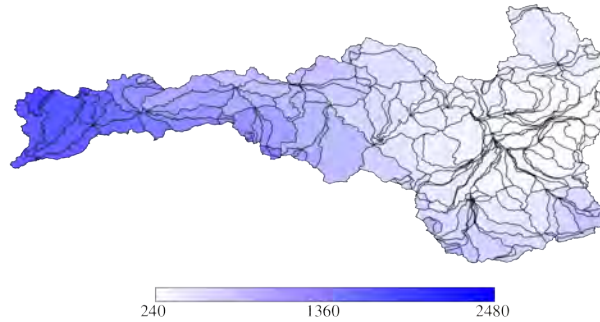
10-Year Average of Annual Precipitation (mm)
ECHAM5 A2-3 wy2030-wy2040



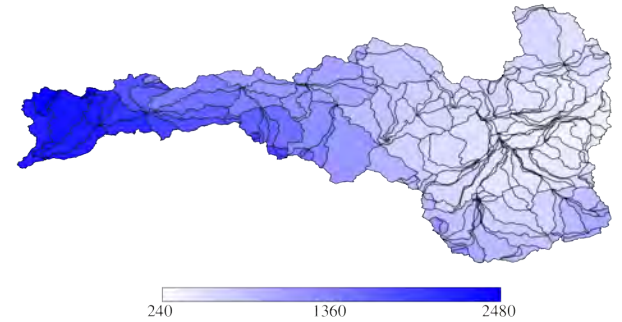
10-Year Average of Annual Precipitation (mm)
ECHAM5 A2-3 wy2040-wy2050



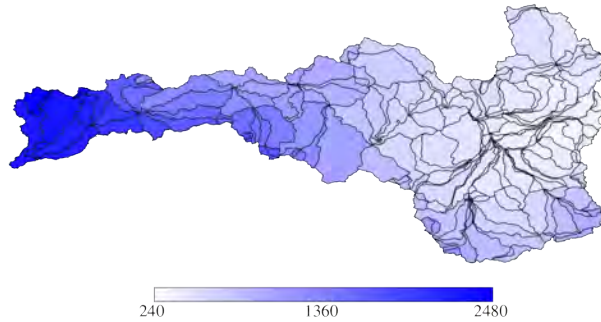
10-Year Average of Annual Precipitation (mm)
ECHAM5 A2-3 wy2050-wy2060



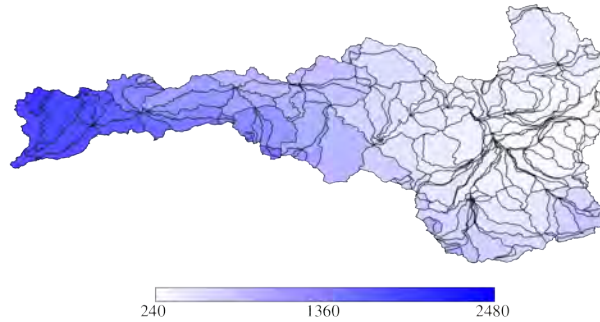
10-Year Average of Annual Precipitation (mm)
ECHAM5 A2-3 wy2060-wy2070



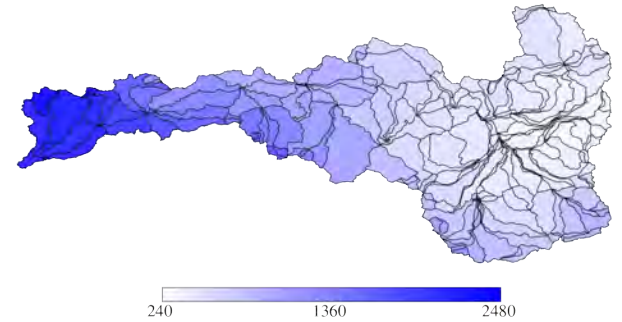
10-Year Average of Annual Precipitation (mm)
ECHAM5 A2-3 wy2070-wy2080



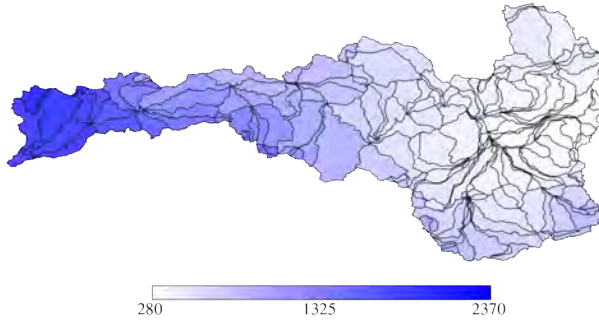
10-Year Average of Annual Precipitation (mm)
ECHAM5 A2-3 wy2080-wy2090



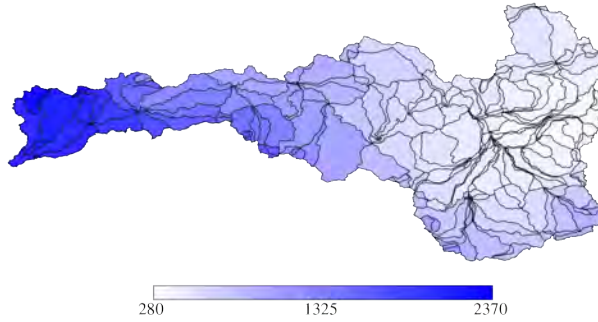
10-Year Average of Annual Precipitation (mm)
ECHAM5 A2-3 wy2090-wy2100



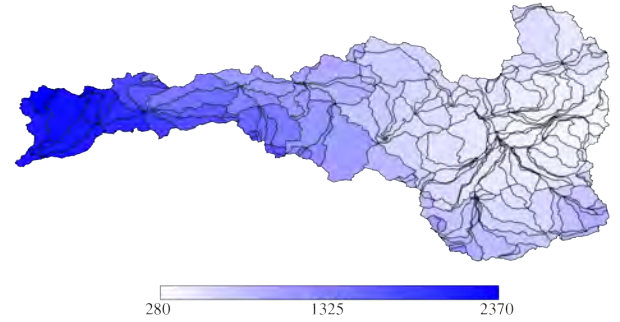
10-Year Average of Annual Precipitation (mm)
ECHAM5 B1-1 wy2010-wy2020



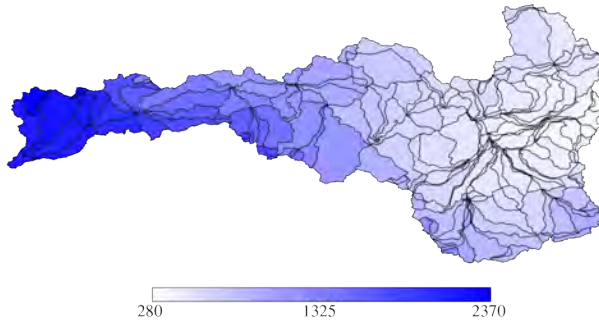
10-Year Average of Annual Precipitation (mm)
ECHAM5 B1-1 wy2020-wy2030



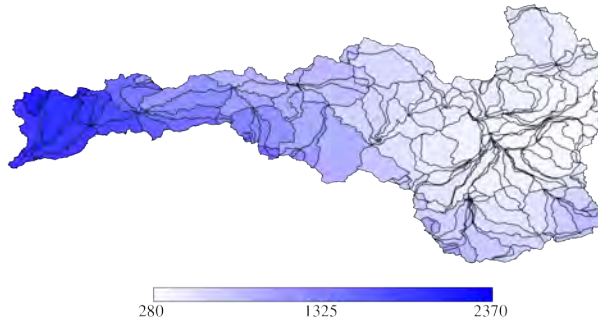
10-Year Average of Annual Precipitation (mm)
ECHAM5 B1-1 wy2030-wy2040



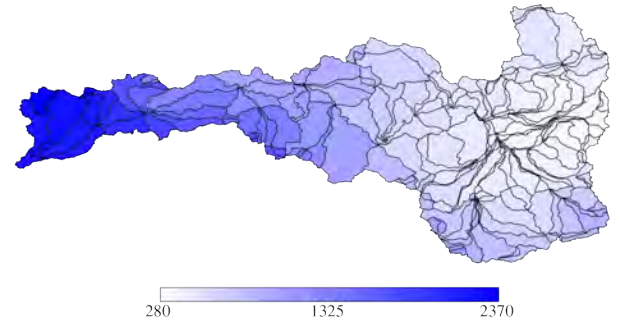
10-Year Average of Annual Precipitation (mm)
ECHAM5 B1-1 wy2040-wy2050



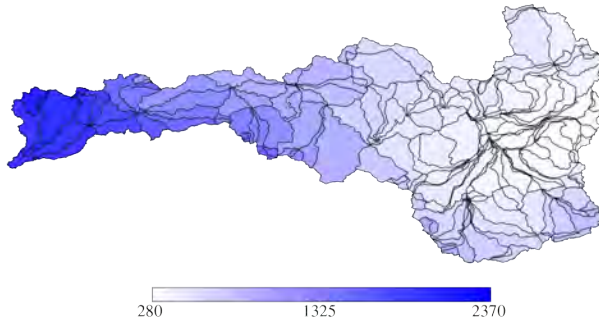
10-Year Average of Annual Precipitation (mm)
ECHAM5 B1-1 wy2050-wy2060



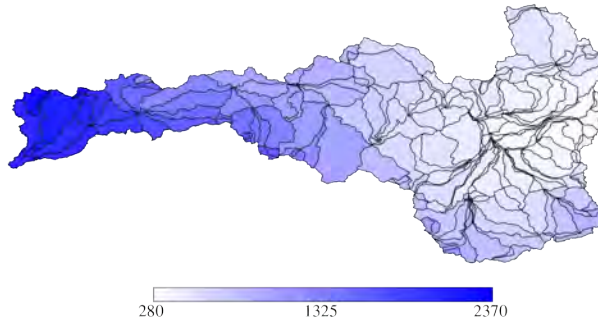
10-Year Average of Annual Precipitation (mm)
ECHAM5 B1-1 wy2060-wy2070



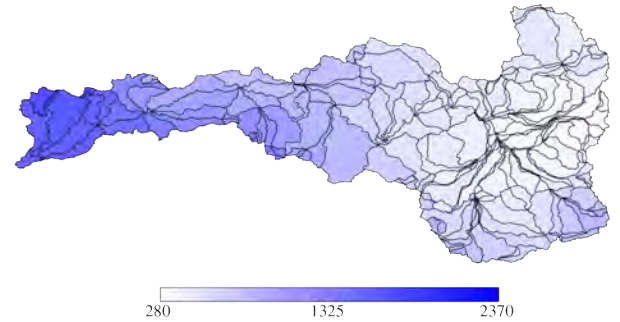
10-Year Average of Annual Precipitation (mm)
ECHAM5 B1-1 wy2070-wy2080



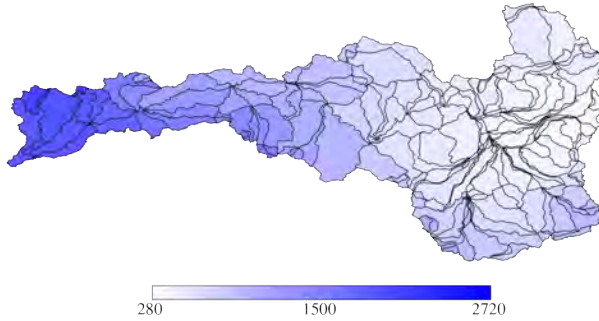
10-Year Average of Annual Precipitation (mm)
ECHAM5 B1-1 wy2080-wy2090



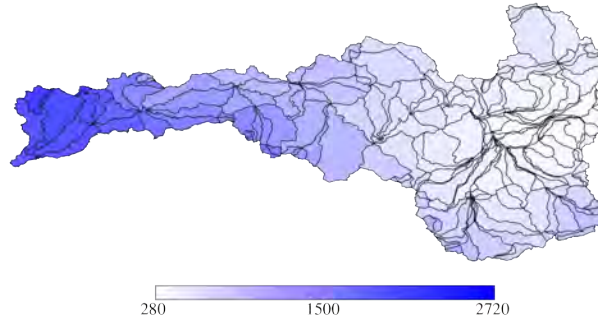
10-Year Average of Annual Precipitation (mm)
ECHAM5 B1-1 wy2090-wy2100



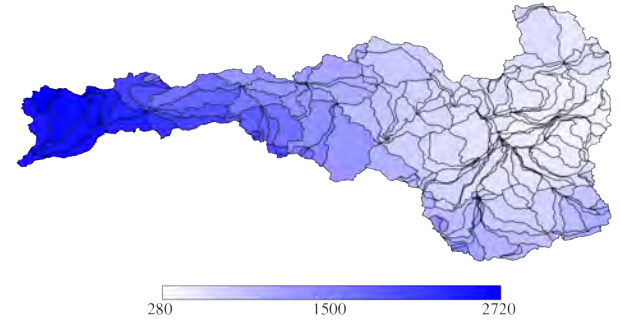
10-Year Average of Annual Precipitation (mm)
ECHAM5 B1-2 wy2010-wy2020



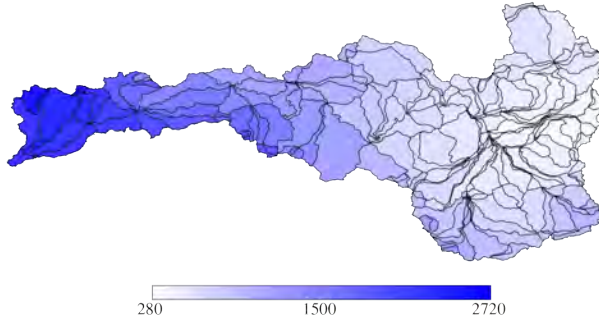
10-Year Average of Annual Precipitation (mm)
ECHAM5 B1-2 wy2020-wy2030



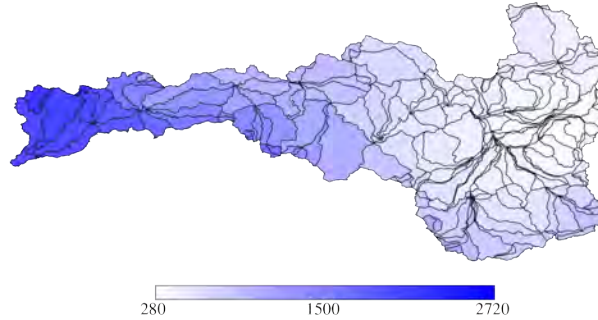
10-Year Average of Annual Precipitation (mm)
ECHAM5 B1-2 wy2030-wy2040



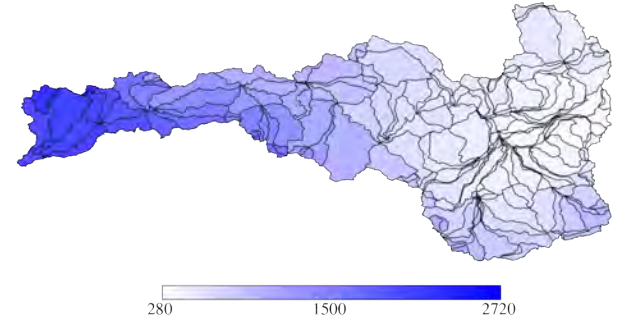
10-Year Average of Annual Precipitation (mm)
ECHAM5 B1-2 wy2040-wy2050



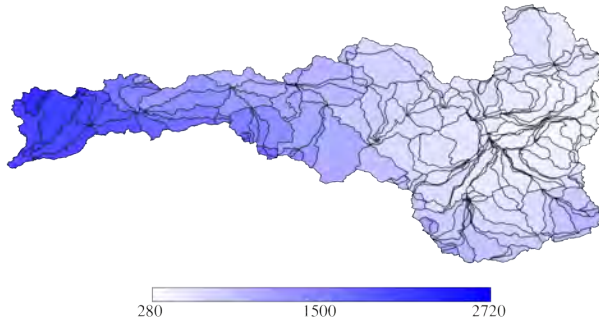
10-Year Average of Annual Precipitation (mm)
ECHAM5 B1-2 wy2050-wy2060



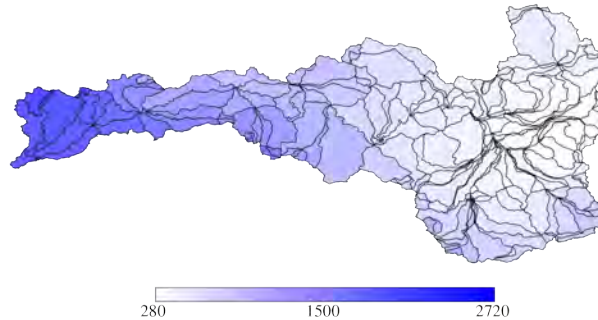
10-Year Average of Annual Precipitation (mm)
ECHAM5 B1-2 wy2060-wy2070



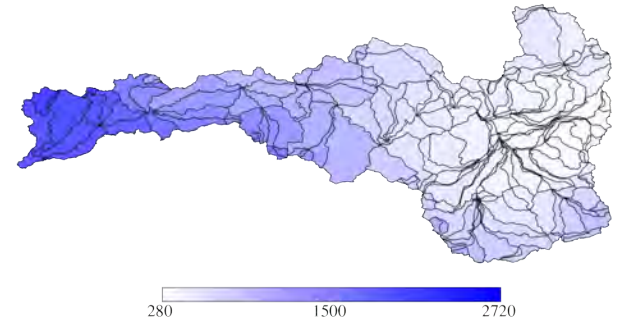
10-Year Average of Annual Precipitation (mm)
ECHAM5 B1-2 wy2070-wy2080



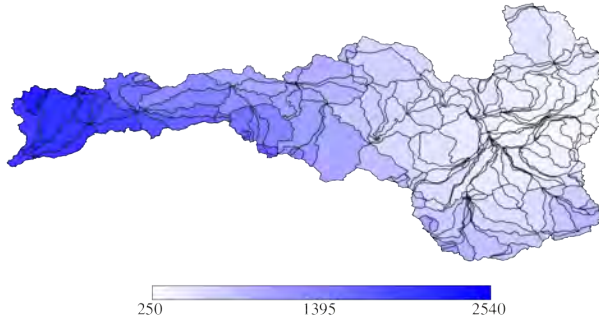
10-Year Average of Annual Precipitation (mm)
ECHAM5 B1-2 wy2080-wy2090



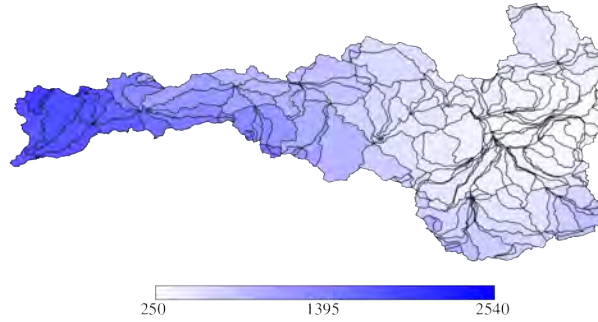
10-Year Average of Annual Precipitation (mm)
ECHAM5 B1-2 wy2090-wy2100



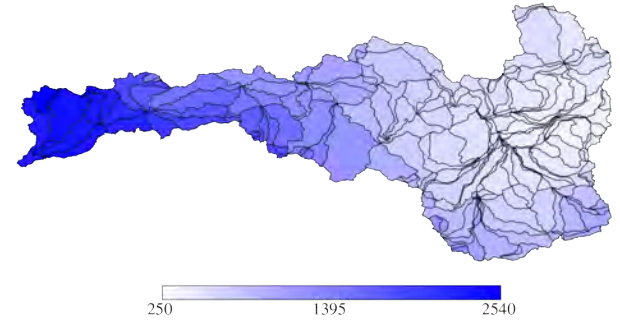
10-Year Average of Annual Precipitation (mm)
ECHAM5 B1-3 wy2010-wy2020



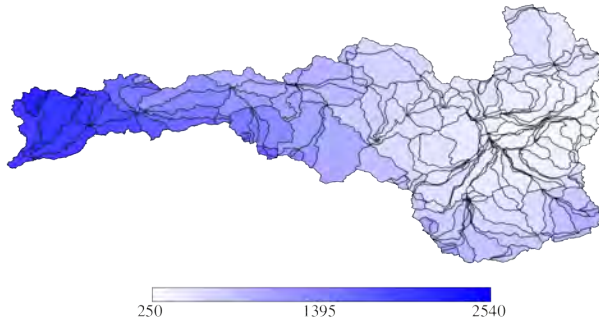
10-Year Average of Annual Precipitation (mm)
ECHAM5 B1-3 wy2020-wy2030



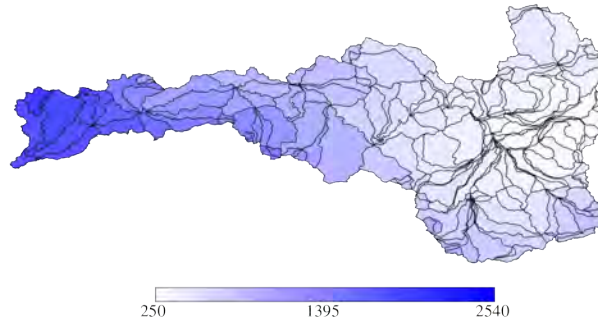
10-Year Average of Annual Precipitation (mm)
ECHAM5 B1-3 wy2030-wy2040



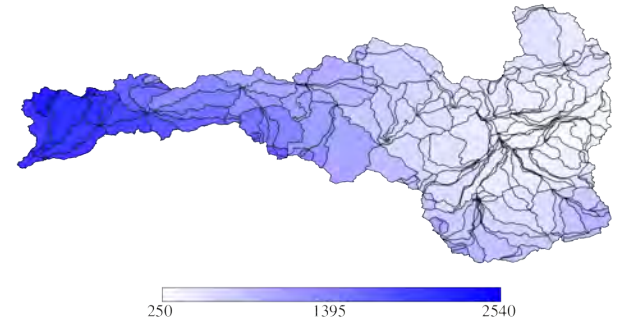
10-Year Average of Annual Precipitation (mm)
ECHAM5 B1-3 wy2040-wy2050



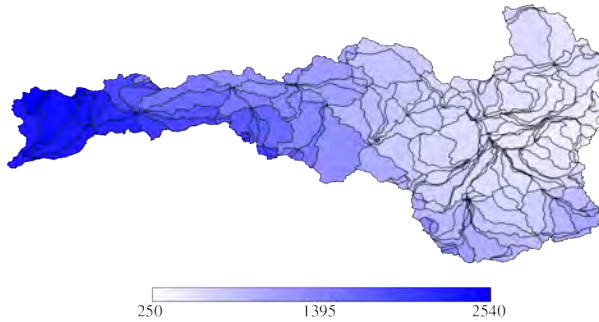
10-Year Average of Annual Precipitation (mm)
ECHAM5 B1-3 wy2050-wy2060



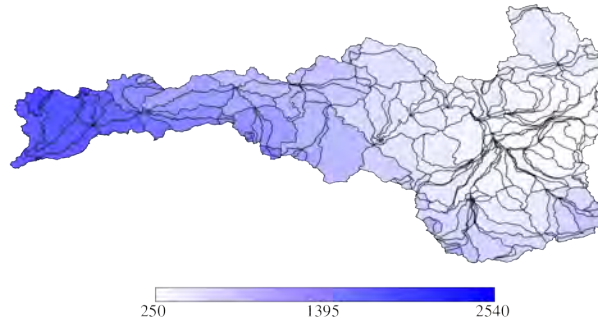
10-Year Average of Annual Precipitation (mm)
ECHAM5 B1-3 wy2060-wy2070



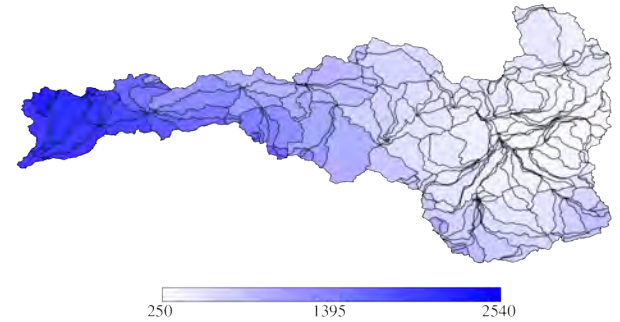
10-Year Average of Annual Precipitation (mm)
ECHAM5 B1-3 wy2070-wy2080



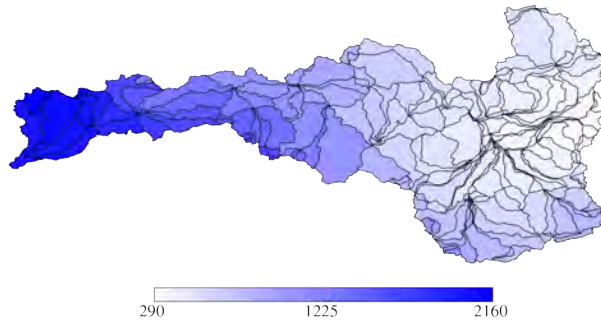
10-Year Average of Annual Precipitation (mm)
ECHAM5 B1-3 wy2080-wy2090



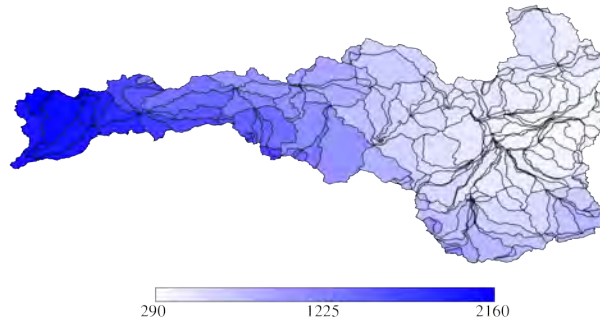
10-Year Average of Annual Precipitation (mm)
ECHAM5 B1-3 wy2090-wy2100



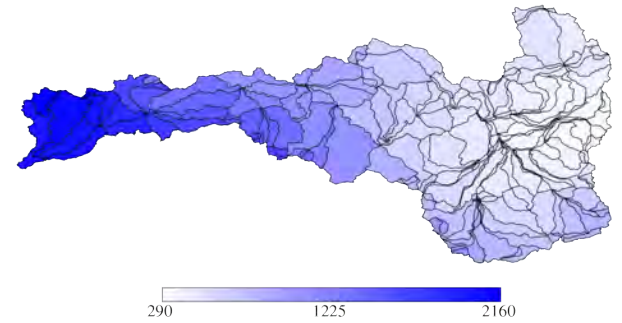
10-Year Average of Annual Precipitation (mm)
Ensemble All wy2010-wy2020



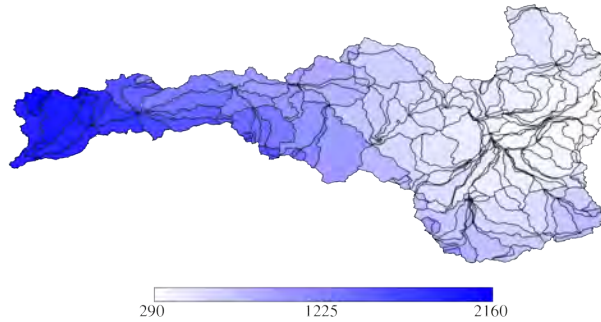
10-Year Average of Annual Precipitation (mm)
Ensemble All wy2020-wy2030



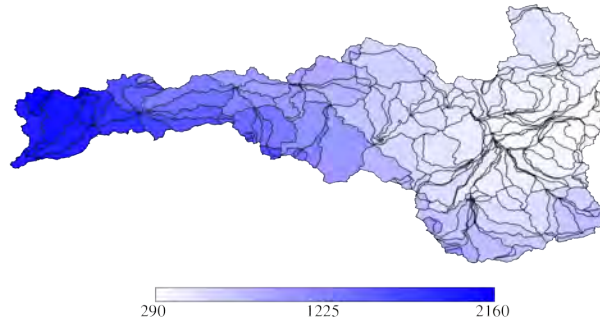
10-Year Average of Annual Precipitation (mm)
Ensemble All wy2030-wy2040



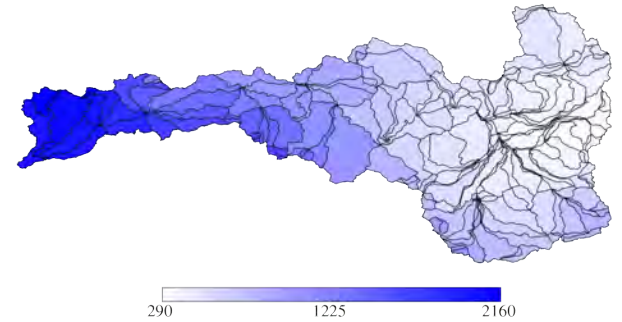
10-Year Average of Annual Precipitation (mm)
Ensemble All wy2040-wy2050



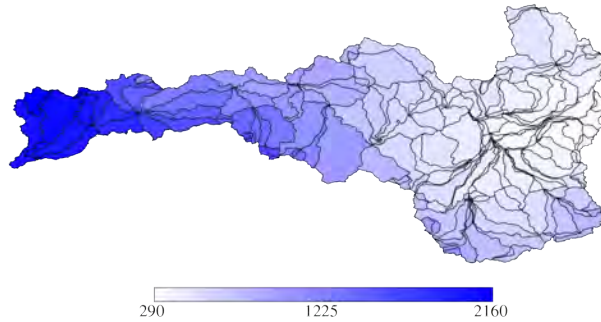
10-Year Average of Annual Precipitation (mm)
Ensemble All wy2050-wy2060



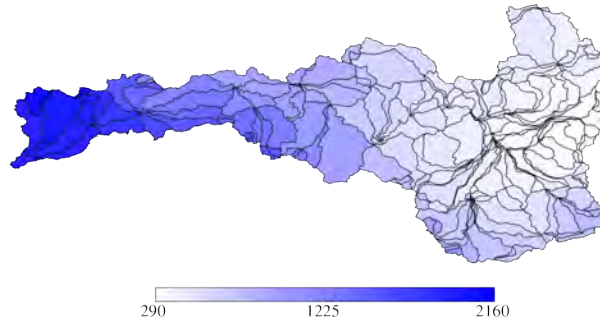
10-Year Average of Annual Precipitation (mm)
Ensemble All wy2060-wy2070



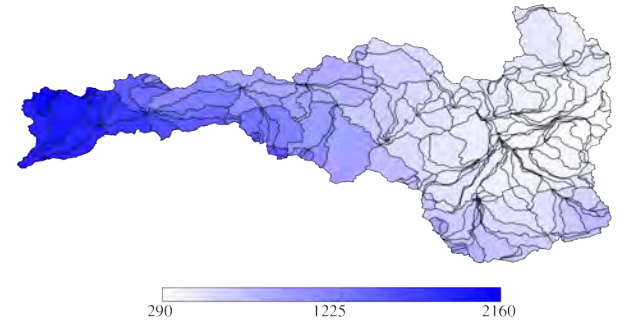
10-Year Average of Annual Precipitation (mm)
Ensemble All wy2070-wy2080



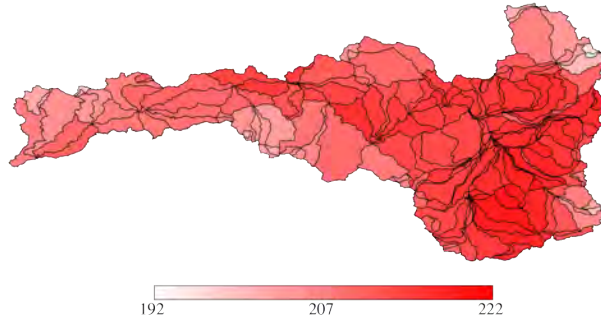
10-Year Average of Annual Precipitation (mm)
Ensemble All wy2080-wy2090



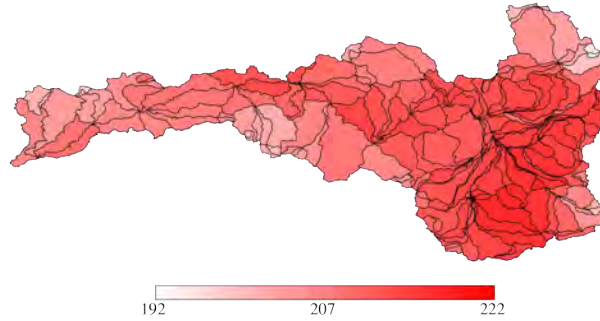
10-Year Average of Annual Precipitation (mm)
Ensemble All wy2090-wy2100



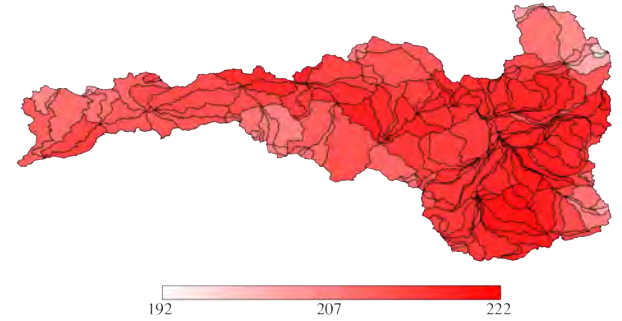
10-Year Average of Annual Average Short-wave Radiation (W/m²)
CCSM3 A1B wy2010-wy2020



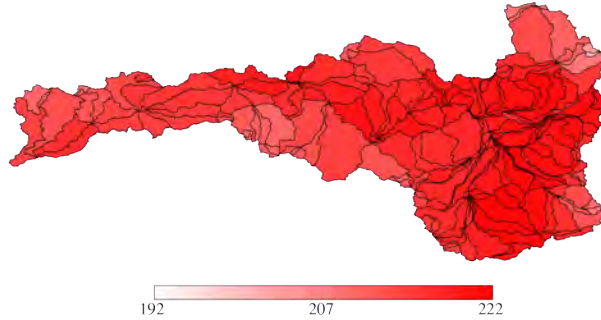
10-Year Average of Annual Average Short-wave Radiation (W/m²)
CCSM3 A1B wy2020-wy2030



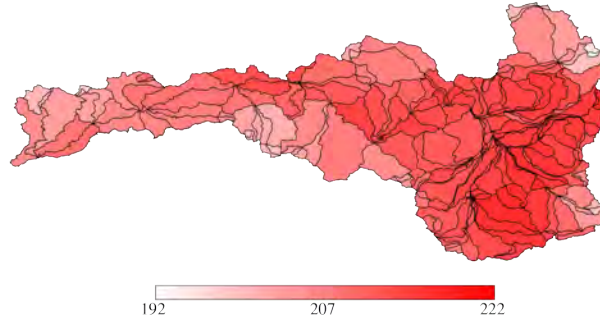
10-Year Average of Annual Average Short-wave Radiation (W/m²)
CCSM3 A1B wy2030-wy2040



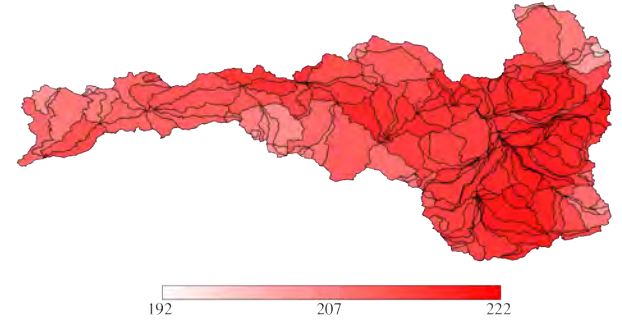
10-Year Average of Annual Average Short-wave Radiation (W/m²)
CCSM3 A1B wy2040-wy2050



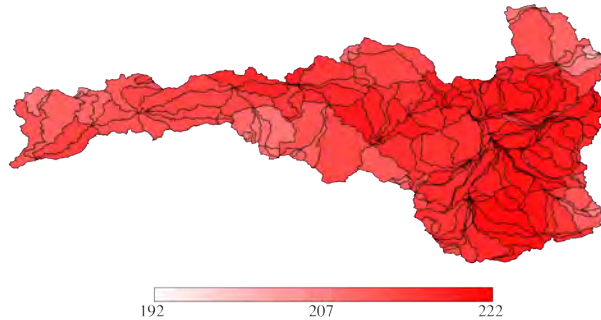
10-Year Average of Annual Average Short-wave Radiation (W/m²)
CCSM3 A1B wy2050-wy2060



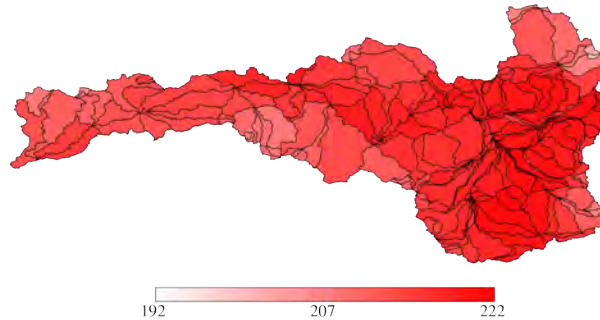
10-Year Average of Annual Average Short-wave Radiation (W/m²)
CCSM3 A1B wy2060-wy2070



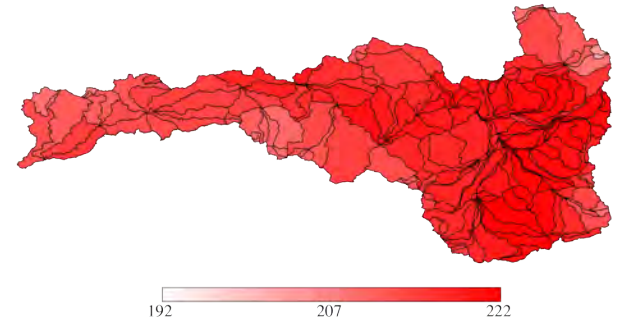
10-Year Average of Annual Average Short-wave Radiation (W/m²)
CCSM3 A1B wy2070-wy2080



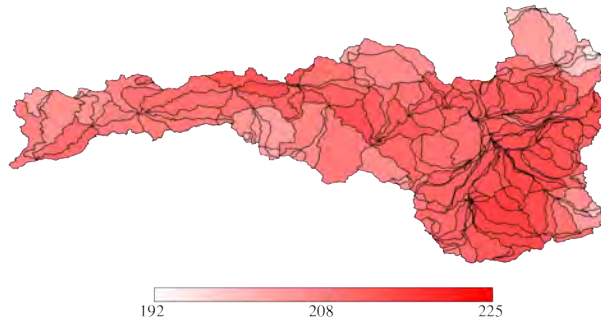
10-Year Average of Annual Average Short-wave Radiation (W/m²)
CCSM3 A1B wy2080-wy2090



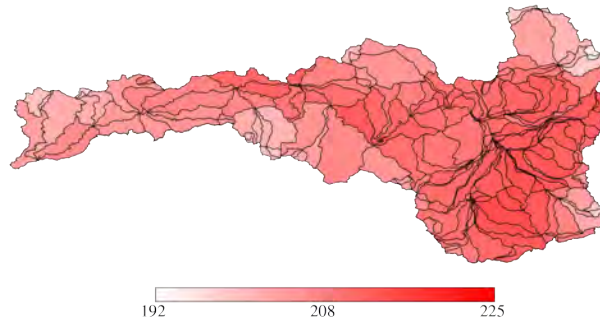
10-Year Average of Annual Average Short-wave Radiation (W/m²)
CCSM3 A1B wy2090-wy2100



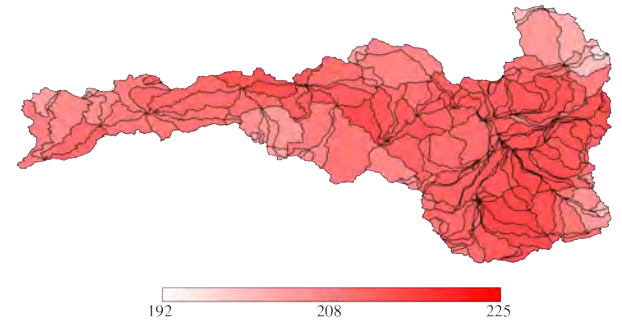
10-Year Average of Annual Average Short-wave Radiation (W/m²)
CCSM3 A1FI wy2010-wy2020



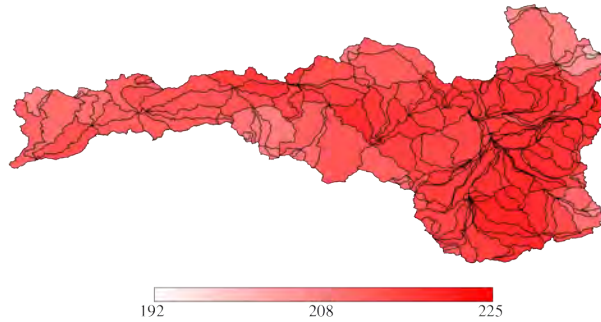
10-Year Average of Annual Average Short-wave Radiation (W/m²)
CCSM3 A1FI wy2020-wy2030



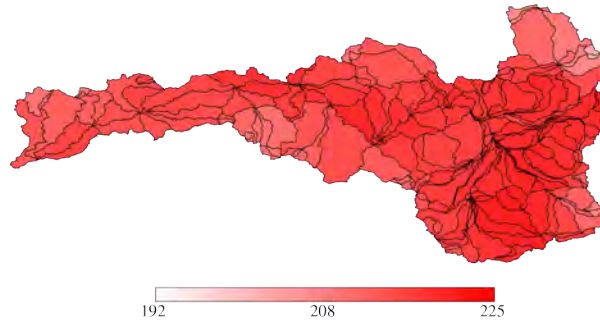
10-Year Average of Annual Average Short-wave Radiation (W/m²)
CCSM3 A1FI wy2030-wy2040



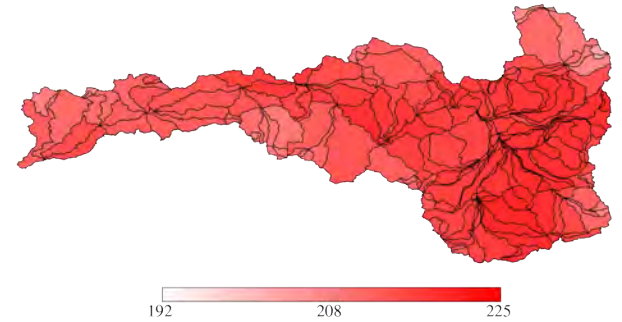
10-Year Average of Annual Average Short-wave Radiation (W/m²)
CCSM3 A1FI wy2040-wy2050



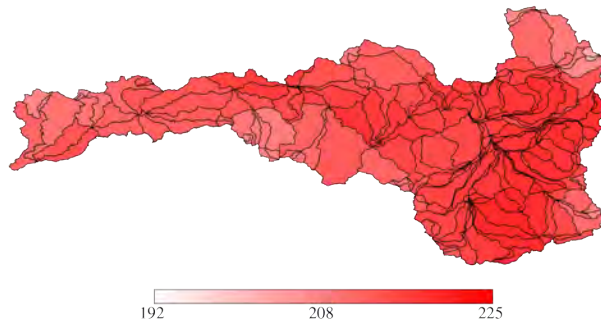
10-Year Average of Annual Average Short-wave Radiation (W/m²)
CCSM3 A1FI wy2050-wy2060



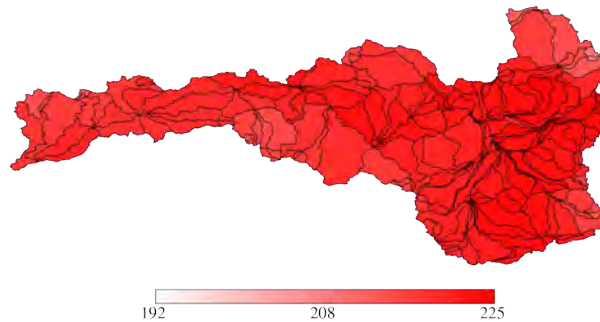
10-Year Average of Annual Average Short-wave Radiation (W/m²)
CCSM3 A1FI wy2060-wy2070



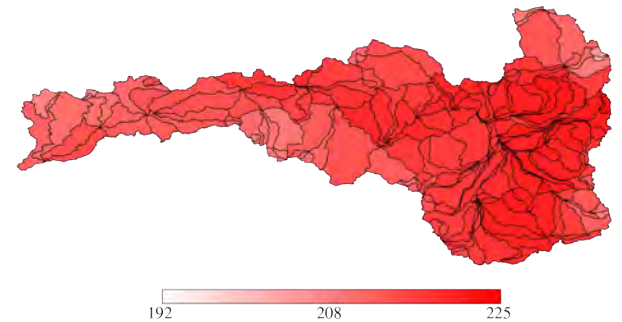
10-Year Average of Annual Average Short-wave Radiation (W/m²)
CCSM3 A1FI wy2070-wy2080



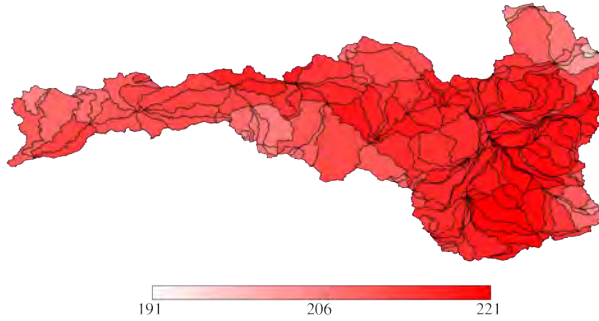
10-Year Average of Annual Average Short-wave Radiation (W/m²)
CCSM3 A1FI wy2080-wy2090



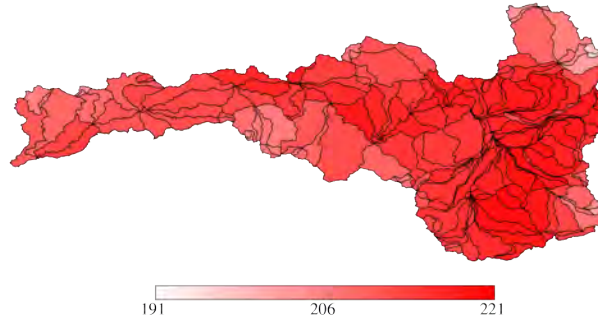
10-Year Average of Annual Average Short-wave Radiation (W/m²)
CCSM3 A1FI wy2090-wy2100



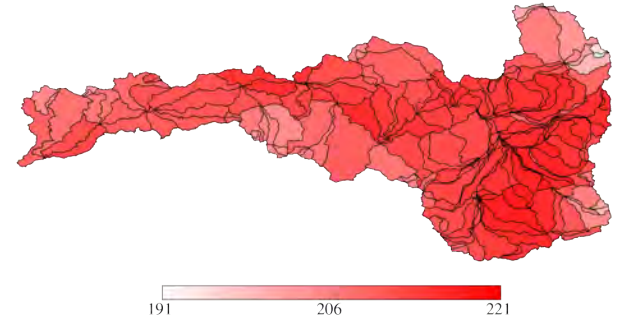
10-Year Average of Annual Average Short-wave Radiation (W/m²)
CCSM3 B1 wy2010-wy2020



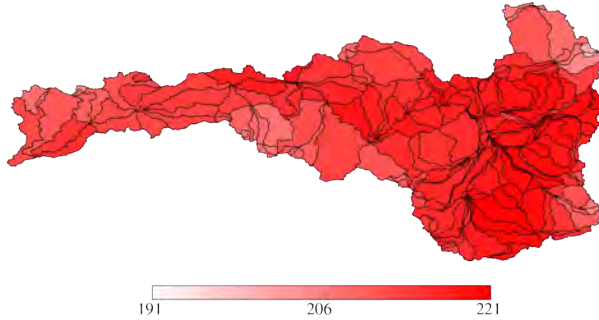
10-Year Average of Annual Average Short-wave Radiation (W/m²)
CCSM3 B1 wy2020-wy2030



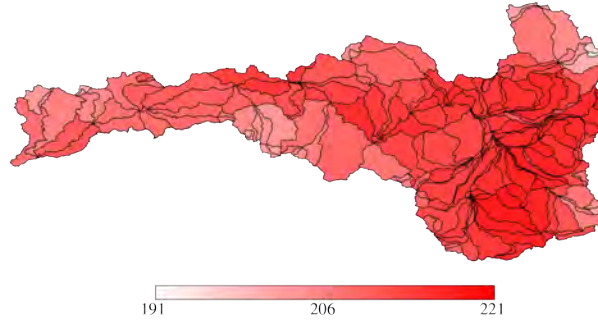
10-Year Average of Annual Average Short-wave Radiation (W/m²)
CCSM3 B1 wy2030-wy2040



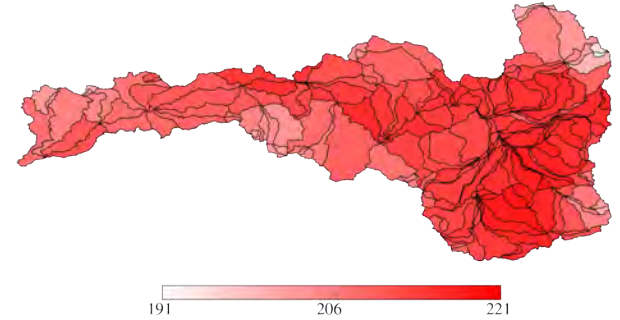
10-Year Average of Annual Average Short-wave Radiation (W/m²)
CCSM3 B1 wy2040-wy2050



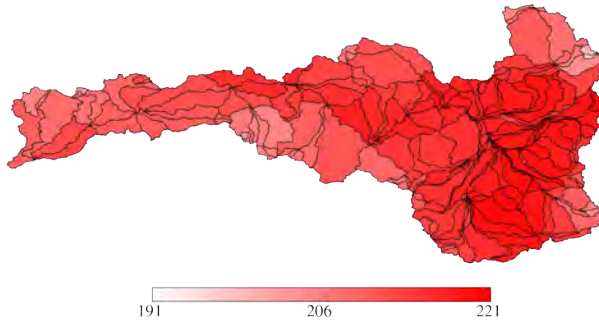
10-Year Average of Annual Average Short-wave Radiation (W/m²)
CCSM3 B1 wy2050-wy2060



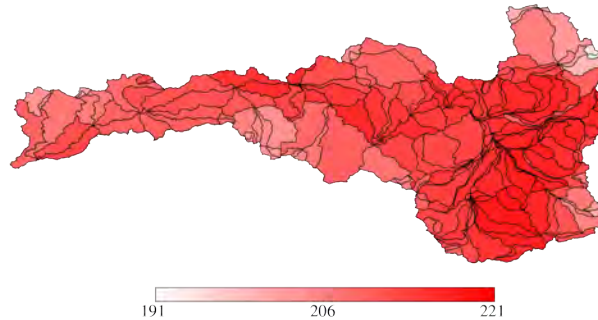
10-Year Average of Annual Average Short-wave Radiation (W/m²)
CCSM3 B1 wy2060-wy2070



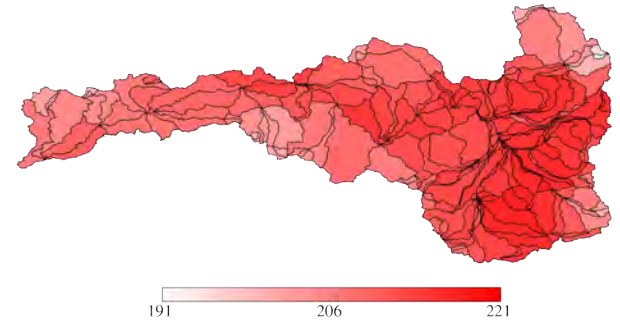
10-Year Average of Annual Average Short-wave Radiation (W/m²)
CCSM3 B1 wy2070-wy2080



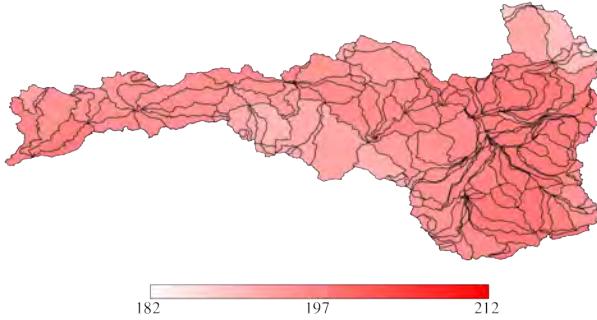
10-Year Average of Annual Average Short-wave Radiation (W/m²)
CCSM3 B1 wy2080-wy2090



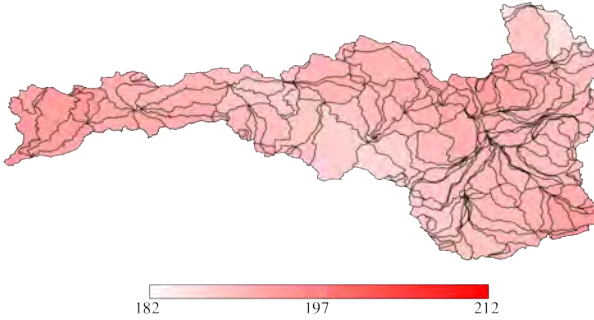
10-Year Average of Annual Average Short-wave Radiation (W/m²)
CCSM3 B1 wy2090-wy2100



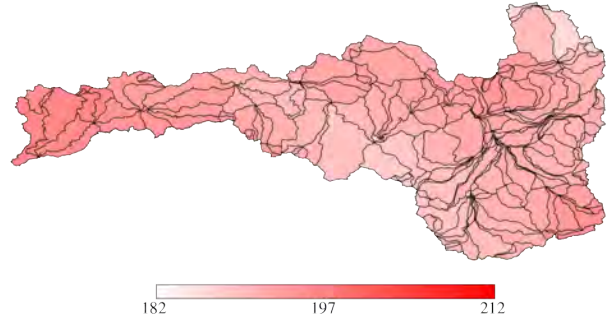
10-Year Average of Annual Average Short-wave Radiation (W/m²)
ECHAM5 A1B1 wy2010-wy2020



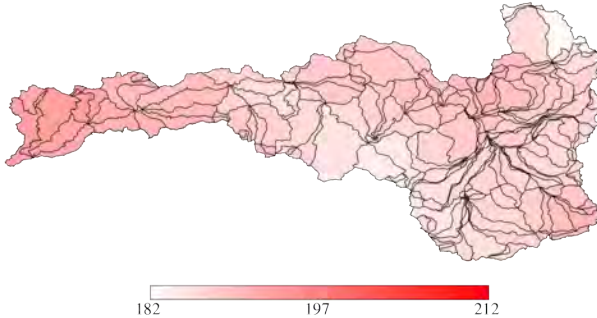
10-Year Average of Annual Average Short-wave Radiation (W/m²)
ECHAM5 A1B1 wy2020-wy2030



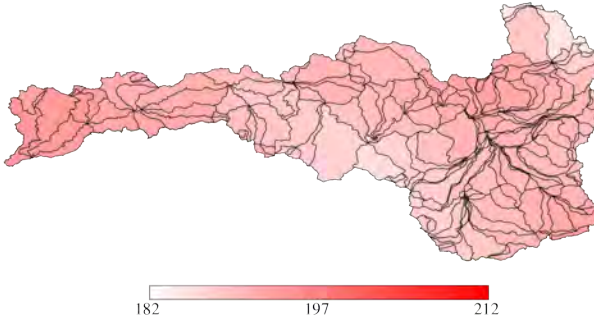
10-Year Average of Annual Average Short-wave Radiation (W/m²)
ECHAM5 A1B1 wy2030-wy2040



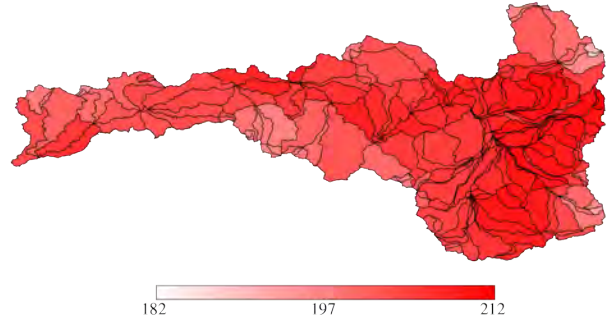
10-Year Average of Annual Average Short-wave Radiation (W/m²)
ECHAM5 A1B1 wy2040-wy2050



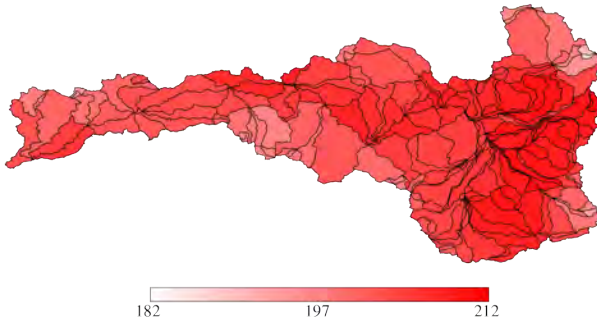
10-Year Average of Annual Average Short-wave Radiation (W/m²)
ECHAM5 A1B1 wy2050-wy2060



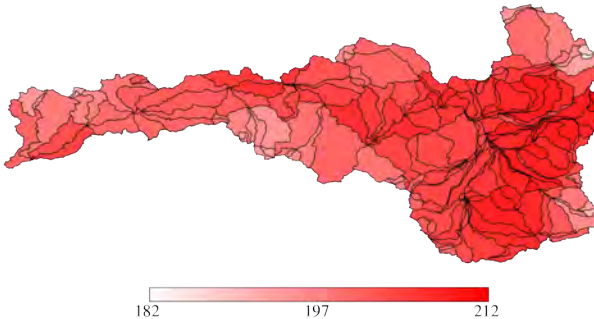
10-Year Average of Annual Average Short-wave Radiation (W/m²)
ECHAM5 A1B1 wy2060-wy2070



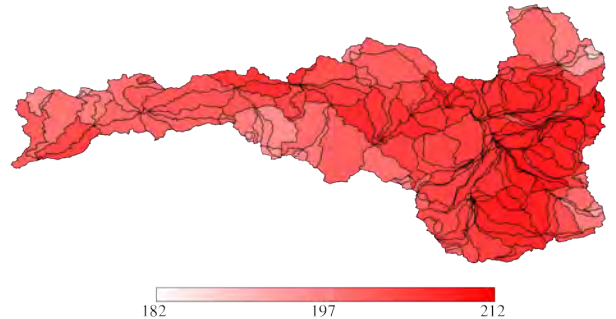
10-Year Average of Annual Average Short-wave Radiation (W/m²)
ECHAM5 A1B1 wy2070-wy2080



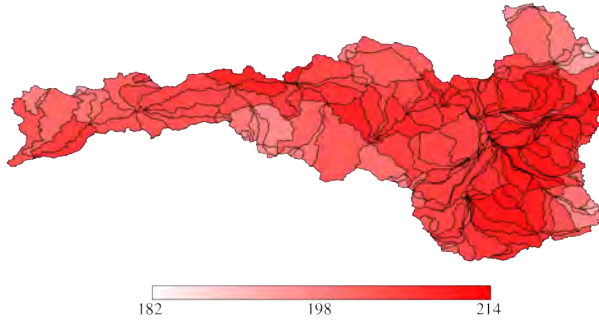
10-Year Average of Annual Average Short-wave Radiation (W/m²)
ECHAM5 A1B1 wy2080-wy2090



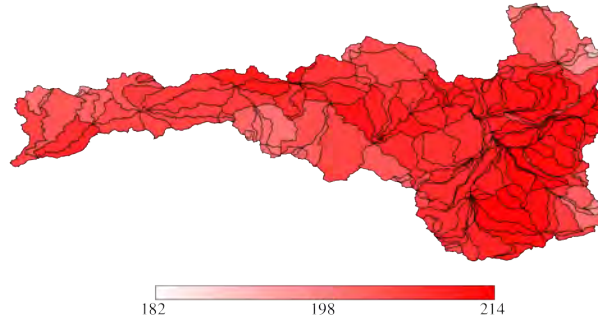
10-Year Average of Annual Average Short-wave Radiation (W/m²)
ECHAM5 A1B1 wy2090-wy2100



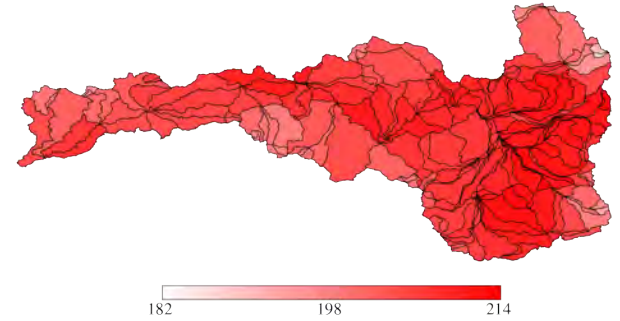
10-Year Average of Annual Average Short-wave Radiation (W/m²)
ECHAM5 A1B2 wy2010-wy2020



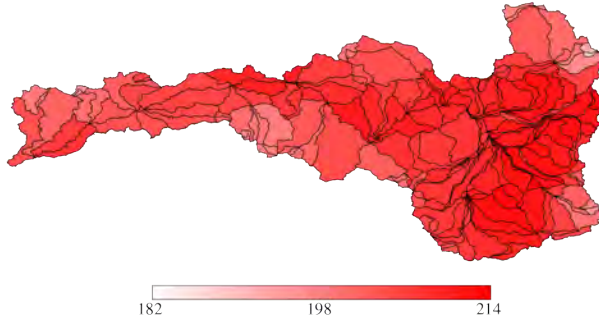
10-Year Average of Annual Average Short-wave Radiation (W/m²)
ECHAM5 A1B2 wy2020-wy2030



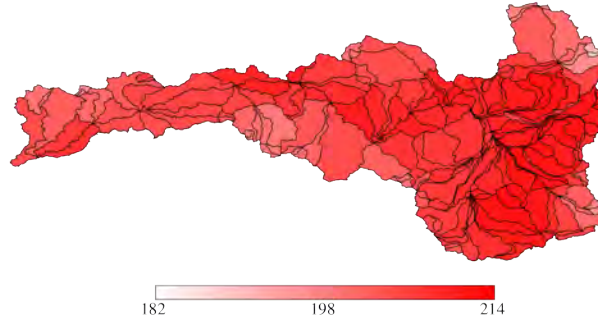
10-Year Average of Annual Average Short-wave Radiation (W/m²)
ECHAM5 A1B2 wy2030-wy2040



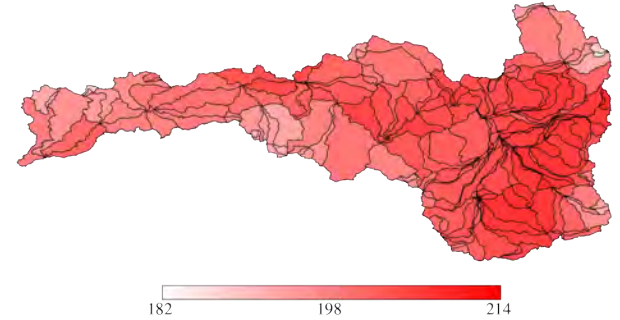
10-Year Average of Annual Average Short-wave Radiation (W/m²)
ECHAM5 A1B2 wy2040-wy2050



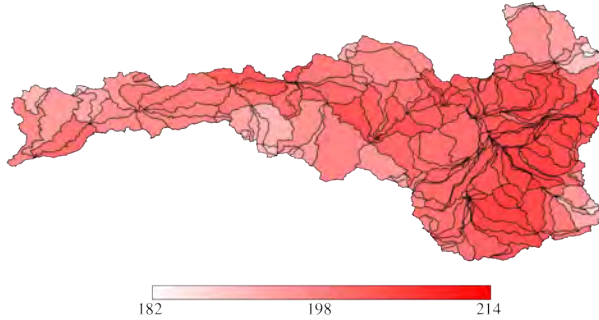
10-Year Average of Annual Average Short-wave Radiation (W/m²)
ECHAM5 A1B2 wy2050-wy2060



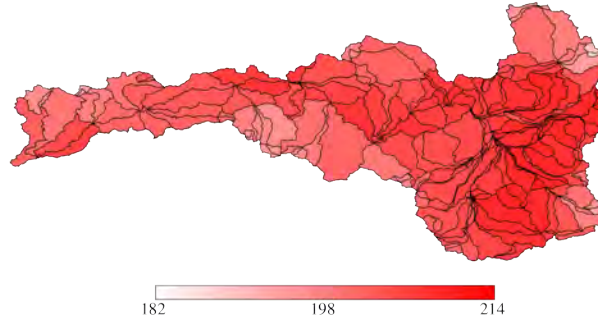
10-Year Average of Annual Average Short-wave Radiation (W/m²)
ECHAM5 A1B2 wy2060-wy2070



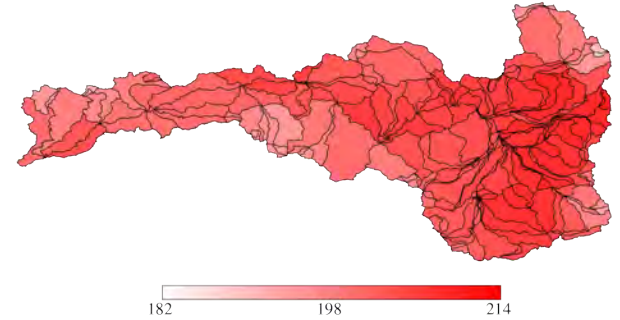
10-Year Average of Annual Average Short-wave Radiation (W/m²)
ECHAM5 A1B2 wy2070-wy2080



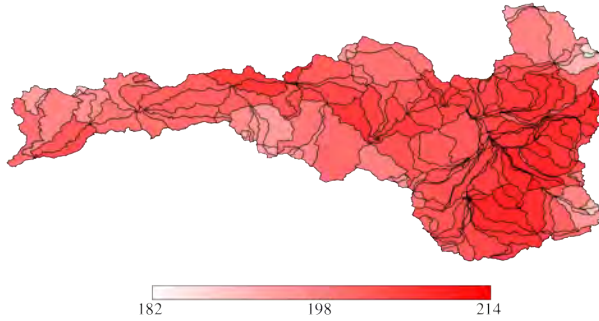
10-Year Average of Annual Average Short-wave Radiation (W/m²)
ECHAM5 A1B2 wy2080-wy2090



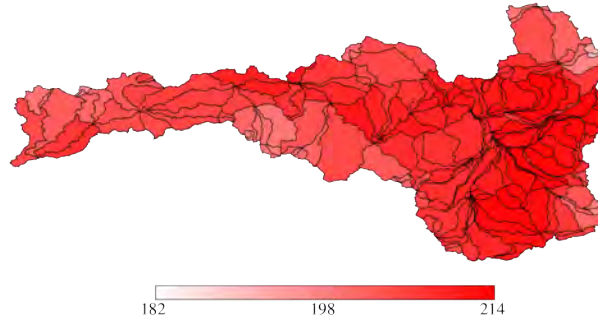
10-Year Average of Annual Average Short-wave Radiation (W/m²)
ECHAM5 A1B2 wy2090-wy2100



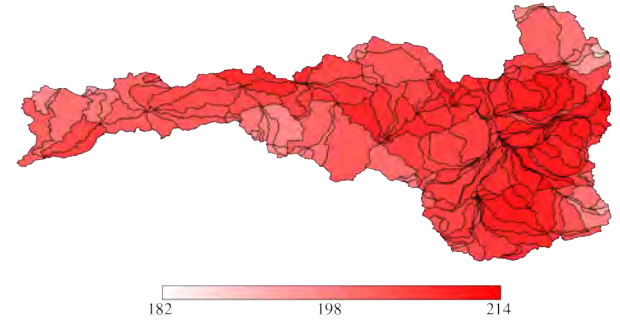
10-Year Average of Annual Average Short-wave Radiation (W/m²)
ECHAM5 A1B3 wy2010-wy2020



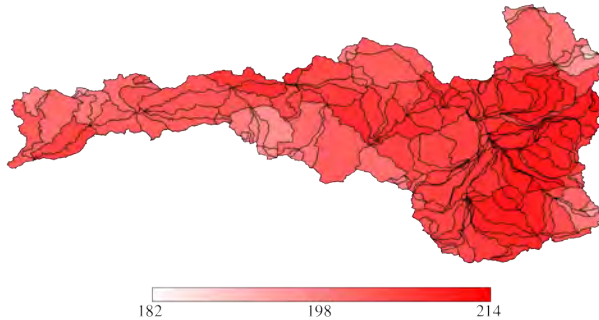
10-Year Average of Annual Average Short-wave Radiation (W/m²)
ECHAM5 A1B3 wy2020-wy2030



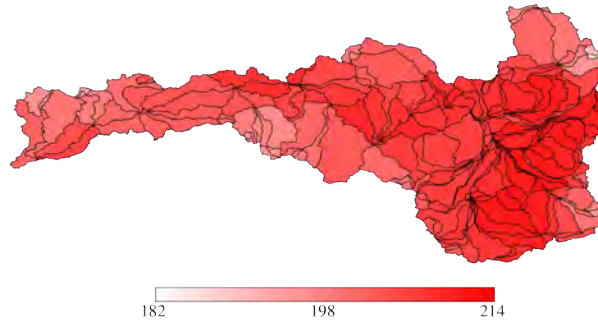
10-Year Average of Annual Average Short-wave Radiation (W/m²)
ECHAM5 A1B3 wy2030-wy2040



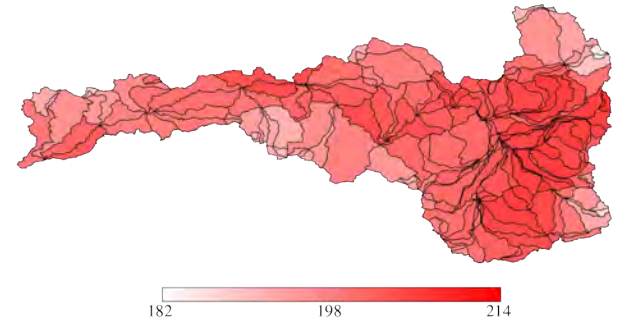
10-Year Average of Annual Average Short-wave Radiation (W/m²)
ECHAM5 A1B3 wy2040-wy2050



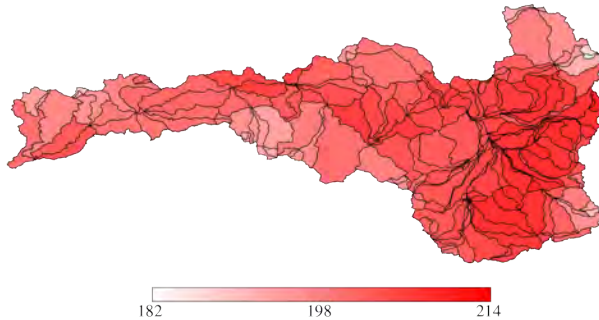
10-Year Average of Annual Average Short-wave Radiation (W/m²)
ECHAM5 A1B3 wy2050-wy2060



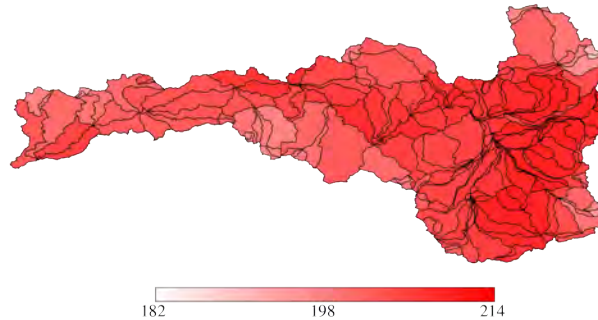
10-Year Average of Annual Average Short-wave Radiation (W/m²)
ECHAM5 A1B3 wy2060-wy2070



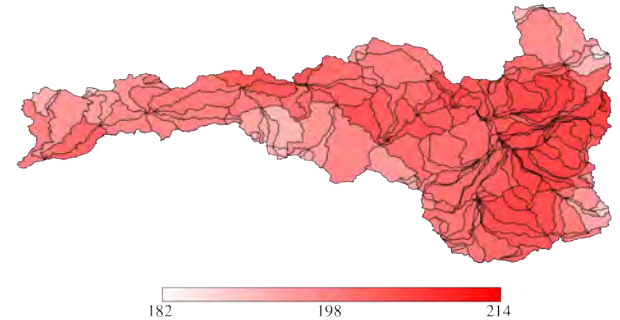
10-Year Average of Annual Average Short-wave Radiation (W/m²)
ECHAM5 A1B3 wy2070-wy2080



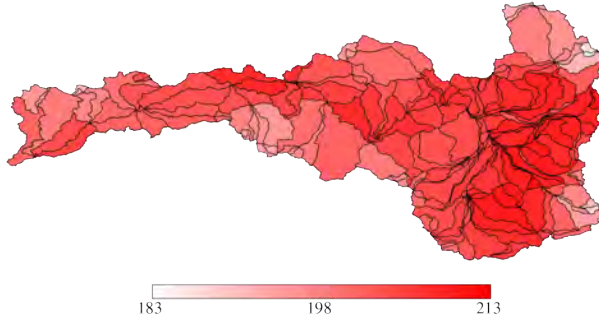
10-Year Average of Annual Average Short-wave Radiation (W/m²)
ECHAM5 A1B3 wy2080-wy2090



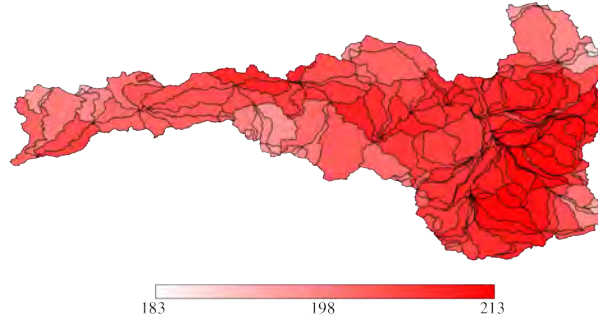
10-Year Average of Annual Average Short-wave Radiation (W/m²)
ECHAM5 A1B3 wy2090-wy2100



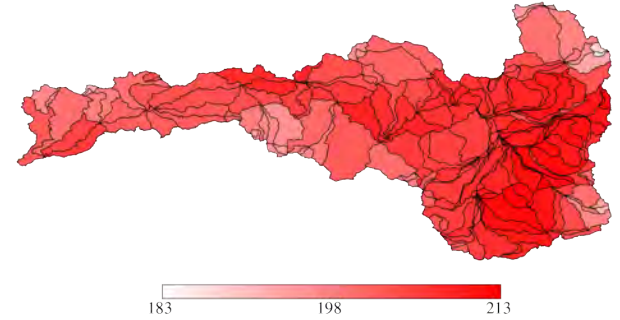
10-Year Average of Annual Average Short-wave Radiation (W/m²)
ECHAM5 A2-1 wy2010-wy2020



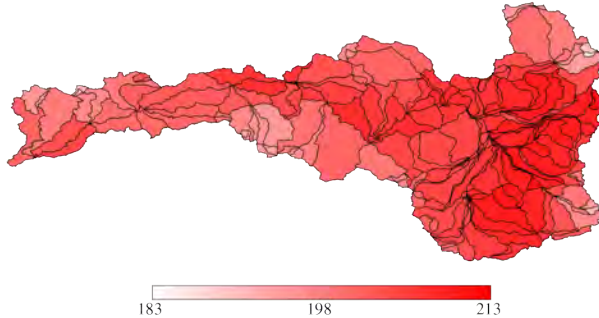
10-Year Average of Annual Average Short-wave Radiation (W/m²)
ECHAM5 A2-1 wy2020-wy2030



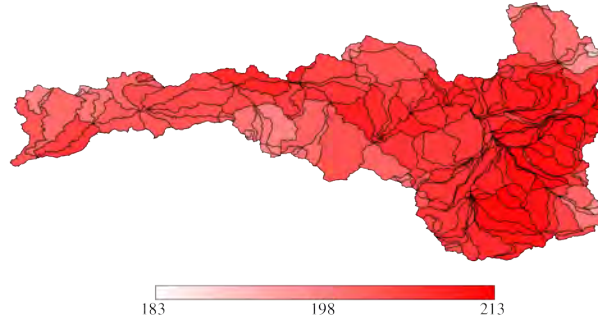
10-Year Average of Annual Average Short-wave Radiation (W/m²)
ECHAM5 A2-1 wy2030-wy2040



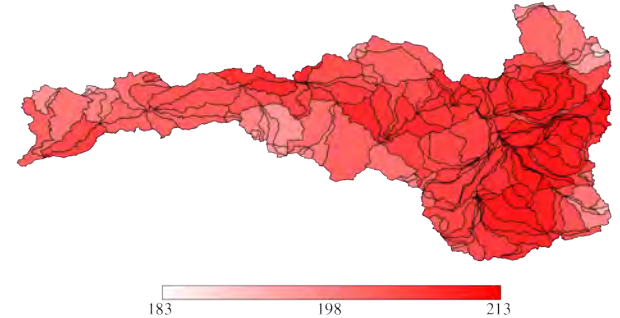
10-Year Average of Annual Average Short-wave Radiation (W/m²)
ECHAM5 A2-1 wy2040-wy2050



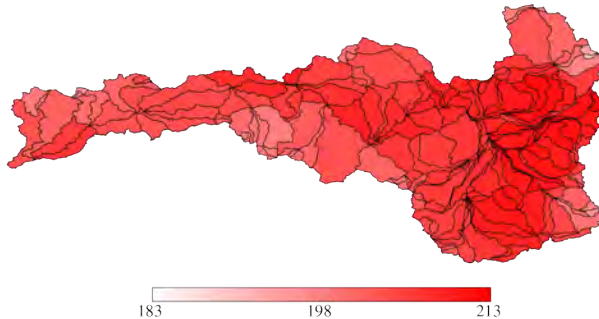
10-Year Average of Annual Average Short-wave Radiation (W/m²)
ECHAM5 A2-1 wy2050-wy2060



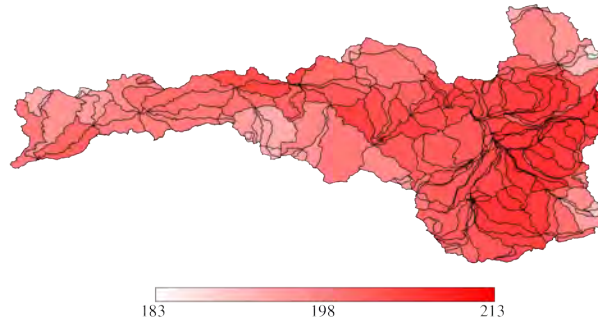
10-Year Average of Annual Average Short-wave Radiation (W/m²)
ECHAM5 A2-1 wy2060-wy2070



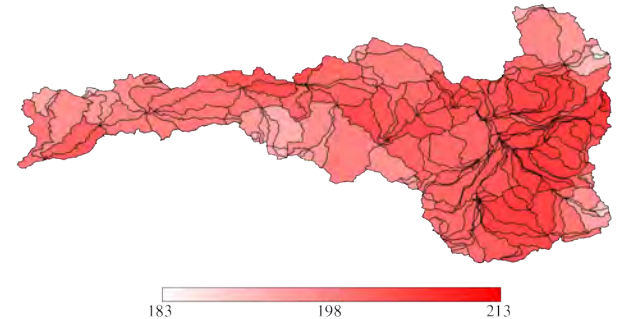
10-Year Average of Annual Average Short-wave Radiation (W/m²)
ECHAM5 A2-1 wy2070-wy2080



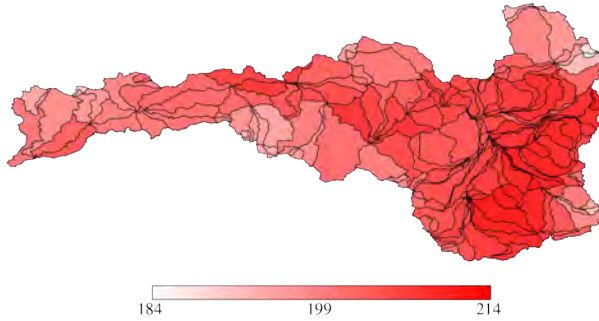
10-Year Average of Annual Average Short-wave Radiation (W/m²)
ECHAM5 A2-1 wy2080-wy2090



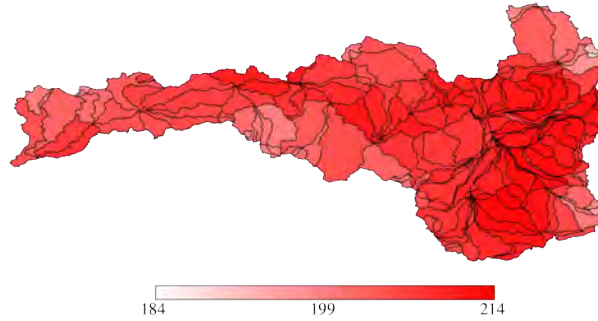
10-Year Average of Annual Average Short-wave Radiation (W/m²)
ECHAM5 A2-1 wy2090-wy2100



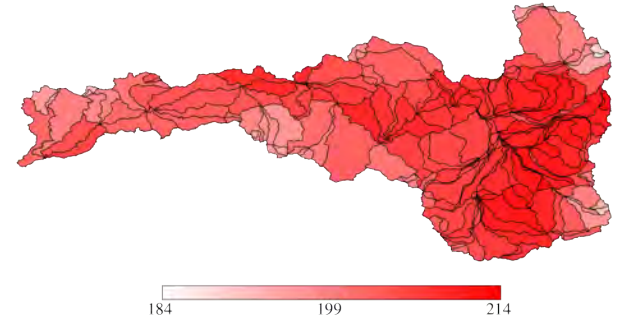
10-Year Average of Annual Average Short-wave Radiation (W/m²)
ECHAM5 A2-2 wy2010-wy2020



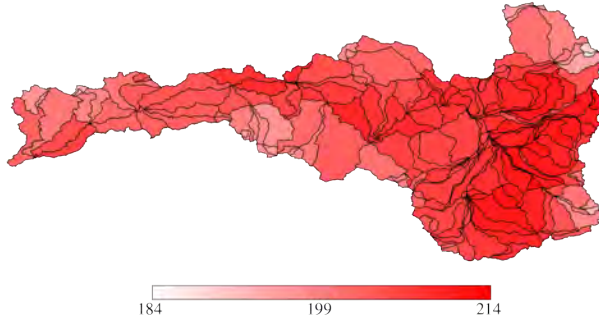
10-Year Average of Annual Average Short-wave Radiation (W/m²)
ECHAM5 A2-2 wy2020-wy2030



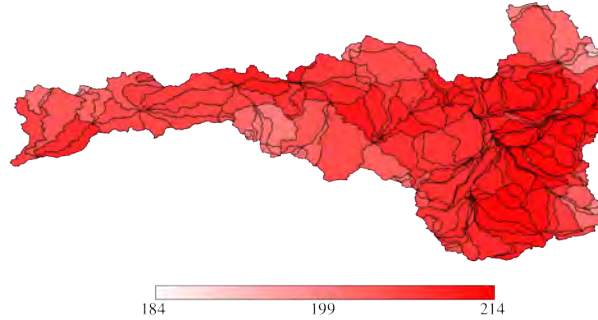
10-Year Average of Annual Average Short-wave Radiation (W/m²)
ECHAM5 A2-2 wy2030-wy2040



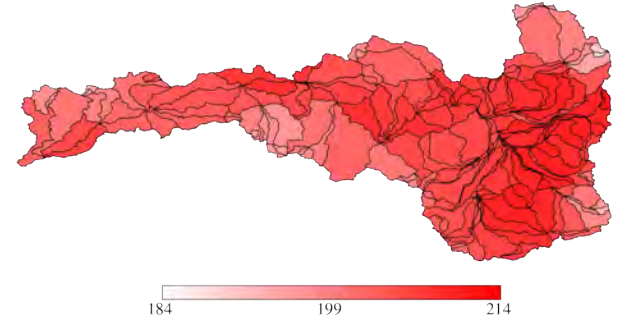
10-Year Average of Annual Average Short-wave Radiation (W/m²)
ECHAM5 A2-2 wy2040-wy2050



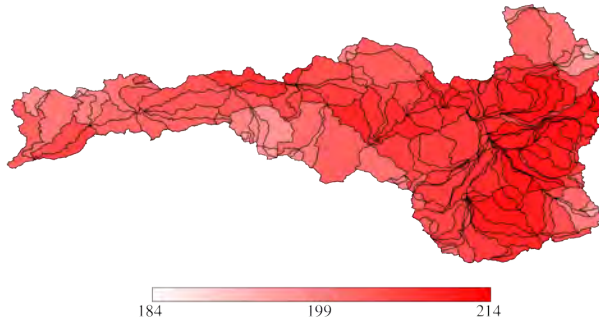
10-Year Average of Annual Average Short-wave Radiation (W/m²)
ECHAM5 A2-2 wy2050-wy2060



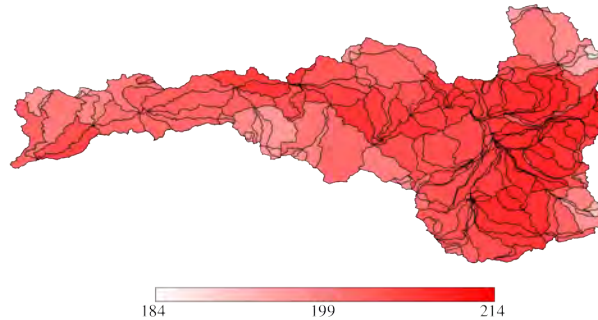
10-Year Average of Annual Average Short-wave Radiation (W/m²)
ECHAM5 A2-2 wy2060-wy2070



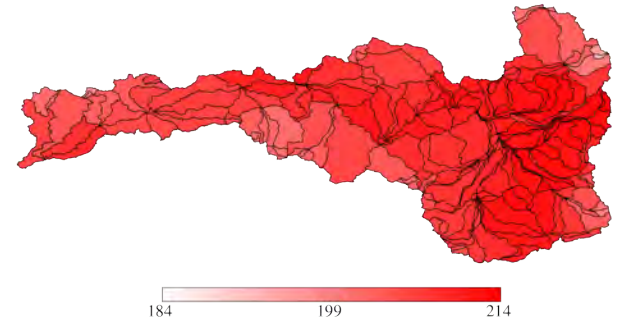
10-Year Average of Annual Average Short-wave Radiation (W/m²)
ECHAM5 A2-2 wy2070-wy2080



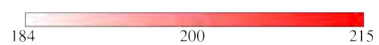
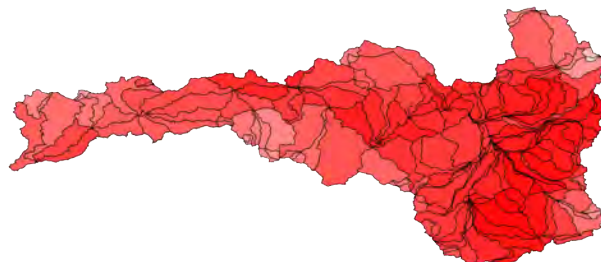
10-Year Average of Annual Average Short-wave Radiation (W/m²)
ECHAM5 A2-2 wy2080-wy2090



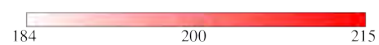
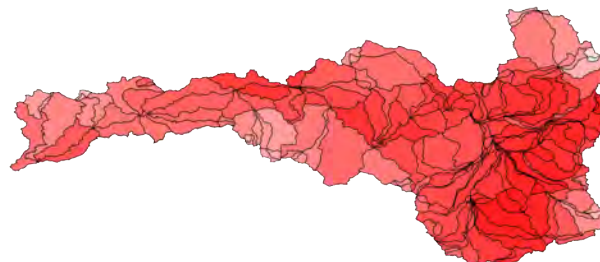
10-Year Average of Annual Average Short-wave Radiation (W/m²)
ECHAM5 A2-2 wy2090-wy2100



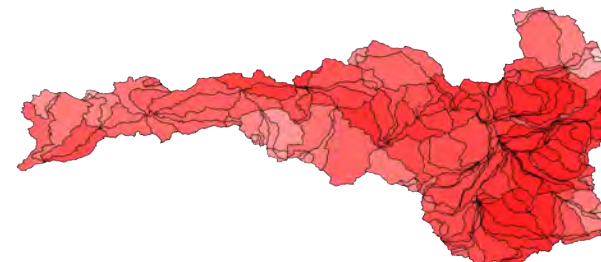
10-Year Average of Annual Average Short-wave Radiation (W/m²)
ECHAM5 A2-3 wy2010-wy2020



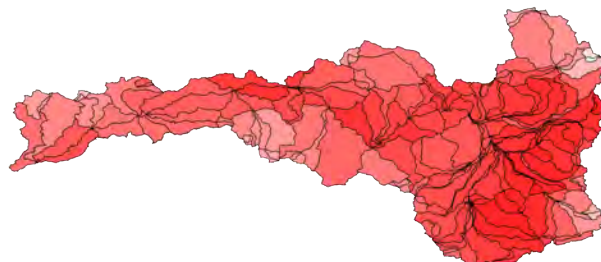
10-Year Average of Annual Average Short-wave Radiation (W/m²)
ECHAM5 A2-3 wy2020-wy2030



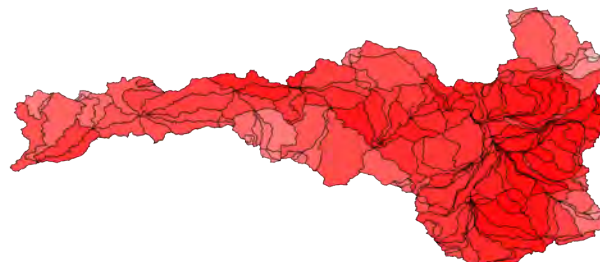
10-Year Average of Annual Average Short-wave Radiation (W/m²)
ECHAM5 A2-3 wy2030-wy2040



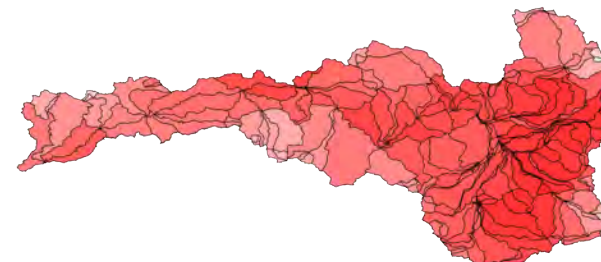
10-Year Average of Annual Average Short-wave Radiation (W/m²)
ECHAM5 A2-3 wy2040-wy2050



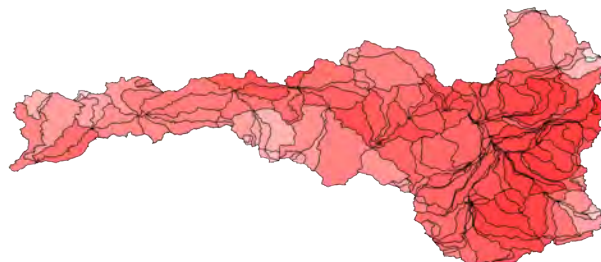
10-Year Average of Annual Average Short-wave Radiation (W/m²)
ECHAM5 A2-3 wy2050-wy2060



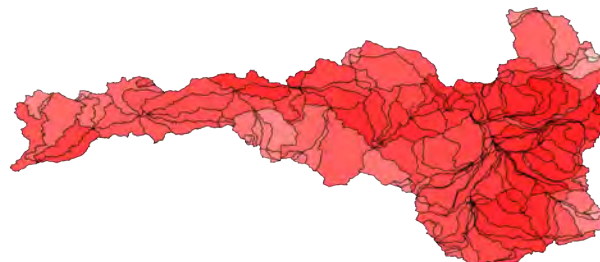
10-Year Average of Annual Average Short-wave Radiation (W/m²)
ECHAM5 A2-3 wy2060-wy2070



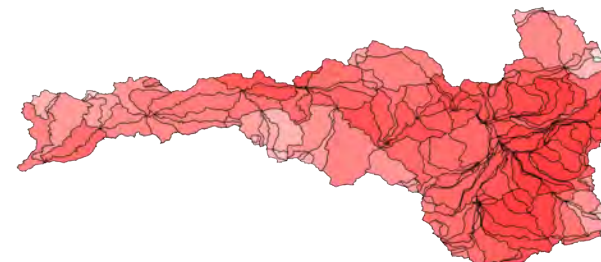
10-Year Average of Annual Average Short-wave Radiation (W/m²)
ECHAM5 A2-3 wy2070-wy2080



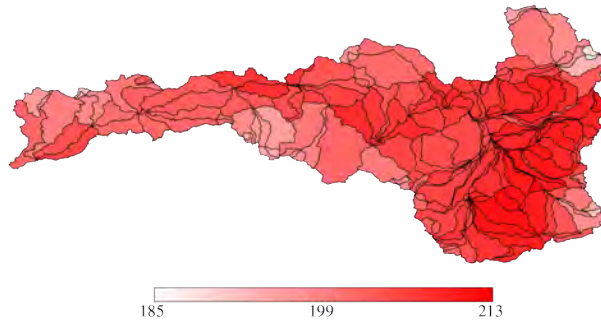
10-Year Average of Annual Average Short-wave Radiation (W/m²)
ECHAM5 A2-3 wy2080-wy2090



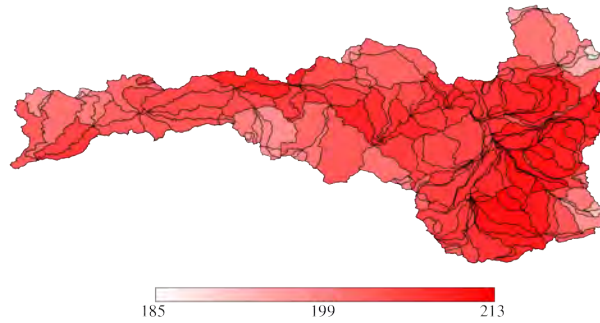
10-Year Average of Annual Average Short-wave Radiation (W/m²)
ECHAM5 A2-3 wy2090-wy2100



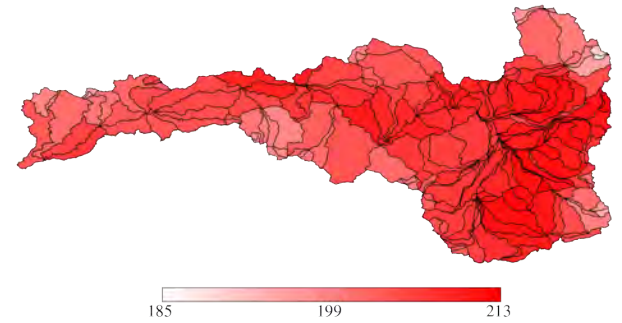
10-Year Average of Annual Average Short-wave Radiation (W/m²)
ECHAM5 B1-1 wy2010-wy2020



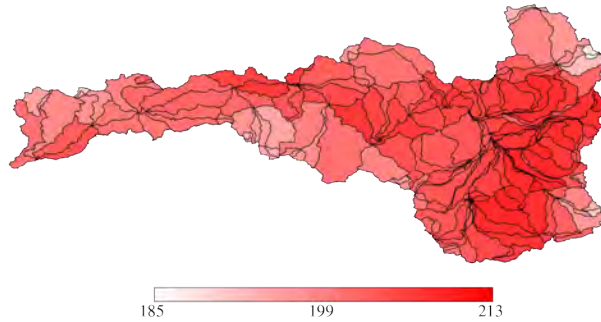
10-Year Average of Annual Average Short-wave Radiation (W/m²)
ECHAM5 B1-1 wy2020-wy2030



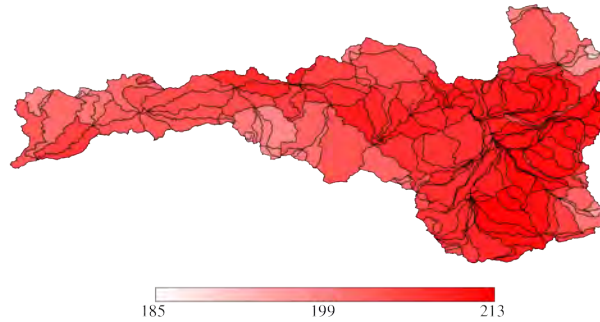
10-Year Average of Annual Average Short-wave Radiation (W/m²)
ECHAM5 B1-1 wy2030-wy2040



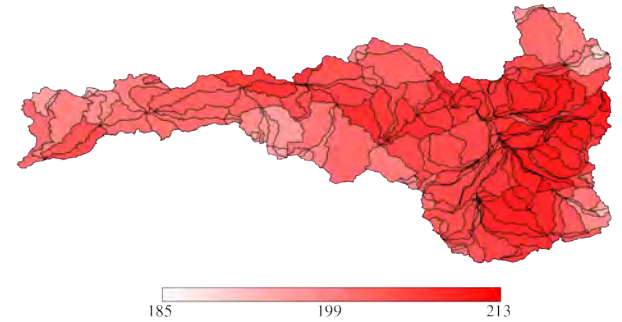
10-Year Average of Annual Average Short-wave Radiation (W/m²)
ECHAM5 B1-1 wy2040-wy2050



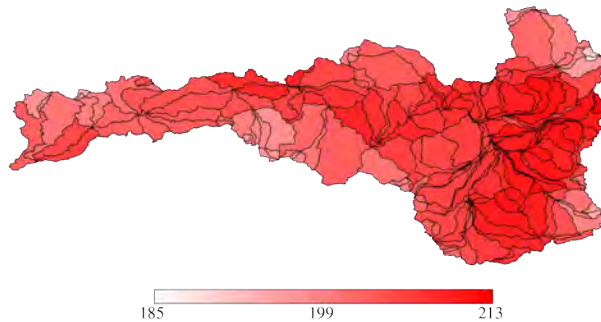
10-Year Average of Annual Average Short-wave Radiation (W/m²)
ECHAM5 B1-1 wy2050-wy2060



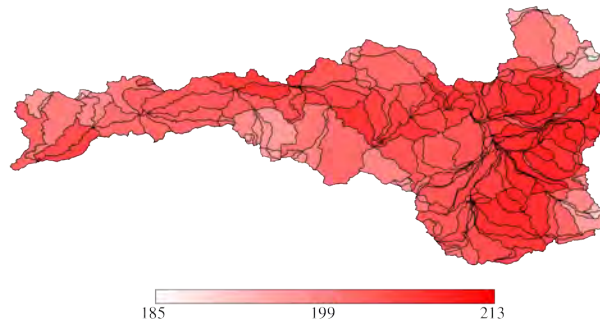
10-Year Average of Annual Average Short-wave Radiation (W/m²)
ECHAM5 B1-1 wy2060-wy2070



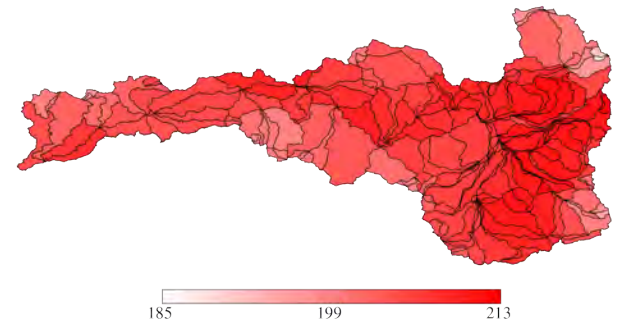
10-Year Average of Annual Average Short-wave Radiation (W/m²)
ECHAM5 B1-1 wy2070-wy2080



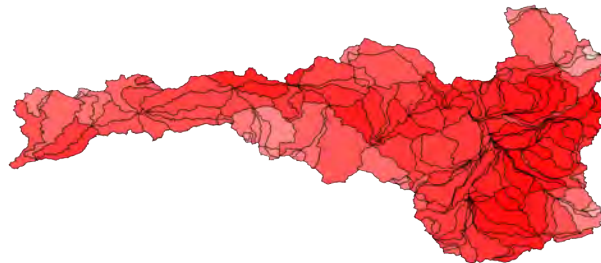
10-Year Average of Annual Average Short-wave Radiation (W/m²)
ECHAM5 B1-1 wy2080-wy2090



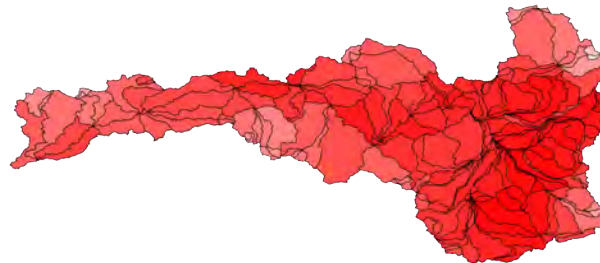
10-Year Average of Annual Average Short-wave Radiation (W/m²)
ECHAM5 B1-1 wy2090-wy2100



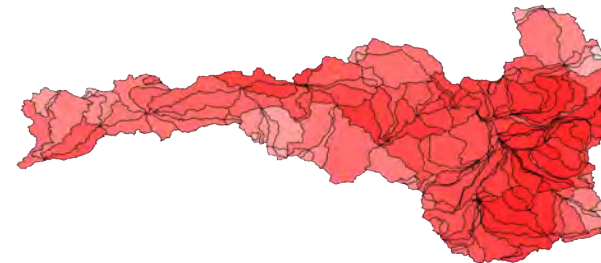
10-Year Average of Annual Average Short-wave Radiation (W/m²)
ECHAM5 B1-2 wy2010-wy2020



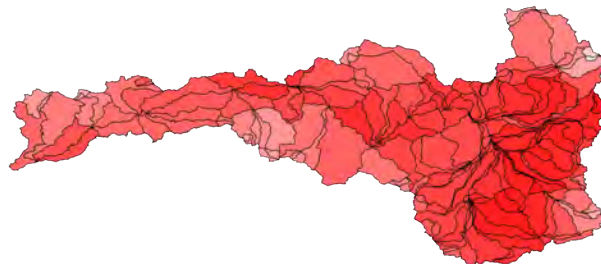
10-Year Average of Annual Average Short-wave Radiation (W/m²)
ECHAM5 B1-2 wy2020-wy2030



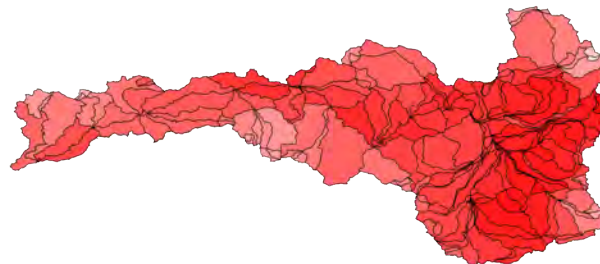
10-Year Average of Annual Average Short-wave Radiation (W/m²)
ECHAM5 B1-2 wy2030-wy2040



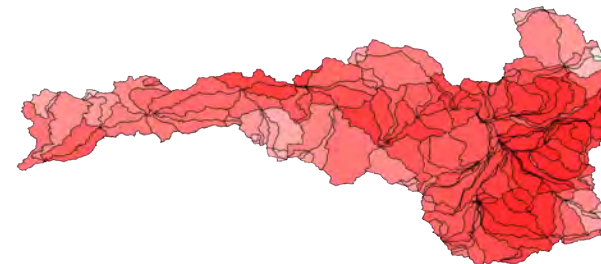
10-Year Average of Annual Average Short-wave Radiation (W/m²)
ECHAM5 B1-2 wy2040-wy2050



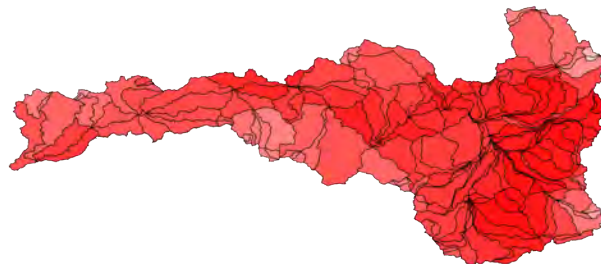
10-Year Average of Annual Average Short-wave Radiation (W/m²)
ECHAM5 B1-2 wy2050-wy2060



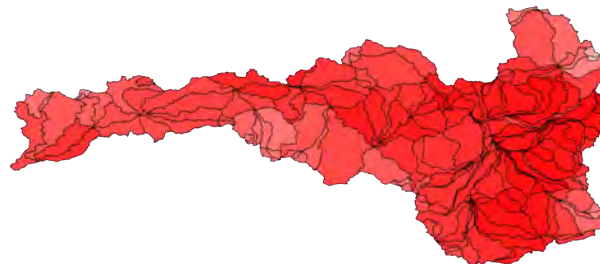
10-Year Average of Annual Average Short-wave Radiation (W/m²)
ECHAM5 B1-2 wy2060-wy2070



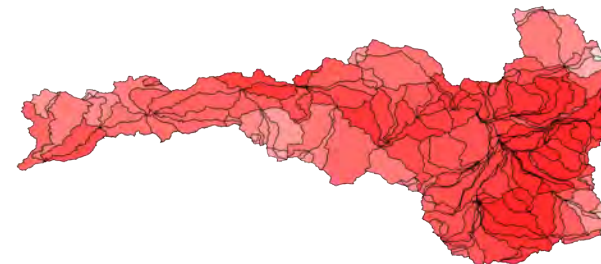
10-Year Average of Annual Average Short-wave Radiation (W/m²)
ECHAM5 B1-2 wy2070-wy2080



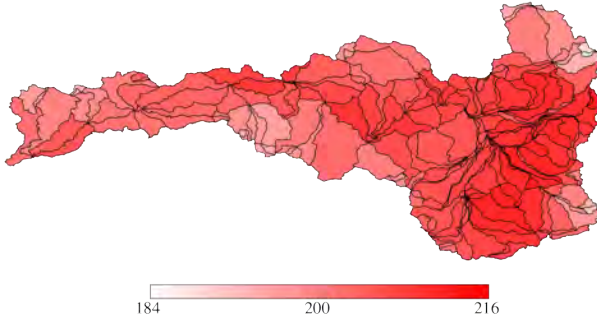
10-Year Average of Annual Average Short-wave Radiation (W/m²)
ECHAM5 B1-2 wy2080-wy2090



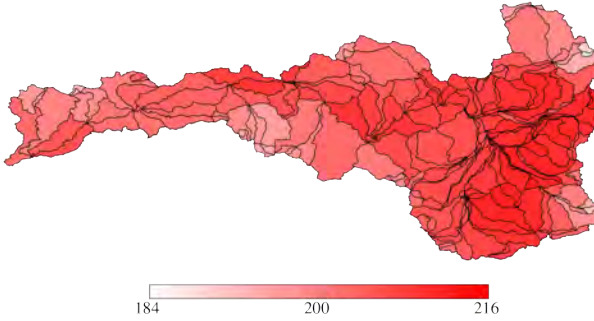
10-Year Average of Annual Average Short-wave Radiation (W/m²)
ECHAM5 B1-2 wy2090-wy2100



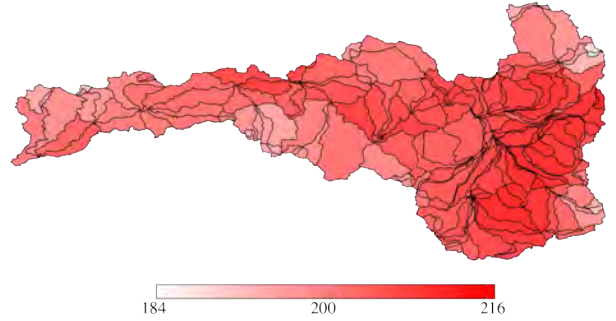
10-Year Average of Annual Average Short-wave Radiation (W/m²)
ECHAM5 B1-3 wy2010-wy2020



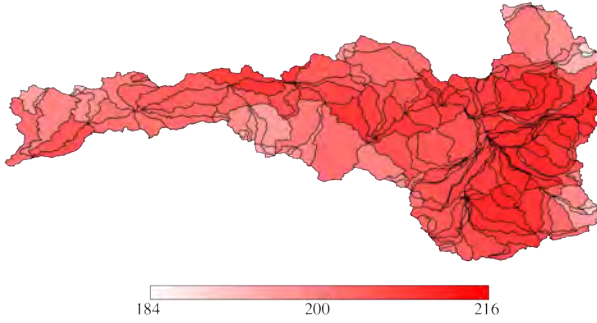
10-Year Average of Annual Average Short-wave Radiation (W/m²)
ECHAM5 B1-3 wy2020-wy2030



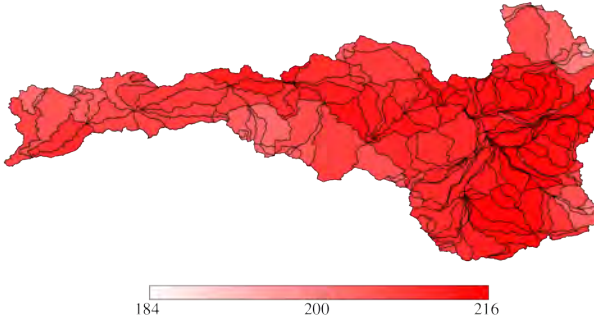
10-Year Average of Annual Average Short-wave Radiation (W/m²)
ECHAM5 B1-3 wy2030-wy2040



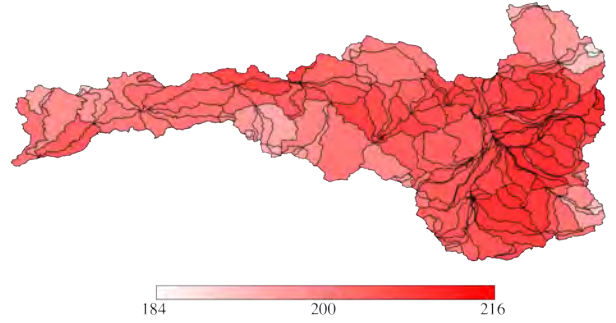
10-Year Average of Annual Average Short-wave Radiation (W/m²)
ECHAM5 B1-3 wy2040-wy2050



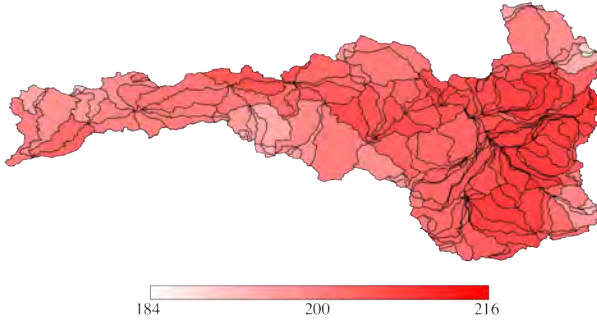
10-Year Average of Annual Average Short-wave Radiation (W/m²)
ECHAM5 B1-3 wy2050-wy2060



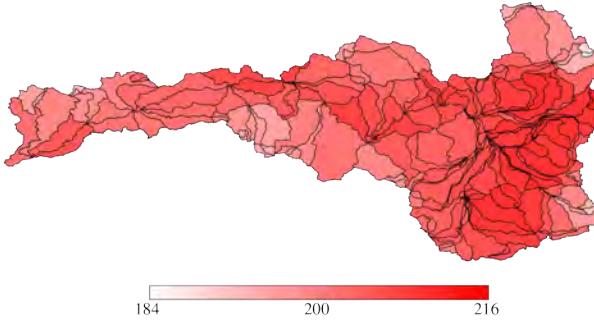
10-Year Average of Annual Average Short-wave Radiation (W/m²)
ECHAM5 B1-3 wy2060-wy2070



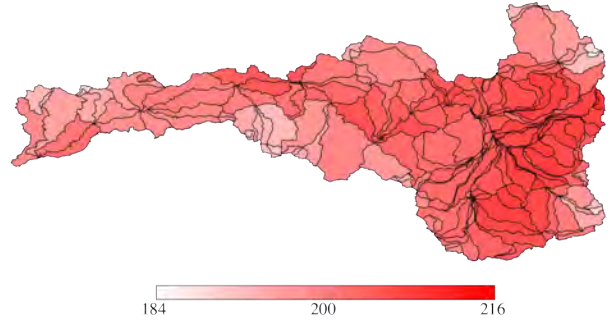
10-Year Average of Annual Average Short-wave Radiation (W/m²)
ECHAM5 B1-3 wy2070-wy2080



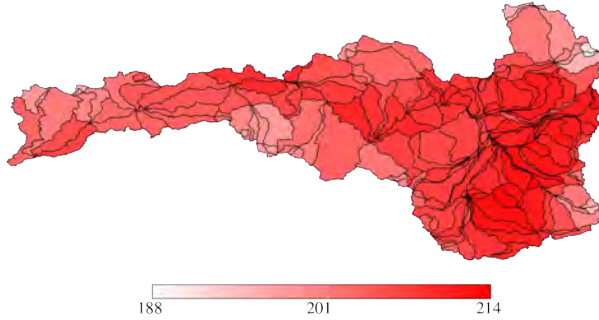
10-Year Average of Annual Average Short-wave Radiation (W/m²)
ECHAM5 B1-3 wy2080-wy2090



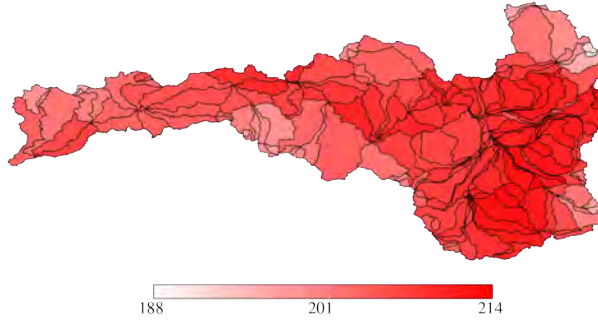
10-Year Average of Annual Average Short-wave Radiation (W/m²)
ECHAM5 B1-3 wy2090-wy2100



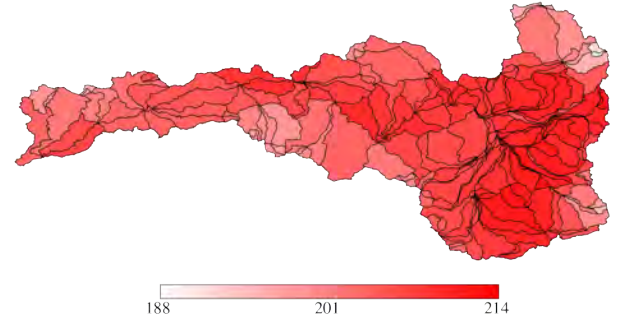
10-Year Average of Annual Average Short-wave Radiation (W/m²)
Ensemble All wy2010-wy2020



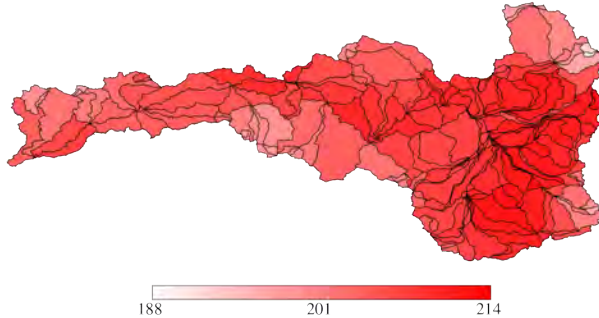
10-Year Average of Annual Average Short-wave Radiation (W/m²)
Ensemble All wy2020-wy2030



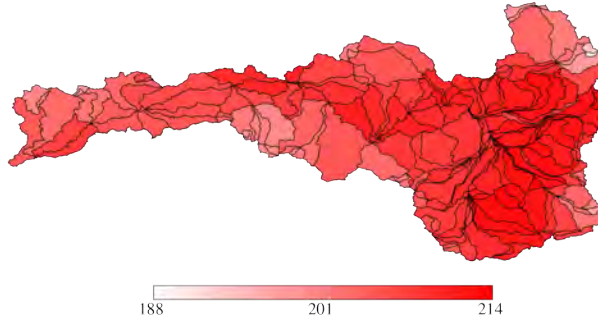
10-Year Average of Annual Average Short-wave Radiation (W/m²)
Ensemble All wy2030-wy2040



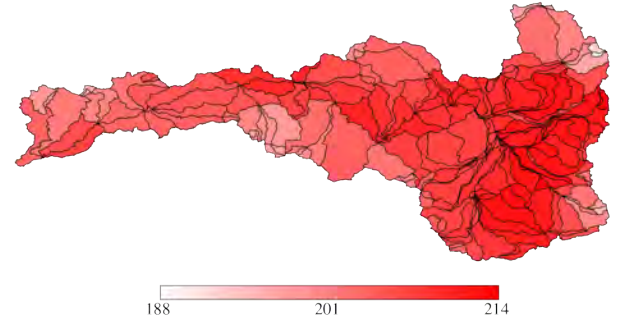
10-Year Average of Annual Average Short-wave Radiation (W/m²)
Ensemble All wy2040-wy2050



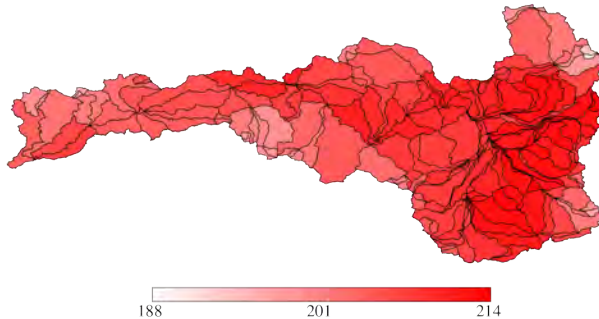
10-Year Average of Annual Average Short-wave Radiation (W/m²)
Ensemble All wy2050-wy2060



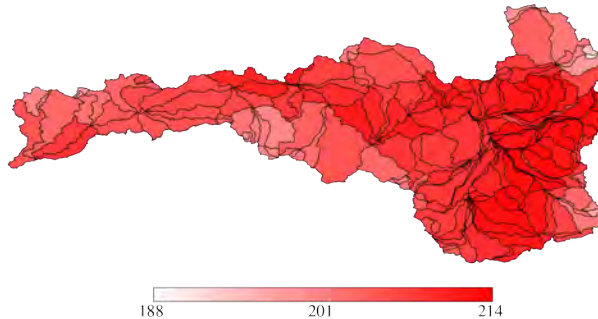
10-Year Average of Annual Average Short-wave Radiation (W/m²)
Ensemble All wy2060-wy2070



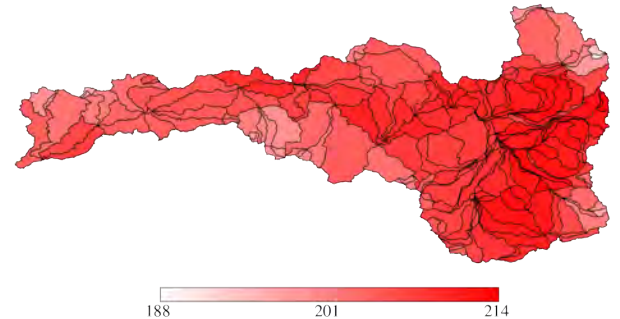
10-Year Average of Annual Average Short-wave Radiation (W/m²)
Ensemble All wy2070-wy2080



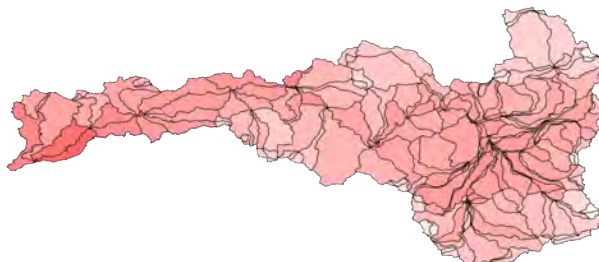
10-Year Average of Annual Average Short-wave Radiation (W/m²)
Ensemble All wy2080-wy2090



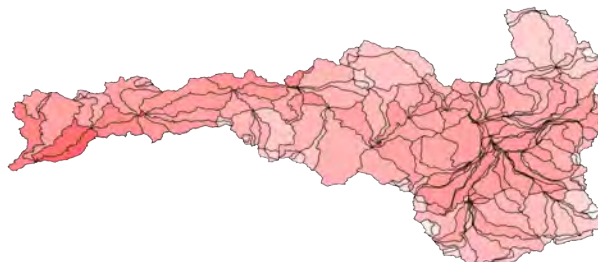
10-Year Average of Annual Average Short-wave Radiation (W/m²)
Ensemble All wy2090-wy2100



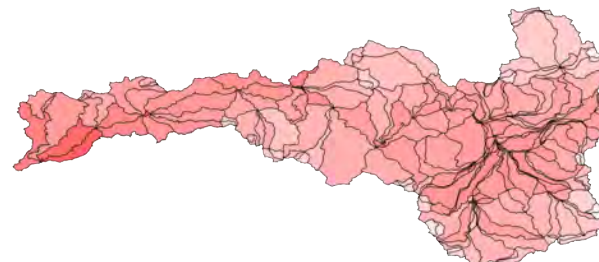
10-Year Average of Annual Average Air Temperature (deg C)
CCSM3 A1B wy2010-wy2020



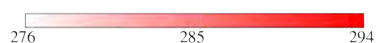
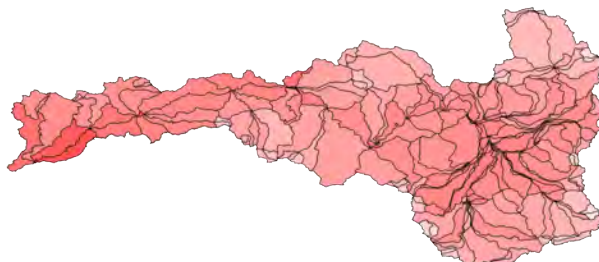
10-Year Average of Annual Average Air Temperature (deg C)
CCSM3 A1B wy2020-wy2030



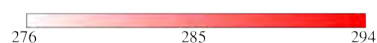
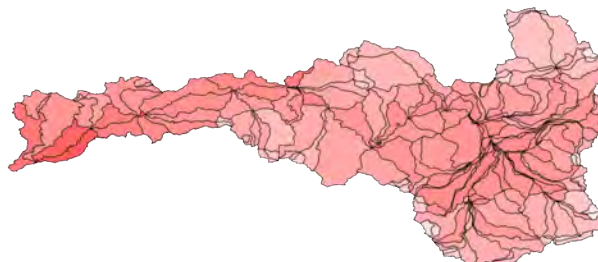
10-Year Average of Annual Average Air Temperature (deg C)
CCSM3 A1B wy2030-wy2040



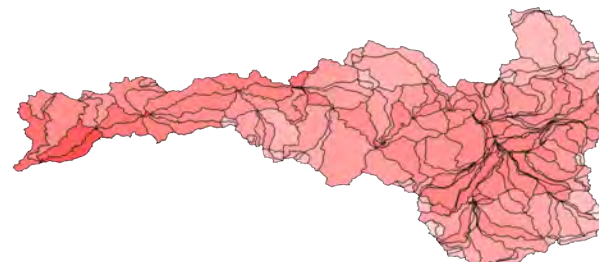
10-Year Average of Annual Average Air Temperature (deg C)
CCSM3 A1B wy2040-wy2050



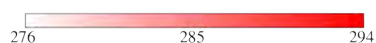
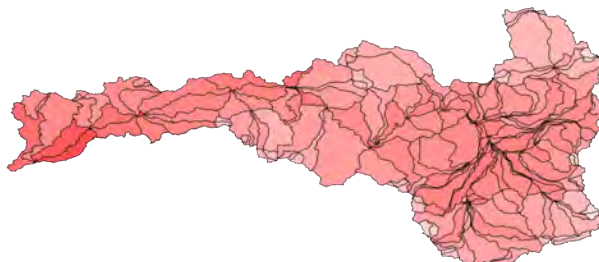
10-Year Average of Annual Average Air Temperature (deg C)
CCSM3 A1B wy2050-wy2060



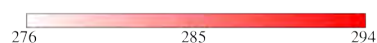
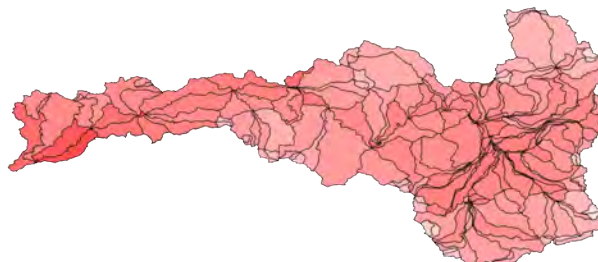
10-Year Average of Annual Average Air Temperature (deg C)
CCSM3 A1B wy2060-wy2070



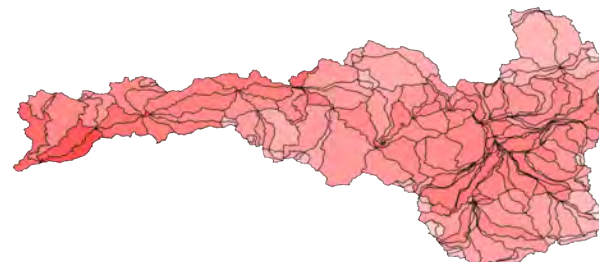
10-Year Average of Annual Average Air Temperature (deg C)
CCSM3 A1B wy2070-wy2080



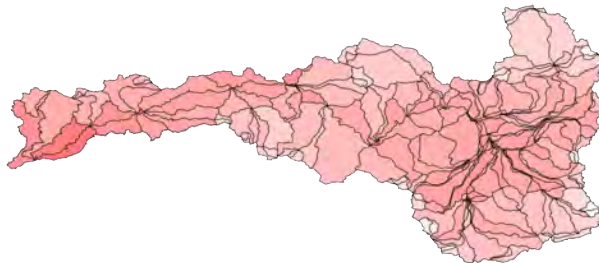
10-Year Average of Annual Average Air Temperature (deg C)
CCSM3 A1B wy2080-wy2090



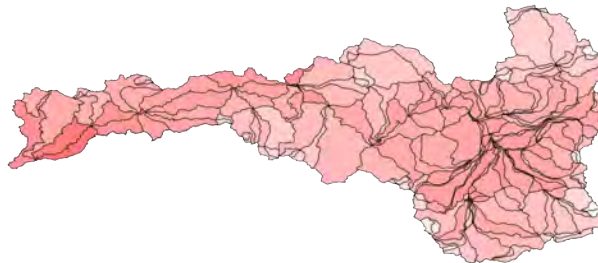
10-Year Average of Annual Average Air Temperature (deg C)
CCSM3 A1B wy2090-wy2100



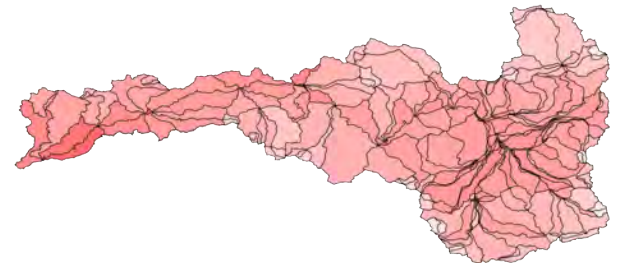
10-Year Average of Annual Average Air Temperature (deg C)
CCSM3 A1FI wy2010-wy2020



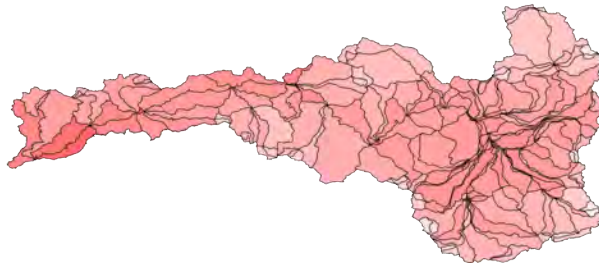
10-Year Average of Annual Average Air Temperature (deg C)
CCSM3 A1FI wy2020-wy2030



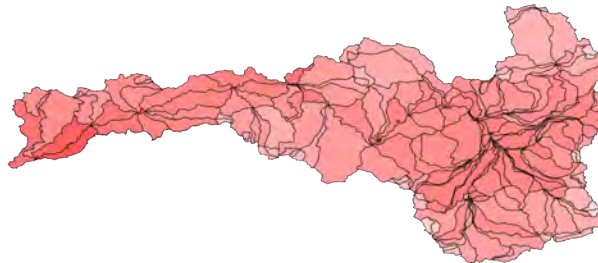
10-Year Average of Annual Average Air Temperature (deg C)
CCSM3 A1FI wy2030-wy2040



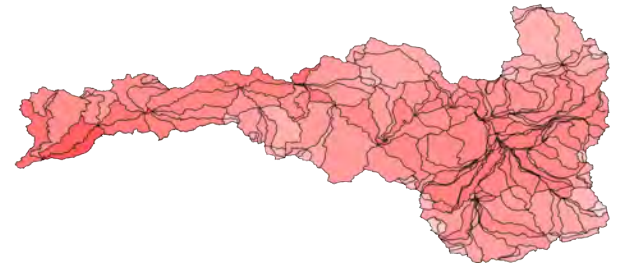
10-Year Average of Annual Average Air Temperature (deg C)
CCSM3 A1FI wy2040-wy2050



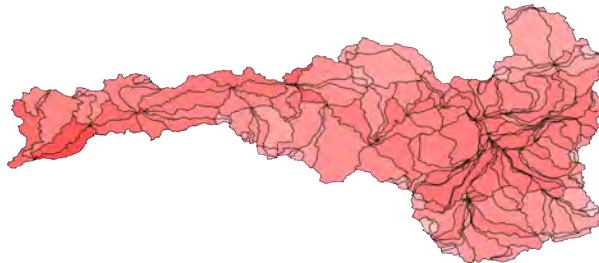
10-Year Average of Annual Average Air Temperature (deg C)
CCSM3 A1FI wy2050-wy2060



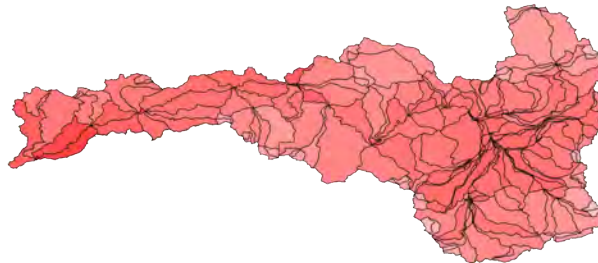
10-Year Average of Annual Average Air Temperature (deg C)
CCSM3 A1FI wy2060-wy2070



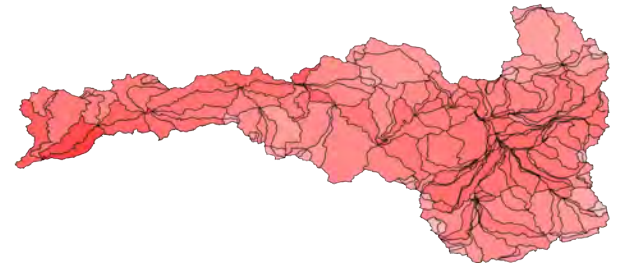
10-Year Average of Annual Average Air Temperature (deg C)
CCSM3 A1FI wy2070-wy2080



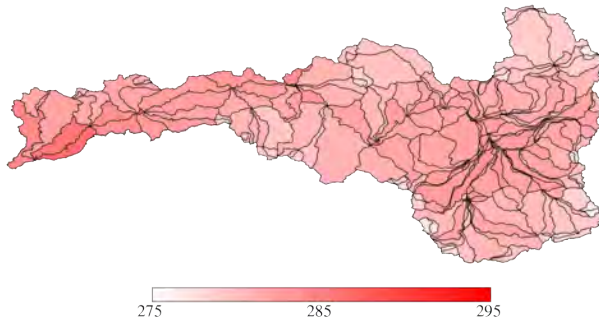
10-Year Average of Annual Average Air Temperature (deg C)
CCSM3 A1FI wy2080-wy2090



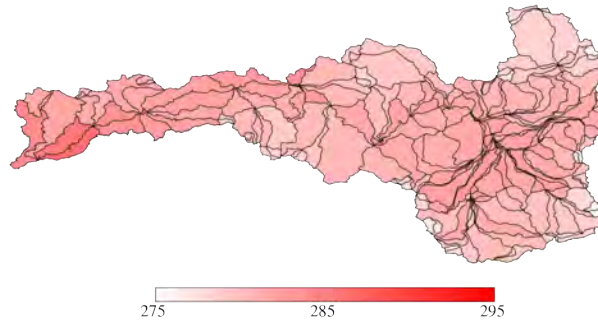
10-Year Average of Annual Average Air Temperature (deg C)
CCSM3 A1FI wy2090-wy2100



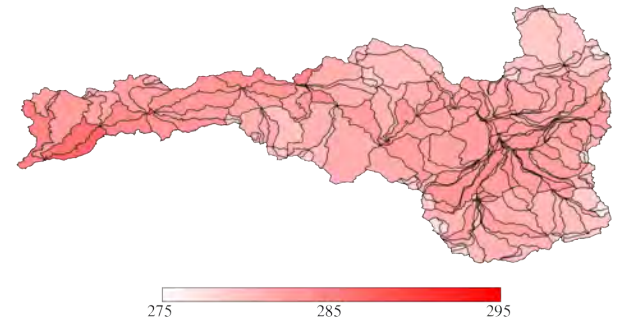
10-Year Average of Annual Average Air Temperature (deg C)
CCSM3 A2 wy2010-wy2020



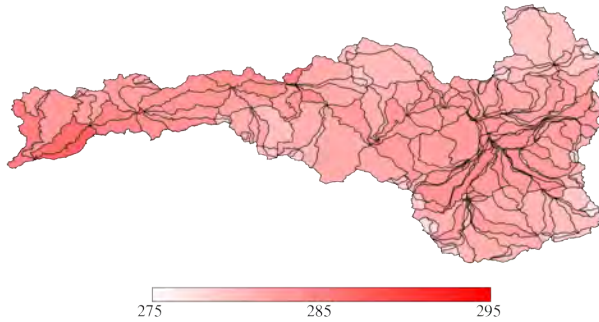
10-Year Average of Annual Average Air Temperature (deg C)
CCSM3 A2 wy2020-wy2030



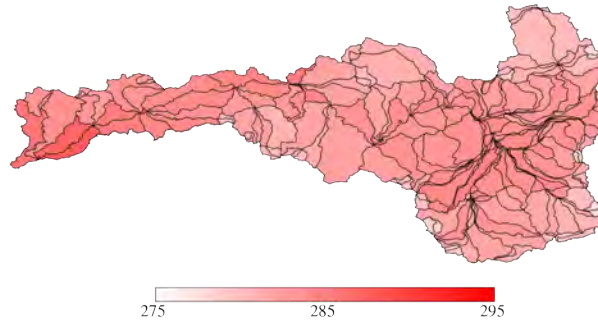
10-Year Average of Annual Average Air Temperature (deg C)
CCSM3 A2 wy2030-wy2040



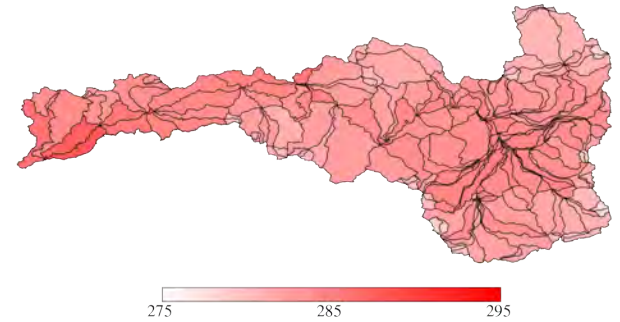
10-Year Average of Annual Average Air Temperature (deg C)
CCSM3 A2 wy2040-wy2050



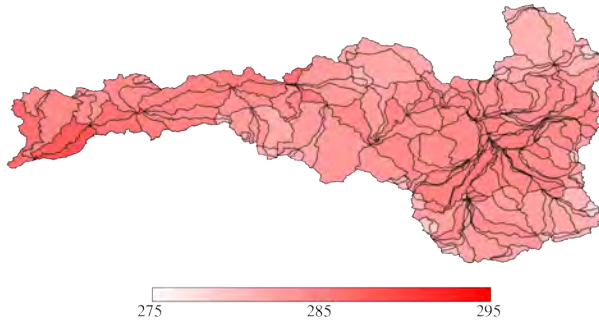
10-Year Average of Annual Average Air Temperature (deg C)
CCSM3 A2 wy2050-wy2060



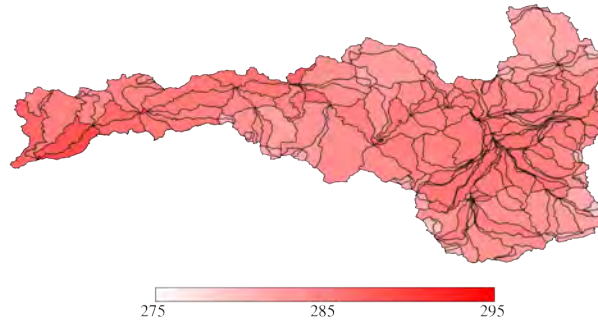
10-Year Average of Annual Average Air Temperature (deg C)
CCSM3 A2 wy2060-wy2070



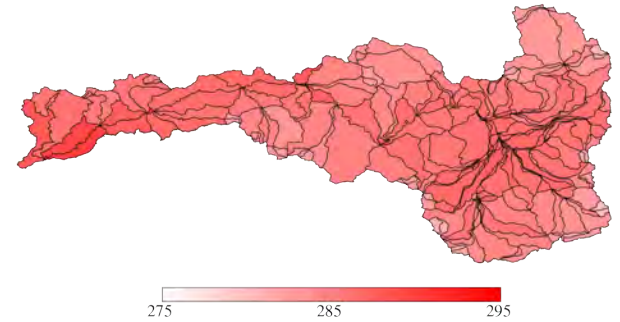
10-Year Average of Annual Average Air Temperature (deg C)
CCSM3 A2 wy2070-wy2080



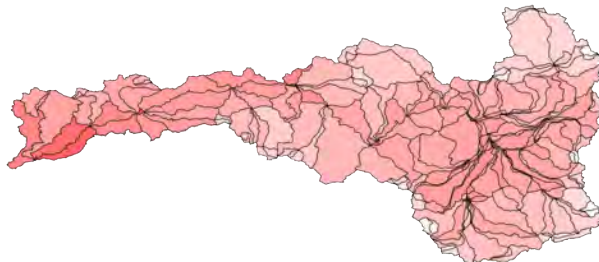
10-Year Average of Annual Average Air Temperature (deg C)
CCSM3 A2 wy2080-wy2090



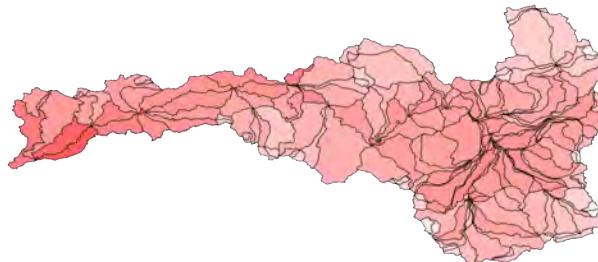
10-Year Average of Annual Average Air Temperature (deg C)
CCSM3 A2 wy2090-wy2100



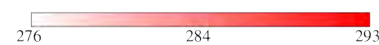
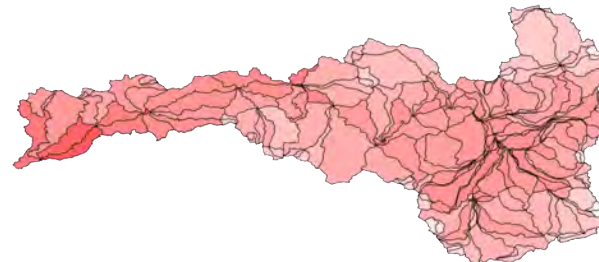
10-Year Average of Annual Average Air Temperature (deg C)
CCSM3 B1 wy2010-wy2020



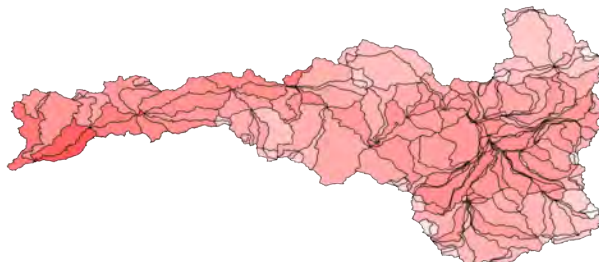
10-Year Average of Annual Average Air Temperature (deg C)
CCSM3 B1 wy2020-wy2030



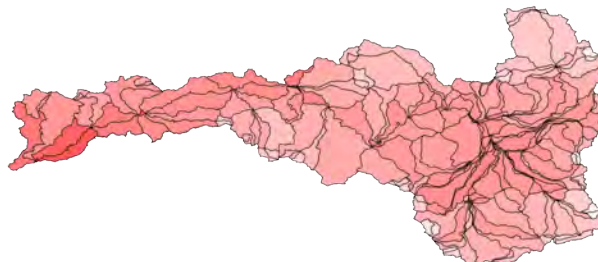
10-Year Average of Annual Average Air Temperature (deg C)
CCSM3 B1 wy2030-wy2040



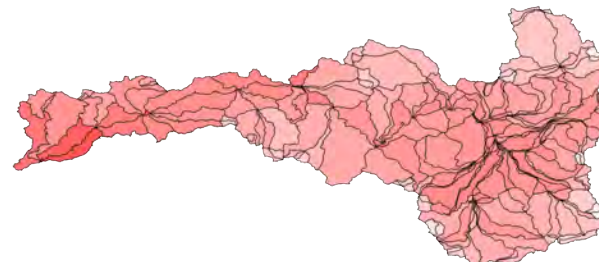
10-Year Average of Annual Average Air Temperature (deg C)
CCSM3 B1 wy2040-wy2050



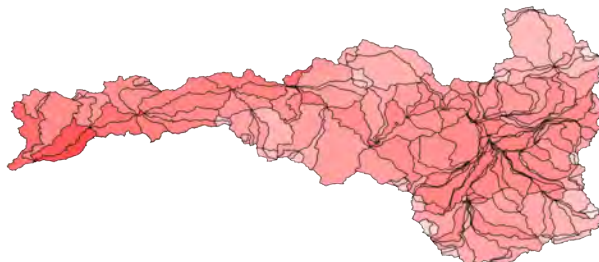
10-Year Average of Annual Average Air Temperature (deg C)
CCSM3 B1 wy2050-wy2060



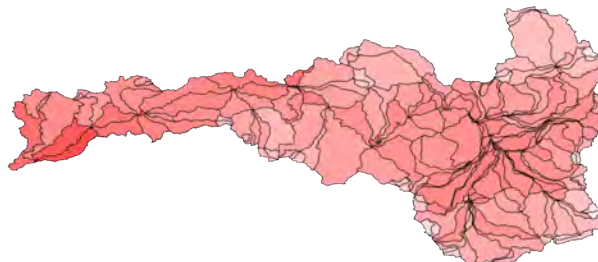
10-Year Average of Annual Average Air Temperature (deg C)
CCSM3 B1 wy2060-wy2070



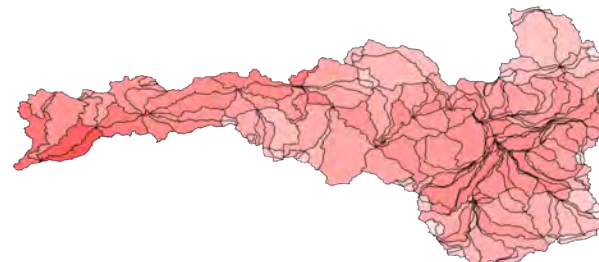
10-Year Average of Annual Average Air Temperature (deg C)
CCSM3 B1 wy2070-wy2080



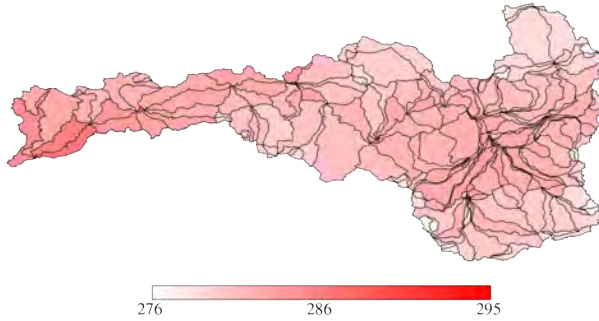
10-Year Average of Annual Average Air Temperature (deg C)
CCSM3 B1 wy2080-wy2090



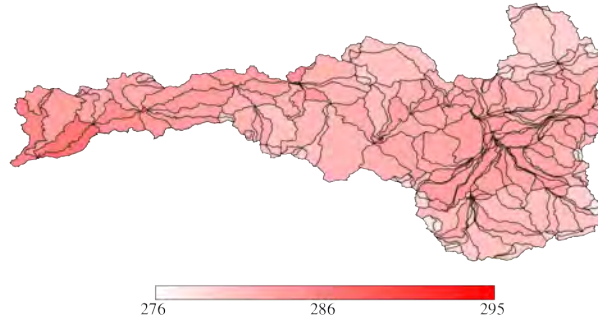
10-Year Average of Annual Average Air Temperature (deg C)
CCSM3 B1 wy2090-wy2100



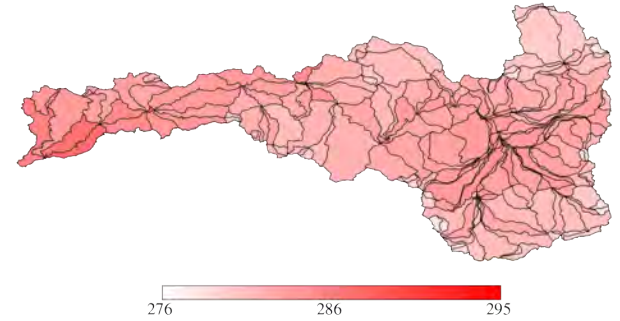
10-Year Average of Annual Average Air Temperature (deg C)
ECHAM5 A1B1 wy2010-wy2020



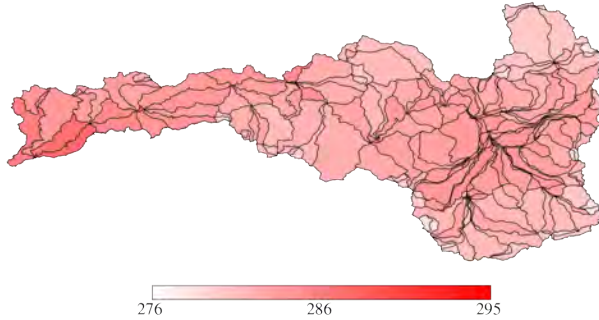
10-Year Average of Annual Average Air Temperature (deg C)
ECHAM5 A1B1 wy2020-wy2030



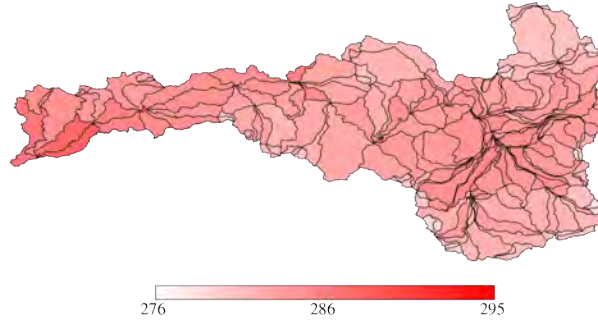
10-Year Average of Annual Average Air Temperature (deg C)
ECHAM5 A1B1 wy2030-wy2040



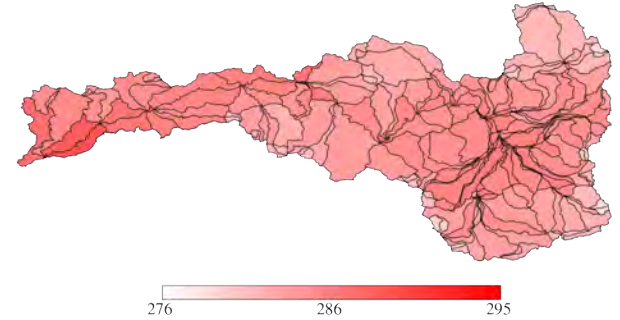
10-Year Average of Annual Average Air Temperature (deg C)
ECHAM5 A1B1 wy2040-wy2050



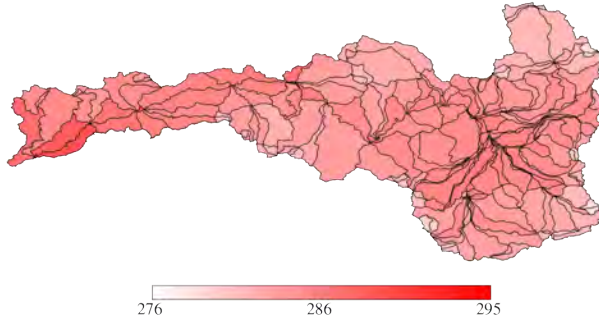
10-Year Average of Annual Average Air Temperature (deg C)
ECHAM5 A1B1 wy2050-wy2060



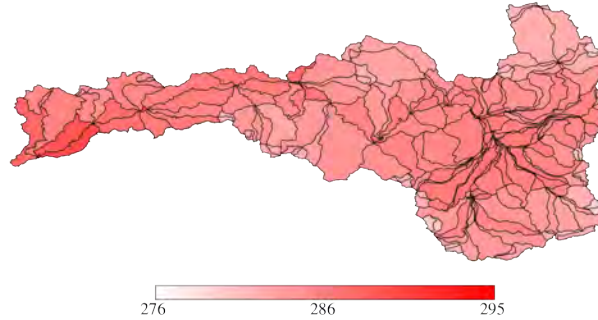
10-Year Average of Annual Average Air Temperature (deg C)
ECHAM5 A1B1 wy2060-wy2070



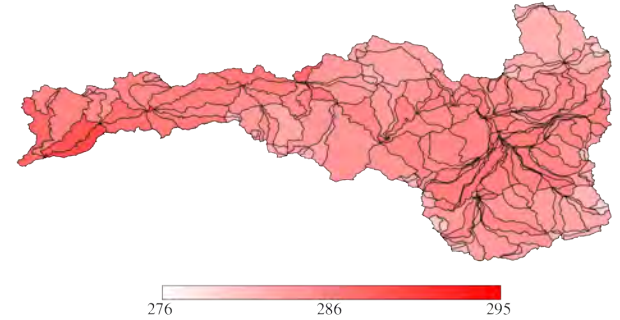
10-Year Average of Annual Average Air Temperature (deg C)
ECHAM5 A1B1 wy2070-wy2080



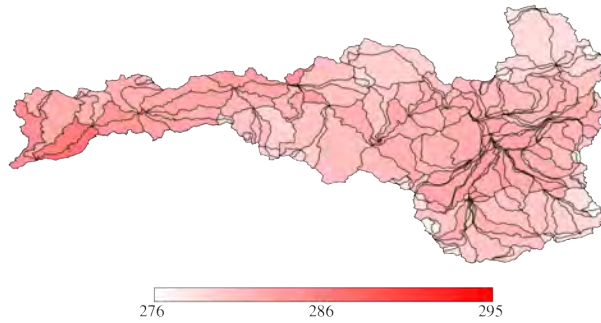
10-Year Average of Annual Average Air Temperature (deg C)
ECHAM5 A1B1 wy2080-wy2090



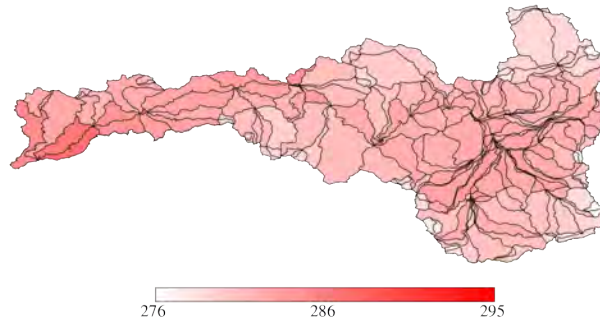
10-Year Average of Annual Average Air Temperature (deg C)
ECHAM5 A1B1 wy2090-wy2100



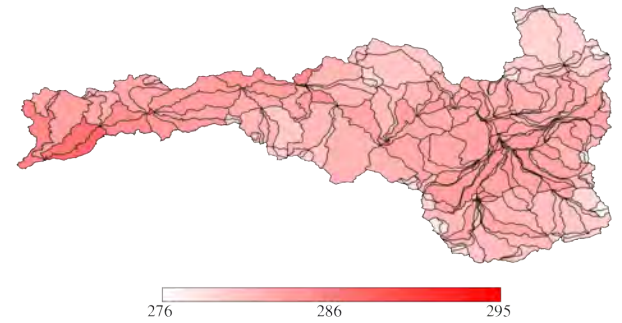
10-Year Average of Annual Average Air Temperature (deg C)
ECHAM5 A1B2 wy2010-wy2020



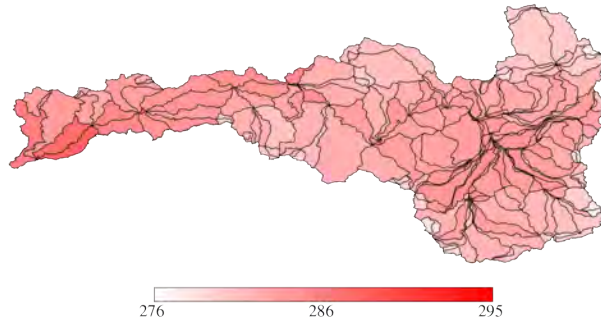
10-Year Average of Annual Average Air Temperature (deg C)
ECHAM5 A1B2 wy2020-wy2030



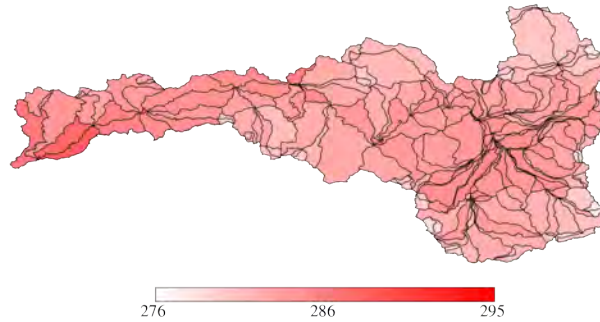
10-Year Average of Annual Average Air Temperature (deg C)
ECHAM5 A1B2 wy2030-wy2040



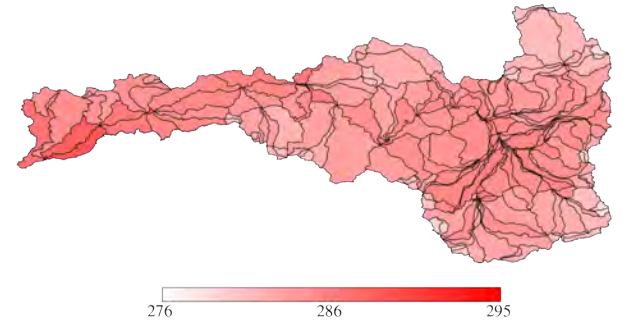
10-Year Average of Annual Average Air Temperature (deg C)
ECHAM5 A1B2 wy2040-wy2050



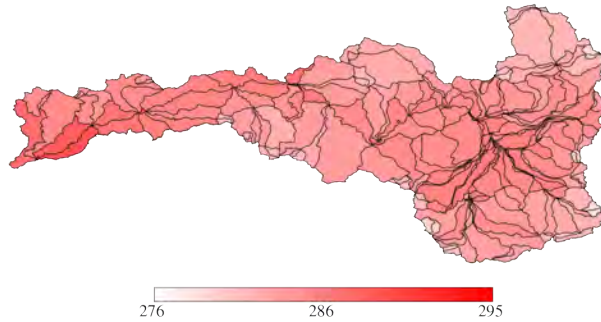
10-Year Average of Annual Average Air Temperature (deg C)
ECHAM5 A1B2 wy2050-wy2060



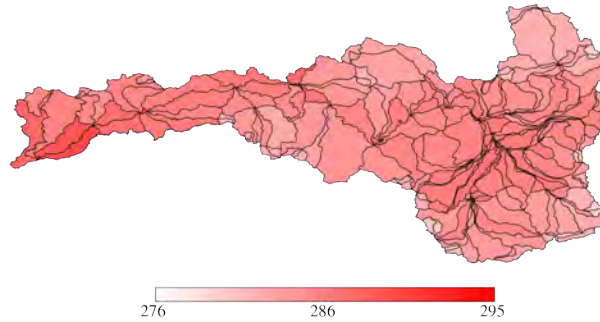
10-Year Average of Annual Average Air Temperature (deg C)
ECHAM5 A1B2 wy2060-wy2070



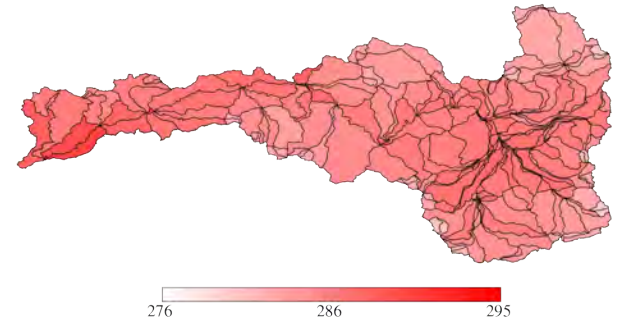
10-Year Average of Annual Average Air Temperature (deg C)
ECHAM5 A1B2 wy2070-wy2080



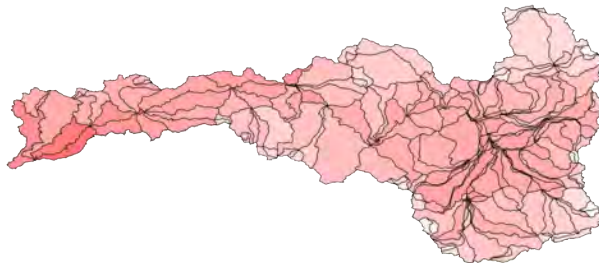
10-Year Average of Annual Average Air Temperature (deg C)
ECHAM5 A1B2 wy2080-wy2090



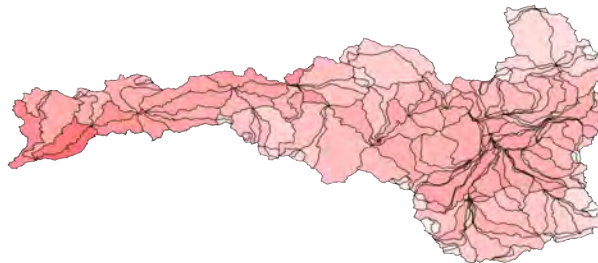
10-Year Average of Annual Average Air Temperature (deg C)
ECHAM5 A1B2 wy2090-wy2100



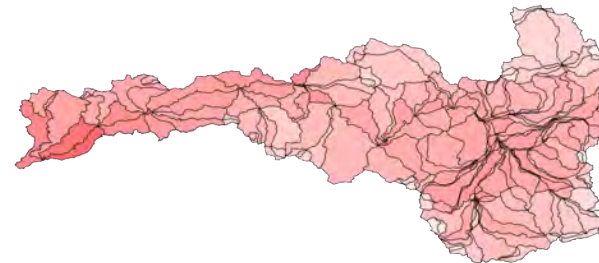
10-Year Average of Annual Average Air Temperature (deg C)
ECHAM5 A2-1 wy2010-wy2020



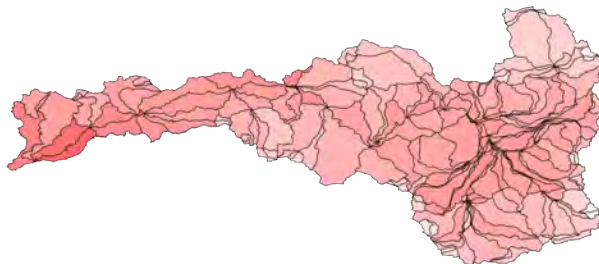
10-Year Average of Annual Average Air Temperature (deg C)
ECHAM5 A2-1 wy2020-wy2030



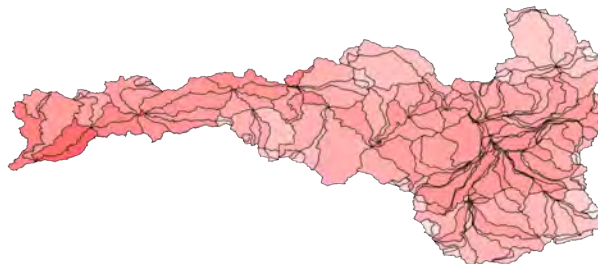
10-Year Average of Annual Average Air Temperature (deg C)
ECHAM5 A2-1 wy2030-wy2040



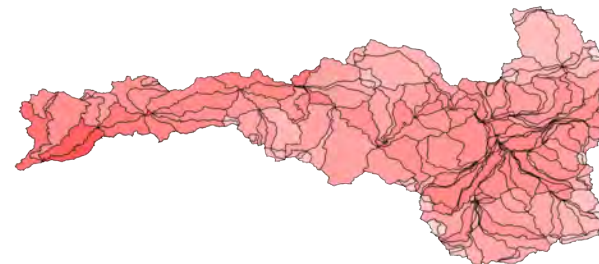
10-Year Average of Annual Average Air Temperature (deg C)
ECHAM5 A2-1 wy2040-wy2050



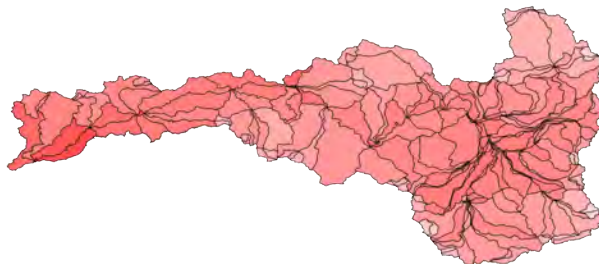
10-Year Average of Annual Average Air Temperature (deg C)
ECHAM5 A2-1 wy2050-wy2060



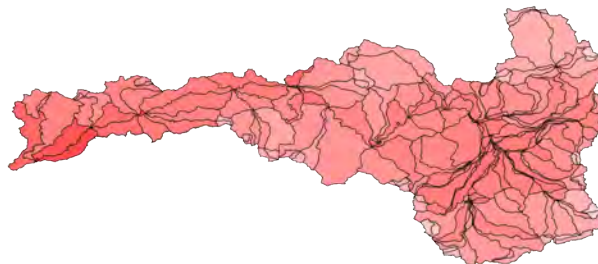
10-Year Average of Annual Average Air Temperature (deg C)
ECHAM5 A2-1 wy2060-wy2070



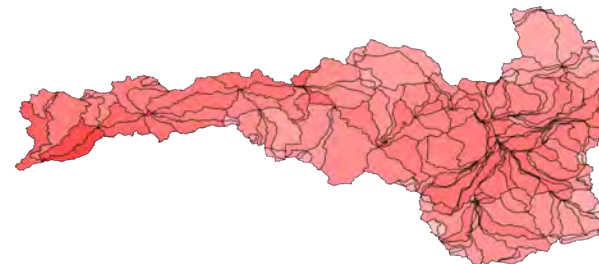
10-Year Average of Annual Average Air Temperature (deg C)
ECHAM5 A2-1 wy2070-wy2080



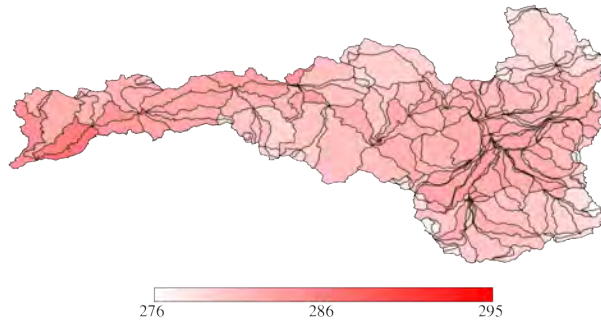
10-Year Average of Annual Average Air Temperature (deg C)
ECHAM5 A2-1 wy2080-wy2090



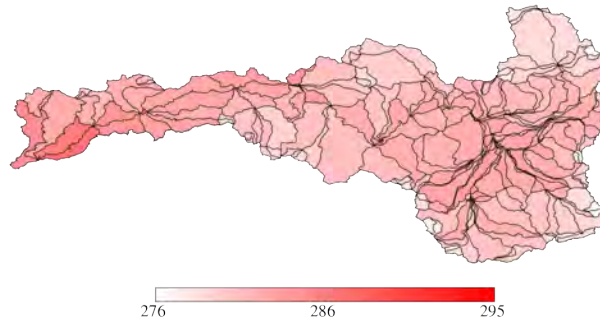
10-Year Average of Annual Average Air Temperature (deg C)
ECHAM5 A2-1 wy2090-wy2100



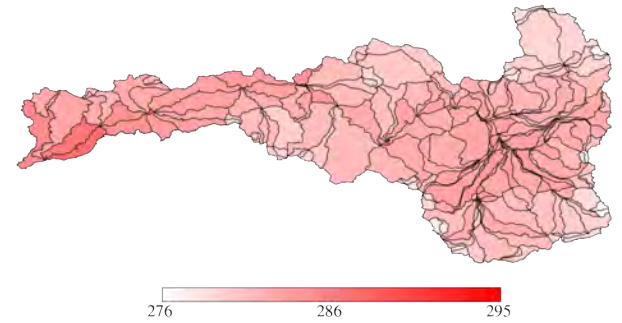
10-Year Average of Annual Average Air Temperature (deg C)
ECHAM5 A2-2 wy2010-wy2020



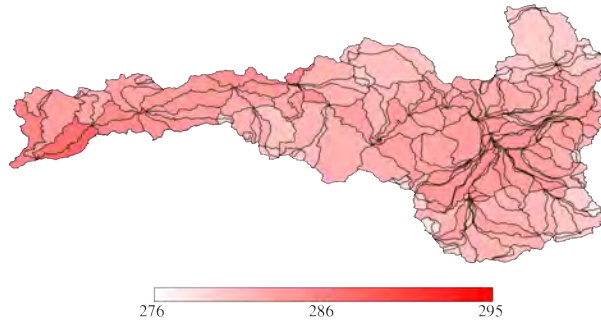
10-Year Average of Annual Average Air Temperature (deg C)
ECHAM5 A2-2 wy2020-wy2030



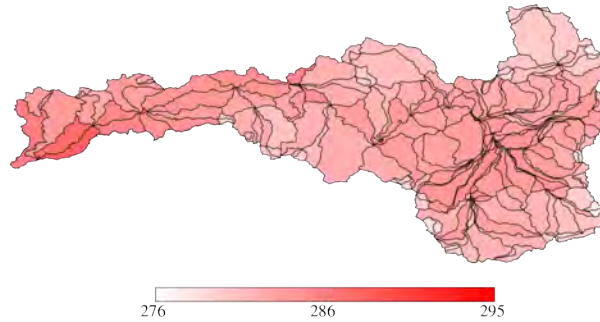
10-Year Average of Annual Average Air Temperature (deg C)
ECHAM5 A2-2 wy2030-wy2040



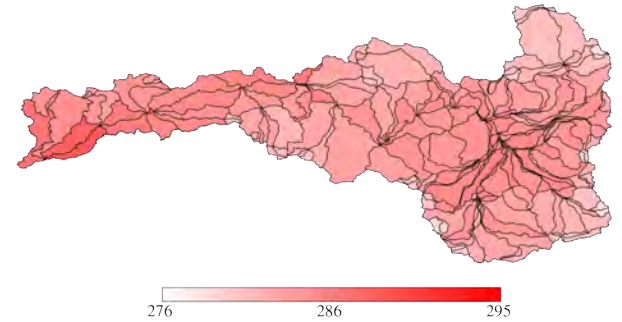
10-Year Average of Annual Average Air Temperature (deg C)
ECHAM5 A2-2 wy2040-wy2050



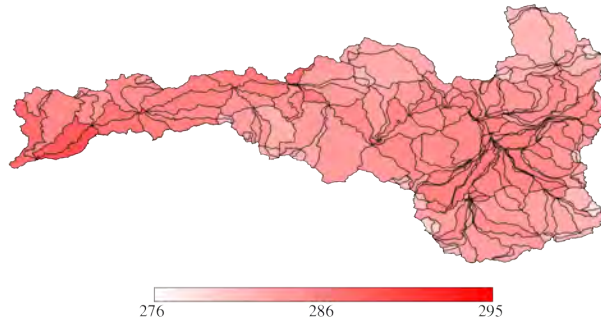
10-Year Average of Annual Average Air Temperature (deg C)
ECHAM5 A2-2 wy2050-wy2060



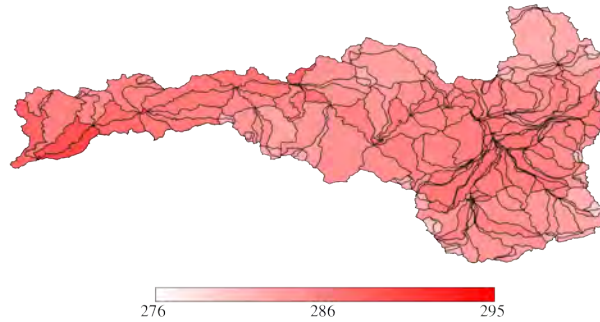
10-Year Average of Annual Average Air Temperature (deg C)
ECHAM5 A2-2 wy2060-wy2070



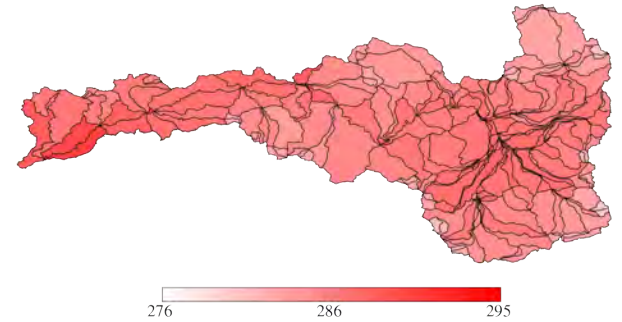
10-Year Average of Annual Average Air Temperature (deg C)
ECHAM5 A2-2 wy2070-wy2080



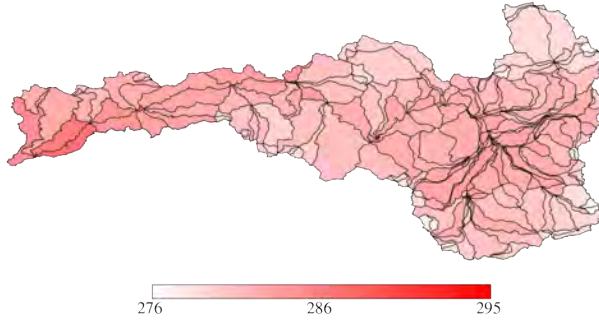
10-Year Average of Annual Average Air Temperature (deg C)
ECHAM5 A2-2 wy2080-wy2090



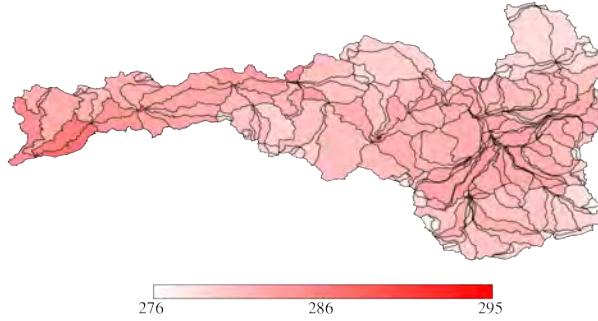
10-Year Average of Annual Average Air Temperature (deg C)
ECHAM5 A2-2 wy2090-wy2100



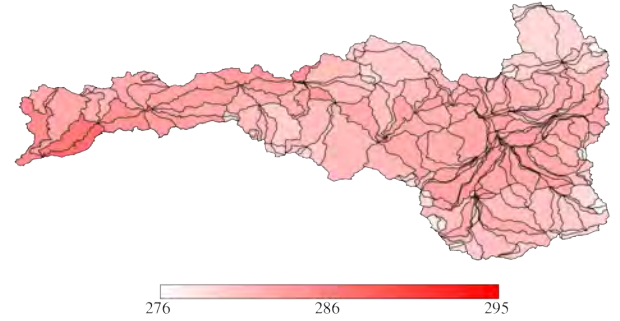
10-Year Average of Annual Average Air Temperature (deg C)
ECHAM5 A2-3 wy2010-wy2020



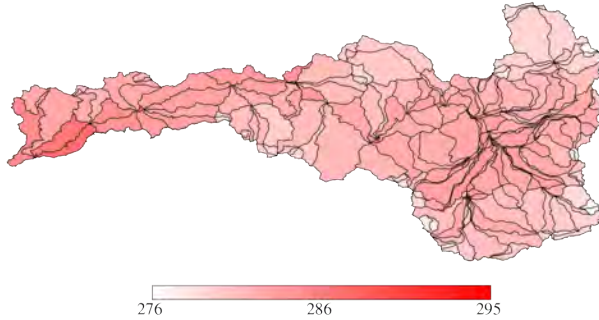
10-Year Average of Annual Average Air Temperature (deg C)
ECHAM5 A2-3 wy2020-wy2030



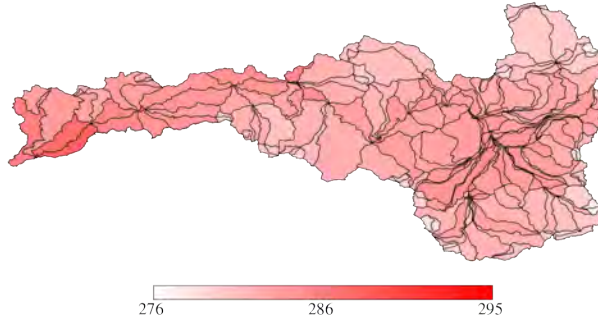
10-Year Average of Annual Average Air Temperature (deg C)
ECHAM5 A2-3 wy2030-wy2040



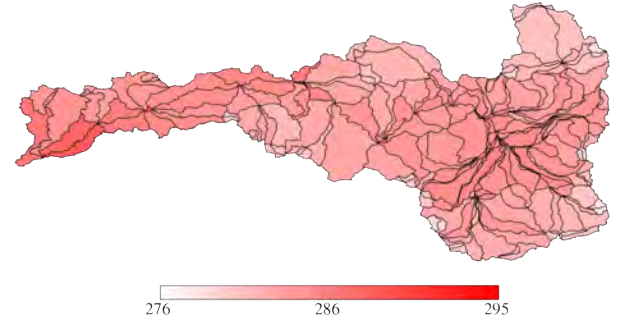
10-Year Average of Annual Average Air Temperature (deg C)
ECHAM5 A2-3 wy2040-wy2050



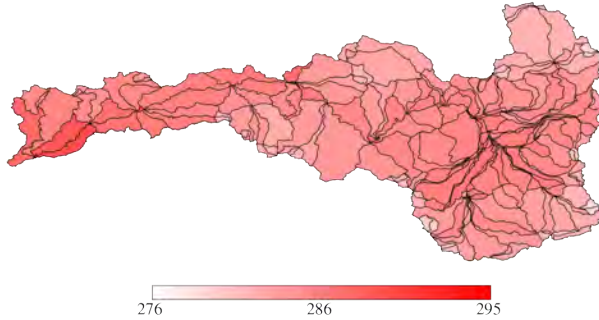
10-Year Average of Annual Average Air Temperature (deg C)
ECHAM5 A2-3 wy2050-wy2060



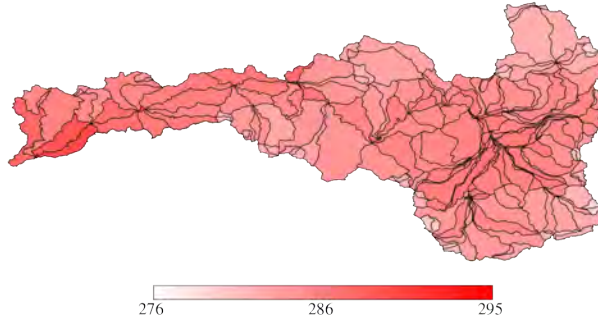
10-Year Average of Annual Average Air Temperature (deg C)
ECHAM5 A2-3 wy2060-wy2070



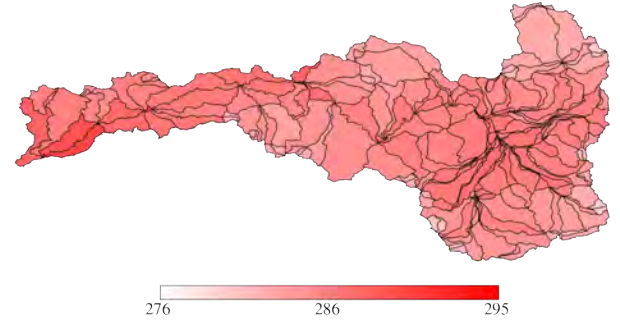
10-Year Average of Annual Average Air Temperature (deg C)
ECHAM5 A2-3 wy2070-wy2080



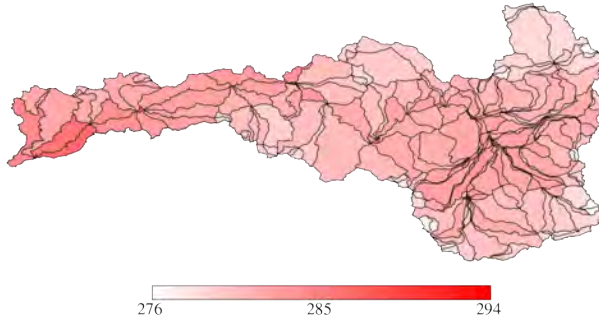
10-Year Average of Annual Average Air Temperature (deg C)
ECHAM5 A2-3 wy2080-wy2090



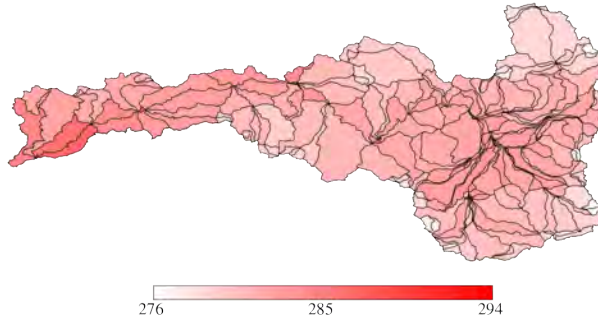
10-Year Average of Annual Average Air Temperature (deg C)
ECHAM5 A2-3 wy2090-wy2100



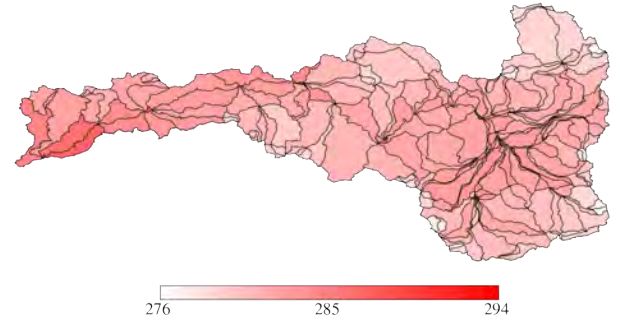
10-Year Average of Annual Average Air Temperature (deg C)
ECHAM5 B1-1 wy2010-wy2020



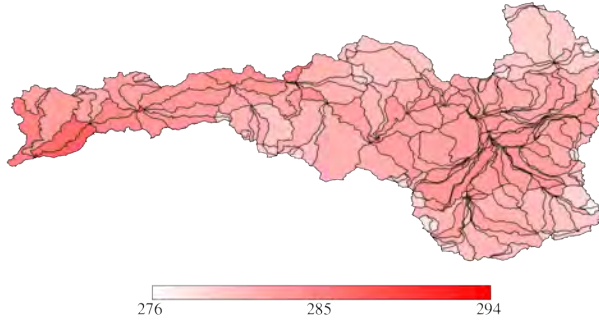
10-Year Average of Annual Average Air Temperature (deg C)
ECHAM5 B1-1 wy2020-wy2030



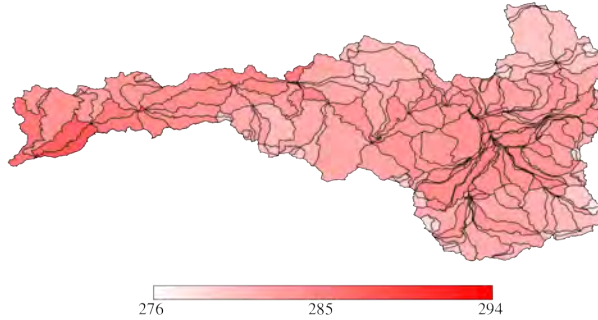
10-Year Average of Annual Average Air Temperature (deg C)
ECHAM5 B1-1 wy2030-wy2040



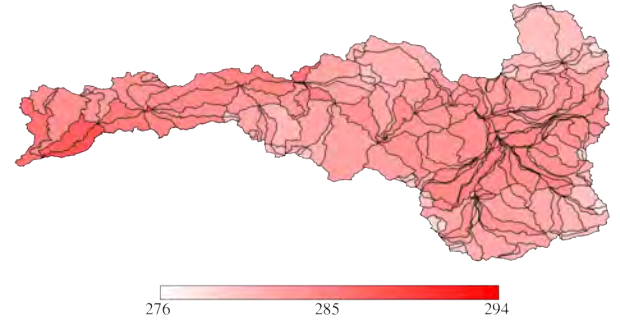
10-Year Average of Annual Average Air Temperature (deg C)
ECHAM5 B1-1 wy2040-wy2050



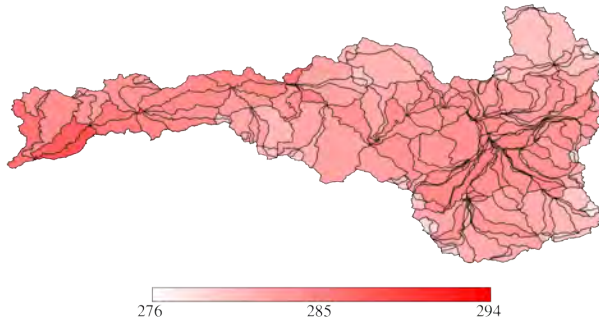
10-Year Average of Annual Average Air Temperature (deg C)
ECHAM5 B1-1 wy2050-wy2060



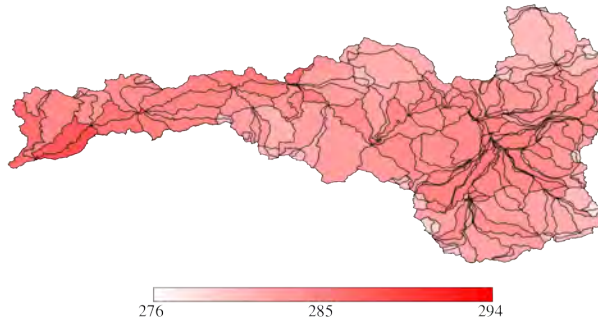
10-Year Average of Annual Average Air Temperature (deg C)
ECHAM5 B1-1 wy2060-wy2070



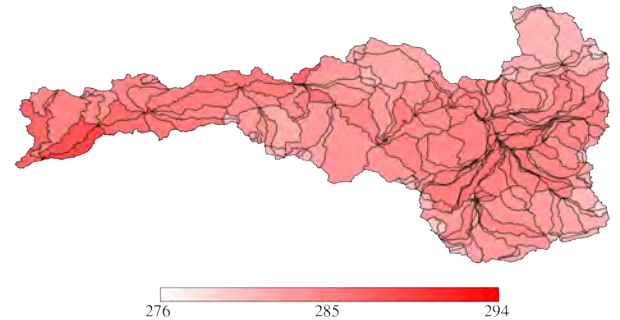
10-Year Average of Annual Average Air Temperature (deg C)
ECHAM5 B1-1 wy2070-wy2080



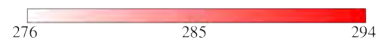
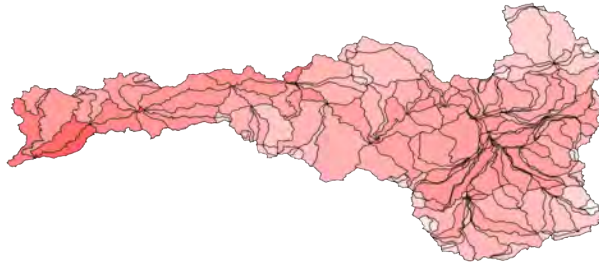
10-Year Average of Annual Average Air Temperature (deg C)
ECHAM5 B1-1 wy2080-wy2090



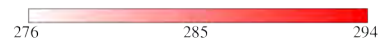
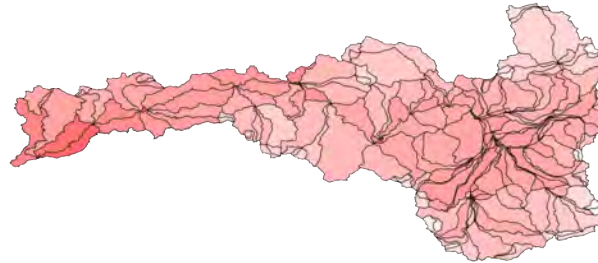
10-Year Average of Annual Average Air Temperature (deg C)
ECHAM5 B1-1 wy2090-wy2100



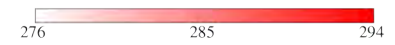
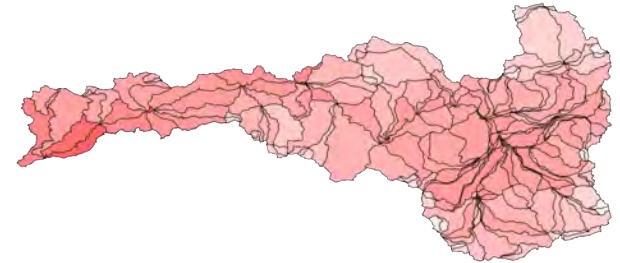
10-Year Average of Annual Average Air Temperature (deg C)
ECHAM5 B1-2 wy2010-wy2020



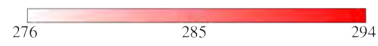
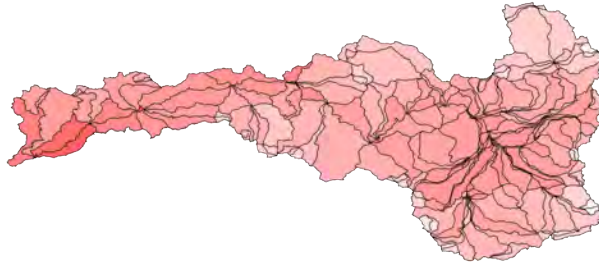
10-Year Average of Annual Average Air Temperature (deg C)
ECHAM5 B1-2 wy2020-wy2030



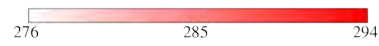
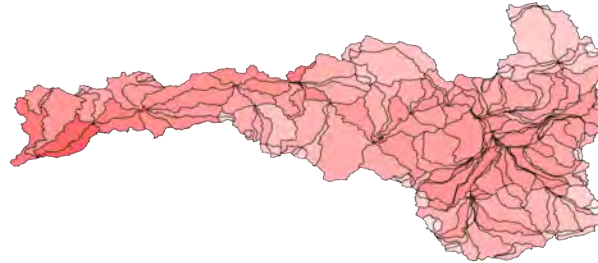
10-Year Average of Annual Average Air Temperature (deg C)
ECHAM5 B1-2 wy2030-wy2040



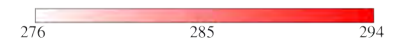
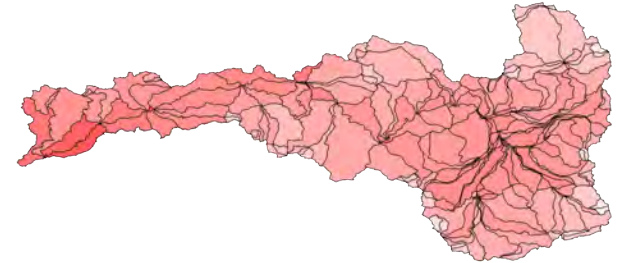
10-Year Average of Annual Average Air Temperature (deg C)
ECHAM5 B1-2 wy2040-wy2050



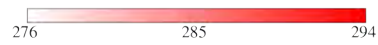
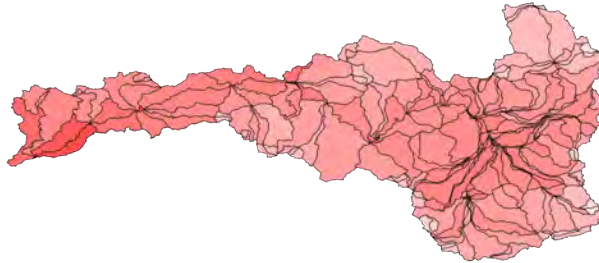
10-Year Average of Annual Average Air Temperature (deg C)
ECHAM5 B1-2 wy2050-wy2060



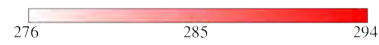
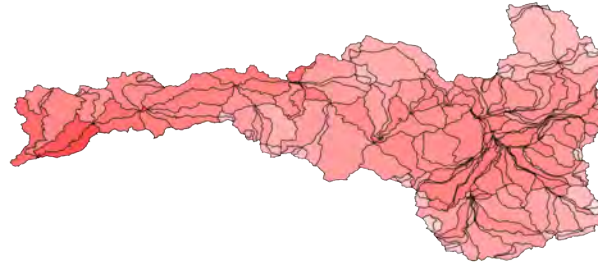
10-Year Average of Annual Average Air Temperature (deg C)
ECHAM5 B1-2 wy2060-wy2070



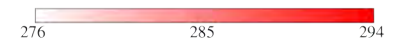
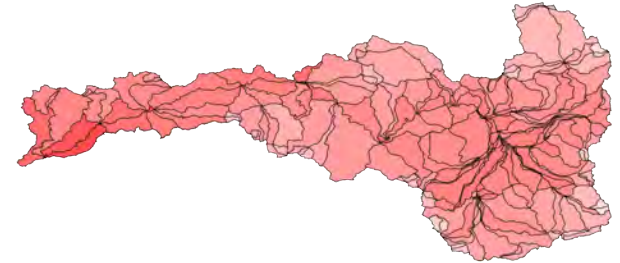
10-Year Average of Annual Average Air Temperature (deg C)
ECHAM5 B1-2 wy2070-wy2080



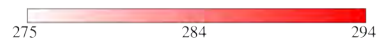
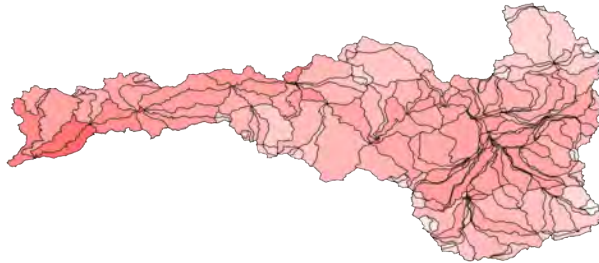
10-Year Average of Annual Average Air Temperature (deg C)
ECHAM5 B1-2 wy2080-wy2090



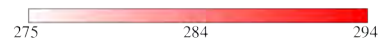
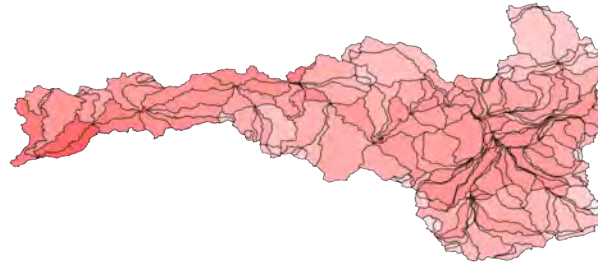
10-Year Average of Annual Average Air Temperature (deg C)
ECHAM5 B1-2 wy2090-wy2100



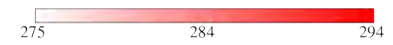
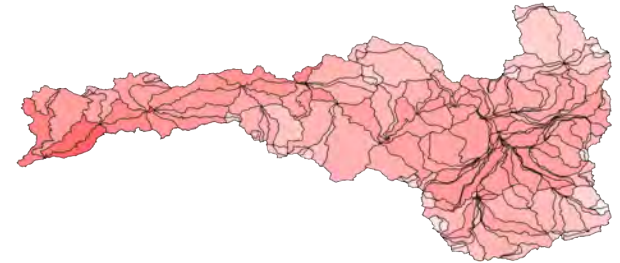
10-Year Average of Annual Average Air Temperature (deg C)
ECHAM5 B1-3 wy2010-wy2020



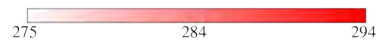
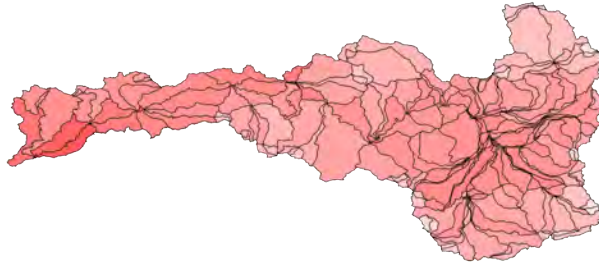
10-Year Average of Annual Average Air Temperature (deg C)
ECHAM5 B1-3 wy2020-wy2030



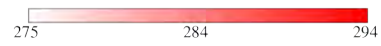
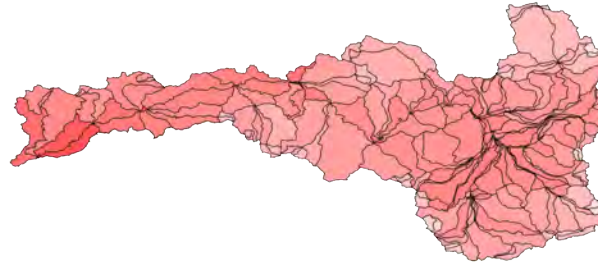
10-Year Average of Annual Average Air Temperature (deg C)
ECHAM5 B1-3 wy2030-wy2040



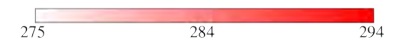
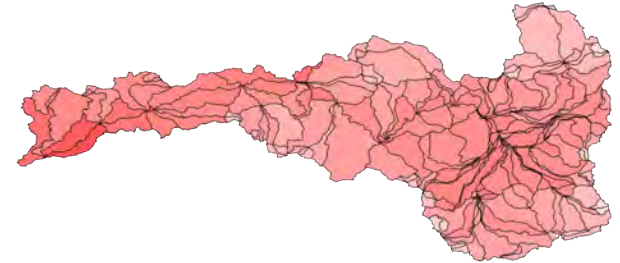
10-Year Average of Annual Average Air Temperature (deg C)
ECHAM5 B1-3 wy2040-wy2050



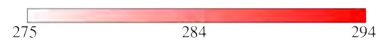
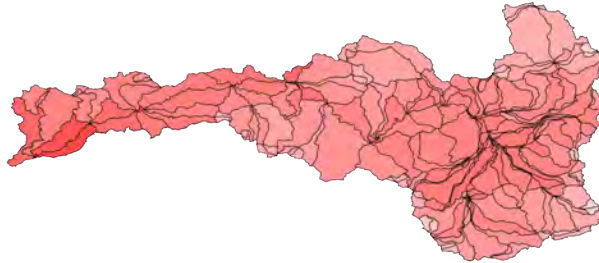
10-Year Average of Annual Average Air Temperature (deg C)
ECHAM5 B1-3 wy2050-wy2060



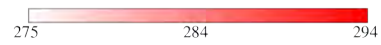
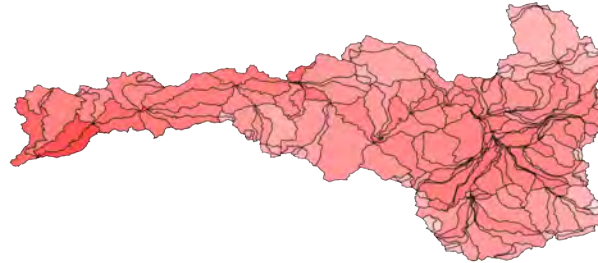
10-Year Average of Annual Average Air Temperature (deg C)
ECHAM5 B1-3 wy2060-wy2070



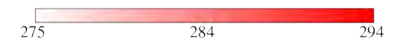
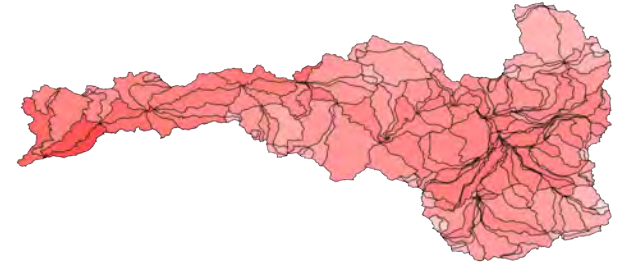
10-Year Average of Annual Average Air Temperature (deg C)
ECHAM5 B1-3 wy2070-wy2080



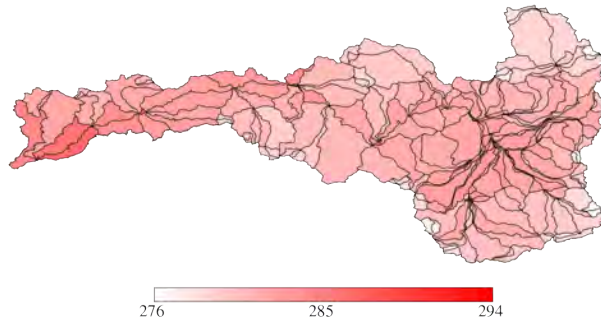
10-Year Average of Annual Average Air Temperature (deg C)
ECHAM5 B1-3 wy2080-wy2090



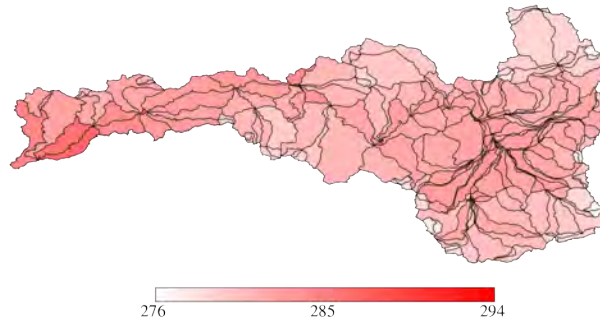
10-Year Average of Annual Average Air Temperature (deg C)
ECHAM5 B1-3 wy2090-wy2100



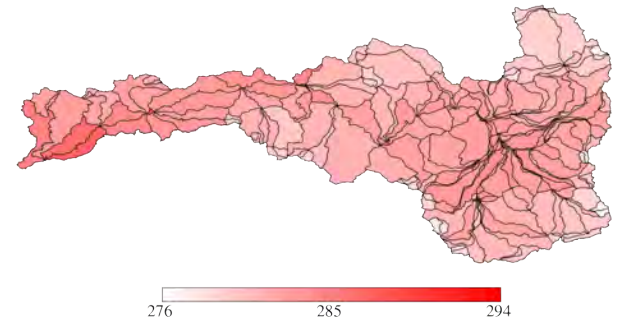
10-Year Average of Annual Average Air Temperature (deg C)
Ensemble All wy2010-wy2020



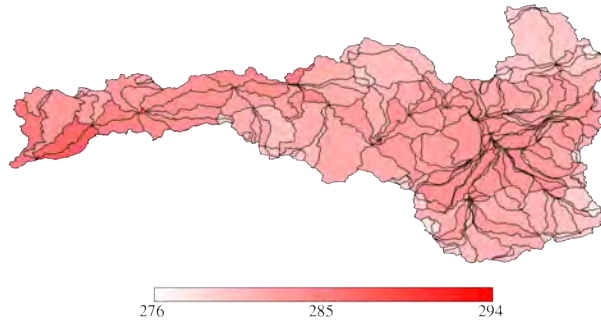
10-Year Average of Annual Average Air Temperature (deg C)
Ensemble All wy2020-wy2030



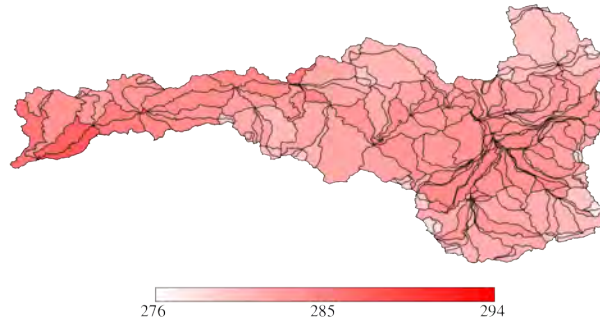
10-Year Average of Annual Average Air Temperature (deg C)
Ensemble All wy2030-wy2040



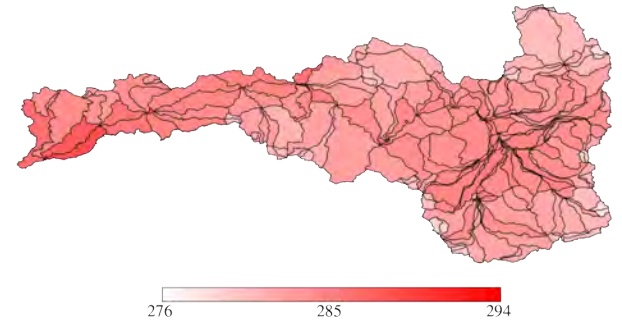
10-Year Average of Annual Average Air Temperature (deg C)
Ensemble All wy2040-wy2050



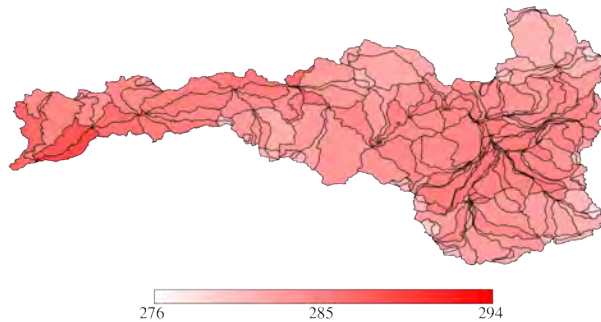
10-Year Average of Annual Average Air Temperature (deg C)
Ensemble All wy2050-wy2060



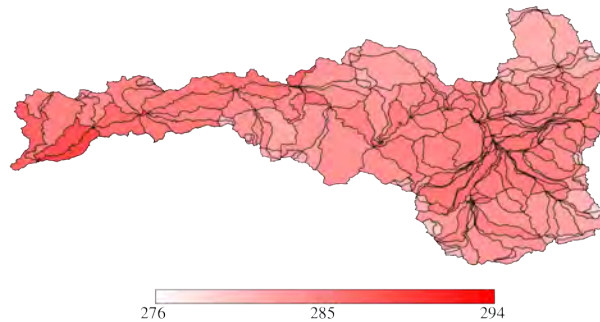
10-Year Average of Annual Average Air Temperature (deg C)
Ensemble All wy2060-wy2070



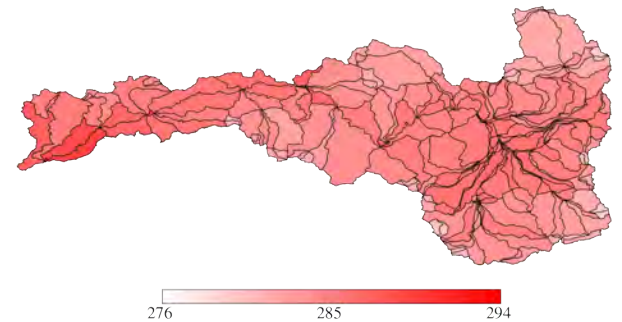
10-Year Average of Annual Average Air Temperature (deg C)
Ensemble All wy2070-wy2080



10-Year Average of Annual Average Air Temperature (deg C)
Ensemble All wy2080-wy2090



10-Year Average of Annual Average Air Temperature (deg C)
Ensemble All wy2090-wy2100



APPENDIX E

Contours of the Piezometric Surface over the Sierra Valley
Aquifer for all 13 Future Projections and their Ensemble
Minimum and Maximum Provided for the End of Each Decade

